

R-05-18

Preliminary site description

Forsmark area – version 1.2

Svensk Kärnbränslehantering AB

June 2005

Svensk Kärnbränslehantering AB

Swedish Nuclear Fuel
and Waste Management Co
Box 5864

SE-102 40 Stockholm Sweden

Tel 08-459 84 00

+46 8 459 84 00

Fax 08-661 57 19

+46 8 661 57 19



ISSN 1402-3091

SKB Rapport R-05-18

Preliminary site description

Forsmark area – version 1.2

Svensk Kärnbränslehantering AB

June 2005

Preface

The Swedish Nuclear Fuel and Waste Management Company (SKB) is undertaking site characterisation at two different locations, the Forsmark and Simpevarp areas, with the objective of siting a geological repository for spent nuclear fuel. An integrated component in the characterisation work is the development of a site descriptive model that constitutes a description of the site and its regional setting, covering the current state of the geosphere and the biosphere as well as those ongoing natural processes that affect their long-term evolution. The present report documents the site descriptive modelling activities (version 1.2) for the Forsmark area.

The overall objectives of the version 1.2 site descriptive modelling are to produce and document an integrated description of the site and its regional environments based on the site-specific data available from the initial site investigations and to give recommendations on continued investigations. The modelling work is based on primary data, i.e. quality-assured, geoscientific and ecological field data available in the SKB databases SICADA and GIS, available July 31, 2004.

The work has been conducted by a project group and associated discipline-specific working groups. The members of the project group represent the disciplines of geology, rock mechanics, thermal properties, hydrogeology, hydrogeochemistry, transport properties and surface ecosystems (including overburden, surface hydrogeochemistry and hydrology). In addition, some group members have specific qualifications of importance in this type of project e.g. expertise in RVS (Rock Visualisation System) modelling, GIS-modelling and in statistical data analysis.

The overall strategy to achieve a site description is to develop discipline-specific models by interpretation and analyses of the primary data. The different discipline-specific models are then integrated into a site description. Methodologies for developing the discipline-specific models are documented in methodology reports or strategy reports. A forum for technical coordination between the sites/projects controls that the methodology is applied as intended and is developed, if deemed necessary. The forum consists of specialists in each field as well as the project leaders of both modelling projects.

The following individuals and expert groups contributed to the project and/or to the report:

- Kristina Skagius – project leader and editor,
- Lennart Ekman – investigation data,
- Michael Stephens, Isabelle Olofsson, Paul La Pointe, Assen Simeonov, Ola Forssberg, Jan Hermanson – geology,
- Flavio Lanaro, Rolf Christiansson, Isabelle Olofsson, Anders Fredriksson – rock mechanics,
- Jan Sundberg and co-workers – thermal properties,
- Sven Follin, Ingvar Rhén, Lee Hartley and the members of the HydroNET Group, – hydrogeology,
- Marcus Laaksoharju and the members of the HAG group – hydrogeochemistry,
- Jan-Olof Selroos, Johan Byegård and co-workers – transport properties,
- Björn Söderbäck, and the members of the SurfaceNET group – surface ecosystems (including overburden),
- Johan Andersson – confidence assessment,
- Anders Lindblom – production of maps and figures.

The report has been reviewed by the following members of SKB's international Site Investigation Expert Review Group (SIERG): Per-Eric Ahlström (Chairman); Jordi Bruno (Enviros, Spain); John Hudson (Rock Engineering Consultants, UK); Ivars Neretnieks (Royal Institute of Technology, Sweden); Lars Söderberg (SKB); Mike Thorne (Mike Thorne and Associates Ltd, UK); Gunnar Gustafson (Chalmers University); Roland Pusch (GeoDevelopment AB). The group provided many

valuable comments and suggestions for this work and also for future work. The latter group is not to be held responsible for any remaining shortcomings of the report. Additional and most valuable review comments were provided by Alan Geoffrey Milnes with a special focus on the geological parts of the site description. Review comments on the details of the geological models were also provided by Raymond Munier (SKB).

Anders Ström
Site Investigations – Analysis

Summary

A site descriptive model constitutes a description of the site and its regional setting, covering the current state of the geosphere and the biosphere as well as those ongoing natural processes that affect their long-term evolution. The main objectives of the site descriptive modelling of the Forsmark area, version 1.2, are to produce this integrated description based on site-specific data available from the initial site investigations as well as to give recommendations on continued investigations. The modelling work is based on quality-assured, geoscientific and ecological field data from Forsmark that were available at the time for data freeze 1.2, July 31, 2004.

The candidate area for site investigations at Forsmark is situated within the north-westernmost part of a tectonic lens. This lens extends along the Uppland coast from north-west of the nuclear power plant south-eastwards to Öregrund and it is approximately 25 km long. The candidate area is approximately 6 km long and the north-western part of the candidate area has been selected as the target area for continued site investigations during the complete site investigation phase.

The primary data available for model version 1.2 originate from surface investigations in the candidate area with its regional environment and from drilling and investigations in boreholes. In addition, old data collected during the construction of the nuclear reactors at the Forsmark power plant and from the pre-investigations and construction of SFR were part of the version 1.2 database. The surface-based data are from geoscientific and ecological investigations on land and off shore. Depth data originate from drilling and investigations in five c. 1,000 m deep, and two shallower cored boreholes, 500 m and 100 m deep, respectively. In addition, data from 19 percussion-drilled boreholes (c. 200 m deep) and from c. 65 boreholes through the Quaternary deposits were available.

Modelling results and main features of the site

A first attempt has been made to provide an integrated description of the surface system. Quantitative modelling of Quaternary cover thickness, shallow groundwater and surface water has been undertaken that supports earlier conceptual models. Terrestrial, limnic and marine ecosystem models have been developed for the drainage area of Lake Bolundsfjärden, which is located within the target area. The results indicate that by far the largest pool of carbon in the ecosystem is stored in soil and sediments and that the largest flux of carbon is driven by the exchange of water between the marine basins and between the marine basins and the open Baltic Sea.

The topography of the Forsmark area is gently undulating and of quite moderate elevation. Unconsolidated Quaternary deposits cover c. 85% of the land area in the regional model area and the overburden is dominated by glacial till of different character. Despite the modest topography, the upper surface of the bedrock is found to undulate over small distances implying large variations in thickness of the Quaternary cover (between 0 and c.17 m). The small-scale topography implies that many local, shallow groundwater flow systems are formed in the Quaternary deposits, overlying more large-scale flow systems associated with groundwater flows at greater depths. The Quaternary deposits are rich in CaCO₃. This together with the recent emergence of the area from the Baltic Sea affects the chemistry of surface and shallow groundwaters giving rise to high pH and high alkalinity.

The bedrock in the candidate area is dominated by one lithological domain, defined as rock domain RFM029. The dominant rock type in this domain is a medium-grained metagranite (84% of the domain volume). This metagranite and subordinate rock types extend downwards to a depth of at least 1,000 m. Rock domains with strongly deformed, and also in part, banded and inhomogeneous rocks occur along the south-western and the north-eastern margins of the tectonic lens and the candidate area.

There is no potential for exploration for metallic and industrial mineral deposits within the Forsmark candidate area. A potential for iron oxide mineralisation has been recognised in an area south-west of the candidate area, but the mineral deposits are small and have been assessed to be of no economic value.

Three major sets of deformation zones have been recognised with high confidence of occurrence at the Forsmark area. Vertical and steeply, SW-dipping zones with WNW-NW strike, form important regional structures at the boundary of the candidate volume (e.g. Forsmark and Singö deformation zones). The second set comprises vertical and steeply-dipping, brittle deformation zones with NE strike that transect the candidate volume at Forsmark and are prominent in the Bolundsfjärden area. The third set comprises gently SE- and S-dipping brittle deformation zones that occur more frequently in the south-eastern part of the candidate volume. Uncertainties still remain concerning the geometry and character of deformation zones, mainly in the regional domain outside the candidate area, as well as in the extension of the gently dipping deformation zones. For these reasons, three alternative deformation zone models were developed.

Statistical analyses of rock mass fractures in between deformation zones indicate a large spatial variability in the size, intensity and properties between different rock domains, but also within rock domain RFM029. In general, the fracture frequency is low in rock domain RFM029, with higher frequency in the upper parts of the rock. However, the fracturing shows no consistent depth dependence, but may be affected by the proximity to deformation zones. This is indicated, for example, by the higher frequency of fractures close to the gently dipping zone ZFMNE00A2 in one of the boreholes and very few fractures at larger depths below this zone.

Site-specific data and rock stress modelling have confirmed that rock stresses at Forsmark are relatively high compared with typical central Scandinavian sites. The major principal stress is aligned with the overall direction of the tectonic lens and the associated regional deformation zones. An average maximum horizontal stress of 45 MPa has been estimated at the depth of 500 m. The stress gradient of this stress component at depths between 350 and 650 m is probably small (0.02 MPa/m) compared with the gradient at shallow depths. More site-specific data and analyses have also confirmed the earlier results of high strength and low deformability of the rock mass in rock domain RFM029. The rock types in rock domain RFM029 have high quartz contents and thermal properties that are favourable for a potential repository, e.g. a mean value for the thermal conductivity of approximately 3.6 W/(m·K).

Hydraulic properties of the deformation zones have been interpreted from hydraulic tests. These tests indicate that the gently dipping deformation zones generally have greater transmissivities than the steeply dipping zones at comparative depths, and that all the deformation zones have much greater transmissivities close to the ground surface compared to that at depth. Analyses of hydraulic data from the boreholes show that the rock mass between the deformation zones in the candidate volume has very low hydraulic conductivity beneath the gently dipping deformation zone ZFMNE00A2 at depths below about the -360 m level. In contrast, the upper part of the rock mass is rather conductive. Therefore, the rock mass, also within rock domain RFM029, was divided into different volumes in the evaluation of the hydraulic properties of the rock mass. Regional groundwater flow simulations indicate that the location and properties of the deformation zones inside the candidate volume predominantly determine the groundwater flow within this volume.

Four main groundwater types have been identified at the Forsmark site. Recent to young meteoric (Na-HCO₃ type) waters are found at shallow depths (0–150 m). Old brackish water of Littorina Sea origin (Na-Ca-Cl(SO₄) type) are found at depths between c. 150 and 500 m. At larger depths, a saline (Na-Ca-Cl type) groundwater with a glacial component is found. At still greater depth, a strongly saline non-marine Ca-Na-Cl type groundwater is probably dominating. Most lines of evidence suggest that the sulphur system, microbiologically mediated, is the main redox controller in the deepest and most saline groundwater. Furthermore, the groundwater composition at repository depth is such that it fulfils the SKB chemical suitability criteria for all the principal components, i.e. Eh, pH, TDS, DOC and Ca+Mg.

Hydrogeological simulations of the past evolution of groundwater composition show good agreement between simulated and measured hydrogeochemical data at depth, whereas poorer matches were obtained in the upper 100 m of the rock. Furthermore, these simulations support the occurrence of Littorina Sea water in the upper 500 m of the rock.

No retardation model has been developed, but site-specific data have allowed for parameterisation of rock matrix porosity and formation factor. For the dominant rock type in rock domain RFM029, mean values of porosity and formation factor are 0.2% and 2×10^{-5} , respectively.

Uncertainties and confidence in the site description

Important modelling steps have been taken in the development of model version 1.2 and many of the uncertainties are now quantified or explored as alternative hypotheses/models. Uncertainties in rock mechanics properties, rock stresses and thermal properties are quantified. Uncertainties in the occurrence and geometry of deformation zones have been illustrated by providing alternative models, which have been explored in the hydrogeological modelling. The hydrogeological modelling has also involved a number of sensitivity analyses to illustrate the importance of uncertainties in e.g. boundary conditions, the hydraulic properties of the deformation zones, and the hydraulic properties of the fractures between the deformation zones. Uncertainties in the hydrogeochemical description have been explored by applying different modelling approaches to the same data set.

Our current understanding of the site has been confirmed by the outcome of the version 1.2 modelling and no major surprises have occurred relative to model version 1.1. The fact that much more sub-surface data have implied only minor changes in the rock domain model has significantly increased the confidence in the lithological description. Enhanced confidence in the models for rock mechanics and thermal properties has also been achieved, since the analyses and modelling, now based on a larger data set and site-specific data, confirm the ranges obtained in model version 1.1.

Sub-surface data have confirmed the existence of deformation zones and supported the significance of seismic reflectors as representing gently dipping zones. The deformation zone model is stabilising and can be treated with enhanced confidence in the local model volume. This also increases the confidence in the hydrogeological description, although much uncertainty still remains regarding the hydraulic properties of the deformation zones and of the fracture network in the rock mass between the deformation zones.

Sammanfattning

En platsbeskrivande modell är en beskrivning av platsen och dess regionala omgivning och omfattar geosfärens och biosfärens nuvarande tillstånd liksom de pågående naturliga processer som påverkar platsens utveckling i ett långtidsperspektiv. Huvudsyftena med version 1.2 av den beskrivande platsmodellen för Forsmarksområdet är att upprätta en integrerad beskrivning baserad på plats-specifika data från de inledande platsundersökningarna och att ge rekommendationer angående de fortsatta undersökningarna. Modellarbetet baseras på de kvalitetssäkrade geovetenskapliga och ekologiska fältdata från Forsmark som var tillgängliga vid tillfället för datafrys 1.2 den 31 juli 2004.

Kandidatområdet där platsundersökningarna i Forsmark genomförs är beläget i den nordvästligaste delen av en tektonisk lins. Denna lins sträcker sig längs Upplandskusten från ett område nordväst om kärnkraftverket i sydöstlig riktning till Öregrund och är ca 25 km lång. Kandidatområdet är ca 6 km långt och den nordvästra delen har valts ut som fokuserat område för fortsatta undersökningar under det kompletta platsundersökningsskedet.

Tillgängliga primärdata för modellversion 1.2 härrör från ytundersökningar inom kandidatområdet och dess regionala omgivningar liksom från borrhningar och undersökningar i borrhål. Dessutom utgör äldre data från byggandet av kärnkraftsreaktorerna samt från förundersökningarna och byggandet av SFR en del av databasen för version 1.2. Ytdata härrör från geovetenskapliga och ekologiska undersökningar på land och utanför kusten. Data på djupet kommer från borrhningar och undersökningar i fem ca 1 000 m djupa och två grundare kärnborrhål, 500 respektive 100 m djupa. Dessutom var data tillgängliga från 19 hammarborrhål (ca 200 m djupa) och från ca 65 borrhål genom de kvartära avlagringarna.

Modellresultat och platsens huvuddrag

Ett första försök har gjorts att tillhandahålla en integrerad beskrivning av det ytliga systemet. Kvantitativ modellering av tjockleken av det kvartära jordlagret, av ytnära grundvatten och ytvatten har utförts och resultaten understödjer tidigare konceptuella modeller. Modeller har upprättats för terrestra, limniska och marina ekosystem inom Bolundfjärdens avrinningsområde som är beläget inom det fokuserade området för fortsatta undersökningar. Resultaten antyder att den särklassigt största förekomsten av kol finns i jord och sediment och att det största kolflödet sker via vattenutbytet mellan avgränsade havsbassänger samt mellan dessa bassänger och öppet vatten i Östersjön.

Topografin i Forsmarksområdet är utpräglad låglänt med små nivåskillnader. Ungefär 85 % av landytan i det regionala modellområdet täcks av lösa kvartära avlagringar. Avlagringarna domineras av glacial morän av varierande karaktär. Bergöverytans nivå varierar mer än markytans vilket medför att de kvartära avlagringarnas tjocklek varierar kraftigt (mellan 0 och ca 17 m). Den småskaliga topografin medför att många lokala grundvattenströmningssystem bildas i de kvartära avlagringarna. Dessa överlagras mer storskaliga strömningceller som sammanhänger med grundvattenströmningen på större djup. De kvartära avlagringarna innehåller mycket CaCO_3 . Detta tillsammans med det faktum att området relativt nyligen har höjt sig över havsytan påverkar kemin i ytvatten och ytnära grundvatten vilket resulterar i höga pH-värden och hög alkalinitet.

Urberget inom kandidatområdet domineras av en litologisk domän som definierats som bergdomän RFM029. Den dominerande bergarten inom denna domän är medelkornig metagranit (84 % av domänvolymen). Metagraniten och underordnade bergarter sträcker sig nedåt till ett djup av minst 1 000 m. Bergdomäner med starkt deformerat och delvis bandat inhomogent berg återfinns längs de sydvästra och nordöstra gränserna av den tektoniska linsen och kandidatområdet.

Det finns ingen potential för utforskning av metaller eller industrimineral inom kandidatområdet i Forsmark. En möjlig järnoxidmineralisering har identifierats i den sydvästra delen av kandidatområdet, men den är liten och har bedömts vara utan ekonomiskt värde.

Inom Forsmarksområdet har tre huvudgrupper av deformationszoner identifierats med hög tilltro till deras existens. Vertikala till brant sydvästligt stupande zoner med västnordvästlig till nordvästlig strykning, bildar viktiga regionala strukturer vid kandidatområdet gränser (t ex Forsmarkszonen och Singözonen). Den andra gruppen utgörs av vertikala till brant stupande spröda deformationszoner med nordöstlig strykning som tvärrar över kandidatvolymen. Dessa zoner är betydande i området rund Brolundfjärden. Den tredje gruppen utgörs av spröddeformerade flacka zoner med svag sydöstlig till sydlig stupning. Dessa zoner uppträder mer frekvent i den sydöstra delen av kandidatområdet. Det finns kvarstående osäkerheter avseende deformationszonernas geometri och karaktär, huvudsakligen inom det regionala området, liksom i de flacka deformationszonernas utsträckning. På grund av dessa osäkerheter har tre alternativa deformationszonsmodeller tagits fram.

Statistiska analyser av sprickor i bergmassan mellan deformationszonerna visar på en stor rumslig variabilitet avseende storlek, frekvens och egenskaper mellan olika bergdomäner i området men även inom bergdomän RFM029. Generellt sett är sprickfrekvensen i bergdomän RFM029 låg, men med något högre värden i den övre delen av berget. Uppsprickningen visar emellertid ingen entydig koppling till djupet utan verkar snarare ha påverkats av närheten till deformationszoner. Detta indikeras t ex av den högre sprickfrekvensen som iakttagits nära den flacka zonen ZFMNE00A2 i ett av borrhålen och den väsentligt lägre sprickfrekvensen på större djup under denna zon.

Platsspecifika data och modellering av bergspänningar har bekräftat att bergspänningarna inom Forsmarksområdet är relativt höga jämfört med typiska förhållanden i centrala Skandinavien. Riktningen för den största huvudspänningen sammanfaller med utsträckningen av den tektoniska linsen och de omgivande regionala deformationszonerna. Medelvärdet av den maximala horisontella spänningen på 500 m djup har uppskattats till 45 MPa. Sannolikt är gradienten av denna spänning liten mellan 350 och 650 m djup (0.02 MPa/m) jämfört med gradienten på mindre djup. Ytterligare platsspecifika data och analyser har också bekräftat de tidigare resultaten som visade på hög styrka och låg deformerbarhet av bergmassan i bergdomän RFM029. Bergarterna inom denna domän har ett högt kvartsinnehåll och termiska egenskaper som är gynnsamma för ett potentiellt slutförvar, t ex är medelvärde för värmekonduktiviteten 3,6 W/(m·K).

Deformationszonernas hydrauliska egenskaper har tolkats från resultat av hydrauliska tester. Dessa visar att flacka deformationszoner generellt har högre transmissiviteter än brantstående zoner vid samma djup samt att alla zoner oavsett stupning har väsentligt högre transmissivitet nära markytan än på större djup. Analyser av hydrauliska data från borrhål visar att berget mellan deformationszonerna i kandidatvolymen är mycket lågkonduktivt under den flacka zonen ZFMNE00A2, dvs på djup större än ca -360 m. Den övre delen av bergmassan är däremot relativt konduktiv. Baserat på dessa observationer har bergmassan inom bergdomän RFM029 delats in i olika volymer för utvärderingen av de hydrauliska egenskaperna. Modellsimuleringar av det regionala grundvattenflödet indikerar att flödet inom kandidatvolymen till övervägande del styrs av deformationszonerna inom kandidatvolymen, i termer av deras läge och egenskaper.

Fyra grundvattentyper har identifierats inom Forsmarksområdet. Nutida eller ungt meteoriskt (Na-HCO₃-typ) vatten hittas i den övre delen av berget (0–150 m). Äldre bräckt vatten med ursprung i Littorinahavet (Na-Ca-Cl(SO₄)-typ) hittas mellan ca 150 och 500 m djup. På större djup återfinns ett salt (Na-Ca-Cl-typ) grundvatten med inslag av glacialt vatten. På ytterligare större djup dominerar sannolikt ett salt grundvatten av Na-Ca-Cl-typ av icke-marint ursprung. Resultaten av analyserna antyder att svavelsystemet, med mikrobiellt understöd, styr redoxförhållandena i det djupaste grundvattnet med de högsta salthalterna. Dessutom är grundvattensammansättningen på förvarsdjup sådan att den uppfyller SKB:s kemiska kriterier för alla huvudkomponenter, dvs Eh, pH, TDS, DOC och Ca+Mg.

Hydrogeologiska simuleringar av den historiska utvecklingen av grundvattensammansättningen visar en god överensstämmelse mellan beräknade och mätta hydrogeokemiska data på djupet medan överensstämmelsen var sämre för data i de övre 100 m av berget. Dessa simuleringar ger också stöd för förekomsten vatten från Littorinahavet i de övre 500 m av berget.

Ingen retardationsmodell har ännu tagits fram, men platsspecifika data har möjliggjort en parametrering av bergmatrixens porositet och formationsfaktor. För den dominerande bergarten i bergdomän RFM029 är medelvärdet för porositet bestämt till 0,2 % och medelvärdet för formationsfaktorn till 2×10^{-5} .

Osäkerheter och tilltro till platsbeskrivningen

I samband med utvecklingen av version 1.2 av den platsbeskrivande modellen har viktiga modelleringssteg tagits. Många av osäkerheterna har nu kvantifierats eller analyserats som alternativa hypoteser/modeller. Osäkerheter i bergmekaniska egenskaper, bergsspänningar och termiska egenskaper har kvantifierats. Osäkerheter kopplade till deformationszoners förekomst och geometri har illustrerats genom upprättande av alternativa modeller som har analyserats i den hydrogeologiska modelleringen. Den hydrogeologiska modelleringen har även omfattat ett antal känslighetsanalyser som illustrerar betydelsen av osäkerheter i t ex randvillkor, i deformationszonernas hydrauliska egenskaper och i de hydrauliska egenskaperna hos sprickorna mellan deformationszonerna. Osäkerheterna i den hydrogeokemiska beskrivningen har studerats genom att använda alternativa modellansatser på samma uppsättning data.

Vår uppfattning av platsens egenskaper har bekräftats av resultaten från version 1.2 av platsmodelleringen och inga väsentliga överraskningar har uppkommit jämfört med modell version 1.1. Det faktum att tillkomsten av stora mängder data från djupet har medfört endast mindre ändringar i bergdomänmodellen har väsentligt ökat tilltron till den litologiska beskrivningen. Även tilltron till modellerna för de bergmekaniska och termiska egenskaperna har ökat då analyser och modellering baserade på större datamängder och platsspecifika data bekräftar de storleksordningarna som redovisades i version 1.1 av modellen.

Underjordsdata har bekräftat förekomsten av deformationszoner och givit stöd för att seismiska reflektorer representerar flacka zoner. Modellen av deformationszonerna är mer stabil än tidigare och tilltron till modellen är högre i den lokala modellvolymen. Detta ökar även tilltron till den hydrogeologiska beskrivningen även om osäkerheterna fortfarande är stora vad det gäller deformationszonernas hydrauliska egenskaper och de hydrauliska egenskaperna hos spricknätverket mellan deformationszonerna.

Contents

1	Introduction	19
1.1	Background	19
1.2	Scope and objectives	20
1.3	Setting	21
1.4	Methodology and organisation of work	22
1.4.1	Methodology	22
1.4.2	Interfaces between disciplines	24
1.4.3	Organisation of work	24
1.4.4	Important changes compared to Forsmark 1.1 work	25
1.5	This report	26
2	Available data and other prerequisites for the modelling	27
2.1	Overview of investigations	27
2.1.1	Investigations and primary data acquired up to data freeze 1.1.	27
2.1.2	Data freeze 1.2 – investigations performed and data acquired	28
2.2	Previous model versions	29
2.2.1	Forsmark model version 0	29
2.2.2	Forsmark model version 1.1	29
2.3	Geographical data	30
2.4	Surface investigations	31
2.4.1	Bedrock geology and ground geophysics	31
2.4.2	Quaternary geology and ground geophysics	32
2.4.3	Meteorology and hydrology	32
2.4.4	Hydrochemistry	32
2.4.5	Surface ecology	33
2.5	Borehole investigations	33
2.5.1	Drilling and measurements while drilling	35
2.5.2	Drill core, drill cuttings and borehole investigations after completion of drilling	38
2.6	Other data sources	40
2.7	Databases	41
2.8	Model volumes	61
2.8.1	General	61
2.8.2	Regional model volume	62
2.8.3	Local model volume	62
3	Evolutionary aspects of the Forsmark site	65
3.1	Crystalline bedrock from c. 1,910 million years ago to the Quaternary period	65
3.1.1	Background	65
3.1.2	Primary geochronological data	69
3.1.3	Timing of crystallisation of the igneous rocks at the Forsmark site	69
3.1.4	Timing of ductile deformation at the Forsmark site	70
3.1.5	Timing of brittle deformation and Phanerozoic fluid movement at the Forsmark site	73
3.2	Late-or post-glacial faulting during the Quaternary period	74
3.3	Quaternary deposits and other regoliths	77
3.3.1	Quaternary development of Sweden	77
3.3.2	The Pleistocene	79
3.3.3	The latest deglaciation	81
3.3.4	Climate and vegetation after the latest deglaciation	81
3.3.5	Development of the Baltic Sea after the latest deglaciation	82
3.3.6	Late Quaternary history of the Forsmark area	83
3.4	Surface and groundwater	85

3.4.1	Premises for surface water evolution	85
3.4.2	Post-glacial conceptual model of groundwater evolution	87
3.5	Surface ecosystems	89
3.5.1	The Baltic Sea	89
3.5.2	Lacustrine ecosystems	90
3.5.3	Vegetation	91
3.5.4	Wild fauna	92
3.5.5	Population and land use	93
4	The surface system	95
4.1	State of knowledge at previous model version	95
4.2	Evaluation of primary data	95
4.2.1	Overburden including Quaternary deposits	96
4.2.2	Climate, hydrology and hydrogeology	96
4.2.3	Chemistry	97
4.2.4	Biota	98
4.2.5	Humans and land use	99
4.3	Model of the overburden including Quaternary deposits	99
4.3.1	Background	99
4.3.2	The surface and stratigraphy of Quaternary deposits	100
4.3.3	Lake sediment and peat	102
4.3.4	Offshore Quaternary deposits	103
4.3.5	Chemical composition of the Quaternary deposits	104
4.3.6	The soil types	104
4.3.7	Soil depth model	104
4.4	Description of climate, hydrology and hydrogeology	106
4.4.1	Conceptual and descriptive modelling	106
4.4.2	Some observations from quantitative flow modelling	107
4.5	Chemistry	109
4.5.1	Methodology	109
4.5.2	Description and conceptual model	110
4.6	Biota	111
4.6.1	Terrestrial producers	111
4.6.2	Terrestrial consumers	114
4.6.3	Limnic producers	115
4.6.4	Limnic consumers	117
4.6.5	Marine producers	118
4.6.6	Marine consumers	120
4.7	Humans and land use	121
4.8	Development of the ecosystem models	121
4.8.1	Terrestrial ecosystem description	122
4.8.2	Limnic ecosystem description	123
4.8.3	Marine ecosystem description	126
4.9	Evaluation of uncertainties	128
4.9.1	Abiotic descriptions	128
4.9.2	Biotic descriptions	129
5	Bedrock geology	133
5.1	State of knowledge at previous model version	133
5.2	Evaluation of primary data	134
5.2.1	Outcrop mapping and complementary analytical studies	134
5.2.2	Rock type distribution on the surface	149
5.2.3	Lineament identification	156
5.2.4	Observation of ductile and brittle structures from the surface	166
5.2.5	Surface geophysics	177
5.2.6	Borehole data – rock types, ductile structures, borehole radar, geophysical logs	186
5.2.7	Fracture statistics from cored borehole data	194
5.2.8	Single hole interpretation	204

5.3	Rock domain model	210
5.3.1	Modelling assumptions and input from other disciplines	210
5.3.2	Conceptual model	211
5.3.3	Division into rock domains and property assignment	213
5.3.4	Evaluation of uncertainties	225
5.4	Deterministic deformation zone modelling	228
5.4.1	Modelling assumptions and input from other disciplines	228
5.4.2	Conceptual model and alternative geometric models	229
5.4.3	Determination and property assignment of deformation zones	233
5.4.4	Evaluation of uncertainties	248
5.5	Statistical model of fractures and deformation zones	254
5.5.1	Modelling assumptions	254
5.5.2	Derivation of statistical model with properties	255
5.5.3	Conceptual model with potential alternatives	263
5.5.4	Verification tests for conceptual models	264
5.5.5	Evaluation of uncertainties	265
5.6	Feedback to other disciplines	266
6	Rock mechanics model	267
6.1	State of knowledge at previous model version	267
6.2	Evaluation of primary data	268
6.2.1	Laboratory tests on intact rock	268
6.2.2	Laboratory tests on natural rock fractures	270
6.2.3	Other data	271
6.2.4	Rock mass properties based on borehole data	272
6.3	Rock mechanics properties	274
6.3.1	Modelling assumptions and input from other disciplines	274
6.3.2	Conceptual model with potential alternatives	275
6.3.3	Assignment of rock mechanics properties to the intact rock	276
6.3.4	Assignment of rock mechanics properties to the rock fractures	277
6.3.5	Empirical approach	277
6.3.6	Theoretical approach	279
6.3.7	Assignment of rock mechanics properties to the model volumes	280
6.3.8	Evaluation of uncertainties	286
6.4	State of stress	288
6.4.1	Stress measurements	288
6.4.2	Modelling assumptions and input from other disciplines	290
6.4.3	Conceptual model with potential alternatives	290
6.4.4	Stress distribution in the model volume	292
6.4.5	Evaluation of the uncertainties	296
7	Bedrock thermal model	299
7.1	State of knowledge at the previous model version	299
7.2	Evaluation of primary data	299
7.2.1	Thermal conductivity from measurements	299
7.2.2	Thermal conductivity from mineral composition	301
7.2.3	Thermal conductivity from density	301
7.2.4	Modelling of thermal conductivity (rock type level)	302
7.2.5	Heat capacity	304
7.2.6	Anisotropy	304
7.2.7	Coefficient of thermal expansion	305
7.2.8	In-situ temperature	305
7.3	Thermal modelling (lithological domain level)	306
7.3.1	Modelling assumptions and input from other disciplines	306
7.3.2	Conceptual model	307
7.3.3	Modelling approaches	308
7.3.4	Conclusions – modelling results	313
7.3.5	Evaluation of uncertainties	315

7.4	Feedback to other disciplines	318
8	Bedrock hydrogeology	319
8.1	State of knowledge at previous model version	319
8.2	Evaluation of primary data	321
8.2.1	Hydraulic evaluation of single-hole tests	321
8.2.2	Hydraulic evaluation of interference tests	340
8.2.3	Joint hydrogeology and geology interpretation	344
8.3	Hydrogeological modelling – general conditions and concepts	348
8.3.1	Modelling objectives and premises	348
8.3.2	General modelling assumptions and input from other disciplines	349
	Data sources	349
8.3.3	Modelling strategy	351
8.3.4	Hydrogeological DFN	352
	Transmissivity of conductive features	356
8.3.5	General assumptions regarding block size properties	361
8.3.6	General assumptions regarding HCD, HRD, HSD, initial and boundary conditions	361
8.4	Assignment of hydraulic properties	362
8.4.1	Assignment of hydraulic properties to the HSDs	362
8.4.2	Assignment of hydraulic properties to the HCDs	362
8.4.3	Assignment of hydraulic properties to the HRDs	364
8.4.4	Block-size properties	381
8.5	Boundary and initial conditions	389
8.5.1	Boundary conditions	389
8.5.2	Initial conditions	391
8.6	Regional groundwater simulations	392
8.6.1	Hydraulic properties	392
8.6.2	Cases for the modelling	395
8.6.3	Comparisons with measured data	397
8.6.4	Palaeo-hydrogeological evolution	407
8.6.5	Flow path simulations and exit locations	409
8.6.6	Sensitivity analyses	411
8.7	Evaluation of uncertainties	415
8.7.1	Overburden and the upper parts of the bedrock	415
8.7.2	Deformation zones	416
8.7.3	Rock mass	417
8.7.4	Boundary and initial conditions	417
8.8	Feedback to other disciplines	418
9	Bedrock hydrogeochemistry	419
9.1	State of knowledge at the previous model version	419
9.2	Hydrogeochemical data	419
9.2.1	Groundwater chemistry data sampled in boreholes	420
9.2.2	Representativeness of the data	420
9.2.3	Explorative analysis	423
9.3	Modelling assumptions and input from other disciplines	456
9.4	Conceptual model with potential alternatives	458
9.5	Hydrogeochemical modelling	458
9.5.1	Calcium carbonate system	458
9.5.2	Silica system	461
9.5.3	Sulphate system	462
9.5.4	Massbalance and mixing calculations using PHREEQC and M4	462
9.5.5	Reaction-path modelling	465
9.5.6	Redox modelling	470
9.5.7	Mixing modelling using M3	473
9.5.8	Visualisation of the groundwater properties	475
9.5.9	Conclusions used for the site descriptive model	478

9.6	Evaluation of uncertainties	483
9.7	Comparison between the hydrogeological and hydrogeochemical models	484
10	Bedrock transport properties	487
10.1	State of knowledge at previous model version	487
10.2	Modelling methodology and input from other disciplines	487
10.3	Conceptual model with potential alternatives	488
10.4	Description of input data	489
	10.4.1 Data and models from other disciplines	489
	10.4.2 Transport data	491
10.5	Evaluation of transport data	491
	10.5.1 Methods and parameters	491
	10.5.2 Porosity	492
	10.5.3 Diffusion	493
	10.5.4 Sorption	495
10.6	Transport properties of rock domains, rock mass fractures and deformation zones	495
	10.6.1 Methodology	495
	10.6.2 Rock domains	496
	10.6.3 Rock mass fractures and deformation zones	496
10.7	Evaluation of uncertainties	498
10.8	Feedback to other disciplines	498
11	Resulting description of the Forsmark site	499
11.1	Surface properties and ecosystems	499
	11.1.1 Quaternary deposits and other regoliths	499
	11.1.2 Climate, hydrology and hydrogeology	500
	11.1.3 Chemistry	501
	11.1.4 Ecosystem description	501
	11.1.5 Humans and land use	503
11.2	Bedrock geological description	503
	11.2.1 Rock domain model	504
	11.2.2 Deterministic deformation zone models	506
	11.2.3 Discrete fracture network (DFN) model	510
11.3	Rock mechanics description	512
	11.3.1 Mechanical properties	512
	11.3.2 In-situ stress state	514
11.4	Bedrock thermal properties	515
	11.4.1 In-situ temperature	515
	11.4.2 Thermal properties	515
11.5	Bedrock hydrogeological description	516
	11.5.1 Hydraulic properties	516
	11.5.2 Boundary and initial conditions	518
	11.5.3 Groundwater flow and salt transport	519
11.6	Bedrock hydrogeochemical description	520
11.7	Bedrock transport properties	522
	11.7.1 Summary of observations	523
	11.7.2 Retardation model	523
	11.7.3 Implications for further work	524
12	Overall confidence assessment	525
12.1	How much uncertainty is acceptable?	525
	12.1.1 Safety assessment needs	525
	12.1.2 Repository Engineering needs	526
	12.1.3 Assessing the importance of the uncertainties	526
12.2	Are all data considered and understood?	527
	12.2.1 Answers to auditing protocol	527
	12.2.2 Overall judgement	532

12.3	Uncertainties and potential for alternative interpretations?	532
12.3.1	Auditing protocol	532
12.3.2	Main uncertainties	533
12.3.3	Alternatives	545
12.3.4	Overall assessment	551
12.4	Consistency between disciplines	551
12.4.1	Important and actually considered interactions	552
12.4.2	Overall assessment	556
12.5	Consistency with understanding of past evolution	556
12.6	Comparison with previous model versions	559
12.6.1	Auditing protocol	559
12.6.2	Assessment	561
13	Conclusions	563
13.1	Major developments since previous model version	563
13.2	Current understanding of the site	564
13.2.1	Main features of the Forsmark site	564
13.2.2	Uncertainties and confidence	568
13.3	Implications for further modelling	569
13.3.1	Technical aspects	570
13.3.2	Modelling procedures and organisation of work	571
13.4	Implications for the ongoing site investigation programme	571
13.4.1	Recommendations provided during the modelling work	571
13.4.2	Recommendations based on uncertainties in the integrated model	572
13.5	General conclusions	576
14	References	577
Appendix 1	Properties of rock domains (RFM001 to RFM042) in the regional model volume	599
Appendix 2	Dominant and subordinate rock types in rock domains – codes and nomenclature	649
Appendix 3	Properties of all deformation zones included in the regional model volume	651
Appendix 4	Overall confidence assessment	701
Appendix 5	Motivation and selection of site for cored boreholes KFM07A, KFM07B, KFM08A, KFM08B, KFM06B, KFM06C, and the associated group of percussion boreholes HFM20, HFM21 and HFM22 (Appendix to SKB Decision paper 1024611)	739
Appendix 6	Revision of the recommended length and orientation of borehole KFM08B (Appendix to SKB decision paper 1038014)	745
Appendix 7	Motivation for and orientation of cored borehole KFM08C (Appendix to SKB decision paper 1038090)	749

1 Introduction

1.1 Background

The Swedish Nuclear Fuel and Waste Management Company (SKB) is undertaking site characterisation at two different locations, the Forsmark and Simpevarp areas, with the objective of siting a geological repository for spent nuclear fuel. The characterisation work is divided into an initial site investigation phase and a complete site investigation phase, /SKB, 2001a/. The results of the initial investigation phase will be used as a basis for deciding on a subsequent complete investigation phase.

An integrated component in the characterisation work is the development of a site descriptive model that constitutes a description of the site and its regional setting, covering the current state of the geosphere and the biosphere as well as those ongoing natural processes that affect their long-term evolution. The site description shall serve the needs of both Repository Engineering and Safety Assessment with respect to repository layout and construction, and its long-term performance. It shall also provide a basis for the environmental impact assessment.

The site description includes two main components:

- a *written synthesis* of each site summarising the current state of knowledge as well as describing ongoing natural processes which affect its long-term evolution, and
- one or several *site descriptive models*, in which the collected information is interpreted and presented in a form which can be used in numerical models for rock engineering, environmental impact and long-term safety assessments.

More about the general principles for site descriptive modelling and its role in the site investigation programme can be found in the general execution programme for the site investigations /SKB, 2001a/.

Before the start of the initial site investigation at Forsmark, version 0 of the site descriptive model was developed /SKB, 2002a/. This version served as a point of departure for the development of new versions of the site description during the site investigation phase. Each model version is coupled to a “data freeze” that defines out the database available for the model version in question. The results of the descriptive modelling also serve to produce feedback to, and set the priorities for the ongoing site characterisation. This interplay between site descriptive modelling, Site Investigation, Repository Engineering (Design) and Safety Assessment is illustrated in Figure 1-1.

The preliminary site description (version 1.2), which completes the initial site investigation phase, is compiled in this report. It is a further development of the version 0 and of the version 1.1 model, the latter being an interim version of the preliminary site description that was published in April 2004 /SKB, 2004a/. The interim version was a learning exercise and the experience gained from the work with developing the interim versions for both Forsmark /SKB, 2004a/ and the Simpevarp sub-area /SKB, 2004b/ have been utilised in the continuing work on the preliminary site description. With reference to Figure 1-1, this preliminary site description (version 1.2) is being used by Repository Engineering to produce the facility description layout D1. Together with layout D1 it also forms the basis for both a Preliminary Safety Evaluation (PSE) of the Forsmark site and a Safety Assessment (SR-Can) of repository layout D1 at Forsmark. The preliminary site description has also provided input to the complete site investigation (CSI) programme for Forsmark /SKB, 2005a/. Another important recipient of the site descriptive model is Environmental Impact Assessment, (the latter entity not illustrated in Figure 1-1).



Figure 1-1. Site descriptive modelling (SDM) and its main product in a context. Illustrated is also the exchange of information (deliveries and feedback) between the main technical activities which provide data to the site modelling, or which makes use of the site modelling and the associated description.

1.2 Scope and objectives

The development of the preliminary site description of the Forsmark area (version 1.2) was made with the main objectives of presenting a site descriptive model on a local and a regional scale with an accompanying synthesis of the current understanding of the site, based on field data collected during the initial site investigation. Furthermore, to give recommendations on continued field investigations based on results and experiences gained during the work with the development of site descriptive model versions.

The specific objectives of the work are to:

- produce and document an integrated description of the site and its regional environment based on the site-specific data available from the initial site investigations,
 - analyse the primary data available in data package Forsmark 1.2,
 - build a three-dimensional site descriptive model,
 - perform an overall confidence assessment, including systematic treatment of uncertainties and evaluation of alternative interpretations,
 - develop, document and evaluate alternative models in a systematic way,
 - perform activities in close interaction with safety analysis and repository engineering,
- perform the safety related geosphere and biosphere analyses that are specified as site modelling in the planning document for the Preliminary Safety Evaluation (PSE) /SKB, 2002b/,
- highlight and, where the available data allow, address all current site-specific geoscientific and ecological key issues for understanding the site,
- give recommendations on continued investigations in the final document as well as on a continuous basis.

The basis for the preliminary site description (model version 1.2) are quality-assured, geoscientific and ecological field data from Forsmark that were available in the SKB databases SICADA and GIS at July 31, 2004. All information that became available up to this date has been used to re-evaluate the pre-existing knowledge built into version 1.1 of the site description, in order to re-assess the validity of the previous model version.

As would be expected at this stage of the site investigation, there are still substantial uncertainties in the site description and in many aspects the confidence is low. However, many significant steps have been taken in the descriptive modelling up to now, and it is expected that future exploratory analyses and modelling based on a larger set of primary data will resolve many of the uncertainties in the preliminary site description.

1.3 Setting

The Forsmark site is located in northern Uppland within the municipality of Östhammar, about 170 km north of Stockholm. The candidate area is located along the shoreline of Öregrundsgrepen and it extends from the Forsmark nuclear power plant and access road to the SFR-facility in the northwest towards Kallrigafjärden in the southeast (Figure 1-2). The candidate area is approximately 6 km long and 2 km wide. The north-westernmost part of the candidate area has been selected as the target area for continued site investigations /SKB, 2005a/.

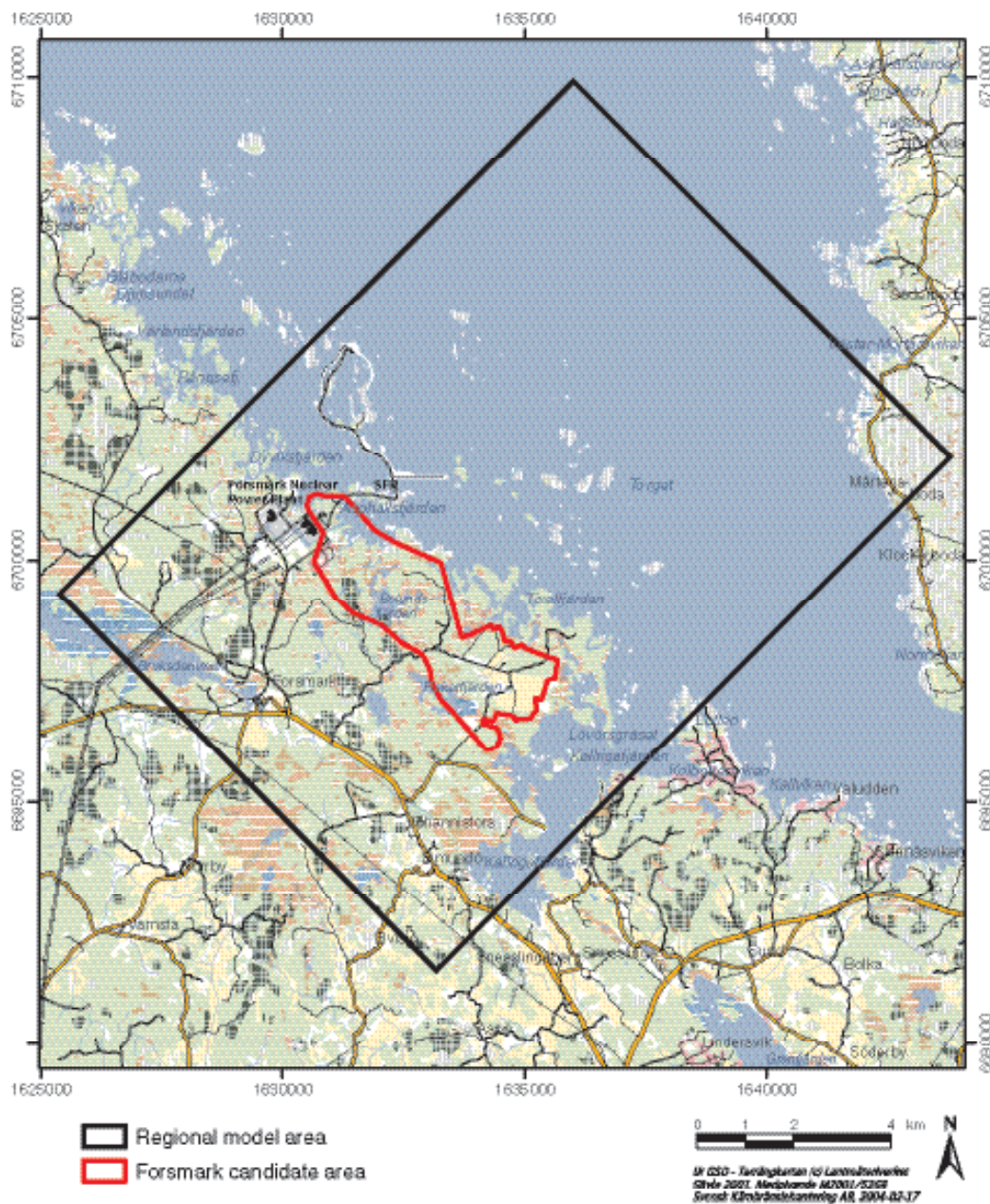


Figure 1-2. The Forsmark candidate area (red) and the regional model area (black) in the preliminary site descriptive model.

The major part of the bedrock was formed about 1,900 million years ago and it has been affected by both ductile and brittle deformation. The ductile deformation has resulted in large-scale ductile high-strain zones and the brittle deformation has given rise to large-scale faults and fracture zones. “Tectonic lenses”, in which the bedrock is much less affected by ductile deformation, are enclosed between the ductile high-strain zones. The candidate area is located in one of these tectonic lenses.

A detailed description of the underlying primary data for the site descriptive model, including geographical information and definition of modelling areas, is provided in Chapter 2.

1.4 Methodology and organisation of work

1.4.1 Methodology

The project is multi-disciplinary, in that it covers all potential properties of the site that are of importance for the overall understanding of the site, for the design of the deep repository, for safety assessment and for the environmental impact assessment. The overall strategy to achieve this (illustrated in Figure 1-3) is to develop discipline-specific models by interpretation and analyses of the quality-assured primary data that are stored in the two SKB databases, SICADA and GIS. The different discipline-specific models are then integrated into a unified site description (see also Figure 1-4 and text below). The quantitative, discipline-specific models are stored in the SKB model database Simone, from where quality-assured versions of the models can be accessed by e.g. the recipients of the site description.

The site descriptive modelling comprises the iterative steps of primary data evaluation, descriptive and quantitative modelling in 3-D and of overall confidence evaluation. A strategy for achieving sufficient integration between disciplines in producing site descriptive models is documented in a

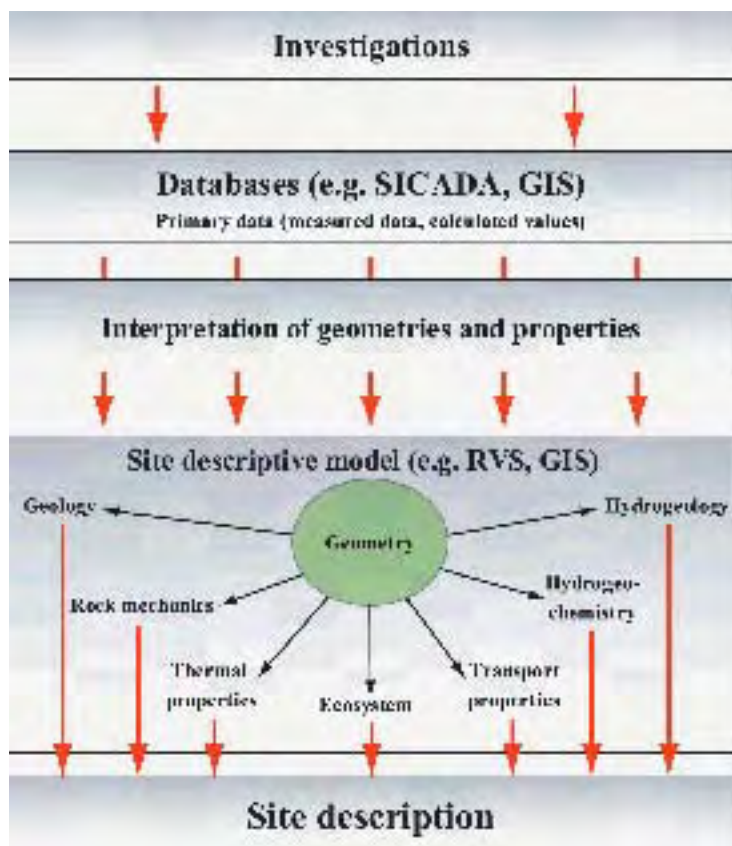


Figure 1-3. From site investigations to site description. Primary data from site investigations are collected in databases. Data are interpreted and presented in a site descriptive model, which consists of a description of the geometry of different units in the model and the corresponding properties of those units and of the site as a whole (from /SKB, 2002a/).

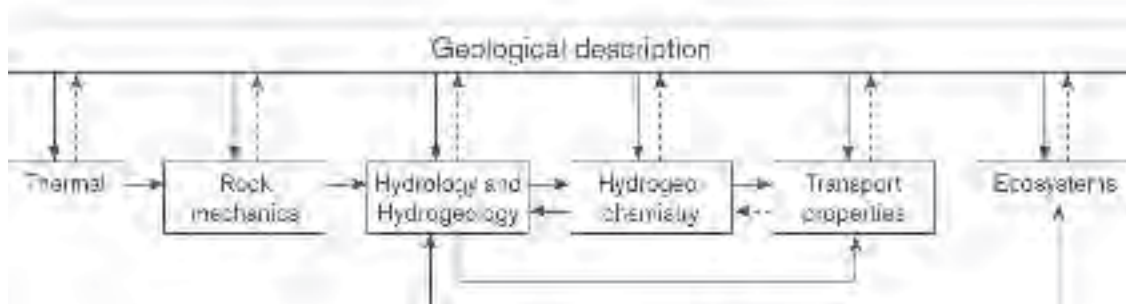


Figure 1-4. Interrelations and feedback loops between the different disciplines in site descriptive modelling where geology provides the geometrical framework (from /Andersson, 2003/).

separate strategy report for integrated evaluation /Andersson, 2003/, but has been developed further during the work with model versions 1.1 for Forsmark and Simpevarp.

Data are first evaluated within each discipline and then the evaluations are cross-checked between the disciplines. Three-dimensional modelling, with the purpose of estimating the distribution of parameter values in space, as well as their uncertainties, follows. The geometrical framework for modelling is taken from the geological model and is in turn used by the rock mechanics, thermal and hydrogeological modelling etc (see Figure 1-4). The three-dimensional description should present the parameters with their spatial variability over a relevant and specified scale, with the uncertainty included in this description. If required, different alternative descriptions should be provided.

Methodologies for developing site descriptive models are based on experience from earlier SKB projects, e.g. the Äspö HRL and the Laxemar modelling projects. Before the underground laboratory in Äspö was built, forecasts of the geosphere properties and conditions were made based on pre-investigations carried out around Äspö. Comparisons of these forecasts with observations and measurements in tunnels and boreholes underground and evaluation of the results showed that it is possible to reliably describe geological properties and conditions with the aid of analyses and modelling /Rhén et al. 1997a,b,c; Stanfors et al. 1997/. The Laxemar modelling project /Andersson et al. 2002a/ was set up with the intention of exploring the adequacy of the available methodology for site descriptive modelling based on surface and borehole data and to identify potential needs for developments and improvements in methodology. The project was a methodology test using available data from the Laxemar area. Subsequently, as previously mentioned, full application of the developed methodologies has been undertaken in the version 1.1 descriptive modelling of the Forsmark /SKB, 2004a/ and Simpevarp /SKB, 2004b/ areas.

The current methodologies for developing the discipline-specific models are documented in methodology reports or strategy reports. In the present work, the guidelines given in those reports have been followed to the extent possible with the data and information available at the time of data freeze for Forsmark model version 1.2. How the work was carried out is described further in Chapters 4 through 11. For more detailed information on the methodologies, the reader is referred to the methodology reports. These are:

- Geological site descriptive modelling /Munier et al. 2003/.
- Rock mechanics site descriptive modelling /Andersson et al. 2002b/.
- Thermal site descriptive modelling /Sundberg, 2003a/.
- Hydrogeological site descriptive modelling /Rhén et al. 2003/.
- Hydrogeochemical site descriptive modelling /Smellie et al. 2002/.
- Transport properties site descriptive modelling /Berglund and Selroos, 2004/.
- Ecosystem descriptive modelling /Löfgren and Lindborg, 2003/.

According to the strategy report for integrated evaluation /Andersson, 2003/, the overall confidence evaluation should be based on the results from the individual discipline modelling and involve the different modelling teams. The confidence is assessed by carrying out checks concerning e.g. the status and use of primary data, uncertainties in derived models, and various consistency checks such

as between models and with previous model versions. This strategy has been followed when assessing the overall confidence in Forsmark model version 1.2. The core members of the project and the activity leaders from the Forsmark site investigation group together utilised protocols addressing uncertainties and biases in primary data, uncertainty in models and potential for alternative interpretations, consistency and interfaces between disciplines, consistency with understanding of past evolution, and consistency with previous model versions. The results are described in Chapter 12.

1.4.2 Interfaces between disciplines

Central in the modelling work is the geological model which provides the geometrical context in terms of the characteristics of deformation zones¹ and the rock mass between the zones (see Figure 1-4). Using the geological and geometrical description as a basis, descriptive models for other geodisciplines (rock mechanics, thermal properties, hydrogeology, hydrogeochemistry and transport properties) are developed. Development of these models has in turn highlighted issues of potential importance for the geological model. Some of these issues have been discussed across the disciplinary interfaces during the course of work, but the main feedback to the geology model has to be addressed in the next version of the site description. The interface between hydrogeology and hydrogeochemistry has been handled e.g. by regional palaeo-hydrogeological simulations of variable-density groundwater flow between 8,000 BC and 2,000 AD.

The interface between the surface and bedrock systems has been considered in the evaluation of deep and shallow groundwater movement, as well as in the groundwater chemistry description. The present conceptualisation of the hydraulic properties of the quaternary deposits is implemented into the hydrogeological modelling and also into modelling and evaluation of the impact of infiltration on the present groundwater composition. A first attempt to model the shallow groundwater system has been made, where also the upper part of the bedrock is included. However, it should be noted that the flow conditions in the bedrock are adopted from the version 1.1 hydrogeological model. The link between water flow and water chemistry in the shallow system is so far restricted to comparisons between the location and extent of discharge and recharge zones from the hydrology modelling and the corresponding characteristics evaluated from the chemical composition of water samples.

The handling of interfaces between disciplines is described in more detail in Chapters 4 through 12.

1.4.3 Organisation of work

The work has been conducted by a project group and other discipline-specific working groups or persons engaged by members of the project group. The members of the project group represent the disciplines of geology, rock mechanics, thermal properties, hydrogeology, hydrogeochemistry, transport properties and surface ecosystems. In addition, some group members have specific qualifications of importance in this type of project e.g. expertise in RVS (Rock Visualisation System) modelling, GIS-modelling and in statistical data analysis.

Each discipline representative in the project group was given the responsibility for the assessment and evaluation of primary data and for the modelling work concerning his/her specific discipline. This task was then done either by the representatives themselves, or together with other experts or groups of experts outside the project group. In this context, discipline-specific groups, set up by SKB, play an important role. These groups are the same for both the Forsmark and Simpevarp/Laxemar site-modelling projects and they are essentially run by the discipline responsible, as assigned by SKB. The purpose of these groups is to carry out site modelling tasks and to provide technical links between the site organisations, the site modelling teams and the principal clients (Repository Engineering, Safety Assessment and Environmental Impact Assessment). The discipline-specific NET-groups actively involved in the site modelling work are identified in Table 1-1. Supporting reports have been produced for some of the discipline-specific work carried out within the framework of Forsmark model version 1.2. References to these supporting reports are given at the appropriate places in the following chapters of this report.

¹ The term deformation zone is used to designate an essentially 2-dimensional structure (sub-planar structure with a small thickness relative to its lateral extent) along which deformation has been concentrated /Munier et al. 2003/. See also Chapter 5 for use in this modelling.

Table 1-1. Discipline-specific analysis groups involved in site descriptive modelling and their mandate/objective.

Discipline	NET-group	Mandate
Geology	GeoNET	Constitutes the group for execution of the geological modelling, as specified by the geological part of the site modelling projects, and to promote technical exchange of experience and coordination between the two modelling projects and the site organisations.
Rock mechanics and thermal properties	MekNET	Coordination of modelling tasks for rock mechanics and thermal properties at both sites. Resource for development and maintenance of method descriptions.
Hydrogeology	HydroNET	Execution of the hydrogeological modelling; constitutes a forum for all modellers within hydrogeology (needs of site modelling and safety assessment and design), and promotes technical exchange of experience.
Hydrogeochemistry	HAG	To model the groundwater data from the sites and assure that the data quality is sufficient. Produce site descriptive hydrogeochemical models. Integrate the description with other disciplines and make recommendations for further site investigations.
Surface system	SurfaceNET	To model and describe the surface system by description by subdiscipline (biotic and abiotic), model the properties in a distributed way (maps and 3D), model the interdisciplinary processes (over space and time), describe the different ecosystems (conceptually and in site-specific terms), describe and model the flow of matter in the landscape, define and connect the biosphere objects, and produce site descriptions to support environmental impact assessment (EIA).

The project group has met at regular intervals to discuss the progress of the work and specific questions that have emerged during the modelling. In addition, the project group has had a workshop together with activity leaders from the Forsmark site investigation team addressing uncertainties and overall confidence in the data gathered and in the models produced. The information exchange between the modelling project and the site investigation team is an important component of the project, which is facilitated by the fact that some of the project members are also engaged as experts in the site investigation team.

1.4.4 Important changes compared to Forsmark 1.1 work

Important changes to the overall modelling strategies include the development of an updated appendix to the strategy document for geological site descriptive modelling /Munier et al. 2003/. This updated appendix /Munier, 2004/ details and clarifies the products expected from the geological discrete fracture network (DFN) modelling.

An additional change in modelling strategy is related to redistribution of work on transport parameters between the site descriptive modelling and safety analysis. This has the effect that flow-related transport parameters are handled by Safety Assessment and are not presented as part of the transport modelling herein. The hydrogeological site descriptive modelling may still use flow-related transport parameters for the analysis, but the results are in this case presented in a context of site understanding, rather than as measures of contaminant transport.

Another change concerns the organisation of work. As compared with the version 1.1, more of the modelling work in version 1.2 has been carried out by the discipline-specific expert groups (NET groups). An implication of this is that these expert groups handle most of the discipline-specific questions, whereas the project group more and more has focussed on handling issues related to the integration between disciplines.

Compared with the structure of the version 1.1 reports, the version 1.2 report has been changed to the effect that all major disciplines are now covered by individual chapters that encompass the full chain going from primary data screening, exploratory analysis to three-dimensional modelling and assessment of uncertainties, cf. Section 1.5.

1.5 This report

The structure of this report differs significantly from that of the version 1.1 reports for Forsmark and Simpevarp. Chapter 2 summarises available primary data and their usage and provide an overview of previous modelling versions and other prerequisites for the modelling. In Chapter 3, the current understanding of the historical development of the geosphere and surface systems is described.

Chapters 4 through 10 in sequence provide accounts of the modelling of the surface system, bedrock geology, bedrock mechanics, bedrock thermal properties, hydrogeology, hydrogeochemistry and bedrock transport properties, respectively. Each chapter includes the discipline-based accounts of evaluation of primary data, three-dimensional modelling and discussion of identified uncertainties associated with the developed models. Chapter 11 summarises the resulting descriptive model of the Forsmark area. In Chapter 12, a discussion on overall consistency between disciplines and possible alternative interpretations in the light of observed uncertainties is provided. Chapter 13 provides the overall conclusions from the work and discusses implications for the continued site investigation work and modelling process.

2 Available data and other prerequisites for the modelling

As more boreholes are drilled and investigated and new types of surface investigations are conducted, successively more data are added to the databases for site descriptive modelling. The modelling has now reached model version 1.2, which was preceded by versions 0 and 1.1. Each defined version is associated with a so called “data freeze”, which is a defined date, after which new data are no longer permitted to be included in the model version in question.

This chapter defines the database used for the Forsmark 1.2 modelling as well as other prerequisites. References are given to actual data sources. However, data per se are neither provided nor discussed. Reports belonging to the P-series¹ display data or references to data in the SKB SICADA and GIS databases and also provide descriptions of the performance of the investigations and other circumstances associated with data acquisition.

2.1 Overview of investigations

This section primarily presents a summary of the investigations made between data freezes 1.1 and 1.2. The majority of these investigations were performed during the period May 1st 2003 – July 31st 2004. Also, a short review is given of data previously acquired, i.e. data used in model version 1.1 /SKB, 2004a/. Model version 0, which served as a platform for model version 1.1, was reported in /SKB, 2002a/ and further commented on in /SKB, 2004a/ and is therefore discussed only to a limited degree.

2.1.1 Investigations and primary data acquired up to data freeze 1.1.

The site investigations leading up to data freeze 1.1 started in February 2002 and continued to the end of April 2003. They comprised geoscientific and ecological surface investigations (including a marine geological/geophysical survey), airborne geophysical measurements and drilling, as well as borehole investigations during and after drilling. Below, a summary of the most important activities of different character is given. A full reference list of P-reports characterising the data included in data freeze 1.1 is presented in Chapter 2 of the version 1.1 report /SKB, 2004a/, and in Section 2.7 of this report.

The *surface investigations* consisted of bedrock mapping including detailed bedrock mapping of two excavated and artificially cleaned sites (KFM02A and KFM03A) with special emphasis on fractures, mapping of Quaternary deposits, airborne geophysical measurements along profiles across the model area, ground geophysical investigations, hydrochemical sampling/analysis of surface waters and ecological investigations. A marine geological/geophysical survey between the island of Gräsö and the mainland at Forsmark was also carried out, but the results were not reported until after data freeze 1.1 and are therefore included in data freeze 1.2.

The *drilling activities* included drilling of one c. 1,000 m deep telescopic borehole, KFM01A, the percussion-drilled part of a second telescopic borehole, KFM02A, eight percussion boreholes in solid rock and 53 boreholes through Quaternary deposits (see also Figures 2-1 and 2-2 in Section 2.5).

Several methods of borehole and drill core investigation after drilling were applied. These were: geological and rock-mechanics sampling and testing of drill cores, colour TV logging using BIPS (Borehole Image Processing System), radar logging, conventional geophysical logging, boremap mapping of core-drilled and percussion-drilled boreholes, different types of hydraulic testing and groundwater sampling.

¹ The P-series report the results of the on-going site investigations at Forsmark and Oskarshamn (Simpevarp and Laxemar subareas). These reports are available on the SKB web page together with reports in the SKB R- and TR-series (www.skb.se).

2.1.2 Data freeze 1.2 – investigations performed and data acquired

The data included in data freeze 1.2 and available for the version 1.2 modelling work are the data used in previous model versions and data acquired between data freezes 1.1 and 1.2 (i.e. during the period May 1st 2003 – July 31st 2004). The investigations associated with data collection during the period between the data freezes 1.1 and 1.2 comprised the following main items:

- Geoscientific and ecological surface investigations. However, airborne measurements have not been performed after data freeze 1.1.
- Drilling, measurements while drilling and drill core/drill cutting and borehole investigations after completion of drilling.

The surface investigations comprised:

- Bedrock mapping (lithology, structural characteristics, geochronology).
- Investigations of Quaternary deposits including marine and lacustrine sediments in the Baltic and in lakes (stratigraphy, element distribution in till, analysis of microfossils in till and sediment samples and peatland investigations).
- Ground geophysical investigations including acquisition of new results and updated/extended interpretations of results from surface investigations carried out prior to data freeze 1.1.
- Meteorological and hydrological monitoring and measurements (snow depth, ground frost, ice cover, surface-water levels, water run-off in brooks).
- Hydrochemical sampling and analysis of precipitation, surface waters and shallow groundwater.
- Various ecological inventories and investigations.

The drilling activities comprised (see Figure 2-1 in Section 2.5 for borehole locations):

- Drilling of the telescopic boreholes KFM02A (from 100 m), KFM03A, KFM04A and KFM05A.
- Drilling of the cored boreholes KFM01B and KFM03B.
- Drilling of percussion boreholes HFM09–19 and KFM04B.
- Drilling of 12 shallow boreholes through Quaternary deposits.

Borehole investigations during drilling of all telescopic, core-drilled and percussion-drilled boreholes were carried out according to special standardised programmes presented in Section 2.5. The measurements and activities performed after drilling can be outlined as follows:

- Borehole geology: Boremap mapping and geological single-hole interpretation of the boreholes that were drilled after data freeze 1.1. For the core-drilled parts of the telescopic boreholes also drill core sampling and analyses of petrographical, geochemical and petrophysical properties as well as fracture mineralogy. Single-hole interpretation was performed also for the telescopic borehole KFM01A and the percussion-drilled boreholes HFM01–08 that were included in data freeze 1.1.
- Borehole geophysics: BIPS- and radar logging, conventional geophysical logging and interpretation of geophysical measurements in the boreholes that were drilled after data freeze 1.1.
- Rock mechanics: Sampling and rock-mechanics testing of drill cores from boreholes KFM01A–05A and, for some investigations, KFM01B and KFM03B.
- Thermal properties: Drill core sampling of boreholes KFM01A–04A and determination of thermal conductivity, specific heat capacity and thermal expansion.
- Hydrogeology: Difference flow logging in telescopic boreholes KFM02A–05A, single-hole injection tests in telescopic boreholes KFM01A–03A, pumping tests and flow logging in the percussion-drilled boreholes HFM01–19 and in the percussion-drilled part (c. 0–100 m) of the telescopic boreholes KFM02A, 03A and 06A, interference tests between percussion-drilled and telescopic boreholes and between various percussion-drilled boreholes.

- Hydrogeochemistry: Hydrochemical logging and complete hydrogeochemical characterisation in telescopic boreholes KFM02A, KFM03A and KFM04A, investigations of microbes in flushing water during drilling, sampling and analysis of groundwater from percussion-drilled boreholes, and investigations of fracture minerals from boreholes KFM01A, KFM02A and KFM03A+B.
- Transport properties: Resistivity measurements on core samples from borehole KFM01A and logging in-situ by electrical methods in KFM01A and KFM02A for determination of the formation factor.

By the field investigations and testing/analyses in laboratories on samples from the Forsmark investigation area, the volume of data representing several disciplines has expanded considerably since data freeze 1.1. Borehole data covering the geosphere from the soil or rock surface to 1,000 m depth with an areal extent including the entire candidate area, and to some extent beyond that, are of special interest, since depth data available at the time of the earlier model versions were very sparse. However, also the greatly increased amount of surface data has much contributed to a successively enhanced understanding of the geoscientific and ecological characteristics of the model area.

2.2 Previous model versions

2.2.1 Forsmark model version 0

The point of departure for all versions of the site descriptive model for the Forsmark area was model version 0 /SKB, 2002a/. Version 0 was developed out of the information available at the start of the site investigations. This information, except data from tunnels and boreholes at the sites of the Forsmark nuclear reactors and the SFR repository, is mainly 2D in nature (areal data), and is general and regional, rather than site-specific, in content. For this reason, the Forsmark site descriptive model, version 0, was developed on a regional scale, covering a rectangular area, 15 km in a south-west-northeast and 11 km in a northwest-southeast direction, see Figure 2-3 in Section 2.8.3. This area, which encloses the area identified in the feasibility study as favourable for further investigations, has been designated the *Forsmark regional model area* (see also Section 2.8.2).

The version 0 reporting provided a site descriptive model for the geosphere covering the disciplines geology, rock mechanics, hydrogeology and hydrogeochemistry. Within each discipline, uncertainties and alternative models were identified and discussed to various levels of detail, given by the available data. For the surface system, version 0 provided a systematic overview of data needs and availability for developing a site descriptive model for the surface ecosystems (biosphere).

An important result of the work with the version 0 model was the data inventory, in which the locations and scope of all potential sources of data were documented, and the evaluation of those data with respect to their usefulness for site descriptive modelling. This inventory contains data that, at that time, already were stored in the SKB databases SICADA and GIS, but also data that had not been evaluated and/or inserted in the databases, but which were, nevertheless, relevant for site descriptive modelling.

2.2.2 Forsmark model version 1.1

Data available for model version 1.1 originated from surface investigations within the candidate area and its regional environment, and from drilling and investigations in boreholes. The surface-based data sets were rather extensive, whereas the data sets from boreholes were limited to information from one c. 1,000 m deep cored borehole (KFM01A) and eight c. 150 to 200 m deep percussion-drilled boreholes in the Forsmark candidate area.

Compared with version 0, there were considerable additional features in the version 1.1, especially in the geological description and in the description of the near surface. The geological models of lithology and deformation zones were based on borehole information and much higher resolution surface data. The existence of highly fractured sub-horizontal zones was verified and included in the model of the deformation zones. A discrete fracture network (DFN) model was also developed. The rock mechanics model was based on strength information from SFR and an empirical, mechanical

classification by depth at KFM01A and at outcrops. A first model of thermal properties of the rock was developed, although still rather immature due to few site-specific data in support of it.

The hydrogeological description was based on the new geological (structure) model and the fracture transmissivity distribution of the DFN model was based on the data from depth (cored borehole KFM01A). The fracture intensity and permeability are very low below 400 m depth. Hydrogeological simulations of the groundwater evolution since the last glaciation were performed and compared with the hydrogeochemical conceptual model. The conceptual model of the development of post-glacial hydrogeochemistry was updated. Also, the salinity distribution, mixing processes and the major reactions altering the groundwaters were described down to a depth of 200 m. A first model of the transport properties of the rock was presented, although still rather immature due to lack of site-specific data. Furthermore, the surface description contained additional information regarding the stratigraphic distribution of glacial till and water-laid sediment.

There was much uncertainty in version 1.1 of the site descriptive model, but the main uncertainties were identified. Some of these uncertainties were also quantified and others were left as input to alternative hypotheses. However, since a main reason for uncertainty in version 1.1 was lack of data and poor data density and as much more data were expected in coming data freezes, it was judged not meaningful to carry the uncertainty quantification or alternative model generation too far.

2.3 Geographical data

The geographical data available for the *site descriptive model, version 0* are described in /SKB, 2004a/. The presentation includes the coordinate system, available maps (general map, topographic map, cadastral² index map), digital orthophotographs³ and elevation data. This information is, with exception for the coordinate system, still relevant for data freeze 1.2. The coordinate system that is valid for data freezes 1.1 and 1.2 is:

- X/Y (N/E): the national 2.5 gon V 0:–15, RT 90 system (“RAK”).
- Z (elevation): the national RHB 70 levelling system.

Elevation data covering the land area are available for the whole of Sweden from the GSD-Elevation database. For most parts of the country, including the Forsmark area, a digital elevation model called 4600DEM (sometimes termed DTM-model, Digital Terrain Model), based on the GSD-Elevation database, is available. This elevation model, which is derived from aerial photographs taken at a height of 4,600 m, is produced on a 50×50 m grid. Metria, National Land Survey of Sweden, guarantees that the average error in elevation data is less than ± 2.5 m for each 50×50 m grid cell, and data are delivered with a resolution of 1 m.

A more detailed digital elevation model of the Forsmark area, called 2300DEM, has also been developed by Metria. This is based on flying at 2,300 m height and uses 10 m grids, i.e. the distance between data points in both X and Y direction is 10 m. In the Z direction the elevation is calculated and stored with a precision of 4 decimal places. With its smaller grid size and thus higher resolution, this DEM is considerably more useful for investigations regarding e.g. surface water and ground-water run-off in the flat Forsmark area than the 4600DEM. The 2300DEM has served as the basis for further elaboration of elevation data in several steps, of which the first was reported in /Brydsten, 2004/.

The 2300DEM in its primary version has served as the standard elevation database in the site investigations performed between data freezes 0 and 1.2 and further developed versions have been applied for special purposes. The most recent version, in which e.g. bathymetric data from shallow and deep parts of the Baltic outside the candidate area are integrated, is described in /Lindborg, 2005/.

² Cadastral map is a map of real estates.

³ Orthophotography is a black and white aerial photography in which perspective and measurement errors have been corrected so that the scale is as correct as in a map. The photograph is also adjusted to the general coordinate system.

2.4 Surface investigations

The surface investigations (including marine and lacustrine investigations) performed in the model area, see Figure 2-3, between the two data freezes 1.1 and 1.2 involved the following disciplines:

1. Bedrock geology.
2. Quaternary geology.
3. Ground geophysics.
4. Meteorology and hydrology.
5. Hydrochemistry.
6. Surface ecology.

In this section, the investigations that have generated the new data sets are described in more detail than in Section 2.1.2. Especially interesting features are commented on. Geophysical data are treated together with bedrock or Quaternary geological data, due to their close interrelation with the geological information. References to the documentation of data are given in tables in Section 2.7.

2.4.1 Bedrock geology and ground geophysics

Bedrock mapping – Stage 2. Stage 2 of the bedrock mapping continued after data freeze 1.1, and the major part of the survey was carried out during the summer and autumn of 2003. Areas not earlier mapped were for example a number of islands in the bay Öregrundsgrepen within the regional model area, and some outcrops south-west of road 76. Moreover, supplementary mapping was performed also within the candidate area. With completion of stage 2, the surface bedrock mapping in Forsmark has, in principle, come to its end, and, in the future, only minor, complementary contributions to the surface geology by surface mapping will be made.

Bedrock mapping with focus on U-Pb, $^{40}\text{Ar}/^{39}\text{Ar}$ and (U-Th)/He geochronology. Dating of the main rock types is essential not only for grasping the geologic history and development of different rock types, but also for understanding the present day character of the site and its future behaviour. Dating of the main rock types will later be complemented with dating of fracture minerals.

The ground content of K, U, Th and ^{137}Cs was recalculated by processing of radiometric data.

Detailed fracture mapping at three sites, Klubbudden and drill sites DS4 and DS5. Fracture mapping of uncovered bedrock serves as a fundamental input to fracture network (DFN) modelling, and a number of representative sites scattered over the model area are needed for that purpose. Detailed fracture mapping will continue after data freeze 1.2. The fracture mapping at DS5 revealed late-glacial block movements and sub-horizontal, sediment-filled fractures, which initiated a special examination.

Updated interpretation of the reflection seismics carried out during 2002. Data regarding the comprehensive reflection seismic study reported in data freeze 1.1 /Juhlin et al. 2002/ were further processed and the results refined /Juhlin and Bergman, 2004/. Many of the seismic reflectors were thereby better constrained and the estimate of bedrock topography (giving regolith thickness) was updated.

Extended analyses of the airborne geophysical survey performed during 2002. Also the airborne geophysical survey executed in 2002 resulted in a vast amount of data. Results were presented in two reports at data freeze 1.1 /Rønnig et al. 2003/ and /Isaksson et al. 2004c/. The analytic work has continued, resulting in three new P-reports, see Section 2.7.

Presentation of the results of the detailed marine geological/geophysical survey of the sea bottom off Forsmark. A detailed marine geological/geophysical survey was performed during the summer of 2002, but data were not available until data freeze 1.2 /Elhammer et al. 2005/.

Ground geophysical surveys (slingram and magnetometer) were conducted prior to siting of the telescopic boreholes KFM04A, KFM05A and KFM06A, covering the areas of interest. Also two SW-NE-lineaments were investigated with the same methods.

The bedrock topography was characterised using seismic tomography along refraction seismic profiles.

2.4.2 Quaternary geology and ground geophysics

The mapping of Quaternary deposits was initiated in 2002 and the field work has continued during 2003 and 2004. Data are both surface-based and of stratigraphical character.

The following data were added to the previously existing data set:

- Stratigraphical and analytical data from auger drilling and pits.
- Stratigraphical investigations of till in machine-cut trenches.
- Ground penetrating radar (GPR) and resistivity (CVES) measurements for overburden investigations (test of methods, ground penetrating radar survey 2003, two interpretation reports, one utilising GPR- and CVES-surveys, the other only GPR measurements).
- Updated information on bedrock topography, and hence the thickness of the regolith, from the reflection seismic survey, Stage 1.
- Estimation of bedrock topography (and regolith thickness) using seismic tomography along refraction seismic profiles.
- Investigations of marine and lacustrine sediments – stratigraphical and analytical data.
- A map and associated description based on the mapping of Quaternary deposits performed in 2002–2003.
- Elemental distribution in till at Forsmark – a geochemical study.
- Microfossil analyses of till and sediment samples from Forsmark.
- Results from peatland investigations.

2.4.3 Meteorology and hydrology

The following meteorological and hydrological data have been added to previously available data.

Meteorological parameters (precipitation, air temperature, wind speed, wind direction, humidity, global radiation) were monitored during the entire period between data freezes 1.1 and 1.2.

Snow depth, ground frost depth and ice cover were measured during the winter 2003/2004.

Surface water levels were monitored at nine observation points (SFM0038–43 and SFM0064–66, see Figure 2-2) for the entire or part of the period between the two latest data freezes.

Surface water run-off in a brook discharging into lake Bolundsfjärden was monitored in a control flume for a relatively short period before data freeze 1.2. Run-off estimates with simpler equipment were made in a number of other brooks within the investigation area. Data from these measurements were available for data freeze 1.2, although the P-report will be presented later.

2.4.4 Hydrochemistry

The hydrochemical surface investigations included in data freeze 1.2 were the following:

- Sampling and analysis of precipitation.
- Sampling and analysis of surface waters from six lakes, four shallow bays and eight running waters. Sampling was performed on 20 occasions during the period March 2003 to March 2004. In other words, the sampling period did not entirely cover the period between data freezes 1.1 and 1.2.
- Sampling and analysis of shallow groundwater (from 21 drill holes in soil, one spring, 3 soil boreholes with BAT filter tips for pore-water sampling in fine-grained soils, and 7 shallow private wells).

The number of sampling points for surface waters, shallow groundwater and private wells has, after evaluation of similarities and differences between the sampling points, been reduced compared with the data set available at data freeze 1.1.

2.4.5 Surface ecology

The discipline “Surface ecosystems” is to some extent dependent on making use of data from other disciplines (e.g. Quaternary geology, hydrogeology, hydrochemistry). Investigations made exclusively for Surface ecology within the site investigation, resulting in data used in data freeze 1.2, are listed below.

- Surface water sampling at the same sampling points as defined above for hydrochemistry, as well as at two additional sampling points in shallow sea bays and two additional points in running waters. In addition to the parameters analysed within the hydrochemical programme, some other parameters are analysed within the ecological programme, e.g. nutrient salts, chlorophyll, carbon species and silica. Also a number of physical parameters are measured in the field, e.g. turbidity, depth visibility and colour.
- Identification of catchments, lake-related drainage parameters and lake habitats.
- Water depth soundings in shallow bays.
- Investigations of soils and solum types.
- Sampling and analyses of surface sediment in lakes and shallow bays.
- Vegetation inventory in part of the municipality of Östhammar and vegetation mapping with satellite data of the Forsmark and Tierp regions.
- Investigation of the amount of dead wood.
- Surveys of mammal populations in the areas adjacent to Forsmark. Results from 2003.
- Sampling of freshwater fish.
- Inventory of amphibians and reptiles.
- Bird monitoring at Forsmark 2002–2003.

The volume and variety of surface ecological data have increased considerably since data freeze 1.1.

2.5 Borehole investigations

Borehole investigations generating data for data freeze 1.2 were performed in the core- and percussion-drilled boreholes displayed in Figure 2-1 and in the soil boreholes illustrated in Figure 2-2. Boreholes included already in model version 1.1 are presented in /SKB, 2004a/. Below, only data from borehole investigations performed between data freezes 1.1 and 1.2 are discussed.

The borehole investigations performed within the site investigation may be subdivided into:

- 1) Investigations made during and immediately after completion of the drilling, and
- 2) Investigations performed after drilling.

Each of the three borehole categories, core-drilled boreholes, percussion-drilled boreholes in solid rock, and boreholes in soil (the last category may be e.g. percussion-drilled or auger-drilled), was associated with a specific investigation programme during drilling and another programme after drilling. These programmes are presented in Sections 2.5.1 and 2.5.2, together with a comment on nonconformities that may have come about for different reasons.



Figure 2-1. Core-drilled and percussion-drilled boreholes in solid rock from which data were included in data freeze 1.2. Telescopic borehole KFM01A and percussion-drilled boreholes HFM01–08 were available in model version 1.1.

2.5.1 Drilling and measurements while drilling

Core-drilled boreholes

Borehole investigations during and immediately after core drilling normally include the following items (cf. SKB MD 620.004): overview mapping of the drill core, hydraulic tests with a special test-tool (the wireline-probe), absolute pressure measurements with the wireline-probe, water sampling with the wireline-probe, measurements of borehole deviation and weighing of drill cuttings. In addition, registration of the following flushing and return water parameters is made: flushing water and return water flow rate, flushing water pressure, content of dissolved oxygen in flushing water and electric conductivity of flushing and return water. Moreover, the flushing and return water is sampled for determination of the content of tracer dye. Drill-technical parameters, of which some may be useful for geoscientific evaluation, e.g. penetration rate and feed pressure, are also registered. If the core-drilled borehole is prioritised for rock mechanics investigations, stress measurements by overcoring are also carried out during the drilling process.

The core-drilled boreholes produced during the site investigation may be divided into two categories: 1) telescopic boreholes and 2) core-drilled boreholes of traditional type. Most of the deep (down to c. 1,000 m) boreholes belong to the first category. Telescopic drilling implies that the upper 100 m is percussion-drilled with a large diameter (≥ 200 mm). Often this part is cased with a stainless steel casing, and the gap between the casing and borehole wall is grouted, in order to prevent shallow groundwater discharging into deeper parts of the rock aquifer during the continued drilling below 100 m. If casing plus grouting is required, the diameter of the upper 100 m has to be increased to c. 250 mm in order to permit a casing with an inner diameter of 200 mm.

The borehole section c. 100–1,000 m, i.e. the major part of the telescopic borehole, is core-drilled. Because a telescopic borehole consists of a percussion-drilled as well as a core-drilled part, the investigation programmes for both percussion-drilled and core-drilled boreholes are applied.

The telescopic boreholes are categorised as boreholes of standard type or of chemistry type. During drilling of both these categories, severe requirements are placed on cleaning the down-hole equipment, in order to avoid contamination of the groundwater and borehole walls. However, the cleaning procedures for boreholes of chemistry type also include disinfection of the down-hole equipment, in addition to the degreasing and washing used for both categories of telescopic boreholes.

Data from four c. 1,000 m deep telescopic boreholes became available after data freeze 1.1 and before data freeze 1.2. These are KFM02A, KFM03A, KFM04A and KFM05A. Two core-drilled boreholes of traditional type were drilled during the same period: KFM01B (c. 500 m) and KFM03B (c. 100 m). The drilling procedure and measurements while drilling are presented in a sequence of P-reports (see Section 2.7).

Comments, telescopic boreholes KFM02A, KFM03A, KFM04A and KFM05A

Boreholes KFM02A and KFM03A are near-vertical and inclined 85° from the horizontal plane, whereas KFM04A and KFM05A are inclined 60° . The percussion drilled part of all boreholes except KFM03A is cased and gap grouted. However, a top casing of c. 10–15 m through the overburden is always installed.

The investigation programme for percussion boreholes was carried out during drilling of section 0–100 m of the telescopic boreholes with only one nonconformity. Weighing of drill cuttings was not regarded as meaningful, since the return water flow was so high that the containers to which the water was discharged were brimming over, making estimates of lost amounts of drill cuttings difficult.

Concerning the investigation programme for core-drilled boreholes, the deviations from plan are described in the respective drilling reports, see Section 2.7. The following nonconformities should be noted:

1. The number of tests performed with the wireline-probe, including water sampling, was less than planned, due to technical problems in boreholes KFM02A and KFM04A, in combination with a very limited inflow of groundwater at depth in all boreholes.

2. Registration of dissolved oxygen in the flushing water had to be almost completely abandoned in boreholes KFM02A, KFM03A+B and KFM04A due to repeated technical problems. For drilling of borehole KFM01B, no oxygen gauge was available.

The technical problems with the wireline probe are now solved. However, the situation with a very low inflow of groundwater at depths below a couple of hundred metres seems characteristic for the entire candidate area. For obvious reasons this entails continued problems for making hydraulic tests and hydrochemical sampling with the wireline probe at these depths. Also the previous technical problems with the oxygen gauge are now solved.

Much concern was devoted to selection of high-quality flushing water sources for the core-drilled part of the telescopic boreholes. Percussion-drilled wells in solid rock were used for all boreholes. Especially the total content of organic constituents (TOC) was evaluated. TOC should preferably not exceed 5 mg/L. The flushing water well used for drilling KFM01A (percussion borehole HFM01) had a TOC-content above the 5 mg limit, entailing that a water filter of activated carbon had to be used. However, analyses from wells later drilled indicated a TOC-content sufficiently low to permit them to be approved without the use of a water filter device. The following percussion drilled boreholes were used as flushing water wells: HFM05 for KFM02A, HFM06 for KFM03A, HFM10 for KFM04A and HFM13 for KFM05A.

Comments, core-drilled boreholes KFM01B and KFM03B

The primary objective of borehole KFM01B was rock stress measurements by both overcoring and hydraulic methods. In addition to that, a drill core from the upper 100 m of the bedrock at drill site DS1 was provided (the upper 100 m of KFM01A is percussion drilled). KFM01B is inclined 79° and the flushing water well used was HFM01 without the use of the active carbon filter for the major part of the borehole (tap water was used at the very beginning of the drilling). The investigation programme for core-drilled boreholes was applied during drilling of KFM01B with the following nonconformities.

1. Registration of drilling- and flushing water parameters was not performed because the drilling equipment used was not provided with a registration system.
2. Absolute pressure measurements were not carried out due to logistic problems.
3. Only one deviation measurement was conducted, after completion of drilling.
4. Weighing of drill cuttings was not performed, because the recovery was very limited.

KFM03B was drilled in order to compensate for the missing drill core in KFM03A. The borehole is inclined 85° and the flushing water well used was HFM06. The investigation programme for core-drilled boreholes was applied during drilling of KFM03B with the following nonconformities.

1. No wireline probe tests were carried out due to the short length of the borehole.
2. Only one deviation measurement was made, after completion of drilling.
3. Weighing of drill cuttings was not performed, because the recovery was very limited.

Percussion-drilled boreholes

Borehole investigations during (and immediately after) percussion drilling in solid rock comprise (see SKB MD 610.003):

- sampling of soil with a frequency of one sample per metre while drilling through the unconsolidated overburden (if any) and a preliminary on-site examination,
- sampling of drill cuttings from the solid rock with a frequency of one sample per metre and a preliminary on-site examination,
- manual measurement of the penetration rate at every 20 cm,
- observation of groundwater flow rate (if any) and water colour every 20 cm.
- measurement of the flow rate at each major flow change observed,

- measurement of the electric conductivity of the groundwater every third metre,
- deviation measurements after completion of drilling.

Comments, percussion drilled boreholes HFM09–19 and KFM04B

No deviations from the measurement programme occurred during performance of the eleven percussion-drilled boreholes included between data freezes 1.1 and 1.2.

Surface water level gauges and boreholes in soil

The position of all surface water level gauges (8), groundwater monitoring wells (54), abstraction wells for hydraulic pumping tests (2), a spring used for shallow groundwater sampling, and BAT-type filter tips (6) available at data freeze 1.2 are displayed on the map in Figure 2-2. The corresponding information at data freeze 1.1 is given in /SKB, 2004a/, and the difference represents new observation points that have been added between the two data freezes.

The surface water level gauges in the Baltic and some of the lakes are attached to a steel pipe or some other, similar facility.

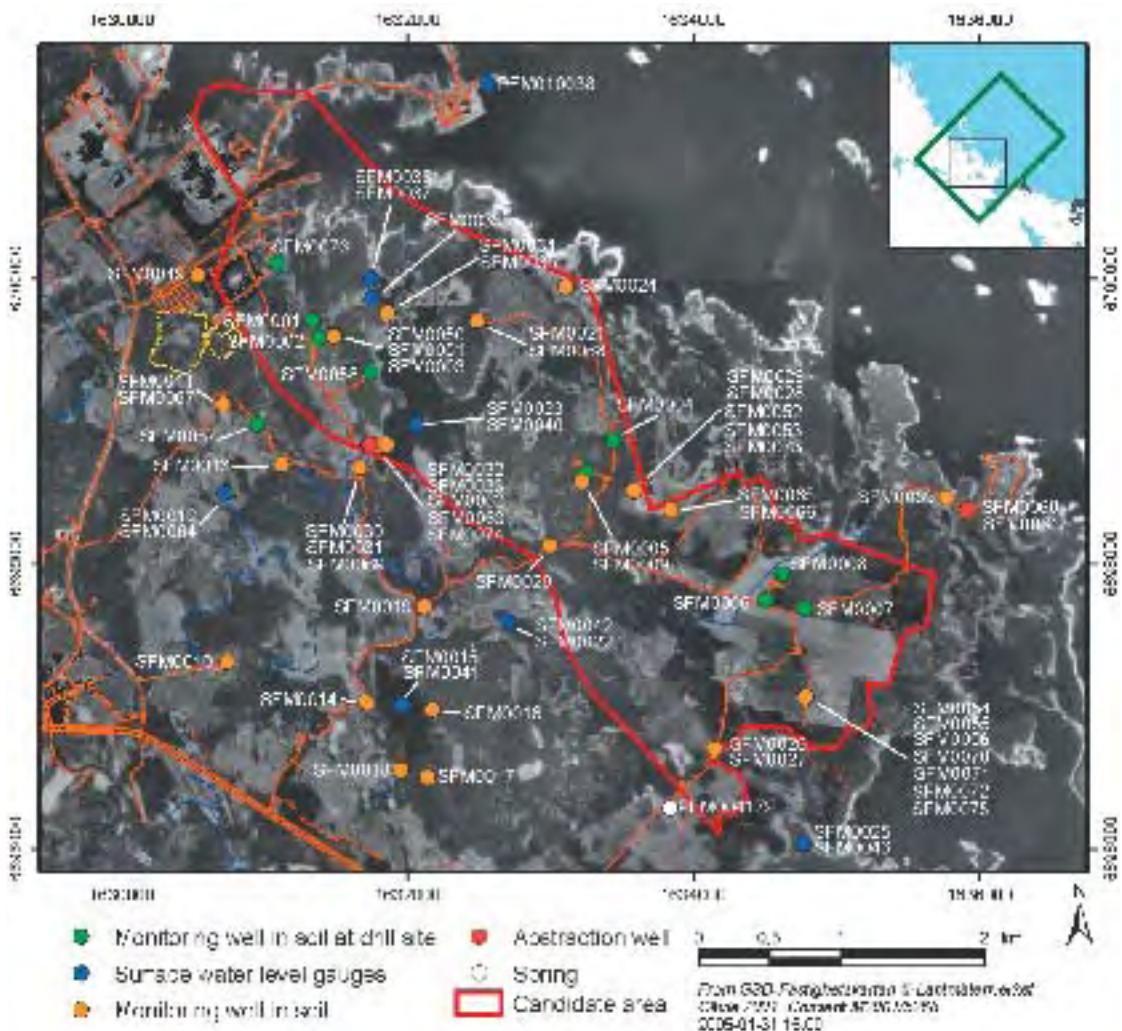


Figure 2-2. Boreholes and other observation points of different character in soil from which data are included in data freeze 1.2. See /SKB, 2004a/ for information as to which boreholes were included in data freeze 1.1.

The groundwater monitoring wells, abstraction wells and BAT-type filter tips all represent boreholes drilled through the unconsolidated overburden (regolith) and sometimes a few decimetres or even some metres into the solid bedrock. Two categories of soil boreholes intended as groundwater monitoring wells may be identified regarding design, performance and position.

1. Boreholes drilled with a large percussion drilling machine. The borehole diameter is 168 mm and the boreholes are supplied with a HDPE well screen and riser pipes 63/50 mm or 90/75 mm (outer/inner diameter), embedded in a sand filter and provided with bentonite sealing for protection against surface-water contamination. These boreholes are exclusively situated close to drill sites for core-drilling. Boreholes of this category that became available between data freezes 1.1 and 1.2 were SFM0057–58 and SFM0076 (results from the last borehole have not yet been described in a P-report). Boreholes SFM0001–08 were included already at data freeze 1.1.
2. Boreholes drilled with a percussion or auger technique with borehole diameter 115 mm and supplied with a well screen, riser pipes, sand filter and bentonite sealing. These boreholes are, with a few exceptions, situated away from drill sites. A simpler category of groundwater monitoring wells is achieved by knocking down a steel pipe, 60.3/51.3 mm, supplied with a well screen in the lower part, with a Pionjär percussion drill rig. All boreholes of this type are driven down into lake bottoms (SFM0012, 0015, 0022–0025, 0062–0063 and SFM0065).

Besides the two mentioned main categories, a number of other soil boreholes have been drilled for special purposes. A number of boreholes are supplied with BAT filter tips. The objectives of these boreholes are water sampling of pore water and determination of hydraulic conductivity in fine-grained soil layers.

Two boreholes were drilled to be used as abstraction wells during hydraulic pumping tests. Borehole SFM0061 at the Börstilåsen esker was percussion-drilled with a large drilling machine through the soil layer and c. 12 m into the bedrock. The stainless steel casing diameter is 154/150 mm and the diameter of the Johnson well screen is 162/148 mm. The casing and screen diameter (non-stainless steel) of the second abstraction well, SFM0074, which was drilled with a smaller machine, is 114/101 mm. The borehole penetrates the soil layer and c. 0.5 m into the bedrock. Two observation wells, SFM0059 and SFM0060 with casing and screen diameter 90/72 mm were also drilled at the Börstilåsen esker.

The borehole investigations during drilling differ between the three borehole categories. The investigation programme applied for the first category was identical to that used for percussion-drilled holes in rock (cf. SKB MD 610.003), except for the deviation measurements.

The investigation programme for the second category of boreholes could differ somewhat from borehole to borehole, but was in most cases carried out at least as comprehensive as according to the instructions in SKB MD 630.003. Special attention was given to soil and groundwater sampling.

Comments, boreholes in soil

The analyses of soil samples that were collected during drilling through the soil layer (soil boreholes and percussion boreholes) are reported as stratigraphic data within the activity characterised as mapping of Quaternary deposits (see Section 2.4.2). Also drill cuttings from the rock surface sampled during drilling of soil boreholes have been analysed and the results reported together with the rest of the bedrock surface mapping data in data freeze 1.2.

2.5.2 Drill core, drill cuttings and borehole investigations after completion of drilling

A base programme was carried out after drilling in all core-drilled boreholes and another base programme in percussion-drilled boreholes. Depending on whether the borehole is prioritised for hydrogeochemical measurements or not, the supplementary data acquired after the base programme may differ from borehole to borehole /SKB, 2000b/. However, all new boreholes included in data freeze 1.2 were, with the exceptions of KFM01B and KFM03B, regarded as prioritised for hydrogeochemical investigations and therefore surveyed by the same methods, one set of methods for core-drilled boreholes, and another for percussion-drilled holes.

Core-drilled boreholes – telescopic

Only data from the telescopic borehole KFM01A were included in data freeze 1.1. Data from the telescopic boreholes KFM02A, KFM03A, KFM04A and KFM05A became available by data freeze 1.2.

The upper c. 100 m long borehole section is percussion drilled in all mentioned telescopic boreholes. Normally, BIPS-logging should be performed in this section (below the upper casing of 10–15 m) after the first drilling step which provides a borehole diameter of 165 mm. Borehole radar, conventional borehole geophysics and HTHB (HydroTestutrustning i HammarBorrhål) tests are a bit tricky to carry out with good results at this borehole dimension. Above all, those investigations are, like BIPS-logging, difficult to accomplish from a logistic point of view, due to the narrow time window available during the different sequences of percussion drilling. Therefore, it has not been possible to perform some of these methods in all telescopic boreholes.

BIPS-logging and the samples of drill cuttings provide the basis for Boremap mapping of the percussion-drilled part. However, BIPS-logging may be difficult to conduct also from a technical aspect, because the available time is not always long enough to permit drill cuttings to settle, entailing the risk of poor water quality in the borehole. BIPS-logging and Boremap mapping were successful in the percussion-drilled sections of KFM02A, KFM03A and KFM04A, but had to be excluded in KFM05A.

Geophysical logging was performed in KFM02A and KFM03A and HTHB-tests were conducted in KFM02A, KFM03A and KFM06A.

The borehole investigations performed in the *borehole section 100–1,000 m* and reported by data freeze 1.2 comprise:

- BIPS-logging (all boreholes), borehole radar logging (all boreholes including re-logging with the directional radar antenna in KFM01A), geophysical logging (all boreholes), Boremap-mapping (all boreholes using drill core and BIPS images with support from geophysical logging), geological and rock mechanics single-hole interpretation (all boreholes including KFM01A).
- Difference flow measurements (all boreholes) and single-hole injection tests with the PSS equipment (all boreholes, but data and P-report not available until data freeze 2.1 for boreholes KFM04A and KFM05A).
- Hydrochemical logging (in KFM02A, KFM03A and KFM04A).
- Complete hydrogeochemical characterisation of selected water-yielding sections (all boreholes, although sampling failed in KFM05A due to limited water yield: a P-report relating to KFM01A is also available).
- Microbial investigations in KFM01A, KFM02A and KFM03A and investigations of fracture minerals from boreholes KFM01A, KFM02A and KFM03A+B.
- Sampling of the drill core for geological, rock mechanics, geochemical and transport laboratory analyses (all boreholes, although not all data and reports available from KFM05A): the rock mechanics testing comprised porosity and density determinations, indirect tensile strength tests, uniaxial and triaxial compression tests, normal stress tests and shear tests on joints, tilt tests, and determination of the P-wave velocity transverse to the drill cores.

Core-drilled boreholes of traditional type

Data from the core-drilled boreholes of traditional type KFM01B and KFM03B became available by data freeze 1.2. The borehole investigations performed and reported are:

- BIPS-logging, borehole radar logging and geophysical logging in both boreholes and Boremap-mapping of both boreholes using drill core and BIPS images with support from geophysical logging.
- Geological single-hole interpretation of both boreholes.
- Sampling of the drill core for geological, rock mechanics, geochemical and transport laboratory analyses (both boreholes).

- Overcoring rock-stress measurements in KFM01B.
- Single-hole injection tests with the PSS equipment in KFM03B, but the data and associated P-report will not be available until data freeze 2.1.

Percussion-drilled boreholes

The borehole investigations performed in the percussion-drilled boreholes in bedrock, HFM09–HFM19 and KFM04B, were:

- BIPS-logging, borehole radar logging, geophysical logging and Boremap-mapping using drill cuttings and BIPS images with support from geophysical logging,
- HTHB-logging, except in KFM04B.

Multi-section equipment for long-term groundwater level monitoring has been installed and monitoring has been initiated in boreholes HFM02–04. Besides that, temporary groundwater level gauges have, with interruptions for hydraulic pumping tests etc, been installed in HFM01 and HFM05–19 during the period between data freezes 1.1 and 1.2.

In addition, hydraulic interference tests have been performed between boreholes HFM01, HFM02 and HFM03, between HFM11 and HFM12, and finally between KFM01B and HFM01, HFM02, HFM03 and KFM01A, respectively, during drilling of KFM01B.

Boreholes in soil

Investigations in soil boreholes after completed drilling normally include slug tests and groundwater sampling. Slug tests were performed in the boreholes SFM0022, SFM0062–63, SFM0065, SFM0067–73 and SFM0075 (see Figure 2-2) between data freezes 1.1 and 1.2. Boreholes tested already before data freeze 1.1 are reported in /SKB, 2004a/.

Groundwater sampling between data freezes 1.1 and 1.2 has been conducted in soil boreholes SFM0001–03, SFM0005–09, SFM0012, SFM0015, SFM0022–23, SFM0025, SFM0027, SFM0029, SFM0031–32, SFM0037, SFM0049, SFM0057 and SFM0060 as well as in the spring PFM004179 (see Figure 2-2). Furthermore, sampling of pore water with BAT filter tips has been undertaken in SFM0051, SFM0053 and SFM0056.

In addition to the investigations mentioned above, pumping tests were carried out in the abstraction wells SFM0061 and SFM0074, whereby pressure responses were observed in nearby situated observation wells.

2.6 Other data sources

The old data identified during compilation of data for model version 0 were evaluated and/or inserted in the SKB databases SICADA and GIS in time for data freeze 1.2, and are included in the compilation tables in Section 2.7. However, it should be noted that these data are of lower “quality” than the data generated under the present site investigation work.

In the rock mechanics evaluation, stress data from Finnsjön, Björkö, Stockholm, and Olkiluoto have been used to estimate the regional state of stress in Central Sweden and eastern Finland. These results have been used in the evaluation of stress and stress boundary conditions at Forsmark. This evaluation and the data used are reported in /Sjöberg et al. 2005/, see also Section 6.4.

In the hydrogeochemical evaluation, available data from SICADA on groundwater conditions at near-by locations, such as SFR, and at other Swedish sites were used as background information together with data from Finnish sites (e.g. /Pitkänen et al. 1999/).

In the hydrogeological evaluation, data from structural and hydraulic characterisation as well as modelling conducted in the Forsmark reactor area /Carlsson, 1979; SSPB, 1982, 1986/, the SFR /Axelsson et al. 2002/, the Finnsjön study site /Andersson et al. 1991; Geir et al. 1992; Ahlbom et al.

1992; Stigsson et al. 1999/ and the Olkiluoto site /Löfman, 1999/ have been considered in various degree in the conceptual and quantitative modelling. Of particular interest has been the information gained about gently dipping deformation zones occurring at these places.

In the description and modelling of the surface system, many site-specific data from sources outside SKB have been used, especially for the biotic components. When site data needed for the modelling of carbon dynamics in the surface system were missing, generic data have been used. A detailed account of all data sources used in the description and modelling of the surface system is given in /Lindborg, 2005/.

2.7 Databases

The data that were available at the time of the data freeze for model version 1.2 are compiled in tables in this section. The purpose of these tables is to give a reference and account of which data were considered in the development of the site descriptive model (columns 1 and 2 in the tables), as well as to give a reference to where in the following sections of the report the data are utilised (columns 3 and 4 in the tables). Data not included in the modelling/site description work are commented upon in the last column of the tables. For simplification and traceability reasons, the information is split into several tables, one for each discipline, and complete references to the site-data reports are given in the last table in this section.

A number of studies involving data interpretation and modelling have been carried out within the framework of developing model version 1.2. In some cases, these studies are reported in separate reports, which are not included as references in the tables in this section. However, references to these supporting documents are given in Chapters 4 through 10.

Table 2-1. Available bedrock geological and geophysical data and their handling in Forsmark model version 1.2. Report numbers in italics show data available already at data freeze 1.1.

Available data Data specification	Ref.	Usage in F1.2 Analysis/Modelling	cf. section	Not utilised in F1.2 Motivation/Comment
Data from core-drilled boreholes				
Technical data in connection with drilling (KFM01A, KFM01B, KFM02A, KFM03A and KFM03B, KFM04A, KFM05A)	<i>P-03-32</i>	Siting and orientation of boreholes in modelling work.	5.3 and 5.4	
	<i>P-04-302</i>			
	<i>P-03-52</i>			
	<i>P-03-59</i>			
	<i>P-03-82</i>			
Radar and BIPS logging, and interpretation of radar logs (KFM01A, KFM01B, KFM02A, KFM03A and KFM03B, KFM04A, KFM05A)	<i>P-04-222</i>			
	<i>P-03-45</i>	Data used in borehole mapping (BIPS) and in single hole interpretation (radar logging) with focus on identification of brittle deformation zones. Input for both rock domain and DZ modelling.	5.2.6, 5.2.8, 5.3, 5.4	
	<i>P-04-79</i>			
	<i>P-04-40</i>			
	<i>P-04-41</i>			
<i>P-04-67</i>				
Geophysical logging (KFM01A, KFM01B, KFM02A and KFM03A/ KFM03B, KFM04A, KFM05A)	<i>P-04-152</i>			
	<i>P-03-103</i>	Data used in borehole mapping and in single hole interpretation. Input for both rock domain and DZ modelling.	5.2.6, 5.2.8, 5.3, 5.4	
	<i>P-04-145</i>			
	<i>P-04-97</i>			
	<i>P-04-144</i>			
<i>P-04-153</i>				
Interpretation of geophysical logs (KFM01A and KFM01B, KFM02A and KFM03A/KFM03B, KFM04A, KFM05A)	<i>P-04-80</i>	Used in single hole interpretation. Input for both rock domain and DZ modelling.	5.2.6, 5.2.8, 5.3, 5.4	
	<i>P-04-98</i>			
	<i>P-04-143</i>			
	<i>P-04-154</i>			

Available data Data specification	Ref.	Usage in F1.2 Analysis/Modelling	cf. section	Not utilised in F1.2 Motivation/Comment
Boremap mapping (KFM01A, KFM01B, KFM02A, KFM03A and KFM03B, KFM04A, KFM05A)	P-03-23 P-04-114 P-03-98 P-03-116 P-04-115 P-04-295	Rock type, ductile deformation in the bedrock, fracture statistics. Data used in identification of rock units and brittle deformation zones in single hole interpretation. Input for rock domain, DZ and DFN modelling.	5.2.6, 5.2.7, 5.2.8, 5.3, 5.4, 5.5	
Mineralogical and geochemical analyses of rock types and fracture fillings (KFM01A, KFM02A, KFM03A and KFM03B)	P-04-103 P-04-149	Mineralogical and geochemical properties of rock types and mineral fracture fillings. Input for rock domain, DZ and DFN modelling.	5.2.6, 5.2.7, 5.3, 5.4, 5.5	
Petrophysical and in-situ gamma-ray spectrometric data from rock types (KFM01A, KFM02A, KFM03A and KFM03B)	P-04-103 P-04-107	Physical properties of rock types. Input for rock domain model. Comment: Data also utilised for the interpretation of geophysical logs.	5.2.6, 5.3	
Mineralogical and microstructural analyses of vuggy metagranite in KFM02A	P-03-77	Understanding the formation of the vuggy metagranite in KFM02A. Input for DZ modelling.	5.2.6, 5.2.7, 5.2.8, 5.4	
Single hole interpretation (KFM01A and KFM01B, KFM02A, KFM03A and KFM03B, KFM04A, KFM05A)	P-04-116 P-04-117 P-04-118 P-04-119 P-04-296	Interpretation used in rock domain, DZ and DFN modelling.	5.2.8, 5.3, 5.4, 5.5	
Data from percussion-drilled boreholes				
Technical data in connection with drilling (HFM01–HFM03, HFM04–HFM05, HFM06– HFM08, HFM09–HFM10, HFM13–HFM15, HFM16, HFM11–HFM12 and HFM17–HFM19)	P-03-30 P-03-51 P-03-58 P-04-76 P-04-85 P-04-94 P-04-106	Siting and orientation of boreholes in modelling work.	5.3 and 5.4	
Radar and BIPS logging, and interpretation of radar logs (KFM01A and HFM01– HFM03, KFM02A and HFM04–HFM05, HFM06– HFM08, KFM04A/4B and HFM09–HFM10, HFM11– HFM12, HFM13–HFM15, HFM16–HFM19)	P-03-39 P-03-53 P-03-54 P-04-67 P-04-39 P-04-68 P-04-69	Data used in borehole mapping (BIPS) and in single hole interpretation (radar logging) with focus on identification of brittle deformation zones. Input for both rock domain and DZ modelling.	5.2.6, 5.2.8, 5.3, 5.4	Data from KFM04B not used. Percussion borehole neither mapped nor interpreted.
Geophysical logging (KFM01A and HFM01– HFM03, repeat HFM01– HFM02, KFM02A and HFM04–HFM05, HFM06– HFM08, HFM10–HFM13, HFM14–HFM18, HFM19)	P-03-39 P-03-103 P-03-53 P-03-54 P-04-144 P-04-145 P-04-153	Data used in borehole mapping and in single hole interpretation. Input for both rock domain and DZ modelling.	5.2.6, 5.2.8, 5.3, 5.4	Geophysical data in P-03-39 not used. Poor quality.
Interpretation of geophysical logs (HFM01–HFM03, HFM04–HFM08, HFM10– HFM13 and HFM16– HFM18, HFM14–HFM15 and HFM19)	P-04-80 P-04-98 P-04-143 P-04-154	Used in single hole interpretation. Input for both rock domain and DZ modelling.	5.2.6, 5.2.8, 5.3, 5.4	

Available data Data specification	Ref.	Usage in F1.2 Analysis/Modelling	cf. section	Not utilised in F1.2 Motivation/Comment
Boremap mapping (HFM01–HFM03, HFM04–HFM05, HFM06–HFM08, HFM09–HFM12, HFM13–15 and HFM19, HFM16–HFM18)	<i>P-03-20</i> <i>P-03-21</i> <i>P-03-22</i> P-04-101 P-04-112 P-04-113	Data mainly used in identification of rock units and brittle deformation zones in single hole interpretation. Input for rock domain, DZ and DFN modelling. Comment: Difficulties with the recognition of rock types and mineral coatings along fractures. Also underestimation of fractures. Latter derived solely from BIPS images.	5.2.6, 5.2.8, 5.3, 5.4, 5.5	
Single hole interpretation (HFM01–HFM03, HFM04–HFM05, HFM06–HFM08, HFM09–HFM10, HFM11–13 and HFM16–HFM18, HFM14–HFM15 and HFM19)	P-04-116 P-04-117 P-04-118 P-04-119 P-04-120 P-04-296	Interpretation used in rock domain, DZ and DFN modelling.	5.2.8, 5.3, 5.4, 5.5	
Older borehole, tunnel and surface data				
Older geological and geophysical data from the Forsmark nuclear power plant and SFR, including seismic refraction data	P-04-81	Rock type data from boreholes and tunnels, lineament identification at the nuclear power plant, brittle structures at or close to the surface in the vicinity of the nuclear power plant and identification of brittle deformation zones. Input for both rock domain and DZ modelling. Comment: Data acquisition in P-04-81.	5.2.2, 5.2.3, 5.2.4, 5.2.5, 5.3, 5.4	
Surface-based data				
Bedrock mapping – outcrop data. Rock type and ductile structures at 2,119 outcrops; frequency and orientation of fractures at 44 outcrops	<i>P-03-09</i> P-04-91 Bedrock geological map, Forsmark, version 1.2 (SKB GIS database)	Rock type, rock type distribution, ductile deformation in the bedrock, fracture statistics and identification of deformation zones at the surface. Input for both rock domain and DZ modelling. Comment: Data also utilised for the interpretation of helicopter-borne geophysical data.	5.2.1, 5.2.2, 5.2.4, 5.3, 5.4	Fracture data from scan-line mapping of 44 outcrops (truncation level 100 cm) were used in the DFN modelling in version 1.1. They are not used in the DFN modelling in version 1.2 (5.5). Possibly provide additional information concerning the spatial variability of fracture intensity and orientation.
Detailed bedrock mapping with special emphasis on fractures (drill sites 2, 3, 4 and 5, and coastal outcrop at Klubbudden)	<i>P-03-12</i> P-03-115 P-04-90	Rock type, ductile and brittle deformation in the bedrock, fracture statistics. Input for DFN modelling.	5.2.1, 5.2.2, 5.2.4, 5.5	
Geochemical analyses of till	P-03-118	Potential for mineral resources at the site.	5.2.2	
Evaluation of the occurrence of late- or post-glacial faulting	<i>P-03-76</i> P-04-123	Evolutionary aspects of the site	3.2	
Mineralogical and geochemical analyses of rock types	<i>P-03-75</i> P-04-87	Mineralogical and geochemical properties of rock types. Input for rock domain model.	5.2.1, 5.3	
Petrophysical and in-situ gamma-ray spectrometric data from rock types	<i>P-03-26</i> <i>P-03-102</i> P-04-155	Physical properties of rock types. Input for rock domain model. Comment: Data also utilised for the interpretation of helicopter-borne geophysical data.	5.2.1, 5.3	

Available data Data specification	Ref.	Usage in F1.2 Analysis/Modelling	cf. section	Not utilised in F1.2 Motivation/Comment
U-Pb, ⁴⁰ Ar/ ³⁹ Ar and (U-Th)/He geochronological data	P-04-126	Evolutionary aspects of the site. Input for conceptual understanding of the rock domain, DZ and DFN modelling work.	3.1, 5.3, 5.4, 5.5	
Production of orthorectified aerial photographs and digital terrain model	P-02-02	Data utilised for the interpretation of lineaments (topographic).	5.2.3	
Methodology for construction of digital terrain model for the site	P-04-03	Utilised for the interpretation of lineaments (topographic and bathymetric).	5.2.3	
Marine geological survey of the sea bottom off Forsmark	P-03-101	Data utilised for the interpretation of lineaments (bathymetric).	5.2.3	
Water depth in shallow lakes	P-04-25	Data utilised for the interpretation of lineaments (bathymetric).	5.2.3	
Water depth in shallow bays	P-04-125	Data utilised for the interpretation of lineaments (bathymetric).	5.2.3	
Helicopter-borne, geophysical data (magnetic, EM, VLF and gamma-ray spectrometry data)	P-03-41	Data utilised for the interpretation of lineaments (magnetic, EM and VLF).	5.2.3	
Electric soundings	P-03-44	These data provide a support in the interpretation of the helicopter-borne EM data.	5.2.3	
Inversion of helicopter-borne EM measurements	P-04-157	Utilised for the interpretation of lineaments (bathymetric).	5.2.3	
Interpretation of topographic, bathymetric and helicopter-borne geophysical data. Alternative interpretation in and immediately around the candidate area	P-03-40 P-04-29 P-04-282 P-04-241	Identification of lineaments. Input for DZ and DFN models.	5.2.3, 5.4, 5.5	
High-resolution seismic reflection data along five separate profiles with a total length c. 16 km. Interpretation of these data in two steps	R-02-43 P-04-158	Identification of seismic reflectors in the bedrock that may correspond to deformation zones or boundaries between different types of bedrock. Input for DZ model.	5.2.5, 5.4	
Ground geophysical data (magnetic and EM data) close to drill sites 1, 2, 3, 4 and 5, and several lineaments (including Interpretation)	P-02-01 P-03-55 P-03-104	Identification of lineaments. Input for DZ and DFN models.	5.2.5, 5.4, 5.5	
Regional gravity data	P-03-42		5.2.5	The data have not yet been interpreted. They are of broad, regional significance.
Previous models				
SFR structural models	R-98-05 R-01-02	The sub-vertical zones 3, 8 and 9 have been extracted from /Axelsson and Hansen, 1997/. The sub-horizontal zone H2 has been extracted from the SAFE model /Holmén and Stigsson, 2001/. On account of its length, the subvertical zone 6 /Axelsson and Hansen, 1997/ has not been included in the DZ modelling carried out for version 1.2.	5.4	
Forsmark site descriptive models, version 0 and version 1.1	R-02-32 R-04-15	Comparison of models.	5.3, 5.4	

Table 2-2. Available rock mechanics data and their handling in Forsmark model version 1.2. Report numbers in italics show data available already at data freeze 1.1.

Available data Data specification	Ref.	Usage in F1.2 Analysis/Modelling	cf. section	Not utilised in F1.2 Motivation/Comment
Data from core-drilled boreholes				
Uniaxial compressive strength – Intact rock		Characterisation of the intact rock;	6.2	
		Empirical determination of the	6.2.1	
KFM01A	P-04-223	rock mass mechanical properties	6.2.4	
KFM02A	P-04-224	by means of RMR and Q;	6.3.3	
KFM03A	P-04-225	Theoretical determination of the	6.3.5	
KFM04A	P-04-226	rock mass mechanical properties	6.3.6	
KFM01A – Independent determination	P-04-176	by means of numerical modelling.		
Triaxial compressive strength – Intact rock		Characterisation of the intact rock;	6.2	
		Empirical determination of the	6.2.1	
KFM01A	P-04-227	rock mass mechanical properties	6.2.4	
KFM02A	P-04-228	by means of RMR and Q;	6.3.3	
KFM03A	P-04-229	Theoretical determination of the	6.3.5	
KFM04A	P-04-230	rock mass mechanical properties	6.3.6	
KFM01A – Independent determination	P-04-177	by means of numerical modelling.		
Indirect tensile strength		Characterisation of the intact rock;	6.2	
		Theoretical determination of the	6.2.1	
KFM01A	P-04-170	rock mass mechanical properties	6.3.3	
KFM02A	P-04-172	by means of numerical modelling.	6.3.5	
KFM03A	P-04-173		6.3.6	
KFM04A	P-04-174		6.4.1	
KFM01A – Independent determination	P-04-171			
Direct shear tests on rock fractures		Characterisation of the rock	6.2	
		fractures – strength and stiffness;	6.2.2	
KFM01A	P-04-175	Theoretical determination of the	6.3.4	
	P-05-08	rock mass mechanical properties	6.3.6	
		by means of numerical modelling.		
KFM02A	P-05-09			
KFM03A	P-05-10			
KFM04A	P-05-11			
Crack initiation stress		Evaluation of the elastic limit of	6.3.3	
		deformation – for addressing		
KFM01A	P-04-223	spalling and core discing		
KFM02A	P-04-224	problems.		
KFM03A	P-04-225			
KFM04A	P-04-226			
Q-logging from KFM01A	<i>P-03-29</i>	Comparison of Q-logging by	6.1	
		different methods; Empirical	6.2.3	
		determination of the rock mass		
		mechanical properties.		
Tilt tests on fractures		Characterisation of the rock	6.2	
		fracture properties and of the	6.2.2	
KFM01A	<i>P-03-108</i>	rock mass by RMR and Q.		
KFM02A	P-04-08			
KFM03A	P-04-178			
KFM04A	P-04-179			

Available data Data specification	Ref.	Usage in F1.2 Analysis/Modelling	cf. section	Not utilised in F1.2 Motivation/Comment
P-wave velocity measurements		Correlation between rock mass stresses and foliation. Intact rock properties at depth.	6.2	
KFM01A	P-03-38		6.2.1	
KFM02A	P-04-09			
KFM03A	P-04-180			
KFM04A	P-04-181			
Empirical characterisation		Characterisation of the rock mass (RMR, Q) – rock mass mechanical properties.	6.1	
KFM01A	P-05-112		6.2.4	
KFM02A	P-05-113		6.3.5	
KFM03A	P-05-114		6.3.7 6.3.8	
KFM04A	P-05-115			
Overcoring measurements – KFM01B	P-04-83			
Evaluation of over-coring result – KFM01B	P-05-66	Stress state determination, core discing and spalling evaluation.	6.4.1	
			6.4.4	
			6.4.5	
HF and HTPF measurements – KFM01A, KFM01B, KFM02A, KFM04A	P-04-311	Stress state determination, core discing and spalling evaluation.	6.4.1	
			6.4.4	
			6.4.5	
HF and HTPF measurements – KFM01A, KFM01B, KFM02A, KFM04A – laboratory testing on cores	P-04-312			
Other borehole and tunnel data				
Young's modulus, Poisson's ratio of intact rock. Point load tests on fractures. Point load tests on core samples from SFR boreholes.	SICADA	Characterisation of the rock mass by RMR, Q; Empirical determination of the rock mass mechanical properties of the deformation zones.	6.1	
			6.2.3	
			6.3.7	
Stress measurements in DBT1, DBT3	SICADA	Re-interpretation of old data, transient strain analysis, stress state determination	6.4.1	
			6.4.4	
			6.4.5	
Stress measurements in KB-21, KB-22, KBS-7, SFR 1/177	SICADA	Stress state determination, core discing and spalling evaluation.	6.4.1	
			6.4.4	
			6.4.5	

Table 2-3. Available rock thermal data and their handling in Forsmark model version 1.2. Report numbers in italics show data available already at data freeze 1.1.

Available data Data specification	Ref.		Usage in F1.2 Analysis/Modelling	cf. section	Not utilised in F1.2 Motivation/Comment
Data from core-drilled boreholes					
Temperature logging	Results	Interpret.	Temperature and temperature gradient distribution.	7.2.8	
KFM01A	P-03-103	P-04-80			
KFM01B	P-04-145				
KFM02A	P-04-97	P-04-98			
KFM03A	P-04-97	P-04-98			
KFM04A	P-04-144	P-04-143			
Density logging			Density distribution to indicate the distribution of thermal properties.	7.2.3	
KFM01A	P-03-103			7.2.4	
KFM01B	P-04-145				
KFM02A	P-04-97				
KFM03A	P-04-97				
KFM04A	P-04-144				
Boremap logging of KFM01A, KFM01B, KFM02A, KFM03A, KFM04A	<i>P-03-23</i> SICADA		Dominant and subordinate rock type distribution	7.2.3 7.3	
Laboratory test of thermal properties			Estimation of thermal conductivity and specific heat capacity.	7.2.1 7.2.4 7.2.5	
KFM01A	P-04-159				
KFM02A	P-04-161				
KFM03A	P-04-162				
KFM04A	P-04-199				
Modal analysis			Estimation of thermal conductivity.	7.2.2 7.2.4	
KFM01A	P-04-159				
KFM02A	P-04-161				
KFM03A	P-04-162				
KFM03B	SICADA				
Anisotropy for KFM04A	P-report in print		Estimation of anisotropy in thermal properties.	7.2.6	
Comparing TPS measurements for KFM01A	P-04-186			7.2.1	
Laboratory test of thermal expansion			Estimation of the thermal expansion coefficient.	7.2.7	
KFM01A	P-04-163				
KFM02A	P-04-164				
KFM03A	P-04-165				
Surface-based data					
Modal analyses	<i>P-03-75</i>		Modelling of thermal conductivity from mineralogical properties of the bedrock. Statistical analysis.	7.2.2 7.2.4	
Measurement of thermal properties	<i>P-03-08</i>		Thermal transport properties for some samples. Comparison with modelled results.	7.2.1 7.2.4 7.2.5	

Table 2-4. Available meteorological, hydrological and hydrogeological data and their handling in Forsmark bedrock hydrogeological model version 1.2. Report numbers in italics show data available already at data freeze 1.1.

Available data Data specification	Ref.	Usage in F1.2 Analysis/Modelling	cf. section	Not utilised in F1.2 Motivation/Comment
Single-hole data from core-drilled boreholes				
Double-packer injection tests (PSS)		Lumped characterisation of rock fracture transmissivities in terms of different test section length transmissivities (5 m, 20 m and 100 m).	8.2, 8.4	
KFM01A	P-04-95			
KFM02A	P-04-100			
KFM03A	P-04-194			
Difference-flow logging (PFL)		Detailed characterisation of individual rock fracture transmissivities in terms of high-resolution test section length transmissivities (0.1 m).	8.2, 8.4	
KFM01A	<i>P-03-28</i> P-04-193			
KFM02A	P-04-188			
KFM03A	P-04-189			
KFM04A	P-04-190			
KFM05A	P-04-191			
Single-hole data from percussion-drilled boreholes				
Pumping tests and impeller flow logging		Characterisation of superficial rock fracture transmissivities in terms of borehole specific capacity and cumulative flow logging.	8.2, 8.4	
HFM01, -02, -03	<i>P-03-33</i>			
HFM04, -05	<i>P-03-34</i>			
HFM06, -07, -08	<i>P-03-36</i>			
HFM09, -10	P-04-74			
HFM11, -12	P-04-64			
HFM13, -14, -15	P-04-71			
HFM16	P-04-65			
HFM17, -18, -19	P-04-72			
Cross-hole (interference) data				
HFM01, -02, -03	<i>P-03-35</i>	Characterisation of the hydraulic contact between boreholes presumably intersected by a swarm of connected fractures forming a transmissive deformations zone.	8.2, 8.4	
HFM11, -12	P-04-200			
Correlation of structural, hydraulic and hydrogeochemical data				
KFM01A, -02A, -03A, -04A, -05A	R-04-77	Correlation of Posiva Flow Log anomalies to core mapped features.	8.2, 8.4	
HFM16, KFM02A	SICADA Field note Forsmark 437	Hydraulic responses during drilling of HFM16.	8.2, 8.4	
KFM03A	P-04-96	Hydraulic evaluation of pumping activities prior to hydrogeochemical sampling – indications of upconing.	8.2, 8.6	
KFM02A, -03A, -04A	P-05-21	Comparison of measured EC in selected fractures – indications of upconing.	8.2, 8.6	
KFM01B, HFM01, -02, -03, KFM01A	P-04-135	Hydraulic responses during drilling of KFM01B.	8.2, 8.4	
Surface data				
Geometrical and topographical data	cf. Table 2-7	Basic input to flow and transport models. Delineation of surface water divides.	8.7	

Available data Data specification	Ref.	Usage in F1.2 Analysis/Modelling	cf. section	Not utilised in F1.2 Motivation/Comment
Geological data	cf. Table 2-7	Conceptual model, distribution of Quaternary deposits, 2D model and input to 3D soil-depth model. Stratigraphical distribution and characterisation of terrestrial, lacustrine and marine Quaternary deposits. Depth to bedrock. Input to 3D soil-depth model.	8.4, 8.7	
Meteorological data	cf. Table 2-7	General description and quantitative modelling of groundwater and surface water flow.	8.7	
Hydrological data	cf. Table 2-7	Delineation of catchment areas. Specific discharge in conceptual and quantitative modelling.	8.4, 8.7	
Hydrogeological data	cf. Table 2-7	General description, conceptual and quantitative modelling. Description of soil depth, basis for groundwater level measurements and hydraulic tests. Basis for assigning hydraulic conductivity of Quaternary deposits in conceptual and quantitative models.	8.4, 8.7	
Supplementary information and models				
Geological data	cf. Table 2-1	General description, conceptual and quantitative modelling. Definition of relevant DZ and DFN models necessary for conceptual and quantitative hydrogeological modelling.	8.4, 8.7	
Hydrogeochemical data	cf. Table 2-5	General description, conceptual and quantitative modelling.	8.5, 8.6, 8.7	
Shoreline displacement	TR-96-24 TR-97-28 TR-00-02 TR-03-17	General description, conceptual and quantitative modelling of the initial condition and variable – density flow.	8.6, 8.7	
Baltic Sea salinity	R-99-08 TR-99-38 TR-04-12	General description, conceptual and quantitative modelling of the initial condition and variable – density flow.	8.6, 8.7	
SFR	R-02-14	General description, conceptual and quantitative modelling. Basis for assigning transmissivity data to some of the deterministically treated deformation zones.	8.2, 8.4	
Forsmark Reactor area	SSPB, 1982 SSPB, 1996 /Carlsson, 1979/	General description, conceptual and quantitative modelling.	8.2, 8.4	
Finnsjön study site	TR-91-24 TR-92-07 TR-92-33 TR-99-18	General description, conceptual and quantitative modelling. Basis for assigning hydraulic conductivity of bedrock outside the candidate area in conceptual and quantitative models.	8.7	
SDM version 0	R-02-32	General description, conceptual and quantitative modelling.	8.1	
SDM version 1.1	R-04-15	General description, conceptual and quantitative modelling.	8.1	
Olkiluoto	/Löfman, 1999/	General description, conceptual and quantitative modelling.	8.1	

Table 2-5. Available hydrogeochemical data and their handling in Forsmark model version 1.2. Report numbers in italics show data available already at data freeze 1.1.

Available data Data specification	Ref.	Usage in F1.2 Analysis/Modelling	cf. section	Not utilised in F1.2 Motivation/Comment
KFM01, KFM02, KFM03; KFM04	P-04-109 P-04-108	Manual evaluation and mathematical modelling such as PHREEQC, M3 and coupled transport modelling. The results of the modelling is presented in the conceptual model of the site. The use of the data in the specific modelling approaches are described in Appendix 8 in SKB R-05-17.	9 and 11.6	Non representative samples were not used in the detailed modelling (see motivation in SKB R-05-17).
Complete chemical characterisation (class 4 and 5), sampling during drilling ,urinine analyses.	P-04-92 P-04-47 P-04-70			
Percussion drilled boreholes HFM01–HFM19	P-03-96 <i>P-03-95</i> <i>P-03-94</i>			
Environmental monitoring boreholes PFM000001-7-9-910-39-2942-4778	<i>P-03-52</i> <i>P-03-49</i> <i>P-03-48</i> <i>P-03-47</i>			
Soil pipes, BAT tubes	<i>P-03-32</i>			
Sea water, Running water, Lake water	<i>P-03-27</i>			
Other available data: Swedish and Nordic site data				

Table 2-6. Available data on transport properties and their handling in Forsmark model version 1.2. Report numbers in italics show data available already at data freeze 1.1.

Available data Data specification	Ref.	Usage in F1.2 Analysis/Modelling	cf. section	Not utilised in F1.2 Motivation/Comment
Data from core-drilled boreholes				
Results from porosity measurements and through-diffusion test on samples from boreholes KFM01A and KFM02A	P-report not yet published	Assignment of porosity and diffusion parameters.	10.4	
Formation factors from electrical resistivity measurements in the laboratory on samples from boreholes KFM01A and KFM02A	P-05-26	Assignment of porosity and diffusion parameters.	10.4	
Formation factors from in situ electrical resistivity measurements in boreholes KFM01A and KFM02A	P-05-29	Assignment of porosity and diffusion parameters.	10.4	
Results from BET surface area measurements on crushed material	P-report not yet published	Qualitative assessment of sorption properties.	10.4	
Fracture mineralogy	P-04-103 P-04-149	Identification of site-specific fracture and fracture zone properties as a basis for a conceptual transport model	10.3	

Table 2-7. Available abiotic data for the surface system and their handling in Forsmark model version 1.2. Report numbers in italics show data available already at data freeze 1.1.

Available data Data specification	Ref.	Usage in F1.2 Analysis/Modelling	cf. section	Not utilised in F1.2 Motivation/Comment
Geometrical and topographical data				
Geometry, topography, bathymetry, Digital Elevation Model (DEM)	P-04-25 P-04-125 R-04-70	Basic input to flow and transport models.	4.3, 4.4	
Geological data				
Geological maps, Quaternary deposit descriptions	<i>P-03-11</i> R-04-39 SKB GIS	Conceptual model, distribution of Quaternary deposits, 2D model and input to 3D soil-depth model.	4.3	
Marine geological map	P-03-101 SKB GIS	Conceptual model, distribution of Quaternary deposits, 2D model.	4.3	
Soil type map	R-04-08 SKB GIS	Conceptual and quantitative model, input to 3D soil-depth model.	4.3	
Stratigraphical and analytical data from boreholes (HFM, SFM, PFM)	<i>P-03-14</i> <i>P-03-64</i> P-04-111 P-04-138 P-04-139 P-04-140 P-04-148	Stratigraphical distribution and characterisation of Quaternary deposits. Depth to bedrock. Input to 3D soil-depth model.	4.3	
Peatland investigations	<i>R-01-12</i> P-04-127	Chemical properties and distribution of organic deposits in two mires. Conceptual model.	4.3	
Mapping of marine and lacustrine sediment	<i>P-03-24</i> P-04-86 <i>TR-03-17</i> <i>R-01-12</i>	Description of stratigraphical distribution and characteristics of sediments in lakes. Input to 3D soil-depth model.	4.3	
Stratigraphical data from machine-cut trenches	P-04-34	Depth and stratigraphical distribution of Quaternary deposits. Conceptual model, input to 3D soil-depth model.	4.3	
Investigation of evidence of neotectonic movements	<i>P-03-76</i> P-04-123	Conceptual understanding.	3.2 4.3	
Textural composition	<i>P-03-14</i> P-04-34 P-04-86 P-04-111 P-04-148 R-04-08	Conceptual model, input to quantitative modelling of hydraulic properties.	4.3	
Chemical analyses of glacial and post-glacial sediments	<i>P-03-14</i> <i>TR-03-17</i> P-04-34 P-04-86 P-04-111 P-04-148 R-04-08	Conceptual model, input to quantitative model of chemical properties.	4.4	
Peat chemistry	P-04-127			
Pollen composition in glacial sediments	P-04-110	Conceptual understanding, glacial/interglacial history.	4.3	
Helicopter-borne survey data	P-03-41			Not yet utilised.

Available data		Usage in F1.2		Not utilised in F1.2
Data specification	Ref.	Analysis/Modelling	cf. section	Motivation/Comment
Ground penetrating radar	P-04-78 P-04-156	Conceptual model and 3D model of soil depth.	4.3	
Reflection seismics	P-04-99			
Meteorological data				
Regional meteorological data up to 2003	R-99-70 TR-02-02 SICADA	General description and quantitative modelling of groundwater and surface water flows.	4.4	
Data from meteorological stations at Högmasten and Storskäret June 2003 to July 2004	SICADA	Comparison with regional meteorological data.	4.4	
Snow depth, ground frost and ice cover	P-03-117 P-04-137	Validation of snow routine in quantitative modelling.	4.4	
Hydrological data				
Catchment characteristics – regional data	SKB GIS	Delineation of catchment areas.	4.4	
Regional discharge data	R-99-70 TR-02-02	Specific discharge in conceptual and quantitative modelling.	4.4	
Geometric data on catchment areas, lakes and water courses	P-04-25 SKB GIS	Delineation and characteristics of catchment areas and lakes.	4.4	
Automatic discharge measurements	SICADA		4.4	Only < 3 months time series at one station.
Simple discharge measurements in water courses	SICADA P-03-27 P-04-146	General description of temporal variability in surface water discharge.	4.4	
Installation of surface water level gauges	P-03-64 P-04-139	Surface water – groundwater level relations, test of quantitative modelling with MIKE SHE.	4.4	
Level measurements in lakes and the sea	SICADA P-04-313			
Hydrogeological data				
Inventory of private wells	R-02-17	Description of available hydrogeological information.	4.4	No attempt is made to infer hydraulic parameters from capacity data.
Data on installed groundwater monitoring wells, abstraction wells and BAT filter tips	P-03-64 P-04-136 P-04-138 P-04-139	Description of soil depth, basis for groundwater level measurements and hydraulic tests.	4.4	
Hydraulic conductivity of Quaternary deposits	P-03-65 P-04-136 P-04-138 P-04-140 P-04-142	Basis for assigning hydraulic conductivity of Quaternary deposits in conceptual and quantitative models.	4.4	
Groundwater levels in Quaternary deposits	P-04-313	General description, conceptual and quantitative modelling.	4.4	
Oceanographic data				
Regional oceanographic data	TR-02-02 TR-99-11	Quantitative modelling (see /Lindborg, 2005/).	–	
Chemistry data				
Surface water sampling	P-03-27	Description.	4.5	
Groundwater sampling	P-03-47 P-03-48	Description.	4.5	

Table 2-8. Available biotic data for the surface system and their handling in Forsmark model version 1.2. Report numbers in italics show data available already at data freeze 1.1.

Available data Data specification	Ref	Usage in F1.2 Analysis/Modelling	cf. section	Not utilised in F1.2 Motivation/Comment
Terrestrial biota				
Compilation of existing information 2002	<i>R-02-08</i>	Description.	4.6, 4.8	
Bird population survey	<i>P-03-10</i> P-04-30	Description.	4.6, 4.8	
Mammal population survey	P-04-04	Description, modelling.	4.6, 4.8	
Amphibians and reptiles	P-04-07	Description, modelling.	4.6, 4.8	
Vegetation inventory	P-03-81	Description.	4.6, 4.8	
Vegetation mapping	<i>R-02-06</i>	Description, modelling.	4.6, 4.8	
Biomass of the dead organic material	P-03-90 P-04-124	Modelling.	4.6, 4.8	
Data from soil mapping	R-04-08	Description, modelling.	4.6, 4.8	
Limnic biota				
Habitat borders	P-04-25	Description.	4.6, 4.8	
Limnic producers	R-02-41 R-03-27	Description, modelling.	4.6, 4.8	
Limnic consumers	R-03-27 P-04-05	Description, modelling.	4.6, 4.8	
Marine biota				
Light penetration depth	SICADA	Description.	4.6, 4.8	
Phytoplankton	SICADA	Description, modelling.	4.6, 4.8	
Zooplankton	SICADA	Description, modelling.	4.6, 4.8	
Macrophyte communi-ties	R-99-69	Description, modelling.	4.6, 4.8	
Macrofauna	R-99-69	Description, modelling.	4.6, 4.8	
Bird population survey	<i>P-03-10</i> P-04-30	Description.	4.6, 4.8	
Hunams and land use				
Humans and land use	R-04-10	Description, modelling.	4.7	

Table 2-9. Reports in the SKB series P-, R- and TR that are referred to in Table 2-1 to Table 2-8. Reports with numbers in italics contain data available already at data freeze 1.1.

<i>P-02-01</i>	Thunehed H, Pitkänen T. Markgeofysiska mätningar inför placering av de tre första kärnborrhålen i Forsmarksområdet.
<i>P-02-02</i>	Wiklund S. Digitala ortofoton och höjdm modeller. Redovisning av metodik för platsundersökningsområdena Oskarshamn och Forsmark samt förstudieområdet Tierp Norra.
<i>P-03-08</i>	Adl-Zarrabi B. Outcrop samples from Forsmark. Determination of thermal properties by the TPS-method.
<i>P-03-09</i>	Stephens M B, Bergman T, Andersson J, Hermansson T, Wahlgren C-H, Albrecht L, Mikko H. Bedrock mapping. Stage 1 (2002) – Outcrop data including fracture data. Forsmark.
<i>P-03-10</i>	Gren M. Fågelundersökningar inom SKB:s platsundersökningar 2002. Forsmark.
<i>P-03-11</i>	Sohlenius G, Rudmark L, Hedenström A. Forsmark. Mapping of unconsolidated Quaternary deposits. Field data 2002.
<i>P-03-12</i>	Hermanson J, Hansen L, Olofsson J, Sävås J, Vestgård J. Detailed fracture mapping at the KFM02 and KFM03 drill sites. Forsmark.
<i>P-03-14</i>	Sohlenius G, Rudmark L. Forsmark site investigation. Mapping of unconsolidated Quaternary deposits. Stratigraphical and analytical data.
<i>P-03-18</i>	Cederlund G, Hammarström A, Wallin K. Surveys of mammal populations in the areas adjacent to Forsmark and Tierp.

- P-03-20* **Nordman, C.** Forsmark site investigation. Boremap mapping of percussion boreholes HFM01–03.
- P-03-21* **Nordman, C.** Forsmark site investigation. Boremap mapping of percussion boreholes HFM04 and HFM05.
- P-03-22* **Nordman, C.** Forsmark site investigation. Boremap mapping of percussion boreholes HFM06–08.
- P-03-23* **Petersson J, Wägnerud A.** Forsmark site investigation. Boremap mapping of telescopic drilled borehole KFM01A.
- P-03-24* **Hedenström A.** Forsmark site investigation. Investigation of marine and lacustrine sediments in lakes. Field data 2003.
- P-03-26* **Mattsson H, Isaksson H, Thunehed H.** Forsmark site investigation. Petrophysical rock sampling, measurements of petrophysical rock parameters and in-situ gamma-ray spectrometry measurements on outcrops carried out 2002.
- P-03-27* **Nilsson A-C, Karlsson S, Borgiel M.** Forsmark site investigation. Sampling and analysis of surface waters. Results from sampling in the Forsmark area, March 2002 to March 2003.
- P-03-28* **Rouhiainen P, Pöllänen J.** Forsmark site investigation. Difference flow logging of borehole KFM01A.
- P-03-29* **Barton N.** KFM01A. Q-logging.
- P-03-30* **Claesson L-Å, Nilsson G.** Forsmark site investigation. Drilling of a flushing water well, HFM01, and two groundwater monitoring wells, HFM02 and HFM03 at drillsite DS1.
- P-03-32* **Claesson L-Å, Nilsson G.** Forsmark site investigation. Drilling of the telescopic borehole KFM01A at drilling site DS1.
- P-03-33* **Ludvigson J-E, Jönsson S, Levén, J.** Forsmark site investigation. Pumping tests and flow logging. Boreholes KFM01A (0–100 m), HFM01, HFM02 and HFM03.
- P-03-34* **Ludvigson J-E, Jönsson S, Svensson T.** Forsmark site investigation. Pumping tests and flow logging. Boreholes KFM02A (0–100 m), HFM04 and HFM05.
- P-03-35* **Ludvigson J-E, Jönsson S.** Forsmark site investigation. Hydraulic interference tests. Boreholes HFM01, HFM02 and HFM03.
- P-03-36* **Källgården J, Ludvigson J-E, Jönsson S.** Forsmark site investigation. Pumping tests and flow logging. Boreholes KFM03A (0–100 m), HFM06, HFM07 and HFM08.
- P-03-38* **Tunbridge L, Chryssanthakis P.** Forsmark site investigation. Borehole KFM01A. Determination of P-wave velocity, transverse borehole core.
- P-03-39* **Gustafsson C, Nilsson P.** Forsmark site investigation. Geophysical, radar and BIPS logging in boreholes HFM01, HFM02, HFM03 and the percussion drilled part of KFM01A.
- P-03-40* **Isaksson H.** Forsmark site investigation. Interpretation of topographic lineaments 2002.
- P-03-41* **Rønning H J S, Kihle O, Mogaard J O, Walker P, Shomali H, Hagthorpe P, Byström S, Lindberg H, Thunehed H.** Forsmark site investigation. Helicopter borne geophysics at Forsmark, Östhammar, Sweden.
- P-03-42* **Aaro S.** Forsmark site investigation. Regional gravity survey in the Forsmark area, 2002 and 2003.
- P-03-44* **Thunehed H, Pitkänen, T.** Forsmark site investigation. Electric soundings supporting inversion of helicopterborne EM-data.
- P-03-45* **Aaltonen J, Gustafsson C.** Forsmark site investigation. RAMAC and BIPS logging in borehole KFM01A.
- P-03-47* **Nilsson A-C.** Forsmark site investigation. Sampling and analyses of groundwater in percussion drilled boreholes and shallow monitoring wells at drillsite DS1. Results from the percussion boreholes HFM01, HFM02, HFM03, KFM01A (borehole section 0–100 m) and the monitoring wells SFM0001, SFM0002 and SFM 0003.
- P-03-48* **Nilsson A-C.** Forsmark site investigation. Sampling and analyses of groundwater in percussion drilled boreholes and shallow monitoring wells at drillsite DS2. Results from the percussion boreholes HFM04, HFM05, KFM02A (borehole section 0–100 m) and the monitoring wells SFM0004 and SFM 0005.
- P-03-49* **Nilsson A-C.** Forsmark site investigation. Sampling and analyses of groundwater in percussion drilled boreholes at drillsite DS3. Results from the percussion boreholes HFM06 and HFM08.
- P-03-51* **Claesson L-Å, Nilsson, G.** Forsmark site investigation. Drilling of a flushing water well, HFM05, and a groundwater monitoring well, HFM04, at drillsite DS2.
- P-03-52* **Claesson L-Å, Nilsson, G.** Forsmark site investigation. Drilling of the telescopic borehole KFM02A at drilling site DS 2.
- P-03-53* **Nilsson P, Gustafsson C.** Forsmark site investigation. Geophysical, radar and BIPS logging in boreholes HFM04, HFM05, and the percussion drilled part of KFM02A.
- P-03-54* **Nilsson P, Aaltonen J.** Forsmark site investigation. Geophysical, radar and BIPS logging in boreholes HFM06, HFM07 and HFM08.
- P-03-55* **Pitkänen T, Isaksson H.** Forsmark site investigation. A ground geophysical survey prior to the siting of borehole KFM04A.
- P-03-58* **Claesson L-Å, Nilsson, G.** Forsmark site investigation. Drilling of a flushing water well, HFM06 and two groundwater monitoring wells, HFM07 and HFM08, at drillsite DS3.

- P-03-59 **Claesson L-Å, Nilsson, G.** Forsmark site investigation. Drilling of the telescopic borehole KFM03A and the core drilled borehole KFM03B at drilling site DS3.
- P-03-64 **Johansson P-O.** Forsmark site investigation. Slug tests in groundwater monitoring wells in soil.
- P-03-65 **Werner K, Johansson P-O.** Forsmark site investigation. Slug tests in groundwater monitoring wells in soil.
- P-03-75 **Stephens M B, Lundqvist S, Bergman T, Anderson J, Ekström M.** Forsmark site investigation. Bedrock mapping. Rock types, their petrographic and geochemical characteristics, and a structural analysis of the bedrock based on Stage 1 (2002) surface data.
- P-03-76 **Lagerbäck R, Sundh M.** Forsmark site investigation. Searching for evidence of late- or post-glacial faulting in the Forsmark region. Results from 2002.
- P-03-77 **Möller C, Snäll S, Stephens M B.** Forsmark site investigation. Dissolution of quartz, vug formation and new grain growth associated with post-metamorphic hydrothermal alteration in KFM02A.
- P-03-81 **Abrahamsson T.** Forsmark site investigation. Vegetation inventory in part of the municipality of Östhammar.
- P-03-82 **Claesson L-Å, Nilsson G.** Forsmark site investigation. Drilling of the telescopic borehole KFM04A and the percussion drilled borehole KFM04B at drilling site DS4.
- P-03-90 **Fridriksson G, Öhr J.** Forsmark site investigations. Assessment of plant biomass of the ground, field and shrub layers of the Forsmark area.
- P-03-94 **Wacker P, Bergelin A, Nilsson A-C.** Forsmark site investigation. Complete hydrochemical characterisation in KFM01A. Results from two investigated sections, 110.1–120.8 and 176.8–183.9 metres.
- P-03-95 **Wacker P, Nilsson A-C.** Forsmark site investigation. Hydrochemical logging and “clean up” pumping in KFM02A.
- P-03-96 **Berg C, Nilsson A-C.** Forsmark site investigation. Hydrochemical logging in KFM 03A.
- P-03-98 **Petersson J, Wängnerud A, Strähle A.** Forsmark site investigation. Boremap mapping of telescopic drilled borehole KFM02A.
- P-03-101 **Elhammer et al.** Forsmark site investigation. Detailed marine geological mapping (in prep).
- P-03-102 **Isaksson H, Mattsson H, Thunehed H, Keisu M.** Forsmark site investigation. Interpretation of petrophysical surface data. Stage 1 (2002).
- P-03-103 **Nielsen U T, Ringgaard J.** Forsmark site investigation. Geophysical borehole logging in borehole KFM01A, HFM01 and HFM02.
- P-03-104 **Pitkänen T, Thunehed H, Isaksson H.** Forsmark site investigation. A ground geophysical survey prior to the siting of borehole KFM05A and KFM06A and control of the character of two SW-NE oriented lineaments.
- P-03-108 **Chryssanthakis P.** Forsmark site investigation. Borehole KFM01A. Results of tilt testing.
- P-03-115 **Hermanson J, Hansen L, Vestgård J, Leiner P.** Forsmark site investigation. Detailed fracture mapping of the outcrops Klubbudden, AFM001098 and drill site 4, AFM001097.
- P-03-116 **Petersson J, Wängnerud A, Danielsson P, Strähle A.** Forsmark site investigation. Boremap mapping of telescopic drilled borehole KFM03A and core drilled borehole KFM03B.
- P-03-117 **Aquilonius K, Karlsson S.** Forsmark site investigation. Snow depth, frost in ground and ice cover during the winter 2002/2003.
- P-03-118 **Nilsson B.** Forsmark site investigation. Element distribution in till at Forsmark – a geochemical study.
- P-04-03 **Brydsten L.** A method for construction of digital elevation models for site investigation program at Forsmark and Simpevarp.
- P-04-04 **Cederlund G, Hammarström A, Wallin K.** Survey of mammal populations in the areas adjacent to Forsmark and Oskarshamn. Results from 2003.
- P-04-05 **Borgiel M.** Forsmark site investigation. Sampling and analyses of surface sediment in lakes and shallow bays.
- P-04-07 **Andrén C.** Forsmark site investigation. Amphibians and reptiles.
- P-04-08 **Chryssanthakis P.** Forsmark site investigation. Borehole KFM02A. Results of tilt testing.
- P-04-09 **Chryssanthakis P, Tunbridge L.** Forsmark site investigation. Borehole KFM02A. Determination of P-wave velocity, transverse borehole core.
- P-04-25 **Brunberg A-K, Carlsson T, Blomqvist P, Brydsten L, Strömgren M.** Forsmark site investigation. Identification of catchments, lake-related drainage parameters and lake habitats.
- P-04-29 **Isaksson H, Thunehed H, Keisu M.** Forsmark site investigation. Interpretation of airborne geophysics and integration with topography.
- P-04-30 **Gren M.** Forsmark site investigation. Bird monitoring in Forsmark 2002–2003.
- P-04-34 **Sundh M, Sohlenius G, Hedenström A.** Forsmark site investigation. Stratigraphical investigation of till in machine cut trenches.

- P-04-39 **Gustafsson J, Gustafsson C.** Forsmark site investigation. RAMAC and BIPS logging in borehole HFM11 and HFM12.
- P-04-40 **Gustafsson J, Gustafsson C.** Forsmark site investigation. RAMAC and BIPS logging in borehole KFM02A.
- P-04-41 **Gustafsson J, Gustafsson C.** Forsmark site investigation. RAMAC and BIPS logging in borehole KFM03A and KFM03B.
- P-04-47 **Berg C, Nilsson A-C.** Forsmark site investigation. Hydrochemical logging of KFM04A.
- P-04-64 **Ludvigson J-E, Jönsson S, Jönsson J.** Forsmark site investigation. Pumping tests and flow logging. Boreholes HFM11 and HFM12.
- P-04-65 **Ludvigson J-E, Jönsson S, Hjerne C.** Forsmark site investigation. Pumping tests and flow logging. Boreholes KFM06A (0–100 m) and HFM16.
- P-04-67 **Gustafsson J, Gustafsson C.** Forsmark site investigation. RAMAC and BIPS logging in borehole KFM04A, KFM04B, HFM09 and HFM10.
- P-04-68 **Gustafsson J, Gustafsson C.** Forsmark site investigation. RAMAC and BIPS logging in borehole HFM13, HFM14 and HFM 15.
- P-04-69 **Gustafsson J, Gustafsson C.** Forsmark site investigation. RAMAC and BIPS logging in borehole KFM06A, HFM16, HFM17, HFM18 and HFM19.
- P-04-70 **Wacker P, Bergelin A, Nilsson A-C.** Forsmark site investigation. Hydrochemical characterisation in KFM02A. Results from three investigated borehole sections; 106.5–126.5, 413.5–433.5 and 509.0–516.1 m.
- P-04-71 **Ludvigson J-E, Jönsson S, Jönsson J.** Forsmark site investigation. Pumping tests and flow logging. Boreholes HFM13, HFM14 and HFM15.
- P-04-72 **Ludvigson J-E, Källgården J, Hjerne C.** Forsmark site investigation. Pumping tests and flow logging. Boreholes HFM17, HFM18 and HFM19.
- P-04-74 **Ludvigson J-E, Källgården J, Jönsson J.** Forsmark site investigation. Pumping tests and flow logging. Boreholes HFM09 and HFM10.
- P-04-76 **Claesson L-Å, Nilsson G.** Forsmark site investigation. Drilling of a flushing water well, HFM10, a groundwater monitoring well in solid bedrock, HFM09, and a groundwater monitoring well in soil, SFM0057, at drilling site DS4.
- P-04-78 **Marek R.** Forsmark site investigation. Ground penetrating radar survey 2003.
- P-04-79 **Gustafsson J, Gustafsson C.** Forsmark site investigation. RAMAC and BIPS logging in borehole KFM01B and RAMAC directional re-logging in borehole KFM01A.
- P-04-80 **Mattsson H, Thunehed H, Keisu M.** Forsmark site investigation. Interpretation of borehole geophysical measurements in KFM01A, KFM01B, HFM01, HFM02 and HFM03.
- P-04-81 **Keisu M, Isaksson H.** Forsmark site investigation. Acquisition of geological information from Forsmarksverket. Information from the Vattenfall archive, Räcksta.
- P-04-83 **Sjöberg J.** Forsmark site investigation. Overcoring rock stress measurements in borehole KFM01B.
- P-04-85 **Claesson L-Å, Nilsson G.** Forsmark site investigation. Drilling of a flushing water well, HFM13, two groundwater monitoring wells in solid bedrock, HFM14–15, and one groundwater monitoring well in soil, SFM0058, at and close to drilling site DS5.
- P-04-86 **Hedenström A.** Forsmark site investigation. Investigation of marine and lacustrine sediments in lakes. Stratigraphical and analytical data.
- P-04-87 **Stephens M B, Lundqvist S, Bergman T, Ekström M.** Forsmark site investigation. Bedrock mapping. Petrographic and geochemical characteristics of rock types based on Stage 1 (2002) and Stage 2 (2003) surface data.
- P-04-90 **Hermanson J, Hansen L, Vestgård J, Leiner P.** Forsmark site investigation. Detailed fracture mapping of excavated rock outcrop at drilling site 5, AFM100201.
- P-04-91 **Bergman T, Andersson J, Hermansson T, Zetterström Evins L, Albrecht L, Stephens M, Petersson J, Nordman C.** Forsmark site investigation. Bedrock mapping. Stage 2 (2003) – bedrock data from outcrops and the basal parts of trenches and shallow boreholes through the Quaternary cover.
- P-04-92 **Nilsson D.** Forsmark site investigation. Sampling and analyses of groundwater from percussion drilled boreholes. Results from the percussion boreholes HFM09 to HFM19 and the percussion drilled part of KFM06A.
- P-04-94 **Claesson L-Å, Nilsson G.** Forsmark site investigation. Drilling of a monitoring well, HFM16, at drilling site DS6.
- P-04-95 **Ludvigson J-E, Levén J, Jönsson S.** Forsmark site investigation. Single-hole injection tests in borehole KFM01A.
- P-04-96 **Ludvigson J-E, Jönsson S, Levén J.** Forsmark site investigation. Hydraulic evaluation of pumping activities prior to hydro-geochemical sampling in borehole KFM03A – Comparison with results from difference flow logging.

- P-04-97 **Nielsen U T, Ringgaard J.** Forsmark site investigation. Geophysical borehole logging in borehole KFM02A, KFM03A and KFM03B.
- P-04-98 **Thunehed H.** Forsmark site investigation. Interpretation of borehole geophysical measurements in KFM02A, KFM03A, KFM03B and HFM04 to HFM08.
- P-04-99 **Bergman B, Palm H, Juhlin C.** Forsmark site investigation. Estimate of bedrock topography using seismic tomography along reflection seismic profiles.
- P-04-100 **Källgård J, Ludvigson J-E, Jönsson J.** Forsmark site investigation. Single-hole injection tests in borehole KFM02A.
- P-04-101 **Nordman C.** Forsmark site investigation. Boremap mapping of percussion holes HFM09–12.
- P-04-103 **Petersson J, Berglund J, Danielsson P, Wängnerud A, Tullborg E-L, Mattsson H, Thunehed H, Isaksson H, Lindroos H.** Forsmark site investigation. Petrography, geochemistry, petrophysics and fracture mineralogy of boreholes KFM01A, KFM02A and KFM03A+B.
- P-04-106 **Claesson L-Å, Nilsson G.** Forsmark site investigation. Drilling of five percussion boreholes, HFM11–12 and HFM17–19, on different lineaments.
- P-04-107 **Mattsson H, Thunehed H, Isaksson H, Kübler L.** Forsmark site investigation. Interpretation of petrophysical data from the cored boreholes KFM01A, KFM02A, KFM03A and KFM03B.
- P-04-108 **Wacker P, Bergelin A, Berg C, Nilsson A-C.** Forsmark site investigation. Hydrochemical characterisation in KFM03A. Results from six investigated borehole sections: 386.0–391.0 m, 448.0–453.0 m, 448.5–455.6 m, 639.0–646.1 m, 939.5–946.6 m, 980.0–1,001.2 m.
- P-04-109 **Wacker P, Bergelin A, Berg C, Nilsson A-C.** Forsmark site investigation. Hydrochemical characterisation in KFM04A. Results from two investigated borehole sections, 230.5–237.6 and 354.0–361.1 metres.
- P-04-110 **Robertsson A-M.** Microfossil analyses of till and sediment samples from Forsmark, northern Uppland.
- P-04-111 **Hedenström A, Sohlenius G, Albrecht J.** Forsmark site investigation. Stratigraphical and analytical data from auger drillings and pits.
- P-04-112 **Nordman C.** Forsmark site investigation. Boremap mapping of percussion boreholes HFM13–15 and HFM19.
- P-04-113 **Nordman C, Samuelsson E.** Forsmark site investigation. Boremap mapping of percussion boreholes HFM16-18.
- P-04-114 **Berglund J, Petersson J, Wängnerud A, Danielsson P.** Forsmark site investigation. Boremap mapping of core drilled borehole KFM01B.
- P-04-115 **Petersson J, Wängnerud A, Berglund J, Danielsson P, Strähle A.** Forsmark site investigation. Boremap mapping of telescopic drilled borehole KFM04A.
- P-04-116 **Carlsten S, Petersson J, Stephens M, Mattsson H, Gustafsson J.** Forsmark site investigation. Geological single-hole interpretation of KFM01A, KFM01B and HFM01–03 (DS1).
- P-04-117 **Carlsten S, Petersson J, Stephens M, Mattsson H, Gustafsson J.** Forsmark site investigation. Geological single-hole interpretation of KFM02A and HFM04–05 (DS2).
- P-04-118 **Carlsten S, Petersson J, Stephens M, Thunehed H, Gustafsson J.** Forsmark site investigation. Geological single-hole interpretation of KFM03B, KFM03A and HFM06–08 (DS3).
- P-04-119 **Carlsten S, Petersson J, Stephens M, Mattsson H, Gustafsson J.** Forsmark site investigation. Geological single-hole interpretation of KFM04A and HFM09–10 (DS4).
- P-04-120 **Carlsten S, Petersson J, Stephens M, Thunehed H, Gustafsson J.** Forsmark site investigation. Geological single-hole interpretation of HFM11-13 and HFM16–18.
- P-04-123 **Lagerbäck R, Sundh M, Johansson H.** Forsmark site investigation. Searching for evidence of late- or post-glacial faulting in the Forsmark region. Results from 2003.
- P-04-124 **Andersson J.** Forsmark site investigation. Investigation of the amount of dead wood.
- P-04-125 **Brydsten L, Strömberg M.** Forsmark site investigation. Water depth soundings in shallow bays in Forsmark.
- P-04-126 **Page L, Hermansson T, Söderlund P, Andersson J, Stephens M B.** Forsmark site investigation. Bedrock mapping U-Pb, ⁴⁰Ar/³⁹Ar and (U-Th)/He geochronology.
- P-04-127 **Fredriksson D.** Forsmark site investigation. Peatland investigation Forsmark.
- P-04-135 **Levén J, Ludvigson J-E.** Forsmark site investigation. Hydraulic interferences during the drilling of borehole KFM01B. Boreholes HFM01, HFM02, HFM03 and KFM01A.
- P-04-136 **Johansson P-O.** Forsmark site investigation. Undisturbed pore water sampling and permeability measurements with BAT filter tips. Soil sampling for pore water analyses.
- P-04-137 **Heneryd N.** Forsmark site investigation. Snow depth, frost in ground and ice cover during the winter 2003/2004.
- P-04-138 **Werner K, Lundholm L, Johansson P-O.** Forsmark site investigation. Drilling and pumping test of wells at Börstilåsen.

- P-04-139 **Werner K, Lundholm L.** Forsmark site investigation. Supplementary drilling and soil sampling, installation of groundwater monitoring wells, a pumping well and surface water level gauges.
- P-04-140 **Werner K.** Forsmark site investigation. Supplementary slug tests in groundwater monitoring wells in soil.
- P-04-142 **Werner K, Lundholm L.** Forsmark site investigation. Pumping test in wells SFM0074.
- P-04-143 **Mattsson H, Keisu M.** Forsmark site investigation. Interpretation of borehole geophysical measurements in KFM04A, KFM06A (0–100 m), HFM10, HFM11, HFM12, HFM13, HFM16, HFM17 and HFM18.
- P-04-144 **Nielsen U T, Ringgaard J.** Forsmark site investigation. Geophysical borehole logging in borehole KFM04A, KFM06A, HFM10, HFM11, HFM12 and HFM13.
- P-04-145 **Nielsen U T, Ringgaard J.** Forsmark site investigation. Geophysical borehole logging in borehole KFM01B, HFM14, HFM15, HFM16, HFM17 and HFM18.
- P-04-146 **Nilsson A-C, Borgiel M.** Forsmark site investigation. Sampling and analyses of surface waters. Results from sampling in the Forsmark area, March 2003 to March 2004.
- P-04-148 **Hedenström A.** Forsmark site investigation. Stratigraphical and analytical data of Quaternary deposits.
- P-04-149 **Sandström B, Savolainen M, Tullborg E-L.** Forsmark site investigation. Fracture mineralogy. Results from fracture minerals and wall rock alteration in boreholes KFM01A, KFM02A, KFM03A and KFM03B.
- P-04-152 **Gustafsson J, Gustafsson C.** Forsmark site investigation. RAMAC and BIPS logging in borehole KFM05A.
- P-04-153 **Nielsen U T, Ringgaard J.** Forsmark site investigation. Geophysical borehole logging in borehole KFM05A and HFM19.
- P-04-154 **Thunehed H, Keisu M.** Forsmark site investigation. Interpretation of borehole geophysical measurements in KFM05A, HFM14, HFM15 and HFM19.
- P-04-155 **Isaksson H, Mattsson H, Thunehed H, Keisu M.** Forsmark site investigation. Petrophysical surface data Stage 2 – 2003 (including 2002).
- P-04-156 **Marek R.** Forsmark site investigation. A co-ordinated interpretation of ground penetrating radar data from the Forsmark site.
- P-04-157 **Thunehed H.** Forsmark site investigation. Inversion of helicopterborne electromagnetic measurements.
- P-04-158 **Juhlin C, Bergman B.** Reflection seismics in the Forsmark area. Updated interpretation of Stage 1 (previous report R-02-43). Updated estimate of bedrock topography (previous report P-04-99).
- P-04-159 **Adi-Zarrabi B.** Forsmark site investigation. Drill hole KFM01A. Thermal properties: heat conductivity and heat capacity determined using the TPS method and mineralogical composition by modal analysis.
- P-04-161 **Adi-Zarrabi B.** Forsmark site investigation. Drill hole KFM02A. Thermal properties: heat conductivity and heat capacity determined using the TPS method and mineralogical composition by modal analysis.
- P-04-162 **Adi-Zarrabi B.** Forsmark site investigation. Drill hole KFM03A. Thermal properties: heat conductivity and heat capacity determined using the TPS method and mineralogical composition by modal analysis.
- P-04-163 **Åkesson U.** Forsmark site investigation. Drill hole KFM01A. Extensometer measurements of the coefficient of thermal expansion of rock.
- P-04-164 **Carlsson L.** Forsmark site investigation. Drill hole KFM02A. Extensometer measurements of the coefficient of thermal expansion of rock.
- P-04-165 **Liedberg L.** Forsmark site investigation. Drill hole KFM03A. Extensometer measurements of the coefficient of thermal expansion of rock.
- P-04-170 **Jacobsson L.** Forsmark site investigation. Drill hole KFM01A. Indirect tensile strength test.
- P-04-171 **Eloranta P.** Forsmark site investigation. Drill hole KFM01A. Indirect tensile strength test (HUT).
- P-04-172 **Jacobsson L.** Forsmark site investigation. Drill hole KFM02A. Indirect tensile strength test.
- P-04-173 **Jacobsson L.** Forsmark site investigation. Drill hole KFM03A. Indirect tensile strength test.
- P-04-174 **Jacobsson L.** Forsmark site investigation. Drill hole KFM04A. Indirect tensile strength test.
- P-04-175 **Chryssanthakis P.** Forsmark site investigation. Drill hole KFM01A. The normal stress and shear tests on joints.
- P-04-176 **Eloranta P.** Forsmark site investigation. Drill hole KFM01A. Uniaxial compression test (HUT).
- P-04-177 **Eloranta P.** Forsmark site investigation. Drill hole KFM01A. Triaxial compression test (HUT).
- P-04-178 **Chryssanthakis P.** Forsmark site investigation. Boreholes KFM03A and KFM03B Tilt testing.
- P-04-179 **Chryssanthakis P, Tunbridge L.** Forsmark site investigation. Borehole KFM04A Tilt testing.
- P-04-180 **Chryssanthakis P, Tunbridge L.** Forsmark site investigation. Borehole KFM03A. Determination of P-wave velocity, transverse borehole core.
- P-04-181 **Chryssanthakis P, Tunbridge L.** Forsmark site investigation. Borehole KFM04A. Determination of P-wave velocity, transverse borehole core.

- P-04-186 **Dinges C.** Forsmark site investigation. Drill hole KFM01A. Thermal properties: heat conductivity and heat capacity determined using the TPS method – compared test.
- P-04-188 **Rouhiainen P, Pöllänen J.** Forsmark site investigation. Difference flow logging in borehole KFM02A.
- P-04-189 **Pöllänen J, Sokolnicki M.** Forsmark site investigation. Difference flow logging in borehole KFM03A.
- P-04-190 **Rouhiainen P, Pöllänen J.** Forsmark site investigation. Difference flow logging in borehole KFM04A.
- P-04-191 **Pöllänen J, Sokolnicki M, Rouhiainen P.** Forsmark site investigation. Difference flow logging in borehole KFM05A.
- P-04-193 **Rouhiainen P, Pöllänen J, Ludvigson J-E.** Forsmark site investigation. Addendum to Difference flow logging in borehole KFM01A.
- P-04-194 **Källgården J, Ludvigson J-E, Hjerne C.** Forsmark site investigation. Single-hole injection tests in borehole KFM03A.
- P-04-199 **Adl-Zarrabi B.** Forsmark site investigation. Drill hole KFM04A. Thermal properties: heat conductivity and heat capacity determined using the TPS method and mineralogical composition by modal analysis.
- P-04-200 **Jönsson S, Ludvigson J-E, Svensson T.** Forsmark site investigation. Hydraulic interference tests. Boreholes HFM11 and HFM12.
- P-04-222 **Claesson L-Å, Nilsson G.** Forsmark site investigation. Drilling of the telescopic borehole KFM05A at drilling site DS5.
- P-04-223 **Jacobsson L.** Forsmark site investigation. Borehole KFM01A. Uniaxial compression test of intact rock.
- P-04-224 **Jacobsson L.** Forsmark site investigation. Borehole KFM02A. Uniaxial compression test of intact rock.
- P-04-225 **Jacobsson L.** Forsmark site investigation. Borehole KFM03A. Uniaxial compression test of intact rock.
- P-04-226 **Jacobsson L.** Forsmark site investigation. Borehole KFM04A. Uniaxial compression test of intact rock.
- P-04-227 **Jacobsson L.** Forsmark site investigation. Borehole KFM01A. Triaxial compression test of intact rock.
- P-04-228 **Jacobsson L.** Forsmark site investigation. Borehole KFM02A. Triaxial compression test of intact rock.
- P-04-229 **Jacobsson L.** Forsmark site investigation. Borehole KFM03A. Triaxial compression test of intact rock.
- P-04-230 **Jacobsson L.** Forsmark site investigation. Borehole KFM04A. Triaxial compression test of intact rock.
- P-04-241 **Korhonen K, Paananen M, Paulamäki S.** Interpretation of lineaments from airborne geophysical and topographic data. An alternative model within version 1.2 of the Forsmark modelling project
- P-04-282 **Isaksson H, Keisu M.** Forsmark site investigation. Interpretation of airborne geophysics and integration with topography. Stage 2 (2002–2004).
- P-04-295 **Petersson J, Berglund J, Wängnerud A, Danielsson P, Strähle A.** Forsmark site investigation. Boremap mapping of telescopic drilled borehole KFM05A.
- P-04-296 **Carlsten S, Petersson J, Stephens M, Thunehed H, Gustafsson J.** Forsmark site investigation. Geological single-hole interpretation of KFM05A, HFM14–15 and HFM19 (DS5).
- P-04-302 **Claesson L-Å, Nilsson G.** Forsmark site investigation. Drilling of borehole KFM01B at drilling site DS1.
- P-04-311 **Klee G, Rummel F.** Forsmark site investigation. Rock stress measurements with hydraulic fracturing and hydraulic testing of pre-existing fractures in borehole KFM01A, KFM01B, KFM02A and KFM04A. Results from in-situ tests.
- P-04-312 **Rummel F, Weber U.** Forsmark site investigation. Rock stress measurements with hydraulic fracturing and hydraulic testing of pre-existing fractures in borehole KFM01A, KFM01B, KFM02A and KFM04A. Laboratory Core Investigations.
- P-04-313 **Nyberg G, Wass E, Askling P, Johansson P-O.** Forsmark site investigation. Hydro monitoring programme. Report for June 2002 – July 2004.
- P-05-08 **Ljunggren B.** Forsmark site investigation. Drill hole KFM01A. Normal loading and shear tests on joints.
- P-05-09 **Ljunggren B.** Forsmark site investigation. Drill hole KFM02A. Normal loading and shear tests on joints.
- P-05-10 **Ljunggren B.** Forsmark site investigation. Drill hole KFM03A. Normal loading and shear tests on joints.
- P-05-11 **Ljunggren B.** Forsmark site investigation. Drill hole KFM04A. Normal loading and shear tests on joints.
- P-05-21 **Ludvigson J-E, Levén J.** Forsmark site investigation. Comparison of measured EC in selected fractures in boreholes KFM02A, KFM03A and KFM04A from difference flow logging and hydro-geochemical characterization – Analysis of observed discrepancies in KFM03A.
- P-05-26 **Thunehed H.** Forsmark site investigation. Resistivity measurements on samples from KFM01A and KFM02A.
- P-05-29 **Löfgren M, Neretnieks I.** Forsmark site investigation. Formation factor logging in-situ and in the laboratory by electrical methods in KFM01A and KFM02A. Measurements and evaluation of methodology.
- P-05-66 **Lindfors U, Perman F, Sjöberg J.** Forsmark site investigation. Evaluation of the overcoring results from borehole KFM01B.
- P-05-112 **Lanaro F.** Forsmark site investigation. Rock mechanics characterisation of borehole KFM01A.

- P-05-113 **Lanaro F.** Forsmark site investigation. Rock mechanics characterisation of borehole KFM02A.
- P-05-114 **Lanaro F.** Forsmark site investigation. Rock mechanics characterisation of borehole KFM03A.
- P-05-115 **Lanaro F.** Forsmark site investigation. Rock mechanics characterisation of borehole KFM04A.
- R-98-05 **Axelsson C-L, Hansen L M.** Update of structural models at SFR nuclear waste repository, Forsmark, Sweden
- R-99-08 **Stigsson M, Follin S, Andersson J.** On the simulation of variable density flow at SFR, Sweden.
- R-99-69 **Kautsky H, Plantman P, Borgiel M.** Quantitative distribution of aquatic plant and animal communities in the Forsmark area.
- R-99-70 **Lindell S, Ambjörn C, Juhlin B, Larsson-McCann S, Lindquist K.** Available climatological and oceanographical data for site investigation programme.
- R-01-02 **Holmén J G, Stigsson M.** Modelling of future hydrogeological conditions at SFR.
- R-01-12 **Bergström E.** Late Holocene distribution of lake sediment and peat in NE Uppland.
- R-02-06 **Boresjö Bronge L, Wester K.** Vegetation mapping with satellite data of the Forsmark and Tierp regions.
- R-02-08 **Berggren J, Kyläkorpi L.** Ekosystemen i Forsmarksområdet. Sammanställning av befintlig information.
- R-02-17 **Ludvigson J-E.** Brunnsinventering i Forsmark.
- R-02-14 **Axelsson C-L, Ekstav A, Lindblad Påsse A.** SFR – Utvärdering av hydrogeologi.
- R-02-32 **SKB.** Forsmark – site descriptive model version 0.
- R-02-41 **Blomqvist P, Nilsson E, Brunberg A-K.** Habitat distribution, water chemistry, and biomass and production of pelagic and benthic microbiota in Lake Eckarfjärden, Forsmark.
- R-02-43 **Juhlin C, Bergman B, Palm H.** Reflection seismic studies in the Forsmark area – stage 1.
- R-03-27 **Andersson E, Tudorancea M-M, Tudorancea C, Brunberg A-K, Blomqvist P.** Water chemistry, biomass and production of biota in Lake Eckarfjärden during 2002.
- R-04-08 **Lundin L, Lode E, Stendahl J, Melkerud P A, Björkvald L, Thorstensson A.** Soils and site types in the Forsmark area.
- R-04-10 **Miliander S, Punakivi M, Kyläkorpi L, Rydgren B.** Human population and activities in Forsmark. Site description.
- R-04-15 **SKB.** Preliminary site description Forsmark area – version 1.1
- R-04-77 **Forsman I, Zetterlund M, Rhén I.** Correlation of Posiva Flow Log anomalies to core mapped features in Forsmark (KFM01A to KFM05A).
- R-04-39 **Sohlenius G, Hedenström A, Rudmark L.** Forsmark site investigation. Mapping of unconsolidated Quaternary deposits 2002–2003. Map description.
- R-04-70 **Brydsten L.** Digital elevation models for site investigation program in Forsmark.
- TR-91-24 **Andersson J-E, Nordqvist R, Nyberg G, Smellie J, Tirén S.** Hydrogeological conditions in the Finnsjön area. Compilation of data and conceptual model.
- TR-92-07 **Geir J E, Axelsson C-E, Hässler L, Benabderrahmane A.** Discrete fracture modelling of the Finnsjön rock mass: Phase 2.
- TR-92-33 **Ahlbom K, Andersson J-E, Andersson P, Ittner T, Ljunggren C, Tirén S.** Finnsjön study site. Scope of activities and main results.
- TR-96-24 **Påsse T.** A mathematical model of the shore level displacement in Fennoscandia.
- TR-97-28 **Påsse T.** A mathematical model of past, present and future shore level displacement in Fennoscandia.
- TR-99-11 **Engqvist A, Andrejev O.** Water exchange of Öregrundsgrepen. A baroclinic 3D-model study.
- TR-99-16 **Brydsten L.** Shore line displacement in Öregrundsgrepen.
- TR-99-18 **Gylling B, Walker D, Hartley L.** Site-scale groundwater flow modelling of Beberg.
- TR-99-38 **Westman P, Wastegård S, Schoning K, Gustafsson B, Omstedt A.** Salinity change in the Baltic Sea during the last 8,500 years: evidence, causes and models.
- TR-00-02 **Brunberg A-K, Blomqvist P.** Post-glacial, land rise-induced formation and development of lakes in the Forsmark area, central Sweden.
- TR-02-02 **Larsson-McCann S, Karlsson A, Nord M, Sjögren J, Johansson L, Ivarsson M, Kindell S.** Meteorological, hydrological and oceanographical information and data for the site investigation program in the communities of Östhammar and Tierp in the northern part of Uppland.
- TR-03-17 **Hedenström A, Risberg J.** Shore displacement in northern Uppland during the last 6,500 calendar years.
- TR-04-12 **Gustafsson B G.** Millennial changes of the Baltic Sea salinity. Studies of the sensitivity of the salinity to climate change.

2.8 Model volumes

In agreement with the general execution programme /SKB, 2001a/, the site descriptive modelling is performed using two different scales of model volume, the *regional* and the *local* model volumes. Generally, the local model is required to cover the volume within which the repository is expected to be placed, including accesses and the immediate environs. In addition to the description on the local scale, a description is also devised for a much larger volume, the regional model, in order to place the local model in a larger context and to allow for a sensitivity analysis of, mainly, hydrogeological boundary conditions. This section presents and justifies the model volumes selected.

2.8.1 General

By necessity, the site characterisation efforts need to focus on the volumes of primary interest for the repository location. Requested information densities are higher in these volumes than outside. The local volume description should be detailed enough for the needs of the design and safety assessment groups. It is primarily these users of the descriptions who can judge whether the local volume is sufficiently large. However, the site modelling needs to ensure a sufficient understanding of the evolution of the natural system. This means that the size and level of resolution needed, especially in the regional volume, should be dictated by what is required in order to capture the most relevant physical phenomena for this evolution.

In selecting the model volumes for version 1.1 the following rules of thumb, taken from the SKB strategy document for integrated evaluation /Andersson, 2003/ were applied:

- The local site descriptive model should cover an area of about 5–10 km², i.e. large enough to include the potential repository and its immediate surroundings. This also means that the location of this model area needs to be agreed upon by both the design and site modelling groups.
- The regional descriptive model should be large enough to allow for a sensitivity analysis of boundary conditions and to provide site understanding to the local model.
- If possible, model domains selected in previous versions should be retained. Deviations should be well motivated and their basis fully documented.
- The models should include the main sources of new information (e.g. deep boreholes and areas of extensive surface geophysics).
- The local domain should be large enough to allow meaningful hydrogeological flow simulations within the domain, though information for boundary conditions or an encompassing regional scale hydrogeological model will often need to be taken from the regional domain – or beyond.
- Potentially important features, such as lineaments, rock type boundaries etc, should be considered when selecting the size of the model volumes.

These rules also apply for version 1.2. It needs also to be understood that the distinct model sizes primarily concern the development of the geological model in the SKB Rock Visualisation System, RVS. This is also the reason why the model areas and volumes have a rectangular shape. The following additional considerations and alternative domain sizes should be noted:

- Model boundaries for numerical simulations, e.g. in the hydrogeological model, are selected for the purposes of these simulations and do not need to be restricted to the size of the RVS-representation.
- In modelling the hydrogeological and hydrogeochemical evolution of the area, the numerical model assesses the importance of the location of boundaries and the importance of different conditions at these boundaries, see Chapter 8. These studies are, in principle, not restricted by the size of the regional volume for the RVS representation.
- The regional and local model volumes differ with respect to the amount of detailed data and degree of determinism, but not with regard to the scale of resolution of the spatial variability. For example, outside the local model volume, the geological model only has large deterministic deformation zones, whereas small zones are represented by expanding the scope of the

DFN-model in this volume, see Chapter 5. This means that in the regional hydrogeological modelling, see Chapter 8, the resolution is the same in the entire model domain, whereas, of course the uncertainty in the domain outside the local volume is much higher than inside this volume.

2.8.2 Regional model volume

Generally, the geographic scope of the regional model depends on the local premises and is controlled by the need to achieve understanding of the conditions and processes that determine the conditions at the site /SKB, 2001a/. The regional model should encompass a sufficiently large area so that the geoscientific conditions that directly or indirectly can influence the local conditions, or help in understanding the geoscientific processes in the repository area, are included. In practical terms, this may entail a surface area of “a few hundred square kilometres”.

Figure 2-3 shows the Forsmark regional model area selected for version 1.2. It is the same as the regional model area in version 1.1 /SKB, 2004a/. The arguments for selection of this volume remain, with some further clarification.

- It includes the candidate area and it is not prohibitively large as it has a surface area of 165 km² (see Figure 2-3).
- It captures relevant portions of the extensive regional deformation zones, which strike in a north-westerly direction and surround the candidate area (see Figure 2-3). Any expansion of the regional model area to the northwest or southeast would not provide any significant changes in the regional geological picture. It should also be noted that the geological evolution, outlined in Chapter 3, is assessed considering a much larger area than the regional model area. Based on this, as far as geological aspects are concerned, the size of the regional model area is sufficient.
- It adequately covers the variations in rock type in the candidate area and its immediate surroundings.
- It captures the main hydrogeological features of the region, as the boundaries perpendicular to the shoreline are judged to be sufficiently far away from each other so that they do not influence the groundwater flow in the candidate area. The boundary to the southwest lies on the south-western side of a local topographic divide and the boundary to the northeast lies northeast of a major bathymetric break in Öregrundsgrepen. The proper locations of the boundaries in the regional hydrogeological model – as well as the proper boundary conditions are assessed through a series of sensitivity analyses, see Chapter 8.
- A depth of 2,100 m below sea-level is considered to provide a reasonable vertical extent for description and is the maximum depth down to which any meaningful extrapolations of deformation zones could be made. To represent this depth in RVS, the vertical dimension is set to 2,200 m since the upper boundary is set to +100 m above mean sea level.

The coordinates defining the regional model volume are (in metres):

(Easting, Northing): (1625400, 6699300), (1636007, 6709907), (1643785, 6702129), (1633178, 6691522)

Z: +100, -2,100

2.8.3 Local model volume

The horizontal area of the deep repository (at repository depth) is ideally about 2 km² in size. This area includes a fully built repository. The surface facility and the access routes to the deep repository are not included in this area, since their plan requirement depends on whether a straight ramp, a spiral ramp or a shaft will be used. The geometrically ideal case will not be achieved in reality, since the layout of the deep repository will be adapted to conditions in the bedrock (deformation zones, etc). The more deposition subareas the deep repository is made up of and the more irregular

these geometries are, the larger total repository area will be required, since intervening un-utilised “corridors” must also be included in the total “encompassing” area. The local investigation and model area should also be considerably larger than the repository area, above all because it is not otherwise possible to try alternative repository layouts and gradually arrive at the optimal placement and adaptation to rock conditions. The local model should therefore encompass a surface area of 5–10 km²/SKB, 2001a/.

Figure 2-3 shows the Forsmark local model area selected for version 1.2. The vertical extent of the model is set to 1,200 m, 1,100 m below sea-level and 100 m above sea-level. The coordinates for the local scale area are (in metres):

(Easting, Northing): (1627916, 6701816), (1630179, 6704079), (1636755, 6697503), (1634492, 6695240)

Again, the local volume for version 1.2 is the same as that selected for version 1.1. The arguments for selection of this volume remain, with some further clarification.

- It provides the minimum volume, which includes the candidate area, the parts of the ‘tectonic lens’ below the current reactor site as well as potential access ramps from the SFR peninsula. Thus, the volume encompasses any possible location of the deep repository at the Forsmark site, i.e. where a high resolution description may be needed.
- Both to the northeast and southwest, it includes the boundaries to more inhomogeneous and banded bedrock outside the candidate area.
- It includes key rock boundaries within and immediately adjacent to the candidate area which help to define the structural framework within the “tectonic lens”.
- A depth of 1,100 m beneath sea-level permits inclusion of all information from the deep boreholes that will be drilled at the site.
- It is larger than the recommended size, but not prohibitively large as it has a surface area of 31.5 km² (see Figure 2-3). In the next version of the site descriptive model, the size of the local domain could be reduced, since the current size is larger than needed.
- The level of confidence in a high-resolution-scale description outside the candidate area will always be quite small, except for patches like the SFR-volume. A too large local volume may thus provide a misleading picture of the actual confidence or may require unmotivated resources to improve confidence in details that are not really required. This restriction should not be seen as a reason for not looking at the ‘old data’. Relevant old geological data have been looked at and assessed, see, for example, Chapter 5, but one must also keep in mind that these data are of lower “quality” and provide far less information relative to the data generated under the present site investigation work.
- The resource requirements needed to handle a very large local model volume are not prohibitive, but are significant. A larger local model volume would still not be sufficiently large to capture all features required in the regional model (see Section 2.8.2).

Evidently, the limits of the model size selected mean that e.g. hydrogeological model simulations usually cannot treat boundaries of the local model as physical boundaries. If a larger model domain is needed, the regional deformation zones surrounding the candidate area as well as the major topographic features will be included. However, this is not a problem for the simulation models as they can handle nested volumes. As already explained, the resolution in the regional hydrogeological modelling, see Chapter 8, is the same in the entire model domain, whereas, of course the uncertainty in the domain outside the local volume is much higher than inside this volume.

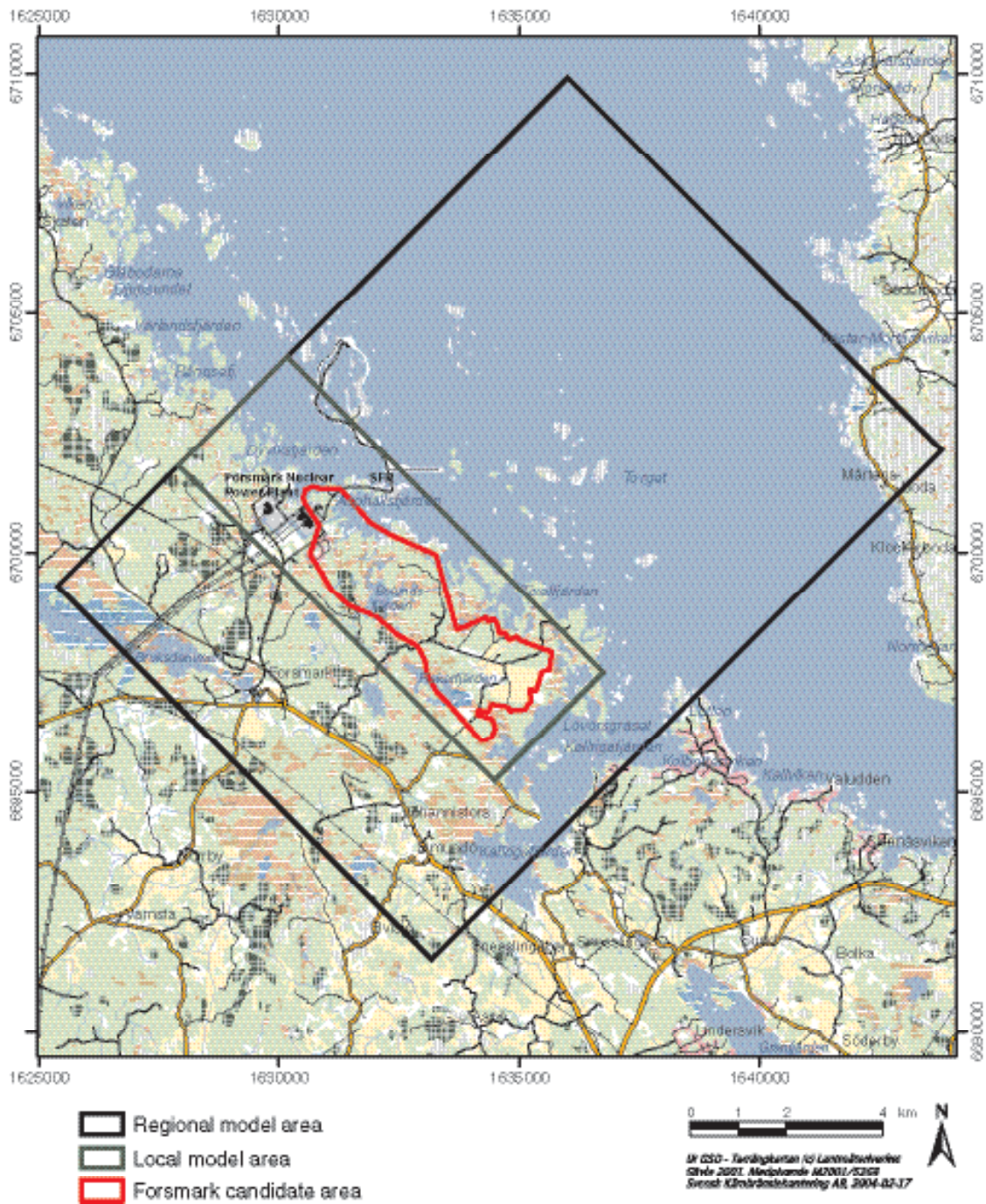


Figure 2-3. Regional and local model areas used in model version 1.2. The regional area is the same as in versions 0 and 1.1. The local volume area (green line) just surrounds the Forsmark candidate area (red line) and is the same as in version 1.1.

3 Evolutionary aspects of the Forsmark site

3.1 Crystalline bedrock from c. 1,910 million years ago to the Quaternary period

3.1.1 Background

The Forsmark regional model area in central Sweden is situated within one of planet Earth's, ancient Precambrian crystalline terrains, referred to as the Fennoscandian Shield. Forsmark lies within the southernmost part of a complex, structural domain with predominantly high-grade metamorphic rocks. This domain extends from the coastal area in the northern part of Uppland to the Hudiksvall-Ånge area to the north and is referred to as structural domain 1 in Figure 3-1. It is characterised by a relatively high concentration of ductile high-strain zones with NW or NNW strike, which anastomose around lenses in which the bedrock is folded and generally displays lower strain. These so-called tectonic lenses are also conspicuous on a smaller scale within the Forsmark regional model area.

Structural domain 1 is situated in the northern part of a broader lithological province, which extends from the Loftahammar-Linköping area in the south to the Hudiksvall-Ånge area in the north. This province consists of metagranitoids with associated metavolcanic and metasedimentary rocks (Figure 3-1). The meta-igneous rocks within this province vary in age from 1,906 to 1,840 million years, rocks younger than 1,870 million years being especially conspicuous north of Gävle. It includes one of Sweden's important ore provinces – Bergslagen and adjacent areas – that is situated between Örebro and Gävle /Frietsch, 1975; Åkerman, 1994/. As with other older Precambrian shields, complex networks of ductile-brittle and brittle deformation zones transect the bedrock in this part of the Fennoscandian Shield.

In order to understand the geological evolutionary aspects of the Forsmark site, it is necessary to view the site in a broader geological context. For this purpose, attention was focused in model version 1.1 /SKB, 2004a/ on the area in the central-eastern part of Sweden that extends from Loftahammar in the south to Ånge in the north, within which the Forsmark regional model area is situated (Figure 3-1). The geological evolution of this segment of the Fennoscandian Shield was described for six key phases related to different time periods. Where the effects of geological events are of more limited character and, in general, less well understood (phases 3–6), information from outside the Loftahammar-Ånge area was taken into account /SKB, 2004a/. A brief summary of the relevance of each phase for the geological evolution of the Forsmark site was also addressed. The sources of information used to establish the geological evolutionary aspects in central-eastern Sweden are listed in /SKB, 2004a/.

Following establishment of version 1.1, a significant improvement in our understanding of the geological evolution of the Forsmark site has occurred with the generation of new geochronological data at the site. The present chapter aims to summarise these new data and place them in the context of the various phases that were established in /SKB, 2004a/. Particular focus is on the tectonic evolution, since this has an important bearing on the establishment of the conceptual model for deformation zones at the site (see Section 5.4.2). The internationally accepted geological time scale that has been used in this report is presented in Figure 3-2 and an overview of phases 1–6, which has been extracted from /SKB, 2004a/, is provided in Table 3-1. The changes in the orientation of the inferred bulk crustal shortening or maximum principal stress directions through geological time are also illustrated in a series of diagrams (Figure 3-3a–e).

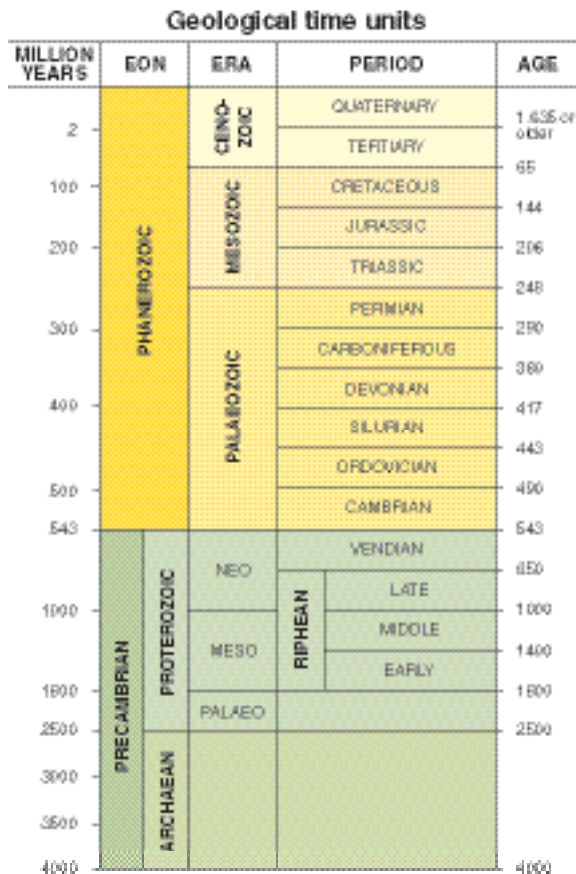


Figure 3-2. Geological time scale used in this report. Modified after /Koistinen et al. 2001/.

Table 3-1. Overview of geological activity in the crystalline bedrock of central-eastern Sweden from 1,910 million years ago to the Quaternary period (modified after /SKB, 2004a/).

Phase	Time period	Geological activity, central-eastern Sweden
1	1,910 to 1,870 (1,860) million years ago	Sedimentation, major igneous activity and crustal deformation/metamorphism, all associated with growth and early-stage reworking of the crust (Svecokarelian orogeny, early stage).
2	1,870 to 1,750 million years ago	Major igneous activity, sedimentation and crustal deformation/metamorphism, associated primarily with reworking of the newly-formed crust (Svecokarelian orogeny, late stage). Slow exhumation of deeper crustal levels and erosion.
3	1,710 to 900 million years ago	Distal effects of : <ul style="list-style-type: none"> • Continued crustal growth and crustal reworking with deformation and metamorphism in south-western Sweden (Gothian and Hallandian orogenies). • Crustal reworking with deformation and metamorphism in south-western Sweden, related to the assembly of the supercontinent Rodinia (Sveconorwegian orogeny). Geological activity in central-eastern Sweden includes: <ul style="list-style-type: none"> • Continued slow exhumation of deeper crustal levels and erosion. • Deformation along discrete deformation zones related to the Gothian orogenic activity to the west. • Igneous activity at high crustal levels.

Phase	Time period	Geological activity, central-eastern Sweden
4	900 to 400 million years ago	<ul style="list-style-type: none"> Local subsidence and formation of sedimentary basins during the Mesoproterozoic. Faulting of Mesoproterozoic rocks in offshore areas, east of Uppland (Timing – phase 3, 4, 5 or 6, or a combination of these possibilities). Deformation along discrete deformation zones related to the Sveconorwegian orogenic activity to the west. Subsidence and formation of a foreland sedimentary basin to the east of the Sveconorwegian orogenic belt, related to the exhumation of deeper crustal levels and erosion within this orogenic belt. <p>Distal effects of:</p> <ul style="list-style-type: none"> The break-up of Rodinia with the formation of the ocean Iapetus and the continent Baltica. The rotation and drift of Baltica northwards over the globe. The destruction of Iapetus and the birth of the continent Laurussia (Caledonian orogeny to the north-west). <p>Geological activity in central-eastern Sweden includes:</p> <ul style="list-style-type: none"> Rifting, erosion and final establishment of the sub-Cambrian peneplain. Marine transgression and deposition of sedimentary cover during the Early Palaeozoic. Subsidence and formation of an Upper Silurian to Devonian, foreland sedimentary basin to the east of the Caledonian orogenic belt, related to the exhumation of deeper crustal levels and erosion within this orogenic belt. Possible disturbance of the sub-Cambrian peneplain. Some faulting of Palaeozoic rocks on land and in offshore areas (Timing – phase 4, 5 or 6, or a combination of these possibilities). Infilling of fractures immediately below the sub-Cambrian peneplain with Cambrian sandstone and various minerals (calcite, fluorite, galena), and the formation of clastic sedimentary dykes (Timing – phase 4, 5 or 6, or a combination of these possibilities).
5	400 to 250 million years ago	<p>Distal effects of:</p> <ul style="list-style-type: none"> Hercynian-Variscan orogeny in central Europe and final assembly of the supercontinent Pangaea. Rifting along the southern margin of the Fennoscandian Shield. <p>Geological activity in central-eastern Sweden includes:</p> <ul style="list-style-type: none"> Possible disturbance of the sub-Cambrian peneplain and fracture infilling (see above).
6	250 million years ago to the start of the Quaternary period	<p>Distal effects of:</p> <ul style="list-style-type: none"> Rifting along the southern and western margins of the Fennoscandian Shield and marine transgression during the Cretaceous (especially the Late Cretaceous). Alpine orogeny in southern Europe. Opening and spreading of the North Atlantic Ocean, and upheaval of the mountain belt in western Scandinavia. <p>Geological activity in central-eastern Sweden includes:</p> <ul style="list-style-type: none"> Some exhumation of deeper crustal levels and erosion. Possible disturbance of the sub-Cambrian peneplain and fracture infilling (see above). Plate motion from 60–0 million years related to opening of the North Atlantic Ocean.

3.1.2 Primary geochronological data

The geochronological analytical programme at the Forsmark site aimed, with the help of different isotopic systems, to reconstruct the temperature-time history for the bedrock at the site. This history extends from the time of crystallisation of the intrusive rocks through to the time when the rocks were uplifted through the c. 70–60°C geotherm. The programme has involved the analysis of different minerals in different isotopic systems with different blocking temperatures. In order of decreasing blocking temperature, these systems are U-Pb zircon with measurements by both the secondary ion and thermal ionisation mass spectrometry techniques, i.e. SIMS and TIMS techniques, respectively, U-Pb titanite (TIMS technique), $^{40}\text{Ar}/^{39}\text{Ar}$ hornblende, $^{40}\text{Ar}/^{39}\text{Ar}$ biotite, and (U-Th)/He apatite.

31 age determinations were completed on 25 samples and the results are presented in /Page et al. 2004/. The analysed samples come from different groups of meta-intrusive rocks at the site, from contrasting ductile structural domains, and from different bedrock blocks between regionally important deformation zones (Forsmark, Eckarfjärden, Singö). All ages cited take into account the errors in the age determinations provided in /Page et al. 2004/.

3.1.3 Timing of crystallisation of the igneous rocks at the Forsmark site

A summary of the age-dating results that bear on the timing of formation of the bedrock at the Forsmark site are summarised in Table 3-2. A more detailed description of the rock types in the various bedrock groups (A to D) is presented in Section 5.2.1.

Bearing in mind the analytical errors, two samples from an older suite of calc-alkaline, meta-intrusive rocks, with tonalitic to granodioritic and gabbroic compositions (Group B), have yielded crystallisation ages in the time range 1,887 to 1,880 million years. The felsic to intermediate metavolcanic rocks (Group A) are older than 1,885 million years. All these rocks formed during phase 1 in the geological evolution (Table 3-1) and the metavolcanic rocks with the associated magnetite mineralisation can be correlated confidently with the Svecofennian metavolcanic rocks in Bergslagen and its surroundings. The metagranite in the candidate area (Group B) has yielded a younger age of $1,865 \pm 3.4$ million years and formed in the transition from phase 1 to phase 2 in the geological evolution (Table 3-1). Amphibolite dykes and irregular minor intrusions in this metagranite are not so well constrained in age. They formed between 1,868 and 1,840 million years ago.

A minor intrusion with granodioritic composition (Group C), which belongs to a younger suite of calc-alkaline rocks, has yielded an age of $1,864 \pm 3.4$ million years. This overlaps with the age of crystallisation of the metagranite in the candidate area. However, the field relationships indicate that the Group C rocks are younger and that they intruded after at least some ductile deformation and metamorphism had affected the rocks in Groups A and B (see Section 5.2.1). A sample from a suite of granite dykes (Group D), which is strongly discordant to the intense tectonic banding in the rocks in the coastal area, has yielded a crystallisation age of $1,851 \pm 5.2$ million years. These results indicate that the younger suite of calc-alkaline rocks in Groups C and D formed between 1,867 and 1,846 million years ago, i.e. during phase 2 of the geological evolution (Table 3-1).

Table 3-2. Age of crystallisation of the igneous rocks at the Forsmark site (after /Page et al. 2004/). Ma = million years. SIMS = Secondary Ion Mass Spectrometry. TIMS = Thermal Ionisation Mass Spectrometry.

Geological feature	Dated rock type	Method	Age
Supracrustal rocks (Group A)	–	–	<i>Comment:</i> Age inferred to be older than 1,885 Ma.
Older calc-alkaline plutons with ultramafic to intermediate, tonalitic and granodioritic compositions (Group B intrusive rocks)	Metagabbro	U-Pb zircon (TIMS)	1,886 ± 0.9 Ma
	Metatonalite to metagranodiorite	U-Pb zircon (SIMS)	1,883 ± 3.4 Ma
Older calc-alkaline plutons with granitic to granodioritic composition (Group B intrusive rocks)	Metagranite inside the candidate area	U-Pb zircon (SIMS)	1,865 ± 3.4 Ma
Mafic dyke-like bodies and irregular minor intrusions in Group B metagranite to metagranodiorite	–	–	<i>Comment:</i> Field relationships indicate similar or younger age relative to the Group B metagranite to metagranodiorite. Age of cooling through the 700–550°C temperature interval is 1,843 ± 3 Ma (see below). Age of intrusion inferred to be 1,868–1,840 Ma.
Younger, calc-alkaline, dyke-like bodies and minor intrusions with granodioritic to tonalitic composition (Group C intrusive rocks)	Metagranodiorite	U-Pb zircon (SIMS)	1,864 ± 3.4 Ma
Younger calc-alkaline dykes and intrusions with granitic composition (Group D intrusive rocks)	Granite	U-Pb zircon (SIMS)	1,851 ± 5.2 Ma <i>Comment:</i> The age is supported by the U-Pb titanite age (see below) from the same rock type.

3.1.4 Timing of ductile deformation at the Forsmark site

Penetrative, ductile deformation occurred in the time interval 1,868 to 1,846 Ma. This range is constrained by the age dating results in the coastal area around Klubbudden. Ductile deformation, which occurred along more discrete, ductile deformation zones and under lower temperature conditions, occurred after 1,856 Ma. This type of deformation has been observed along the Singö and Eckarfjärden deformation zones (see Section 5.2.4). It is also inferred to be present along the other deformation zones that strike WNW or NW (see Section 5.4). Since the bedrock started to cool below 500°C at c. 1,830 million years ago and below 300°C at c. 1,700 million years ago (Table 3-3), it is inferred that the ductile deformation along discrete zones occurred during phase 2 in the regional geological evolution, i.e. during the later part of the Svecokarelian orogeny.

Table 3-3. Timing of ductile deformation as well as cooling and exhumation ages at the Forsmark site (after /Page et al. 2004/). Ma = million years. TIMS = Thermal Ionisation Mass Spectrometry.

Geological feature	Dated rock type	Method	Age
Penetrative ductile deformation under amphibolite-facies metamorphic conditions	–	–	<i>Comment:</i> Field relationships indicate that penetrative deformation in the coastal area (Klubudden) affected the Group B rocks and was complete prior to intrusion of the Group D dykes, <i>i.e. is constrained to the time interval 1,868–1,846 Ma.</i> The intense tectonic banding in this area affected the Group B rocks and was established prior to intrusion of the Group C rocks, <i>i.e. developed around 1,865 Ma.</i>
Discrete ductile deformation under lower amphibolite- or greenschist-facies metamorphic conditions	–	–	<i>Comment:</i> Field relationships indicate that this type of deformation affects the Group D rocks, <i>i.e. developed after 1,856 Ma.</i>
Cooling below 700–550°C	Group B amphibolite Group D granite	U-Pb titanite (TIMS)	1,843 ± 3 Ma
		U-Pb titanite (TIMS)	1,844 ± 4 Ma
Cooling below c. 500°C	Group B amphibolite (eight samples) and metagabbro (one sample)	⁴⁰ Ar/ ³⁹ Ar hornblende	1,834–1,793 Ma <i>Comment:</i> Variation in age in different structural domains.
Cooling below c. 300°C	Various Group B and Group C felsic meta-intrusive rocks (eight samples)	⁴⁰ Ar/ ³⁹ Ar biotite	1,704–1,635 Ma <i>Comment:</i> Variation in age at the surface in different bedrock blocks and a younger age with depth in KFM01A. Age difference between the samples in KFM01A suggests an uplift rate of c. 25 m/Ma.
Cooling below c. 70–60°C	Group B metagranite to metagranodiorite, predominantly from KFM01A (seven samples)	(U-Th)/He apatite	c. 630–250 Ma <i>Comment:</i> (U-Th)/He ages are younger with depth in KFM01A, with a possible exhumation event between c. 300 and 250 Ma. Borehole data indicate an uplift rate of c. 4 m/Ma. Variation also at the surface in different bedrock blocks.

During both phase 1 and phase 2, the geodynamic regime in the central-eastern part of Sweden involved transpressive strain. This deformation was related to an oblique collision against the older continental margin to the north-east, with a N to NNW bulk crustal shortening direction (Figure 3-3a, see also /SKB, 2004a/). The transpressive strain was absorbed by dextral displacement along ductile high-strain zones with WNW or NW strike, combined with more local-scale shortening in a NE direction across the zones /Stephens and Wahlgren, 1996; Högdahl, 2000; Beunk and Page, 2001/, *i.e.* by partitioning of the strain. Weaker mineral fabric development and major folding in the crustal segments between the ductile high-strain zones are also an expression of this strain.

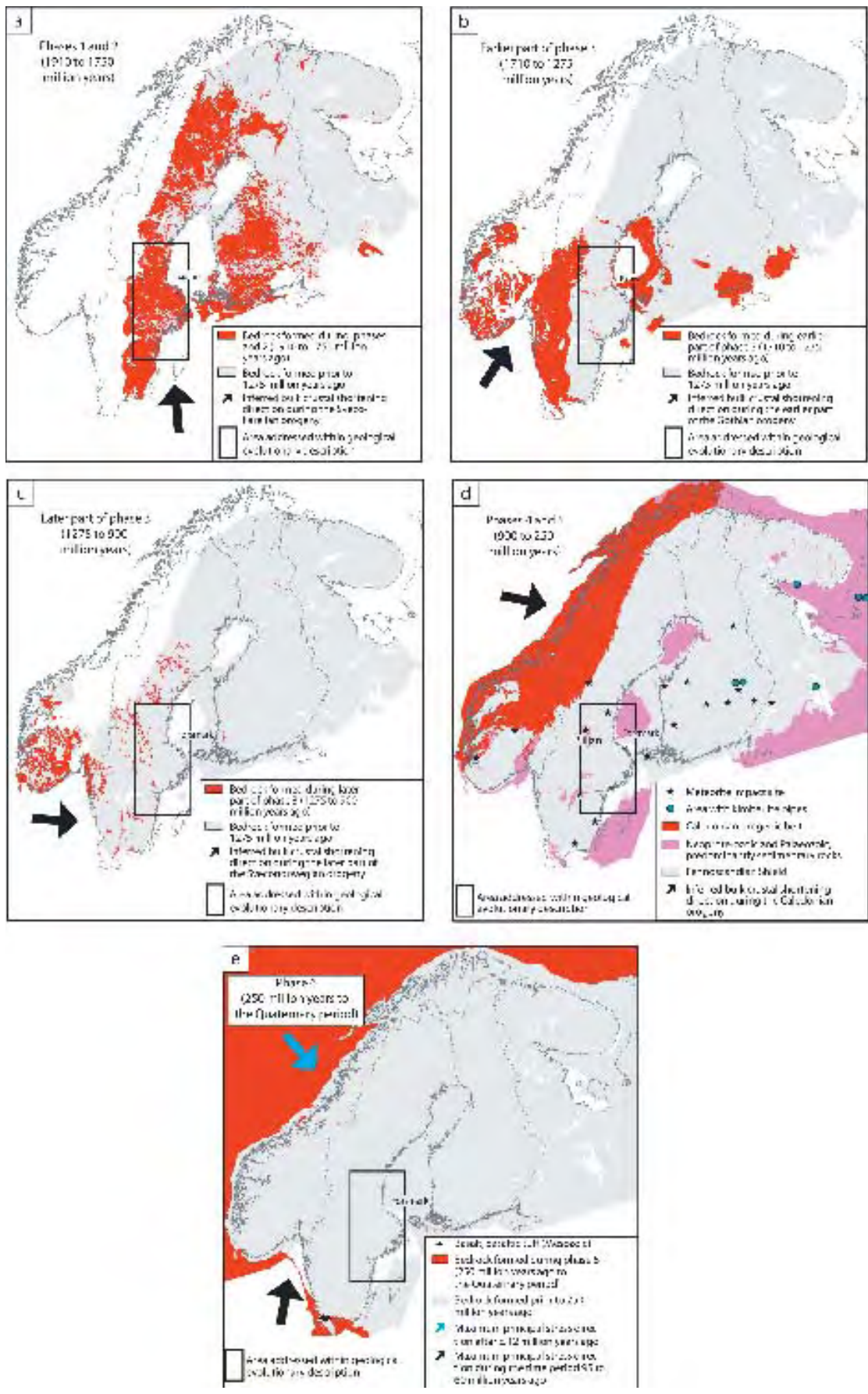


Figure 3-3. Formation of rock units and variation in the inferred directions of bulk crustal shortening (phases 1 to 5) and maximum principal stress (phase 6) through geological time in the Fennoscandian Shield. The sources of these inferred directions are presented in the text (Sections 3.1.4 and 3.1.5).

3.1.5 Timing of brittle deformation and Phanerozoic fluid movement at the Forsmark site

Proterozoic faulting

The $^{40}\text{Ar}/^{39}\text{Ar}$ biotite ages (Table 3-3) indicate that the advent of sub-greenschist facies metamorphic conditions, with the growth of prehnite and a predominantly brittle response to regional deformation, initiated prior to c. 1,700 million years ago, i.e. probably during the waning stages of phase 2. However, different $^{40}\text{Ar}/^{39}\text{Ar}$ biotite ages are present in different bedrock blocks at the surface, between the regionally important Forsmark, Eckarfjärden and Singö deformation zones /Page et al. 2004/. Thus, these ages also show that reactivation occurred after c. 1,675 million years ago, i.e. after phase 2 in the geological evolution of the region.

Structural analyses of low-temperature, ductile high-strain zones, which were active during the earlier part of the Gothian (1,700–1,560 million years ago) and during the later part of the Sveconorwegian (1,100–920 million years ago) orogenies, have been completed north of Mora /Bergman and Sjöström, 1994/ and close to Vänern /Wahlgren et al. 1994; Stephens et al. 1996/, respectively. In particular, west of Örebro, in the frontal part of the Sveconorwegian orogen, ductile-brittle high-strain zones with NE strike show dextral transpressive deformation /Wahlgren et al. 1994/. These data provide some constraints on the direction of bulk crustal shortening during the earlier and later stages of phase 3 in the geological evolution /SKB, 2004a/. No data are available that provide constraints on the geodynamic evolution during the Hallandian orogeny (1,460–1,420 million years ago).

Bulk crustal shortening to the NE and to the ESE have been inferred for the early Gothian and late Sveconorwegian tectonic events, respectively (Figure 3-3b and Figure 3-3c). Furthermore, a radical change in the bulk crustal shortening direction occurred between phases 2 and 3 (cf. Figure 3-3a). Eastwards in the Fennoscandian Shield, including the Forsmark site, the crust would have responded to the important Gothian, Hallandian and Sveconorwegian tectonic events (Table 3-1) in a predominantly brittle manner. A lower intercept, U-Pb (titanite) age of 909 ± 200 million years provides some indication that loss of lead in connection with the Sveconorwegian tectonic activity has indeed affected the Forsmark site /Page et al. 2004/.

The dating of minerals along fractures can also provide constraints on the timing of brittle deformation. So far no geochronological data of this type are available at the Forsmark site. However, in the northern part of Uppland, where Forsmark is situated, U-Pb dating of pitchblende in quartz-, calcite- and chlorite-filled fractures /Welin, 1964/ and Rb-Sr dating of epidote-filled fractures /Wickman et al. 1983/ have yielded mineral ages in the time interval 1,590 to 1,450 million years. Furthermore, Rb-Sr dating of prehnite- and calcite-filled fractures in the same region has yielded younger ages in the time interval 1,250 to 1,100 million years. It is necessary to understand the blocking temperatures for the different minerals within the selected isotope system, before a direct coupling can be made between a mineral age and the actual timing of movement along a brittle deformation zone. Nevertheless, these data suggest that brittle deformation occurred during or prior to these time intervals, i.e. during the Proterozoic.

Faulting and fluid movement after the establishment of the sub-Cambrian peneplain

(U-Th)/He apatite ages (Table 3-3) decrease in age with depth in the cored borehole KFM01A /Page et al. 2004/. A maximum age of c. 630 million years is present at the surface and an age of c. 250 million years occurs at a depth of 1,000 m. However, a marked change in slope on the age-depth diagram at c. 600 m depth is apparent /Page et al. 2004/. This change in slope indicates a possible exhumation event between c. 300 and 250 million years ago, i.e. during the later part of the Carboniferous or the Permian during phase 5 of the geological evolution (Table 3-1). Rifting and igneous activity prevailed in the southern part of Scandinavia during this time period (Table 3-1). Movements along brittle deformation zones at this time would have disturbed the sub-Cambrian peneplain. Such disturbances have been documented at several places in northern Uppland /Lidmar-Bergström, 1994/, in particular along the Forsmark deformation zone /Bergman et al. 1999; SKB, 2002a/.

In the late Cretaceous through to the early part of the Tertiary (95 to 60 million years ago), the maximum principal stress direction was oriented close to NNE (Figure 3-3e and /Muir Wood, 1995/). From 60 million years and onwards, the North Atlantic Ocean started to open and to spread (Table 3-1). During this time, plate movements associated with spreading of the North Atlantic Ocean appear to have dominated the geodynamics of northern Europe. Furthermore, upheaval of the western coastal area of Scandinavia occurred. After c. 12 million years ago, a maximum principal stress in a SE direction has prevailed in this region (Figure 3-3e and /Muir Wood, 1995/).

The occurrence of asphaltite along near-surface (< 100 m) fractures in the cored boreholes KFM01B and KFM05A (see Section 5.2.7) is reminiscent of the occurrence of clastic sedimentary dykes immediately beneath the sub-Cambrian peneplain in south-eastern Sweden. In the latter case, the source of material is the Cambrian sandstone, in the former possibly the Upper Cambrian oil-bearing shales. It is suggested that fluids have moved downwards through the pile of Lower Palaeozoic sedimentary cover rocks, which once covered the crystalline bedrock, into either newly formed or reactivated older fractures in the bedrock. Movement of fluids took place after the Cambrian period and prior to or in connection with removal of this sedimentary cover. At Forsmark, fluids that contained glacial sediment also migrated downwards and filled fractures that either formed or were reactivated during the later part of the Quaternary period (/Carlsson, 1979/, see also Section 5.2.4).

Different mechanisms for such fluid movement and sediment infill are discussed in /Carlsson, 1979; Röshoff and Cosgrove, 2002/. The interplay between sediment loading or unloading and the effects of these processes on the local stress field, in the uppermost part of the bedrock, is of importance. The effects of stress release due to unloading and the development or reactivation of new or old fractures, respectively, is also discussed in Section 5.4.2.

3.2 Late-or post-glacial faulting during the Quaternary period

Far away from any plate boundaries, the current seismicity of Sweden is very low. Present-day tectonics is dominated by regional uplift due to isostatic rebound after depression of the crust during the latest glaciation. Earthquakes are few and seldom exceed magnitude 4–5 on the Richter scale. This is particularly true for the Forsmark region, since most of the seismic activity in Sweden is concentrated in a zone that extends from south-western Sweden via the coastal areas of Norrland to inland Norrbotten (Figure 3-4).

The present-day situation contrasts markedly with the conditions that prevailed some 10,000 years ago, when at least northern Sweden and the adjacent parts of Finland and Norway were affected by major faulting in connection with the disappearance of the inland ice-sheet. A significant number of late- or post-glacial, reverse fault scarps have been identified in northern Fennoscandia /e.g. Lagerbäck, 1990; Kuivamäki et al. 1998; Olesen et al. 2004/ and accompanying earthquakes have been estimated to reach magnitudes of c. 6–8.2 /e.g. Muir Wood, 1993; Arvidsson, 1996/. Abundant liquefaction structures in the fault region, which developed in sandy sediments, fit well with the pattern of coseismic faulting. Faults of these dimensions are completely abnormal for intraplate regions and can probably best be explained by release of tectonic strain that accumulated during glaciation /e.g. Johnston and Muir Wood in Stanfors and Ericsson, 1993/.

Since vertical displacements on the late- or post-glacial faults in northern Fennoscandia generally exceed 5 m and the fault scarps stand out as anomalous features in the generally, glacially smoothed relief, they are relatively easily detected by means of the interpretation of aerial photographs. A brief investigation by means of aerial photograph interpretation was not able to identify similar features in the Forsmark region or elsewhere in central Sweden /Lagerbäck, 1979/. However, possible evidence for seismically induced liquefaction phenomena has been reported from the southern parts of Sweden /e.g. Mörner, 2003/. Nevertheless, as yet, conclusive evidence for corresponding fault movements is lacking.

Earthquakes 1375 through 2003

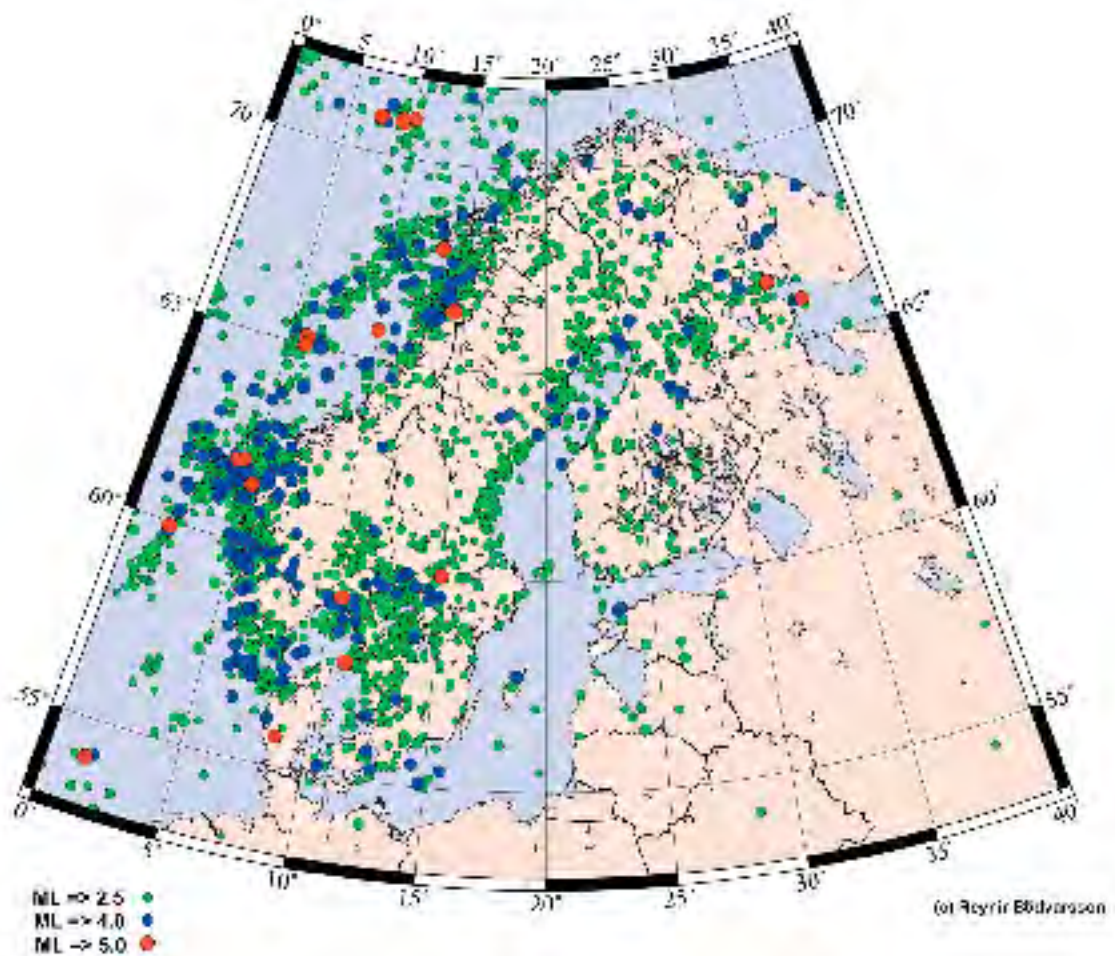


Figure 3-4. Map of recent seismicity in northern Europe during historical time, up to and including 2003.

A targeted investigation programme, which aimed to trace possible, major late- or post-glacial fault movements at the Forsmark site or in its vicinity, was initiated in 2002 /Lagerbäck and Sundh, 2003; Lagerbäck et al. 2004/. “Major faulting” in this context was defined as dislocations in the order of several metres along faults of several kilometres length. Faults of these dimensions may, if conditions are favourable, be detected by means of the interpretation of aerial photographs. Furthermore, they would have generated high magnitude earthquakes, which may produce characteristic distortions in waterlogged sandy or silty sediments. An interpretation of aerial photographs was carried out in a relatively large area (Figure 3-5) in north-eastern Uppland, with the purpose to look for morphologically conspicuous lineaments that are late- or post-glacial fault candidates. A number of fairly prominent escarpments and crevasses were noted but, when later field-checked, they turned out to be more or less strongly, glacially abraded, i.e. they are not late- or post-glacial in age.

In order to search for seismically induced distortions, all gravel and sand quarries in operation within the investigation area (Figure 3-5) were visited and seventeen machine cut trenches along the Börstil esker to the south-east of Forsmark were examined. Strongly contorted and folded sequences of glacial clay were encountered at several localities (Figure 3-6), but the disturbances were interpreted to be caused by sliding. A seismic origin for the sliding was not excluded but no conclusive evidence for this was found. As no major distortions that could be associated with seismically induced liquefaction were identified (Figure 3-7), it was concluded that no major (magnitude > 7 on the Richter scale) earthquakes had occurred in the Forsmark area after the disappearance of the last inland ice sheet.

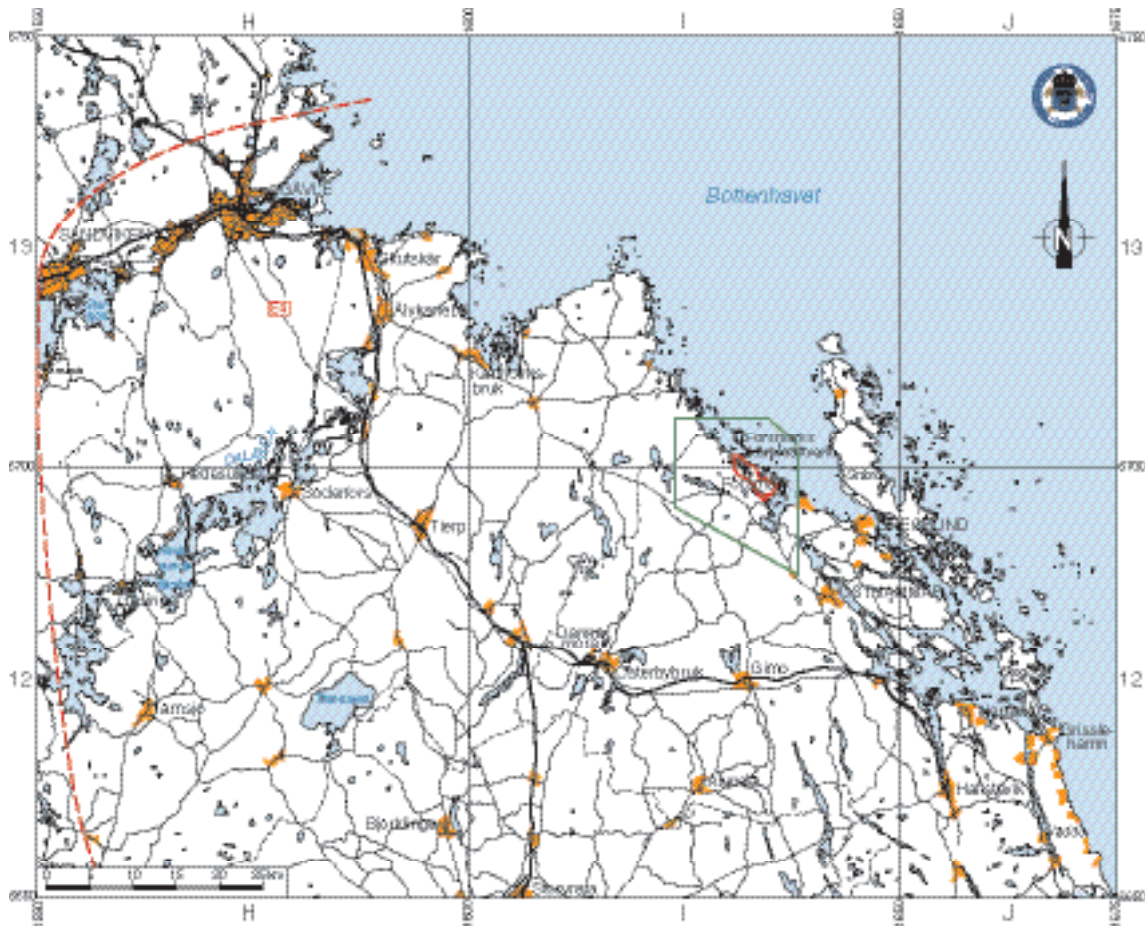


Figure 3-5. Map of the area investigated for the detection of late- or post-glacial faults in north-eastern Uppland.



Figure 3-6. Chaotically mixed slide deposits of fine sand, silt and glacial clay along the Börstil esker to the south-east of Forsmark.



Figure 3-7. This section is typical of the stratigraphy along the Börstil esker. The trench section shows a bed of fine sand and coarse silt covered by a bed of clay-laminated silt. Extended excavation revealed loosely packed and saturated glaciofluvial sand to a depth of at least 5 m. Although the stratigraphy is considered to be highly susceptible to liquefaction, no disturbances related to seismically induced liquefaction were discovered here or elsewhere along the Börstil esker.

3.3 Quaternary deposits and other regoliths

3.3.1 Quaternary development of Sweden

The Quaternary is the present geological period and it is characterised by alternating cold glacial and warm interglacial stages. The glacial stages are further subdivided into cold phases, stadials, and relatively warm phases, interstadials (Figure 3-8). A combination of climatic oscillations of high amplitude, together with the intensity of the colder periods, is characteristic of the Quaternary period. At the Geological Congress in London, 1948 the age of the Tertiary/Quaternary transition, as used here, was determined to be 1.65 million years. More recent research, however, suggests that the Quaternary period started c. 2.4 million years ago /e.g. Šibrava, 1992; Shackelton, 1997/. The Quaternary period is subdivided into two epochs: the Pleistocene and the Holocene. The latter represents the present interglacial, which began c. 11,500 years ago (Figure 3-8).

Results from studies of deep-sea sediment cores suggest as many as fifty glacial/interglacial cycles during the Quaternary /Shackelton et al. 1990/. The climate during the past c. 900,000 years has been characterised by 100,000 years long glacial periods interrupted by interglacials lasting for approximately 10,000–15,000 years. The coldest climate, and largest ice sheets, occurred toward the end of each of the glacial periods. Most research indicates that the long-term climate changes (> 10,000 years) are triggered by variations in the earth's orbital parameters. However, there is not a universal agreement on this point. Quaternary climatic conditions, with focus on Sweden, have been reviewed by e.g. /Morén and Pässe, 2001/.

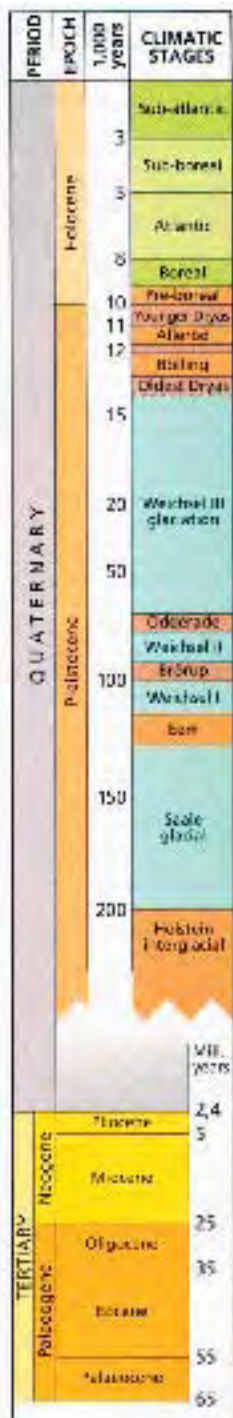


Figure 3-8. The geological timescale showing the subdivision of the late Quaternary period with climatic stages. The ages are approximate and given in calendar years before present (from: Sveriges Nationalatlas, /Fredén, 2002/).

The most complete stratigraphies used in Quaternary studies are from the well-dated sediment cores retrieved from the deep sea, which have been used for studies of e.g. oxygen isotopes /e.g. Shackleton et al. 1990/. The marine record has been subdivided into different Marine Isotope Stages (MIS), which are defined based on changes in the global climatic record. Quaternary stratigraphies covering the time before the Last Glacial Maximum (LGM) are sparse in areas that have been repeatedly glaciated, such as Sweden. Furthermore, these stratigraphies are often disturbed by erosion and are difficult to date absolutely. Our knowledge of the pre-LGM Quaternary history of Sweden is therefore to a large extent based on indirect evidence from non-glaciated areas.

In most parts of Sweden, the relief of the bedrock is mainly of Pre-Quaternary age and has only been slightly modified by glacial erosion /Lidmar-Bergström et al. 1997/. The magnitude of the glacial erosion seems, however, to vary considerably geographically. Pre-Quaternary deep weathered bedrock occurs in areas such as the inland of eastern Småland, southern Östergötland and the inner parts of northernmost Sweden /Lundqvist, 1985; Lidmar-Bergström et al. 1997/. The occurrence of saprolites indicates that these areas have been affected only to a minor extent by glacial erosion.

In some areas, such as in large parts of inner northern Sweden, deposits from older glaciations have been preserved, which indicates that the subsequent glaciations have had a low erosional capacity /e.g. Hättestrand and Stroeven, 2002; Lagerbäck and Robertsson, 1988/. Such deposits occur also in areas, e.g. Skåne, which have been glaciated over a relatively short period of time (see also Section 3.3.2).

3.3.2 The Pleistocene

The global oxygen isotope record indicates numerous glaciations during the Quaternary Period. Several of these glaciations have probably affected Sweden. It is, however, at present impossible to state the total number of Quaternary glaciations in Sweden.

In Sweden, the preserved geological information from Pleistocene is, as mentioned above, fragmentary. Pleistocene deposits have mainly been found in areas which have been subjected to glaciations during a short period of time, e.g. Skåne, or where the glacial erosion has been low due to cold-based ice conditions. It has been suggested that these latter conditions occurred in the inner parts of northern Sweden during the middle and late parts of the latest glaciation, the Weichselian. Most Pleistocene deposits have been correlated with the stadials and interstadials, of the latest glaciation. There are, however, a few sites with older Pleistocene deposits. Inorganic deposits such as glacial till have not been dated with absolute methods and such deposits from early stages of the Quaternary Period may therefore exist.

There are traces of three large glaciations, Elster (MIS 8), Saale (MIS 6) and Weichsel (MIS 2–5d), that reached as far south as northern Poland and Germany /e.g. Fredén, 2002/. Saale had the largest maximum extension of any known Quaternary ice sheet. There were two interstadials, Holstein and Eem, between these three glacials.

The oldest interglacial deposits in Sweden, dated by fossil composition, were probably deposited during the Holstein interglacial (MIS 7, c. 230,000 years ago) /e.g. Ambrosiani, 1990/. The till underlying the Holsteinian deposits may have been deposited during Elster and is the oldest known Quaternary deposit in Sweden.

Deposits from the Eemian interglacial (MIS 5e, 130,000–115,000 years ago) are known from several widely spread sites in Sweden /e.g. Robertsson et al. 1997/. The climate during this interglacial was periodically milder than it has been during the present interglacial, Holocene. The sea level was, at least periodically, higher than at present and large parts of the Swedish lowland were probably covered with brackish or marine water.

The latest glacial, the Weichselian started c. 115,000 years ago. It was characterised by colder phases, stadials, interrupted by milder interstadials. Numerous sites with deposits from the early part of Weichsel are known from the inner parts of northern Sweden. The model presented by e.g. /Fredén, 2002/ and /Lundqvist, 1992/ is often used to illustrate the history of Weichsel (Figure 3-9). Two interstadials took place during the early part of Weichsel, approximately 100,000–90,000 (MIS 5c) and 80,000–70,000 years ago (MIS 5a). Most of Sweden was free of ice during these interstadials, but the climate was considerably colder than today and tundra climate with shrub vegetation probably characterised northern Sweden. Southern Sweden was covered with coniferous forests during the first of these interstadials.

The second interstadial (correlated with MIS 5a) was colder and the vegetation in southern Sweden was probably characterised by a sparse birch forest. Most researchers agree that the ice did not reach further south than the Mälaren Valley during the Early Weichselian stadials. The ice advanced south and covered southern Sweden first during Mid Weichselian (c. 70,000 years ago). Most of Sweden was thereafter covered by ice until the deglaciation at around 12,000 years BP. Parts of Skåne were, however, free from ice until a few thousand years before LGM.

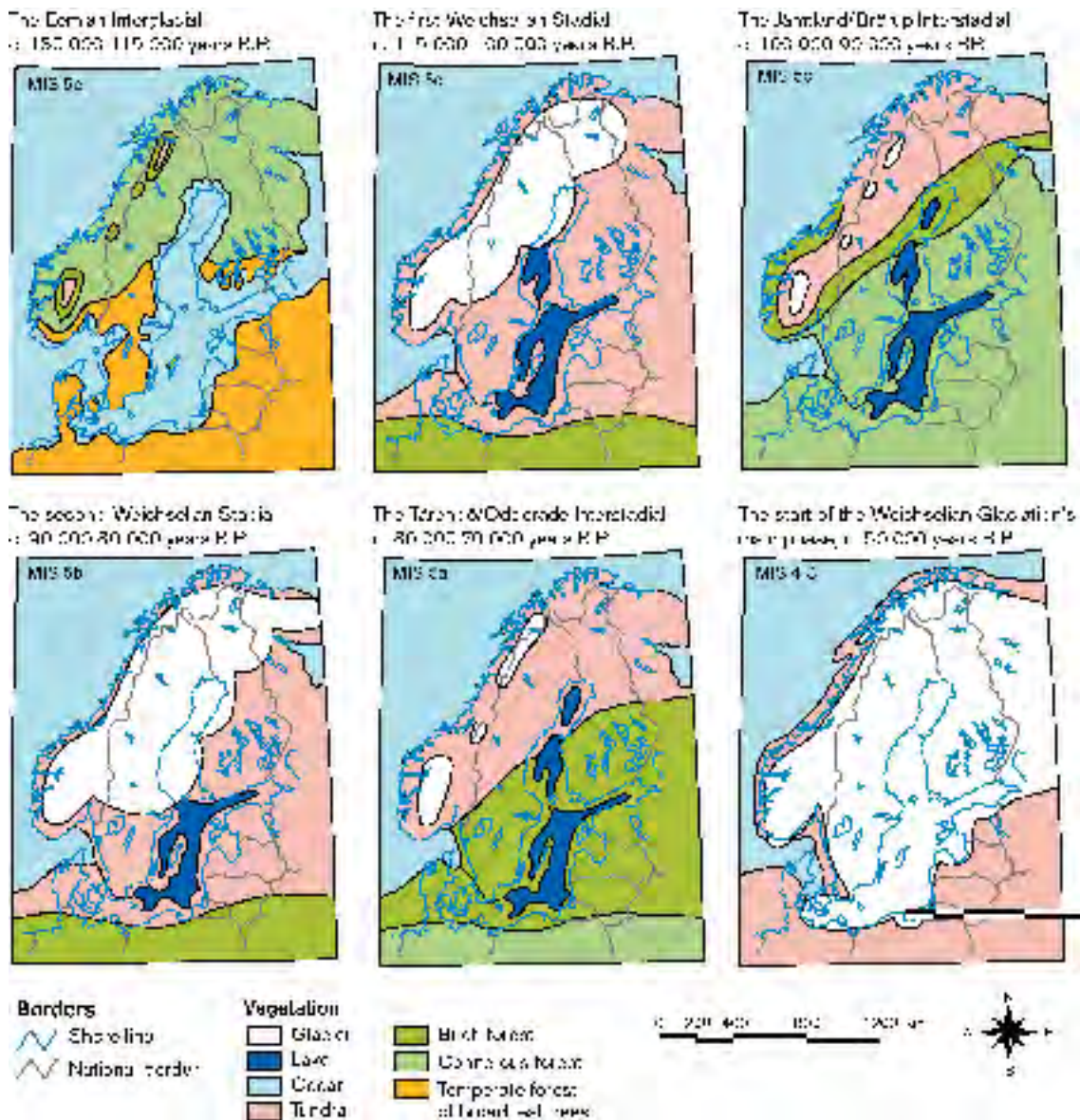


Figure 3-9. The development of vegetation and ice cover in northern Europe during the latest interglacial (Eem) and first half of the last ice age (Weichsel). The different periods have been correlated with the Major Isotope Stages (MIS). The maps should be regarded as hypothetical due to the lack of well-dated deposits from the different stages (from: *Sveriges Nationalatlas* /Fredén, 2002/).

The model presented by /Fredén, 2002/ and /Lundqvist, 1992/ (Figure 3-9) has been questioned. Most researchers agree that at least two interstadials with ice-free conditions did occur during the Weichselian glaciation. However, since the dating of such old deposits is problematic, the timing of these interstadials is uncertain. Investigations from both Finland and Norway suggest that most of the Nordic countries were free from ice during parts of Mid Weichselian (MIS 3–4) /e.g. Olsen et al. 1996; Ukkonen et al. 1999/. That may imply that one of the interstadials attributed to Early Weichselian by /Fredén, 2002/ may have occurred during Mid Weichsel. In large parts of Sweden, the total time of ice cover during Weichsel may therefore have been considerably shorter than previously suggested by e.g. /Fredén, 2002/.

During the last glacial maximum c. 20,000 years ago (MIS 2), the continental ice reached its southernmost extent (Figure 3-10). The Weichselian ice sheet reached as far south as the present Berlin, but had a smaller maximal extent than the two preceding glacials (Saale and Elster).

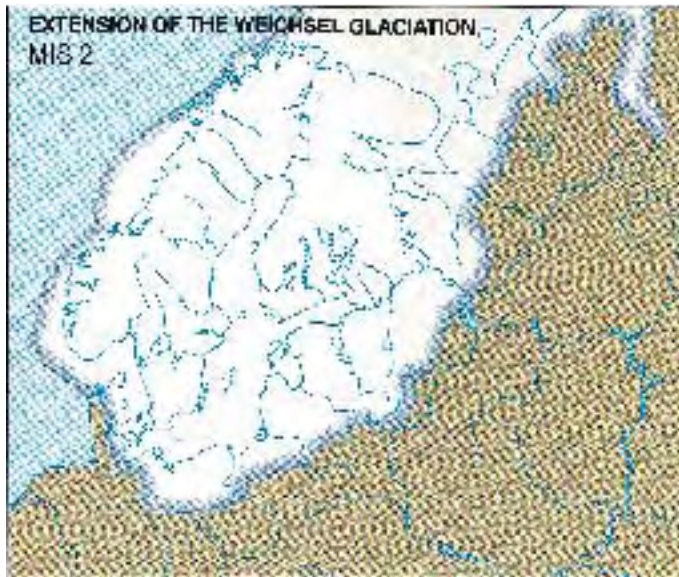


Figure 3-10. The maximum extent of the Weichselian ice sheet during MIS 2 approximately 20,000 years ago (from: Sveriges Nationalatlas /Fredén, 2002/).

3.3.3 The latest deglaciation

A marked improvement in climate took place about 18,000 years ago, shortly after the LGM and the ice started to withdraw, a process that was completed after some 10,000 years.

The timing of the deglaciation of Sweden has been determined with ^{14}C dates and clay-varve chronology. The deglaciation of eastern Sweden, including the Simpevarp and Forsmark areas, has mainly been studied by using clay-varve chronologies /Kristiansson, 1986; Strömberg, 1989; Brunberg, 1995; Ringberg et al. 2002/, whereas the timing of the deglaciation in other parts of Sweden has been determined with ^{14}C dates. These two chronologies have recently been calibrated to calendar years /e.g. Fredén, 2002; Lundqvist and Wohlfarth, 2001/.

There were several standstills and even re-advances of the ice front during the deglaciation of southern Sweden. In western Sweden, zones with end moraines reflect these occasions. The correlations of ice marginal zones across Sweden are, however, problematic. In southeastern Sweden few end moraines developed, because a lot of stagnant ice remained in front of the retreating ice sheet.

There was a major standstill and in some areas a re-advance of the ice front during a cold period called the Younger Dryas (c. 13,000–11,500 years ago). The ice front then had an east west extension across Västergötland and Östergötland (cf. Figure 3-11). The end of Younger Dryas marks the onset of the present interglacial, the Holocene. The ice retreated more or less continuously during the early part of the Holocene.

3.3.4 Climate and vegetation after the latest deglaciation

Pollen investigations from southern Sweden have shown that a sparse *Betula* (birch) forest covered the area soon after the deglaciation /e.g. Björck, 1999/. There was a decrease in temperature during the Younger Dryas (c. 13,000–11,500 years ago) and the deglaciated parts of Sweden were consequently covered by a herb tundra. At the beginning of the Holocene c. 11,500 years ago, the temperature increased and southern Sweden was covered by forests, first dominated by *Betula* and later by *Pinus* (pine) and *Corylus* (hazel). The timing and climatic development of the transition between the Pleistocene and the Holocene has been discussed by e.g. /Björck et al. 1996/ and /Andrén et al. 1999/.

Northern Sweden was deglaciated during the early part of Holocene when the climate was relatively warm. These areas were therefore covered by forest, mainly birch and pine, shortly after deglaciation.

Between 9,000 and 6,000 years ago, the summer temperature was approximately 2° warmer than at present and forests with *Tilia* (lime), *Quercus* (oak) and *Ulmus* (elm) covered large parts of southern Sweden. These tree species then had a much more northerly distribution than at present. The temperature has subsequently decreased after this warm period, and the forests have become successively more dominated by coniferous trees. During the Holocene, *Picea* (spruce) has spread from northernmost Sweden towards the south. This tree has not yet spread to Skåne and the Swedish west coast. The composition of vegetation has changed during the last few thousand years due to human activities, which have decreased the areas covered by forest. The ecological history of Sweden during the last 15,000 years has been reviewed by e.g. /Berglund et al. 1996/.

3.3.5 Development of the Baltic Sea after the latest deglaciation

A major crustal phenomenon that has affected and continues to affect northern Europe, following the melting of the latest continental ice, is the interplay between isostatic recovery on the one hand and eustatic sea level variations on the other. During the latest glaciation, the global sea level was in the order of 120 m lower than at present, due to the large amounts of water stored in ice /Fairbanks, 1989/.

In northern Sweden, the heavy continental ice depressed the Earth's crust by as much as 800 m below its present altitude. As soon as the pressure started to decrease, due to thinner ice coverage, the crust started to rise (isostatic land uplift). This uplift started before the final deglaciation and is still an active process in most parts of Sweden. In Sweden, the highest identified level of the Baltic Sea or the West Sea is called the highest shoreline. This shoreline is situated at different altitudes throughout Sweden depending on how much the crust had been depressed. The highest levels, nearly 300 m, are found along the coast of northern Sweden and the level sinks to below 20 m in southernmost Sweden.

The development of the Baltic Sea since the last deglaciation is characterised by changes in salinity, which have been caused by variations in the sea level. This history has therefore been divided in four main stages /Björck, 1995; Fredén, 2002/, which are summarised in Table 3-4 and Figure 3-11. The most saline period occurred 6,500–5,000 years ago when the surface water salinity in the Baltic proper (south of Åland) was 10–15‰ compared with approximately 7‰ today /Westman et al. 1999/.

The shoreline displacement in northern Sweden has been mostly regressive due to a large isostatic component. Along the southern part of the Swedish east and west coasts, the isostatic component was less pronounced and declined earlier during the Holocene, resulting in a complex shoreline displacement with alternating transgressive and regressive phases. The shoreline displacement in Sweden has been summarised by e.g. /Risberg, 1991/ and /Påsse, 2001/.

Table 3-4. Summary of the stages of the Baltic Sea, years before present /Fredén, 2002; Westman et al. 1999/. Note that the Littorina Sea stage is based on the palaeogeography in the threshold areas and includes e.g. the Mastogloia Sea stage and the present Baltic conditions. Note also that the altitudes and ages are approximate values, based on regional extra- and interpolations.

Baltic stage	Calendar year BP	Salinity	Environment in Forsmark
Baltic Ice Lake <i>not applicable in Forsmark</i>	15,000–11,550 <i>not applicable in Forsmark</i>	Glacio-lacustrine <i>not applicable in Forsmark</i>	Covered by inland ice
Yoldia Sea	11,500–10,800	Lacustrine/Brackish /Lacustrine	Deglaciation, regressive shoreline from c. 150 m.a.s.l.* Minor (or no) influence of brackish water.
Ancylus Lake	10,800–9,500	Lacustrine	Regressive shoreline from c. 140–75 m.a.s.l.
Littorina Sea <i>sensu lato</i>	9,500–present	Brackish	Regressive shoreline from 75–0 m.a.s.l. Most saline period 6,500–5,000 calendar years BP. Present Baltic Sea during approximately the last 2,000 years.

* m.a.s.l. = metre above sea level.

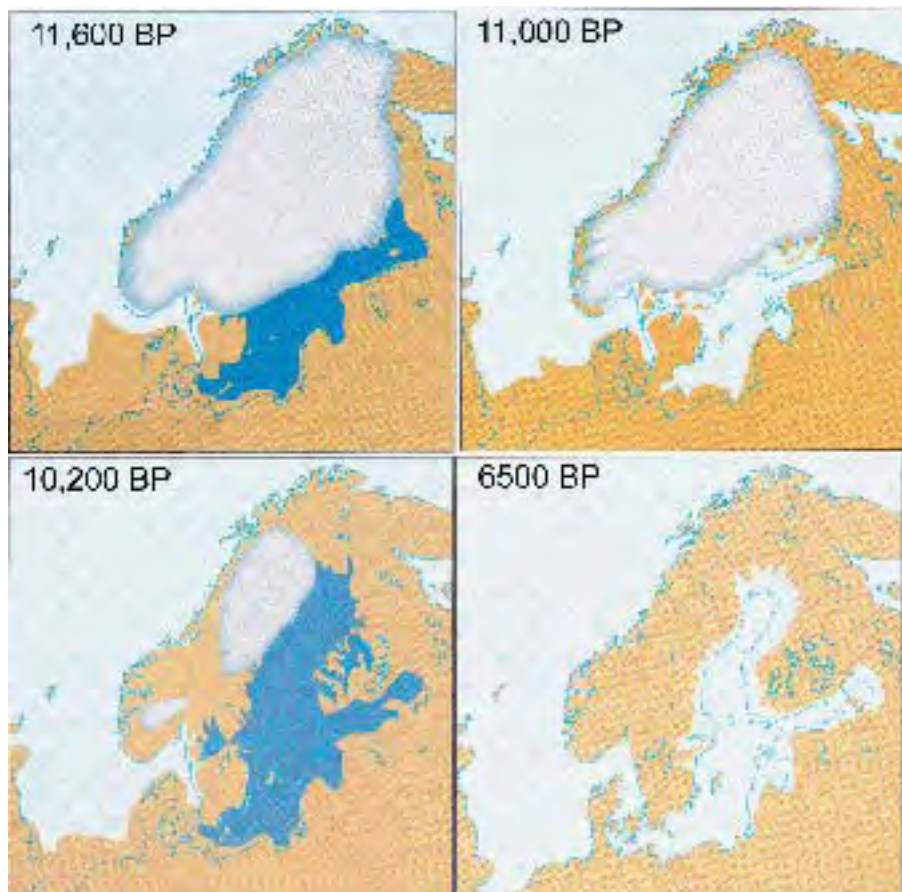


Figure 3-11. Four main stages are characterising the development of the Baltic Sea since the latest deglaciation: the Baltic Ice Lake (15,000–11,550), the Yoldia Sea (11,500–10,800), the Ancylus Lake (10,800–9,500) and the Littorina Sea (9,500–present). Fresh water is symbolised with dark blue and marine/brackish water with light blue (from: *Sveriges Nationalatlas /Fredén, 2002/*). The Forsmark area was deglaciated during the Yoldia Sea stage.

3.3.6 Late Quaternary history of the Forsmark area

The marine isotope record suggests numerous glaciations during the Quaternary Period. The number of glaciations covering the Forsmark area is, however, unknown. End moraines from three glaciations are known from northern Poland and Germany. It can therefore be concluded that the Forsmark area has been glaciated at least three times, but probably more, during the Quaternary Period.

During the last interglacial, the Eemian (MIS 5e, 130,000–115,000 years ago), the Baltic Sea level was higher than at present and it is therefore likely that the Forsmark area was covered with brackish water during a substantial part of that interglacial /Robertsson et al. 1997/.

The area was probably free of ice during the first Weichselian stadial and interstadials. The inland ice during the second Weichselian stadial probably reached as far south as the Stockholm region, thus covering the Forsmark area (Figure 3-9). It has been assumed that tundra conditions prevailed during the stadials /Fredén, 2002/. The vegetation during the first Weichselian interstadial was probably dominated by coniferous forest whereas the second interstadial was colder, the forest sparse and dominated by *Betula* (Birch). The exact timing of the Mid Weichselian glaciation is, however, unknown and there are indications of ice free condition in large parts of Fennoscandia during parts of Mid Weichsel /Ukkonen et al. 1999/. The total time of ice coverage in the Forsmark area may therefore have been considerably shorter than in the model presented by /Fredén, 2002/.

According to mathematical and glaciological models, the maximum thickness of the ice cover in the Forsmark region was more than 1.5 km at 18,000 years BP /Näslund et al. 2003/.

Glacial striae on bedrock outcrops are formed at different stages of the glaciations, thus several generations of striae may be identified. The oldest glacial striae observed in north-eastern Uppland are orientated from the north-west, a younger system from the north-north west and the youngest striae are formed by an ice moving approximately from the north /Persson, 1992/. All known overburden in the Forsmark regional model area has been deposited during, or after, the Weichselian glaciation.

The latest deglaciation took place during the Preboreal climatic stage, c. 10,800 years ago /Fredén, 2002; Persson, 1992; Strömberg, 1989/. According to extrapolations from clay varve investigations from central and northern Uppland and Åland, the ice recession had a rate of c. 300–350 m per year in northern Uppland. The ice at the front was in the order of 300 m thick, retreating into the open water of the Yoldia Sea stage of the Baltic.

In north-eastern Uppland, the highest Holocene shoreline was developed at the de-glaciation in the Yoldia Sea stage of the Baltic. The closest shore/land area at that time was situated c. 80 km to the west of Forsmark and the Forsmark area was covered with approximately 150 m of Yoldia Sea water.

The Holocene shoreline displacement in northern Uppland has been studied with stratigraphical methods by e.g. /Robertsson and Persson, 1989/ and /Hedenström and Risberg, 2003/.

/Påsse, 2001, 1997/ has made mathematical modelling of the shoreline displacement in Fennoscandia. The modelled curve, together with the results from dated isolation events of lakes and mires are presented together in Figure 3-12. Påsse's curve is similar to the curve presented by /Hedenström and Risberg, 2001/. Påsse's mathematical model, however, continues back to the deglaciation whereas the stratigraphical investigations only cover the last 6,500 years.

In Forsmark, the shoreline has been continually regressive since the deglaciation. Initially, during the Yoldia Sea and Ancylus Lake stages of the Baltic, the regression rate was in the order of 4 m/100 years. The brackish water phase of the Yoldia Sea lasted c. 120 years, as recorded e.g. by ostracods and foraminifers in varved clay from central Sweden /Wastegård et al. 1995; Schoning, 2001/. Marine water entered the Baltic basin through the topographic lowland in Närke, known as

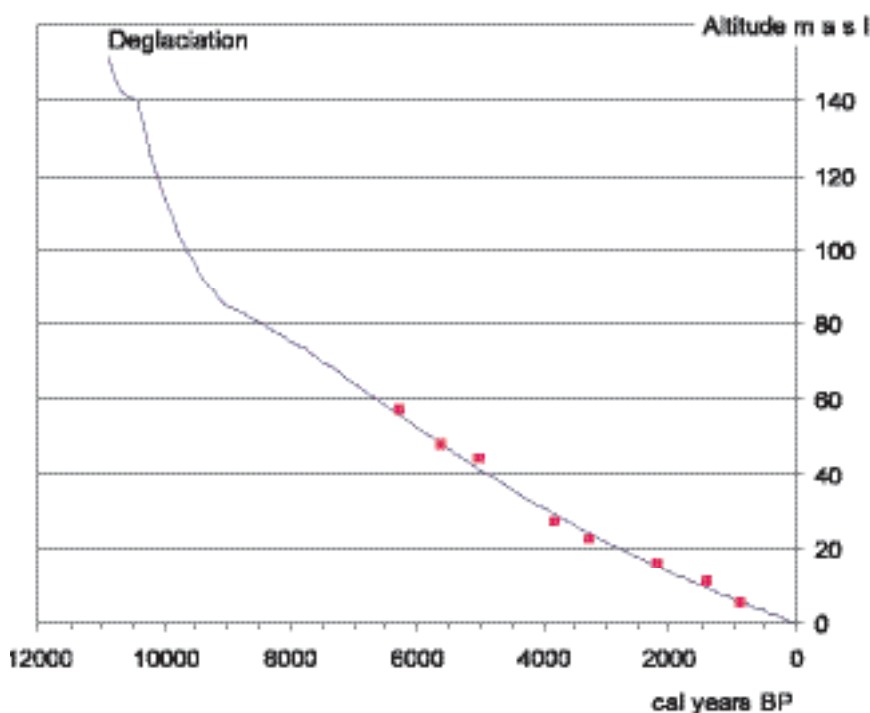


Figure 3-12. The shoreline displacement in the Forsmark area after the latest deglaciation. The purple symbols show a curve established by dating the isolation of lakes /Hedenström and Risberg, 2001/. The blue solid curve has been calculated by the use of a mathematical model /Påsse, 2001/.

the Närke Strait. The short duration of the brackish phase, the lateness of the deglaciation, together with freshwater supply from the melting ice, probably resulted in only minor, if any, influence of saline water in north-eastern Uppland during the brackish water phase of the Yoldia Sea.

The next Baltic stage, the Ancyclus Lake, was lacustrine with an initial outlet through the Lake Vänern basin (Figure 3-11). The isostatic uplift was faster in the north, resulting in the Ancyclus transgression in regions situated south of the outlet, for example the Oskarshamn area /e.g. Svensson, 1989/. Ongoing eustatic sea level rise, in combination with reduced isostatic rebound in the southern Baltic basin enabled marine water to enter the Baltic basin through the Danish straits, marking the onset of the Littorina Sea *sensu lato*. This stage includes an initial phase when the salinity was stable and low, the Mastogloia Sea, that lasted for approximately 1,000 years in Southern Uppland, before the onset of the brackish water Littorina *sensu stricto* /Hedenström, 2001/.

During the last c. 9,000 years the average regression rate has been lower, in the order of 9 mm/year (Figure 3-12). This means that neither the transgressions during the Ancyclus Lake or the Littorina Sea stages have affected the Forsmark area. An effect of the ongoing regressive shoreline displacement is that the new land areas have not been flooded after emerging from the Baltic.

Within northern Uppland, the first land areas emerged c. 6,500 years ago /Robertsson and Persson, 1989; Bergström, 2001; Hedenström and Risberg, 2003/, i.e. during the most saline phase of the Littorina Sea (correlated with the Holocene climatic optimum during the Atlantic climatic stage /Westman et al. 1999/). The major part of the Forsmark regional model area was still covered by water until c. 2,500 years ago (Figure 3-12). A few scattered islands, situated close to the church of Forsmark, are the first land areas to emerge from the Baltic c. 2,500 years ago. At present, the land in north-eastern Uppland is rising with respect to the sea level at the rate of c. 6 mm/year /Ekman, 1996b/.

Pollen-analytical changes recorded in northern Uppland are the Elm decline, c. 5,200 cal years BP and the spread of spruce at c. 3,400–2,700 cal years BP /Robertsson and Persson, 1989/. At the Hållnäs peninsula, c. 35 km north of the regional model area, biostratigraphical investigations have been performed in connection with archaeological investigations /Ranheden, 1989/. Settlements from the Viking age and medieval period were identified in the fossil record, i.e. humans have been occupying the archipelago successively as new land emerged from the Baltic. A survey of the pollen content in sediment collected in the Kallrigafjärden indicated that the area was used for cultivation shortly after its emergence from the Baltic /Bergkvist et al. 2003/.

3.4 Surface and groundwater

3.4.1 Premises for surface water evolution

As shown in Figure 3-12, almost the whole regional model area was covered by sea water until 2,500 years ago. There are no direct records from the site which can be used to depict the past salinity. The past salinity in the Baltic Proper since the onset of the Littorina period has been reviewed by /Westman et al. 1999/ and /Gustafsson, 2004a/. From proxy data they estimated a range within which the salinity of the Baltic Proper can be described over time. They also showed a model, which uses knowledge of the sills in the southern Baltic Sea together with river runoff to the Baltic Sea, to estimate the past and future salinity changes in the Baltic Sea, and which also can be used to evaluate differences in salinity between the different basins of the Baltic Sea /Gustafsson, 2004a,b/.

The model by /Gustafsson, 2004a,b/ has, together with proxy records of salinity in the Baltic proper, been used to make a rough estimation of the likely range of past salinity in the Bothnian Sea, i.e. the basin where the Forsmark area is situated (Figure 3-13). The difference in estimated salinity between the Baltic Proper and the Bothnian Sea back in time is generally low (< 1 ppt), due to the wide sill in Ålands hav.

In Figure 3-14, the time since the land emerged from the Baltic Sea is presented as an iso-chronic map based on /Brydsten, 1999/. From the map it can be seen that the whole candidate area was covered by the sea until less than 1,500 years ago. This means that the Quaternary deposits in the area have been exposed to groundwater recharge and soil forming processes for a very limited time.

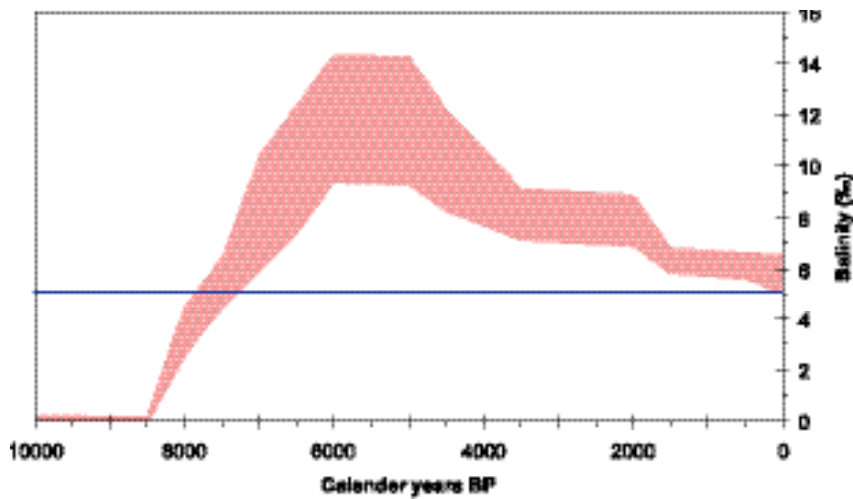


Figure 3-13. Estimated range for the salinity of sea water in the Forsmark area from the onset of the Littorina period until today. Maximum and minimum estimates are derived from /Westman et al. 1999/ and /Gustafsson, 2004a,b/. The present salinity in the area is shown as a horizontal reference line.

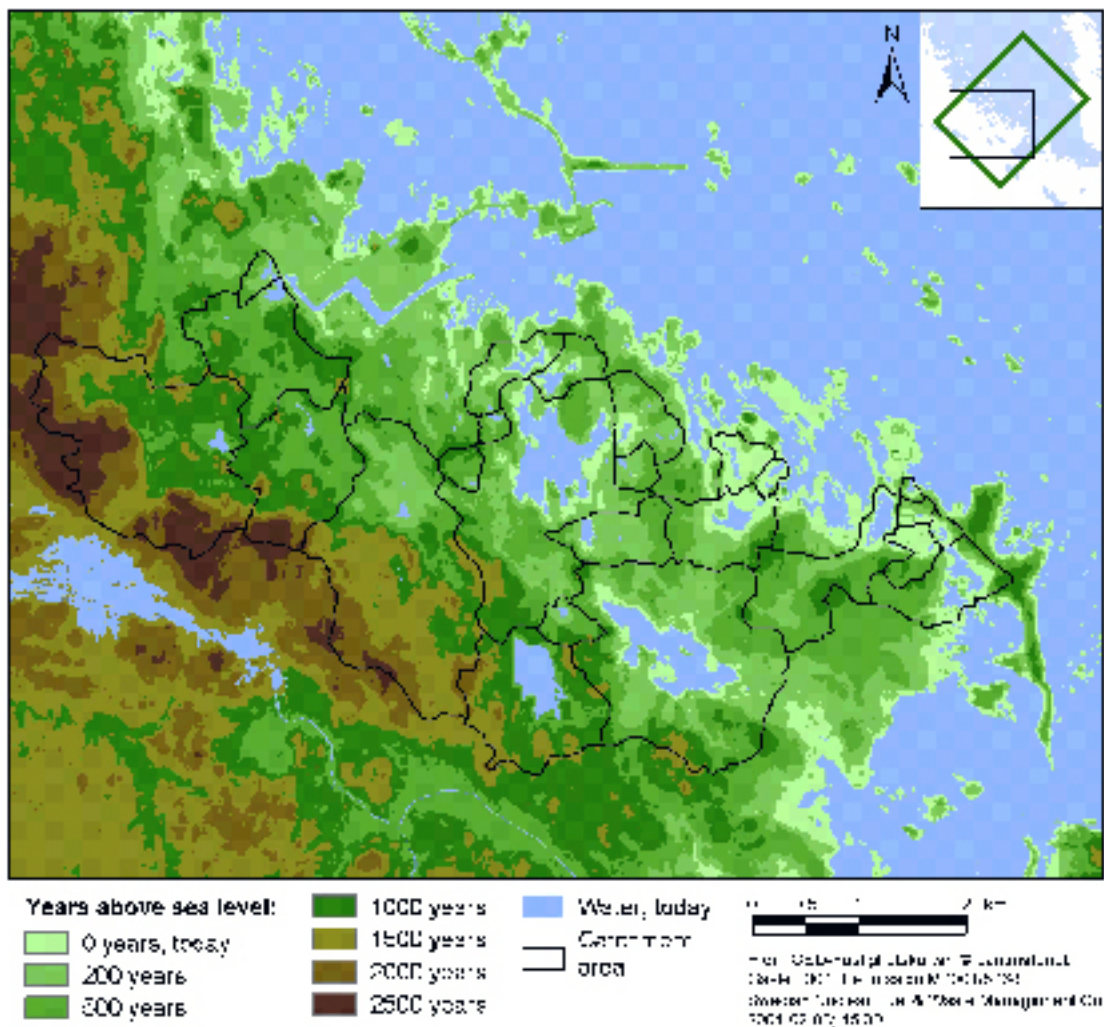


Figure 3-14. Iso-chronic map showing the time since the land emerged from the Baltic Sea.

Processes which may affect the drainage-network mainly took place prior to isolation from the Baltic. It is therefore reasonable to assume that no major topographical changes due to e.g. erosion or sedimentation have occurred after the Forsmark area emerged above the sea level, with the exception of sedimentation in lakes. Sediment accumulation will probably not change the drainage areas, since thresholds generally are formed in glacial till or bedrock. Peat formation may lead to damming, resulting in expanding peatlands. However, damming due to peat formation is considered to be of minor importance for the drainage-network evolution in the area, and it is probably only in the most elevated areas that peat formation may have caused any changes in the drainage pattern.

3.4.2 Post-glacial conceptual model of groundwater evolution

The first step in the groundwater evaluation is to construct a conceptual postglacial scenario model for the site (Figure 3-15), based largely on known palaeo-hydrogeological events indicated by Quaternary geological investigations. This model can be helpful when evaluating data, since it provides constraints on the possible groundwater types that may occur. Interpretation of the glacial/post-glacial events that might have affected the Forsmark site is based on information from various sources including /Fredén, 2002; Pässe, 2001; Westman et al. 1999; SKB, 2002a; Hedenström and Risberg, 2003/. This recent literature provides background information, which is combined with more than 10 years of studies of groundwater chemical and isotopic information from sites in Sweden and Finland in combination with various modelling studies of the postglacial hydrogeological events /Laaksoharju and Wallin, 1997; Pitkänen et al. 1998; Svensson, 1996/. The presented model is therefore based on Quaternary geology, fracture mineralogical investigations and groundwater observations. These facts have been used to describe possible palaeo events that may have affected the groundwater composition in the bedrock.

Development of permafrost and saline water

When the continental ice sheet was formed at about 100,000 BP, permafrost formations ahead of the advancing ice sheet probably extended to depths of several hundred metres. According to /Bein and Arad, 1992/ the formation of permafrost in a brackish lake or sea environment (e.g. similar to the Baltic Sea) produced a layer of highly concentrated salinity ahead of the advancing freezing front. Since this saline water would be of high density, it would subsequently mix and sink to lower depths and potentially penetrate into the bedrock where it would eventually mix with formational groundwaters of similar density. Where the bedrock was not covered by brackish lake or sea water, similar freeze-out processes would occur on a smaller scale within the hydraulically active fractures and fracture zones, again resulting in formation of a higher density saline component which would gradually sink and eventually mix with existing saline groundwaters. Whether the volume of high salinity water produced from brackish waters by this freeze-out process would be adequate to produce widespread effects is presently under debate.

With continued evolution and movement of the ice sheet, areas previously subject to permafrost would eventually be covered by ice, accompanied by a rise in temperature at the base of the ice sheet and slow decay of the underlying permafrost layer. Hydrogeochemically, this decay may have resulted in distinctive signatures being imparted to the groundwater and fracture minerals.

Deglaciation and flushing by meltwater

During subsequent melting and retreat of the ice sheet, the following sequence of events is thought to have influenced the Forsmark area:

When the continental ice melted and retreated, glacial meltwater was hydraulically injected under considerable head pressure into the bedrock (> 11,500 BP) close to the ice margin. The exact penetration depth is still unknown, but depths exceeding several hundred metres are possible according to hydrodynamic modelling /e.g. Svensson, 1996/. Some of the permafrost decay groundwater signatures may have been disturbed or destroyed during this stage.

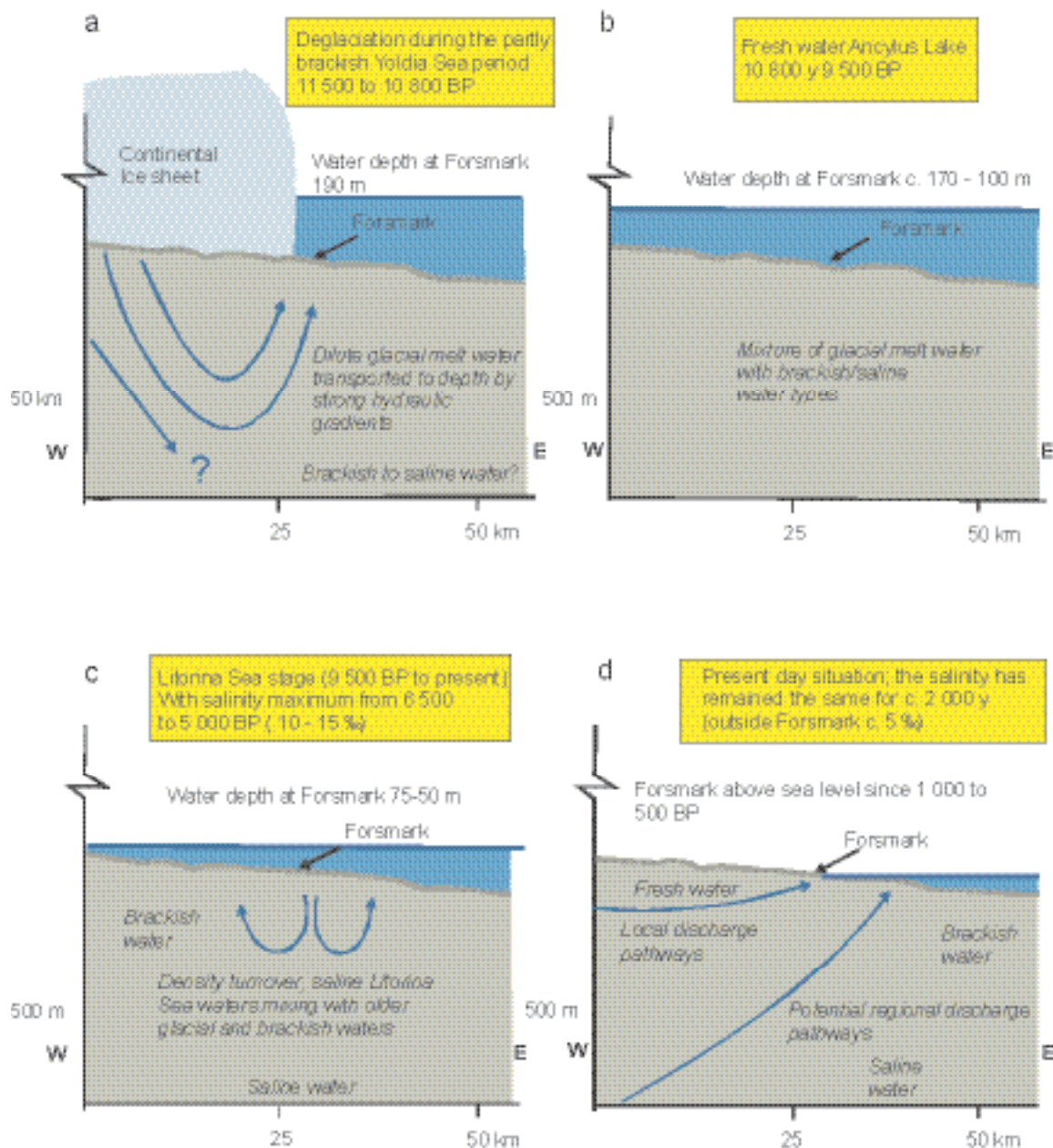


Figure 3-15. An updated (from model version 1.1) conceptual postglacial scenario model for the Forsmark site. The figures show possible flow lines, density driven turnover events and non-saline, brackish and saline water interfaces. Possible relation to different known post-glacial stages such as land uplift which may have affected the hydrochemical evolution of the site is shown: a) Yoldia Sea stage including deglaciation, b) Ancylus Lake stage, c) Littorina Sea stage, and d) present day Baltic Sea stage. From this conceptual model, it is expected that glacial meltwater and deep and marine water of various salinities have affected the groundwater. Based on information from /Fredén, 2002/, /Hedenström and Risberg, 2003/, /Westman et al. 1999/ and /SKB, 2002a/.

Different non-saline and brackish lake/sea stages then transgressed the Forsmark site during the period c. 11,000–500 BP. Of these, two periods with brackish water can be recognised; the Yoldia Sea (11,500 to 10,800 BP) and the Littorina Sea (9,500 BP to the present cf. Table 3-4) with the Baltic Sea from 2,000 BP to the present. The Yoldia period has probably resulted in only minor contributions to the subsurface groundwater, since the water was very dilute to brackish in type from the large volumes of glacial meltwater it contained. Furthermore, this period lasted only for 700 years. The Littorina Sea period in contrast had a salinity maximum of about twice the present Baltic Sea and this maximum prevailed from 6,500 to 5,000 BP. During the last 2,000 years, the salinity has remained almost equal to the present Baltic Sea values /Westman et al. 1999 and references therein/. Dense brackish seawater, such as the Littorina Sea water, was able to penetrate the bedrock resulting in a density turnover which affected the groundwater in the more conductive parts of the bedrock. The density of the intruding seawater in relation to the density of the groundwater determined the final penetration depth. As the Littorina Sea stage comprised the most saline groundwater, it is assumed to have had the deepest penetration depth eventually mixing with the glacial/brine groundwater mixtures already present in the bedrock.

When the Forsmark region was gradually raised above sea level during the last 1,500 years, fresh meteoric recharge water formed a lens on top of the saline water because of its low density. As the present topography of the Forsmark area is flat and the time elapsed since the area rose above the sea is short, the out flushing of saline water has been limited and the freshwater lens remains at shallow depths (from the surface down to 25–100 m depending on hydraulic conditions).

Many of the natural events described above may be repeated during the lifespan of a repository (thousands to hundreds of thousands of years). As a result of the described sequence of events, brine, glacial, marine and meteoric waters are expected to be mixed in a complex manner at various levels in the bedrock, depending on the hydraulic character of the fracture zones, groundwater density variations and borehole activities prior to groundwater sampling. For the modelling exercise, which is based on the conceptual model of the site, groundwater end-members reflecting, for example, Glacial meltwater and Littorina Sea water composition, were added to the data set (cf. Appendix 4 in /SKB, 2005b/).

The uncertainty of the updated conceptual model increases with modelled time. The largest uncertainties are therefore associated with the stage associated with flushing of glacial melt water. The driving mechanism behind the flow lines in Figure 3-15 is the shore level displacement due to the land uplift.

3.5 Surface ecosystems

Patterns in the present-day surface ecosystems are a result of physical and biological processes over time, e.g. land uplift, climate change, vegetation development and human impact. These processes are often combined, where one process sets the limits for others. For example, climate and land uplift often determine vegetation development, which in turn affects human settlements and land use. The strongest impact on the historical development of the surface ecosystems in the Forsmark area is caused by direct or indirect effects of the latest glaciation. A direct effect, still strongly affecting the systems, is shoreline displacement, but other factors like soil evolution, altitude, and the prerequisites for creation of lakes and watersheds are also determined by the latest glaciation.

3.5.1 The Baltic Sea

When the glacial ice cover started to retreat about 11,000 years ago, the Forsmark regional model area was situated about 190–170 m below the surface level of the Yoldia Sea, at that time a freshwater stage of the Baltic Sea (cf. Table 3-4). The conditions in the Forsmark area remained principally lacustrine for approximately 1,500 years, until the onset of the Littorina Sea stage. From Littorina until today, the Baltic Sea has been brackish with varying salinity and with an estimated maximum salinity level about twice as high as today, occurring during the period 6,500–5,000 BP

/Westman et al. 1999/. The post-glacial climate in the Baltic Sea area has changed several times between cold and warm periods, and the varying salinity may at least partly be related to climate variations with decreased salinity during periods of climate deterioration /Westman et al. 1999/.

As described above, the first islands in the Forsmark regional model area appeared approximately 2,500 years ago (cf. Figure 3-14). Accordingly, the post-glacial ecosystems have been dominated by marine stages, and no terrestrial or lacustrine ecosystems have existed in the area until the last 2,500 years. Today, the Forsmark area is situated on the border between two different landscape types: “Woodlands south of Limes Norrlandicus” and “Coasts and archipelagos of the Baltic sea” /NMR, 1984/. Because of the shoreline displacement, all terrestrial and freshwater parts of the model area have relatively recently belonged to the latter type and the border between the two types is continuously moving to the east. This means that both the aquatic and the terrestrial ecosystems have gone through substantial changes during the post-glacial period, and they are still changing continuously, especially near the shoreline.

3.5.2 Lacustrine ecosystems

In Scandinavia, a majority of the present lakes were formed during the last glaciation, when geomorphological processes substantially altered the entire landscape. As the glacier retreated, erosion, transport, and deposition of material resulted in the formation of numerous lake basins in the landscape. Due to present land uplift in the Forsmark area, freshwater lake basins are continuously formed along the coast as bays become isolated from the brackish water of the Baltic Sea. Immediately after the formation of a lake, an ontogenetic process starts, where the basin ultimately is filled with sediments, and thereby develops towards extinction of the lake. Depending on local hydrological and climatic conditions, the lake may be converted to a final stage of a bog or to forest /Wetzel, 2001/. A usual pattern for lake ontogeny is the subsequent development of more and more eutrophic conditions as lake depth and volume decrease. In later stages, aquatic macrophytes speed up the process by colonising large areas of the shallow sediments /Wetzel, 2001/.

All lakes in the Forsmark area, as well as all other lakes below the highest shoreline of the Baltic Sea (and its previous lake and sea stages), have their origin as depressions at the bottom of these large aquatic systems /Brunberg and Blomqvist, 2000/. The lakes of Uppsala County can be divided into three categories, based on their ecosystem functioning: shallow and oligotrophic hardwater lakes, shallow alkaline brownwater lakes, and deeper highly eutrophic lakes /Brunberg and Blomqvist, 2000/. All three lake categories occur within the vicinity of or in the Forsmark area, but the lakes in the area differ in several aspects from lakes in Uppsala County in general /Brunberg and Blomqvist, 2000/. Because of their location close to the Baltic Sea in a low-land area, they are generally younger than the inland, more elevated lakes. Other characteristics of the Forsmark lakes are that they are smaller in area, shallower and have a smaller volume of water than the lakes of Uppsala County in general.

Shallow oligotrophic hardwater lakes, which are totally dominant among the present lakes in the Forsmark regional model area, can be regarded as ephemeral in that they shift to alkaline brownwater conditions approximately 1,000–1,500 years after isolation from the sea /Brunberg and Blomqvist, 2003/. Thereafter, they are successively filled with allocthonous (from the drainage area) and autocthonous material (produced in the lake basin itself), the final stage being a wetland forest or a bog (Figure 3-16). Due to the small catchment areas with minor topographic variation dominated by wave-washed till and wetlands, there are few sources of allocthonous material. Thus, the sediment of the lakes in the area shows a high degree of autocthonous origin compared with many other lakes. There seems to be very few, if any, lakes or previous lakes in the Forsmark area that have followed the general pattern of more and more eutrophic conditions during lake ontogeny /Brunberg and Blomqvist, 2000/. Several lakes connected to the river Forsmarksån have been strongly affected by anthropogenic activity.

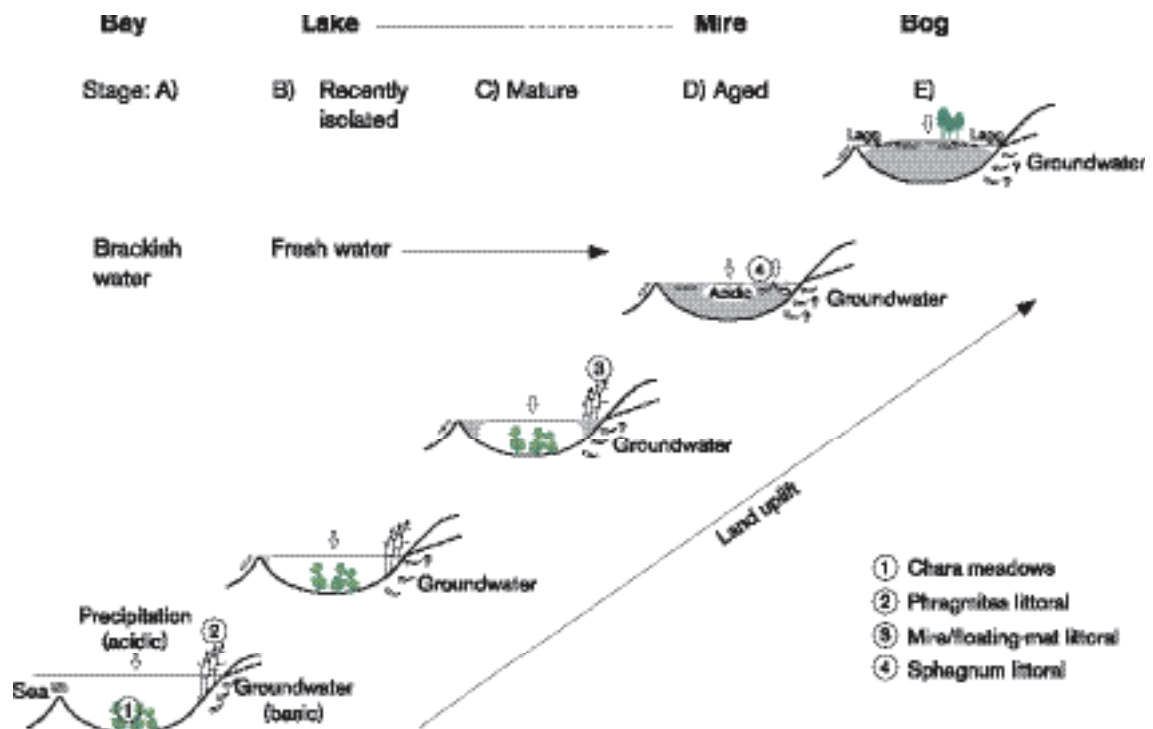


Figure 3-16. Suggested ontogeny of the oligotrophic hardwater lakes in the Forsmark area. The numbers in the figure represent different major components of the ecosystem: 1 = Chara meadow, 2 = *Phragmites littoral*, 3 = mire/floating-mat littoral, 4 = *Sphagnum littoral* /from Brunberg and Blomqvist, 2000/.

3.5.3 Vegetation

Vegetation development after the latest glaciation has been primarily controlled by land uplift and climatic changes. The general vegetation development, after the retreat of the glacial ice cover, is very much the same all over Stockholm archipelago /Jerling et al. 2001/. However, the first islets appears in the Forsmark area around 2,500 years BP, which is some 4,000 years later than for the earliest parts of the archipelago. This affects the time period of vegetation development, unaffected by humans, which is quite short compared with other areas in the archipelago. On the other hand, the general processes controlling the successional development of vegetation are the same, regardless of when the succession begins.

The historical vegetation development has been examined by using data from pollen analysis /Jerling et al. 2001/. Such analyses have shown that the first vegetation in the Stockholm archipelago was dominated by typical early colonising tree species like Pine (*Pinus sylvestris*), Birch (*Betula spp*) and Hazel (*Corylus avellana*). Some tree species are fast colonisers and occur early in succession (Figure 3-17). However, a major part of the early succession species is short-lived herbs and grasses, but since they are light dependent they disappear later in the succession, when the vegetation canopy is closing. The Boreal period was totally dominated by Birch (*Betula spp*) and Pine (*Pinus sylvestris*), whereas the Atlantic period was characterised by the expansion of nemoral (thermophilous) forest trees, like Oak (*Quercus robur*), Elm (*Ulmus glabra*), Lime (*Tilia cordata*), Ash (*Fraxinus excelsior*), because of warmer climate. Spruce (*Picea abies*) had its expansion much later, about 2,500 BP /Jerling et al. 2001/. In conclusion, a major part of the immigrating plants were already established in the coastal area of Uppsala County when the first islands in the Forsmark area emerged from sea. There is a consensus that Uppsala county never has been so forested as today /Lindborg and Schüldt, 1998/. Thus, in several areas today's forests are the first generation of woodlands since the first settlement, as a result of agriculture.

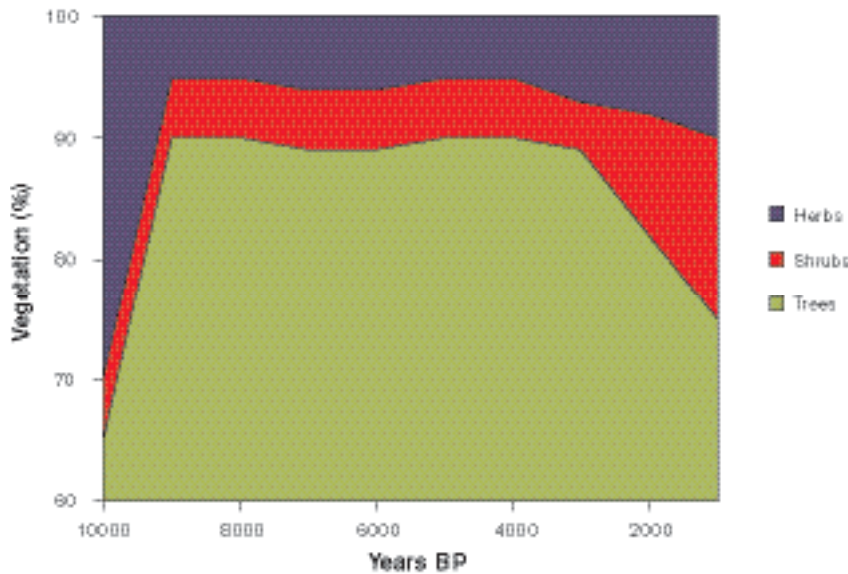


Figure 3-17. Pollen diagram showing the relative amount of trees, shrubs and herbs in the Stockholm archipelago /after Jerling et al. 2001/.

During the last 200 years, human activities have had a major impact on the development of the vegetation in the Forsmark area. Historical vegetation and land use development can be reconstructed by combining data from pollen analysis, old cadastral maps, soil and bedrock maps and archaeological data, with shoreline displacement models /Cousins, 2001/. Although land use alters the “natural” vegetation processes, all of the area has not been equally exploited through time, depending on differences in Quaternary deposits. For example, deposits on the flat sub-Cambrian peneplain are naturally rich in nutrients and thus frequently used in agriculture, but the areas closer to the coast have more exposed bedrock, resulting in less opportunity for agriculture /Jerling et al. 2001/. Moreover, as new land emerges, new immigrating species can establish and the primary succession, comparable to the one occurring after the glaciation, continues. Thus, the land class distribution on the border of the coastal region changes little even though local spatial patterns are continuously changing.

Due to the strong influence by man on terrestrial ecosystems, it is difficult to evaluate the relative importance of natural factors affecting the conifer forests. As the iron industry became more organised in the 16th century, forests were cut down to feed furnaces and mines with wood and charcoal. Many regions, including Forsmark, were almost depleted of trees at the end of this period /Welinder et al. 1998/. Tar and lumber also became commercially important.

3.5.4 Wild fauna

Archaeological excavations make it possible to document the diet of early settlers by identifying bones from animals /cf. Bratt, 1998/. However, abundances of specific species are not possible to estimate based on these findings. Food remains from the Stone Age imply that seal and different fish species were common in the food of man in the Stockholm archipelago. Further inland there are frequent traces of moose, red deer, wild boar and bear in the remains /Bratt, 1998/. During the most intense hunting period, some two hundred years ago, many large mammals were locally extinct in Uppsala County, e.g. bear, beaver, and wolf /Lindborg and Schüldt, 1998/. Documenting earlier fauna in the Forsmark area specifically has not been done, and may be difficult due to few excavations in this area. However, information on the occurrence of large mammals during the last 50 years are available for the Forsmark area, based on bag records registered by local hunters /Cederlund et al. 2004/.

3.5.5 Population and land use

The first documented settlement close to the Forsmark area is from c. 4,000 BP, when people began to cultivate the large peneplain of Uppsala /Lindborg and Schüldt, 1998/. However, due to the low altitude in the Forsmark area, the first settlers were not able to colonise until after 1,500 BP, by which time a substantial land area had emerged from the sea /Brydsten, 1999/.

Some estimations of the population size in the area, from the medieval and onwards, are presented in /Jansson et al. 2004/ and /Lindborg, 2005/. However, since no comprehensive source material on the Swedish population size exists before c. 1,750, estimates before this time are approximations. The settlement situation in Forsmark in the early-modern period is strongly dependent on the establishment of the ironworks *Forsmarks bruk* in the 17th century. As a consequence of the need of labour to the ironwork, the population increased from the 17th century and onwards. The physical mark of the population increase can be seen in that many crofters' places were established in the area during this period. The crofters had small areas of arable land and meadows near their houses, and the places were localised in small valleys with fruitful soil in the woodlands. The population in the Forsmark area reached a maximum in the beginning of the 20th century, when the area was quite densely settled /Jansson et al. 2004/.

The historical land use may be studied by using cadastral maps from the late 17th century and written historical documents. However, only land close to villages was mapped and only when the villagers asked for land redistribution. Generally, the cultural landscape (i.e. field boundaries) described in such maps was to a large extent established in the late Iron Age /Widgren, 1983; Welinder et al. 1998/. During the period 1,700–1,850, the communally owned land was divided into individual farms, and the fields were reorganised. Technology also altered the landscape as lakes and wetlands were drained and cultivated, which is also documented in the Forsmark area. Better iron tools made it possible to till the earth deeper and dig ditches and thus drain sodden areas. During the late 19th century, much of the former forested and more unsuitable areas also became agricultural land.

The forests in the landscape have not been mapped over historical time to the same extent as the cultivated landscape. Forests and wood have only recently been regarded as an economic resource, which has implications for the historical documentation of forestry in the Forsmark area. Forestry was, however, a major industry in the northern part of the Uppland County between the 11th and the 19th century. Iron mining has played an important role in the region since the Iron Age /Mattson and Stridberg, 1980/.

The life close to the mines shaped the landscape into a mosaic of a small-scale traditional agricultural landscape, ironworks and forest industry. The water from the river Forsmarksån was also regulated for mining. These places are today of national interest for their cultural history /Lindborg and Schüldt, 1998/. If we look at the changes over the last 100 years, it is clear that there has been an increase in arable land in Forsmark from the late 19th century to the mid 20th century. One of the dramatic changes was the reduction of numbers and areas of the meadows. More than one hundred years ago the landscape was to some extent dominated by the often wet meadows. During the last few hundred years, a major part of the Forsmark region has been used for forestry, first owned by *Forsmarks bruk* and later by Assi-Domän and Sveaskog.

4 The surface system

This chapter presents results from the work that has been performed within the site modelling for Forsmark 1.2 concerning the surface system, i.e. meteorology, overburden characterisation, hydrology, hydrochemistry, oceanography, biota and development of ecosystem models. A comprehensive surface description is reported separately in /Lindborg, 2005/.

The surface system starts where the deep bedrock ends, except where the bedrock reaches the surface and thereby becomes a part of the surface system as outcrops, and extends to processes in the atmosphere affecting the investigated site (e.g. climate). This means that a number of different disciplines are represented in covering discipline specific patterns and processes at various spatial and temporal scales. The chapter starts with a section describing the evaluation of primary data. Then discipline-specific descriptions for geology (overburden), hydrology and hydrogeology, chemistry, biotic characteristics, and humans and land use, are presented. Each description should be considered inter-dependent aiming at a deepened understanding of the patterns and processes at the site.

At the end of this chapter, three descriptive ecosystem models are presented, describing terrestrial, limnic and marine environments. The overall aim of the ecosystem modelling is to describe the carbon cycle for the different environments. This is done in two steps; 1) a conceptual model is presented for each of the three environments, 2) site specific quantitative data are used to create carbon budgets for the terrestrial part of a discharge area, a lake and three marine basins. These descriptive ecosystem models use data from a number of disciplines, e.g. overburden characterisation (Quaternary deposits), hydrology, biota etc, which are presented in the earlier sections within the surface ecosystem description. These carbon budgets will be one important tool to estimate and predict flows and accumulations of matter and radionuclides at a landscape scale in the subsequent safety assessment.

The overall aim of the modelling is to produce a detailed description of the present conditions at the site. However, it is equally important to know the history of the studied site, not only to understand the present patterns, but also to be able to make projections of possible future conditions.

4.1 State of knowledge at previous model version

In the Forsmark 1.1 site descriptive model, the modelling of the abiotic components of the surface system was included in the discipline-specific geological, hydrogeological and hydrogeochemical modelling. In addition, an integrated description of the surface system was provided in Chapter 7 of the version 1.1 report /SKB, 2004a/. The site data available for the descriptions of the abiotic components were quite limited. The geology of the Quaternary deposits was described based on the detailed map of the Quaternary deposits within the Forsmark area, and available data from soil drillings within that area. The descriptions of surface hydrology and oceanography were based on regional (version 0) data only, and, as no hydraulic tests in the Quaternary deposits had been performed, the hydrology model was based on literature data.

The version 1.1 description of the biotic components of the surface system included a vegetation map over the regional model area, results of biomass and production calculations for different vegetation types, some data on aquatic producers, and a description, to large extent based on generic data, of terrestrial and aquatic consumers. In addition, an assessment of the available information on humans and land use was provided. No quantitative ecosystem models were presented in the version 1.1 site descriptive model.

4.2 Evaluation of primary data

A complete list of abiotic and biotic data from the surface system available for use in Forsmark 1.2 is found in Tables 2-7 and 2-8.

4.2.1 Overburden including Quaternary deposits

The data included in this model version are summarised in Table 2-7. For a detailed description of the data and the methods used, see /Lindborg, 2005/.

The description of the Quaternary deposits is focused on the spatial distribution of the different units, together with a description of physical and chemical properties. The physical properties are used as input data for the hydrogeological modelling, whereas the chemical properties contribute to the biological models of the upper geosphere and to the hydrogeochemical modelling.

This model version comprises initial data, compiled in connection with the Östhammar feasibility study /Bergman et al. 1996/ together with the results from the initial site investigations in Forsmark. Between the data freeze Forsmark 1.1 (April 30, 2003) and Forsmark 1.2 (July 31, 2004), the investigations of the overburden resulted in maps of the distribution of Quaternary deposits on land /Sohlenius et al. 2004/ and offshore /Elhammer et al. 2005/ as well as a map showing the distribution of the soil types in Forsmark /Lundin et al. 2004/. Stratigraphical data comprise information on the spatial distribution of the different layers of Quaternary deposits. This information has been gained from the large number of soil/rock drillings, machine cut trenches, corings in sediment and peat, stratigraphical observations from the geological mapping and geophysical data. The stratigraphical data were compiled into an outline of a 3D soil depth model of the catchment area of Lake Bolundsfjärden /Vikström, 2005/.

The analyses performed on the overburden comprises physical as well as chemical properties: grain size composition, CaCO₃ content, geochemical analyses of till and sediment, elemental composition in peat and till, clay mineral analyses of till and clay and microfossil analyses of till. In respect of soil type, texture, pH, and carbon and nitrogen contents were analysed for the different horizons in each soil class.

4.2.2 Climate, hydrology and hydrogeology

As the Forsmark model version 0 /SKB, 2002a/ was developed prior to the site investigations in the Forsmark area, it was mainly based on generic and regional (rather than site-specific) data compiled for the Östhammar feasibility study /SKB, 2000a/. Some information was available from drill holes, shafts and tunnels from the construction of the Forsmark nuclear power plant and the underground low and medium active radioactive waste storage facility, SFR. The site-specific investigations that provided the basis for the Forsmark model version 1.1 /SKB, 2004a/ in terms of climate, hydrology and near-surface hydrogeology included a delineation of catchment areas, manual discharge measurements, installation of surface-water level gauges, drilling of boreholes and excavation of pits in Quaternary deposits (QD). In addition, groundwater monitoring wells were installed in QD, and hydraulic (slug) tests were performed in these wells. Local meteorological and hydrological stations were not established before the data freeze for model version 1.1, and there was no time to collect time series of surface water and groundwater levels. Hence, the very limited amount of site-specific data meant that also model version 1.1 was also mainly based on generic and/or regional data.

Between the data freezes for model version 1.1 (April 30, 2003) and model version 1.2 (July 31, 2004), the amount of data from meteorological, hydrological and near-surface hydrogeological investigations has increased considerably. Table 2-7 provides references to site investigations and other reports that contain data used in the version 1.2 modelling. For a detailed presentation and evaluation of the *primary* data, the reader is referred to /Johansson et al. 2005/. In the version 1.2 dataset, local meteorological data are available (from May 2003 to July 2004) from the weather stations Högmasten, situated in the vicinity of the nuclear power plant, and Storskäret, located in the south-eastern part of the regional model area.

Hydrological data include surface-water levels from six lakes and two locations in the Baltic Sea. Moreover, manual discharge measurements have been performed in water courses at eight locations since March 2002. Near-surface hydrogeological data include hydraulic conductivities in Quaternary deposits (QD), measured by means of slug tests in a total of 48 groundwater monitoring wells, pumping tests at two locations (in Börstilåsen and close to lake Bolundsfjärden). Moreover, permeability tests have been performed in six BAT-type filter tips installed in QD. Figure 4-1 shows the locations of these hydraulic tests, as well as the locations of the surface-water level gauges.

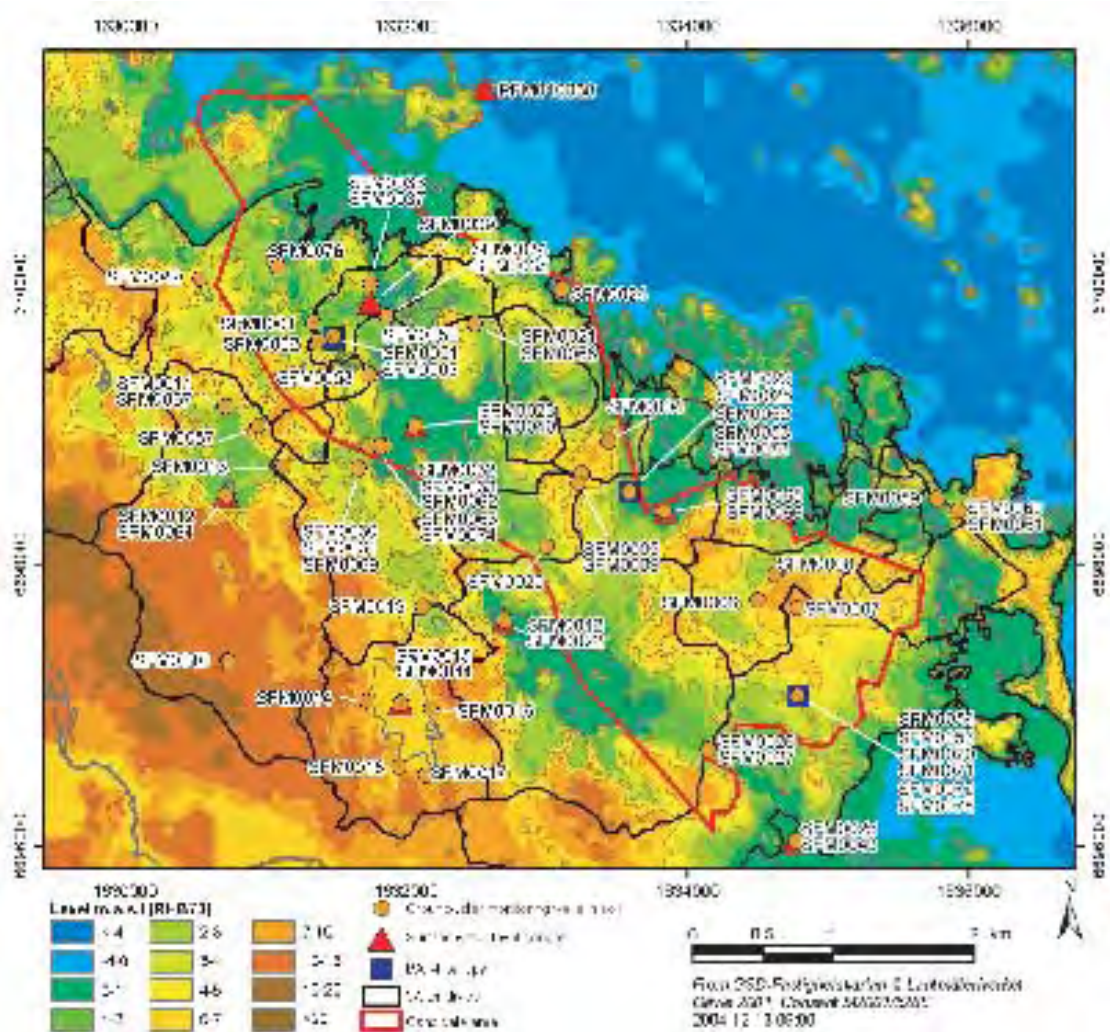


Figure 4-1. Location of groundwater monitoring wells, abstraction wells, BAT-type filter tips and surface water level gauges (SKB-GIS).

The background colours are different altitude classes, obtained from the Digital Elevation Model (DEM) of the regional model area.

Private wells and water prospecting wells in the Forsmark area were investigated by /Ludvigson, 2002/. A total of 40 wells (27 private wells and 13 water prospecting wells) were identified. The investigation included a gathering of basic well data, field checks, and water sampling in 25 of the private wells. For more details, the reader is referred to /Johansson et al. 2005/.

4.2.3 Chemistry

A comprehensive description of the chemical properties in surface ecosystems will include a wide array of parameters (concentration of elements and compounds as well as aggregate measures such as pH and electrical conductivity) and processes, varying both in time and space in several different media. Water is by far the most important medium for transport of elements and matter, and the site investigations concerning chemical properties in the surface system have so far been concentrated on analyses of samples from surface water and near-surface groundwater, and to some extent also on samples from the overburden. The site investigation programme for 2005 is planned to include further analyses of chemical properties of the overburden and also of biota. No new information concerning the chemical composition of wet deposition in the Forsmark area is available for the current version of the site descriptive model.

The results presented in this chapter represent only a part of the total data produced within the programme, and the aim is mainly to give an overall impression and understanding of the site-specific data. The surface water sampling programme is described in detail in /Nilsson et al. 2003/, and an evaluation of surface water data is presented in /Sonesten, 2005/. For the current analysis, all available data at data freeze for model version 1.2 have been included in the analyses, unless stated otherwise.

4.2.4 Biota

Terrestrial producers

The descriptive model contains a large number of components that describe biomass, NPP (Net Primary Production) and turnover of plant tissues. For information about the site specificity of the data, where it is published and some information about the methods used to estimate/calculate results, see /Lindborg, 2005/. The data sources are shown in Table 2-8. A number of conversion factors have been used, and these are described in /Lindborg, 2005/.

Terrestrial consumers

Site-specific data and generic data obtained from different reports are listed in Table 2-8. The other data used, such as weight figures for many species and consumption data, have been gathered from Internet sites, such as Svenska Jägareförbundet (Swedish Association for Hunting and Wildlife Management), Jägarnas Riksförbund (The National Associations of Huntsmen), BBC – Nature wildfacts and the Mammal Society. The production figures have been calculated very simplistically and are therefore associated with considerable uncertainty.

A bird survey has been performed in the Forsmark area, mainly to evaluate the possible effects of the site investigation on the numbers of breeding birds and in some cases also on their breeding success /Green, 2004/. The number of birds registered per kilometre on line transects, as well as numbers of territories in the survey area are provided in /Green, 2004/.

Limnic producers

A total of eight small water systems, which are situated partly or entirely within the site investigation area, have been identified, and the total number of lakes and ponds within these catchments is 25 /Brunberg et al. 2004/. The three largest lakes in the Forsmark area are Lake Bolundsfjärden, Lake Eckarfjärden and Lake Fiskarfjärden. Primary producers in Lake Eckarfjärden have been thoroughly investigated for several years. During 2000–2002, biomass of microbiota was investigated monthly during winter and every second week during summer /Blomqvist et al. 2002/. Production by microbiota was measured during the summer of 2001. During 2002, biomass of zooplankton, benthic fauna and macrophytes, as well as production of microbiota, were investigated /Andersson et al. 2003/. Biomass data for phytoplankton and microphytobenthos from Lake Bolundsfjärden are available for the period August–October 2001 /Franzén, 2002/. No data on primary production are available from Lake Bolundsfjärden. No biomass or production data are available for Lake Fiskarfjärden. The borders between different habitats within the lakes have been determined and dominant species within each habitat identified /Brunberg et al. 2004/.

Site-specific data and generic data obtained from various reports are shown in Table 2-8.

Limnic consumers

During 2002, biomasses of zooplankton and benthic fauna were investigated in Lake Eckarfjärden /Andersson et al. 2003/. Biomasses of bacterioplankton and benthic bacteria were investigated during the period 2000–2002. Bacterial production in the pelagic zone as well as in the top five centimetres of the sediments in Lake Eckarfjärden was measured during 2002. Fish data have been collected from four of the larger lakes in the area (Lake Bolundsfjärden, Lake Eckarfjärden, Lake Fiskarfjärden and Lake Gunnarsbo-Lillfjärden) in August 2003 /Borgiel, 2004/.

Site-specific data and generic data obtained from different reports are shown in Table 2-8.

Marine producers

Phytoplankton have been studied in the area twice, in a recent study performed by /Huononen and Borgiel, 2005/ in Asphällsfjärden, where the biomass was determined on five occasions during 2003 and 2004, and an earlier study by /Lindahl and Wallström, 1980/ in Öregrundsgrepen where both biomass and primary production were measured during 1977 and 1978. The phytoplankton productivity was estimated with the ¹⁴C-method /Steemann-Nielsen, 1952/ and presented as net primary production, NPP, and therefore their respiration was omitted in the further calculations in that study. In the descriptive model presented in this report, the biomass values from the most recent study /Huononen and Borgiel, 2005/ were used whereas the primary production was estimated from the production to biomass relationship found by /Lindahl and Wallström, 1980/ and the biomass by /Huononen and Borgiel, 2005/. Macrophytes comprise both macroalgae and vascular plants and the biomass estimates for this group originate from diving surveys conducted during 1999 /Kautsky et al. 1999/. The microphyte biomass data originate from studies performed in and around the biotest basin off Forsmark nuclear power plant during 1985 and 1986 /Snoeijs, 1985, 1986/.

The site-specific input data used in the descriptive modelling of the primary producers at the site are identified and referenced in Table 2-8.

Marine consumers

Bacterioplankton, benthic meiofauna and microfauna, and seals have not been studied in the area. Generic data for these groups were used. Zooplankton biomass was studied both in a survey by /Eriksson et al. 1977/ and more recently by /Huononen and Borgiel, 2005/. Fish in the Forsmark area were sampled by the National Board of Fisheries (Fiskeriverket) /e.g. Neuman, 1982/. Unfortunately, the results in these surveys were presented as catches per unit effort (e.g. individuals per gill net), which are very difficult to convert to a biomass estimate per unit surface or volume. Also, these types of surveys mainly sample medium to large pelagic fish and cannot estimate the abundance of small sized fish, benthic fish or fish larvae. There is an ongoing survey on fish biomass in the sea in the Forsmark area, which probably can be used in a future version of the model. In this study, fish data from another area were used instead. As for the macrophytes the biomass estimates for grazing macrofauna, filter feeders and other macrofauna originate from diving surveys conducted during 1999 /Kautsky et al. 1999/.

There has been an extensive bird investigation in the terrestrial part of the modelling area /Green, 2003, 2004/ describing e.g. the amount of bird species and territories, abundance of terrestrial birds along transects and in certain areas etc. However, since the abundance of the waterfowl was not estimated, it was difficult to use the presented data in ecosystem modelling.

The site-specific input data used in the descriptive modelling of the consumers at the site are identified and referenced in Table 2-8.

4.2.5 Humans and land use

In order to arrive at a justified description of the human population and human activities in the model area, a wide range of different human-related statistics were acquired from SCB (Statistics Sweden). These statistics include data and times series on demography, labour, health situation, land use, agriculture etc. Beside this, some additional information was searched for and acquired from other sources, such as Fiskeriverket (the National Board of Fisheries), Jägareförbundet (the Swedish Association for Hunting and Wildlife Management) and Länsstyrelsen (the County Administrative Board). A comprehensive presentation of the data and results is given in /Miliander et al. 2004/.

4.3 Model of the overburden including Quaternary deposits

4.3.1 Background

The regolith, also referred to as the overburden, includes all unconsolidated Quaternary deposits, both glacial deposits such as till, glaciofluvial sediment and clay, as well as postglacial deposits such as marine and lacustrine sediment and peat. The upper part of the overburden, affected by soil-forming processes, is referred to as *the soil*.

All known Quaternary deposits in the Forsmark area were formed during or after the latest glaciation. The oldest deposits are of glacial origin, deposited directly from the inland ice, or by water from the melting ice. The whole area is located far below (> 120 m) the highest coastline, thus the area has been located under the sea during the major part of the Holocene (see Section 3.2 in the historical description). Fine-grained sediment has been deposited in local depressions such as the bottom of the lakes and on the present sea floor. Wave action and currents have partly eroded the upper surface of the overburden. Isostatic uplift at Forsmark is still ongoing (6 mm/year) resulting in new land areas emerging from the Baltic. The most notable change in the areas uplifted from the Baltic is the development of organic soils, for example the sedimentation of gyttja in the lakes and the formation of peat in the wetlands. The minerogenic Quaternary deposits are affected by coastal and soil-forming processes at the surface, but no major redistribution of these deposits has occurred after the area has been isolated from the Baltic. For a complete description of the present knowledge of the Quaternary deposits in the Forsmark area, see /Lindborg, 2005/.

4.3.2 The surface and stratigraphy of Quaternary deposits

The ground surface of the Forsmark area is flat, dominated by glacial till. Unconsolidated Quaternary deposits cover c. 85% of the land area in the regional model area and artificial fill, c. 3%. Exposed bedrock occupies c. 13% of the land area in the regional model area and only 5% in the central part of the model area (see Table 4-1). Glacial striae occur frequently on the bedrock outcrops, a majority formed from the north (350–360°), but an older system from the northwest has also been observed.

Glacial till is the oldest known Quaternary deposit in the Forsmark area, deposited directly from the inland ice. The distribution of till in Forsmark is characterised by heterogeneity, in textural composition as well as spatial distribution. The complex composition of the till types makes some generalisations necessary. Based on the composition of the surface layer, three till areas have been distinguished /Sohlenius et al. 2004/. The major part, especially in the west and south, of the model area is dominated by sandy till with medium boulder frequency. At Storskäret and on the island of Gräsö, clayey till with low boulder frequency dominates (see Figure 4-2). At Storskäret, the clayey till is used as arable land and the frequency of bedrock outcrops is generally low. The hydraulic properties, described in Table 4-3 in the hydrology section, refer to the sandy till (coarse) and clayey till (fine-grained). In the area close to the Börstilåsen esker, the till is characterised by a high frequency of large boulders.

Table 4-1. Aerial coverage of the different types of Quaternary deposits and bare bedrock in the different sub-areas. For the land areas, the till is subdivided into sandy and clayey. The first column includes the regional model area and the calculations are based both on the detailed mapping performed within the site investigations and the initial geological map from /Persson, 1985, 1986/. The second column is based solely on the detailed mapping (Figure 4-2), and the third column is based on the marine geological mapping, (Figure 4-3).

	Forsmark land, total	Forsmark land, detailed	Forsmark sea
Bedrock exposures	13	5	6
Glacial clay	4	4	41
Post-glacial clay (including gyttja clay and gyttja)	4	4	17
Post-glacial sand and gravel	2	4	2
Post-glacial fine sand	–	–	4
Till	65 (58/7)	74 (63/11)	30
Glaciofluvial sediment	1	2	0
Peat	8	3	–
Artificial fill	3	4	–

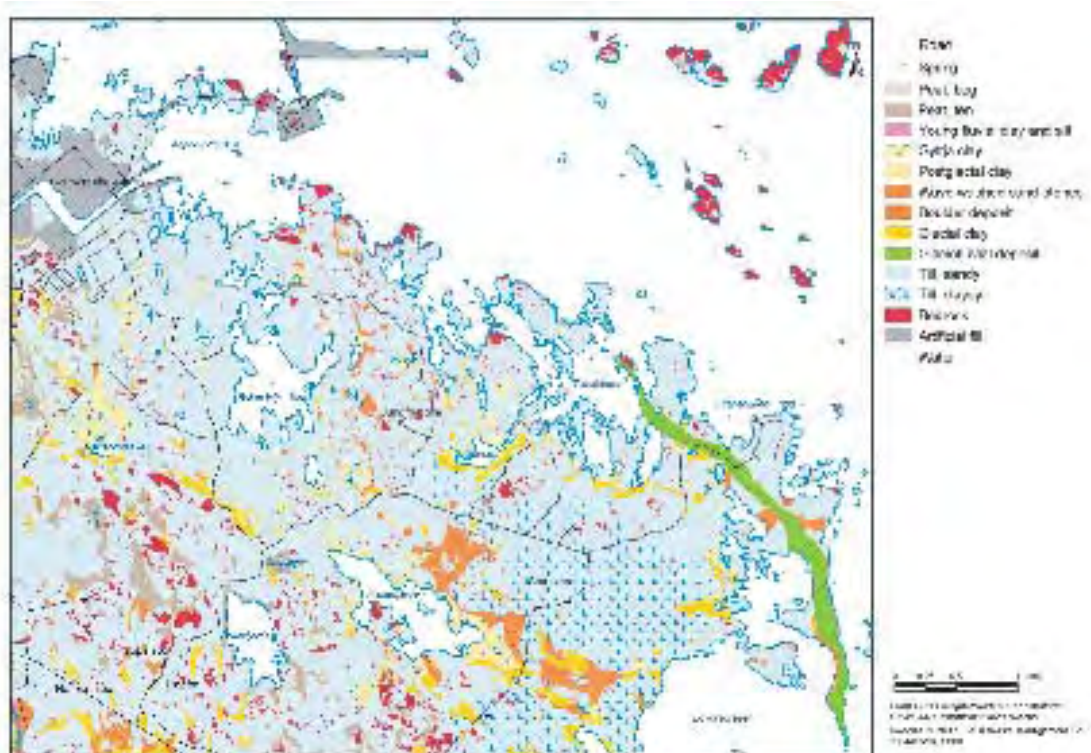


Figure 4-2. Map showing the spatial distribution of Quaternary deposits in the central part of the Forsmark regional model area, from /Sohlenius et al. 2004/.

The stratigraphical investigations confirm the general pattern of the distribution of the different till types. However, the stratigraphic relations between the different units are complex and have not been fully understood. One example of a complex till stratigraphy is located north of Lake Gällsboträsket. A dark clayey till was revealed under a 1.9 m deep layer of sandy-silty till /Sundh et al. 2004/. The most striking feature about the dark clayey till is the extreme degree of consolidation. Pollen analysis was performed in order to give information on the age of the dark clayey till /Robertsson, 2004/. Re-deposited pollen grains observed in the dark clayey till showed an interglacial composition known from Eemian deposits. The pollen composition gives the maximum age of deposition of the unit to be post Eemian, i.e. some time during the Weichselian glaciation.

The thickness of the Quaternary deposits, as observed in corings, varies between 0 and 17 m within the investigated area /e.g. Johansson, 2003/. The depth to bedrock is generally greater in the area covered by clayey till. In the north-western part of the investigated area, the depth to bedrock is generally between 4 and 8 m in the corings performed /Johansson, 2003/. Close to drill site 1, the thickness of the till varies between 12 and 4 m although the upper surface of the overburden is quite flat. These variations in depth to bedrock support the concept of a small-scale undulating upper surface of the bedrock, and Quaternary cover that fills out the depressions. Another example of this was observed at the nearby located drill site 5, where a small-scale undulating, fractured bedrock was revealed at excavation.

Glaciofluvial sediments are deposited in a small esker, the Börstilåsen esker, with a flat crest reaching c. 5 m above the present sea level. Drilling at the crest (SFM0060) showed c. 7 m of glaciofluvial sediments (gravel) that rested directly on the bedrock /Werner et al. 2004/. Open sections from abandoned small gravelpits also contain coarse, well-sorted sediment consisting of gravel and stones.

After the deglaciation, c. 10,800 years ago, the water level was c. 150 m higher than at present. The distal glaciofluvial sediments, which consist of glacial clay, deposited in stagnant water at some distance from the retreating inland ice, are concentrated in local depressions such as the bottom of lakes and small ponds. Small areas with glacial clay were frequently found during the geological mapping. These deposits are often only a few dm thick and are probably remnants after erosion.

Large areas of glacial clay associated with lakes or wetland are situated e.g. south east of Lake Fiskarfjärden and south of Lillfjärden (see Figure 4-2). At these localities, the uppermost surface is often covered by organic sediment.

Postglacial sediments were eroded and re-deposited by waves and streams during the last c. 10,000 years. Clay, gyttja clay, sand and peat occur frequently as the superficial Quaternary deposits and cover many small (less than 50×50 m) areas (see Figure 4-2). These small deposits are frequent, but cover only a small part of the total area under investigation (see Table 4-1). Larger areas of postglacial sediment are e.g. gyttja clay along the shore of Lake Fiskarfjärden and Lake Gällsboträsket. Peat accumulations are restricted to the south-western part of the investigated area, corresponding to the most elevated part of the area that has been situated above the sea level for long enough for peat to form. The wetlands in the north-eastern part of the map may have peat cover of < 0.5 m and have therefore not been marked as peat on the geological map.

4.3.3 Lake sediment and peat

The marine and lacustrine sediments in the Forsmark region are fairly uniform within each broad landscape element. A generalised outline of sediment types, together with some chemical characteristics of the investigated sediments at Forsmark, is presented in Table 4-2. It should be noted that not all strata were present at every basin. In a majority of the lakes investigated, the total thickness of the sediments (not including glacial till) was less than 2 m and only two lakes contained sediments thicker than 4.5 m.

The sediment in Lake Eckarfjärden has been subject to detailed stratigraphical investigations in order to reconstruct the shore displacement in northern Uppland /Hedenström and Risberg, 2003/. A continuous layer of glacial clay covers the till. A sand layer, representing the end of a hiatus overlies the clay. The isolation of Lake Eckarfjärden has been dated at c. 850 cal years BP, recorded approximately at the transition between clay gyttja and gyttja. After the isolation, algal gyttja and calcareous gyttja have been deposited in the freshwater lake. The sediment sequence in Lake Eckarfjärden is consistent with the schematic profile shown in Figure 4-6 in the hydrology section.

Another typical example of sedimentary sequence is represented in Lake Bolundsfjärden. The sediment is generally less than two metres thick with sediment focusing in the central part of the lake. The sequence starts with a thin layer of sand covered by gyttja clay and gyttja /Hedenström, 2004/. Probably, the erosion has been more effective in this basin compared with e.g. Eckarfjärden since there is almost no protection from wave activity from the north.

Peat covers c. 3% of the central part of the Forsmark area (see Table 4-1). One example is the peat formation in the Stenrösmossen mire /Fredriksson, 2004/. Stenrösmossen is a shallow minerotrophic mire of fen type, formed after isolation from the Baltic at approximately 1,500 years ago. Stratigraphical investigations showed a thin gyttja layer, resting directly on till in the bottom of the mire. A thin layer of *Phragmites* peat with *Equisetum* remnants overlies the gyttja. Further up, *Carex* peat and at the top *Carex-Sphagnum* peat represents a typical succession of an infilling of a shallow pond and the succession into a mire. The pH in the surface water is between 5 and 6 in the nutrient poor, central part. In the south-western part, the mire vegetation is more nutrient demanding and the pH in the surface water is between 6 and 7, indicating contact with the nutrient-rich groundwater from the surrounding mineral soil.

Table 4-2. The general types of marine and lacustrine sediments in lakes in Forsmark, based on data from /Hedenström, 2004/. The average contents of C, N and S in glacial clay and algal gyttja have been calculated (algal gyttja n=27, clay gyttja n=14). Note that not all lakes yielded a complete sedimentary sequence.

Environment	Lithology		C	N	S
Freshwater lake	Calcareous gyttja	Youngest			
Freshwater lake and coastal lagoons	Algal gyttja		14.0	1.3	1.9
Postglacial Baltic Basin	Clay gyttja	↑	4.7	0.6	1.6
Shallow coast	Sand and gravel				
Postglacial Baltic Basin	Postglacial clay	↑			
Late glacial Baltic Basin	Glacial clay	Oldest			

4.3.4 Offshore Quaternary deposits

Compared with the map of Quaternary deposits on land areas, the sea floor is to a larger extent covered by sediments (see Figure 4-3). Offshore Quaternary deposits are dominated by glacial and post-glacial clay, together covering c. 55% of the sea floor (see Table 4-1). The clay in this area occurs most conspicuously in a narrow belt, which trends in NNW and N-S directions. /Carlsson et al. 1985/ have speculated that the occurrence of clay may be linked, in some cases, to fracture zones in the bedrock. The thickness of the offshore Quaternary deposits varies considerably from < 2.5 m to > 10 m /Carlsson et al. 1985/. In the area above SFR, till varies in thickness between

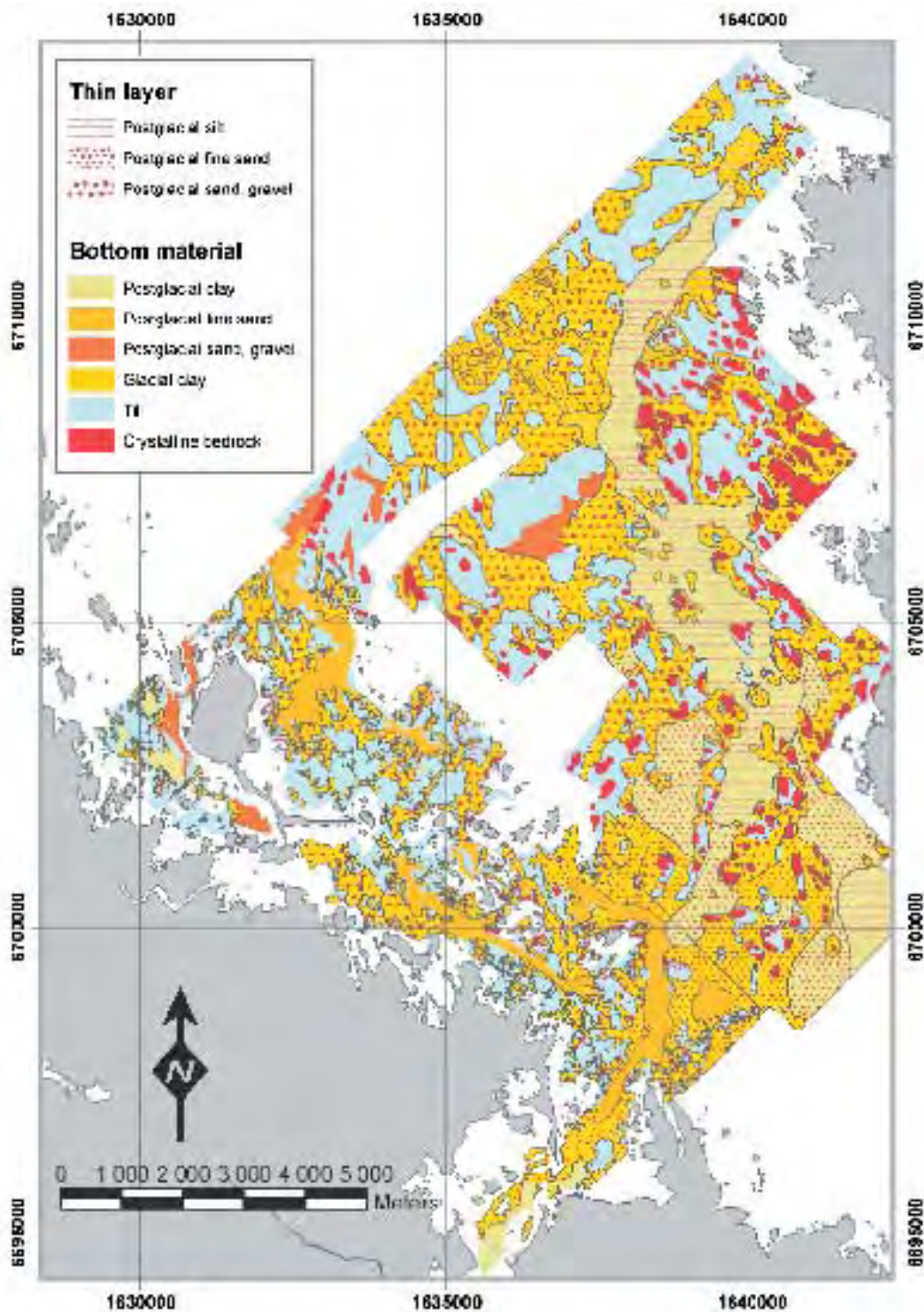


Figure 4-3. Map showing the distribution of Quaternary deposits on the sea floor /Elhammer et al. 2005/.

4 and 14 m and clay between 0 and 4 m. In the next model version, analyses from the detailed marine geological investigations offshore of Forsmark will provide the sediment depth on the sea floor. The area covered by glacial till on land is c. 75% but only c. 30% on the bottom of the Sea. The discrepancy is partly the result of erosion and re-deposition of fine-grained material, e.g. postglacial clay, in the deeper parts still situated below sea level. The discrepancy may also, to some extent, be caused by the different methods used in the mapping.

4.3.5 Chemical composition of the Quaternary deposits

The glacial till in the Forsmark area is characterised by its high content of calcium carbonate. The calcite originates from Ordovician limestone present at the sea bottom north of the Forsmark area. The tills with a clay content higher than 5% have a slightly higher content of calcite (average content 24%, n=84) in the fine fraction (grain sizes < 63 µm) compared with the sandy till (average content 18%, n=52). Results from the quantitative XRD analyses show small variations in the contents of most silicate minerals in the till. The samples contain almost 40% of quartz, which is similar to most of the bedrock in the investigated area. The results show that the chemical and mineralogical compositions of the till mainly reflect those of the local bedrock. The high CaCO₃ content of the till shows, however, that one fraction of the till has been transported several tens of kilometres.

The carbonate content in groundwater in Forsmark is high due to chemical weathering of calcite from the soils. When calcite precipitates and accumulates in the sediments, calcareous gyttja and lake marl forms for example in Lake Eckarfjärden and Lake Stocksjön. The highest calcite content (> 60%) in lacustrine sediment was recorded at Lake Stocksjön /Hedenström, 2004/.

4.3.6 The soil types

The soils in the Forsmark area are typically poorly developed soil types on till or sedimentary parent material influenced by calcareous material /Lundin et al. 2004/. The poor soil development is a result of young age; since most of the candidate area emerged from the sea during the last 1,500 years. The calcareous soil material has yielded nutrient-rich conditions, which can be observed in the rich and diverse flora of the area. This can also be seen in the predominant humus forms of mull type and of the intermediate moder type, which indicate a rich soil fauna. Because of the young age of the soils, the Forsmark area exhibits less soil of the Podsol type than most similar areas in Sweden. Instead, the typical soil types are the less developed Regosols, together with Gleysols and Histosols, which are formed under moist conditions (see Figure 4-4).

4.3.7 Soil depth model

One way of visualising the spatial variations in the thickness of the Quaternary cover is the compilation of a depth model /Vikström, 2005/. The program used in the modelling of soil depths is the GeoEditor, which is an ArcView 3.3-extension. GeoEditor is compatible with other modelling tools such as the catchment-scale hydrological model MIKE SHE.

In Figure 4-5, the calculated depth to bedrock is displayed. In the areas with low data density, the average soil depth from the data imported to the model was used (1.9 m). The basis for this calculation is the input data used in the Geo Editor modelling after excluding the bedrock outcrops, where the soil depth is 0.

The deepest till cover (13 m) recorded within the modelled area was observed north of Lake Stocksjön. This site is situated within a zone striking NW-SE, where there are relatively few bedrock outcrops. This zone continues towards the southeast to the Lake Fiskarfjärden basin. The deepest total cover noted in the Forsmark area is located along this zone at the outlet from Lake Fiskarfjärden (SFM0026). The depth to bedrock was approximately 16 m, with a cover consisting mainly of clay and till /Johansson, 2003/. This site, however, is situated outside the area modelled for soil depth. Although outside the model area, it is also evident that thick Quaternary deposits cover the eastern area of Storskäret.

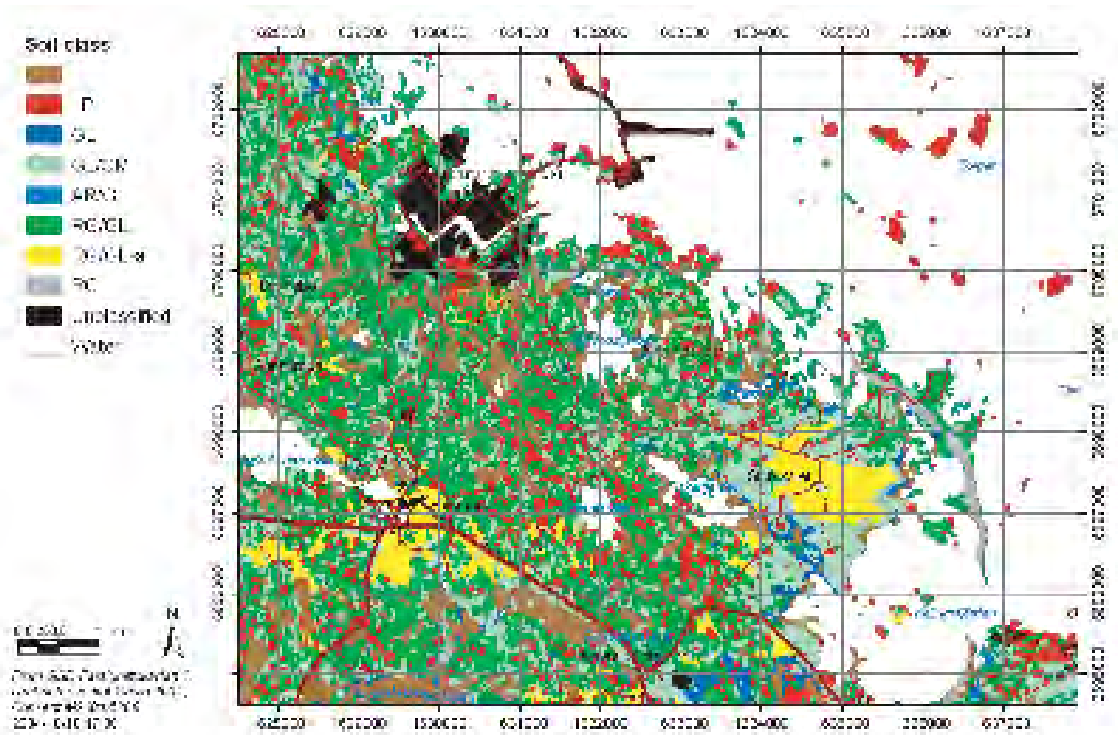


Figure 4-4. Map showing the spatial distribution of the soil types in the Forsmark regional model area /Lundin et al. 2004/ (HI: Histosol, LP: Leptosol, GL: Gleysol, GL/CM: Gleysol/Cambisol, AR/GL: Arenosol/Gleysol, RG/GL: Regosol/Gleysol, RG/GL-a: Regosol/Gleysol, arable land, RG: Regosol).

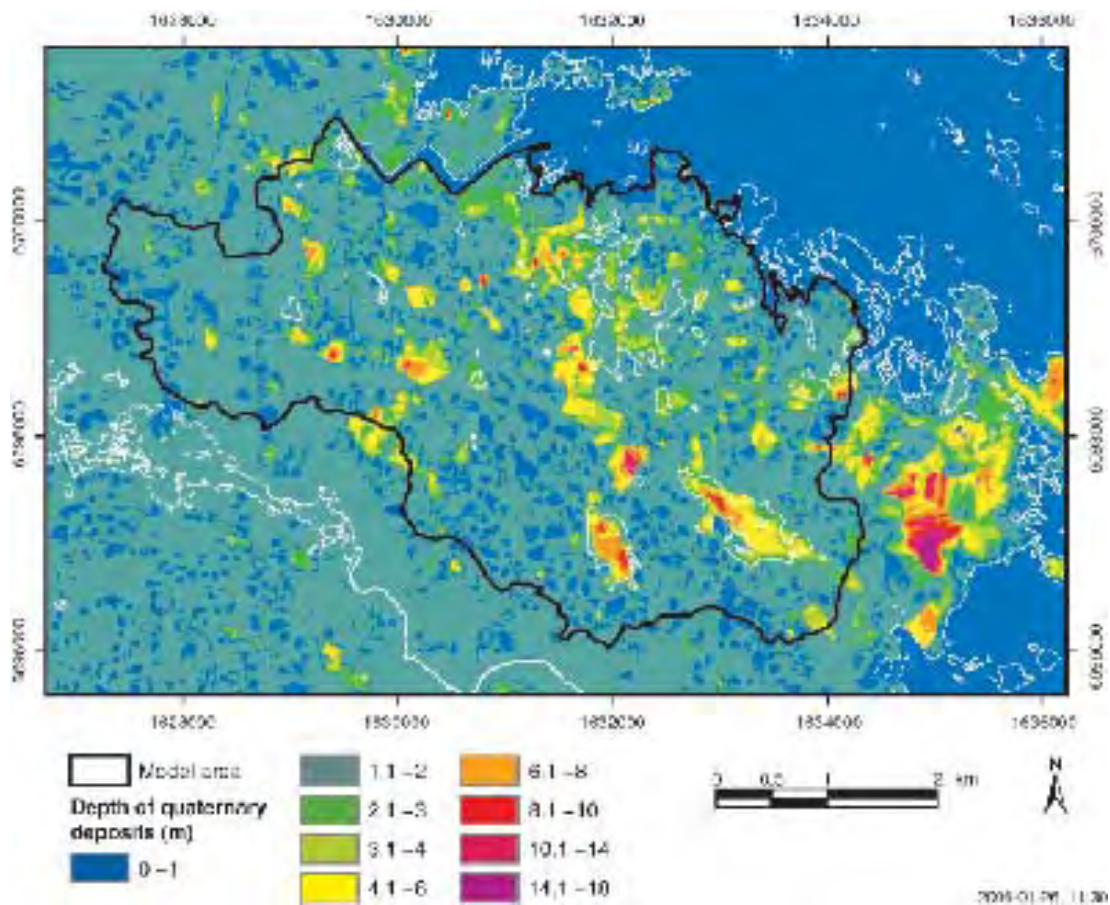


Figure 4-5. Map showing the depth to bedrock, based on the soil depth modelling in Geo Editor. The model is valid for the area within the black solid line, corresponding to the catchment area for Lake Bolundsfjärden.

The small-scale bedrock topography in the area close to drill site 1 can be seen as a deep soil cover north west of Lake Bolundsfjärden. The data density around Lake Eckarfjärden and Bolundsfjärden is sufficient for the model. The depth data from Lake Fiskarfjärden, however, should be regarded as minimum values since the model is based on lake sediment corings, but only a single coring within the till and no geophysical data have been available. New seismic profiles and updated depths calculated from seismic profiles will be available for the next model version, as well as interpretations of depth from air-borne geophysical investigations. The next model version will aim at including also the sediment depth on the sea floor.

4.4 Description of climate, hydrology and hydrogeology

4.4.1 Conceptual and descriptive modelling

The conceptual and descriptive modelling of the meteorological, surface hydrological and near-surface hydrogeological conditions in the Forsmark area is presented in /Johansson et al. 2005/. The model area is characterised by a low relief and a small-scale topography; almost the whole area is located below 20 metres above sea level. The corrected mean annual precipitation is 600–650 mm and the mean annual evapotranspiration can be estimated to a little more than 400 mm, leaving approximately 200 mm/year for runoff. In total, 25 “lake-centered” catchments, ranging in size from 0.03 to 8.67 km² have been delineated and described within the model area. The 25 mapped lakes range in size from 0.006 to 0.752 km². The lakes are very shallow with maximum depths ranging from 0.4 to 2.0 m. No major watercourses flow through the model area. Wetlands are frequent and cover 10–20% of the areas of the three major catchments, and up to 25–35% of some sub-catchments. The conceptual model of the near-surface hydrogeological conditions is illustrated in Figure 4-6. In the version 1.2 modelling, the HSDs (Hydraulic Soil Domains, in QD) are assigned hydraulic properties (hydraulic conductivity, and total and effective porosity) according to Table 4-3.

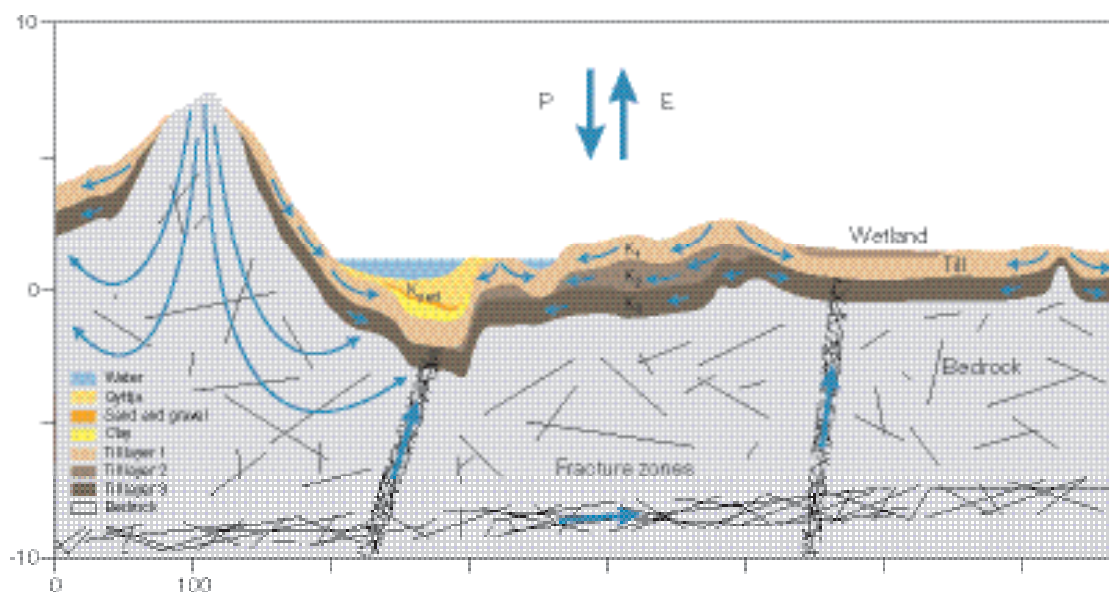


Figure 4-6. Schematic profile illustrating a conceptual model of the near-surface hydrogeological conditions (note that horizontal and vertical scales are different).

Table 4-3. Proposed mean values of horizontal saturated hydraulic conductivity, porosity and effective porosity for a simplified 3-layer till profile.

Layer	Horizontal saturated hydraulic conductivity (m/s)	Porosity (%)	Effective porosity (%)
0 to 1 m below ground	1.5×10^{-5}	35	15
Middle layer			
Coarse till	1.5×10^{-6}	25	5
Fine-grained till	1.5×10^{-7}		3
0 to 1 m above bedrock	1.5×10^{-5}	25	5

4.4.2 Some observations from quantitative flow modelling

In order to provide input to the ecological system modelling, the hydrology extension in ArcGIS 8.3 was used to calculate flow directions and mean discharges in the regional model area, based on topographical information (DEM) and regional data on the specific discharge. The MIKE SHE modelling tool (MIKE SHE User guide, DHI Water and Environment, DHI Software 2003) was used for detailed process modelling of near-surface groundwater flow and surface water flow within a modelling area covering most of the land area within the regional model boundaries.

The water balance for the Forsmark area, as calculated with the MIKE SHE modelling tool using regional meteorological data, agrees with the presented conceptual and descriptive models of the flow system. The transient model simulations for the selected reference year (1989) result in an annual total runoff of 226 mm and a total evapotranspiration of 441 mm. These values, which are average values for the considered model area, are considered to be reasonable for the Forsmark area. At present, however, they cannot be tested against site-specific measurements.

The results of the GIS modelling showed that there were only small differences between the model-calculated and the field-controlled /Brunberg et al. 2004/ water divides in most of the model area. However, the GIS modelling also illustrated the importance of incorporating ditches, diverted water courses and other man-made structures in some catchment areas, and that the flat topography in the model area implies that the results could be sensitive to the representation of such objects in the model.

Another important model application is the identification of recharge and discharge areas. Figure 4-7 shows the distribution of these areas within the regional model area, as calculated by the ArcGIS model of the Forsmark area /Johansson et al. 2005/. The results show that the detailed locations of recharge and discharge areas are strongly influenced by the local topography, which creates a small-scale recharge-discharge pattern. Areas of colours other than blue and red in Figure 4-7 are “intermediate areas”, i.e. neither recharge nor discharge areas. It should be noted that the spatial extents of recharge areas, “intermediate areas” and discharge areas depend on definitions made by the modeller. In this case, recharge areas were defined such that their extent represented a minimum at the used $10 \times 10 \text{ m}^2$ grid resolution, i.e. they consisted of cells without any upstream cells that provided inflow, whereas areas receiving water from an upstream area larger than 0.05 km^2 were defined as discharge areas.

The MIKE SHE model has been applied to calculate transient groundwater and surface water flows in the regional model area. Hence, the model takes into account temporally variable meteorological parameters (e.g., precipitation, snow melt and temperature). Figure 4-8 shows “snapshots” of the distribution of recharge and discharge areas during a wet (left) and a dry (right) period. The distribution of permanent recharge (high altitude) areas and permanent discharge areas depends on the topography. However, in “intermediate” areas, the results show that the actual extent of recharge and discharge areas varies during the year, due to the temporal variability in meteorological conditions.

In the flow modelling reported by /Johansson et al. 2005/, near-surface groundwater levels and the hydrogeological interactions between QD and fractured rock were also investigated. Particle-tracking simulations, in which particles were introduced in the rock at a depth of 150 m, were also performed. For the aspects of the model that were tested, it was found that the quantitative modelling provided evidence supporting the descriptive model of the site. However, this support should be regarded as merely qualitative, since no calibration exercises or other quantitative comparisons with field data were carried out.



Figure 4-7. Identification of recharge and discharge areas using a GIS model. Areas with colours other than blue and red are “intermediate areas”, i.e. neither recharge nor discharge areas based on the definitions of those in the modelling (see text).

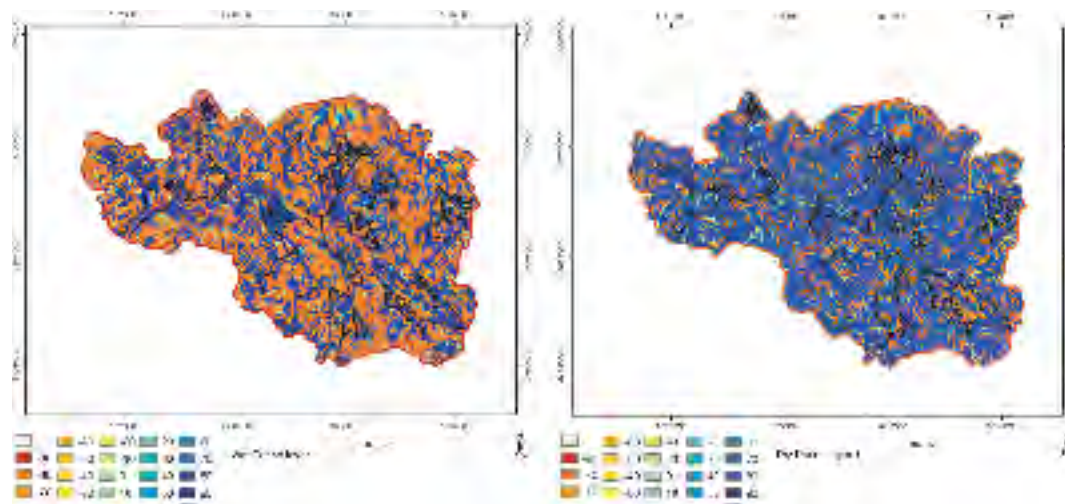


Figure 4-8. Examples of results from detailed process modelling of the regional model area, illustrating the calculated distribution of recharge and discharge areas during a wet (left) and a dry (right) period. The colours represent different classes in terms of the angle between the groundwater flow velocity vector in the xy -plane and the velocity component in the z -direction. Discharge areas (upward flow) are defined as areas where the resulting angle is from -90° to -45° , whereas the angle in recharge areas (downward flow) is in the interval $+45^\circ$ to $+90^\circ$. Areas with a flow vector angle between -45 to $+45^\circ$ are “intermediate” areas, with predominantly horizontal flow.

4.5 Chemistry

4.5.1 Methodology

Data on surface water chemistry have been collected biweekly to monthly from March 2002, and the sampling programme includes 8 stream, 6 lake and 3 sea sampling sites (Figure 4-9). Data on near-surface groundwater have been collected from a total of 41 wells (shallow boreholes, see Figure 4-1). The wells are sampled 4 times per year, and at the time for data-freeze 1.2, most of the wells have been sampled on more than one sampling occasion. Analysed parameters include, for most samples, major cations and anions, nutrients, organic compounds and O₂. Water temperature, pH, conductivity, salinity and turbidity were determined in the field. Moreover, trace elements and stable and radiogenic isotopes were analysed on 1–4 sampling occasions per year. For a more detailed description of the chemical parameters analysed in the site investigation programme, see /Nilsson, 2003a,b/.

Results from chemical investigations of the overburden are presented in Section 4.3.5 and a comprehensive account of the chemical characteristics of the overburden is given in /Lindborg, 2005/. Data on the water chemistry of precipitation have regularly been collected from one sampling location; however, no evaluation of the chemical composition of the precipitation has yet been performed. No data on the chemistry of biota have so far been collected in the site investigations.

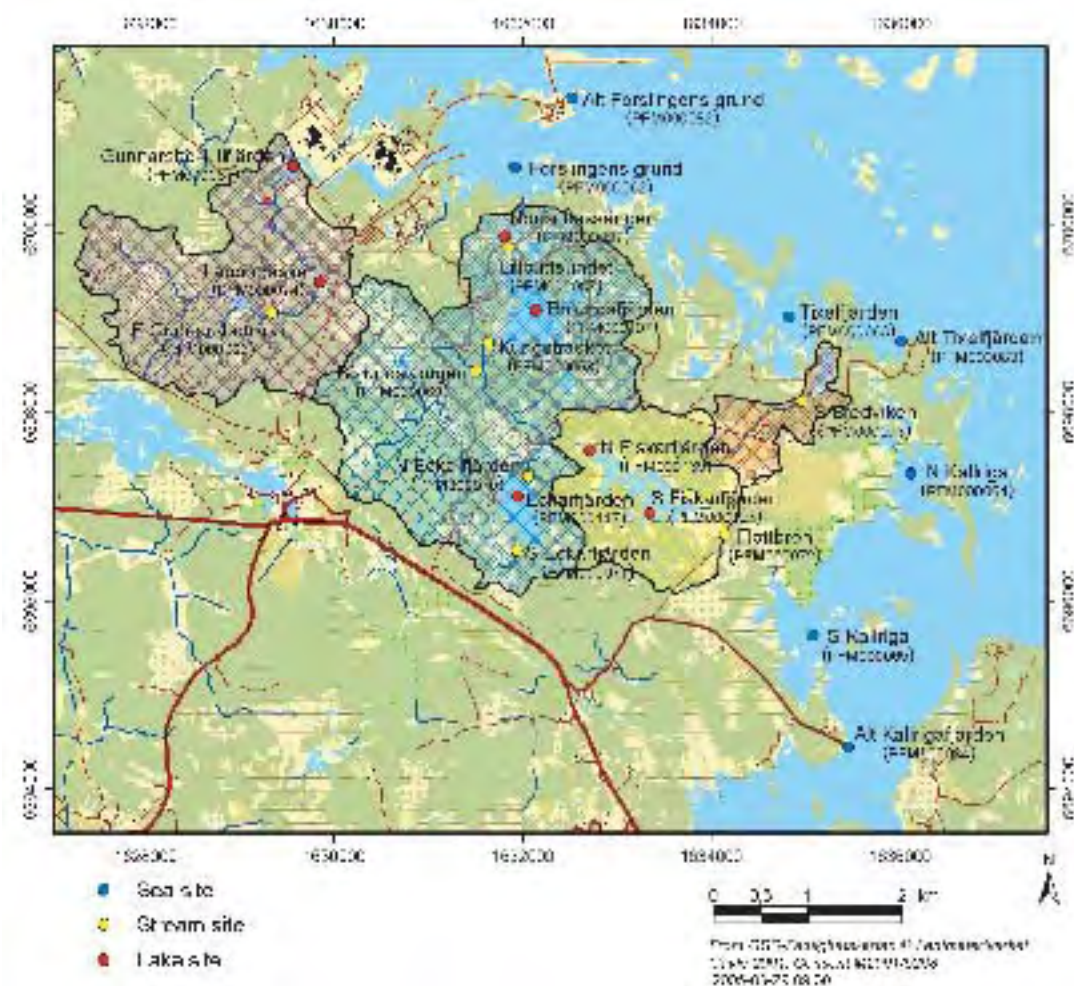


Figure 4-9. Location of sampling sites for surface water in lakes, streams and sea in the Forsmark area.

4.5.2 Description and conceptual model

Surface water

The lakes and streams in the Forsmark model area are, similar to most surface waters in the north-eastern parts of Uppland, characterised by high pH, high concentrations of major ions and high electrical conductivity. As mentioned above, this is a combined effect of the calcium rich deposits in the area and of the recent emergence of the area from the Baltic Sea. Due to both chemically and biologically induced processes in the lake water, the amount of phosphorus transported to the lake is effectively reduced by precipitation of calcium-rich particulate matter. Because of this, the P concentration in lakes and streams is generally low. The nitrogen concentration, on the other hand, tends to be high, or even very high, due to a combination of high input and low biotic utilisation /Brunberg and Blomqvist, 1999, 2000/. Taken together, these conditions give rise to a unique type of lake in the Forsmark area, the oligotrophic hardwater lake.

Two of the sampling sites in the sea are situated close to the open sea, which means that these sites show similar and relatively constant chemical conditions. The third site is situated in the shallow bay Kallrigafjärden, which is strongly influenced by the outflow of two rivers entering the bay. The chemical conditions at this site are therefore much more variable, depending on the mixing between the ion-rich brackish water and the ion-poor, nutrient-rich freshwater from the two rivers. Generally, the chemical conditions in both the fresh and marine surface waters in the Forsmark area are relatively unaffected by anthropogenic influence.

Many of the investigated chemical parameters show pronounced seasonal variations, coupled either to the production and degradation of organic matter, or to seasonal changes in the amount or composition of inflowing water. The production of organic matter directly affects the availability of substances needed for primary production, e.g. phosphate, nitrate, ammonium and silica. An indirect effect of primary production in the Forsmark lakes is the biogenic precipitation of calcite, caused by increased pH during periods of high primary production, which gives rise to predictable variations of Ca and P concentrations in lake water.

Several of the Forsmark lakes are still not completely isolated from the Baltic Sea because of the small altitude differences in the area. The lakes Norra Bassängen and Bolundsfjärden are both strongly affected by episodic intrusions of brackish water, and there have also been indications on intruding brackish water in Lake Fiskarfjärden during the site investigations. For a comprehensive compilation of surface water chemistry data in the Forsmark area, the reader is referred to /Lindborg, 2005/.

Near-surface groundwater

The groundwater in northern Uppland is, similar to the surface waters, characterised by relatively high pH and high Ca concentrations /Naturvårdsverket, 1999/. This is an effect of the high calcite content in many Quaternary deposits in the area. The Cl concentrations are also higher than the average concentration in Sweden, an effect of relict brackish water, which remains since the area was covered by seawater. Median concentrations of Ca, Mg and especially Cl and HCO₃ in the Forsmark area are, however, even above the median values for Uppland (see Table 4-4).

There are two main factors which determine the characteristic chemical composition of the groundwater in the Forsmark region. The first factor is the occurrence of relict saline water, which remains since the sea covered the area. The lowest topographical areas were quite recently covered by the sea, which explains the high concentrations of e.g. Cl in some of the wells. The most saline groundwater is found in Quaternary deposits below lakes, wetlands and bays. Interestingly, the highest concentration of Cl in groundwater in the area (3.9 gL⁻¹), noted below Lake Bolundsfjärden, is higher than the Cl concentration in the present Baltic (Bothnian) Sea (2.6 gL⁻¹). The reason for this high salinity has to be elucidated in coming model versions. Generally, the groundwater salinity in the area will probably decrease with time as the area is further uplifted.

The second factor affecting the chemical characteristics is the occurrence of CaCO₃ in most of the Quaternary deposits, which causes a high pH and high concentrations of Ca and HCO₃. Weathering processes are now slowly dissolving the calcite. These processes have not been active for a long period since the area recently was covered by water. Studies from higher altitudes west of Forsmark

Table 4-4. Compilation of the chemical characteristics of groundwater from 37 monitoring wells in the Forsmark area. Median values for some elements in groundwater in till and wave washed sediments > 4 m from northern Uppland are shown in the right column /Naturvårdsverket, 1999/.

	Average	Median	Max	Min	N	Median Uppl.
Na (mg/l)	230	32.3	1,596	5.76	37	
Ca (mg/l)	131	110	541	29.0	37	89 (Ca+Mg)
Mg (mg/l)	29.7	11.7	177	4.40	37	
K (mg/l)	12.8	8.22	64.9	1.82	37	
HCO ₃ (mg/l)	376	378	721	150	37	180
Cl (mg/l)	437	50.9	3,894	5.1	36	21
SO ₄ (mg/l)	86.4	48.7	359	1.04	36	40
Si (mg/l)	5.73	5.43	9.89	3.30	37	
Mn (mg/l)	0.261	0.20	0.990	0.023	21	0.03
Li (mg/l)	0.016	0.011	0.116	0 (below detection limit)	33	
Sr (mg/l)	0.590	0.233	3.90	0.080	37	
Cond. (mS/m)	305	90.0	2,250	51.6	24	
pH	7.31	7.26	7.83	6.65	24	7.4

have shown that the CaCO₃ has been dissolved in the uppermost metres of the till /Ingmar and Moreborg, 1976/. In the future, the chemistry of the groundwater will probably change (e.g. lower pH and alkalinity) as the calcite content in the Quaternary deposits decreases.

4.6 Biota

4.6.1 Terrestrial producers

Description

The vegetation is strongly influenced by the characteristics of the bedrock and the Quaternary deposits, and by human land management. The bedrock mainly consists of granites, but outcrop is not a major substrate, making pine forest on acid rocks quite scarce. The Quaternary deposits are mainly wave-washed till, typically covered with conifer forests. Scotch pine (*Pinus sylvestris*) and Norway spruce (*Picea abies*) dominate the forests. In depressions, a deeper regolith layer is found typically with fairly high lime content. The lime influence is typical for the northeast of Uppland and is manifested in the flora. The field layer is characterised by herbs and broad-leaved grasses along with a number of orchid species. The Forsmark area has had a long history of forestry and this is also seen today as a fairly high percentage of younger and older clear-cuts in the landscape. The spatial distribution of different vegetation types is presented by /Boresjö Bronge and Wester, 2002/.

Species composition and red-listed species

The flora in this region has been investigated within the project “Upplands Flora” /Aronsson, 1993/. The Hållnäs parish north of Forsmark has been thoroughly investigated /Jonsell and Jonsell, 1995/ and is very similar to the Forsmark region. The flora has also been investigated within the “National survey of forest soil and vegetation” in 36 sample plots in the area. Moreover, an additional 38 sample plots were located within the area using the same methodology for taxa identification as under the “National survey of forest soil and vegetation” /Abrahamsson, 2003/. This was made to get a more even distribution of future monitoring opportunities. All information concerning red-listed plants from the site has been obtained from the Swedish Species Information Centre (sw. Artdatabanken) and is presented in /Kyläkorpi, 2005/ and /Berggren and Kyläkorpi, 2002/.

Protected areas

A number of sensitive areas of conservation interest are located within the site. Some areas have extensive protection whereas others so far are unprotected, but for several of them protection strategies are under planning. These areas are listed in /Kyläkorpi, 2005/. There are today two areas that are legally protected as nature reserves. These are Kallrigafjärden and part of Skaten-Rångsen.

Woodland key habitats

Woodland key habitats are areas where red-listed animals and plants exist or could be expected to exist /Nitare and Norén, 1992/. A nationwide survey of these habitats has been conducted in Sweden, administrated by the Swedish Board of Forestry /SBF, 1999/. As a complement to this survey, SKB initiated a more in depth survey at the site. A total of 31 habitats were identified with a total area of 100 ha /Eklund, 2004/. The dominating key habitat type in the area, both in number of objects and in total area, is conifer forests, representing approximately 70% of the different woodland key habitat types.

Wetlands

The wetlands in the Forsmark area are characterised by moderately to extreme rich fens /Jonsell and Jonsell, 1995/, due to a high calcareous influence. However, bogs are also present at higher locations.

Descriptive biomass and NPP models – introduction

The vegetation constitutes a major part of living biomass and vegetation biomass and necromass will therefore be an important measure of how much carbon may be accumulated in a specific ecosystem. Similarly, the net primary production (NPP) will be an estimate of how much carbon (and other elements) are incorporated in living tissue. Combining net primary production and decomposition rates will give a rough estimate of the carbon turnover in the ecosystem. The primary producers covering the terrestrial landscape are described using biomass and NPP in order to feed a conceptual ecosystem model with data (see Section 4.8). This section describes the components, the resolution and the methodology that are used to build the descriptive models of biomass and NPP.

The plant biomass in an area consists of a number of different components that all have to be measured or estimated to estimate the total biomass (Figure 4-10).

Photosynthesis provides the carbon and energy that are essential for many important processes in ecosystems. Photosynthesis directly supports plant growth and produces organic matter that is consumed by animals and soil microbes. The photosynthesis at an ecosystem level is termed gross primary production (GPP). Approximately half of the GPP is respired by plants to provide the energy that supports the growth and maintenance of biomass /Chapin et al. 2002/. The net carbon gain is termed net primary production (NPP) and is the difference between GPP and plant respiration. However, GPP cannot be measured directly and total respiration is difficult to measure, especially in multi-species forests /Gower et al. 1999/. In contrast, the different components constituting the NPP for a certain ecosystem may be measured separately /Clark et al. 2001/ (Figure 4-11).

NPP is sometimes (e.g. for trees) equated to the net accumulation of biomass during one year. In those cases the NPP and the turnover are different. Sometimes the NPP and turnover are set equal, as a simplification, meaning that there is no net accumulation of biomass between years.

Descriptive models

Below, the methodology and procedure applied in the modelling of biomass and NPP are described. The results are given in /Lindborg, 2005/ and the figures are used in the subsequent terrestrial ecosystem model as described in Section 4.8.

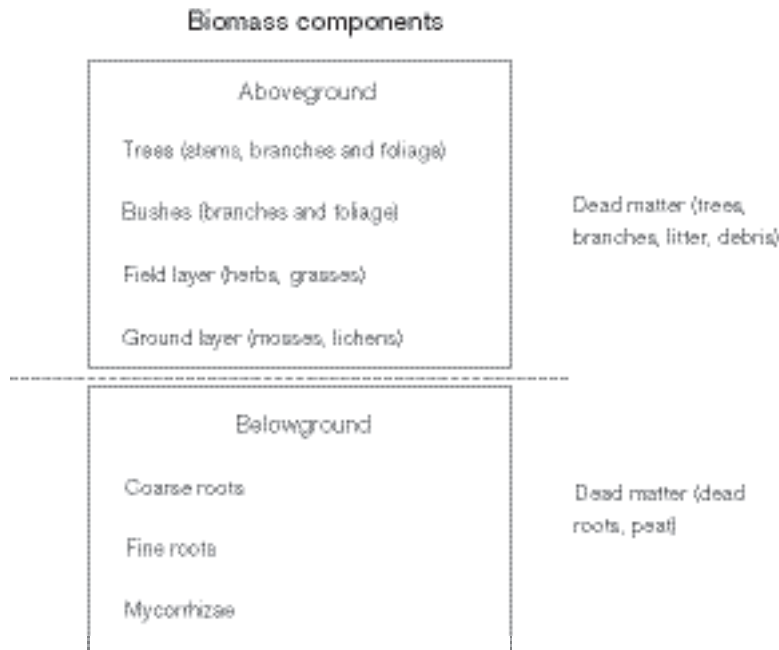


Figure 4-10. The different biomass components in a forest.

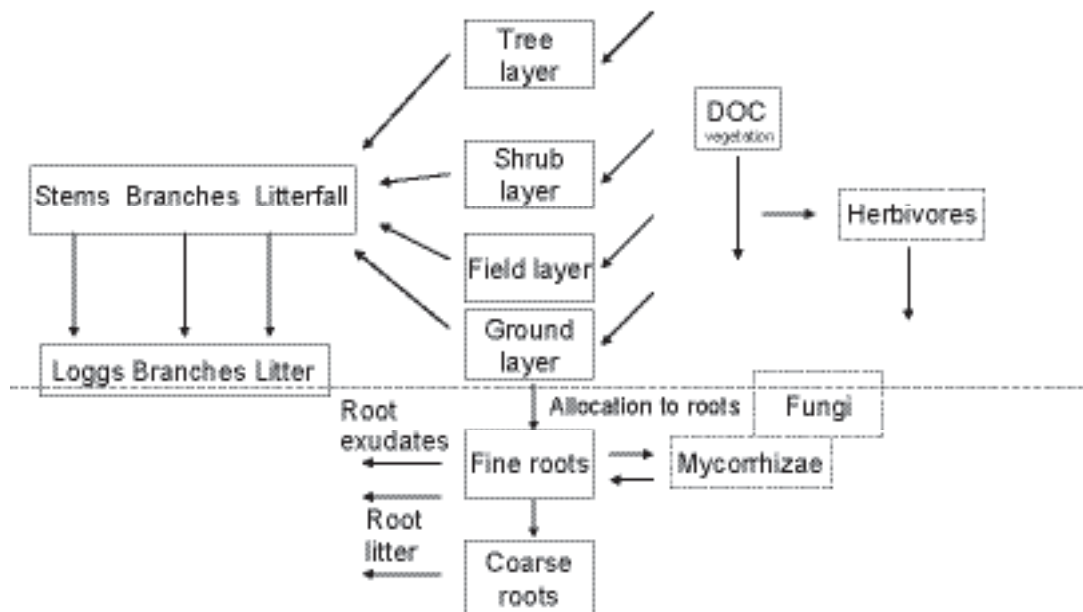


Figure 4-11. An illustration of the different pools and fluxes of matter in a terrestrial ecosystem with the focus on the producers. Boxes with broken line are consumers.

Tree layer

Biomass and NPP for four fractions of the tree layer have been calculated (woody parts (above ground), green parts, coarse roots and fine roots). Furthermore, the annual amount of litterfall and other falling components have been calculated for the four forest classes. The forest classes used to describe the tree layer (young-, dry- and old coniferous forest and deciduous forest) and the GIS sources from which the information were obtained to construct the classes are described in /Lindborg, 2005/ as well as the methodology and the data used in the calculations.

Shrub layer

Biomass and NPP of the shrub layer have been calculated. Field inventories /Abrahamsson, 2003/ indicated that the shrub layer most often is insignificant when a tree layer is present in this area. A habitat that had a very significant shrub layer was clear cuts of varying age where *Betula pendula* is very dominant. *Salix* sp. can be abundant on mires and was identified by /Boresjö Bronge and Wester, 2002/ in their shrub layer. Therefore, the focus has been on *Betula* and *Salix* in the shrub layer. However, due to lack of biomass and NPP data for *Salix* sp., the values for *Betula* have been used.

The classes used to describe the shrub layer and the GIS sources from which the information was obtained to construct the classes are described in /Lindborg, 2005/ jointly with the methodology and the data used in the calculations.

Dead wood

The biomass of dead wood has been calculated according to the description in /Lindborg, 2005/. The results, expressed as dry weight of logs (gC m^{-2}) for different forest classes, are presented in /Lindborg, 2005/.

Field and ground layer

Biomass and NPP of the field and ground layer have been calculated. The classes used to describe the field and ground layer and the GIS sources from which the information were obtained to construct the classes are described in /Lindborg, 2005/ as well as the methodology and the data used in the calculations. The resulting biomass and NPP values (expressed as gC m^{-2}) for the different field, ground and litter layer classes are presented in /Lindborg, 2005/.

Fungi/mycorrhizae

Biomass and NPP for fungi in the forest habitats (young-, dry- and old coniferous forest and deciduous forest) have been calculated according to the description in /Lindborg, 2005/.

4.6.2 Terrestrial consumers

Description

Mammals

The most common mammal species in the Forsmark regional model area is roe deer (9.4 deer km^{-2}) /Cederlund et al. 2004/. Moose is also fairly common ($1.2 \text{ moose km}^{-2}$), but unevenly distributed, which is normal for this part of Sweden due to hunting pressure, snow depth variations and distribution of food. European and mountain hare are fairly low in abundance, compared with other regions (see Table 4-5). A comprehensive description of the mammals is found in /Lindborg, 2005/.

Birds

In total, 96 bird species were found along the line transect in the regional model area, compared to 86 in 2002. The most common species on land were Chaffinch (sw. *Bofink*) and Willow warbler (sw. *Lövsångare*). For detailed information on each species found in the Forsmark area see /Green, 2004/.

Cattle

There is one producing farm within the Forsmark area today, with a few beef cattle /Miliander et al. 2004/. Therefore, domestic animals represent an important part of the terrestrial biomass for consumers in the Forsmark region.

Table 4-5. Estimated abundances of mammal species in 2003 in the Forsmark regional model area /Cederlund et al. 2004/.

Species	Animals per km ²
European hare (field)	0.32
Mountain hare (forest)	0.23
Fox	Observed
Lynx	Observed (0.02 in 2002)
Marten (Swe: Mård)	0.24
Mink	Observed
Moose	1.23
Otter	Observed
Red deer	0.01
Roe deer	9.36
Small mammals field (mice and voles) ¹	1,500
Small mammals forest (mice and voles) ¹	1,200
Wild Boar	0.01

¹ New figures from 2004 obtained from Göran Cederlund (personal comm.)

No observations of Badger, Beaver, Fallow deer or Wolf were made during the investigations in 2003.

Amphibians and reptiles

Site-specific data concerning the species that are likely to occur in the Forsmark area have been obtained through field studies by /Andrén, 2004a/. There are no site-specific density data for amphibians and reptiles. Generic data concerning these species have been obtained from /Andrén, 2004b/. These data are compiled in /Lindborg, 2005/.

Soil fauna

There are no site-specific data concerning soil fauna. Three examples of soil fauna densities and biomass figures have been obtained from Prof. Tryggve Persson, Dept of Soil Biology, SLU (pers. comm.). The three examples come from a pine moor in Gästrikland, a deciduous forest in Uppland (Andersby-Ängsbacka in Dannemora) and a grassland in Uppland /Lohm and Persson, 1979/. The densities and biomass for the different soil species are given in /Lindborg, 2005/.

Quantitative model

A carbon budget for the terrestrial consumers in the drainage area of Lake Bolundsfjärden has been calculated based on the site-specific density data for mammals and humans. There is no active agriculture in the Lake Bolundsfjärden drainage area, but as there is some grazing- and arable land in the area, five milk cows have been included in the model. No biomass figures have been calculated for birds, since no site-specific density data are available for the Forsmark model version 1.2. The applied methodology with carbon pools and flows are presented in full in /Lindborg, 2005/ and the resulting numbers are used in the terrestrial ecosystem model, described in Section 4.8.1.

4.6.3 Limnic producers

Methodology

The delimitations between different habitats in the lakes were determined in connection with the *lake characterisation*, which included identification of the watershed, data collection and field investigations /Brunberg et al. 2004/. The extension of different lake habitats was identified in the field and the borders were recorded using DGPS (Differential Geographical Position System) equipment.

Microbiota were sampled at 15 sites monthly or biweekly from January 2000 to March 2003 /Andersson et al. 2003/. Species composition and biomass of planktonic microbiota (phytoplankton and heterotrophic nanoflagellates) and microphytobenthos were determined using an inverted phase-contrast microscope. Primary production was measured *in-situ* by ¹⁴C-incorporations on 9 and 14 occasions in the sediment and pelagial zones, respectively.

Descriptive model

The Forsmark lakes were divided into five different habitats; the Littoral type I, II and III, the Pelagial and the Profundal, according to /Blomqvist et al. 2002/ (see Figure 4-12). Littoral type III is defined as a littoral habitat with submerged vegetation. Littoral type II is a wind-exposed habitat with a hard substrate. Photosynthesizing organisms colonizing these areas include species that are able to attach to the hard substrate, e.g. periphytic algae. Littoral type I is a wind-sheltered habitat in shallow areas, where the substrate is soft and allows emergent and floating-leaved vegetation to colonise.

General characteristics for lakes in the Forsmark area

Since the Forsmark lakes are small and shallow, only three of these habitats were found, namely the Littoral types I and III and the pelagial /Brunberg et al. 2004/. The dominating habitat in the larger lakes in the area is the littoral with submerged vegetation (Littoral type III). In Lakes Eckarfjärden, Bolundsfjärden and Fiskarfjärden this habitat makes up at least 50% of the lake area, whereas 20 of the other 22 lakes in the area have a larger share of the littoral with emergent and floating-leaved vegetation (Littoral type I) /Brunberg et al. 2004/. This is not surprising since these lakes are smaller, shallower and in a later successional stage.

Lake Eckarfjärden is by far the most investigated lake in the area, and in the parameterisation of quantitative models for the other lakes in Forsmark, most of the data used will, therefore, be data from this lake. However, Lake Bolundsfjärden is described below, as Lake Bolundsfjärden is used in the limnic ecosystem model presented below.

Lake Bolundsfjärden

Lake Bolundsfjärden has three major habitats, Littoral type I, Littoral type III and the pelagic habitat. The open water surface, i.e. the pelagic habitat, covers 66% of the lake area (Figure 4-13). Due to the shallowness and clear water of the lake, light penetrates down to all bottom areas and no profundal areas are present. Hence, the littoral with submerged vegetation has the same distribution as the pelagic habitat.

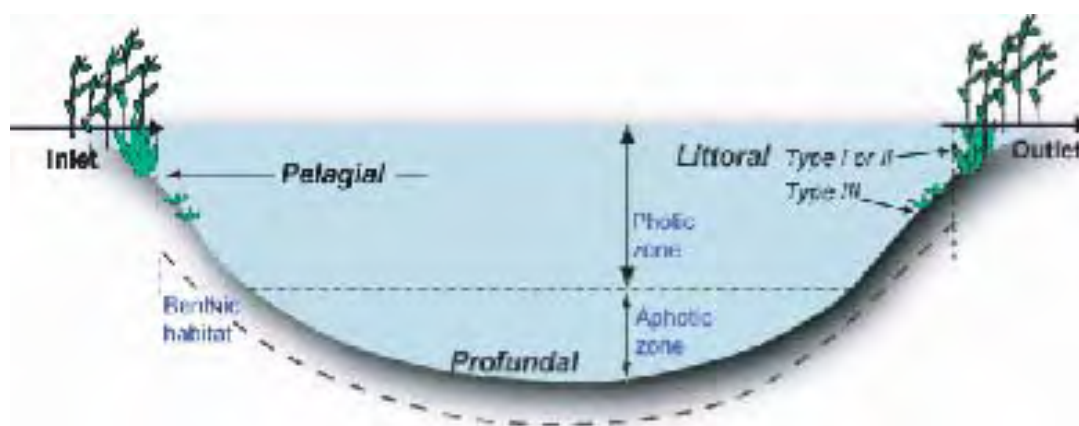


Figure 4-12. Conceptual illustration of a lake ecosystem with the conventional division into littoral, pelagial and profundal habitats. In the quantitative modelling, the benthic habitat includes all bottom areas, except the littoral areas with emergent vegetation (Littoral Type I).

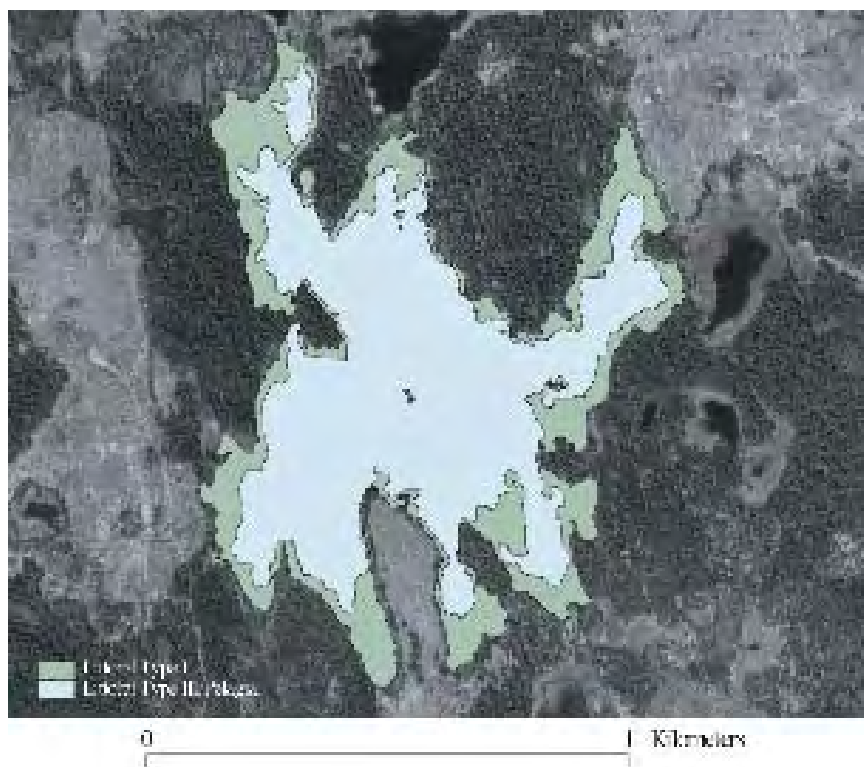


Figure 4-13. Distribution of major habitats in Lake Bolundsfjärden /from Brunberg et al. 2004/. Litoral Type 1 represents areas with emergent and floating-leaved vegetation and Litoral Type 3 areas with submerged vegetation.

Biomass data for phytoplankton and microphytobenthos from Lake Bolundsfjärden are available for the period August–October 2001 /Franzén, 2002/. Phytoplankton biomass seemed to be in the same order of magnitude as in Lake Eckarfjärden, but no direct comparison was possible for microphytobenthos. However, due to the short time series of these data and the considerable temporal variation in biomasses shown in Lake Eckarfjärden, phytoplankton and microphytobenthos data from Lake Eckarfjärden were used in the quantitative model. No data on primary production are available from Lake Bolundsfjärden.

4.6.4 Limnic consumers

Methodology

Heterotrophic bacterioplankton and sediment bacteria were sampled, counted and measured in 2002. *Bacterial production* in the water column as well as in the upper sediment in Lake Eckarfjärden was measured /Andersson et al. 2003/.

Zooplankton was sampled at 15 sites monthly or biweekly from January 2002 to March 2003. The biovolumes were transformed to biomass and calculations of carbon content were slightly differently depending on species /Andersson et al. 2003/.

Benthic fauna was sampled in March 2002 at 10 randomly chosen sites in Lake Eckarfjärden /Andersson et al. 2003/. The benthic animals were identified to species, counted and weighed.

The *fish survey* was performed so that the result could be compared with other studies and so that the weight values per unit effort could be transferred into biomass per hectare /Borgiel, 2004/. For this conversion, a factor of 33 has been used (1 kg fish in the net represents 33 kg fish/ha in the lake) (Per Nyberg, National Board of Fisheries, pers. comm.).

Descriptive model

Data concerning zooplankton and benthic fauna are only available from one of the lakes in the area, Lake Eckarfjärden. However, considering the large similarities in lake morphology and water chemistry between lakes in the area, data from Lake Eckarfjärden can be regarded as valid also for the other lakes, at least those with similar size and habitat distribution. *Zooplankton* biomass in Lake Eckarfjärden was dominated by copepods and showed an opposite seasonal trend compared with most other Swedish lakes, with a summer minimum and winter maximum. The biomass of *benthic fauna* was low compared to other lakes. The benthic fauna was dominated by herbivores, both in terms of number of individuals and in terms of biomass.

Fish data from all four investigated lakes in the area show that benthivorous fish generally is the dominating functional group. This is not surprising since species which are not sensitive to low oxygen levels belong to this group. Due to shallow conditions and high organic content in the sediments, oxygen levels in all lakes in the area are strongly reduced during ice cover in winter, and it is relatively common with more or less anoxic conditions in the whole water column. The benthivorous fish biomass range from 68% in Lake Eckarfjärden to 89% in Lake Fiskarfjärden of the total fish biomass. The share of planktivorous fishes is generally low, ranging from 0.1% in Lake Bolundsfjärden to 8% in Lake Fiskarfjärden.

4.6.5 Marine producers

The marine system in the Forsmark modelling area is located in Öregrundsgrepen, Southern Bothnian Sea. The marine area in Forsmark has been divided into seven basins (Figure 4-14). An ecosystem model for two of these basins, Basin SAFE-area and Basin Stånggrundsfjärden is presented in /Lindborg, 2005/.



Figure 4-14. The Forsmark model area including its seven basins. In the map, the location of the drainage area of Bolundsfjärden (Forsmark 2) is indicated.

The marine system in the Forsmark area is a relatively productive coastal area in a region of otherwise fairly low primary production. This is due to upwelling along the mainland /Eriksson et al. 1977/. The surface water has a nutrient concentration ranging from 330 to 790 $\mu\text{g/L}$ tot-N and 12 to 25 $\mu\text{g/L}$ tot-P (field measurements, SICADA). The seabed is dominated by erosion and transport bottoms with heterogeneous and mobile sediment consisting mainly of sand and gravel with varying fractions of glacial clay /Mo and Smith, 1988/. The seabed close to the mainland has some areas of rocky bottoms, which are partly covered with coarse moraine /Sigurdsson, 1987/.

Methodology

The marine basins in the Forsmark area were classified into three different habitats; the phytobenthic habitat, the soft bottom habitat and the pelagial (see Figure 4-15).

The light penetration depth was of major importance to enable estimates of the total biomass of the various groups of primary producers. This was because the borders between different habitats where the organisms reside, in each basin were defined by reference to the light penetration depths, i.e. by dividing each basin into a photic and an aphotic zone, assuming that the photic zone reaches twice the light penetration depth.

Phytoplankton has been studied in the area twice, in a recent study performed by /Huononen and Borgiel, 2005/ and by /Lindahl and Wallström, 1980/. These studies gave estimates of the integrated phytoplankton biomass in 0–20 m water column, and were normalised to square metres. In this study, the estimates per square metre were normalised to volumes (cubic metres) by assuming that phytoplankton mainly were present in the photic zone, i.e. in the uppermost ten metres. The phytoplankton productivity was estimated with the ^{14}C -method /Steemann-Nielsen, 1952/ and presented as net primary production. Therefore, their respiration was omitted in the further calculations in this study.

In the descriptive model presented in this report, the biomass from the most recent study /Huononen and Borgiel, 2005/ were used, whereas the primary production was estimated from the P/B-relationship found by /Lindahl and Wallström, 1980/ and the biomass values given by /Huononen and Borgiel, 2005/.

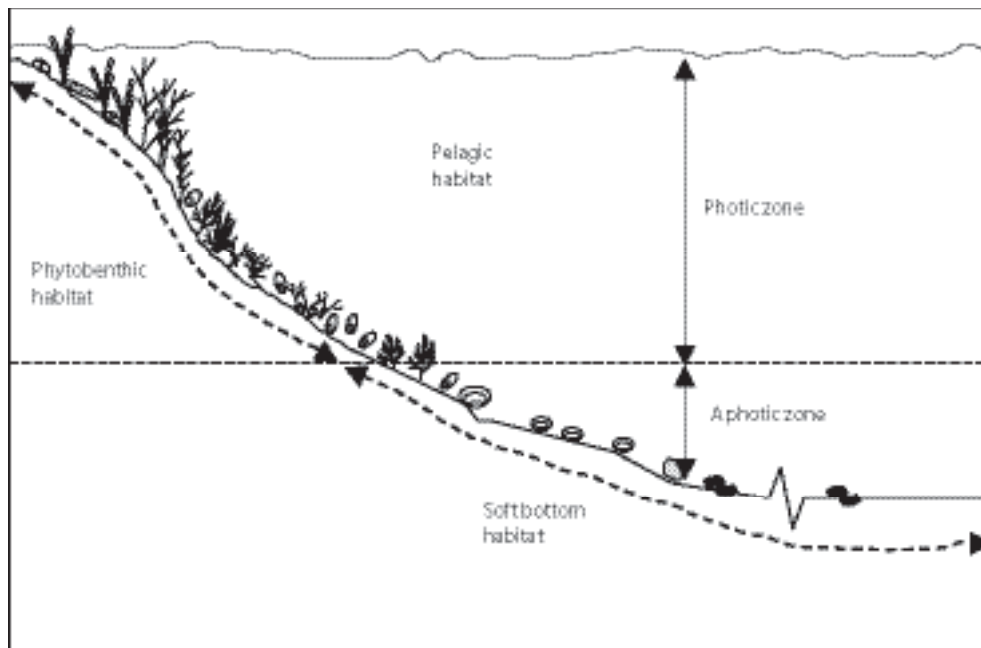


Figure 4-15. Conceptual figure of the marine coastal ecosystem in Forsmark including illustrations of the habitats (phytobenthic, soft bottom and pelagic).

The biomass estimates for macrophytes were reported as biomass per square metre depth interval (0–1 m, 1–2 m, 2–4 m, 4–6 m, 6–10 m and 10–15 m) at species level /Kautsky et al. 1999/, which were then integrated by calculating the biomass of each species per depth interval, summing over the depth intervals and dividing by the surface of the photic zone to normalise the biomass per square metre. These values were then used in the budget calculations for the basins in this study.

Results

The major groups among primary producers in the Forsmark area are macrophytes (including macroalgae), microphytobenthos and phytoplankton. This grouping of primary producers has also been used in the quantitative model of the marine ecosystem (see Section 4.8).

Several studies on flora have been carried out in the Öregrundsgrepen area, of which many were conducted in the defined modelling area. In the photic zone, the seabed is to a large extent covered with a layer of micro algae, mainly diatoms, with a relatively high species diversity and large amount of macrophytes (both macroalgae and vascular plants) /Kautsky et al. 1999; Snoeijs, 1985, 1986/. The macrophyte species that contribute most to the macrophyte biomass of the benthic community in Forsmark are the red algae *Polysiphonia nigrescens*, the brown algae *Fucus vesiculosus* and *Sphacelaria arctica* and the vascular plant *Potamogeton filiformis* /Kautsky et al. 1999/.

The phytoplankton are strongly dominated by diatoms and dinoflagellates during springtime, whereas the plankton community in summer and autumn mainly consists of blue-green algae and small flagellates /Lindahl and Wallström, 1980/.

4.6.6 Marine consumers

The major groups of consumers present in the area have been identified to be bacterioplankton, zooplankton, fish (zooplankton feeding, benthic feeding and carnivorous), benthic herbivores, benthic filter feeders, benthic detritivores (including meiofauna), benthic carnivores, benthic bacteria, birds (fish feeding and benthic feeding), seals and humans.

Methodology

The biomass estimates for grazing macrofauna, filter feeders and other macrofauna were also reported as biomass per square metre depth interval (0–1 m, 1–2 m, 2–4 m, 4–6 m, 6–10 m and 10–15 m) at species level /Kautsky et al. 1999/, which were then integrated by calculating the biomass of each species per depth interval, summing over the depth intervals and dividing by the surface of the photic zone to normalise the biomass per square metre. The resulting biomass values were used in the budget calculations for the basins in this study.

Results

Several studies on fauna have been carried out in the Öregrundsgrepen area of which many were conducted in the defined modelling area. Herbivorous gastropods together with both herbivorous and omnivorous crustaceans dominate the grazing macrofauna and the most common filter feeder in the area has been found to be the bivalve *Cardium* spp. /Kautsky et al. 1999/. The major meiofauna taxa present in the area are nematodes, acarins, cladocerans, copepods and ostracods /Snoeijs and Mo, 1987/. The seabed below the photic zone has a lower species diversity, which may be due to the heterogeneous and mobile sediment /Mo and Smith, 1988/. Among the macrobenthos found in this community, the detritus- and filter feeding bivalve *Macoma baltica* strongly dominates the biomass /Kautsky et al. 1999/.

The zooplankton community has low species diversity. Two copepod species constitute about 80% of the zooplankton biovolume, with the rest composed of cladocerans, rotatorians, ciliates and different larvae stages from benthic animals /Eriksson et al. 1977; Persson et al. 1993/. The most common fish species in Öregrundsgrepen are herring (*Clupea harengus*), roach (*Rutilus rutilus*) and perch (*Perca fluviatilis*) /Neuman, 1982/. The method used in the fish survey was not well adapted to catching small-sized species such as sticklebacks (Gasterosteidae) and gobies (Gobiidae), which may possibly have affected the species distribution results.

4.7 Humans and land use

Input data sources and calculated values for the parameters used to describe humans and land use in the Forsmark area and its surroundings are provided in detail in /Miliander et al. 2004/ and more briefly in /Lindborg, 2005/. The Forsmark area is not inhabited on a permanent basis. Nevertheless, there are five holiday houses and three farms within the Forsmark area, which indicates that the area has a small holiday population. There is only one active agricultural enterprise within the Forsmark area, situated at Storskäret. The agricultural component in the Forsmark area is only 4% of the total area, considerably lower than in the County of Uppsala as a whole, where it represents 25%. The forest area represents as much as 72.5% of the land area.

The short description below illustrates the situation in the parish of Forsmark, since many of the data were available on the parish level. The Forsmark parish is very similar in size to the model area and covers some 90% of its land area.

The assessment of the data acquired can be summarised as follows.

- The parish of Forsmark is very scarcely populated.
- The main employment sector is within electricity supply. There is a clear net daily in-migration to the parish of Forsmark due to the dominant employer; the Forsmark nuclear power plant.
- The land use is dominated by forestry; wood extraction is the only significant outflow of biomass from the area.
- The dominant leisure activity, by far, is hunting. Besides this, the area is only occasionally used for leisure. This is probably a result of both the scarce population and the relative inaccessibility of the area and distance from major urban areas.
- The agriculture in the parish is limited in extent and the major crop is barley.

The Forsmark area is uninhabited. Nevertheless, there are five holiday houses and three farms within the Forsmark area, which indicates that the area has a small holiday population. There is only one agricultural enterprise in use within the Forsmark area and that one is situated at Storskäret. The agricultural area in the Forsmark area is only 4% of the total area, considerably lower than in the County of Uppsala where it represents 25%. The forest area represents as much as 72.5% of the land area.

The carbon flow to humans from the drainage area of Lake Bolundsfjärden has been calculated according to the methodology described in /Lindborg, 2005/. The result is presented in /Lindborg, 2005/. The figures are used in the terrestrial ecosystem model.

4.8 Development of the ecosystem models

The drainage area Forsmark 2 (drainage area of Lake Bolundsfjärden) was chosen as the model area when developing the terrestrial and limnic ecosystem model (see Figure 4-16). The total drainage area is 8.7 km² and the surface area of Lake Bolundsfjärden is 0.6 km². A limnic model has been developed for Lake Bolundsfjärden as well as for Lake Eckarfjärden, which is also within the drainage area of Bolundsfjärden. The limnic model of Lake Eckarfjärden is not discussed here, but is described in /Lindborg, 2005/.

The Forsmark marine ecosystem has been divided into seven basins, shown in Figure 4-14. Two of these basins, Basin Stånggrundsfjärden and Basin SAFE-area, were used for the marine modelling. These two basins are recipients of the drainage area of Bolundsfjärden. The model for Basin SAFE-area is described in /Lindborg, 2005/. The ecosystem models were developed as stand-alone models. No efforts have been made in this version to connect the models.

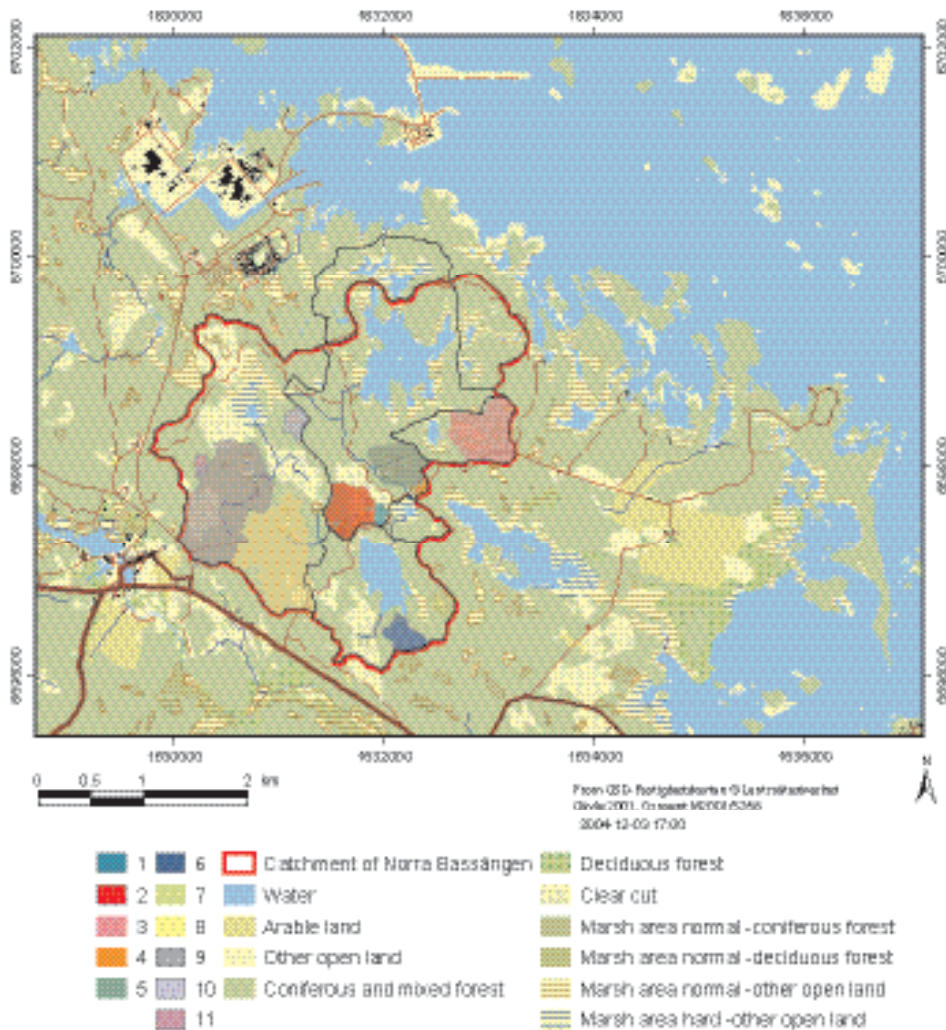


Figure 4-16. The drainage area of Bolundsfjärden within the Forsmark area to which the descriptive ecosystem model was applied in order to construct a large-scale carbon budget. The numbers 1 to 11 represents wetlands in the drainage area. The input, output and accumulation of dissolved organic carbon (DOC) were calculated for the wetlands as well as the rate of peat accumulation, see /Lindborg, 2005/.

4.8.1 Terrestrial ecosystem description

The dominating vegetation types in the drainage area of Bolundsfjärden are old Norway spruce and Scotch pine forests of mesic-wet type, together constituting 35% of the area. Clear-cuts represent 11%, water 9%, young conifer forest 8% and reed-dominated wetlands 8% of the vegetation types in the drainage area /Brunberg et al. 2004/.

The large amount of information describing pools and fluxes and the different spatial resolution of this information called for an implementation of the conceptual model on a number of the vegetation types before a carbon budget could be presented for a complete catchment area. Three vegetation types were therefore chosen using the vegetation map, to represent a forest, a mire and agriculture land. Data describing pools and fluxes were extracted for these vegetation types. These data are presented in /Lindborg, 2005/.

The descriptive model has been reduced in number of boxes and fluxes, and is presented in Figure 4-17. Where measures of biomass and faeces and mortality were missing, the simple assumption was made that it was on average the same as for those animals for which these figures were known. The arrow from vegetation to humans represents crops from the agriculture land in the

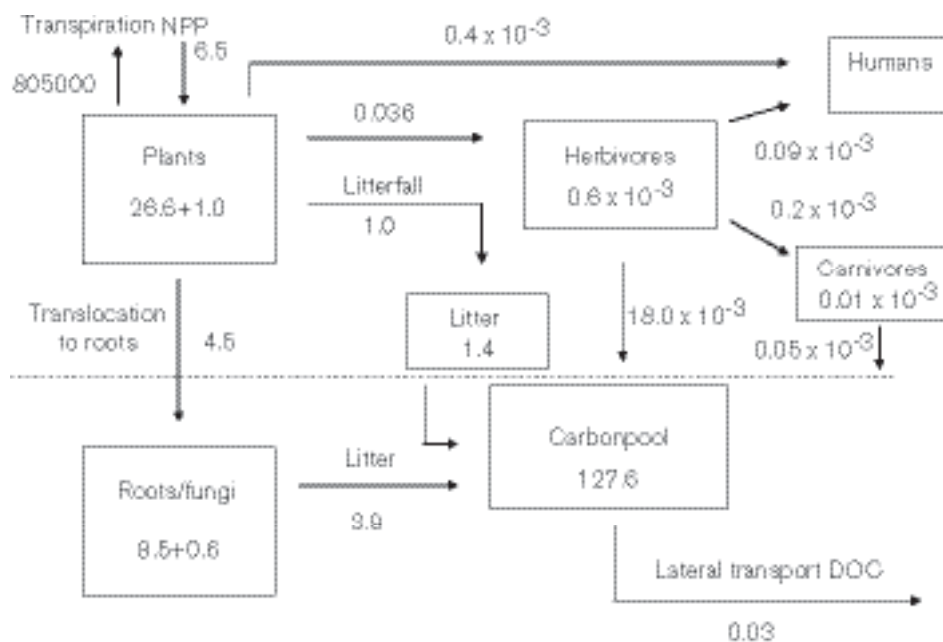


Figure 4-17. Major pools and net fluxes of carbon for the drainage area in Forsmark 2. Transpiration is in m^3y^{-1} , figures in boxes are in units of $1 \times 10^9 \text{gC}$ and figures describing fluxes in units of $1 \times 10^9 \text{gCy}^{-1}$. Annual net changes (in units of $1 \times 10^9 \text{gCy}^{-1}$) for plants and roots/fungi are shown within the boxes.

discharge area, and berries and fungi that are utilised (see /Lindborg, 2005/ for more information behind these figures). The arrow from herbivores to humans is the meat utilised after slaughter. If a steady state between carbon input to SOC and C-mineralisation is assumed the C-mineralisation should approximate $1.24 \times 10^9 \text{gCy}^{-1}$.

The total lateral transport of DOC was calculated using a figure from /Canhem et al. 2004/ that estimated leaching of DOC from conifer forests into lakes as $3.5 \text{gCm}^{-2}\text{y}^{-1}$. This figure was multiplied with the total discharge area (lake area subtracted). This resulted in the total amount of $0.03 \times 10^9 \text{gCy}^{-1}$ that was transported as DOC from the terrestrial land types in the discharge area.

4.8.2 Limnic ecosystem description

The larger lakes in the Forsmark area, and probably also the smaller ones that have not been investigated, can be classified as oligotrophic hardwater lakes. This means that they show very unusual chemical conditions, with high alkalinity, conductivity, pH-value and nitrogen concentrations, very high concentrations of slightly coloured DOC, whereas phosphorus concentrations are very low. Phytoplankton and bacterioplankton biomasses are low, and the microbial community (including both autotrophs and heterotrophs) is mainly confined to the sediments where a 10–15 cm thick microbial mat, mainly consisting of cyanobacteria, is found. Preliminary primary production measurements in the lake show that while the production in the pelagial is always low, the production in the microbial mat may potentially be very high /Blomqvist et al. 2002/.

An important group of underwater vegetation of the lakes in the Forsmark area is the stoneworts (*Chara spp.*). Large parts of the bottoms of the larger lakes are covered with *Chara*. The biomass of benthic fauna is low compared to other Swedish lakes /Andersson et al. 2003/ and the benthic fauna is dominated by herbivores, both in terms of number of individuals and in terms of biomass.

Carbon budget for Lake Bolundsfjärden

Lake Bolundsfjärden is the largest of eleven lakes in the drainage area Forsmark 2. The lake has a total surface area of 0.61km^2 , a maximum depth of 1.8 m and a mean depth of 0.6 m.

In the modelling work for Forsmark 1.2, carbon budgets have been developed for both Lake Bolundsfjärden and Lake Eckarfjärden. For details the reader is referred to /Lindborg, 2005/, here only major results from Lake Bolundsfjärden are presented. Both production and biomass of primary producers in Lake Bolundsfjärden is dominated by macrophytes (reed) and macroalgae (*Chara*), whereas lake respiration and total consumption are strongly dominated by bacteria, both benthic and pelagic (Table 4-6, Figure 4-18).

By assuming the same sedimentation rate as for Lake Eckarfjärden ($15 \text{ gC m}^{-2} \text{ y}^{-1}$ in the whole area of the pelagial), the annual sedimentation in Lake Bolundsfjärden is estimated to $6.1 \times 10^6 \text{ gC y}^{-1}$. This corresponds to approximately 10% of the estimated annual POC excess in the carbon budget.

Whereas Lake Eckarfjärden constantly acts as a carbon source in a drainage area context, Lake Bolundsfjärden is a carbon sink during the main parts of the year (Figure 4-19). By combining measured TOC concentrations with estimated specific discharge, the annual net transport of carbon to Lake Bolundsfjärden (amount of C transported to the lake minus amount of C transported from lake) is estimated to $6.6 \times 10^5 \text{ gC y}^{-1}$. The annual gross transport of carbon from the lake is estimated to $3.6 \times 10^7 \text{ gC y}^{-1}$, and this figure can be viewed as a rough approximation of the total annual transport of carbon from the drainage area Forsmark 2 to the sea.

Table 4-6. Total average biomass (gC) and annual metabolic rates (gC y⁻¹) of functional organism groups in Lake Bolundsfjärden. Note that phytoplankton includes both autotrophic and mixotrophic species and hence has primary production as well as respiration and consumption.

Functional group	Biomass gC	Prod. gC y ⁻¹	Cons. gC y ⁻¹	Resp. gC y ⁻¹	Supply ¹ gC y ⁻¹	Graz. or pred. ² gC y ⁻¹	Excess ³ gC y ⁻¹
Pelagic habitat							
Phytoplankton	1.5E+04	6.9E+06	7.2E+06	3.6E+06	6.9E+06	3.4E+05	6.6E+06
Bacterioplankton	2.0E+04		2.5E+07	1.9E+07	6.4E+06	4.5E+06	1.9E+06
Zooplankton	2.4E+04		1.0E+06	3.3E+05	6.7E+05	2.8E+05	3.6E+05
Z-fish (zooplanktivore)	4.3E+02		4.0E+03	2.3E+03	1.7E+03	6.0E+02	1.1E+03
M-fish (benthivore)	2.7E+05		2.6E+06	1.5E+06	1.1E+06	3.8E+05	7.1E+05
F-fish (carnivore)	4.8E+04		4.5E+05	2.6E+05	1.9E+05	6.7E+04	1.2E+05
Benthic habitat							
Macroalgae	3.8E+06	4.2E+07			4.2E+07	3.4E+06	4.0E+07
Microphytobenthos	1.6E+06	2.3E+07			2.2E+07	1.4E+06	2.1E+07
Benthic bacteria	1.5E+06		6.8E+07	5.1E+07	1.7E+07	4.4E+06	1.2E+07
Benthic fauna	4.5E+05		6.7E+06	2.2E+06	4.5E+06	7.5E+05	3.7E+06
Littoral habitat							
Macrophytes	6.0E+06	3.9E+07			3.9E+07	0	3.9E+07
Epiphytic algae	6.4E+04	2.9E+06			2.9E+06	3.0E+05	2.6E+06
Epiphytic bacteria	6.4E+04		2.0E+06	1.5E+06	4.9E+05	3.0E+05	1.9E+05
Epiphytic fauna	1.2E+03		1.5E+04	5.2E+03	1.0E+04	5.3E+03	5.05E+03
Lake total	1.4E+07	1.1E+08	1.1E+08	7.9E+07	1.4E+08	1.6E+07	1.3E+08
Lake carbon pools							
gC							
DOC	6.8E+06				2.2E+07	2.7E+07	-5.0E+06
POC	1.9E+05				1.3E+08	6.9E+07	5.9E+07

¹ Supply = For biota: consumption – respiration, for DOC: calculated from assumed DOC excretion by the different functional groups (see text for specification), for POC: excess from all functional groups.

² Grazing or consumption upon the respective functional group/carbon pool.

³ Excess = supply – grazing or predation.

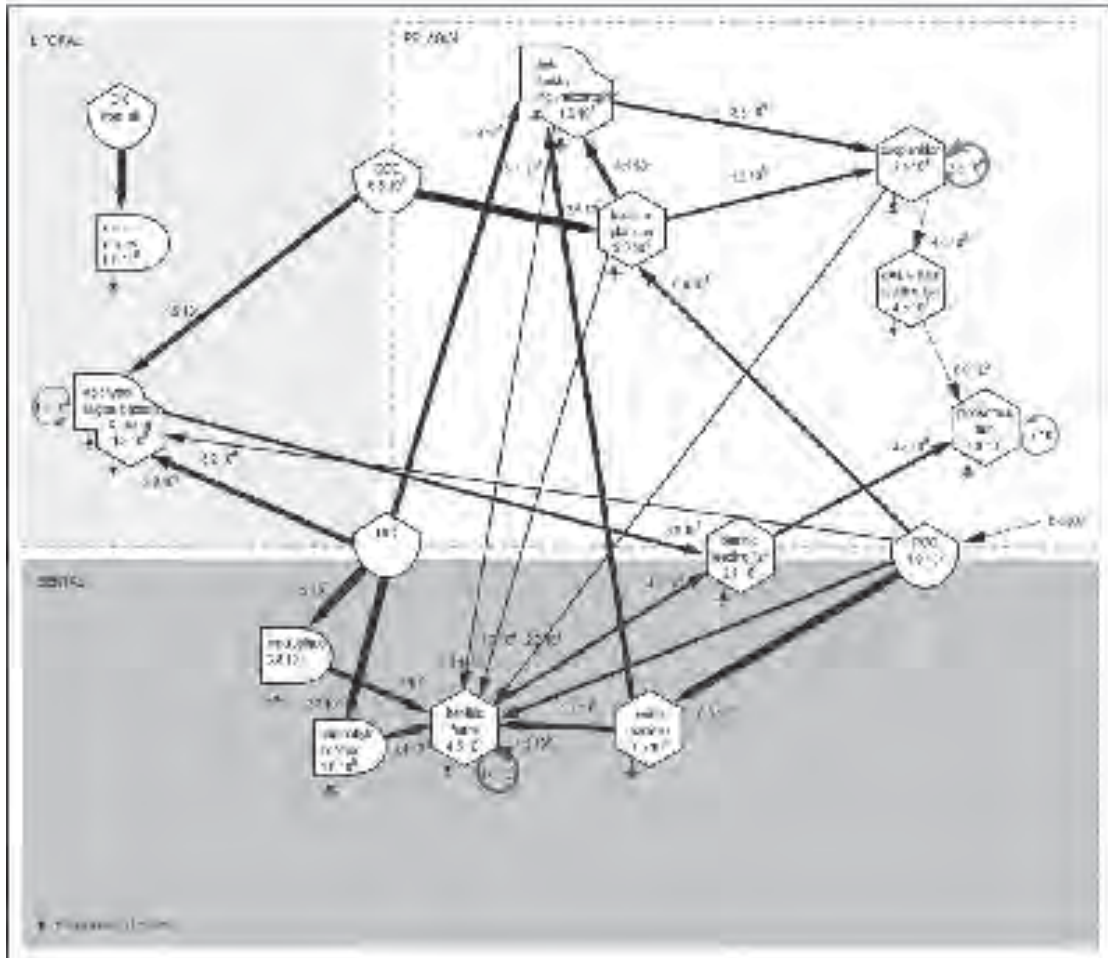


Figure 4-18. Carbon budget for Lake Bolundsfjärden. Arrow sizes indicate the magnitude of carbon flow between different functional groups. Since the biomasses of all epiphytic groups (algae, bacteria and fauna) are so small, they have been treated as a single epiphyte group in the picture.

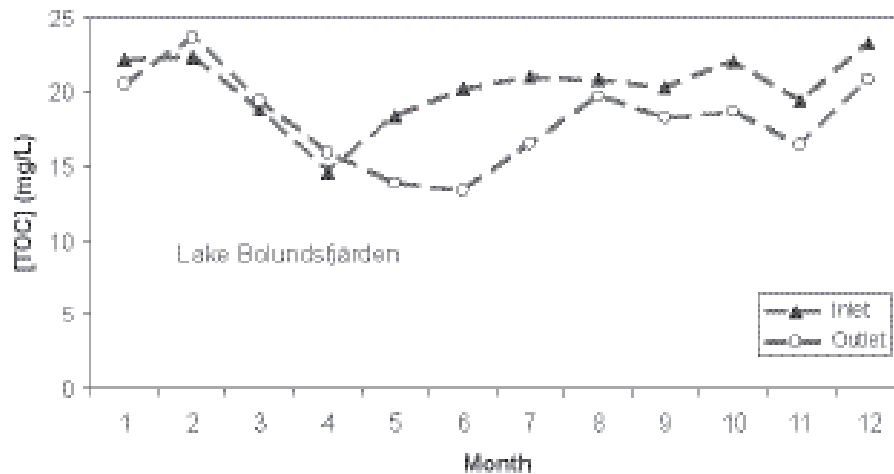


Figure 4-19. Monthly mean values for total organic carbon in the inlet and outlet of Lake Bolundsfjärden, based on all sampling occasions during the period March 2002 to June 2004 (N varies between 2 and 7 for the different sampling sites/months).

The carbon budget clearly demonstrates the importance of the benthic and littoral habitats in the oligotrophic lakes in the Forsmark area. The major part of the biomass and primary production clearly occurs in these two habitats. The pelagial is mainly supported with carbon from the benthic habitat, but also from the littoral. The major flows of carbon originate from carbon fixed by macroalgae and microphytobenthos, which are further channelled up through the food web either by benthic herbivores, or by bacteria utilising DOC exudates from the primary producers. The benthic bacteria make up about 2/3 of the respiration as well as the consumption, whereas bacterioplankton contribute the smaller part (1/3).

4.8.3 Marine ecosystem description

The marine ecosystem in Forsmark has a varied bathymetry, with a few enclosed bays clearly affected by fresh water effluence, a shallow but exposed archipelago and open sea areas heavily exposed to currents and wave action. As a result, elements discharged into the marine environment from the adjacent terrestrial and limnic environments will have a different fate depending on where they enter the marine system.

The Forsmark marine ecosystem has been divided into seven basins, shown in Figure 4-14. Two of these basins, Basin Stånggrundsfjärden and Basin SAFE-area, were used for the marine modelling. Only Basin Stånggrundsfjärden is described below, but both are described in /Lindborg, 2005/.

The basins are parts of the marine environment, but are bathymetrically separated from each other. The basins have in the descriptions been treated as separate units, based on the assumption that relevant flows of carbon will be greater within the basins than between the basins. The flows of carbon between the basins could be quantified with estimations of abiotic carbon flows (runoff and oceanographic flows) or biotic flows (i.e. migration of organisms).

The modelling assumptions related to habitat preferences and occurrence of the functional groups, biomass estimates, calculation of primary production, respiration and consumption, and the conversion factors used are presented in /Lindborg, 2005/.

Basin Stånggrundsfjärden in the Forsmark area is located just outside the drainage area of Lake Bolundsfjärden (Figure 4-14). The basin has a total surface area of 5.5 km² and water volume of 0.021 km³. The maximum depth in this basin is about 13 m, the average depth 6 m and light penetration depth is about 6.7 m (field measurements, SICADA). The average annual retention time for the water in this basin is less than half a day /Lindborg, 2005/.

Carbon budget for Basin Stånggrundsfjärden

The total biomass (excluding DIC and POC) in Basin Stånggrundsfjärden amounts to about 1.1×10^8 gC, where 96% of the biomass is associated to the benthic habitats (52% flora and 44% fauna) (Table 4-7). The biomass is, as in Basin SAFE-area, clearly dominated by benthic primary producers and detritivores. The phytoplankton, macrophytes and microphytes contribute with about one third each of the total primary production (see Figure 4-20). As for the SAFE-area, the annual amount of primary production (4.9×10^8 gC yr⁻¹) approximately equals the respiration (4.7×10^8 gC yr⁻¹) (Table 4-7). The supply of carbon available for consumption (grazing or predation) (1.3×10^9 gC yr⁻¹) is about three times higher than the carbon demand resulting in an excess of carbon (biotic biomass) of 4.3×10^8 gC yr⁻¹ (this estimate does not include the inflow of POC to the area). As a consequence of a positive net excess value and a total primary production exceeding the total respiration, the basin could be considered as net autotrophic. However, as for the SAFE-area, the estimated predation on zooplankton and benthic bacteria is higher than the estimated supply of carbon from these groups. For zooplankton this is possibly due to the poor estimations of fish biomass and fish consumption because of the lack of site-specific data for fish. The reason for the over-predation of the benthic bacteria by the benthic detritivores may be related to the model being a static illustration of the ecosystem.

Table 4-7. Biomass (gC/basin), annual primary production or consumption of carbon by each functional group (gC/yr/basin), respiration (gC/yr/basin), supply (available for grazing or predation) (gC/yr/basin), grazing or predation on the functional groups (gC/yr/basin) and excess (gC/yr/basin) in the ecosystem in Basin Stånggrundsfjärden. (Birds and humans have been excluded due to lack of data.)

Basin	Biomass (gC/basin)	Prod. or Cons. (gC/yr/basin)	Respiration (gC/yr/basin)	Supply ¹ (gC/yr/basin)	Graz. or pred. ² (gC/yr/basin)	Excess ³ (gC/yr/basin)
Stånggrundsfjärden						
Phytoplankton	1.8×10 ⁵	1.4×10 ⁸	–	1.4×10 ⁸	2.7×10 ⁶	1.4×10 ⁸
Microphytes	1.3×10 ⁷	1.4×10 ⁸	–	1.4×10 ⁸	4.3×10 ⁶	1.4×10 ⁸
Macrophytes	4.4×10 ⁷	2.0×10 ⁸	–	2.0×10 ⁸	1.4×10 ⁷	1.9×10 ⁸
Bacterioplankton	4.9×10 ⁵	7.9×10 ⁷	4.0×10 ⁷	4.0×10 ⁷	7.4×10 ⁶	3.2×10 ⁷
Zooplankton	2.4×10 ⁵	9.7×10 ⁶	3.2×10 ⁶	6.5×10 ⁶	3.0×10 ⁷	–2.3×10 ⁷
Zoopl. feeding fish	2.5×10 ⁶	2.9×10 ⁷	9.8×10 ⁶	2.0×10 ⁷	1.6×10 ⁶	1.8×10 ⁷
Benthic feeding fish	6.6×10 ⁵	7.9×10 ⁶	2.6×10 ⁶	5.2×10 ⁶	4.3×10 ⁵	4.8×10 ⁶
Predatory fish	1.7×10 ⁵	2.0×10 ⁶	6.5×10 ⁵	1.3×10 ⁶	1.1×10 ⁵	1.2×10 ⁶
Benthic herbivores	1.5×10 ⁶	1.8×10 ⁷	6.1×10 ⁶	1.2×10 ⁷	9.5×10 ⁵	1.1×10 ⁷
Benthic filter feeders	6.8×10 ⁵	5.0×10 ⁶	1.7×10 ⁶	3.3×10 ⁶	4.4×10 ⁵	2.9×10 ⁶
Benthic detritivores	4.2×10 ⁷	1.0×10 ⁹	3.4×10 ⁸	6.7×10 ⁸	2.7×10 ⁷	6.5×10 ⁸
Benthic carnivores	5.8×10 ⁵	2.1×10 ⁷	6.8×10 ⁶	1.4×10 ⁷	1.0×10 ⁵	1.4×10 ⁷
Benthic bacteria	4.7×10 ⁶	7.8×10 ⁷	3.9×10 ⁷	3.9×10 ⁷	3.4×10 ⁸	–3.0×10 ⁸
Fish feeding birds	–	–	–	–	–	–
Benthic feeding birds	–	–	–	–	–	–
Seals	2.0×10 ⁴	1.9×10 ⁵	–	1.9×10 ⁵	–	1.9×10 ⁵
Humans	–	–	–	–	–	–
DIC	2.2×10 ⁸	–	–	2.2×10 ⁸	4.9×10 ⁸	–2.7×10 ⁸
POC	9.2×10 ⁶	–	–	9.2×10 ⁶	8.3×10 ⁸	–8.2×10 ⁸
Total (only biota)	1.1×10 ⁸	(prod.) 4.9×10 ⁸ (cons.) 1.3×10 ⁹	4.5×10 ⁸	1.3×10 ⁹	4.3×10 ⁸ net excess	8.7×10 ⁸ 4.8×10 ⁷

¹ Supply = consumption – respiration.

² Grazing or predation upon the respective functional group.

³ Excess = supply – grazing or predation.

In these calculations, the net inflow of DIC and POC from runoff and exchange with other sea basins has not been included. For Basin Stånggrundsfjärden, the annual terrestrial runoff was assumed to be insignificant compared to the water exchange rate between the marine basins. The basin has a modelled Average Transit Residence (ATR) time of 0.30 days, which possibly generates an exchange of POC corresponding to 1.2×10¹⁰ gC. The total excess of biota, i.e. supply – grazing or predation, also contributes to the POC pool, but is two orders of magnitudes lower than the POC flow caused by the water fluxes. The exchange with surrounding water also results in a potential inflow of 2.7×10¹¹ gC DIC.

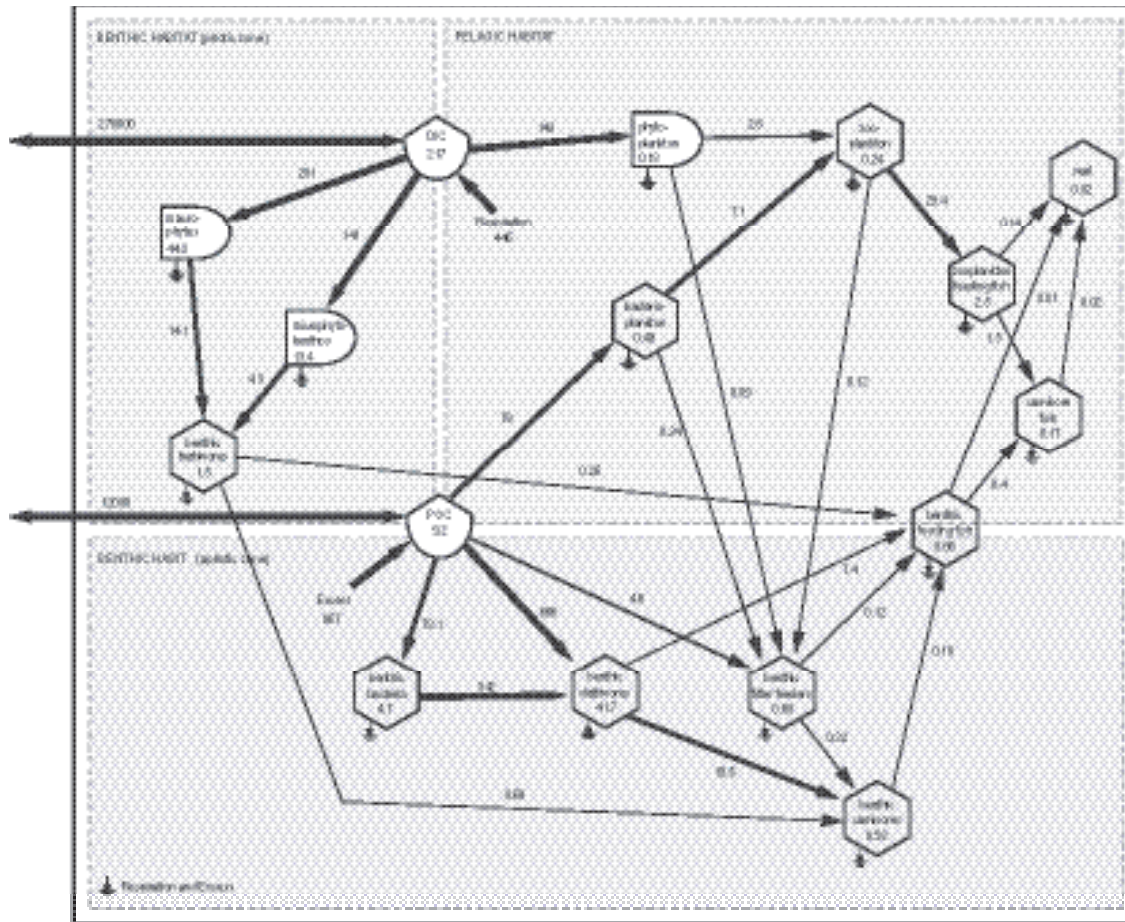


Figure 4-20. Carbon flow model for Basin Stånggrundsfjärden in Forsmark. Biomass (10^6 gC) and flow of carbon between the functional groups, i.e. consumption (10^6 gC yr⁻¹).

4.9 Evaluation of uncertainties

4.9.1 Abiotic descriptions

Hydrology and meteorology

A relatively large amount of new data has been available for the Forsmark version 1.2 modelling. Specifically, the evaluation of time series of local meteorological data and surface water and groundwater levels, enabling comparisons between different processes and hydrological sub-systems, has led to an improved understanding of the site, supporting some of the fundamental aspects of the descriptive model. However, significant uncertainties still exist regarding the interactions between different sub-systems and the spatial and temporal variability of model parameters. In particular, the site-specific basis for setting boundary conditions in hydrological models (i.e. meteorological data) and for evaluating calculated water balances and surface water discharges (i.e. discharge measurements) is still quite weak.

The main uncertainties in the present descriptive model can be summarised as follows:

- The available local meteorological time series are very short (one year) and longer time series, at least a couple of years, are needed to get reliable correlations to nearby regional SMHI-stations that will allow for long-term hydrological and near-surface hydrogeological modelling.
- Local continuous discharge measurements were not available for model version 1.2. Time series from these measurements will be most valuable for the derivation of a more accurate total water balance, and can be used for calibration and validation of the quantitative models. Four discharge stations are now running, producing data that will be used in forthcoming model versions.

- The groundwater levels in the area are very shallow. However, there is a bias to local topographical minima in the location of the monitoring wells. The implications of this bias should be analysed and some additional wells should be located to typical local topographical maxima (recharge areas).
- The evident difference in groundwater levels between the soil and the upper bedrock observed at some of the core-drill sites should be further investigated for a better understanding of hydraulic contact between the soil and the rock. The sites studied are considered to be recharge areas. A similar study in a local discharge area is recommended.
- More information on the hydraulic conditions at and below lakes and wetlands is essential since they have been identified as important discharge areas. Further field investigations including drillings and hydraulic tests are recommended to reduce this uncertainty.
- The locations of recharge and discharge areas at different scales are crucial for the understanding of groundwater system. A combination of complementary field investigations, including hydrogeological and hydrogeochemical methods, and modelling exercises using models based on morphological parameters as well as hydrogeological modelling is recommended. The models should be compared with the vegetation map, the soil map and the map of the Quaternary deposits.

4.9.2 Biotic descriptions

Terrestrial ecosystem

For the overall carbon budget, the importance of the different pools and fluxes is set by their relative size. This means that large variation or uncertainties in relative large pools/fluxes overshadow the influence of relatively smaller pools/fluxes. This has often been an argument as to why some smaller pools or fluxes have been left out. There is a large spatial variation within the regional area as an effect of different abiotic conditions and due to disturbances, such as logging and thinning in the forestry industry. The biomasses of trees are probably the data that have the best estimates in this carbon budget, and they are also sampled from a fairly large regional area covering a large number of age classes and abiotic conditions.

It should be noticed that the production figures of mammals given by Göran Cederlund, Svensk Naturförvaltning, as a percentage of the biomass, are roughly calculated and are not to be regarded as well-established values. More adequate estimates of the production will hopefully come out of a new report on mammals.

The largest stocks and flows are associated with trees (except the SOC). This means that a low confidence in these values would have a large effect on the overall confidence in the descriptive models. The estimates of tree properties are, however, the best estimates there are (in terms of all the data used) in the sense of number of replicates, coverage of the region and the allometric functions used within Riksskogstaxeringen (the National Forest Inventory, NFI), to calculate biomass for the above ground fractions. There is a large variation depending on a number of factors such as nutrient status and wetness.

An assumption of a steady state has repeatedly been applied when quantifying turnover of plant tissue. This assumption in some cases entails an overestimation of the actual turnover, because there is some net accumulation perennial taxa, but there are a lack of data describing these processes on the community level. In other cases, the assumption is more justified e.g. root turnover /Majdi, 2001/.

Interestingly, few or no single studies have been identified in which all the properties that have been treated above have been studied. Partly, because of the laborious work involved, but also because many of the pools and fluxes are small in comparison with the major system components, and are therefore expected to have a small influence on the overall carbon budget.

Limnic ecosystem

The lake carbon budgets in this study are mainly based on site-specific data from extensive studies in Lake Eckarfjärden. Since the biomasses of most functional groups, as well as many of the important ecosystem processes, have been measured directly in the lake, and since missing data were estimated from studies in lakes similar to Lake Eckarfjärden, the uncertainties in estimated stocks and flows of carbon can be considered as small. This makes the confidence of the carbon budget relatively high, although some uncertainties of course exist.

Generic data were used for biomass and production of *Chara* and epiphytic algae, bacteria and fauna. The magnitude of these parameters may therefore be over- or underestimated. Concerning *Chara*, it is likely that the two parameters have been underestimated, since local observations are that the biomass is very high and the literature value used is the average biomass from several studies /Kufel and Kufel, 2002/. The rate of primary production for *Chara* spp. used /Pereya-Ramos, 1981/ was also chosen from the low end of reported studies /Kufel and Kufel, 2002/.

Due to a small area available for colonisation by epiphytic algae, this functional group contributes little to the total primary production. The small substrate area is a consequence of a large part of the reed belt being above the water surface during the summer. The estimates used for primary production by epiphytic algae per substrate area of *P. australis* /Muelemanns, 1988/ was about 10 times higher than productivity estimates reported by e.g. /Gessner et al. 1996/, but in the same order of magnitude as reported by /Allen and Osceviski, 1981/. However, because of the small area available for colonisation by epiphytes, overestimation has little effect on the budget.

Fish data have been collected by standardised and generally accepted methods; however, the generated data are only semi-quantitative. The conversion of catch per unit effort (CPUE) data to an absolute estimate of biomass per area unit is associated with large uncertainties. To our knowledge, no study exists to validate any conversion factor, and the proposed conversion factor which is used in this report may be regarded as an “expert guess”.

The estimated net and gross transport of carbon from the lakes is of course associated with large uncertainties, since site-specific chemistry data have to be coupled with regional discharge data. This uncertainty will, however, be considerably reduced in the next model version, when site specific discharge data will be available. Similarly, the values of annual sedimentation in Lakes Eckarfjärden and Bolundsfjärden are associated with large uncertainties and the calculations should be regarded as an attempt to obtain rough estimates of the magnitude of sedimentation.

Marine ecosystem

The quality and representativity of the data are summarised in Table 4-8 and are discussed below. A more detailed discussion is presented in /Lindborg, 2005/.

The bathymetric data used to estimate the areas and volumes of the basins originate from a combination of recent site-specific measurements and existing digital nautical charts and have a very high quality /Lindborg, 2005/.

The estimates of the extensions of the photic and aphotic zones are based on the rough assumption that the photic zone is twice the light penetration depth (which has been measured in the field). This assumption is probably fairly accurate.

The primary production was generally estimated from the biomass, conversion factors, and the solar insolation during the year. An optimal approach would have been to measure the primary production at the sites during the year. However, the calculated primary production probably has a sufficient good quality, since the conversion factors used are species-specific in most cases and mostly obtained from the Baltic Sea, and the insolation measurements used in the calculations are site-specific with a high resolution. The assumption that the epiphyte biomass and primary production were included in the macrophyte estimates probably contributes to an underestimation in total biomass and primary production.

Table 4-8. Estimations of the quality of input data and their representativeness for the basins in the Forsmark area. Higher values indicate high quality or better representativity.

Functional group	Quality of data (1–4)	Representativity of data (1–4)
Areas and volumes	4	4
Photic zone	3	3
Carbon transport	2	2
DIC	2	4
POC	2	4
Phytoplankton	2	4
Macrophytes	3	4
Bacterioplankton	3	2
Zooplankton	2	4
Zooplankton feeding fish	2	1
Benthic fauna feeding fish	2	1
Predatory fish	2	1
Benthic herbivores	3	4
Benthic filter feeders	3	4
Benthic detritivores	3	4
Benthic carnivores	3	4
Benthic bacteria	3	2
Seal	3	2

The reasoning applicable for the estimates of the primary production also applies to the estimates of the respiration, i.e. that real measurements probably would have given better estimates than the calculations used in this study. However, as in the case of primary production, the use of species-specific conversion factors probably makes the calculations fairly correct. The assumption that the respiration to consumption ratio is approximately 1:3 is a fairly well accepted relationship, as is also that it is less for bacteria (1:2), since their metabolism has a higher rate.

Human population description

Most of the data were obtained from Statistics Sweden (SCB). When only a single object is found within a geographic area, SCB adjusts this single object to a “false” zero for reasons of individual privacy. If two objects are found, the count is adjusted to three /SCB, 2003/. This can result in incoherence between the sum of values for different categories and the total number (as an example the total number of inhabitants and the sum of inhabitants per age class). As the parish of Forsmark is a very sparsely populated area this is a potentially significant source of error. Also, in sparsely populated areas, the data becomes more statistically unreliable, irrespective of the above deliberate reporting bias.

Furthermore, there are some uncertainties concerning the data from the National Board of Fisheries (Fiskeriverket). The catch statistics within the offshore grid (EU-grid) only comprise the catch from the logbook-keeping vessels, as they report the tackle position. Second, the catch is registered in the square where the tackle is placed, but that does not necessarily mean that the fish has been caught in that particular square. Fishing boats can trawl a long distance and therefore catch the main part of the fish in a neighbouring square. The catch data at each EU-square therefore varies considerably between the years.

5 Bedrock geology

The bedrock geological model consists of three components; the rock domain model, the deterministic deformation zone model, and the statistical description of fractures and possible deformation zones inferred from lineaments, the discrete fracture network (DFN) model. The work has been carried out with the assistance of the SKB guidelines described in /Munier et al. 2003/. As in the model version 1.1, the rock domain and deterministic deformation zone models are presented for the whole regional model volume. The DFN model has utilised fractures from essentially within the local model volume and addresses possible deformation zones inferred from lineaments in the mainland area. Only fractures that are situated outside deformation zones have been included in the DFN model.

One rock domain model is presented. Despite a significant increase in the amount of new data, there are only minor changes when a comparison is made with model version 1.1. The model can be described as stable. A base model, a variant of this model and an alternative model for the deterministic deformation zones in the regional volume are presented. Compared with model version 1.1, there is a more confident and a more detailed presentation of a conceptual model for the deformation zones at the site. Furthermore, there is a marked increase in the number of high confidence zones. This part of the geological modelling work is stabilising, but important changes are anticipated when new data become available in future modelling work. The assessment of the version 1.2 data in the DFN model shows that the spatial variability in the size, intensity and properties of fractures outside deformation zones is large. This part of the geological model remains unstable.

One or more components of the bedrock geological model provide a foundation for the modelling work in rock mechanics, thermal properties, hydrogeology (bedrock) and, to less extent, even hydrogeochemistry (bedrock) and transport properties (bedrock). All components of the geological model have a direct impact on the location and design of the repository volume. They also provide a significant input for certain aspects of the safety analysis.

5.1 State of knowledge at previous model version

The same three components of the bedrock geological model are present in model version 1.1 as are present in version 1.2. In the former model, these three components were developed on the basis of an incomplete assembly of surface information and a very limited amount of borehole information. Geological and geophysical data with a high resolution were only available at the surface in the area between road 76 and the coast. For this reason, the bedrock geological map at the surface and the lineament map were both at an incomplete stage in their development when compilation was carried out for model version 1.1. Detailed fracture data from only two surface sites were used.

Data bearing on the character of the bedrock at depth was even more restricted in extent. Only data from one cored borehole (KFM01A) and from eight percussion boreholes (HFM01–HFM08) were included in model version 1.1. Furthermore, rigorous single hole interpretations of these boreholes had not been completed prior to the establishment of the version 1.1 geological model. There was also little information that could help to calibrate the seismic reflection data. For this reason, the reflectors were utilised in a supportive rather than a deterministic manner. Finally, an assessment of older geological and geophysical data from the nuclear power plant and from SFR had not been completed prior to the modelling work.

With this restricted information, particularly at depth, the first rock domain, deterministic deformation zone, and DFN models were presented for the site, in the context of the site investigation programme /SKB, 2004a/. The rock domain and deformation zone models were presented for the regional model volume and the DFN model was presented for the local model volume. As pointed out above, the rock domain model in version 1.2 strongly resembles that presented in version 1.1. However, major changes have occurred in the deformation zone and DFN models. Nevertheless, both models contain the same orientation sets for both deformation zones and fractures in the bedrock.

The following major uncertainties were identified during the development of the version 1.1 rock domain model.

- The quality and resolution of surface data south of road 76 and, especially, in the sea area to the north-east of the candidate area. It was anticipated that this problem would reduce dramatically when new data became available for model version 1.2. However, the problem would remain for the offshore sea area at Öregrundsgrepen.
- The precision in the location of the boundaries between rock units that show different degrees of homogeneity and of ductile deformation.
- The extension of rock domain boundaries at depth, especially outside the local model volume where data at depth are absent. It was anticipated that the problem outside the local model volume would almost certainly remain in future model versions.
- The proportions of various rock types in each rock domain, especially outside the local model volume. It was anticipated that this problem would reduce inside the local model volume when more borehole data became available.

In a similar manner, the following uncertainties were recognised in the version 1.1, deterministic deformation zone and DFN models.

- The geological feature (features) that gives (give) rise to the seismic reflectors.
- The geological feature (features) that is (are) represented in the inferred lineaments. The key question raised concerned the correlation of lineaments with deformation zones in the bedrock.
- The position at the surface and, especially, the length, dip, thickness and extension at depth of the deformation zones that have been inferred from lineaments. Two points of high uncertainty were recognised – the continuity and the dip of these possible deformation zones.
- The extension in both the strike and dip directions of the gently dipping deformation zones.
- The interpretation that fractures and lineaments can be represented by the same statistical distributions for orientation, size and intensity.
- The orientation, size and intensity of fractures that are longer than those documented in connection with the detailed fracture mapping at the surface and shorter than that inferred to be represented by lineaments.
- The variability of the geometric properties of fracturing at depth.
- The variability of the fracturing in rock domains outside the domain that dominates the candidate volume.

As the following text will show, several of these uncertainties have been removed in model version 1.2 whereas other uncertainties remain. For example, there is now a much better understanding of the geological character of the seismic reflectors and even of some of the lineaments. Furthermore, the development of a more detailed conceptual model for the deformation zones at the site provides a better geological basis for tackling the continuity of, especially, the gently dipping deformation zones.

5.2 Evaluation of primary data

5.2.1 Outcrop mapping and complementary analytical studies

Data

The character of the various rock types at the Forsmark site is defined primarily on the basis of two data sets:

- Outcrop mapping data.
- Complementary analytical results from representative, surface bedrock samples.

These data are essential for the development of a bedrock geological map of the site (see Section 5.2.2). Furthermore, in combination with the corresponding, more limited borehole information (see Section 5.2.6), they yield the properties of the different rock types in the rock domain model (see Section 5.3).

The intensity of outcrop mapping data varies within the regional model area. Three areas, which contain data of markedly different intensity, are recognised (Figure 5-1):

- The mainland.
- The archipelago in the coastal area.
- The open sea area at Öregrundsgrepen.

Detailed mapping of the bedrock outcrops and follow-up analytical work were carried out in both the mainland and archipelago areas during 2002 and 2003. The results of these activities were reported during 2003 to 2005. Apart from some poorly exposed areas, e.g. in the critical north-western part of the candidate area close to and north-west of Bolundsfjärden, there is a relatively even dispersion of these high-quality, outcrop data on the mainland (Figure 5-1). The quality of exposure on most of the islands is excellent. However, the bedrock exposure in the archipelago is limited and, for this reason, there is an uneven distribution of high-quality outcrop mapping data in this area (Figure 5-1). In the open sea area at Öregrundsgrepen, surface outcrop data are absent (Figure 5-1). Furthermore, in the small area on Gräsö, in the easternmost part of the regional model area, only outcrop information that was generated in connection with an older bedrock map compilation at the scale 1:50,000 /Svenonius, 1887/ is available. These outcrop data have not been used in the present work and an evaluation of their character and quality is lacking.

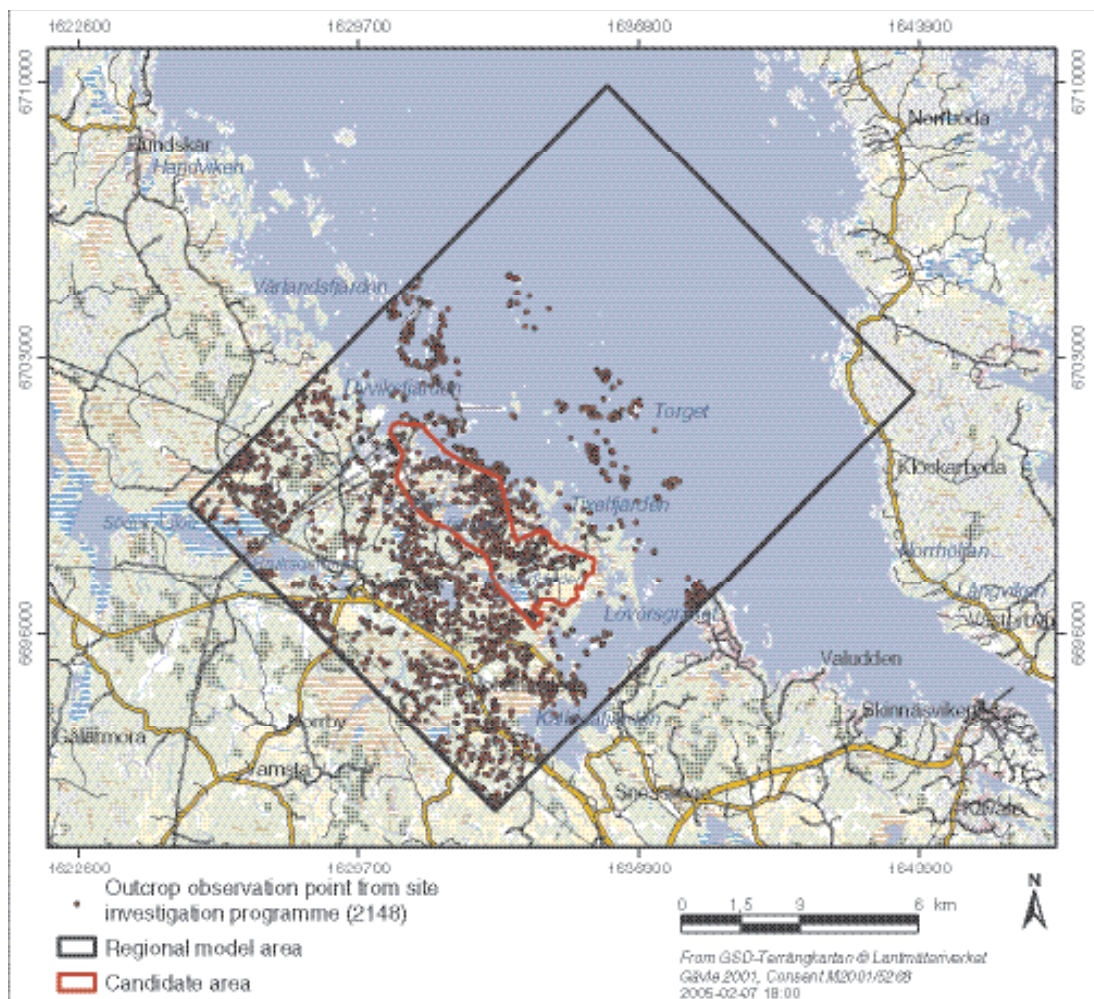


Figure 5-1. Summary of outcrop data generated by the site investigation programme in the regional model area.

The following outcrop mapping data, with complementary analytical material from representative samples, are available from the mainland and the archipelago areas. Geochronological data from the Forsmark site /Page et al. 2004/ are discussed under the evolutionary aspects of the site (see Section 3.1):

- Character of the rock type at 2,119 outcrop observations, at the base of eight, temporarily exposed minor trenches and at 21 shallow boreholes in the Quaternary cover (Figure 5-1). These objects were studied in connection with the bedrock mapping programme at the scale 1:10,000, and the field data were subsequently synthesised in /Stephens et al. 2003a; Bergman et al. 2004/. The data also include repetitive measurements (commonly eight) of the magnetic susceptibility of different rock types at 1,832 of the outcrops. These data were subsequently evaluated and interpreted in /Isaksson et al. 2004a,b/.
- Character of the rock type that was documented in connection with the detailed fracture mapping of five sites at the scale 1:50 (see Section 5.2.4). These sites include Klubbudden, which has an areal extent of c. 325 m², and four temporarily exposed outcrops at drill sites 2, 3, 4 and 5, which range in areal extent from c. 500 to c. 600 m² /Hermanson et al. 2003a,b, 2004/.
- Petrographic data from 159 surface rock samples (Figure 5-2a) and the evaluation and interpretation of these data in /Stephens et al. 2003b, 2005a/. This data set includes 122 modal analyses that have been recalculated to QAP(F=0) values, in order to permit a mineralogical classification of the different rock types /Streckeisen, 1976, 1978/.
- Geochemical data from 90 surface rock samples (Figure 5-2b) and the evaluation and interpretation of these data in /Stephens et al. 2003b, 2005a/. These data permit, for example, a geochemical classification of the different rock types /Winchester and Floyd, 1977; Debon and Le Fort, 1983; Le Bas et al. 1986; Middlemost, 1994/.
- Laboratory measurements of the density, magnetic properties, electrical properties and porosity of 139 surface rock objects (Figure 5-2c), and the evaluation and interpretation of these data /Mattsson et al. 2003; Isaksson et al. 2004a,b/. For the most part, measurements were carried out on four samples of each rock.
- In-situ measurements of gamma-ray spectrometry properties of 169 surface rock objects (Figure 5-2d), and the evaluation and interpretation of these data /Mattsson et al. 2003; Isaksson et al. 2004a,b/.

On account of the release of stress during unloading and exhumation of the bedrock, it is probable that the porosity values included in the published data reports are too high. For this reason, these values need to be handled with care. In the same data reports, calculations of the natural exposure rate have been carried out on the basis of the in-situ gamma-ray spectrometry measurements. The unit microR/h has been used in these calculations. It should be noted that 1R = 0.01 Gray (Gy).

Rock types

Overview

Intrusive igneous rocks dominate the Forsmark site. Supracrustal rocks, which are predominantly volcanic in origin and contain calc-silicate rocks and iron oxide mineralisation, form a subordinate component. Apart from some younger granite, pegmatitic granite and pegmatite, all rocks are affected, to a variable extent, by penetrative ductile deformation. This deformation is associated with recrystallization that occurred under amphibolite-facies (> 500–550°C) metamorphic conditions and at depths probably greater than 15 km. For this reason, most of the rock names are prefixed with the term “meta”.

Outcrop mapping on the mainland and in the archipelago area indicates that four major groups of rock types – Groups A to D – are present (Table 5-1). The candidate area on the mainland is dominated by a medium-grained, biotite-bearing metagranite that belongs to the Group B intrusive suite. Amphibolite, fine- to medium-grained metagranitoid that belongs to Group C, and pegmatitic granite, pegmatite and fine- to medium-grained granite that belong to Group D form subordinate components (see also Sections 5.2.2 and 5.2.6).

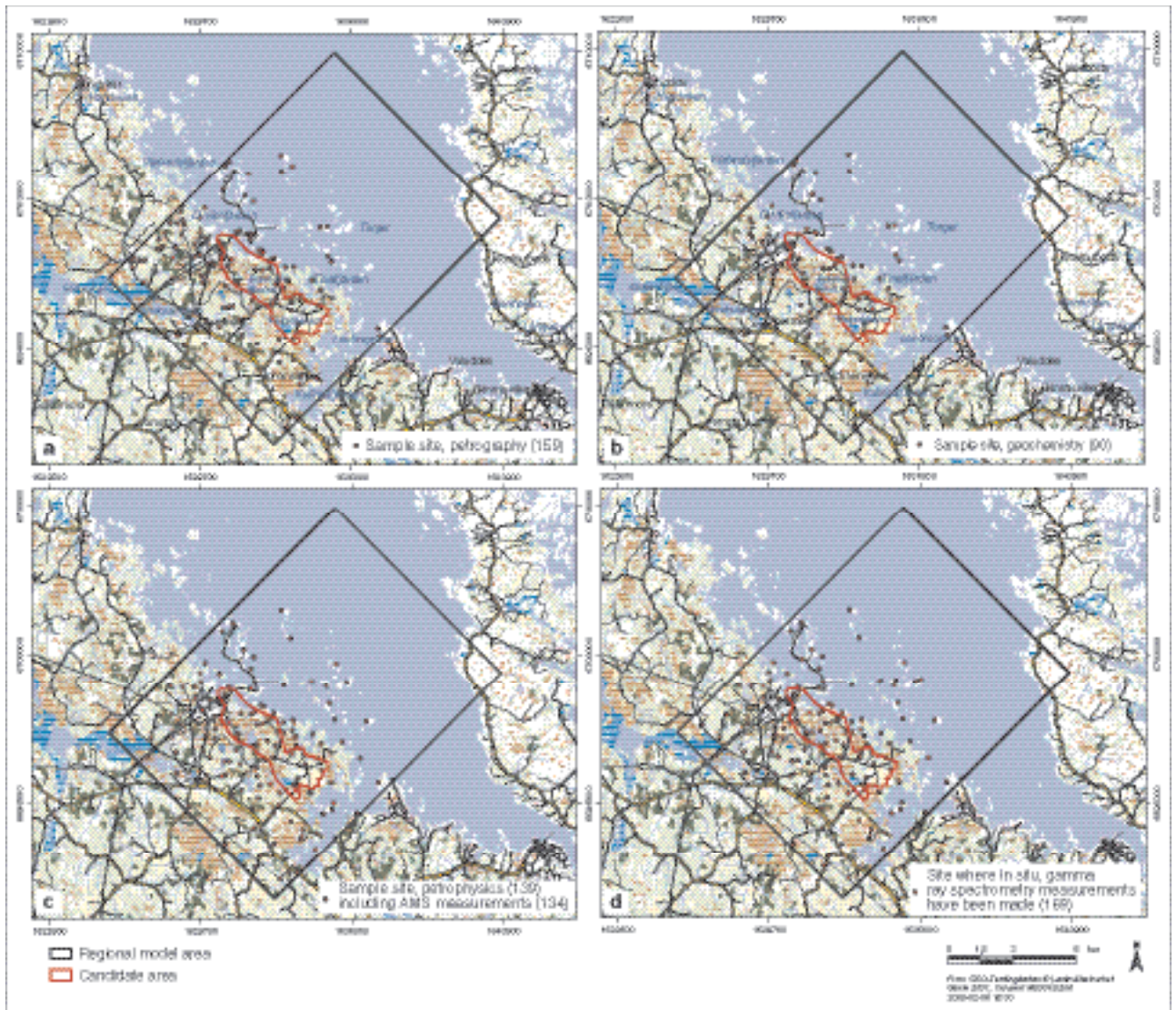


Figure 5-2. Sites where samples have been taken for the measurements of petrographic (a), geochemical (b) and petrophysical (c) data and where in-situ, gamma-ray spectrometry measurements have been carried out (d).

The rocks in Group A form the oldest rocks and are dominated by metavolcanic rocks and iron oxide mineralisation. They belong to the Svecofennian, predominantly supracrustal rocks in the Bergslagen area and its surroundings in central Sweden. These rocks formed during phase 1 in the geological evolution of this part of the Fennoscandian Shield (see Section 3.1).

The rocks in Group B consist of major plutonic rocks with variable compositions. They belong to the early-tectonic suite of intrusive rocks that also formed during phase 1 in the geological evolution of this part of the shield (see Section 3.1). Such plutonic rocks dominate large areas in the eastern part of central Sweden.

The predominantly minor intrusive rocks in Groups C and D are younger than the rocks in Group A and most of the rocks in Group B. However, their absolute ages overlap with the youngest rocks in Group B, including the biotite-bearing metagranite in the candidate area (see Section 3.1). Furthermore, there are variable time relationships between the rocks in Groups C and D. These intrusive rocks are correlated with the early-tectonic suite of intrusive rocks that formed during phase 2 in the geological evolution of this part of the Fennoscandian Shield (see Section 3.1). Plutonic rocks that belong to this evolutionary phase dominate northwest of Gävle, in the central part of Sweden.

Table 5-1. Major groups of rock types recognised during outcrop mapping at the Forsmark site. The geochronological data are discussed in Section 3.1. SKB rock codes are shown in brackets after each lithology.

Rock types	
<i>All rocks are affected by brittle deformation. The fractures generally cut the boundaries between the different rock types. The boundaries are predominantly not fractured.</i>	
<i>Rocks in Group D are affected only partly by ductile deformation and metamorphism.</i>	
Group D (c. 1,851 million years)	<ul style="list-style-type: none"> Fine- to medium-grained granite and aplite (111058). Pegmatitic granite and pegmatite (101061) <p>Variable age relationships with respect to Group C. Occur as dykes and minor bodies that are commonly discordant and, locally, strongly discordant to ductile deformation in older rocks</p>
<i>Rocks in Group C are affected by penetrative ductile deformation under lower amphibolite-facies metamorphic conditions.</i>	
Group C (c. 1,864 million years)	<ul style="list-style-type: none"> Fine- to medium-grained granodiorite, tonalite and subordinate granite (101051). <p>Occur as lenses and dykes in Groups A and B. Intruded after some ductile deformation in the rocks belonging to Groups A and B with weakly discordant contacts to ductile deformation in these older rocks.</p>
<i>Rocks in Groups A and B are affected by penetrative ductile deformation under amphibolite-facies metamorphic conditions.</i>	
Group B (c. 1,886–1,865 million years)	<ul style="list-style-type: none"> Biotite-bearing granite (to granodiorite) (101057) and aplitic granite (101058), both with amphibolite (102017) as dykes and irregular inclusions. Tonalite to granodiorite (101054) with amphibolite (102017) enclaves. Granodiorite (101056). Ultramafic rock (101004). Gabbro, diorite and quartz diorite (101033).
Group A (supracrustal rocks older than 1,885 million years)	<ul style="list-style-type: none"> Sulphide mineralisation, possibly epigenetic (109010). Volcanic rock (103076), calc-silicate rock (108019) and iron oxide mineralisation (109014). Subordinate sedimentary rocks (106001).

Metavolcanic rocks and iron oxide mineralisation (Group A)

Due to the effects of ductile deformation and recrystallisation under amphibolite-facies metamorphic conditions, an uncertainty remains concerning whether the metavolcanic rocks represent juvenile pyroclastic rocks, lavas, synvolcanic intrusions, resedimented volcanoclastic deposits or even volcanogenic sedimentary rocks. It is likely that several of these rock types are present in this group.

The metavolcanic rocks are fine-grained and show, at several outcrops, a compositional layering (Figure 5-3a). Apart from two samples with an andesitic composition, the Group A rocks are felsic in character and contain between 24 and 39% quartz (Figure 5-4). Plagioclase is the dominant feldspar and biotite and/or hornblende comprise the mafic minerals (Figure 5-4). Secondary alteration includes saussuritization and/or sericitization of plagioclase feldspar, and growth of epidote, chlorite (after biotite), goethite (after pyrite), prehnite and calcite.

Mineralogically, the metavolcanic rocks show a dacitic to andesitic composition (Figure 5-5a). However, both geochemical (Figure 5-6a) and density (Figure 5-7a) data indicate a more varied rhyolitic to andesitic composition. This discrepancy may be related to early-stage (pre-tectonic) hydrothermal alteration. The local occurrences of anomalously high SiO₂ (> 74%) and low K₂O (< 1.5%) values, muscovite and sillimanite (fibrolite), and ghost alteration textures indicate that early-stage alteration has affected some of the rocks. The range of porosity values (0.20–0.62%) is restricted (Figure 5-8a) and the uranium contents (2.5–6.8 ppm) are normal (Figure 5-9a).

Calc-silicate rock with actinolite, garnet and commonly more than 50% magnetite is the most important type of mineralisation in the Forsmark area. Locally, these iron oxide mineralisations also contain base metal sulphides. The metavolcanic rocks form their host rock. As expected, the analysed samples of magnetite mineralisation show anomalously high values for density (Figure 5-7a), magnetic susceptibility and porosity (Figure 5-8a), and anomalously low values for electric resistivity.

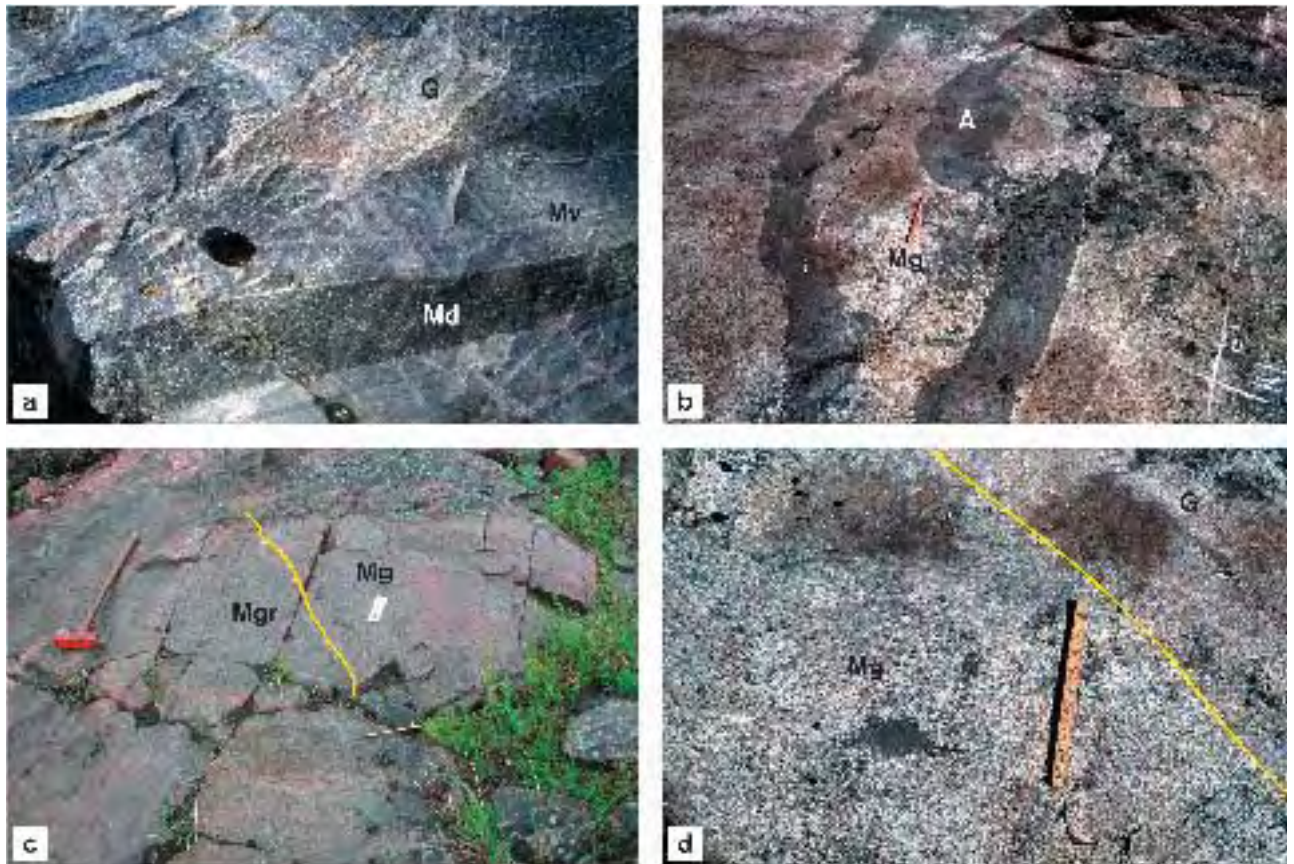


Figure 5-3. a) Group A felsic metavolcanic rock with compositional layering (Mv) intruded by metadiorite dyke with plagioclase phenocrysts (Md) and a younger Group D granite (G). Camera lens cap is c. 5 cm. Observation point PFM001264. b) Group B metagranite (Mg) in candidate area intruded by mafic dyke that is amphibolitic (A). Pencil is c. 10 cm. Observation point PFM001172. c) Group B metagranite (Mg) intruded by Group C metagranodiorite (Mgr). Contact marked with yellow line. Hammer is c. 40 cm. Observation point PFM000718. d) Group B metagranite (Mg) in candidate area intruded by Group D granite dyke (G). Contact is marked with yellow line. Marker is c. 10 cm. Observation point PFM001176.

Ultramafic mafic, intermediate and felsic (quartz-rich) meta-intrusive rocks (Group B)

Medium-grained, equigranular intrusive rocks dominate the Forsmark site (Figure 5-3b). These rocks formed as deep-seated, major intrusions (plutons) and were subsequently affected by ductile deformation and recrystallisation under amphibolite-facies metamorphic conditions. They show a wide variety of compositions that range from ultramafic (partly serpentinized pyroxenite) to mafic (gabbro), intermediate (diorite, quartz diorite) and felsic (tonalite, granodiorite and granite). The felsic rocks belong to the family of intrusive rocks that are referred to as granitoids.

Plagioclase feldspar and hornblende form the dominant minerals in the mafic and intermediate rocks (Figure 5-4). Subordinate amounts of biotite (< 15%) and quartz (< 10%) are also present in the intermediate rocks (Figure 5-4). The high quartz content in the felsic varieties is an important mineralogical feature from the point of view of the thermal characteristics of the site (see Chapter 7). Apart from some of the tonalites and granodiorites, the quartz content in the felsic rocks exceeds 20% and ranges up to 45% (Figure 5-4). The tonalites and granodiorites contain both hornblende and biotite as mafic minerals, hornblende decreasing consistently with increasing quartz content (Figure 5-4). The granites only contain biotite. Growth of epidote, chlorite, prehnite and calcite in combination with saussuritization and/or sericitization of plagioclase feldspar indicate the effects of secondary alteration processes following the crystallisation of these intrusive rocks.

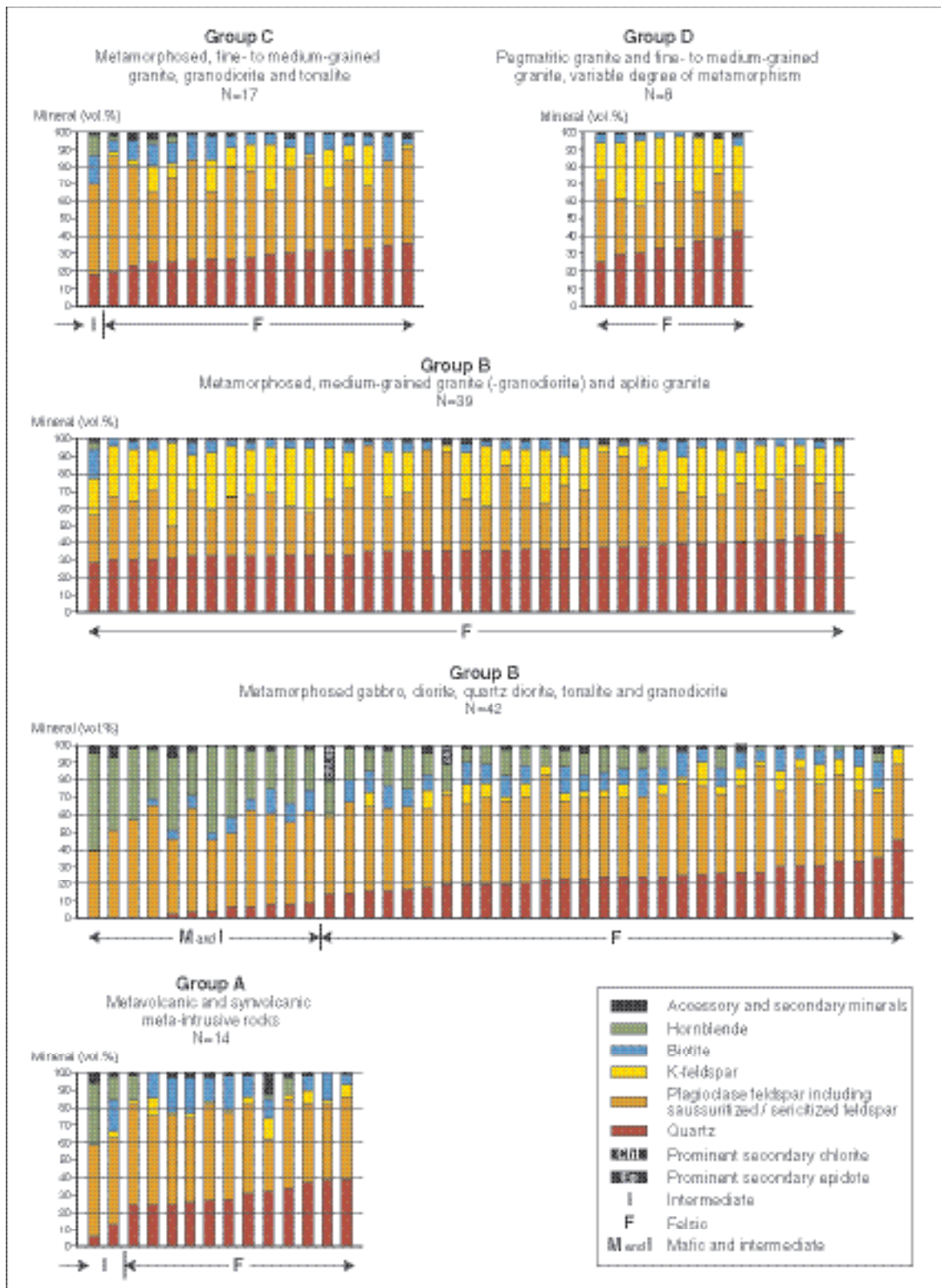


Figure 5-4. Mineralogical composition of the analysed samples in the different rock groups (after /Stephens et al. 2005a/).

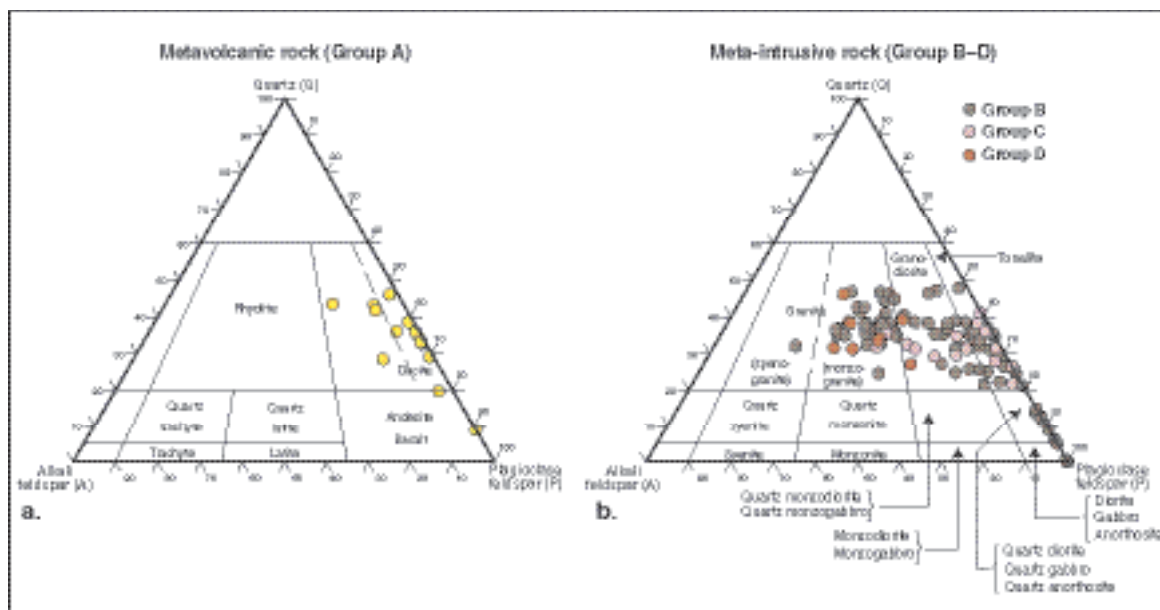


Figure 5-5. $QAP(F=0)$ modal classification of the analysed samples in the different rock groups (modified after /Stephens et al. 2003b, 2005a/). The classification is based on /Streckeisen, 1978/ for the volcanic rocks (a) and /Streckeisen, 1976/ for the intrusive rocks (b).

The wide range in composition of the Group B intrusive rocks is confirmed on the basis of the mineralogical (Figure 5-5b), geochemical (Figure 5-6b) and density (Figure 5-7b) data. However, some of the Group B felsic rocks, which, on the basis of other criteria, resemble the normal, biotite-bearing metagranite in the candidate area or the aplitic metagranite, show anomalously high contents of plagioclase feldspar and low contents of K-feldspar (e.g. PFM001229B and PFM001627A). These samples yield apparent tonalitic or granodioritic compositions on the $QAP(F=0)$ plot and an anomalous trend into the tonalite field on the QP geochemical classification diagram (Figure 5-6c). Anomalous depletion of potassium in some of the metagranites has also been detected in the in-situ gamma ray spectrometry measurements. It appears that early-stage (pre-tectonic) hydrothermal alteration has given rise to higher Na_2O and lower K_2O contents in these granites and has affected their position on various mineralogical and geochemical classification diagrams.

As for the metavolcanic rocks, the range of porosity values for the Group B intrusive rocks (0.25–0.58%) is restricted (Figure 5-8b). Two serpentinized pyroxenites show somewhat higher values (Figure 5-8b). These two samples also show anomalously low values for electric resistivity. The uranium contents of the Group B rocks (0.0–7.6 ppm) do not yield any anomalously high values (Figure 5-9b).

Felsic (quartz-rich) meta-intrusive rocks (Group C)

The Group C rocks are fine- to medium-grained and equigranular. They predominantly occur as minor intrusions in the form of dyke-like bodies, lens-shaped massifs or possible boudins in the rocks belonging to both Groups A and B (Figure 5-3c). The Group C rocks have been affected by penetrative ductile deformation under lower amphibolite-facies metamorphic conditions. However, at several places, the contacts of these bodies are discordant to a planar mineral fabric or a tectonic banding in the adjacent host rocks (Figure 5-3c). They intruded after at least some deformation had affected the rocks within Groups A and B but prior to later ductile deformation and metamorphism.

The quartz content in the Group C samples lies between 18 and 35% (Figure 5-4). In general, plagioclase dominates over K-feldspar, and biotite and/or hornblende comprise the mafic minerals (Figure 5-4). Secondary alteration includes saussuritization and/or sericitization of plagioclase feldspar, and growth of epidote, chlorite (after biotite), goethite (after pyrite), prehnite and calcite.

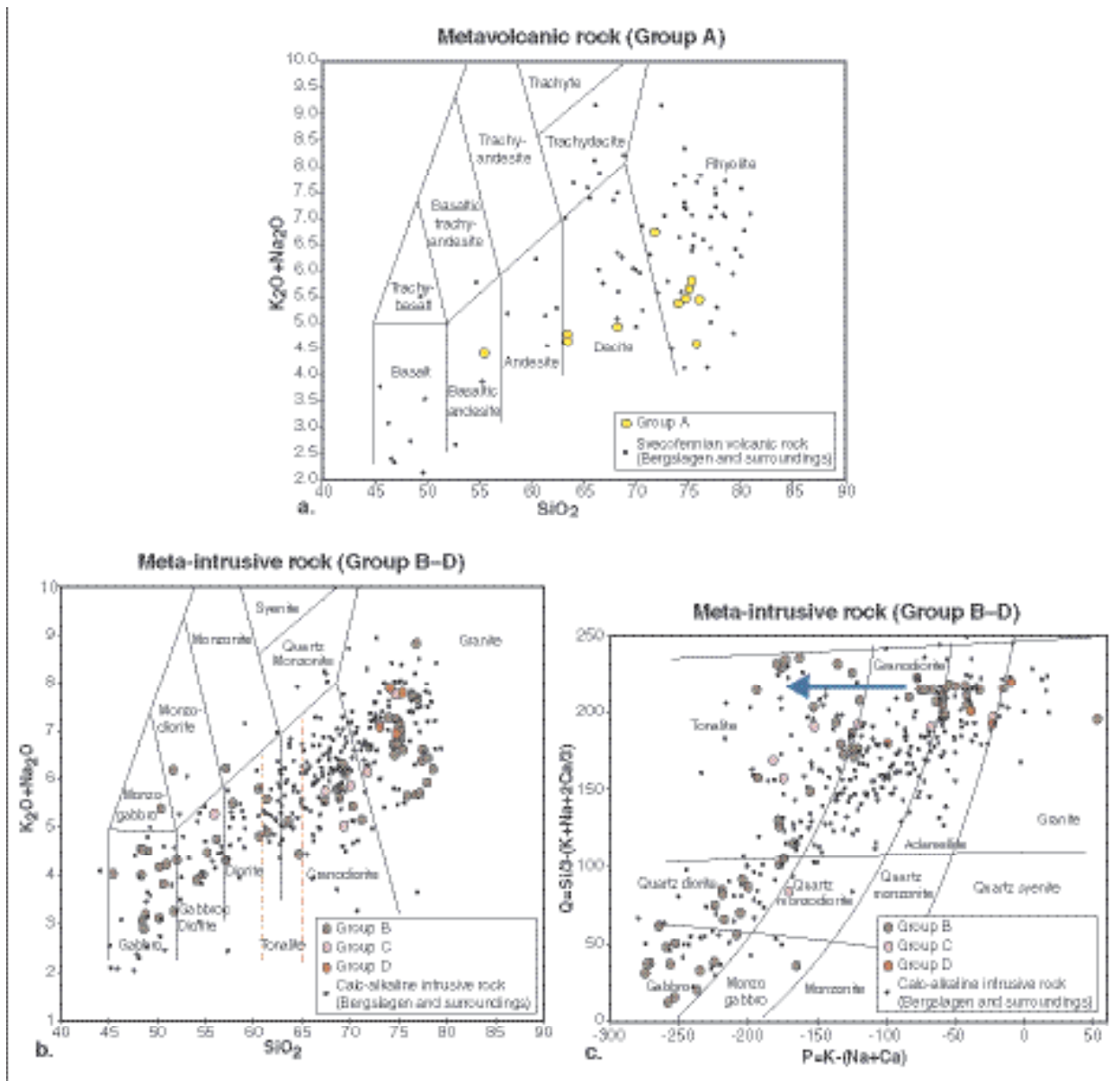


Figure 5-6. Geochemical classification of the analysed samples in the different rock groups (modified after /Stephens et al. 2003b, 2005a/). The classification is based on /Le Bas et al. 1986/ for the volcanic rocks (a), and /Middlemost, 1994/ and /Debon and Le Fort, 1983/ for the intrusive rocks, (b) and (c), respectively.

The Group C intrusive rocks show a compositional bias towards granodioritic and tonalitic compositions in the granitoid family of felsic intrusive rocks (Figure 5-5b). Plots of analysed samples on geochemical classification diagrams (Figure 5-6b and Figure 5-6c) as well as density data (Figure 5-7c) confirm this assessment. The restricted range of porosity values (0.39–0.59%) and the uranium contents (1.9–7.5 ppm) in these rocks (Figure 5-8c and Figure 5-9c, respectively) confirm the similarities of the Group C meta-intrusive rocks to the older Group A and Group B felsic rocks. They can only be distinguished from the older felsic rocks on the basis of their grain size and field occurrence.

Granite, aplite, pegmatitic granite and pegmatite (Group D)

The Group D granites are fine- to medium-grained, equigranular and, in part, leucocratic; aplite (fine-grained, leucocratic granite) is included in this subgroup. These rocks occur as dykes with sealed contacts to the older host rocks or, locally, as larger bodies. Some dykes are zoned in

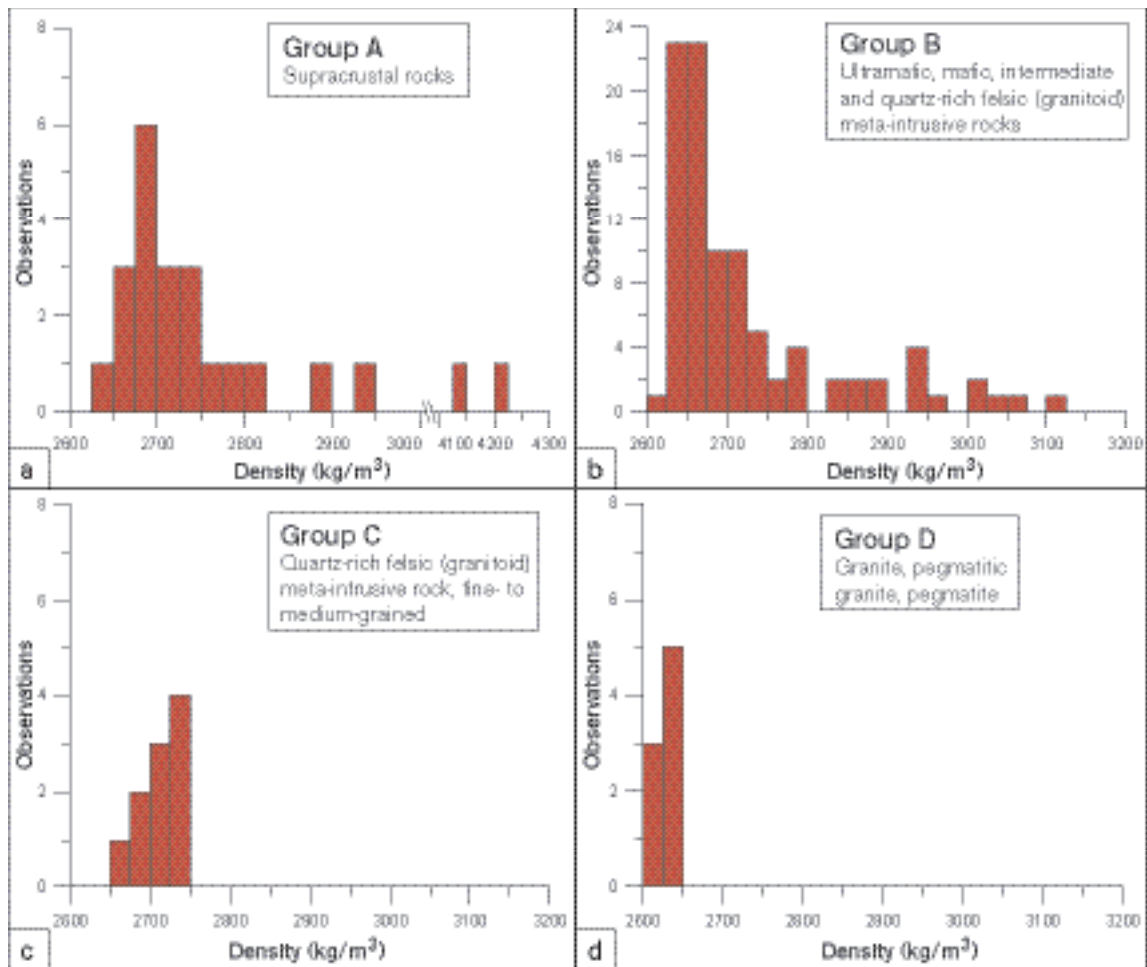


Figure 5-7. Histograms showing the density values for the analysed samples in the different rock groups (modified after /Isaksson et al. 2004b/).

character with a thin pegmatitic rim along the margins of the dyke (Figure 5-3d). In several outcrops, the granites are strongly discordant to the banding and mineral fabric in the host rocks (Figure 5-3d). For this reason, they are inferred to have intruded after much of the ductile deformation had affected the older rocks that belong to Groups A, B and C.

The term pegmatitic granite has been applied to those rocks where the grain size is highly variable and irregularly distributed, often from pegmatite to fine- to medium-grained granite to aplite, in a single body. Pegmatitic granite commonly occurs as irregular concentrations along the contacts to and as injections within the Group C rocks. These field relationships suggest that pegmatitic granite intruded close in time to or after intrusion of the Group C rocks.

Pegmatite occurs as discontinuous bands, lenses and segregations, as more irregular bodies and as dykes. The pegmatites show highly variable relationships to the ductile deformation in the rocks that belong to Groups A, B and C. Some pegmatites are tightly folded and concordant to the banding and mineral fabric in the host rocks. Other pegmatites show distinctly discordant relationships but are, nevertheless, commonly weakly folded. Different generations of pegmatite are inferred to be present.

The quartz content in the granites and pegmatitic granites lies in the range 25 to 43% (Figure 5-4). Plagioclase and K-feldspar are present in approximately equal proportions, and the content of mafic minerals (biotite) is generally low (Figure 5-4). These mineralogical features confirm their predominantly granitic composition (Figure 5-5b). Plots of analysed samples on geochemical classification diagrams (Figure 5-6b and Figure 5-6c) as well as density data (Figure 5-7d) confirm this assessment. Epidote, chlorite (after biotite), prehnite, muscovite and a conspicuous saussuritization/sericitization of plagioclase feldspar form the main secondary minerals.

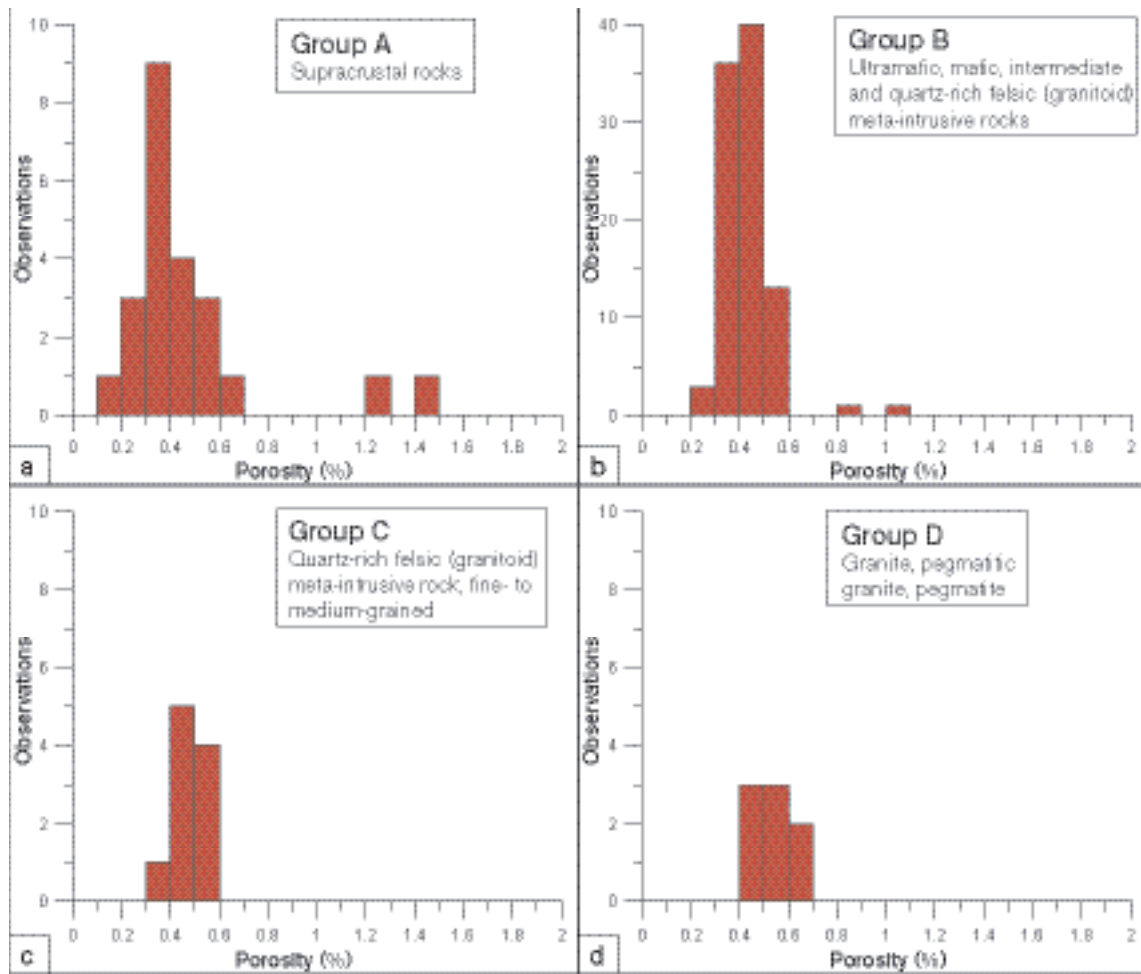


Figure 5-8. Histograms showing the porosity values for the analysed samples in the different rock groups (modified after /Isaksson et al. 2004b/).

The porosity values (0.45–0.64%) resemble the values obtained in all the other rock groups (Figure 5-8d). By contrast, a distinctive feature of the Group D rocks and, especially, the pegmatites is the more variable content of uranium (Figure 5-9d), in part with anomalously high values (> 16 ppm U). The pegmatites and pegmatitic granites that are rich in uranium and show high natural exposure rates are, with one exception, exposed outside the candidate area.

Properties

A statistical evaluation of the mineralogical composition of the different rock types at the Forsmark site is presented in Table 5-2. This table also documents the grain size of the different rock types. Similar assessments of the physical properties of these rocks and their uranium contents are listed in Table 5-3 and Table 5-4, respectively. The values for the various parameters include the data from the boreholes KFM01A, KFM02A, KFM03A and KFM03B (see Section 5.2.6). For this reason, the values in the tables correspond to the values used in the property assignment for the dominant rock type in the various rock domains (see Section 5.3.3). Only gamma-ray spectrometry values are shown for the determination of uranium contents. Geochemical values for uranium are also available /Stephens et al. 2003b, 2005a/. Knowledge of this parameter in the bedrock is important, since anomalously high values of uranium, and, in particular, the dominant isotope uranium-238, can give rise to high values of radon-222.

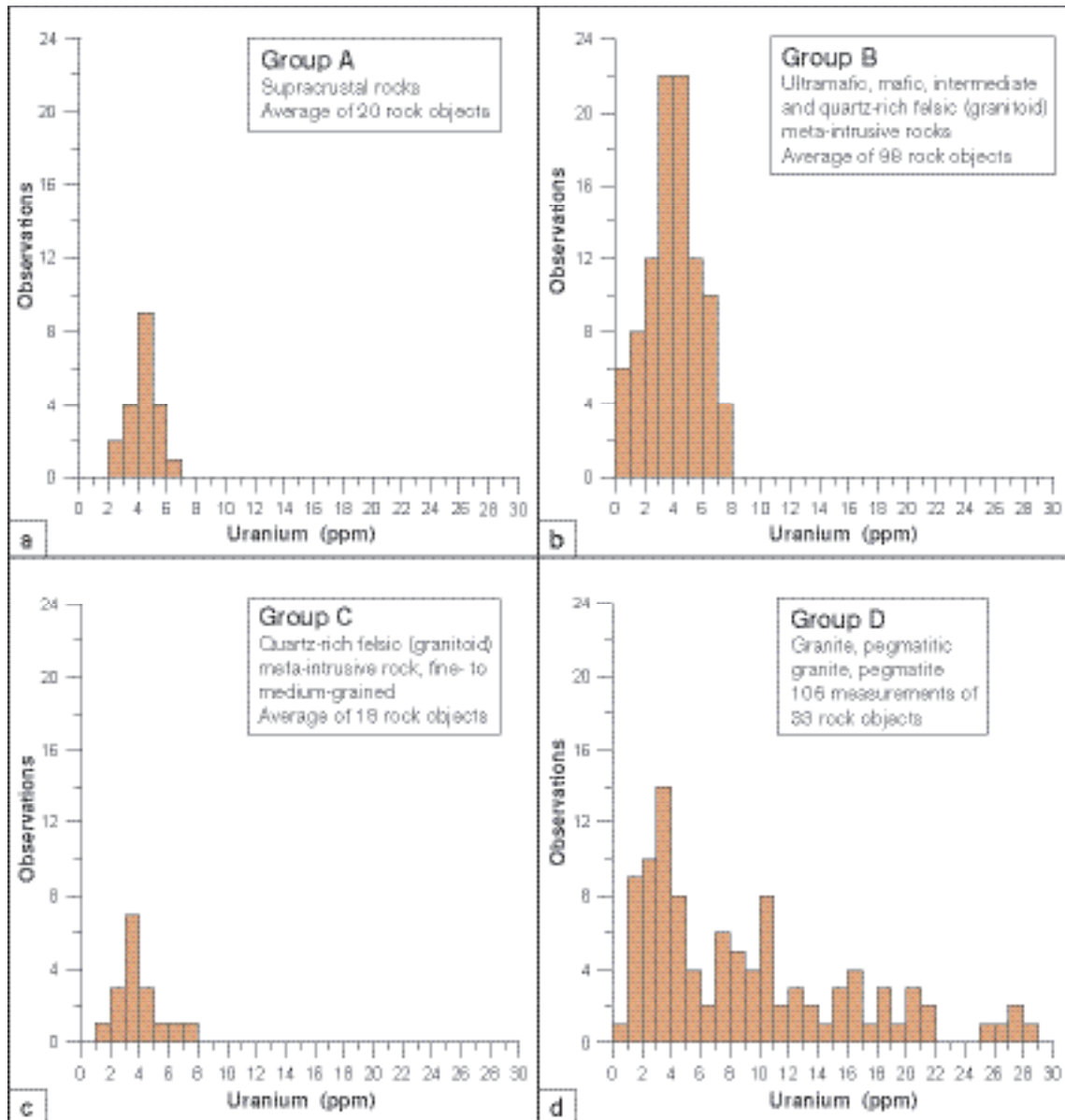


Figure 5-9. Histograms showing the uranium content (ppm) for the analysed samples in the different rock groups (based on data reported in /Isaksson et al. 2004b/). The uranium contents are based on *in situ*, gamma-ray spectrometry measurements.

Table 5-2. Composition and grain size of the different rock types at the Forsmark site (based on surface data in /Stephens et al. 2003b, 2005a/ and data from boreholes KFM01A, KFM02A, KFM03A and KFM03B in /Pettersson et al. 2004e/). The code classification of each sample is based on that assigned during the surface or borehole mapping.

Code (SKB)	Composition									Grain size	
		Quartz (%)		K-feldspar (%)		Plagioclase (%)		Biotite (Bi), Hornblende (Hb) (%)			N (No. of samples)
		Range	Mean/Std	Range	Mean/Std	Range	Mean/Std	Range	Mean/Std		
103076	Felsic to intermediate volcanic rock, metamorphic	5.2–39.2	26.0/10.3	0–12.6	3.4/4.1	29.2–53.2	48.6/6.5	Bi 0–22.8 Hb 0–35.6	Bi 12.0/8.0 Hb No estimate	15. Hb in 6 samples	Fine-grained

Code (SKB)	Composition										Grain size	
	Name (IUGS/SGU)	Quartz (%)		K-feldspar (%)		Plagioclase (%)		Biotite (Bi), Hornblende (Hb) (%)		N (No. of samples)		Class (SGU)
		Range	Mean/Std	Range	Mean/Std	Range	Mean/Std	Range	Mean/Std			
106001	Sedimentary rock, metamorphic, veined to migmatitic	No data available										
108019	Calc-silicate rock (skarn)	No data available										Finely medium-grained
109010	Pyrite-pyrrhotite-chalcopyrite-sphalerite mineralisation	No data available										Fine-grained
109014	Magnetite mineralisation associated with calc-silicate rock	No data available										Fine-grained
101004	Ultramafic rock (olivine-hornblende pyroxenite)	Not relevant. Quartz, K-feldspar and plagioclase feldspar are absent. 46.6–61.2% pyroxene, 9.6–31.0% hornblende (actinolite) and 0–35.2% olivine (serpentine) in two samples.										Medium-grained
102017	Amphibolite	6.4	No estimate			39.2–42.8	No estimate	Bi 9.0 Hb 40.6–55.6	Bi, Hb No estimates	Qz and Bi in 1 sample. Pl and Hb in 2 samples. Kf not present	Finely medium-grained	
101033	Diorite, quartz diorite and gabbro, metamorphic	0–24.6	8.3/7.7			40.4–64.6	51.3/5.0	Bi 0–14.2 Hb 10.6–50.6	Bi 8.3/5.0 Hb 27.6/11.5	11. Kf not present	Medium-grained	
101054	Tonalite to granodiorite, metamorphic	0–45.4	23.4/9.1	0–21.8	5.9/5.4	19.6–61.4	47.4/9.1	Bi 0–15.6 Hb 0–41.8	Bi 9.5/4.7 Hb 10.0/0.1	25	Medium-grained	
101056	Granodiorite, metamorphic	24.4–36.0	29.6/4.4	8.6–16.6	12.5/3.0	37.2–51.4	44.6/5.5	Bi 7.6–12.4 Hb 0–13.4	Bi 9.3/1.5 Hb No estimate	7. Hb in 2 samples	Medium-grained	
101057	Granite (to granodiorite), metamorphic	27.8–45.8	35.6/4.2	0.2–36.0	22.5/8.6	24.0–63.8	35.6/8.5	Bi 0.8–8.2	Bi 5.1/1.6	46	Medium-grained	
111057	Granite (to granodiorite), metamorphic, veined to migmatitic	No data available. Rock type affected by veining and migmatization is similar to 101057										
101058	Granite, metamorphic	30.8–44.4	37.3/4.4	4.0–47.0	22.9/15.9	18.8–58.2	37.1/15.8	Bi 0–2.0	Bi 1.1/0.9	7	Fine-grained (aplitic)	
111051	Granitoid, metamorphic	No data available										
101051	Granodiorite, tonalite and subordinate granite, metamorphic	15.4–35.4	27.3/5.6	0–38.0	12.2/12.0	29.4–67.0	46.4/10.0	Bi 1.8–19.4 Hb 0–25.2	Bi 9.1/4.8 Hb No estimate	23. Hb in 10 samples	Fine- to medium-grained	
101061	Pegmatitic granite, pegmatite	29.2–38.1	34.0/3.7	19.2–45.0	31.3/9.5	20.6–39.0	31.4/7.4	Bi 0.3–5.2	Bi 1.7/2.0	5	Coarse-grained (pegmatitic)	
111058	Granite	25.4–42.8	32.4/6.4	22.6–37.8	29.6/5.6	22.0–46.2	33.0/9.3	Bi 0.6–4.4	Bi 2.7/1.6	5	Fine- to medium-grained	

Table 5-3. Physical properties of the different rock types at the Forsmark site (based on surface data in /Isaksson et al. 2004b/ and data from boreholes KFM01A, KFM02A, KFM03A and KFM03B in /Mattsson et al. 2004a/). The code classification of each sample is based on that assigned during the surface or borehole mapping.

Code (SKB)	Composition (and grain size)	Physical properties								
		Density (kg/m ³)		Porosity (%)		Magnetic susceptibility (SI units)		Electrical resistivity in fresh water (ohm m)		N (No. of samples)
		Range	Mean/ Std	Range	Mean/ Std	Range	Geometric mean/ Std above mean/ Std below mean	Range	Geometric mean/ Std above mean/ Std below mean	
103076	Felsic to intermediate volcanic rock, metamorphic	2648–2946	2732/79	0.20–0.62	0.37/0.11	0.00006–0.24000	0.00235/0.04163/0.00222	1725–81878	14374/22146/8716	
106001	Sedimentary rock, metamorphic, veined to migmatitic	Value = 2691		Value = 0.48		Value = 0.00270		Value = 10888		1
108019	Calc-silicate rock (skarn)	No data available								
109010	Pyrite-pyrrhotite-chalcopyrite-sphalerite mineralisation	No data available								
109014	Magnetite mineralisation associated with calc-silicate rock	4130–4225		1.24–1.47		0.12220–0.12400		168–324		2
101004	Ultramafic rock (olivine-hornblende pyroxenite)	Value = 3045		Value = 1.04		Value = 0.04572		Value = 52		1
102017	Amphibolite	2928–3048	2988/60	0.24–0.32	0.29/0.04	0.00067–0.00071	0.00069/0.00002/0.00002	11211–38904	22062/15840/9220	3 (5 for elec. resis.)
101033	Diorite, quartz diorite and gabbro, metamorphic	2738–3,120	2934/100	0.25–0.54	0.37/0.07	0.00036–0.05592	0.00293/0.01914/0.00254	5412–34227	15315/12575/6905	14
101054	Tonalite to granodiorite, metamorphic	2674–2831	2737/43	0.31–0.53	0.40/0.07	0.00020–0.03507	0.00185/0.01049/0.00157	5921–25249	14380/6715/4578	21 (22 for elec. resis.)
101056	Granodiorite, metamorphic	2661–2706	2689/18	0.38–0.55	0.45/0.08	0.00673–0.01563	0.00963/0.00409/0.00287	16962–76646	27810/23612/12770	5
101057	Granite (to granodiorite), metamorphic, medium-grained	2639–2722	2657/15	0.28–0.66	0.43/0.08	0.00007–0.02548	0.00442/0.01591/0.00346	3352–54100	14727/11237/6374	64 (82 for elec. resis.)
111057	Granite (to granodiorite), metamorphic, medium-grained, veined to migmatitic	No data available. Rock type affected by veining and migmatisation is similar to 101057								
101058	Granite, metamorphic, aplitic	2620–2646	2635/9	0.36–0.48	0.40/0.05	0.00179–0.01722	0.00657/0.00691/0.00337	11467–27915	15876/5288/3967	7
111051	Granitoid, metamorphic	No data available								
101051	Granodiorite, tonalite and granite, metamorphic, fine- to medium-grained	2642–2832	2715/52	0.28–0.59	0.45/0.09	0.00014–0.02539	0.00096/0.00445/0.00079	5862–18252	9932/4220/2962	16 (17 for mag. susc. and 22 for elec. resis.)

Code (SKB)	Composition (and grain size) Name (IUGS/SGU)	Physical properties								N (No. of samples)
		Density (kg/m ³)		Porosity (%)		Magnetic susceptibility (SI units)		Electrical resistivity in fresh water (ohm m)		
		Range	Mean/Std	Range	Mean/Std	Range	Geometric mean/Std above mean/Std below mean	Range	Geometric mean/Std above mean/Std below mean	
101061	Pegmatitic granite, pegmatite	2621–2637	2627/6	0.45–0.64	0.55/0.07	0.00019–0.02028	0.00208/0.00746/0.00163/	10600–33483	15289/6744/4680	7 (9 for mag. susc. and 8 for elec. resis.)
111058	Granite, fine- to medium-grained	2627–2645	2638/9	0.48–0.69	0.50/0.02	0.00010–0.00573	0.00085/0.00408/0.00070	6974–13017	8849/2770/2115	3 (4 for mag. susc. and elec. resis.)

Table 5-4. Uranium contents and natural exposure rates of the different rock types at the Forsmark site, defined by in-situ, gamma-ray spectrometry measurements (based on surface data in /Isaksson et al. 2004b/ and data from boreholes KFM01A, KFM02A, KFM03A and KFM03B in /Mattsson et al. 2004a/). The code classification of each sample is based on that assigned during the surface or borehole mapping.

Code (SKB)	Composition (and grain size) Name (IUGS/SGU)	Gamma-ray spectrometry measurements				N (No. of samples)
		Content of uranium (ppm)		Natural exposure rate (microR/h)		
		Range	Mean/Std	Range	Mean/Std	
103076	Felsic to intermediate volcanic rock, metamorphic	2.5–6.8	4.3/1.0	5.2–13.4	9.4/2.5	19
106001	Sedimentary rock, metamorphic, veined to migmatitic	Value = 5.3		Rate = 9.2		1
108019	Calc-silicate rock (skarn)	No data available				
109010	Pyrite-pyrrhotite-chalcopyrite-sphalerite mineralisation	No data available				
109014	Magnetite mineralisation associated with calc-silicate rock	5.2–6.2		6.6–6.7		2
101004	Ultramafic rock (olivine-hornblende pyroxenite)	Value = 0.0		Rate = 0.0		1
102017	Amphibolite	0.2–2.4	1.3/0.9	2.1–3.8	3.3/0.8	4
101033	Diorite, quartz diorite and gabbro, metamorphic	0.0–2.8	1.2/0.9	0.2–6.4	2.7/1.9	14
101054	Tonalite to granodiorite, metamorphic	1.2–7.4	3.6/1.4	4.7–10.9	7.8/1.8	21
101056	Granodiorite, metamorphic	3.3–5.1	4.0/0.7	6.9–9.6	8.2/1.1	5
101057	Granite (to granodiorite), metamorphic, medium-grained	0.8–19.0	4.9/2.3	6.3–19.3	12.4/2.0	66
111057	Granite (to granodiorite), metamorphic, medium-grained, veined to migmatitic	No data available. Rock type affected by veining and migmatization is similar to 101057				
101058	Granite, metamorphic, aplitic	3.3–7.6	5.3/1.4	8.3–18.9	12.8/3.3	9
111051	Granitoid, metamorphic	No data available				
101051	Granodiorite, tonalite and granite, metamorphic, fine- to medium-grained	1.9–8.2	4.1/1.8	5.7–22.8	11.0/4.6	21
101061	Pegmatitic granite, pegmatite	2.3–61.7	14.5/12.9	11.5–54.3	21.7/8.9	26
111058	Granite, fine- to medium-grained	3.4–14.9	8.3/3.8	12.7–22.9	19.0/3.6	6

5.2.2 Rock type distribution on the surface

Data and interpretation of magnetic anomaly maps

The compilation of a bedrock geological map for the Forsmark site, which shows, amongst other features, the distribution of rock types on the surface, is a key component in the establishment of a rock domain model for the site (see Section 5.3). Six different types of information have been used in the compilation of the bedrock geology over the whole regional model area (Figure 5-10).

- Outcrop data from 2,119 observation points on the mainland and in the archipelago area that were generated in connection with the bedrock mapping of the Forsmark site at the scale 1:10,000 (Figure 5-1 and /Stephens et al. 2003a; Bergman et al. 2004/). The character of the bedrock on the mainland has also been documented at the base of eight, temporarily exposed minor trenches and 21 shallow boreholes in the Quaternary cover (Figure 5-1 and /Bergman et al. 2004/).
- Rock type distribution at five sites where detailed mapping of fractures has been carried out at the scale 1:50 (see Section 5.2.4 and /Hermanson et al. 2003a,b, 2004/). One of these sites is an outcrop along the coast at Klubbudden, which has an areal extent of c. 325 m². The other sites are temporarily exposed outcrops at drill sites 2, 3, 4 and 5, which range in areal extent from c. 500 to c. 600 m².
- Rock type data from cored boreholes that were drilled in connection with the construction work at the nuclear power plant and at SFR, and from various shallow tunnels in the vicinity of these facilities /Stephens et al. 2005b/. Most of the boreholes are also shallow (generally < 50 m).
- An interpretation of the detailed magnetic anomaly map over the mainland and the archipelago area (Figure 5-11). The interpretation of the patterns on the magnetic anomaly map, as well as the data input and the data processing used in the interpretation work, are presented in /Isaksson et al. 2004c/. This work was carried out independently of the analysis of the outcrop data. The data behind the magnetic anomaly map are discussed briefly in Section 5.2.3.
- An interpretation of the older magnetic anomaly map over the Forsmark area, especially in the areas where the new, high-quality, airborne geophysical data are either absent or disturbed (Figure 5-11). The data input and the data processing used in the interpretation work are summarised in /Isaksson et al. 2004c/ and the data behind the magnetic anomaly map are discussed briefly in Section 5.2.3.
- An old map compilation of the bedrock geology of Gräsö at the scale 1:50,000 /Svenonius, 1887/.

The construction of the bedrock geological map on the mainland is based predominantly on the interpretation of the outcrop observations (Figure 5-10). The conclusions drawn from an interpretation of the magnetic anomaly maps have played a subordinate role. By contrast, in the archipelago area, the overall exposure of the bedrock is considerably lower and the interpretation of the magnetic anomaly maps is of greater significance (Figure 5-10). In the open sea area, at Öregrundsgrepen, construction of the boundaries between bedrock units is based entirely on the conclusions drawn from the older magnetic anomaly map (Figure 5-10). Since outcrop information is lacking, the bedrock geological map in this area is far less reliable in comparison with the areas to the south-west. The map compilation over the small part of Gräsö that lies within the regional model area is based on both the older compilation of /Svenonius, 1887/ and the conclusions drawn from the interpretation of the older magnetic anomaly map (Figure 5-10).

Bedrock geological map

Work within the site investigation programme has generated a new bedrock geological map at the scale 1:10,000 that covers the mainland and the archipelago area at the Forsmark site (Bedrock geological map, Forsmark, version 1.2). A description of this map is presented in /Stephens et al. 2005b/ and only a brief summary is presented here. The bedrock geological map shows the following:

- A two-dimensional model for the surface distribution of major rock units.
- The occurrence of subordinate rock types, abandoned mines, exploration prospects, and key minerals.

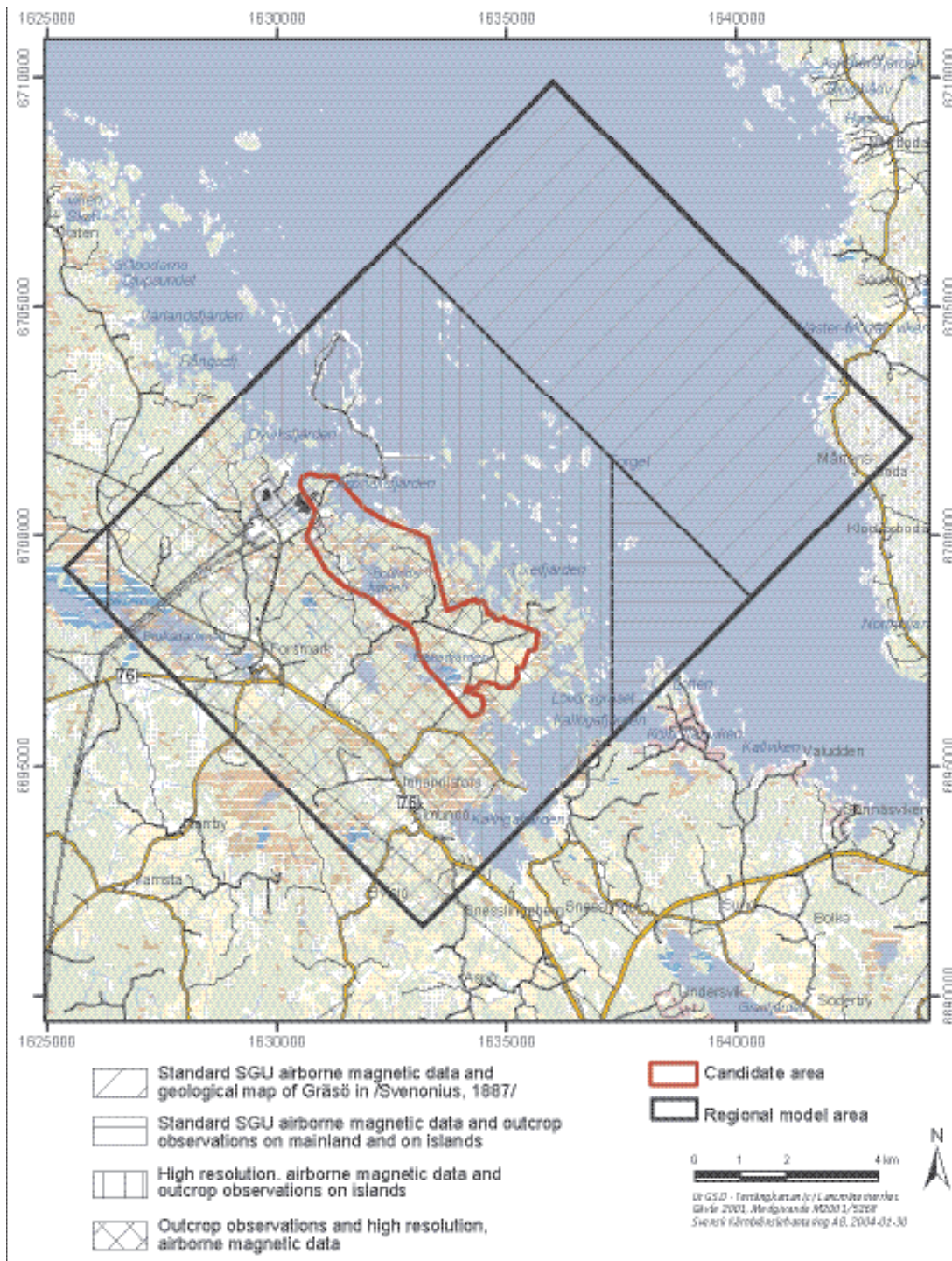


Figure 5-10. Summary of base data that have been used to compile the bedrock geology over the regional model area.

- The structures formed in connection with high-temperature, ductile deformation at deeper crustal levels (see Section 5.2.4).
- The structures formed in connection with brittle and low-temperature, ductile deformation at shallower crustal levels (see Section 5.2.4). Lineaments (see Section 5.2.3) and the deformation zones that were modelled to intersect the surface in model version 1.1 (SKB, 2004a) are included here.

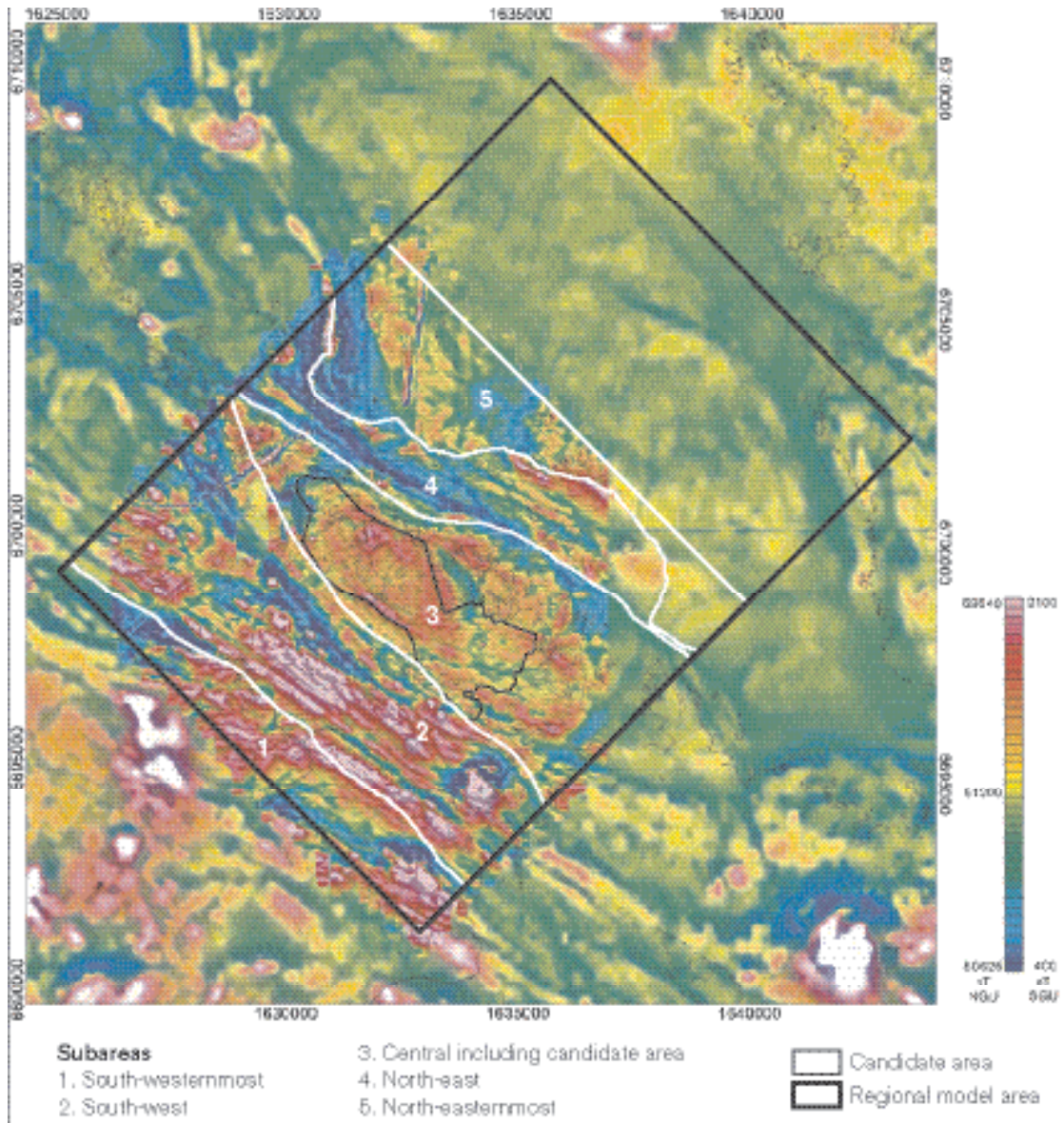


Figure 5-11. Map of the magnetic total field over the regional model area. The results of the airborne (helicopter), geophysical survey in a north-south direction are included here (see Section 5.2.3). The sub-areas that were recognised in connection with the bedrock geological mapping are also shown (see text below). The red-lilac end of the colour spectrum indicates strongly magnetic bedrock and the blue end of the spectrum indicates weakly magnetic bedrock. The strong, positive magnetic anomaly in the square 1634000–1635000/6694000–6695000 corresponds to a major Group B ultramafic intrusion. Helicopter data are lacking in the vicinity of the nuclear power plant. They are also disturbed by power lines, and a DC-cable in the area north-west of the power plant and at Öregrundsgrepen along co-ordinate grid line 1633000.

A simplified version of a part of this map, focused on the candidate area, is shown in Figure 5-12. The principles that have been used to further simplify the bedrock geological map of the Forsmark site, and to combine it with the poorly understood areas to the north-east (Öregrundsgrepen and Gräsö), are described in connection with the rock domain modelling (see Section 5.3.3). This procedure is necessary in order to compile a map of rock domains over the whole regional model area.

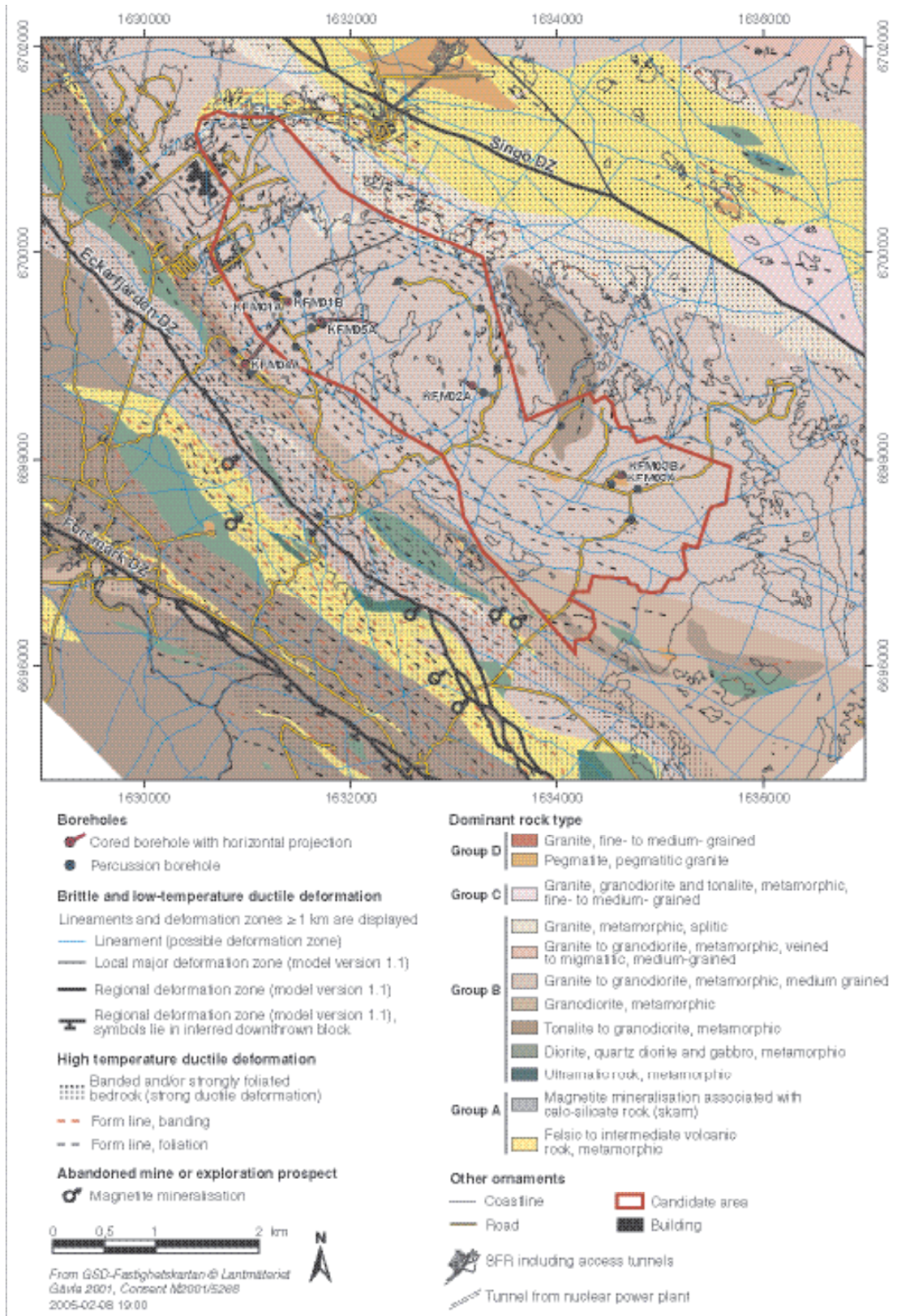


Figure 5-12. Bedrock geological map of the candidate area and its surroundings at the Forsmark site.

Subordinate rock types and division into sub-areas

The colour for each rock unit on the geological map shows the dominant rock type in the unit. Subordinate rock types observed at an outcrop are illustrated on the map with the help of point information. For purposes of clarity, subordinate rock types as well as other geological features (occurrence of key minerals, structural measurements) have been omitted from the simplified geological map shown in Figure 5-12. The subordinate rock types occur as:

- Xenoliths of predominantly Group A supracrustal rocks within younger, intrusive rocks.
- Amphibolite enclaves in metatonalite (Group B).
- Amphibolite dykes and irregular inclusions in biotite-bearing metagranite and aplitic metagranite (Group B).
- Bands and lenses of one rock type within another. The bands and lenses may be deformed dykes, deformed inclusions or both these possibilities.
- Dykes and minor intrusions of rocks that belong to the younger, Group C and Group D suites.

The amphibolite enclaves, dykes and irregular inclusions, and the various bands and lenses generally trend parallel or sub-parallel to the tectonic foliation, whereas the younger Group C and Group D rocks display a more varied orientation.

The bedrock geological map can be divided into five distinctive sub-areas that trend north-west (Figure 5-11). These sub-areas are defined on the basis of the degree of homogeneity of the bedrock and the character of the ductile deformation (see Section 5.2.4). The brief description presented below focuses on the surface distribution of the major rock units within these different sub-areas.

Sub-area in the south-westernmost part of the mapped area

In general, the bedrock in this sub-area is inferred to be homogeneous and affected by a relatively low degree of ductile strain. Group B rocks that are tonalitic and granodioritic in composition are dominant (Figure 5-12). However, some lensoid bodies of Group B ultramafic to intermediate rocks as well as a unit of more strongly deformed, felsic to intermediate metavolcanic rocks, banded together with amphibolite and calc-silicate rock, are conspicuous. Metagranite, similar to that observed in the candidate area, is present in the southernmost part of the mapped area.

Sub-area south-west

The sub-area that is situated immediately south-west of the candidate area contains several major rock units (Figure 5-12). An inhomogeneous bedrock that also displays high ductile strain is conspicuous up to c. 1,000 m across the strike, on both sides of the Eckarfjärden and Forsmark deformation zones. These features are also expressed in the form of a banded anomaly pattern with north-west trend on the magnetic anomaly map (Figure 5-11). The detailed geological map at drill site 4 (Figure 5-13) illustrates the strong bedrock inhomogeneity and the high ductile strain on an outcrop scale. Larger pockets of more homogeneous rocks with an inferred lower degree of ductile deformation are present in the north-western part of the sub-area, and in the inferred strain shadow close to the major ultramafic-mafic intrusion, in the south-eastern part of the sub-area.

Group B rocks that are tonalitic and granodioritic in composition form an important bedrock component in this sub-area (Figure 5-12). A strongly foliated, tectonic sheet that consists of metagranite, similar to that observed in the candidate area, and aplitic metagranite is also present (Figure 5-12). Furthermore, major lensoid bodies of metamorphosed ultramafic, mafic and intermediate rocks, locally with garnet, and commonly associated with pegmatite and pegmatitic granite, are conspicuous (Figure 5-12). The ultramafic body in the south-eastern part of the sub-area yields a well-defined, magnetic maximum (Figure 5-11).

Felsic to intermediate metavolcanic rocks form a major rock unit with north-west trend (Figure 5-12). They also occur as minor tectonic sheets within the Group B metatonalites and metagranodiorites. This is apparent on both map (Figure 5-12) and outcrop (Figure 5-13) scales.

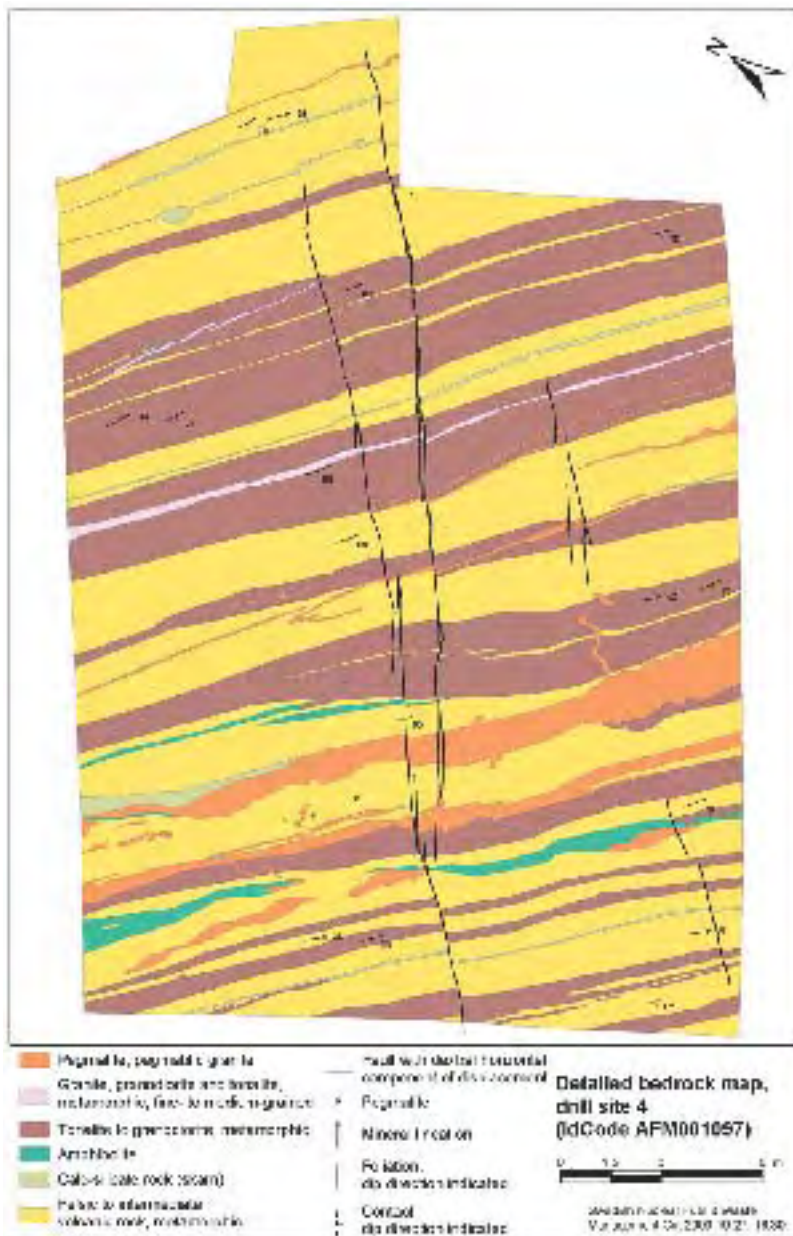


Figure 5-13. Detailed geological map of drill site 4 (after Persson Nilsson in /Hermanson et al. 2003b/). With the exception of some faults, all fractures in the bedrock have been omitted from the map for purposes of clarity.

The local occurrence of thin layers rich in biotite and garnet within the metavolcanic rocks indicate a dispersal of volcanic material within an originally shale-rich, sedimentary basin. The metavolcanic rocks also form the host rock to calc-silicate rocks and iron oxide mineralisations, several of which (e.g. Skomakargruvan) have been the focus of exploration and mining activity in historical time.

An assessment of the potential of the Forsmark area for exploration for metallic and industrial mineral deposits has been presented in /Lindroos et al. 2004/. A potential for iron oxide mineralisation and possibly base metals was recognised. A mineral resource map (Figure 5-14) shows how the areas that bear this potential are situated in sub-area south-west, predominantly in the felsic to intermediate metavolcanic rocks. Geochemical analyses of till at Forsmark provide support to this conclusion /Nilsson, 2003c/. However, the small iron mineralisations in the Forsmark area have no economic value and this judgement is also deemed to be valid in a long-term perspective /Lindroos et al. 2004/.

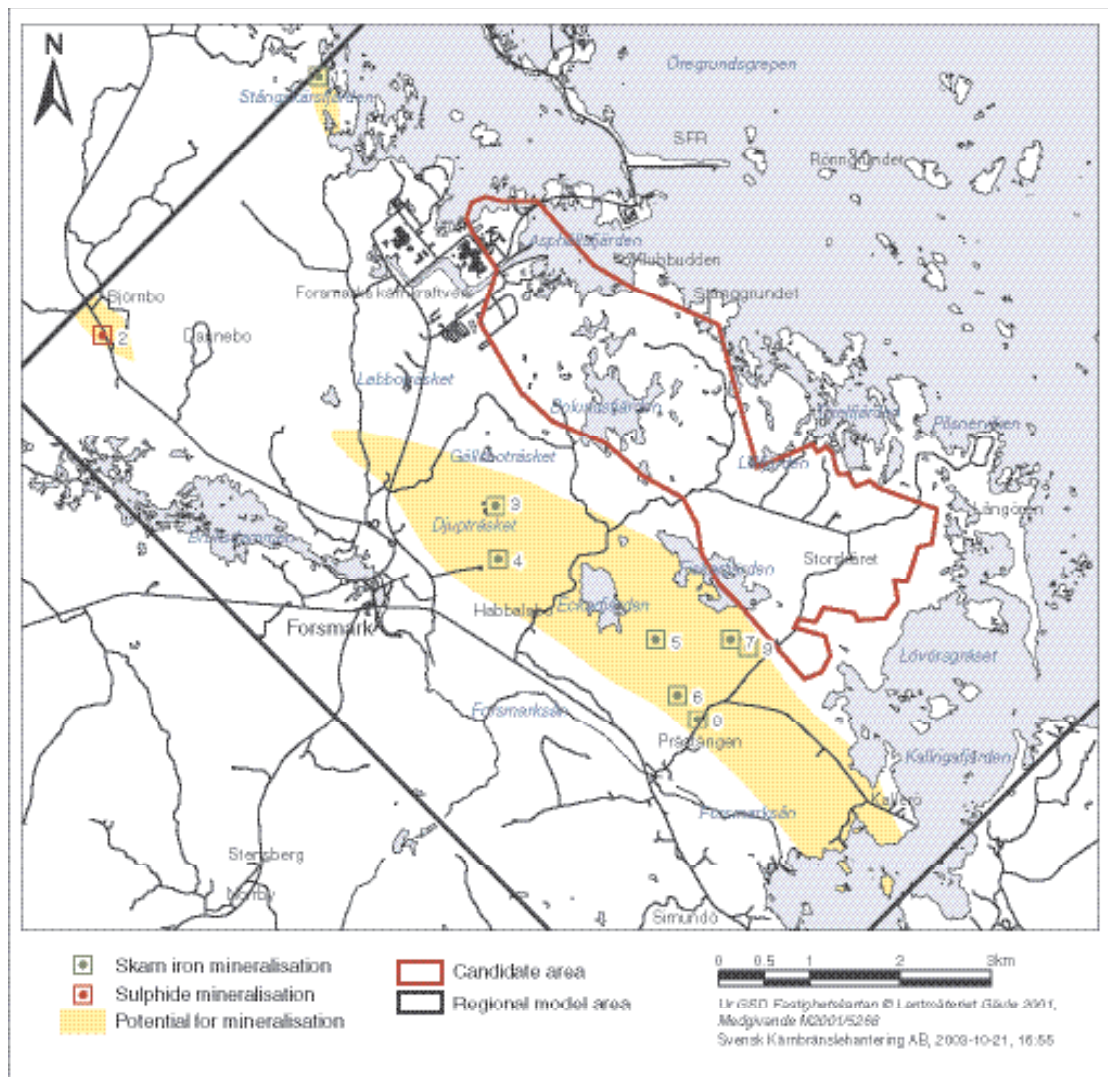


Figure 5-14. Mineral resources map of the Forsmark area. The map shows the areas on the surface that are judged to have some exploration potential for mineral deposits (modified after Lindroos et al. 2004).

Sub-area central including the candidate area

Sub-area central, which includes the candidate area, is dominated by medium-grained metagranite that belongs to the Group B suite of intrusive rocks (Figure 5-12). Although amphibolite, fine- to medium-grained metagranitoid (Group C), and pegmatitic granite, pegmatite and fine- to medium-grained granite (Group D) commonly form subordinate components at outcrop scale (see, for example, Figure 5-15), this rock unit is relatively homogeneous. A conspicuous variation at the surface is an increase in the proportion of pegmatitic granite and pegmatite to the south-east, in the area around Storskåret. Other mappable rock units in this sub-area include (Figure 5-12):

- A large-scale xenolith of Group B metatonalite, close to Lillfjärden, which corresponds to a low magnetic area on the magnetic anomaly map (Figure 5-11).
- Group B aplitic metagranite that, west and north-west of Asphällsfjärden and along Klubbudden, occurs in a heterogeneous mixture together with metavolcanic rocks, medium-grained metagranite, amphibolite, Group C metagranodiorite and Group D pegmatitic granite and pegmatite, and defines a major fold structure. This structure is evident on the magnetic anomaly map as a folded, low magnetic area (Figure 5-11).
- A heterogeneous mixture of metagranodiorite and metatonalite with subordinate metagabbro, metadiorite, pegmatitic granite and pegmatite in the south-eastern part of the sub-area.



Figure 5-15. Detailed geological map of drill site 2 (after Andersson and Bergman in /Hermanson et al. 2003a/). With the exception of some faults, all fractures in the bedrock have been omitted from the map for purposes of clarity.

Apart from the marginal parts of the sub-area and the area in the vicinity of the major fold structure, close to Asphällsfjärden, the bedrock shows relatively low ductile strain. This feature is expressed on the magnetic anomaly map as an irregular anomaly pattern with a few low magnetic areas (Figure 5-11).

Sub-area north-east

The bedrock in sub-area north-east resembles that in sub-area south-west in terms of both the increased degree of inhomogeneity and the high ductile strain. This feature is reflected in the banded anomaly pattern on the magnetic anomaly map in both sub-areas, in sharp contrast to the predominantly irregular anomaly pattern in sub-area central (Figure 5-11).

Felsic to intermediate metavolcanic rocks dominate sub-area north-east (Figure 5-12). They are generally banded and occur together with pegmatitic granite and pegmatite and, locally, with fine- to medium grained granite, all of which belong to the Group D suite of intrusive rocks. In the north-western part of the sub-area, the metavolcanic rocks are more homogeneous, muscovite-bearing and are inferred to be hydrothermally altered. In earlier compilations (e.g. /Hansen, 1989/), these mica-rich, altered metavolcanic rocks have been mapped as metasedimentary rocks. Other subordinate rock units in sub-area north-east include Group B aplitic metagranite, similar to that observed at Klubbudden, Group B metagabbro and metadiorite, and Group C metagranodiorite and metatonalite (Figure 5-12). Two larger bodies of Group C intrusive rocks are inferred to be present in the south-eastern part of the sub-area.

Sub-area in the north-easternmost part of the mapped area

The bedrock in this sub-area consists of several, major rock units that are relatively homogeneous and generally show a low degree of ductile strain. The bedrock is more inhomogeneous in its eastern part. The sub-area shows an irregular anomaly pattern on the magnetic anomaly map (Figure 5-11).

A rock unit dominated by medium-grained, equigranular metagranite, similar to that observed in the candidate area, forms an important bedrock component in this sub-area (Figure 5-12). In the eastern part of the sub-area, this rock unit merges gradually into more inhomogeneous, veined to migmatitic metagranite. Strongly veined to migmatitic metasedimentary rocks intruded by Group C metagranodiorites are also present. A finer grained, equigranular granite that shows only weak ductile deformation and is devoid of amphibolite dominates the northern part of the sub-area, on the small Länsmän islands. This granite contains xenoliths of metavolcanic rock and is tentatively inferred to be a larger Group D intrusion. The western part of the sub-area consists of a major body of metadiorite. It corresponds to a low magnetic area on the magnetic anomaly map (Figure 5-11). The metadiorite is spatially associated with pegmatite and pegmatitic granite, and is intruded by a Group C metagranitoid.

5.2.3 Lineament identification

Data

The identification and interpretation of lineaments is an indirect method that can be used to define possible deformation zones in the bedrock (see Section 5.4). They are also used in the establishment of orientation and size distributions in the DFN model for the site (see Section 5.5). However, lineaments are related to different geological features. For this reason, independent data (e.g. outcrop data, trenching, borehole data, surface geophysics) are necessary to interpret the anomalies and, thereby, confirm or refute the presence of deformation zones.

Lineaments have been identified with the help of essentially three different sets of data:

- Airborne magnetic, electromagnetic (EM) and very low frequency electromagnetic (VLF) data.
- Topographic and bathymetric data.
- Refraction seismic data.

Ground EM (slingram) and magnetic data are available in restricted areas inside the candidate area and close to the nuclear power plant 3, and the latter have also been used to identify lineaments. The evaluation of this subordinate data set is presented in Section 5.2.5.

Airborne geophysical data

Two sets of airborne geophysical data, which differ markedly in their degree of resolution, are available for the regional model area (Figure 5-16). A detailed description of the input geophysical data and the processing of these data can be found in /Isaksson et al. 2004c/.

The entire regional model area is covered by airborne geophysical data that were generated predominantly by the Geological Survey of Sweden (SGU), in connection with their standard mapping activities (Figure 5-16). They were available prior to the onset of the site investigation programme and were already utilised in the feasibility study work at Östhammar /Bergman et al. 1996, 1998/ and Tierp /Bergman et al. 1999/. These data have been processed on a 40 m grid.

In connection with the site investigation programme during 2002, a denser population of high-resolution, helicopter geophysical measurements was generated over most of the land area close to Forsmark, over the lakes in this area, and over the sea area near to the coast at Forsmark (Figure 5-16 and /Rønning et al. 2003/). These data have been processed in a 10 m grid. In the vicinity of the candidate area, this survey involved measurements in both north-south and east-west directions (Figure 5-16). However, no measurements were carried out around the nuclear power plant. There are also disturbances along power lines and a DC-cable.

A magnetic anomaly map, which has been generated from an integration of the two distinct data sets, is shown in Figure 5-11. In the vicinity of the candidate area, the integration includes the results of the north-south helicopter geophysical survey. This map is the most important component in the interpretation of lineaments from geophysical data.

Topographic and bathymetric data

A variety of topographic and bathymetric data (Figure 5-17) have been used to generate an integrated, topographic map over the land, and over the lake and sea bottoms. This topographic map provides an important basis for the interpretation of topographic lineaments in the regional model area. The quality and resolution of the data in the open sea area at Öregrundsgrepen are considerably lower compared with those on the land, beneath the lakes in the Forsmark area and on the sea bottom close to the Forsmark coast. The disturbance of the topography, which occurred in connection with the construction work at the nuclear power plant, renders all modern topographic data in this area as unsuitable for the interpretation of lineaments. A detailed description of the input topographic and bathymetric data as well as the processing of these data can be found in /Isaksson, 2003; Isaksson and Keisu, 2005/.

High-resolution topographic and bathymetric data are available over the land area, the lakes close to Forsmark and the sea area close to the Forsmark coast (Figure 5-17). The data in these areas have been generated during the site investigation programme and include:

- Detailed elevation data on land on a 10 m grid /Wiklund, 2002/.
- A sea bottom digital terrain model on a 10 m grid /Isaksson and Keisu, 2005/, which is based on the inversion of airborne EM data measured in a north-south direction /Thunehed, 2005/. These data have not been used in the development of the standard digital elevation model for the Forsmark area.
- Water depth soundings in shallow sea areas and lakes /Brunberg et al. 2004; Brydsten and Strömgren, 2004/.

In the open sea area at Öregrundsgrepen, a sea bottom digital terrain model on a 50 m grid, which was compiled in connection with the SKB project “SAFE” /Brydsten, 1999/, has mainly been used in the interpretation of topographic lineaments (Figure 5-17). This terrain model is based on sea charts from the Swedish National Administration of Shipping and Navigation.

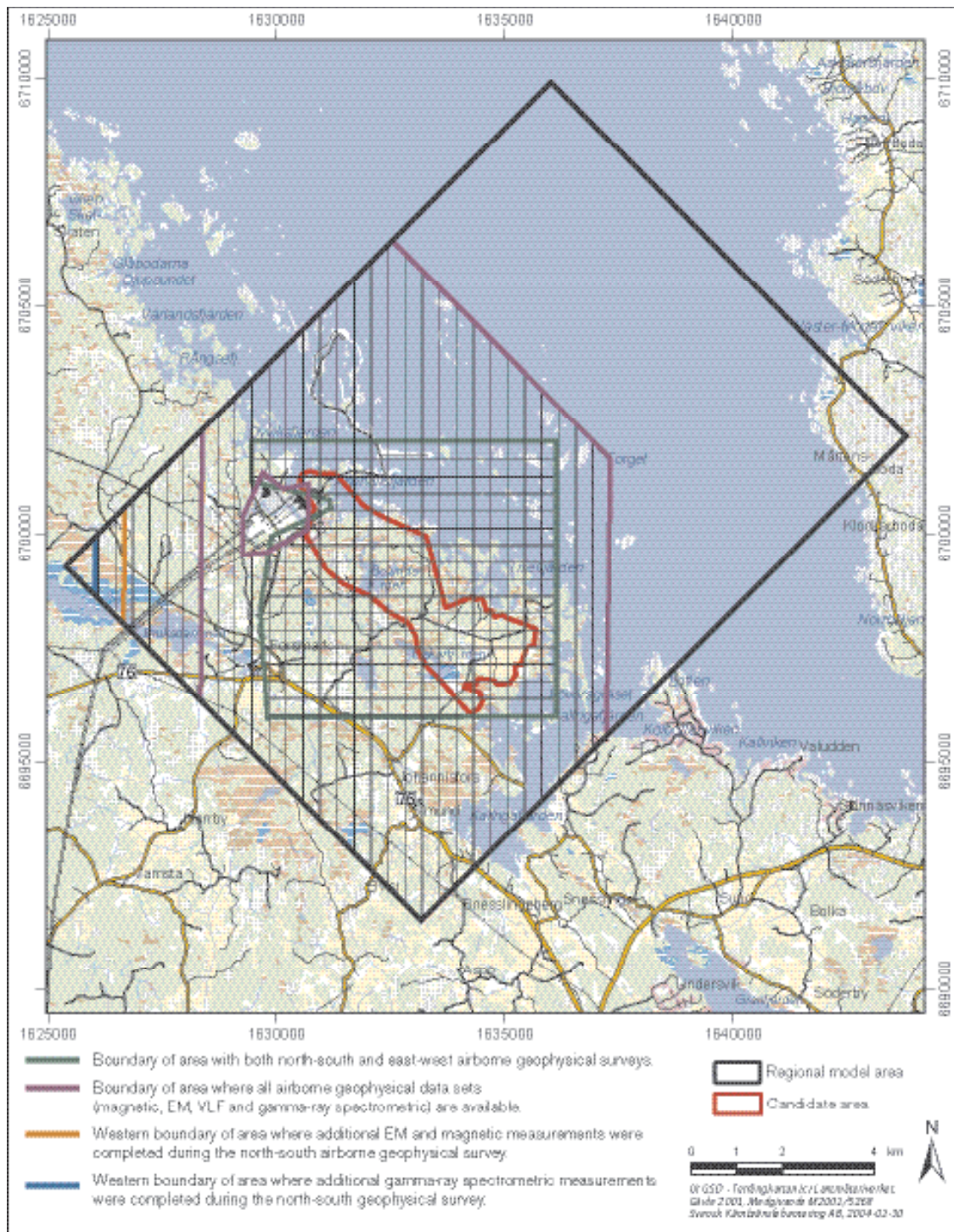


Figure 5-16. Map showing high-resolution, helicopter geophysical data coverage. It was not possible to acquire new data during the site investigation programme in the vicinity of the nuclear power plant. Disturbance of the data also occurred along power lines, and close to a DC-cable in the area north-west of the power plants and at Öregrundsgrepen north-east of the power plant (along co-ordinate grid line 1633000).

Bathymetric data, which were generated during 2002 in connection with a marine geological and geophysical survey of the site /Elhammer et al. 2005/, have also been processed and utilised to identify topographic lineaments in the sea area. These data were assembled along north-east survey lines. They permit an independent interpretation of topographic lineaments on both the sea bottom and the bedrock surface beneath the Quaternary cover.

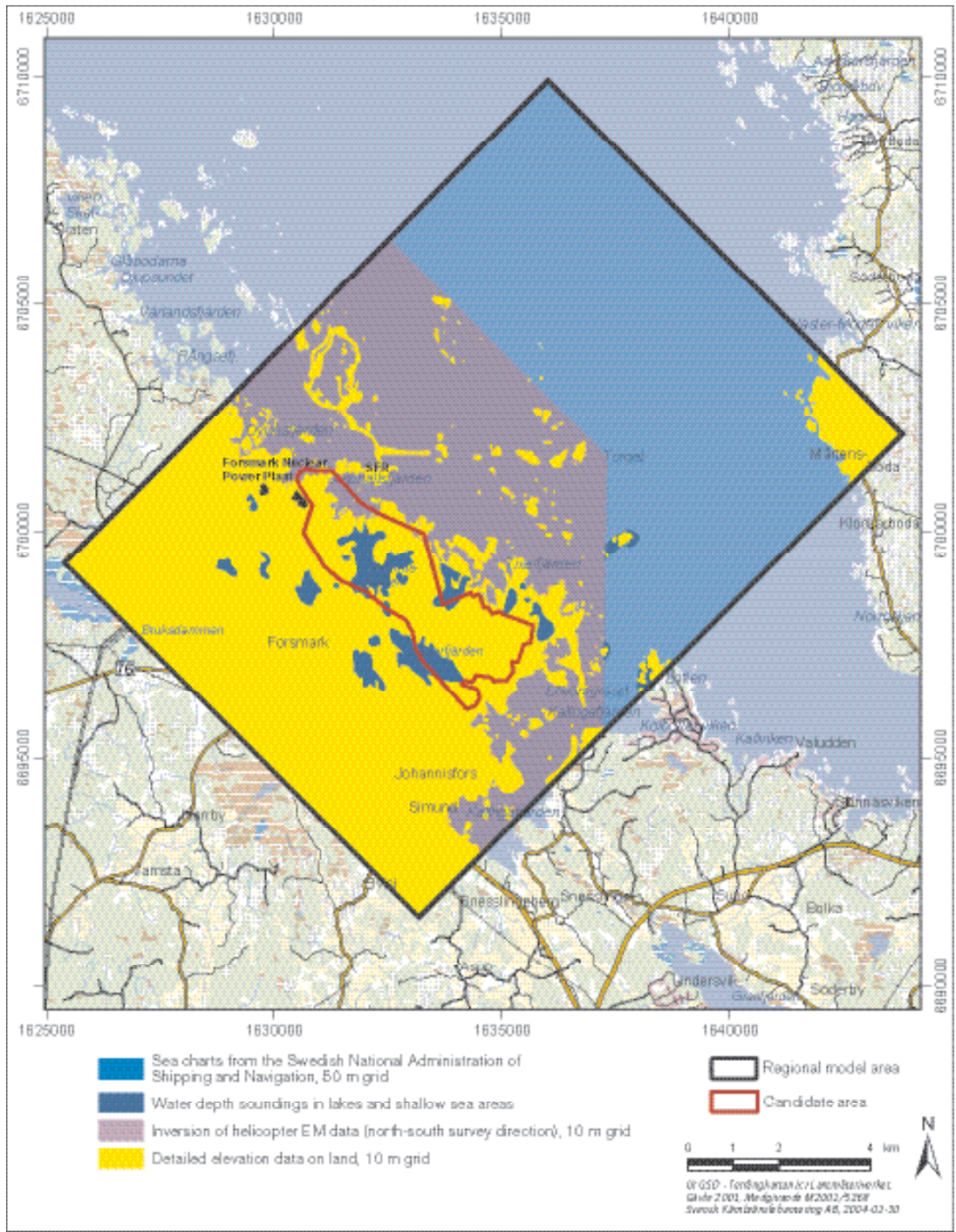


Figure 5-17. Map showing the compilation of base data used in the construction of an integrated topographic map (land and sea bottom surfaces) for the Forsmark site (modified after /Isaksson and Keisu, 2005/).

Refraction seismic data

Neither airborne geophysical data nor modern topographic data can be used to interpret lineaments in the area close to the nuclear power plant. However, considerable refraction seismic data, which were generated in connection with the construction work at both the nuclear power plant and later at SFR, are available (Figure 5-18 and /Keisu and Isaksson, 2004/).

The refraction seismic data permit an estimation of both the elevation of the land (or the sea bottom) and the elevation of the bedrock surface beneath the Quaternary cover. These two sets of elevation values have been processed in a 10 m grid and topographic maps for both surfaces have

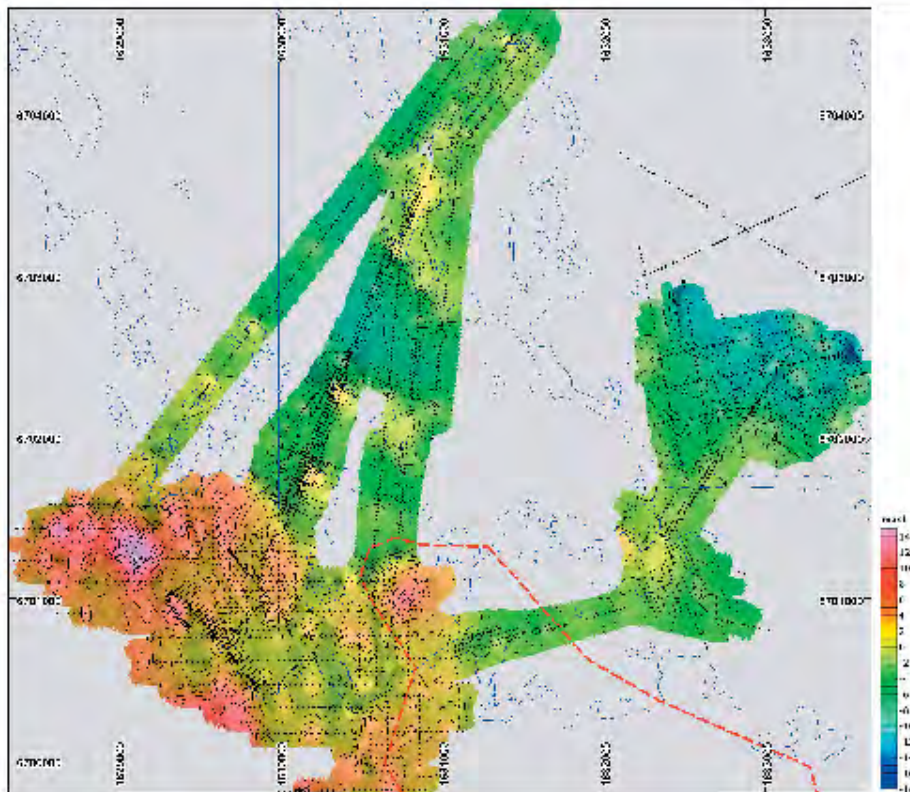


Figure 5-18. Topographic map (land and sea bottom surfaces) based on refraction seismic data in the vicinity of the nuclear power plant, the tunnels from this plant and SFR. The refraction seismic survey lines are also shown (after /Isaksson and Keisu, 2005/). The north-western boundary of the candidate area is shown by a red line.

been generated and interpreted (Figure 5-18) and /Isaksson and Keisu, 2005/). Furthermore, in the area around the nuclear power plant, old maps, which provide information on the topography prior to the construction work /Keisu and Isaksson, 2004/, complement the interpretation of topographic lineaments from the refraction seismic data. A detailed description of all these input data as well as the data processing can be found in /Isaksson and Keisu, 2005/. The identification of bedrock segments with low rock velocity from the refraction seismic data is discussed later under Section 5.2.5.

Interpretation

Methodology

The interpretation of lineaments over the whole regional model area was carried out during 2002–2003 /Isaksson, 2003; Isaksson et al. 2004c/ and 2004 /Isaksson and Keisu, 2005/. The lineaments interpreted from the two sets of airborne geophysical data and the topographic data on land were used in model version 1.1 /SKB, 2004a/. These lineaments underwent minor revision and have been complemented with topographic lineaments in off-shore areas and around the nuclear power plant for use in version 1.2. The complementary interpretation of topographic lineaments is based primarily on the bathymetric data of variable quality, the inverted airborne EM data and the refraction seismic data.

The interpretation of lineaments in the site investigation programme follows a three-stage process that is described briefly below /Isaksson et al. 2004c; Isaksson and Keisu, 2005; Korhonen et al. 2004/. These stages involve the identification of method-specific, co-ordinated and linked lineaments (Figure 5-19). Attribute tables are completed at each stage in the interpretation procedure:

- *Method-specific lineament.* Each set of data (e.g. magnetic, topographic – land or sea bottom surface, topographic – bedrock surface) is interpreted individually and method-specific lineaments are identified and described (Figure 5-19).

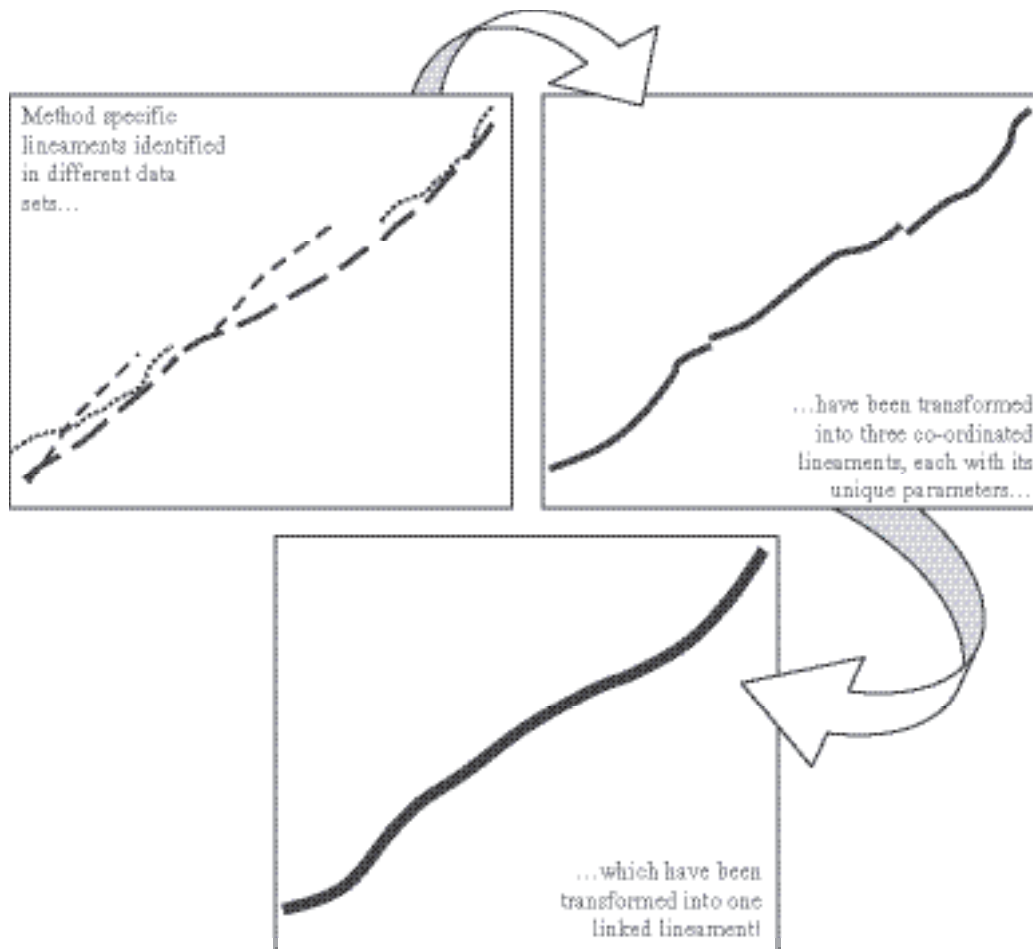


Figure 5-19. Three-stage process in the interpretation of lineaments (after /Triumpf, 2004/).

- *Co-ordinated lineament.* A visual inspection is carried out and a decision made concerning which method-specific lineaments can be integrated into a single, co-ordinated lineament. The method-specific lineament that is judged to provide the best representation of the linear feature is selected for location purposes. Splitting of each lineament is carried out so that segments that have been defined by different methods or combination of methods can be distinguished from each other (Figure 5-19). This step is vital in order to trace the basis for the interpretation work. Each segment that has been identified on the basis of one or more method-specific lineaments is referred to as a co-ordinated lineament.
- *Linked lineament.* The co-ordinated lineaments that are judged to form the same linear feature are linked together (Figure 5-19). Some minor adjustment of node locations at the termination of a co-ordinated lineament may occur during the linking procedure.

Only linked lineaments are utilised in the geological modelling work (see Section 5.4). These lineaments have been assigned the following key attributes:

- ID-number according to SKB's protocol (XFM*****).
- The number of co-ordinated segments along the lineament.
- The methods that have been used to identify the lineament (magnetics, topography – total, topography – land or sea bottom surface, topography – bedrock surface, electrical conductivity based on combined EM and VLF). A weighted average has been calculated for each method that takes into account the length of each segment in the lineament divided by the total length of the lineament. This value ranges continuously from 0 to 1.

- An assessment of the uncertainty factor for each lineament that is a judgement concerning its degree of clarity. A weighted average has been calculated that takes into account the length of each segment in the lineament divided by the total length of the lineament. This value ranges continuously from 1 (low uncertainty) to 3 (high uncertainty).
- An overall assessment of the confidence of the lineament interpretation. This is based on both the number of methods (1 to 3) upon which the lineament has been identified and the degree of uncertainty (1 to 3). A weighted average has been calculated that takes into account the length of each segment in the lineament divided by the total length of the lineament. This value grades continuously from 1=low confidence to 5=high confidence.
- Length.
- Average trend.

Results

1,169 linked lineaments have been identified in the analysis of the various data sets (Figure 5-20). Twelve lineaments are shorter segments that lie along what are judged, with confidence, to be longer lineaments (XFM0014A0, XFM0015A0, XFM0017A0, XFM0025A0). Furthermore, one lineament links to an adjacent lineament, but with lower confidence (XFM0137A0). For this reason, only 1,156 lineaments have a unique identity number (first seven positions of the ID-number, XFM****) and the remaining thirteen segments are simply distinguished by a different denomination in the

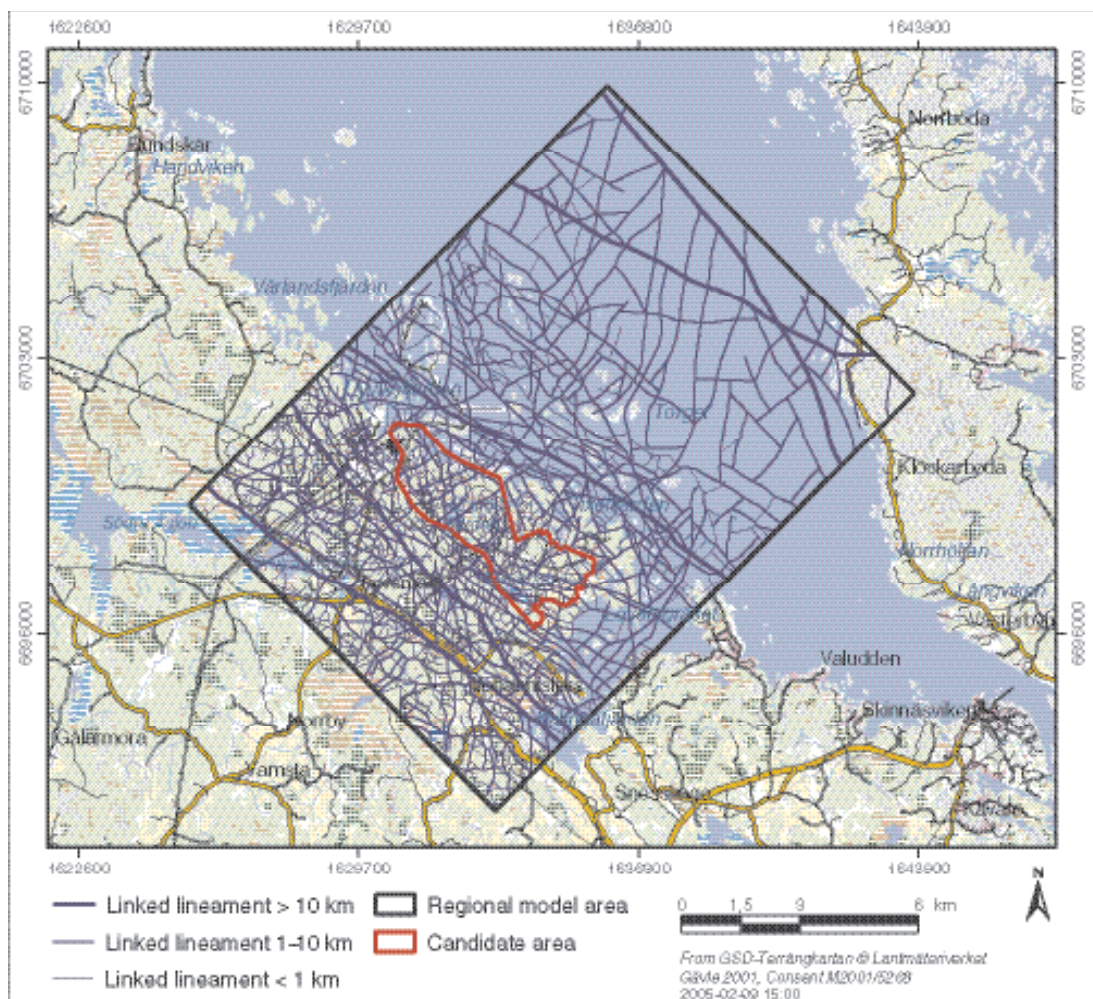


Figure 5-20. Linked lineaments in the regional model area.

final two positions in the ID-number. Inside the regional model area, five of the 1,156 lineaments show a length more than 10 km and 271 of these lineaments lie between 1 and 10 km in length. A statistical evaluation of the orientation and size distributions of the linked lineaments is provided in Section 5.5.

There is a consistent increase in the number of lineaments from the open sea area at Öregrundsgrepen to the coastal area near to Forsmark to the land area (Figure 5-20). This feature is an inherent bias associated with the radically better quality and resolution of the base data in the coastal area and, especially, on land. This bias is especially relevant for the topographic data, but is also relevant where the airborne geophysical data are concerned. This data bias diminishes markedly when only lineaments that are longer than 1 km and that show, at least partly, a magnetic signature are considered (Figure 5-21). It is likely that the variation in intensity of these lineaments over the regional model area is controlled more strongly by geological rather than by data bias factors. A distinctive feature of the candidate area is the array of low magnetic lineaments that trend north-east across this area (Figure 5-22). This array is most intense in the north-western part of the candidate area, around Bolundsfjärden.

Uncertainties

Several important uncertainties are present in the interpretation of lineaments. First and foremost, the exercise is subjective in character and questions arise concerning the reproducibility of the results.

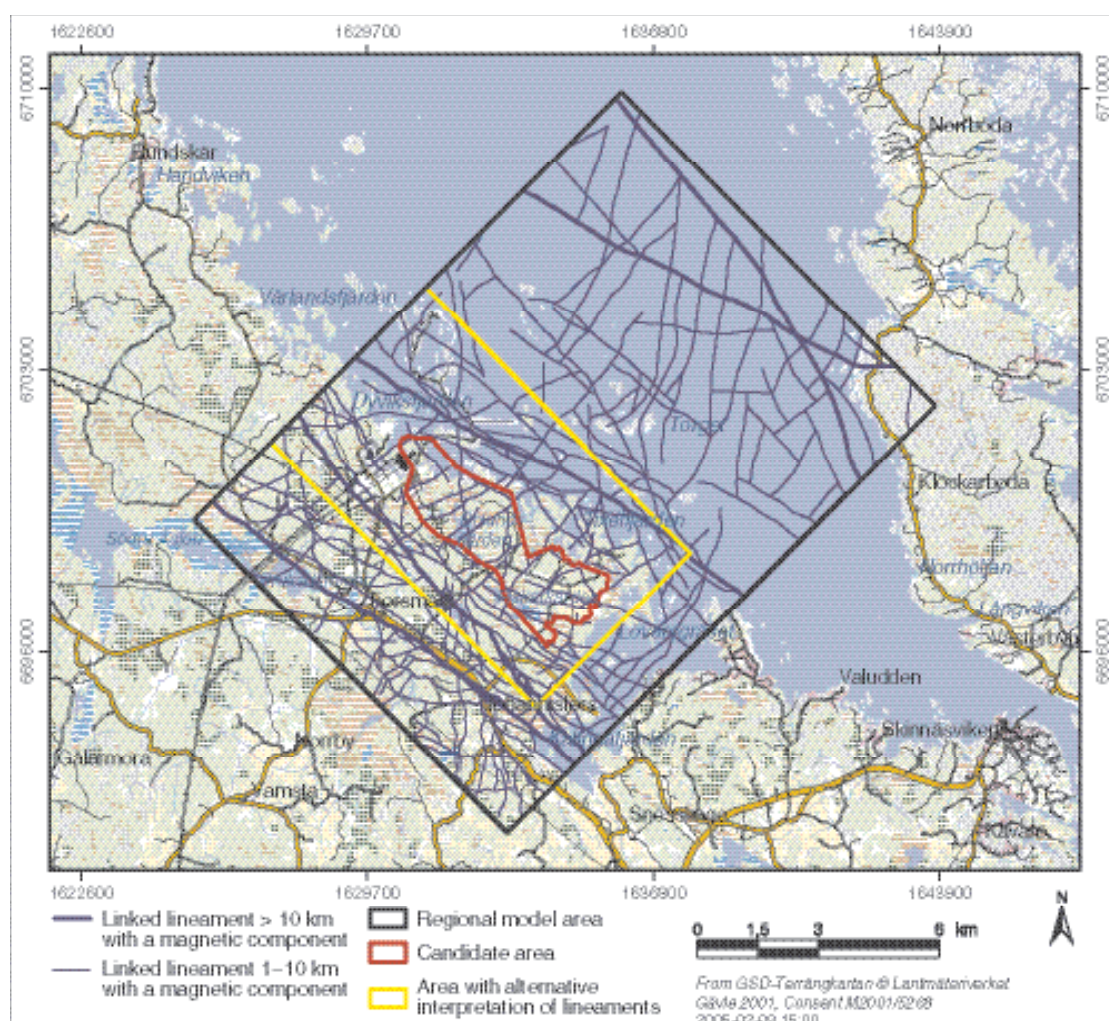


Figure 5-21. Regional and local major linked lineaments. The map only displays lineaments that show, at least partly, a magnetic signature. The area in which an alternative interpretation of lineaments has been carried out is also shown.

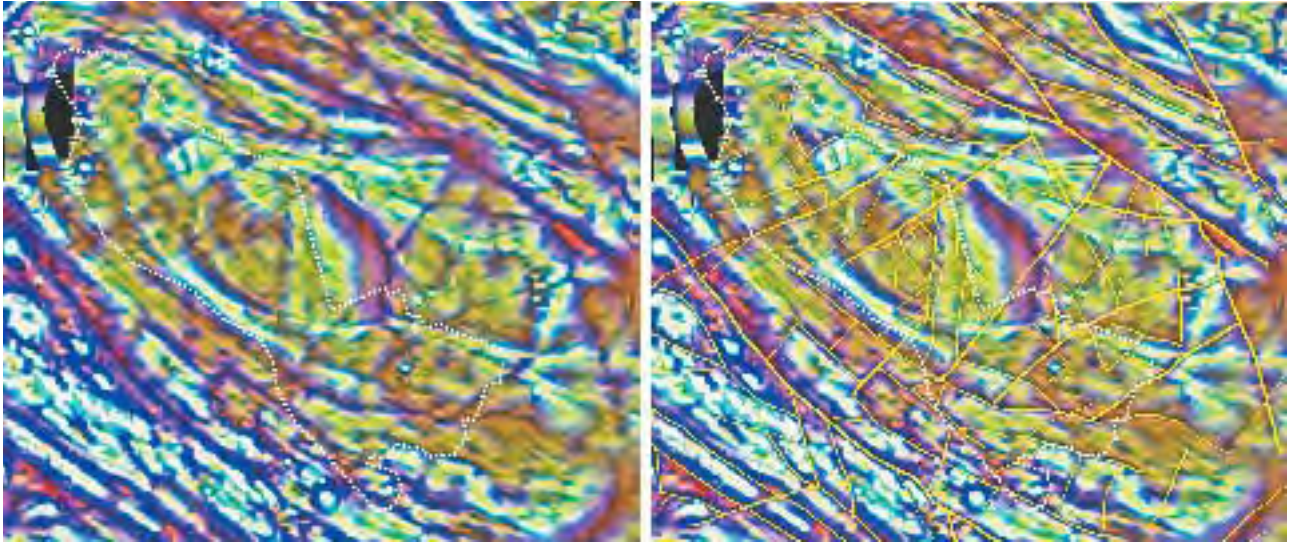


Figure 5-22. Contrast-enhanced airborne magnetics over the candidate area at Forsmark (north-south survey). The lilac areas indicate low magnetic anomalies and the inferred low magnetic lineaments (method-specific) are shown in the right hand picture as yellow lines. The thick and thin lines indicate low and high uncertainty lineaments, respectively. The candidate area is marked with a dotted white line (for a more detailed description, see /Isaksson et al. 2004c/).

This factor is most relevant where it concerns the establishment of the end points and, thereby, the length of an individual lineament. Assessment of uncertainty and, thereby, the overall assessment of the confidence in a lineament are also factors that are difficult to register in an objective manner. This is the case irrespective of whether the lineament is method-specific, co-ordinated or linked. However, this problem increases in importance at each stage in the interpretation procedure.

Secondly, since individual method-specific lineaments may represent different geological features, there is an intrinsic problem with the formation of both co-ordinated and linked lineaments. Thirdly, the low topographic relief gives rise to serious difficulties in the interpretation of even the high-resolution topographic data. Finally, there is a specific problem in the Forsmark area in relation to the interpretation of the magnetic data. Since bedrock units with variable magnetisation are aligned in a north-west direction in the strongly deformed areas, it is difficult to separate lineaments, in these areas, that are related to rock types with low magnetisation from deformation zones where magnetite has been affected by fluids and hematisation. This problem is also relevant to possible trails of Group D dykes that show low magnetisation.

Alternative interpretation

Bearing in mind the uncertainties listed above, an alternative interpretation of lineaments was carried out in a restricted area that includes the candidate area (Figure 5-21). This interpretation made use of the airborne geophysical and topographic data that were available for model version 1.1 /SKB, 2004a/. The same methodology for the interpretation work, as that used in the base model, has been adopted and the results have been presented in /Korhonen et al. 2004/. A comparative study of the two lineament interpretations has also been completed /Johansson, 2005/.

In general, it appears that many of the lineaments that were identified in the base interpretation are present in the alternative interpretation. However, there are important discrepancies, for example, in the north-western part of the candidate area (Figure 5-23). These discrepancies must be taken into consideration. There are also significant differences concerning the estimation of the length of a lineament. This parameter is clearly difficult to define and there are no objective criteria available to define when two lineaments should be kept separate or combined to form one single lineament. This concerns both the stages from method-specific to co-ordinated lineament and from co-ordinated to linked lineament. Furthermore, the factor “uncertainty” is too subjective to be used as a stand-alone criterion for further assessment of the inferred lineaments.

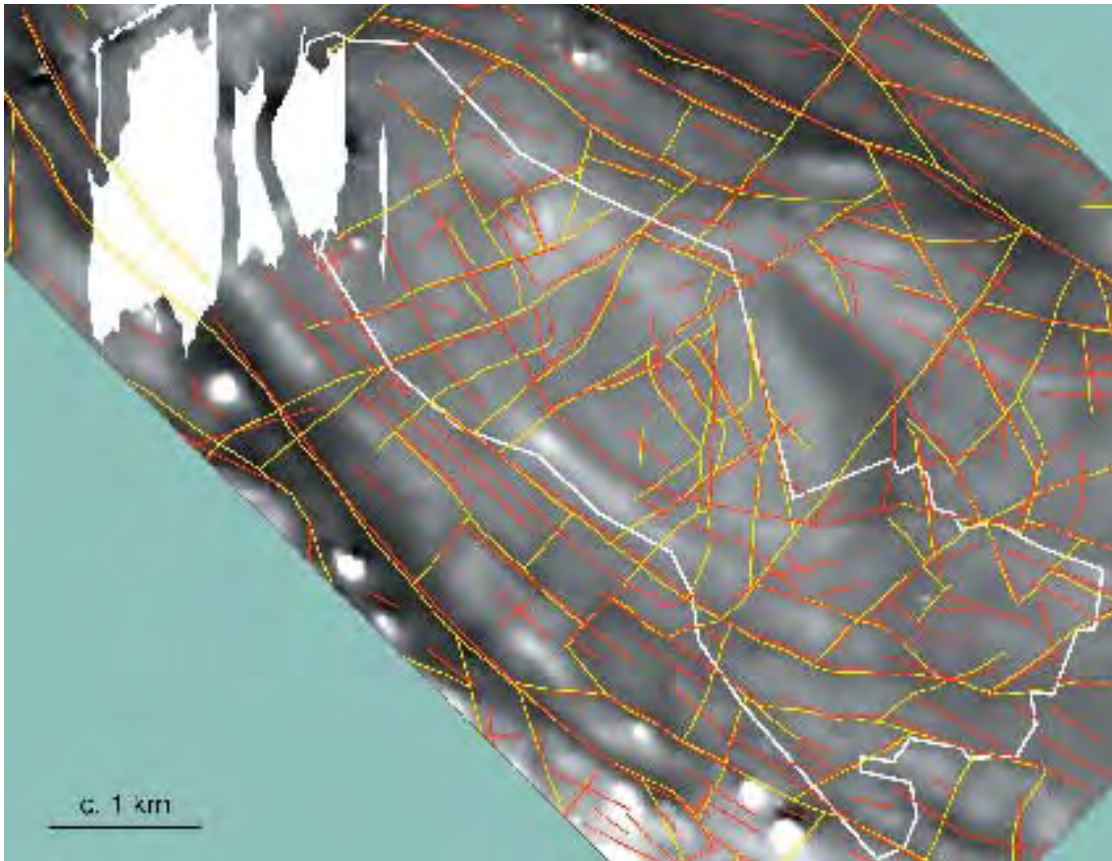


Figure 5-23. Comparison of the two interpretations inside the candidate area for the method-specific lineaments based on magnetic minima. The original interpretation is shown with yellow lines and the alternative interpretation with red lines. The boundaries of the candidate area are marked with a white line. The white areas lie close to the nuclear power plant where high-resolution, helicopter-borne geophysical data are lacking. Note the long lineament with north-west trend in the alternative interpretation (red) that passes through the candidate area and is not present in the original interpretation (yellow). Note also the difference in the style of the lineaments. The lineaments in the original interpretation tend to be longer and are documented in more detail. The lineaments in the alternative interpretation are commonly shorter, straight lines.

It is concluded that there is no single criterion or combination of criteria that can be used for further evaluation of the lineaments as a group. Each lineament, or set of similar lineaments, has to be evaluated individually based on all available information. If no outcrops are available, lineaments of critical importance for further assessment of the site must be subject to investigations by means of direct methods, in the first hand by trenching and in the second hand by drilling. Other lineaments could be investigated by, for example, surface geophysics (e.g. seismic refraction studies).

5.2.4 Observation of ductile and brittle structures from the surface

Data

The ductile structural data at the surface, in combination with the corresponding, more limited borehole information (Section 5.2.6), provide a key input for the development of the geometry of rock domains in the rock domain model (Section 5.3). Furthermore, the investigation of brittle structures at the surface, in combination with the extensive borehole data on fractures (Section 5.2.7), are critical for the development of both the deterministic deformation zone and DFN models (Sections 5.4 and 5.5, respectively).

The following data are available that document the character and orientation of ductile and brittle structures at or close to the surface:

- Measurements of the orientation of predominantly ductile structures and bedrock contacts at 1,661 of the 2,119 outcrops (Figure 5-1) that were mapped in connection with the bedrock mapping programme /Stephens et al. 2003a; Bergman et al. 2004/. Mylonites and cataclastic rocks are also documented in these outcrop data. The structural data were subsequently evaluated and interpreted in /Stephens et al. 2003b, 2005b/.
- Laboratory measurements of the anisotropy of magnetic susceptibility (AMS) from 134 surface rock objects (Figure 5-2c). For the most part, measurements were carried out on four samples of each rock. Data assembly, evaluation and interpretation were presented in /Mattsson et al. 2003; Isaksson et al. 2004a,b/.
- Various studies of fractures in the near-surface bedrock that were carried out during construction of the nuclear power plant, the inlet channel for cooling water, the two discharge tunnels and SFR (see, for example, /Larsson, 1973; Stephansson and Ericsson, 1975; Carlsson and Olsson, 1977; Carlsson, 1979; Carlsson and Christiansson, 1987; Pusch et al. 1990/).
- Detailed mapping of fractures (including fracture fillings) that are longer than 50 cm at the scale 1:50 at five sites (Figure 5-24). These sites include Klubbudden, which has an areal extent of c. 325 m², and four temporarily exposed outcrops at drill sites 2, 3, 4 and 5, which range in areal extent from c. 500 to c. 600 m² /Hermanson et al. 2003a,b, 2004/).

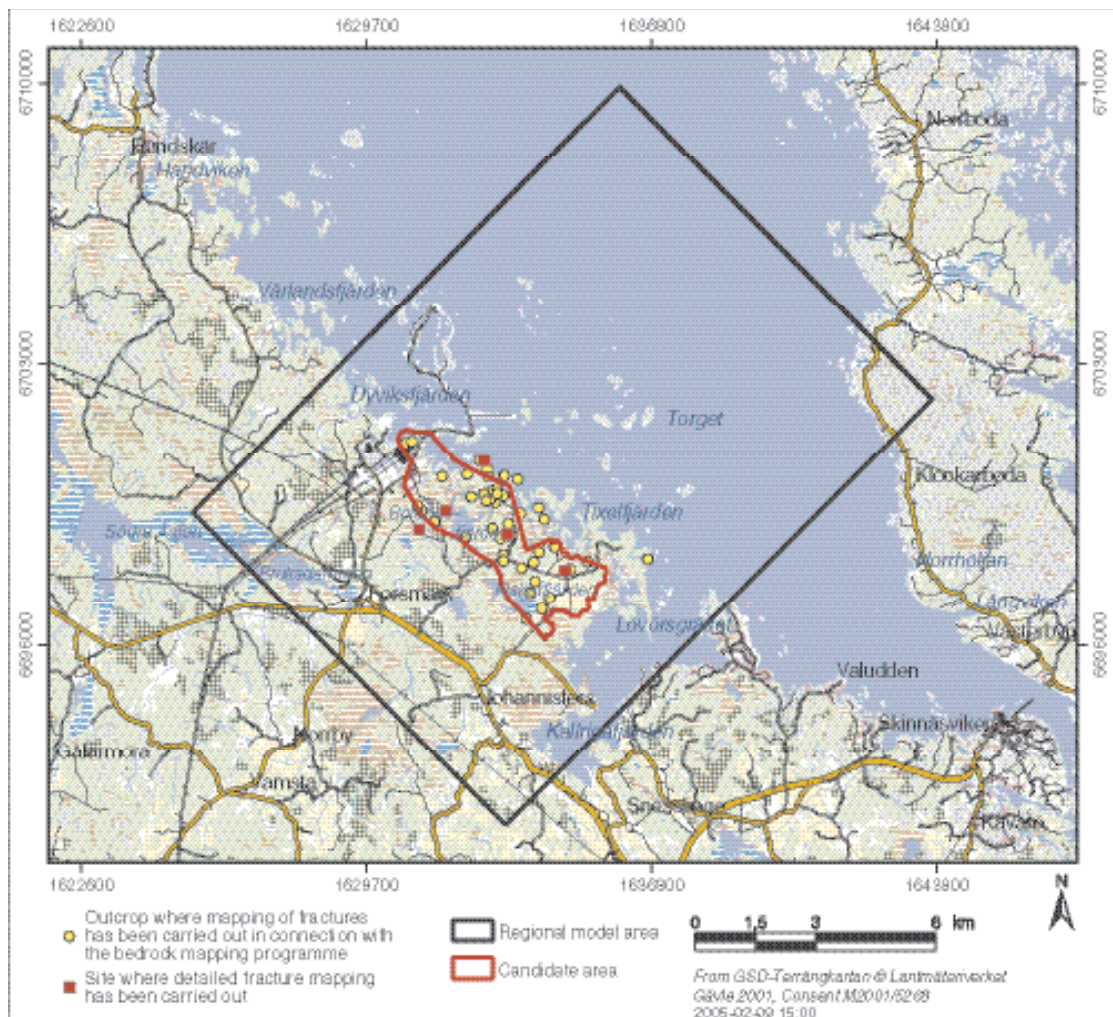


Figure 5-24. Summary of surface field data used to assess the character and orientation of brittle structures in the regional model area. Ductile structural data are available from most of the outcrop observation points visited during the bedrock mapping programme (see Figure 5-1).

- Measurements of the frequency and orientation of fractures that are longer than 100 cm at 44 of the 2,119 outcrops referred to above /Stephens et al. 2003a/. Fracture fillings were also noted at some of these outcrops. The 44 outcrops are located predominantly within the candidate area (Figure 5-24) and the data were subsequently evaluated and interpreted in /Stephens et al. 2003b/. No new data of this type have been generated after model version 1.1.
- The documentation of minerals that fill fractures at 115 of the 2,119 outcrops referred to above /Stephens et al. 2003a; Bergman et al. 2004/.

This section focuses attention on the ductile structures, including the magnetic susceptibility (AMS) values. These data are assessed according to the sub-areas defined in Section 5.2.2 (Figure 5-11). Only a brief summary of the results of the detailed fracture mapping at the five sites is included here. A more detailed analysis is presented in Section 5.5. Evaluation of the brittle structures from the 44 outcrops, where a simplified fracture mapping has been carried out, was completed and described in /SKB, 2004a/. No further comments are included here.

Ductile structures

Character of the ductile structures

Ductile planar structures at the Forsmark site consist of a foliation, a tectonic banding or a combined foliation and banding. These structures vary considerably in their degree of development and this variation is interpreted to reflect a variation in the degree of ductile deformation over the area (see below). The foliation corresponds to a planar grain-shape fabric. In the dominant felsic rocks that belong to Groups A and B, this fabric is defined by oriented grains of biotite and, less commonly, hornblende, as well as elongate aggregates of recrystallised quartz and feldspar.

A ductile linear structure that corresponds to a linear grain-shape fabric is conspicuous over the whole area. This mineral lineation is inferred to mark the direction of stretching during the ductile deformation. Oriented hornblende crystals in the Group B mafic and intermediate rocks define this fabric most conspicuously. Oriented biotite grains and elongate aggregates of recrystallised quartz and feldspar also form the lineation in the felsic rocks that belong to Groups A, B and C. Minor folds that deform the foliation or tectonic banding define a second type of ductile linear structure.

The structures defined by the anisotropy of magnetic susceptibility (AMS) formed in connection with the regional ductile deformation in the bedrock /Isaksson et al. 2004a,b/. AMS measurements permit calculations of the mean directions of the principal AMS axes and, thereby, the orientation of the magnetic foliation and magnetic lineation at the sample sites. The AMS measurements also permit a calculation of the mean values of the principal magnetic susceptibilities ($K_1 \geq K_2 \geq K_3$) for each sample locality. With the help of these mean values, estimates of the degree of anisotropy (K_1/K_3) and the shape of the anisotropy ellipsoid can also be made for each locality. The ellipsoid may be prolate (with a dominance of magnetic lineation), spherical, or oblate (with a dominance of magnetic foliation). These calculations provide some quantitative estimates of the degree and character of the ductile strain at different locations in the Forsmark area.

Structures in the south-westernmost and north-easternmost sub-areas

In both these sub-areas, a linear grain-shape fabric dominates the bedrock that, in a structural sense, is predominantly composed of LS-tectonites (Figure 5-25a and Figure 5-25e). In the south-westernmost sub-area, all structures show well-constrained orientations. Both the mineral lineations and the fold axes plunge moderately to the south-east and the planar structures dip steeply to the south-west. By contrast, in the north-easternmost sub-area, both the mineral lineations and the planar structures show more variable orientations. The linear structures also commonly show a gentler plunge and the majority of the planar structures dip to the north-east and east.

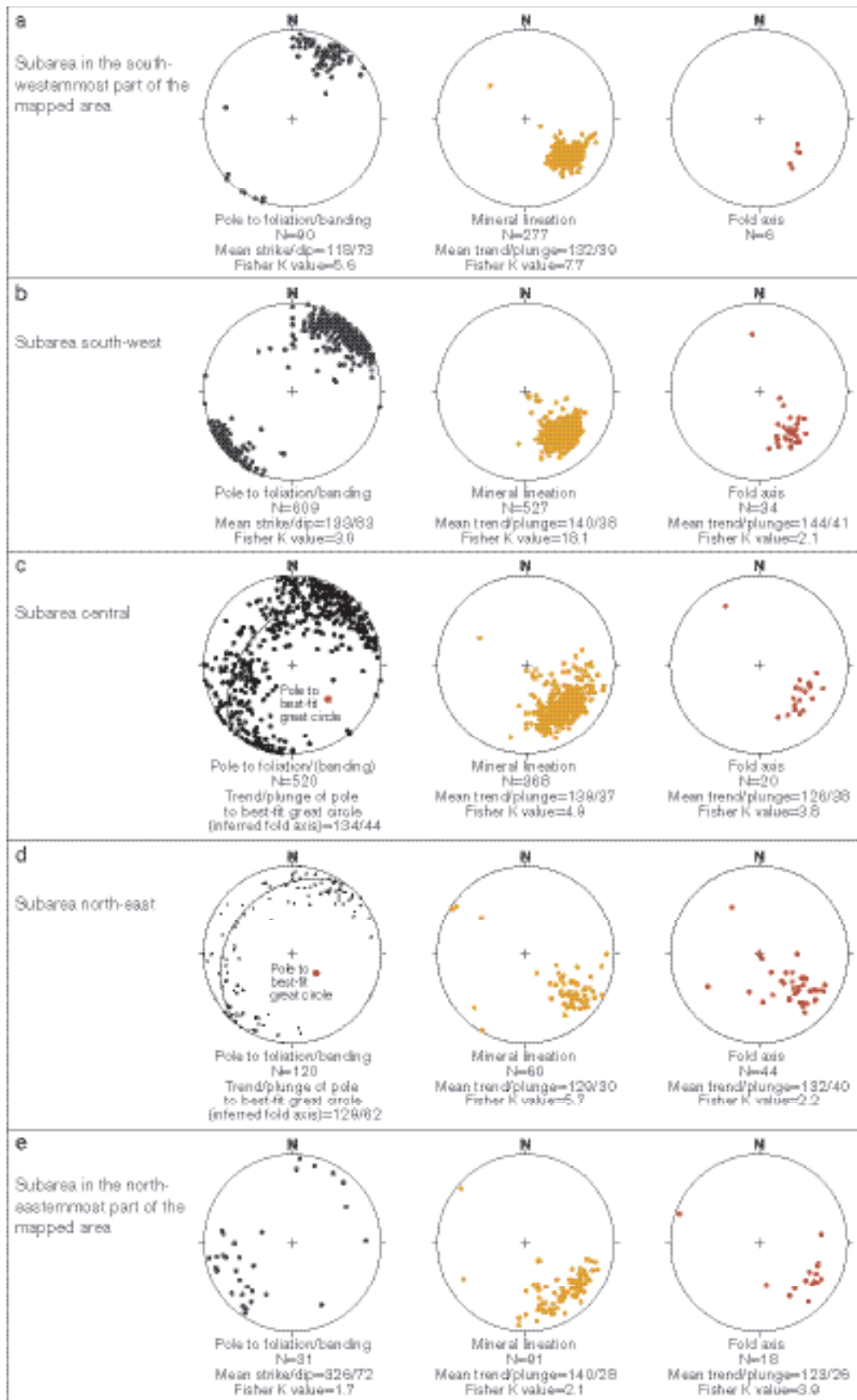


Figure 5-25. Orientation of ductile structures in the different sub-areas (after /Stephens et al. 2003b, 2005b). All structures have been plotted on the lower hemisphere of a Schmidt, equal area stereographic plot. Planar structures have been plotted as poles to planes. The sub-areas are defined in Figure 5-11.

Structures in the sub-areas south-west and north-east

The bedrock in sub-areas south-west and north-east generally shows a high level of ductile strain and contains both planar and linear ductile structures, i.e. the bedrock is predominantly composed of SL-tectonites. Exceptions to this general rule include several of the ultramafic, mafic and intermediate plutons, two areas in the western and eastern, marginal parts of sub-area south-west, and the Group C intrusive rocks in sub-area north-east (Figure 5-12). Linear mineral fabrics and lower ductile strain dominate in these segments. Winged porphyroclasts /Passchier and Trouw, 1998/ in highly-strained rocks in both sub-areas indicate a component of dextral horizontal movement (Figure 5-26a). Minor folds, which contain an intense, mineral stretching lineation along the fold axes, deform the planar fabric in these highly-strained rocks (Figure 5-26b). An eye-shaped, tubular fold has been observed at one locality in sub-area north-east.

Concentration of high ductile strain is evident along the Eckarfjärden deformation zone /SKB, 2002a, 2004a/. An intense banding structure (Figure 5-26c), which formed under amphibolite facies metamorphic conditions and even affected the Group D rocks, characterises an early stage in the development of this zone. Mylonites as well as extensive hematization and epidotisation of the rocks characterise a later stage of development under greenschist facies metamorphic conditions (Figure 5-26d). ^{40}Ar - ^{39}Ar hornblende ages close to the Eckarfjärden deformation zone (see Section 3.1) suggest that the deformation under greenschist facies metamorphic conditions occurred more recently than 1,812 million years ago.

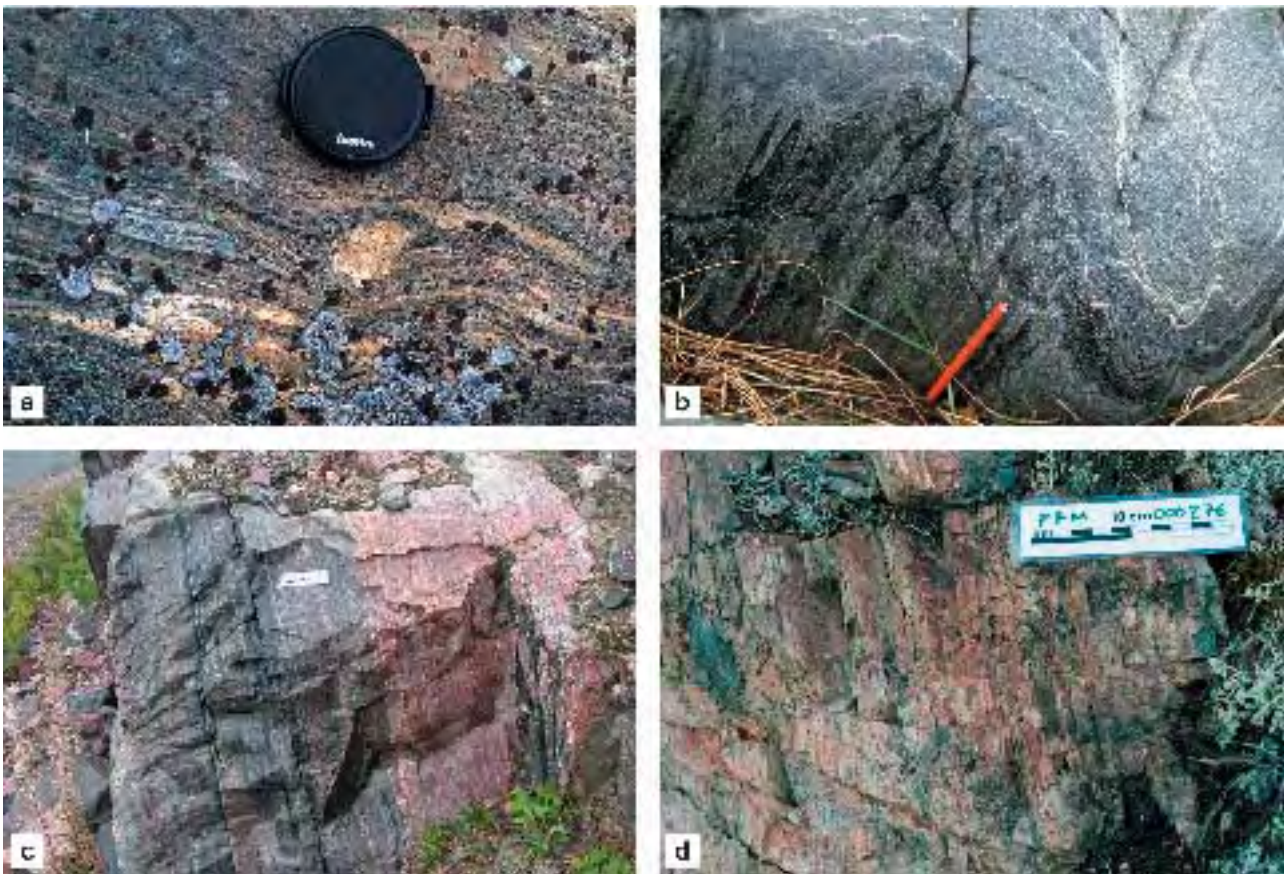


Figure 5-26. a) Winged porphyroclast (δ -type), which indicates a component of dextral horizontal movement, in rocks affected by high ductile strain at field observation point PFM001235. b) Folding of the highly-strained rocks at PFM001235. Folds of this type are dominated by an S-symmetry in this outcrop. c) Intense ductile strain under amphibolite facies metamorphic conditions along the Eckarfjärden deformation zone. A Group D pegmatite is also affected by the high strain. Field observation point PFM000834. d) Low-temperature mylonite and hematization/epidotisation along the Eckarfjärden deformation zone. Field observation point PFM000276.

In sub-area south-west, the ductile structures show a regular orientation pattern similar to that observed in the south-westernmost sub-area (compare Figure 5-25a and Figure 5-25b). By contrast, in sub-area north-east, the poles to the planar structures lie along a great circle (Figure 5-25d) that is related to the folding of these structures around the metadiorite in the western part of the sub-area. This fold structure is inferred to plunge steeply to the south-east (129/62). Both the mineral lineation and the measured fold axes in this sub-area also plunge to the south-east (Figure 5-25d).

Structures in sub-area central including the candidate area

The bedrock in sub-area central is inferred to show a low level of ductile deformation relative to that observed in the adjacent areas to the south-west and north-east. A linear grain-shape fabric with subordinate, planar structures dominates this sub-area, i.e. the bedrock is predominantly composed of LS-tectonites.

Folding on different scales dominates the structural framework in sub-area central. North-west of Asphällsfjärden, the heterogeneous rock unit dominated by aplitic metagranite and metavolcanic rocks is folded in a synformal structure, whereas, close to Lillfjärden, the Group B metatonalite unit is folded in an open antiform (Figure 5-12). The folding is also expressed in the great circle pattern defined by the poles to planar structures in the sub-area (Figure 5-25c). These structural data indicate that the folding affected not only the boundaries to rock units but also the planar grain-shape fabric in the rocks. The folds plunge moderately to the SE (Figure 5-25c). Both the fold axis inferred from the pole to the great circle on the foliation plot (134/44) and the measured fold axes are more or less parallel to the mineral stretching lineation (Figure 5-25c). These geometric features are reminiscent of oblique folds /Passchier and Trouw, 1998/ or tubular-shaped structures that are referred to as sheath folds /Cobbold and Quinquis, 1980/.

AMS data

The AMS measurements have been carried out on samples from all five sub-areas. However, the majority of these samples are from the candidate area in sub-area central.

The minimum, principal AMS axes (poles to magnetic foliation) for the rocks in Groups A and B plot along a great circle on the lower hemisphere of a Schmidt, equal-area stereographic projection, with a strong cluster in the north-eastern part of the diagram (Figure 5-27). The great circle distribution indicates a folding of the magnetic foliation with an axis that plunges moderately to the south-east. The inferred fold axis (132/44) is similar in orientation to the maximum, principal AMS axes (magnetic lineation) for these rocks (Figure 5-27). This distribution, including the inferred fold axis orientation, is more or less identical to that indicated from the measured structural data for sub-area central (see above).

The inferred higher degree of ductile deformation in sub-area south-west compared to that in sub-area central is confirmed by the higher degree of magnetic anisotropy values in the south-western sub-area (Figure 5-28a). Furthermore, the more frequent occurrence of strongly banded and foliated rocks south-west of the candidate area is consistent with the more oblate character of the shape ellipsoid in this area (Figure 5-28b).

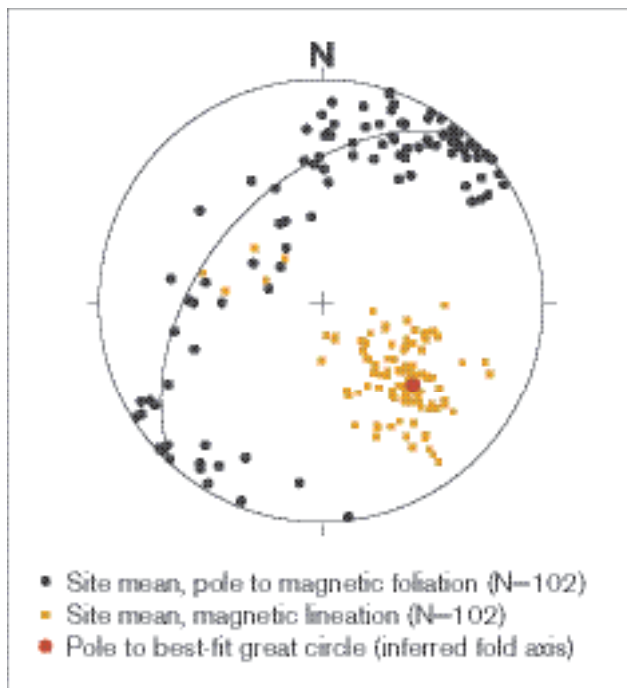


Figure 5-27. Orientation of the site mean values of magnetic foliation and magnetic lineation for the rocks in Groups A and B. The poles to the magnetic foliation define a great circle, the pole to which is also shown. All structures have been plotted on the lower hemisphere of a Schmidt, equal area stereographic plot.

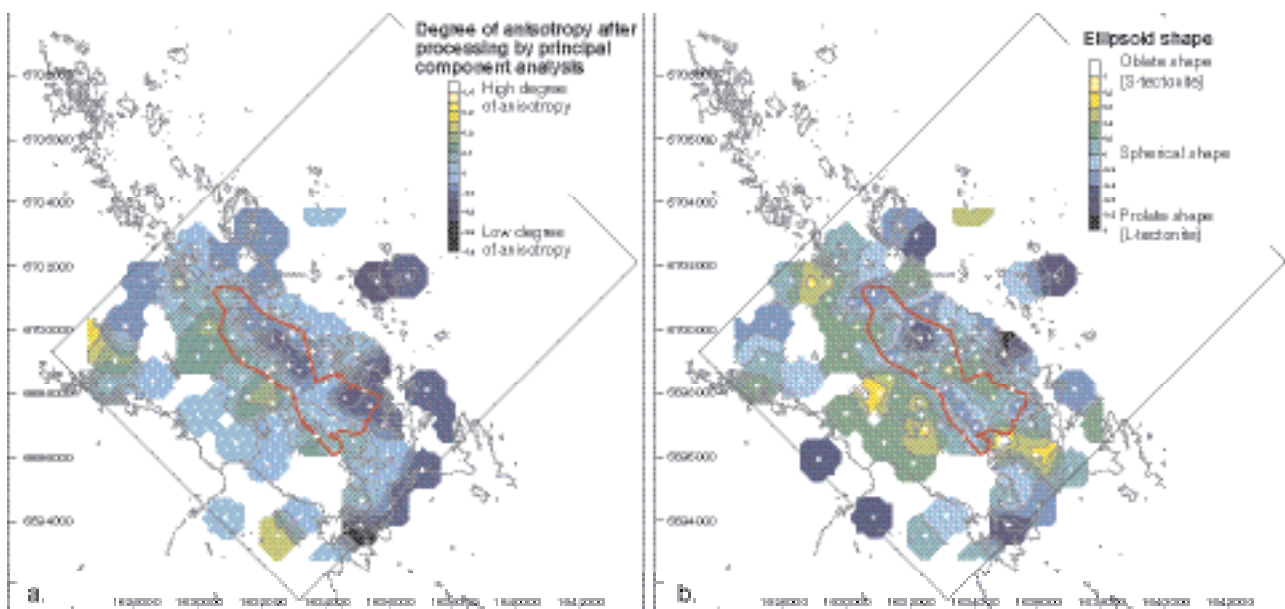


Figure 5-28. Contoured diagrams that show a) the normalised degree of magnetic anisotropy and b) the ellipsoid shape parameter in the Forsmark area. Only the felsic Group B rocks are included and the sample locations (84) are shown with a white cross (after /Isaksson et al. 2004b/). It has been assumed that the degree of magnetic anisotropy is dependent on a linear combination of grain shape and volume susceptibility. On the basis of this assumption, a principal component analysis has been applied to the degree of magnetic anisotropy and the corresponding volume susceptibility values, in order to correct the former for the effects of the volume susceptibility. A more detailed discussion of this procedure is presented in /Isaksson et al. 2004a,b/.

Brittle structures

Summary of older work at the nuclear power plant and SFR

Significant fracture sets are vertical or dip steeply and strike NW, NE and EW /Carlsson and Christiansson, 1987/. However, an important finding of the studies carried out during the construction work at the nuclear power plant concerns the occurrence of horizontal and sub-horizontal (dip $< 10^\circ$) fractures, especially in the upper part of the bedrock, i.e. probably down to a few tens of metres /Carlsson, 1979/. These fractures commonly show wide apertures, locally > 50 cm and up to 82 cm, and are also commonly filled with glacial sediment (Figure 5-29a). This feature suggests that these fractures either formed or were reactivated (opened) during late- or post-glacial time. Chlorite is by far the most important mineral that fills the fractures in all four fracture sets. Laumontite is also present in each set of vertical or steeply-dipping fractures /Carlsson and Christiansson, 1987/.

The Singö deformation zone, a splay from this zone that intersects tunnel 3 and the Forsmark deformation zone, which all strike north-west, as well as a zone that strikes north-east along Kallrigaffjärden were all recognised as regional fault lines in /Carlsson and Christiansson, 1987/. Furthermore, the drilling and tunnel work demonstrated that both the Singö deformation zone and its splay are complex zones with both ductile and brittle components of deformation. Cross-cutting relations between fractures with different mineral fillings along the Singö deformation zone indicate that at least this zone has been active at different periods /Larsson, 1973; Carlsson, 1979/.

The Singö deformation zone and other subordinate, vertical or steeply dipping zones that strike NW (zone 8), NE (zones 3 and 9) and NS (zone 6) have been recognised at the SFR repository /Axelsson and Hansen, 1997; Holmén and Stigsson, 2001/. However, the geological structure that has attracted most attention at SFR is the sub-horizontal zone H2 that is present beneath the repository. This zone dips $15\text{--}20^\circ$ to the south-east, and consists of horizontal lenses of highly fractured and altered rock that define a 5–15 m thick, hydraulically conductive zone. The continuity of this zone, especially in a horizontal direction, has provoked considerable discussion (see summary in /SKB, 2002a/).

Data from the detailed mapping of fractures

Detailed mapping of fractures has been carried out at five sites in the Forsmark local model area (Figure 5-30a). The data from two of the sites, drill sites 2 and 3, were already made use of in the statistical analysis of fractures in model version 1.1, but these data have been re-analysed in the present model version.



Figure 5-29. a) Sub-horizontal fracture that is filled with glacial sediment, located in the excavation for unit 3 at the nuclear power plant (after /Carlsson, 1979/). b) Gently dipping, open fracture at drill site 5.



Figure 5-30. a) View to the south-west of the temporarily exposed outcrop at drill site 4 where a detailed mapping of fractures was carried out. Note the brittle deformation zone that strikes north-east and dips steeply to the north-west to the right in the picture. This is the surface expression of the local minor zone ZFMNE1188 (see Section 5.4.3). b) Component of dextral horizontal movement along the brittle deformation zone at drill site 4 shown in Figure 5-30a.

Fracture trace maps that visualise fracture geometry were produced for each outcrop where detailed fracture mapping has been carried out (Figure 5-31). The orientation of fractures has been recorded (Figure 5-31) and the physical properties associated with each fracture have been mapped. These include mineralogy, aperture, trace length and termination characteristics. The censoring of fractures includes trace lengths from 50 cm up to the maximum extent mapped in the exposed outcrop area. The number of fractures mapped varies from 869 to 1,188 (Table 5-5). Scan line measurements were also carried out along two orthogonal profiles at each of the five sites. The minimum trace length mapped was 20 cm. A statistical evaluation of the orientation, size and intensity of the brittle structures at the five sites is included in Section 5.5. Unfortunately, due to shortage of analysis time, the scan line data were not used in the modelling work.

Over 50% of the fractures at drill site 5 (AFM100201) are inferred to have formed or to have been reactivated during late glacial time /Hermanson et al. 2004/. These fractures are both steeply and gently dipping, and several are open or filled in part with glacial sediment (Figure 5-29b). These features are reminiscent of the horizontal and sub-horizontal fractures observed during the construction work at the nuclear power plant (see above). However, several of the fractures that are filled with glacial sediment at drill site 5 dip more steeply (c. 25°).

Quartz, hematite-stained quartz, chlorite, calcite, a mineral that is inferred to belong to the zeolite group and one or more unidentified minerals have been observed along the fractures studied during the detailed fracture mapping programme. Furthermore, many fractures show a thin altered border zone that is reddish and is inferred to be composed of tiny hematite grains. A component of dextral horizontal movement is present along the brittle deformation zone that strikes north-east and dips steeply to the north-west at drill site 4 (Figure 5-30b).

Table 5-5. Number of fractures (trace length > 0.5 m) mapped at the five sites selected for detailed fracture mapping.

Outcrop ID	Area (m ²)	All fractures	Open fractures	Sealed fractures
AFM000053	c. 600	968 ¹⁾	246	720
AFM000054	c. 600	1,182	44	1,138
AFM001097	525	1,188	68	1,120
AFM001098	325	1,130	23	1,107
AFM100201	501	869	552	317

¹⁾ Two fractures have not been classified as open or sealed.

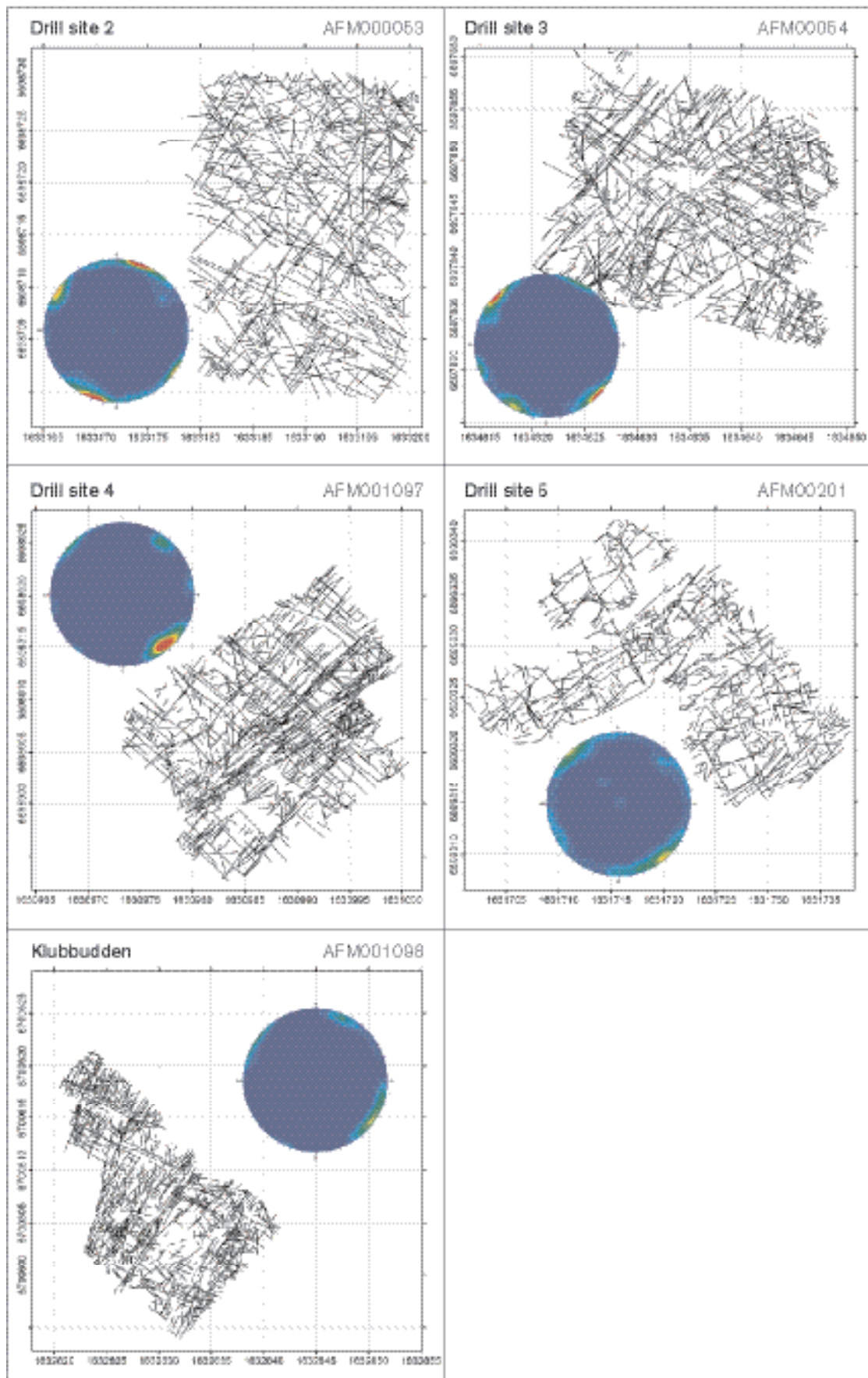


Figure 5-31. Fracture trace maps and fracture orientations that are compiled in the lower hemisphere of Schmidt stereographic plots.

Data from the bedrock mapping programme

Cataclastic rocks and brecciated mylonites are exposed along the Eckarfjärden deformation zone (Figure 5-32a). These observations demonstrate the complex character of this zone (see also ductile structures). It apparently formed under amphibolite-facies metamorphic conditions, continued to be active under greenschist-facies metamorphic conditions, and was also active, possibly more than once, under lower temperature metamorphic conditions, when the bedrock responded to crustal deformation in a brittle manner. Kinematic data are more or less absent at the site. One steeply-dipping fracture along the line survey LFM000363, which strikes in a north-east direction, contains inferred Riedel shear fractures (Figure 5-32b). This relationship indicates a sinistral component of horizontal movement along the fracture (cf. drill site 4).

Data generated during the bedrock mapping programme show that epidote and quartz are the dominant minerals that have been observed to fill fractures in outcrops. Chlorite, hematite, pyrite and magnetite have also been observed. At several outcrops, a hard, reddish-coloured mineral has been documented which, at some outcrops, has been interpreted as hematite-stained quartz but may possibly be hematite-stained adularia. Larger segregations or veins of hydrothermal quartz, in places stained with hematite, are also present. Reddish, alteration zones that border many fractures consist of tiny hematite grains. It is important to bear in mind that the dominant occurrence of epidote and quartz in the surface outcrops reflects the hard nature of these minerals and their ability to survive surficial weathering and/or erosional processes. Mineral fillings along fractures at depth, as observed in boreholes (see Section 5.2.7), are far more representative.

Due to the removal of much of the mineral fracture fillings at the surface, there are insufficient data to assess with confidence the relationship between the occurrence of the different fracture-filling minerals and the orientation of the fractures. Nevertheless, epidote has been observed along at least one fracture in each of the steeply dipping NW, NS, NE and subordinate EW sets, as defined in the DFN modelling work (see Section 5.5). It is suggested that hydrothermal fluids, which were at temperatures corresponding to greenschist-facies metamorphic conditions, moved along the fractures that are filled with epidote. This indicates that at least some of the fractures in each of the sets are geologically old structures.

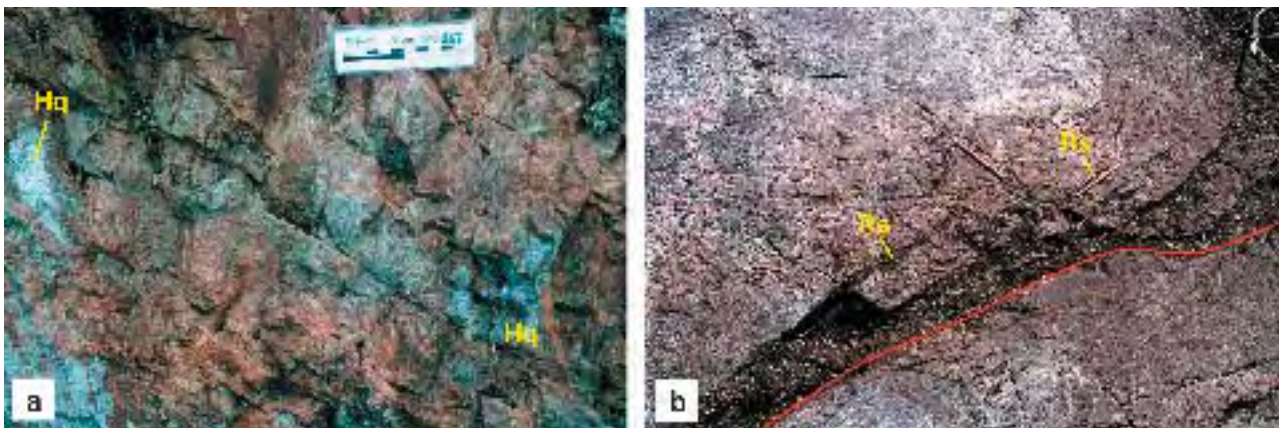


Figure 5-32. a) Strongly altered cataclastic rock along the Eckarfjärden deformation zone. Note the abundant occurrence of hydrothermal quartz (Hq). Field observation point PFM000267. b) Splay of inferred Riedel shear fractures (Rs) that emanate from a main fracture with north-east strike (red line). The orientation of these shear fractures relative to the main fracture indicates a component of sinistral horizontal movement. The pencils are c. 10 cm in length. Compare Figure 5-30b. Line survey LFM000363.

5.2.5 Surface geophysics

Data

Different types of surface geophysical data provide indirect methods to study the occurrence of possible deformation zones and provide a basis for the modelling of geological structures (see Section 5.4). As for lineaments, independent data (e.g. outcrop data, trenching, borehole data) are necessary to calibrate the geophysical anomalies and, thereby, confirm or refute the presence of the inferred zones. Many of the data that have been generated during the ongoing site investigation programme and during older construction work at Forsmark were focused on the identification of deformation zones. Gravity data have also been acquired /Aaro, 2003/. However, these data are of a broad regional character and have, as yet, neither been interpreted nor used in the modelling work.

Older data

Two types of older surface geophysical data /Keisu and Isaksson, 2004/ have been utilised during the site investigation work:

- Refraction seismic data.
- Ground EM (slingram) and magnetic data.

The refraction seismic data were generated predominantly in connection with the construction of the nuclear power plant and, at a later stage, the SFR facility /Keisu and Isaksson, 2004/. The processing of these data to form various topographic maps, and the interpretation of lineaments from these maps were discussed earlier (see Section 5.2.3). However, these data have also been processed to evaluate the velocity distribution in the bedrock and to identify low velocity ($\leq 4,000$ m/s) anomalies /Isaksson and Keisu, 2005/. The survey lines, the inferred low velocity anomalies in the bedrock, and the identification of some possible zones are shown in Figure 5-33.

Ground EM and magnetic data surveys were carried out in a restricted area in the vicinity of unit 3 at the nuclear power plant /Keisu and Isaksson, 2004/. The interval between the measurement stations in all these surveys varies between c. 10 and 20 m. A number of method-specific lineaments have been identified with the help of these data /Isaksson and Keisu, 2005/ and have been incorporated in the lineament identification study (see Section 5.2.3).

A combination of various surface geophysical measurements (refraction seismic data, EM/VLF data, magnetic data) are also available from short line surveys in the area between the Eckarfjärden and Forsmark deformation zones, as well as along the Forsmark zone /Keisu and Isaksson, 2004/. No systematic evaluation of these data has been carried out.

Data generated inside the candidate area

Two types of surface geophysical data inside the candidate area have been generated and utilised during the site investigation work:

- High-resolution reflection seismic data /Juhlin et al. 2002/.
- Ground EM (slingram) and magnetic data /Thunehed and Pitkänen, 2002; Pitkänen and Isaksson, 2003; Pitkänen et al. 2004b/.

The high-resolution reflection seismic survey was carried out to investigate the occurrence of gently dipping structures in the bedrock. The data were obtained along five separate, cross-cutting profiles, each of which varies in length from 2 to 5 km. The total survey length is approximately 16 km and the profiles are restricted more or less entirely to the candidate area (Figure 5-34). The shot and receiver spacing intervals along the profiles were 10 m (c. 1,300 shot points) and a dynamite source that weighed 15 to 75 g was employed. Most of the shots were also recorded on a stationary network of 11 Orion 3-component seismometers in order to provide a velocity model. Interpretation of the reflectors was presented in /Juhlin et al. 2002/ and a minor re-interpretation of the data was presented in /Juhlin and Bergman, 2004/.

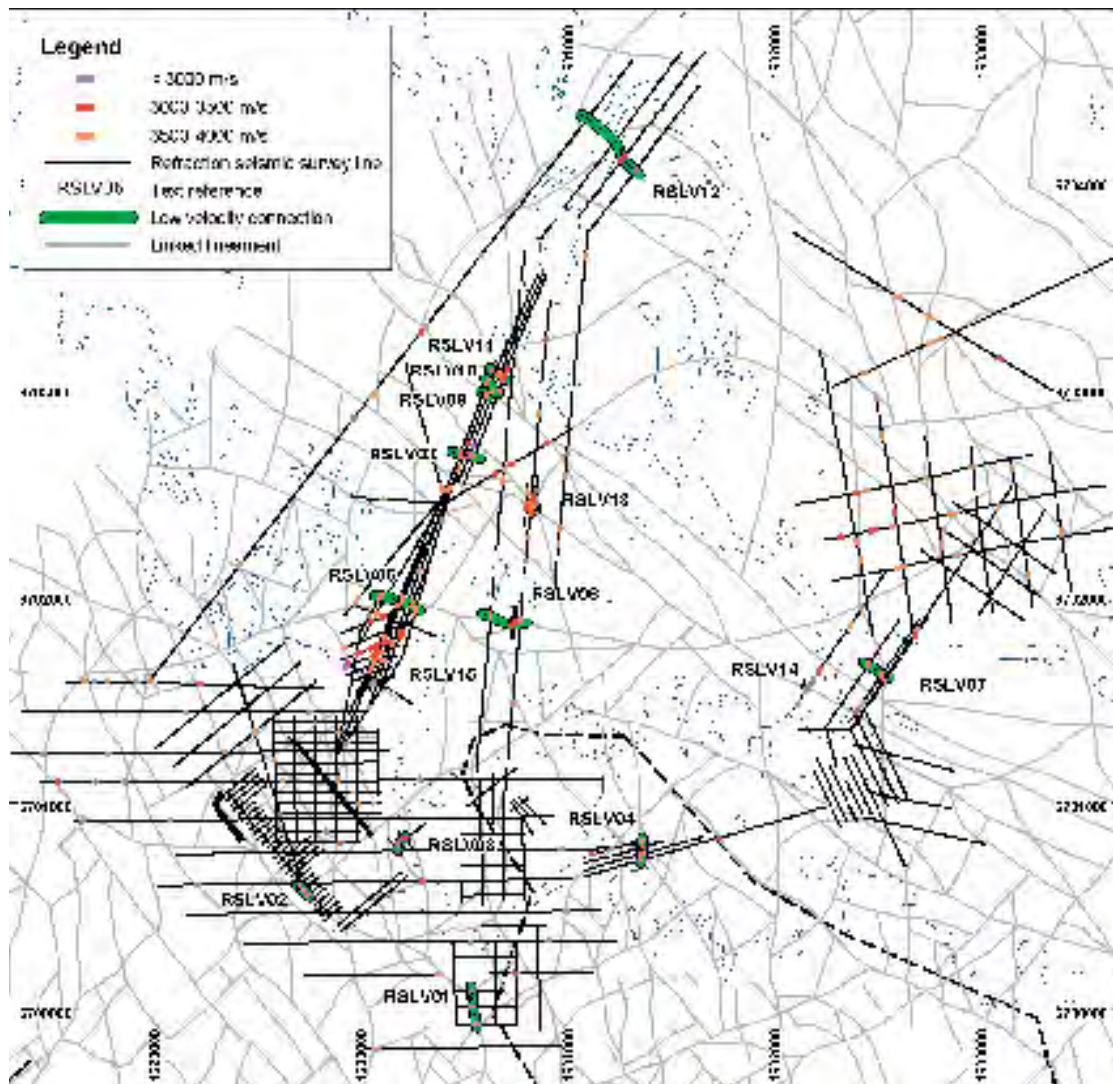


Figure 5-33. Refraction seismic survey lines and low velocity anomalies in the bedrock based on the line data. Some low velocity lineaments (marked in green), where the information on adjacent lines is consistent, are also shown. The Forsmark candidate area is outlined by a dashed black line (after /Isaksson and Keisu, 2005/).

The ground EM (slingram) and magnetic data measurements were carried out (Figure 5-35) in the vicinity of drill sites 1, 2 and 3 /Thunehed and Pitkänen, 2002/, in the vicinity of drill site 4 /Pitkänen and Isaksson, 2003/, and in the vicinity of drill sites 5 and 6 /Pitkänen et al. 2004b/. A ground survey was also completed along a north-easterly continuation of one of the east-west profiles at drill site 1, in order to investigate, in more detail, the NS lineaments that transect the candidate area at Forsmark /Thunehed and Pitkänen, 2002/. This profile extends c. 600 m along the land strip that lies between Bolundsfjärden and Norra Bassängen (Figure 5-35). Ground surveys across the Eckarfjärden deformation zone with NW strike /SKB, 2004a/ and two lineaments (XFM0062A0 and XFM0065A0), which strike NE across the candidate area, have also been carried out (Figure 5-35 and /Pitkänen and Isaksson, 2003; Pitkänen et al. 2004b/). The interval between the measurement stations in all these surveys was 10 m.

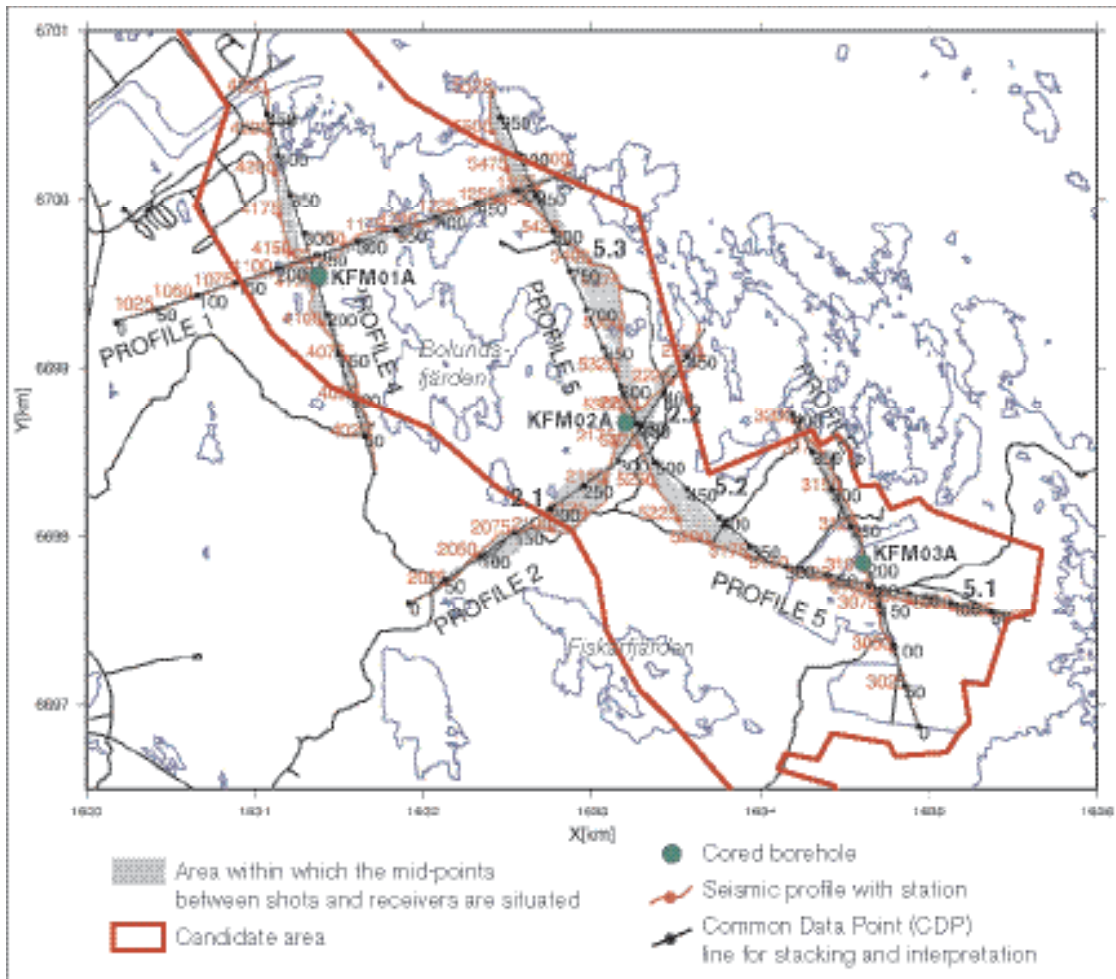


Figure 5-34. Common Data Point (CDP) lines along which the reflection seismic data have been projected for stacking and interpretation (after /Juhlin et al. 2002/). Lines 2 and 5 were split into separate linear segments and referred to as 2.1 and 2.2, and 5.1, 5.2 and 5.3, respectively, in /Cosma et al. 2003/.

Evaluation

High-resolution reflection seismic data

The reflection seismic survey has been able to image reflectors in the bedrock down to depths of at least 3 km. Groups of reflectors with different orientations have been recognised and have been labelled with different letters (A to I) in /Juhlin et al. 2002/. Gently dipping reflectors that strike ENE or NE are dominant. There is a much stronger concentration of well-defined, gently dipping reflectors in the upper 2 km of bedrock in the south-eastern part of the candidate area (Figure 5-36), relative to that observed in the north-western part, closer to the nuclear power plant (Figure 5-37). Nevertheless, possibly the most conspicuous group of reflectors (referred to as A0–A1 in /Juhlin et al. 2002/) are seen in the results for profile 4, in the north-western part of the candidate area (Figure 5-37). Apart from a possible correlation of reflectors A0–A1 with lineament XFM0134A0 and reflector A5 with lineament XFM0067A0, there is no simple correlation of the surface projection of the reflectors and the inferred lineaments.

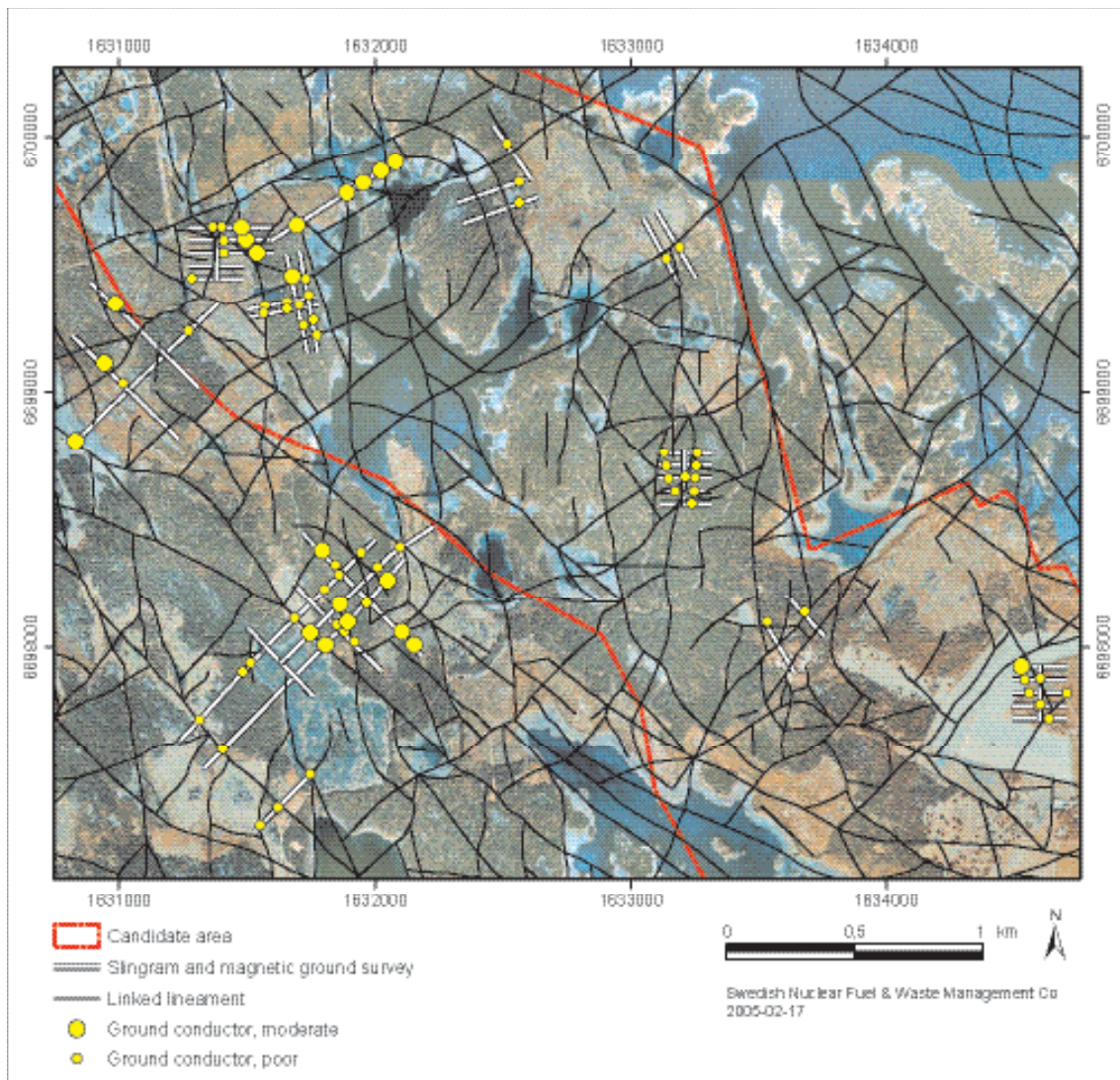


Figure 5-35. Ground EM (slingram) and magnetic survey lines carried out during the site investigation programme at the Forsmark site. EM (slingram) minima, which are inferred to represent ground conductors, and linked lineaments are also shown.

Bearing in mind the importance of the reflection seismic data to detect possible, gently dipping deformation zones and the uncertainties that arise in their interpretation /SKB, 2004a/, an independent assessment was carried out /Cosma et al. 2003/, in connection with the version 1.1 modelling work. This assessment also aimed to place the reflectors in 3D space. On the basis of a comparison study between the two studies /Juhlin et al. 2002; Cosma et al. 2003/, only the reflectors included in groups A, B, C, E and F /Juhlin et al. 2002/ were recommended for use in the modelling procedure /SKB, 2004a/. Since no constraints on the geological significance of the reflectors were available at the time of presentation of the version 1.1 model, they were utilised as supportive rather than deterministic information in this model.

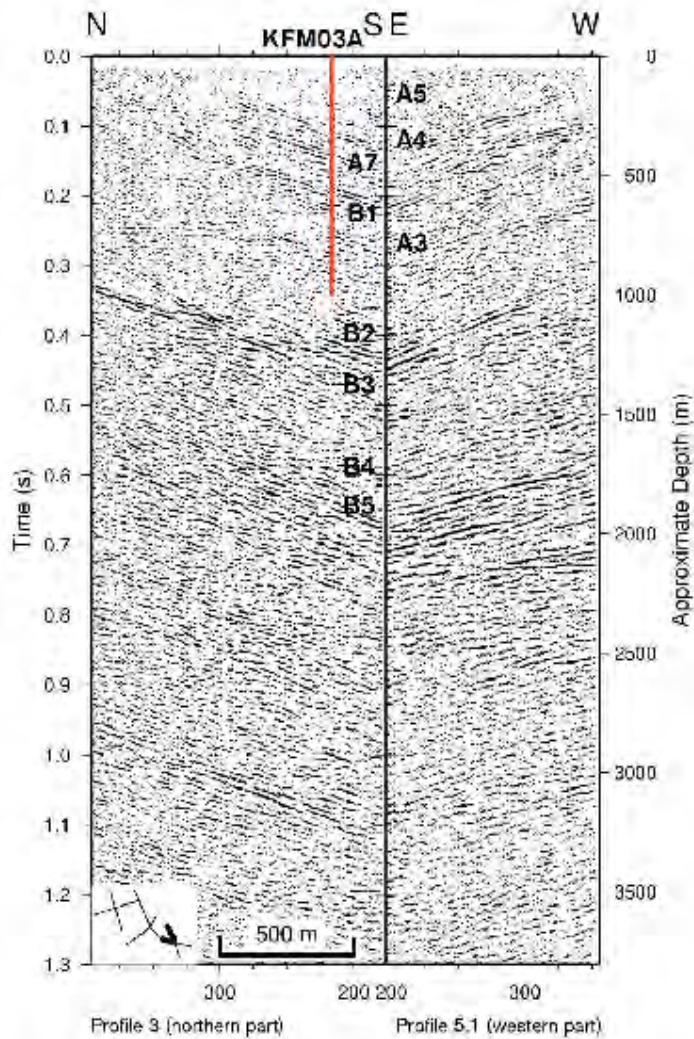


Figure 5-36. Correlation of stacks from profiles 3 and 5 at their crossing points, in the south-eastern part of the candidate area. The location of each section is shown in the lower left-hand part of the figure. The depth scale along the vertical axis is only valid for sub-horizontal reflectors. The numbers along the horizontal axis refer to the CDP line along which the data have been projected for stacking and interpretation (after /Juhlin et al. 2002/). Only the reflectors in groups A, B and C (definite reflectors) are labelled.

A major development since the establishment of model version 1.1 concerns the results from the cored boreholes KFM02A, KFM03A and KFM03B. These boreholes were predicted to intersect at depth many of the reflectors classified as definite /Juhlin et al. 2002/. In these boreholes, the seismic reflectors correlate excellently with gently dipping, brittle deformation zones along which ground-water is present (see Section 5.2.8 and Chapter 8).

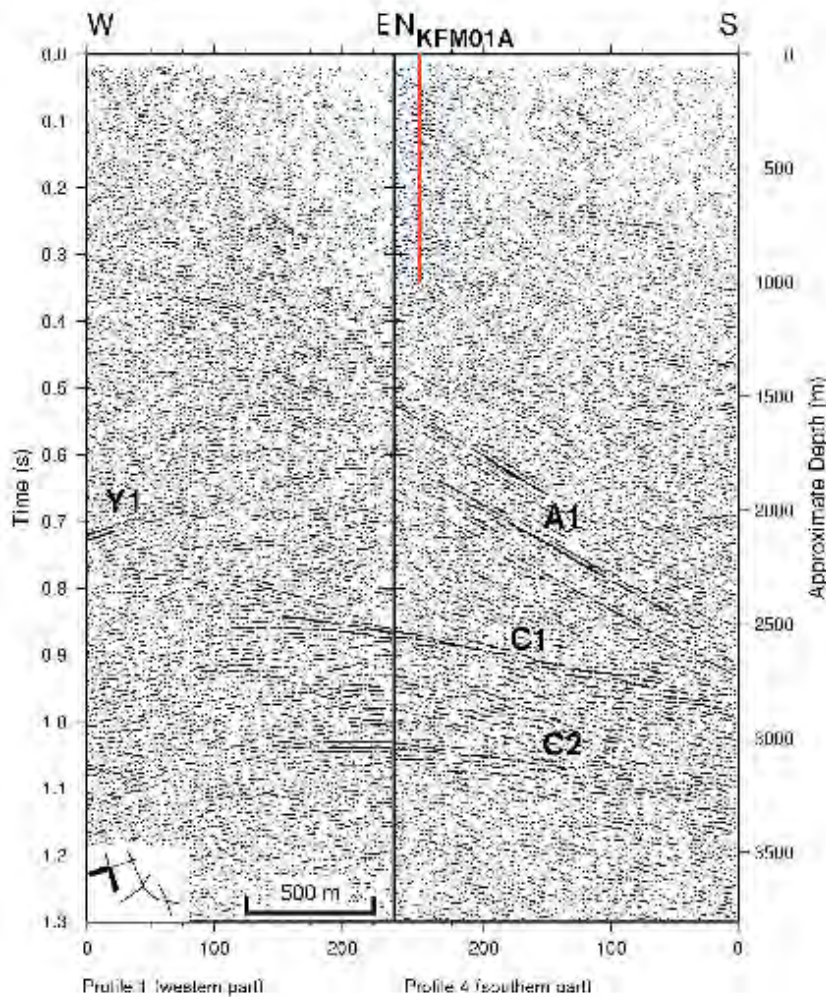


Figure 5-37. Correlation of stacks from profiles 1 and 4 at their crossing points, in the north-western part of the candidate area. The location of each section is shown in the lower left-hand part of the figure. The depth scale along the vertical axis is only valid for sub-horizontal reflectors. The numbers along the horizontal axis refer to the CDP line along which the data have been projected for stacking and interpretation (after /Juhlin et al. 2002/). Only the reflectors in groups A, B and C (definite reflectors) are labelled.

The minor re-interpretation of the data carried out in /Juhlin and Bergman, 2004/ has resulted in the following new features:

- Three reflectors, referred to as A7 (ranked as definite), B6 (ranked as definite) and B7 (ranked as probable), have been added to the reflectors interpreted in /Juhlin et al. 2002/.
- The orientations of four of the reflectors in /Juhlin et al. 2002/ have been slightly modified (A3, B2, B3 and D3).
- The extensions of two of the reflectors in /Juhlin et al. 2002/ have been slightly modified (A2 and B4).

An independent assessment of these changes /Balu and Cosma, 2005/ confirms the occurrence of the reflectors A7, B6 and B7. A comparison of the orientation estimates for the reflectors A7, B6, B7 and A3, as recommended in /Juhlin et al. 2002; Juhlin and Bergman, 2004/ and /Balu and Cosma, 2005/, is provided in Table 5-6. There is good agreement between the two sets of orientation estimates. No changes for the orientation of reflectors B2, B3 and D3, as recorded in /Cosma et al. 2003/, have been recommended in the later assessment /Cosma et al. 2005/.

Table 5-6. Comparison of the orientation estimates in /Juhlin et al. 2002; Juhlin and Bergman, 2004/ and /Balu and Cosma, 2005/ for the seismic reflectors A7, B6, B7 and A3.

Definite and probable reflectors					
Reflector ID	Values without brackets from /Juhlin and Bergman, 2004/. Values in brackets from /Juhlin et al. 2002/		/Balu and Cosma, 2005/		
	Strike	Dip	Strike	Dip	Profile
A7 (definite)	055	23	052	23	3
			052	16	3
			052	23	5.1
			045	16	5.2
B6 (definite)	030	32	030	32	3
			030	32	5.1
B7 (probable)	025	20	016	22	1
			016	22	5.3
A3 (definite)	050 (065)	23 (25)	050	23	3
			050	23	5.1
			050	23	5.2
			050	23	5.3

Relationship between ground EM (slingram) anomalies, magnetic anomalies and lineaments

Table 5-7 summarises the relationship between the anomalies that are associated with EM (slingram) and magnetic minima along the surface line surveys, at and close to the various drill sites, and the inferred lineaments in the Forsmark area. The lineament correlation takes into account the uncertainty in the position of the lineament (generally ± 20 m).

All except one of the moderate conductors, which have been recognised in the surface geophysical surveys at and close to the various drill sites, correspond to lineaments that have been recognised with the help of airborne geophysical and topographic data. However, the ground geophysical surveys have detected a number of weaker conductors that are classified as poor in Figure 5-35. It is worth noting that the character of these conductors is such that they could hardly have been detected with the airborne EM survey that was carried out. Correlation of the moderate conductors in the ground surveys with distinct minima in the ground magnetic data is generally poor.

Five moderate conductors have been recognised along the extended line survey from drill site 1, between Bolundsfjärden and Norra Bassängen. Three of these conductors correlate well with lineaments that trend NS (XFM0127A0), NW (XFM0164A0) and either NS (XFM0402A0) or NW (XFM0163A0). The remaining two conductors lie on both sides of a NS lineament (XFM0098A0). Apart from XFM0163A0, all these lineaments show no or only a minor magnetic signature along their length.

A magnetic minimum and a weak EM minimum, which is consistent with a poor conductor, characterise the surface measurements along the Eckarfjärden deformation zone. These features are consistent with the character of the lineament (XFM0015A0) that corresponds to this zone. Unfortunately, the measurements along the line surveys across the NE lineaments XFM0062A0 and XFM0065A0 were seriously disturbed by buried cables, a fence and possibly also by a cattle grid.

In summary, it appears that the ground EM (slingram) and magnetic data, which were carried out on a coarse survey line basis, provide only a limited complement to the recognition of possible deformation zones based on the interpretation of airborne geophysical and topographic data. However, poor conductors, which were not detected in the airborne survey, have been recognised in the ground surveys. Compared with the lineament interpretation, the surface geophysical data provide a better control on the position of the anomalies and, thereby, the position and continuity of possible deformation zones. Furthermore, an even better interpretation of the position and continuity of lineaments would have been possible if the survey lines had been more closely spaced.

Table 5-7. Correlation of EM (slingram) minima based on surface measurements, magnetic minima based on surface measurements, and linked lineaments based on airborne geophysical and topographic data for the line surveys at and close to drill sites 1 to 6. Only the EM (slingram) minima that are inferred to represent moderate conductors (see Figure 5-35) are addressed in this table.

Investigation object	Number of EM (slingram) minima that represent a moderate conductor (surface data)	Correlation with magnetic minima (surface data)	Correlation with linked lineament	Comment
Drill site 1 and vicinity	3	Moderate	XFM0099A0 (three moderate conductors)	The lineament shows no magnetic signature.
Drill site 2 and vicinity	No conspicuous moderate conductor			
Drill site 3 and vicinity	1	Difficult to judge. Whole area is low magnetic	XFM0067A0	XFM0067A0 is based on magnetic, electrical conductivity and topographic data. Possible correspondence also to surface projection of seismic reflector A5 /Juhlin et al. 2002/.
Drill site 4 and vicinity (SE alternative)	8	Poor	XFM0017A0 (two moderate conductors) XFM0240A0 (two) XFM0707A0 (one) XFM0705A0 (one) XFM0063A0 or XFM0238A0 (one) No lineament (one)	The lineaments XFM0017A0, XFM0063A0 and XFM0238A0 show a magnetic signature along their length. The other lineaments do not.
Drill site 4 and vicinity (NW alternative)	3	Poor	XFM0017A0 XFM0060A0 XFM0416A0	Both XFM0017A0 and XFM0060A0 are based on a combination of magnetic, electrical conductivity and topographic data.
Drill site 5 and vicinity	1	Poor	XFM0406A0 or XFM0060A0	XFM0406A0 shows no magnetic signature. XFM0060A0 is based on magnetic, electrical conductivity and topographic data.
Drill site 6 and vicinity	No conspicuous moderate conductor			

Relationship between connected low velocity ($\leq 4,000$ m/s) anomalies in the bedrock and lineaments

Low velocity zones in the bedrock can represent brittle deformation zones that contain an anomalous concentration of open fractures or one or more incohesive fault breccias. A possible correlation between some connected low velocity ($\leq 4,000$ m/s) anomalies in the bedrock (Figure 5-33) and the linked lineaments is presented in Table 5-8. Once again, the lineament correlation takes into account the uncertainty in the position of the lineament (generally ± 20 m).

There is a good correlation between the connected low velocity anomalies and linked lineaments (Table 5-8). The lineaments are based solely on topographic or a combination of magnetic and topographic or bathymetric data. However, some of the lineaments are situated in the area close to the nuclear power plant where detailed magnetic data are absent.

These observations provide a support to the interpretation that at least the lineaments listed in Table 5-8 represent brittle deformation zones where open fractures dominate or where incohesive fault breccias are present close to the surface. It is important to keep in mind the uncertainty concerning the position of the data assembly points in the older seismic refraction surveys and the difficulties in quantifying this uncertainty. Furthermore, care needs to be taken in the interpretation work concerning the influence of an older, well-packed boulder clay that shows a higher P-wave velocity relative to the normal Quaternary cover and a lower velocity relative to the normal bedrock. Finally, it needs to be emphasised that the methodology is not suitable where it concerns the detection of brittle deformation zones that are dominated by sealed fractures and sealed fracture networks or are of limited thickness (< 5 m).

Table 5-8. Correlation of connected, low velocity ($\leq 4,000$ m/s) anomalies in the vicinity of the nuclear power plant and SFR /Isaksson and Keisu, 2005/ and linked lineaments based on airborne geophysical and topographic data.

Identity: Low velocity anomaly in refraction seismic data (see Figure 5-33)	Identity: Linked lineament	Comment
RSLV01	XFM0100A0	
RSLV02	XFM1068A0	
RSLV03	No linked lineament	
RSLV04	XFM1064A0 Possible connection with XFM0099A0	
RSLV05	XFM0137A0 Possible correlation also with XFM1105A0	Possible correspondence also to surface projection of seismic reflector A0-A1 /Juhlin et al. 2002/.
RSLV06	XFM0137A0 Possible correlation also with XFM1099A0	Possible correspondence also to surface projection of seismic reflector A0-A1 /Juhlin et al. 2002/.
RSLV07	XFM1035A0 Possible correlation also with XFM1022A0	
RSLV08	XFM1124A0 Possible correlation also with XFM0803A0	XFM0803A0 corresponds to ZFMNW0001 (Singö deformation zone) in /SKB, 2004a/.
RSLV09	XFM0804A0	XFM0804A0 corresponds to ZFMNW0002 (splay from Singö deformation zone in tunnel 3) in /SKB, 2004a/.
RSLV10	No linked lineament.	Situated between RSLV09 and RSLV11.
RSLV11	XFM1038A0 Possible correlation also with XFM1036A0	
RSLV12	XFM 1012A0	
RSLV13	XFM 0803A0 Possible correlation also with XFM1040A0, XFM1101A0, XFM1125A0	XFM0803A0 corresponds to ZFMNW0001 (Singö deformation zone) in /SKB, 2004a/.
RSLV14	XFM0803A0 Possible correlation also with XFM1127A0	XFM0803A0 corresponds to ZFMNW0001 (Singö deformation zone) in /SKB, 2004a/.
RSLV15	XFM1092A0	

5.2.6 Borehole data – rock types, ductile structures, borehole radar, geophysical logs

Boreholes and geological mapping

The geological mapping and geophysical logging programmes for the boreholes generate sub-surface data that bear on the character of rock type (including alteration), ductile deformation and brittle deformation including fractures. These programmes are of vital importance for all three components in the geological modelling work (see Sections 5-3, 5-4 and 5-5).

Data from approximately 5,100 m of cored boreholes, which were drilled at five separate sites (Figure 5-38), have been used in model version 1.2. Four of these boreholes entered the bedrock at an angle of 85° (KFM01A, KFM02A, KFM03A and KFM03B), one at an angle of 80° (KFM01B), and two at an angle of 60° (KFM04A, KFM05A). The boreholes also entered the bedrock in different directions (NW, NE, W and E). Complementary data from approximately 2,850 m of percussion boreholes (HFM01–HFM19), which were drilled either close to these sites or at separate locations (Figure 5-38), are also available.

The length and orientation of the boreholes, and a description of the drilling activities have been presented in a series of reports (Table 5-9). Old cored borehole data from KFO01 (Figure 5-38), summarised in /Ekman, 1996a/, have also been used in the rock domain modelling work. No deviation measurements were available digitally in the SICADA database for this borehole. However, the borehole deviation was constructed from images that show the deviation and that were presented in /Ekman, 1996a/. KFO01 is 478.3 m in length and entered the bedrock at an angle of 90°.

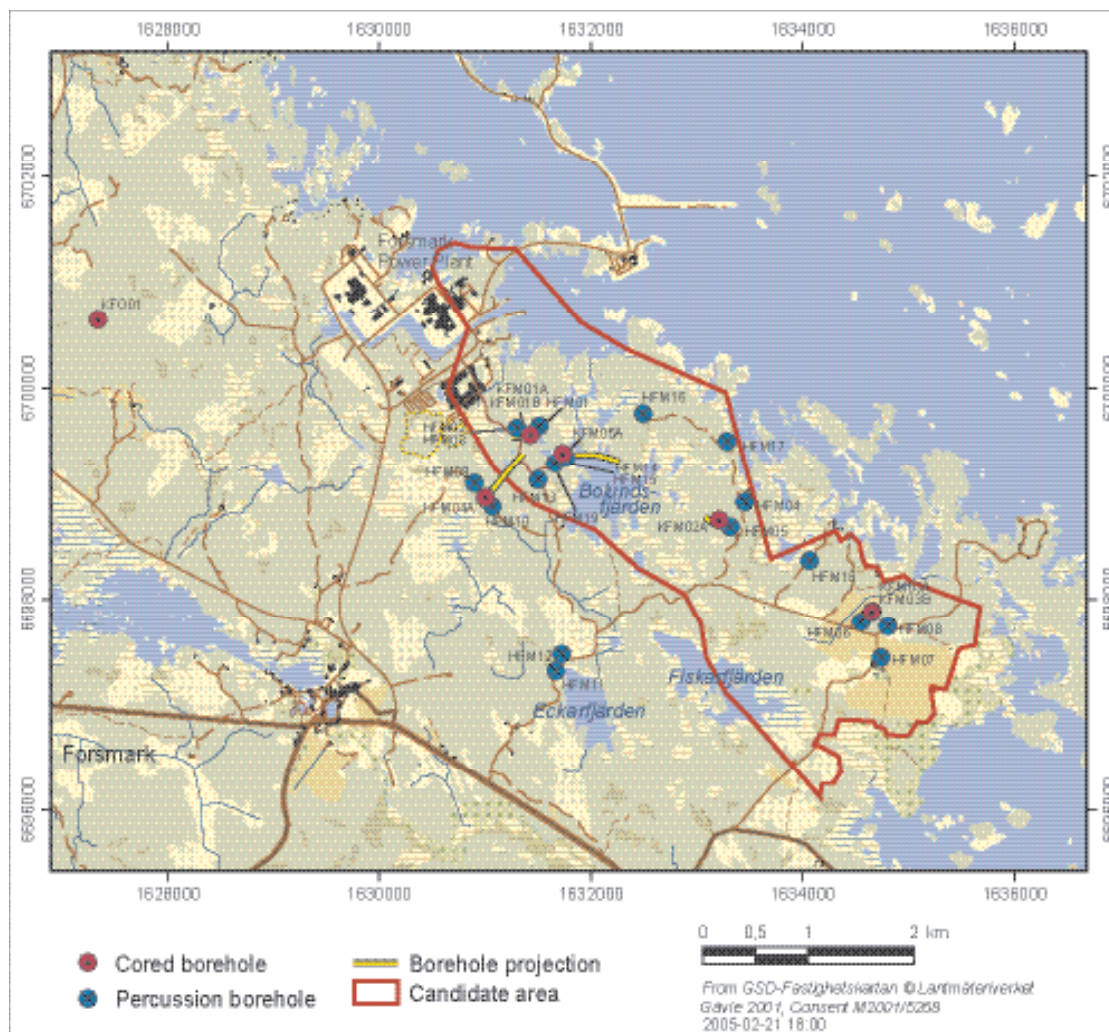


Figure 5-38. Location of boreholes from which data were available for model version 1.2.

Table 5-9. Summary of borehole length, borehole orientation and the literature concerned with the drilling activities and the geological mapping work.

Borehole	Borehole length	Borehole orientation	Drilling activity	Borehole mapping (Boremap data)	
Drill site 1	KFM01A	Percussion: 100.48 Cored: 901.01	318.35/84.73	/Claesson and Nilsson, 2004a/	/Petersson and Wängnerud, 2003//
	KFM01B	Cored: 500.52	267.59/79.04	Claesson and Nilsson, /2004b/	/Berglund et al. 2004/
	HFM01	Percussion: 200.20	034.06/77.50	/Claesson and Nilsson, 2004c/	/Nordman, 2003a/
	HFM02	Percussion: 00.00	006.52/87.79	/Claesson and Nilsson, 2004c/	/Nordman, 2003a/
	HFM03	Percussion: 26.00	264.53/87.28	/Claesson and Nilsson, 2004c/	/Nordman, 2003a/
Drill site 2	KFM02A	Percussion: 100.42 Cored: 902.02	275.76/85.38	/Claesson and Nilsson, 2004d/	/Petersson et al. 2004a/
	HFM04	Percussion: 221.70	336.87/84.26	/Claesson and Nilsson, 2004e/	/Nordman, 2003b/
	HFM05	Percussion: 200.10	335.59/84.96	/Claesson and Nilsson, 2004e/	/Nordman, 2003b/
Drill site 3	KFM03A	Percussion: 100.34 Cored: 900.85	271.52/85.75	/Claesson and Nilsson, 2004f/	/Petersson et al. 2004b/
	KFM03B	Cored: 101.54	264.49/85.30	/Claesson and Nilsson, 2004f/	/Petersson et al. 2004b/
	HFM06	Percussion: 110.70	002.44/84.60	/Claesson and Nilsson, 2004g/	/Nordman, 2003c/
	HFM07	Percussion: 122.55	342.32/84.52	/Claesson and Nilsson, 2004g/	/Nordman, 2003c/
	HFM08	Percussion: 143.50	348.69/84.44	/Claesson and Nilsson, 2004g/	/Nordman, 2003c/
Drill site 4	KFM04A	Percussion: 107.42 Cored: 894.00	045.24/60.08	/Claesson and Nilsson, 2004i/	/Petersson et al. 2004c/
	HFM09	Percussion: 50.25	139.36/68.90	/Claesson and Nilsson, 2004h/	/Nordman, 2004d/
	HFM10	Percussion: 150.00	092.93/68.70	/Claesson and Nilsson, 2004h/	/Nordman, 2004d/
Drill site 5	KFM05A	Percussion: 100.35 Cored: 902.36	080.90/59.98	/Claesson and Nilsson, 2004m/	/Petersson et al. 2004d/
	HFM14	Percussion: 150.50	331.75/59.81	/Claesson and Nilsson, 2004i/	/Nordman, 2004e/
	HFM15	Percussion: 99.50	314.31/43.70	/Claesson and Nilsson, 2004i/	/Nordman, 2004e/
HFM11	Percussion: 182.35	63.51/49.32	/Claesson and Nilsson, 2004j/	/Nordman, 2004d/	
HFM12	Percussion: 209.55	245.16/49.05	/Claesson and Nilsson, 2004j/	/Nordman, 2004d/	
HFM13	Percussion: 175.60	051.19/58.85	/Claesson and Nilsson, 2004i/	/Nordman, 2004e/	
HFM16	Percussion: 132.50	327.96/84.22	/Claesson and Nilsson, 2004k/	/Nordman and Samuelsson, 2004/	
HFM17	Percussion: 210.65	318.58/84.19	/Claesson and Nilsson, 2004j/	/Nordman and Samuelsson, 2004/	
HFM18	Percussion: 180.65	313.30/59.36	/Claesson and Nilsson, 2004j/	/Nordman and Samuelsson, 2004/	
HFM19	Percussion: 185.20	280.91/58.10	/Claesson and Nilsson, 2004j/	/Nordman, 2004e/	

All the cored and percussion boreholes have been mapped using the Boremap methodology adopted by SKB and the relevant reports are listed in Table 5-9. A key input in the mapping procedure is the oriented image of the borehole walls that is obtained with the help of the *Borehole Image Processing System (BIPS)*.

Some problems have been encountered during the borehole mapping programme. Firstly, no routine has been developed to measure linear structural features in the boreholes and, for this reason, lineations have not been measured at depth. This omission is potentially of significance for the rock domain modelling and is addressed again in Chapter 13. Secondly, there are difficulties involved with the mapping of the percussion boreholes. In particular, problems have arisen with the interpretation of the finely crushed material generated during the drilling, especially where it concerns the recognition of rock types and mineral coatings along fractures. Furthermore, since fractures can essentially be identified only from the BIPS images, it is judged that there is an underestimation of fractures, particularly sealed fractures, in the percussion boreholes. This feature is enhanced by the larger diameter size of these boreholes and its influence on the quality of the BIPS images. For these reasons, focus is addressed in this and the following sections on the cored borehole data. Data from the percussion boreholes have primarily been used as a help in the recognition of rock units and deformation zones in the single hole interpretation (see Section 5.2.8).

Rock types in cored boreholes

The borehole mapping logs (Table 5-9) have been complemented with analytical data from rock samples in KFM01A, KFM02A, KFM03A and KFM03B. These data provide a support to the geological mapping procedure. In particular, they provide tighter constraints on the classification of rock types and the identification of minerals along fractures. Furthermore, the petrophysical data provide a quality control and assist in the interpretation of the geophysical logs (see below). Finally, together with the more extensive surface data, the petrographic and petrophysical data yield the properties of the different rock types in the rock domain model (see Section 5.2.1). The following data are available:

- Petrographic data from 45 rock samples, including 29 modal analyses that have been recalculated to QAP(F=0) values /Pettersson et al. 2004e/. A special study of the alteration associated with the formation of a vuggy metagranite in KFM02A has also been completed /Möller et al. 2003/.
- Geochemical data from 34 rock samples /Pettersson et al. 2004e/.
- XRD analyses of mineral coatings along fractures, both randomly oriented grain samples (46) and oriented grain samples (32) of fine fractions (< 2 µm) for clay mineral identification /Pettersson et al. 2004e/.
- Geochemical data from 12 samples of mineral fracture coatings /Pettersson et al. 2004e/.
- Laboratory measurements of the density, magnetic properties, electrical properties and porosity of 33 rock samples /Mattsson et al. 2004a; Pettersson et al. 2004e/.
- Gamma-ray spectrometry measurements of the 34 powdered rock samples that were selected for geochemical analysis /Mattsson et al. 2004a; Pettersson et al. 2004e/.

Samples from KFM01A have also been included in a geochronological study /Page et al. 2004/. The results of this work are discussed together with the geochronological data from surface samples (see Section 3.1).

Metamorphosed diorite associated with pegmatite dominates the upper part (0–270.7 m) of KFO01 /Ekman, 1996a/. The lower part of this borehole (270.7–478.3 m) is dominated by gneiss that is predominantly grey in colour /Ekman, 1996a/. Surface data suggests that this rock is equivalent to a Group B metagranodiorite.

The proportions of different rock types in each of the cored boreholes drilled during the site investigation programme are summarised in Table 5-10. Rock occurrences that are less than 1 m in borehole length were not included in this analysis but will be incorporated in future modelling work. Medium-grained, biotite-bearing metagranite, which belongs to the Group B intrusive suite,

Table 5-10. Proportions of different rock types that are greater than 1 m in borehole length in the cored boreholes.

Code (SKB)	Composition and grain size	KFM01A	KFM01B	KFM02A	KFM03A	KFM03B	KFM04A	KFM05A
103076	Felsic to intermediate volcanic rock, metamorphic	No occurrence > 1 m	No occurrence > 1 m	No occurrence > 1 m	No occurrence > 1 m	No occurrence > 1 m	4.2%	0.3%
108019	Calc-silicate rock (skarn)	0.2%	No occurrence > 1 m	No occurrence > 1 m	No occurrence > 1 m	No occurrence > 1 m	No occurrence > 1 m	No occurrence > 1 m
102017	Amphibolite	1.9%	0.3%	4.1%	1.9%	8.5%	2.8%	3.4%
101054	Tonalite and granodiorite, metamorphic	No occurrence > 1 m	No occurrence > 1 m	No occurrence > 1 m	4.2%	No occurrence > 1 m	No occurrence > 1 m	No occurrence > 1 m
101056	Granodiorite, metamorphic	No occurrence > 1 m	No occurrence > 1 m	No occurrence > 1 m	No occurrence > 1 m	No occurrence > 1 m	10.8%	No occurrence > 1 m
101057	Granite (to granodiorite), metamorphic, medium-grained	85.3%	92.6%	79.5%	74.8%	50.3%	68.3%	89.2%
101051	Granodiorite, tonalite and granite, metamorphic, fine- to medium-grained	10.0%	6.1%	14.3%	9.9%	1.2%	10.5%	5.0%
101061	Pegmatitic granite, pegmatite	1.4%	1.0%	0.9%	6.8%	38.7%	2.3%	1.2%
111058	Granite, fine- to medium-grained	1.2%	No occurrence > 1 m	1.2%	2.4%	1.3%	1.1%	0.8%
No information		No occurrence > 1 m	No occurrence > 1 m	No occurrence > 1 m	No occurrence > 1 m	No occurrence > 1 m	No occurrence > 1 m	0.1%

dominates strongly in all the boreholes. A finer-grained variant of this rock type, which has not been documented in the surface outcrops, is present in the upper part (102–286 m) of KFM05A. Subordinate (generally < 10%) rock types, which occur throughout all the boreholes, include fine- to medium-grained metagranitoid that belongs to the Group C suite of intrusive rocks, amphibolite, and pegmatitic granite, pegmatite and fine- to medium-grained granite that belong to the Group D suite. Pegmatitic granite, pegmatite and amphibolite are prominent in KFM03B.

Rock types that are restricted to particular borehole intervals occur in KFM03A and KFM04A. Medium-grained metatonalite that belongs to the Group B suite is prominent in the borehole section 220–293 m in KFM03A, and Group B metagranodiorite is conspicuous in the upper part (< 176 m) of KFM04A. The metagranodiorite is intermingled with felsic to intermediate metavolcanic rock (Group A) in the uppermost, percussion-drilled part of KFM04A. This association is reminiscent of the surface features at drill site 4 (Figure 5-13) and the results from the percussion boreholes HFM09 and HFM10. However, there is some discrepancy concerning whether the Group B intrusive rock is granodioritic or tonalitic in composition. The density measurements from the geophysical logs for KFM04A (log beneath 110 m) and HFM10 (log in interval c. 15–150 m) indicate that metatonalite is common closer to the surface. Felsic to intermediate metavolcanic rock is also prominent between 275 and 342 m in KFM04A.

Apart from a sample of Group B metatonalite that is restricted to KFM03A and two Group C metatonalites, all the rock samples contain between 25 and 46% quartz. The trends on both the QAP(F=0) modal analysis (Figure 5-39) and QP geochemical (Figure 5-40) plots are identical to those observed in the equivalent plots for the surface samples. In particular, the anomalous flat trend into the tonalite field is once again apparent in the geochemical data (see Section 5.2.1). With some exceptions, the density and porosity values as well as the uranium contents of the rock samples lie in the same range as those observed in the surface samples (see Section 5.2.1). One exception concerns a sample near the base of KFM02A that has been mapped as a Group B metagranite but contains 19 ppm uranium.

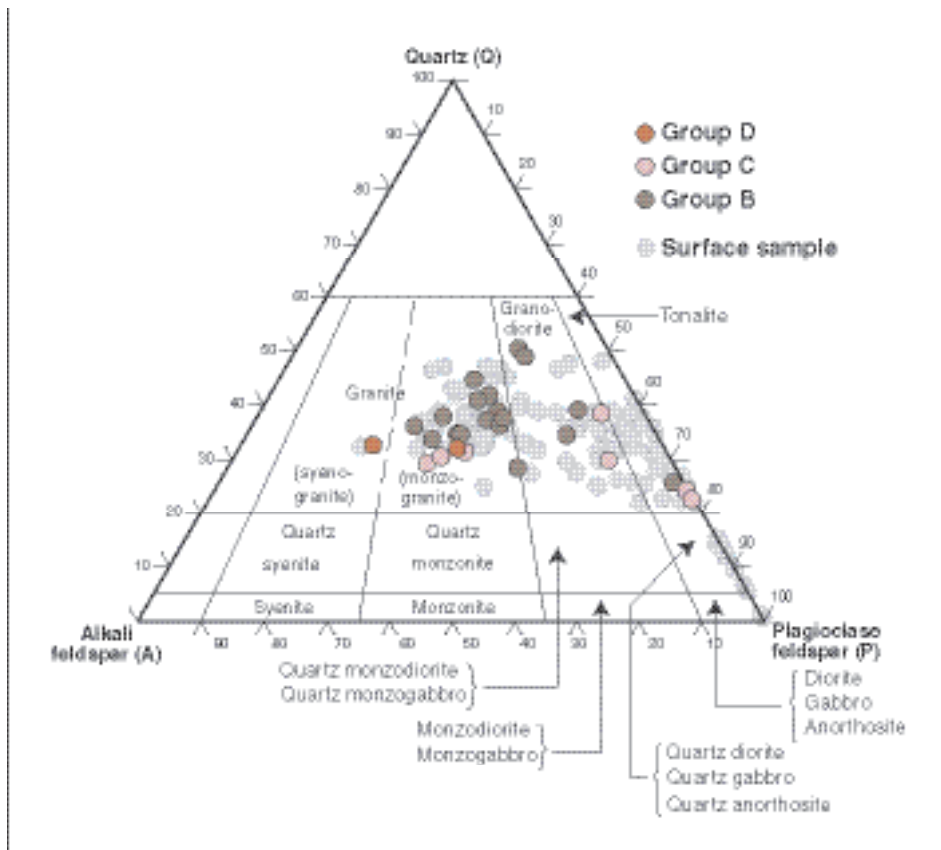


Figure 5-39. $QAP(F=0)$ modal classification of the analysed borehole samples in the different rock groups (modified after /Pettersson et al. 2004e/). The classification is based on /Streckeisen, 1976/. A comparison is also presented with the surface samples (see Figure 5-5b).

Anomalous, strongly reddened and vuggy metagranite (Figure 5-41a) occurs in the depth intervals 171–180 m and 240–310 m in KFM02A. Subordinate rock types in these two sections (e.g. amphibolite, pegmatitic granite) are also affected by the alteration (Figure 5-41a). The alteration involved /Möller et al. 2003/:

- Dissolution and removal of quartz to form vugs (Figure 5-41b).
- Resorption of K-feldspar (Figure 5-41b).
- Intense albite-chlorite-hematite-Ti-oxide alteration of plagioclase feldspar, biotite (and hornblende).
- Precipitation of albite, quartz, chlorite and hematite in the vugs (Figure 5-41b).

The vuggy metagranite shows anomalously low density (2,064–2,568 kg/m³), high porosity (1.97–13.06%) and low resistivity (1,060–3,610 ohm m) values. This strongly altered rock also shows a low magnetic susceptibility. It contains normal uranium (3.7–5.9 ppm), low gold (< 0.2–0.7 ppb) and low sulphur (0.02–0.07%) contents /Lindroos et al. 2004; Mattsson et al. 2004a/ and there is nothing to suggest that the altered metagranite has any ore potential /Lindroos et al. 2004/. The formation of the vugs and the intense alteration are younger than, and genetically unrelated to, both the intrusion of the granite and the subsequent ductile deformation and metamorphism. Comparison with other examples in granites suggests that the vugs and associated hydrothermal alteration occurred under relatively low pressures and at temperatures corresponding to the greenschist facies /Möller et al. 2003/.

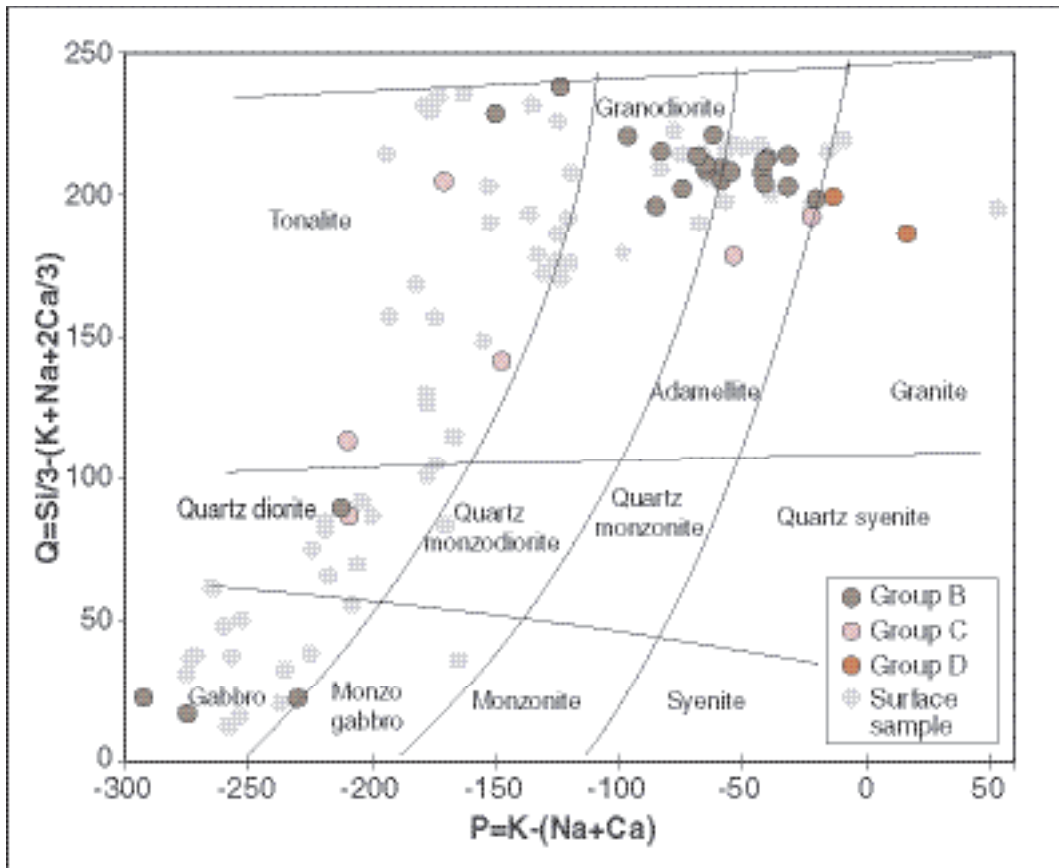


Figure 5-40. Geochemical classification of the analysed borehole samples in the different rock groups (modified after /Pettersson et al. 2004e). The classification is based on /Debon and Le Fort, 1983/. A comparison is also presented with the surface samples (see Figure 5-6c). As for the surface samples, an anomalous, flat trend into the tonalite field for, especially, some of the granitic Group B rocks is apparent. This is related to an early-stage alteration.

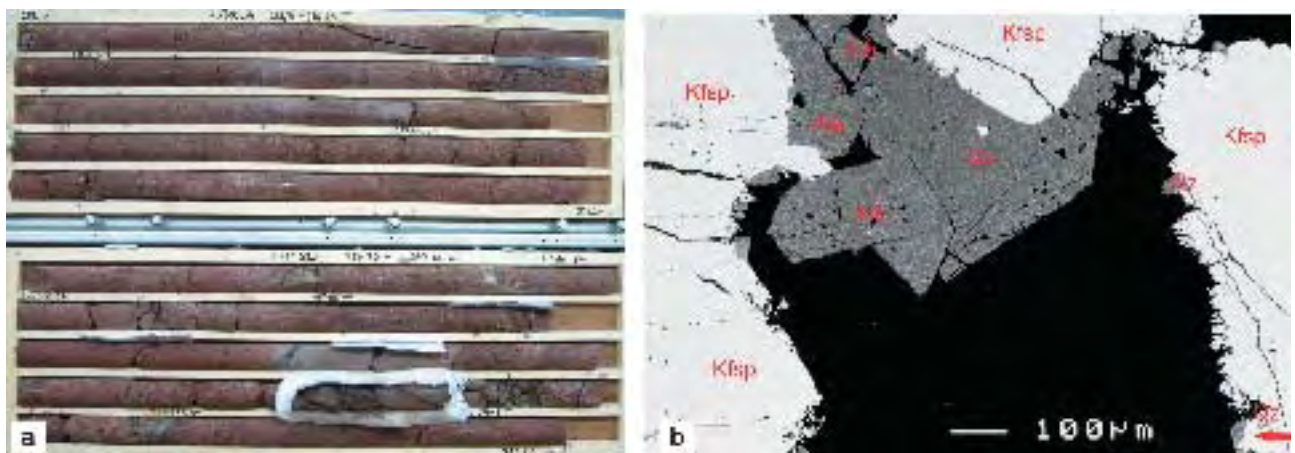


Figure 5-41. a) Strongly altered and vuggy metagranite in KFM02A. The incoherent section (in plastic casing) is a strongly altered amphibolite that has been modified to a rock composed of chlorite, albite, hematite, Ti-oxide and quartz. b) Back-scatter electron (BSE) image that shows euheedral crystals of albite and quartz (medium grey) on a vug wall (black = cavity). The thin rims on K-feldspar grains (light grey) along the vug walls are irregular fringes of K-feldspar (resorbed grains) and small, euheedral crystals of albite and quartz. Scale bar is 0.1 mm. Alb = albite, Kfsp = K-feldspar and Qz = Quartz.

Ductile structures in cored boreholes

The bedrock in all the boreholes shows ductile, planar and linear mineral fabrics. These fabrics are defined by oriented mineral grains and mineral grain aggregates (see also Section 5.2.4).

A planar grain-shape fabric (tectonic foliation) is dominant in the boreholes that lie closer to the south-west margin of the candidate area (KFM01A and KFM01B). By contrast, a mineral lineation prevails in the boreholes that enter the bedrock in the more internal parts of the candidate area (KFM02A, KFM03A and KFM03B). A mineral lineation is also dominant in the lower part (500–1,001.5 m) of KFM04A. The tectonic foliation shows a variable orientation and the mineral lineation is judged to plunge gently to moderately to the south-east. These features strongly resemble the character of the ductile deformation at the surface in sub-area central (see Section 5.2.4 and Figure 5-25c).

By contrast, the upper part (12–500 m) of KFM04A shows stronger ductile strain, with a well developed tectonic foliation and a conspicuous reduction in grain-size induced by the strong deformation. The foliation is more regular in orientation compared to that in the other borehole intersections. It strikes south-east with a steep dip to the south-west. These features resemble the character of the ductile structures observed at the surface in subarea south-west (see Section 5.2.4 and Figure 5-25b).

A few occurrences of strongly foliated rocks that show a grain size reduction have been documented in all the boreholes except KFM01A. These occurrences are generally up to a few decimetres wide and have been interpreted as minor, ductile shear zones. However, in the borehole interval between 322 and 440 m in KFM04A, several zones are present. They range up to 5 m wide and show, in part, strong phyllonitisation with the development of secondary muscovite.

Borehole radar and geophysical logs

Besides production of an oriented image of the wall of each borehole with the help of the *Borehole Image Processing System* (BIPS) for use in the mapping work, borehole radar measurements and geophysical logs have been generated in all the boreholes (Table 5-11). A combination of some of the geophysical data (e.g. density, natural gamma radiation) with the relevant petrophysical data provides a support to the mapping of the bedrock in the boreholes, especially in the percussion boreholes (see above). The borehole radar measurements and geophysical logs also provide an important input to the geological single hole interpretation (see Section 5.2.8).

The interpretation of borehole radar reflectors has been carried out for each borehole (Table 5-11). An attempt has been made in several boreholes to document the orientation of these reflectors. However, this approach has been of varied success and the results must be treated with care.

The following geophysical data have been generated in the logging procedure for each borehole:

- Density (gamma-gamma).
- Magnetic susceptibility.
- Natural gamma radiation.
- A variety of electrical measurements in the bedrock (e.g. focused guard resistivity, normal resistivity, single point resistance or SPR).
- Fluid resistivity.
- Fluid temperature.
- P-wave velocity (sonic) measurements.
- Caliper measurements.

The interpretation of the geophysical logs has been carried out in a separate exercise (Table 5-11). Density, magnetic susceptibility and natural gamma radiation rate measurements have been combined to provide an independent control on the compositional and even stratigraphic interpretation of the rock types. The calculated silicate density, for example, can be linked

Table 5-11. Summary of literature concerned with the generation of BIPS, borehole radar and geophysical logs and the interpretation of those logs.

Borehole	BIPS and borehole radar logging including interpretation	Geophysical logging	Interpretation of geophysical log
Drill site 1	KFM01A	/Aaltonen and Gustafsson, 2004; Gustafsson and Gustafsson, 2004a/	/Gustafsson and Nilsson, 2003; Nielsen and Ringgaard, 2004a/
	KFM01B	/Gustafsson and Gustafsson, 2004a/	/Nielsen and Ringgaard, 2004b/
	HFM01–HFM03	/Gustafsson and Nilsson, 2003/	/Gustafsson and Nilsson, 2003; Nielsen and Ringgaard, 2004a/
Drill site 2	KFM02A	/Gustafsson and Gustafsson, 2004b/	/Nielsen and Ringgaard, 2004c/
	HFM04–HFM05	/Nilsson and Gustafsson, 2003/	/Nilsson and Gustafsson, 2003/
Drill site 3	KFM03A/ KFM03B	/Gustafsson and Gustafsson, 2004c/	/Nielsen and Ringgaard, 2004c/
	HFM06–HFM08	/Nilsson and Aaltonen, 2003/	/Nilsson and Aaltonen, 2003/
Drill site 4	KFM04A	/Gustafsson and Gustafsson, 2004d/	/Nielsen and Ringgaard, 2004d/
	HFM09–HFM10	/Gustafsson and Gustafsson, 2004d/	/Nielsen and Ringgaard, 2004d/
Drill site 5	KFM05A	/Gustafsson and Gustafsson, 2004h/	/Nielsen and Ringgaard, 2004e/
	HFM14–HFM15	/Gustafsson and Gustafsson, 2004e/	/Nielsen and Ringgaard, 2004b/
HFM11–HFM12	/Gustafsson and Gustafsson, 2004f/	/Nielsen and Ringgaard, 2004d/	/Mattsson and Keisu, 2004/
HFM13	/Gustafsson and Gustafsson, 2004e/	/Nielsen and Ringgaard, 2004d/	/Mattsson and Keisu, 2004/
HFM16–HFM18	/Gustafsson and Gustafsson, 2004g/	/Nielsen and Ringgaard, 2004b/	/Mattsson and Keisu, 2004/
HFM19	/Gustafsson and Gustafsson, 2004g/	/Nielsen and Ringgaard, 2004e/	/Thunehed and Keisu, 2004/

to the composition of igneous rocks (Table 5-12). However, the effects of alteration can disturb the simple correlation between density and composition. The natural gamma radiation rate measurements provide some help in the recognition of Group D granites and pegmatitic rocks that commonly show higher contents of uranium (see Section 5.2.1). Finally, the magnetic susceptibility measurements provide some constraints on the occurrence of bedrock alteration that is related to oxidation processes and the conversion of magnetite to hematite.

Table 5-12. Relationship between silicate density and the igneous composition of granitoids and associated quartz-poor and quartz-deficient rocks.

Silicate density (kg/m ³)	Inferred igneous composition
< 2,680	Granite
2,680 to 2,730	Granodiorite
2,730 to 2,800	Tonalite
2,800 to 2,890	Diorite
> 2,890	Gabbro

The occurrences of larger individual fractures have been inferred from a combined analysis of the resistivity, SPR, P-wave velocity and mean caliper measurements. Furthermore, the fracture frequency along sections that are 5 m in length has been calculated with the help of a calibration against the fracture frequency that was established during the mapping of several cored boreholes.

5.2.7 Fracture statistics from cored borehole data

Fracture terminology and general features

Fractures in the boreholes have been mapped according to whether they part the core or not. Those that part the core are referred to as broken fractures while the remainder are referred to as unbroken fractures. Broken fractures include both truly open fractures and originally sealed fractures that opened in connection with the drilling activity. In order to decide if a fracture was originally open or sealed in the rock volume, SKB has developed a confidence classification based on the weathering and fit of the fracture planes with the help of the BIPS technique.

Broken fractures with fresh fracture planes that fit well together are inferred to represent sealed fractures. They are presented with an aperture = 0. Fractures that show signs of weathering and/or fit poorly are inferred to have been open, and hence, given an aperture of > 0. The unbroken fractures, on the other hand, are divided into partially open and sealed fractures. A partially open fracture is an unbroken fracture with aperture > 0, whereas a sealed fracture has an aperture = 0. A more detailed description of the nomenclature for fractures and the practical aspects of the mapping procedure are provided in the SKB method description for mapping with the help of the Boremap system (SKB MD 143.006, version 2.0). The terms “crush zone” and “sealed fracture network”, which have been used in the mapping work, correspond to an incohesive fault breccia and a cohesive crush breccia, respectively, according to the fault rock terminology of /Sibson, 1977/.

As for the other primary data, the fracture data included in the following analysis were extracted from SKB’s SICADA database. These data have been generated during the borehole mapping programme (Table 5-9). The parameters that have been analysed in this report are summarised in Table 5-13.

The numbers of different categories of fractures that have been documented during the mapping of the boreholes are shown in Table 5-14. The same parameters for fractures outside deformation zones are listed in Table 5-15. The deformation zones have been adopted from the single hole interpretations of the boreholes (see Section 5.2.8). Bearing in mind the uncertainty in the calculation of the number of fractures in so-called crush zones and sealed fracture networks, the values in both tables do not include the fractures that have been estimated in these structures.

Table 5-13. Parameters from SKB’s SICADA database that have been used in the analysis of fractures (Sections 5.2.7, 5.4 and 5.5).

Parameter	Comments
BHID	Borehole ID.
Strike	Strike orientation (degrees).
Dip	Dip, right hand rule (degrees).
SEC_UP	Fracture location in the borehole, i.e. length along the borehole (m).
TYPE	Open, partly open or sealed fracture.
CONFIDENCE	Certain, probable or possible.
ROCKTYPE	Rock type at fracture location. For analysis of fractures outside deformation zones, see Section 5.5.
DZID	Deformation zone ID at fracture location based on single hole interpretation (see Section 5.2.8). For analysis of fractures along deformation zones, see Section 5.4.
RD	Rock domain based on rock domain model (see Section 5.3). For analysis of fractures outside deformation zones, see Section 5.5.
MIN1– MIN4	Mineral coating along fractures.

Table 5-14. All fractures analysed in boreholes (excluding crush zones and sealed fracture networks).

Borehole	Total number of fractures	Open fractures	Partly open fractures	Sealed fractures	Percent of open fractures in the borehole	Fracture frequency per metre (all)	Fracture frequency per metre (open)
Cored borehole							
KFM01A	1,638*	775	41	820	47	1.68	0.79
KFM01B	1,753	571	89	1,093	33	3.59	1.17
KFM02A	2,354	343	138	1,873	15	2.37	0.35
KFM03A–B	2,019	297	114	1,608	15	2.03	0.30
KFM04A	4,426	1,226	232	2,968	28	4.48	1.24
KFM05A	2,835	591	42	2,202	21	3.14	0.65
Percussion borehole							
HFM01	361	177	1	183	49	1.84	0.90
HFM02	140	79	1	60	56	1.57	0.89
HFM03	13	12	0	1	92	0.94	0.86
HFM04	294	151	12	131	51	1.30	0.67
HFM05	238	132	8	98	55	1.14	0.63
HFM06	222	107	12	103	48	2.06	0.99
HFM07	251	134	14	103	53	2.18	1.16
HFM08	272	145	13	114	53	1.99	1.06
HFM09	107	30	24	53	28	2.33	0.65
HFM10	297	94	34	169	32	2.04	0.65
HFM11	512	109	32	371	21	2.83	0.60
HFM12	630	182	53	395	29	3.06	0.88
HFM13	428	230	20	178	54	2.48	1.33
HFM14	422	334	24	64	79	2.80	2.22
HFM15	156	145	1	10	93	1.58	1.47
HFM16	362	256	14	92	71	3.07	2.17
HFM17	263	203	8	52	77	1.29	1.00
HFM18	436	357	8	71	82	2.52	2.06
HFM19	391	272	13	106	70	2.17	1.51

*2 fractures of unknown type

The following sections present an analysis of the frequency, orientation and mineralogy of the fractures in each of the cored boreholes. For the reasons outlined above, the data from the percussion boreholes have not been included in this statistical treatment. As for the lineaments and the fractures documented in the detailed mapping of outcrops, the fractures in boreholes are an important input for the DFN modelling. For this reason, a more detailed analysis of these fractures is presented in Section 5.5.

Fracture frequency

Fracture frequency has been calculated from fracture observations registered during the mapping of the bedrock in the boreholes. The frequency values for the fractures outside deformation zones, along the total lengths of boreholes KFM01A, KFM02A and KFM03A–B, lie inside the interval 1–2 fractures/metre (Table 5-15). KFM01B, which is only c. 500 m in length, and KFM05A show slightly higher frequency values of 2.24 and 2.74 fractures/metre, respectively. The values for the open fractures that are situated outside deformation zones in these boreholes are all less than 1 fracture/metre. There is also a very strong dominance of sealed fractures in KFM02A and KFM03A–B (Table 5-15).

Table 5-15. All fractures analysed in boreholes that are situated outside deformation zones (excluding crush zones and sealed fracture networks). The deformation zones have been adopted from the single hole interpretation (see Section 5.2.8).

Borehole	Total number of fractures	Open fractures	Partly open fractures	Sealed fractures	Percent of open fractures in the borehole	Fracture frequency per metre (all)	Fracture frequency per metre (open)
Cored borehole							
KFM01A	1,196*	639	37	519	53	1.34	0.71
KFM01B	863	222	17	624	26	2.24	0.58
KFM02A	1,005	79	22	904	8	1.37	0.11
KFM03A–B	1,578	182	83	1,313	12	1.77	0.20
KFM04A	3,592	934	149	2,509	26	3.98	1.03
KFM05A	2,242	435	34	1,773	19	2.74	0.53
Percussion borehole							
HFM01	329	162	1	166	49	1.76	0.87
HFM02	104	58	1	45	56	1.24	0.69
HFM03	13	12	0	1	92	0.94	0.86
HFM04	252	128	9	115	51	1.15	0.58
HFM05	237	131	8	98	55	1.14	0.63
HFM06	179	86	10	83	48	1.83	0.88
HFM07	153	75	9	69	49	1.48	0.73
HFM08	232	126	10	96	54	1.76	0.96
HFM09	54	8	12	34	15	1.94	0.29
HFM10	252	80	23	149	32	1.90	0.60
HFM11	303	97	27	179	32	1.71	0.55
HFM12	358	157	35	166	44	2.78	1.22
HFM13	347	199	9	139	57	3.71	2.13
HFM14	272	213	9	50	78	1.99	1.56
HFM15	104	93	1	10	89	1.26	1.12
HFM16	125	76	6	43	61	1.16	0.70
HFM17	263	203	8	52	77	1.29	1.00
HFM18	250	216	2	32	86	1.94	1.68
HFM19	180	138	5	37	77	1.32	1.01

*1 fracture of unknown type

The results from borehole KFM04A, which penetrates a large segment of bedrock outside the candidate volume, are different. The total number of fractures is more or less double that observed in the other cored boreholes of the same length. Furthermore, the corresponding frequency values for all fractures and for open fractures are 3.98 and 1.03 fractures/metre, respectively.

The analysis of fracture frequency along the length of each borehole is presented in the form of both moving average (Figure 5-42) and cumulative fracture frequency (Figure 5-43) curves for each borehole. The fractures documented in crush zones and in sealed fracture networks are included in these diagrams. Since the fracture frequency is one of the more important factors used in the definition of possible deformation zones in the single hole interpretations (see Section 5.2.8), these zones are also shown on the moving average plot.

The mode of variation of fracture frequency with depth varies considerably for each borehole (Figure 5-42 and Figure 5-43). In KFM01A and KFM01B, there is a high concentration of both open and sealed fractures in the upper part of these two boreholes, i.e. down to c. 290 and 140 m depths, respectively (Figure 5-43). By contrast, KFM03A–B shows a much more even distribution where it concerns the distribution of fractures at depth. This applies to both open and sealed fractures.

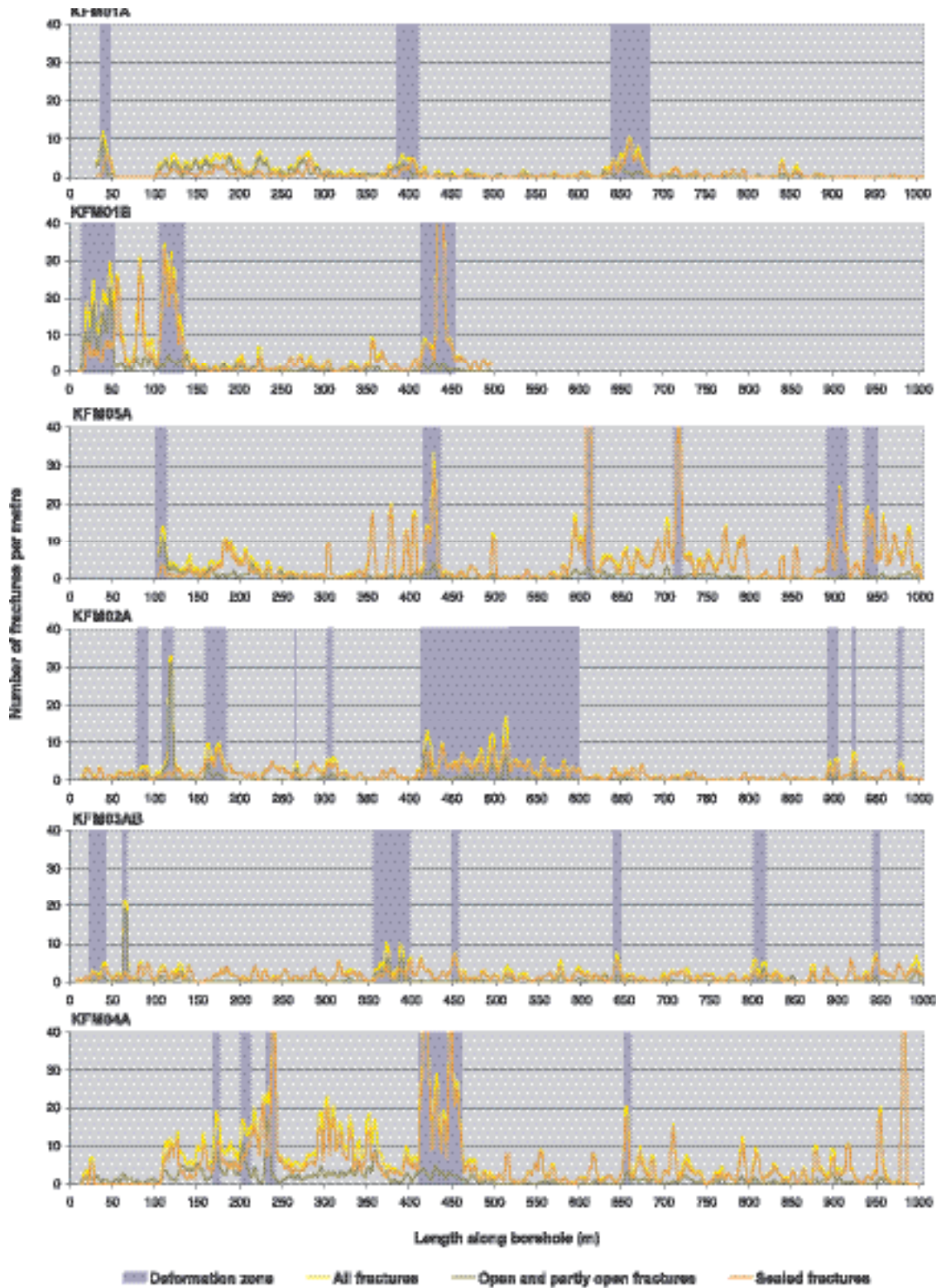


Figure 5-42. Fracture frequency plots for the cored boreholes. Moving average with a 5 m window and 1 m steps. Crush zones and sealed fracture networks are included. The locations of deformation zones, as defined in the single hole interpretation (see Section 5.2.8), are also shown.

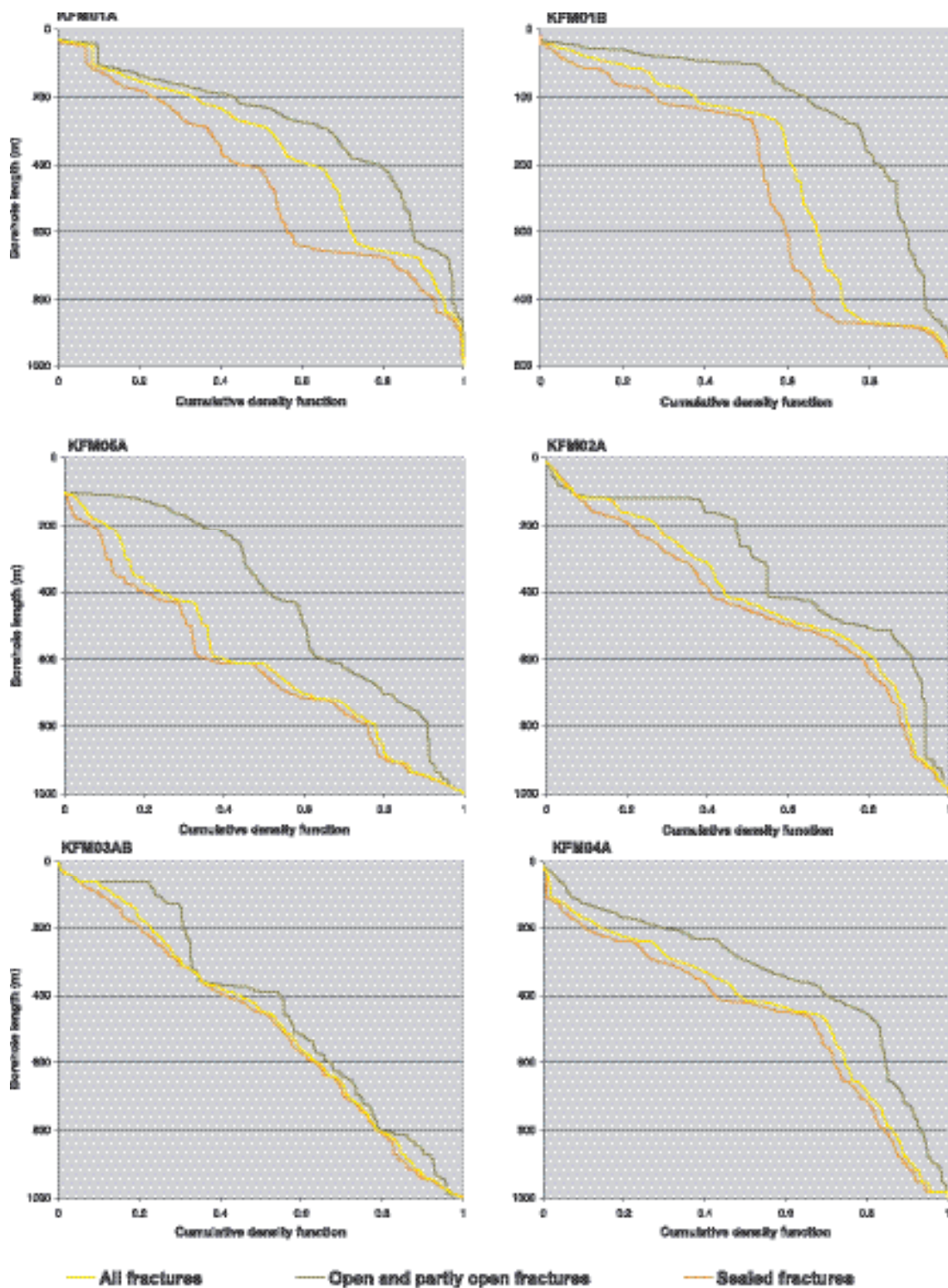


Figure 5-43. Cumulative fracture frequency plots for the cored boreholes. Crush zones and sealed networks are included. Flatter intervals on these diagrams correspond to borehole sections with a relatively high frequency of fractures. In general, these correspond to the deformation zones shown in Figure 5-42. The steeper intervals correspond to borehole sections with a relatively low frequency of fractures.

Both KFM02A and the inclined borehole KFM04A show distinctive breaks in the cumulative fracture frequency curves at c. 600 m and c. 400 m depths, respectively. The latter corresponds to a borehole length of c. 460 m (see Figure 5-42 and Figure 5-43). Only c. 20% of all the fractures in borehole KFM02A occur beneath c. 600 m, while, in KFM04A, only c. 30% of all the fractures in the borehole are present beneath c. 400 m depth. The two boreholes differ somewhat where it concerns the behaviour of the open and sealed fractures. These follow each other in a consistent manner in KFM04A but the open fractures show a more irregular pattern in the upper part of KFM02A.

The inclined borehole KFM05A shows a more complex pattern relative to all the other boreholes (Figure 5-42 and Figure 5-43). The distribution of open fractures is reminiscent of boreholes KFM01A and KFM01B with a relatively high concentration down to c. 215 m depth (c. 250 m borehole length). By contrast, the sealed fractures and even the total number of fractures increase somewhat beneath c. 520 m depth (c. 600 m borehole length).

In summary, it appears that there is no simple pattern for the variability in the frequency of fractures at depth. In particular, there are marked contrasts between boreholes KFM01A, KFM03A–B and KFM05A. It needs to be emphasised that the distributions are only slightly modified, if the possible deformation zones from the single hole interpretations are omitted from the analysis (see Section 5.5). Bearing in mind the significant occurrence of steeply dipping fractures with SE strike in the upper half of KFM04A (see below and /La Pointe et al. 2005/), it is suggested that the high frequency of fractures in the upper part of KFM04A is related to the strongly anisotropic bedrock in this part of the borehole, with ductile planar structures that strike SE and dip steeply to the SW (see above and /Petersson et al. 2004c/).

Fracture orientation (excluding deformation zones)

The orientations of fractures that are situated outside the identified deformation zones in the cored boreholes are presented in Figure 5-44 and Figure 5-45. In a complementary manner, the orientations of fractures within deformation zones are presented in /Stephens and Forssberg, 2005/.

All fractures, the open or partly open fractures and the sealed fractures, are distinguished for each borehole. No data are available for the fractures in crush zones and in sealed fracture networks. A Terzhagi correction has been applied to each of the stereographic plots that helps to reduce the bias related to the borehole orientation. However, it needs to be kept in mind that there is considerable variation in the trend of the boreholes and that the boreholes are both sub-vertical and inclined (Table 5-9).

All fractures in boreholes KFM01A, KFM01B and KFM05A display distinctive orientation sets that are both steeply dipping and sub-horizontal (Figure 5-44). The steeply dipping fractures are grouped into different sets, the most prominent of which strikes NE. The other sets of steeply dipping fractures strike N or N to NW. Both the open or partly open and sealed fractures occur in all the different orientation sets. However, there is a concentration of open and partly open fractures in the sub-horizontal set and a concentration of sealed fractures in the steeply dipping sets.

The orientations of fractures in boreholes KFM02A and KFM03A–B show a somewhat more dispersed pattern relative to that observed in KFM01A, KFM01B and KFM05A (Figure 5-45). There are concentrations of sub-horizontal and gently, SE- or S-dipping fractures as well as steeply dipping fractures that strike NE, SE and N.

Borehole KFM04A, with its high concentration of fractures (Table 5-15), shows four well-defined orientation sets. These include one sub-horizontal set and three steeply dipping sets. The latter strike SE, SW and N. The open or partly open fractures are conspicuous in the SE and SW, steeply dipping sets, and in the sub-horizontal set. They are of little importance in the steeply dipping set that strikes N. By contrast, the sealed fractures are prominent in all the three steeply dipping sets, but are less prominent in the sub-horizontal set.

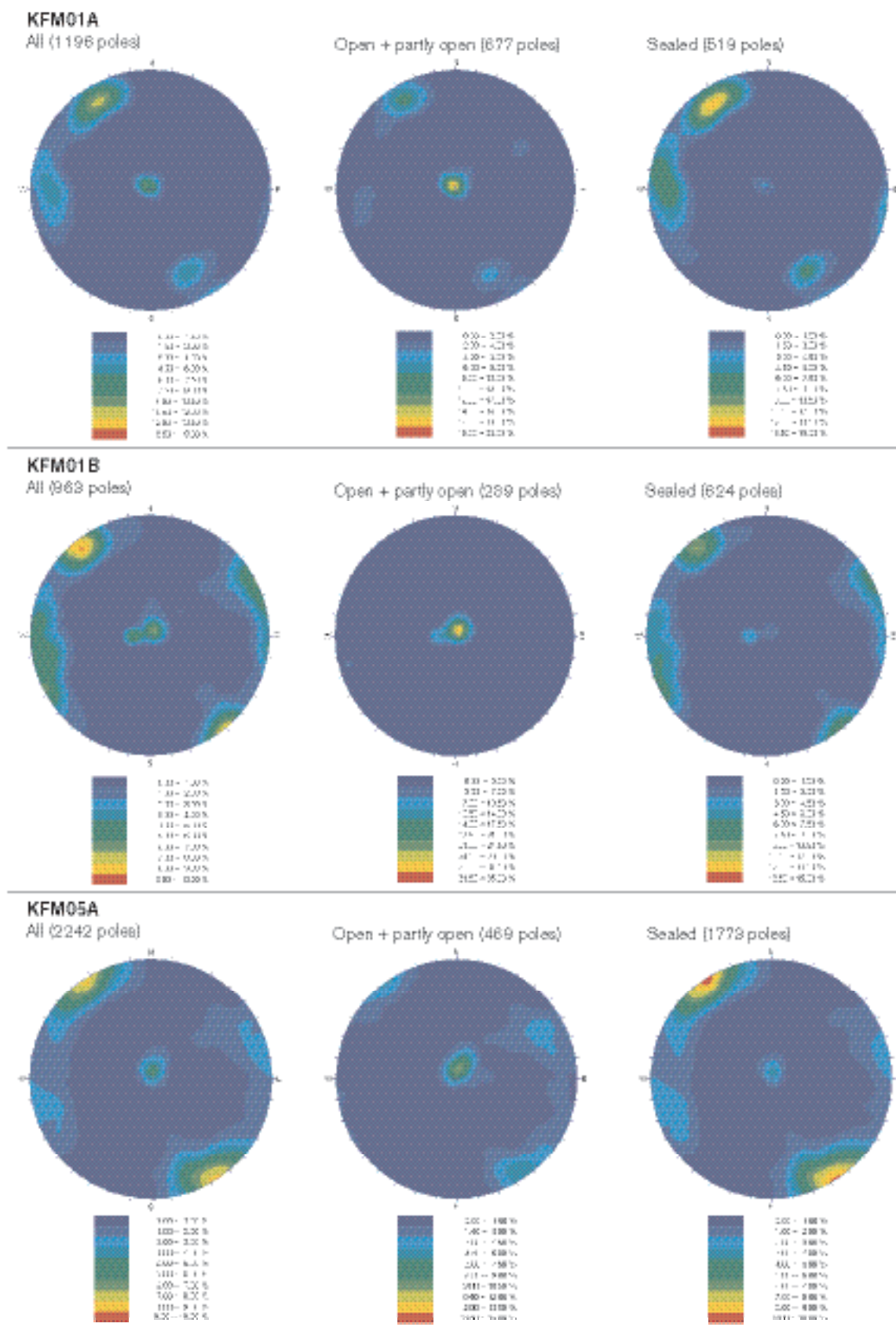


Figure 5-44. Orientation of fractures in boreholes KFM01A, KFM01B and KFM05A, as shown in the lower hemisphere of Schmidt equal area, stereographic plots. Fisher concentrations are shown in % of total per 1.0% area. Terzaghi correction applied.

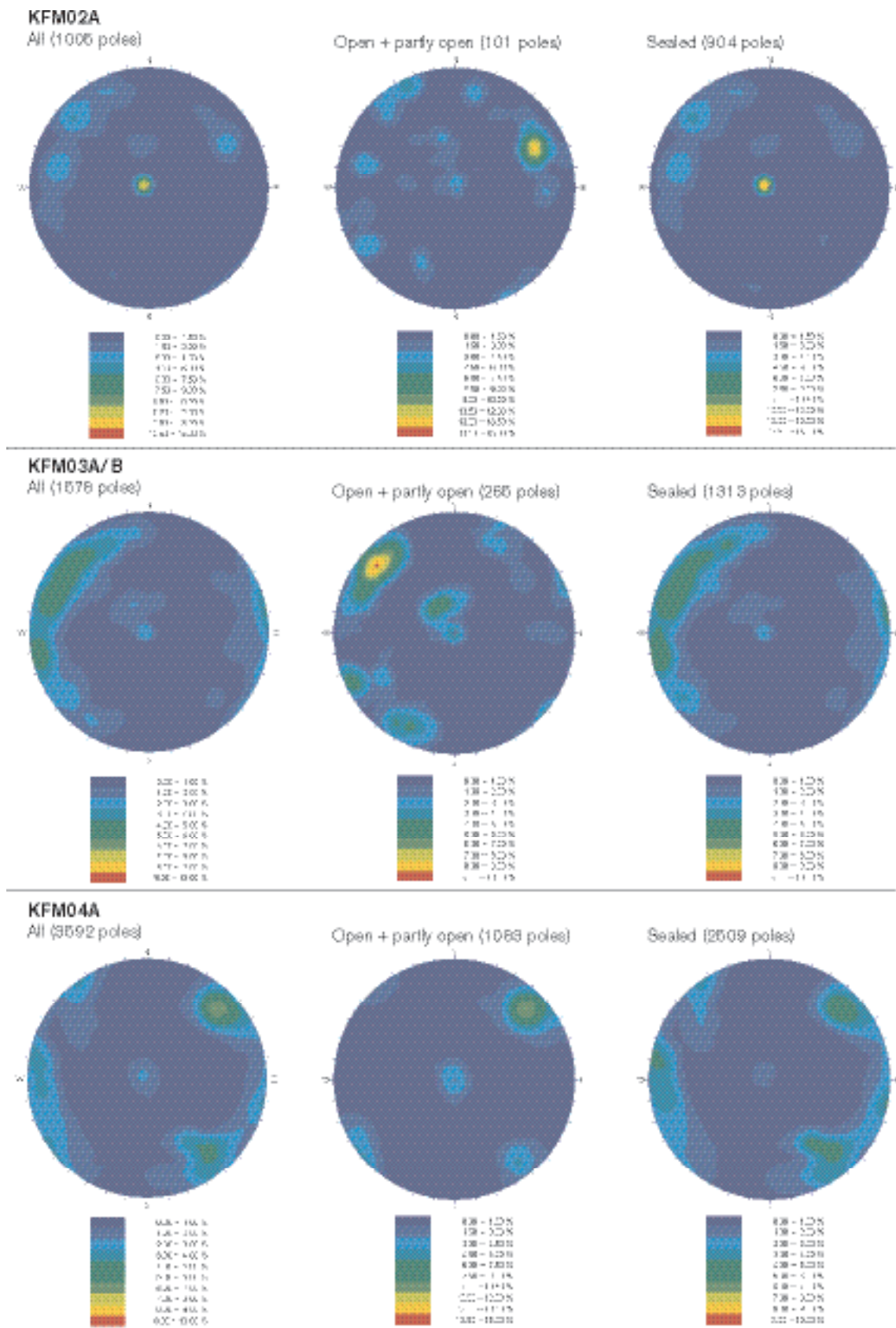


Figure 5-45. Orientation of fractures in boreholes KFM02A, KFM03A–B and KFM04A, as shown in the lower hemisphere of Schmidt equal area, stereographic plots. Fisher concentrations are shown in % of total per 1.0% area. Terzhagi correction applied.

Fracture mineralogy

The identification of mineral coatings along fractures is present in the borehole mapping data set. Further refinements in mineral identification and the characterisation of wall-rock alteration have been presented for selected samples from KFM01A, KFM02A, KFM03A and KFM03B in /Petersson et al. 2004e; Sandström et al. 2005/.

The following minerals (arranged in alphabetical order) have been identified as coatings along fractures: Adularia (low-temperature K-feldspar), albite, analcime (a zeolite), apophyllite (a hydrothermal sheet silicate), calcite, chlorite, clay minerals, epidote, fluorite, hematite, laumontite (a zeolite), prehnite, pyrite and quartz. A common clay mineral is corrensite, which is a mixed layer clay with alternating layers of chlorite and smectite or vermiculite. Other clay minerals are illite, smectite and a mixed layer clay that is composed of illite and smectite. The mineral asphaltite has been observed along fractures in the upper parts of KFM01B and KFM05A. A comparison of the results from the borehole mapping and from the follow-up mineralogical work indicates that the occurrence of certain minerals (e.g. adularia, albite, analcime) is underestimated in the Boremap data. It is likely that many of the minerals that have been mapped as hematite are hematite-stained adularia.

Wall rock alteration adjacent to fractures involved growth of very small grains of hematite under oxidizing conditions. This alteration is most prominent around the epidote- and laumontite-filled fractures.

On the basis of their growth relationships, six generations of fracture mineralisation have been identified /Sandström et al. 2005/. These are summarised below in order of decreasing age:

- *Generation 1 (oldest)*: Epidote, quartz and chlorite.
- *Generation 2/Generation 3*: Prehnite/Laumontite. In addition, growth of calcite, chlorite-corrensite, adularia and quartz. Generations 2 and 3 are grouped together since stable isotope data on calcite indicate a close relationship between the generation of prehnite and laumontite /Sandström et al. 2004/.
- *Generation 4/Generation 5*: Quartz, adularia, albite, analcime, chlorite-corrensite and calcite/calcite and pyrite. Generations 4 and 5 are also grouped together on the basis of the stable isotope composition of the calcite in the two generations /Sandström et al. 2005/.
- *Generation 6 (youngest)*: Calcite, clay minerals, possibly also asphaltite.

In the following analysis, attention is focused on a selection of eight common minerals. In alphabetical order, these minerals are calcite, chlorite, clay minerals, epidote, hematite, laumontite, prehnite and quartz. The fractures where either other minerals or no mineral coating has been identified, and the occurrences of oxidized wall-rock alteration, adjacent to the fractures, are also included in the analysis.

Histograms that show the number of fractures along which a particular mineral has been identified are presented for each borehole (Figure 5-46). The mineral coatings along open and partly open fractures have been separated from those along sealed fractures in each histogram. Some control on the frequency of occurrence of the different mineral coatings is provided in these diagrams.

Chlorite and calcite are prominent along the fractures in all the boreholes. Indeed, in boreholes KFM02A and KFM03A–B, where sub-horizontal and gently dipping fractures are conspicuous, these minerals dominate together with fractures where a mineral coating is lacking. The minerals laumontite and hematite as well as the oxidized walls to fractures are common in boreholes KFM01A, KFM01B, KFM04A and KFM05A. Epidote, prehnite, quartz and other minerals form a subordinate group. Apart from KFM01B, clay minerals yield a low score on the histograms in all the boreholes.

The prime purpose of the statistical analysis was to identify the orientation distribution of the different mineral coatings. For this reason, the orientations of fractures that are coated by a particular mineral have been plotted in the lower hemisphere of a series of Schmidt equal area, stereographic diagrams. These plots have been constructed for each borehole (not shown here) and for all the boreholes together (Figure 5-47). Fracture fillings along crush zones or sealed fracture networks are not included in this analysis.

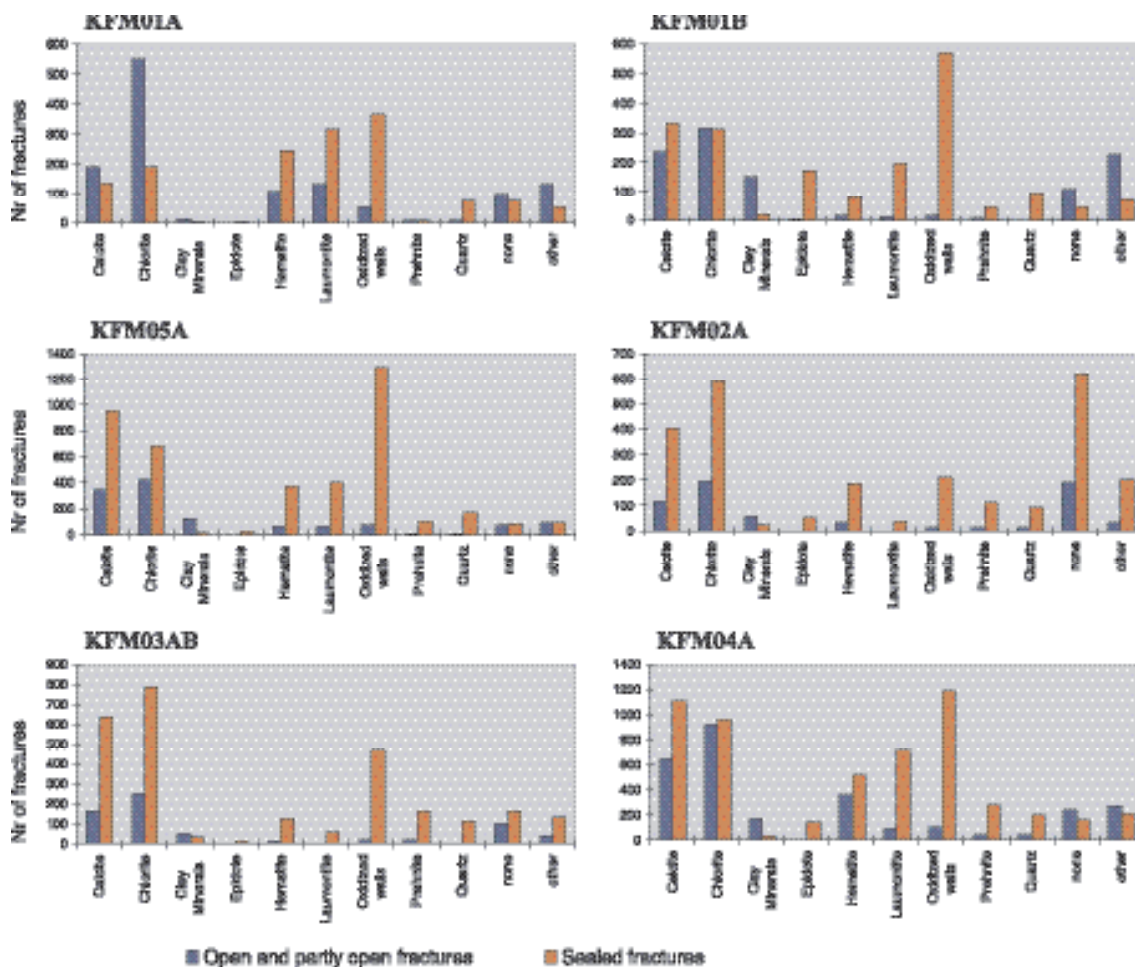


Figure 5-46. Histograms showing the frequency of mineral coatings along fractures in each cored borehole.

The minerals chlorite, calcite, laumontite, hematite as well as the oxidised walls to fractures occur in all the different orientation sets of fractures that were recognized in the previous section, i.e. the NE, SE, N, and sub-horizontal and gently dipping sets. This feature is most prominent in the data for boreholes KFM04A and KFM05A. A similar tendency is also apparent for prehnite and quartz. There is also a conspicuous concentration of laumontite along the NE set of fractures in boreholes KFM01A, KFM04A and KFM05A. Furthermore, there is a high concentration of prehnite along the SE set of fractures in KFM04A. In strong contrast to all these features, epidote and even the clay minerals are more or less restricted to the NW and gently dipping fracture sets.

5.2.8 Single hole interpretation

Aims and methodology

In the same way that the bedrock geological map (see Section 5.2.2) forms an important, intermediate step between outcrop data (see Section 5.2.1) and geological modelling work (see Sections 5.3 and 5.4), the single hole interpretation (SHI) forms a key step between the borehole data and the modelling. A SHI provides a synthesis of all the geological and geophysical information in a borehole. It aims to document the rock units that show a minimum length of 5–10 m along the borehole as well as all the deformation zones that are intersected in the borehole, i.e. fixed data points for these zones at depth. The identification of these geological features is unique for each borehole. Correlation of these features between boreholes and with surface data forms part of the modelling work.

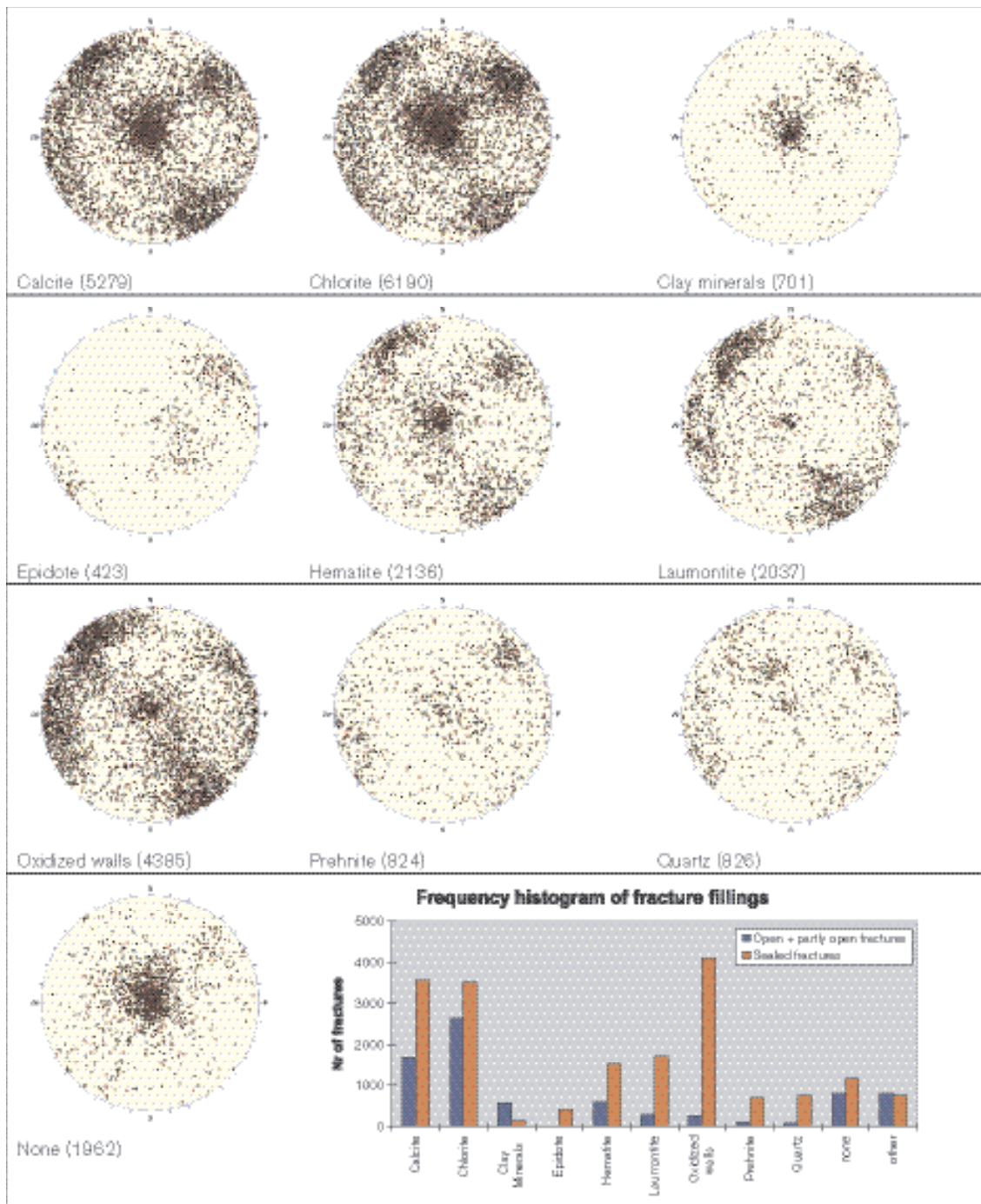


Figure 5-47. Orientation of the fractures along which the mineral coatings have been documented in all the boreholes. The orientations are shown in the lower hemisphere of a series of Schmidt equal area, stereographic plots.

The following input data have been used in all the SHI:

- Geological mapping data using BIPS and the Boremap system.
- Borehole radar data and their interpretation.
- Geophysical logs and their interpretation.

Short descriptions of the rock units and deformation zones in each cored and percussion borehole are provided in /Carlsten et al. 2004a, b, c, d, e and f/. The orientation of fractures in each rock unit and each deformation zone is synthesised in these reports. Sealed fractures are distinguished from

open and partly open fractures in the fracture orientation plots. The confidence in the interpretation of the different geological components has been assessed on the following basis: 3 = certain, 2 = probable, 1 = possible. A summary of the location of rock units and deformation zones that have been identified in each borehole is provided in Table 5-16.

Rock units

All boreholes, with the exception of one section (220–293 m) in KFM03A, one section (9–30 m) in HFM18, the upper half (12–500 m) of KFM04A and the percussion boreholes HFM09–HFM12, are dominated by a rock unit that contains medium-grained, biotite-bearing metagranite (Group B) as a major component (Figure 5-48). Fine- to medium-grained metagranodiorite and metatonalite (Group C), amphibolite, and pegmatitic granite form subordinate rock types in this unit. The Group C metagranodiorite and metatonalite locally dominates or is intermingled with the medium-grained metagranite in minor rock units that do not exceed 70 m in borehole length (Figure 5-48). These features are identical to those observed in the surface outcrops in a large part of the candidate area (see Section 5.2.2). The finer grained variety of the biotite-bearing metagranite forms a separate, minor rock unit at the top of KFM05A (Figure 5-48).

The common occurrence of pegmatitic granite and pegmatite at the surface in the south-eastern part of the candidate area is consistent with the high proportion of pegmatitic granite throughout KFM03B (Figure 5-48) and in several rock units in HFM06–HFM08. This rock type is also dominant in the rock unit that is situated between 349–377 m in KFM03A (Figure 5-48).

Medium-grained metatonalite (Group B), identical to that distinguished at the surface close to Lillfjärden (see Section 5.2.2), dominates one interval (220–293 m) in KFM03A (Figure 5-48) and occurs in the upper part (9–30 m) of HFM18. The interval between 12 and 177 m in KFM04A (Figure 5-48), as well as HFM09 and HFM10, consist of rock units that contain a high proportion of metagranodiorite and metatonalite. Felsic metavolcanic rocks and amphibolite are also common components. Strongly foliated metagranite, that is similar in composition to that observed in the candidate area, is an important component in the rock units in the borehole interval 177–500 m in KFM04A (Figure 5-48) and in the percussion boreholes HFM11 and HFM12. Several of the rock units in these borehole sections are also inhomogeneous. In particular, felsic metavolcanic rocks are prominent in the interval 275–342 m in KFM04A (Figure 5-48).

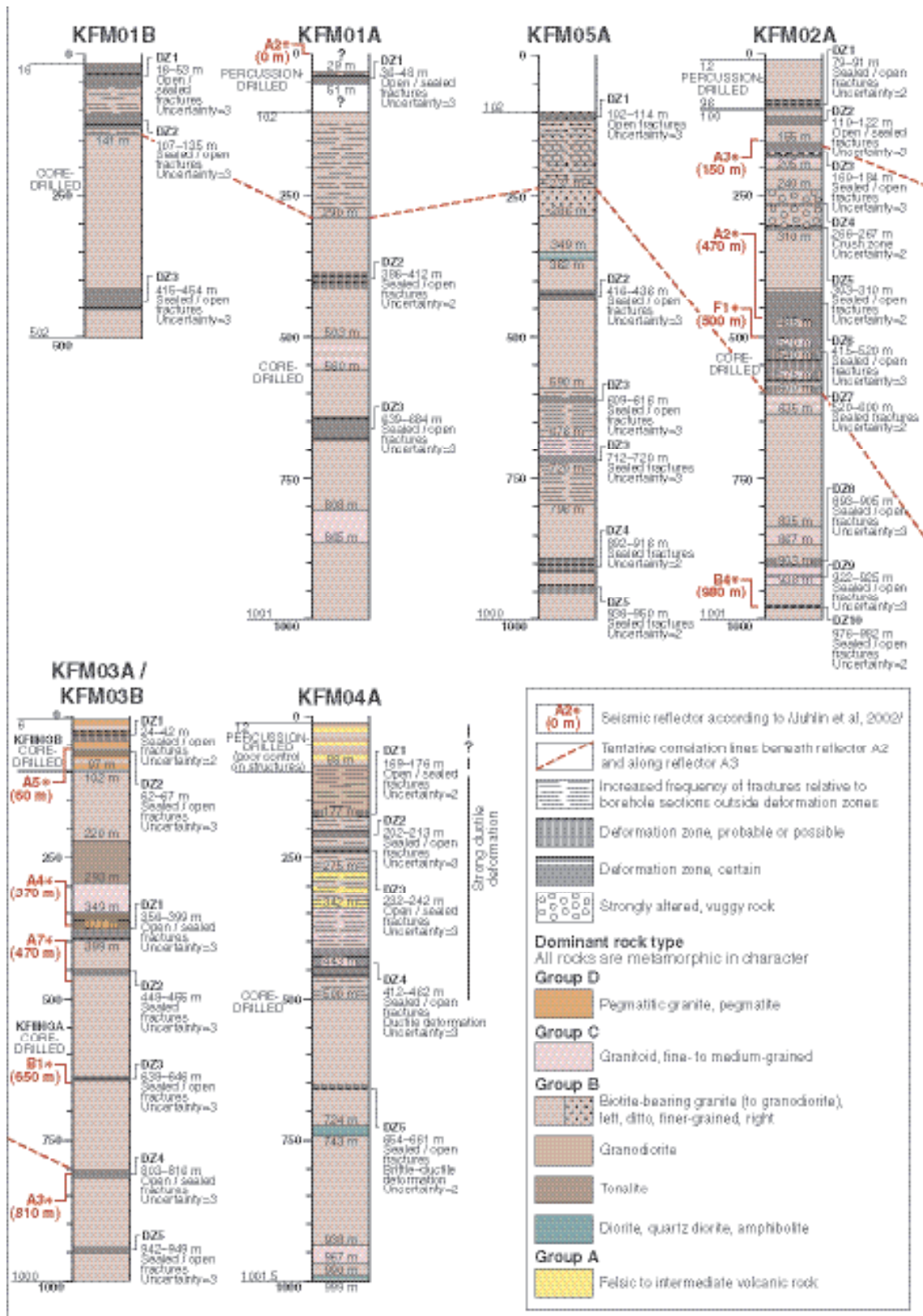
Deformation zones

Deformation zones have been identified primarily on the basis of the frequency of fractures (see Section 5.2.7), according to the recommendations in /Munier et al. 2003/. Both the transitional part, with a fracture frequency in the range 4–9 fractures/m, and the core part, with a fracture frequency > 9 fractures/m, have been included in each zone (Figure 5-49). The frequencies of both open and sealed fractures and the character of dominant mineral coatings along fractures have been assessed in the identification procedure, and the character of the zone has been described accordingly. The presence of bedrock alteration, the occurrence and, locally, the inferred orientation of radar reflectors, and the resistivity, SPR, P-wave velocity, caliper and magnetic susceptibility logs have assisted in the identification of the zones. Anomalies in these logs are presented in the description of each zone intersection. Virtually all the deformation zones that have been recognised in the SHI are solely brittle in character. Two zones are composite with both ductile and brittle components. The terminology for deformation zones as recommended in /Munier et al. 2003/ is followed.

Deformation zones, which are characterised by the occurrence of incohesive fault breccias (crush zones) and an increased frequency of gently dipping, open fractures (Figure 5-50a), are present in the upper part of all the boreholes that have been drilled at or close to drill sites 1 and 5 (Figure 5-48) as well as in HFM16 at drill site 6. Furthermore, with the exception of the deformation zones, there is a generally higher frequency of fractures down to 290 m, 141 m and 237 m borehole length in KFM01A, KFM1B and KFM05A, respectively, relative to the deeper parts of these boreholes (Figure 5-48. See also Section 5.2.7). Only zones that are characterised by an increased frequency of steeply dipping, predominantly sealed fractures and sealed fracture networks, i.e. cohesive structures, are present at deeper levels in the cored boreholes (Figure 5-48).

Table 5-16. Identification of rock units and deformation zones from the SHI of KFM01A, KFM01B, KFM02A, KFM03A, KFM03B, KFM04A, KFM05A and HFM01–19. The ID codes for the rock units (RU) and deformation zones (DZ) are not transferable from borehole to borehole.

Borehole	Rock unit	Borehole section (m)	Deformation zone	Borehole section (m)	
Drill site 1	KFM01A	RU1–RU3	29–503, 560–808 and 865–1,001 (RU1), 808–865 (RU2), 503–560 (RU3)	DZ1–DZ3	36–48 (DZ1), 386–412 (DZ2), 639–684 (DZ3)
	KFM01B	RU1	16–502	DZ1–DZ3	16–53 (DZ1), 107–135 (DZ2), 415–454 (DZ3)
	HFM01	RU1	31–197	DZ1	35–44
	HFM02	RU1	25–99	DZ1	42–47
	HFM03	RU1	13–26	No zone	No zone
Drill site 2	KFM02A	RU1–RU4	12–155, 205–240, 310–485, 520–540, 575–600, 635–835, 867–903 and 938–1,001 (RU1), 240–310 (RU2), 155–205, 485–520, 540–575, 600–635 and 835–867 (RU3), 903–938 (RU4)	DZ1–DZ10	79–91 (DZ1), 110–122 (DZ2), 160–184 (DZ3), 266–267 (DZ4), 303–310 (DZ5), 415–520 (DZ6), 520–600 (DZ7), 893–905 (DZ8), 922–925 (DZ9), 976–982 (DZ10)
	HFM04	RU1	12–222	DZ1–DZ2	61–64 (DZ1), 183–187 (DZ2)
	HFM05	RU1	12–199	DZ1	153–154
Drill site 3	KFM03A/ KFM03B	RU1–RU5	102–220 and 399–1,000 (RU1), 220–293 (RU2), 293–349 and 377–399 (RU3), 349–377 (RU4), 6–97 (RU5)	DZ1–DZ5 in KFM03A and DZ1–DZ2 in KFM03B	24–42 (DZ1 in KFM03B), 62–67 (DZ2 in KFM03B), 356–399 (DZ1 in KFM03A), 448–455 (DZ2 in KFM03A), 638–646 (DZ3 in KFM03A), 803–816 (DZ4 in KFM03A), 942–949 (DZ5 in KFM03A)
	HFM06	RU1	11–108	DZ1	61–71
	HFM07	RU1	11–109	DZ1	54–66
	HFM08	RU1–RU3	17–27, 41–78 and 115–142 (RU1), 27–41 (RU2), 78–115 (RU3)	DZ1	136–141
Drill site 4	KFM04A	RU1–RU8	12–88 (RU1), 88–177 (RU2), 177–275 and 443–500 (RU3), 275–342 (RU4), 342–443 (RU5), 500–724, 743–938, 967–990 and 999–1,001.5 (RU6), 724–743 and 990–999 (RU7), 938–967 (RU8)	DZ1–DZ5	169–176 (DZ1), 202–213 (DZ2), 232–242 (DZ3), 412–462 (DZ4), 654–661 (DZ5)
	HFM09	RU1	17–50	DZ1	18–28
	HFM10	RU1	12–149	DZ1–DZ2	65–69 (DZ1), 108–117 (DZ2)
Drill site 5	KFM05A	RU1–RU4	102–286 (RU1), 286–349, 362–676 and 720–1,000 (RU2), 349–362 (RU3), 676–720 (RU4)	DZ1–DZ5	102–114 (DZ1), 416–436 (DZ2), sections 609–616 and 712–720 in the interval 590–796 (DZ3), 892–916 (DZ4), 936–950 (DZ5)
	HFM14	RU1	3–149	DZ1–DZ2	68–76 (DZ1), 92–104 (DZ2)
	HFM15	RU1	4–99	DZ1	86–96
HFM11	RU1–RU2	13–83 (RU1), 83–183 (RU2)	DZ1	83–160	
HFM12	RU1	14–209	DZ1	91–170	
HFM13	RU1	14–93	DZ1	162–176	
HFM16	RU1–RU2	12–18 and 35–130 (RU1), 18–35 (RU2)	DZ1	12–71	
HFM17	RU1	8–209	No zone	No zone	
HFM18	RU1–RU2	9–30 (RU1), 30–182 (RU2)	DZ1–DZ3	9–11 (DZ1), 36–49 (DZ2), 119–148 (DZ3)	
HFM19	RU1	11–185	DZ1–DZ2	121–148 (DZ1), 168–185 (DZ2)	



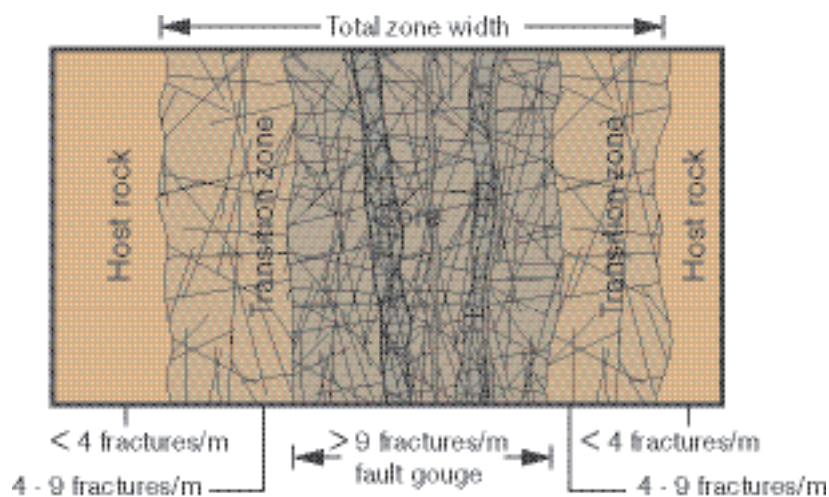


Figure 5-49. Terminology for brittle deformation zones (after /Munier et al. 2003/).

Steeply dipping, sealed fractures and sealed fracture networks are common along the section 590–796 m in KFM05A. However, brittle deformation zones, which have been inferred with a high degree of confidence, are restricted to the sections 609–616 m and 712–720 m (Figure 5-50b). The fractures in these two cohesive fault structures, as well as in similar brittle zones at 416–436 m, 892–916 m and 936–950 m in KFM05A, strike predominantly north-east /Stephens and Forsberg, 2005/. These data do not provide support for intersections with steeply dipping deformation zones that correspond to the lineaments through Bolundsfjärden with a north-south trend.

The results from the boreholes at or close to drill sites 2 and 3 are quite different. Brittle deformation zones that have been graded as certain or probable occur in the upper (79–310 m), middle (415–600 m) and lower (893–982 m) parts of KFM02A (Figure 5-48). They also occur at regular intervals throughout the total borehole length in KFM03A–B (Figure 5-48). The most conspicuous zone is present between 415 and 520 m in KFM02A. All these zones are characterised by an increased frequency of gently (or moderately) dipping fractures that are both sealed and open. Furthermore, there is an excellent correlation between these inferred zones and the predicted intersection of definite and probable seismic reflectors in the boreholes (Figure 5-48). The predicted intersections were estimated in /Juhlin et al. 2002; Juhlin and Bergman, 2004/, predominantly prior to the drilling at these two sites. This calibration work allows a correlation to be made between the deformation zones in different boreholes (Figure 5-48).

The results from the boreholes at or close to drill site 4 are also quite specific. A distinctive feature of KFM04A is the higher degree of ductile deformation (see Section 5.2.6) and a generally higher frequency of fractures above relative to beneath 500 m borehole length (Figure 5-48). A brittle deformation zone, which contains an incohesive fault breccia (crush zone) and an increased frequency of gently dipping, open fractures, occurs at 232–242 m in KFM04A. Fractures of this type are also present in the inferred zones at 169–176 m and 202–213 m. As in the boreholes at drill sites 1 and 5, deformation zones at deeper levels have been identified primarily by an increased frequency of steeply dipping, sealed fractures, i.e. the structures are more cohesive in character.

The rock unit with vuggy metagranite in KFM02A (borehole depth interval 240–310 m) contains an incohesive fault breccia (crush zone) at 266–267 m and a probable brittle deformation zone at its base (303–310 m). Furthermore, vuggy metagranite is also present within the brittle deformation zone at 160–184 m in KFM02A. These observations suggest that the formation of vugs and the associated hydrothermal alteration are related to the discrete channelling of fluids along brittle deformation zones /Möller et al. 2003/.

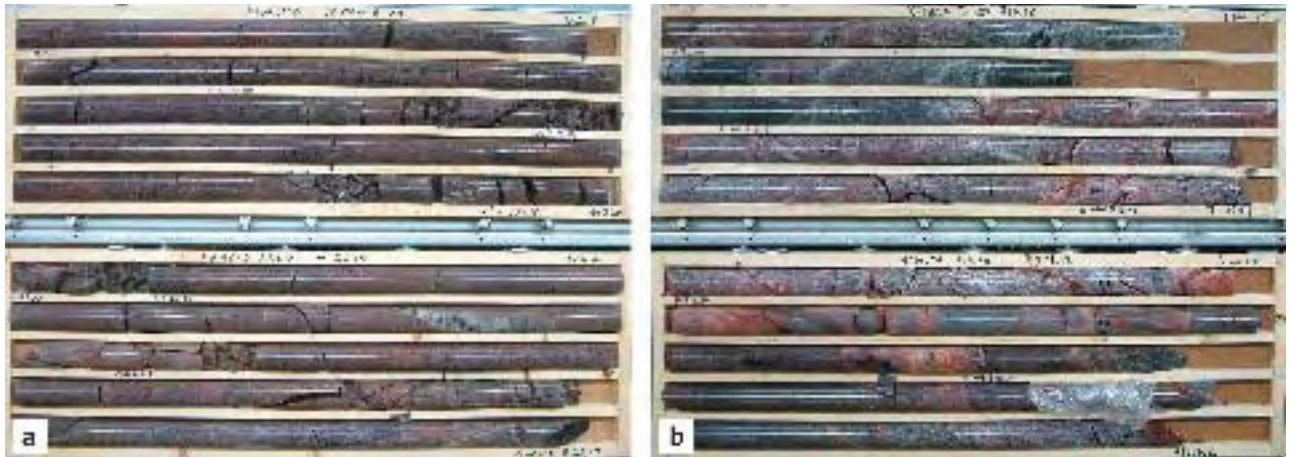


Figure 5-50. a) Incohesive fault breccias (crush zones) and gently dipping fractures (high angle to borehole length) within DZ1 in the uppermost part of KFM01B. This zone is correlated with seismic reflector A2. b) Steeply dipping fractures in the 712–720 m borehole section in KFM05A (part of DZ3). Laumontite, calcite and chlorite are prominent fracture coatings. Although several fractures are broken, they are inferred to have been sealed prior to the drilling activity and this part of DZ3 is interpreted as a cohesive fault structure.

The percussion boreholes that were drilled some distance away from drill sites 1–5 (HFM11, HFM12, HFM13, HFM17, HFM18 and HFM19) were designed to test the correlation between deformation zones and lineaments. When the results of the SHI for these boreholes are assessed, it is important to keep in mind the difficulties encountered during the mapping of all the percussion boreholes.

Strong ductile deformation and an increased frequency of steeply dipping, sealed fractures characterise the borehole sections 83–160 m and 91–170 m in HFM11 and HFM12, respectively. These results are consistent with the outcrop observations /Stephens et al. 2003a/ in the vicinity of the lineament (XFM0015A0) that corresponds to the Eckarfjärden deformation zone /SKB, 2004a/. The borehole data confirm the composite character of this deformation zone and show that the brittle deformation is most prominent in the south-western part of the zone.

One probable, brittle deformation zone that is characterised by an increased frequency of steeply dipping fractures is present at the base of HFM13 (162–176 m). However, the borehole does not penetrate the base of this zone. No zones were identified in HFM17. A deformation zone, which contains two incohesive fault breccias (crush zones) and an increased frequency of especially gently dipping, open fractures, is present in the upper part (36–49 m) of HFM18. A more complex zone (or zones) with both gently and steeply dipping fractures is present in the lower part (119–148 m) of this borehole. Both the zones that have been identified in HFM19 are dominated by gently dipping, open fractures. As in KFM05A, there is little support for an intersection with any steeply dipping deformation zone that corresponds to a lineament with north-south trend.

5.3 Rock domain model

5.3.1 Modelling assumptions and input from other disciplines

The work connected with the establishment of the rock domain model for the Forsmark site has made use of the following information:

- The rock domain models that were presented in version 0 /SKB, 2002a/ and version 1.1 /SKB, 2004a/ of the site descriptive models. The three-dimensional version 1.1 model forms the basis for the present model.
- Data bearing on the character of rock types that are exposed at the surface (see Section 5.2.1) and that are present at depth in the boreholes (see Section 5.2.6).
- The distribution of rock units at the surface, as expressed in the bedrock geological map of the area (see Section 5.2.2), and at depth, as recognised in the single hole interpretations of the cored and percussion boreholes (see Section 5.2.8).
- Data bearing on the penetrative ductile deformation in the bedrock, both at the surface (see Section 5.2.4) and at depth (see Section 5.2.6).
- Data bearing on the timing of crystallization of the igneous rocks and their cooling history to below various temperatures (see Section 3.1).

Most of these data have been generated at the surface. However, data from eight cored boreholes, down to a depth of c. 1,000 m, and from nineteen percussion boreholes, in average down to a depth of 200 m, have also been used in the modelling work. The borehole data are restricted predominantly to the candidate volume. Furthermore, these data show that the dominant rock domain in this volume (RFM029) extends to a depth of c. 1,000 m. For these two reasons, the surface data are of prime importance for the modelling work.

The terms rock units and rock domains are used here according to the terminological guidelines in /Munier et al. 2003/. Rock units are defined on the basis of the composition and grain size of the dominant rock type or the degrees of bedrock homogeneity and ductile deformation. The modelling procedure has involved the use of ten rock units that have been distinguished on the basis of the mineralogical composition and grain size of the dominant rock type, and four rock units that show different degrees of bedrock homogeneity and ductile deformation (see below). Rock domains are defined on the basis of an integration of these different geological criteria.

A single model for the three-dimensional distribution of rock domains in the regional model volume has been established. The following assumptions have been adopted in the modelling procedure.

- The strike and dip of the planar ductile structures (banding and tectonic foliation), as measured at the surface (see Section 5.2.4), are assumed to provide an estimate of the strike and dip of the contacts between the major rock domains, i.e. those domains that can be followed at the surface over several kilometres.
- Since the contacts between the major rock domains are commonly estimated to be steeply dipping, virtually all these domains are assumed to extend downwards to, at least, the base of the regional model volume (–2,100 m).
- The lenses of ultramafic, mafic and intermediate rocks at the surface (SKB codes 101033 and 101004) are assumed to trend downwards in the direction of the mineral stretching lineation (see Section 5.2.4) and to extend to, at least, the base of the regional model volume.

The modelling of rock domains is an important base input to several other disciplines in the site descriptive modelling work (see Section 5.6). However, the rock domain modelling has also benefited from a feedback from the modelling of the thermal properties of the site.

5.3.2 Conceptual model

The candidate area at Forsmark is situated within the north-westernmost part of a tectonic lens in which folding, LS-tectonites, where linear ductile mineral fabrics dominate over planar equivalents, and a generally lower degree of ductile strain are present. This lens was identified during the earlier feasibility study work /Bergman et al. 1996, 1999/ and extends along the Uppland coast from north-west of the nuclear power plant south-eastwards to Öregrund (Figure 5-51). The lens is c. 25 km long and up to c. 4 km wide. It developed when the rock units were situated at mid-crustal depths and were affected by penetrative but variable degrees of ductile deformation under amphibolite-facies metamorphic conditions.

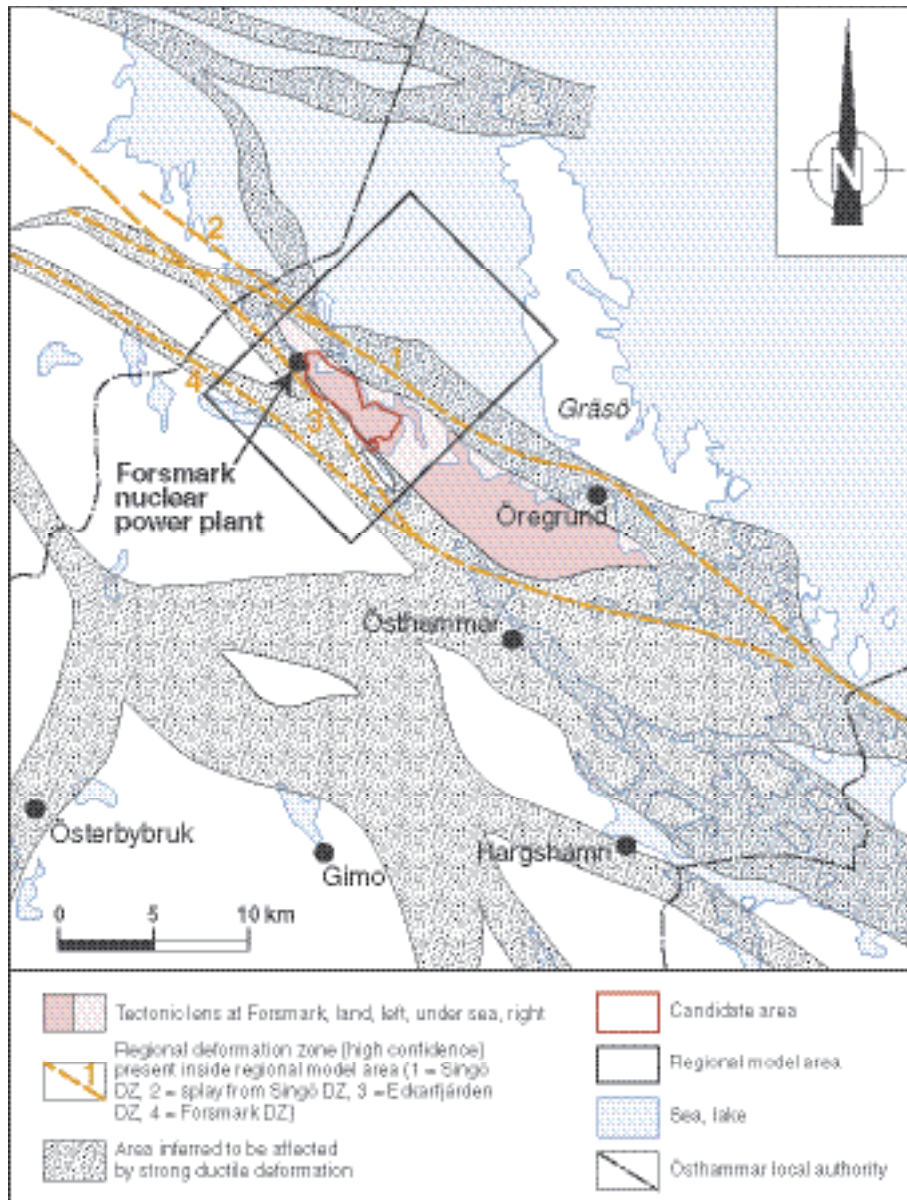


Figure 5-51. Structural geological map of the coastal area in the local authority of Östhammar showing the extension of the tectonic lens within which the candidate area at Forsmark is situated (based on /Bergman et al. 1996, 1999/). The regional deformation zones with high confidence that transect the regional model area are also shown (based on Section 5.4).

At the Forsmark site, the bedrock inside the lens is relatively homogeneous and is dominated by a metagranite with between 28 and 46% quartz. This rock domain can be traced from the surface to at least c. 1,000 m depth. Folds at different scales within the lens deform a planar grain-shape fabric, the boundaries between the metagranite and a rock unit composed of metatonalite, and, in a limited area north-west of Asphällsfjärden, a heterogeneous rock unit that is inferred to show a higher degree of ductile strain.

The lens at Forsmark is surrounded by various domains that strike north-west, dip steeply to the south-west and are dominated by SL-tectonites, i.e. contain both planar and linear ductile mineral fabrics. In general, the rocks in these domains show a considerably higher degree of ductile deformation relative to that observed inside the tectonic lens. The bedrock in these domains is heterogeneous and composed of various types of felsic to intermediate metavolcanic rocks and metagranitoids, with quartz contents in the felsic varieties that range from 14 to 44%. Major, intermediate to ultramafic intrusive bodies that are quartz-poor or quartz-deficient are also present. Iron oxide mineralisation occurs in the metavolcanic rocks.

Fold axes and mineral stretching lineation show a similar, moderate to gentle plunge to the south-east, both inside the candidate volume and in the marginal domains. Tubular-shaped folding is present on an outcrop scale in the highly deformed, marginal domain to the north-east of the candidate area. All the isolated bodies of metamorphosed intrusive rocks have been modelled as major rod-like structures that extend at depth parallel to the mineral stretching lineation. One younger granite body that is situated in the archipelago north of the candidate area has been modelled as a laccolith that does not extend to the base of the regional model volume. It shows a broad extension at the surface and a rapidly decreasing extension at depth.

The structural features summarised above are characteristic of regions where planar grain-shape fabric development, mineral stretching lineation and folding are intimately related during strong, non-coaxial, progressive deformation. The tectonic lens generally shows more prolate structures and is inferred to be situated in the hinge of an oblique or sheath fold that plunges to the south-east. It is sandwiched between steeply dipping slabs of bedrock that generally show stronger ductile deformation and more oblate structures. The ductile strain in the highly deformed bedrock on both sides of the tectonic lens shows a component of dextral horizontal movement. These observations are consistent with bulk crustal shortening in an approximately north-south direction (see also Section 3.1).

The intrusive rocks in the Forsmark area formed during the time interval 1,887 to 1,840 million years ago. In particular, the metagranite in the candidate area crystallised $1,865 \pm 3.4$ million years ago. The supracrustal rocks are older and formed prior to 1,885 million years ago. The penetrative ductile deformation and the amphibolite-facies metamorphism occurred during the time interval 1,868 to 1,846 million years. However, strong ductile strain at the peak of the amphibolite-facies metamorphism had occurred prior to the intrusion of the Group C rocks, between 1,868 and 1,861 million years ago.

At least a part of the bedrock that is exposed at the surface had cooled beneath 700–550°C and beneath 500°C at 1,840 and 1,828 million years ago, respectively. However, the cooling ages below 500°C vary somewhat over the surface and extend in age downwards to 1,793 million years. These results, in combination with the observation that subordinate ductile deformation affects the younger intrusive rocks in the marginal domains, suggest that ductile deformation, under lower grade metamorphic conditions, continued along discrete zones within the marginal parts of the tectonic lens, probably until at least 1,790 million years ago.

At least a part of the bedrock at the surface had cooled beneath 300°C at 1,704 million years ago. This cooling age suggests that the bedrock had started to deform in a brittle manner at an earlier stage, i.e. probably during the waning stages of the Svecokarelian orogeny (see Section 3.1). These results have important implications for the conceptual model for deformation zones (see Section 5.4.2). Cooling ages beneath 70–60°C vary with depth from c. 630 million years at the surface to c. 250 million years at 1,000 m depth. The implication of these cooling ages awaits further assessment.

5.3.3 Division into rock domains and property assignment

Division into rock domains

A primary step in the modelling procedure has been the recognition of rock domains at the surface and a combination with information from boreholes KFM03A, KFM04A, HFM18 and KFO01 that intersect rock domain boundaries (see Section 5.2.8).

The geometrical modelling has followed the principles that were applied in the model version 1.1 work. The rock domain model has been modified in accordance with the updated version of the bedrock geological map and the data from the new cored and percussion boreholes (see Sections 5.2.1, 5.2.2, 5.2.4, 5.2.6 and 5.2.8).

Six working stages have been followed during the geometric modelling:

- Simplification of the bedrock geological map, version 1.2 /Stephens et al. 2005b/.
- Construction of two geological maps that show the distribution at the surface of the two types of rock units defined in Table 5-17. The base information was extracted from the bedrock geological map, version 1.2.
- Interpretation of standard, SGU airborne magnetic data and a study of the bedrock map compilation in /Svenonius, 1887/ at Öregrundsgrepen and on Gräsö, in the north-easternmost part of the regional model area. Development of the same two types of map compilation as described above.
- Definition of the areal extension of thirty-five rock domains at the surface that are based on an integration of the two types of rock units defined in Table 5-17.
- Definition of rock domains in the boreholes based on the results of the single hole interpretations.
- Downward projection of the thirty-five rock domains throughout the regional model volume and integration with the sub-surface data.

In order to carry out the modelling procedure efficiently, it was necessary to simplify the version 1.2 bedrock geological map of the Forsmark area (see Section 5.2.2). Minor rock units on the geological map were included in the modelling procedure as subordinate rock types within the adjacent major rock unit. This simplification affected the recognition of sulphide and magnetite mineralisations on the map, the Group D pegmatitic granite and pegmatite, and the minor occurrences of Group C metagranitoid. Furthermore, the ultramafic rocks were modelled together with the metamorphosed gabbro, diorite and quartz diorite, and the metatonalite together with the metagranodiorite. These changes reduced the fourteen rock units on the bedrock geological map to nine rock units in the modelling work.

The integration with the results of the work in the north-easternmost part of the regional model area, at Öregrundsgrepen and on Gräsö, resulted in the addition of one rock unit, a metamorphosed metagranitoid. The absence of complementary analytical data in this area does not permit any division of this rock unit into tonalitic, granodioritic or granitic components.

The simplification and integration procedures of the surface data have yielded three important products:

- A simplified geological map over the regional model area that shows the distribution of rock units distinguishable in the field (Figure 5-52). Each rock unit on this map is dominated by one of the ten rock types defined in Table 5-17.
- A geological map that shows the variation in the degree of both bedrock homogeneity and ductile deformation over the regional model area (Figure 5-53). The four units displayed on this map are also defined in Table 5-17. This assessment utilises the results from the bedrock mapping work (see Sections 5.2.2 and 5.2.4).
- A geological map that shows rock domains over the regional model area (Figure 5-54). They have been defined by identifying all the combinations in the two products described above. The rock domains are identified by different numbers in Figure 5-54.

Table 5-17. Bedrock components that have been used in the modelling procedure.

Rock units defined on the basis of composition and grain size of dominant rock type				
Code (SKB)	Composition	Complementary characteristics		
111058	Granite		Fine- to medium-grained	Group D on SDM version 1.2 geological map
101051	Granodiorite, tonalite and granite	Metamorphic	Fine- to medium-grained	Group C on SDM version 1.2 geological map
111051	Granitoid	Metamorphic		Inferred group B
101058	Granite	Metamorphic	Aplitic	Group B on SDM version 1.2 geological map
111057	Granite (to granodiorite)	Metamorphic, veined to migmatitic		Group B on SDM version 1.2 geological map
101057	Granite (to granodiorite)	Metamorphic	Medium-grained	Group B on SDM version 1.2 geological map
101054 and 101056 combined	Tonalite and granodiorite	Metamorphic		Group B on SDM version 1.2 geological map
101033 and 101004 combined	Diorite, quartz diorite, gabbro and ultramafic rock	Metamorphic		Group B on SDM version 1.2 geological map
103076	Felsic to intermediate volcanic rock	Metamorphic		Group A on SDM version 1.2 geological map
106001	Sedimentary rock	Metamorphic, veined to migmatitic		Group A on SDM version 1.2 geological map
Rock units defined on the basis of degrees of bedrock homogeneity and ductile deformation				
Rock unit	Degree of homogeneity	Degree of ductile deformation		
1	Inhomogeneous	Banded, foliated and lineated (BSL-tectonites).		Inferred higher degree of ductile deformation
2	Inhomogeneous	Lineated and weakly foliated (LS-tectonites).		Inferred lower degree of ductile deformation
3	Homogeneous	Foliated and lineated (SL-tectonites).		Inferred higher degree of ductile deformation
4	Homogeneous	Lineated and weakly foliated (LS-tectonites).		Inferred lower degree of ductile deformation

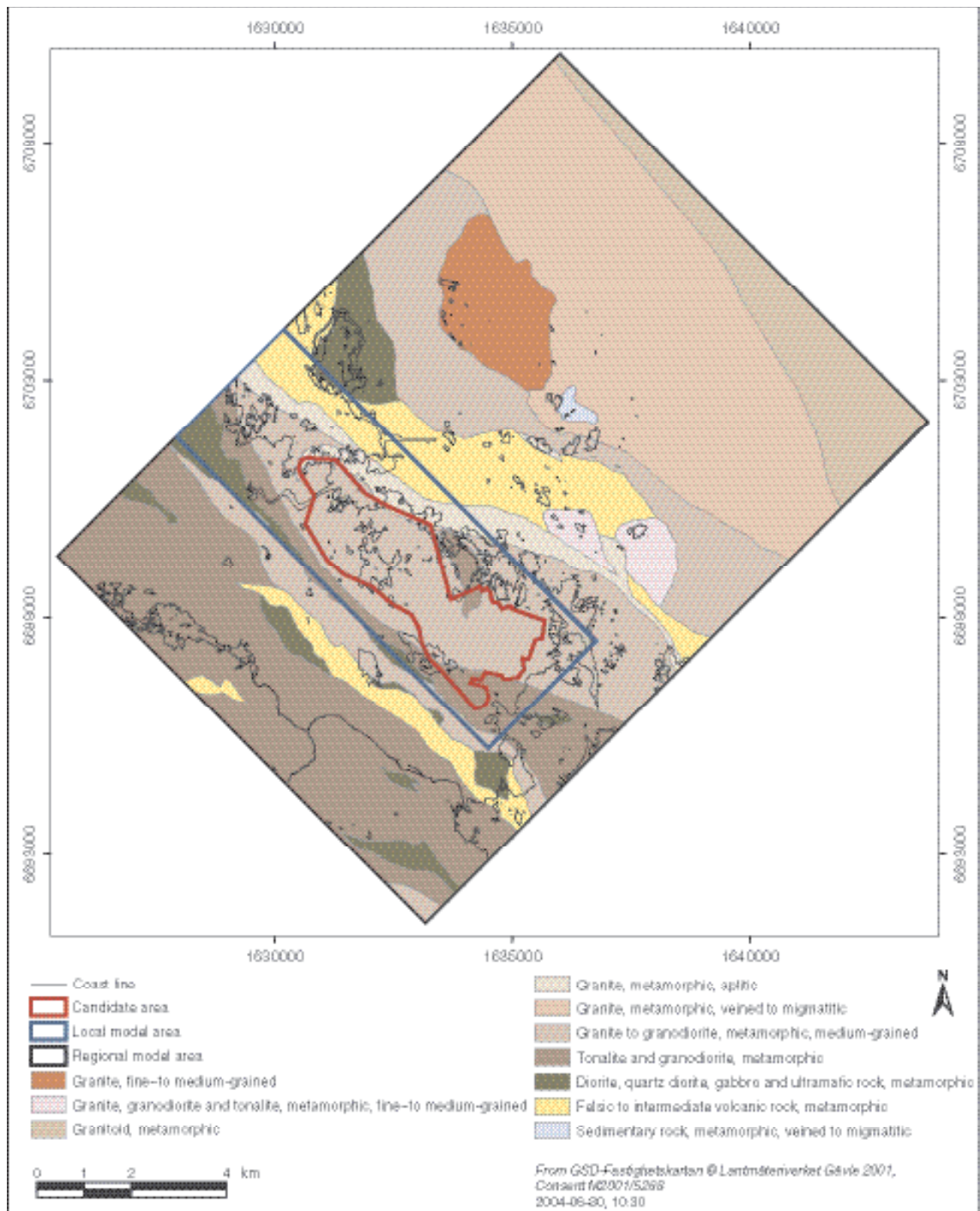


Figure 5-52. Rock units defined by different dominant rock types. Surface view of the regional model volume.

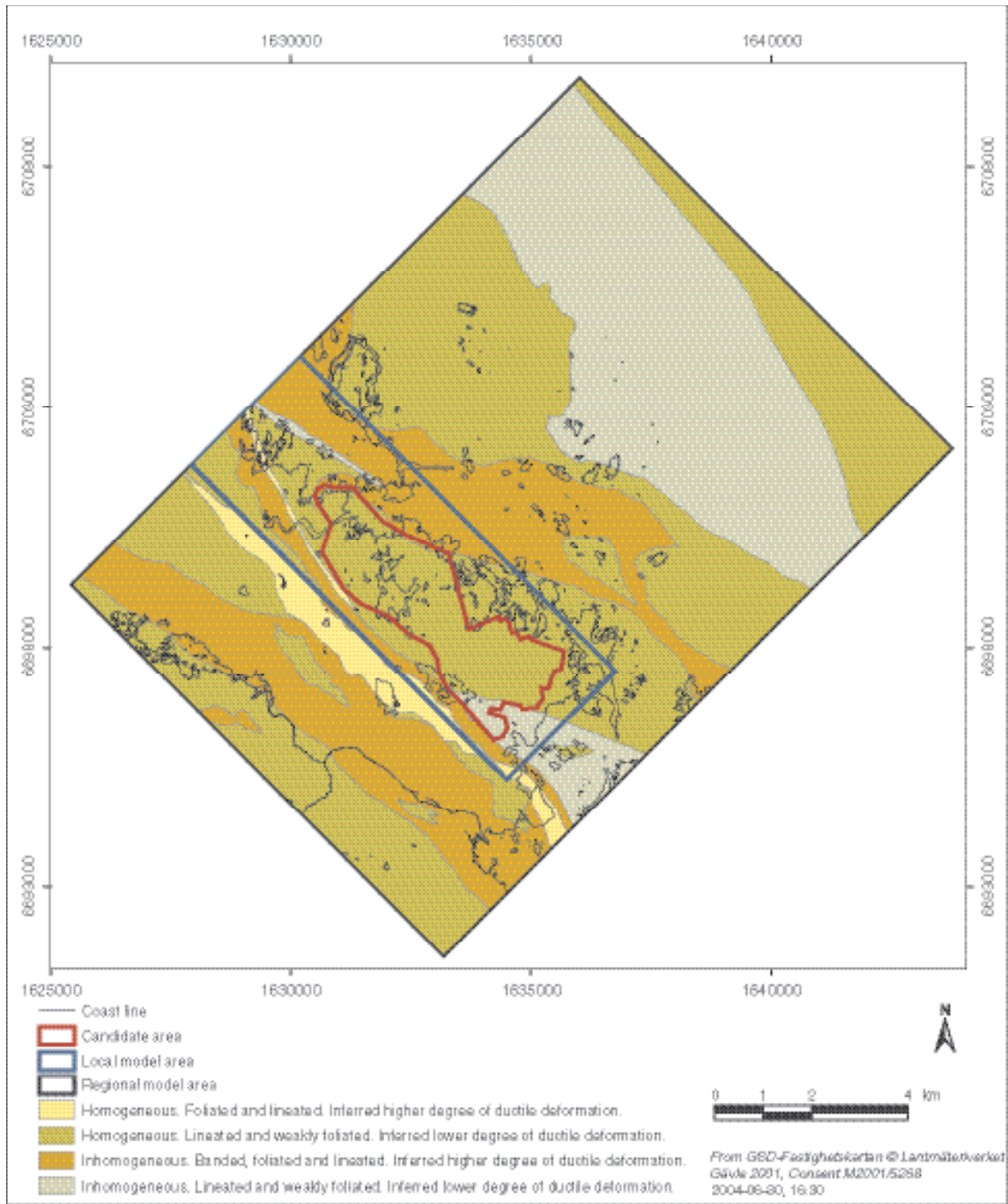


Figure 5-53. Rock units distinguished on the basis of degree of homogeneity and ductile deformation in the bedrock. Surface view of the regional model volume.

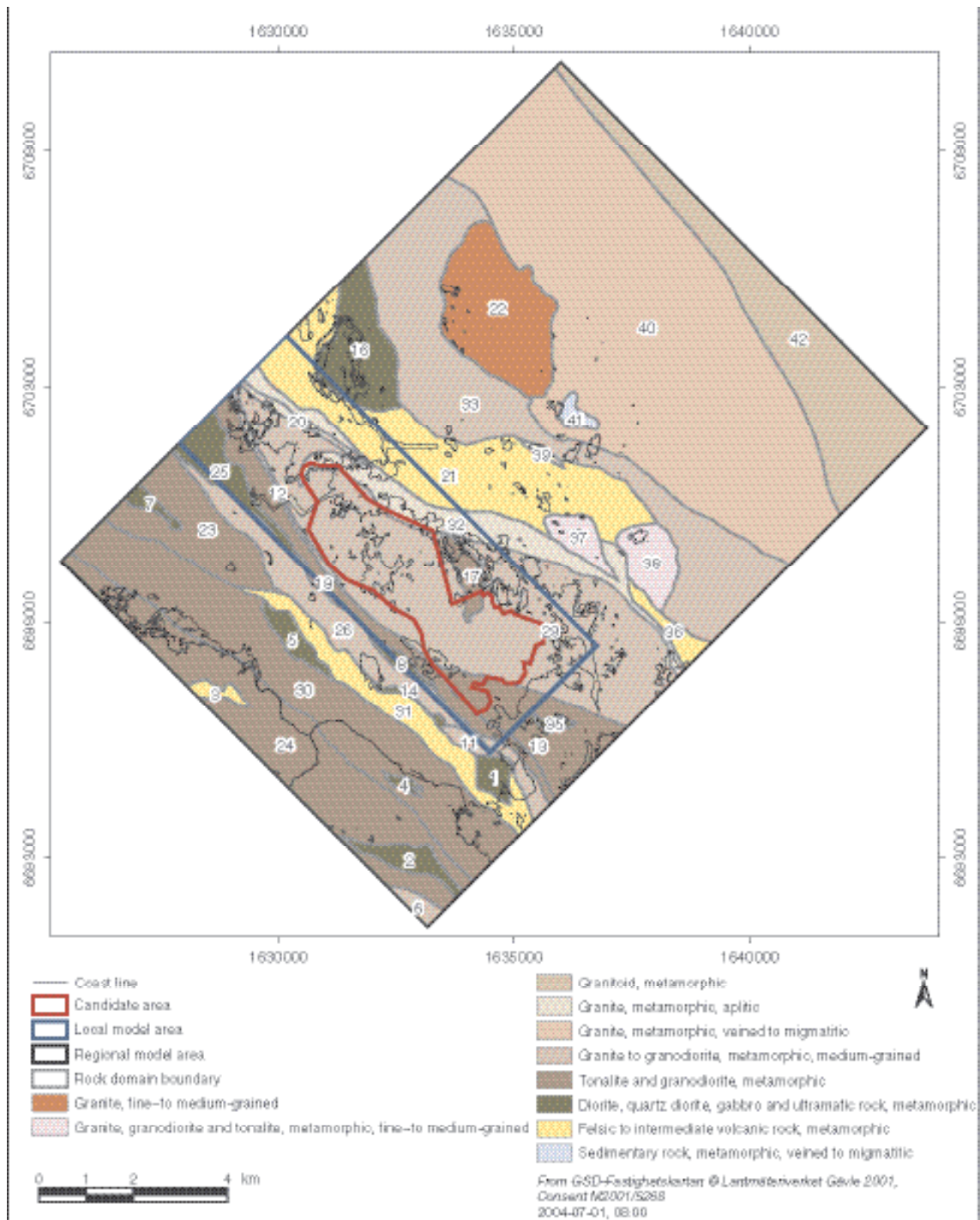


Figure 5-54. Rock domains used in the modelling procedure numbered from 1 to 42. The colours show the rock units that were defined on the basis of dominant rock type. These units are identical to those shown in Figure 5-52. Surface view of the regional model volume.

On this basis, thirty-five rock domains have been identified at the surface in the regional model volume. All these rock domains are identified with the help of unique ID-numbers (RFMxxx). For traceability purposes, the ID-numbers for the rock domains, which are present in model version 1.1 /SKB, 2004a/ but have been omitted in the present model (Table 5-18), have not been used. Furthermore, new rock domains in model version 1.2 have been provided with new ID-numbers (Table 5-18). The rock domain model at the surface resembles that in model version 1.1 for the mainland area (compare Figure 5-54 and Figure 5-6 in /SKB, 2004a/). However, more conspicuous changes have occurred in the coastal area and in the open sea area at Öregrundsgrepen, primarily on account of the results of the bedrock mapping work during 2003.

Inspection of the single hole interpretations (Section 5.2.8) suggests that most of the rock units that have been identified in the boreholes can be included in rock domain RFM029. Other domains are present in parts of cored boreholes KFM03A and KFM04A, in the percussion boreholes HFM09, HFM10, HFM11, HFM12 and HFM18, and in the older cored borehole KFO01 (Table 5-19). These intersections provide sub-surface constraints on the boundaries between rock domains RFM017 and RFM029, RFM012 and RFM029, RFM012 and RFM018, and RFM007 and RFM023.

The final stage in the modelling work concerns the projection of the rock domains that have been recognised at the surface to a depth of –2,100 m, i.e. to the base of the regional model volume. The key assumptions and conceptual model adopted in this procedure have been summarised earlier. An important working component has been to define sub-areas that are structurally and lithologically homogeneous.

Table 5-18. Summary of the changes in rock domains, model versions 1.1 and 1.2.

Rock domains in SDM version 1.1, omitted in SDM version 1.2	Rock domains added in SDM version 1.2
RFM009	RFM035
RFM010	RFM036
RFM015	RFM037
RFM019	RFM038
RFM027	RFM039
RFM028	RFM040
RFM034	RFM041
	RFM042

Table 5-19. Summary of the correlation of rock units and rock domains in boreholes KFM03A, KFM04A, HFM09, HFM10, HFM11, HFM12, HFM18 and KFO01. All other rock units in the single hole interpretations have been included in RFM029.

Borehole	Rock unit	Rock domain
KFM03A	RU1, RU3, RU4, RU5	RFM029
KFM03A	RU2	RFM017
KFM04A	RU1, RU2	RFM018
KFM04A	RU3, RU4, RU5	RFM012
KFM04A	RU6, RU7, RU8	RFM029
HFM09	RU1	RFM018
HFM10	RU1	RFM018
HFM11	RU1, RU2	RFM026
HFM12	RU1	RFM026
HFM18	RU1	RFM017
HFM18	RU2	RFM029
KFO01	0–270.7 m	RFM007
KFO01	270.7–478.3 m	RFM023

The strike and dip of banding and tectonic foliation, the trend and plunge of the mineral stretching lineation, and the trend and plunge of measured fold axes have been assembled on Schmidt, equal area stereographic plots for each domain /Stephens and Forsberg, 2005/. Once again surface data dominate. However, the data from boreholes have also been included. The mean orientations of the planar structures and the mineral stretching lineation and, where relevant, the pole to the best-fit great circle in folded domains have been calculated in the different domains (Table 5-20). These values have then been used to assist in the projection of the various rock domains at depth and to visualise the variation in plunge of the stretching lineation within the rock domains. A view of the rock domain is presented in Figure 5-55.

Table 5-20. Dominant rock type, degree of homogeneity and mean values of the orientation of geological structures that have been used in the projection of rock domains at depth in the 3D-modelling work. The strike and dip of a tectonic foliation/banding are provided with the help of the right-hand-rule method, i.e. 108/75 = N72W/75SW.

Rock domain ID	Dominant rock type (SKB code)	Degree of homogeneity	Strike and dip of tectonic foliation/banding (mean orientation)	Trend and plunge of mineral stretching lineation (mean orientation)	Comment
RFM001	Ultramafic rock, metamorphic (101004)	High	No data	No data	Extension to base of model.
RFM002	Diorite, quartz diorite and gabbro, metamorphic (101033)	High	Dip 77	124/36	Extension to base of model. Dip from RFM006.
RFM003	Felsic to intermediate volcanic rock, metamorphic (103076)	Low	108/75	136/40	Extension to base of model.
RFM004	Ultramafic rock, metamorphic (101004)	High	No data	No data	Extension to base of model.
RFM005	Diorite, quartz diorite and gabbro, metamorphic (101033)	High	136/89	137/41	Extension to base of model.
RFM006	Granite (to granodiorite), metamorphic (101057)	High	127/77	143/44	Extension to base of model.
RFM007	Diorite, quartz diorite and gabbro, metamorphic (101033)	High	No data	147/34	Extension to base of model. 0–270.7 m in KFO01.
RFM008	Diorite, quartz diorite and gabbro, metamorphic (101033)	High	133/82	137/41	Extension to base of model.
RFM011	Granite (to granodiorite), metamorphic (101057)	High	Variable	141/46	Extension to base of model.
RFM012	Granite (to granodiorite), metamorphic (101057)	High	139/79 (surface data and data from KFM04A)	155/37 (surface data)	Extension to base of model. 177–500 m in KFM04A.
RFM013	Tonalite to granodiorite, metamorphic (101054)	Low	112/57 (undulating)	144/36	Extension to base of model.
RFM014	Diorite, quartz diorite and gabbro, metamorphic (101033)	High	No data	145/41	Extension to base of model.

Rock domain ID	Dominant rock type (SKB code)	Degree of homogeneity	Strike and dip of tectonic foliation/ banding (mean orientation)	Trend and plunge of mineral stretching lineation (mean orientation)	Comment
RFM016	Diorite, quartz diorite and gabbro, metamorphic (101033)	High	344/74 (undulating) Pole to best-fit great circle is 124/64	163/27	Extension to base of model. Pole to best-fit great circle from RFM021 (northern part).
RFM017	Tonalite to granodiorite, metamorphic (101054)	High	Pole to best-fit great circle is 126/23 (surface data and data from KFM03A)	134/32 (surface data)	No extension to base of model. Thins out to the south-east. 220–293 m in KFM03A and 9–30 m in HFM18.
RFM018	Tonalite to granodiorite, metamorphic (101054)	Low	141/81 (surface data and data from KFM04A)	143/35 (surface data)	Extension to base of model. 0–177 m in KFM04A.
RFM020	Granite, metamorphic, aplitic (101058)	Low	120/84	123/40	Extension to base of model.
RFM021 (northern part)	Felsic to intermediate volcanic rock, metamorphic (103076)	Low	Pole to best-fit great circle is 124/64	Few data, variable	Extension to base of model. Fisher mean value of fold axes is 134/58.
RFM021 (southern part)	Felsic to intermediate volcanic rock, metamorphic (103076)	Low	127/83	127/30 (variable plunge)	Extension to base of model. Fisher mean value of fold axes is 136/37.
RFM022	Granite, fine- to medium-grained (111058)	High	319/72 (few data and uncertain geological significance)	137/22	No extension to base of model. Laccolithic shape.
RFM023	Tonalite to granodiorite, metamorphic (101054)	High	Variable	144/33	Extension to base of model. 270.7–478 m in KFO01.
RFM024	Tonalite to granodiorite, metamorphic (101054)	High	118/73	131/38	Extension to base of model. RFM030 steers contact between RFM024 and RFM030.
RFM025	Diorite, quartz diorite and gabbro, metamorphic (101033)	High	146/88	145/42	Extension to base of model.
RFM026	Granite (to granodiorite), metamorphic (101057)	High	138/87	139/41	Extension to base of model.
RFM029	Granite (to granodiorite), metamorphic (101057)	High	Pole to best-fit great circle is 143/45 (surface data) Pole to best-fit great circle is 163/41 (data from KFM01A, KFM01B, KFM02A, KFM03A, KFM03B, KFM04A) Pole to best-fit great circle is 154/45 (all surface and borehole data)	142/38 (surface data)	Extension to base of model.

Rock domain ID	Dominant rock type (SKB code)	Degree of homogeneity	Strike and dip of tectonic foliation/ banding (mean orientation)	Trend and plunge of mineral stretching lineation (mean orientation)	Comment
RFM030	Tonalite to granodiorite, metamorphic (101054)	Low	126/81	136/40	Extension to base of model.
RFM031	Felsic to intermediate volcanic rock, metamorphic (103076)	Low	131/85	139/41	Extension to base of model.
RFM032 (whole domain)	Granite, metamorphic, aplitic (101058)	Low	Pole to best-fit great circle is 126/65	118/37	Extension to base of model.
RFM032 (eastern part)	Granite, metamorphic, aplitic (101058)	Low	135/84	No data	Extension to base of model.
RFM033	Granite (to granodiorite), metamorphic (101057)	High	Few data and variable	129/24	Extension to base of model.
RFM035	Diorite, quartz diorite and gabbro, metamorphic (101033)	High	No data	137/32 (few data)	Extension to base of model.
RFM036	Felsic to intermediate volcanic rock, metamorphic (103076)	Low	No data	No data	Extension to base of model. Use structural data from RFM032 (eastern part).
RFM037	Granodiorite, tonalite and granite, metamorphic, fine- to medium-grained (101051)	High	Few data and variable	129/25	Extension to base of model. Use structural data from RFM021 (southern part).
RFM038	Granodiorite, tonalite and granite, metamorphic, fine- to medium-grained (101051)	High	Few data and variable	126/24	Extension to base of model. Use structural data from RFM021 (southern part).
RFM039	Granite, metamorphic, aplitic (101058)	Low	303/81 (few data)	133/29	Extension to base of model. Fisher mean value of fold axes is 128/26.
RFM040	Granite (to granodiorite), metamorphic, veined to migmatitic (111057)	Low	Few data	123/32	Extension to base of model, Fisher mean value of fold axes is 126/27.
RFM041	Sedimentary rock, metamorphic, veined to migmatitic (106001)	Low	Few data	122/29	Extension to base of model. Fisher mean value of fold axes is 116/30.
RFM042	Granitoid, metamorphic (111051)	High	No data	No data	Extension to base of model.

The data from rock domain RFM029, which forms a major part of the candidate volume, indicate large-scale folding of the tectonic foliation with a fold axis that plunges moderately to the south-east, parallel to the mineral stretching lineation /Stephens and Forsberg, 2005/. The results naturally mimic those obtained for sub-area central that includes the candidate area (Figure 5-25). Structural data from the adjacent rock domain RFM032, which lies partly embedded in a major fold structure within rock domain RFM029 (Figure 5-55), show a similar pattern. The pole to the best-fit great circle in this domain has a trend and plunge of 126/65° /Stephens and Forsberg, 2005/. This value has been used to construct the downward projection of the fold structure in RFM032 (Figure 5-55).

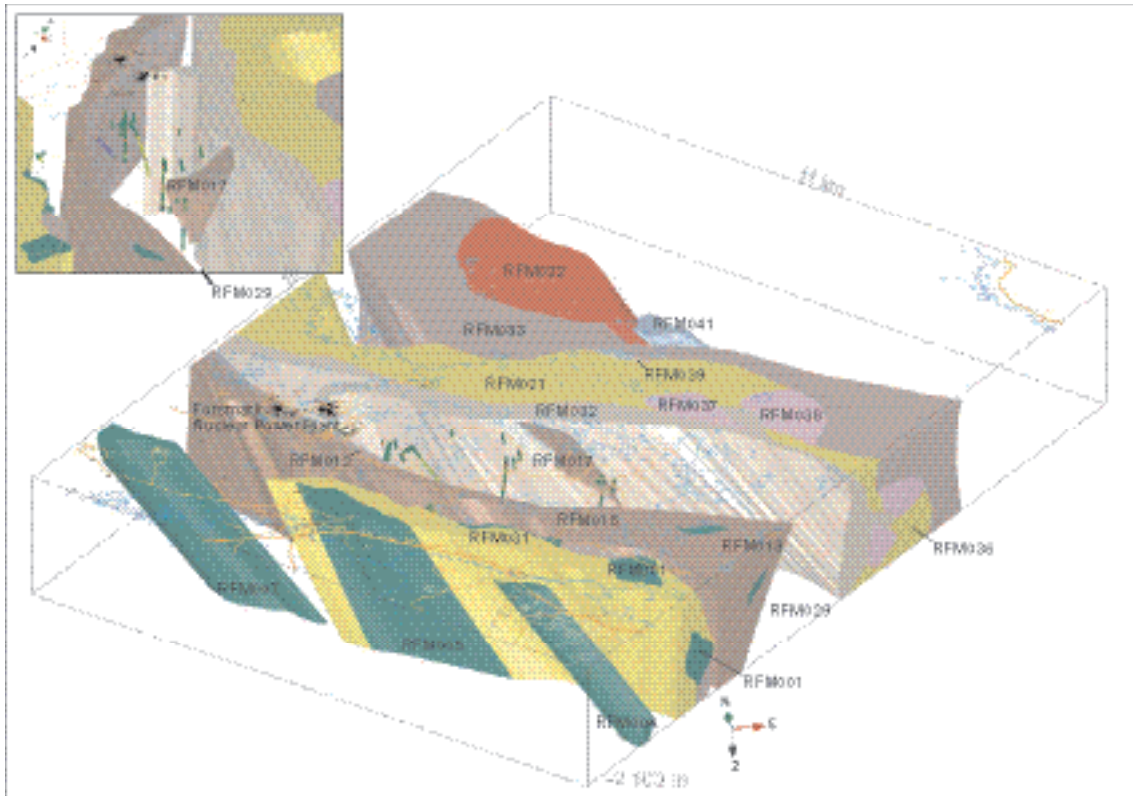


Figure 5-55. a) Rock domain model, version 1.2, viewed to the north. Rock domain RFM029 is unshaded in order to show the major folding within the tectonic lens at the Forsmark site. Other domains are unshaded in order to show the modelled, south-eastern elongation of several domains. The dominant rock type in each domain is illustrated with the help of different colours (see Figure 5-54). Boreholes are also shown. b) Detailed view of the tectonic lens and rock domain RFM029 within which most of the boreholes are situated. Note the drilling through rock domains RFM017 and RFM029 (KFM03A) and RFM018, RFM012 and RFM029 (KFM04A).

The structural data from the rock domains RFM012 and RFM018, which are situated immediately south-west of the candidate area, are considerably more homogeneous. As expected, the results are similar to those observed in sub-area south-west (Figure 5-25). The planar structures strike in a north-west direction and dip steeply to the south-west, and the linear structures plunge moderately to the south-east (Figure 5-55).

Property assignment

Each rock domain has been assigned a list of properties (Table 5-21) that includes, for example, the dominant and subordinate rock types in the domain. The dominant rock type and the degree of homogeneity in each domain are shown in Table 5-20. Key properties (Table 5-22) have also been assigned to the dominant rock type in each domain. The range, mean and standard deviation values as well as the number of samples analysed are provided for each property and rock type. These values have been extracted from Table 5-2, Table 5-3 and Table 5-4 (see Section 5.2.1). The quantitative estimates or qualitative assignment of the properties of all the thirty-five domains are listed in tabular format in Appendix 1. The basis for the estimation of a particular property in each domain is also provided in these tables.

Table 5-21. Properties assigned to each rock domain.

Property
Rock domain ID. RFM, according to the nomenclature recommended by SKB.
Dominant rock type. Quantitative proportion only for RFM012 and RFM029.
Subordinate rock types. Quantitative proportions only for RFM012 and RFM029.
Degree of homogeneity.
Metamorphism/alteration.
Mineral fabric. Type and orientation with Fisher mean and K value. Orientation according to right-hand-rule method.

Table 5-22. Properties assigned to the dominant rock type in each domain.

Property
Mineralogical composition (%). Only the dominant minerals are listed. Range/mean/standard deviation/number of samples.
Grain size (classification according to SGU).
Age (million years). Range or value and 95% confidence interval.
Structure.
Texture.
Density (kg/m ³). Range/mean/standard deviation/number of samples.
Porosity (%), Range/mean/standard deviation/number of samples.
Magnetic susceptibility (SI units). Range/mean/standard deviation/number of samples.
Electric resistivity in fresh water (ohm m). Range/mean/standard deviation/number of samples.
Uranium content based on gamma ray spectrometry data (ppm). Range/mean/standard deviation/number of samples.
Natural exposure rate (microR/h). Range/mean/standard deviation/number of samples.

Critical properties for, for example, thermal modelling work are the mineralogical composition and the proportions of different rock types in the various domains. The mineralogical composition of the various rock types is provided in the property tables (Appendix 1). It has been possible to estimate qualitatively the relative amounts of the different rock types in each domain from the outcrop database (see Section 5.2.1). For example, in rock domain RFM029, the lithology that forms the dominant rock type in over 75% of the outcrops that have been studied (488) is a medium-grained, metamorphosed granite to granodiorite (Figure 5-56). In over 100 outcrops, this lithology is the only rock type that has been recorded (Figure 5-56). However, pegmatitic granite and pegmatite, amphibolite, metamorphosed aplitic granite, and various finer-grained, younger granitoids that show variable effects of metamorphism form common, yet subordinate rock types (Figure 5-56). Similar qualitative information concerning the proportions of dominant and subordinate rock types in most of the remaining rock domains are presented in /Stephens and Forssberg, 2005/.

It has only been possible to estimate quantitatively the proportions of different rock types in rock domains RFM012 and RFM029 using data from the cored boreholes (Table 5-23). Borehole intersections for these two domains are assumed to be sufficiently long to provide such estimates. It is important to keep in mind that rock occurrences that are less than 1 m in borehole length have not been included in the present analysis. This procedure will be modified in future modelling work. Nevertheless, these data conform well to the qualitative surface estimates. The borehole intersections in rock domains RFM007, RFM017, RFM018, RFM023 are too short to provide reliable quantitative estimates.

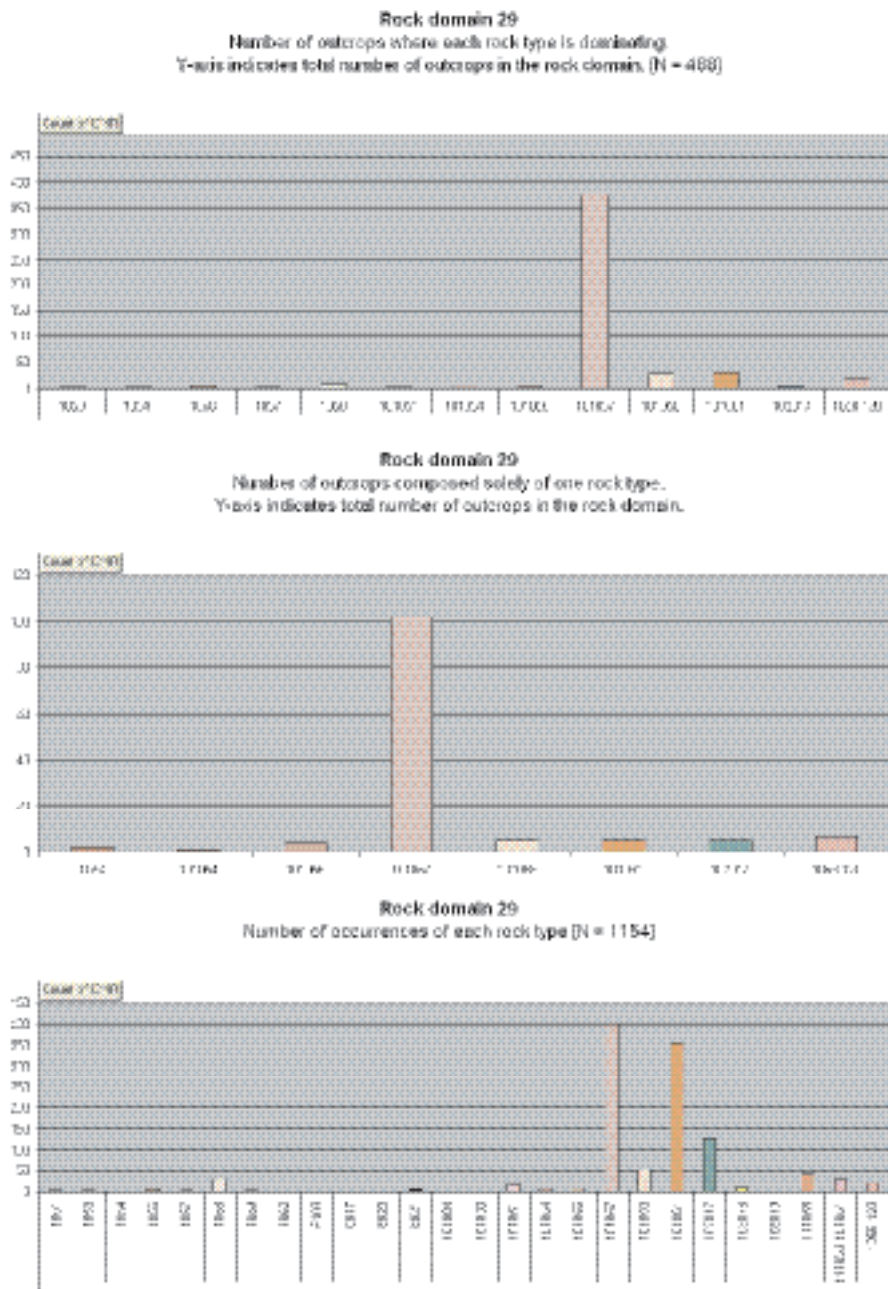


Figure 5-56. Qualitative assessment of dominant and subordinate rock types in rock domain RFM029 based on surface outcrop data. The translation of the rock codes to rock type is provided in Appendix 2.

Table 5-23. Quantitative estimates of the proportions of different rock types in RFM012 and RFM029. Rock occurrences that are less than 1 m in borehole length have not been included in the calculations.

Code (SKB)	Composition and grain size	RFM012 (rock domain directly to the south-west of RFM029)	RFM029 (major part of candidate volume)
101057	Granite (to granodiorite), metamorphic, medium-grained	68%	84%
101051	Granodiorite, tonalite and granite, metamorphic, fine- to medium-grained	24%	10%
102017	Amphibolite	2%	3%
101061	Pegmatitic granite, pegmatite	4%	2%
111058	Granite, fine- to medium-grained	No occurrence > 1 m	1%
103076	Felsic to intermediate volcanic rock, metamorphic	2%	No occurrence > 1 m

5.3.4 Evaluation of uncertainties

The variation in the quality of the surface geological data over the regional model area (see Section 5.2.1) is an important source of uncertainty in the modelling procedure. Relative to model version 1.1, this problem has been reduced dramatically south-west of road 76 and in the coastal area north-east of the candidate area, because the new data from the outcrop mapping 2003 have been incorporated in the compilation of the revised bedrock geological map. However, uncertainties at Öregrundsgrepen and in the areas between the islands close to the coast will remain throughout the site investigation programme.

An important uncertainty concerns the location of the boundaries between the rock units that have been defined on the basis of composition and grain size, and the rock units that have been defined on the basis of degree of homogeneity and degree of ductile deformation. High outcrop frequency and access to the new airborne, geophysical data (see Sections 5.2.1, 5.2.2 and 5.2.3) are two factors that help to reduce the uncertainty in the definition of these boundaries on the bedrock geological map. This uncertainty is of special significance where it concerns the position of the rock unit boundaries in the north-western and south-easternmost parts of the candidate area, i.e. under Asphällsfjärden, between the nuclear power plant and Bolundsfjärden, and around Storskäret. There also remains an uncertainty concerning the actual occurrence of a rock domain since, in some cases, data are completely absent, e.g. rock domain RFM042 at Öregrundsgrepen, or are limited in extent, e.g. rock domains RFM022, RFM033, RFM040 and RFM041.

Since the three-dimensional projection of the rock domain boundaries at depth has predominantly made use of structural data from surface outcrops, there remain uncertainties concerning the extension of rock domains to a depth of –2,100 m. Considerable compositional and structural data exist at depth in rock domain RFM029, but only down to c. 1,000 m. Furthermore, lineation data are lacking. Limited borehole information is available from rock domains RFM007, RFM012, RFM017, RFM018 and RFM023 but such data are totally lacking in the other rock domains. This problem will remain throughout the site investigation programme for most of the rock domains. Future reduction of this uncertainty may be obtained by modelling of airborne or ground geophysical data.

With the above considerations in mind, a judgement has been carried out to assess, at least qualitatively, the confidence in the occurrence and geometry of the thirty-five rock domains (Table 5-24). Confidence is generally expressed at three levels, “high”, “medium” and “low”. The confidence level referred to as “very low” has been used for the down-dip extension of the rock domain RFM042 at Öregrundsgrepen where information, even at the surface, is totally lacking.

Table 5-24. Table of confidence for the occurrence and geometry of rock domains.

Domain ID	Basis for interpretation	Confidence at the surface	Confidence at a depth of -2,100 m
RFM001	Surface data (29 observed outcrops, airborne magnetic data), bedrock geological map SDM version 1.2	High	Medium
RFM002	Surface data (27 observed outcrops, airborne magnetic data), bedrock geological map SDM version 1.2	High	Medium
RFM003	Surface data (17 observed outcrops, airborne magnetic data), bedrock geological map SDM version 1.2	High	Medium
RFM004	Surface data (8 observed outcrops, airborne magnetic data), bedrock geological map SDM version 1.2	High	Medium
RFM005	Surface data (21 observed outcrops, airborne magnetic data), bedrock geological map, SDM version 1.2	High	Medium
RFM006	Surface data (21 observed outcrops, airborne magnetic data), bedrock geological map, SDM version 1.2	High	Medium
RFM007	Surface data (18 observed outcrops, airborne magnetic data), bedrock geological map, SDM version 1.2, borehole data from KFO01	High	Medium
RFM008	Surface data (11 observed outcrops, airborne magnetic data), bedrock geological map, SDM version 1.2	High	Medium
RFM011	Surface data (17 observed outcrops, airborne magnetic data), bedrock geological map, SDM version 1.2	High	Medium
RFM012	Surface data (7 observed outcrops, airborne magnetic data), borehole data from KFM04A, borehole data), bedrock geological map, SDM version 1.2, predominantly shallow borehole data close to nuclear power plant 3, borehole data from KFM04A	High	Medium
RFM013	Surface data (45 observed outcrops, airborne magnetic data), bedrock geological map, SDM version 1.2	High	Medium
RFM014	Surface data (8 observed outcrops, airborne magnetic data), bedrock geological map, SDM version 1.2	High	Medium
RFM016	Surface data (60 observed outcrops, airborne magnetic data), bedrock geological map, SDM version 1.2	High	Medium
RFM017	Surface data (40 observed outcrops, airborne magnetic data), bedrock geological map, SDM version 1.2, borehole data from HFM18 and KFM03A	High	High
RFM018	Surface data (99 observed outcrops, airborne magnetic data), bedrock geological map, SDM version 1.2, predominantly shallow borehole data close to nuclear power plant 3, borehole data from HFM09, HFM10 and KFM04A	High	Medium
RFM020	Surface data (7 observed outcrops, airborne magnetic data), bedrock geological map, SDM version 1.2, data along tunnels 1-2 and 3, shallow borehole data close to tunnels 1-2 and 3	High	Medium
RFM021	Surface data (98 observed outcrops, airborne magnetic data), bedrock geological map, SDM version 1.2, data along tunnels 1-2, 3 and SFR, shallow borehole data close to tunnels 1-2, 3 and SFR	High	Medium
RFM022	Surface data (18 observed outcrops, airborne magnetic data), bedrock geological map, SDM version 1.2	High	Medium
RFM023	Surface data (77 observed outcrops, airborne magnetic data), bedrock geological map, SDM version 1.2, borehole data from KFO01	High	Medium
RFM024	Surface data (228 observed outcrops, airborne magnetic data), bedrock geological map, SDM version 1.2	High	Medium
RFM025	Surface data (43 observed outcrops, airborne magnetic data), bedrock geological map, SDM version 1.2	High	Medium
RFM026	Surface data (144 observed outcrops, airborne magnetic data), bedrock geological map, SDM version 1.2, borehole data from HFM11 and HFM12	High	Medium

Domain ID	Basis for interpretation	Confidence at the surface	Confidence at a depth of -2,100 m
RFM029	Surface data (488 observed outcrops, airborne magnetic data), bedrock geological map, SDM version 1.2, data along tunnels 1-2 and 3, shallow borehole data close to nuclear power plant 1-2, barrack area and tunnels 1-2 and 3, borehole data from HFM01-08, HFM13-19, KFM01A, KFM01B, KFM02A, KFM03A, KFM03B, KFM04A and KFM05A	High	High (down to 1,000 m), medium (below 1,000 m)
RFM030	Surface data (274 observed outcrops, airborne magnetic data), bedrock geological map, SDM version 1.2	High	Medium
RFM031	Surface data (129 observed outcrops, airborne magnetic data), bedrock geological map, SDM version 1.2	High	Medium
RFM032	Surface data (99 observed outcrops, airborne magnetic data), bedrock geological map, SDM version 1.2, data along tunnels 1-2 and 3, shallow borehole data close to tunnels 1-2 and 3	High	Medium
RFM033	Surface data (18 observed outcrops, airborne magnetic data), bedrock geological map, SDM version 1.2	Medium	Low
RFM035	Surface data (6 observed outcrops, airborne magnetic data), bedrock geological map, SDM version 1.2	High	Medium
RFM036	Surface data (2 observed outcrops, airborne magnetic data), bedrock geological map, SDM version 1.2	Medium	Low
RFM037	Surface data (17 observed outcrops, airborne magnetic data), bedrock geological map, SDM version 1.2	Medium	Low
RFM038	Surface data (9 observed outcrops, airborne magnetic data), bedrock geological map, SDM version 1.2	Medium	Low
RFM039	Surface data (9 observed outcrops, airborne magnetic data), bedrock geological map, SDM version 1.2	Medium	Low
RFM040	Surface data (13 observed outcrops, airborne magnetic data), bedrock geological map, SDM version 1.2	Medium	Low
RFM041	Surface data (9 observed outcrops, airborne magnetic data), bedrock geological map, SDM version 1.2	Medium	Low
RFM042	Bedrock geological map, SKB report PR D-96-016 and SDM version 0	Low	Very low

The information concerning the properties of the different rock domains (Table 5-21) once again arises primarily from the surface outcrop data (see Section 5.2.1). Sub-surface data are only available for a limited number of rock domains. Although it has been possible to estimate from the surface data, in a qualitative manner, the relative importance of the different rock types in a specific domain, quantitative estimates of the proportions are generally lacking. Bearing in mind this data deficiency, there exists an incomplete property characterisation for most of the domains. However, since quantitative estimates of these proportions are available from borehole data for rock domains RFM012 and RFM029, the uncertainty is of limited significance for the candidate volume and its immediate margin to the south-west.

The range, mean and standard deviation values of the properties of most rock types (Table 5-22) are available (see Section 5.2.1). There remain uncertainties concerning the properties of the rock types referred to as “granite to granodiorite, metamorphic, veined to migmatitic” (SKB code 111057), “sedimentary rock, metamorphic, veined to migmatitic” (SKB code 106001) and “granitoid, metamorphic” (SKB code 111051). No data are available for these rock types, which dominate in rock domains RFM040, RFM041 and RFM042, respectively. However, since these domains are situated in the marginal parts of the regional model area, this uncertainty is judged to be of little significance.

5.4 Deterministic deformation zone modelling

5.4.1 Modelling assumptions and input from other disciplines

The work connected with the establishment of deterministic, deformation zone models for the Forsmark site has made use of:

- The summary of the geology at the nuclear power plant and at SFR in /Carlsson and Christiansson, 1987/.
- The deformation zone models for SFR /Axelsson and Hansen, 1997; Holmén and Stigsson, 2001/.
- The deformation zone models that were presented in model version 0 /SKB, 2002a/ and model version 1.1 /SKB, 2004a/.
- The identification and brief description of inferred deformation zones in the single hole interpretation of the cored and percussion boreholes (see Section 5.2.8).
- The fracture orientation sets and their truncation relationships that have been identified in the DFN modelling work (see Section 5.5).
- Data bearing on the frequency, orientation and mineral filling of fractures in the deformation zones as recognised in the single hole interpretation. Where necessary, attention has also been focused on ductile structural data along these zones. These data come from the geological mapping of the boreholes (see Section 5.2.6).
- Data from the few ductile and brittle deformation zones that are exposed at the surface (see Section 5.2.4).
- The interpretation of reflection seismic data (see Section 5.2.5) and a correlation of reflectors with the single hole interpretations in the cored boreholes KFM01A, KFM02A and especially KFM03A (see Section 5.2.8).
- The interpretation of linked lineaments (see Section 5.2.3) and the relationship of these lineaments to ground EM (slingram) anomalies and low velocity, refraction seismic anomalies (see Section 5.2.5).
- Geochronological data at the Forsmark site and their relationship to the bedrock geological evolution in the central part of Sweden (see Section 3.1).

The modelling work has primarily addressed deformation zones that are inferred to be 1,000 m or longer, i.e. local major and regional deformation zones according to the terminology of /Andersson et al. 2000a/. Some local minor zones are also included. Only models for the regional model volume are presented. Gently dipping zones have been detected by an integration of data from boreholes and tunnels with the interpretation of seismic reflectors. By contrast, vertical and steeply dipping zones have been recognised by an integration of data from boreholes, tunnels and the surface with the interpretation of lineaments. The consequences of variable data resolution inside the regional model volume are addressed in connection with the presentation of alternative models (see Section 5.4.2).

The gently dipping zones are assumed to truncate, both along their strike and in the down-dip direction, against a limited number of regional or local major, vertical and steeply dipping zones. In the working conceptual model, the vertical and steeply dipping zones have a higher order of importance in the structural hierarchy (see Section 5.4.2). Such considerations have also steered the truncation relationships between some individual, gently dipping zones. This procedure has resulted in a number of splay patterns.

In the cases where a deformation zone that is observed in a borehole is inferred to correspond at the surface to a linked lineament, the strike of the zone is assumed to be the same as the trend of the matching lineament. On the basis of structural data from borehole and tunnel intersections, these zones are vertical or steeply dipping. Bearing in mind this observation, the dip of other deformation zones that are related to lineaments but lack information on their dip is assumed to be 90°. The surface length of the vertical and steeply dipping zones that correspond to linked lineaments is determined from the length of the matching lineament. The along-strike truncation of such zones is also determined by the lineament pattern.

A truncation relationship for the vertical and steeply dipping zones in the down-dip-direction is determined by their inferred order of importance in the working conceptual model (see Section 5.4.2). The deformation zones that are not truncated at depth by an adjacent zone are extended in a down-dip direction according to the procedure outlined in Table 5-25. This procedure assumes a relationship between the length of the lineament at the surface and its extension at depth. It has been applied especially to the deformation zones that are related solely to linked lineaments at the surface and that have been modelled with a dip of 90°. An inherent consequence of this procedure is that the frequency of such deformation zones decreases with depth. The degree of reduction is related to the negative correlation between the size and the frequency of lineaments that are inferred to represent deformation zones (see Section 5.5).

Table 5-25. Relationship between length of a zone at the surface and its down-dip extension.

Classification	Length at the surface	Truncation at depth
Local minor zone	< 1,000 m	1,100 m
Local major zone	1,000–1,550 m	1,275 m
Local major zone	1,550–2,100 m	1,825 m
Local major and regional zones	> 2,100 m, i.e. longer than the depth of the regional model volume	Base of regional model volume

The modelling of deterministic deformation zones is an important base input to the other disciplines in the site descriptive modelling work. However, a feedback from the work carried out in connection with the establishment of, particularly, the hydrogeological and rock mechanics models has assisted or potentially can assist with the establishment of the structural geological model for the site. Information that addresses the hydraulic contact between some of the inferred deformation zones has already provided support for the modelling of these zones. This support is especially relevant for some of the gently dipping structures. Consideration of the present day orientation of principal stress axes in the bedrock and the stress distribution in the model volume can also potentially provide greater confidence for a particular deformation zone model.

5.4.2 Conceptual model and alternative geometric models

Three observations motivate the establishment of alternative deformation zone models for the site.

- There is a major variation in the resolution of different data sets over the regional model volume. In particular, data at depth from especially boreholes are only available within and close to the candidate area. Reflection seismic data are also restricted to the candidate area.
- There is an uncertainty concerning the extension of the gently dipping zones, both in the down-dip and especially the along-strike directions.
- There is an uncertainty concerning the geological significance and, to a less extent, even the identification of lineaments.

Three models for deterministic deformation zones have been developed that are referred to as the base model, the base model variant, and the alternative model. The conceptual basis for these three models, as described below, is identical. However, these models adopt different strategies for the gently dipping zones, and for the vertical and steeply dipping zones, bearing in mind the three observations listed above.

In essence, the difference between the base model and the base model variant concerns the extension of four gently dipping zones. Furthermore, the difference between the base model (and its variant) and the alternative model concerns how lineaments have been handled in the different models (see Section 5.4.3). In essence, there are far more vertical and steeply dipping zones in the alternative model compared to that in the base model (and its variant). Zones that are based solely on the interpretation of seismic reflectors or lineaments as well as comparison studies, i.e. lack direct data in the form of, for example, borehole intersections, have been graded with medium or low confidence in all three models.

Four sets of deformation zones, all of which are associated with oxidised bedrock that contains a fine-grained hematite dissemination, have been recognised in the regional model volume.

- Vertical and steeply, SW-dipping deformation zones that strike WNW-NW, that contain mylonites, cataclastic rocks and cohesive crush breccias, and that are dominated by sealed fractures. These zones initiated their development in the ductile regime but continued to be active as faults in the brittle regime, i.e. they are composite structures. On the basis of their length, both regional and local major zones are present. The model also includes one local minor zone, which has been recognised with high confidence, as well as subordinate zone segments that are situated close to and are attached to regional and local major zones. These segments are both local minor and local major in character.
- Vertical and steeply dipping deformation zones that strike NE and are also dominated by sealed fractures with the development of cohesive crush breccias. These zones formed in the brittle regime and length estimates indicate that regional zones are absent. Several local major zones and two local minor zones, which have been recognised with high confidence, have been modelled. Furthermore, the model includes two subordinate zone segments that are local minor in character, and are situated close to and are attached to two local major zones. A zone that does not extend to the surface has also been included.
- Vertical and steeply dipping deformation zones that strike NS and are also dominated by sealed fractures. These zones formed in the brittle regime and length estimates indicate again that regional zones are absent. On the basis of their low frequency of occurrence, the NS set is judged to be of lower significance in the regional model volume, relative to the other three sets. Furthermore, with the exception of one local minor zone, which has been identified with medium confidence, all zones have been recognised with low confidence. Relative to the other three sets, there is a far higher degree of uncertainty concerning the existence of deformation zones in this set.
- Gently SE- and S-dipping deformation zones that formed in the brittle regime and that, relative to the other sets, contain a higher frequency of open fractures and incoherent fault breccias. Length estimates indicate that regional zones are absent. However, on account of truncation or their gentle dip, several zones fail to reach the surface inside the regional model volume and, for this reason, estimates of length are lacking.

In summary, three sets of deformation zones with distinctive orientations (WNW-NW, NE and gently dipping), each of which contains zones with a high confidence of occurrence, are recognised. This is in good agreement with the structural models for SFR (Figure 5-57). Attention is focused on these three sets in the development of a conceptual model for the site.

Several properties of the deformation zones (see Section 5.4.3) and the geochronological data (see Section 3.1) help to define a working conceptual model:

- Fractures that belong to the NW, NE, gently dipping and even NS orientation sets, as defined in the DFN model (see Section 5.5), are present along individual zones in each of the three major sets of deformation zones (see /Stephens and Forssberg, 2005/).
- Fractures that are coated or sealed by chlorite and calcite occur in all the deformation zones that belong to the WNW-NW, NE and gently dipping sets. Furthermore, epidote and quartz are present along fractures in at least one of the deformation zones in each of these sets (see /Stephens and Forssberg, 2005/).
- Low-temperature mylonites and the occurrence of epidote in fracture fillings, which formed at temperatures under c. 500–550°C, characterise the WNW-NW set. Laumontite and, to a lesser extent prehnite, which formed at temperatures under c. 250°C and c. 300–350°C, respectively, characterise the fractures in the NE set. Clay minerals are present along fractures in many of the gently dipping zones. Furthermore, asphaltite has been recognised above c. 100 m along fractures in one of these zones (ZFMNE00A2).
- Outcrop and tunnel investigations (see Section 5.2.4) indicate that the Singö and Eckarfjärden deformation zones (ZFMNW0001 and ZFMNW003A, respectively) were active under different metamorphic conditions at different time periods.

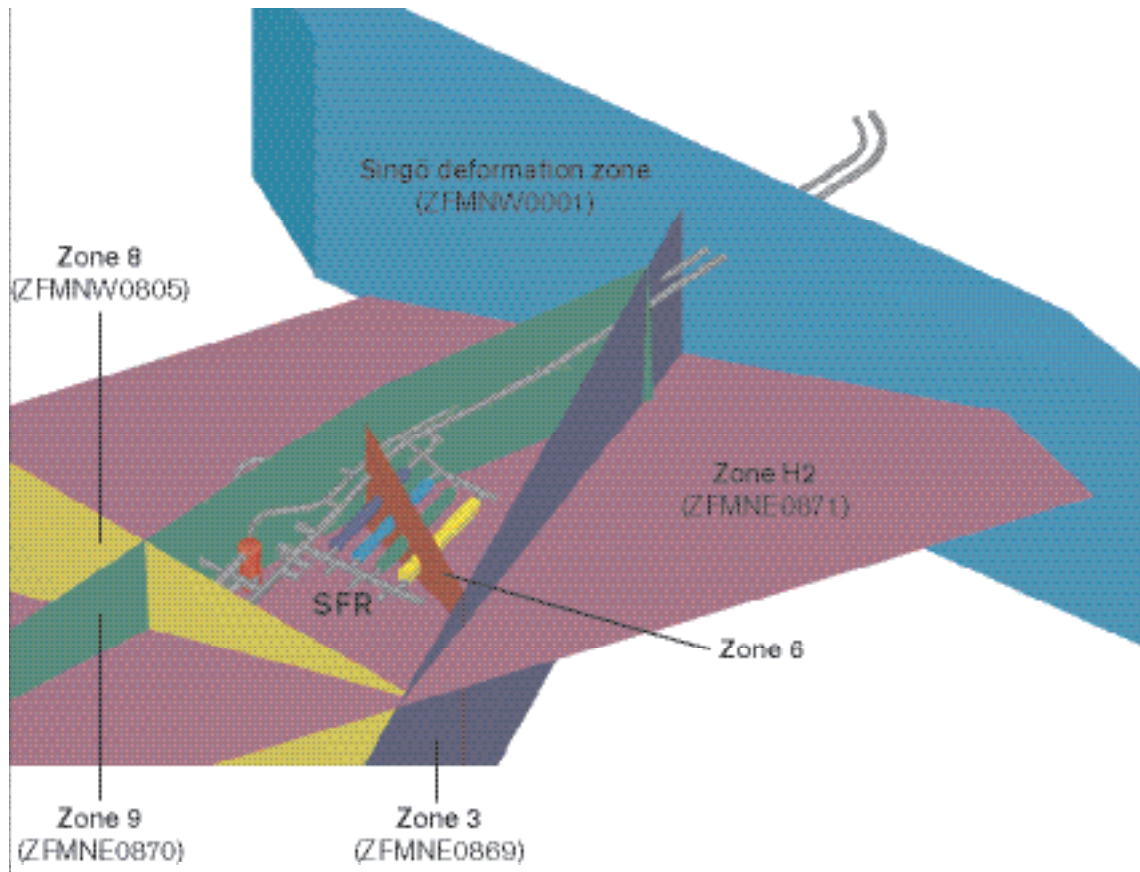


Figure 5-57. Deformation zones within the structural model for the SFR area based on /Holmén and Stigsson, 2001/. View to the south. Note the occurrence of the regionally important Singö deformation zone with WNW strike, zone 8 that strikes NW, zones 3 and 9 that strike NE, and zone H2 that dips gently to the SE.

- Geochronological data (see Section 3.1) indicate that crustal cooling through c. 500°C had initiated in the surface bedrock at c. 1,830 million years ago and through c. 300°C at c. 1,700 million years ago.
- The topographic surface which is inferred to mark the sub-Cambrian peneplain /Lidmar-Bergström 1994/ lies up to c. 10 m lower on the south-western relative to the north-eastern side of the Forsmark deformation zone (ZFMNW004A). A bulk southwest-side-down direction of movement has tentatively been inferred /Bergman et al. 1999/.

On the basis of these observations, it is inferred that:

- The WNW-NW deformation zones comprise the oldest set.
- The WNW-NW, NE and gently dipping sets of deformation zones *formed* close to each other in geological time, at temperatures under 500–550°C and in response to the same tectonic regime.
- *Reactivation* of deformation zones occurred at temperatures under c. 300–350°C (growth of prehnite) and under 250°C (growth of laumontite). This is especially relevant for the NE set. Bearing in mind the cooling ages, this phase (or phases) of reactivation occurred after c. 1,700 million years ago. On the basis of these data, it is apparent that reactivation must have occurred in response to a new tectonic regime (see Section 3.1). This inference is supported by the variable sense of horizontal movement along fractures that strike NE (see Section 5.2.4). However, at the present stage, it cannot be excluded that the zones in the NE set, with a predominance of lower temperature minerals, actually formed later than c. 1,700 million years ago.

- The disturbance of the sub-Cambrian peneplain indicates that movement along at least the Forsmark deformation zone occurred after formation of the peneplain, probably during the Phanerozoic.

The regionally important Forsmark and Singö deformation zones with WNW strike, and the NW splays from these zones (e.g. Eckarfjärden deformation zone), are ranked as first order and second order structures, respectively, in a strike-slip fault system (Figure 5-58). This structural hierarchy reflects a variation in both the regional significance and relative timing of formation of these structures. It is proposed that these structures formed in response to bulk crustal shortening in a N to NNW direction (Figure 5-58). It is assumed that the steeply dipping NE zones initiated as third order structures, and that the gently SE- and S-dipping structures are fourth order structures in the same system (Figure 5-58). In this manner, a strategy for truncation of zones has been developed.

The conceptual model predicts a component of dextral horizontal movement along the first-order zones, and their second-order splays, during their initial phase of development (Figure 5-58). This kinematics is consistent with the component of horizontal movement that has been observed in connection with the older ductile deformation under higher-grade metamorphic conditions (see Section 5.2.4). The model also predicts an early sinistral component of movement along the NE zones (Figure 5-58) and a reverse movement along the gently dipping structures, i.e. the development of thrust faults sandwiched between the first-order structures (Figure 5-58).

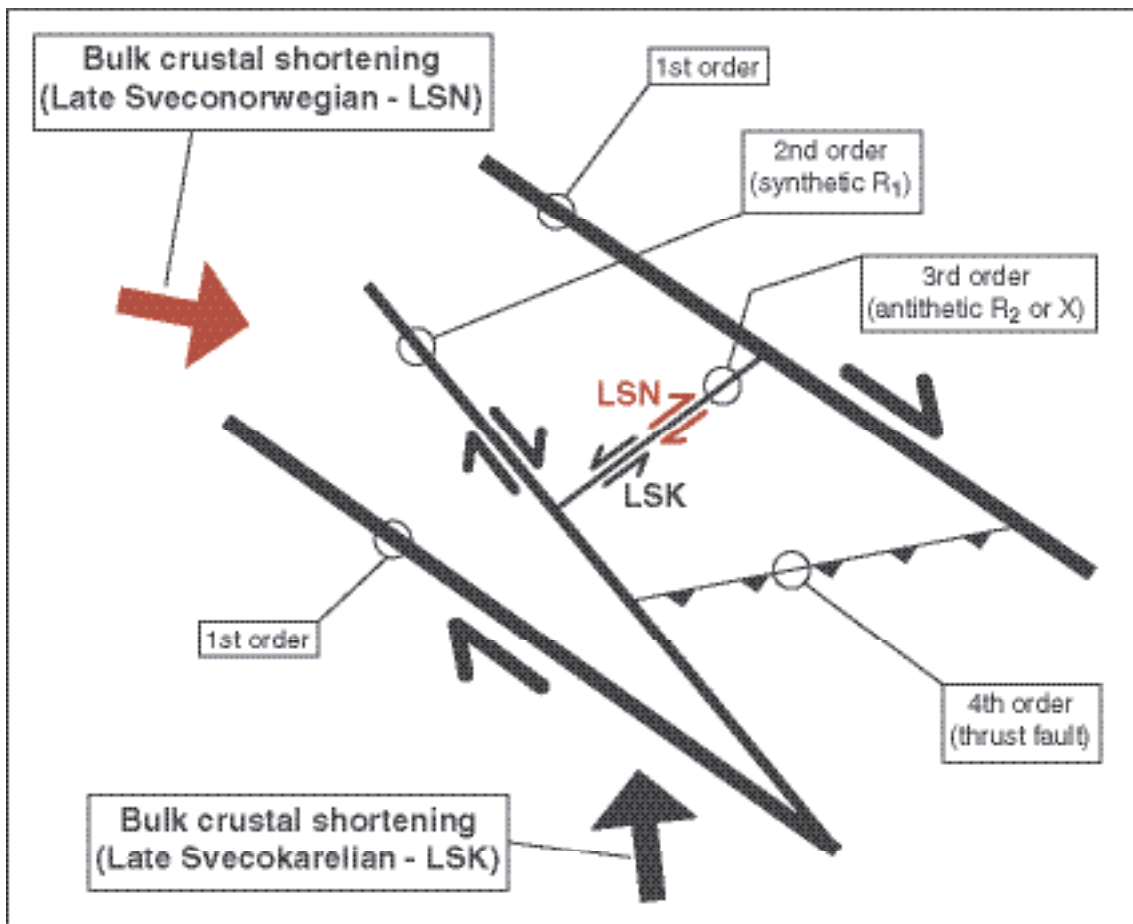


Figure 5-58. Two dimensional, working conceptual model for the three major sets of deformation zones (WNW-NW, NE and gently dipping) at the Forsmark site. It is suggested that all sets formed in a dextral, strike slip fault system, during the waning stages of the Svecokarelian orogeny. Faults with decreasing order of importance in this system include master faults (WNW), synthetic Riedel (R_1) shear faults (NW), antithetic Riedel (R_2) or X shear faults (NE) and thrust faults (gently dipping). Significant reactivation along at least the NE set, during the later part of the Sveconorwegian orogeny, is also incorporated in the model. Note, for example, /McClay, 1989/ for a summary of the features of strike-slip fault systems.

The geochronological data in combination with the properties of the zones suggest that the three sets of deformation zones formed during the waning stages of the Svecokarelian orogeny (see Section 3.1). It is apparent that deformation zones, which formed during this major tectonic event, would have evolved under progressively cooler metamorphic conditions and would have been progressively more discrete in character. At an earlier stage, deformation was ductile and occurred under greenschist facies metamorphic conditions. The formation of low-temperature mylonites is predicted at this stage. Progressively more brittle deformation under lower grade metamorphic conditions and along narrower zones is predicted during the later stages of the deformation, with growth of epidote and quartz along fractures.

Bearing in mind the occurrence of dextral horizontal movement along some fractures with NE strike (see Section 5.2.4), it is proposed that at least the NE set of deformation zones were subject to significant reactivation during the Sveconorwegian orogeny (Figure 5-58). It is suggested that this reactivation occurred in response to bulk crustal shortening in an ESE direction (see Chapter 3.1). Reactivation along at least the Forsmark deformation zone during the Phanerozoic is also apparent.

At least some of the fractures with wide apertures in the uppermost part of the bedrock (see Section 5.2.4), which are oriented more or less parallel to the ground surface and are commonly filled with glacial sediment, are inferred to represent sheet joints. Such joints developed in response to unloading and the release of stress. Such structures are not necessarily related to deformation zones that involved shear displacement. The effects of the change in state of stress in connection with the removal of ice during the waning stages of the last deglaciation, in combination with the effects of hydraulic lifting, have been discussed /Carlsson, 1979; Pusch et al. 1990/. The effects of the earlier removal of the Phanerozoic sedimentary cover rocks, which include relatively dense Ordovician limestone, also needs to be assessed. However, the fractures with glacial sediment infill at drill site 5 (see Section 5.4.2) are possibly related to the surface intersection of the gently dipping deformation zone ZFMNE00A2. This observation opens the question to what extent the horizontal or gently dipping fractures, close to the surface, are *reactivated* older fractures that are related to the gently dipping set of deformation zones.

The conceptual model raises a second question concerning the character of the gently dipping zones. This question concerns how much the increased frequency of open fractures, incohesive fault breccias and clay minerals along the gently dipping zones are controlled by the favourable orientation of these structures for reactivation, in relation to the present orientation of principal stresses. In this concept, the special character rather than the occurrence of the gently dipping zones is steered by the orientation of these zones with respect to the present stress regime. Finally, it needs to be stated that the conceptual model urgently requires independent testing with the establishment of more kinematic data along the deformation zones and with the help of age dating of mineral fillings.

5.4.3 Determination and property assignment of deformation zones

Determination of deformation zones

All the thirteen deformation zones, which were recognised with high confidence in model version 1.1 /SKB, 2004a/, have been identified and utilised in the present model. These include Zones 3, 8, 9, H2 and the Singö deformation zone at SFR. Changes have only been made with the along-strike and down-dip extensions of the gently dipping zones that were recognised in the earlier model inside the candidate area (ZFMNE0865, ZFMNE0866, ZFMNE0866 and ZFMNE0868). These changes are motivated by a better geological understanding of the seismic reflectors and a revised concept for their extension in three-dimensional space. For purposes of clarity, the names of three of these gently dipping zones have been modified in order to emphasise their correlation with a specific reflector. In the following text, only the main segment in a deformation zone (ZFM*****A) is addressed in the documentation of the number of zones. The subordinate zone segments (ZFM*****B, C etc) are not included in the figures cited.

The base model and its variant have been constructed in order to emphasise the uncertainty in the along-strike extension of the gently dipping zones. In both models, gently dipping brittle deformation zones have only been assessed deterministically in a restricted volume close to the coast. This volume corresponds at the surface approximately to the candidate area and its extension to the north-west (Figure 5-59). It contains considerable borehole and tunnel data, as well as reflection seismic data.

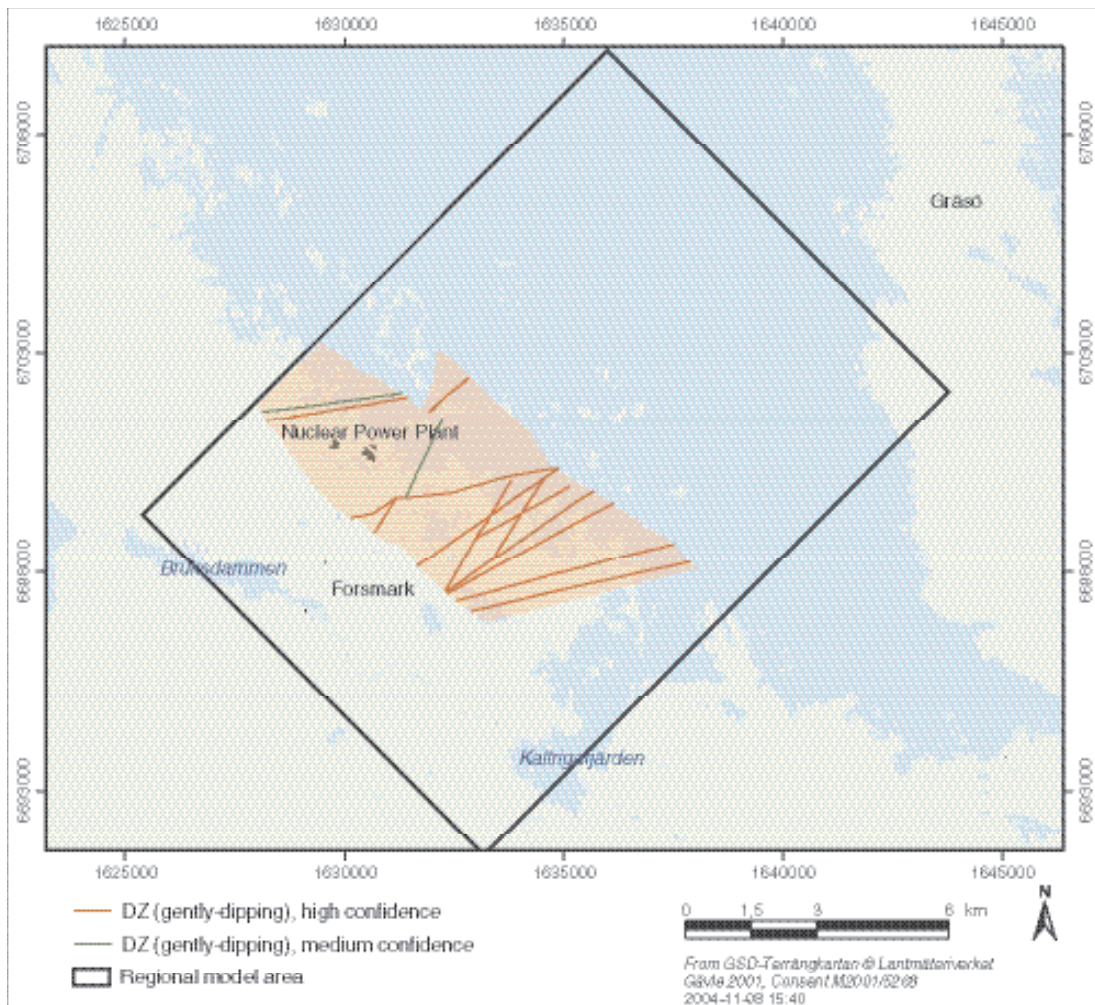


Figure 5-59. Map showing the area in the base model and its variant (beige colour) in which gently dipping deformation zones, which are predominantly longer than 1,000 m, have been handled deterministically. The surface traces of all these zones in the base model are also shown.

Four conspicuous zones (ZFMNE00A1, ZFMNE00A2, ZFMNE00C1 and ZFMNE00C2) have been modelled in different ways in the two models. In the base model, these zones are truncated against the Singö deformation zone (ZFMNW0001) to the north-east and the main segment of the Eckarfjärden deformation zone (ZFMNW003A) to the south-west. By contrast, in the base model variant, these zones are truncated against the Singö deformation zone (ZFMNW0001) to the north-east but have been extended to the main segment of the Forsmark deformation zone (ZFMNW004A) to the south-west. The surface traces of all the gently dipping deformation zones in the base model are shown in Figure 5-59. More reflection seismic data, especially to the south-west of the candidate area, are needed to test the relative suitability of the two models.

In the base model and its variant, the interpretation of lineaments is mainly supportive in character for the determination of vertical and steeply dipping deformation zones. In both models, vertical and steeply dipping zones, which are mostly longer than 1,000 m, have only been assessed deterministically in two small volumes in the north-western part of the candidate area and close to SFR. The corresponding areas at the surface are shown in Figure 5-60. It is only in these volumes that there is a relatively high concentration of deeper borehole and tunnel data. Outside these two volumes, where such data are considerably reduced or are absent, only vertical and steeply dipping deformation zones that, for the most part, are longer than 4,000 m have been included in the deterministic model. Most of these longer zones are based solely on lineament and comparison studies, and only lineaments that are based on magnetic data or a combination of magnetic and other data have been

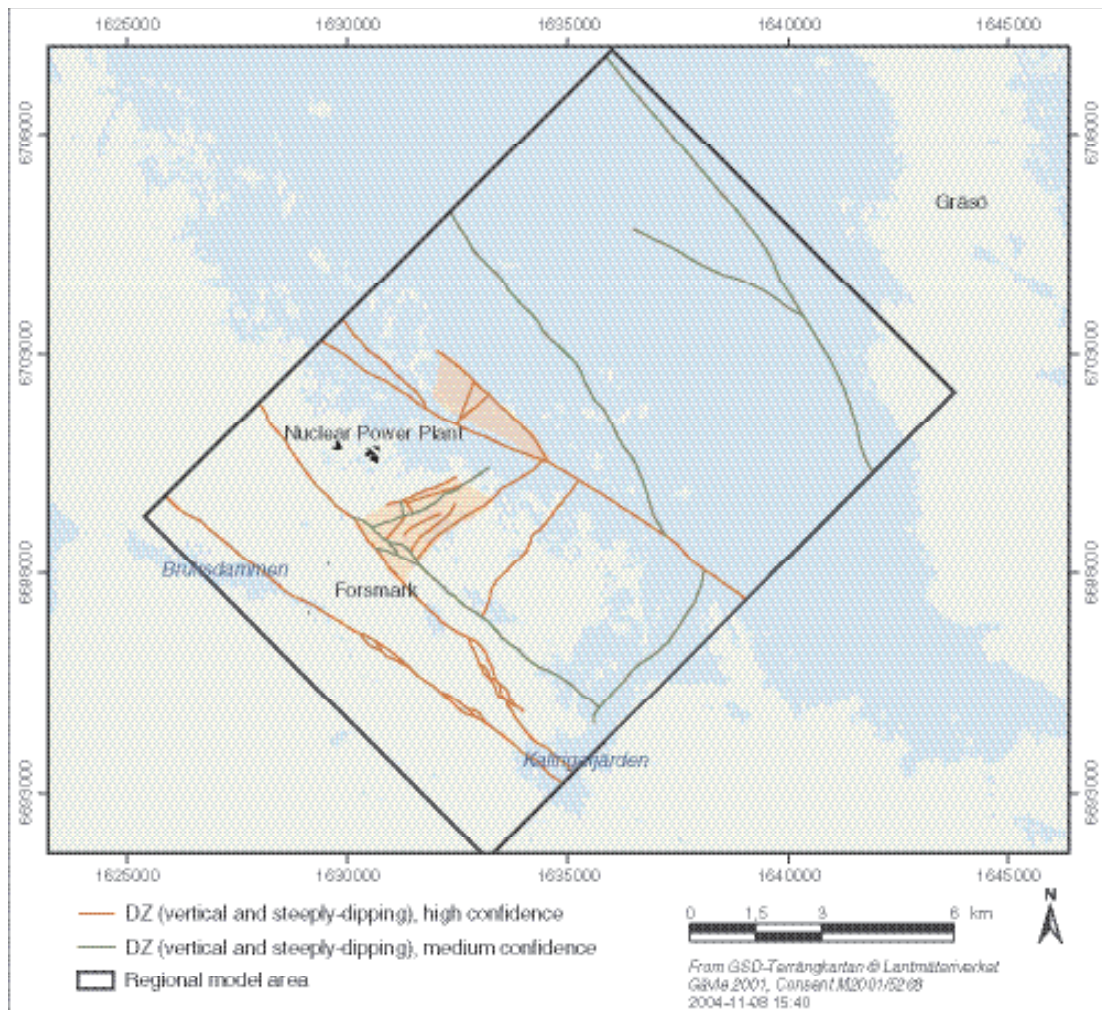


Figure 5-60. Map showing the two areas in the base model and its variant (beige colour) in which vertical and steeply dipping deformation zones, which are predominantly longer than 1,000 m, have been handled deterministically. Outside these two areas, only vertical and steeply dipping zones mostly longer than 4,000 m have been handled deterministically. The surface traces of all the vertical and steeply dipping zones in the two models are also shown.

included. Bearing in mind safety analysis considerations, the choice of this length restriction is under further review. Zones that are longer than 3,000 m will probably be addressed in future model versions. The surface traces of all the vertical and steeply dipping deformation zones in the base model are shown in Figure 5-60.

In the alternative model, the gently dipping zones have been recognised and treated in the same manner as in the base model. The contrast between the alternative model and the other models concerns the treatment of the vertical and steeply dipping zones. In the alternative model, the interpretation of lineaments plays a far more active role in the determination of these zones.

Zones that are vertical or steeply dipping and that show lengths generally longer than 1,000 m have been modelled deterministically within the whole regional volume. As far as these zones are concerned, the model is identical to the base model where it concerns the high and medium confidence zones. The main difference between the two models concerns the inclusion of low confidence zones that lie between 1,000 and 4,000 m in length and that are based solely on the interpretation of lineaments. Once again, only lineaments that are defined by either magnetic data or a combination of magnetic and other data have been included in this group. The surface traces of all the vertical and steeply dipping zones in the alternative model are shown in Figure 5-61.

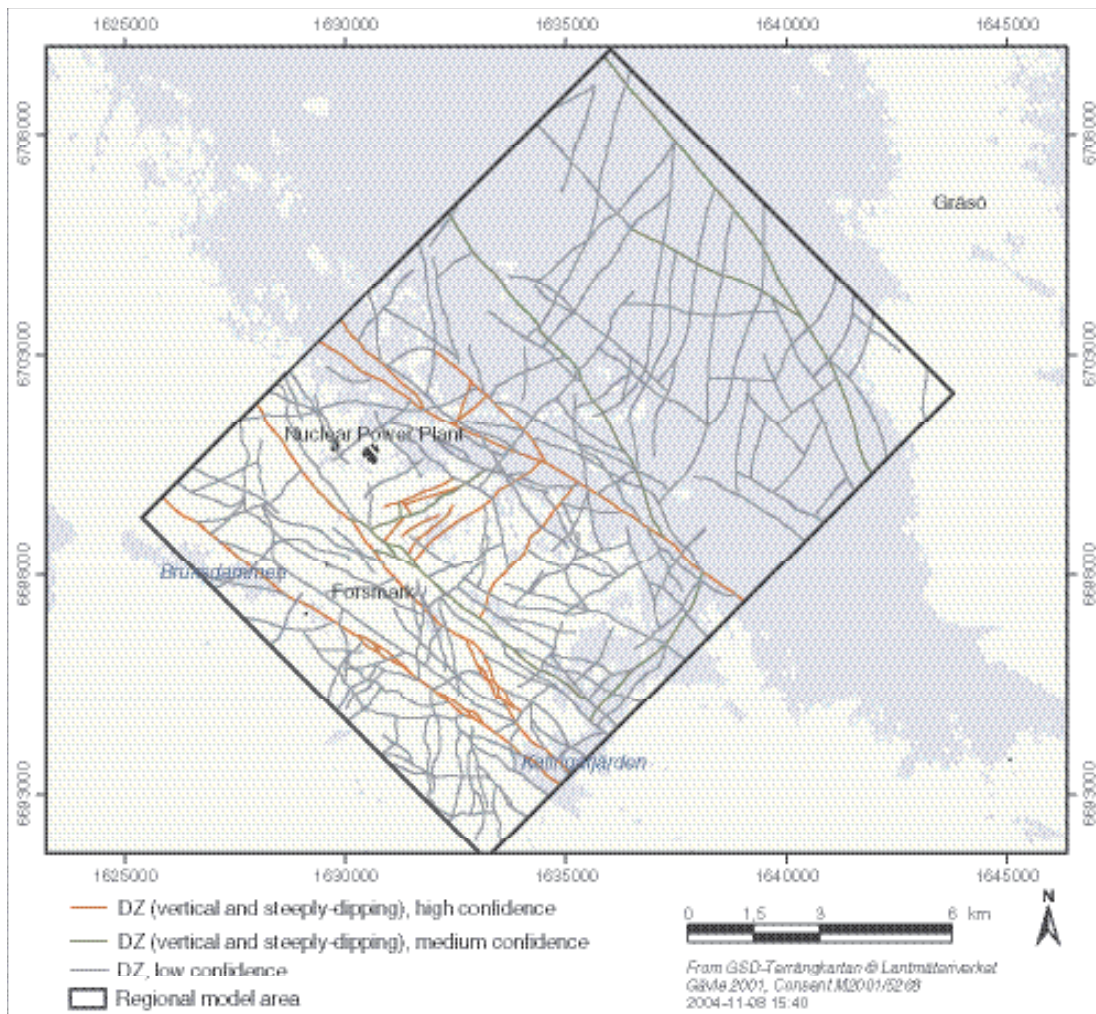


Figure 5-61. Map showing the surface traces of all vertical and steeply dipping zones in the alternative model.

31 deformation zones have been identified on the basis of an integration of direct observational information and indirect information obtained from the interpretation of geophysical data. The direct information includes the documentation and fracture characteristics of deformation zones, which have been recognised along tunnels and in the single hole interpretation (SHI) of the cored and percussion boreholes. These occurrences represent fixed point intersections of deformation zones in the regional model volume. The orientation and mineralogy of fractures along the deformation zones are presented for each zone in /Stephens and Forsberg, 2005/. The indirect information includes reflectors that have been interpreted from seismic reflection data and linked lineaments that have been interpreted from a variety of airborne and surface geophysical measurements. All these 31 zones, including the subordinate zone segments, are present in all three models.

Seven deformation zones are based solely on the interpretation of seismic reflection data. These zones are also present in all three models. 176 deformation zones are based on the interpretation of linked lineaments. In a few cases, they are supported by surface geophysical measurements. Only six of these zones, which are predominantly longer than 4,000 m, are included in all three models. The majority (170) are restricted to the alternative deformation zone model.

49 of the 56 deformation zones that were recognised in the SHI have been included in all three deterministic models. Five of the seven zones that have not been modelled (DZ1 in HFM10, DZ1 in HFM18, DZ4 in KFM02A, DZ9 in KFM02A and DZ5 in KFM03A) occur along short borehole intersections (1 to 7 m). Furthermore, several of these zones were graded only as probable in the SHI

work. The zones DZ7 in KFM02A and DZ3 in KFM05A occur along longer borehole intersections, but have been graded only as probable or possible, respectively, in the SHI work. The borehole interval along which DZ3 in KFM05A occurs (590–796 m) has been re-assessed as an interval with a high frequency of mostly sealed fractures, and with two brittle deformation zones with a high degree of confidence at 609–616 m and 712–720 m.

Following the important calibration work along KFM02A and, especially, KFM03A, all the seismic reflectors labelled as A, B, C, E and F have been inferred to be brittle deformation zones and included in all three deterministic models. All the linked lineaments that are longer than 1,000 m (and even a few that are shorter) have been scanned in the modelling procedure. However, only those lineaments that contain a magnetic minimum along a part of or along the total length of the lineament have been interpreted as deformation zones and included in one or more of the deterministic models. One exception is lineament XFM0098A0 which was not confirmed by the drilling of KFM05A.

The modelling procedure has made use of the assumptions concerning the dip and both the along-strike and down-dip extensions of a deformation zone, as outlined in Section 5.4.1. The procedure has also utilised the conceptual model for the truncation of one zone against another. The methods used to identify an individual deformation zone and to calculate its orientation are shown in Tables 5-26 to 5-29 and briefly summarised below. The procedures used for the determination of vertical and steeply dipping zones differ somewhat from those used for the determination of gently dipping zones. For this reason, each set of zones in the conceptual model is presented separately. Views of the three-dimensional models for the vertical and steeply dipping zones in the base model (and its variant) and in the alternative model are shown in Figure 5-62 and Figure 5-63, respectively. A view that focuses on the gently dipping zones, with their consistent dip to the south and south-east, is shown in Figure 5-64.

Vertical and steeply, SW-dipping ductile and brittle deformation zones with WNW-NW strike

Four zones in this set (ZFMNW0001, ZFMNW0002, ZFMNW003A and ZFMNW0805) have been identified using a combination of intersections in boreholes and/or tunnels, and the interpretation of linked lineaments (Table 5-26). Zones ZFMNW0001 and ZFMNW0805 correspond to the Singö deformation zone and Zone 8 in the structural model for SFR in /Holmén and Stigsson, 2001/, respectively. All the linked lineaments are composite in character and show a magnetic minimum along their total length. Seismic refraction data have also contributed to the definition of three of the zones, and surface geological data to one of them (Table 5-26). The orientation of these four zones has been determined by integration of the sub-surface and surface information. Subordinate zone segments have been identified solely by the interpretation of linked lineaments.

One zone (ZFMNW004A) is based on a combination of surface geological and geophysical data and the interpretation of linked lineaments (Table 5-26). The corresponding lineament is composite in character and includes a magnetic minimum along its total length. Neither boreholes nor tunnels intersect this zone (Forsmark deformation zone), which is probably the most important zone in the region. The strike of this zone is based on the mean trend of the corresponding lineament. The dip is assumed to be 90° on the basis of a comparison with ZFMNW0001. Once again, the subordinate zone segments have been identified solely by the interpretation of linked lineaments.

One local minor zone (ZFMNW1194) is based on a single borehole intersection in KFM01B (DZ2). The zone is dominated by sealed fractures that contain, amongst other minerals, epidote and quartz as mineral fillings. On the basis of these observations, it is assumed that the set of fractures that strikes north-west and dips steeply to the south-west /Stephens and Forsberg, 2005/ provides the best estimate of the orientation of the zone (Table 5-26).

82 deformation zones in this set are based on the interpretation of linked lineaments (Table 5-26) and a few of these lineaments coincide with surface geophysical anomalies (see Section 5.2.5). Each of these lineaments shows a magnetic minimum either along a part of or along the total length of the lineament. The strike of these zones has been determined from the mean trend of the corresponding lineament while the dip is assumed to be 90°. Four zones are longer than 4,000 m (ZFMNW017A, ZFMNW0806, ZFMNW0853 and ZFMNW0854).

Table 5-26. Basis for the interpretation of the geometry of the vertical and steeply, SW-dipping deformation zones with WNW-NW strike. The strike and dip of the zone are provided with the help of the right-hand-rule method, i.e. 140/85 = N40W/85SW.

Zone ID	Occurrence in older models	Basis for interpretation	Basis for calculation of strike and dip	Strike and dip in degrees
ZFMNW0001. Singö deformation zone	SFR (Singö Zone) SDM version 0 SDM version 1.1	Intersections along tunnels 1–2, 3 and SFR, and boreholes along tunnels, seismic refraction data, linked lineament XFM0803A0	Intersections along tunnels 1–2, 3 and SFR, boreholes along tunnels, linked lineament XFM0803A0	120/90
ZFMNW0002. Splay from Singö deformation zone through tunnel 3	SDM version 0 SDM version 1.1	Intersection along tunnel 3, seismic refraction data, linked lineament XFM0804A0	Intersection along tunnel 3, linked lineament XFM0804A0	135/90
ZFMNW003A–F. Eckarfjärden deformation zone	SDM version 0 SDM version 1.1	Intersections along HFM11 (DZ1) and HFM12 (DZ1), surface geology, linked lineament XFM0015A0	Intersections along HFM11 (DZ1) and HFM12 (DZ1), linked lineament XFM0015A0	140/85. Refers to ZFMNW003A
ZFMNW004A–E. Forsmark deformation zone	SDM version 0 SDM version 1.1	Surface geology outside regional model volume, surface geophysics, linked lineament XFM0014A0	Strike based on linked lineament XFM0014A0. Dip by comparison with ZFMNW0001	125/90. Refers to ZFMNW004A
ZFMNW0805. Splay from Singö deformation zone	SFR (Zone 8) SDM version 0 SDM version 1.1	Borehole intersections, seismic refraction data, linked lineament XFM0805A0	Borehole intersections, linked lineament XFM0805A0	135/90
ZFMNW1194	Not present in other models	Intersection along KFM01B (DZ2)	Orientation of fractures in KFM01B (DZ2)	145/81
ZFMNW017A–C	SDM version 1.1	Linked lineament XFM0017A0	Strike based on trend of linked lineament. Dip based on comparison with high confidence, vertical and steeply-dipping zones with NW strike	127/90
ZFMNW0806. Splay from Singö deformation zone	SDM version 1.1	Linked lineament XFM0806A0	Strike based on trend of linked lineament. Dip based on comparison with high confidence, vertical and steeply-dipping zones with NW strike	146/90
ZFMNW0853	SDM version 1.1	Linked lineament XFM0853A0	Strike based on trend of linked lineament. Dip based on comparison with high confidence, vertical and steeply-dipping zones with NW strike	117/90
ZFMNW0854	SDM version 1.1	Linked lineament XFM0854A0	Strike based on trend of linked lineament. Dip based on comparison with high confidence, vertical and steeply-dipping zones with NW strike	147/90
78 deformation zones based solely on lineament and comparison studies			Strike based on trend of linked lineament. Dip based on comparison with high confidence, vertical and steeply-dipping zones with NW strike	Strike in interval 85–154/dip 90

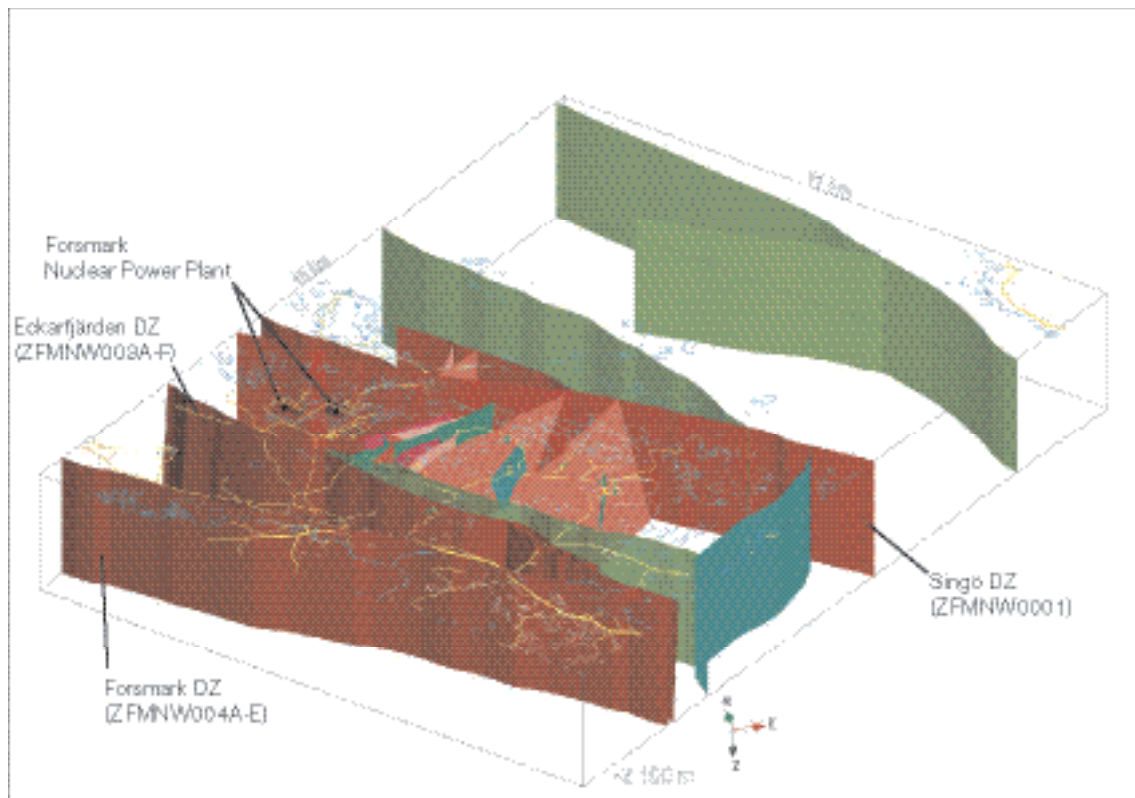


Figure 5-62. Vertical and steeply dipping deformation zones in the version 1.2, base model (and its variant) for the site, viewed to the north. The zones coloured in red-brown shades are high confidence zones and the zones coloured in green shades are medium confidence zones. No low confidence zones are present in these two models.

Vertical and steeply dipping, brittle deformation zones with NE strike

Five zones in this set (ZFMNE0061, ZFMNE062A, ZFMNW065, ZFMNW103A and ZFMNE0401) have been identified using a combination of intersections in boreholes and the interpretation of linked lineaments (Table 5-27). All the linked lineaments are composite in character and show a magnetic minimum along a major part, or along the total length, of the lineament. The orientation of these zones has been determined by integration of the sub-surface and surface information. The subordinate zone segments ZFMNE062B and ZFMNE103B have been identified solely by the interpretation of borehole information in KFM05A (DZ4 and 609–616 m in DZ3, respectively).

Five zones (ZFMNE0869, ZFMNE0870, ZFMNE1188, ZFMNE1189 and ZFMNE1192) are based predominantly on borehole intersections (Table 5-26). Four of these zones are predicted to intersect the surface. However, there appears to be no expression at the surface in the form of a lineament.

Zones ZFMNE0869 and ZFMNE0870 have been adopted from the structural model for SFR in /Holmén and Stigsson, 2001/. They correspond to zones 3 and 9, respectively, in this model. Tunnel and seismic refraction data have also contributed to the definition of these zones and their orientation is based on the tunnel intersections. An integration of surface data from drill site 4, where a component of dextral horizontal movement has been observed (Figure 5-30b), with two separate intersections in the middle and lower parts of KFM04A have helped to identify and to define the orientation of ZFMNE1188. Indeed, borehole KFM04A is inferred to be situated close to this brittle deformation zone along its entire length. The orientations of zones ZFMNE1189 and ZFMNE1192 have been determined from the orientation of fractures in the inferred borehole intersections (DZ5 in KFM02A and DZ2 in KFM01A, respectively).

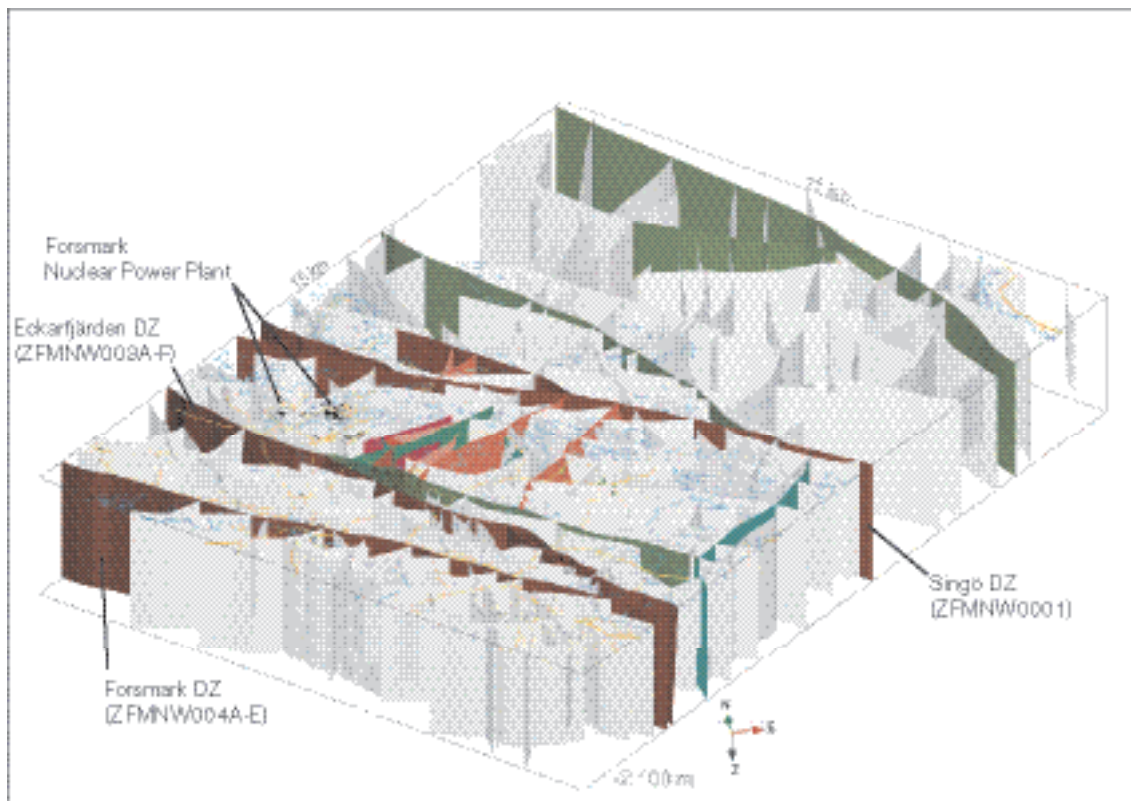


Figure 5-63. All vertical and steeply dipping deformation zones included in the version 1.2, alternative model for the site, viewed to the north. The zones coloured in red-brown shades are high confidence zones, the zones coloured in green shades are medium confidence zones, and the zones coloured in grey shades are low confidence zones.

53 deformation zones in this set are based on the interpretation of linked lineaments (Table 5-26) and a few of these lineaments coincide with surface geophysical anomalies (see Section 5.2.5). As in the other sets, each of these lineaments shows a magnetic minimum either along a part, or along the total length, of the lineament. The strike of these zones has been determined from the mean trend of the corresponding lineament while the dip is assumed to be 90°.

Zones ZFMNE0060 and ZFMNE0828 correspond to lineaments, which are longer than 3,000 m and 4,000 m, respectively. These lineaments belong to a family of lineaments that cross-cut the tectonic lens at Forsmark. Five other lineaments in this family have been successfully linked to deformation zones in boreholes and help to define the zones discussed above (ZFMNE0061 to ZFMNE0401). This comparison strengthens the interpretation that these two lineaments correspond to brittle deformation zones in the vertical and steeply dipping, north-east set.

The magnetic data measured along two of the surface geophysical survey lines (LFM000650 and LFM000651) have been modelled in order to estimate the dip of two possible deformation zones that are recognised as magnetic minima /Pitkänen et al. 2004b/. The geophysical modelling indicates that both zones dip towards the north-west. The magnetic minima lie directly north and directly south of the linked lineaments XFM0060A0 and XFM0062A0, respectively. Assuming that the minima can be correlated with these lineaments, then the modelling work provides some constraints on the dip of the brittle deformation zones ZFMNE0060 and ZFMNE0062, respectively. The inferred dips to the north-west provide an independent estimate of the dips modelled for these two zones, which are based on an integration of borehole and lineament data.

Table 5-27. Basis for the interpretation of the geometry of the vertical and steeply dipping, brittle deformation zones with NE strike. The strike and dip of the zone are provided with the help of the right-hand-rule method, i.e. 068/81 = N68E/81SE.

Zone ID	Occurrence in older models	Basis for interpretation	Basis for calculation of strike and dip	Strike and dip in degrees
ZFMNE0061	SDM version 1.1	Intersection along KFM01A (DZ3), linked lineament XFM0061A0	Intersection along KFM01A (DZ3), linked lineament XFM0061A0	068/81
ZFMNE062A, B	SDM version 1.1, but based solely on lineament study	Intersections along KFM05A (DZ4 and DZ5), linked lineament XFM0062A0	Intersections along KFM05A (DZ4 and DZ5), linked lineament XFM0062A0	234/73
ZFMNE0065	SDM version 1.1, but based solely on lineament study	Intersection along HFM18 (DZ3), linked lineament XFM0065A0	Intersection along HFM18 (DZ3), linked lineament XFM0065A0	036/75
ZFMNE103A, B	SDM version 1.1, but based solely on lineament study (ZFMNE103A)	Intersections along KFM05A (609–616 m and 712–720 m borehole depth intervals in DZ3), linked lineament XFM0103A0	Intersections along KFM05A (609–616 m and 712–720 m borehole depth intervals in DZ3), linked lineament XFM0103A0	232/79
ZFMNE0401	Not present in other models	Intersections along KFM05A (DZ2) and HFM13 (DZ1), linked lineament XFM0401A0	Intersections along KFM05A (DZ2) and HFM13 (DZ1), linked lineament XFM0401A0	239/80
ZFMNE0869	SFR (Zone 3) SDM version 0 SDM version 1.1	Intersection along SFR tunnel and boreholes, seismic refraction data	Intersection along SFR tunnel	020/90
ZFMNE0870	SFR (Zone 9) SDM version 0 SDM version 1.1	Intersection along SFR tunnel and boreholes	Intersection along SFR tunnel	050/90
ZFMNE1188	Not present in other models	Surface geology (drill site 4) and intersections along KFM04A (DZ4, DZ5)	Surface geology (drill site 4) and intersections along KFM04A (DZ4, DZ5)	220/88
ZFMNE1189	Not present in other models	Intersection along KFM02A (DZ5)	Orientation of fractures in KFM02A (DZ5)	040/65
ZFMNE1192	Not present in other models	Intersection in KFM01A (DZ2)	Orientation of fractures in KFM01A (DZ2)	073/82
ZFMNE0060	SDM version 1.1	Linked lineament XFM0060A0	Strike based on trend of linked lineament. Dip based on comparison with high confidence, steeply-dipping zones with NE strike and lack of intersection in the boreholes at drill site 1	242/87
ZFMNE0828	Not present in other models	Linked lineament XFM0828A0	Strike based on trend of linked lineament. Dip based on comparison with high confidence, steeply-dipping zones with NE strike	216/90
51 deformation zones based solely on lineament and comparison studies			Strike based on trend of linked lineament. Dip based on comparison with high confidence, steeply-dipping zones with NE strike	20–84/90

Vertical and steeply dipping, brittle deformation zones with NS strike

Only one zone in this set (ZFMNS0404) has been identified using a combination of an intersection in a borehole (DZ3 in KFM01B) and a linked lineament (Table 5-28). The linked lineament (XFM0404A0) has been interpreted solely from topographic data. However, the lineament occurs in a generally low magnetic area and is, therefore, difficult to recognise in the magnetic data. The orientation of this zone has been determined by integration of the sub-surface and surface information (Table 5-28).

Table 5-28. Basis for the interpretation of the geometry of the vertical and steeply dipping, brittle deformation zones with NS strike. The strike and dip of the zone are provided with the help of the right-hand-rule method, i.e. 352/85 = N8W/85NE.

Zone ID	Occurrence in older models	Basis for interpretation	Basis for calculation of strike and dip	Strike and dip in degrees
ZFMNS0404	Not present in other models	Intersection along KFM01B (DZ3), linked lineament XFM0404A0	Intersection along KFM01B (DZ3), linked lineament XFM0404A0	352/85
41 deformation zones based solely on lineament and comparison studies			Strike based on trend of linked lineament. Dip based on comparison with ZFMNS0404	Strike in interval 335–19/dip 90

There are several observations that cast some question marks concerning the presence of a zone with NS strike along DZ3 in KFM01B.

- The alteration observed in DZ3 along KFM01B (hematite dissemination associated with bedrock oxidation) does not agree with the character of lineament XFM0404A0 at the surface.
- Laumontite, which is characteristic along fractures in the NE set, is a significant mineral fracture filling along the fractures in DZ3 along KFM01B.
- If zone ZFMNE1192 is not truncated by ZFMNW1194 (see property assignment tables in Appendix 3), then it will intersect KFM01B at DZ3. In such a model, DZ3 in KFM01B is the same zone as DZ2 in KFM01A, i.e. ZFMNE1192. However, the orientations of the fractures along these two zones are distinctly different /Stephens and Forssberg, 2005/.

In summary, zone ZFMNS0404 is retained in all the present models, but with a lower level of confidence (see also below).

41 deformation zones in this set are based on the interpretation of linked lineaments (Table 5-26) and a few of these lineaments coincide with surface geophysical anomalies (see Section 5.2.5). The lineaments are of the same character and have been modelled in the same manner as the lineaments that are related to deformation zones in the WNW-NW and NE sets.

Gently, SE- and S-dipping brittle deformation zones

Nine zones in this set (ZFMNE00A2, ZFMNE00A3, ZFMNE00A4, ZFMNE00A5, ZFMNE00A6, ZFMNE00A7, ZFMNE00B1, ZFMNE00B4 and ZFMNE00B6) have been identified using a combination of intersections in boreholes and the interpretation of the reflection seismic data (Table 5-29). The orientation of ZFMNE00A2 is based on an integration of the various borehole intersections with the strike and dip recorded in /Juhlin et al. 2002/. The orientation of the remaining eight zones is based on the orientation of the corresponding seismic reflector in /Juhlin et al. 2002; Juhlin and Bergman, 2004; Cosma et al. 2003; Balu and Cosma, 2005/. The strike and dip that has been adopted for each zone is specified in Table 5-29. The inferred correlation of ZFMNE00A2 and ZFMNE00A3 between different cored boreholes is summarised in Figure 5-48.

One zone (ZFMNE0871) has been adopted from the structural model for SFR in /Holmén and Stigsson, 2001/. It corresponds to zone H2 at SFR. Both tunnel and borehole intersections are available for this zone (Table 5-29). Furthermore, there is a possible correlation with a linked lineament (XFM0137B0) that is based on both magnetic and bathymetric data. The orientation of this zone has been determined from the intersection along the SFR tunnel system.

Table 5-29. Basis for the interpretation of the geometry of the gently SE- and S-dipping, brittle deformation zones. The strike and dip of the zone are provided with the help of the right-hand-rule method, i.e. 080/24 = N80E/24SE.

Zone ID	Occurrence in older models	Basis for interpretation	Basis for calculation of strike and dip	Strike and dip in degrees
ZFMNE00A2	Incorporates ZFMEW0865 in SDM version 1.1	Borehole intersections along KFM01A (DZ1), KFM01B (DZ1), KFM02A (DZ6), KFM04A (DZ1, DZ2 and DZ3), KFM05A (DZ1), HFM01 (DZ1), HFM02 (DZ1), HFM14 (DZ1 and DZ2), HFM15 (DZ1), HFM16 (DZ1), HFM19 (DZ1 and DZ2) in combination with seismic reflector A2	/Juhlin et al. 2002/ in combination with borehole intersections listed in previous column	080/24
ZFMNE00A3	Not present in other models	Intersections along KFM02A (DZ3) and KFM03A (DZ4), seismic reflector A3	Mean value of strike and dip estimates in /Cosma et al. 2003/	055/23
ZFMNE00A4	Not present in other models	Intersections along KFM03A (DZ1) and HFM18 (DZ2), seismic reflector A4	Strike from /Cosma et al. 2003/, dip from /Juhlin et al. 2002/.	061/25
ZFMNE00A5	Corresponds to ZFMNE0867 in SDM version 1.1	Intersections along KFM03B (DZ1), KFM03B (DZ2), HFM06 (DZ1) and HFM08 (DZ1), seismic reflector A5. Possible correlation with linked lineament XFM0067A0	Mean value of strike and dip estimates in /Juhlin et al. 2002; Cosma et al. 2003/	075/31
ZFMNE00A6	Corresponds to ZFMNE0868 in SDM version 1.1	Intersection along HFM07 (DZ1), seismic reflector A6	Strike from /Juhlin et al. 2002/, dip from /Cosma et al. 2003/	075/31
ZFMNE00A7	Not present in other models	Intersections along KFM03A (DZ2) and HFM18 (DZ3), seismic reflector A7	/Juhlin and Bergman, 2004/	055/23
ZFMNE00B1	Not present in other models	Intersection along KFM03A (DZ3), seismic reflector B1	/Cosma et al. 2003/	032/27
ZFMNE00B4	Not present in other models	Intersection along KFM02A (DZ10), seismic reflector B4	/Cosma et al. 2003/. Consistent with /Juhlin et al. 2002/	050/29
ZFMNE00B6	Not present in other models	Intersections along KFM02A (DZ2) and HFM04 (DZ2), seismic reflector B6	/Balu and Cosma, 2005/. Consistent with /Juhlin and Bergman, 2004/	030/32
ZFMNE0866	Corresponds to ZFMNE0866 in SDM version 1.1	Intersections along KFM02A (DZ1), HFM04 (DZ1) and HFM05 (DZ1)	Intersections along KFM02A (DZ1), HFM04 (DZ1) and HFM05 (DZ1)	061/31
ZFMNE0871	SFR (Zone H2) SDM version 0 SDM version 1.1	Intersection along SFR tunnel and boreholes. Possible correlation with linked lineament XFM0137B0	Intersection along SFR tunnel	048/16
ZFMNE1187	Not present in other models	Intersections along HFM09 (DZ1) and HFM10 (DZ2). Intersects also KFM04A (c. 75 m) and KFM04B (c. 80 m). Report during drilling	Intersections along HFM09 (DZ1), HFM10 (DZ2). Intersects also KFM04A (c. 75 m) and KFM04B (c. 60 m). Report during drilling	032/15
ZFMNE1193	Not present in other models	Intersection along borehole length 316–322 m in DBT1 (KFK001)	Comparison with ZFMNE00A2. Minor modification in dip so as to avoid intersection in DBT3 (KFK003)	080/27

ZFMNE1195	Not present in other models	Intersection along KFM02A (DZ8)	Orientation of fractures in KFM02A (DZ8)	080/39
ZFMNE00A1	Not present in other models	Seismic reflector A1/A0. Possible correlation with linked lineament XFM0137A0	/Cosma et al. 2003/	082/45
ZFMNEB23A, B	Not present in other models	Seismic reflectors B2 and B3	/Cosma et al. 2003/. Consistent with /Juhlin et al. 2002/	028/24
ZFMNE0B5A, B	Not present in other models	Seismic reflector B5	/Cosma et al. 2003/	050/9 for ZFMNE0B5A and 062/26 for ZFMNE0B5B
ZFMNE00B7	Not present in other models	Seismic reflector B7	/Juhlin and Bergman, 2004/	025/20
ZFMNE00C1	Not present in other models	Seismic reflector C1	/Cosma et al. 2003/	037/18
ZFMNE00C2	Not present in other models	Seismic reflector C2	/Cosma et al. 2003/	035/13
ZFMNW00E1	Not present in other models	Seismic reflector E1	/Cosma et al. 2003/	297/12

Four zones in this set (ZFMNE0866, ZFMNE1187, ZFMNE1193 and ZFMNE1195) are based solely on the character of deformation zones in borehole intersections (Table 5-29). The orientation of these zones has been modelled using the inferred intersections in several boreholes (ZFMNE0866, ZFMNE1187), a comparative study with ZFMNE00A2 (ZFMNE1193) or the orientation of fractures in a single borehole intersection (ZFMNE1195).

Seven zones (ZFMNE00A1, ZFMNEB23A, ZFMNE0B5A, ZFMNE00B7, ZFMNE00C1, ZFMNE00C2 and ZFMNE00E1) and the two complementary segments (ZFMNEB23B and ZFMNE0B5B) have been identified solely on the basis of the interpretation of seismic reflectors (Table 5-29). The orientation of these zones is once again based on the orientation of the corresponding reflector /Juhlin et al. 2002; Juhlin and Bergman, 2004; Cosma et al. 2003; Balu and Cosma, 2005/. The strike and dip that has been adopted for each zone is specified in Table 5-29.

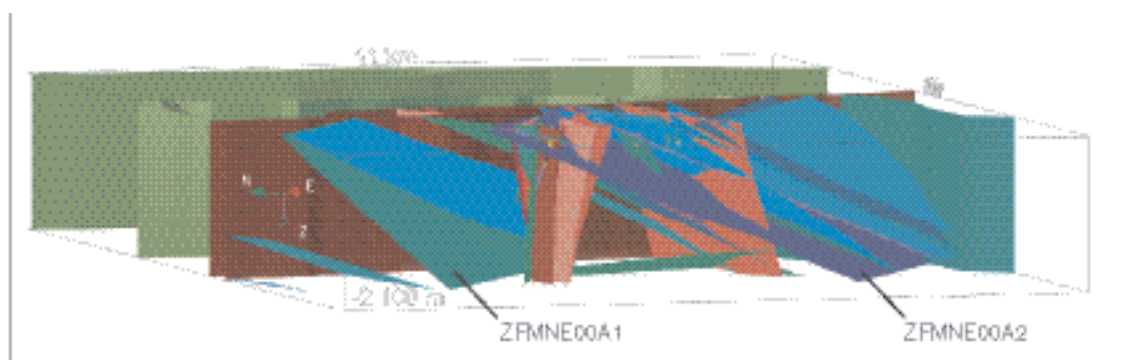


Figure 5-64. View to the north-east of the version 1.2 base model for the deformation zones at the site. Several vertical and steeply dipping zones in the foreground have been removed so that the view can focus on the gently dipping deformation zones in the candidate volume. The zones coloured in red-brown shades are vertical and steeply dipping zones with high confidence, the zones coloured in blue shades are gently dipping zones with high confidence, and the zones coloured in green shades are medium confidence zones irrespective of their dip (see also Section 5.4.4)

Property assignment

Key properties have been assigned to each deformation zone that has been identified with the help of one or more intersections in boreholes and tunnels, or by an integration of surface information and such intersections (Table 5-30). The quantitative estimates or qualitative assignments of key properties for each of these zones are listed in tabular format in Appendix 3. The basis for the estimation of a particular property in each zone is also provided in these tables. Properties are only assigned to the main segment in the complex zones (e.g. ZFMNW003A in the group ZFMNW003A–F).

Table 5-30. Properties assigned to deterministic deformation zones.

Property	Comment
Deformation zone ID code	ZFM* ***** . Eight deformation zones (ZFMNW003*, ZFMNW004*, ZFMNW017*, ZFMNW025*, ZFMNE062*, ZFMNE103*, ZFMNEB23*, ZFMNE0B5*) contain two or more segments along the same zone. These sixteen segments are distinguished by placing a letter (A, B, C, etc) in the final ID code position.
Position	With numerical estimate of uncertainty.
Orientation (strike/dip)	With numerical estimate of uncertainty. Orientation according to right-hand-rule method.
Thickness	With numerical estimate of uncertainty.
Length	With numerical estimate of uncertainty.
Ductile deformation	Indicated if present along the zone.
Brittle deformation	Indicated if present along the zone.
Alteration	Indicated if present along the zone. Type of alteration specified.
Fracture orientation	With numerical estimate of uncertainty.
Fracture frequency	With numerical estimate of uncertainty.
Fracture filling	Mineral coating or filling specified.

It has not been possible to assign certain properties (e.g. alteration, fracture orientation, fracture frequency, fracture filling) to the deformation zones that are based solely on an interpretation of seismic reflection data or lineament studies. Furthermore, several properties of these zones (e.g. thickness, type of deformation present along the zone) have been estimated solely by a comparison with zones that have been identified both with the help of this indirect information as well as borehole and tunnel intersections. The limited assessment of the properties of all these zones is also presented in tabular format in Appendix 3. The zones (six in combination with two subordinate zone segments) that are based solely on indirect information and that occur in all three models are presented individually. The low confidence deformation zones, which are based solely on lineament studies and are restricted to the alternative model (170 in combination with one subordinate zone segment), are presented in separate, orientation sets (WNW-NW, NE, NS).

The thickness of a deformation zone refers to the total thickness of the zone, including both the transition and core parts of the zone (Figure 5-49), according to the terminology in /Munier et al. 2003/. The length of a zone concerns its along-strike extension on the surface. No length is estimated for the zones that fail to intersect the surface. Some zones are truncated by the boundaries to the regional model volume. With one exception, the total length of all the high and medium confidence zones (see Section 5.4.4) in the base model, including their extension outside the regional model volume, is provided. However, only a minimum length is documented for the medium confidence zone ZFMNE00A1 in the variant of the base model and for some of the low confidence zones in the alternative model. All these zones extend outside the regional model volume and their total length is not known. Estimates and span values for the thickness and length of the deformation zones in the base model and its variant are shown in Table 5-31. This table also summarises how each zone has been truncated in the model volume, which in turn constrains its along-strike and down-dip extension.

Table 5-31. Thickness, length and truncation of deformation zones in the base model and its variant. Basis for the thickness and length estimates are provided in Appendix 3.

Zone ID	Thickness	Span	Length	Span	Truncation
Vertical and steeply, SW-dipping brittle and ductile deformation zones with WNW-NW strike					
ZFMNW0001. Singö deformation zone	200 m	± 50 m	30 km	+ 25 km	Extension to base of model
ZFMNW0002. Splay from Singö deformation zone through tunnel 3	75 m	± 10 m	13 km	± 1 km	Extension to base of model. Truncated to the south-east against ZFMNW0001
ZFMNW003A–F. Eckarfjärden deformation zone	60 m	± 20 m	35 km	± 5 km	Extension to base of model
ZFMNW004A–E. Forsmark deformation zone	200 m	± 50 m	70 km	± 5 km	Extension to base of model
ZFMNW0805. Splay from Singö deformation zone	10 m	± 5 m	3,632 m	± 200 m	Extension to base of model. Truncated to the south-east against ZFMNW0001
ZFMNW1194	3 m	Only one borehole intersection	379 m	± 25 m	Truncated at depth against ZFMNE0060 and ZFMNE0061
ZFMNW017A–C	130 m	± 70 m	7,223 m	± 500 m	Extension to base of model. Truncated against ZFMNW003A and ZFMNE0828
ZFMNW0806. Splay from Singö deformation zone	130 m	± 70 m	16 km	± 2 km	Extension to base of model. Truncated to the south-east against ZFMNW0001
ZFMNW0853	10 m	± 5 m	4,348 m	± 200 m	Extension to base of model. Truncated to the east against ZFMNW0854
ZFMNW0854	130 m	± 70 m	26 km	± 2 km	Extension to base of model
Steeply-dipping brittle deformation zones with NE strike					
ZFMNE0061	15 m	Only one borehole intersection	1,727 m	± 100 m	Truncated at depth against ZFMNE0060
ZFMNE062A, B	10 m in sub-zone ZFMNE062A and 19 m in sub-zone ZFMNE062B	Only one borehole intersection for each segment	3,704 m	± 200 m	Extension to base of model
ZFMNE0065	23 m	Only one borehole intersection	3,895 m	± 200 m	Extension to base of model. Truncated against ZFMNW0001 and ZFMNW017A
ZFMNE103A, B	7 m in sub-zone ZFMNE103A and 6 m in sub-zone ZFMNE103B	Only one borehole intersection for each segment	1,542 m	± 100 m	ZFMNE103A truncated against ZFMNW0017A and at depth against ZFMNE0060 and ZFMNE0062
ZFMNE0401	8 m	± 2 m	965 m	± 50 m	Truncated at depth against ZFMNE0060
ZFMNE0869	10 m	± 1 m	1,077 m	± 50 m	Truncated against ZFMNW0001 and ZFMNW0805 and extended to 1,100 m depth
ZFMNE0870	2 m	± 1 m	1,029 m	± 50 m	Truncated against ZFMNW0001 and ZFMNW0805 and extended to 1,100 m depth
ZFMNE1188	1.5 m	± 0.5 m	741 m	± 50 m	Truncation against ZFMNE0060 and ZFMNW017A and extended to 1,100 m depth

Zone ID	Thickness	Span	Length	Span	Truncation
ZFMNE1189	4 m	Only one borehole intersection			ZFMNE1189 does not extend to the surface. Truncated at depth against ZFMNE00A2, ZFMNE00A3 and ZFMNE00B6, and along strike against the downward projection (90°) of two arbitrarily chosen lineaments XFM0047A0 and XFM0101A0
ZFMNE1192	5 m	Only one borehole intersection	1,326 m	± 50 m	Truncated against ZFMNE0060 and ZFMNW1194
ZFMNE0060	10 m	± 5 m	3,012 m	± 200 m	Truncated against ZFMNW017A and extension to base of model
ZFMNE0828	10 m	± 5 m	4,402 m	± 200 m	Truncated against ZFMNW0001 and extension to base of model
Steeply-dipping brittle deformation zones with NS strike					
ZFMNS0404	16 m	Only one borehole intersection	336 m	± 25 m	Truncated against ZFMNE0060, ZFMNE0061 and ZFMNW1194. Note comments under Section 5.4.3 (zones with NS strike)
Gently SE- and S-dipping brittle deformation zones					
ZFMNE00A2	65 m	± 35 m	4,874 m in base model. 7,894 m in alternative model	± 200 m ± 500 m	Extension to base of model. Truncated against ZFMNW0001 and ZFMNW003A in base model and against ZFMNW0001 and ZFMNW004A in variant of base model. Uncertain whether ZFMNE00A2 extends as far as KFM03A (see /Juhlin and Bergman, 2004/)
ZFMNE00A3	13 m	± 9	3,889 m	± 200 m	Truncated at depth against ZFMNW0001, ZFMNW017A, ZFMNE0828 and ZFMNE00A2
ZFMNE00A4	25 m	± 13 m	4,298 m	± 200 m	Truncated at depth against ZFMNW0001, ZFMNE0828 and ZFMNW017A
ZFMNE00A5	10 m	± 5 m	5,116 m	± 200 m	Truncated at depth against ZFMNE00A4, ZFMNW0001, ZFMNW017A and ZFMNE0828
ZFMNE00A6	10 m	Only one borehole intersection	5,091 m	± 200 m	Truncated at depth against ZFMNW0001, ZFMNW017A and ZFMNE0828
ZFMNE00A7	17 m	± 10 m	4,090 m	± 200 m	Truncated at depth against ZFMNE00A4, ZFMNW0001, ZFMNW017A and ZFMNE0828
ZFMNE00B1	7 m	Only one borehole intersection	2,208 m	± 100 m	Truncated at depth against ZFMNE00A3, ZFMNE00A7, ZFMNE00A4, ZFMNW017A and ZFMNE0828
ZFMNE00B4	5 m	Only one borehole intersection			ZFMNE00B4 does not extend to the surface but extends to base of model. Truncation against ZFMNW0001 in the north-east, against ZFMNW017A in the south-west and against ZFMNE0062 in the north-west. Truncation to the north-west takes account of recommendation in /Juhlin and Bergman, 2004/
ZFMNE00B6	7 m	± 4 m	2,950 m	± 200 m	Extension to base of model. Truncated against ZFMNW0001 and ZFMNW017A
ZFMNE0866	5.5 m	± 4.5 m	2,417 m	± 100 m	Truncated at depth against ZFMNE00A3, ZFMNE00B6 and ZFMNE0065
ZFMNE0871	10 m	± 9 m	1,168 m	± 100 m	Truncated at depth against ZFMNW0001, ZFMNW0002 and ZFMNW0805
ZFMNE1187	7 m		911 m	± 100 m	Truncated at depth against ZFMNE00A2, ZFMNW017A and ZFMNE062A
ZFMNE1193	5 m	Only one borehole intersection	3,288 m	± 200 m	Truncated at depth against ZFMNW0001, ZFMNW003A, ZFMNW0017A and ZFMNE0060

Zone ID	Thickness	Span	Length	Span	Truncation
ZFMNE1195	9 m	Only one borehole intersection			ZFMNE1195 does not intersect the surface. Truncated at depth against ZFMNE0062, ZFMNE0065, ZFMNE00A2, ZFMNE00B4 and ZFMNE00B6
ZFMNE00A1	65 m	± 35 m	3,213 m in base model 3,669 m (minimum) in alternative model	± 200 m	Extension to base of model. Truncated against ZFMNW0001 and ZFMNW003A in base model and against ZFMNW0001 and ZFMNW004A in variant of base model
ZFMNEB23A, B	15 m	± 10 m			ZFMNEB23A, B does not intersect the surface but extends to base of model. Truncated against ZFMNW0001, ZFMNW017A, ZFMNE0062 and arbitrarily against the downward projection (90°) of lineament XFM0101A0
ZFMNE0B5A, B	15 m	± 10 m			ZFMNE0B5A, B does not intersect the surface but extends to base of model. Truncated against ZFMNW0001, ZFMNW017A, ZFMNE0062 and arbitrarily against the downward projection (90°) of lineament XFM0101A0
ZFMNE00B7	15 m	± 10 m	1,999 m	± 100 m	Truncated at depth against ZFMNW0001, ZFMNE0060 and ZFMNE00A2
ZFMNE00C1	65 m	± 35 m			ZFMNE00C1 does not intersect the surface but extends to base of model. In the base model, ZFMNE00C1 is truncated against ZFMNW0001 and ZFMNW003A. In the variant of the base model, ZFMNE00C1 is truncated against ZFMNW0001 and ZFMNW004A
ZFMNE00C2	65 m	± 35 m			ZFMNE00C2 does not intersect the surface but extends to base of model. In the base model, ZFMNE00C2 is truncated against ZFMNW0001 and ZFMNW003A. In the variant of the base model, ZFMNE00C2 is truncated against ZFMNW0001 and ZFMNW004A
ZFMNW00E1	15 m	± 10 m			ZFMNE00E1 does not intersect the surface but extends to base of model. Truncated against ZFMNW017A, ZFMNE0062 and ZFMNE0065

If there is a match between a deformation zone and a lineament, then the strike and length of each zone concurs with the trend and length, respectively, of the corresponding lineament. The quantitative estimates of the strike and length of the low confidence deformation zones in the alternative model are documented in the form of intervals for each orientation group (WNW-NW, NE, NS). Apart from a few exceptions (see Appendix 3), fracture orientation sets in an individual zone have been defined on the basis of DFN modelling work (see also /Stephens and Forssberg, 2005/).

5.4.4 Evaluation of uncertainties

A judgement concerning the level of confidence for the occurrence of the 214 deformation zones in the alternative model is provided in Table 5-32. A similar confidence table is available for the 44 deformation zones in the base model and its variant. This table is identical to the confidence table in the alternative model, apart from the exclusion of low confidence zones.

Table 5-32. Table of confidence for the occurrence of deformation zones in the alternative, deterministic deformation zone model. This model only differs from the base model and its variant by the inclusion of low confidence zones that are vertical or steeply dipping.

Zone ID	Basis for interpretation	Confidence of existence																				
Vertical and steeply, SW-dipping brittle and ductile deformation zones with WNW-NW strike																						
ZFMNW0001 (Singö deformation zone)	Tunnels, boreholes, seismic refraction data, linked lineament based on airborne geophysics (magnetic 100% along the length) and bathymetry.	High																				
ZFMNW0002 (splay from Singö deformation zone through tunnel 3)	Tunnel, seismic refraction data, linked lineament based on airborne geophysics (magnetic 100% along the length) and bathymetry.	High																				
ZFMNW003A, B, C, D, E, F (Eckarfjärden deformation zone)	Boreholes, surface geology, linked lineament based on airborne geophysics (magnetic 100% along the length, electrical data) and topography/bathymetry.	High																				
ZFMNW004A, B, C, D, E (Forsmark deformation zone)	Surface geology, surface geophysics, linked lineament based on airborne geophysics (magnetic 100% along the length, electrical data) and topography/bathymetry.	High																				
ZFMNW0805 (Zone 8, SFR; splay from Singö deformation zone)	Borehole, seismic refraction data, airborne geophysics (magnetic 100% along the length) and bathymetry.	High																				
ZFMNW1194 (DZ2 in KFM01B)	Borehole.	High																				
Vertical and steeply, SW-dipping brittle and ductile deformation zones with NW strike, based solely on lineament and comparison study																						
ZFMNW017A, B, C	High confidence linked lineament longer than 4,000 m, based on airborne geophysics (magnetic 57% along the length, electrical data) and topography/bathymetry.	Medium																				
ZFMNW0806 (splay from Singö deformation zone)	High confidence linked lineament longer than 4,000 m, based on airborne geophysics (magnetic 94% along the length) and bathymetry.	Medium																				
ZFMNW0853	High confidence linked lineament longer than 4,000 m, based on airborne geophysics (magnetic 100% along the length).	Medium																				
ZFMNW0854	High confidence linked lineament longer than 4,000 m, based on airborne geophysics (magnetic 100% along the length).	Medium																				
ZFMNW0016	Linked lineaments with variable confidence that predominantly lie between 1,000 and 4,000 m in length, and that have been defined solely on magnetic data or on a combination of magnetic data and topographic/bathymetric and/or electrical data. An initial assessment of the seismic refraction data in the vicinity of the nuclear power plants and SFR has also been carried out.	Low																				
ZFMNW0018																						
ZFMNW0019																						
ZFMNW0020																						
ZFMNW0021																						
ZFMNW0022																						
ZFMNW0023																						
ZFMNW0024																						
ZFMNW025A, B																						
ZFMNW0026																						
ZFMNW0027																						
ZFMNW0028																						
ZFMNW0029																						
ZFMNW0031																						
ZFMNW0032																						
ZFMNW0033																						
ZFMNW0034																						
ZFMNW0035																						
ZFMNW0036																						
ZFMNW0037																						
ZFMNW0039																						
ZFMNW0042																						
ZFMNW0044																						
ZFMNW0136	ZFMNW0289	ZFMNW0351	ZFMNW0658	ZFMNW0809	ZFMNW0813	ZFMNW0815	ZFMNW0816	ZFMNW0818	ZFMNW0833	ZFMNW0835	ZFMNW0836	ZFMNW0837	ZFMNW0841	ZFMNW0849	ZFMNW0851	ZFMNW0855	ZFMNW0856	ZFMNW0888	ZFMNW0895	ZFMNW0914	ZFMNW0927	ZFMNW0936

Zone ID	Basis for interpretation	Confidence of existence
ZFMNW0045	ZFMNW0970	
ZFMNW0046	ZFMNW0974	
ZFMNW0049	ZFMNW1006	
ZFMNW0050	ZFMNW1033	
ZFMNW0052	ZFMNW1043	
ZFMNW0053	ZFMNW1053	
ZFMNW0054	ZFMNW1127	
ZFMNW0055	ZFMNW1131	
ZFMNW0056	ZFMNW1146	
ZFMNW0058	ZFMNW1147	
ZFMNW0059	ZFMNW1148	
ZFMNW0110	ZFMNW1149	
ZFMNW0118	ZFMNW1150	
ZFMNW0121	ZFMNW1154	
ZFMNW0122	ZFMNW1156	
ZFMNW0123	ZFMNW1173	
Steeply-dipping brittle deformation zones with NE strike		
ZFMNE0061 (DZ3 in KFM01A)	Borehole, linked lineament based on airborne geophysics (magnetic 100% along the length, electrical data) and topography.	High
ZFMNE062A, B (DZ5 and DZ4 in KFM05A)	Borehole, linked lineament based on airborne geophysics (magnetic 94% along the length, electrical data) and topography.	High
ZFMNE0065 (DZ3 in HFM18)	Borehole, linked lineament based on airborne geophysics (magnetic 100% along the length, electrical data) and topography.	High
ZFMNE103A, B (712–720 m and 609–616 m levels within DZ3 in KFM05A)	Borehole, linked lineament based on airborne geophysics (magnetic 80% along the length) and topography.	High
ZFMNE0401 (DZ2 in KFM05A/DZ1 in HFM13)	Boreholes, linked lineament based on airborne geophysics (magnetic 100% along the length) and topography.	High
ZFMNE0869 (Zone 3, SFR)	Tunnel, boreholes, seismic refraction data.	High
ZFMNE0870 (Zone 9, SFR)	Tunnel, boreholes.	High
ZFMNE1188 (surface at drill site 4/DZ4 and DZ5 in KFM04A)	Surface geology, borehole.	High
ZFMNE1189 (DZ5 in KFM02A)	Borehole.	Medium
ZFMNE1192 (DZ2 in KFM01A)	Borehole.	High
Vertical and steeply-dipping brittle deformation zones with NE strike, based solely on lineament and comparison study		
ZFMNE0060	High confidence linked lineament longer than 3,000 m, based on airborne geophysics (magnetic 70% along the length, electrical data) and topography.	Medium
ZFMNE0828	High confidence linked lineament longer than 4,000 m, based on airborne geophysics (magnetic 97% along the length) and topography/bathymetry.	Medium
ZFMNE0063	Linked lineaments with variable confidence that predominantly lie between 1,000 and 4,000 m in length, and that have been defined solely on magnetic data or on a combination of magnetic data and topographic/bathymetric and/or electrical data. An initial assessment of the seismic refraction data in the vicinity of the nuclear power plants and SFR has also been carried out.	Low
ZFMNE0064		
ZFMNE0066		
ZFMNE0067		
ZFMNE0068		
ZFMNE0070		

Zone ID	Basis for interpretation	Confidence of existence
ZFMNE0071	ZFMNE0842	
ZFMNE0072	ZFMNE0844	
ZFMNE0075	ZFMNE0846	
ZFMNE0076	ZFMNE0850	
ZFMNE0077	ZFMNE0860	
ZFMNE0078	ZFMNE0876	
ZFMNE0079	ZFMNE0894	
ZFMNE0082	ZFMNE0957	
ZFMNE0084	ZFMNE0958	
ZFMNE0086	ZFMNE1016	
ZFMNE0087	ZFMNE1020	
ZFMNE0097	ZFMNE1137	
ZFMNE0120	ZFMNE1138	
ZFMNE0128	ZFMNE1139	
ZFMNE0135	ZFMNE1141	
ZFMNE0138	ZFMNE1142	
ZFMNE0159	ZFMNE1144	
ZFMNE0807	ZFMNE1162	
ZFMNE0808	ZFMNE1177	
ZFMNE0810		
Steeply-dipping brittle deformation zones with NS strike		
ZFMNS0404 (DZ3 in KFM01B)	Borehole, linked lineament based solely on topography.	Medium DZ3 in KFM01B is possibly the same zone as ZFMNE1192
Vertical and steeply-dipping brittle deformation zones with NS strike, based solely on lineament and comparison study		
ZFMNS0089	ZFMNS0487	Linked lineaments with variable confidence that predominantly lie between 1,000 and 4,000 m in length, and that have been defined solely on magnetic data or on a combination of magnetic data and topographic/bathymetric and/or electrical data. An initial assessment of the seismic refraction data in the vicinity of the nuclear power plants and SFR has also been carried out.
ZFMNS0090	ZFMNS0821	
ZFMNS0092	ZFMNS0822	
ZFMNS0095	ZFMNS0823	
ZFMNS0096	ZFMNS0839	
ZFMNS0100	ZFMNS0843	
ZFMNS0101	ZFMNS0848	
ZFMNS0104	ZFMNS0857	
ZFMNS0106	ZFMNS0858	
ZFMNS0107	ZFMNS0859	
ZFMNS0108	ZFMNS0861	
ZFMNS0109	ZFMNS0929	
ZFMNS0111	ZFMNS0990	
ZFMNS0112	ZFMNS0999	
ZFMNS0113	ZFMNS1132	
ZFMNS0114	ZFMNS1133	
ZFMNS0115	ZFMNS1134	
ZFMNS0116	ZFMNS1135	
ZFMNS0117	ZFMNS1136	
ZFMNS0119	ZFMNS1140	
ZFMNS0125		
Gently SE- and S-dipping brittle deformation zones		
ZFMNE00A2 (ZFMEW0865 in SDM version 1.1 is included here as a sub-zone within ZFMNE00A2; type intersection DZ6 in KFM02A)	Boreholes, seismic reflection data.	High

Zone ID	Basis for interpretation	Confidence of existence
ZFMNE00A3 (DZ3 in KFM02A/DZ4 in KFM03A)	Boreholes, seismic reflection data.	High
ZFMNE00A4 (DZ1 in KFM03A/DZ2 in HFM18)	Boreholes, seismic reflection data.	High
ZFMNE00A5 (ZFMNE0867 in SDM version 1.1 has been renamed to ZFMNE00A5; DZ1 and DZ2 in KFM03B/DZ1 in HFM06/DZ1 in HFM08)	Boreholes, seismic reflection data.	High
ZFMNE00A6 (ZFMNE0868 in SDM version 1.1 has been renamed to ZFMNE00A6; DZ1 in HFM07)	Borehole, seismic reflection data.	High
ZFMNE00A7 (DZ2 in KFM03A/DZ3 in HFM18)	Boreholes, seismic reflection data.	High
ZFMNE00B1 (DZ3 in KFM03A)	Borehole, seismic reflection data.	High
ZFMNE00B4 (DZ2 in KFM02A/DZ2 in HFM04)	Borehole, seismic reflection data.	High
ZFMNE00B6 (DZ10 in KFM02A)	Boreholes, seismic reflection data.	High
ZFMNE0866 (DZ1 in KFM02A/DZ1 in HFM04/DZ1 in HFM05)	Boreholes.	High
ZFMNE0871 (Zone H2, SFR)	Tunnel, boreholes, possible correlation with linked lineament based on airborne geophysics (100% magnetic along the length) and bathymetry.	High
ZFMNE1187 (DZ1 in HFM09/DZ2 in HFM10)	Boreholes.	High
ZFMNE1193 (316–322 m level in DBT1/KFK001)	Borehole.	High
ZFMNE1195 (DZ8 and possibly DZ9 in KFM02A)	Borehole.	High
Gently SE- and S-dipping brittle deformation zones, based solely on seismic reflection data and comparison study		
ZFMNE00A1	Seismic reflection data, possible correlation with linked lineament based on airborne geophysics (76% magnetic along the length, electrical data) and topography/bathymetry.	Medium
ZFMNEB23A, B	Seismic reflection data (combination of reflectors B2 and B3).	Medium
ZFMNE0B5A, B	Seismic reflection data.	Medium
ZFMNE00B7	Seismic reflection data.	Medium
ZFMNE00C1	Seismic reflection data.	Medium
ZFMNE00C2	Seismic reflection data.	Medium
ZFMNW00E1	Seismic reflection data.	Medium

A high confidence of occurrence is restricted to those zones in which direct and unequivocal geological and geophysical data from boreholes, tunnels or the surface have played a role in their identification. Zones that have been recognised indirectly by either the interpretation of seismic reflectors or the interpretation of longer (predominantly 4,000 m) linked lineaments are considered to show a medium confidence of occurrence. Supporting geological and geophysical data are lacking. A low confidence of occurrence is applied to those zones that have been recognised indirectly by the interpretation of shorter (1,000 to predominantly 4,000 m) linked lineaments. Once again, supporting geological and geophysical information is absent.

In the alternative model, 29 deformation zones are allocated a high confidence of occurrence, 15 zones a medium confidence of occurrence and 170 zones a low confidence of occurrence. Only deformation zones that have been recognised with high and medium confidence are present in the

set of zones that is gently SE- and S-dipping. Furthermore, all except one of the vertical and steeply dipping zones with NS strike have been recognised with low confidence. The exception has only been rated with medium confidence and certain arguments (see Section 5.4.3) suggest that this zone may be the continuation of a modelled zone that belongs to the NE set. It is apparent that, although fractures that belong to a NS orientation set exist in the bedrock (see Section 5.5), there are major uncertainties concerning the existence of deformation zones with this orientation.

An important development since the version 1.1 model concerns a better geological understanding of the seismic reflectors. The results from boreholes KFM02A and, especially, KFM03A have radically improved our confidence in the geological interpretation of these structures as brittle deformation zones, commonly with water-bearing open fractures. By contrast, the uncertainty concerning the geological significance of many of the linked lineaments, which was recognised in model version 1.1, remains.

The results from especially the drilling activities have confirmed the existence of deformation zones, with a high proportion of sealed fractures and the presence of cohesive crush breccias, along lineaments that trend WNW, NW and NE. All the lineaments along these zones are based partly or entirely on magnetic data. However, the drilling results close to Bolundsfjärden indicate that predominantly topographic lineaments that trend NS do not appear to correspond to deformation zones. These results emphasise the difficulties in the evaluation of the geological significance of individual lineaments when direct calibration data are lacking. It is also noteworthy that the alternative interpretation of lineaments raises questions concerning the identification of lineaments and the reproducibility of the interpretation work.

A major uncertainty in virtually all the deformation zones concerns their along-strike continuity and their down-dip extension. The alternative interpretation of lineaments inside and close to the candidate area focuses attention on the uncertainty concerning the length of an individual lineament. This observation has direct implications for the along-strike extension of all the vertical and steeply dipping zones that partly or solely are based on the interpretation of lineaments. In particular, the down-dip extension of the low confidence zones in the alternative model is highly uncertain. The along-strike and down-dip continuity of the gently dipping deformation zones is determined with the help of the working conceptual model. Modifications in this model can radically change the continuity of these zones.

Although considerable progress has been made in the present model concerning the establishment of the dip of the high and medium confidence zones, the dip of the low confidence zones in the alternative model remains unknown and the modelled dip of 90° is an assumption. An attempt has been made to provide some quantitative estimates of the uncertainty in the position, orientation, thickness and length of most of the deformation zones. Numerical estimates of the uncertainty in the orientation and frequency of fractures along the majority of the high and medium confidence zones have also been made. Furthermore, a judgement concerning the level of confidence in the establishment of an individual property for a deformation zone has been made. All these estimates and confidence judgements are provided in the tabulation of the properties of deformation zones in Appendix 3.

Bearing in mind the uncertainties concerning, for example, the length of lineaments, the length of zones that have made use of the lineament interpretation is graded no higher than medium in the confidence level assessment in the property tables. Most estimates of the thickness, fracture orientation, fracture frequency and fracture mineralogy of the deformation zones come from the fixed point intersections in boreholes. However, since there are only one or a few borehole intersections for most zones, the confidence grading for these parameters is set at medium. An exception to this judgement concerns, for example, zone ZFMNE00A2, where data has been extracted from many borehole intersections.

Finally, it is apparent that there are several high confidence deformation zones in the area between drill site 2 and the nuclear power plant, i.e. in the north-western part of the candidate area (Figure 5-59 and Figure 5-60). These zones strike NE or ENE and are both steeply and gently dipping. This feature naturally reflects the higher amount of borehole and seismic reflection data in this area. Only a few zones with low or medium confidence are present in the north-westernmost

part of the candidate area, i.e. directly south-east of the nuclear power plant (Figure 5-59 and Figure 5-61). These observations are of considerable significance, bearing in mind the selection of the area between drill site 2 and the nuclear power plant for further investigations during the complete site investigation phase (see Chapters 12 and 13 and /SKB, 2005a/). A better knowledge of the character of the low and medium confidence zones as well as an open-minded attitude to the occurrence of, as yet, undetected zones in this area are required. Steeply dipping zones that strike NE and less confidently NS, all of which should contain a high frequency of sealed fractures and coherent crush breccias, are the most likely candidates. Furthermore, the extension in this area of some gently dipping zones with high and medium confidence, which contain a higher frequency of open fractures and especially close to the surface incoherent fault breccias, also remains uncertain.

5.5 Statistical model of fractures and deformation zones

5.5.1 Modelling assumptions

There are several assumptions that have been made in order to construct the stochastic DFN model for the Forsmark site. Each assumption is described below, along with its impact on the model, a rationale for why the assumption is reasonable, and recommendations for future re-evaluation of the assumption.

Assumption 1: Lineaments represent possible deformation zones, which in this report are treated as individual fractures.

Much care was taken to ensure that the lineaments in the delivered data set (see /La Pointe et al. 2005/ for references) were structural features likely to be fractures, but this does not guarantee that each and every lineament trace is truly a mechanical fracture. Because of the care and protocols followed, however, it is likely that a very high proportion of the lineaments do represent mechanical fractures, and the error that may arise from considering the few data that are not fractures in orientation and size statistics is likely to be small.

Assumption 2: The length of a linked lineament or a linked fracture in outcrop is an accurate and appropriate measure of a fracture's trace length for the purpose of building a stochastic DFN model.

This assumes that the linked lineament is a sufficiently accurate measure of a fracture's length, and that it is the appropriate one for computing size statistics. The purpose of linking lineaments is to develop a DFN model that has fracture sizes and intensities that adequately reproduce flow and transport over large and small scales simultaneously. Linking approximately straight-line individual rupture segments into a single lineament requires consideration of several factors, such as geology, data source and resolution, and lineament geometry. Particularly where an individual lineament splits into several, or where lineaments cross, the disposition of which segments belong to which linked lineaments contains uncertainty. These difficulties have been discussed earlier in connection with the alternative interpretation of lineaments (see Section 5.2.3).

Although the size model depends on the lengths of the linked lineaments and the way outcrop segments are linked, the uncertainty can be bracketed and quantified. The potential uncertainties in trace lengths at the outcrop scale are manifested (along with other uncertainties) as the variance among area-normalized frequency values for the outcrops. It is likely that the variance due to outcrop differences is greater than the uncertainty produced by the linkage algorithm, and in any case, the uncertainty is quantified by calculating an envelope of parameters for the size of a specific fracture set.

Assumption 3: Fractures in outcrops may represent the smaller portion of a population of much larger fractures if the orientation of the sets in outcrops is similar to the orientation of lineaments, and the trace lengths conform at both outcrop and lineament scales to a single size probability distribution.

The size calculation for lineament-related sets is based upon fitting a power law curve to lineament trace length values and outcrop trace length values. However, the fracturing at Forsmark is likely to be very old /SKB, 2000a/ and, whatever the origin of the outcrop fracturing may have been, it is

likely to have been re-activated many times (see Section 5.4.2). In this respect, large-scale lineaments may be fractures that have been more intensely re-activated because of higher stress or more focused deformation through time, and as such, share a common tectonic evolution with the outcrop fractures.

We recommend to further evaluate the fractures mapped on outcrops to determine what evidence for re-activation exists, and perhaps to construct an alternative size model based only on outcrop fractures that have clear evidence for re-activation or shear movement. Another assessment could come from mapping fracture traces between individual outcrops, thereby providing trace length frequency data at a scale intermediate between lineaments and outcrops. If these intermediate sized fractures have orientations and sizes consistent with both outcrop and lineament data, then the assumption could be further assessed.

Assumption 4: Variations in fracture intensity as a function of rock type, alteration zone or other geological control can be estimated for un-sampled rock units based on the inference of the controlling parameters for those units.

So far, information on geological controls for fracture intensity variation suggests that lithology and degree of alteration may be important controls. However, five outcrops and a limited number of boreholes have not provided data for all possible combinations of lithology and degree of alteration. In order to specify fracture intensity throughout the model region, it is necessary to infer similarity of un-sampled rock types to sampled ones. It would be useful to validate this extrapolation to un-sampled rock types by acquiring data in one of these un-sampled units, and comparing with predictions.

5.5.2 Derivation of statistical model with properties

The strategy for calculating the parameter values required for the stochastic DFN model focuses firstly on defining fracture sets and then on calculating properties for each set. Since each set may have its own distinct parameter values, the specification of the sets impacts the uncertainty in the parameter values. For example, if all fractures were combined into a single set, the variance in parameters such as size or orientation could be quite high. The separation of the fractures into multiple sets makes it possible to reduce the parameter variance associated with each group, thereby lowering the overall variance or uncertainty in the DFN model.

After sets have been specified, it is necessary to determine the stochastic geometrical description of each set. For each set, this geometry is composed of:

- Fracture orientations, expressed as the trend and plunge of the mean pole, with variability quantified by one or more of the following models and its associated parameters: Fisher, Bivariate Fisher, Bingham, Bivariate Normal, Bootstrap,
- Fracture sizes, expressed as a size-frequency distribution following one or more of the following distributions and their associated parameters: normal, lognormal, exponential, power law, uniform; and any minimum or maximum truncation values,
- Fracture shape,
- Fracture intensity, specified as P_{32} , the amount of fracture surface area per unit volume of rock, where surface area is measured as the area of one of the adjacent sides of a fracture,
- Fracture spatial controls; these might be such models as Poissonian, fractal, geostatistical, or more complex combinations of these processes within specific geological domains,
- Fracture terminations.

Additional parameter values may be included depending upon the model's intended use, but no additional items have been identified for this model version.

The workflow for analysing the individual borehole, outcrop and lineament data sets (Figure 5-65) is presented within its context for achieving the overall characterisation objectives. These are to determine regional controls on fracture pattern geometry. In particular, to develop a predictive algorithm to specify fracture intensity, orientation and size throughout the spatial and depth extent at the Forsmark site. The workflow diagram begins with the analysis of data sets for each individual

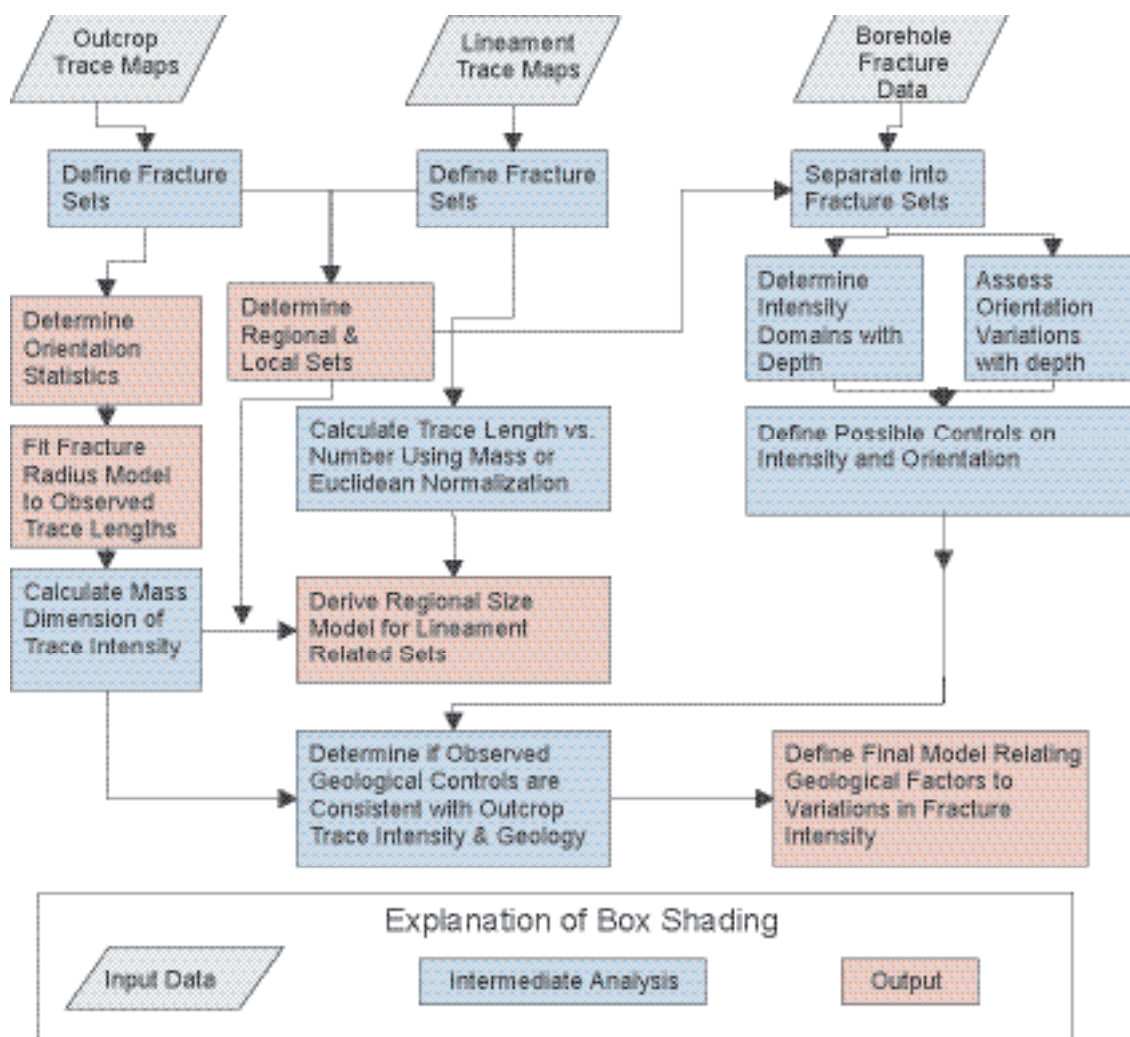


Figure 5-65. Data analysis flow chart

borehole, outcrop trace map or lineament data set. These individual data sets are described as “local” in the sense that it is not initially known whether the fracture controls and geometry determined for each individual set are found elsewhere; they may not have any regional consistency among boreholes or outcrops. The results from the analyses for each borehole or outcrop are initially assumed to represent only the fracturing of the rock in the immediate proximity of the outcrop or borehole, unless comparative analysis later demonstrates that fracture orientations, geological controls on intensity, and so on, exhibit regional consistency. The term, local fracture set, should not be confused with the local DFN model, which comprises the fracture model for the Forsmark site. The local DFN model is independent of whether it is composed of local fracture sets where individual borehole or outcrop data sets show little spatial consistency, or of regional sets, which show great spatial consistency, or of some combination of regional and local sets.

The flowchart shows the components of the analysis of the local data sets. Any box that can be traced to an original input data source without connection to another data source is part of the local fracture data set analyses. For example, the chart shows that calculating the mass dimension of the trace intensity is part of the local data analysis for the outcrop trace data, but the derivation of the regional size model for lineament-related sets is not, as it relies upon the joint analysis of both the lineament and outcrop trace data sets, and whether the outcome of these analyses suggest that lineaments and smaller scale fracturing ought to be combined. In contrast, the stages in determining the possible regional controls on fracturing are based on the borehole data, as these data sets contain the most detailed geological information. Any controls identified in the borehole data set are then

extended to the outcrop data to see if the controls appear to persist for these data sets as well. All of the analyses eventually flow towards the conceptual basis and parameters values for the stochastic DFN model inside the local model volume. This model consists of all of the pink-shaded output data sets and relations.

Determination of fracture sets and their orientation statistics

A fracture set is essentially a group of fractures whose orientations are either similar over a large spatial domain, or whose orientations, intensity or other properties can be closely related to geological factors in a statistically significant, predictable manner. The first step in the analysis of data available for the Forsmark model version 1.2 /La Pointe et al. 2005/ was to identify statistically homogeneous subpopulations for each of the five outcrops independently of any other outcrop, borehole or lineament data set. This analysis consists of evaluating the outcrop fracture trace patterns to look for families of consistently oriented fractures that show consistent abutting relations with other fracture sets (Figure 5-66). Next, these sets identified from trace data were plotted as stereoplots of the fracture data (Figure 5-67), expressed as poles to the fracture planes. Statistics were calculated for each set by assessing the goodness-of-fit of alternative statistical models for orientation. The statistical models derived are shown in Table 5-33.



Figure 5-66. Fracture trace maps with the different sets identified in outcrop shown with different colours. North is directed upwards in the figure. The different trace maps are at different scales (see also Figure 5-31).

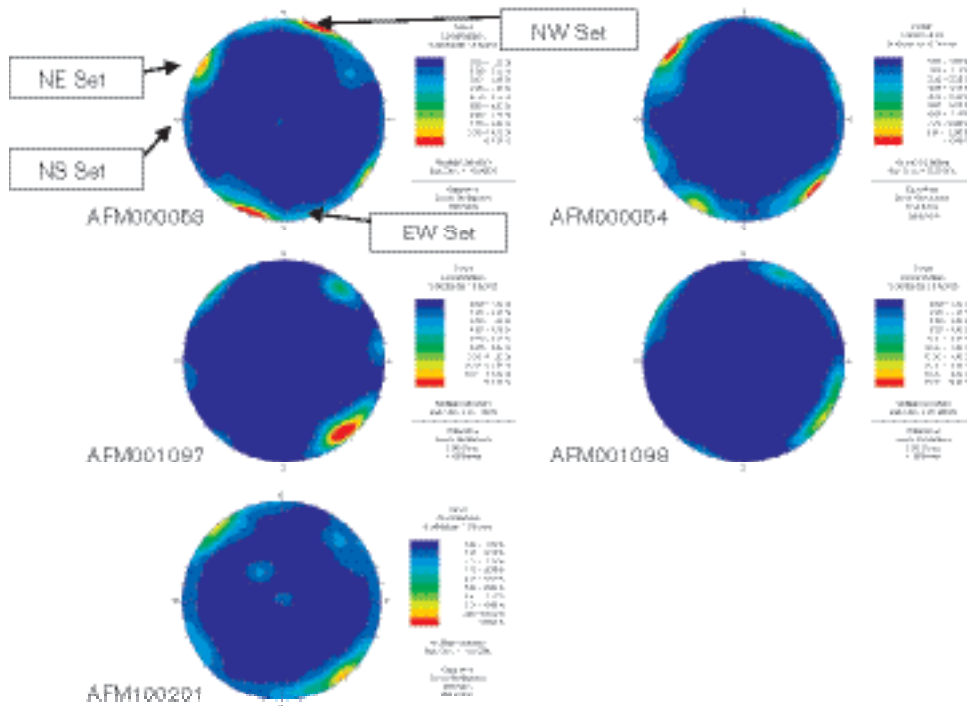


Figure 5-67. Stereoplots of poles to all fractures mapped in outcrops.

Table 5-33. Definitions of fracture set orientations derived from outcrop fracture data.

Set	Best model	Other acceptable models	Mean pole trend	Mean pole plunge	Dispersion
NS (L1)	Bivariate Fisher	None	92.4	5.9	k1 = 19.31, k2 = 19.69
NE (L2)	Bivariate Bingham	Bivariate Fisher at 2.2%	137.3	3.7	k1 = -17.9, k2 = -9.1
NW (L3)	Fisher	None	40.6	2.2	k = 23.9
EW (L4)	Fisher	None	190.4	0.7	k = 30.63
HZ	Fisher	All others	342.9	80.3	k = 8.18
Set	Major axis trend	Major axis plunge	KS Statistics	Significance	
NS (L1)	355.3	50.2	0.06	8.80%	
NE (L2)	38.1	68.2	0.045	10.30%	

The next step in defining sets was to determine what fracture sets might be present in the lineament data and assess whether they might be related to the sets identified in outcrop. The lineaments have been classified (see Section 5.2.3 and Figure 5-20) as regional and local major (> 1 km) or local minor (< 1 km). Figure 5-68 shows the rosette for traces from all the lineaments that are confined to the mainland area. This rosette shows sets that correspond well to the four sub-vertical sets identified in the outcrop data.

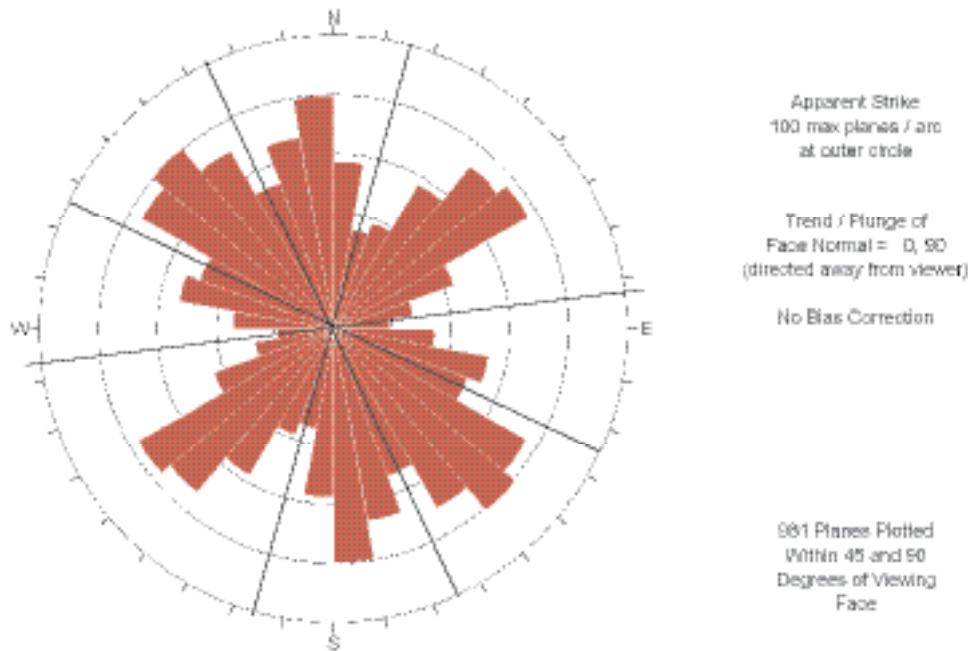


Figure 5-68. Rosettes for lineaments that are present on the mainland. The black lines on the rosette indicate the set boundaries.

Estimation of fracture sizes

The fracture size model was determined by combining trace lengths from outcrops and lineaments longer than 1 km for the same set, and fitting a scaling function to them (La Pointe et al. 2005). This calculation begins by determining whether the fracture intensity scales in a Euclidean manner or according to a different function, such as a fractal function. The type of scaling was determined through calculation of the mass dimension of the number of fractures per unit area. In a rock mass in which fractures scale according to a Euclidean function, doubling the area doubles the number of fractures. In a rock mass where the number of fractures per unit area follows a power law function, the scaling is fractal.

Tests of the scaling behaviour were carried out through the calculation of the mass dimension, and it was found that virtually all of the sets in all of the outcrops scaled approximately as a Euclidean function (Figure 5-69). This result means that it is possible to combine lineament trace length data and outcrop trace length data on a single plot simply by normalising for the different areas of each data set. The trace lengths for each data set were sorted from the shortest to the longest and numbered from n to l , where n was the number of traces in the data set. The n :th trace was the shortest trace in the data set, while the trace numbered l was the longest. This value was divided by the area of the outcrop or lineament map. The resulting plot is referred to as the normalised number/trace length plot. An example is shown in Figure 5-70.

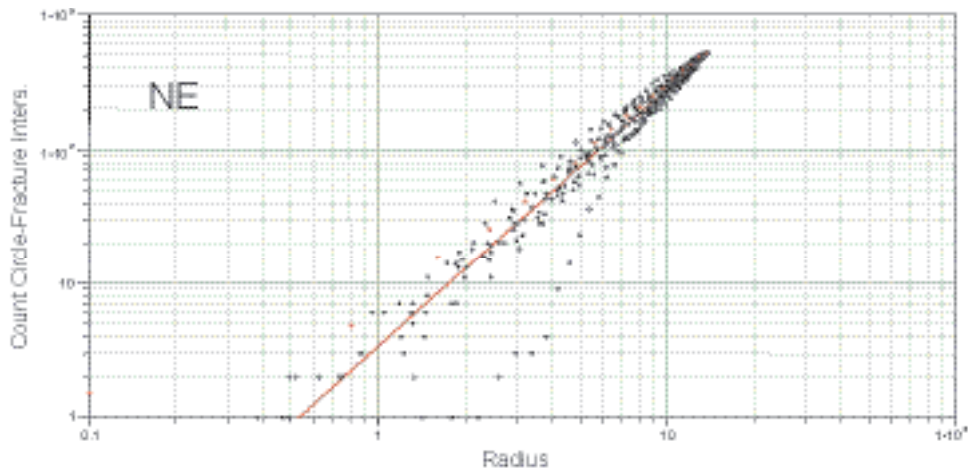


Figure 5-69. Mass dimension calculations for the northeast sub-vertical fracture set identified on outcrop ASM000053. The slope of the line is approximately 2.0, which indicates Euclidean intensity scaling.

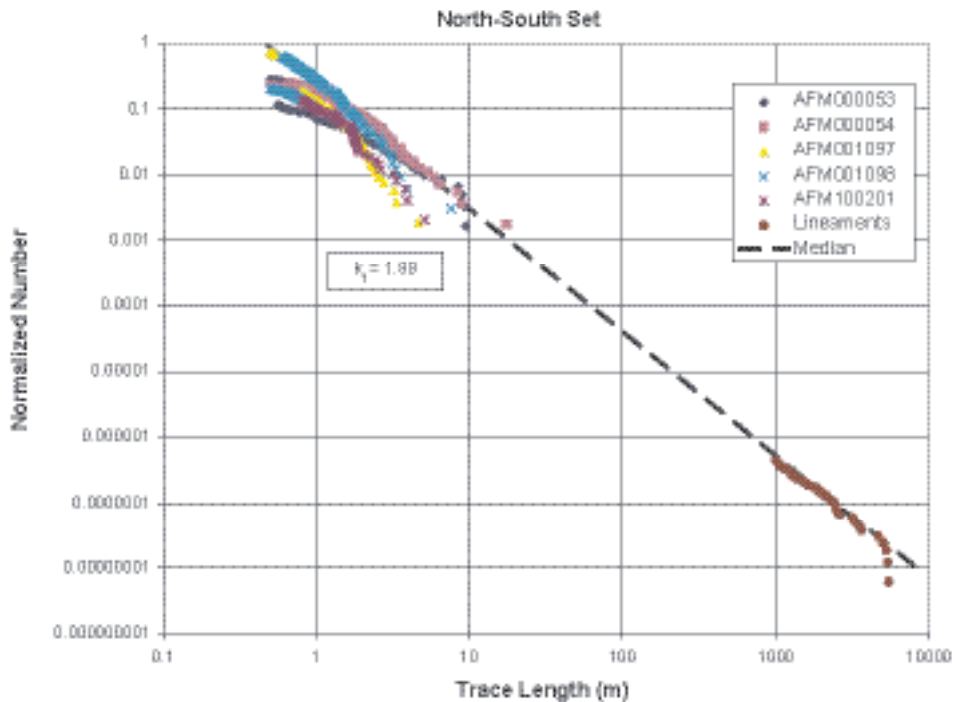


Figure 5-70. Example of trace length model estimation plot resulting from fractal mass dimension normalisation of fracture intensity with area. Plot shown is for the NS lineament-related regional fracture set.

The probability distribution that describes the size of the fractures was derived from these area-normalised number/trace length plots for each set through numerical simulation and theory. Mathematical derivation shows that the power law scaling exponent of the fracture radius distribution is equal to 1.0 plus the slope of the area-normalised number/trace length plot. The other parameter in the power law distribution, referred to as the location parameter, was derived through stochastic simulations that simultaneously matched the fracture trace length intensity in outcrops and the mean fracture intensity in cored boreholes.

The form of the power law size model is:

$$Prob(X \geq x) = \left(\frac{x_r}{x} \right)^k \quad (5-1)$$

where

x_r is the location parameter,

X is any fracture radius greater than or equal to x ,

k_r is the fracture radius shape parameter, and

$Prob(X \geq x)$ is the probability that X is greater than or equal to x .

The results are shown in Table 5-34. This table also shows the power laws which represent the upper and lower boundaries of the data, and thus quantify the uncertainty in the scaling exponent. The median values are somewhat steeper than the scaling exponent deduced in the trace length analysis of historic data from the Finnsjön study site in SR97, which suggested a value of 2.7. Note that the values of x_r reported in Table 5-34 are derived solely from the trace length plots matched to borehole mean intensity. New methodology has been developed and applied to the Laxemar/Simpevarp area, subsequent to the development of the DFN model for Forsmark, which simultaneously incorporates borehole, outcrop and deformation zone data, and provides an improved estimate of fracture sizes. It is suggested that this new methodology is also applied in future modelling work at Forsmark. Shortage of time did not permit its application at this stage.

Table 5-34. Fracture size parameters for fracture sets.

Set	Size model	Power law (parent radius distribution)		
		Upper k_r	Median k_r/x_r	Lower k_r
NS (L1)	Power law	2.94	2.88/0.28	2.78
NE (L2)	Power law	3.05	3.02/0.25	2.94
NW (L3)	Power law	2.87	2.81/0.14	2.71
EW (L4)	Power law	3.03	2.95/0.15	2.77
SubH	Power law	3.02	2.92/0.25	2.97

Intensity

The determination of geological controls on fracture intensity relies upon comparing fracture intensity from boreholes with borehole geology, and subsequent evaluation of possible controls with intensity variations at outcrop. The boreholes form the primary source of data since:

1. They provide a record of fracturing from the surface or near-surface to beyond the depth of the proposed repository.
2. There are large volumes of fracture data from the boreholes, leading to better statistical power for hypothesis testing.
3. The data encounter a wider variety of geological settings than do the outcrops.

Outcrop fracture data are much more limited. However, borehole data may be biased towards sub-horizontal fracturing and hence be better suited for investigating controls on sub-horizontal fracture intensity. Possible biases towards sub-horizontal fracturing in boreholes was investigated by separating fractures into sub-horizontal and sub-vertical sets to see if there were any significant differences. Only fractures outside the deterministic deformation zones were included (see Sections 5.2.8 and 5.4).

It was found that fracture intensity was often relatively constant through borehole intervals of hundreds of metres. It was also found that these intervals of homogeneous fracture intensity were associated with both identifiable geological factors and also with some as yet unknown factors. Rock domain, as defined in Section 5.3, was an important factor, so intensities were measured separately by rock domain. Fracture type (open, partially open, sealed) was also important; thus fracture intensities were calculated separately by fracture type. The different types are defined in Section 5.2.7. Finally, each fracture set exhibited its own intensity as well. The results are shown in Table 5-35.

The data analysis also showed that there were sub-domains of homogeneous fracture intensity that did not correspond to any mapped geological factors. These sub-domains often extended hundreds of metres, and many were associated with the presence or absence of specific fracture sets. The reasons for the presence or absence of specific fracture sets at this scale, and for the variations in intensity even when the same sets are present, are not known. These variations are likely to be important for repository-scale modelling, and should be investigated further.

Table 5-35. Intensity parameters as a function of rock domain, fracture type and fracture set.

Rock Domain ID	Fracture set	Intensity ($P_{32} - m^2/m^3$)			Total
		Open	Partly open	Sealed	
RFM029	NS	0.12	0.01	0.47	0.60
	NE	0.46	0.05	1.56	2.07
	NW	0.16	0.01	0.27	0.45
	EW	0.05	0.00	0.17	0.23
	HZ	0.34	0.01	0.26	0.61
	All	1.13	0.09	2.73	3.95
RFM018	NS	0.26	0.05	0.43	0.74
	NE	1.01	0.18	1.43	2.62
	NW	0.36	0.05	0.25	0.66
	EW	0.11	0.02	0.15	0.29
	HZ	0.73	0.04	0.24	1.01
	All	2.47	0.34	2.50	5.31
RFM017	NS	0.01	0.01	0.51	0.53
	NE	0.02	0.04	1.70	1.77
	NW	0.01	0.01	0.30	0.32
	EW	0.00	0.00	0.18	0.19
	HZ	0.02	0.01	0.28	0.31
	All	0.06	0.08	2.98	3.12
RFM012	NS	0.22	0.10	1.04	1.36
	NE	0.84	0.37	3.46	4.67
	NW	0.30	0.11	0.60	1.01
	EW	0.09	0.04	0.37	0.51
	HZ	0.61	0.09	0.57	1.27
	All	2.06	0.71	6.05	8.82

Spatial model

The spatial model was based on a combination of two components: the scaling of fracture intensity and the horizontal and vertical spatial correlation of fracture intensity in intervals /La Pointe et al. 2005/.

The mass dimension calculations described in this section demonstrate that a Euclidean model approximates the fracture trace intensity scaling observed on the scale of individual outcrops. A second series of tests was conducted in which the fracture intensity was calculated over 10 m depth intervals for all percussion boreholes. A non-parametric correlation analysis of these intervals showed that there were nearly no statistically significant correlations among these depth intervals for any pair of wells. This suggests that horizontal spatial correlation is negligible. Examination of intensity patterns with depth in individual wells also showed no systematic changes with depth. For these reasons, the data suggests that a Poissonian spatial model within an individual rock domain is appropriate.

5.5.3 Conceptual model with potential alternatives

The conceptual model consists of four sub-vertical sets and one sub-horizontal set. The sets suggest, based upon their mineral fillings, orientations and structural geometry, that the fractures were active at different times during the geological evolution of the region (see Section 3.1). Formation of at least some fractures as early as phase 2 in the geological evolution is considered probable (see also Section 5.4.2). There is no evidence to suggest that recent processes, such as deglaciation and crustal unloading following this period, have produced significant new fractures. Even the sub-horizontal fractures appear to be of similar age to the vertical fractures, based upon their fillings with epidote and intensity patterns with depth that track the vertical set intensities. Furthermore, they do not show shallow zones of higher open fracture intensity as might be expected if surficial stress relief produced new fractures or opened old ones. The relation of the sub-horizontal fractures to tectonic fabric or processes is not known. Some discussion on this question is presented in the conceptual model for the deterministic deformation zones (see Section 5.4.2).

The four sub-vertical sets appear to be related to structural lineaments in terms of orientation, relative intensity and size. This relation suggests that each sub-vertical fracture set consists of a single population of fractures that varies in size from centimetres to kilometres. This model implies that there are fractures in the tens of metres to hundreds of metres size range that are not well represented in outcrops or in the lineament data, but do exist in the rock mass.

The intensity of the fractures does not appear to vary with depth in any systematic way that could be related to stress relief. Rather, the fracturing outside of identified deformation zones is often found in intervals hundreds of metres in extent with relatively constant intensity. However, the intensity can vary significantly among the intervals, even in the same borehole, rock domain and lithology, as can the presence or absence of any of the fracture sets. The reasons for this are not currently known, but it is clear that each domain consists of sub-domains, often hundreds of metres in extent, with internally homogeneous fracture properties, and substantial variations between the sub-domains.

Within each rock domain, the spatial pattern of fracturing is well approximated by a Poissonian model in which there is no correlation in fracture intensity and the location of each fracture is independent of the location of other fractures.

In summary, the conceptual fracture model consists of five sets that probably formed during the early deformational stages of the craton (see also Section 5.4.2). There is no need to call upon recent deglaciation to explain the fracturing. The fractures show different intensity characteristics in different rock domains, and even within a single rock domain, there are sub-domains of different intensity and orientation that show low variation within the sub-domain and large variation among sub-domains. There is no variation of fracture intensity with depth that is consistent. The four sub-vertical sets are probably part of much larger fracture sets that also include structural lineaments.

5.5.4 Verification tests for conceptual models

Validation consists of a series of formal, documented steps that addresses whether a particular model is adequate for its intended purposes. One of the intended purposes is to predict fracture intensity at un-sampled or un-drilled locations. Validation includes confidence building exercises during model development, such as prediction of existing laboratory or field tests, as well as one or more post-model activities such as formal peer review, pre-model prediction of a post model experiment, comparison with other models, and comparison with published, peer-reviewed laboratory studies. The validation carried out for Forsmark model version 1.2 /La Pointe et al. 2005/ is quite limited in scope, as it focuses on using the DFN model to predict the fracturing in a single borehole, thus not validating the model for all rock domains, and only for fracture intensity and to a qualitative extent, fracture orientation. More thorough validation is warranted in future model versions as additional validation test data become available.

The purpose of model validation is to build confidence in the stochastic parameters determined for the DFN model. The validation of the DFN model has been carried out for the fractures recorded in KFM01A that is situated in rock domain RFM029. Most of the shallow high intensity intervals are identified within or in the possible zone of influence of ZFMNE00A2. This model suggests that the gently dipping deformation zone ZFMNE00A2, which includes DZ1 in KFM01A (see Section 5.4), is a major structure that controls the fracture frequency in the rock mass. The value of fracture intensity below DZ2 in KFM01A probably best reflects the intensity in the rock away from deformation zones (see Section 5.4). The intensity for the DFN model is based on the specific P_{10} values for the mean fracture frequency for the intervals presented in Table 5-36.

Twenty-five realisations of the fracture model for open and partly open fractures were simulated. Each realisation was sampled by a borehole in the same orientation (and with the same diameter) as KFM01A. The mean value of P_{10} was 0.67 m^{-1} , about twice the value measured in KFM01A below DZ2, but considerably less than the values measured above DZ2. The value for sealed fractures was 1.51 m^{-1} , about three times greater than the values measured in KFM01A below DZ2.

Although the results of the simulation are only a factor of 2 or 3 different from observations, this difference could have an impact on the behaviour of models at the well scale. What this simple validation exercise shows is that, however good the current model may be for matching rock domain average values, it probably does not accurately predict intensities on a more local borehole scale at the level required. A borehole interval of 300 m is sufficiently large to be significant in a hydrological model, and whether over- or under-prediction of fracture intensity by a factor of three is acceptable is not determined here, but could possibly be significant.

More importantly, this very preliminary validation exercise points out the need to better understand why intensity values change significantly in the same rock domain and in the same borehole. The results so far have shown that in some intervals, the changes in intensity coincide with the presence or absence of certain fracture sets, whereas in other cases, they do not. The size of these intervals of relatively constant intensity often is several hundred metres, which is clearly large enough to be of consequence in hydrological and mechanical modelling. The lack of predictive accuracy in the validation shows that further investigations are needed to determine why there are large intervals of varying intensity within a particular rock domain and borehole, and to develop a means to predict local intensity variations within a rock domain.

Table 5-36. P_{10} calculated for the sub-domains in RFM029 (outside of deformation zones).

Borehole interval	Range (m)	Length (m)	P_{10} – Open and partly open	P_{10} – Sealed
Above DZ1	30.5–35.9	5.43	4.05	0.55
DZ1–DZ2	47.8–386.1	338.24	1.61	0.88
DZ2–DZ3	412.9–639.0	226.10	0.35	0.33
Below DZ3	684.3–993.8	309.50	0.10	0.47

5.5.5 Evaluation of uncertainties

Quantification and propagation of uncertainty

Uncertainty in the model derives from several sources, including the uncertainty inherent in the data variability among the various outcrops and boreholes, as well as in the conceptual model which the data are used to construct.

The uncertainty in fracture orientation has been quantified by calculating the orientation dispersion for each set at each of the five outcrops, as well as through the consideration of alternative dispersion models that are statistically significant.

The uncertainty in the fracture intensity has been quantified by calculating the mean and standard deviation for intensity, stratified by fracture type (open vs. sealed), rock domain and depth. Users of this information may choose to propagate the uncertainty into their own models or calculations according to stratified Monte Carlo sampling or by analytical techniques as is appropriate and adequate for the intended purpose.

The uncertainty in size is quantified in two different ways. For the horizontal fracture set, the size model for the parent fracture radius distributions is based on aggregating all of the outcrop data for that set, and estimating a model for the distribution of fracture radii. There is also a conceptual uncertainty for this set, as its relation to other tectonic features is unknown, and the current method for calculating the size of the fractures assumes that it is not related to any other tectonic feature such as a lineament. For the lineament-related sets, three values are given: two bounding cases and a "best-guess". Since the artefacts have to do with censoring of trace length data, the trace length model fit to the normalised data is done visually rather than through non-linear regression. The "best-guess" is the best visual fit through all of the outcrop and lineament data. The two bounding cases are lines that approximate the shallowest and steepest lines that could be fit through the data. These represent the span of possible size variation given the existing data. As in the case of orientations, it is up to the user of this data to decide which parameter values to select.

Uncertainty in the spatial model is not completely specified except at the conceptual level. Because of current outcrop and borehole coverage, fracture data are not available for all specified rock domains. However, as emphasised earlier, it is possible that these un-sampled domains are best represented by different spatial models from the sampled domains. Moreover, the mass fractal analysis showed a slight departure in the spatial model from Poissonian towards a slightly fractal spatial pattern. The conceptual uncertainty as to whether to specify the spatial model as Poissonian or slightly fractal will affect the size calculations in a minor way, as the treatment of size uncertainty probably overshadows the impact. It will also slightly affect the number of fractures in the larger-scale models which extrapolate the P_{32} from small scales, like outcrops, to entire model regions. Depending upon whether the mass dimension is slightly below or above 2.0, the large-scale model will overestimate or underestimate, respectively, the number of fractures that would be inferred from the Poissonian spatial model. However, the uncertainty inherent in the P_{32} intensity for the small domain probably has a far greater impact than the scaling uncertainty.

Overall, the uncertainty in the model has been reduced by stratifying the DFN geometry as a function of rock domain.

Unresolved aspects of uncertainty

The primary unresolved uncertainty that seems likely to have the largest impact on models is the intensity, and perhaps the fracture size, as a function of rock domain. The current outcrop and borehole data are very limited as to the number of domains for which there are adequate data. Extrapolation of the values calculated for these few domains is a major uncertainty for site-scale modelling.

Another important unresolved uncertainty is the size model for the sub-horizontal set. If these fractures are on the order of tens or hundreds of metres in radius, which is not possible to resolve from outcrop trace data for the current outcrop data sets, then this could have a major impact on flow and transport behaviour of the rock mass.

Related to this uncertainty is the overall conceptual uncertainty of linking outcrop fracture sets to lineaments that represent possible deformation zones, to form a single, continuous population of fractures from metres to kilometres in size. As little data are available on fractures in the 20 m (approximate maximum length of outcrop trace) to 500 m (approximate minimum size of lineament traces) size range, the existence of fractures in this intermediate, yet hydrologically significant size range is unconstrained.

A final unresolved uncertainty is the impact of intervals of high and low intensity in the boreholes, and how to incorporate this in site-scale models. The data and validation exercise showed that there were zones of open and sealed fracture intensity, extending from a few metres to a few hundred metres in vertical extent, where intensity is higher or lower. The changes in intensity within a single borehole are often associated with the consistent presence or absence of some of the fracture sets. Why these bands of high and low intensity occur, and why they are associated with the presence or absence of sets has not been resolved. They do not correspond either to clusters in a Poissonian spatial model or clusters in a fractal spatial model. Moreover, the impact on calculating a single intensity value from borehole information, or prescribing a single orientation model for a borehole, when in fact most boreholes do not follow this simplified conceptual model, is not known. Since the controls on these intervals are not understood, the manner to best propagate this uncertainty to a larger-scale model is also not known.

5.6 Feedback to other disciplines

One or more components of the bedrock geological model provide a foundation for the modelling work in several other disciplines. However, since the challenges offered to the bedrock geological modelling group in their modelling work vary from discipline to discipline, each discipline needs to make a qualified judgement bearing on the relevance of each part of the geological model to their specific activity. For instance, the bedrock hydrogeology teams need to consider not only the spatial variations in the total fracture area per unit volume but also variations in the connected fracture area per unit volume.

The rock types at the site have been defined and their mineralogical, geochemical, petrophysical and geochronological characteristics quantified. The distribution of both rock units and rock domains has been presented at the surface, in the form of various bedrock geological maps over the site. The distribution of both these geological features has also been presented at depth, in especially the critical rock domain RFM029, in the form of borehole logs. Subsequently, the domains have been modelled in three-dimensional space. Furthermore, a numerical estimate of the proportions of different rock types, both dominant and subordinate, has been calculated for two rock domains RFM012 and RFM029. Finally, the variation in the character and intensity of the ductile deformation in the bedrock at the site, which steers its anisotropy, has also been addressed. All these features provide a feedback to especially the discipline thermal modelling in the bedrock. They are also of significance for the disciplines rock mechanics, hydrogeology (bedrock) and, to a less extent, hydrogeochemistry (bedrock) and transport properties (bedrock).

The locations of deformation zones that are predominantly longer than 1,000 m have been defined in three-dimensional space in three separate geometric models. The properties of each zone in the models, including, for example, thickness, length, character of deformation, fracture orientation and fracture mineralogy, have been documented. Furthermore, a conceptual model for the formation and reactivation of different orientation sets has been developed. This concept integrates the wealth of quality new data that has been generated at the site with the regional tectonic evolution in central Sweden. The orientation, size and intensity of fractures in the bedrock between the deformation zones has been presented with the help of a statistical analysis in the complementary, DFN modelling work. All these aspects of the bedrock geological model provide a necessary structural framework for the hydrogeological and even rock mechanics modelling. The information on fracture mineralogy also provides a feedback to the disciplines hydrogeochemistry (bedrock) and transport properties (bedrock).

All the three components of the geological model have had a direct impact on the location and the design of the repository volume, version D1. They also provide necessary background information for certain aspects of the safety analysis work.

6 Rock mechanics model

The task of rock mechanics is to use the geological information summarised in the geological model, together with the quantification of the mechanical properties of the different components of the rock mass (intact rock, rock fractures and, their assemblage in the rock mass), to provide the necessary information for rock mechanics analyses of the site. The quantification of mechanical properties and boundary conditions are input to the calculations for stability analysis and design of the underground facilities, and the safety analysis of the possible repository at the site. The rock mechanics model consists of a set of constitutive models and parameters that allow for analytical and numerical simulations of the mechanical behaviour of the rock mass. The rock mechanics model is constructed in accordance with the SKB strategy report /Andersson et al. 2002b/ that implies:

- i) Analysis of the primary data (laboratory tests and in-situ observations and measurements).
- ii) Estimation of the mechanical properties of the intact rock (matrix) and rock fractures.
- iii) Estimation of the rock mass mechanical properties by means of empirical and theoretical methods. Rock domains and deformation zones, particularly those with of brittle character, are studied.
- iv) Estimation of the rock stress field by means of the analysis of in-situ measurements and numerical modelling.
- v) Compilation of a set of parameters and boundary conditions that describes the behaviour and the in-situ constraints at the site based on the results achieved in i) through iv).

Geomechanical information from boreholes KFM01A, KFM02A, KFM03A and KFM04A was used for rock mechanics purposes (see Figure 2-1).

6.1 State of knowledge at previous model version

In the version 1.1 of the Forsmark site descriptive model /SKB, 2004a/, a rock mechanics model was set up based on the information available at the time. This information consisted of laboratory testing and excavation experience from the construction of the power plants and of the SFR repository. Moreover, borehole KFM01A had been drilled and new core data were available (for rock domain RFM029) together with information from new outcrop surveys (for rock domains RFM017, RFM018, RFM032 and RFM033).

Laboratory results available from SFR on “gneissic granite” were considered representative of the “granite to granodiorite” rock type (code 101057) in RFM029. On average, the uniaxial compressive strength (UCS) of such rock was estimated to be 230 MPa, whereas its Young’s modulus and Poisson’s ratio were 75 GPa and 0.24, respectively. The tensile strength of the intact rock was also estimated.

By means of the empirical methods Q and RMR, the mechanical properties of the rock mass were estimated. This task was also carried out by different persons for the purpose of evaluation of the robustness of the methods and for verification. The independently-determined results were very consistent. From the empirical methods, the equivalent UCS of the rock mass was estimated to be between 100 and 170 MPa, the deformation modulus between 40 and 70 GPa, the Poisson’s ratio between 0.10 and 0.24, whereas the equivalent cohesion and friction angle (for rock stresses between 10 and 30 MPa) were evaluated to be between 20 and 35 MPa and 20° and 45°, respectively. Based on the rock-mass classification during construction of the SFR’s access tunnels, the deformation modulus of the Singö deformation zone (ZFMNW0001) was estimated to range between 3 and 10 GPa. Other minor deformation zones were reported to have a deformation modulus between 15 and 30 GPa.

The determined parameters were assumed to increase with depth, as the geological information along borehole KFM01A would suggest. The actual spatial variability was not very well known. These mechanical properties were quantified for the characterisation of the rock mass. Thus, the effects of rock stresses, water conditions and orientation of the underground excavations had to be considered separately.

The stress field at the site was inferred based on the reinterpretation of rock stress measurements carried out in the late Seventies in boreholes DBT-1 and DBT-3. The maximum and minimum (vertical) principal stresses were estimated to be, respectively, 49.0 and 13.5 MPa at 500 m depth. The intermediate principal stress was estimated to be very close in magnitude to the vertical stress. The spatial variability of the stresses was quantified to be 15% or 50% of the mean value for the stresses outside or within fractured rock, respectively. The uncertainty of the stress estimations was judged to be about 20% of the mean values. The trend of the major principal stress was rather uncertain ($134^\circ \pm 15^\circ$), probably due to the effect of gently dipping fracture zones that affected, not only the aspect of the surface outcrops, but also the stress orientation from depth to depth. The orientation of the local stress field seemed to agree with the available data in central Sweden and with the strike of the regional deformation zones (e.g. Singö, Forsmark and Eckarfjärden deformation zones). Furthermore, the stress field at shallower depth may also be affected by the presence of horizontal sediment-filled fractures generated by the vertical stress release in the last post-glacial period. The frequency of the horizontal fractures usually diminishes below a depth of around 100 m.

6.2 Evaluation of primary data

For model version 1.2, a new experimental campaign was carried out on samples from four boreholes: KFM01A, KFM02A, KFM03A and KFM04A. The amount of available laboratory test results has noticeably increased; 68 uniaxial compressive tests, 59 triaxial compressive tests, and 143 tensile strength determinations were performed on intact rock, 96 shear tests were performed on 28 samples and 142 tilt tests were undertaken on rock fractures (see Table 6-1).

Samples were collected of the two most dominant rock types (granite to granodiorite and tonalite to granodiorite) and several natural fracture samples. Also, other data collected during the construction of the power plants and of the SFR repository /SKB, 2004a/ were considered in the evaluation, mainly for comparison with the new data.

Table 6-1. New laboratory tests carried out for the Forsmark model version 1.2.

Laboratory test	KFM01A	KFM02A	KFM03A	KFM04A
Uniaxial compressive tests	21	15	17	15
Triaxial tests	19	12	16	12
Indirect tensile tests	40	30	40	33
Shear tests on fractures	33 (7 samples)	21 (7 samples)	24 (8 samples)	18 (6 samples)
Tilt tests on fractures	41	40	35	26
P-wave velocity on core samples	34	79	68	37

* See Table 2-2 in Chapter 2.

6.2.1 Laboratory tests on intact rock

All the available new data on intact rock samples, consisting of results of uniaxial, triaxial and indirect tensile strength tests, were analysed. Based on the testing results, deformational parameters such as Young's modulus and Poisson's ratio were determined. The parameter "crack initiation stress" was also evaluated to be used for the evaluation of rock burst and spalling potential /Martin and Chandler, 1994/. The crack initiation stress defines the limit of elastic deformation in the intact rock under compression.

Two metamorphic rocks with a granitic to granodioritic and tonalitic to granodioritic composition were sampled along the borehole cores. A few samples of metamorphic granodiorite were also collected (totally 7). In model version 1.1, the properties of the gneissic granite from SFR were assumed for the "granite to granodiorite" rock type. /Lanaro and Fredriksson, 2005/ showed that the average mechanical properties of the intact rock for the rock types do not significantly differ from the SFR's results (Table 6-2) whereas the frequency distributions do (Figure 6-1). This is probably due to the

fact that the gneissic samples were collected at the border of the local model volume, where the influence of the Singö deformation zone and associated metamorphic processes might have affected the rock strength and thereby producing a wider variation compared with the samples of granite from the inner part of the local model volume.

Considering the variation with depth, there seems to be no change of intact rock properties with depth above 500 m (Figure 6-2). Below this depth, some sample disturbance due to the release of high rock stresses might occur. Moreover, the presence of sealed fractures in some samples of the intact rock did not significantly affect the uniaxial compressive strength (between 145 and 188 MPa) and the Young's modulus (about 80 GPa) of the samples.

Table 6-2. Mechanical properties of the intact rock from uniaxial (UCS), triaxial (TCS) and tensile (TS) tests. Samples from borehole KFM01A, KFM02A, KFM03A and KFM04A.

	SFR: Gneissic granite*	SFR: Gneiss*	Granite to granodiorite**	Tonalite to granodiorite**
Number of tests	20 UCS	28 UCS	52 UCS 47 TCS 112 TS	8 UCS 8 TCS 20 TS
Uniaxial Compressive Strength (mean)	230 MPa	248 MPa	225 MPa	156 MPa
Young's modulus (mean)	75 MPa	78 MPa	76 GPa	72 GPa
Poisson's ratio (mean)	0.24	0.23	0.24	0.27
Tensile Strength (mean)	13 MPa	–	13 MPa	15 MPa

* Estimated in SDM version 1.1.

** Estimated in SDM version 1.2.

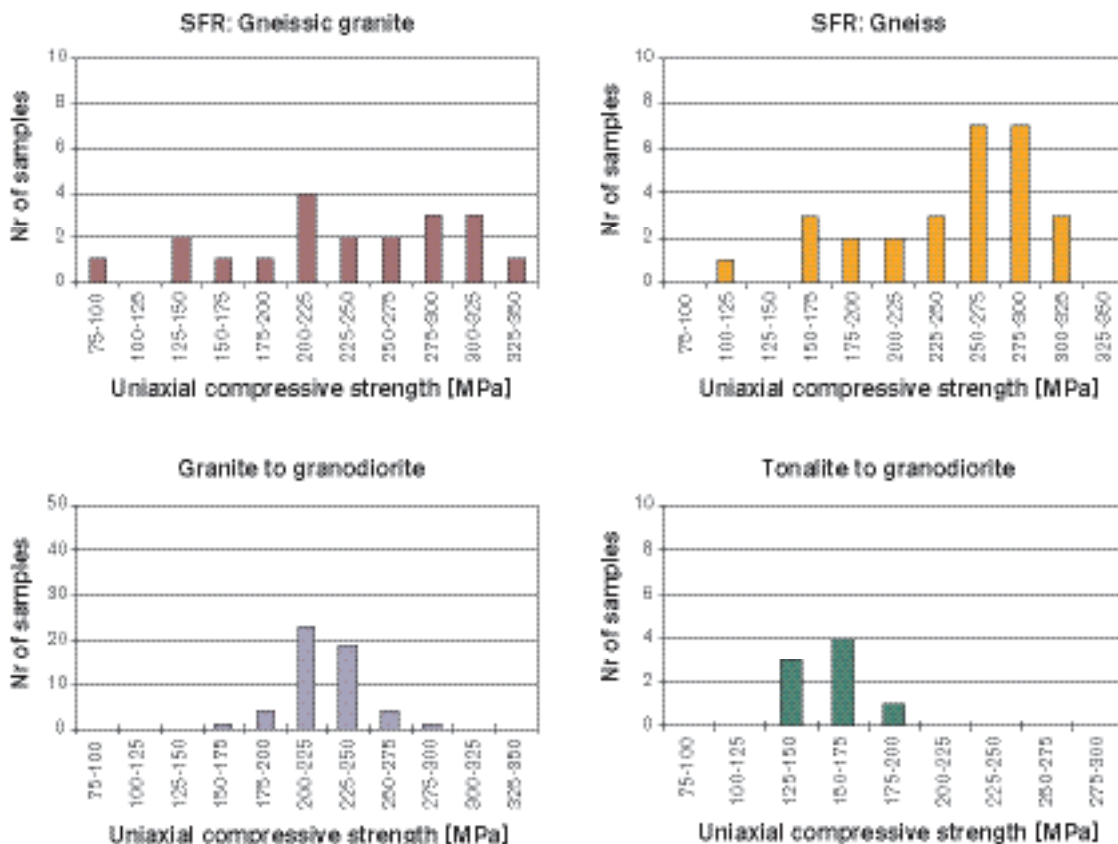


Figure 6-1. Histograms of the uniaxial compressive strength of the samples collected during the construction of the SFR Repository (upper row) and of samples collected for the Forsmark model version 1.2 (lower row).

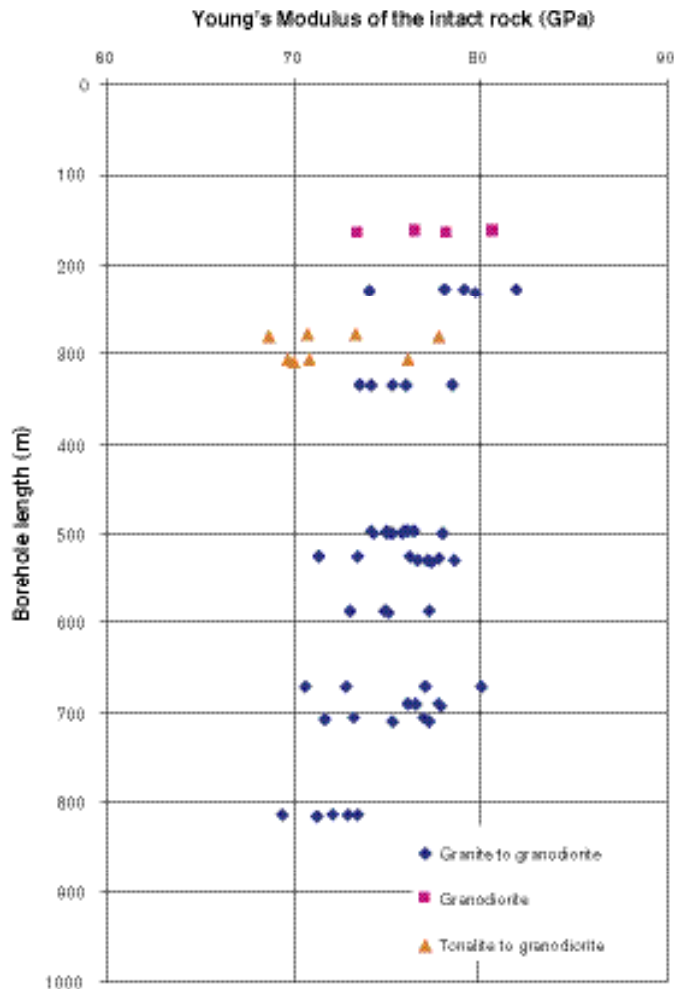


Figure 6-2. Young's modulus of the intact rock samples under uniaxial loading. The Young's modulus is plotted versus sample location along boreholes KFM01A, KFM02A, KFM03A and KFM04A.

6.2.2 Laboratory tests on natural rock fractures

The results of direct shear tests were provided in terms of strength and strain-stress curves. Tilt tests on similar samples were also carried out and provided fracture strength parameters. The cohesion and the friction angle values were then determined based on results from both kinds of tests. The results from different samples are very consistent independently of the orientation of the fractures, thus the mechanical properties are calculated as an average for all fracture sets /Lanaro and Fredriksson, 2005/. Also the tilt tests showed that there are not significant differences between the mechanical properties obtained from tilt tests and direct shear tests. The newly obtained values of the peak cohesion and friction angle (Table 6-3) agree very well with the earlier results by /Stille et al. 1985/ that quantified the cohesion and friction angle of fractures in rock samples from SFR as 0.6 MPa and 35°, respectively, as adopted in model version 1.1 /SKB, 2004a/. The same does not apply to the fracture stiffness values obtained in the earlier study. The normal and shear stiffness of the fractures were quantified as 32 and 5.4 MPa/mm, respectively, which are between 3 and 7 times smaller than the newly determined values. Although the new tests should have higher accuracy than the earlier tests that provided data to model version 1.1 /SKB, 2004a/, problems were still encountered when determining the normal and shear stiffness of the fractures. The problems are probably due to the different size of the tested samples and to the imprecise knowledge of the deformability of the shear apparatus, sample holders and rock blocks. Corrections to these problems are planned for the coming test campaigns.

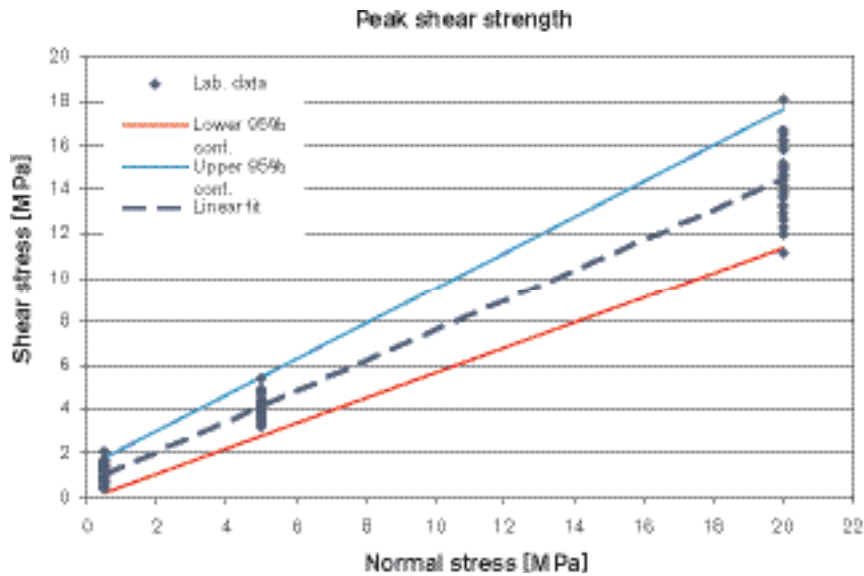


Figure 6-3. Peak shear strength envelope for the fracture samples tested under direct shear. The samples came from boreholes KFM01A, KFM02A, KFM03A and KFM04A.

Table 6-3. Mechanical properties of the natural rock fractures from direct shear and tilt tests (boreholes KFM01A, KFM02A, KFM03A and KFM04A). All fractures are grouped together independent of the fracture set.

Parameter for single fractures – All fracture sets	Direct shear		Tilt tests	
	Mean/standard deviation	Truncation interval: min–max	Mean/standard deviation	Truncation interval: min–max
Peak cohesion, $c_p^{1)}$	0.6/0.3 MPa	0.0–1.1 MPa	0.36/0.4 MPa	0.1–0.6 MPa
Peak friction angle, $\phi_p^{1)}$	34.0°/2.8°	27.3°–39.1°	34°/3.6° ²⁾	27°/41° ³⁾
Residual cohesion, $c_r^{1)}$	0.5/0.3 MPa	0.0–1.1 MPa	0.3/0.1 MPa	0.1–0.6 MPa
Residual friction angle, $\phi_r^{1)}$	31°/4°	22°–38°	29.6°/4.4°	21°/38°
Normal stiffness, $K_n^{4)}$	128.4/51.6 MPa/mm	68.0–288.4 MPa/mm	–	–
Shear stiffness, $K_s^{5)}$	38.8/10.8 MPa/mm	12.2–55.1 MPa/mm	–	–

¹⁾ Shear strength for normal stress between 0.5 and 20 MPa.

²⁾ The basic friction angle has a mean value and standard deviation of: 31°/2°.

³⁾ The basic friction angle has a truncation interval: 23°–35°.

⁴⁾ Secant normal stiffness for normal stress between 0 and 10 MPa.

⁵⁾ Secant shear stiffness for normal stress between 0 and half the peak shear strength.

6.2.3 Other data

In the late Seventies, the construction works for the power plant produced a certain amount of engineering-geological information. In particular, information was obtained about the superficial rock mass, characterised by extensive horizontal fracturing, sometimes with a width of more than half a metre and sediment infilled, and about the regional Singö deformation zone. This was crossed by two discharge tunnels. The seismic velocity measured along the tunnels was on average over 5 km/s but it dropped to 3.6 km/s in the zones of weakness.

Also, the investigations and the construction of the SFR repository provided a better insight on the rock mass quality and properties east of the Singö deformation zone. Here, earlier editions of the RMR_{79} (determined based on /Bieniawski, 1979/) and Q_{74} method (determined based on /Barton et al. 1974/) were applied to infer the mechanical properties of the rock mass. These studies, even

though not completely in agreement, classified the rock mass as “good” or “very good”. The average RMR_{79} varied between 62 and 83, whereas Q_{74} was determined to vary between 5 and 10. From the rock mass quality, the rock mass uniaxial compressive strength, deformation modulus and Poisson’s ratio were derived. The rock mass compressive strength ranged between 5 and 29 MPa with an average around 10 MPa; the deformation modulus varied between 2 and 43 GPa with an average of 20 GPa; the Poisson’s ratio was estimated between 0.08 and 0.1. Based on these parameters, numerical modelling by FEM codes was carried out.

The characterisation of the rock mass by means of the Q-system was also carried out based on the surveying of surface outcrops and SFR tunnel walls /Barton, 2004/. The survey of the outcrops highlighted the presence of rock mass quality contrasts within the “target area” with Q values ranging from 5 to 15 that almost corresponded to the maximum and minimum observed for all the surveyed outcrops, i.e. between 2.8 and 16.6. A tentative extrapolation of these surface data down to a depth of 250 m was done, resulting in a range of expected Q values between 6 and 58.

A direct Q-logging was performed on the core of borehole KFM01A /Barton, 2003/. This was done to verify the extrapolation of the surface Q-logging to depth, but also for comparing the results obtained with the Q-loggings based on Boremap data (Section 6.2.4). The direct logging of the core identified four fracture zones with Q frequently between 17 and 38. The overall quality of the rock mass ranged between very good and excellent (frequent values around 100). Thus, the extrapolation of the surface data to depth underestimated the rock mass quality at depth. This is probably due to the poor connectivity of the fractures and the almost dry conditions of the borehole at depth that did not reflect the values of the Q parameter for water, J_w , suggested in the literature.

6.2.4 Rock mass properties based on borehole data

Based on Boremap geological loggings along four boreholes (KFM01A, KFM02A, KFM03A and KFM04A), the characterisation of the rock mass at depths between 100 and 1,000 m was carried out using the empirical systems RMR /Bieniawski, 1989/ and Q /Barton, 2002/. For this purpose, the SKB methodology for rock mass characterisation was followed /Andersson et al. 2002b; Röshoff et al. 2002/. The characterisation implies that the rock mass properties are determined independently of the boundary conditions (e.g. rock stresses, water pressure, micro-cracking, excavation shape). Thus, the values of Q and RMR reported here assume low rock stresses and dry conditions /Lanaro, 2005a–d/ (Table 6-4). For the purpose of the rock mechanics modelling of the site, the effect of the boundary conditions on the mechanical properties of the rock mass is illustrated in Section 6.3.

The use of Boremap mapping implies that most of the rock mass characterisation is based on digital data regarding fractures (orientation, frequency, roughness, infilling, etc), intact rock (rock types, I_s , UCS, TCS, TS, etc), crushed zones, clay occurrences, etc. This technique was validated against direct Q-logging of the cores and shown to give very similar statistics of Q and its input parameters /SKB, 2004a/. The characterisation (Figure 6-4) was also based on the geological “single-hole” interpretation of the boreholes and the DFN model. For controlling scale effects and reducing biases, the empirical methods were applied to equally long sections of core/borehole of 5 and 20 m (for KFM01A) or 30 m (for the other boreholes). It could be observed that RMR stays the same with changing core section length whereas Q diminishes when longer core sections are analysed (30% for KFM01A /Lanaro et al. 2004/). This is mainly due to the fact that the longer the core sections, the larger the number of fracture sets occurring in the section. This produces lower Q values.

The mechanical properties of the rock mass were also determined through empirical relations with RMR (and GSI /Hoek and Brown, 1997; Hoek et al. 2002/) and Q. The mechanical properties of the rock mass are given as frequency distributions of the apparent uniaxial compressive strength, cohesion and friction angle, tensile strength, deformation modulus and Poisson’s ratio. These properties characterise the rock mass as an equivalent continuum at the tunnel scale.

Table 6-4. Results of the characterisation by means of Q and RMR for boreholes KFM01A, KFM02A, KFM03A and KFM04A.

		KFM01A mean (min-max)	KFM02A mean (min-max)	KFM03A mean (min-max)	KFM04A mean (min-max)
Competent rock	Q	100* (7.6-2,133)	71* (4.3-2,133)	40.2* (1.8-2,133)	104* (4.7-2,133)
	RMR	88 (73-96)	84 (74-96)	85 (74-96)	89 (76-99)
Deformation zones	Q	51* (15-1,067)	12.7* (2.8-85)	10.8* (3.0-600)	34.5* (9.7-167)
	RMR	82 (77-94)	81 (68-87)	79 (72-91)	82 (77-86)

* Most frequent value.

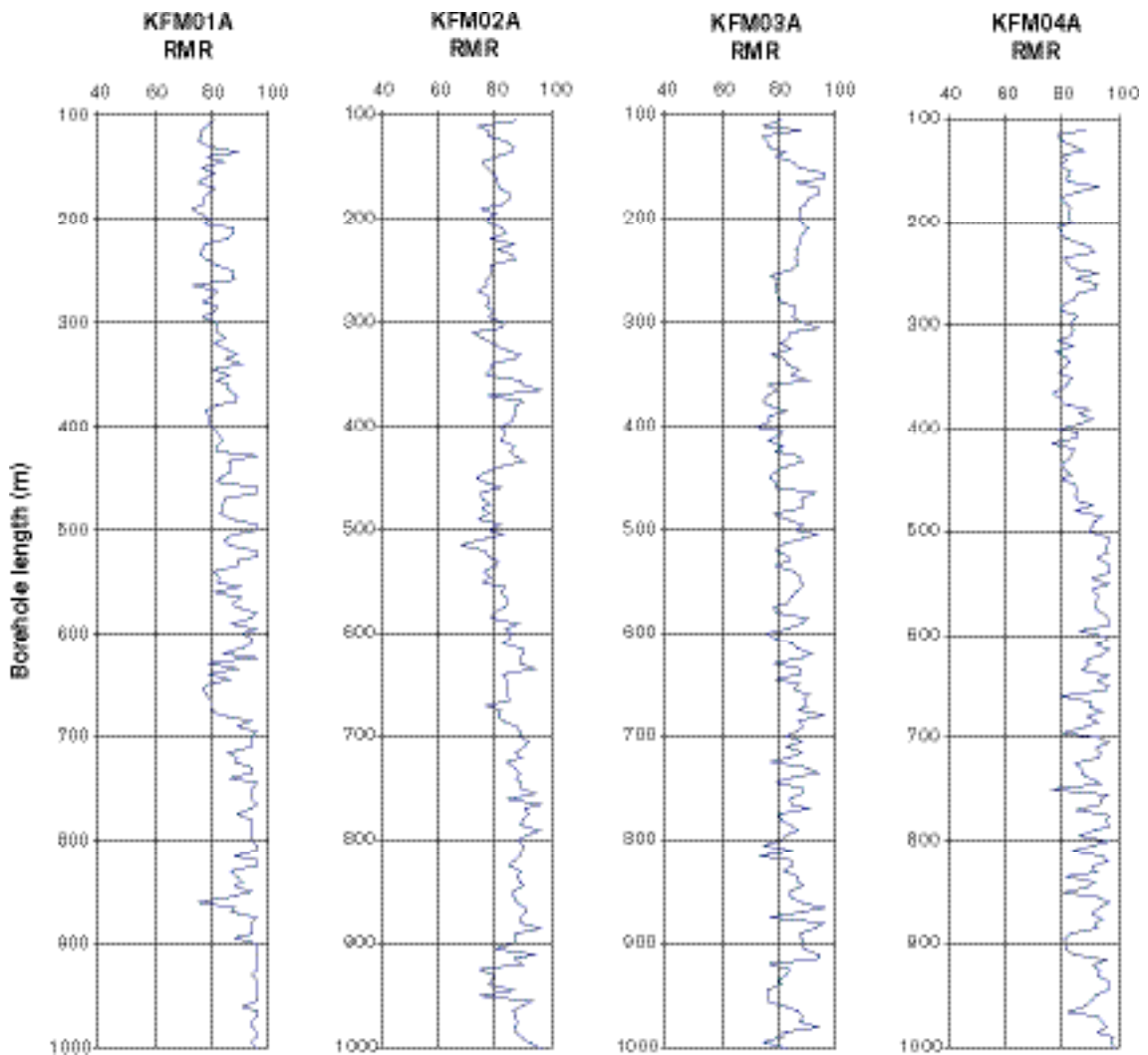


Figure 6-4. Variation of RMR along boreholes KFM01A, KFM02A, KFM03A and KFM04A.

6.3 Rock mechanics properties

The current rock mechanics model assigns the deformability and strength properties to the rock domains and deformation zones indentified in Chapter 5 where geological information is available, and it estimates the properties when no data are available by means of extrapolations and deductions. The properties regard the intact rock, the rock fractures and the rock mass.

6.3.1 Modelling assumptions and input from other disciplines

The background to the rock mechanics modelling was provided by the new geological models proposed for the site: the rock domain, the deformation zone and the discrete fracture network (DFN) models (Sections 5.3 to 5.5). The main assumptions of the rock mechanics model are that:

- The mechanical properties were assigned to the rock domains and deformation zones as they were defined and described by the rock domain and deformation zone models (Figure 6-5).
- The mechanical properties of the intact rock and fractures were obtained from the laboratory results. Only the properties of two rock types are provided.
- The rock mechanics properties can be estimated by means of empirical and theoretical methods applied to the available geomechanical information.
- It is possible to superimpose the effect of rock stresses, water pressure and temperature onto the mechanical properties of the rock mass “at rest” (i.e. for characterisation according to /Andersson et al. 2002/: low stress, dry conditions and in-situ temperature).
- The uncertainties of the rock mechanics model can be quantified by using the same methods applied for the determination of the mechanical properties.

At different scales, the main features of the rock mass are:

- i) The intact rock matrix, i.e. the solid rock.
- ii) The natural rock fractures.
- iii) The competent rock mass inside each rock domain (sometimes called also “background rock”), i.e. the assembly of intact rock and fractures where the repository may be located.
- iv) The deterministic deformation zones (DDZ), which are the zones judged to be important components of the deformation zone model of the site due to their size, deformation, alteration and fracture frequency.
- v) The minor deformation zones (SDZ). These zones were identified as rock mass volumes with higher fracture frequency and weathering than the nearby competent rock in the geological single-hole interpretation of the borehole data. In the DFN model, these zones are included and modelled as stochastic features. At Forsmark, these minor zones are not very frequent. Their definition has been retained for coherence with the Simpevarp site descriptive model version 1.2.

The intact rock properties are given in Section 6.3.3 and the mechanical properties of the rock fractures are given in Section 6.3.4 based on the laboratory results. Sections 6.3.5 and 6.3.6 provide the mechanical properties of the rock mass obtained by means of two independent approaches: the empirical and the theoretical approach. Finally, in Section 6.3.7, the two approaches are combined into a single rock mechanics model that merges the two sets of results and describes the mechanical properties of the rock mass at the Forsmark local model volume.

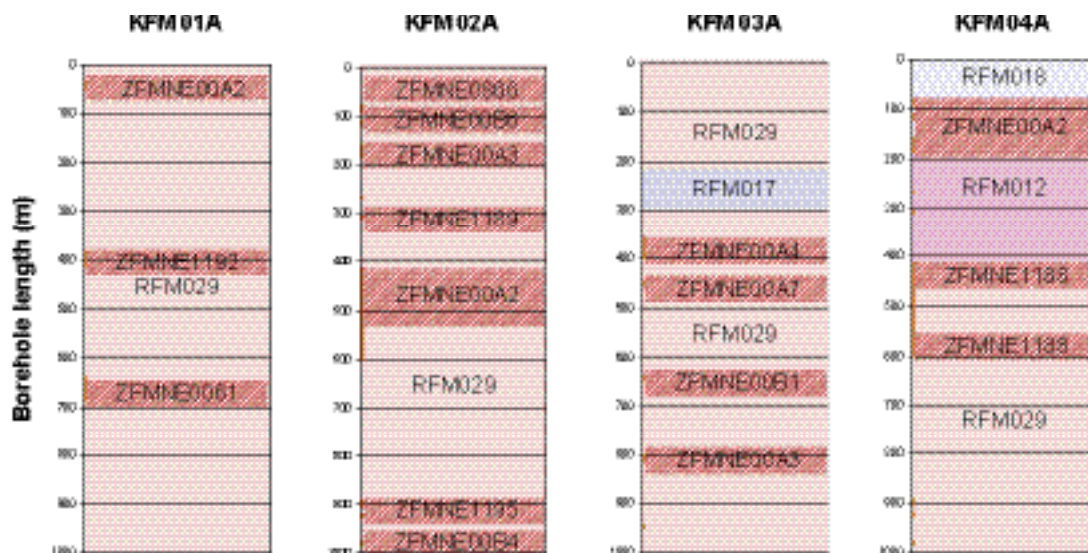


Figure 6-5. Rock domains (different colours) and deformation zones (raster and orange lines) along the analysed boreholes. The lettering indicates the name of the rock domains and deformation zones according to the rock domain and deformation zone model in Chapter 5. The values of Q and RMR in Table 6-4 show that the competent rock and the deformation zones intercepted by the boreholes in general present rather good rock quality.

6.3.2 Conceptual model with potential alternatives

Two conceptual models are used for describing the behaviour of the rock mass from a rock mechanics point of view:

- 1) Discrete medium composed by intact rock and rock fractures.
- 2) Continuous equivalent medium.

The description of the behaviour was kept as simple as possible to mirror the provided laboratory results, their sparseness and the constitutive models to be used for the numerical analyses. Thus, both conceptual models listed above were assigned the same deformability and strength criteria:

- a) Linear elasticity is assumed for the intact rock and the rock fractures (i.e. the deformation is linearly proportional to the applied stresses). Typical parameters are: i) for intact rock: Young's modulus, Poisson's ratio; ii) for the rock mass: deformation modulus, Poisson's ratio; and iii) for the rock fractures: normal and shear stiffness. The intact rock and the fracture were also assumed to be isotropic (i.e. the properties do not vary in different direction).
- b) Linear (Coulomb) or truncated bi-linear strength criteria for the intact rock, fractures and equivalent rock mass. Model parameters for intact rock, rock mass and rock fractures are: apparent cohesion and friction angle for a defined normal stress interval (e.g. between 10 and 30 MPa). For the intact rock and the rock mass, the uniaxial compressive and tensile strength are also provided. The use of these parameters can lead to a truncated bi-linear strength criterion that approximates the concave strength criteria often exhibited by natural materials. The strength criteria apply in term of effective stresses.

These conceptual models satisfy the requirements imposed by the Underground Design Premises /SKB, 2004c/. The boundary conditions to the rock mechanics model are provided by the state of stress and by the hydrogeological model (Chapter 8). Moreover, exactly the same parameter definition and stress ranges were adopted for the Simpevarp model version 1.2, so that comparison of the mechanical properties of the rock mass at the two sites can be made.

The rock mechanics parameters of the rock mass are provided for equivalent rock volumes of about 20 to 30 m edge. This size was chosen because it allows a certain degree of averaging of the mechanical properties and it is comparable to the size of the numerical models used for the analysis of an ordinary tunnel (about 5 m in diameter).

The parameters are all described by means of truncated normal distribution functions. In fact, the normal distribution approximates most of the frequency distributions of most of the parameters, either obtained in laboratory or inferred empirically or numerically. The truncations are not always symmetrical with respect to the mean value due to the skewness (i.e. asymmetry) of some of the experimentally determined or estimated frequency distributions.

6.3.3 Assignment of rock mechanics properties to the intact rock

The two rock types tested in laboratory (Section 6.2.1) can be assumed to coincide with the most predominant rock types in rock domains RFM012 and RFM029 (granite to granodiorite) and rock domain RFM17 (tonalite to granodiorite), respectively. Rock domain RFM18 is composed of a mixture of several rock types. Consequently, the properties of the rock types in Table 6-3 can be assumed as upper and lower boundaries of the properties of the intact rock in rock domain RFM018. The mechanical properties of the intact rock are obtained by means of internationally established standard methods and procedures (i.e. ISRM Suggested Methods).

The uncertainty of some of the mechanical properties (i.e. uniaxial compressive strength, Young's modulus, Poisson's ratio and tensile strength) was evaluated by comparing the experimental results obtained from different laboratories on two sets of samples from the same borehole, rock type and depth. The resulting uncertainty of the mean value for all the properties is reported in Table 6-5 in percentage. For the friction angle and cohesion, the uncertainty was estimated based on engineering considerations. For assigning the mechanical properties of the rock types to the rock in the rock domains, the hypothesis that the rock samples are representative of the intact rock inside each rock domain is also made. This is an approximation, because it assumes that the variation of the laboratory samples is representative of the spatial variation and volumetric distribution of each rock type in the rock domains. Thus, sampling bias cannot *a priori* be excluded.

Table 6-5. Mechanical properties of the intact rock matrix (i.e. solid rock without any fractures) for the main rock types in the Forsmark local model volume. The mean value and the standard deviation of the properties are given with the truncation intervals for the normal distribution. The samples were collected from boreholes KFM01A to KFM04A. The properties of the two rock types are assumed to coincide with the intact rock properties of rock domains RFM029 and RFM012 (granite), and RFM017 (tonalite), respectively. The range of variation of the mean value due to uncertainty is also given (see definition in Section 6.3.8).

Parameter for intact rock (drillcore scale)	Intact rock in RFM029 and RFM012		Intact rock in RFM017	
	Granite to granodiorite		Tonalite to granodiorite	
	Mean/standard deviation <i>Uncertainty of the mean</i>	Truncation interval: min and max <i>Uncertainty of the mean</i>	Mean/standard deviation <i>Uncertainty of the mean</i>	Truncation interval: min and max <i>Uncertainty of the mean</i>
Uniaxial compressive strength, UCS	225/22 MPa ± 3%	180–270 MPa	156/13 MPa ± 3%	130–180 MPa
Young's modulus, E	76/3 GPa ± 1%	70–82 GPa	72/3 GPa ± 1%	65–80 GPa
Poisson's ratio, ν	0.24/0.04 ± 9%	0.15–0.30	0.27/0.04 ± 9%	0.20–0.35
Tensile strength, TS	13/2 MPa ± 9%	10–17 MPa	15/1.5 MPa ± 9%	13–18 MPa
Coulomb's cohesion, $c^{1)2)}$	28/3 MPa ± 10%	22–34 MPa	30/2.5 MPa ± 10%	25–35 MPa
Coulomb's friction angle, $\phi^{1)2)}$	60°/0.4° ± 1°	59°–61°	47°/0.2° ± 1°	46°–48°
Crack initiation stress, σ_{ci}	120/20 MPa ± 3%	85–190 MPa	82/9 MPa ± 3%	70–95 MPa

1) The cohesion and friction angle according to the Coulomb's Criterion are assumed to be non-correlated.

2) The cohesion and friction angle are determined for a confinement stress between 0 and 15 MPa.

6.3.4 Assignment of rock mechanics properties to the rock fractures

The definition of the fracture sets, the fracture intensity, orientation and size distributions are described in detail in Section 5.5. To complete the description of the fracture sets, the mechanical properties are also assigned. The resulting cohesion and the friction angle values in Table 6-6 are given based on results from both tilt tests and direct shear tests (Section 6.2.2). The results for different fractures are very consistent independent of the rock domain and orientation. Thus, the mechanical properties are calculated on average for all fracture sets in the Forsmark local model volume.

In Table 6-6, an attempt to quantify the uncertainty of the fracture parameters is made. For the friction angle and cohesion, the uncertainty is based on the available results from earlier studies /SKB, 2004a/, new tilt tests and shear tests. After the completion of the direct shear test campaign, problems were encountered for the determination of the shear and normal stiffness of the fractures. These problems were due to the sample preparation and experimental test set-up. Reviewed testing procedures are expected to produce more correct and higher values of the shear and normal stiffness compared with the values in Table 6-6.

Table 6-6. Rock mechanics properties for single rock fractures in the Forsmark local model volume. The mean value and the standard deviation of the properties are given with the truncation intervals for the normal distribution. The range of variation of the mean value due to uncertainty is also given (see definition in Section 6.3.8).

Parameter for single fractures (small scale)	All fracture sets	
	Mean/standard deviation <i>Uncertainty of the mean</i>	Truncation interval: min–max
Normal stiffness, K_n	128/55 MPa/mm ²)	60–230 MPa/mm
Shear stiffness, K_s	39/11 MPa/mm ²)	10–55 MPa/mm
Peak cohesion, $c_p^{1)}$	0.6/0.3 MPa $\pm 20\%$	0.0–1.1 MPa
Peak friction angle, $\phi_p^{1)}$	34°/3° $\pm 3^\circ$	27°–40°
Residual cohesion, $c_r^{1)}$	0.5/0.3 MPa $\pm 20\%$	0.1–0.9 MPa
Residual friction angle, $\phi_r^{1)}$	31°/4° $\pm 3^\circ$	22°–38°
Peak dilation angle at 0.5 MPa ³⁾	19.5°/7° $\pm 2^\circ$	4°–33°
Peak dilation angle at 5 MPa ⁴⁾	4°/2.5° $\pm 1^\circ$	0°–11°

¹⁾ For normal stresses smaller than 0.5 MPa, a linear envelope should be assumed. This envelope should have zero cohesion and should have the shear strength obtained from the properties in this table when a normal stress of 0.5 MPa is considered. A maximum friction angle of 70° should be adopted when higher values are obtained from the linear envelope for low normal stresses.

²⁾ The uncertainty is high. See Sections 6.2.3 and 6.3.4.

³⁾ A linear decrease of the dilation angle is assumed between 0.5 and 5 MPa.

⁴⁾ For normal stresses larger than 5 MPa, the dilation angle is assumed constant.

6.3.5 Empirical approach

As prescribed by the SKB methodology, two independent empirical systems were applied for the characterisation of the rock mass along the four boreholes /Lanaro, 2005/. Combined with the rock stresses and water pressure conditions, their Q and RMR values quantify the rock mass quality. Moreover, they can be used for estimating the rock mass deformational and strength properties. When comparing the deformation modulus of the rock mass obtained from RMR and Q, some differences can be observed. These can be explained because: i) there is no direct relation between the Young's modulus of the intact rock and that obtained from RMR and Q; ii) the methods are at their limit of applicability due to the high quality of the rock mass. For this last reason, the deformation modulus of the rock mass should be very close to that of the intact rock. Considering that RMR gives higher values of the deformation modulus compared with the deformation modulus

obtained from Q, RMR seems to provide slightly more realistic values for the almost fracture-free rock of high Young's modulus at Forsmark. Moreover, RMR is provided with a more extensive set of equations that relates it with the mechanical properties of the rock mass than for Q. RMR also seems to be insensitive to the scale of application. Thus, this empirical system was chosen for the estimation of the rock mass mechanical properties. The same conclusion was also reached during the rock mechanics modelling of Simpevarp version 1.2.

The analysed boreholes were partitioned into rock domains and deterministic deformation zones (DDZ) according to the rock domain and deformation zone model. Furthermore, the rock within each rock domain was subdivided into "competent rock" (COMP) and "minor deformation zones" (SDZ) based on the partitioning provided by the "single-hole" interpretation. The mechanical properties for each component of the rock mass were empirically evaluated. Figure 6-6 shows the

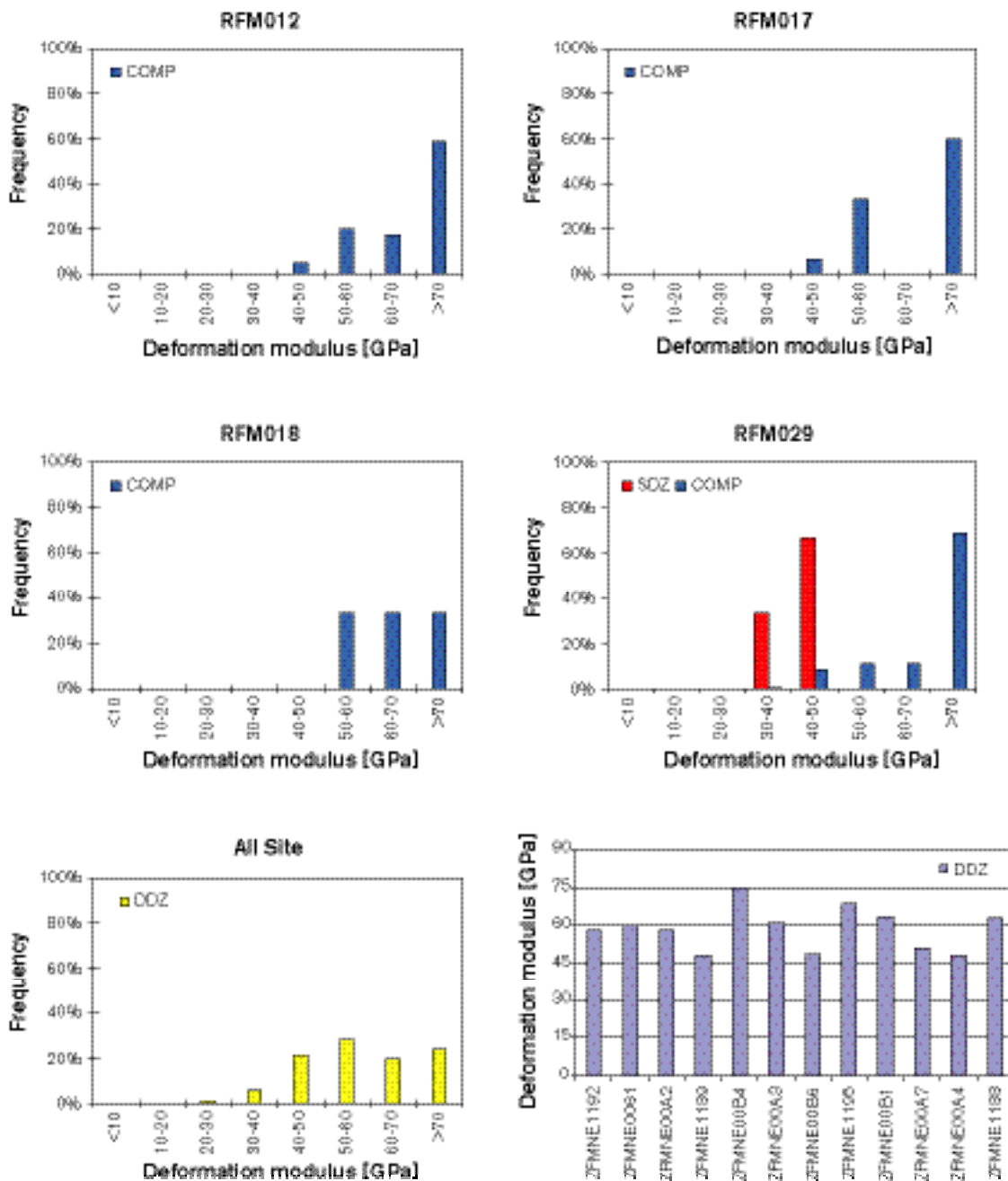


Figure 6-6. Histograms of the deformation modulus of the rock mass obtained by means of RMR for the "competent rock" (COMP) and "minor deformation zones" (SDZ) in rock domains RFM12, RFM017, RFM018 and RFM029, and for the deterministic deformation zones (DDZ) intercepted by Boreholes KFM01A, KFM02A, KFM03A and KFM04A.

deformation modulus of the rock mass for the rock domains and deformation zones intercepted by the four boreholes. It can be noticed that RFM029 presents a slightly higher frequency of high values of the deformation modulus than the other rock domains.

6.3.6 Theoretical approach

Numerical modelling of the behaviour of rock mass blocks of equivalent edge of 20 m were carried out by /Fredriksson and Olofsson, 2005/ based on two alternative DFN models for rock domain RFM029 and on the mechanical properties of intact rock and rock fractures (Sections 6.2.1 and 6.2.2) (Figure 6-7). These DFN models are judged to be within the uncertainty of the DFN model presented in Section 5.5. A consistency check has also been made using the DFN parameters reported in Section 5.5 that basically confirmed the results summarised here. The parameters resulting from the modelling are the equivalent deformation modulus, Poisson's ratio, cohesion and friction angle of the rock mass.

To limit the number of numerical simulations, the effect of the fracture network geometry was assumed independent of the mechanical properties of the intact rock and rock fractures, which are also assumed to be uncoupled from each other. In this way, the principle of superposition can be applied on the results obtained for:

- 1) Geometry: 3DEC model simulations representing slices of the geometry of the fracture network (20×20×1 m) parallel and perpendicular to the mean orientation of the maximum horizontal stress were carried out with mean values of the intact rock and fracture properties of the rock domain. Figure 6-8 (left) shows that the deformation modulus changes very little depending on the stress level and the direction of loading with respect to the fracture geometry. This would indicate that the rock mass behaves isotropically. These results also provide the frequency distributions of the rock mass equivalent properties depending on the model geometry only.
- 2) Material properties: one 3DEC model simulation for each of the two horizontal directions was run with maximum and minimum values of each material parameter in different combinations. These results provided the range of the increase/decrease of the mean equivalent properties of the rock mass depending only on the intact rock and fracture properties.

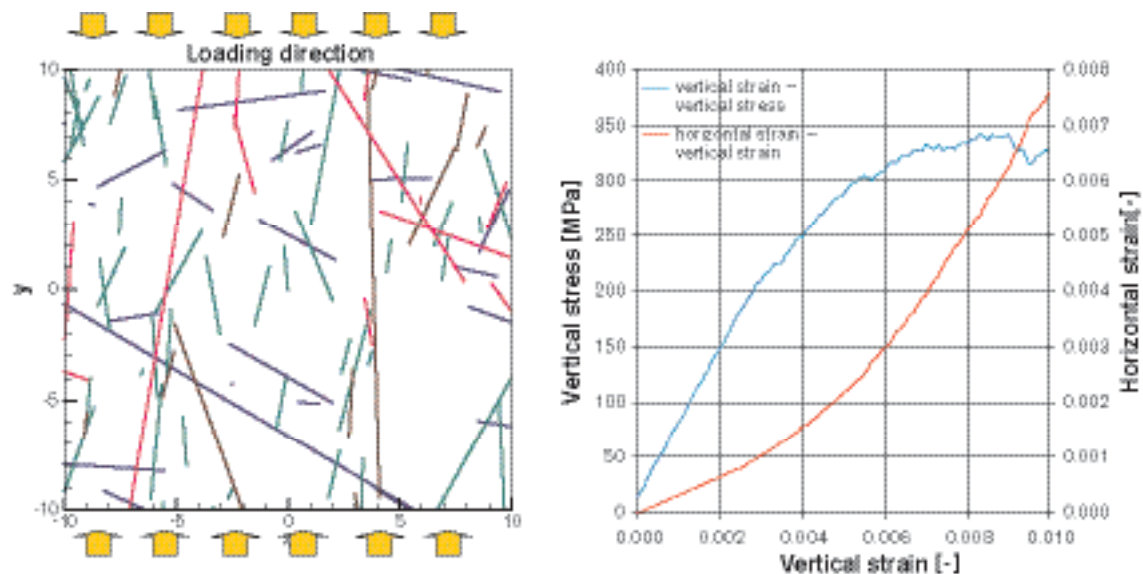


Figure 6-7. Fracture network (left) and mechanical behaviour of the same rock mass volume by 3DEC modelling (right) in a direction parallel to the maximum horizontal in-situ stress and for a confinement horizontal pressure of 45 MPa.

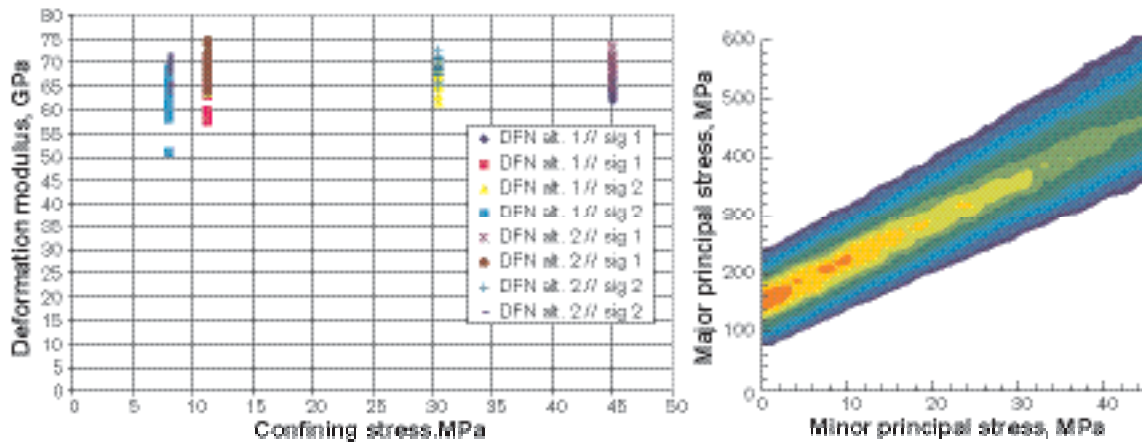


Figure 6-8. Effect of the fracture network geometry (e.g. DFN parameters and direction of loading) and of the stress on the equivalent deformation modulus of the rock mass (left); Monte-Carlo simulations of the rock mass strength (right, for DFN alt. 2 // sig 1). The colours indicate the frequency of occurrence from low (blue) towards high (red).

100,000 Monte-Carlo simulations were carried out based on the frequency distributions obtained in 1) and 2). The Monte-Carlo simulations of the rock mass strength are shown in Figure 6-8 (right) for the direction parallel to the maximum horizontal rock stress. The range of variation of the minor principal stress is small compared with the strength of the rock mass, thus the strength envelope looks linear. The frequency distributions of the equivalent rock mass properties were also derived. A set of representative results were chosen for RFM029 for two levels of stress (11.3 and 45 MPa). The combined effects of data uncertainty and spatial variability were considered in the theoretical approach, but no evaluation of the conceptual uncertainties was attempted.

6.3.7 Assignment of rock mechanics properties to the model volumes

The results of the empirical and theoretical approach are based on the same geomechanical information, but this is treated in two different ways: the empirical approach directly uses BOREMAP information and applies relations based on engineering experience, whereas the theoretical model uses the DFN model, which processes the BOREMAP information, and utilises constitutive laws for the intact rock and the fractures. However, the two approaches make use of the same experimental data. The approaches can be considered as two independent interpretations of the geomechanical data to obtain the same rock mass parameters: deformability and strength.

The deformability of the rock mass (i.e. deformation modulus and Poisson's ratio) depends on the level of applied stress. Since the boundary conditions at the site (e.g. rock stresses, water pressure and temperature) vary depending on the spatial location and depth, the empirical approach is applied to determine the rock mass deformability for low stresses and dry conditions so that the rock mass quality at different locations can be compared (i.e. for "characterisation"). These conditions typically correspond to a low level of stress (i.e. to a depth of about 50 m). Conveniently, the effect of the boundary conditions can be superimposed to determine the behaviour of the rock mass under different constraints. The theoretical approach, which has problems constraining the numerical models at low stresses, can be used to simulate the stress effect on rock mass deformability. The combination of the empirical results for low rock stresses with the theoretical results for in-situ rock stresses provides an estimation of the deformability of the rock mass under the whole range of rock stresses. Since, up to now, there is no overlapping of the results, the two approaches are given the same reliability (i.e. no weighting is applied).

The strength of the rock mass is implicitly stress dependent and can be obtained by the empirical and theoretical methods. In this case the two results, in terms of equivalent and apparent uniaxial compressive strength, apparent cohesion and friction angle, can directly be compared. Rock mechanics modelling consist in choosing rock mass parameters representative of the results of the two models. For this purpose, averaging is applied to the mean values of the parameters without weighting. The differences in the mean values provided by the empirical and theoretical approach may help to quantify the uncertainty of the parameter determination (Section 6.3.8). Since the plots of Q and RMR along the borehole do not show a clear depth dependence, and the numerical models indicate that the rock mass should be isotropic despite the orientation of the fractures and the in-situ stress state, the standard deviation of the parameters is assumed to quantify their spatial variability. Rock mechanics modelling assumes that the maximum standard deviation for each parameter from the empirical and theoretical approach is representative of the spatial variability of the parameter.

According to Section 6.3.5 and 6.3.6, the mechanical properties of rock domains RFM012, RFM017, RFM018 and RFM029 can be evaluated. However, the empirical characterisation of the boreholes mainly provides data from RFM029 (78% of the total characterised borehole length), and the theoretical approach only gives results for this rock domain.

Properties of the competent rock mass

The empirical and theoretical results were combined for the two purposes of reciprocal verification and of coverage of the whole range of confinement stresses relevant for the material description. The deformation modulus and Poisson's ratio of the rock mass in RFM029, where this comparison was possible, seem to be independent on stress (Figure 6-9). This is probably due to the relatively low fracture frequency in this rock domain. Furthermore, the theoretical models show that the orientation of loading with respect to the geometry of the fractures does not significantly affect the equivalent deformation modulus of the rock mass (see Figure 6-8). Based on the results in Section 6.3.6, the deformability of the rock mass in rock domain RFM029 can be considered isotropic.

The other rock domains were assigned the same properties as obtained by the empirical approach with minor changes. This implies the sensible hypothesis that the other rock domains also do not have deformability properties dependent on stress thanks to their relatively good rock quality. As a first approximation, these rock domains are also assumed to be isotropic, although the state of stress is strongly anisotropic (see Section 6.4).

The rock mechanics modelling of the strength material properties was carried out in the same way as for deformability. For the apparent cohesion and friction angle of the rock mass for stresses between 10 and 30 MPa, there is agreement between the empirical and theoretical approaches as shown in Figure 6-10. Table 6-7 shows all the predicted mechanical properties of the competent rock mass in rock domains RFM012, RFM017, RFM018 and RFM029. Here, the minimum, mean and maximum values, the standard deviation of the deformability and strength parameters are summarised.

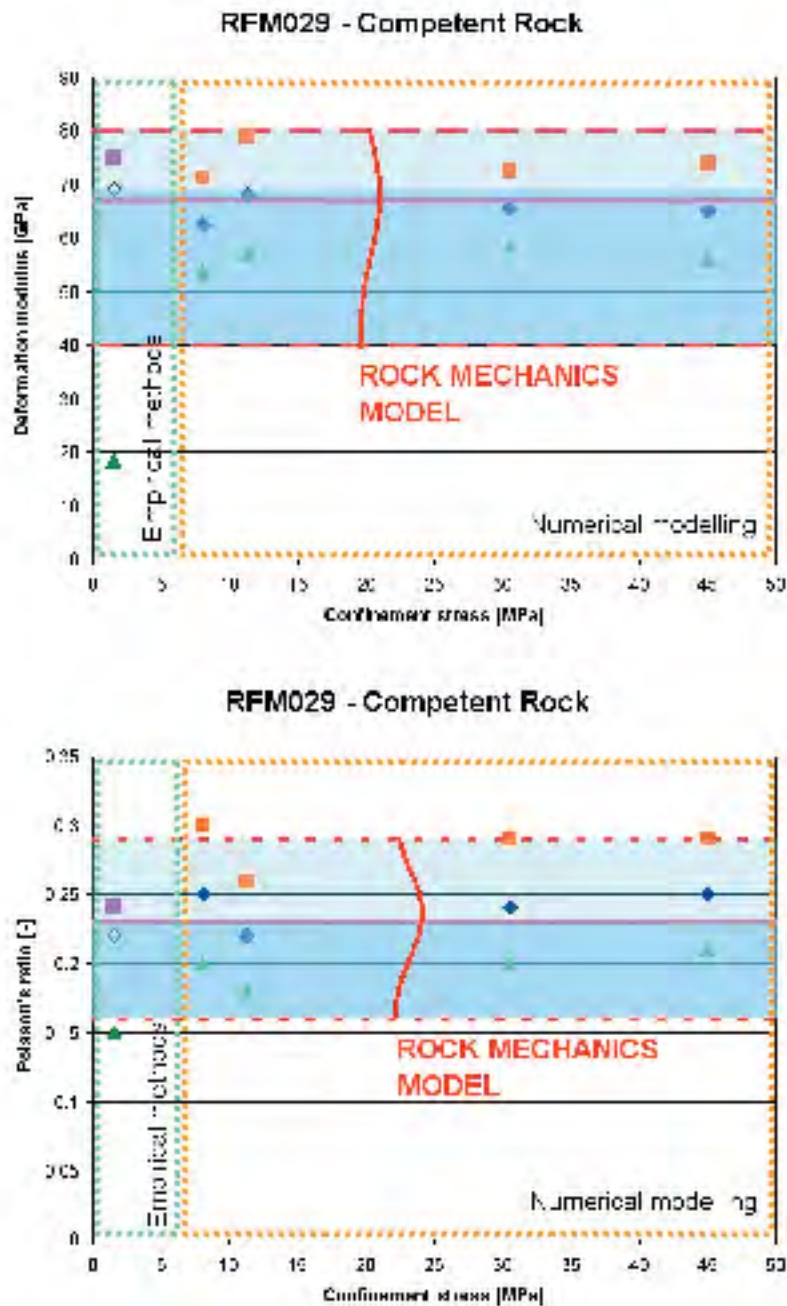


Figure 6-9. Deformation modulus (above) and Poisson's ratio (below) of the rock mass as a function of the confinement stress. The diagrams show the results of the empirical (low stress – green boxes) and theoretical approach (higher stress – orange boxes) and the rock mechanics modelling results for the competent rock in rock domain RFM029 at Forsmark (deformation zones excluded). The maximum (squares), average (rhomboids) and minimum (triangles) values are shown for the deformation modulus and the Poisson's ratio. The frequency distribution of the deformation modulus and Poisson's ratio resulting from the rock mechanics modelling are also shown.

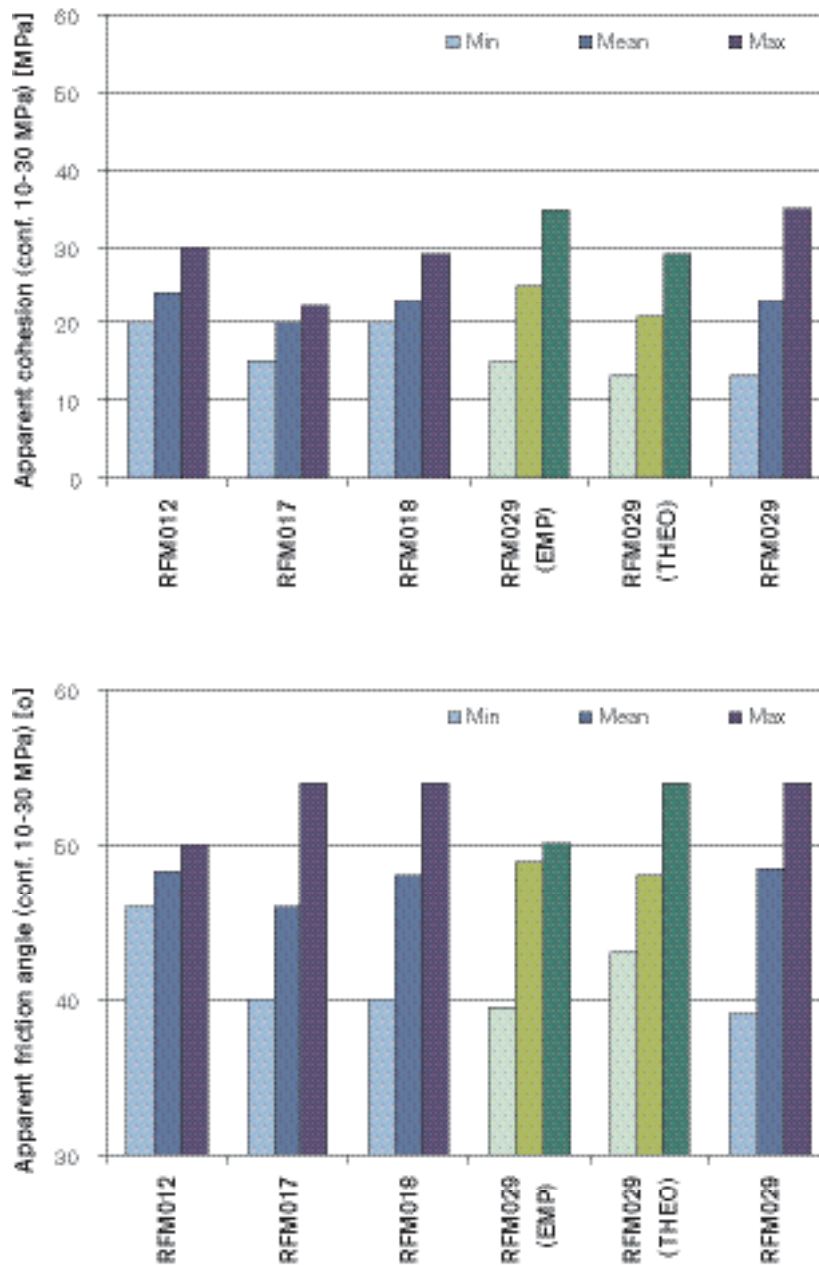


Figure 6-10. Apparent cohesion (above) and friction angle (below) of the rock mass for stresses between 10 and 30 MPa and for four rock domains at Forsmark. The diagrams show in green the results of the empirical and theoretical approach (when available), and in blue the rock mechanics modelling results for the competent rock (deformation zones excluded).

Table 6-7. Predicted rock mechanics properties of the rock mass in the rock domains in the Forsmark local model volume (deformation zones excluded). The mean value and the standard deviation of the properties are given with the truncation intervals for the normal distribution. The range of variation of the mean value due to uncertainties is also given (see definition in Section 6.3.8).

Rock domain	RFM012	RFM017	RFM018	RFM029
Prevalent rock type	Granite to granodiorite	Tonalite to granodiorite ³⁾	Tonalite to granodiorite ⁴⁾	Granite to granodiorite
Properties of the rock mass	Mean/st. dev.	Mean/st. dev.	Mean/st. dev.	Mean/st. dev.
	Min–max	Min–max	Min–max	Min–max
	<i>Uncertainty on the mean</i>	<i>Uncertainty on the mean</i>	<i>Uncertainty on the mean</i>	<i>Uncertainty on the mean</i>
Uniaxial compressive strength (Coulomb) ¹⁾	127/17 MPa 90–170 MPa ± 12%	100/8 MPa 60–120 MPa ± 12%	121/16 MPa 60–160 MPa ± 20%	122/26 MPa 60–195 MPa ± 10%
Uniaxial compressive strength (Hoek and Brown) ⁵⁾	74/19 MPa 45–120 MPa ± 16%	46/9 MPa 30–60 MPa ± 22%	68/18 MPa 50–110 MPa ± 32%	80/30 MPa 18–150 MPa ± 8%
Friction angle ¹⁾	48.3°/1.0° 46°–50° ± 3%	46.0°/2.0° 40°–54° ± 4%	48.0°/2.0° 40°–54° ± 5%	48.5°/2.7° 39°–54° ± 1%
Cohesion ¹⁾	24/2.5 MPa 20–30 MPa ± 15%	20/1.5 MPa 15–22 MPa ± 15%	23/3 MPa 20–29 MPa ± 15%	23/4 MPa 13–35 MPa ± 10%
Deformation Modulus ²⁾	68/9 GPa 40–80 GPa ± 7%	67/10 GPa 40–80 GPa ± 12%	64/9 GPa 40–80 GPa ± 15%	67/10 GPa 40–80 GPa ± 3%
Poisson's ratio ²⁾	0.22/0.03 0.15–0.24 ± 15%	0.24/0.04 0.18–0.27 ± 15%	0.20/0.03 0.15–0.24 ± 15%	0.23/0.03 0.16–0.29 ± 9%
Tensile strength ⁶⁾	1.9/0.7 MPa 0.5–3.6 MPa ± 20%	1.0/0.3 MPa 0.4–1.3 ± 20%	1.7/0.7 MPa 0.3–3.5 MPa ± 20%	2.0/1.0 MPa 0.3–5.0 MPa ± 10%

¹⁾ The apparent uniaxial compressive strength, cohesion and friction angle are obtained from the Coulomb's Strength Criterion between 10 and 30 MPa confinement stress.

²⁾ The deformation modulus and the Poisson's ratio of the rock mass are assumed independent on the state of stress due to their high values.

³⁾ Tonalite predominates.

⁴⁾ Granodiorite predominates.

⁵⁾ The uniaxial compressive strength is obtained from the curvilinear Hoek and Brown's Criterion of the rock mass from the RMR-GSI relation.

⁶⁾ The tensile strength is obtained from the curvilinear Hoek and Brown's Criterion of the rock mass from the RMR-GSI relation.

Properties of the deformation zones

Twelve deterministic deformation zones were intercepted by the four boreholes analysed from a rock mechanics point of view. The orientation of these deformation zones seems to have a very consistent strike in the N-E direction and lengths of up to 10 km (Figure 6-11 left).

Experience regarding the Singö deformation zone (length 30+25 km) seem to indicate that regional features present weaker material properties (Figure 6-11 right). For this reason, two groups of deformation zones were identified and described as:

- 1) Minor and deterministic deformation zones with length ≤ 10 km: their characterisation is based on the borehole information.

- 2) Regional deterministic deformation zones with length > 10 km and strike NW-SE: their characterisation is based on the experience during excavation of tunnels across the Singö regional deformation zone.

Short portions of borehole were identified as minor deformation zones during the geological single-hole interpretation (total about 15 m). These zones are given the same mechanical properties as the deterministic deformation zones. The regional deformation zones are important because their extension and weakness are important from an engineering point of view and they might also affect the stress field at the site.

The rock mechanics characterisation of the deformation zones is based on the results of the empirical approach and on construction experience. Table 6-8 shows all the predicted mechanical properties of the deformation zones of the local model volume at Forsmark. Here, the minimum, mean and maximum values and the standard deviation of the deformability and strength parameters are summarised.

For the deformation zones shorter than 10 km, the deformational properties were assumed independent of the stresses. The deformation modulus of these zones is almost as high as the competent rock in the rock domains. On the other hand, for the regional deformation zones, a linear increase was assumed for low stresses, between about 1.5 and 10 MPa, and, for stresses larger than 10 MPa, the deformation zone is considered to exhibit constant properties. The values of the deformation modulus were estimated based on the seismic velocity measured in the rock mass along the discharge tunnels of the power plant. Velocities between 3.6 and 4.7 km/h were recorded and could be related to a deformation modulus between 3 and 10 GPa. These values are also supported by the observation in the tunnels, where a zone of about 10 m of crushed material was observed together with several clay sections.

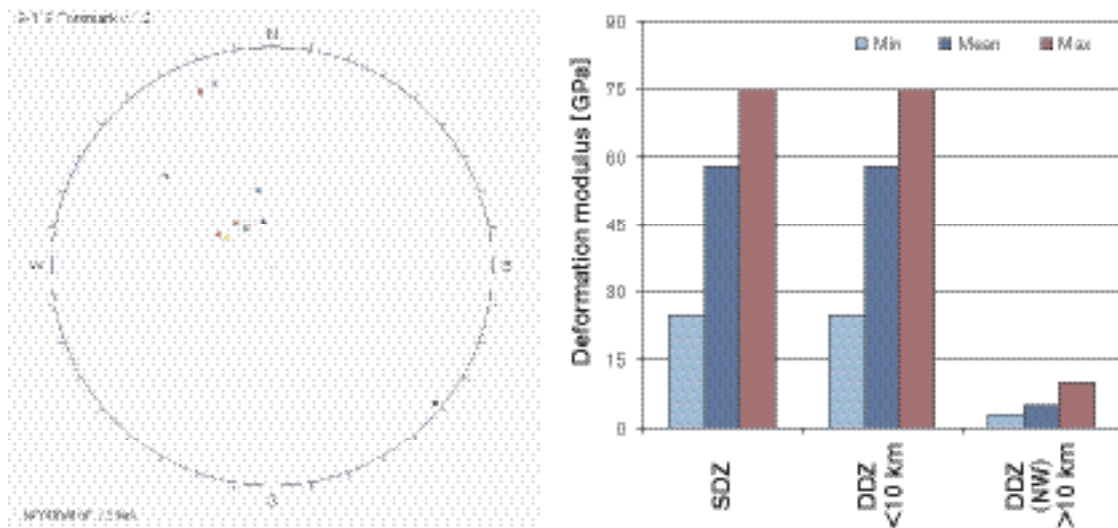


Figure 6-11. Orientation (left) and deformation modulus (right, for low stress) of the rock mass in the deformation zones obtained based on the empirical approach and construction experience through the Singö deformation zone.

Table 6-8. Predicted rock mechanics properties of the rock mass in the deformation zones of the Forsmark local model volume. The mean value and the standard deviation of the properties are given with the truncation intervals for the normal distribution. The interval of variation of the mean value due to uncertainties is also given (see definition in Section 6.3.8).

Deformation zones	Minor and deterministic deformation zones ³⁾	Regional deterministic deformation zones ZFMNWYYYY ⁴⁾
Properties of the rock mass	Mean/st. dev. Min–max <i>Uncertainty on the mean</i>	Mean Min–max <i>Uncertainty on the mean</i>
Uniaxial compressive strength (Coulomb) ¹⁾	112/16 MPa 55–160 MPa ± 20%	40 MPa 20–60 MPa ± 40%
Uniaxial compressive strength (Hoek and Brown) ⁵⁾	56/16 MPa 14–110 MPa ± 45%	20 MPa 10–40 MPa ± 90%
Friction angle ¹⁾	47°/2° 38°–51° ± 7%	35° 30°–40° ± 14%
Cohesion ¹⁾	22/2.2 MPa 14–29 MPa ± 17%	10 MPa 5–15 MPa ± 40%
Deformation modulus ²⁾	58/13 GPa ⁷⁾ 25–75 GPa ± 20%	5 GPa (30 GPa) ⁸⁾ 3–10 GPa (10–60 GPa) ⁸⁾ ± 40%
Poisson's ratio ²⁾	0.19/0.04 0.09–0.24 ± 20%	0.10 0.03–0.20 ± 40%
Tensile strength ⁵⁾	1.2/0.5 MPa 0.2–2.9 MPa ± 30%	0.2 MPa 0.0–0.4 MPa ± 60%

¹⁾ The apparent uniaxial compressive strength, cohesion and friction angle are obtained from the Coulomb's Strength Criterion between 10 and 30 MPa confinement stress.

²⁾ The deformation modulus and the Poisson's ratio of the rock mass are given for low stress confinement.

³⁾ These values apply to all deterministic deformation zones shorter than 10 Km.

⁴⁾ These values apply to all regional deterministic deformation zones striking NW-SE (i.e. ZFMNWYYYY) and longer than 10 Km.

⁵⁾ The tensile strength is obtained from the curvilinear Hoek and Brown's Criterion of the rock mass from the RMR-GSI relation.

⁶⁾ The uniaxial compressive strength is obtained from the curvilinear Hoek and Brown's Criterion of the rock mass from the RMR-GSI relation.

⁷⁾ This value is high, thus no variation with stress is considered.

⁸⁾ The deformation modulus is given for a stress level of low stress (about 1.5 MPa) and 10 MPa (upper threshold), respectively. Intermediate values can be obtained by linear interpolation.

6.3.8 Evaluation of uncertainties

The rock mechanics properties of the rock mass are statistically described by means of the mean value and standard deviation. The standard deviation is assumed to quantify the spatial variability of the parameters within the rock domain. Minimum and maximum truncation values, not necessarily symmetrical about the mean, are also assumed as limits of the statistical distribution.

A measure of the uncertainty on the parameter determination is provided by means of an interval ($\pm u$) of possible variability of the mean value (Figure 6-12). This interval of possible variability of the mean is, when possible, determined based on the difference between the mean values of the same parameter determined with two different methods. For example, the mean values of the test results for the properties of the intact rock are available from two laboratories. Thus, the interval u is determined as half of the difference between the two available mean values. The same technique is applied to the mean values of the mechanical properties of the rock mass obtained from the empirical and numerical approach. Some of the mechanical properties were obtained based on results from just one method and their uncertainty interval was estimated based on engineering judgement.

The size of the uncertainty interval u quantifies the reliability of the parameter determination (Table 6-2, Table 6-3, Table 6-7, Table 6-8): the smaller the interval, the more confident the parameter determination. In this report, the uncertainties are assumed to be unrelated to the spatial variability of the parameter. Hence, the statistical distribution is simply shifted when the uncertainty of the mean value of the parameter is considered. The uncertainty produces an identical shift in the truncation values as for the mean value.

Some measurements on core samples (see Chapter 10) show an increase of porosity of about 30% between about 500 and 1,000 m depth. For KFM01A and KFM02A, a slight degeneration of the sample condition is also shown by the decrease of the P-wave velocity transversally to the cores for depths larger than 500 m. This is probably due to the unfavorable stress-path that the core samples are subjected to during drilling that induces microcracking. Despite these observations, the strength and deformational properties of the intact rock do not seem to be affected, except for samples taken below about 700 m (Figure 6-2).

In practice, the empirical approach has developed a technique for evaluating the uncertainty interval of the mean. This is done by assuming the maximum and minimum possible value of each geomechanical parameter involved in the empirical characterisation, and by combining these extreme values in the most favourable and unfavourable ways. This is an attempt to quantify intrinsic uncertainties that originate from the limits of the empirical methods (e.g. qualitative observations, lack of constitutive laws, subjectivity). However, when only empirical results are available, the possible bias of the results cannot be avoided. The theoretical approach did not provide an evaluation of the uncertainties but only the span of expected parameter values.

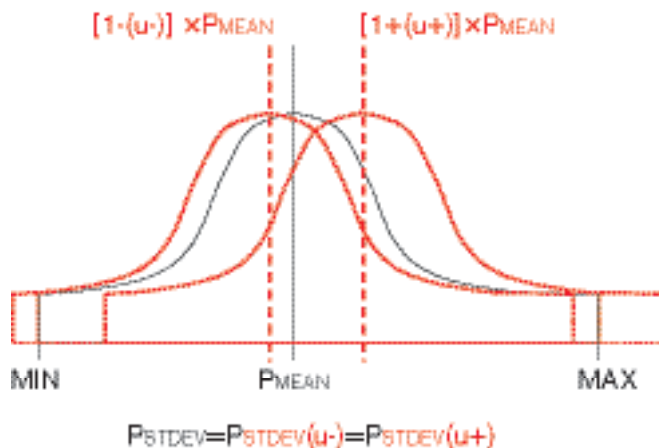


Figure 6-12. Description of the statistical distribution and uncertainty of the parameters determined by the rock mechanics model.

The uncertainty on the rock mechanics model parameters is determined as follows:

- a) Rock domains with parameters available from the empirical and theoretical approaches: the uncertainty of the mean value is determined as half of the difference between the empirical and the theoretical mean values. Thus, the same reliability is assigned to the two methods.
- b) Rock domains with only empirical parameters available: the uncertainty is taken as the uncertainty provided by the empirical approach.
- c) Rock domains with construction data only: the uncertainty is estimated based on engineering judgment.

6.4 State of stress

In the following sections, the state of stress in the rock mass at Forsmark is inferred based on the available in-situ measurements and some scoping numerical models. Then, an evaluation of the uncertainties of the produced stress model is given.

6.4.1 Stress measurements

Stress measurements at the Forsmark site were carried out in two periods: between 1977 and 1984 (boreholes DBT-1, DBT-3, KB-21, KB-22, KBS-7, SFR 1/177) and between 2003 and 2004 (KFM01A and B, KFM02A and KFM04A) for the present site characterisation. The methods used for the stress determination were an overcoring technique and hydraulic methods /Amadei and Stephansson, 1997/. Other results from direct (e.g. door-stopper method) and indirect methods (e.g. core diskings and borehole spalling analyses) are also available. The following measurement campaigns were conducted.

Overcoring in DBT-1 and DBT-2: The measurements were carried out at depths between 10 and 500 m with the SSPB probe between 1977 and 1979 and corrected in 1982. In 2003, the data were analysed by means of the “transient strain analysis” and some outliners were also removed based on the criterion of “unexplained strain” /Perman and Sjöberg, 2003/.

Overcoring near the SFR facility in KB-21, KB-22, KBS-7, SFR 1/177: The measurements were taken in the SFR area between 40 and 140 m by means of a Borre probe between 1982 to 1985.

HF (Hydraulic Fracturing tests) in DBT-1: Measurements were performed in 1984 between 25 to 500 m depth. These data are not directly used in this report because they do not satisfy the requirements regarding fracture orientation and traceability.

Overcoring in KFM01B: The stress measurements were conducted in 2003–2004 using the Borre probe at two depth levels (233–236 and 399–455 m). Of the 18 measurement attempts, only 5 were considered successful and were used in the modelling presented here. These results were analysed by means of classical stress analysis and “transient strain analysis”. Moreover, a correction was applied because the overcoring data tend to return unrealistically high values of the vertical stress, known to be very close to the weight of the overburden /Lindfors et al. 2004/.

HF and HTPF (Hydraulic Testing of Pre-existing Fractures) in KFM01A, KFM01B, KFM02A and KFM04A: 85 tests were performed in 2004 /Klee and Rummel, 2004/. Several of the HTPF did not succeed in reopening the pre-existing fractures and resulted instead in classic break down. The normal stresses measured on 12 vertical and 22 horizontal fractures have being re-interpreted /Sjöberg et al. 2005/ so that the minimum horizontal and the vertical stress could be determined. The data show a wide scatter in the stress magnitude.

The location of boreholes for stress measurements are given in Figure 6-13. An overview of the results of old and new measurements are given in Figure 6-14.

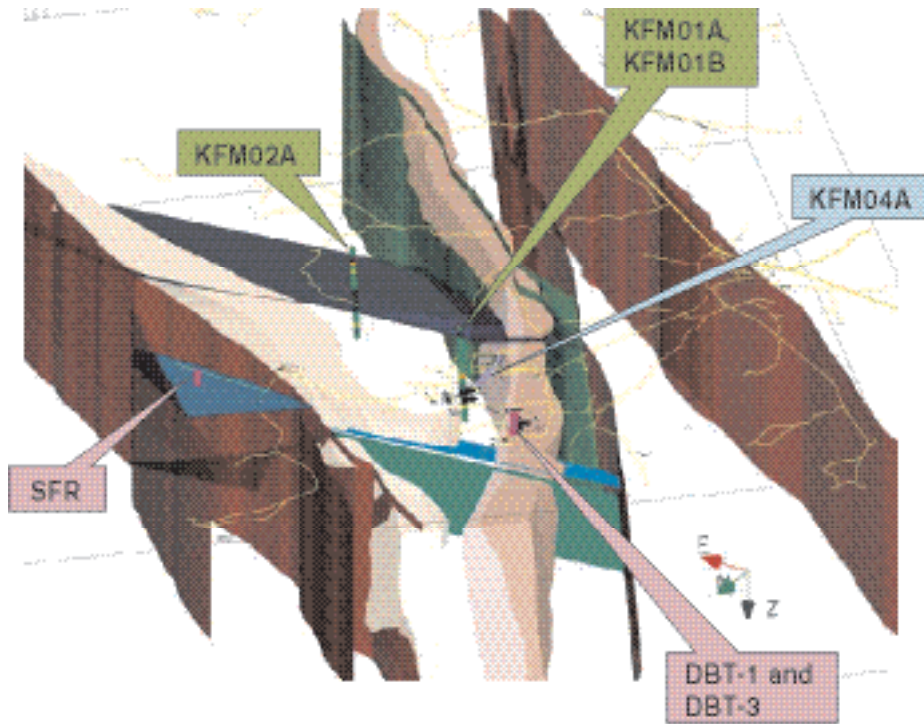


Figure 6-13. Location of boreholes for in-situ stress measurements at the Forsmark site. Birds view looking south into the Forsmark local model volume. Only the new data are from inside the local volume.

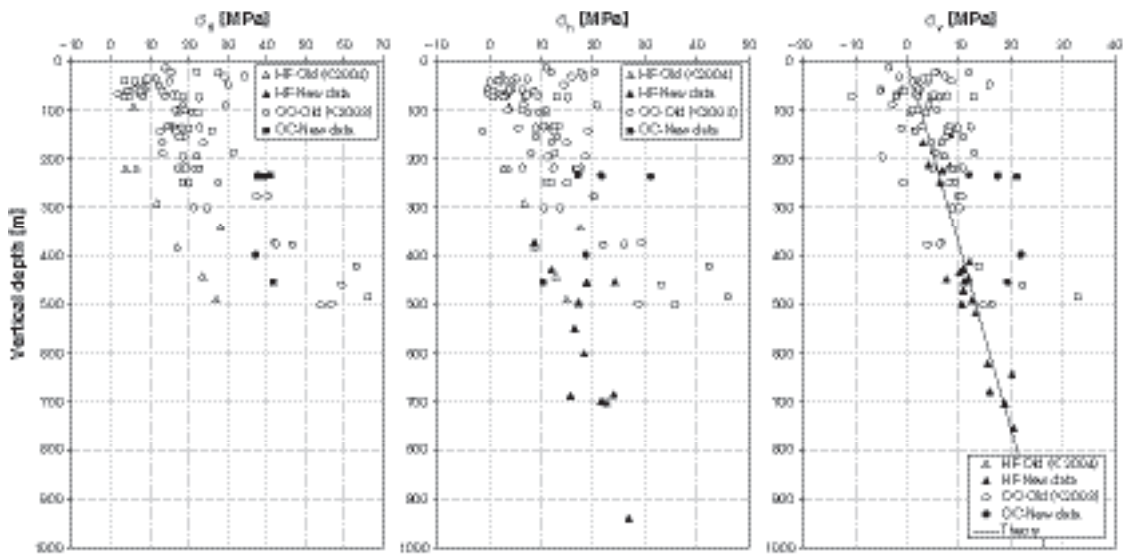


Figure 6-14. Summary of all measurements used for the rock stress modelling. The maximum and minimum horizontal stress and vertical stress are shown. For details see /Sjöberg et al. 2005/.

All the new boreholes at Forsmark, including KFM05A, exhibited minor diskings of the solid and hollow cores at various depths, except for KFM04A deeper than 500 m. An analysis of the spacing of the core diskings could then be carried out /Lindfors et al. 2004/ based on the loggings and the nomogram technique by /Hakala, 1999/. This analysis concluded that, for a rock with tensile strength of 14 MPa and a minimum-to-maximum horizontal stress ratio between 0.25 and 0.5, the maximum horizontal stress causing core diskings can be as low as 55 MPa. These stress conditions are considered applicable as an upper limit for the maximum horizontal stress at Forsmark down to a depth of about 500 m, even though some of the core diskings was observed in weaker pegmatitic rocks.

All newly measured stresses within the site investigation programme have been subject to a thorough quality procedure, following principles by ISRM Suggested methods for stress estimation – Quality control /Christiansson and Hudson, 2003/. Overcoring is following ISRM Suggested Methods /Sjöberg, 2004/. In addition, confidence in the overcoring method can be improved using the “transient strain analysis” /Hakala et al. 2003/. This analysis checks for consistency in the overcoring results, which is particularly useful as the elastic limit of the rock response is approached. The use of hydraulic methods for stress estimation is also following the ISRM Suggested Methods /Haimson and Cornet, 2003/. For these reasons, new data are considered to have higher confidence than old data, even if the methods and parts of the equipments are in principle the same.

The rock stress data are summarised together with the results of the stress modelling in the following sections.

6.4.2 Modelling assumptions and input from other disciplines

The rock stress modelling has been carried out according to the methodology and recommendations developed by /Hakami et al. 2002/. The bases for the rock stress modelling are:

- The in-situ data; all the data available have been scrutinised to determine quality, traceability, appropriate application of expert judgment and uncertainties of the measuring technique /Sjöberg et al. 2005/. Thus, only a sub-set of the data available was used for the stress modelling. Similar data for the Scandinavian Region as a whole were also considered.
- The geological model, in particular the rock domain (Section 5.3) and deformation zone model (Section 5.4); they geometrically define the rock mass volume in which the rock stresses are estimated.
- The evolutionary aspects (Chapter 3); the focus is on plate tectonic and post-glaciation effects.
- The mechanical properties evaluated by the rock mechanics model; it assigns the material properties to the rock mass for the rock stress modelling.

The stresses are defined according to the geomechanical sign convention that implies positive compressive stresses. The stress orientations are given as trend and plunge with respect to the geographic North and using a right-hand rule.

6.4.3 Conceptual model with potential alternatives

The conceptual model for the state of stress at Forsmark is based on the present-day tectonic plate motion as a stress-build-up phenomenon. According to /Müller et al. 1992; Gölke and Coblenz, 1996/, Scandinavia is characterised by a W NW-E SE directed maximum compressive horizontal stress sub-parallel to the direction of relative plate motion between Africa and Europe (Figure 6-15). The European plate has been involved in this plate collision since the time of the Alpine orogeny in the Late Cretaceous /Hakami et al. 2002/.

The almost completely planar topography of the Uppland region where Forsmark is located also implies that the principal stresses at the site should be confined to the horizontal plane and the vertical direction.

The rock stress measurements available in middle-east Sweden and western Finland indicate that the rock stresses measured at Forsmark are generally higher than the neighboring areas, but the orientation of the major horizontal stress is rather consistent, at least at the Swedish side of the

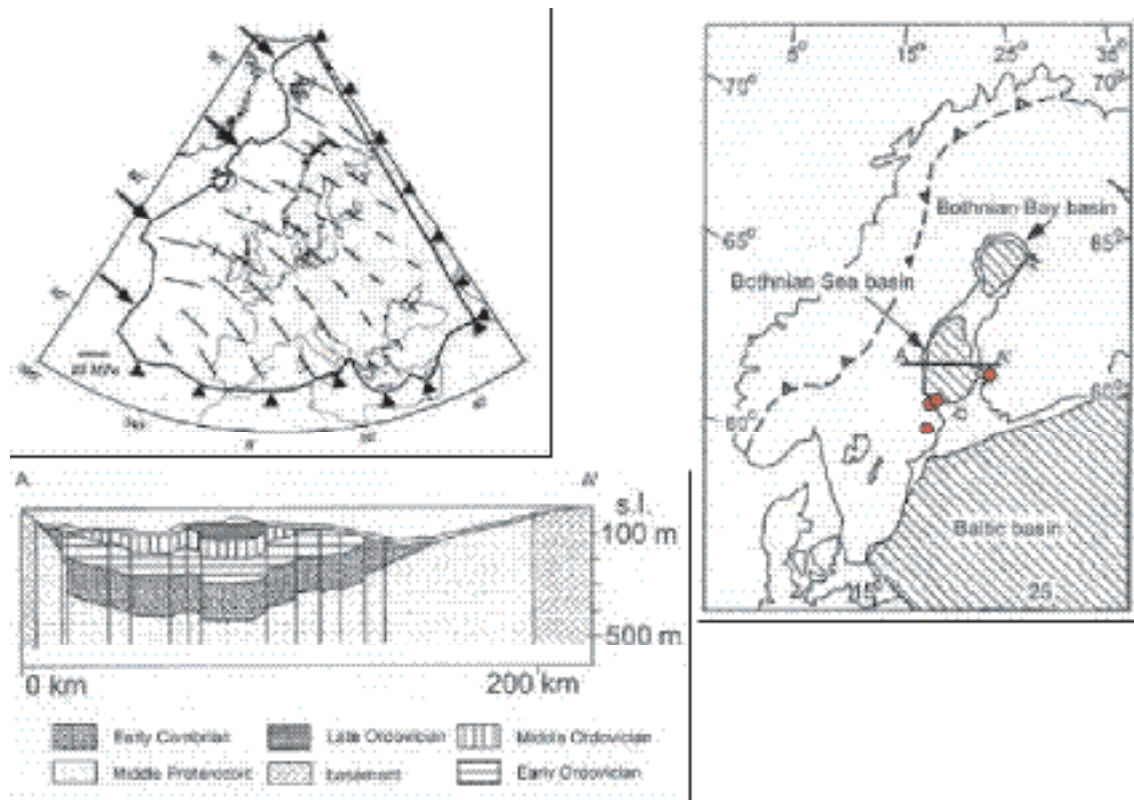


Figure 6-15. European tectonic stresses originated from plate collision (top, left) /Gölke and Coblentz, 1996/ and plan view and cross section of the Bothnian Sea basin (bottom and right) /van Balen and Heeremans, 1998/.

Baltic Sea (Table 6-9) /Sjöberg et al. 2005/. /Gregersen, 1992/ and /Hakami et al. 2002/ affirm that, although there have been major modifications of the stress field due to the latest glaciation, no evidence in the stress orientation and magnitude remains today. Thus, it is suggested that the present stress state reflects only plate motion. A tentative explanation of the high stresses at the Forsmark site could be based on the presence of the Bothnian See Basin /van Balen and Heeremans, 1998/. This basin, mainly composed of weaker sedimentary rocks (e.g. Cambrian and Ordovician) and extending to a depth of 500 m below the bottom of the Baltic See (Figure 6-15), could cause the plate collision-push to deepen under the basin bottom or deviate towards the more competent hard rock at the Swedish east coast. Alternatively, the geometrical distribution of the larger deformation zones at the Forsmark site together with the stiff rock in the tectonic lens may contribute to elevate the stresses.

The relation between the magnitudes of the stress components in Table 6-9 indicates a thrust faulting regime because: $\sigma_H > \sigma_h > \sigma_v$. Moreover, the levels of the stress magnitudes indicate that the ratio between the magnitude of the maximum horizontal stress and the vertical stress is about 3.5.

Table 6-9. Comparison of the stresses at Forsmark and in geographically near Scandinavian sites (depth of about 500 m) (after /Sjöberg et al. 2005/).

Site	σ_H	σ_h	σ_v	Trend of σ_H
Björkö (Sörmland, Sweden)	22 MPa	13 MPa	13 MPa*	130°
Finnsjön (Uppland, Sweden)	20 MPa	16 MPa	13 MPa*	120°–150°
Olkiluoto (Finland)	25 MPa	15 MPa	14 MPa	90°
Forsmark (Uppland, Sweden)**	45 MPa	18 MPa	13 MPa	142°

* Estimations based on the weight of the overburden.

** Site descriptive model version 1.2.

Based on this information, the basic hypotheses for the state of stress at the Forsmark regional model volume can be stated:

- The vertical stress (σ_v) is only due to the weight of the overburden.
- The maximum horizontal stress (σ_H) is trending NW-SE, sub-parallel to the plate-collision push and to the regional deformation zones at the site. The magnitude is significantly higher, at least at some 200–500 m depth, compared with other sites in Scandinavia.
- The minimum horizontal stress (σ_h) seems to be in the range of what is commonly found in Scandinavia at 200–500 m depth, but the data exhibit large scatter.

The geomechanical and stress data show that the upper crust, down to about 100–200 m depth, exhibits a more varying stress state characterised by local changes in magnitude and orientation /Carlsson and Christiansson, 1987; Sjöberg et al. 2005/. Fractures and fracture zones at the site are sparsely distributed, and sub-vertical or sub-horizontal. The superficial horizontal fracturing extends down to a depth of about 100 m only. High hydraulic transmissivities have been observed associated with this kind of fracturing, indicating significant apertures. The sparsely fractured rock mass below 100 m has the possibility to hold high stresses up to relatively shallow depths. Stress-induced initiation and reopening of fractures would then cause locally large apertures as well as varying stress state. The stress gradient in the upper part of the crust at the site will therefore be much dependent on local variations in fracturing. Thus, the present rock stress modelling primarily considers the rock mass within rock domain RFM029 and at the depth of the possible repository, where the superficial effects are probably negligible, and where available data are considered to have the highest confidence.

The potential alternatives to this model originate from working hypotheses that have been discarded from the basic model because they are not supported by the measurement results.

- a) The tectonic lens in rock domain RFM029 has higher stresses than the bedrock outside the lens. This hypothesis seems not to be supported by the data. In fact, the comparison of the measurements taken west and east of the Singö deformation zone seem to be very consistent with each other at least for depths larger than 60 m /Sjöberg et al. 2005/ (see also Section 0).
- b) The gently dipping deformation zones (12 with high confidence and 7 with medium confidence striking prevalently NE) might affect the stress gradient at several locations. However, the frequency of such gently dipping zones might indicate that the phenomenon should extend to the whole of RFM029 and not only to particular locations (see also Section 6.4.4).
- c) The NW part of rock domain RFM029 might have a slightly different stress state from the SE part. This is suggested by the fact that the density of gently-dipping zones striking NE seems to increase in the SE part (borehole KFM03A) compared with the NW part of the tectonic lens. Since there are no stress measurements in the SE part of the tectonic lens, this hypothesis can neither be supported nor discarded.

In the next section, the basic model for the rock stress state in rock domain RFM029 is presented together with the evidence that could invalidate the alternative models. The possible stress distribution down to at least 500 m is also discussed.

6.4.4 Stress distribution in the model volume

New stress data have been obtained since model version 1.1 and the proposed stress state in RFM029 at Forsmark incorporates those findings. Table 6-10 provides the stress gradients for depths ranging from 250 to 650 m and Figure 6-16 shows the data on which Table 6-10 is based. It is evident from Figure 6-16 and Table 6-10 that there is good confidence in the vertical stress. Estimating the horizontal stress is more challenging because the stress data in Figure 6-16 are compiled from boreholes that are located hundreds of metres apart from each other. Hence, there is always the risk that Figure 6-16 combines data from different geological domains and thus also stress domains. For example, borehole DBT-1, for which the highest stress magnitudes are reported (Figure 6-16), is located north of the candidate area (near the power plant) and is located in a local geology that differs from the geology found in KFM01A and KFM01B. These spatial differences have been factored into the stress gradients given in Table 6-10.

Table 6-10. Estimated maximum stresses as a function of depth (in metres) for rock domain RFM029. The equations are valid for depths between 350 and 650 m.

Magnitude and orientation	Min (MPa)	Average (MPa)	Max (MPa)
Vertical stress (σ_v)	$0.0260 z$	$0.0265 z$	$0.027 z$
Maximum horizontal stress (σ_H)	Average -10%	$35+0.020 z$	Average +10%
Minimum horizontal stress (σ_h)	Average -20%	$19+0.025 z$	Average +20%
Orientation of the maximum horizontal stress (σ_H)	-	140°	-

* z is the depth from the ground surface in metres.

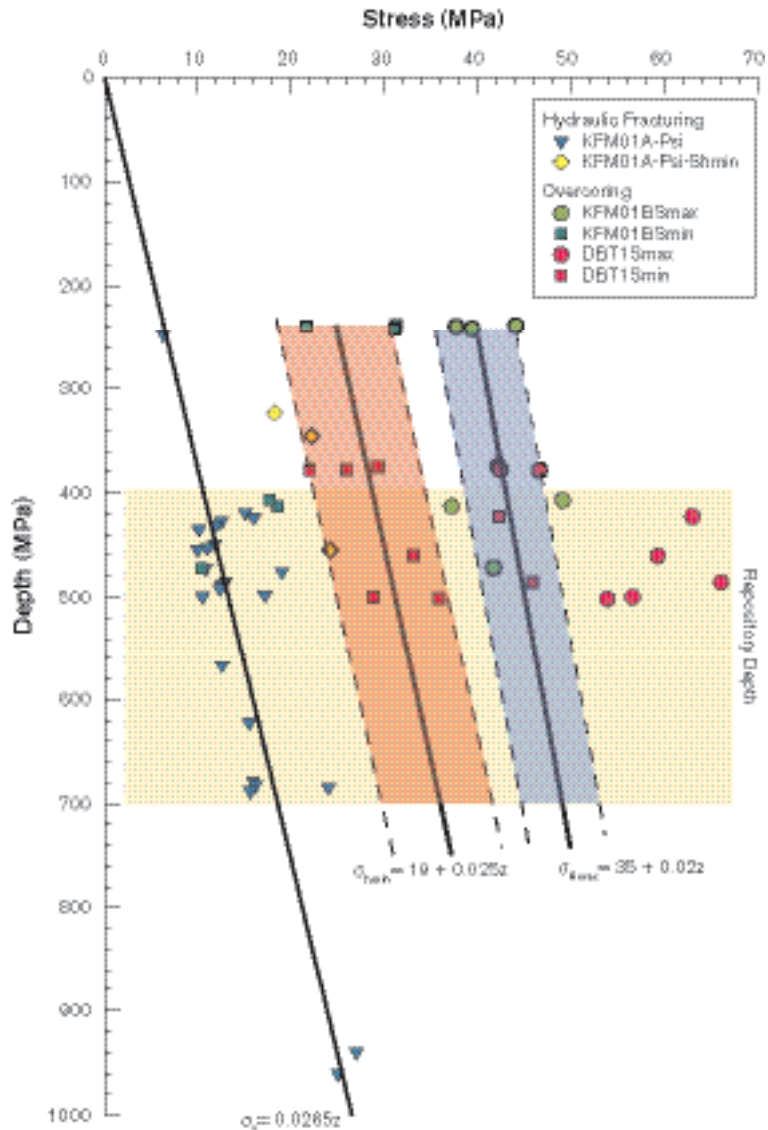


Figure 6-16. Stress measurements and stress modelling results for RFM029 at Forsmark (data from /Sjöberg et al. 2005/).

Vertical stress (σ_v)

The determination of the vertical stress mainly relied on the successful hydraulic test measurements in KFM01A, KFM01B and KFM02A /Sjöberg et al. 2005/. For this purpose, only the results obtained on fractures dipping less than 20° were considered. The vertical stress mainly depends on the rock mass density. At Forsmark, intact rock densities varying between 2,650 and 2,810 kg/m³ were measured, with an average of about 2,700 kg/m³. This variation does not significantly affect the average stress gradient with depth that is 0.0265 MPa/m. This gradient can be extrapolated to the whole RFM029 (depth from 0 to 1,000 m). A maximum and minimum interval for the vertical stresses can be estimated from data in Table 6-10.

Maximum horizontal stress (σ_H)

The maximum horizontal stress was evaluated using results of different techniques: i) overcoring data from KFM01B corrected to fit the vertical stress; ii) stress estimates from core diking and spalling in KFM01B; iii) stress estimates from core diking of solid cores in KFM01A, KFM02A, KFM04A and KFM05A; iv) re-interpreted overcoring results from DBT-1.

The estimates in Table 6-10. take into account the fact that core diking was present but not extensive in the solid and hollow core specimens. The rather high stress gradients are also confirmed by /Sjöberg et al. 2005/. The maximum horizontal stress is oriented NW-SE with a wide scatter of values in the interval 120–170°.

Minimum horizontal stress (σ_h)

The minimum horizontal stress is the most uncertainly determined. Its evaluation is based on: i) results from hydraulic fracturing from DBT-1 and; ii) hydraulic tests results from fractures dipping at least 75° in KFM01A, KFM01B and KFM02A. By using the values of the maximum horizontal and vertical stress, the variation of the minimum horizontal stress can be determined in plain-strain conditions when the Poisson's ratio and the density of the overburden rock are known. For density values varying between 2,650 and 2,810 kg/m³, and Poisson's ratios between 0.16 and 0.29 (see Section 6.3.7), the gradient of the minimum horizontal stress is estimated between 0.009 and 0.013 MPa/m, with an average value of 0.011 MPa/m. For simplicity, the maximum and minimum expected gradient for this stress component are assumed equal. The offsets at the ground surface are slightly changed compared to the theory to better fit the stress measurements.

Stresses outside rock domain RFM029

One of the alternative models is based on the assumption that the rock stresses in the tectonic lens represented by rock domain RFM029 could be higher than for the surrounding rock domains. This stress increase could be explained by a possible stiffness contrast between the rock domains with different competence. However, Figure 6-17 shows that the stress state is very similar inside (west of the Singö deformation zone) and outside rock domain RFM029 (east of the Singö deformation zone). Figure 6-17 also show that the presence of the Singö deformation zone does not much affect the stress state at Forsmark, probably because the maximum principal stresses are almost parallel to the strike of the zone.

Stresses above 350 m

As mentioned, it is very common in Scandinavia that the upper bedrock exhibits a different stress regime from the deeper crust. This can be due to local features, such as particular positions of the fracture zones and folding axes, the presence of superficial fracturing and its orientation, topographical variations, rock type heterogeneities and rock intrusions. These features often produce a decrease of the stress gradient from the shallow bedrock to the deep bedrock, as shown by numerical modelling in the next section. In particular, superficial stresses are more isotropic than deep stresses, and the orientation of the maximum horizontal stress close to the surface is often very scattered (Figure 6-17).

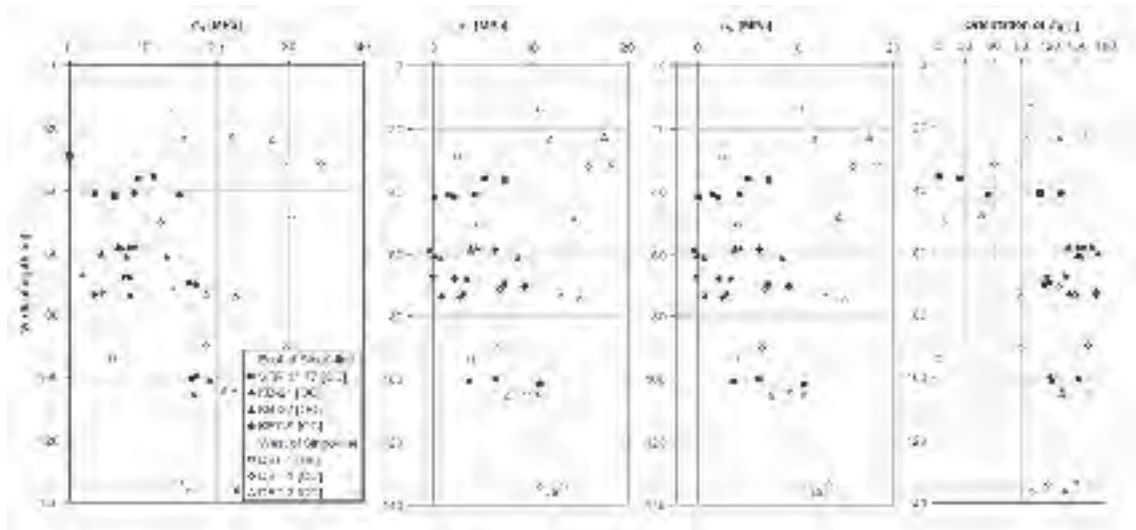


Figure 6-17. Stress measurements east and west of the Singö deformation zone (ZFMNW0001). The maximum and minimum horizontal and vertical stresses and the trend of the maximum horizontal stress are plotted for the upper 140 m depth.

Effect of gently dipping deformation zones

To study the effect of gently dipping deformation zones within rock domain RFM029, a 3DEC numerical model simulation was performed on a simplified geometry of the tectonic lens and some of the regional deformation zones (Singö and Forsmark) /Mas Ivars and Hakami, 2005/. The tectonic lens is also cut by deformation zone ZFMNE00A2, which is considered in some of the modelling cases. This zone is laterally limited by the regional zones (Figure 6-18). The numerical modelling indicates that the difference in stiffness of the tectonic lens and the rest of the bedrock do not significantly affect the rock stress distribution. This result is probably influenced by the simplified geometry of the model that does not consider some of the “splays” of the Singö deformation zone, which could give rise to high stresses in the “sand glass” shaped rock volume between the regional zones.

The presence of the gently dipping zone, on the other hand, produces a deepening of the stress trajectories toward the toe of the zone itself. This effect tends to diminish the maximum principal stress (sub-horizontal) for a certain depth above the zone. Another interesting effect is that the minimum principal stress (sub-vertical) exhibits a larger gradient approaching the surface and in relation to the gently-dipping zone. This stress can sometimes even be in extension. It is worth pointing out that the boundary stresses used for the modelling were the same as assumed in model version 1.1. Thus, the modelling stress gradients are different from those in Table 6-1.

If the effect of several gently dipping zones can be obtained by superposition of the effects of one zone, the result could be an increase of: i) the variability of the maximum principal stress at the surface and; ii) the gradient of the vertical stress in the upper 100–200 m. Thus, the presence of numerous gently-dipping deterministic deformation zones at the site implies that the numerical modelling exaggerates the effect of such structures, as the measurements along KFM01A, KFM01B and KFM02A seem to indicate /Sjöberg et al. 2005/.

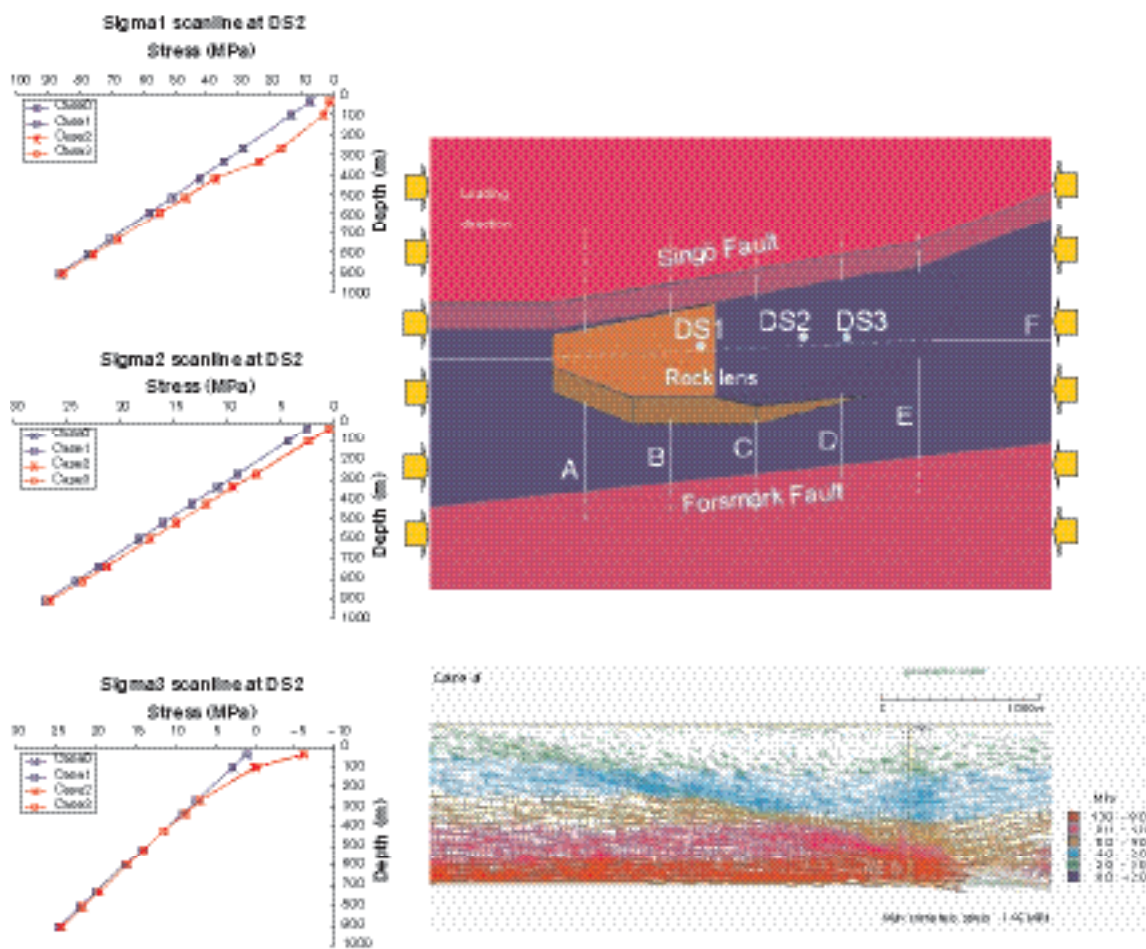


Figure 6-18. Summary of the 3DEC modelling for the simplified structural geometry of the Forsmark regional area (top). The principal stresses along the scan line DS 2 are shown on the left. At the bottom, a plot of the stress directions on a vertical cross section along scan line F is given. Cases 0 and 1 (the gently dipping zone is absent), Case 2 and 3 (the gently dipping zone is activated) with stress boundaries. Case 4 with displacement boundaries /Mas Ivars and Hakami, 2005/.

6.4.5 Evaluation of the uncertainties

All the stress measurement methods suffer from different kinds of uncertainties that often derive from the assumptions behind the processing technique. The overcoring technique, for instance, has a more robust theoretical basis, making no assumption about the ratio between the principal stresses, than that of the hydraulic techniques. The overcoring technique is applied at the limit of applicability of the method when non-elastic behaviour occurs (e.g. diskings of the hollow core), as often happens at Forsmark. However, accuracy is improved by the “transient strain analysis” /Hakala et al. 2003/, since this takes into account measurements at different depths at the same time.

The hydraulic test techniques measure directly the vertical and minimum horizontal stress at Forsmark (hydraulic fracturing of intact rock and hydraulic testing of pre-existing horizontal and vertical fractures), and potentially have a higher accuracy than the overcoring technique for these stress components. In some cases, the orientation of the hydraulically generated fractures cannot be accurately measured and may even rotate toward the ends of the packer section of the borehole. There is also a concern in highly stressed rock, whether an induced vertical fracture propagates in the same direction or turns to become more horizontal away from the borehole.

Some of the uncertainties in the in-situ stress data are related to the scatter introduced by the measurement technique. Traditional overcoring methods provide more scatter in the results compared with large scale back-calculation methods (Figure 6-19, upper). However, the scatter from overcoring measurements does not imply that the in-situ stress magnitudes will show the same scatter, particularly not when the rock mass is relatively massive and homogeneous. Figure 6-19 (lower) shows the scatter in both the overcoring and hydraulic fracturing methods compared with the uncertainty in the in-situ stress magnitudes determined by back analysis of the Mine-by Experiment /Martin and Read, 1996/. Consequently, the stress gradients provided in Table 6-10 have been adjusted to reflect the findings shown in Figure 6-19.

The considerations in this section were kept in mind when processing the rock stress measurements available at Forsmark. For the present modelling: i) the maximum horizontal stress determined by hydraulic methods was never used; ii) the overcoring results were re-calculated based on more realistic values of the vertical stress; iii) only hydraulic test results on almost horizontal and vertical fractures were used. Moreover, results from independent analyses on the solid and hollow core disk, and of the spalling phenomena in the boreholes were carried out /Sjöberg et al. 2005/.

The uncertainty on the mean values of the maximum and minimum horizontal stress magnitude for depths between 250 and 650 m in rock domain RFM029 are provided in Table 6-10 and is estimated to be $\pm 10^\circ$ for the mean trend. The intervals in Table 6-10 consider the spatial variability of the stress component in the rock volume considered.

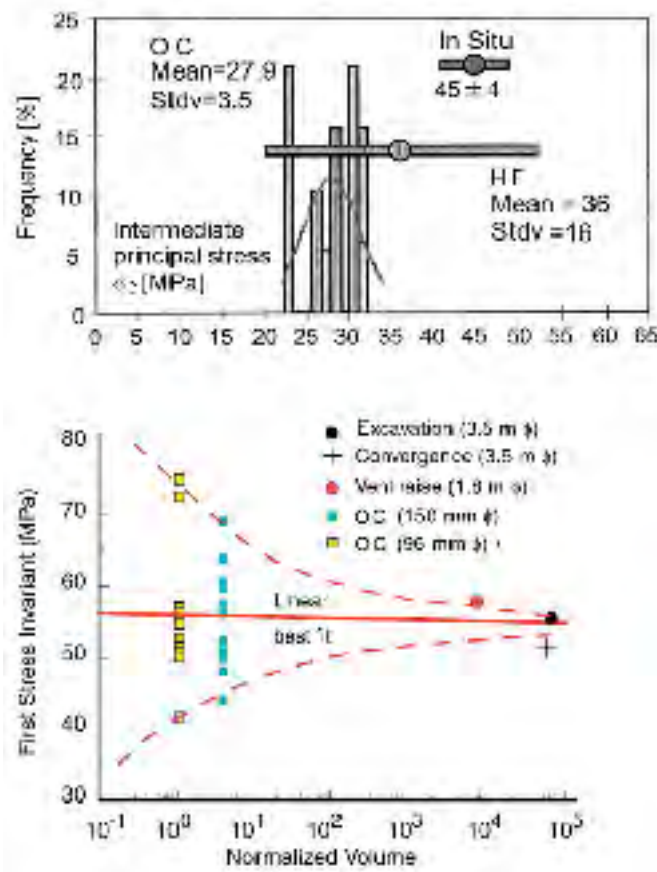


Figure 6-19. Comparison of rock stress measurements from different techniques (upper) and their scale dependence (lower) at the AECL's Mine-by Experiment, URL (Canada, after /Martin and Read, 1996/).

7 Bedrock thermal model

The bedrock thermal model describes thermal properties at the domain level, which is of importance, since the thermal properties of the rock mass affects the possible distance, both between canisters and between deposition tunnels, and therefore puts requirements on the necessary repository volume. Of main interest is the thermal conductivity, since it directly influences the design of a repository. Measurements of thermal properties are performed at the cm scale, but values are required at the canister scale, at which scale the spatial variability is required to be considered. Therefore, the thermal modelling includes elements of upscaling of thermal properties from rock type level to lithological domain level, described in more detail in a supporting document for the thermal model version Forsmark 1.2 /Sundberg et al. 2005b/. The work has been performed according to a strategy presented in /Sundberg, 2003/.

7.1 State of knowledge at the previous model version

In model version 1.1 of the Forsmark area /SKB, 2004a/, the thermal properties of samples were evaluated at both rock unit and rock domain level, and a Monte Carlo simulation of borehole KFM01A was undertaken.

Thermal conductivity properties were given separately for each rock unit with the lowest values for rock type “Felsic to intermediate volcanic rock” (103076), 2.79 W/(m·K) and the highest for rock type “Granite to granodiorite” (101057), 3.33 W/(m·K). The rock domains (RFM029 and RFM017) had conductivities with mean values 3.41 W/(m·K) and 2.73 W/(m·K), respectively. Comparison between measured and calculated (from mineral composition) thermal conductivities showed differences of –6.8 to 8.8%. The in-situ temperature of the Forsmark area increased from 7°C at 100 m depth to about 13°C at 600 m.

The main uncertainties of the thermal model in version 1.1 arose because:

- Temperature loggings were only available for one borehole and the gradient with depth could not fully be explained,
- Few measurements of thermal properties were available, giving rise to a weak statistical basis and uncertainties in the representativeness of calculated thermal conductivities.
- Upscaling from core samples to rock domains was required.
- There was a lack of data concerning properties at elevated temperatures and the anisotropy of thermal properties.

7.2 Evaluation of primary data

In Table 2-3 sources of available data on thermal properties are identified.

7.2.1 Thermal conductivity from measurements

Laboratory measurements of the thermal conductivity on rock samples have been performed with the TPS (Transient Plane Source) method, see description in /Sundberg, 2003/. The measurements are made on a defined rock volume (approximately 10 cm³) determined by the size of the sensor. The variability in the results is probably higher, due to the small scale of measurement, compared to determinations at larger scales. Results from the laboratory measurements are presented in Table 7-1. Samples from different elevations in the boreholes were used for the measurements /Adl-Zarrabi, 2004a,b,c,d/. The samples are, with a few exceptions, spatially located close to each other with approximately 3–5 samples in each group. For illustration, see /Sundberg et al. 2005b/.

Table 7-1. Measured thermal conductivity (W/(m·K)) of samples using the TPS method. Samples are from boreholes KFM01A, KFM02A, KFM03A and KFM04A together with 5 surface samples.

Rock type	Rock name	Sample location	Mean	St. dev.	Number of samples
101057	Granite to granodiorite, metamorphic, medium-grained	Boreholes KFM01A, KFM02A, KFM03A and samples PFM001159 and PFM001164	3.71	0.16	49
101054	Tonalite to granodiorite, metamorphic	Borehole KFM03A, and samples PFM001157 and PFM001162	2.73	0.19	5
101051	Granite, granodiorite and tonalite, metamorphic, fine- to medium-grained	Borehole KFM03A	2.51	0.08	3
101056	Granodiorite, metamorphic	Borehole KFM04A	3.04	0.09	5
101033	Diorite, quartz diorite and gabbro, metamorphic	PFM001158	2.28	–	1

The temperature dependence of the thermal conductivity has been investigated by measuring 18 samples within rock type 101057, granite to granodiorite, at three different temperatures (20, 50 and 80°C) /Adl-Zarrabi, 2004a,c,d/. Table 7-2 summarises the temperature dependence of the thermal conductivity for rock type 101057. The thermal conductivity decreases by 6.2–12.3%/100°C temperature increase, see /Sundberg et al. 2005b/.

As a step in the quality assurance of thermal data, 10 samples from KFM01A within rock type 101057 were selected for comparing TPS measurements at two different laboratories, Hot Disk AB and SP (Swedish National Testing and Research Institute). The samples have been measured at three different temperatures and the results are presented in Table 7-3. The differences in mean value for all samples are small between the two laboratories, especially for thermal conductivity.

For the thermal conductivity, the measured differences on the individual samples varied between –6.6 and 4.8%. The differences in heat capacity, measured on individual samples, varied between –12.4 and 9.7%.

Table 7-2. Measured temperature dependence of thermal conductivity (per 100°C temperature increase) on samples from boreholes KFM01A, KFM02A and KFM03A.

Rock type	Rock name	Sample location	Mean	St. dev.	Number of samples
101057	Granite to granodiorite	boreholes KFM01A, KFM02A and KFM03A	–10.0%	0.019	18

Table 7-3. Comparison of results from TPS measurements performed by two different laboratories on the same samples at three different temperatures.

	Thermal conductivity Mean (W/(m·K))	Heat capacity Mean (MJ/(m ³ ·K))
Measured SP	3.65	2.41
Measured Hot Disk	3.63	2.34
Diff. (Hot Disk-SP)/SP	–0.5%	–2.6%

7.2.2 Thermal conductivity from mineral composition

Thermal conductivity of rock samples can be calculated with the SCA (Self Consistent Approximation) method using mineral compositions from modal analyses and reference values of the thermal conductivity of different minerals /Horai, 1971; Sundberg, 1988; Sundberg, 2003/. The calculations are performed at the mm scale and values have earlier been shown to be in good agreement with measured values /Sundberg, 1988; Sundberg, 2002/.

The following data were used for calculations with the SCA method:

- Modal analyses from surface samples included in Forsmark site descriptive model version 1.1, but with reclassified rock codes /Stephens, 2004/.
- New modal analyses from boreholes KFM01A, KFM02A, KFM03A and KFM03B, where some are made in connection with sampling for measurements of thermal properties.

The results of the SCA calculations are presented in Table 7-4 subdivided according to rock type.

Table 7-4. Thermal conductivity (W/(m·K)) of samples from different rock types, calculated from the mineralogical compositions (SCA method).

Rock type	Rock name	Mean	St. dev.	Number of samples
101057	Granite to granodiorite, metamorphic, medium-grained	3.56	0.24	56
101051	Granite, granodiorite and tonalite, metamorphic, fine- to medium-grained	3.10	0.24	21
101054	Tonalite to granodiorite, metamorphic	3.03	0.42	17
101061	Pegmatite, pegmatitic granite	3.54	0.12	4
101033	Diorite, quartz diorite and gabbro, metamorphic	2.36	0.21	2
101004	Ultramafic rock, metamorphic	3.50		1
101056	Granodiorite, metamorphic	3.20	0.19	3
101058	Granite, metamorphic, aplitic	3.47	0.12	2
102017	Amphibolite	2.43	–	1
103076	Felsic to intermediate volcanic rock, metamorphic	3.01	0.37	10
111058	Granite, fine- to medium-grained	3.35	0.05	2

7.2.3 Thermal conductivity from density

For the Simpevarp site investigation area a relationship between density and thermal conductivity for Ävrö granite (501044) has been found and is presented in /Sundberg et al. 2005c/. The corresponding relationship within a rock type has not been found for any of the present rock types in the Forsmark site investigation area. The background to the relationship for Ävrö granite is described in /Sundberg et al. 2005a/

Figure 7-1 illustrates samples where both density and thermal conductivity have been measured and shows no valid relationship for any of the measured rock types within the Forsmark site investigation area. However, an obvious relationship exists across investigated rock types.

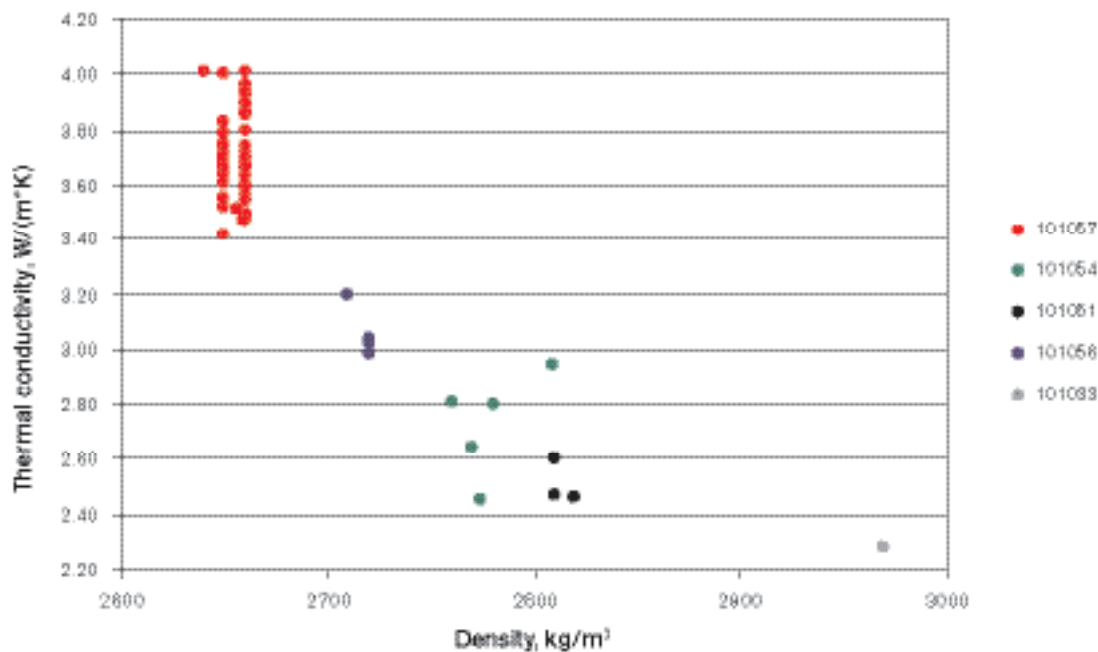


Figure 7-1. Based on available data of rock types present at the Forsmark site investigation area, a trend between density and thermal conductivity is obvious between different rock types. However, a useful relationship within each rock type has not been found.

7.2.4 Modelling of thermal conductivity (rock type level)

There are different data sets of thermal conductivity for the dominant rock types. The most reliable data comes from TPS measurements, but these samples are probably not representative of the rock type due to limited number of samples and the strategy for sample selection (cluster sampling of dominant rock type). Therefore, also SCA calculations from the mineral distribution are included in the rock type model since they have a larger spatial distribution in the rock mass.

In Table 7-5, thermal conductivity values calculated using the SCA method are compared with measured values of the same sample (not always the identical sample although closely located). For the tonalite to granodiorite (101054) and for the granite, granodiorite and tonalite (101051) there are only two and one samples, respectively, available for comparison. Table 7-5 indicates that the difference between calculated and measured values is small for granite to granodiorite (101057), while there are not enough values for comparison for the other rock types.

Rock type models have been developed for the different rock types, see Table 7-6. Distributions of different data sets and the rock type model for granite to granodiorite, (101057) are specified in Figure 7-2. For other rock types, see illustrations in /Sundberg et al. 2005b/. The different mean values for calculated (SCA) and measured (TPS) distributions in the table indicate representativity problems for some rock types.

Table 7-5. Comparison of thermal conductivity (W/(m·K)) for comparable samples for different rock types calculated from mineralogical compositions with the SCA method (samples from thermal programme), and measured with the TPS method. Samples are from boreholes KFM01A, KFM02A and KFM03A together with 4 surface samples.

Method		Rock type 101057 20 samples	Rock type 101054 2 samples	Rock type 101051 1 sample
Calculated (SCA)	Mean	3.63	2.97	3.15
	St. dev.	0.23	0.30	–
Measured (TPS)	Mean	3.69	2.63	2.47
	St. dev.	0.17	0.25	–
Diff. (SCA-TPS)/TPS		–1.5%	12.8%	27.6%

Table 7-6. Model properties of thermal conductivity (W/(m·K)) from different methods and combinations divided by rock type. For some of the samples, there are values from both SCA calculations and TPS measurements for thermal conductivity. In these cases only the measured value (TPS) has been used in the rock type model. All rock type models are based on normal (Gaussian) distributions.

Rock name (rock type)	Samples	Mean	St. dev.	Number of samples
Granite to granodiorite (101057)	TPS	3.71	0.16	49
	SCA	3.56	0.24	56
	Rock type model: TPS+SCA	3.63	0.22	85
Granodiorite (101056)	TPS	3.04	0.09	5
	SCA	3.20	0.19	3
	Rock type model: TPS+SCA	3.10	0.15	8
Tonalite to granodiorite (101054)	TPS	2.73	0.19	5
	SCA	3.03	0.42	17
	Rock type model: TPS+SCA	2.96	0.41	20
Granite, granodiorite and tonalite (101051)	TPS	2.51	0.08	3
	SCA	3.10	0.24	21
	Rock type model: TPS+SCA	3.02	0.31	23
Pegmatite, pegmatitic granite (101061)	Rock type model: SCA	3.54	0.12	4
Felsic to intermediate volcanic rock (103076)	Rock type model: SCA	3.01	0.37	10
Diorite, quartz diorite and gabbro (101033)	TPS	2.28	–	1
	SCA	2.36	0.21	2
	Rock type model: TPS+SCA	2.33	0.16	3
Granite (101058)	Rock type model: SCA	3.47	0.12	2
Granite (111058)	Rock type model: SCA	3.35	0.05	2

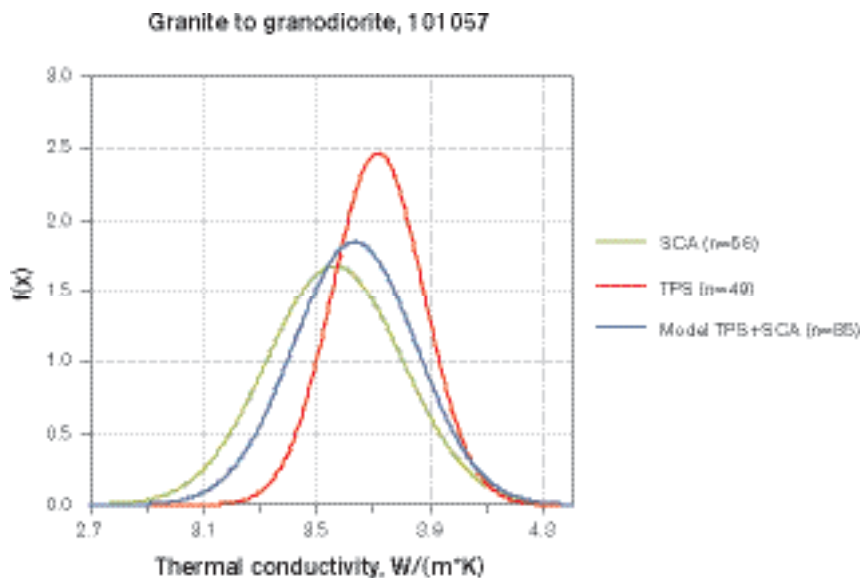


Figure 7-2. PDFs for calculated values (SCA), measured values (TPS) and a summarising rock type model for rock type granite to granodiorite (101057).

The rock type models are used to model thermal properties for domains, see Section 7.3. Density loggings have not been used for the rock type models since no valid relationship between density and thermal conductivity has been found for any of the rock types (within rock type). All rock types are assumed to be characterised by normal (gaussian) PDFs /Sundberg et al. 2005b/.

7.2.5 Heat capacity

No direct laboratory measurements of the heat capacity have been carried out, but the heat capacity has been calculated from conductivity and diffusivity measurements performed with the TPS method. Results are presented in Table 7-7. Determination of heat capacity has been performed on the same samples as used for measurement of thermal conductivity, cf. Section 7.2.1. Therefore the same problem concerning representativeness of the rock mass exists. There are no other sources for heat capacity values and therefore rock type models are based on data in Table 7-7 /Sundberg et al. 2005b/. Heat capacity exhibits a rather large temperature dependence which is shown in Table 7-8.

Table 7-7. Determined heat capacity (MJ/(m³·K)) of samples of different rock types, using the TPS method. Samples are from boreholes KFM01A, KFM02A, KFM03A and KFM04A together with 5 surface samples.

Rock name (rock type)	Sample location	Mean	St. dev.	Number of samples
Granite to granodiorite (101057)	Borehole KFM01A, KFM02A, KFM03A and sample PFM001159 and PFM001164	2.17	0.17	49
Tonalite to granodiorite (101054)	Borehole KFM03A, PFM001157 and PFM001162	2.12	0.20	5
Granite, granodiorite and tonalite (101051)	Borehole KFM03A	2.17	0.05	3
Granodiorite (101056)	Borehole KFM04A	2.25	0.07	5
Diorite, quartz diorite and gabbro (101033)	PFM001158	2.33	–	1

Table 7-8. Determined temperature dependence of heat capacity (per 100°C temperature increase) on samples of rock type (101057) “granite to granodiorite” from boreholes KFM01A, KFM02A and KFM03A. The mean of temperature dependence was estimated by linear regression.

Rock name (rock type)	Sample location	Mean	St. dev.	Number of samples
Granite to granodiorite (101057)	Boreholes KFM01A, KFM02A and KFM03A	27.5%	0.086	18

7.2.6 Anisotropy

Anisotropic conductivity and diffusivity have been investigated for samples from borehole KFM04A /Dinges, 2004/. Measurements were carried out with the TPS-method. The summary of the results for thermal conductivity from the measurements is presented in Table 7-9. Samples showing a clear lineation/foliation were selected for the measurements. The samples were taken in the granite that is the dominant rock type in rock domain RFM029, but rather close to the border to rock domain RFM012. This may imply that the samples have a higher degree of anisotropy compared with the rock in the central parts of domain RFM029.

Table 7-9. Results of the anisotropic thermal conductivity measurements. The measurements were made in the two principle directions; perpendicular to foliation (λ_{axial}) and parallel to the foliation (λ_{radial}). The estimated specific heat capacity of 2.271 MJ/m³·K was used for the measurement.

Borehole, sampling depth (Sec Low)	λ_{axial} (W/(m·K))	Std- λ_{axial} (W/(m·K))	λ_{radial} (W/(m·K))	Std- λ_{radial} (W/(m·K))	$\lambda_{radial}/\lambda_{axial}$
KFM04A, 530.95–531.03	2.13	0.17	5.18	0.22	2.43
KFM04A, 531.03–531.12	2.84	0.15	4.04	0.18	1.42
KFM04A, 531.12–531.20	2.98	0.02	4.01	0.04	1.35
KFM04A, 531.20–531.29	3.06	0.07	4.39	0.08	1.43
KFM04A, 531.29–531.37	0.98	0.02	6.34	0.15	6.47

However, the evaluation of the measurements uses the heat capacity as input. Results of the heat capacity were not available for the current model version. Instead a fixed value for all samples of 2.271 MJ/m³·K were used. By increasing the specific heat by 10%, λ_{axial} is decreased by roughly 10% and λ_{radial} is increased by 10% (and vice versa). The values in Table 7-9 may be both over- and underestimated.

7.2.7 Coefficient of thermal expansion

The coefficient of thermal expansion has been measured on samples from the Forsmark area and the results are presented in Table 7-10. Samples from three different boreholes, KFM01A, KFM02A and KFM03A, have been investigated /Åkesson, 2004a,b,c; Carlsson, 2004; Liedberg, 2004/. The mean value of measured thermal expansion varies for the different rock types between 7.2×10^{-6} and 8.0×10^{-6} m/(m·K). For the dominant rock type 101057 in domain RFM029 and RFM012, a mean value of the thermal expansion coefficient is suggested as 7.7×10^{-6} m/(m·K).

Table 7-10. Measured thermal expansion (m/(m·K)) between 20°C and 80°C on samples of different rock types from boreholes KFM01A, KFM02A and KFM03A in the Forsmark area.

Rock type	Rock name	Sample location	Mean	St. dev.	Number of samples
101057	Granite to granodiorite	Borehole KFM01A, KFM02A, KFM03A	7.7E-06	2.2E-06	44
101054	Tonalite to granodiorite	Borehole KFM03A	7.2E-06	1.6E-06	3
101051	Granite, granodiorite and tonalite	Borehole KFM03A	8.0E-06	1.8E-06	3

7.2.8 In-situ temperature

The temperature of the borehole fluid was logged in boreholes KFM01A, KFM01B, KFM02A, KFM03A and KFM04A. Measured temperature results are presented in Figure 7-3. For a methods description and presentation of borehole results see /Sundberg et al. 2005b/. Temperatures at specified depths and borehole inclination are presented in Table 7-11. There is an uncertainty in the temperature logging results due to disturbance from the drilling and water movements along the boreholes. This difference in temperature is relatively small for a specified depth. However, the influence on the design of a repository may be significant. The temperature of borehole KFM01B is anomalous compared to the other boreholes. The reason for this is not known. Borehole KFM01B is not included in the calculation of mean temperature in Table 7-11.

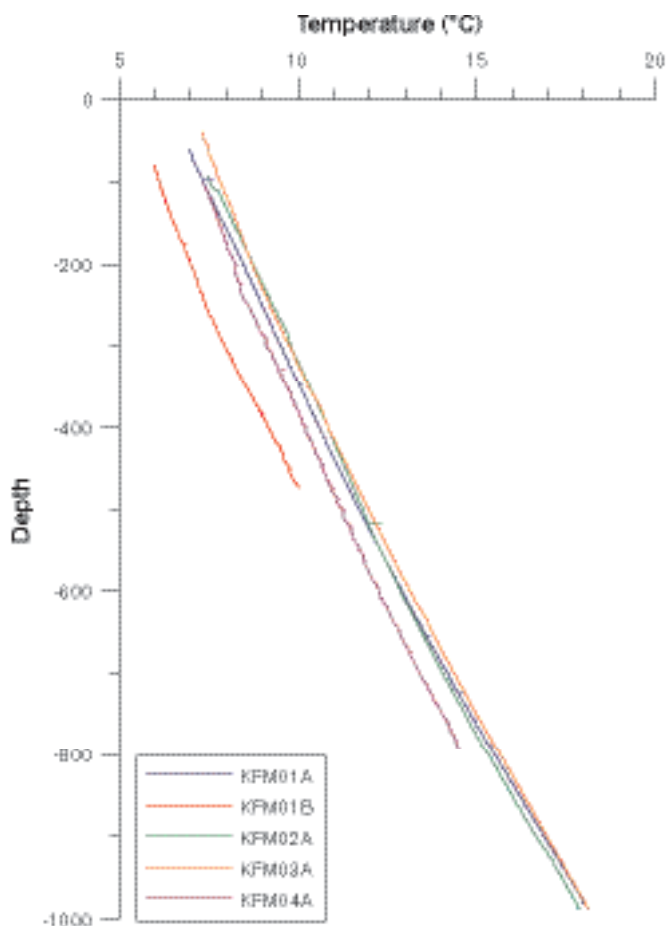


Figure 7-3. Temperature loggings in boreholes within the Forsmark site investigation area.

Table 7-11. Measured temperature (°C) at different vertical depths; 400, 500 and 600 m from ground surface. Approximate inclination of the boreholes is also indicated.

Borehole	400 m	500 m	600 m	Approximate inclination (°)
KFM01A	10.6	11.7	12.9	80
KFM01B	(9.2)	–	–	75
KFM02A	10.8	11.8	12.9	84
KFM03A	10.8	12.0	13.1	85
KFM04A	10.2	11.2	12.3	54
Mean (KFM01B excluded)	10.6	11.7	12.8	

7.3 Thermal modelling (lithological domain level)

7.3.1 Modelling assumptions and input from other disciplines

The lithological model version 1.2 for the Forsmark area is the geometrical basis for the thermal model and is described in Section 5.3. The geological Boremap log of the boreholes, showing the distribution of dominant and subordinate rock types, has been used as input to the thermal modelling jointly with a lithological domain classification of borehole intervals. However, the rock type distributions per domain used in the thermal domain modelling differ from those presented in Section 5.3, due to slightly different data (for example rock occurrences of less than 1 m length

from the Boremap logs are included in the thermal modelling). For the dominant rock type 101057 (granite to granodiorite) this results in a 74% content in domain RFM029 to be compared with 84% stated in the geological model.

7.3.2 Conceptual model

There are three main causes for the spatial variability of thermal conductivity at the domain level; (1) small scale variability between minerals, (2) spatial variability within each rock type, and (3) variability between the different rock types making up the domain. The first type results in variability in small samples (as determined by TPS measurements and modal analysis). At this scale, the small scale variability can be substantial. However, the variability is reduced when the scale increases.

The second type of variability is caused by spatial variability in sample data within a rock type and cannot be explained by small-scale variations. This variability has different importance depending on the rock type. The reason for the spatial variability within a rock type is the process of rock formation, but also the system of classifying the rock types. The variability cannot be reduced, but the uncertainty in the variability may be reduced. This is achieved by collecting large number of samples at varying distances from each other, so that reliable variograms can be created.

A large number of samples are needed to study spatial variability within a rock type. For rock type granite to granodiorite (101057) a variogram is presented in Figure 7-4. The result indicates quite a short range of variability. Variogram for larger scales could not be produced, due to too few samples.

The third type of variability is due to the presence of different rock types in the lithological domain. This variability is more pronounced where the difference in thermal conductivity is large between the most common rock types of the domain. Large variability of this type can also be expected in a domain of many different rock types. It is only reduced significantly when the scale becomes large compared with the spatial extent of occurrence of the various rock types.

Of importance at the domain level is the scale representative for the canister, i.e. at which the thermal conductivity is important for heat transfer from the canister. At present, this scale is not well defined, but it is believed to be in the order of 1 to 10 m. Therefore, the approach in the domain modelling is to use different scales to study the scale effect, and to draw conclusions on representative thermal conductivity values from the range of results obtained.

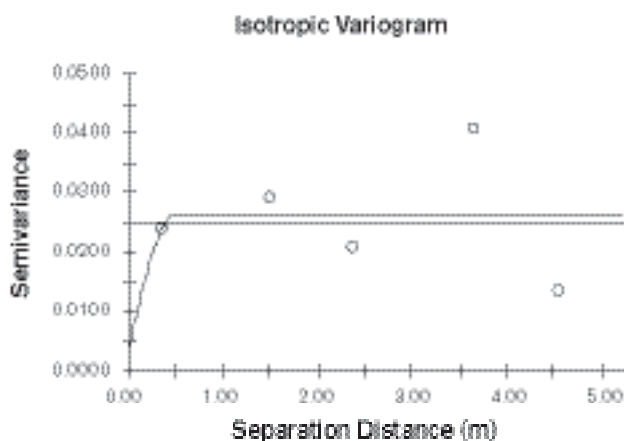


Figure 7-4. Variogram of the thermal conductivity for granite to granodiorite (101057) with a separation distance of up to 5 m. Data are based on TPS measurements and the straight line indicates the sample variance.

7.3.3 Modelling approaches

The methodology for domain modelling and the modelling of scale dependency were developed for the Prototype Repository at the Äspö HRL /Sundberg et al. 2005a/. In parallel, the domain modelling of Forsmark was performed /Sundberg et al. 2005b/. A number of different approaches have been used in the modelling of the two domains RFM029 and RFM012. Modelling of domain RFM017 has not been possible due to lack of borehole and sample data within the domain. Modelling of the mean of the thermal conductivity at the lithological domain level has been performed according to the main approach (Approach 1) described in Figure 7-5. This approach was applied to the two domains RFM029 and RFM012 (both dominated by the granite to granodiorite (101057)). In order to evaluate the spatial variability at domain level, two alternative/complementary approaches were applied (Approaches 2 and 3). Mean value results on a domain level and associated standard deviations are presented in Table 7-13.

Thermal conductivity modelling for domain RFM029 and RFM012

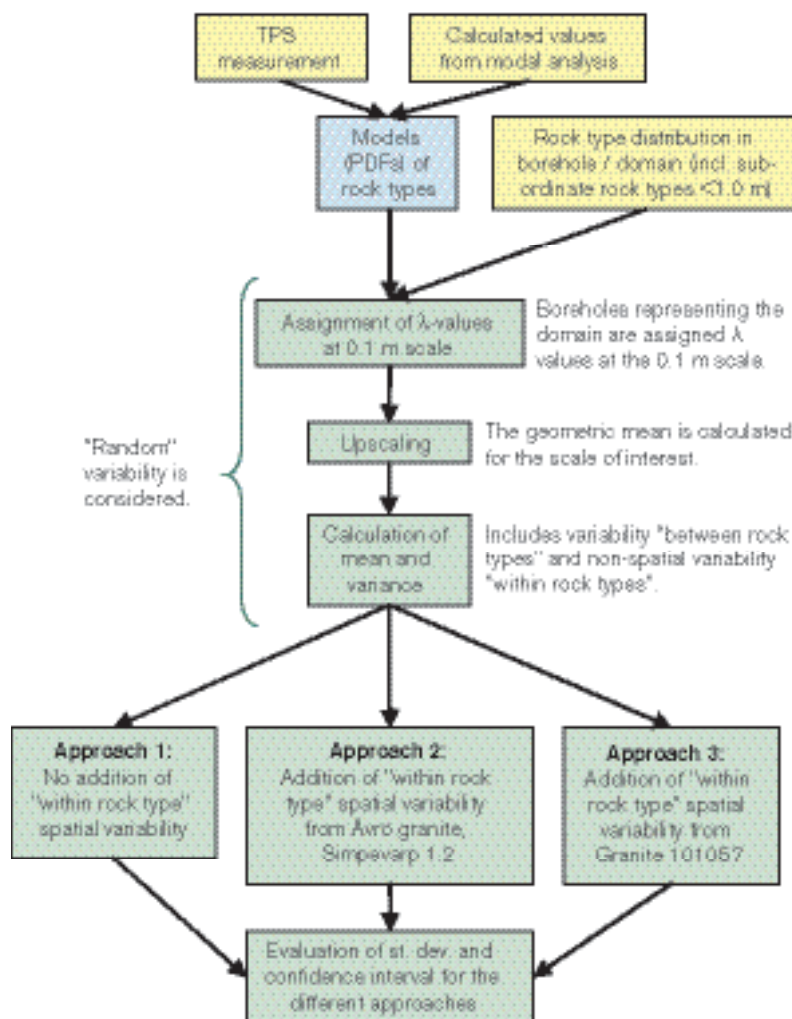


Figure 7-5. Approach for estimation of thermal conductivity for domain RFM029 and RFM012, both dominated by granite to granodiorite (101057). Yellow colour indicates the data level, blue the rock type level and green the domain level.

Approach 1: Main approach

The main approach for the two domains RFM029 and RFM012 is as follows:

Measured and calculated values from modal analysis were used to produce a PDF (Probability Density Function) model for rock types present in the domains, according to Table 7-6.

The summed length of boreholes, or parts of boreholes, belonging to a domain were assumed to be a representative realisation of the domain. Each borehole belonging to a domain was divided into 0.1 m long sections and each section was assigned a thermal conductivity value according to the lithological classification of that section. Both dominant and subordinate rock types are considered in this context. Thermal conductivity values were randomly selected according to the distribution model (PDF) based on measured (TPS) and calculated conductivities from mineral compositions (SCA).

An example illustrating the principle for assigning thermal conductivity for the rock types is shown in Figure 7-6.

For rock types where no rock type model (PDF) is available (due to lack of data), no value was assigned to that 0.1 m section (i.e. the section was ignored in the subsequent upscaling). Such rock types, primary amphibolite (102017), have a low degree of occurrence in the domains and are therefore assumed not to influence the results significantly.

The next step is the upscaling from 0.1 m scale to larger scales. To study scale effects, upscaling was performed on scales ranging from 0.1 m to 50 m. The upscaling was performed in the following way:

1. The boreholes representing the domain were divided into a number of sections with a length according to the desired scale (0.1–50 m).
2. Thermal conductivity was calculated for each section as the geometric mean of the values at the 0.1 m scale.
3. The mean and the variance of all sections of the domain were calculated. For each scale, the calculations were repeated at least 10 times with different assignment of thermal conductivity values at the 0.1 m scale, according to principle above. This produces representative values of the mean and the standard deviation for the desired scale.
4. The calculations are repeated for the next scale.

The principle for upscaling of data for different rock types is illustrated both in Figure 7-6 and Figure 7-7. In Figure 7-6, 24 sections are indicated, each with a length of 0.1 m. For the scale 0.5 m, the thermal conductivity $\lambda_{0.5-1}$ is estimated as the geometric mean of the five 0.1 m sections, $\lambda_{0.5-2}$ as the geometric mean for the next five 0.1 m sections, and so on. The mean and variance is then easily computed for the 0.5 m scale. This sequence is repeated for the other scales of interest. In Figure 7-7 the effects of upscaling are shown. The geometric mean equation is simple to use and is often applied for mean estimation of transport properties /Dagan, 1981; Sundberg, 1988/. In 3D, the effective transport properties are influenced by the variance. However, in this thermal application the variance is low and therefore the geometric mean is sufficient.

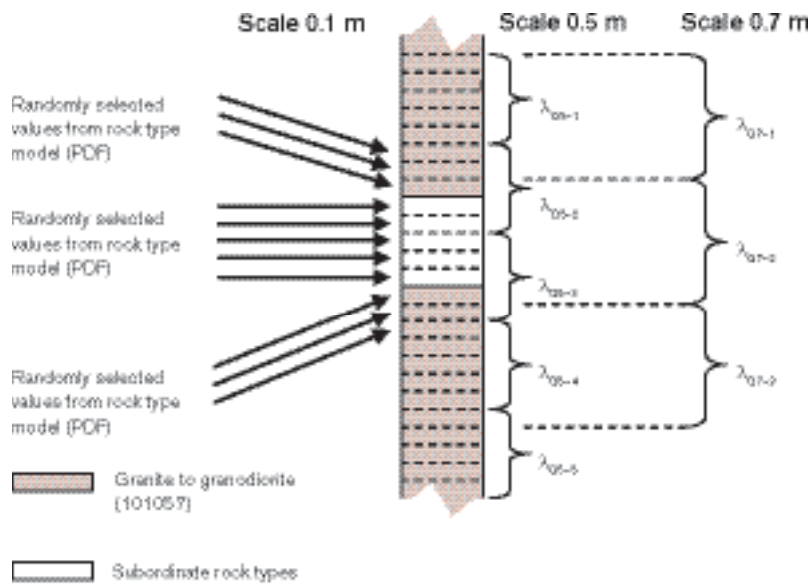


Figure 7-6. Thermal conductivity is assigned to 0.1 m sections by calculation from density loggings or randomly selected from the rock type models. Upscaling is done by calculating geometric means for different scales, for example 0.5 and 0.7 m.

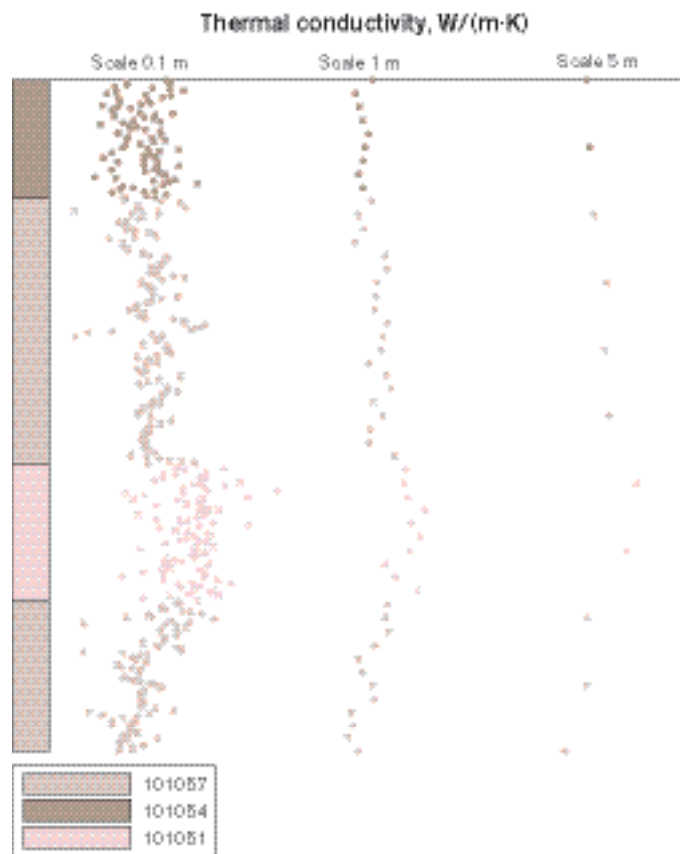


Figure 7-7. Effects of applying the principle for upscaling of thermal conductivity, as given in Figure 7-6. As illustrated in the figure the spatial variability within rock type is averaged out. The figure illustrates the effects of upscaling in general and is not typical for the actual rock types or a specific borehole.

Alternatives to main approach

The approach of randomly selecting thermal conductivity values from rock type models without consideration of spatial variability “within rock types” is described above in the main approach. The reason for not considering the variation “within rock type” is that the density loggings could not be used, since there is no relationship between density and thermal conductivity within a rock type and therefore the spatial correlation within the dominant rock types could not be addressed. This modelling resulted in estimates of thermal conductivity at different scales, see Table 7-12. The variance in the main approach includes variability due to rock type changes in the boreholes (“between rock type” variability), but the variability within each rock type is effectively and rapidly reduced when the scale is increased because of the random assignment of thermal conductivity values. The resulting variance is therefore mainly a result of the presence of different rock types in the boreholes and for domains RFM029 and RFM012 the variance is underestimated.

One way of compensating for the variance reduction caused by ignoring spatial variability is to add the spatial variability within the dominant rock type in the domain. The spatial variability within the dominant rock type can be estimated in different ways, which are presented here in two alternative/ complementary approaches (2 and 3). For approach 2, the variation within rock type is performed by looking at domain RSMA01 (Ävrö granite) from the Simpevarp area, but in approach 3 it is achieved by studying TPS measurements within the dominant rock type of the considered domain.

The total variance for the domain can be estimated as the sum of variances due to different rock types /Sundberg et al. 2005b/ and the variance due to spatial variability within the dominant rock type: $V_{tot} = V_{between\ rock\ type} + V_{within\ rock\ type}$

The “between rock type” variability is qualitatively different from, and therefore likely to be independent of, the “within rock type” variability. Therefore, the addition of variances is reasonable.

Approach 2: Addition of “within rock type” variance from the Simpevarp area

Variance caused by spatial variability (non-random) within rock type 501044 has been estimated for domain RSMA01 (Ävrö granite) in the Simpevarp area /Sundberg et al. 2005c/. In this approach, the variance caused by spatial correlation within rock type 501044 is assumed to be the same as for domains RFM029 and RFM012. Therefore, a spatial contribution of the variance of 0.037 W/(m·K) is added to the variance for domains RFM029 and RFM012, see Figure 7-8 /Sundberg et al. 2005c/ and Table 7-12.

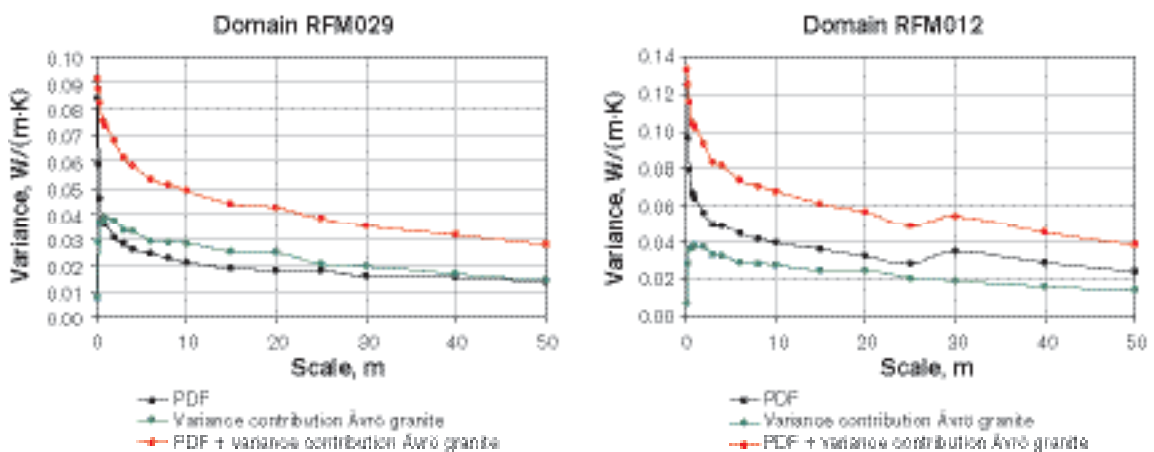


Figure 7-8. Variance contribution from non-random spatial variability in the dominant rock type 501044 of domain RSMA01 (Simpevarp area) added to domain RFM029 and RFM012. The shape of the curve for RFM012 at larger scale is a result of the distribution of rock types in the boreholes used for modelling.

However, the results are probably an overestimation of the variance, since the spatial variation within rock type granite to granodiorite (101057) seems to be much smaller than in Ävrö granite (501044) in Simpevarp.

Approach 3: Addition of “within rock type” variance from TPS measurements

For 101057 (granite to granodiorite), TPS measurements can provide a rough estimate of the non-random spatial variability within the rock type. The variance as a function of scale was calculated with the geometric mean for each scale and the results are presented in Figure 7-9. This type of variance is denoted “within rock type” below in Table 7-12. Although this approach only provides a rough estimate of the total variability, it encompasses all the major types of variability within the domain.

It is not easy to assess whether this approach under- or overestimates the total variance for the domain. There are several factors that may influence this, such as the spatial variability in subordinate rock types compared to dominant rock type. In addition, the variance “within rock type” in Figure 7-9 is rather uncertain due to relatively few measurements and questions of representativeness. Still, it is believed that this approach gives a quite reasonable estimate of the variability compared with the other approaches.

The estimated mean thermal conductivity and the total variance estimated for each domain using the three defined approaches are presented in Table 7-13 and Table 7-12, respectively.

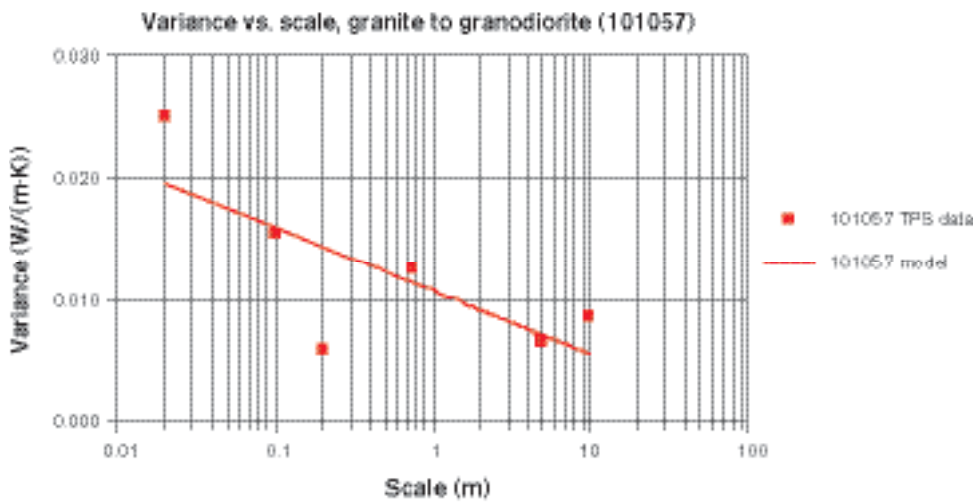


Figure 7-9. Variability within rock type granite to granodiorite, 101057. Note that data are sparse and based on 47 TPS measurements.

7.3.4 Conclusions – modelling results

Thermal conductivity

Modelling results at the 2 m scale for domain RFM029, according to the main approach, are showed in Figure 7-10. The influence of subordinate rock type sections is clearly visible as spikes in the figure, but the variability within rock types may be underestimated according to the modelling approach (1).

Mean values representative for the thermal conductivity at domain level are presented in Table 7-13 based on modelling according to the main approach. Data for the 0.75 m scale are chosen, which are assumed to be representative for the canister scale.

Table 7-13 also summarises the suggested standard deviation of thermal conductivity per domain at the canister scale. The standard deviation has been estimated with two complementary approaches, where the results are summarised in Table 7-12. For approach 1, mean values and standard deviations are calculated for each scale under the assumption of normally distributed data at the scale of interest /Sundberg et al. 2005b/. As described in the table, and also in previous sections, approach 1 probably underestimates the standard deviation and approach 2 overestimates it. Approach 3 is believed to underestimate the standard deviation for domains RFM029 and RFM012 at larger scales, but modelling at the 0.75 m scale may give a reasonable estimation of the standard deviation at the canister scale, a value in between approaches 1 and 2. Therefore, the standard deviations for the two domains are given the values of 0.22 W/(m·K) and 0.28 W/(m·K), which is the result from approach 3 at the 0.75 m scale. The variability contribution due to spatial variability within rock type seems to be rather small and the total variability is dominated by variability between different rock types within the domains.

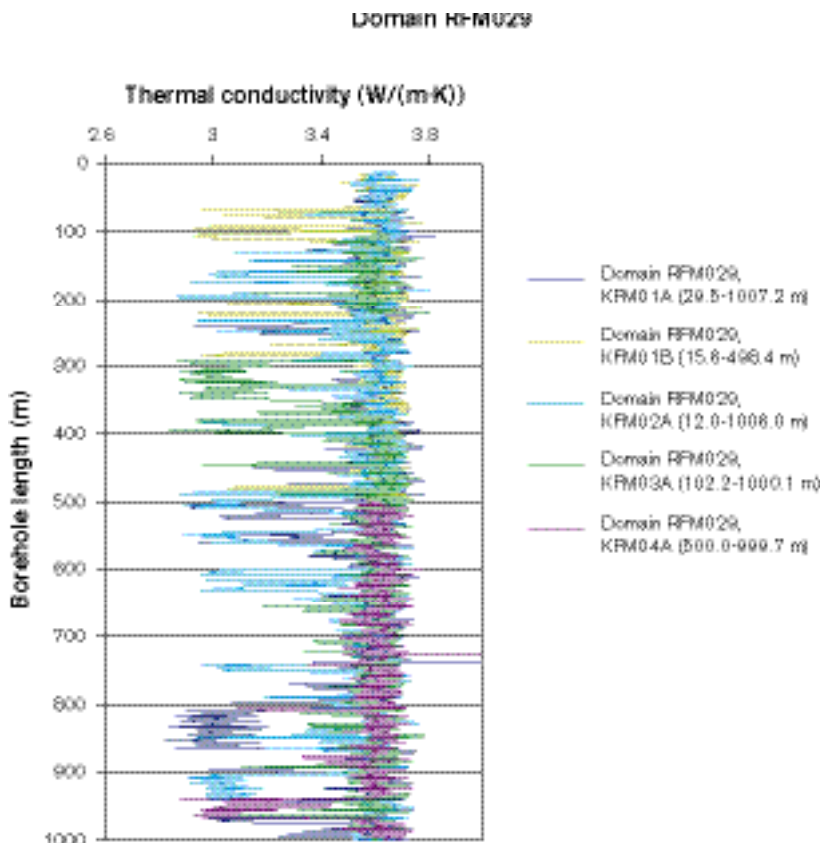


Figure 7-10. Modelling results (approach 1) at the 2 m scale for the domain RFM029 shown separately for each borehole which enters the domain. Thermal conductivity values are calculated as the geometrical mean over 2 m long sections (moving average). The results originate from only one realisation.

Table 7-12. Summary of standard deviations (W/(m·K)) from modelling results on domain level with the main approach (Approach 1) compared to the two alternative/ complementary approaches 2 and 3. Numbers within parenthesis are calculated variances with the resulting standard deviation in bold.

Appr.	Scale (m)	RFM029	RFM012	Comment
1	0.75	0.20 (random from PDF)	0.26 (random from PDF)	Approach 1: possible underestimation of the standard deviation.
	2	0.17 (random from PDF)	0.24 (random from PDF)	
2	0.75	0.27 (0.038+0.037=0.075) (random+variance contr.)	0.32 (0.068+0.037=0.105) (random+variance contr.)	Approach 2 gives an overestimation of the standard deviation.
	2	0.26 (0.030+0.037=0.067) (random+variance contr.)	0.30 (0.056+0.037=0.093) (random+variance contr.)	
3	0.4	0.24 (0.046+0.013=0.059) (between+within rock type)	0.30 (0.080+0.013=0.093) (between+within rock type)	Approach 3 is believed to underestimate the standard deviation for larger scales. The modelling in 0.75 m scale may give a reasonable estimation of the standard deviation for the domain in canister scale. The value is in between approach 1 and 2.
	0.75	0.22 (0.038+0.011=0.049) (between+within rock type)	0.28 (0.068+0.011=0.079) (between+within rock type)	
	2	0.20 (0.030+0.0091=0.039) (between+within rock type)	0.26 (0.056+0.0091=0.065) (between+within rock type)	

It is not possible to fit any simple distribution model (e.g. normal distribution) to the data for the two domains RFM012 and RFM029. Therefore, it is not possible to use the evaluated standard deviations from Table 7-12 to calculate confidence limits. However, it is easy to determine confidence limits for a specified scale based on the data set resulting from modelling approach 1. Approach 1 may result in underestimation of the variability in data, according to the discussion above, and the 0.75 m scale for approach 3 may give a better estimation. In Table 7-13 lower and upper confidence limits are indicated. They are based on modelling results according to approach 1 at the 0.75 m scale but are rounded off to one digit precision to compensate for the increased variability according to approach 3 (rounded off downwards for the lower confidence limit and upwards for the upper confidence limit). This results in the same confidence limits for the two domains.

The distribution in Table 7-13 is bimodal. In further modelling it is possible to use different distributions for different parts of the rock mass.

The effect of anisotropy within the dominant rock type in the two domains could be significant in parts with lineation/foliation, see Section 7.2.6.

A comparison of the results at domain level presented in model version 1.1 /SKB, 2004a/ and model version 1.2 is given in Table 7-14.

Table 7-13. Mean and evaluated standard deviation of thermal conductivity (W/(m·K)) per domain at the possible canister scale. Two-sided 95% confidence intervals are indicated, see discussion in text. The values are valid at 20°C. At higher temperatures the thermal conductivity for the dominant rock type Granite (101057) decreases with about 10%/100°C, see 7.2.1.

Domain	Mean	St. dev.	Indicated two-sided 95% confidence interval	
			Lower confidence limit	Upper confidence limit
RFM029	3.55	0.22	2.9	3.8
RFM012	3.46	0.28	2.9	3.8

Table 7-14. Comparison of modelling results (the mean and the standard deviation) from Forsmark model versions 1.1 and 1.2.

Domain	Mean (W/(m·K))		Diff. (F1.2-F1.1)/F1.1	St. dev. (W/(m·K))	
	Version F1.1	Version F1.2		Version F1.1	Version F1.2
RFM029	3.41	3.55	4.1%	0.21	0.22
RFM012	*	3.46		*	0.28

* Data unavailable.

Heat capacity

Modelling of heat capacity at domain level is performed as a Monte Carlo simulation where the occurrence of different rock types in the domain is weighted together with the rock type models. Results are presented in Table 7-15 and rock type models with an extended methodology are presented in /Sundberg et al. 2005b/.

Table 7-15. Heat capacity MJ/(m³·K) per domain with two-sided 95% confidence intervals under assumption of normal distribution. The data are valid at 20°C. At higher temperatures the heat capacity for rock type 101057 increase with about 25%/100°C, see 7.2.5.

Domain	Mean	St. dev.	Lower confidence limit	Upper confidence limit
RFM029	2.17	0.163	1.85	2.50
RFM012	2.17	0.149	1.86	2.49

Coefficient of thermal expansion

No domain modelling has been performed. For all domains a mean value for the coefficient of thermal expansion is suggested as 7 to 8×10^{-6} m/(m·K), see Section 7.2.7.

In-situ temperature

No domain modelling has been performed. For all domains, mean values of the in-situ temperature at 400, 500 and 600 m depth are estimated at 10.6, 11.7 and 12.8°C, respectively, see Section 7.2.8.

7.3.5 Evaluation of uncertainties

A general description of uncertainties is provided in the strategy report for the thermal site descriptive modelling /Sundberg, 2003/. In the supporting document for the thermal model version 1.2 /Sundberg et al. 2005b/, the uncertainties are further described.

Thermal conductivity

Data level

– TPS data.

The accuracy of TPS measurements is better than 5% and the repetitive consistency is better than 2% according to the manufacturer of the measurement equipment /Sundberg, 2002/. Note that this uncertainty refers to the measurement volume (approx. 10 cm³) and not the volume of the sample, since only a subvolume of the sample is subject to measurement. If the TPS-measurement is supposed to represent the sample scale (approx. 0.1 dm³) the uncertainty is larger and depends on the small-scale heterogeneity of the rock.

There is a potential bias (underestimation) in thermal conductivity data. The reason is that stress dependence has not been assessed. Measurements are made on stress released samples. However, the effect is assumed to be low since the samples are water saturated before measurement.

– SCA data.

The uncertainty associated with SCA data is significantly larger than for TPS data. For SCA data there are two important main sources of uncertainty; (1) determination of the volume fraction of each mineral in the sample and (2) representative values of thermal conductivity of the different minerals.

When comparing TPS and SCA data, there is an uncertainty due to the fact that the modal analysis is not performed for the whole volume of the TPS sample, only a surface of the sample. In addition, the SCA calculation method presumes isotropic conditions. Because of anisotropy at Forsmark the orientation of the sample will effect the modal analysis and the calculated thermal conductivity.

Rock type level

– Representativeness of data.

The representativeness of samples selected for TPS measurements can be questioned since they were not taken with the purpose of statistically representing the rock mass. Similarly, the question of representativeness applies to the calculated values based on modal analyses (SCA method). For both measured and calculated data, non-probabilistic selection of samples has resulted in bias of unknown magnitude. The potential for bias is largest for rock types with few thermal conductivity samples, such as granite, granodiorite and tonalite (101051), pegmatite (101061), and granite (111058).

– Rock type models.

The rock-type models were selected as normal distributions. There is a slight deviation between data and model and one contributing factor can be a lack of representativeness of the samples. Generally, the rock type models slightly overestimate the occurrence of small thermal conductivity values and underestimate the number of large values. Rock type models are required in the domain modelling.

The data set is very small for several rock types, which implies that these rock type models are highly uncertain. This applies to tonalite to granodiorite (101054), granite, granodiorite and tonalite (101051), granodiorite (101056), and diorite, quartz diorite and gabbro (101033).

– Anisotropy.

The anisotropy at rock type level is depending on foliation or lineation. Measurements of samples have suggested anisotropic characteristics, but the interpretation is uncertain and the degree of anisotropy might be overestimated even at the small scale. The samples were taken in the dominant granite in domain RFM029, but quite close to the border to domain RFM012. This may imply that the samples have a higher degree of anisotropy compared with the rock in the central parts of domain RFM029.

There is an uncertainty in the anisotropy measurements since the heat capacity values used have not been measured separately.

– Spatial variability within rock type.

Models of the spatial variability within the rock types occurring in the Forsmark area have not been developed. The spatial variability is only considered in the domain modelling.

Domain level

– Geological model.

Uncertainty in the geological model results from uncertainty in the Boremap logging, alternative interpretations of the spatial occurrence of different rock types, and the extension of lithological domains both at the surface and at depth.

Influences from fractures, deformation zones, and water movements on thermal properties have not been considered. No thermal data are presently available from the deformation zones. This uncertainty may be of minor importance since canisters are not supposed to be situated in or close to deformation zones, so high thermal flow would not be expected to occur in such zones.

– Representativeness of boreholes.

It is not known how representative the boreholes are for the different domains. Since the number of boreholes in each domain is low, it is reasonable to believe that there is a bias present. This bias can only be reduced with additional boreholes, or a more complete understanding of the lithology.

– Spatial variability within the domain.

Spatial variability within the domain is handled in the domain modelling approaches but there are uncertainties as to spatial variability within each rock type.

– Anisotropy.

The anisotropy at a domain level depends on the frequency and orientation of subordinate rock types occurring as dykes of significant extension and with different thermal characteristics. At the present stage, no evaluation of the extent of such anisotropic occurrences has been made.

– Significant scale for the canister.

The significant scale is believed to be 1–10 m. It has not yet been investigated in detail at what scale changes in thermal conductivity are significant for the heat transfer from the canister. This implies a source of uncertainty in the thermal modelling. It can be reduced by numerical simulations of heat flow. Here, the uncertainty is handled by selecting a sufficiently small scale not to underestimate the variability.

– Upscaling methodology.

For all rock types, thermal conductivity values are randomly assigned at the 0.1 m scale based on the rock type models. These rock type models probably overestimate the variance at the 0.1 m scale. The reason is that TPS and SCA data represent a smaller scale. At the 0.1 m scale, some reduction of variance should already have taken place. Therefore, this approach overestimates the likelihood of small values.

In the main modelling approach, spatial variability within rock types is ignored. This results in a too large variance reduction when the scale increases. To compensate for this, the variance due to spatial variability within other rock types is assumed to be equal the spatial variability within the Ävrö granite present in the Simpevarp area (approach 2). This is probably an overestimation of the variance. In modelling approach 3, an addition of variance estimated from TPS data is used to compensate for spatial variability within rock types. This approach is assumed to give the most reasonable estimate of the variability compared with the other approaches.

Uncertainties in the modelling arise from lack of knowledge of spatial variability within the rock types present within the domains. The most straight-forward way of reducing this uncertainty is to collect considerably more data.

– Statistical assumptions.

The confidence intervals calculated for each domain are based on the assumption that domain data at the appropriate scale are normally distributed. This is an uncertain assumption. As long as knowledge of spatial variability is insufficient, it is not possible to check the validity of this assumption. However, data at other scales indicate that assumptions of normality are reasonable.

The rock type models have been considered in terms of normal distributions although the data are somewhat skewed. This results in a too small change of the mean value for the domain when the scale increases. The effect is however insignificant compared with the other uncertainties.

Heat capacity

There exists a problem with the representativeness of measured values (TPS data). The samples are relatively few and focused on certain parts of the rock volume.

When modelling the heat capacity, only the four most commonly occurring rock types have been considered, 16–21% of the domains has not been taken into account. Calculations of the most widely occurring rock types are based on Boremap loggings including rock types with an occurrence length of less than 1 m.

No direct laboratory measurements of heat capacity have been performed. Instead, heat capacity has been determined through conductivity and diffusivity measurements performed with the TPS method.

In-situ temperature

Temperature loggings from different boreholes show a variation in temperature at specified depth. The difference implies an uncertainty in temperature loggings and even small uncertainties may influence the design of the repository. Possible sources of uncertainty are timing of the logging after drilling (drilling adds to temperature disturbance), water movements along the boreholes, calibration error in the temperature logging output or uncertainty in the measured inclination of the boreholes. The uncertainty imposed by water movements may be evaluated jointly with the hydrogeologists. However, this has not yet been done.

Thermal expansion

The representativeness of samples selected for thermal expansion measurements can be questioned. The samples are few and focused on certain parts of the rock volume.

There is a potential bias (underestimation) in thermal expansion data. The reason is that stress dependence has not been assessed. Measurements are made on stress-released samples.

7.4 Feedback to other disciplines

In the thermal modelling, geological and geophysical information have been used. Cooperation with the geologists has been established. Mineralogical data and Boremap data have been used and interpreted during the thermal modelling and comparative calculation of rock type distributions has been performed.

One important question for further modelling is the orientation and extension of subordinate rock types that may influence thermal anisotropic conditions at larger scales. A detailed description of the foliation/lineation in the rock is important for the layout of a repository (anisotropy in thermal properties at smaller scales).

Design is the main receiver of the result from the thermal modelling. It is suggested that the design methodology is developed to take into account the variability in thermal conductivity.

8 Bedrock hydrogeology

Following the methodology described in the SKB strategy report /Rhén et al. 2003/ the bedrock hydrogeological model is divided into hydraulic rock domains (HRD) and hydraulic conductor domains (HCD). At Forsmark, the geometries of the HRDs and HCDs coincide with the geological rock domains and the deterministically modelled deformation zones, respectively. The HRDs consist of two components, a statistical description of flowing fractures, i.e. the flowing discrete fracture network model (hydrogeological DFN), and the less permeable rock matrix between the flowing fractures not readily accessed by flow but through diffusion mainly. The characterisation of the HRDs' two components by means of borehole measurements is a major task for the site investigations.

Primary objectives of the bedrock hydrogeological model are to provide a general conceptual understanding and to determine and justify the assignment of hydraulic properties, boundary and initial conditions based on primary data useful for Repository Engineering, Safety Assessment and Environmental Impact Assessment studies. The importance of identified uncertainties in the hydrogeological description is addressed by numerical simulations, the results of which are used to underpin the development of the bedrock hydrogeological model and to suggest necessary supplements in the investigations.

The level of detail at which the HCDs and the HRDs are represented in a numerical simulation model depends largely on the information at hand (data freeze version), the size of the model domain and the chosen grid resolution. The treatment of the bedrock hydrogeological model follows that of the geological model, which effectively means that the modelling is done on a regional scale, although the body of the data used for the hydraulic parameterisation come from the site investigations within the candidate area. A regional-scale model implies a constraint on the grid resolution and hence the possible level of detail in the representation of hydraulic heterogeneity and anisotropy. For large parts of the model domain, the grid resolution is of the order of 100 m in the work presented here.

Two modelling teams carried out numerical simulations, /Hartley et al. 2005/ and /Follin et al. 2005/. The numerical simulations treat the effects of the regional shoreline displacement process during Holocene between 8,000 BC and 2,000 AD, which means that the density turnover associated with the Littorina Sea period (cf. Table 3-4 and Figure 3-13) is taken into account. Besides studying the impact of variable density groundwater flow, the palaeo-hydrogeological simulations lend themselves to integration with hydrogeochemistry. Since the two disciplines deal with the same geological and hydrodynamic properties, they should be able to complement each other in describing/modelling the bedrock groundwater system.

One or more components of the bedrock hydrogeological model provide a foundation for the integration with and modelling work in rock mechanics, bedrock hydrogeochemistry and bedrock transport properties. Being strongly coupled to the geological model, all components of the bedrock hydrogeological model have a direct impact on the location and design of the shafts and tunnels for the deep repository. They also provide a significant input for the safety analysis work in terms of hydraulic properties relevant for preliminary simulations of radionuclide transport.

8.1 State of knowledge at previous model version

The hydrogeological description of the regional model domain presented in Forsmark model version 1.1 was based on a tentative structural model. The transmissivities of the deterministically modelled deformation zones were based on sparse hydraulic data from the bedrock characterisation of the SFR facility (located outside the candidate area). Furthermore, the rock mass transmissivities between the deformation zones (HRD) were based on hydraulic measurements conducted in a single borehole (KFM01A) inside the candidate area. The conductivity model derived was strongly influenced by the depth trend encountered.

Despite the sparse information, numerical simulations were performed. In addition to an uncertain structural model, the numerical simulations also treated a mathematical-geological model of the shoreline displacement during Holocene, which included a preliminary description of the variable salinity/density of the different lacustrine and marine stages prior to present-day brackish conditions of the Baltic Sea.

The main uncertainties of the bedrock hydrogeological model version 1.1 were related to the following issues.

- The interpretation of lineaments as deformation zones. This was associated with an uncertainty concerning the preliminary structural model. The uncertainty was pronounced by the assignment of uncertain geometrical properties (shape, thickness, dip and penetration depth). Another example of a structural uncertainty affecting the hydrogeology was in the interpretation of the rock fracturing between the deformation zones, i.e. rock fracture orientation, size distribution, intensity variations and spatial model (geological DFN model).
- Lack of hydraulic measurements in boreholes to support interpretations on anisotropy and spatial distribution for the assignment of hydraulic properties to the deterministically modelled deformation zones. In particular, there was an uncertainty in the transmissivity distribution of the deformation zones and the potential relation between deformation zone properties, rock stresses and the transmissivity assignment.
- Lack of hydraulic measurements in boreholes to support interpretations on anisotropy and spatial distribution for the assignment of hydraulic properties to the geological DFN, the result of which is a hydrogeological DFN. The modelled spatial variability and anisotropy in the “rock mass” hydraulic conductivity as used in the numerical simulations was obtained indirectly from the intensity variation with depth of the geological DFN model.
- Lack of hydrogeochemical and hydrological measurements in boreholes for the assignment of initial and boundary conditions required by the numerical simulations used to underpin the development of the conceptual model. In particular, the unknown salinity distribution at depth gave rise to an uncertainty in the palaeo-hydrogeological interpretation of the simulations performed.

The above uncertainties were not quantified in version 1.1, since they originated from the general character of the interpretations (i.e., were qualitative) and suffered from lack of data or bias in the data available. Some of the settings/assumptions used were tentatively tested by means of exploration simulations, although there was no obvious answer to compare the solutions with, e.g., in respect of palaeo-hydrogeological characteristics of the site. More hydraulic data, especially hydrogeochemical measurements, cross-hole tests and additional support for the structural model to be obtained in later data freezes, were stated to be needed to allow for a more meaningful quantification of the uncertainties.

Identified hypotheses for alternative models of the bedrock hydrogeological model version 1.1 encompassed:

- Alternatives in the structural model, in particular, extent of gently dipping deformation zones and depth decrease of rock fracture intensity.
- Alternative values of the factor a and the exponent b in the power-law correlation between fracture transmissivity T and fracture size used in the numerical simulations, i.e. $T = a x_r^b$, or, indeed, no correlation whatsoever.
- A correlation between fracture transmissivity, fracture orientation, fracture position and the stress field.

Due to lack of data, none of these hypotheses were explored further in Forsmark model version 1.1, but various possibilities existed to explore these alternative hypotheses using new data to be obtained in coming data freezes. In particular, it was stated that the assignment of rock mass transmissivities based on hydraulic measurements is a critical conceptual issue to be explored further in forthcoming site descriptions beginning with Forsmark version 1.2.

8.2 Evaluation of primary data

8.2.1 Hydraulic evaluation of single-hole tests

Methods for single-hole testing

A number of hydraulic test methods are used in a more or less standardised fashion for the hydraulic characterisation of the bedrock penetrated by the boreholes drilled during the site investigations. The hydraulic characterisation of the uppermost part of the bedrock down to c. 200 m depth is conducted mainly by single-hole hydraulic tests in 140 mm diameter percussion drilled boreholes (HFMxx). The hydraulic characterisation of the interval 100–1,000 m depth is conducted by single-hole hydraulic tests in 76 mm diameter cored drilled boreholes (KFMxxx). Table 8-1 presents an overview of the single-hole test methods used.

Deep core-drilled boreholes are characterised by two kinds of single-hole test methods, difference flow logging during pumping (PFL) and double-packer injection (PSS). The main reason for using two test methods is that the pros and cons differ. Cross plots of the data from the two methods allow for consistency checks, which improve the detailed characterisation and strengthen the general uncertainty assessment of the conceptual model. Table 2-4 presents a summary of the primary data deduced from the hydraulic characterisation. This information constitutes the hydraulic basis for the hydrogeological modelling and numerical simulations.

Table 8-1. Hydraulic test methods used during the initial site investigations for the hydraulic characterisation of percussion and core drilled boreholes.

Test method and type of borehole	Acronym of method	Acronym of variant	Type of test performed	Comments
Pipe string system Core-drilled boreholes	PSS		Injection tests performed as constant pressure tests (100 m, 20 m, 5 m)	Transient data collected; evaluation of test section T is based on transient or stationary conditions
Hydraulic test system Percussion-drilled boreholes	HTHB		Pumping tests performed as constant rate tests, generally combined with impeller flow logging and, if needed, injection tests above the submersible pump	Transient data collected, evaluation of test section T is based on transient or stationary conditions
Wire line probe Core-drilled boreholes	WLP	WLP-Q	Pumping tests and early water samples	Transient data collected, evaluation of test section T is based on transient or stationary conditions
		WLP-p	Pressure build-up measurements	Transient data collected, evaluation of initial test section pressure
Posiva flow log Core-drilled boreholes	PFL	PFL-s	Flow logging in sequential test sections	Pseudo-steady state data collected; evaluation of test section T and initial pressure is based on the difference of two logging sequences.
		PFL-f	Fracture flow logging in overlapping test sections	Also measured: Electrical conductivity (EC) and temperature of the bore-hole fluid as well as single point resistance (SP) Pseudo-steady state data collected, used in combination with PFL-s to estimate fracture T. Also measured: Fracture fluid EC

Models for single-hole test interpretation

The interpretation of hydraulic tests requires a conceptual model of the flow medium in order to transform the measured constitutive parameters (pressure, flow rate and time) into hydraulic parameters useful for other applications, e.g. numerical simulations. The interpretation depends also on the hydraulic test method used for the measurements.

The interpretation of hydraulic test data available for version 1.2 is based on established (traditional) models for well test interpretation in porous and/or fractured media used in hydrogeology and/or reservoir (petroleum) engineering. The P-reports describing the performance of the hydraulic testing, the data management and the interpretation models used are listed in Table 2-4.

The working hypothesis used in version 1.2 is that the key hydraulic entity deduced from the use of traditional interpretation models, the radial transmissivity, is relevant for forward modelling of the heterogeneity and anisotropy of undisturbed groundwater flow and salt transport in fractured rocks on a regional scale. The assumption implies that the interpretations of the hydraulic tests (and the numerical simulations used to underpin the interpretations) must take the detailed geometric description of the borehole structures into account. The joint hydrogeology and geology single-hole interpretation follows the division of the bedrock into HCDs and HRDs.

Overview of single-hole tests

Data from five core-drilled boreholes and 19 percussion-drilled boreholes are available for hydrogeological evaluation in version 1.2. The locations of the boreholes are shown in Figure 8-1. Table 8-2 shows in which boreholes a particular type of hydraulic test was conducted.

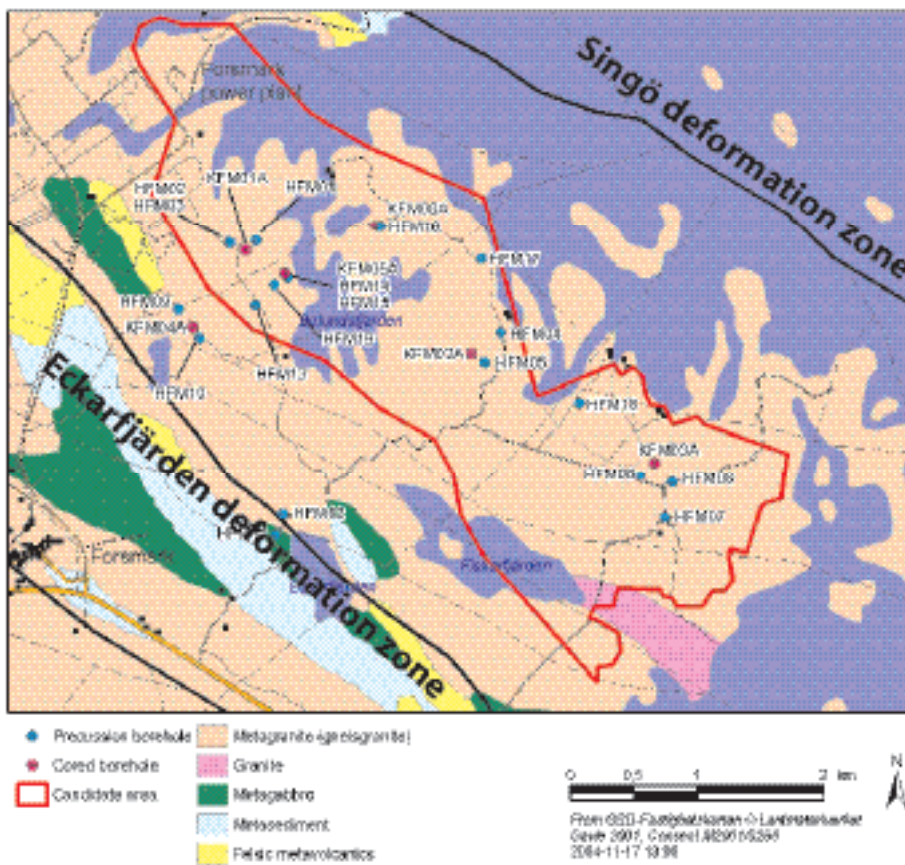


Figure 8-1. Schematic geological map of the Forsmark area showing the candidate area and the location of the five core-drilled boreholes (KFMxxx) and the 19 percussion-drilled boreholes (HFMxx) from which data are available in version 1.2.

Table 8-2. Overview of single-hole hydraulic tests conducted in the core-drilled and the percussion-drilled boreholes available in model version 1.2.

Test method and type of borehole	Acronym of method	Acronym of variant	Type of test performed	Borehole
Pipe string System Core drilled boreholes	PSS		Injection tests performed as constant pressure tests (100 m, 20 m, 5 m)	KFM01A–KFM03A
Hydraulic test system Percussion drilled boreholes	HTHB		Pumping tests performed as constant rate tests, generally combined with impeller flow logging and, if needed, injection tests above the submersible pump	HFM01–HFM06 HFM08–HFM13 HFM015–HFM019
Wire line probe Core drilled boreholes	WLP	WLP-Q	Pumping tests and early water samples	KFM02A–KFM05A KFM01B
		WLP-p	Pressure build-up measurements	KFM03A–KFM05A
Posiva flow log Core drilled boreholes	PFL	PFL-s	Flow logging in sequential test sections	KFM01A–KFM04A
		PFL-f	Fracture flow logging in overlapping test sections	KFM01A–KFM05A

The single-hole hydraulic tests conducted in KFM01B discussed in Chapter 6 are not listed in Table 8-2. This is because these tests concern stress measurements by means of hydraulic fracturing and do not represent undisturbed permeability conditions. Furthermore, a large number of the planned WLP (Wire line probe) tests were not conducted or unsuccessful due to problems with the down-hole device and/or the low permeability rock, see Table 8-3.

Table 8-3. Overview of the WLP (Wire line probe) testing in Forsmark. A large number of the planned WLP tests were never put into practice due to mechanical problems with the down-hole device. Also, some attempts were unsuccessful due to low permeability rock.

Borehole	Pressure build-up		Transmissivity		Water samples		Reference
	Attempts	Successes	Attempts	Successes	Attempts	Successes	
KFM01A	0	0	0	0	0	0	/Claesson and Nilsson, 2004a/
KFM01B	0	0	1	1	1	1	/Claesson and Nilsson, 2004b/
KFM02A	0	0	3	2	1	1	/Claesson and Nilsson, 2004d/
KFM03A	5	5	3	2	1	1	/Claesson and Nilsson, 2004f/
KFM04A	6	5	3	1	3	0	/Claesson and Nilsson, 2004l/
KFM05A	3	3	3	0	1	1	/Claesson and Nilsson, 2004m/

Brief description of the PFL testing and interpretation

The flow logging with the Posiva Flow Log in sequential sections (section logging, PFL-s) was made with a test section length of 5 m and a step length of 0.5 m (5/0.5), with the purpose of measuring transmissivity in 5 m sections and to indicate flowing sections with a resolution of 0.5 m, useful for planning the hydrogeochemistry sampling and the flow-anomaly logging. The flow-anomaly logging (PFL-f) was made with a test section length of 1 m and a step length of 0.1 m (1/0.1) when moving the test section along the borehole, with the purpose of identifying individual flowing fractures. The flow logging (1/0.1) was performed where the (5/0.5) logging identified flow anomalies. Estimates of transmissivity from PFL-s are based on two established heads (or drawdowns) (h_1 , h_2). The head h_1 is established without pumping (h_1 = undisturbed water level in borehole) and h_2 with pumping (h_2 generally = $h_1 - 10$ m) in the borehole associated with two corresponding flow rates (Q_{n1} , Q_{n2}) from the test section. If the upper measurement limit of the flow rate is reached in a test, the test in that test section is later repeated with a smaller drawdown.

The flow logging in overlapping sections (flow-anomaly logging, PFL-f), is only performed with one head (h_2) and the fracture flow (Q_{f2}) is measured, therefore the h_1 and flow Q_{f1} must be approximated as follows: The same h_1 as for the corresponding section with (5/0.5) measurement, that straddles the flow anomaly, is used as well as setting $Q_{f1} = Q_{n1}$. If Q_{n1} could not be estimated for the section it was assumed that $Q_{f1} = 0$.

Thiem's equation /Thiem, 1906/ was used to calculate the transmissivity (denoted by T_s for a 5 m section and by T_f for a distinct inflow, i.e. localised within a dm or so) and the undisturbed hydraulic head in the formation outside the test section (denoted by h_s for PFL-s and by h_f for PFL-f). If $Q_{f1} = 0$ the fracture transmissivity T_f is estimated only.

It was assumed that the influence radius divided by the borehole radius can be approximated to 500. It was thus assumed that undisturbed formation pressure exists at a radial distance of c. 19 m. Since a steady state solution was used the evaluated transmissivity may be affected by a skin factor, particularly if the skin is positive.

Brief description of the PSS testing and interpretation

Injection tests with the Pipe String System were made in a telescopic fashion starting with 100 m test sections followed by 20 m sections within all 100 m sections with flow rates above the lower measurement limit, and, finally, in 5 m sections within all 20 m sections with flow rates above the lower measurement limit. The 20 and 5 m sections not measured were assigned the value of the lower measurement limit of the specific capacity Q/s for the 100 m and 20 m sections, respectively. These Q/s values were then applied in the steady state solution by /Moye, 1967/ to estimate a measurement limit as a transmissivity value.

Tests above the lower measurement limit were evaluated as transient tests giving a transmissivity T_T and skin factor ζ (assuming a storage coefficient $S = 1 \times 10^{-6}$). Different transient test interpretation models were used depending on the response of the transient flow regime, and "the most representative value" of the transient transmissivity interpretations was denoted by T_R . Steady state evaluations of transmissivity T_M based on /Moye, 1967/ were also made. If it was not possible to evaluate a transient T_R , the T_M value was used as "the most representative" for the test section in question.

Strategy of single-hole testing of deep core-drilled boreholes

All deep core-drilled boreholes are tested with both PFL and PSS, but the testing is done at different times. Thus, the differences in usage shown in Table 8-2 are simply due to the fixed date of the data freeze of version 1.2, which happened to make the PSS testing conducted in KFM04A and KFM05A belong to the next data freeze.

The PFL tests are run immediately after the completion of the drilling, whereas the PSS tests are run after the 1–2 month long hydrogeochemical characterisation that follows after the PFL tests. There are several reasons for this strategy.

- The PFL tests allow for an accurate measurement of the initial pressure, EC and temperature profiles along the borehole after the drilling is completed. This information is important for the drilling impact assessment and the characterisation of how the borehole short-circuits different fractures, hydraulically and chemically.
- Pumping of the entire borehole is used for all PFL tests, whereas water of a different chemical composition is injected between the PSS packers. This means that the chances for hydrogeochemical disturbance are probably less for the PFL method.
- The PFL tests are run after several days of pumping, whereas the PSS tests are run for c. 20 minutes of injection. This allows for several kinds of cross plots and a comparison between steady state and transient interpretation methods, which improves the detailed characterisation of the borehole and strengthens the general uncertainty assessment of the hydrogeological model regarding far-field/near-field fracture connectivity.

- The shortest overlap of the PFL-f tests allows a test section resolution of 0.1 m, whereas the test section resolution of the PFL-s and the PSS tests is set to 5 m. Thus, the PFL-f tests allow for a detailed discussion of the most interesting positions for the hydrogeochemical test equipment. The high spatial resolution of discrete fracture transmissivities is also of great importance for the development of the hydrogeological DFN model.
- The PSS tests have a better transmissivity cut-off (lower value of the lower measurement limit) than the PFL tests and is less sensitive to borehole disturbances such as a rough borehole perimeter, gas bubbles, drilling debris, clay particles, high flow rates along the borehole, etc. On the other hand, it does not have such a high spatial resolution, which means that the overall test section fracture transmissivity is measured in contrast to the PFL-f tests.
- The PSS tests allow for other interpretation models than the PFL tests. The interpretation of the PSS tests available for version 1.2 is based on established (traditional) models for well test interpretation in porous and/or fractured media used in hydrogeology and/or reservoir (petroleum) engineering. Other kinds of interpretation models, e.g. generalised radial flow (fractional flow) models, may prove useful for the forthcoming development of the hydrogeological DFN model.

The P-reports provide exhaustive information on the pros and cons of the two test methods and the different interpretation models. The performance of the testing in each core-drilled borehole is described in detail and the possible sources for the problems encountered in the subsequent interpretations are analysed. A demonstration of the different kinds of cross-plots used for checking the consistency between the different tests and interpretation methods is given below. The demonstration is made for the most complicated core-drilled borehole in Forsmark so far, KFM03A.

Consistency between PFL test section transmissivities vs. PFL fracture transmissivities

Fracture transmissivities are summed up to make them comparable with measurements using a 5 m long test section. The agreement between the two data sets is considered excellent in KFM01A, KFM02A, KFM04A and KFM05A /Rouhiainen et al. 2004; Rouhiainen and Pöllänen, 2004a,b; Pöllänen et al. 2004/. The results of the PFL tests conducted in KFM03A /Pöllänen and Sokolnicki, 2004/ are shown in Figure 8-2. Given the extremely difficult test conditions for difference flow logging in this particular borehole the agreement between the two data sets is considered very good. It is noted that at a few (6) positions, low transmissive single inflows (below the practical measurement limit) are reported from the PFL-f tests that are not seen in the PFL-s tests. Apart from these six single-fracture inflow observations, all matches close to or above the practical measurement limit are considered excellent.

The difficult test conditions in KFM03A are due to one high transmissivity deformation zone at c. 60 m borehole length (ZFMNE00A5) and another one at c. 389 m borehole length (ZFMNE00A4). High transmissivity deformation zones effectively prohibit a sufficiently large Δp (pressure drawdown) in the borehole below the deformation zones. A large Δp is required because the practical measurement limit is proportional to $1/\Delta p$. The problems associated with the high transmissivity deformation zone at c. 60 m borehole length are due to the fact that no casing was installed in the percussion drilled uppermost part of KFM03A /Källgård et al. 2004/.

An example of the difference between the theoretical (nominal) and the practical (empirical) lower measurement limit is shown in Figure 8-2. The differences are due to the aforementioned sensitivity of the PFL method to various disturbances in the in-situ conditions. The experience gained so far of using the difference flow logging method at Forsmark suggests that the mean value of the practical lower measurement limit of the PFL method is of the order of $(1 \text{ to } 2) \times 10^{-9} \text{ m}^2/\text{s}$ (cf. Figure 8-2). It is noted that observations below the practical measurement limit are not uncommon. Moreover, the PFL method has a practical upper measurement limit and the high-transmissive deformation zone at c. 388 m borehole length exceeded this value, see Figure 8-2.

Borehole KFM03A

Comparison of transmissivity of borehole sections (5m) and fracture transmissivities

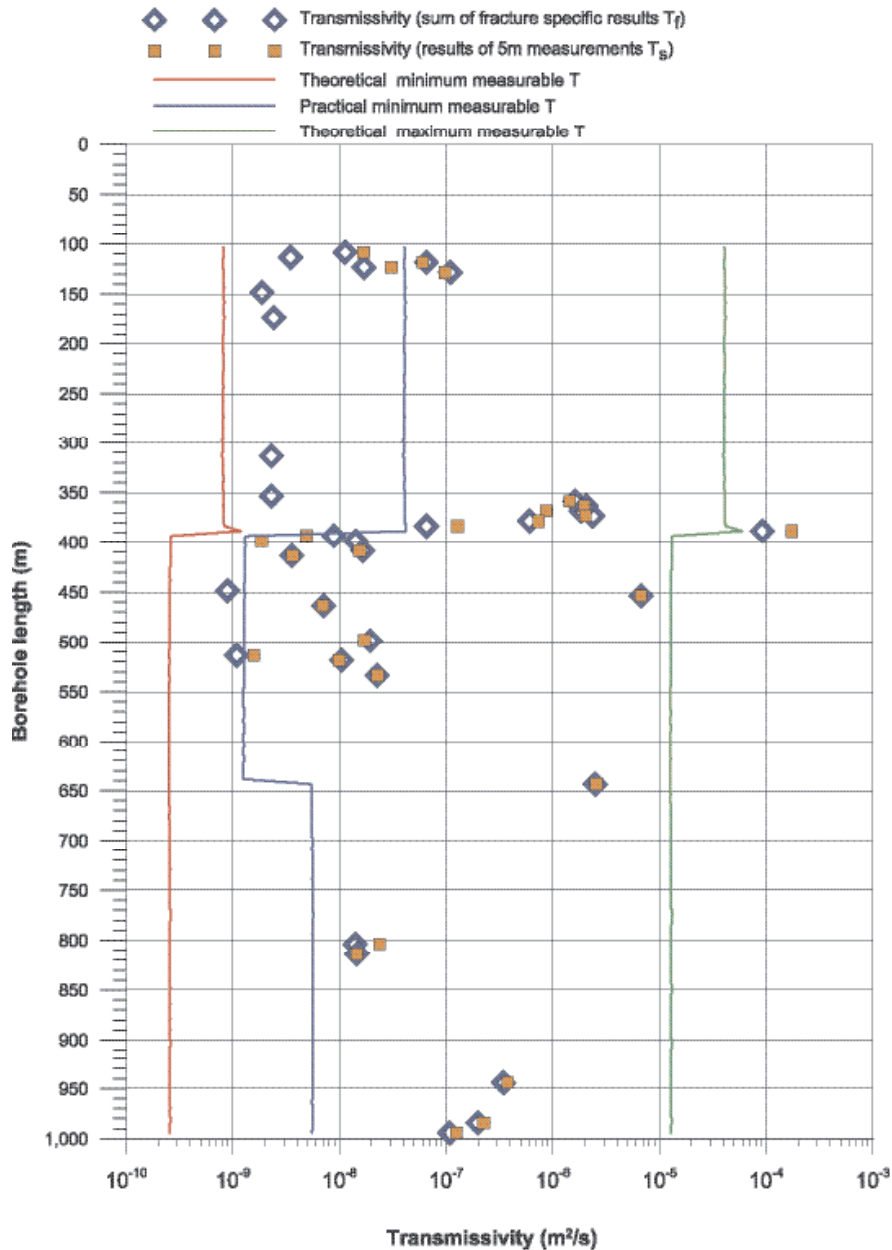


Figure 8-2. Comparison between transmissivities of 5 m test sections (determined by PFL-s tests) and the sum of individual fracture transmissivities in the corresponding intervals (determined by PFL-f tests) in KFM03A. It is noted that at a few positions (6) low transmissive single inflows (below the practical measurement limit) are reported from the PFL-f tests that are not seen in the PFL-s tests. Apart from these six single-fracture inflow observations, all matches close to or above the practical measurement limit are considered excellent. Modified after /Pöllänen and Sokolnicki, 2004/.

Consistency between PSS steady-state transmissivities vs. PSS transient transmissivities

Transmissivities in 5 m test sections calculated from transient evaluations T_T and steady-state evaluations T_M of PSS data are compared. The comparison for KFM03A is shown in Figure 8-3. The agreement between the two data sets is considered good. The lower measurement limit of the T_M transmissivity in 5 m test sections is indicated in the plot. The value $6.7 \times 10^{-10} \text{ m}^2/\text{s}$ is c. two to three times lower than the aforementioned typical practical lower measurement limit of the PFL tests, $(1 \text{ to } 2) \times 10^{-9} \text{ m}^2/\text{s}$.

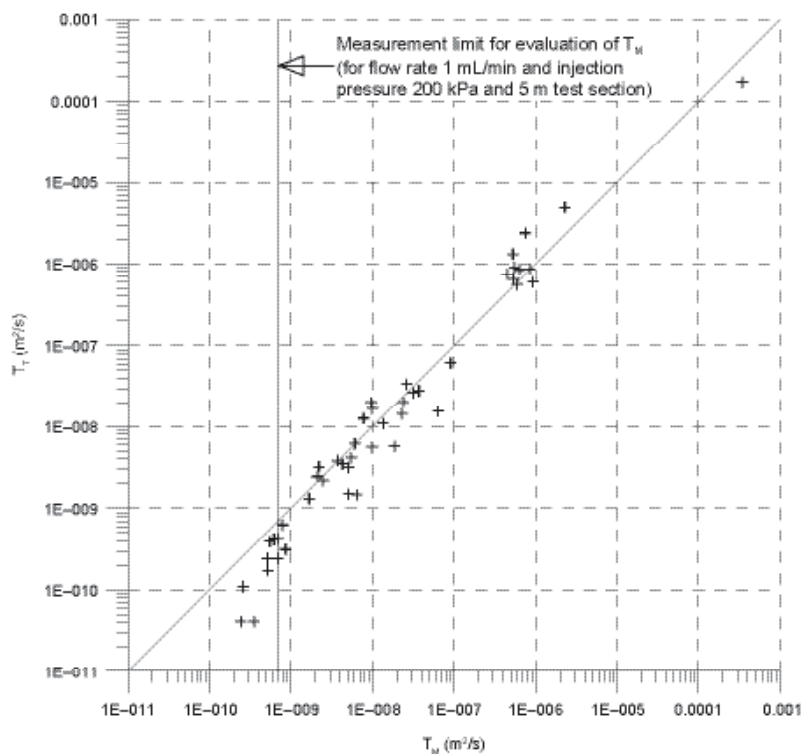


Figure 8-3. Transient (T_T) versus steady-state (T_M) test section transmissivities. The data sets refer to the 5 m long injection tests in KFM03A /Källgården et al. 2004/.

Consistency between PSS 20 m and 100 m transmissivities vs. PSS 5 m transmissivities

The most representative transient transmissivity values of 20 m and 100 m long test sections ($T_R(20\text{ m})$ and $T_R(100\text{ m})$) are compared with the sum of the transient transmissivity values of 5 m long test sections in the corresponding intervals ($SUM\ T_R(5\text{ m})$). The comparison is shown in Figure 8-4. The agreement between the data sets is considered good. The deviation towards the lower limit is caused by the fact that values at the measurement limit are accumulated in the summation process, which most likely results in overestimated values of $SUM\ T_R(5\text{ m})$. The lower measurement limit values of T_M for the different section lengths together with the cumulative measurement limit for the sum of the 5 m test sections are also shown in the plot.

Consistency between PSS transmissivities vs. PFL transmissivities

Calculated steady-state (T_M) and transient (T_R) transmissivity values from the injection tests in 5 m test sections are compared with the calculated transmissivity values (T_D) in the corresponding 5 m test sections from the previously performed sequential difference flow logging in KFM03A /Pöllänen and Sokolnicki, 2004/. The comparison is shown in Figure 8-5. The different values of the lower measurement limit of the difference flow logging refer to the varying practical lower measurement limit commented above. In the summation of the transmissivities over the 5 m test sections, estimated values at the lower practical measurement limit are included.

Figure 8-5 indicates a good agreement between the estimated transmissivity values from the injection tests and the difference flow logging. It should, however, be noted that the two methods differ regarding assumptions and associated uncertainties. For instance, the difference flow logging was performed after several days of pumping for two different drawdowns in the borehole, c. 7 m and 2.3 m with pumping rates of c. 108 L/min and 29 L/min, respectively, whereas the injection tests were conducted over 20 minutes using an excess injection pressure of c. 200 kPa. Potential uncertainties in difference flow logging results are discussed in /Ludvigson et al. 2001/ and in injection tests in /Andersson et al. 1993/.

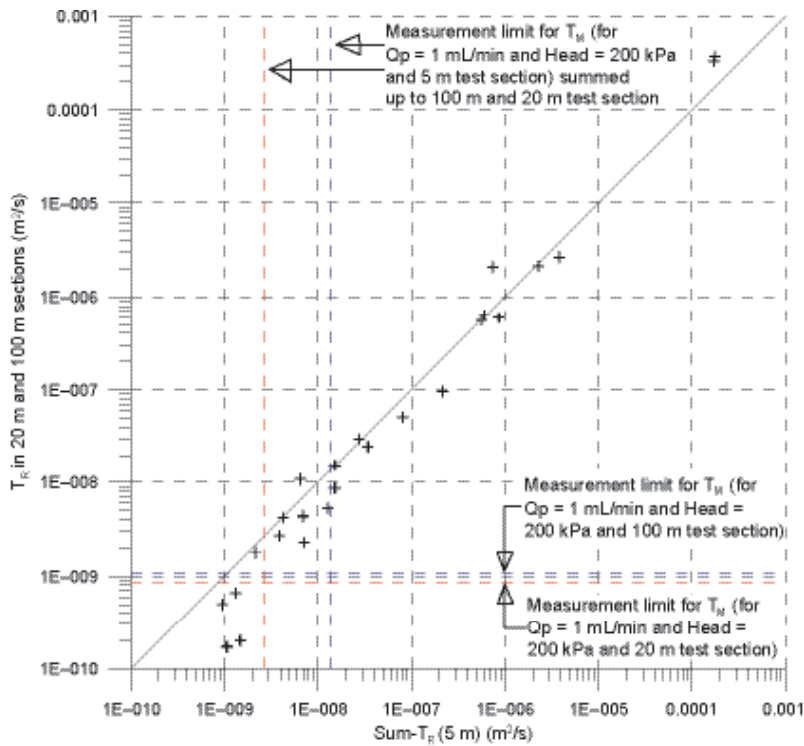


Figure 8-4. Plot of transmissivity values for 100 m and 20 m test sections ($T_R(20\text{ m})$ and $T_R(100\text{ m})$) versus the sum of transmissivity values in 5 m sections in the corresponding borehole intervals ($SUM\ T_R(5\text{ m})$) from the injection tests in KFM03A /Källgården et al. 2004/.

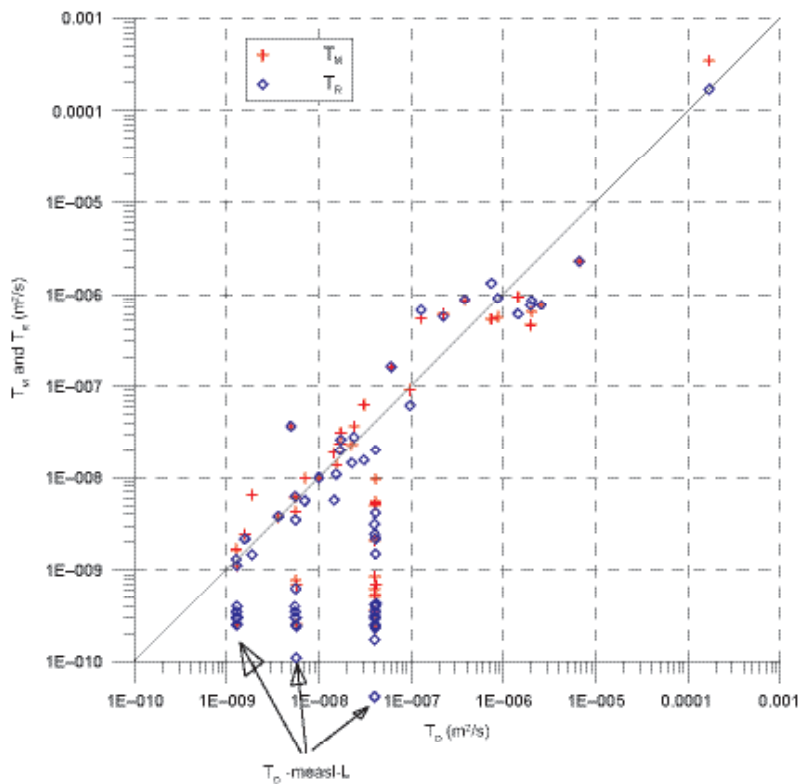


Figure 8-5. Comparison of estimated steady-state (T_M) and transient (T_R) transmissivity values from the injection tests in 5 m test sections with estimated transmissivity values in the corresponding 5 m sections from the previous difference flow logging (T_D) in KFM03A /Källgården et al. 2004/.

Three values for the lower limit for transmissivity were estimated for the difference flow logging in KFM03A, approximately at $4.1 \times 10^{-8} \text{ m}^2/\text{s}$, $5.6 \times 10^{-9} \text{ m}^2/\text{s}$ and $1.3 \times 10^{-9} \text{ m}^2/\text{s}$. These limits are significantly higher than the corresponding measurement limits for the injection tests in KFM03A. This is clearly seen in Figure 8-5 as a difference between T_D , T_M , and T_R , respectively, particularly for low transmissivity values. Discrepancies between injection tests and difference flow logging may also result from small differences in the positions of the test sections in the borehole.

Figure 8-6 shows a comparison between estimated steady-state (T_M) transmissivity values from the injection tests in 100 m and 20 m test sections with the sum of the 5 m test section transmissivity values ($\text{SUM } T_D(5 \text{ m})$) from the difference flow logging in the corresponding intervals in borehole KFM03A. Figure 8-6 shows that the estimated steady-state transmissivity values from the injection tests in 100 m and 20 m test sections are distributed over a much wider range than the sum of the 5 m test section transmissivity values from the difference flow logging. This is partly a result of the lower measurement limit being included in the sum for the difference flow logging. These results are consistent with the results shown in Figure 8-5.

Strategy of single-hole testing of percussion-drilled boreholes

Percussion-drilled boreholes in the proximity of core-drilled boreholes generally have the objective of serving as flush-water wells to the subsequent core drillings. Distant percussion-drilled boreholes often have the objective of checking a structural interpretation, e.g. the interpretation of lineaments as deformation zones. Among the 19 percussion-drilled boreholes available for model version 1.2, 14 are drilled in the proximity of core-drilled boreholes and five at some distance away (HFM07, HFM13, HFM17–19), see Figure 8-1.

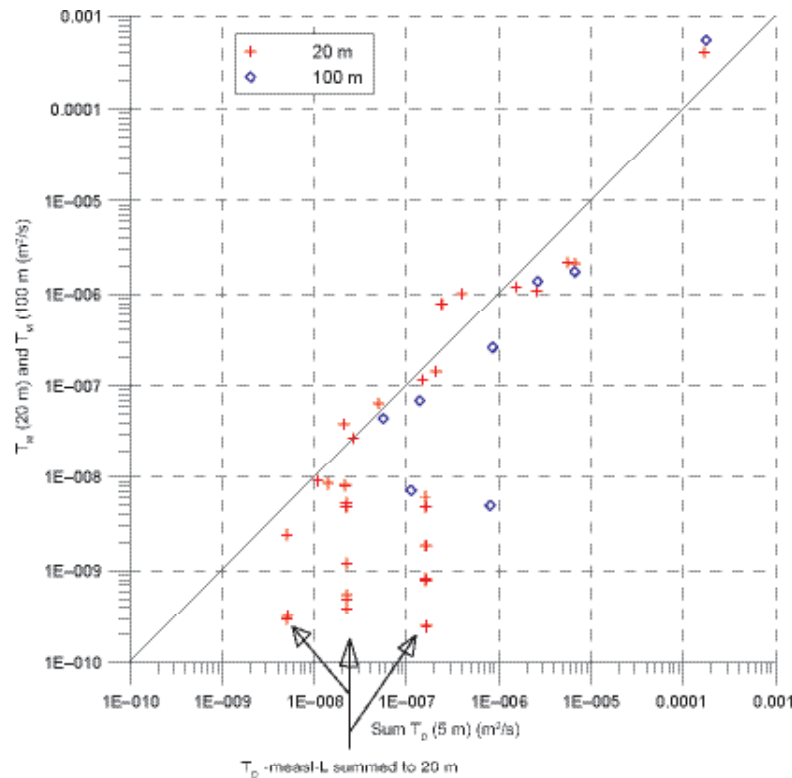


Figure 8-6. Comparison of estimated steady-state (T_M) transmissivity values from injection tests in 20 m and 100 m long test sections with summed transmissivity values in 5 m long test sections ($\text{SUM } T_D(5 \text{ m})$) in the corresponding borehole intervals from difference flow logging in KFM03A /Källgården et al. 2004/.

Another important objective of the regular percussion-drilled boreholes is to study the extent (magnitude, thickness and spatial variability) of the increased near-surface hydraulic conductivity. This information is needed for several reasons, one of which is the hydrogeological description of the interface between the Quaternary deposits (cf. Chapter 4) and the bedrock. It is noted that the uppermost 100 m of the deep core-drilled boreholes are always percussion drilled. This is because the flushing system of the core-drilling equipment needs a larger diameter. However, a casing is generally installed in the percussion-drilled hole. This is to stabilise the borehole and protect the deeper parts from dirt.

All percussion-drilled boreholes are tested with the HTHB method provided that they yield water. The HTHB tests are run immediately after the completion of the drilling and performed as constant rate pumping tests, generally combined with impeller flow logging and water sampling for hydrogeochemical analyses. Inflows from fractures above the submersible pump are tested by means of injection tests between packers. The impeller flow logging and the injection tests are used to delineate the individual contributions to the total borehole transmissivity from intersected fractures and deformation zones. The experience gained so far of using the impeller logging together with the HTHB method in Forsmark suggests that the mean value of the practical lower measurement limit of the impeller logging is of the order of $5 \times 10^{-6} \text{ m}^2/\text{s}$.

Overview of results from PFL single-hole tests

Figure 8-7 illustrates a fracture coupled to a flow anomaly. Figure 8-8 through Figure 8-12 show the results from the PFL-f tests together with fracture data from the core mapping and the interpreted rock domains and deformation zones. The classification of “flow indication open fractures” is defined as the distance between the anomaly and the interpreted fracture. For instance, if the anomaly has a flow indication in class 1, the interpreted fracture is within 1 dm from the anomaly. In the same way, the anomaly has the flow indication class 2, if the interpreted fracture is within 2 dm from the anomaly. Four classes have been defined: Class 1: 0–1 dm; Class 2: 1–2 dm; Class 3: 2–3 dm; and Class 4: 3–4 dm.

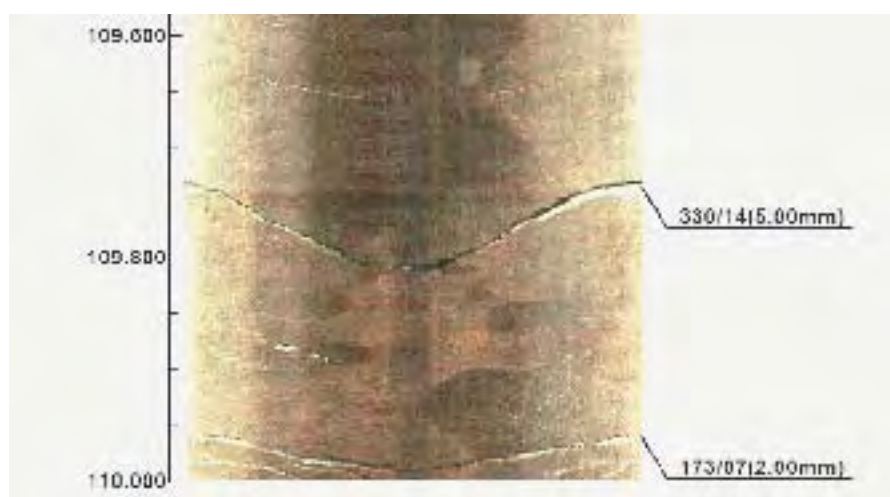


Figure 8-7. Close-up of a BIPS image showing a borehole section in borehole KFM05A. The open fracture in the centre is associated with a flow anomaly.

In the core mapping, each fracture is classified as Sealed, Open or Partly Open and with a judgement of how certain the geologist is of this classification – expressed as Certain, Probable and Possible. Partly Open fractures refers to all fractures that do not cut the core entirely but have (1) altered or weathered fracture planes or are (2) associated with a measurable aperture in the borehole wall using BIPS to indicate an edge of a fracture. The number of Partly Open fractures is small but not negligible. Moreover, a Partly Open fracture may not necessarily intersect the centre line of the core.

The existence of a PFL flow anomaly is classified as Certain or Uncertain. Both the core mapped data and the PFL anomalies are rigorously length corrected and it is expected that the positions of objects along the boreholes normally can be correlated to within 0.2–0.3 m.

/Forsman et al. 2004/ made a joint interpretation between the PFL-f tests and the fracture data from the core mapping. As a first assumption, all Open and Partly Open fractures as well as Crush Zones were assumed to be possible flowing features. In most cases, one or several Open fractures were identified within 0.2 m from a given flow anomaly. Only in a few cases could no Open fractures, Partly Open fractures or Crush Zones be linked to within 0.5 m of a flow anomaly, probably indicating that a fracture mapped as Sealed should have been classified as Open. In such cases one could generally find Sealed fractures classified as Probable or Possible and mapped as broken near the flow anomaly.

Table 8-4 provides a compilation of the classification results provided by /Forsman et al. 2004/. The uncertainties in the classification give rise to requirements for sensitivity analyses. This is to be focus of future work.

The data shown in Figure 8-8 through Figure 8-12 have been a major input data to the hydrogeological DFN modelling conducted by the modelling teams, see Section 8.4.3.

Table 8-4. Compilation of the results obtained from a joint interpretation between PFL-f tests and Boremap data /Forsman et al. 2004/.

Object	KFM01A	KFM02A	KFM03A	KFM04A	KFM05A
Total No of PFL-f anomalies	34	125	52	71	27
No of PFL-f anomalies mapped as "Certain"	13	100	34	50	21
No of Geological features identified with distance < 0.2 m from PFL-f anomaly	76	185	110	195	80
No of Geological features identified with distance 0.2–0.4 m from PFL-f anomaly	5	7	2	9	0
No of Geological features identified with distance 0.4–0.5 m from PFL-f anomaly	0	3	0	1	0
No of Geological features identified with distance > 0.5 m from PFL-f anomaly	0	3	2	1	0
No of PFL-f anomalies not correlated to open fractures	0	14	8	1	2
No of sealed fractures (broken/unbroken) within a distance of 1 dm from PFL-f anomalies not correlated to open fractures	0/0	29/1	10/2	1/0	4/0

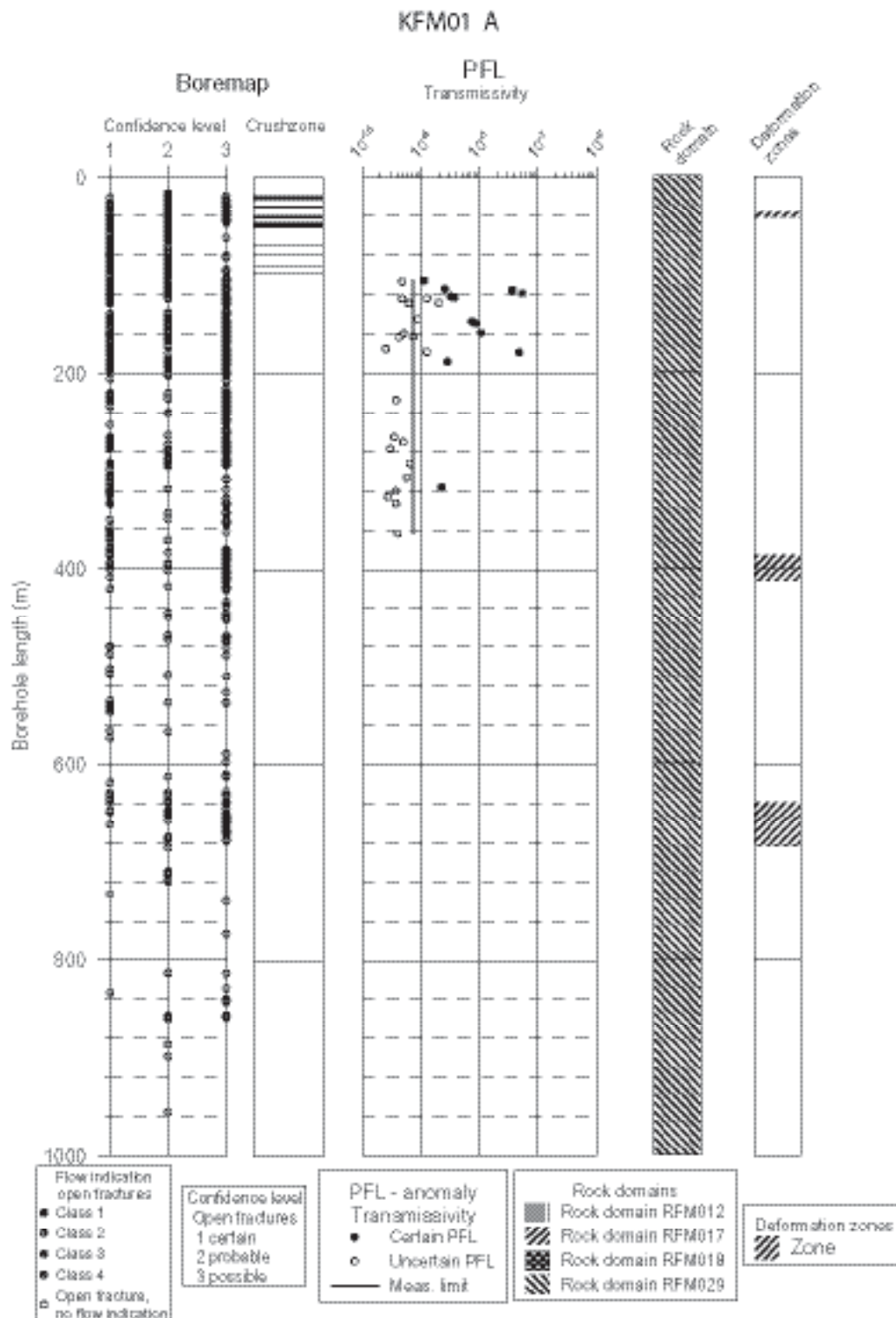


Figure 8-8. Correlation of hydraulic features, based on PFL-f overlapping measurements, to mapped open/partly open fractures (all plotted as open fractures above) or crush zones. Interpreted deformation zones (mainly brittle or ductile) and rock domains shown to the right. Fractures with PFL confidence (flow indication class) > 4 are not plotted /Forsman et al. 2004/.

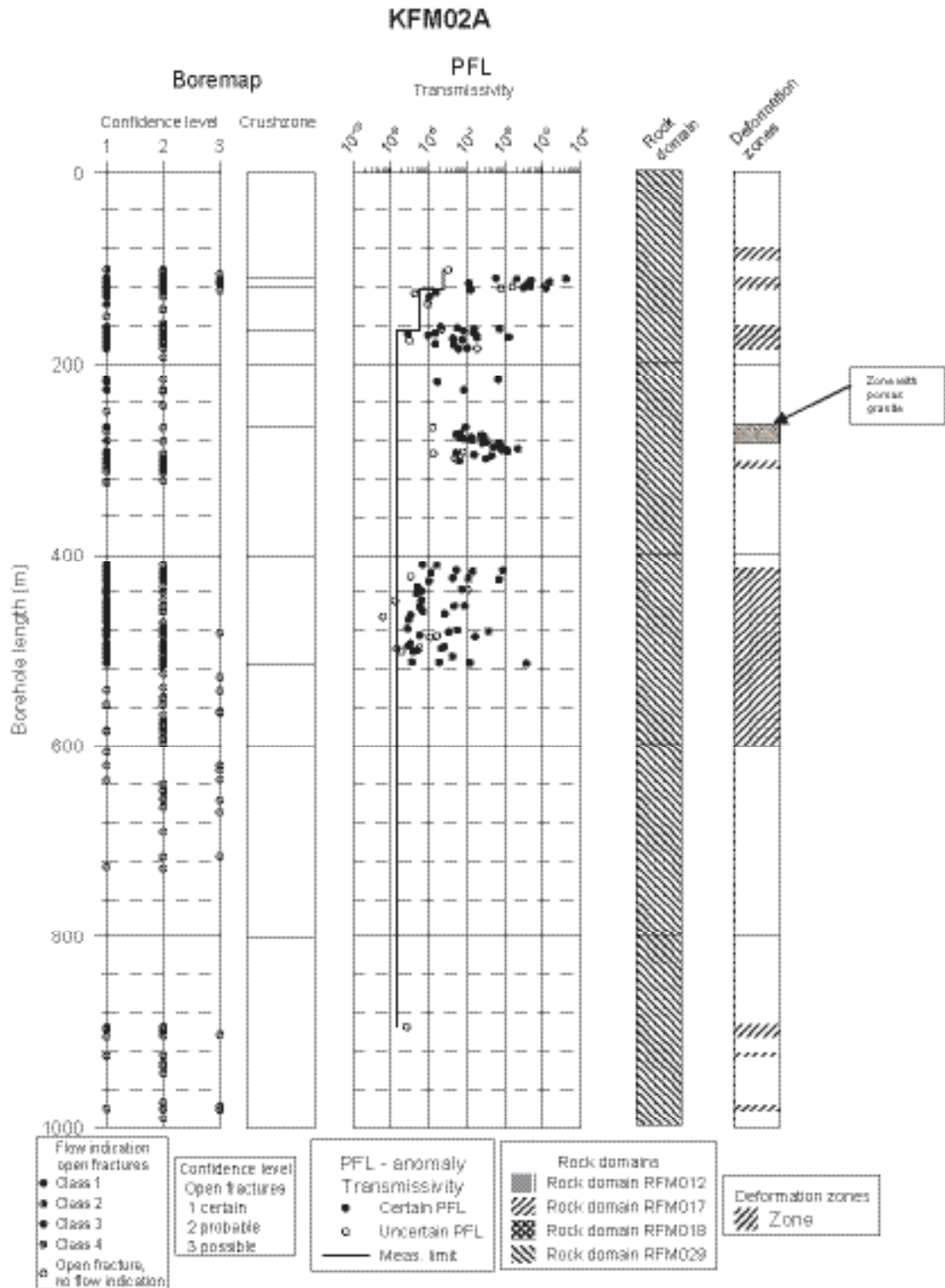


Figure 8-9. Correlation of hydraulic features, based on PFL-f overlapping measurements, to mapped open/partly open fractures (all plotted as open fractures above) or crush zones. Interpreted deformation zones (mainly brittle or ductile) and rock domains shown to the right. Fractures with PFL confidence (flow indication class above) > 4 are not plotted /Forsman et al. 2004/.

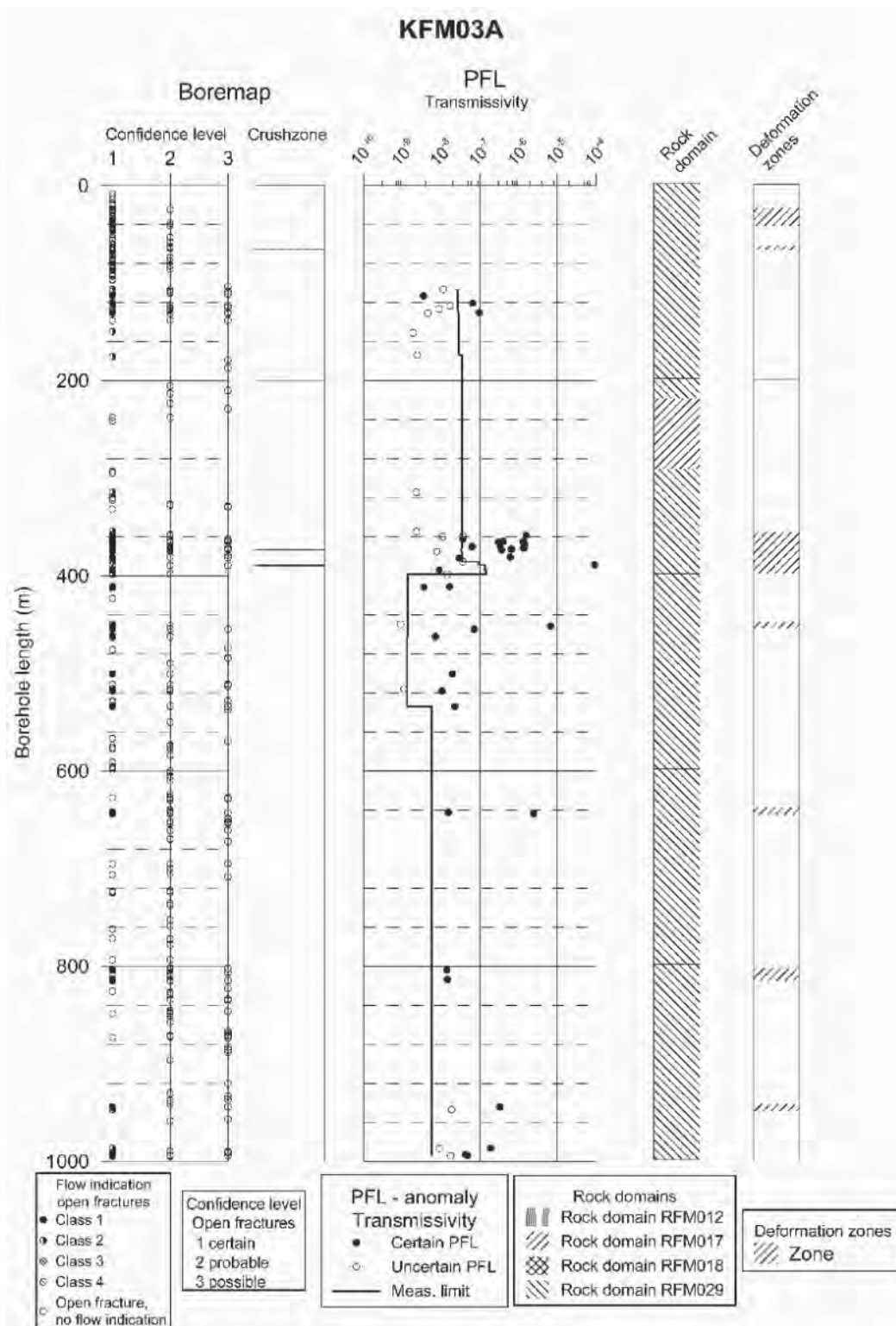


Figure 8-10. Correlation of hydraulic features, based on PFL-f overlapping measurements, to mapped open/partly open fractures (all plotted as open fractures above) or crush zones. Interpreted deformation zones (mainly brittle or ductile) and rock domains shown to the right. Fractures with PFL confidence (flow indication class above) > 4 are not plotted /Forsman et al. 2004/.

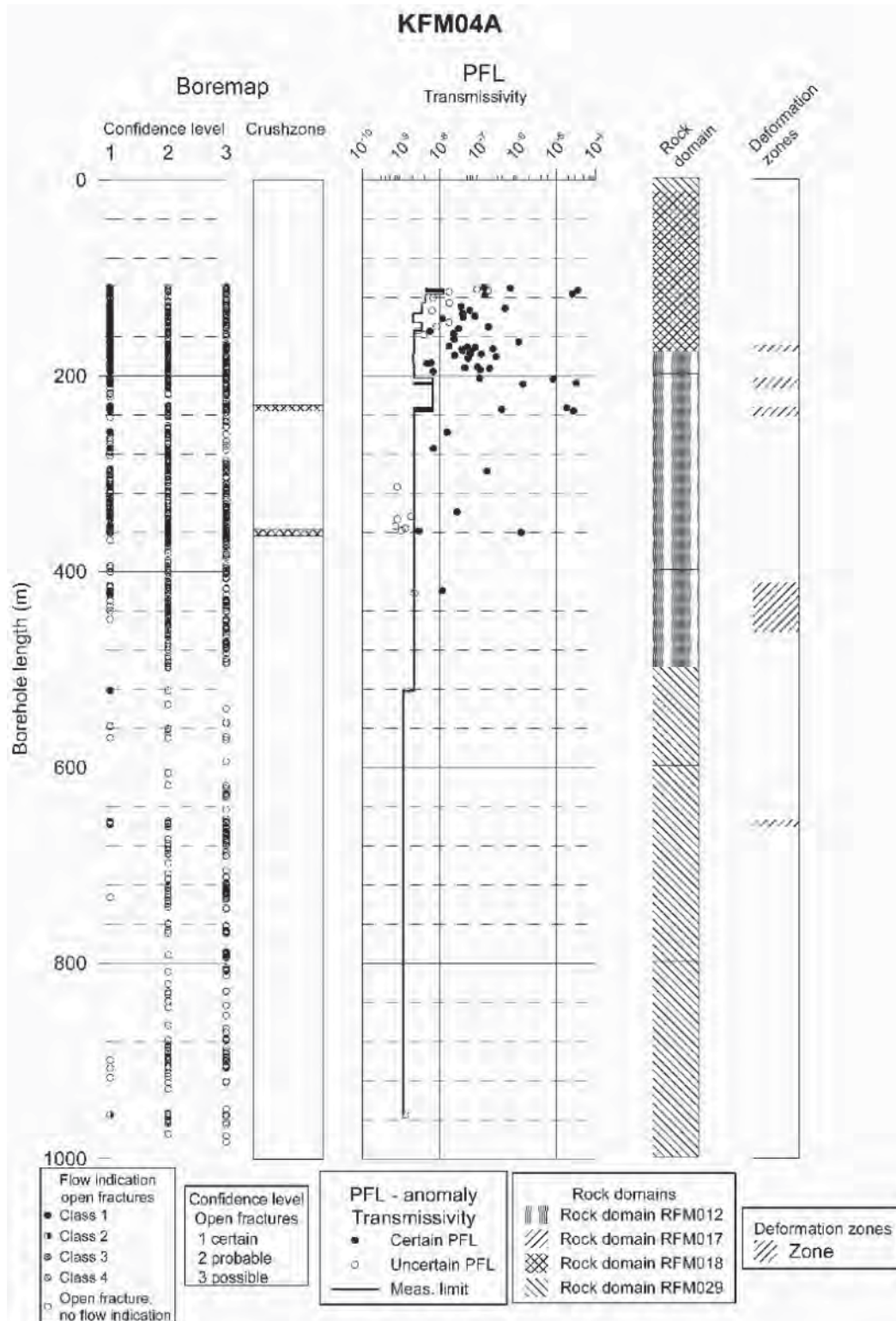


Figure 8-11. Correlation of hydraulic features, based on PFL-f overlapping measurements, to mapped open/partly open fractures (all plotted as open fractures above) or crush zones. Interpreted deformation zones (mainly brittle or ductile) and rock domains shown to the right. Fractures with PFL confidence (flow indication class above) > 4 are not plotted /Forsman et al. 2004/.

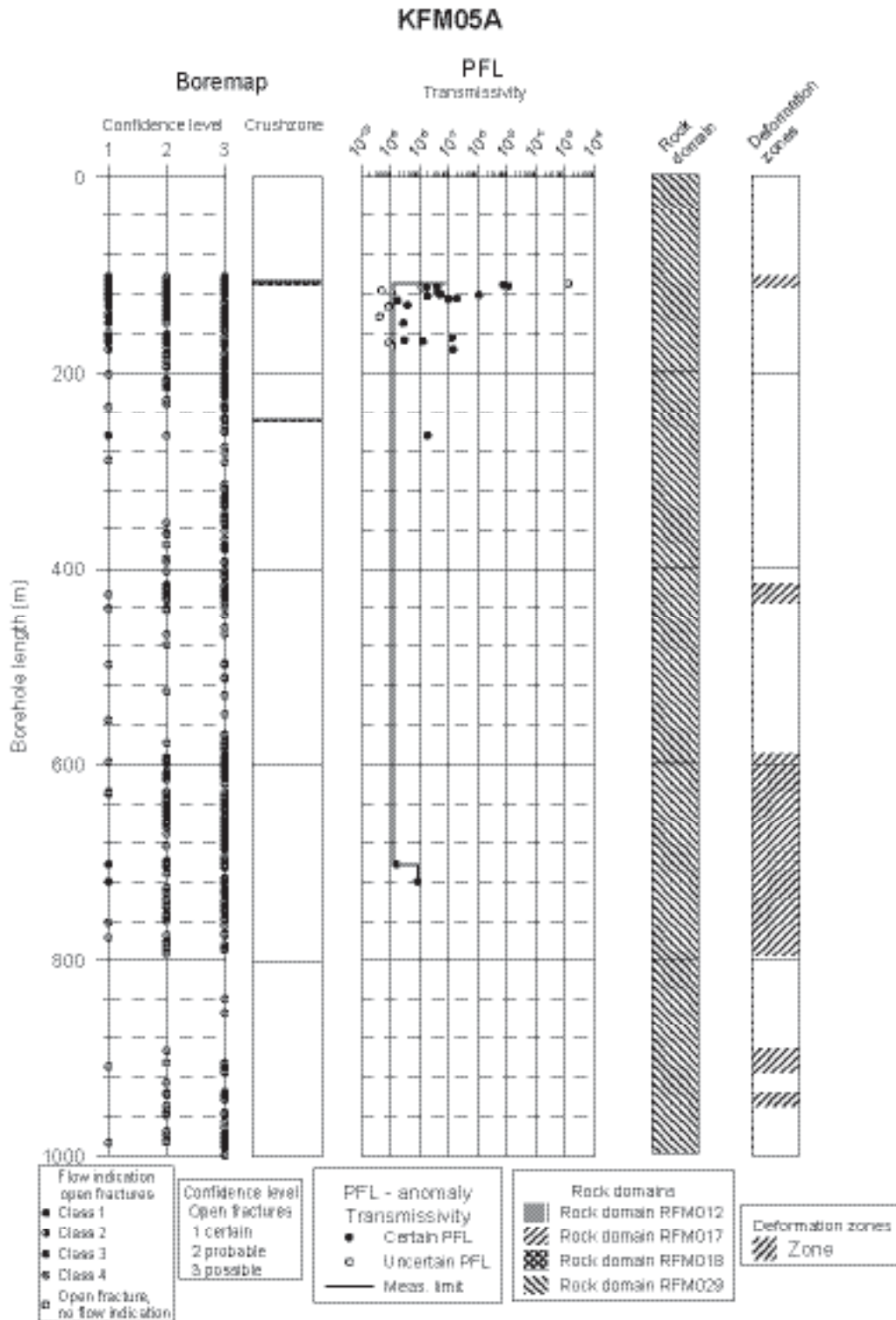


Figure 8-12. Correlation of hydraulic features, based on PFL-f overlapping measurements, to mapped open/partly open fractures (all plotted as open fractures above) or crush zones. Interpreted deformation zones (mainly brittle or ductile) and rock domains shown to the right. Fractures with PFL confidence (flow indication class above) > 4 are not plotted /Forsman et al. 2004/.

Overview of results from PSS single-hole tests

Figure 8-13 displays the PSS test results (5 m, 20 m and 100 m test section lengths) for the three boreholes for which PSS hydraulic tests are available, i.e. KFM01A–03A. The three boreholes are drilled at different locations along the centre line of the candidate area, see Figure 8-1. In addition, the PFL-s test results are displayed together with the aforementioned lower measurement limits of the PSS and PFL methods.

Table 8-5 presents a simplistic comparison between the PFL and PSS tests. The comparison is expressed in terms of the percentage of test sections above the lower measurement limit for each method assuming a 5 m test section length. The difference in lower measurement limit (LML) between the PFL and PSS tests is discussed in detail in the P-reports, see e.g. /Källgårdén et al. 2004/, the conclusions of which are commented on below. The difference in lower measurement limit is visualised in Figure 8-13.

Figure 8-13 reveals significant hydraulic differences between the three boreholes, e.g. in terms of the number of test intervals above the lower measurement limit at different elevations. These differences constitute a major observation of the bedrock hydrogeology at Forsmark as we currently know it. An integrated assessment between the hydraulic test results and intercepted deformation zones is presented in Section 8.2.3.

The 5 m PSS data shown in Figure 8-13 have been a major input data to the hydrogeological DFN modelling conducted by the modelling teams, see Section 8.4.3.

Table 8-5. Simplistic comparison between all PFL and PSS tests conducted in KFM01A–05A assuming a 5 m test section length. The comparison is expressed in terms of the percentage of test sections above the practical lower measurement limit (LML) for each method. Circa 24% of the PSS tests are above the LML and 15% of the PFL tests. It is noted that the mean magnitude of the LML of the 5 m PSS tests is c. two to three times lower (better) than the mean magnitude of the LML of the PFL tests, cf. Figure 8-13.

PSS					
Borehole	Secup* m	Seclow* m	Number of 5 m tests		% above LML
			above LML	below LML	
KFM01A	105	995	26	152	15
KFM02A	104	1,000	53	126	30
KFM03A	106	1,000	51	127	29
Total			130	405	24

PFL					
Borehole	Secup* m	Seclow* m	Number of 5 m tests		% above LML
			above LML	below LML	
KFM01A	100	1,001	22	158	12
KFM02A	101	997	45	134	25
KFM03A	102	997	26	152	15
KFM04A	111	993	33	143	19
KFM05A	106	993	13	177	7
Total			139	764	15

* Secup and Seclow are SICADA acronyms denoting borehole lengths.

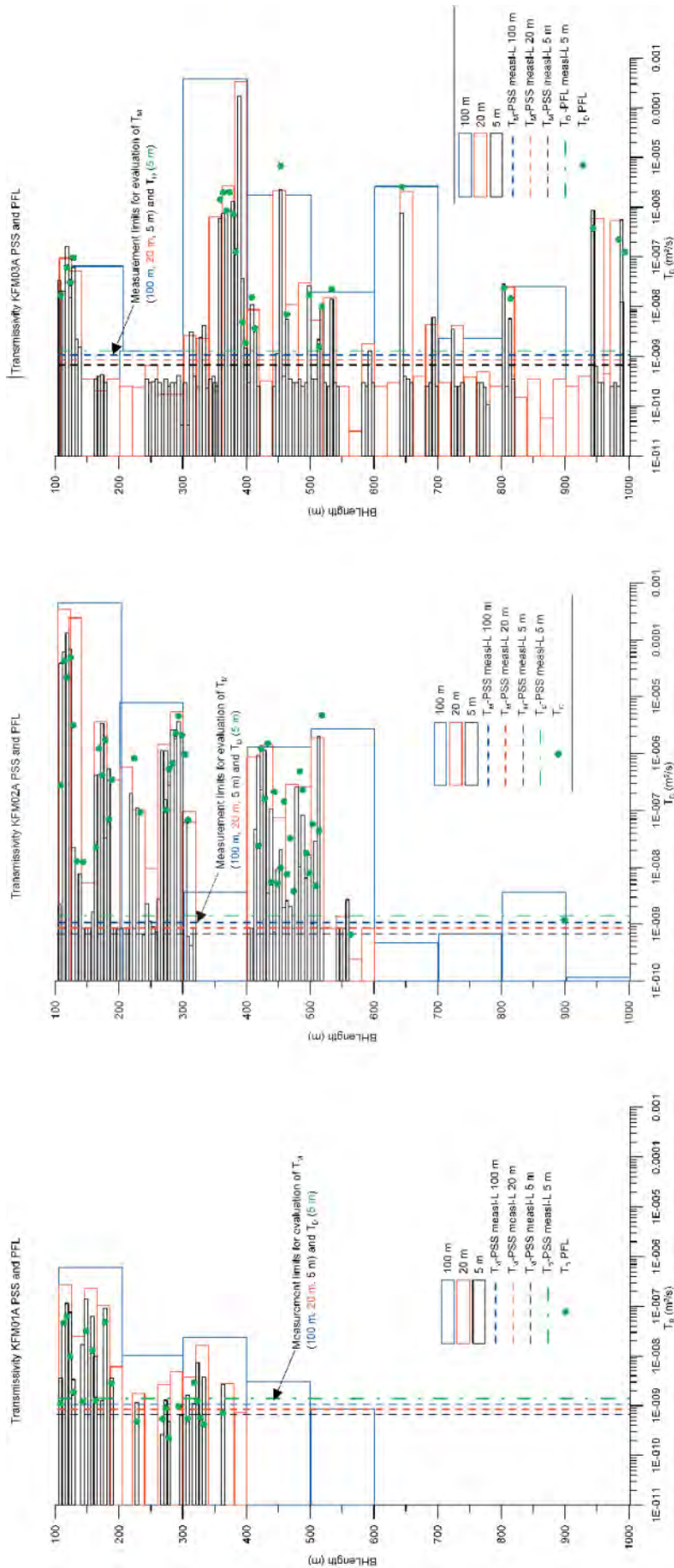


Figure 8-13. Comparison between PFL test results (5 m test section length) and PSS test results (5 m, 20 m and 100 m test section lengths) for the three boreholes where both types of hydraulic test data are available, KFM01A–03A. The three boreholes are drilled at different locations along the centre line of the candidate area, see Figure 8-1. The test results reveal significant hydraulic differences between the three boreholes, e.g. in terms of the number of 5 m test intervals above the practical lower measurement limit. These differences constitute a major observation of the bedrock hydrogeology at Forsmark as we currently know it. It is noted from the plots shown that the two test methods generally show consistent results and that reliable measurements below the practical lower measurement limit occur in all three boreholes but are less frequent for the PFL method. An integrated interpretation between the hydraulic test results and intercepted deformation zones is presented in 8.2.3 /Follin et al. 2005/.

Overview of results from HTHB single-hole tests

Among the 19 percussion-drilled boreholes available, 17 boreholes have been tested with the HTHB method in combination with impeller flow logging. The tested boreholes intercept all together 49 inflows, i.e. an average of c. three intercepts per borehole. The transmissivity distribution of the intercepted inflows is shown in Figure 8-14. The measurement limit of the HTHB method is somewhat dependent on the in-situ conditions. The geometric mean for 17 boreholes is indicated in the histogram. The range in transmissivity of the near-surface inflows varies c. three orders of magnitude.

Figure 8-15 shows a histogram of the apparent hydraulic conductivity of the near-surface rock adjacent to the percussion-drilled boreholes. The apparent hydraulic conductivity values were obtained by dividing the cumulative transmissivity by the borehole length. The borehole lengths vary between 14–220 m with a mean value of 134 m.

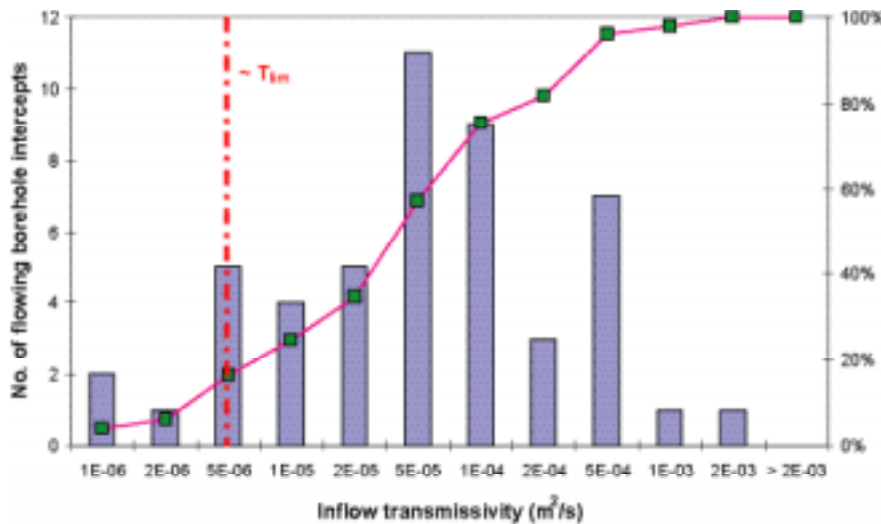


Figure 8-14. Histogram of inflow transmissivities for all percussion-drilled boreholes available for version 1.2 except HFM07 and HFM14. The borehole lengths in the bedrock range between 14–220 m with a mean value of 134 m /Follin et al. 2005/.

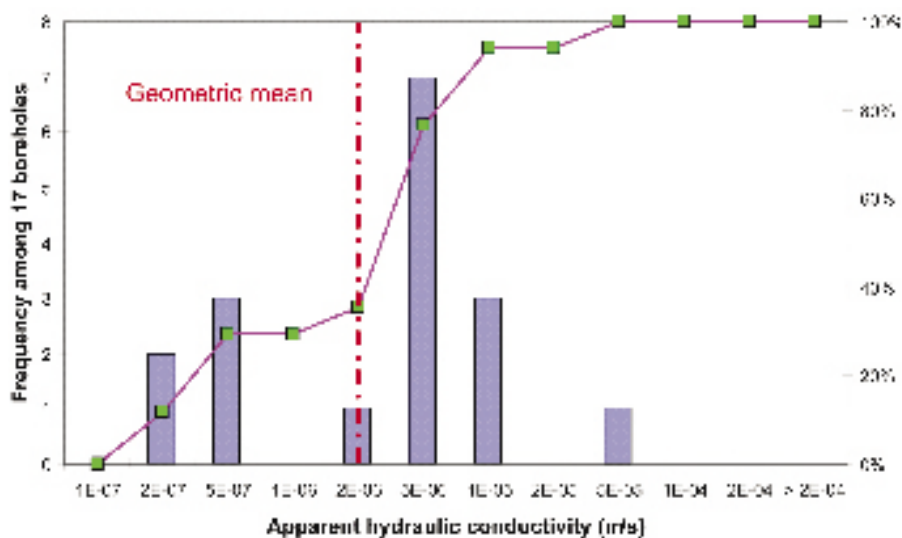


Figure 8-15. Histogram of the apparent hydraulic conductivity of the near surface rock adjacent to the HTHB tested percussion-drilled boreholes /Follin et al. 2005/.

8.2.2 Hydraulic evaluation of interference tests

Methods for testing and models for interpretation

Interference tests (cross-hole tests) are of uttermost importance as they reveal valuable information about the hydraulic connectivity of the network of fractures and deformation zones penetrated by the boreholes and modelled by geologists in 3D. However, a quantitative evaluation of hydraulic tests conducted between two or several boreholes in fractured rock requires a very good geometric perception of the structure in order to produce reliable results, e.g. cross-hole transmissivity and storativity. Assuming a homogeneously distributed (space filling) radial flow regime around the pumped borehole at all distances is a doubtful assumption, in particular if the observation boreholes are located far away from the pumping borehole. Apart from these complexities, the methods for testing and the models for interpretation are the same as those used in single boreholes.

A second kind of interference test is the pressure response observed in other boreholes when a new borehole is being drilled and flushed. Drilling-induced pressure responses are extremely important in the structural discussions with geology and in the planning of new boreholes as well as forthcoming regular interference tests. As the drilling-induced pressure responses may appear unexpectedly it is important that the multi-packer hydrologic monitoring system (HMS) is installed in each new borehole as soon as possible after completion. The documentation of drilling-induced pressure responses is governed by the HMS programme, whereas pressure responses from regular interference tests are documented in P-reports. Occasionally, drilling-induced pressure responses are recorded by temporary divers or by pressure transducers belonging to other multi-packer borehole equipments, e.g. hydrogeochemical sampling devices. The documentation of such responses is made in SICADA for future reference.

A third kind of interference test is the pressure response observed by the hydrologic monitoring system although there is no drilling and/or hydraulic test in operation. An example of such a response is the daily tidal pressure response of c. ± 0.1 m amplitude seen in almost every borehole. Barometric changes are also seen in some boreholes. The barometric-induced pressure responses generally have a long wave length, several days or weeks, and amplitudes of several decimetres are not uncommon. High frequency natural pressure responses are sometimes also seen in the monitoring data, e.g. in the spring at times of intense snow melting, or in the fall when bad weather is approaching and rapid sea level changes occur in the Baltic Sea. A systematic evaluation of tidal, barometric and seasonal transients will be a valuable piece of information in due time, but requires a lot of other geological and hydraulic information to be conclusive. In model version 1.2 the available information is too sparse.

Overview of interference tests

Regular interference tests have been conducted between boreholes HFM01 and HFM02 at drill site 1 /Ludvigson and Jönsson, 2003/ and between boreholes HFM11 and HFM12 close to Lake Eckarfjärden, south of the candidate area /Jönsson et al. 2004/. The results from these tests support the structural model, i.e. the anticipated hydraulic connectivity between the boreholes was observed. In the former case, the two boreholes are vertical, c. 220 m apart and intersect several fractures presumably belonging to the gently dipping deformation zone, ZFMNE00A2. The hydraulic interference was obvious within 4–5 minutes. In the latter case, the two boreholes are drilled with an inclination of 50°, c. 130 m apart, and intersecting several fractures presumably belonging to the steeply dipping deformation zone, ZFMNW003A, see Figure 8-16. The hydraulic interference was obvious within 8–15 minutes. The interpretation models used for the deduction of model parameters from these two interference tests were chosen with regards to the assumed structural model in each case /Ludvigson and Jönsson, 2003; Jönsson et al. 2004/. The results are commented on below.

Pressure responses observed in existing boreholes when a new borehole is being drilled and flushed are common at Forsmark in spite of the sometimes long distances between the drill sites. Figure 8-17 and Figure 8-18 show an example. The boreholes involved are HFM16 at drill site 6 (the borehole being drilled), KFM02A at drill site 2 (monitored by a hydrogeochemical sampling device), HFM13 (monitored by HMS), and HFM14–15 at drill site 5 (monitored by HMS). The pressure responses are shown in Figure 8-18.

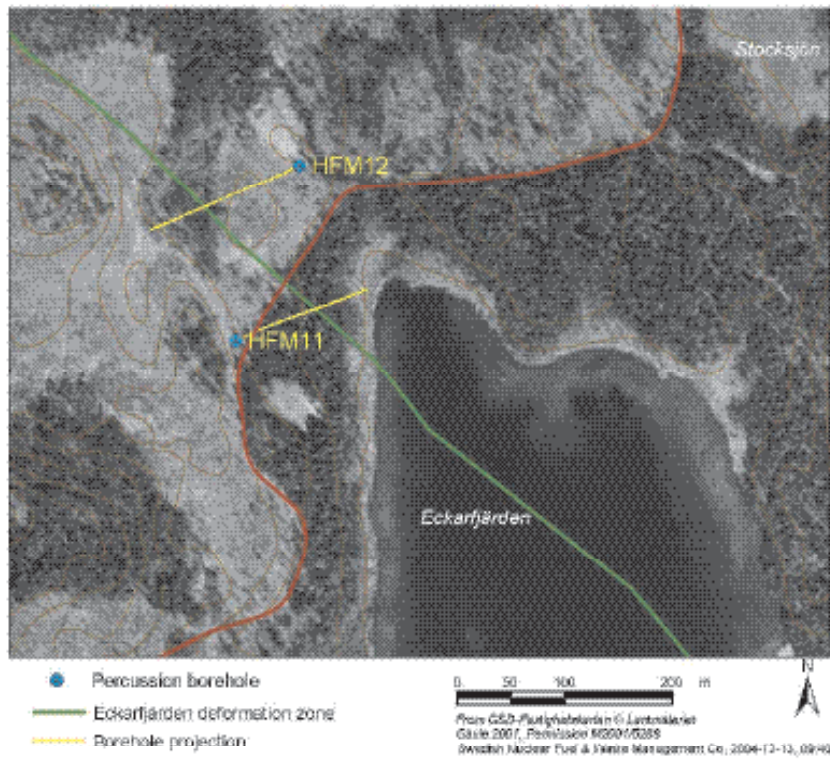


Figure 8-16. Map showing the location and the azimuth of HFM11 and HFM12. The two boreholes were used for used for interference test of the indicated deformation zone (lineament) /Jönsson et al. 2004/.

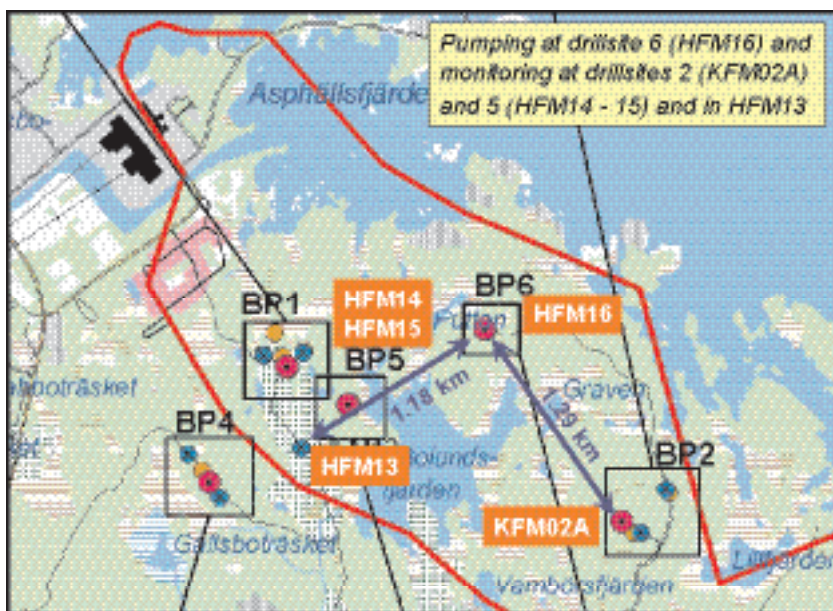


Figure 8-17. Schematic map showing boreholes at the drill sites in the north-western part of the candidate area. While HFM16 was being drilled and flushed at drill site BP6 pressure responses were observed in KFM02A at drill site BP2, in HFM14–15 at drill site BP5 and in HFM13, see Figure 8-18.

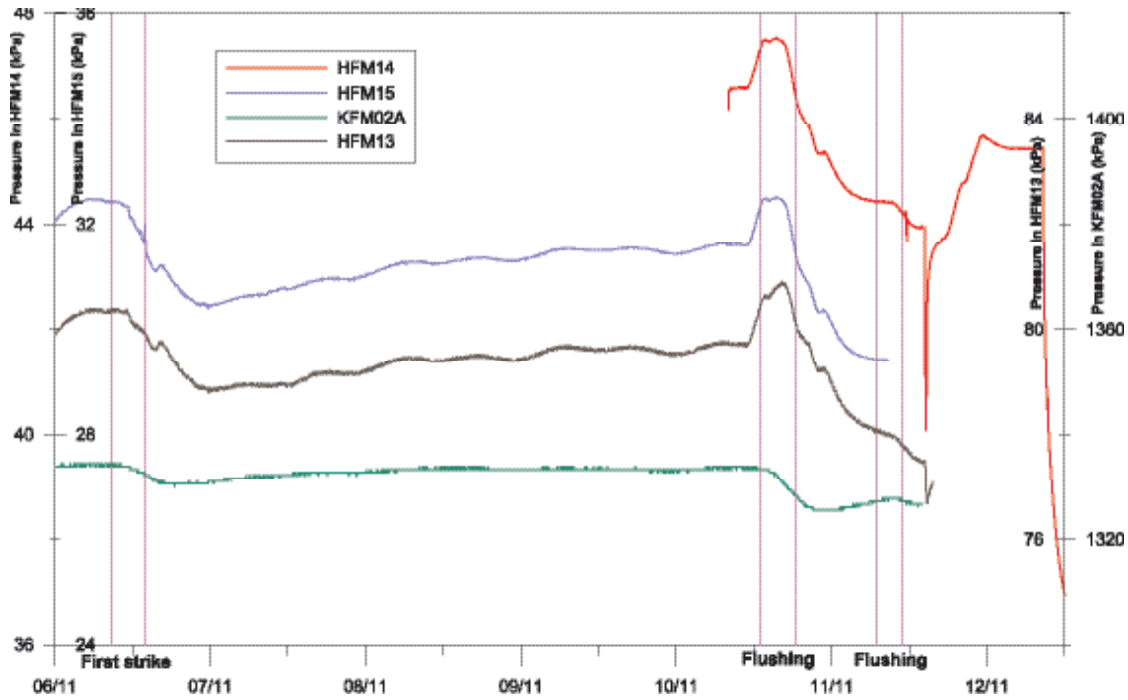


Figure 8-18. The pressure responses observed in KFM02A (Field note: Forsmark 437) and in HFM13–15 (excerpt from HMS, 2003-11-06–2003-11-13) while drilling and flushing HFM16.

Figure 8-19 and Figure 8-20 show an example of the third kind of interference, i.e. responses observed although there is no drilling and/or hydraulic test in operation. The borehole involved is KFM03A, which is intersected by several gently dipping deformation zones (cf. Chapter 5). One of these deformation zones, ZFMNE00A4, intercepts KFM03A at c. 388 m borehole length and outcrops c. 800 m northwest of KFM03A, partly in the Baltic Sea. ZFMNE00A4 is a relatively thin deformation zone and highly transmissive, cf. Figure 8-13. It is also an excellent seismic reflector.

Prior to the hydrogeochemical sampling in borehole KFM03A, a long-term constant-pressure pumping was performed in a five metre long section, (386–391) m borehole length, with the Pipe String System (PSS). The objective of the pumping was to rinse the section from flushing water and drilling debris in order to obtain representative water samples.

During the rinsing, it was noted that the pressure in the pumped section was strongly affected by natural pressure variations. The pressure disturbances affected the pump regulator used to keep the pressure drawdown at a constant level, see Figure 8-20. Subsequent correlation analyses suggest that the pressure variations were caused by variations in the sea water level in the adjacent Baltic Sea and by variations in the barometric pressure /Ludvigson et al. 2004a/. Due to the high transmissivity and the possible association to an outcropping seismic reflector it was tentatively assumed that the fracture zone at c. 388 m in KFM03A is hydraulically connected to the Baltic Sea. /Ludvigson et al. 2004a/ noted that there was a time lag between the sea level variations and the flow rate variations of four hours. The plot in Figure 8-20 takes this time lag into account to make the correlation more obvious.

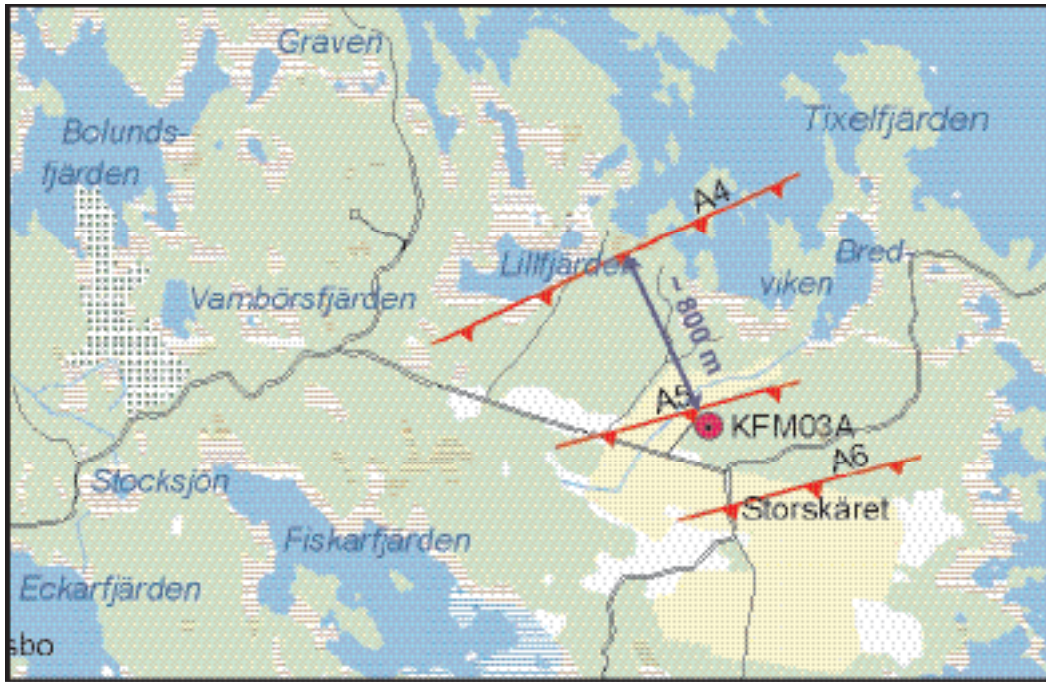


Figure 8-19. Schematic map showing the location of KFM03A and the interpreted outcropping of a seismic reflector modelled as deformation zone ZFMNE00A. Modified after /Ludvigson et al. 2004a/.

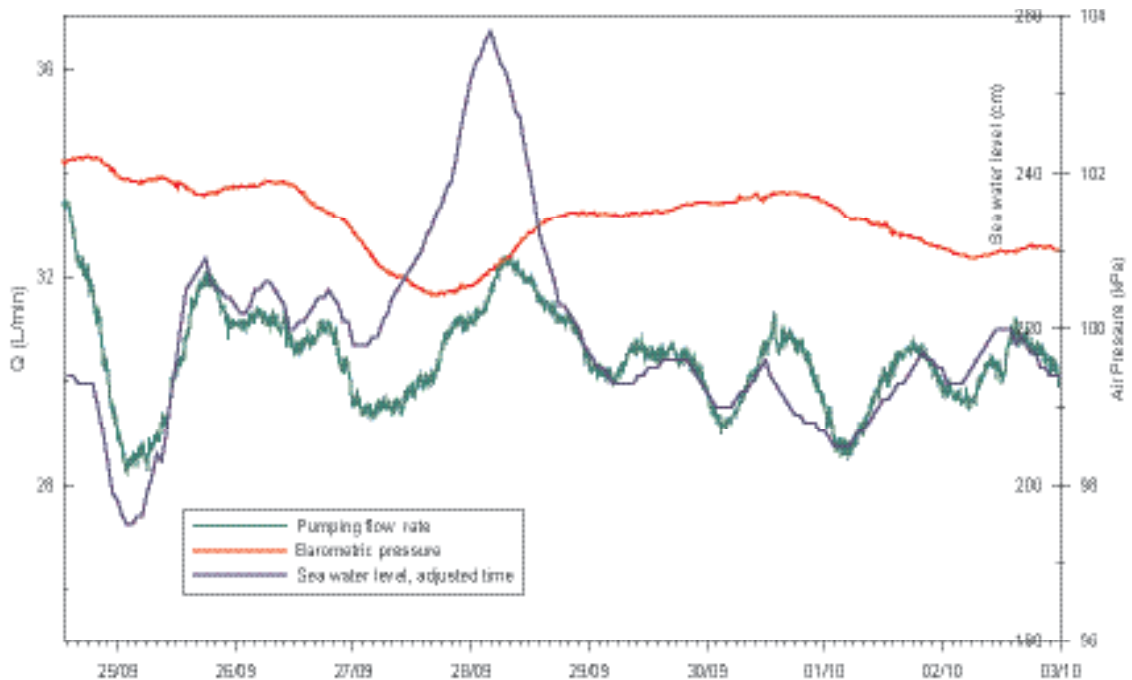


Figure 8-20. Plot showing the observed correlation between sea water level variations and variations in the flow rate of the constant-pressure long-term pumping conducted in a section enclosing deformation zone ZFMNE00A4 in KFM03A. The variations in the pumping flow rate are also disturbed by the relatively great fluctuation the barometric pressure between September 26 and 28 indicating that the flow rate is dependent on both the sea water level and the barometric pressure. Modified after /Ludvigson et al. 2004a/.

8.2.3 Joint hydrogeology and geology interpretation

As part of the geological single-hole evaluation, borehole sections with intercepting deformation zones (ZFM) were identified. The lithological rock domains (RFM) along the boreholes were also identified. Significant characteristics of geological single-hole interpretation in Forsmark are as follows:

- Almost all of the bedrock within the candidate area consists of a single rock domain RFM029.
- Almost all deformation zone intercepts are possible to explain deterministically by the base model given our current understanding of the area and the data collected. A major reason for this situation is the nature of the deformation zones, many of which are gently dipping. Secondly, the combined results from the reflection seismics /Juhlin et al. 2002/ and the drilling-induced hydraulic cross-hole responses have allowed quite confident extrapolations to be made.

During the joint interpretation with hydrogeology, it was noted that almost all PFL and PSS tests could be coupled to the deterministically treated deformation zones leaving very little hydraulic test data above the measurement limit to be associated with the rock domains in between, see Figure 8-8 through Figure 8-13. From a site characterisation point of view, it is therefore obvious to talk about a hydrogeological system consisting of transmissive deformation zones and very low conductivity rock masses in between the deformation zones, i.e. at or below the lower measurement limit.

Hydraulic rock domains (rock domains)

The PSS and the PFL-f test data that are not associated with the deterministically treated deformation zones have been the main input data for the hydrogeological DFN analysis of the HRDs. The outcome of a joint interpretation with the core mapping based of the PFL-f data is provided below.

Out of a total of 309 flow anomalies determined by the PFL-f testing in the five 1,000 m long core-drilled boreholes, 240 flow anomalies were associated with rock domain RFM029. 69 flow anomalies were found in other rock domains outside the candidate area (KFM04A). 149 of the 240 flow anomalies in RFM029 are associated with deterministically treated deformation zones and the remaining 91 with the rock between the deterministically treated deformation zones. 35 of these 91 flow anomalies occur below c. 200 m depth – 11 in KFM01A, 6 in KFM02A, 15 in KFM03A, 2 in KFM04A and 1 in KFM05A. At repository depth, below the gently dipping deformation zone ZFMNE00A2, there are 2 flow anomalies. Figure 8-21 shows the 91 flow anomalies in rock domain RFM029, coloured according to borehole. The left hand plot shows the transmissivities, the centre plot shows the dips and the right hand plot shows the strikes. From these plots it may be noted that most of the flow anomalies, 77%, coincide with gently dipping fractures and there is weak preference for NW and NE fractures concerning strike.

A similar analysis cannot be made for the PFL-s and the PSS tests as they comprise several fractures within each test section interval. A comparison between these latter types of tests is shown in Figure 8-13.

Hydraulic conductor domains (Deformation zones)

Table 8-6 shows a compilation of the transmissivities of intercepted deformation zones deduced from a joint interpretation of the single-hole tests and single-hole deformation zone interpretation. The reference P-report for each hydraulic test is given together with an indicator about the deformation zone dip, **S** for steeply dipping and **G** for gently dipping. There are 14 deformation zones of each kind. Some of the deformation zones have two or more hydraulic test interpretations associated with them. For instance, deformation zone ZFMNE00A2 has 13 hydraulic test interpretations associated to it. During the period between the first and second data freeze, 34 single-hole test interpretations provided hydraulic information about the base model corresponding to 16 deformations zones not previously characterised hydraulically.

The interference tests conducted between boreholes HFM01 and HFM02 /Ludvigson and Jönsson, 2003/ and between boreholes HFM11 and HFM12 /Jönsson et al. 2004/ provide cross-hole transmissivity and storativity values of the deformation zones ZFMNE00A2 and ZFMNW003A

(Eckarfjärden deformation zone), respectively. The transmissivity values deduced from the interference tests are in accordance with the values reported from the single testing of the corresponding boreholes and the deduced values of the storativity from the interference test is 5×10^{-5} in both cases /Ludvigson and Jönsson, 2003; Jönsson et al. 2004/.

Transmissivity values marked as “< 1.0E–09” in Table 8-6 indicate that the value is less than the lower practical measurement limit of the PFL method, i.e. no flow was measured. Figure 8-22 shows a scatter plot of all transmissivity values listed in Table 8-6 columns F1.1 and F1.2. The values are coloured with regards to the dip of the deformation zones, red squares for steeply dipping and blue for gently dipping. Blue squares with a white infilling refer to the hydraulic test interpretations associated to the gently dipping deformation zone ZFMNE00A2.

The two data sets – gently and steeply dipping – show different tendencies for a depth trend, where the transmissivities of the steeply dipping set appears to decrease at a higher rate. The data plotted in Figure 8-22 do not prove that the deformation zones become impervious at greater depth. There may still be several transmissive zones at depth. For instance, the data exposed in Figure 8-13 show quite high transmissivity values below 950 m borehole length in KFM03A. According to /Ludvigson et al. 2004a/ and /Källgården et al. 2004/ the PSS tests at the bottom of KFM03A indicate that the different transmissivities represent several vertical features that are interconnected at some distance away from the borehole, however, not necessarily meaning that they belong to the same deformation zone. The base model does not provide a structural explanation for these transmissivities. This is the reason why the features at the bottom of KFM03A are treated as rock domain flow anomalies in Figure 8-21.

Overall, Figure 8-22 leaves a strong impression of a hydraulic contrast in transmissivity between steeply and gently dipping deformation zones. Close to ground surface the contrast appears to be less than at c. 400 m depth, where the contrast appears to be at least one order of magnitude. However, the 13 hydraulic test interpretations associated with deformation zone ZFMNE00A2 suggest that the deformation zones may also be heterogeneous, which implies an uncertainty about the exact magnitude of the contrast.

The thickness values shown in Table 8-6 are of interest as they provide information about the hydraulic nature of the deformation zones. This is because the transmissivity divided by the thickness yield the homogenised mean value of the hydraulic conductivity of the deformation zone. Moreover, the deformation zone dip and thickness are of interest for the choice of resolution of the computational grid used in the numerical simulations. From Table 8-6 it may be concluded that almost all of the gently dipping deformation zones are much less than 50 m thick except for ZFMNE00A2, which seems to vary a lot.

Table 8-6. Compilation of the transmissivities deduced from a joint interpretation of the single-hole tests and the single-hole deformation zone interpretation. The last column provides information about the deformation zone dip, S for steeply dipping and G for gently dipping. There are 14 deformation zones of each kind. Transmissivity values marked as “< 1.0E–09” indicate that the magnitude is less than the lower practical measurement limit of the PFL method as no flow was measured.

SDM 0 (7)	SDM 1.1 (9)	SDM 1.2 (34)	Borehole	Name of DZ	Approx. elevation of intercept (m.a.s.l.)	Thickness (m)	T (m ² /s)	Reference	Category
x			SFR holes	ZFMNW0001	< –100	30	2.4E–05	R0214	S
x			SFR holes	ZFMNW0002	< –100	30	2.4E–05	R-02-14	S
x			SFR holes	ZFMNW0805	< –100	10	8.0E–06	R-02-14	G
x			SFR holes	ZFMNE0869	< –100	7	2.0E–05	R-02-14	S
x			SFR holes	ZFMNE0870	< –100	5	2.0E–07	R-02-14	S
x			SFR holes	ZFMNE0871	< –100	10	2.0E–06	R-02-14	S
x			FKA DBT1	ZFMNE1193	–319	6	> 1.0E–05	R-02-32	G

SDM 0 (7)	SDM 1.1 (9)	SDM 1.2 (34)	Borehole	Name of DZ	Approx. elevation of intercept (m.a.s.l.)	Thickness (m)	T (m ² /s)	Reference	Category
	x		HFM01	ZFMNE00A2	-36	8	4.5E-05	P-03-33	G
	x		HFM02	ZFMNE00A2	-44	5	5.9E-04	P-03-33	G
	x		HFM04	ZFMNE0866	-62	3	7.9E-05	P-03-34	G
	x		HFM04	ZFMNE00B6	-184	4	2.4E-05	P-03-34	G
	x		HFM05	ZFMNE0866	-153	1	4.0E-04	P-03-34	G
	x		HFM06	ZFMNE00A5	-66	10	1.8E-04	P-03-36	G
	x		HFM08	ZFMNE00A5	-138	5	1.2E-03	P-03-36	G
		x	HFM09	ZFMNE1187	-22	9	3.3E-04	P-04-74	G
		x	HFM10	ZFMNE1187	-104	8	3.1E-04	P-04-74	G
		x	HFM11	ZFMNW003A	-92	58	3.0E-05	P-04-64	S
		x	HFM12	ZFMNW003A	-98	60	7.8E-06	P-04-64	S
		x	HFM13	ZFMNE0401	-145	12	2.9E-04	P-04-71	S
		x	HFM14	ZFMNE00A2	-62	7	1.5E-03	P-04-71	G
		x	HFM15	ZFMNE00A2	-63	7	1.0E-04	P-04-71	G
		x	HFM16	ZFMNE00A2	-41	59	5.0E-04	P-04-72	G
		x	HFM18	ZFMNE00A4	-36	11	1.6E-04	P-04-72	G
		x	HFM18	ZFMNE0065 ZFMNE00A7	-114	25	2.0E-05	P-04-72	G G
			HFM19	ZFMNE00A2	-114	23	1.6E-05	P-04-72	G
		x	HFM19	ZFMNE00A2	-150	14	2.8E-04	P-04-72	G
		x	KFM01A	ZFMNE00A2	-42	12	2.3E-03	P-03-33	G
		x	KFM01A	ZFMNE1192	-398	26	3.2E-09	P-04-95	S
	x		KFM01A	ZFMNE0061	-660	45	< 1.0E-09	P-04-95	S
	x		KFM02A	ZFMNE0866	-85	12	4.0E-04	P-03-34	G
		x	KFM02A	ZFMNE00B6	-116	12	1.1E-04	P-04-188	G
		x	KFM02A	ZFMNE00A3	-171	24	3.5E-06	P-04-188	G
		x	KFM02A	ZFMNE1189	-306	7	1.3E-06	P-04-100 P-04-188	S
		x	KFM02A	ZFMNE00A2	-466	105	7.8E-06	P-04-100 P-04-188	G
		x	KFM02A	ZFMNE1195	-896	12	2.6E-09	P-04-188	G
		x	KFM02A	ZFMNE00B4	-976	6	< 1.0E-09	P-04-100	G
		x	KFM03A	ZFMNE00A4	-376	43	1.0E-04	P-04-189	G
		x	KFM03A	ZFMNE00A7	-450	7	6.7E-06	P-04-189 P-04-194	G
		x	KFM03A	ZFMNE00B1	-640	8	2.5E-06	P-04-189 P-04-194	G
		x	KFM03A	ZFMNE00A3	-807	13	2.9E-08	P-04-189 P-04-194	G
		x	KFM03B	ZFMNE00A5	-33	18	1.4E-05	P-04-278	G
		x	KFM04A	ZFMNE00A2	-132	5	5.0E-07	P-04-190	G
		x	KFM04A	ZFMNE00A2	-159	8	4.2E-05	P-04-190 P-04-293	G
		x	KFM04A	ZFMNE00A2	-182	8	5.0E-05	P-04-190 P-04-293	G
		x	KFM04A	ZFMNE1188	-335	38	1.4E-08	P-04-190 P-04-293	S
		x	KFM04A	ZFMNE1188	-504	5	1.0E-09	P-04-293	S
		x	KFM05A	ZFMNE00A2	-83	9	1.3E-03	P-04-191	G
		x	KFM05A	ZFMNE0401	-326	15	< 1.0E-09	P-04-191	S
		x	KFM05A	ZFMNE103A ZFMNE103B	-531	158	1.0E-08	P-04-191	S S
		x	KFM05A	ZFMNE062B	-693	24	< 1.0E-09	P-04-191	S
		x	KFM05A	ZFMNE062A	-722	14	< 1.0E-09	P-04-191	S

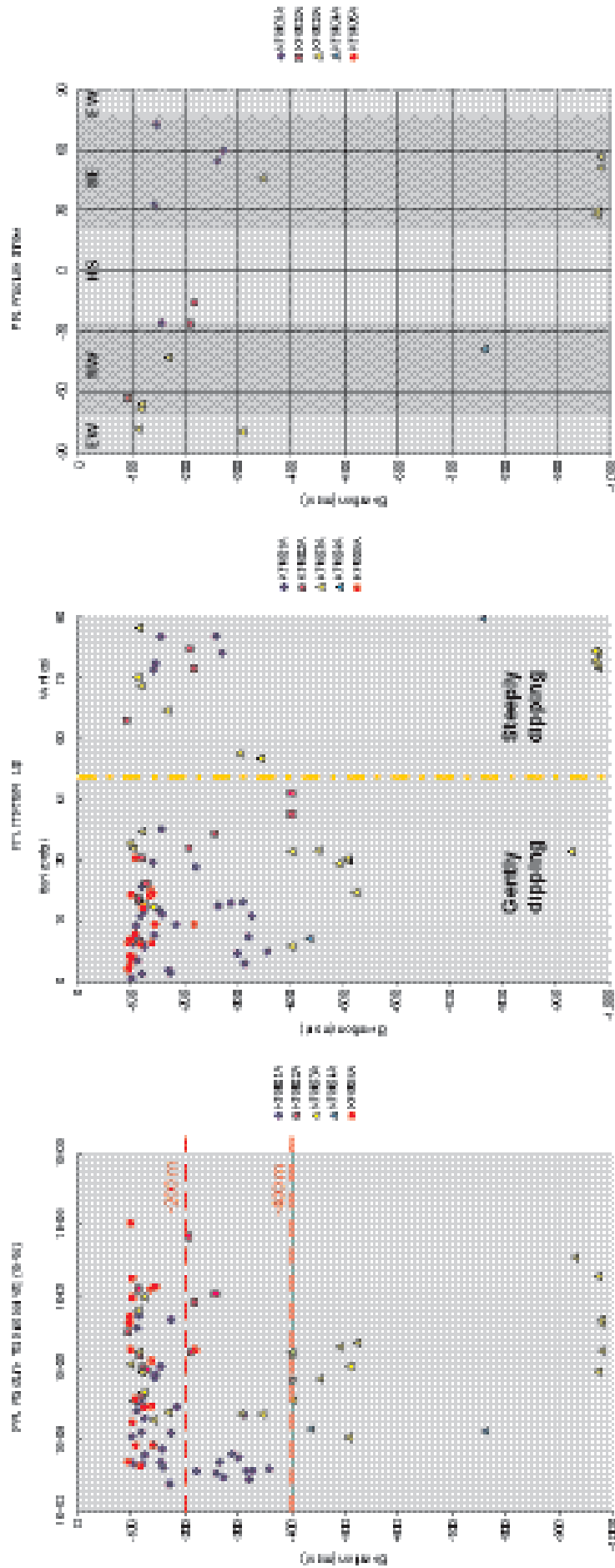


Figure 8-21. Plots showing the 91 PFL-f flow anomalies in rock domain RFM029 between the deterministically treated deformation zones. The anomalies are coloured according to borehole. The left hand plot shows the transmissivities, the centre plot shows the dips and the right hand plot shows the strikes. 35 of the 91 flow anomalies occur below c. 200 m depth – 11 in KFM01A, 6 in KFM02A, 15 in KFM03A, 2 in KFM04A and 1 in KFM05A. At repository depth below the gently dipping deformation zone ZFMNE00A2 there are 2 flow anomalies, i.e. the whole of KFM03A is above ZFMNE00A2. The division of the PFL-f anomalies into sets follows the geological DFN definitions (see Chapter 5) /Follin et al. 2005/.

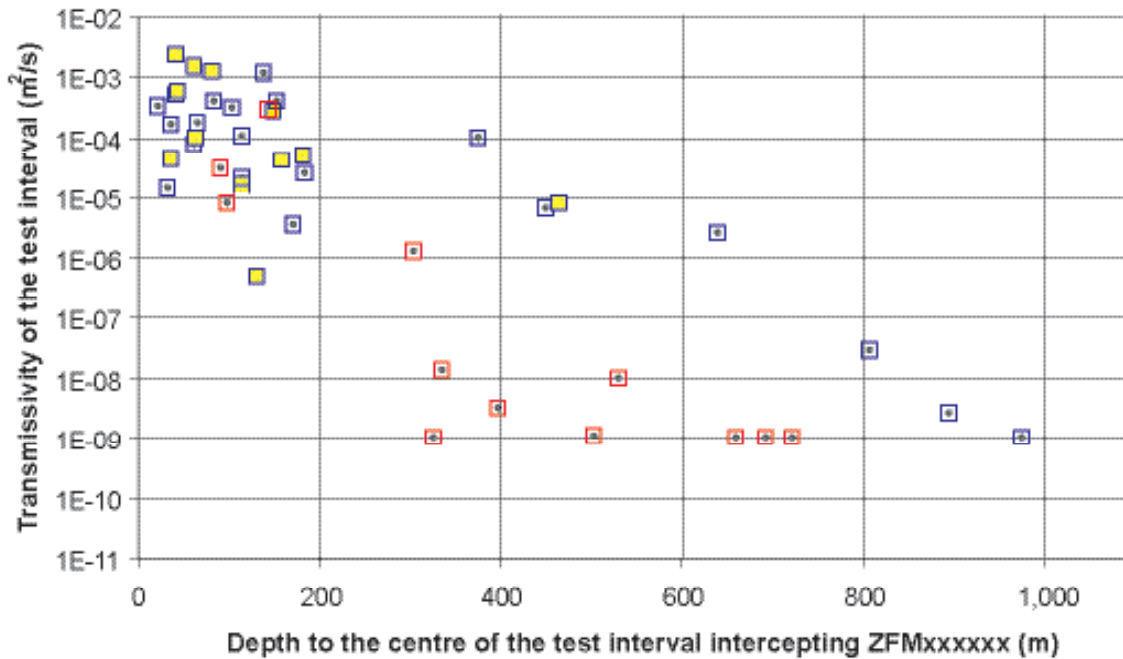


Figure 8-22. Scatter plot of the transmissivity values listed in Table 8-6 columns SDMI.1 and SDMI.2. Red squares indicate steeply dipping deformation zones and blue gently dipping. Blue squares with a yellow infilling refer to the hydraulic test interpretations associated with ZFMNE00A2 /Follin et al. 2005/.

8.3 Hydrogeological modelling – general conditions and concepts

This section describes the modelling strategy and the conceptual models used. It forms the basis for the numerical simulations presented in the following sections.

8.3.1 Modelling objectives and premises

The hydrogeological descriptive model should provide data that are useful for variable-density groundwater flow modelling. More specifically, groundwater flow models should be able to simulate groundwater flow within a given volume under natural (undisturbed) conditions. Hydrogeological modelling, that includes the fully open or back-filled deep repository is subsequently carried out by Repository Engineering and Safety Assessment. In the undisturbed system, the flow paths to the potential repository area are of interest, as they provide a description of the rate at which potential corrodants are introduced. Likewise, the flow paths from the recharge areas to the potential repository area within the modelled volume are important for a reasonable assessment of the palaeo-hydrogeological evolution and hydrogeochemical interpretation, whereas the flow paths from the repository area to discharge areas are important for Safety Assessment. Of particular importance in this context is the shoreline displacement, which must be taken into account when modelling the long-time evolution of the groundwater flow (and chemical evolution).

The numerical groundwater flow simulations serve three main purposes:

- Model testing, i.e. simulations of different major geometric alternatives or boundary conditions in order to disprove a given geometric interpretation or boundary condition, and thus reduce the number of alternative conceptual models of the system.
- Calibration and sensitivity analyses in order to explore the impact of different assumptions of hydraulic properties, boundary and initial conditions.
- Description of flow paths and flow conditions, which is useful for the general understanding of the groundwater flow system (and hydrogeochemistry) at the site.

The numerical groundwater flow simulations are helpful for the uncertainty assessment of the hydraulic properties, boundary and initial conditions, as well as for enhancing the general understanding of the site. The interaction between the geology and hydrogeology disciplines, but also involving the disciplines of hydrogeochemistry, transport and surface ecosystems, in interpreting the available data, is essential in order to obtain consistent models, and the numerical groundwater flow models play an important role in this context.

A given version of the site description, with its groundwater flow models, subsequently forms the basis for further analysis by Repository Engineering and Safety Assessment and for the planning of new investigations. Exploratory groundwater flow simulations are considered when planning field investigations or addressing specific Repository Engineering and Safety Assessment questions.

8.3.2 General modelling assumptions and input from other disciplines

The hydrogeological modelling presented in the subsequent sections is based on the current geological (structural) descriptive models presented in Chapter 5, i.e. the base model (Base Case, BC), the alternative model (Alternative Case, AC) and the base variant model (Variant Case, VC). The modelling utilises estimates of hydraulic properties based on data from the initial site investigations within the Forsmark candidate area mainly. Historic data from single-hole tests and interference tests conducted prior to the site investigations are incorporated into the modelling to the extent possible depending on the objectives. However, the historic data used come from investigations conducted outside the candidate area mainly, e.g. the SFR facility /Axelsson et al. 2002/, the Forsmark Nuclear Power Plant area /SSPB, 1982, 1986; Carlsson, 1979/, and, to a less extent, the Finnsjön study site /Andersson et al. 1991; Geir et al. 1992; Ahlbom et al. 1992; Gylling et al. 1999/.

The groundwater flow simulations were performed by two different modelling teams using the numerical codes DarcyTools /Svensson et al. 2004; Svensson and Ferry, 2004; Svensson, 2004/ and ConnectFlow /Hartley et al. 2003a,b; Hartley and Holton, 2003; Hoch and Hartley, 2003; Hoch et al. 2003/, respectively. The simulations conducted focus mainly on the hydrogeology models of the rock domain between the deterministically treated deformation zones.

Data sources

The descriptive hydrogeological model is based on four different sources of information. These sources are: (i) mapping of Quaternary deposits and bedrock geology (rock type, lineaments and deformation zones), (ii) meteorological and hydrological investigations, (iii) hydraulic borehole investigations and monitoring, and (iv) hydrogeological interpretation and analysis. The modelling may be described by means of parameters, boundary conditions and initial conditions, which detail:

- The geometrical description and hydraulic properties of the crystalline bedrock and the Quaternary deposits.
- The hydrological processes that govern the hydraulic boundary conditions and the hydraulic interplay between surface water and groundwater, including groundwater flow at repository depth.

Systems approach

Figure 8-23 illustrates schematically SKB's general systems approach to hydrogeological modelling of groundwater flow. The division into three hydraulic domains (overburden (soil), rock and conductors (deformation zones)) constitutes the conceptual basis for the numerical simulations carried out in support of the site descriptive modelling.

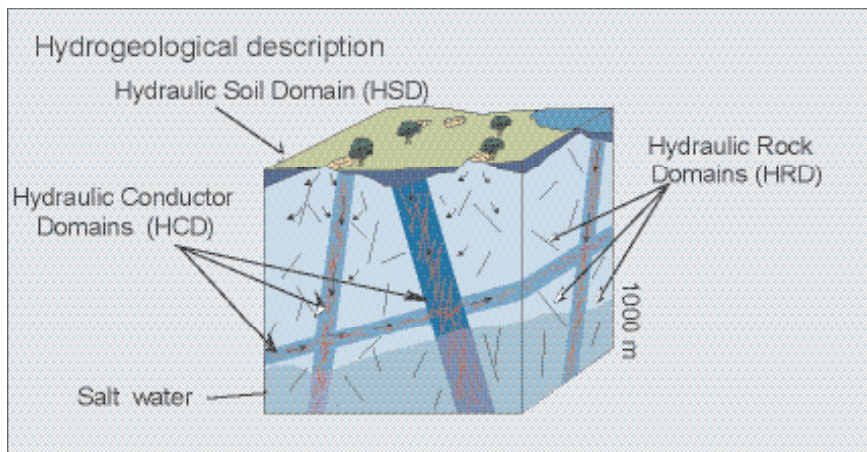


Figure 8-23. Division of the crystalline bedrock and the overburden (Quaternary deposits) into hydraulic domains representing the overburden (HSD) and the rock mass volumes (HRD) between major fracture zones (conductors, HCD). Within each domain, the hydraulic properties are represented by equivalent values, or by spatially distributed statistical distributions /Rhén et al. 2003/.

From a hydrogeological perspective, the geological data and related interpretations constitute the basis for the geometrical modelling of the different hydraulic domains. Thus, the investigations and documentation of the bedrock geology and the overburden (Quaternary deposits) provide input to:

- The geometry of deterministic deformation zones (HCD) and the bedrock in between (HRD).
- The distribution of Quaternary deposits (overburden, HSD), including genesis, composition, stratification and thickness.

Likewise, the investigations and documentation of the present-day meteorology, hydrology and near-surface hydrogeology (in terms of mapping of springs, wetlands and streams, surveying of land use (ditching and dam projects), resources for water supply, etc), together with the shoreline displacement throughout the Holocene, cf. Chapters 3 and 4, constitute the basis for the hydrological process modelling. This information provides input to:

- Present-day interpretation of drainage areas, as well as the distribution of recharge and discharge areas.
- Estimates of the average present-day precipitation and run-off, distribution of hydraulic head and flow in watercourses.
- Estimates of boundary conditions since the last glaciation.

Results from hydraulic borehole investigations and monitoring are of interest for the assignment of hydraulic properties to the different hydraulic domains. There are basically two main sources of information for the assignment of hydrogeological properties:

- Hydraulic tests and hydrogeological monitoring in deep boreholes within the Forsmark area, cf. Section 8.2.
- Hydraulic tests and other hydrogeological observations in boreholes drilled in the overburden (Quaternary deposits) in the Forsmark area, cf. Chapter 4.

Hydrogeological interpretation and analysis form the hydrogeological part of the site descriptive model. The work has three main parts:

- Primary interpretation of hydrogeological data.
- Integrated evaluation between disciplines to obtain consistent models.
- Groundwater flow simulations for testing and evaluating the implications of the site descriptive model.

8.3.3 Modelling strategy

The modelling strategy for the HCDs is pretty straight forward, as the HCDs generally correspond to important large features, such as deterministically treated deformation zones defined by geology. This means that the uncertainty of the geometry of the HCDs is fairly low in the target volume (cf. Chapter 5). Still, the HCD properties may be modelled in different ways due to hydraulic uncertainties. The alternatives here are broadly characterised as homogeneous (constant values), as semi-heterogeneous (values according to defined spatial trends) or as heterogeneous (stochastic values).

It is noted that the geological uncertainties increase when the size of the objects treated deterministically decreases. The geological uncertainties are also larger in areas not well covered by surface mapping and drillings, e.g. under the Baltic Sea. These uncertainties, and many more, call for alternative deterministic structural models as the groundwater flow occurs on all scales, regional and local, in particular in a coastal region as Forsmark where the boundary conditions are continuously changing due to the ongoing shoreline displacement.

The modelling strategy for the HRDs is more complex and consists of several alternative approaches. This is because of the greater uncertainties involved as the description of the bedrock structure becomes more detailed. The HRDs represent the rock between the HCDs, generally coinciding with the lithological rock domains defined by geology. Several rock domains may be merged into one HRD or one rock domain may be divided into several HRDs depending on the hydraulic complexities.

The HRD properties may be modelled in a similar way to those of the HCD, i.e. as homogeneous or heterogeneous. The simplest homogeneous case (from a hydrogeological point of view) is that of a low-conductive uniform continuous porous medium and the most complex heterogeneous case is a fractured rock where the geometric properties do not lend themselves to be simulated by means of simple statistical distributions. The moderately heterogeneous case can be more or less elaborated ranging from complex Discrete Fracture (or Pipe) Network (DFN) realisations or Equivalent Porous Media representations thereof (EPM), as an ergodic Stochastic Continuum (SC) representation, or simply as a composite system consisting of several different Continuous Porous Media (CPM). The premises of different model representations (DFN, EPM, SC or CPM) is an essential part of the overall hydrogeological uncertainty assessment and different conceptions may or may not be used in parallel dependent on the objectives and scale of the flow problem treated.

Figure 8-24 illustrates the workflow of the Equivalent Porous Medium representation of a complex hydrogeological Discrete Fracture Network realisation (hydrogeological DFN). The details of the workflow shown in Figure 8-24 may be described as follows.

1. *A hydrogeological DFN analysis is carried out based on core mapping data, PFL and PSS test data and pump test data.*
2. *The output parameters (connected fracture intensity and fracture transmissivity) are applied to a geological DFN model (characterised by fracture orientation, size, geological intensity and spatial distribution) to estimate block size hydraulic parameters and to analyse possibilities for anisotropy in flow.*
3. *The block size simulations are requested by Repository Engineering, but are useful also for the inclusion of the hydrogeological DFN findings into a regional scale groundwater flow model. In the latter case, Equivalent Porous Media (EPM) parameters are calculated on the scale of the computational grid resolution.*
4. *The EPM model is combined with the models defined for the HCDs and HSDs and calibrated against hydraulic test data and hydrogeochemical data, e.g. chemical elements (salinity), water types, or natural isotopes.*
5. *The calibrated EPM regional model is used for sensitivity analyses of ground water flow paths and transport of solutes.*

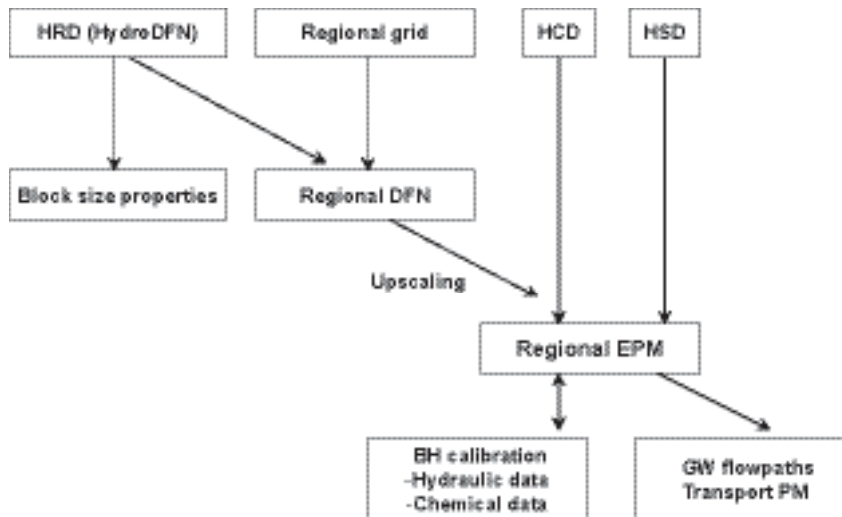


Figure 8-24. Workflow of the hydrogeological modelling. Modified after /Hartley et al. 2005/.

The modelling strategy used for version 1.2 follows to a large extent the workflow shown in Figure 8-24. The details of the modelling approaches used by the two modelling teams are presented in /Hartley et al. 2005/ and /Follin et al. 2005/.

It is noted that the outcome of the initial component, the hydrogeological DFN analysis, has strong implications for the subsequent parts of the workflow as it affects the computation of block size properties and the assignment of parameter values on the scale of the computational grid resolution. Depending on the DFN properties alternative descriptions may or may not be advocated/needed, e.g. EPM, SC and CPM. Apart from this complexity, the workflow is unchanged in this alternative approach.

8.3.4 Hydrogeological DFN

Recognising the important role of the output of the hydrogeological DFN analysis for the workflow shown in Figure 8-24, it is equally important to reveal the assumptions invoked in the DFN analysis. Both modelling teams used numerical simulations with multiple geological DFN realisations around a hypothetical borehole for their analyses. Below, the basic concepts and assumptions invoked by the two modelling teams are outlined. The specific results for version 1.2 are commented on in Section 8.4.3. It is stressed that the assumptions made are due to the huge size of the regional model domain treated in version 1.2. On a local scale a better resolution of the flow modelling is required and some of the assumptions have to be revised.

Conductive features and modelling methodologies

Both modelling teams considered initially all naturally Open and Partially Open fractures, regardless of their geological confidence (Certain, Probable and Possible), to be potential candidates for flow from the onset in the connectivity analysis. Sealed fractures, on the other hand, were considered impervious. This simplification is known to be incorrect on the scale of the fracture aperture, but, as already stated, mainly due to the scale of the problem treated.

An Open fracture is by definition associated with a naturally broken core, i.e. the natural fracture is as large as or larger than the core diameter. Consequently, a Partly Open fracture is by definition a fracture that does not break the core, but still have some kind of aperture associated to it. According to (SKB MD 143.008), all Partly Open fractures are mapped to the extent possible. In effect, Partly Open and Open fractures are treated alike as they both contribute to the fracture intensity (borehole fracture frequency P_{10}).

/Follin et al. 2005/ analysed the geometric connectivity of the geological DFN realisations and tried a hypothesis where the transmissivities interpreted from the PFL-f tests were associated to the largest interconnected fractures intersecting the borehole in each realisation. In comparison, /Hartley et al. 2005/ used a radial flow model and calculated the percentage of Open and Partly Open fractures needed in order to match the interpreted PSS and PFL transmissivity distributions in a statistical sense. The unconditional statistical matching conducted by /Hartley et al. 2005/ was carried out for three different transmissivity models. The analysis by /Follin et al. 2005/ treated one of these transmissivity models.

Deformation zones and conductive features

Large fractures of trace lengths on the order of 100 m may exist as single breaks. However, it is more common that discontinuities of trace lengths greater than about 50 m exist as deformation zones or ‘fracture swarms’. A number of fracture swarms are observed in the boreholes. Some of the swarms are modelled as deterministic deformation zones, other as uncertain (i.e. stochastic) deformation zones. Hence, it is useful to characterise these features to get some indication of the width and fracture intensities within these zones. However, at this regional modelling stage, fracture swarms interpreted as certain or uncertain deformation zones will be approximated as large fracture planes in a continuous range of fracture sizes, as shown in Figure 8-25. It is important that data, such as fracture intensity and the PFL-f flow anomalies, are handled in a manner consistent with this concept. Also, transport parameters, such as fracture porosity and flow-wetted surface, may have to be enhanced in the larger fractures to reflect their zonal characteristics.

Figure 8-25 implies that the fracturing within a given deformation zone is not studied in terms of its components, but treated as one single object. Both (minor) stochastic and interpreted deterministic deformation zones are treated in the same way.

If N_{TOT} is the total number of Open and Partly Open fractures in a borehole and N_{DZ} is the number of Open and Partly Open fractures in an intercepted stochastic deformation zone, the remaining number of potentially flowing Open and Partly Open fractures in the borehole to be matched in the modelling process N_{CAL} may be written as:

$$N_{CAL} = N_{TOT} - \sum (N_{DZ} - 1) \tag{8-1}$$

The summation in equation (8-1) is made over all intercepted stochastic deformation zones. The subtraction by 1 is made as the zone itself is one feature to be included in the modelling process. This is found to be important in cases where the rock is sparsely fractured. In analogy with equation (8-1) the transmissivity of a potentially flowing stochastic deformation zone is considered equal to its geological thickness-hydraulic conductivity product and the storativity is equal to its geological thickness-specific storativity product. This implies that the transmissivity of a stochastic deformation zone, as determined at its intersection with a borehole, is equal to the sum of the transmissivities of the flowing fractures:

$$T_{DZ} = \sum (T_f) \tag{8-2}$$



Figure 8-25. An important assumption in the hydrogeological DFN analysis is the representation of fracture swarms (zones) as single planar features /Follin et al. 2005/.

The summation in equation (8-2) is made over all PFL-f anomalies belonging to the intercepted stochastic deformation zone. In case of heterogeneous deformation zone properties, equivalent homogeneous values are considered. It is noted that equation (8-2) may overestimate the deformation zone transmissivity T_{DZ} if the flowing fractures intersecting the borehole merge at some distance away from the borehole. The similarity in results between the aforementioned test methods, the difference flow logging (PFL) and the double-packer injection tests (PSS), does not indicate that this is a major problem, however.

Spatial distribution of conductive features

The spatial pattern of *all* Open and Partly Open fractures in the rock mass outside the deformation zones is assumed to be Poissonian in the geological DFN. However, the resulting spatial pattern of the connected Open and Partly Open fracture network may be non-Poissonian. The discrimination of isolated features in a Poissonian simulation model leads to a connected network of features that is governed by the positions of the largest features.

Flow in conductive features

Conductive features are assumed to be completely flat surfaces with homogenous macroscopic hydraulic properties, i.e. transmissivity T_f and storativity S_f . In case of heterogeneous fracture properties, equivalent homogeneous (effective) values are considered. In reality, the flow is distributed through channels across the fracture plane. Possibly, also intersections between fractures can be considered as potential channels. The physical channels are formed by the undulating fracture surfaces (spatial distribution of the fracture asperity) that do not exactly match, thus creating channels. The distribution of flow channels is, however, governed by the acting boundary conditions, which may be transient (cf. Figure 8-20). The flow channels in the fracture plane occupy only a minor part of the fracture volume, and parts of the fracture surface are closed due to its undulating nature.

Exchange of solutes to stagnant pools of water, outside the flow channels, is governed by diffusion in more or less free water, which is faster than the diffusive exchange with the rock matrix. It can also be expected that parts of the fracture are filled with fault gouge material, i.e. fine-grained, clayey material. All these characteristics cannot, and need not always, be modelled in detail, but must be approximated in some way. For the diffusion processes, DarcyTools uses a multi-rate diffusion model (diffusion of different rates) and ConnectFlow, a single-rate diffusion process (presently the most well-known approach). Details on how these processes are treated in DarcyTools are provided by /Svensson et al. 2004; Svensson and Ferry, 2004; Svensson, 2004/ and in ConnectFlow by /Hartley et al. 2003a,b; Hartley and Holton, 2003; Hoch and Hartley, 2003; Hoch et al. 2003/.

Size distribution of conductive features

One of the most difficult fracture characteristics to measure directly in the subsurface is fracture size. Fracture trace lengths can be measured on outcrops for fractures on the scale of metres to tens of metres, and data are available for lineaments on the scale of 500 m to several kilometres, but this leaves a gap between the scales. A widely used assumption in geology is one of a continuum of fracturing that spans all scales and that can be described by a power-law relationship between fracture intensity and size. That is, if the slope of the parent size distribution in 3D is k_r , in a complementary cumulative density function plot then the slope of the fracture intensity (fracture area per unit volume) versus size on a log-log plot is $(k_r - 2)$.

A schematic illustration of a power-law relationship is shown in Figure 8-26 and is compared with a log-normal distribution, which is another commonly used model for fracture size. The key parameters of the power-law relationship providing the number of features of different sizes are the slope k_r and the reference size, X_{r0} . The distribution is often used only in a truncated range, $X_{r,min} < X_r < X_{r,max}$.

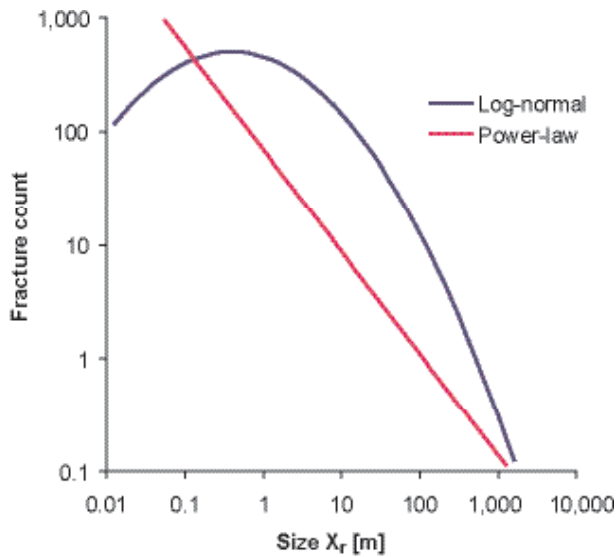


Figure 8-26. Example of a power-law and a log-normal fracture size distribution. When a fracture network is simulated, it is often necessary for practical reasons to truncate the distributions and use data between a lower and upper limit. Modified after /Hartley et al. 2005/.

The size distributions used for the different fractures sets modelled by geology for version 1.2 are all power-law distributed, but with different slopes and reference sizes. Figure 8-27 illustrates the conceptual relationship between the deterministically treated deformation zones and the stochastic geological DFN using a power-law size distribution.

It is noted that fracture shapes are modelled as squares with a side length L by both /Hartley et al. 2005/ and /Follin et al. 2005/, whereas fracture shapes are modelled as circles in the geological DFN model provided by /La Pointe et al. 2005/. The parent fracture radius in the geological DFN model is denoted by X_r , and the reference radius by X_{r0} . The latter varies between 0.14 m to 0.28 m, see Section 5.5. The transformation needed when comparing details in the different studies is that of an equivalent area:

$$X_r = L / \sqrt{\pi} \quad (8-3)$$

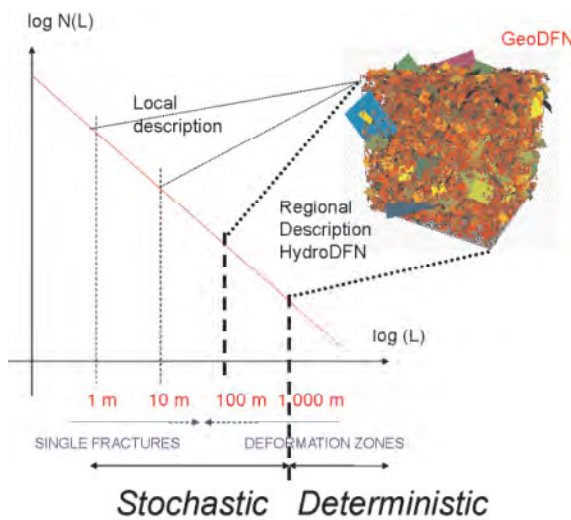


Figure 8-27. Illustration of the power-law size distribution and the conceptual relationship between deterministically treated deformation zones and the stochastic geological DFN /Follin et al. 2005/.

Reference size of conductive features

The reference size of all Open and Partly Open fractures is a difficult issue as the numbers of features increase significantly for a power-law distribution when the sizes of features get smaller, cf. Figure 8-27. Observations of fracture trace lengths on outcrops down to 0.5 m can generally be mapped, whereas a lower cut-off becomes quite cumbersome. The issue is not trivial as one of the significant differences between a log-normal model and a power-law model is in the lower end, see Figure 8-26.

Most probably one cannot observe very small fractures on rough outcrop surfaces but, if present, they will probably show up more easily in the cored borehole as the scale of resolution here is on the order of the borehole radius and the surface is very smooth. Therefore, one should test different assumptions and see what the implications are. Two assumptions have been tested.

1. The number of Open and Partly Open fractures seen in a cored borehole (the geological fracture intensity) is assumed to be in proportion to the size of borehole diameter, which is 0.076 m. The equivalent square thus is 0.067 m. This assumption was tested by /Follin et al. 2005/, who tested other settings as well.
2. The number of Open and Partly Open fractures seen in a cored borehole (the geological fracture intensity) is assumed to reflect intercepts with fractures larger than the borehole diameter. This assumption was tested by /Hartley et al. 2005/ who assumed a radius of 0.282 m, i.e. an equivalent square of 0.5 m. This setting was also tested by /Follin et al. 2005/.

Assuming a Poissonian point distribution for the positions of the fracture centres and circular shaped fractures of reference radius X_{r0} the equivalent trace length reference value is $X_{l0} = (\frac{1}{2} \pi X_{r0})$. For example, a reference trace length of 0.443 m corresponds to a fracture radius of 0.282 which according to equation (8-3) corresponds to a square of 0.5 m. It should be noted that the cut-off value used in the trace mapping on outcrops, 0.5 m, is not equivalent to X_{l0} . Still, the calculation shows the order of magnitudes involved.

It is vital to note that the conversion from borehole fracture frequency P_{10} to fracture area per unit volume P_{32} is insensitive to the size of the reference fracture simulated X_{r0} provided that the borehole used for the statistical matching of simulated versus observed borehole fracture frequency is treated as a scan line, i.e. $r_w = 0$. In contrast, if the borehole used for the statistical matching is simulated as a cylinder with a finite radius, a portion of all fractures intersecting the perimeter of the cylinder will not intersect the scan line, i.e. the centre line. In effect, it is necessary to adjust the fracture area per unit volume P_{32} to retain the match to the observed borehole fracture frequency P_{10} .

The sensitivity to the borehole radius was commented by /Follin et al. 2005/, who noted that it makes a significant difference if the smallest fracture radius is set to 0.038 m or 0.282 m (cf. the two assumptions listed above). This observation raises concerns about the procedures used for fracture mapping and simulation of Partly Open fractures, as these may not necessarily intersect the scan line (the centre of the borehole diameter).

According to the geological DFN model /La Pointe et al. 2005/, the borehole fracture intensity P_{10} associated with Partly Open fractures in RFM029 is c. 8% of the total P_{10} of Open and Partly Open fractures in this rock domain. Recognising the conceptual difficulties associated with the mapping of Partly Open fractures and the relatively large number of Partly Open fractures seen in the cored boreholes it is obvious that the fracture mapping procedures and the techniques used to simulate and condition borehole fracture intercepts have to be consistent. This becomes even more important as c. 9% of the PFL flow anomalies may be associated with what are mapped as Partly Open fractures, see /Forsman et al. 2004/.

Transmissivity of conductive features

A transmissivity model is required in addition to the geometrical properties of the DFN. An important topic for hydrogeology concerns the tentative relationship between the transmissivities of conductive features and the transmissivities deduced from hydraulic single-hole tests. As previously mentioned in Section 8.2.1, the assumption made in version 1.2 is that the key hydraulic entity deduced from the use of traditional hydraulic test interpretation models, the radial transmissivity,

is relevant for forward modelling of the heterogeneity and anisotropy of undisturbed groundwater flow and salt transport in fractured rocks.

Transmissivity data from single-hole tests often show a wide range of variability and it is common to use statistical distributions for the fracture transmissivity assignment, e.g. the power-law distribution or the log-normal distribution (Figure 8-26). Figure 8-28 shows an example where PFL-f transmissivity data from KFM03A are plotted in a complementary cumulative density function (CCDF) plot and in log-normal cumulative density function (CDF) plot, respectively. The straight lines fitted indicate the level by which data above the lower measurement limit conform to the tested distributions. The behaviour seen in Figure 8-28 is quite characteristic for flow in sparsely fractured rocks.

- It is generally quite difficult to discriminate between a power-law fit versus a log-normal fit (the question if it is necessary to make the distinction in version 1.2 is commented on below).
- There is a substantial amount of data below the lower measurement limit, which, in fact, is a decisive piece of information for the conceptual modelling. A vital component for the statistical fitting shown in Figure 8-28 is the determination of the number of connected fractures below the lower measurement limit.

From a statistical point of view, the assignment of transmissivities to the discrete features can be made in an uncorrelated, correlated or semi-correlated fashion. From a hydraulic perspective, however, one can advocate that a correlated model is more logical. This comes from the consideration that hydraulic test transmissivities of different magnitudes have different scales of support, i.e. radius of influence. In other words, a hydraulic test in a feature of high transmissivity implies a large radius of influence and vice versa. If the physical radius (size) of the high transmissive feature is less than its theoretical hydraulic radius of influence, the hydraulic test will sensor this limitation as a physical boundary and in effect a lower transmissivity may be interpreted if the “boundary” is constraining the flow.

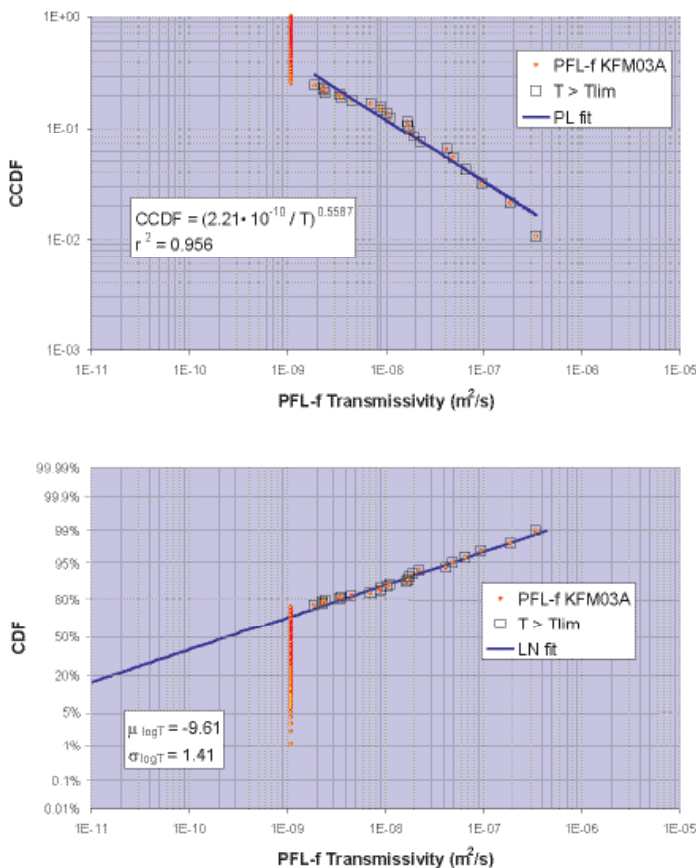


Figure 8-28. Example of a power-law fit and a log-normal fit of PFL-f transmissivity data. The data in the plot come from the rock between the deformation zones in KFM03A /Follin et al. 2005/.

An important difference between the hydrogeological DFN modelling conducted for version 1.1 and the modelling conducted in version 1.2 concerns the transmissivity models analysed. In version 1.1, a direct correlation between fracture transmissivity and radius was assumed. In order to illustrate the implications of this assumption, three alternative models were considered for version 1.2, see Figure 8-29:

1. Transmissivity is uncorrelated to fracture radius X_r , but with a specified log-normal variability (mean, μ , and standard deviation σ of $\log_{10}(T)$);

$$T = 10^{N(\mu, \sigma)} \quad (8-4a)$$

2. Transmissivity is correlated to fracture radius X_r without variability (by a factor, a , and an exponent, b);

$$T = a (X_r)^b \quad (8-4b)$$

3. Transmissivity is semi-correlated to fracture radius X_r with a specified random log-normal variability about a mean based on a correlated function (factor, a , exponent, b , and standard deviation, σ);

$$T = 10^{\left[\log_{10} \left(a (X_r)^b \right) + \sigma N(0,1) \right]} \quad (8-4c)$$

Each of the three concepts has an associated set of parameters, as given in the brackets above, and it is the objective of the hydrogeological DFN to explore what ranges of parameters required in the DFN simulations to give a match to the hydrogeological data. The second relationship was proposed in /Dershowitz et al. 2003/. One argument for it is that, at least for deformation zones, the zone width often increases with size (length), and thus generally so does the number of individual conductive fractures associated with a zone (cf. Figure 8-25). If the transmissivity distribution for individual fractures is the same, then based on the above assumption it follows that the effective transmissivity for the fracture zone should increase with the size of the fracture zone.

/Hartley et al. 2005/ treated all three models, whereas the connectivity-based approach used by /Follin et al. 2005/ was restricted to treat the correlated model (2). However, as there is variability between stochastic realisations there will be uncertainty also in the correlated model simulated by /Follin et al. 2005/. Although the final model has unique values of a and b , a semi-correlated model could in fact be produced as an alternative. In contrast, the semi-correlated model (3) specifies this variability a priori.

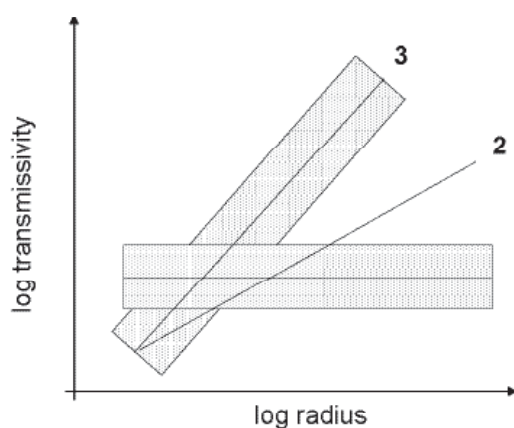


Figure 8-29. Schematic of transmissivity models: 1) Uncorrelated with a specified uncertainty; 2) Correlated without specified uncertainty; 3) Semi-correlated with a specified uncertainty.

Transmissivity limit and connectivity of conductive features

The most transmissive of the potentially flowing Open and Partially Open fractures are assumed to be detected by the Posiva Flow Log, i.e.:

$$N_{PFL} \leq N_{CAL} \tag{8-5}$$

N_{PFL} refers to the number of PFL-f flow anomalies above the lower measurement limit and N_{CAL} is the number of potentially conductive features as defined in equation (8-1). An important component of the connectivity-based approach used by /Follin et al. 2005/ is the determination of N_{CON} , i.e. the geometrically connected feature intensity. N_{CON} is determined by sorting out all isolated features and isolated clusters of features. The probabilistic framework between the simulated connected feature intensity and the interpreted transmissivities is illustrated in Figure 8-30. The intuitive relationship between N_{PFL} , N_{CON} , N_{CAL} and N_{TOT} becomes:

$$N_{PFL} \leq N_{CON} \leq N_{CAL} \leq N_{TOT} \tag{8-6}$$

/Hartley et al. 2005/ did not specifically deal with the geometric connectivity of the generated geological DFN realisations, but computed the number of features needed in order to match (in a statistical sense) the interpreted transmissivity distributions above the lower measurement limit. As the numbers of PFL-f anomalies above the lower measurement limit is quite sparse in version 1.2, this approach made more use of the PSS hydraulic data that often have a lower practical measurement limit than the PFL data.

However, since the PSS data are only available as transmissivity of 5 m long intervals rather than as flow rates in individual fractures, it was necessary to compare simulated flow rates in fractures in a consistent way. This was achieved by inferring a transmissivity for each flowing fracture that intersects the borehole in the model using Dupuit's formula, and then grouping them according to the positions of the 5 m intervals for which PSS data were supplied. The transmissivity of the measured PFL-f anomalies was converted in the same way for comparison.

Once the simulation model had been matched against the measured transmissivity distributions for PSS and PFL-f on a 5 m scale, then the unconditional fit was cross-checked on flow-rate, Q , of individual fractures from the PFL-f analyses.

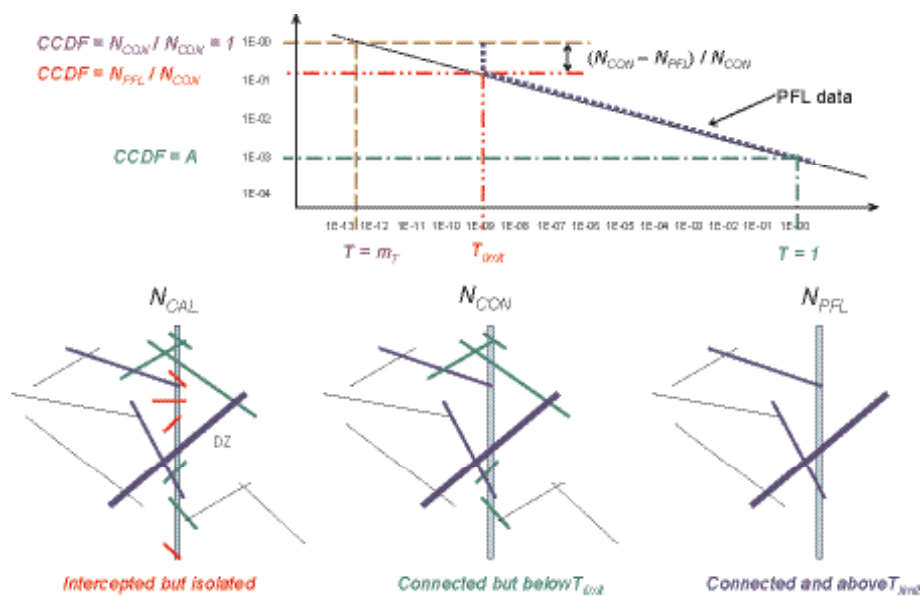


Figure 8-30. Top: Illustration showing how the CCDF plot of the measured fracture transmissivities is used together with information about $N_{PFL} \leq N_{CON} \leq N_{CAL} \leq N_{TOT}$. Bottom: Illustration showing the concepts behind N_{CAL} , N_{CON} and N_{PFL} /Follin et al. 2005/.

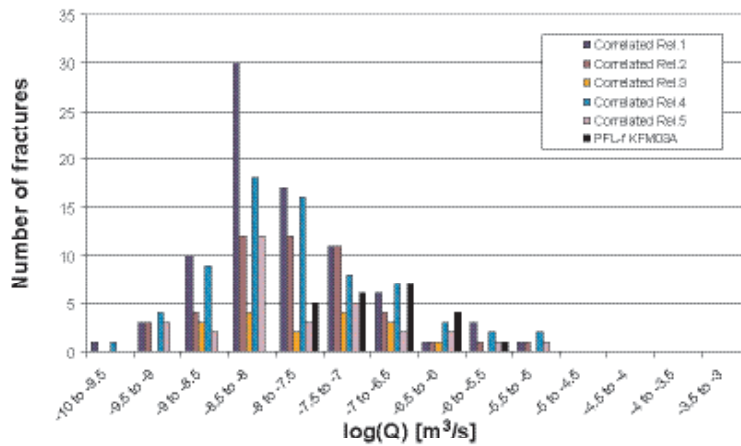
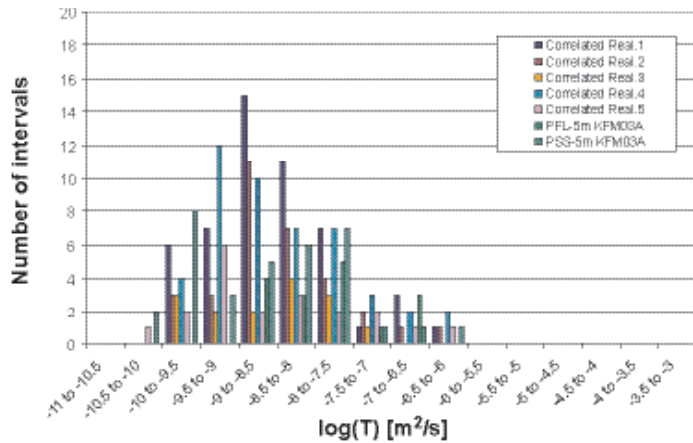


Figure 8-31. Two plots showing the statistical matching of flow simulations against measured data made by /Hartley et al. 2005/. Upper: Histogram showing the conditioning of the simulated transmissivity distribution against the measured transmissivity distributions for PSS and PFL-f on a 5 m scale. Lower: Histogram showing the subsequent cross-check on the simulated flow-rate distribution of individual fractures against the flow-rate distribution from the PFL-f analyses. All data refer to borehole KFM03A.

Figure 8-31 shows an example of the procedure used by /Hartley et al. 2005/. The upper plot shows the unconditional matching of simulated transmissivity distribution against the measured transmissivity distributions for PSS and PFL-f on a 5 m scale. The lower plot shows the subsequent cross-check on flow-rate, Q , of individual fractures from the PFL-f analyses. The cross-checking was also made in a statistical sense. The data shown in Figure 8-31 refer to hydraulic tests conducted in between the deterministically treated deformation zones in KFM03A.

Intensity correction of conductive features

To mitigate against under-predicting the intensity of fractures sub-parallel to the borehole trajectories it is common practice to use the Terzaghi correction method. This method applies a weighting factor for each fracture that is calculated based on the angle (θ) between the pole to the fracture plane and the borehole trajectory. An alternative procedure is to carry out explorative simulations for one fracture set at the time, assuming a linear relationship between the three dimensional fracture intensity P_{32} (fracture area per unit volume) and the borehole fracture intensity P_{10} (fractures per unit length). The latter approach was used by /La Pointe et al. 2005/.

The Terzaghi correction method was applied by the two hydrogeological modelling teams as it provides a rapid means for correcting all sets simultaneously. Moreover, the general experience is that the computed $P_{10,corr}$ values provide a good first guess of the desired three dimensional fracture intensity P_{32} .

An alternative correction factor was proposed by /Darcel et al. 2004/ posterior to Simpevarp 1.2 for the case where the fractures encountered in the borehole are dominated by small ones with sizes comparable to the borehole diameter. Based on a power-law size model, they proposed a correction factor around $1/(\cos(\theta))^3$ for Simpevarp data, which emphasises the steeply dipping fractures more, and perhaps gives more consistency when comparing the relative intensity of fracture sets measured in boreholes against outcrops. The significance of this alternative correction factor was not evaluated in the hydrogeological DFN modelling for version 1.2.

8.3.5 General assumptions regarding block size properties

The objectives for the hydraulic block property task can be summarised as follows:

- Calculate the statistics of the hydraulic conductivity, including the anisotropy, of 100 m and 20 m blocks using the results of the hydrogeological DFN analysis.
- Include DFN porosity in the block calculations.
- Evaluate effects of size-truncation of stochastic features and cell-background properties (to be added to cells after applying the hydrogeological DFN) to determine the minimum fracture size that can be used in the regional DFN models.

The main modelling assumptions in the studies performed for version 1.2 were:

1. The hydraulic conductivity in the host rock is completely dominated by the connected fracture system and can be modelled by the DFN concept.
2. Flow within fractures can be approximated by Darcy's law.
3. The heterogeneity between blocks on a specified scale can be modelled by calculating the hydraulic conductivity of an array of sub-blocks within a much larger domain (as big as the largest stochastic fracture, and ten times the block size) and use this as an ensemble.
4. Fracture transmissivity can be described by one of three alternative models.
5. Fracture kinematic porosity (transport aperture) is correlated to fracture transmissivity as envisaged by Äspö Task Force – Task 6 /Dershowitz et al. 2003/.

8.3.6 General assumptions regarding HCD, HRD, HSD, initial and boundary conditions

The primary concepts and assessments used in the regional scale groundwater flow modelling are:

- The current hydrogeological and hydrogeochemical situation in Forsmark is the result of natural transient processes that have evolved over the post-glacial period beginning at c. 8,000 BC.
- The integration with hydrogeochemistry can be evaluated by assuming appropriate initial and boundary condition for the advective flow of different types of particles representing, ideally, the reference waters treated by hydrogeochemistry – Rain 1960, Brine, Littorina and Glacial – using the reference water fractions as conservative tracers.
- The natural transient processes (land-rise, marine transgressions, dilution/mixing of sea water) can be modelled by appropriate choice of flow and reference water boundary conditions,
- The spatial variability of hydraulic properties of the HRDs that conform to the assumption of a flowing DFN can be correctly represented by means of an Equivalent Porous Media (EPM) model by choosing a suitable grid resolution in combination with appropriate upscaling algorithms,
- The low-conductive HRDs that cannot be clearly associated with a flowing DFN above the measurement limit for transmissivity can be correctly represented by one or several Continuous Porous Media (CPM) models,
- The HCDs can be treated as homogeneous (constant values), as semi-heterogeneous (values according to defined spatial trends) or as heterogeneous (stochastic values),
- For the hydraulic surface domains (HSD), the properties (hydraulic conductivity, thickness, and porosity) may be treated in a simplistic fashion with homogeneous properties over the whole top surface of the model.

8.4 Assignment of hydraulic properties

The hydraulic tests conducted in the overburden and in the bedrock constitute the basis for assigning preliminary hydraulic properties to the defined geological domains. Vis-à-vis the property assignment of the HSDs and the HCDs, the property assignment of the HRDs is associated with a larger uncertainty. The reason for this is twofold, (i) the stochastic nature of the geometry of the underlying geological DFN, and (ii) the scarce amount of hydraulic information about the large volumes of rock that are of interest. In effect, the hydraulic properties of the HSDs and HCDs are assigned in a more or less direct fashion as the geometries are predetermined, whereas the hydraulic properties of the HRDs are assigned by means of numerical simulations that invoke an unconditional statistical matching against available data – both geometric and hydraulic. The matching process is named hydrogeological DFN analysis, the major assumptions of which are described in Section 8.3.5.

8.4.1 Assignment of hydraulic properties to the HSDs

The hydrogeology of the overburden (predominantly Quaternary deposits) is described in Chapter 4. The overburden in the Forsmark area is dominated by sandy till, except in the south east where more clayish conditions pertain. In small parts of the area, eskers with coarse grained material are found. In raised areas or on small islands, the thickness of the till is small or the rock is out-cropping. The thickness of the clayish till can be quite large, the maximum thickness recorded so far is c. 17 m, but the average depth is probably of the order of a couple of metres. The average thickness of the sandy till is probably even less. The outcrop areal coverage within the terrestrial part of the regional model domain is c. 13%.

It is noted that the detailed hydrogeological conditions in large parts of the regional model domain are essentially unknown, but that existing data suggest a considerable heterogeneity. For the bedrock hydrogeological modelling it was decided to work with a simplistic description of the near surface hydrogeological conditions. The simplification was further motivated by the need of a sufficient detailed description of the bedrock conditions at depth, which put constraints on the numerical modelling. Hence, a good geometric and hydraulic description of the bedrock conditions at depth within the regional model domain $15 \times 11 \times 2.1$ km was prioritised. In conclusion, it was decided to assume a thin layer of sandy till except in small discrete areas where the bedrock is outcropping.

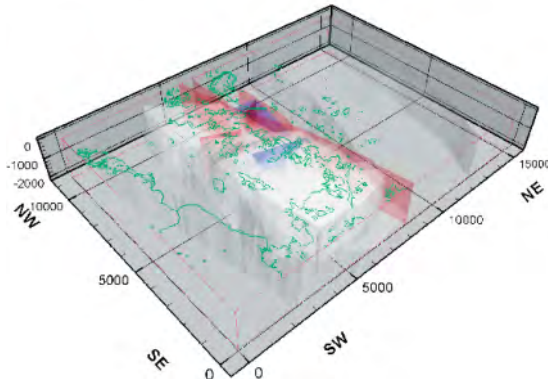
The surface properties were represented explicitly in the model and properties were assigned to each element according to whether the element is predominantly covered by till or outcrop. The outcrop map was provided on a 10 m resolution. A main alternative, denoted by HSD1, with homogeneous properties over the entire model domain was used away from the outcrops. The HSD1 properties were as follows: a constant thickness of 4 m sandy till with homogeneous values for the hydraulic conductivity $K = 7.5 \times 10^{-6}$ m/s, the kinematic porosity $n_e = 0.05$, and the specific storativity $S_s = 1 \times 10^{-4}$ m⁻¹. A variant, HSD2, with three layers was also considered by /Hartley et al. 2005/. The uppermost layer of HSD2 had a thickness of 1 m, $K = 1.5 \times 10^{-5}$ m/s, $n_e = 0.1$ and $S_s = 1 \times 10^{-4}$ m⁻¹; the second layer had a thickness of 2 m, $K = 1.5 \times 10^{-6}$ m/s, $n_e = 0.05$ and $S_s = 1 \times 10^{-4}$ m⁻¹; and the third layer has a thickness of 1 m, $K = 1.5 \times 10^{-5}$ m/s, $n_e = 0.05$ and $S_s = 1 \times 10^{-4}$ m⁻¹. The values of the hydraulic conductivity data were based on the slug test results reported by /Werner and Johansson, 2003/, see Chapter 4. The values for the kinematic porosity and the specific storativity are generic and estimated from /Knutsson and Morfeldt, 2003/.

8.4.2 Assignment of hydraulic properties to the HCDs

The assignment of hydraulic parameter values to the three deterministic structural models presented by geology, i.e. the base model (Base Case, BC), the alternative model (Alternative Case, AC) and the base variant model (Variant Case, VC), was based on the data presented in Table 8-6. The BC and VC models consist of 44 deterministically treated deformation zones, whereas the AC model consists of 215 deterministically treated deformation zones. In version 1.2, every deterministically treated deformation zone was assigned hydraulic properties, thus synonymous to a hydraulic conductor domain.

Historic data available at the time of model version 0 /SKB, 2002a/ provide data for about seven of the 44 HCDs of the BC model. The corresponding figure from version 1.1 /SKB, 2004a/ is twelve, i.e. seven plus five. In comparison, version 1.2 treats data for all together 28 HCDs. A demonstration

F1.1 - HCDs



F1.2 - HCDs

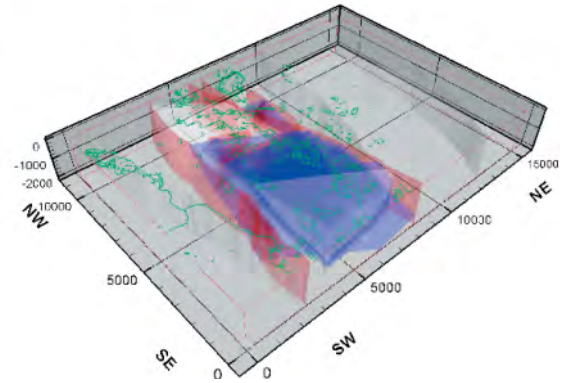


Figure 8-32. Two views showing the difference in hydraulic information between model versions 1.1 and 1.2 with regard to the version 1.2 base model. All deformation zones were treated as HCDs. Red shades are steeply dipping HCDs that are hydraulically tested and blue shades are gently dipping HCDs that are hydraulically tested. White shades indicate that the HCDs in question are not tested hydraulically /Follin et al. 2005/.

of the difference in information between versions 1.1 and 1.2 is schematically illustrated in Figure 8-32, which shows a perspective view of the regional model domain with the 44 HCDs as translucent shades. Red shades are steeply dipping HCDs that are hydraulically tested, and blue shades are gently dipping HCDs that are hydraulically tested. White shades indicate that the HCDs in question are not tested hydraulically.

The measured HCD properties are shown in the scatter plot in Figure 8-22. In order to handle the variability and complexity of the information, three different cases, HCD1, HCD2 and HCD2, were suggested. In HCD1, the initial approach, different deterministic spatial trends were assumed for the gently and steeply dipping deformation zones in the numerical simulations:

$$T_G (\text{Depth}) = \max(4.1 \cdot 10^{-4} \exp(-0.0116 \text{ Depth}), 1 \cdot 10^{-8}) \quad (8-7a)$$

$$T_S (\text{Depth}) = \max(4.6 \cdot 10^{-5} \exp(-0.0174 \text{ Depth}), 1 \cdot 10^{-8}) \quad (8-7b)$$

The exponential regression models shown in equations (8-7a) and (8-7b) indicate tendencies among the data plotted only and do not prove that the deformation zones become impervious at greater depth. There may still be several transmissive zones at depth. The two deterministic trends are plotted in Figure 8-33. Note that both trends were halted at $1 \times 10^{-8} \text{ m}^2/\text{s}$.

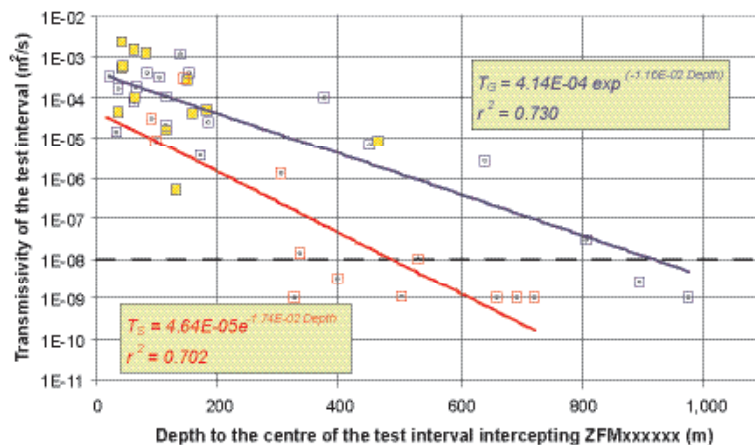


Figure 8-33. Replicate of Figure 8-22 with the addition of two depth trends. Red squares indicate steeply dipping HCDs and blue gently dipping. Blue squares with a yellow infilling refer to the hydraulic test interpretations associated to the gently dipping deformation zone ZFMNE00A2 /Follin et al. 2005/.

A semi-homogeneous HCD2 case was applied to the VC model. A constant (non-trending) transmissivity value of 1×10^{-5} m²/s was assigned to the dominating deformation zones in the area, i.e. the steeply dipping regional deformation zones known as Forsmark, Eckarfjärden and Singö deformation zones, plus four of the gently dipping local major deformation zones denoted by ZFMNE00A1, -A2, -C1 and -C2, respectively. (In the VC model the four gently dipping local major deformation zones are extended until they terminate against the Forsmark deformation zone.) All other deformation zones were assigned depth trends in accordance to equations (8-7a) and (8-7b).

Finally, a fully heterogeneous HCD3 case was applied to the BC model. This case assumed a stochastic component on top of the deterministic trend. The transmissivity models of the fully heterogeneous case were:

$$T_{G,HD} (Depth) = \max(10^{\log[1 \cdot 10^{-4} \exp(-0.0116 \cdot Depth)] + N(0,1) \cdot 2(-Depth / 2,100)}, 1 \cdot 10^{-8}) \quad (8-8a)$$

$$T_{F,HD} (Depth) = \max(10^{\log[6 \cdot 10^{-5} \exp(-0.0174 \cdot Depth)] + N(0,1) \cdot 2(-Depth / 2,100)}, 1 \cdot 10^{-8}) \quad (8-8b)$$

where $N(0,1)$ is a normally distributed random deviate (RD) with mean zero and standard deviation 1.0. The magnitude of the standard deviation, 1.2, was chosen in consideration to previous results reported from the investigations in the Finnsjön area /Andersson et al. 1991/. This value reproduces the spread seen in Figure 8-33 quite well.

In all cases, steeply dipping deformation zones outside this volume encompassed by the Singö and Eckarfjärden deformation zones were assigned the same trend as for the gently dipping deformation zones. This assumption is of importance for the AC model, as there is no hydraulic information available for the low-confidence deformation zones.

General formulae were used for assigning effective values of the transport aperture,

$$e_t = 0.5 T^{0.5} \quad (8-9)$$

the kinematic porosity,

$$n_e = e_t / b_{hyd} \quad (8-10)$$

and the storativity,

$$S = 7 \cdot 10^{-4} T^{0.5} \quad (8-11)$$

These formulae were taken from the findings reported in /Rhén et al. 1997c/, /Rhén and Forsmark, 2001/, /Andersson et al. 1998, 2000b/ and /Dershowitz et al. 2003/. Furthermore, all deformation zones were assumed to be good hydraulic contact with the top boundary.

The thicknesses of the intercepted deformation zones b_{hyd} were inferred from the geological single-hole interpretation. For details about the data, see the supporting documents /Follin et al. 2005/ and /Hartley et al. 2005/.

8.4.3 Assignment of hydraulic properties to the HRDs

Hydraulic properties are assigned to the HRDs by hydrogeological DFN analyses. The two modelling teams, partly applied different approaches.

- The hypothesis of /Follin et al. 2005/ entails a correlated model between feature transmissivity and feature size. As noted in Section 5.5, the fracture size distributions of the geological DFN in version 1.2 are all power-law distributed. The connectivity-based approach by /Follin et al. 2005/ specifically tests the hypothesis that the largest intersecting features in each realisation correspond to the interpreted transmissivities deduced from the measured PFL-f anomalies. A pragmatic motive for this assumption is that the measured PFL-f anomalies represent fractures that are flowing after several days of pumping.

- The hydrological DFN analysis carried out by /Hartley et al. 2005/ did not constrain the relationship between feature transmissivity and feature size to a correlated model, but treated also a non-correlated model and a semi-correlated model. The geometric properties of the underlying geological DFN realisations were the same as in /Follin et al. 2005/, however. It is of interest to learn if the transmissivity model chosen make a difference when comparing simulated inflows with measured. Equally important are the implications of using one or the other transmissivity model for the assignment of block properties and the subsequent regional groundwater flow simulations based on an Equivalent Porous Medium concept.

Workflow of the hydrogeological DFN modelling

The hydrogeological DFN modelling undertaken by /Hartley et al. 2005/ and /Follin et al. 2005/ encompasses four main steps:

1. Assessment of geological data.
2. Assessment of hydraulic data.
3. Determination of connectivity and assessment of correlated hydraulic properties.
4. Hydraulic simulation and assessment of hydraulic properties using three different transmissivity models.

Step 1 covers an examination of the global geological DFN and the geological single-hole interpretations followed by an analysis of the fracture properties and intensities as well as orientations within each deformation zone and each rock domain in the boreholes.

Step 2 includes an analysis of hydraulic data to obtain a representative value for each stochastic deformation zone treated as a part of the hydrological DFN model. Deterministically defined deformation zones intersecting the borehole were excluded from the analysis. A second component was to define the transmissivity distribution.

Step 3 was carried out by /Follin et al. 2005/ but not by /Hartley et al. 2005/. Step 3 aims at generating stochastic fracture models that compare with the mapped orientations and intensities of Open and Partly Open fractures. (The geological DFN model is used, but the fracture intensities required adjustment to better represent the specific boreholes studied.) Once the geological intensity of intercepts is calibrated, the connected fracture area is determined by a connectivity analysis, see Figure 8-30. Subsequently, parameter values for the correlated transmissivity model in Figure 8-29 are derived. The variability between the realisations gives input to an uncertainty assessment of the correlated transmissivity model. The scattering around the mean trend reflects the uncertainty invoked by the assumption that it is the largest features intercepting the borehole in each realisation that correspond to the measured transmissivities.

Step 4 was carried out by /Hartley et al. 2005/, but not by /Follin et al. 2005/, for the different relationships between fracture transmissivity and size shown in Figure 8-29. A 200 by 200 m² large model domain was constructed with similar test conditions as those used for the execution and interpretation of the PFL tests. The simulated fracture inflows were transferred to fracture transmissivities using Dupuit's formula and then grouped into 5 m test section transmissivities. Finally, a statistical comparison was made with the 5 m test section PSS and grouped PFL-f transmissivities reported from the site investigations. The procedure was repeated a couple of times for each transmissivity model tested. An example of the unconditional statistical matching is given in Figure 8-34, which shows the chosen fits for the comparison with the PFL and PSS data outside the deformation zones (the uppermost plot in Figure 8-34) using data from KFM03A. The three lowermost histograms show the fits for the correlated, the uncorrelated and the semi-correlated model, respectively. The goodness-of-fit was judged by eye and from univariate statistics. These results are commented on below.

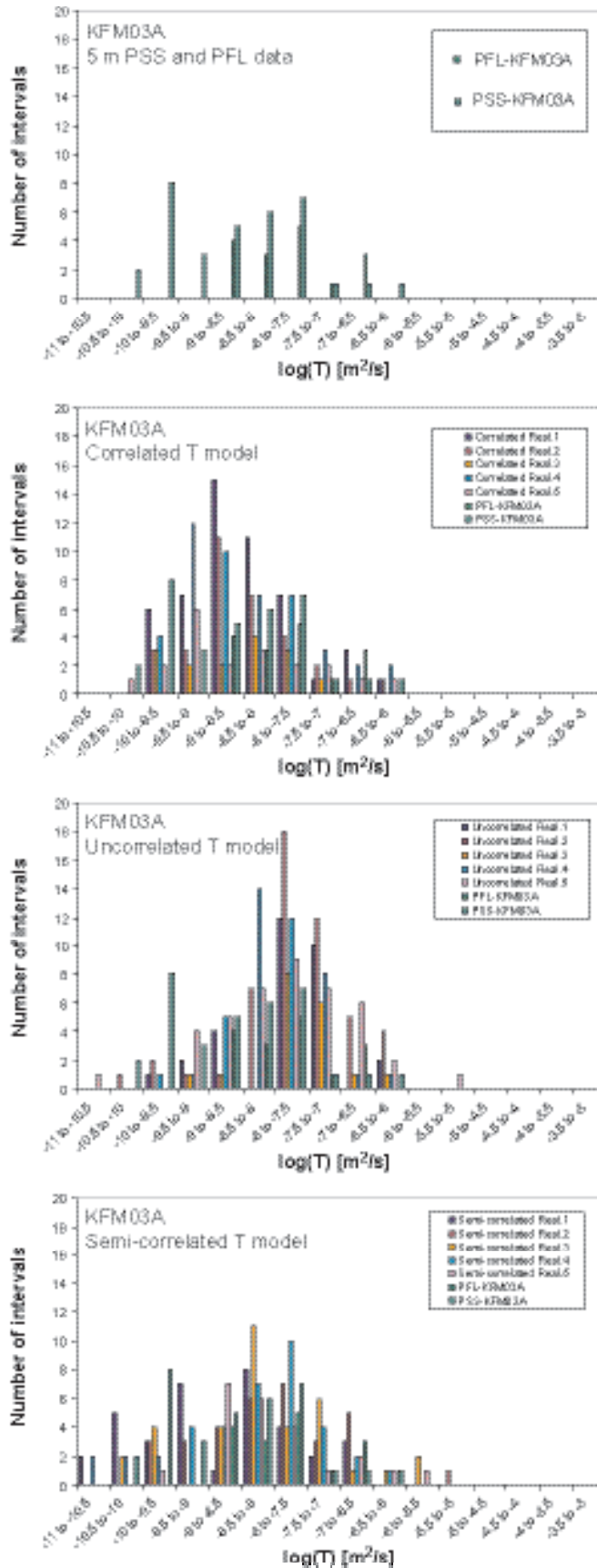


Figure 8-34. Histograms showing the final results of the unconditional statistical matching of simulated transmissivities against interpreted 5 m PSS transmissivities and grouped PFL-f transmissivities in borehole KFM03A. The field data to be matched in borehole KFM03A are shown in the uppermost histogram. The other three histograms show the obtained fits for the correlated, the uncorrelated and the semi-correlated model, respectively. Modified after /Hartley et al. 2005/.

Geological DFN cross-validation

Table 8-7 presents the geological DFN parameter values of Open and Partly Open fractures reported for RFM029. The main motive for using the Univariate Fisher distribution for the NS and NE sets instead of the main alternative – the Bivariate Fisher and the Bivariate Bingham distributions, respectively – is twofold: (i) the actual differences are in this particular case considered to be small, and (ii) the Univariate Fisher distribution is simpler to generate. The most important component of the orientation model is to get relative proportions between the identified steeply and gently dipping sets fairly correct. Moreover, it is vital to note that uncertainties in the details of the orientation model are of second order significance vis-à-vis the assumptions of a Poisson distribution for the spatial correlation between fracture centre points and a power-law distribution for fracture size.

The geological DFN model parameter values listed in Table 8-7 were used to cross-validate the different computer codes used by geology and hydrogeology for generating discrete fracture networks. For the flow simulations, the fracture intensities required adjustment to better represent the specific boreholes studied. That is, from Section 5.5 it is concluded that the methodology used by /La Pointe et al. 2005/ does not allow for a description of the intra-domain heterogeneity of RFM029. This is because all borehole data and outcrop data outside the deformation zones were pooled to form data sets useful for a description of the inter-domain heterogeneity only.

The implications of using a global geological DFN model for the hydrogeological DFN analysis can be best understood by an example: The result of 25 simulations using the geological DFN parameter values listed in Table 8-7 gives a mean value of the borehole fracture intensity P_{10} for RFM029 between the deformation zones of 0.67 m^{-1} /La Pointe et al. 2005/. The simulated mean value is plotted as a dashed line in Figure 8-35 together with a moving average of all Open and Partly Open fractures between the deformation zones in KFM01A–05A. Figure 8-35 indicates that the geological DFN predicts fairly well the borehole fracture intensity between 400–600 m depth, but underestimates the borehole fracture intensity between 0–200 m depth by a factor of 3 and the borehole fracture intensity between 200–400 m depth by a factor of 2. The observed heterogeneity in the borehole fracture intensity is fundamental for the hydrogeological DFN analysis, in particular if there is a depth trend component in the hydraulic properties to.

/Follin et al. 2005/ concluded by means of simulations using the parameter values shown in Table 8-7 that the different codes used for fracture network simulations by /La Pointe et al. 2005/ and /Follin et al. 2005/ yield consistent results for a common setup of model parameters. However, /Follin et al. 2005/ also noted that the aforementioned homogenised borehole fracture intensity P_{10} reported for the global geological DFN decreases by 30%, i.e. $P_{10} = 0.47 \text{ m}^{-1}$ if a scan line is used in the numerical simulations instead of a finite borehole radius. Hence, the statistical matching of simulated intensities against measured is *very* sensitive to the assumption about the borehole radius. As already mentioned in Section 5.5 /La Pointe et al. 2005/ tacitly assumed a finite borehole radius in their analyses.

Table 8-7. Compilation of DFN parameter settings for rock domain RFM029. The following probability distributions are applied: Univariate Fisher distribution for fracture orientation (Trend, Plunge, Kappa), Power law distribution for fracture size and intensity (k_r , X_{r0} , P_{32}), and Poisson distribution for the spatial correlation between fracture centre points.

Set	Trend	Plunge	Kappa	k_r	X_{r0}	P_{32}^*	Rel. P_{32}
NS	87.2	1.7	21.66	2.88	0.28	0.13	11%
NE	135.2	2.7	21.54	3.02	0.25	0.51	42%
NW	40.6	2.2	23.90	2.81	0.14	0.17	14%
EW	190.4	0.7	30.63	2.95	0.15	0.05	4%
HZ	342.9	80.3	8.18	2.92	0.25	0.35	29%
Sum						1.21	100%

* The P_{32} values refer to Open and Partly Open fractures for the given values of k_r and X_{r0} .

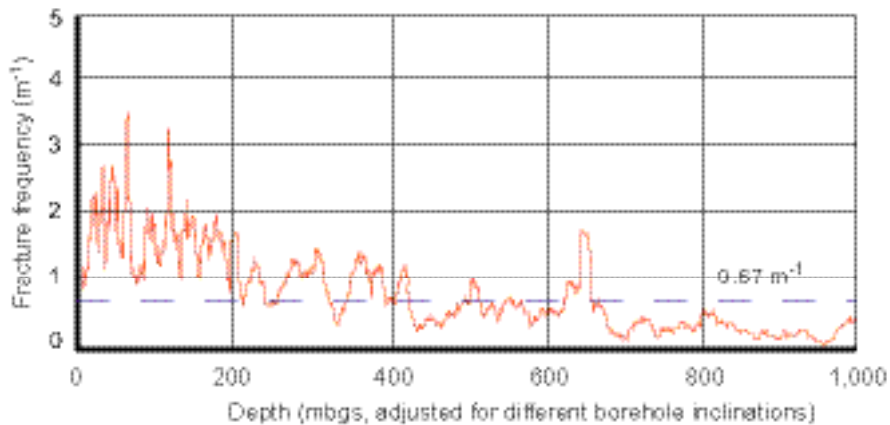


Figure 8-35. Plot showing a moving average of all Open and Partly Open fractures between the deformation zones in KFM01A–05A. The dashed line indicate the predicted fracture intensity of the geological DFN /Follin et al. 2005/.

Motives for dividing RFM029 into sub-volumes

The heterogeneity in borehole fracture intensity P_{10} seen in Figure 8-35 is important for hydrogeology as it suggests that the global geological DFN underestimates the fracture intensity of the uppermost parts of the rock, i.e. between repository depth and ground surface. For instance, Figure 8-13 shows that all 5 m test section transmissivities above the lower measurement limit in borehole KFM01A occur above 400 m borehole length implying that a correct estimation of the geological DFN properties in this interval is of great interest.

Another geometric aspect that is as important for the matching process as the fracture intensity is the change in relative proportions between gently and steeply dipping fractures. As further discussed by /Follin et al 2005/, these proportions vary with depth.

It is important for the conceptual hydrogeological model to note that boreholes KFM01A, KFM02A, KFM04A and KFM05A all indicate a very low-conductive rock mass at depth below deformation zone ZFMNE00A2, see Figure 8-21. For instance, in KFM05A there is one flow anomaly between 200–1,000 m borehole length judged as certain, but many flow anomalies above 200 m depth.

The observed differences between boreholes KFM01A–05A regarding:

- the borehole fracture intensity P_{10} ,
- the relative proportions between the fracture sets, and
- the uneven distribution of flow anomalies above the lower measurement limit

make it difficult to defend a homogenised geological DFN description covering large volumes.

A division of RFM029 into sub-volumes seems more rational. However, as it is not feasible, from a practical point of view, to collect lots of data for each sub-volume, the uncertainties due to lack of data have to be understood and the sensitivities of various assumptions addressed by means of simulations. Improving the understanding of the reasons for the observed spatial variability in the fracturing and the distribution of flow anomalies by integration with other disciplines, as well as assessing the importance of the uncertainties seen by means of numerical simulations using alternative concepts for flow and salt transport have been two major tasks for hydrogeology in version 1.2.

Figure 8-36 shows two schematic cross-sections through the tectonic lens from NE to SW illustrating the division of RFM029 into smaller volumes as analysed by the two modelling teams. The relative locations of the five core-drilled boreholes in relation to the gently dipping deformation zone ZFMNE00A2 are also indicated. The uppermost cross-section shows the division treated by /Follin et al. 2005/ and the lowermost cross-section the division analysed by /Hartley et al. 2005/. Based on the results from the analyses undertaken by the two modelling teams, three conceptual descriptions

have been defined. These will be presented below after a short review of the analyses and modelling carried out.

In terms of borehole flow information, Volumes A and E are associated with flow data in KFM03A and in the upper part of KFM02A. These two boreholes have a limited number of PFL-f anomalies and 5 m PSS data above the measurement limit outside the deterministically treated deformation zones. Volumes C and F are associated with data from the upper parts of KFM01A, KFM04A and KFM05A. Volumes D and G are associated with KFM01A below c. 400 m depth, with KFM05A below c. 200 m depth and with the deeper half of the inclined KFM04A. These borehole intervals have very few PFL-f anomalies and 5 m PSS data above the lower measurement limits.

Volumes A and E in Figure 8-36 may thus be considered equivalent. The same note applies also to Volumes D and G. The main difference between the two cross-sections concerns the division of Volume F into Volumes B and C. The main motive for this division as advocated by /Follin et al. 2005/ is that c. 2/3 of the fractures as well as the inflows observed in Volume F occurs in Volume C.

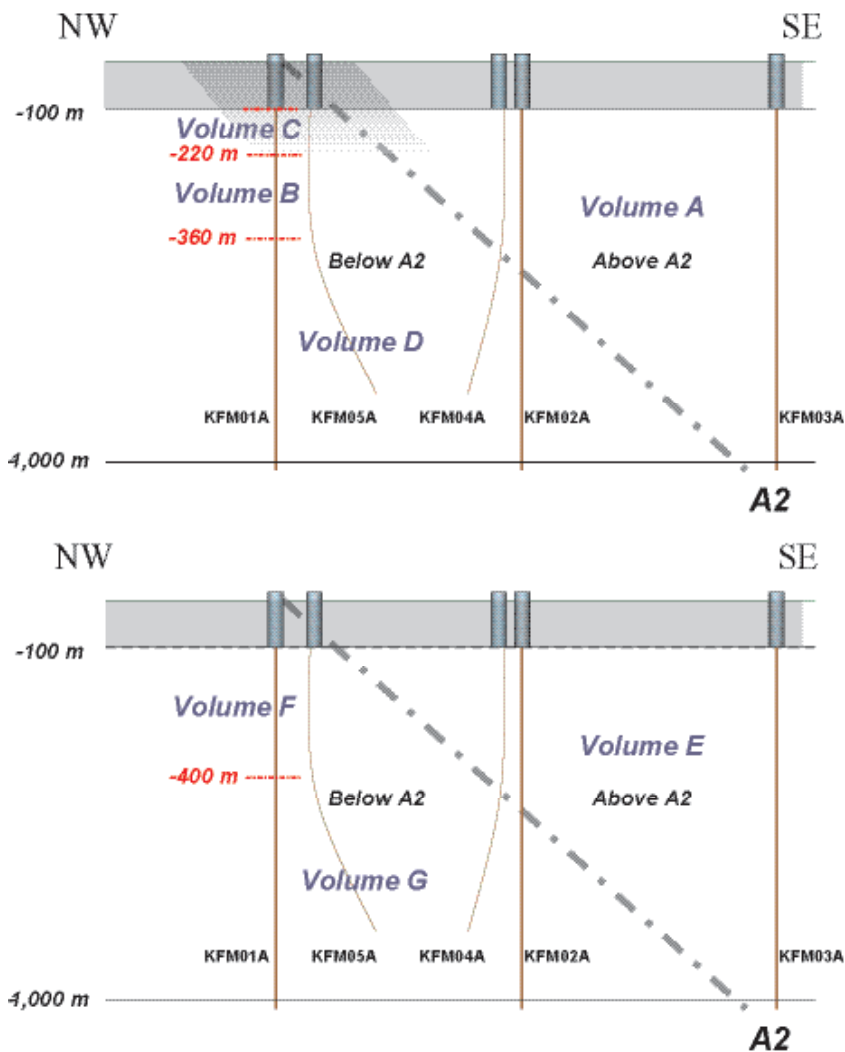


Figure 8-36. Schematic cross-sections through RFM029 illustrating the division into smaller volumes. The upper model was treated by /Follin et al. 2005/ and the lower by /Hartley et al. 2005/. The difference between the two cross-sections concerns the division of Volume F into volumes B and C mainly. Thus, Volumes A and E may be considered equivalent as may Volumes D and G, respectively. Volume C is the most transmissive, whereas Volume D (G) has almost no measurable inflows according to the data available for model version 1.2.

Exploratory simulations

Based on the findings and the many uncertainties described above, different simulation models were constructed for the identified HRDs. /Follin et al. 2005/ treated Volumes A–D and utilised the PFL-f flow anomalies in combination with the size model provided by the geological DFN. /Hartley et al. 2005/ treated Volumes E–G and utilised 5 m PSS data as well as PFL-f data grouped into 5 m intervals in combination with different geological DFN models.

The simulations conducted by /Follin et al. 2005/ revealed the sensitivity of the correlated transmissivity model and the connected fracture area per unit volume P_{32con} to uncertainties concerning:

- the borehole radius (i.e. scan line versus finite radius), and
- the choice of reference feature size.

The simulations conducted by /Hartley et al. 2005/ provided:

- the percentage of Open and Partly Open fractures needed to provide an unconditional statistical match to the interpreted transmissivity distribution, and
- comparisons of the unconditional statistical matches of three different transmissivity models.

The different approaches taken by the two modelling teams are valuable for the overall hydrogeological DFN analysis. Three important questions to keep in mind are:

- I. *What is the motive for assuming a constant value of the reference size X_{r0} ?*
- II. *Is a local increase in the fracture intensity (cluster) in the rock mass outside the deformation zones a result of a local decrease in the reference size X_{r0} mainly or a greater number of fractures of all size categories above the reference size X_{r0} ?*
- III. *What are the practical implications of a very sparsely connected fracture network of low to moderate transmissivities?*

The work associated with the simulation of discrete two-dimensional features in a three-dimensional volume involves a significant amount of geometric algebra and hydraulic simulations. Details on how this was done in practice are provided in the reports by the two modelling teams. The presentation given below aims at showing the main results and the sensitivities involved as well as the similarities in the end results between the two modelling teams, in spite of the many uncertainties and differences in the modelling methodology.

Resulting properties when dividing RFM029 into volumes A–D

Table 8-8 presents the basic fracture frequency data outside the deformation zones that were used in the analysis carried out by /Follin et al. 2005/. N_{CAL} is the number of potentially flowing Open and Partly Open fractures in each borehole (Volume) to be matched in the modelling process (cf. equation (8-1)) and N_{PFL} is the number of flow anomalies in the connected network of flowing features above the lower measurement limit of the PFL method (cf. equation (8-5)). T_{PFLmin} is the smallest transmissivity value measured and may be considered as an estimate of the lower measurement limit T_{lim} . As noted several times in this chapter, the lower measurement limit of the PFL method is not a threshold with a fixed magnitude, but varies in space dependent on the in-situ borehole conditions.

Table 8-8. Basic fracture frequency data outside the deformation zones used in the analysis carried out by /Follin et al. 2005/.

Borehole	Volume	Interval	N_{CAL} (-)	P_{10CAL} ((100 m) ⁻¹)	N_{PFL} (-)	P_{10PFL} ((100 m) ⁻¹)	T_{PFLmin} (m ² /s)	T_{PFLmax} [m ² /s]
KFM03A	A	106–994	248	27.9	24	2.70	1.09E–09	3.46E–07
KFM01A	B	222–363	210	149	11	7.80	2.71E–10	2.22E–09
KFM01A	C	103–222	304	255	23	19.3	2.47E–10	5.35E–08
KFM01A	D	367–956	134	22.8	< 1	< 0.170	3.94E–10	3.94E–10

The frequency of potentially flowing Open and Partly Open borehole fractures P_{10CAL} varies an order of magnitude between the Volumes A–D. In comparison, the aforementioned P_{10} value of the geological DFN, 67 fractures per hundred metres, falls in between the P_{10CAL} values shown in Table 8-8. The value of P_{10PFL} in each Volume is at least one order of magnitude lower than the corresponding value of P_{10CAL} . Between Volume C and Volume D the P_{10PFL} value varies more than two orders of magnitude.

Table 8-9 summarises the outcome of the connectivity-based approach /Follin et al. 2005/. An explanation to the notation is provided below the table. The important entity in Table 8-9 is N_{CON} , the number of interconnected potentially flowing features. The relationship between N_{CAL} , N_{CON} and N_{PFL} on which the methodology of /Follin et al. 2005/ was based is given by equation (8-6).

Four models were tested in Volume B and two of these, 3a and 3b, were also tested in Volumes C, A and D. Model 1 made use of the geological DFN settings, but the intensity of features larger than the reference size of each set was increased to match $N_{CAL} = 210$ in Table 8-8. Model 2 tested the alternative of decreasing the reference size of each set instead of increasing the number of features. Both Model 1 and Model 2 explored the assumption of finite borehole radius. In contrast, Models 3a and 3b explored the scan line assumption. Model 3a challenged a small value of the reference size and Model 3b a larger value. The size of the simulation domain was set to one cubic kilometre in order to allow for large random features, but small features were simulated in the proximity of the borehole only.

The main conclusions of the connectivity analysis drawn by /Follin et al. 2005/ are:

- Depending on the assumptions made for the reference size X_{r0} and the borehole radius r_w different hydrogeological DFN solutions are obtained. This shows that both the reference size and the borehole radius are important for the calibration against the borehole fracture frequency, which is a fundamental component of the DFN analysis. Indeed, the concept of borehole fracture frequency implies that core-drilled boreholes are treated as scan lines in the geological mapping of intersecting fractures.

The choice of reference size is a geological uncertainty that needs to be treated with concern. In order to make progress in the uncertainty assessment in this matter during the remaining part of the site investigations, it is necessary to compare fracture data from outcrop measurements with fracture data from a number of shallow core-drilled boreholes. In model version 1.2 this information is absent due to the telescoping drilling technique used for the deep core drilling of KFM01A–05A. Fracture data from underground measurements in shafts, drifts and tunnels will be another valuable piece of information in due time.

- Volumes A–D may be modelled as percolating networks of discrete features, but with quite different hydrogeological DFN properties depending on the assumption of the reference size. This is an important observation that demonstrates the significance of using a connectivity-based analysis in combination with flow simulations.

If a small value of the reference size is assumed (Model 3a), the body of N_{CAL} in Volumes B and C represents isolated features rendering, relatively speaking, smaller values of P_{32CON} , 17% and 20%, respectively. This means that the rock masses between the deformation zones in Volumes B and C consist of very sparsely connected hydrogeological DFNs, with c. 30–40% of the connectivity above T_{PFLmin} . For Volumes A and D, a small value of the reference size results in no connectivity at all, suggesting impervious rock matrix properties of these HRDs.

If a large value of the reference size is assumed (Model 3b), the hydrogeological DFNs of Volumes B and C become, relatively speaking, well connected, but with less than 10% of the connectivity above T_{PFLmin} . Moreover, Volumes A and D now become sparsely connected. In Volume A, c. 25% of the connectivity is above T_{PFLmin} , whereas in Volume D zero percent is above T_{PFLmin} . The mean spacing between the flowing features above T_{PFLmin} in Volume D is c. 600 m, see Table 8-8, whereas the mean spacing between the connected features below T_{PFLmin} becomes c. 30 m, see Table 8-9.

- A small or a large value of the reference size calls for quite different DFN conceptions for the hydrogeological modelling of groundwater flow within the four HRDs. However, the body of connectivity is below T_{PFLmin} in all volumes, regardless of the reference size studied. The approximation of the different DFNs as EPMs or low-conductive CPMs is strongly coupled to the objectives and scale of the flow problem treated (cf. Section 8.3.3).

Table 8-9. Compilation of the outcome of the connectivity-based approach used by /Follin et al. 2005/. Each model was tested by ten realisations.

X_{i0} (m)	r_w (m)	N_{CON} (-)	P_{i0CON} ((100 m) ⁻¹)	P_{32} (m ² /m ³)	$\sim P_{32CON}$ (%)	$\sim P_{32CON}$ (m ² /m ³)	$P_{32CON} < T_{min}$ (% of P_{32CON})	$P_{32CON} > T_{min}$ (% of P_{32CON})	a (-)	b (-)	T_{10m} (m ² /s)	T_{100m} (m ² /s)
Volume B												
Model 1	0.14-0.28	190	135	2.70	90	2.44	94	6	9.04E-11	0.669	4.21E-10	1.96E-09
Model 2	0.10	103	73.0	2.76	49	1.35	89	11	2.27E-10	0.737	1.24E-09	6.77E-09
Model 3a	0.038	27	19.1	3.98	13	0.512	59	41	8.30E-10	0.645	3.67E-09	1.62E-08
Model 3b	0.28	209	148	3.97	100	3.95	95	5	5.12E-11	0.767	2.99E-10	1.75E-09
Volume C												
Model 3a	0.038	80	67.2	4.70	26	1.238	71	29	3.56E-09	1.451	1.01E-07	2.84E-06
Model 3b	0.282	303	255	4.66	100	4.66	92	8	4.17E-11	1.618	1.73E-09	7.18E-08
Volume A												
Model 3a	0.038	0	0.00	0.786	0	0.000	N/A	N/A	-	-	-	-
Model 3b	0.282	95	10.7	0.786	38	0.301	75	25	7.14E-10	1.459	2.05E-08	5.91E-07
Volume D												
Model 3a	0.038	0	0.00	0.523	0	0.000	N/A	N/A	-	-	-	-
Model 3b	0.282	19	3.23	0.523	14	0.0741	100	0	7.23E-11	0.408	1.85E-10	4.73E-10

X_{i0} Reference feature size.

r_w Borehole radius.

N_{CON} Number of the connected potentially flowing features.

P_{i0CON} Frequency of N_{CON} .

P_{32} Area per unit volume of all $X_i > X_{i0}$.

P_{32CON} Area per unit volume of the connected features $X_i > X_{i0}$.

a Factor of the correlated transmissivity model (cf. equation (8-4b)).

b Exponent of the correlated transmissivity model (cf. equation (8-4b)).

Figure 8-37 and Figure 8-38 show the outcome of the hypothesis of /Follin et al. 2005/ in which the transmissivities interpreted from the PFL-f tests were associated to the largest interconnected fractures intersecting the borehole in each realisation. The plots in Figure 8-37 apply to Models 1, 2 and 3a in Volume B and to Model 3a in Volume C. Similar plots for Model 3b are given in Figure 8-38. The different plots in Figure 8-37 and Figure 8-38 demonstrate the variability between the stochastic realisations conducted. Although the final model in each case has unique values of the factor a and the exponent b , a semi-correlated model could in fact be produced as an alternative. In comparison, the semi-correlated model (equation (8-4c)) specifies this variability *a priori*.

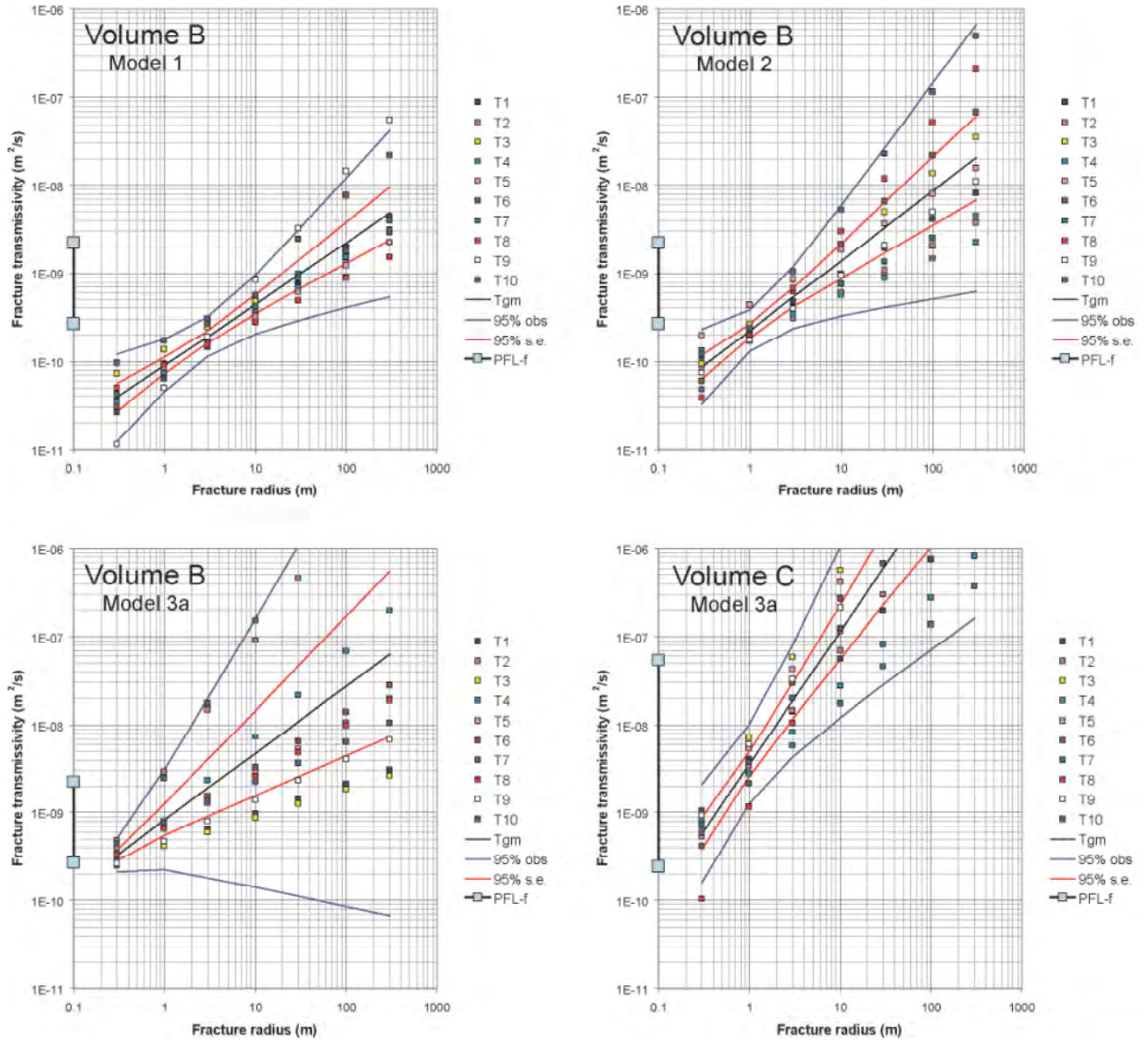


Figure 8-37. Outcome of using the correlated transmissivity model in the work by /Follin et al. 2005/. The results are for Models 1, 2 and 3a in Volume B and 3a in Volume C. T1–T10 = realisations, Tgm = geometric mean, 95% obs = 95% confidence interval for a new observation, 95% s.e. = 95% confidence interval for the standard error.

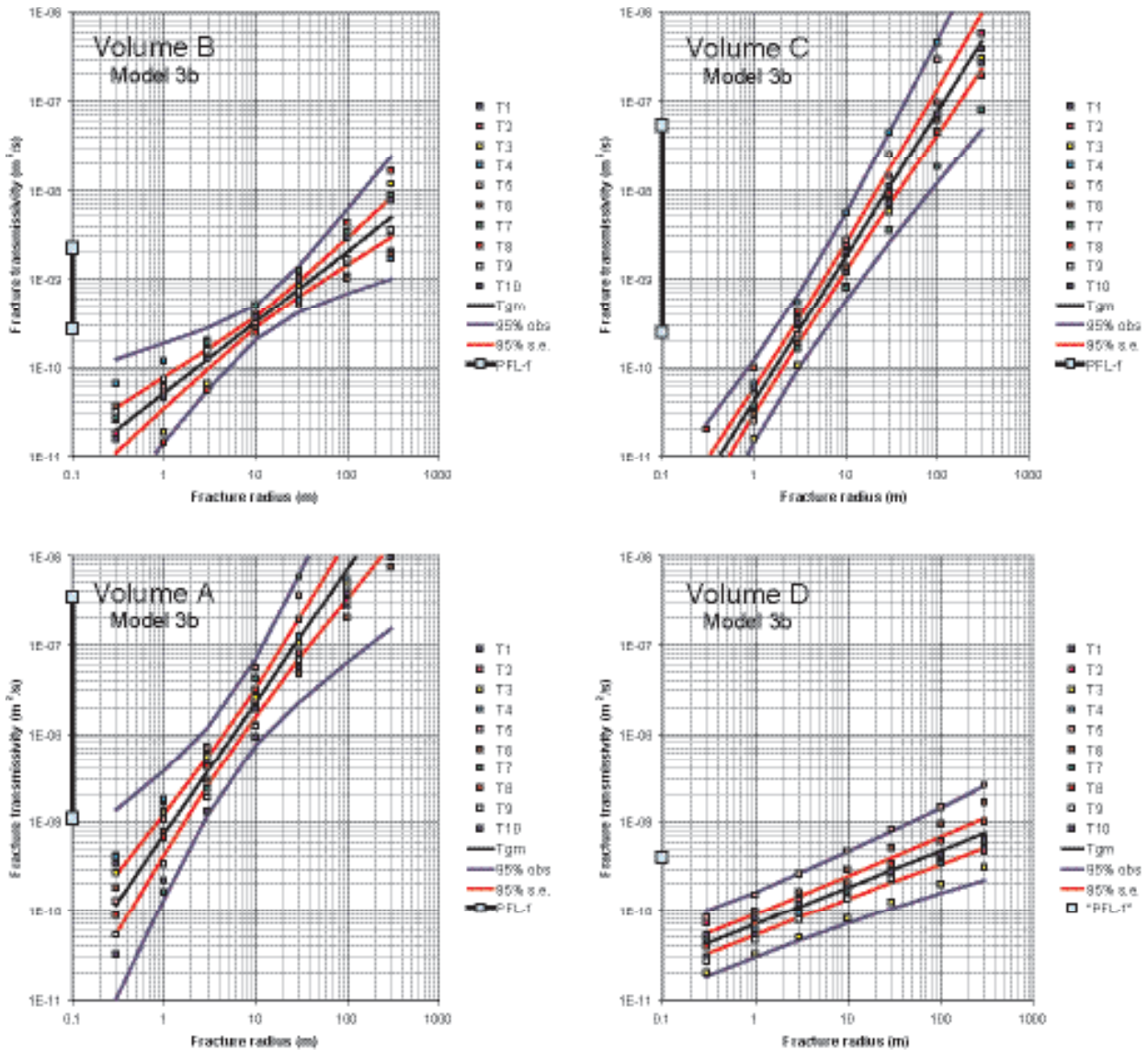


Figure 8-38. Outcome of using the correlated transmissivity model in the work by /Follin et al. 2005/. The results are for Model 3b in Volume A–D. T1–T10 = realisations, Tgm = geometric mean, 95% obs = 95% confidence interval for a new observation, 95% s.e. = 95% confidence interval for the standard error.

Resulting properties when dividing RFM029 into volumes E–G

/Hartley et al. 2005/ tested three different geological DFN models in Volume E, and for each of these models, three transmissivity models were tested. The geological DFN-1 model was based on the specific fracture orientations seen in each borehole and was derived in order to test the importance of using borehole-specific orientations in the unconditional statistical matching of simulated versus measured test section transmissivities. Hence, the parameter values of this model for borehole KFM03A were different from those for KFM01A. The geological DFN-2 model was identical to the aforementioned global geological DFN model derived by /La Pointe et al. 2005/, see Section 5.5. The geological DFN-3 model was a variant of the DFN-2 model, which considered a lower value of the slope k_r of the power-law size distributions than the global DFN model, thus putting more emphasis on the intensity of larger features. The k_r value of the DFN-3 model was 2.75, as suggested by /Follin et al. 2005/. This value is close to the value presented by /La Pointe et al. 1999/ in their regional analysis for northern Uppland (cf. Section 5.5).

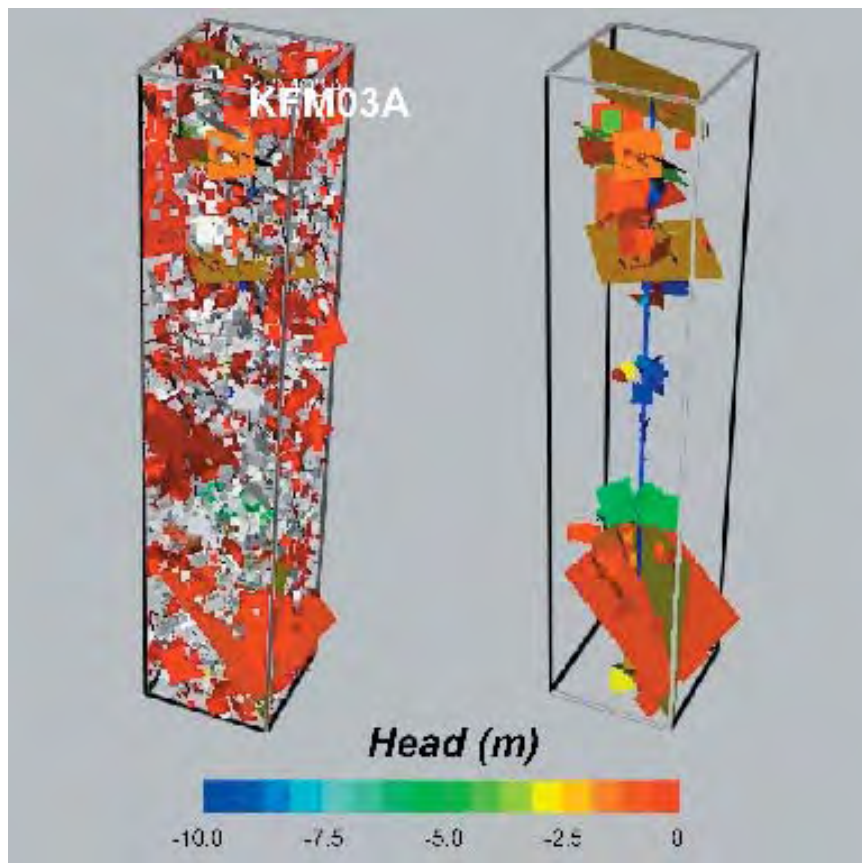


Figure 8-39. DFN realisation for a region of a 200 m square cross-section used in the PSS/PFL simulations. Only features with an equivalent radius greater than 0.56 m were used. Left: Features are coloured by the average head on the feature or grey where they are either isolated or dead-ends. Right: Features around the borehole with a significant drawdown. Modified after /Hartley et al. 2005/.

The size of the model domain used for the radial flow simulation was 200 m by 200 m in the horizontal directions. The hydraulic boundary conditions mimicked those of radial steady-state constant head test.

The differences between the geological DFN-1 and DFN-2 models were found to be moderate in both Volume E and Volume F, but it was a lot easier to produce a good match to measured data in Volume F.

Figure 8-34 shows the outcome of the unconditional matching using the three transmissivity models in combination with the geological DFN-1 model in Volume E. In order to make a reasonable match against the rather broad peak of the 5 m PSS and PFL histograms (cf. the uppermost plot in Figure 8-34), /Hartley et al. 2005/ concluded that it was necessary to use a higher intensity of Open and Partly Open fractures in the flow model compared with the geological intensity of Open and Partly Open observed in the borehole (KFM03A). The statistical match seen in Figure 8-34 corresponds to a fracture area per unit volume of $0.903 \text{ m}^2/\text{m}^3$, which is c. 130% of the P_{32} value deduced for Volume E by /Hartley et al. 2005/, based on the Terzaghi corrected borehole fracture intensity, $0.695 \text{ m}^2/\text{m}^3$.

In comparison, the P_{32} and P_{32CON} values of Volume A, as inferred by /Follin et al. 2005/, were $0.786 \text{ m}^2/\text{m}^3$ and $0.301 \text{ m}^2/\text{m}^3$, respectively, see Table 8-9. It is noted that /Follin et al. 2005/ used other set limits than /Hartley et al. 2005/. However, the value of the reference size X_{r0} in Figure 8-34 was identical to that of Model 3b in Volume A used by /Follin et al. 2005/.

The difficulty encountered when using the geological DFN-1 and DFN-2 models in Volume E was the main reason for testing the DFN-3 model in this volume. Figure 8-40 compares the outcome of using the geological DFN-1 and DFN-3 models for the correlated transmissivity model. The best match for the DFN-3 model was found using an effective intensity of Open and Partly Open of $0.530 \text{ m}^2/\text{m}^3$. It is important to recall that the DFN-3 model is a working hypothesis developed to test the sensitivity to the value of the slope of the power-law size distribution, k_r .

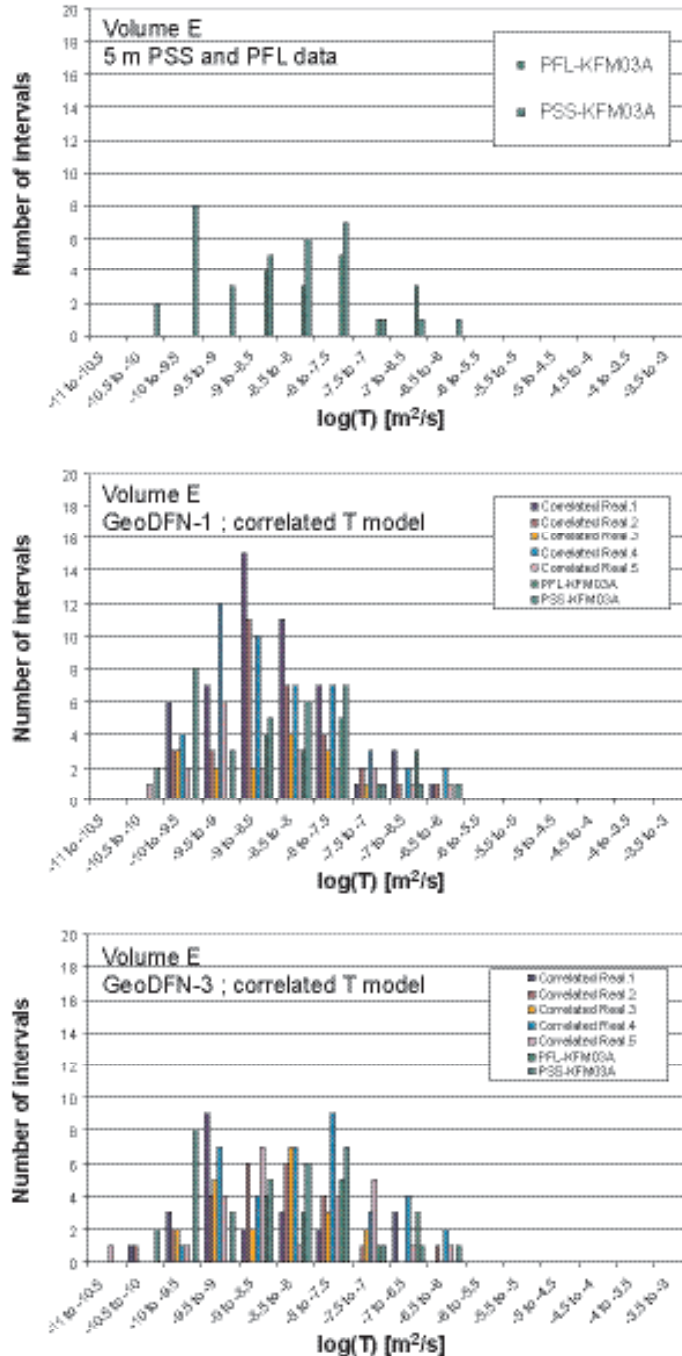


Figure 8-40. Histograms showing the results of the unconditional statistical matching of simulated transmissivities against interpreted 5 m PSS transmissivities and grouped PFL-f transmissivities in Volume E using a correlated transmissivity model in combination with the geological DFN-1 and DFN-3 models. The field data to be matched in Volume E are shown in the uppermost histogram. The other two histograms show the obtained fits for the DFN-1 and DFN-3 models, respectively. Modified after /Hartley et al. 2005/.

Figure 8-41 shows the outcome of using the geological DFN-1 and DFN-2 models in Volume F, respectively. The statistical matches shown correspond to a correlated transmissivity model. The fracture area per unit volume in Figure 8-41 was $1.20 \text{ m}^2/\text{m}^3$, which means that 26% of the P_{32} value deduced by /Hartley et al. 2005/, $4.70 \text{ m}^2/\text{m}^3$, provided a good fit. The model of /Follin et al. 2005/ in Volumes B and C, that compares best with the findings of /Hartley et al. 2005/, is Model 3a see Table 8-9. Using an X_{r0} value of 0.038 m rendered weighted P_{32} and P_{32con} values of Volumes B and C of $4.48 \text{ m}^2/\text{m}^3$ and $0.826 \text{ m}^2/\text{m}^3$, respectively.

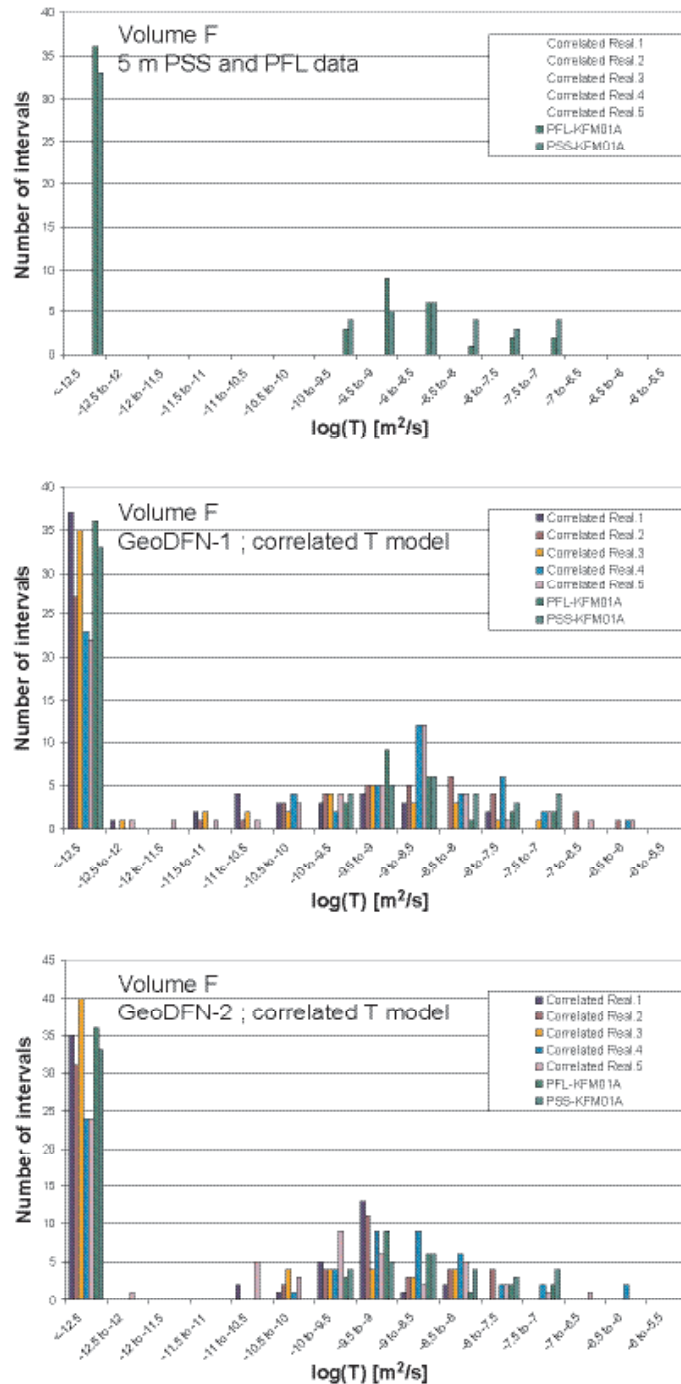


Figure 8-41. Histograms showing the results of the unconditional statistical matching of simulated transmissivities against interpreted 5 m PSS transmissivities and grouped PFL-f transmissivities in Volume F using a correlated transmissivity model in combination with the geological DFN-1 and DFN-2 models. The field data to be matched in Volume F are shown in the uppermost histogram. The other two histograms show the obtained fits for the DFN-1 and DFN-2 models, respectively. Modified after /Hartley et al. 2005/.

As already noted, Volume G is a HRD of almost no flow above the measurement limit between the deterministically treated deformation zones. It is as important to understand the characteristics of this HRD as it is to consider the HRDs with groundwater flow above the measurement limit. /Hartley et al. 2005/ suggested that the lower section of KFM01A may be treated as a poorly connected DFN based on the Terzaghi corrected value for fracture frequency of Open and Partly Open fractures observed below 410 m borehole length, 0.4 m^{-1} . This value is c. one order of magnitude smaller than the corresponding value reported for Volume F. In comparison, the P_{32} value of Volume D, defined to start at 360 m borehole length, was c. $0.5 \text{ m}^2/\text{m}^3$, see Table 8-9.

/Hartley et al. 2005/ simulated flow into KFM01A in Volume G assuming a correlated transmissivity model $(a, b) = (5 \times 10^{-10}, 1)$. Based on the result from five flow simulations, /Hartley et al. 2005/ made the suggestion that a P_{32} around $0.3 \text{ m}^2/\text{m}^3$ is the threshold below which the rock exhibits no flowing features. The results from the five simulations are shown in Figure 8-42. Two simulations predicted 100% non-flowing intervals, and the other three simulations predicted 93%, 94% and 98% non-flowing intervals.

Concerning the three transmissivity models /Hartley et al. 2005/ concluded that the differences between the three models are small in Volume E and Volume F. The best match was obtained for the correlated transmissivity model but further fits were produced for the uncorrelated and semi-correlated transmissivity models as well. Table 8-10 summarises the parameter values suggested for the uncorrelated, correlated and semi-correlated transmissivity models in Volumes E–G.

Table 8-10. Parameter values suggested by /Hartley et al. 2005/ for the uncorrelated, correlated and semi-correlated transmissivity models in Volumes E–G. The values given in the table refer to the geological DFN-1 and DFN-2 models.

Object	Uncorrelated		Correlated		Semi-correlated		
	$\mu_{\log(T)}$	$\sigma_{\log(T)}$	a	b	a	b	$\sigma_{\log(T)}$
Volume E	-6.5	0.9	1.8×10^{-9}	1	5.3×10^{-8}	0.6	1
Volume F	-6.5	0.9	1.8×10^{-9}	1	5.3×10^{-8}	0.6	1
Volume G	–	–	8.9×10^{-10}	1	–	–	–

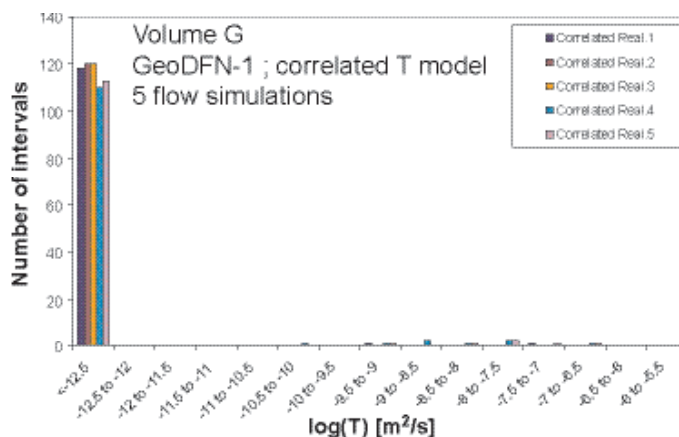


Figure 8-42. Histogram of $\log(T)$ in 5 m intervals for 5 flow simulations around borehole KFM01A (Volume G) using the geological DFN-1 model and a correlated T distribution. Modified after /Hartley et al. 2005/.

Discussion of hydrogeological DFN findings

A summary of the results presented by the two modelling teams is given in Table 8-11. This information should be used together with the orientation data and the power-law slopes of the different sets provided by the global geological DFN model, Table 8-7. Thus, the combination of information in these two tables constitutes the preliminary hydrogeological DFN model of RFM029 in version 1.2 of the Forsmark site descriptive model.

The significant differences between the five core-drilled boreholes demonstrate that the geological and hydrogeological conditions within RFM029 do not lend themselves to a single (global) fracture network model covering large volumes. The pragmatic approach taken by hydrogeology is to divide the rock mass between the deterministically treated deformation zones into sub-volumes based on the heterogeneities observed in the structural (orientation and intensity) and hydraulic (transmissivity) information. However, the key statistical assumptions of the global geological DFN model need to be taken for granted, i.e. the Poisson process and the power-law size distribution. The profit of assuming a globally valid model are in the mathematics providing powerful analytical equations useful for both general and detailed design and safety assessment calculations. The weak point is in the adaptation to local heterogeneities. This is particularly true in RFM029, where large volumes of rock between the deterministically treated deformation zones are at or below the practical measurement limits of the hydraulic testing equipments, thus difficult to challenge by traditional hydraulic test methods.

Table 8-11. Summary of the simulations results presented by the two modelling teams.

Parameter	Volume						
	A	B	C	D	E	F	G
r_w (m)	0	0	0	0	0	0	0
P_{32} (m ² /m ³)	0.786	3.98	4.70	0.523	0.695	4.70	~ 0.4
X_{r0} (m)	0.282	0.038	0.038	0.282	0.282	0.282	0.282
P_{32CON} (m ² /m ³)	0.301	0.512	1.238	0.0741	0.903	1.20	~ 0.3
Rel P_{32} : NS (-)	0.173	0.920	0.111	0.251	0.124	0.110	0.285
Rel P_{32} : NE (-)	0.312	0.558	0.230	0.315	0.291	0.449	0.246
Rel P_{32} : NW (-)	0.164	0.027	0.068	0.034	0.191	0.085	0.050
Rel P_{32} : EW (-)	0.075	0.025	0.056	0.000	0.100	0.049	0.000
Rel P_{32} : HZ (-)	0.276	0.299	0.535	0.400	0.294	0.306	0.418
Corr. T: a (-)	7.1E-10	8.3E-10	3.6E-09	7.2E-11	1.8E-09	1.8E-09	8.9E-10
Corr. T: b (-)	1.46	0.645	1.45	0.408	1.00	1.00	1.00
Variability	Figure 8-38	Figure 8-37	Figure 8-37	Figure 8-38	N/A	N/A	N/A
Uncorr. T: $\mu_{\log(T)}$ (-)	-	-	-	-	-6.5	-6.5	-
Uncorr. T: $\log(T)$ (-)	-	-	-	-	0.9	0.9	-
Semi-corr. T: a (-)	-	-	-	-	5.3E-08	5.3E-08	-
Semi-corr. T: b (-)	-	-	-	-	0.600	0.600	-
Semi-corr. T: $\log(T)$ (-)	-	-	-	-	1.00	1.00	-

As noted in Section 5.5, a major uncertainty of the current geological DFN modelling concerns the reference fracture size X_{r0} of the different power-law size distributions. The sensitivity analysis conducted by /Follin et al. 2005/ demonstrated that local differences in the reference size is vital for the connectivity assessment of the hydrogeological DFN. An integrated interpretation of the simulation results presented by the two modelling teams leads to some interesting observations regarding this matter. The premise for these observations lays in the different approaches taken by the two modelling teams. /Hartley et al. 2005/ used an *a priori* fixed value of the reference size in combination with the (reasonable) assumption that the borehole radius is a scan line. In comparison, /Follin et al. 2005/ tested the sensitivity to different reference sizes and two different assumptions about the borehole radius.

Using a fixed value of the reference size it was necessary to adjust the number of fractures above the reference size to make reasonable good fits to the measured 5 m PSS and grouped PFL-f transmissivities. For example, in Volume F the best match required that the fracture intensity was decreased to 26% and in Volume E the best match required that the fracture intensity was increased to 130%. Interestingly equally good matches were readily obtained by decreasing or increasing the reference size instead of decreasing or increasing the number of features. In Volumes B and C good matches were obtained using a small reference size and in Volume A using a large. The connectivity analyses suggested that the resulting networks had relative connected fracture area per unit volume values of 17%, 20% and 38% of the corresponding total fracture area per unit volume values.

There are no simple proofs or verification tests that can be used to discriminate between the possible explanations to these findings. However, using a small reference size in Volume A led to a non-connected DFN, which is obviously unrealistic given the fact that there are 24 flow anomalies between the deterministically treated deformation zones in Volume A. Likewise, the good match for 130% Open and Partly Open fractures in the identical Volume E is equally unrealistic. According to /Follin et al. 2005/, a larger reference size in Volume A led to a weakly connected DFN that readily explained the 24 flow anomalies.

The hydrogeological DFN analyses of Volumes D and G are more uncertain as there are no flow anomalies in KFM01A. /Follin et al. 2005/ concluded that Volume D becomes non-connected when assuming a small reference size and very poorly connected when assuming a larger value, however, with all flow below the lower measurement limit. The latter finding goes well together with the sensitivity test conducted by /Hartley et al. 2005/, which suggests that this HRD is close to the percolation threshold.

Concerning the transmissivity model, the simulations conducted by /Follin et al. 2005/ demonstrated variability between the realisations if a correlated transmissivity model was stipulated *a priori*. The variability between the realisations increased the more sparsely the network was that was simulated. Although the final model in each case has unique values of the factor a and the exponent b , a semi-correlated model could in fact be produced as an alternative.

The hydrogeological DFN modelling conducted by /Hartley et al. 2005/ incorporates a hydraulic assessment of all of the aforementioned transmissivity models. The conclusion drawn from their work is that the three transmissivity models can be used as alternative cases with the parameterisation derived from the analysis of the 5 m PSS and grouped PFL-f data presented above. However, the direct correlation transmissivity model is probably the easiest to match to the borehole flow data. It is noted that the geometry-based stochastic analysis conducted by /Follin et al. 2005/ gives compatible results with the correlated transmissivity model deduced by /Hartley et al. 2005/ in spite of the difference in methodology, i.e. flow simulations versus connectivity analyses.

Finally, the sensitivity to the magnitude of the slopes of the power-law size distributions was superficially addressed by /Hartley et al. 2005/, based on a proposal suggested by /Follin et al. 2005/ (cf. Section 5.5). The results of the simulations show that a lower value of the slope of the power-law size distribution produced an excellent fit for Volume E. This is a major issue to be resolved by geology.

8.4.4 Block-size properties

Workflow for the assessment of block properties

The remit for this study, as specified by SKB's Design Team, was to calculate Equivalent Porous Media (EPM) statistics of the hydraulic conductivity tensor of 20 m and 100 m blocks using the results from the hydrogeological DFN, see Table 8-11. The block-size simulations are useful also for the implementation of the DFN findings into a regional scale groundwater flow model. In the latter case, Equivalent Porous Media (EPM) parameters are calculated on the scale of the computational grid resolution, which was of the order 50–100 m.

/Hartley et al. 2005/ performed flow simulations through several DFNs representing the relatively speaking well connected Volumes E and F, and used a least-squares fit for the deduction of the block conductivity of an array of blocks within a much larger simulation domain (as big as the largest stochastic fracture and ten times the block size). Two block sizes, 20 m and 100 m, were treated and different fracture size truncations were considered.

/Follin et al. 2005/ generated a single huge DFN representing the sparsely connected Volume B located above the even sparser connected target volume, i.e. Volume D. In comparison with Volumes E and F the conception of an EPM in Volumes B and D is a difficult matter due to the low fracture intensity. For instance, the connected feature area per unit volume in Volume B is 46% of the connected feature area per unit volume in Volume E and 46% of that in Volume F, see Table 8-11. Tentative block-size properties were estimated by /Follin et al. 2005/ for a single block size, 20 m, and a single fracture size truncation using the upscaling algorithm by /Svensson, 2001a,b/.

Anisotropy was addressed in different ways. /Follin et al. 2005/ rotated their simulation domain 45° to make the principal axes of the computational grid parallel to the principal stresses, with the y-axis pointing NW and the x-axis pointing NE. /Hartley et al. 2005/ used a grid system, where the principal y-axis of the computational grid pointed N and the x-axis pointed E. The overall hydraulic conductivity of the simulation domain was calculated by /Hartley et al. 2005/ as the geometric mean of the axial components. A principal component analysis was used to derive the maximum and minimum horizontal hydraulic conductivities together with the strike of the maximum hydraulic conductivity for each of the blocks. This showed how much anisotropy can be expected in any given block and whether there is a general trend toward certain directions over all blocks.

Fracture kinematic porosity of the grid blocks was also calculated by /Hartley et al. 2005/ by summing the fracture area multiplied by transport aperture for each connected fracture within each block and dividing by the block volume. The basis for the calculation is the relationship between transport aperture and transmissivity in equation (8-9).

Volume B

Figure 8-43 illustrates the conception used by /Follin et al. 2005/. The simulation domain was positioned in the target area representing Volume B below the gently dipping deformation zone ZFMNE00A2, see Figure 8-36. The 1,400 m square domain was rotated 45° to make the principal axes of the computational grid parallel to the principal stresses.

Figure 8-44 shows the simulation domain in perspective view together with an example of a DFN realisation using parameter values representative for Volume B, see Table 8-11. Two 1,400 m long horizontal scan lines were inserted at 400 m depth striking NW and NE, respectively.

As further discussed by /Follin et al. 2005/, the resulting block properties depend on the feature truncation size. It is shown that the percentage of 20 m blocks that are completely non-connected decreases as the fracture truncation size decreases. For instance, c. 50% of the 20 m blocks positioned along the two scan lines were completely non-connected when a truncation size of 5.64 m was used. By decreasing the truncation size to 4.23 m, this figure decreased to 45%. The additional fracturing had a small but noticeable contribution to the bulk flow and increased also the probability for a few intermediate large flow channels.

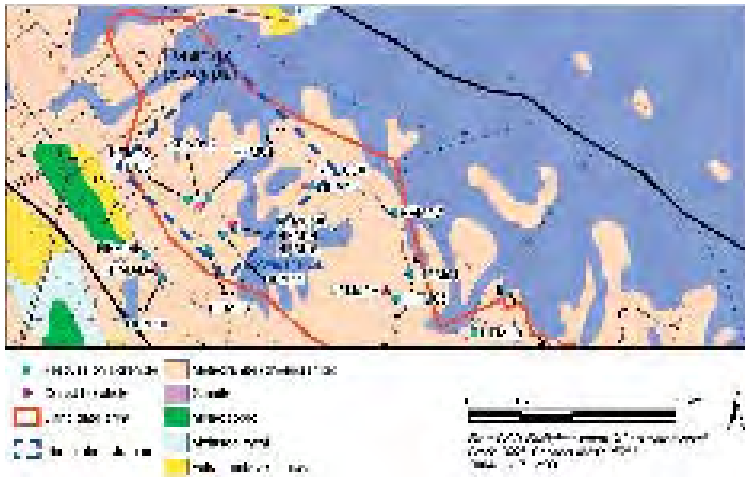


Figure 8-43. Schematic of the conception treated by /Follin et al. 2005/. The simulation domain is positioned in the target area representing Volume B below the gently dipping deformation zone ZFMNE00A2, see Figure 8-36.

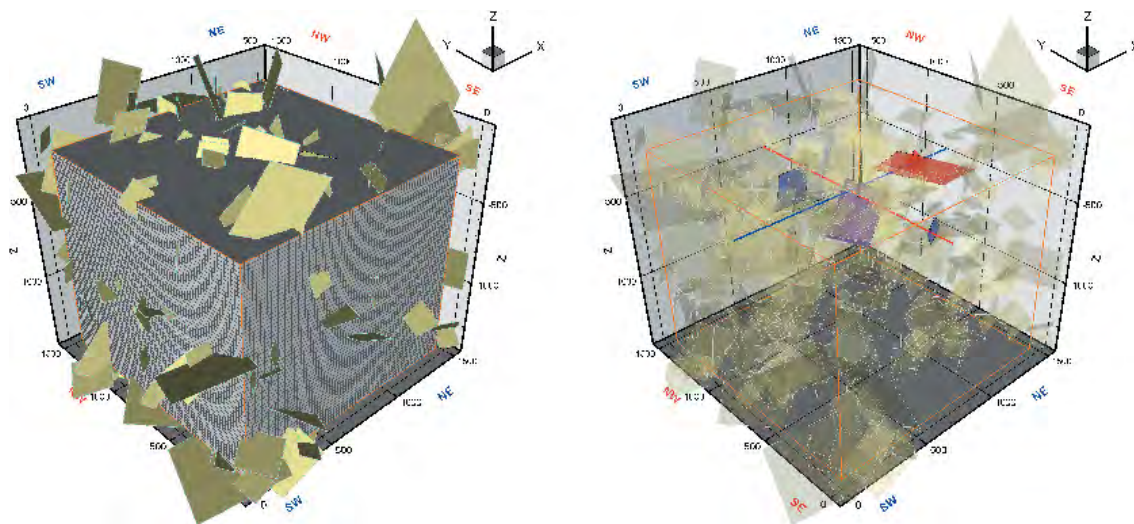


Figure 8-44. Perspective view of the simulation domain together with a DFN realisation using parameter values representative for Volume B, see Table 8-11. Two 1,400 m long scan lines were inserted at 400 m depth striking NW and NE, respectively. Connected features with an equivalent radii X , greater than 56.4 m ($L = 100$ m) are shown only. Features intersecting the scan lines are coloured in red and blue depending on their strike. In the case shown, there are more intersecting features striking NE but the intersecting features striking NW are larger. This behaviour follows directly from the settings of the geological DFN model, see Table 8-11 /Follin et al. 2005/.

The probability of having large connected features intersecting the scan lines is sensitive to the absolute number of features generated, which in turn is dependent on the truncation size used. This suggests that the occurrence of long pathways in the simulation model may be underestimated depending on the truncation size chosen. The implication of this uncertainty needs to be addressed in model applications where a detailed DFN is treated, e.g. in near-field hydrogeological modelling.

In conclusion, the importance of aiming at a perfect representation of the sparsely connected DFN in Volumes B and C is an open question due to the low transmissivities. It may be advocated that moderately large features of, relatively speaking, moderately high transmissivities may not necessarily have much flow in them. This is because the flow rate through a sparsely connected network can be seen as a serial flow system, e.g. a one dimensional pipe-network, and thus governed

by the minimum transmissivity value (cf. the harmonic mean). It is the probability of occurrence of very large single conduits, which do not need other features to form connectivity to the nearest deformation zone, that constitute the key uncertainty. Such features may exist in Forsmark, e.g. see the tentative flow anomalies at depth in boreholes KFM02A, KFM04A and KFM05A (Figure 8-9, Figure 8-11, Figure 8-12 and Figure 8-13). Some of these flow anomalies are reported as uncertain, whereas others have been possible to tie to deterministically treated deformation zones, thus are not stochastic features. The point made here is that such features apparently exist in an otherwise “impermeable” rock mass.

From a pragmatic point of view, there is a trade off between using the best fit truncation size and the limit of the simulation that is possible to run computationally. Therefore, it is important to study the sensitivity of calculated EPM block properties to the feature size truncation $X_{r,min}$. /Follin et al. 2005/ performed bracketing calculations with the objective to grasp the range of uncertainty in the log geometric mean hydraulic of 20 m blocks in Volume B. The calculations were made for a truncation size of 5.64 m. An estimate of the upper bound was made by discarding all 20 m grid cell values that were not hydraulically connected in the three directions x , y and z . An estimate of the lower bound was made by assuming that the non-connected 20 m blocks had a threshold hydraulic conductivity of 1.6×10^{-13} m/s, which was the lowest directional hydraulic conductivity value next to zero that was deduced for a 20 m block.

Table 8-12 shows the percentiles of the effective hydraulic conductivity K_{eff} , i.e. the logarithm of the geometric mean of K_x , K_y and K_z of each 20 m block for the two bounds. The percentiles of the lower bound of the bracketing study were estimated from the log-normal probability plot shown in Figure 8-45.

Table 8-12. Block-size effective hydraulic conductivity simulated in Volume B using two different assumptions. The scale and truncation size are in metres. The percentiles for the upper bound were estimated by discarding all 20 m grid cell values that were not hydraulically connected in all three directions. The percentiles of the lower bound were estimated by assigning a low hydraulic conductivity value to the non-connected 20 m blocks and plot the resulting data in a log-normal probability plot, see Figure 8-45 /Follin et al. 2005/.

Corr. T model	Scale	$X_{r,min}$	$\text{Log}_{10}(K_{eff})$ (m/s)					
			10%	25%	50%	75%	90%	1σ
Upper bound	20	5.64	-10.17	-9.89	-9.65	-9.14	-9.03	0.60
Lower bound	20	5.64	-15.58	-14.15	-12.55	-10.94	-9.52	2.42

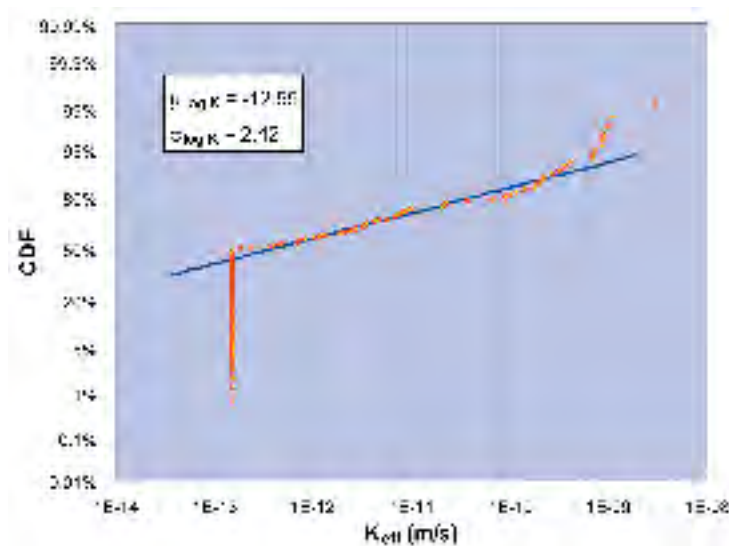


Figure 8-45. Log-normal probability plot of block-size effective hydraulic conductivity data simulated in Volume B /Follin et al. 2005/.

The span in the 50% percentile of log geometric mean between the two bounds is huge, almost three orders of magnitude. The geometric mean of the two medians is -11.00 . One way to estimate if this is a reasonable value is to compare more directly with hydraulic test data in KFM01A, the key borehole for the delineation of Volume B. According to Figure 8-13, about four out of seven 20 m PSS tests are below the measurement limit of the test equipment in Volume B, thus there is an empirical support for the deduced non-connectivity of 20 m blocks. Further, the frequency of PFL-f flow anomalies in Volume B is 0.078 m^{-1} , cf. Table 8-8, which implies a low average of c. 1.56 flow anomalies per 20 m block when assuming a uniform spacing between the flowing fractures. The product of this frequency times the geometric mean of the PFL-f transmissivities ($4.65 \times 10^{-10} \text{ m}^2/\text{s}$) suggests a 20 m block log conductivity of -10.44 ($3.63 \times 10^{-11} \text{ m/s}$), a value which is pretty close to the aforementioned geometric mean of the two medians obtained from the bracketing calculations.

Volume E

Figure 8-46 illustrates the conception used by /Hartley et al. 2005/; a 1,000 m cube with a hydro-geological DFN realisation and calculated hydraulic conductivities in the EW direction for a $9 \times 9 \times 9$ array of 100 m blocks. The model input parameters are shown in Table 8-11. The connected fracture area per unit volume, P_{32CON} , used was 130% of the total fracture area per unit volume of Open and Partly Open fractures.

The results shown in Table 8-13 demonstrate some characteristic properties, in particular to the uncorrelated model, as there is considerable heterogeneity but little correlation between adjacent blocks. The explanation for this is twofold. First, a high transmissivity feature can be of any size in the uncorrelated model. Secondly, because of the steep power-law size distributions, the high transmissivity fractures are relatively small and therefore affect only 1 or 2 blocks. The combination of these two facts leads to few, if any, continuous features of high hydraulic conductivity. The random variability makes the geometric mean larger and the variance smaller for the 20 m block than for the 100 m block. This is one of several reasons making the uncorrelated transmissivity model unattractive. The values shown for the correlated model scale are as expected.

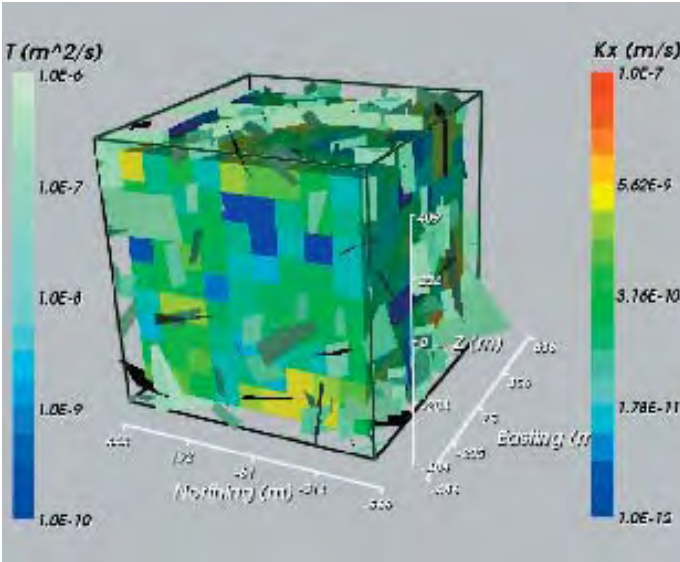


Figure 8-46. Visualisation of hydraulic conductivities in the EW direction for a $9 \times 9 \times 9$ array of 100 m blocks. The underlying DFN model is that of Volume E using a correlated transmissivity model. Features with large transmissivity are superimposed /Hartley et al. 2005/.

Table 8-13. Effective hydraulic conductivity for correlated, uncorrelated, semi-correlated transmissivity concepts for Volume E, see Table 8-11. Scale (cell size) and the $X_{r,min}$ truncation size are in metres. The P_{32CON} used was 130% of the total P_{32} of Open and Partly Open fractures /Hartley et al. 2005/.

T model	Scale	$X_{r,min}$	Log ₁₀ (K_{eff}) (m/s)					
			10%	25%	50%	75%	90%	(1 σ)
Corr.	20	0.28	-11.07	-10.44	-9.77	-9.07	-8.49	0.93
Corr.	100	5.64	-10.87	-10.12	-9.42	-8.78	-8.39	0.89
Corr.	100	14.1	-23.00	-10.68	-9.58	-8.79	-8.33	0.92
Uncorr.	20	0.28	-9.62	-9.00	-8.47	-7.99	-7.61	0.84
Uncorr.	100	5.64	-10.61	-9.84	-9.35	-8.81	-8.40	0.91
Semi-corr.	20	0.28	-9.99	-9.35	-8.76	-8.16	-7.84	0.85
Semi-corr.	100	5.64	-10.32	-9.61	-9.12	-8.64	-8.23	0.79
Corr. $k_r = 2.75$	20	0.28	-13.20	-11-13	-10.19	-9.41	-8.82	1.00

The results for these cases are also presented in Table 8-14 in terms of the individual axial components of hydraulic conductivity (K_x , K_y and K_z); the median ratios of maximum horizontal and minimum horizontal conductivities; the median ratios of maximum horizontal and vertical conductivities; and the strike of any general trend in the maximum horizontal conductivity. The ratios of anisotropy are calculated block-by-block and then the median is computed over the ensemble of blocks. The ratio of K_{hmax} to K_{hmin} is generally around 6, suggesting clear horizontal anisotropy. The ratio between K_{hmax} to K_z is between 1 and 1.5, showing only a very slight contrast with regard to the vertical direction. This result is dependent on the assumption made that there is no depth trend in the transmissivity field. For the correlated and semi-correlated cases, the anisotropy is orientated towards a strike direction between about 120° to 150°, as shown by the horizontal K_{hmax} . In contrast, there is no obvious regional anisotropy orientation for the uncorrelated case. The preference for a major anisotropy in the NW-SE direction is caused by the, relatively speaking, lower k_r value of the NW set, which means that this set generates the longest fractures. A quick glance at Table 8-11 explains the difference in horizontal hydraulic anisotropy relative to Volume B. In Volume B, the relative proportion of the NW set is c. 3% and in Volume E c. 19%.

Table 8-14. Comparison of anisotropy for correlated, uncorrelated and semi-correlated transmissivity concepts for Volume E. Scale (cell size) and the $X_{r,min}$ truncation size are in metres. The P_{32CON} used was 130% of the total P_{32} of Open and Partly Open fractures /Hartley et al. 2005/.

T model	Scale	$X_{r,min}$	Median log ₁₀ (K_x) (m/s)	Median log ₁₀ (K_y) (m/s)	Median log ₁₀ (K_z) (m/s)	Median K_h -ratio K_{max}/K_{min}	Median ratio K_{hmax}/K_z	Strike of K_{hmax} (°)
Corr.	20	0.28	-9.90	-9.74	-9.77	6.26	1.39	170-180
Corr.	100	5.64	-9.47	-9.46	-9.36	6.63	1.35	120-150
Uncorr.	20	0.28	-8.53	-8.49	-8.39	5.36	1.34	120-150
Uncorr.	100	5.64	-9.32	-9.32	-9.27	6.30	1.44	no trend
Semi-corr.	20	0.28	-8.80	-8.75	-8.63	6.29	1.25	40-60, 120-150
Semi-corr.	100	5.64	-9.10	-9.10	-9.03	5.88	1.38	120-150
Corr. $k_r = 2.75$	20	0.28	-10.28	-10.15	-10.16	7.24	1.32	30-60

Table 8-15. Block kinematic porosity for correlated, uncorrelated and semi-correlated transmissivity concepts for Volume E. Scale (cell size) and the $X_{r,min}$ truncation size are in metres. The P_{32CON} used was 130% of the total P_{32} of Open and Partly Open fractures /Hartley et al. 2005/.

T model	Scale	$X_{r,min}$	$\log_{10}(n_e)$ (-)				
			10%	25%	50%	75%	90%
Corr.	20	0.28	-4.93	-4.90	-4.85	-4.78	-4.70
Corr.	100	5.64	-5.39	-5.33	-5.25	-5.16	-5.09
Uncorr.	20	0.28	-3.73	-3.72	-3.70	-3.69	-3.67
Uncorr.	100	5.64	-4.69	-4.66	-4.64	-4.61	-4.57
Semi-corr.	20	0.28	-4.25	-4.24	-4.21	-4.18	-4.15
Semi-corr.	100	5.64	-4.91	-4.89	-4.85	-4.81	-4.77
Corr. $k_r = 2.75$	20	0.28	-5.12	-5.08	-5.02	-4.95	-4.88

The corresponding block kinematic porosity percentiles (10, 25, 50, 75 and 90) are given in Table 8-15. In a 20 m block, the median $\log(\text{porosity})$ is greatest for an uncorrelated case ($\log(n_e) = -3.7$) and lowest for a correlated case ($\log(n_e) = -4.9$). For a 100 m block, a one order of magnitude lower porosity is obtained. However, since the pore space of a DFN model is associated with the number of fractures, the decrease in kinematic porosity for a 100 m block is simply due to the higher value of the truncation.

Volume F

/Hartley et al. 2005/ carried out an analysis also for Volume F. A major difference between Volumes E and F is that Volume F has c. 45% of its fracture intensity in NE, whereas Volume E has c. 29%. On the other hand, the largest value of the power-law slope k_r is for the NE set and smallest value for the NW set. These differences lead to a slight horizontal hydraulic anisotropy $K_{h,max}$ with a strike direction of about 030° – 060° in Volume F, regardless of the transmissivity model assumed. For Volume E, the direction of a horizontal hydraulic anisotropy is less clear, with the uncorrelated transmissivity model showing no directional trend, and the correlated and semi-correlated cases showing a trend in 120° – 150° . The latter result is consistent with the smallest principal regional stress being in NE-SW. The results for Volume F are summarised in Table 8-16 through Table 8-18. The block-scale hydraulic conductivities are visualised as cumulative density functions in Figure 8-47 for the uncorrelated case, the correlated case, and for the semi-correlated case.

Table 8-16. Effective hydraulic conductivity for correlated, uncorrelated, semi-correlated transmissivity concepts for Volume F, see Table 8-11. Scale (cell size) and the $X_{r,min}$ truncation size are in metres. The P_{32CON} used was 26% of the total P_{32} of Open and Partly Open fractures /Hartley et al. 2005/.

T model	Scale	$X_{r,min}$	$\log_{10}(K_{eff})$ (m/s)					(1σ)
			10%	25%	50%	75%	90%	
Corr.	20	0.28	-10.56	-10.10	-9.54	-8.96	-8.48	0.79
Corr.	100	5.64	-10.19	-9.73	-9.15	-8.62	-8.31	0.75
Corr.	100	11.3	-10.84	-9.96	-9.19	-8.58	-8.28	0.88
Corr.	100	14.1	-11.19	-10.06	-9.27	-8.66	-8.32	0.84
Corr.	100	28.2	-23.00	-18.85	-9.52	-8.76	-8.83	0.83
Uncorr.	20	0.28	-9.56	-9.04	-8.62	-8.20	-7.94	0.63
Uncorr.	100	5.64	-10.01	-9.63	-9.29	-9.01	-8.77	0.49
Semi-corr.	20	0.28	-10.02	-9.36	-8.64	-7.89	-7.49	0.97
Semi-corr.	100	5.64	-10.09	-9.58	-8.93	-8.33	-7.85	0.89

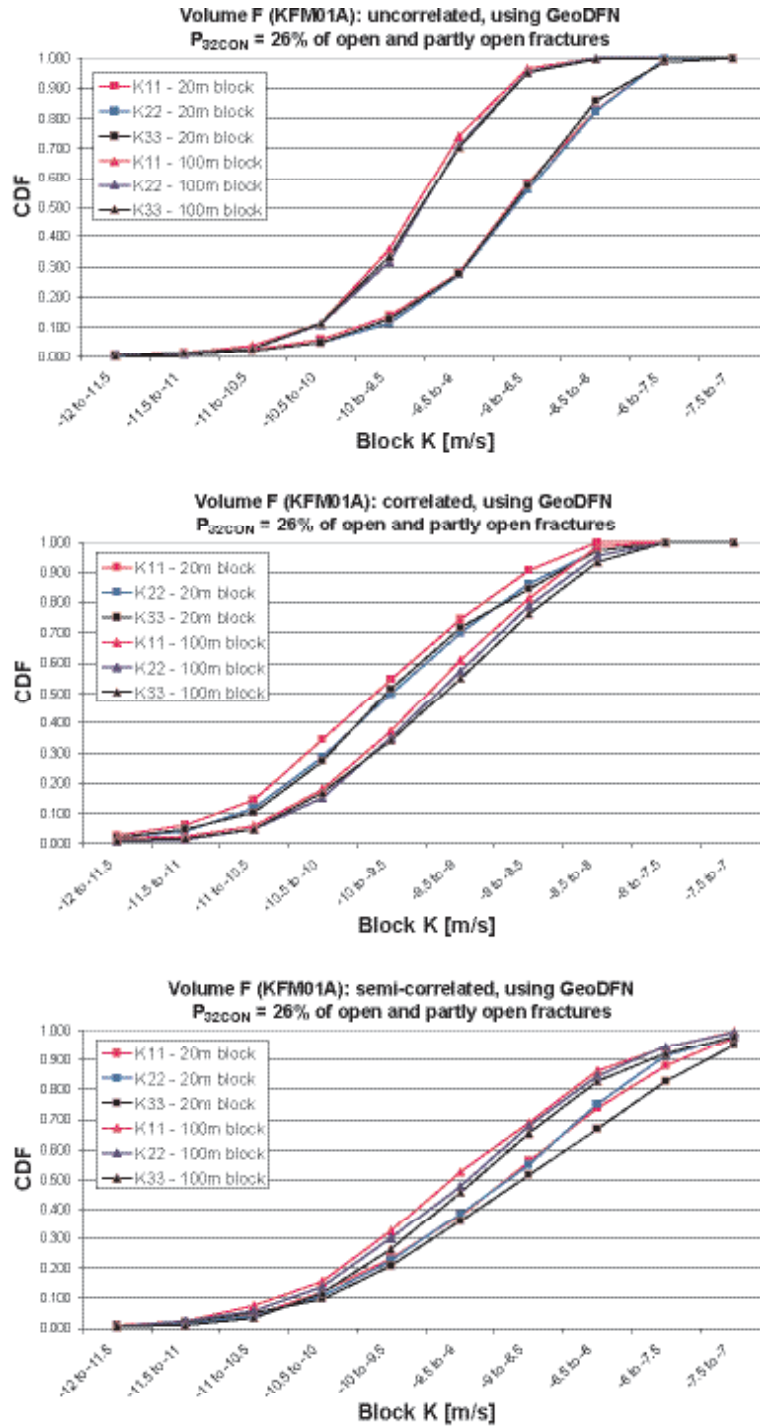


Figure 8-47. Hydraulic conductivity distributions for Volume F for an uncorrelated (top), a correlated (middle) and semi-correlated transmissivity model (bottom). K11, K22, and K33 correspond to K_x (Easting), K_y (Northing) and K_z (vertical), respectively. Model input parameters are shown in Table 8-11. The P_{32CON} used was 26% of the total P_{32} of Open and Partly Open fractures /Hartley et al. 2005/.

Table 8-17. Comparison of anisotropy for correlated, uncorrelated and semi-correlated transmissivity concepts for Volume F. Scale (cell size) and the $X_{r,min}$ truncation size are in metres. The P_{32CON} used was 26% of the total P_{32} of Open and Partly Open fractures /Hartley et al. 2005/.

T model	Scale	$X_{r,min}$	Median $\log_{10}(K_x)$ (m/s)	Median $\log_{10}(K_y)$ (m/s)	Median $\log_{10}(K_z)$ (m/s)	Median K_h -ratio K_{max}/K_{min}	Median ratio K_{hmax}/K_z	Strike of K_{hmax} ($^\circ$)
Corr.	20	0.28	-9.65	-9.50	-9.55	5.17	1.36	30-60
Corr.	100	5.64	-9.24	-9.15	-9.10	4.68	1.33	130-140
Uncorr.	20	0.28	-8.62	-8.57	-8.62	3.61	1.45	30-60
Uncorr.	100	5.64	-9.31	-9.25	-9.26	3.42	1.38	30-60
Semi-corr.	20	0.28	-8.69	-8.64	-8.55	6.98	1.32	30-60
Semi-corr.	100	5.64	-9.04	-8.95	-8.89	6.52	1.30	30-60

Table 8-18. Block kinematic porosity for correlated, uncorrelated and semi-correlated transmissivity concepts for Volume F. Scale (cell size) and the $X_{r,min}$ truncation size are in metres. The P_{32CON} used was 26% of the total P_{32} of Open and Partly Open fractures /Hartley et al. 2005/.

T model	Scale	$X_{r,min}$	$\log_{10}(n_e)$ (-)				
			10%	25%	50%	75%	90%
Corr.	20	1.12	-4.98	-4.94	-4.89	-4.82	-4.73
Corr.	100	5.64	-5.27	-5.22	-5.16	-5.07	-4.99
Uncorr.	20	1.12	-4.21	-4.19	-4.17	-4.14	-4.12
Uncorr.	100	5.64	-4.88	-4.87	-4.85	-4.83	-4.81
Semi-corr.	20	1.12	-4.22	-4.19	-4.16	-4.11	-4.06
Semi-corr.	100	5.64	-4.77	-4.74	-4.70	-4.65	-4.59

Discussion of findings

The sensitivity of the block-scale properties with regard to all the assumptions listed in Section 8.3.6 has been considered. The effect of truncation of lower fracture size limit has also been considered, a requirement of the follow-on regional groundwater flow modelling. The statistical properties inferred by the two modelling teams are summarised in Table 8-12 through Table 8-18.

Exploration simulations together with field data suggest a median value of the 20 m log geometric mean that is at least one order of magnitude lower for Volume B compared with Volume F. The corresponding value in Volume E is similar to that in Volume F, but this value is more difficult to appreciate as it is based on the assumption that the connected fracture area per unit volume is 130% the total fracture area per unit volume of Open and Partly Open fractures. The difference between Volumes F and B is possible to explain by recognising the findings of Volume C, which lies on top of Volume B. The connected fracture area per unit volume in Volume C is quite comparative to that in Volume F and at the same time 240% the value in Volume B, see Table 8-11. For this reason it is suggested that the effective conductivity findings deduced for Volume F are treated as preliminary estimates for Volume C primarily and to keep Volumes B and C separated. Concerning Volume D (G), there are no hydraulic data above the lower measurement limit available for a more elaborated analysis. In conclusion, the findings presented for Volume B may be regarded as an upper bound estimate for the conditions in Volume D.

Concerning anisotropy, things are a bit more complicated. First of all it is important to distinguish between hydraulic anisotropy and structural. The former depends on the latter but not solely. The hydraulic anisotropy depends also on the fracture transmissivities. These have been assumed to be free from a depth trend in the block-scale property modelling. This means that the findings reported on hydraulic anisotropy mainly reflects the differences seen in the total fracture intensity, in the relative intensity proportions and in the power-law slopes. The values of these entities vary between sets and between volumes in a complicated manner. For instance, there are clear differences

between Volumes B and C in terms of relative intensity proportions see Table 8-11. In Volume B, the steeply dipping NE set is the dominating set followed by the gently dipping HZ set. This situation is reversed in Volume C. The relative intensity proportions reported for Volume F, however, resemble the conditions in Volume B better than the conditions in Volume C, despite the greater total fracture intensity in Volume C. This ambiguity probably comes from that /Follin et al. 2005/ used the predefined set bounds of the global geological DFN for their delineation of the relative intensity proportions, whereas /Hartley et al. 2005/ challenged different geological DFN models in the hydrogeological DFN analysis and prioritised a slightly different definition of the set bounds compared with the global geological DFN.

Common to Volumes B, C and F is the low relative intensity proportion of the NW set. In contrast, the relative intensity proportion is more pronounced in Volumes A and E, see Table 8-11. In effect, the simulations conducted in Volume E suggests a slight horizontal anisotropy striking NW, where the strike is NW in Volume F, see Table 8-14 and Table 8-17.

The upscaling of the effective hydraulic conductivity from 20 m blocks to 100 m blocks seems to work pretty straightforward for the correlated and semi-correlated transmissivity models. The uncorrelated transmissivity model, however, produced quite peculiar results, such as a decreasing log geometric mean when the size of the block was increased. Given the findings of the two modelling teams, it is suggested that the semi-correlated model is the main conceptual model to work with, but that more concern is put into the definition of the variability (uncertainty).

Finally, the aforementioned trade off between using the best fit truncation size and the limit of the simulation that is possible to run computationally is a matter that needs to be treated with great care. By decreasing the truncation size, the fracture connectivity of the generated DFN will without doubt increase. However, depending on the objectives of the flow model, the effect of using a truncation size may be more or less severe. From a rock engineering point of view it may be advocated that the site investigations conducted in Forsmark demonstrate that the additional rock mass fracturing that comes from a low truncation size will probably not contribute significantly to the bulk flow because of the low transmissivities. Notwithstanding, from a safety assessment point of view it is noted that the extra connectivity that comes from a lower truncation size will increase the probability of having features in the intermediate size range. Based on the block-scale property findings, the two modelling teams suggest as a rule of thumb that the minimum value of the truncation size should not exceed half the size of the computational grid cell. The preferred value is 25% of the grid cell.

8.5 Boundary and initial conditions

8.5.1 Boundary conditions

The boundary conditions used in version 1.2 of the Forsmark site descriptive model represent the transient processes of (i) shoreline displacement due to postglacial rebound sea level changes, and (ii) the variations in the salinity of the Baltic Sea. The uncertainties in the evolution of the two processes during the considered postglacial period are discussed in Chapter 3, see Figure 3-12 and Figure 3-13, respectively. Figure 8-48 shows the descriptions used for the regional flow simulations.

The general modelling approach was to hold the model domain fixed (*i.e.* same x, y and z coordinates), but modify the head and salinity on the top surface in time. The rate of the land rise is fairly constant over the time period considered, although it is initially greater for about the first thousand years until 7,000 BC. The maximum current elevation in the regional-scale model is about 26 m, so the area has only emerged from sea in the last 3,000 years.

Salinity rises gradually at the start of the Littorina period about 7,500 BC, reaches a maximum at 4,500 BC, and then gradually starts to reduce toward modern salinity levels from 3,000 BC. It is noted that there is a considerable uncertainty associated with the exact looks of the lower graph in Figure 8-48. The uncertainty concerns both the timing and the magnitude of the salinities, see Figure 3-13. In particular, there is a difference in salinity between the shallow waters close to the coast and the deeper parts of the Baltic Sea outside Forsmark. For example, the present-day salinity close to the coast is of the order 0.5%. This discrepancy has no impact on the historic evolution, however.

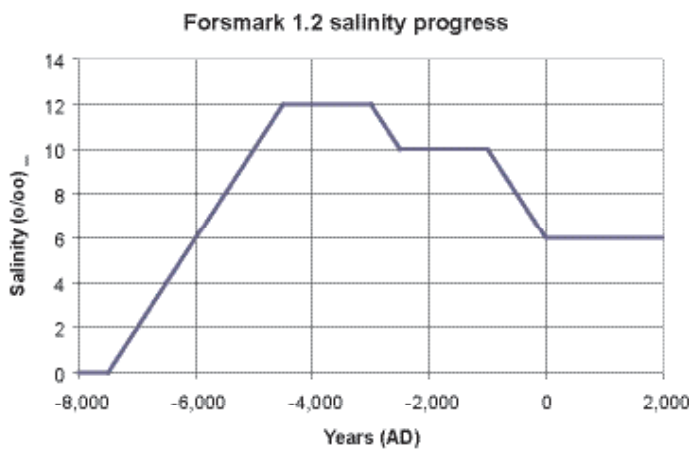
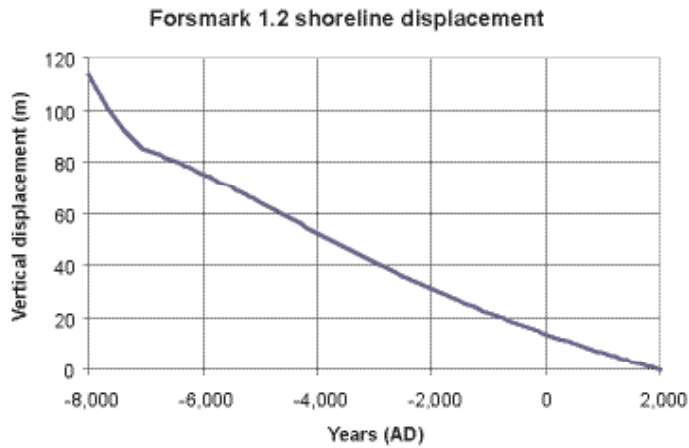


Figure 8-48. Upper: The shoreline displacement in Forsmark relative to the current sea-level for the time period considered in the regional flow simulations cf. Figure 3-12. Lower: The salinity change of the Baltic Sea at Forsmark considered in the regional flow simulations cf. Figure 3-13.

It is also important to have a more general hypothesis of the evolution of surface and sub-surface reference waters. The current understanding of the evolution during Holocene is discussed in Chapter 3 in Figure 3-15. The simulations start when the area is covered by the Ancylus Lake, which is a mixture of glacial melt water and meteoric water. This is followed by the Littorina Sea period, whose salinity first increase and the gradually decreases, and eventually the land emerges from the sea and so becomes exposed to infiltration of modern meteoric water.

For flow, the head on the top surface was set to the topographic height that evolves in time due to changes in the height relative to the shoreline (see Figure 8-48). Offshore, the head was equal to the depth of the sea multiplied by the relative density of the Baltic Sea to freshwater. A variant considered by /Hartley et al. 2005/ was to use a flux-type boundary condition with a potential infiltration of 200 mm per year. Another variant considered by /Follin et al. 2005/ was to fix the head at ground surface in the discharge areas only and lower it in the recharge areas by an amount that was in accordance with the observed variability in the elevation of the water table, see Figure 8-49. The objective of the two variants was to study the implications of a topographic head for groundwater flow at repository depth by reducing the impact of local topographic gradients relative to the topographic regional gradient.

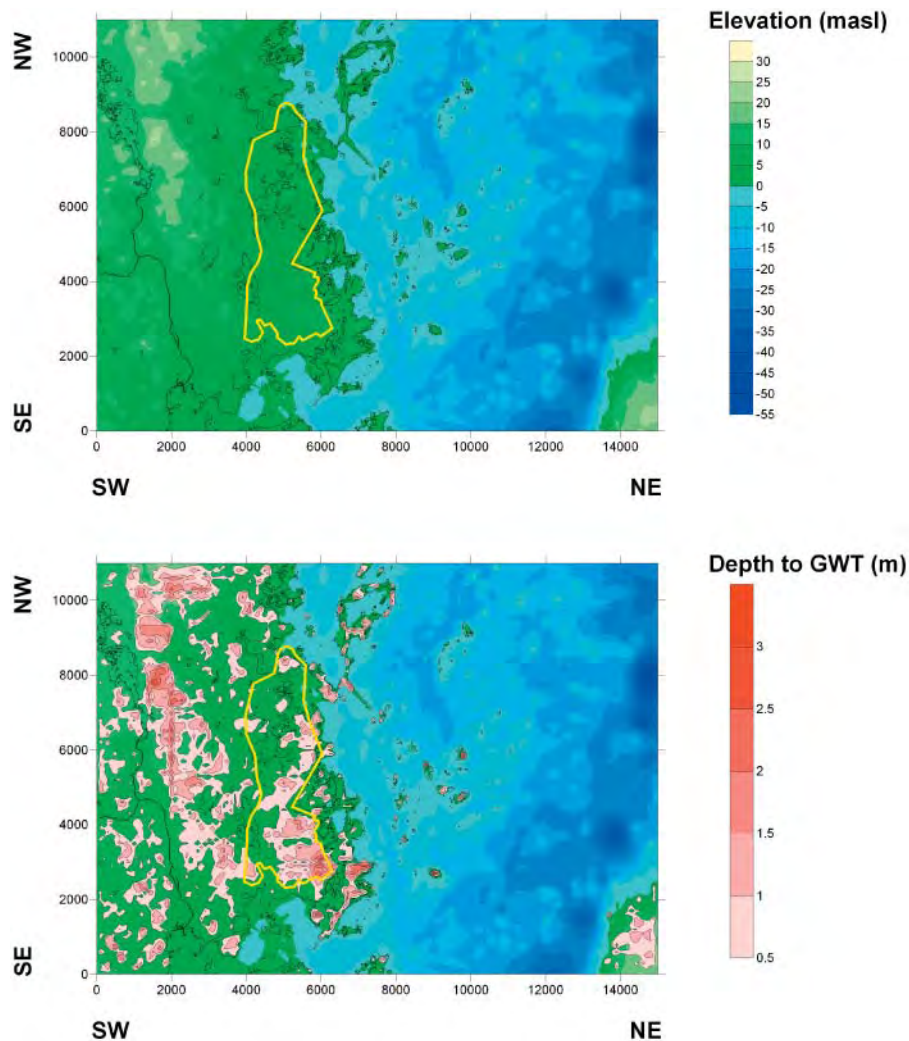


Figure 8-49. Examples of two different top boundary conditions. The upper inset shows the variability in the head if fixed at the present-day topography. The lower inset shows an alternative where the head is lowered in the recharge areas /Follin et al. 2005/.

8.5.2 Initial conditions

The initial condition for the reference waters assumes a profile of Brine at depth and Glacial water at the surface, with a start time of 10,000 BP (8,000 BC). In early models, the initial condition derived in the Simpevarp 1.2 modelling /Hartley et al. 2005b/ and /Follin et al. 2005b/ was adopted, i.e. piecewise linear with full Glacial to 700 m depth, then a gradual rise in Brine to full Brine at 1,500 m depth. This gave reasonable results, but was not entirely consistent with the only deep salinity data in KFM03A. KFM03A has three groups of data points at depth (there are groups of data relating water samples that have been taken from the same location, but at several different times): one at about 640 m depth that has a salinity of around 9‰ and low magnesium content, suggesting predominantly Brine origin for the salinity; one at about 940 m depth that has a salinity of around 14‰ and very low magnesium, suggesting the salinity is entirely of a Brine origin, and a similar sample at 990 m depth with around 16‰ salinity from Brine. Assuming a simple linear profile in Brine, KFM03A suggests that Brine starts to occur at about 500 m depth and rises to about 22‰ at 1,000 m depth which extrapolates to full Brine at about 2,700 m depth /Hartley et al. 2005/.

The simulated advective flows at depth are small due to the aforementioned low hydraulic conductivity of the rock domains and the depth trend in the transmissivity of the deformation zones. Together with the tendency toward stagnant flow within the dense Brine, the initial conditions for reference water composition tends to be preserved up to the present-day, and hence the measured

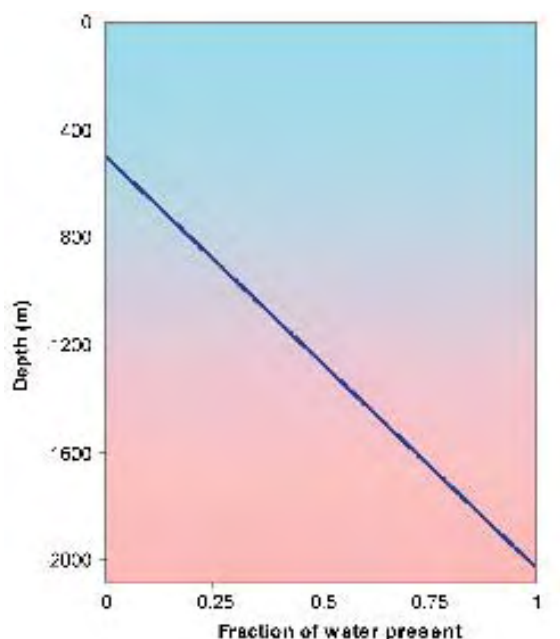


Figure 8-50. Initial condition for reference water transport, at 10,000 BP. Above 500 m the water is pure Glacial (coloured cyan). There is then a linear transition between Glacial and Brine (coloured red) toward pure Brine below 2,000 m.

hydrogeochemistry at depth is a good guide for choosing initial conditions at 10,000 BP. The ultimate initial condition used in the models reported here has full Glacial to –500 m, and then Brine rises linearly to full Brine at –2,000 m, as illustrated in Figure 8-50. This gradient is perhaps too large and gives an over-prediction of Brine at the base of KFM03A as shown below.

The initial condition for flow was calculated by holding the reference water fractions fixed, and calculating the flow field that represents hydrostatic equilibrium at the initial time of 8,000 BC. Moreover, the initial conditions of the salinity profile in the kinematic porosity field were assumed to be in equilibrium with the salinity profile in the matrix porosity field.

8.6 Regional groundwater simulations

The final two steps of the workflow shown in Figure 8-24 involve calibration of the regional flow model against hydraulic and hydrogeochemical measurements and palaeo-hydrogeological simulations, respectively. The latter task comprises flow path simulations and sensitivity tests. In practice, there are not clear distinctions between these steps. For instance, calibration becomes meaningful only if the flow model is free from uncertainties in respect of the size of model domain, choice of boundary conditions and the resolution of the computational grid. Simulations with a non-calibrated model can also be of importance provided that the questions asked are correct vis-à-vis the hydrogeological simplifications (uncertainties). For example, if regional hydrogeological uncertainties can be shown to have little effect on the flow system within the target volume, although the model domain is simulated to be much more conductive than suggested by the hydraulic field tests, the conclusions drawn from the simulations still ought to be of significance.

8.6.1 Hydraulic properties

The significant differences in the deduced conductive fracture intensity together with the measured differences in transmissivity of the rock mass fracturing, as demonstrated in Section 8.4, have important implications for the conception of groundwater flow through RFM029. Different conceptions may be discussed ranging from a very low conductive rock mass characterised by an impermeable

rock matrix and a very sparsely connected and low-transmissive DFN to a moderately conductive rock mass characterised by a pretty well connected and moderately-transmissive DFN. The pertinent examples in mind are of course Volumes D (G) and C (upper part of F), see Figure 8-36.

The choice of conception is also related to the scale of the flow problem. By scale we mean both the size of the model domain that is invoked by the flow problem, and the resolution of the computational grid. On a regional scale, it is generally necessary to use some kind of continuum approach and a grid resolution of about 100 m. Discrete approaches are generally limited to much smaller model domains. As already mentioned in Section 8.3.3, different conceptions may or may not be used in parallel dependent on the objectives and scale of the flow problem treated.

Figure 8-51 illustrates two alternative continuum approximations suggested by the two modelling teams for regional groundwater flow and mass (salt) transport simulations, which is the flow problem dealt with in version 1.2. The uppermost cross-section shows a multicomponent Continuous Porous Medium (CPM). The lowermost cross-section shows a stationary Equivalent Porous Medium (EPM).

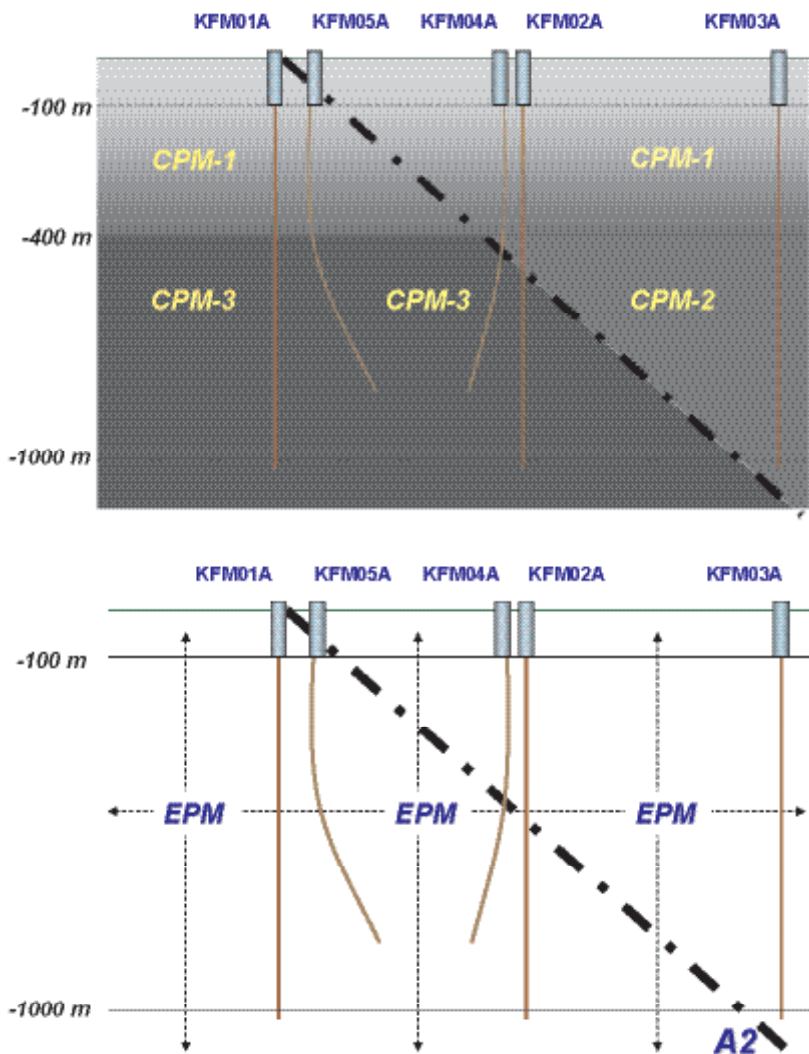


Figure 8-51. Schematic cross-sections showing two alternative conceptual models of RFM029 suggested by the two modelling teams for numerical simulation of regional groundwater flow and mass (salt) transport in version 1.2. The uppermost cross-section shows a multicomponent CPM model with three different CPM bodies. This conception was analysed by /Follin et al. 2005/. The lowermost cross-section shows a uniform EPM model underpinned by statically homogeneous hydrogeological DFN. This conception was analysed by /Hartley et al. 2005/.

The hypothesis suggested by /Follin et al. 2005/ was to simplify the local representation of the rock mass heterogeneity between the Eckarfjärden and Singö deformation zones by using a few more or less low-conductive CPMs. The spatial dimensions of the CPMs were based on the hydrogeological DFN analysis of Volumes A–D, see Figure 8-51. The rest of the regional model domain was characterised as a single CPM, see Figure 8-52. This was because there were little data from outside the tectonic lens with which to parameterise a more sophisticated model conception.

The hypothesis suggested by /Hartley et al. 2005/ was to maintain the local representation of the rock mass heterogeneity within RFM029 by using an EPM representation of each stochastic hydrogeological DFN generated, but simplifying the modelling by using uniform hydrogeological DFN statistics over the whole rock domain RFM029. Hence, spatial variations of the EPM properties in the tectonic lens only occur due to the stochastic nature of the DFN parameters. The choice made by /Hartley et al. 2005/ was to use the DFN statistics inferred for Volume E, i.e. $P_{32CON} = 130\% P_{32}$ of all Open and Partly Open features. Moreover, only the local-scale area composed of rock domain RFM029 was modelled by the EPM concept. The rest of the regional model was treated as a single CPM, see Figure 8-52. This was because there were little fracture data from outside the tectonic lens with which to hydraulically parameterise a geological DFN in this region, although a section of borehole KFM04A indicates higher fracture intensity outside the tectonic lens.

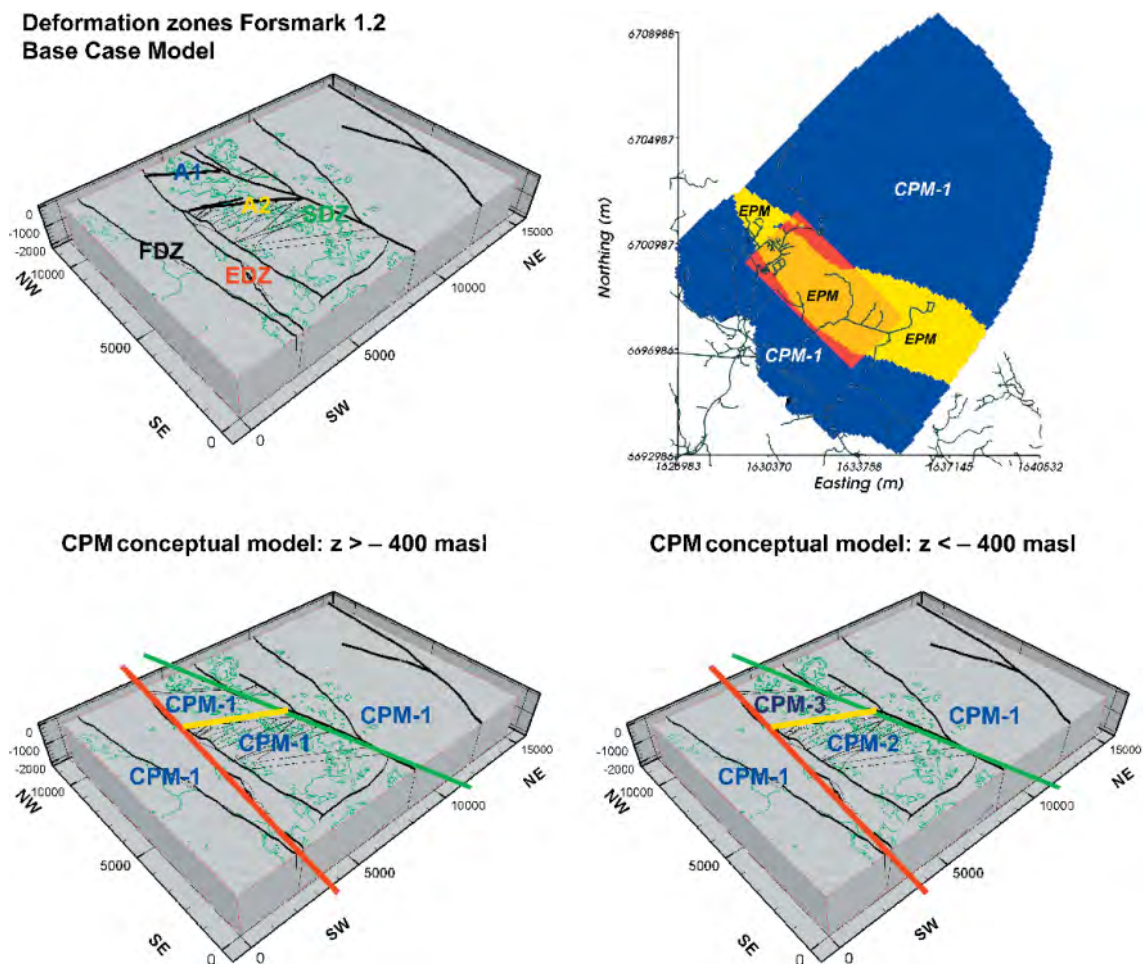


Figure 8-52. Upper left: The base model with labels on the major deformation zones: FDZ = Forsmark DZ, EDZ = Eckarfjärden DZ, SDZ = Singö DZ, A1 = ZFMNE00A1 and A2 = ZFMNE00A2. Upper right: The local-scale area composed of rock domain RFM029 (yellow and orange) was modelled using an EPM model, whereas the rest of the regional model was treated as a CPM (blue and red). A grid size of 50 m was used in the orange and red areas. Outside of that, a grid size of 100 m was used /Hartley et al. 2005/. Lower left and right: The volume between the Eckarfjärden and Singö deformation zones was characterised by a few more or less low-conductive CPM models. Outside of that a single CPM was assumed /Follin et al. 2005/.

Table 8-19. Parameter values selected for the multicomponent CPM conceptual model /Follin et al. 2005/.

Property	CPM-1	CPM-2	CPM-3	Comment
Hydraulic conductivity K (m/s)	1×10^{-6} – 5×10^{-10}	5×10^{-10}	1×10^{-11}	PSS 100 m, Figure 8-13 Table 8-13, 8-16
Kinematic porosity n_e (–)	1×10^{-4} – 2×10^{-5}	2×10^{-5}	5×10^{-6}	Table 8-15, 8-18
Specific storativity S_s (m^{-1})	7×10^{-6} – 2×10^{-8}	2×10^{-8}	2×10^{-9}	Assumed analogous to equation (8-11) in Section 8.4.2

Table 8-19 shows the parameter values selected for the multicomponent CPM model. The hydrogeological DFN parameters underpinning the EPM conceptual model are those shown in Table 8-11. The truncation size of the DFN was set to 25% of the grid size. In order to avoid numerical problems, a value of 5×10^{-11} m/s was used as the minimum hydraulic conductivity for the grid cells hydraulic conductivity. The parameter values in both models were altered during the course of the simulations as a means of studying the sensitivity of the regional groundwater flow system to different hydrogeological uncertainties.

Formulae analogous to equations (8-9), (8-10) and (8-11) were used for assigning effective values of the fracture transport aperture (e_t), kinematic porosity (n_e) and storativity (S) to the hydrogeological DFN underpinning the EPM. These formulae were taken from the findings reported in /Rhén et al. 1997b/, /Rhén and Forsmark, 2001/, /Andersson et al. 1998, 2000b/ and /Dershowitz et al. 2003/.

8.6.2 Cases for the modelling

The main objectives of the regional flow modelling using a reasonably matched flow model are to achieve the following:

- I. **Palaeo-hydrogeological understanding:** An improved understanding of known and unknown palaeo-hydrogeological conditions is necessary in order to gain credibility for the site descriptive model in general and the hydrogeological description in particular. This requires modelling of the groundwater flow from the last glaciation up to present-day with different boundary conditions and hydraulic properties, and comparison with measured TDS and other hydro-geochemical measures.
- II. **Simulation of flow paths:** The simulation and visualisation of flow paths from a tentative repository area is a means for describing the role of the current understanding of the modelled hydrogeological conditions in the target volume, *i.e.* the conditions of primary interest for Safety Assessment. Of particular interest here is demonstration of the need for detailed far-field realism in the numerical simulations. The motivation for a particular model size (and resolution) and set of boundary conditions for a realistic description of the recharge and discharge connected to the flow at repository depth is an essential part of the groundwater flow path simulations.

Several model cases were constructed to quantify the effects of and illustrate each of these issues. During the initial stages of the modelling, a significant number of other cases, including the simple rock domain models were created on route to gain an understanding of how individual model parameters affect the calibration, and ultimately to what ranges of parameters that gave a reasonable match to the field data. The approach was to first define a Reference Case of properties and conditions that gives a reasonable match of the present-day salinity and mixing fractions, and then to consider variants from this to illustrate the sensitivity to the various issues. Hence, the concept of Reference Case properties is not necessarily equivalent to the best parameter setup. Indeed, there may be more than one parameter setup that provides a good match.

Due to the great spatial variability in the rock mass fracture intensity and the uneven distribution of rock mass related flow anomalies properties it was decided to start the assignment of HRD properties for the regional flow simulations with simple homogeneous CPM models and then gradually develop to include more sophisticated concepts. Table 8-20 shows a summary of all properties and conditions for RFM029 arrived at by /Hartley et al. 2005/ and /Follin et al. 2005/. The defined properties and conditions are here called the EPM Reference Case and the CPM Reference Case, respectively.

Table 8-20. Summary of hydrogeological properties and conditions for RFM029 as arrived at by /Hartley et al. 2005/ and /Follin et al. 2005/.

Parameter	EPM Reference Case	CPM Reference (Modified) Case
Model domain and grid resolution	About 15×11×2.3 km with a 50 m grid covering the potential repository area and the five boreholes KFM01A–KFM05A. A 100 m grid was used elsewhere. No flow model boundaries aligned with regional water divides and large deformation zones	15×11×2.1 km with a 100 m cell size in the horizontal and an increased discretisation in the vertical between ground surface and 400 m depth (mean cell size c. 30 m). Artificial no-flow model boundaries aligned with the perimeter of the model domain
Initial condition	Full Glacial 0–500 m; then linear gradient to no Glacial/full Brine at 2,000 m depth	Full Glacial 0–450 m; then linear gradient to no Glacial/full Brine at 1,900 m depth For the sensitivity cases full brine was assumed at 1,450 m depth
Top surface BC	Head equals topography	Head equals topography
Top surface waters	Before 7,500 BC – Baltic Ice Ancylus Ice Lake (Glacial) 4,500 BC – Littorina Sea reaches its maximum salinity After 2,500 BC – Meteoric precipitation with land rise	Before 7,500 BC – Baltic Ice Ancylus Ice Lake (Glacial) 4,500 BC – Littorina Sea reaches its maximum salinity After 2,500 BC – Meteoric precipitation with land rise
HCD hydraulic conductivity K	As HCD1 (8-7a,b) with slightly modified depth dependence on hydraulic conductivity for a few DZ	As HCD1 (8-7a,b) with slightly modified depth dependence on hydraulic conductivity for a few DZ
HCD kinematic porosity n_e	(8-9)	(8-9)
HRD hydraulic conductivity K	Single EPM based on Table 8-11 and a corr T-model. This had block-scale properties of $K_{50\%} \sim 4 \times 10^{-10}$ m/s, $K_{10\%} = 1 \times 10^{-11}$ m/s. A $K_{\min} = 5 \times 10^{-11}$ m/s was adopted for cells without fractures	Multicomponent CPM with properties according to Table 8-19 For the sensitivity cases a single CPM with a $K = 5 \times 10^{-10}$ m/s was adopted
HRD kinematic porosity n_e	1×10^{-5}	Multicomponent CPM with properties according to Table 8-19
Matrix porosity n_m	3.7×10^{-3}	Not applicable
Ratio of immobile volume to mobile α_c	Not applicable	0 For the sensitivity cases a single CPM with a $\alpha_c = 10$ was adopted
Multi-rate coefficients (s^{-1})	Not applicable	0 For the sensitivity cases a single CPM with $(a_{\min}, a_{\max}) = 1 \times 10^{-10} - 1 \times 10^{-3}$ was adopted
FWS for rock matrix diffusion a_r (m^2/m^3)	1	0 For the sensitivity cases a single CPM with $FWS = 2 \text{ m}^2/(b \cdot m^2)$ where b is the geological fracture thickness was adopted (Nota bene: HCDs only)
Matrix diffusion length into matrix blocks L_D (m)	1	Not applicable
Intrinsic diffusion coefficient into matrix D_e (m^2/s)	5×10^{-13}	Not applicable

Both modelling teams carried out a series of sensitivity cases about the two Reference Cases, their properties and conditions. These cases were analysed in order to assess the sensitivity on the comparison with data for the resulting palaeo-hydrogeological simulations, and for current-day flow simulations, as further explained by /Hartley et al. 2005; Follin et al. 2005/. The text shown in red in Table 8-20 indicate the changes made for a variant called the CPM Modified Case that was used as a basis for the sensitivity analyses by /Follin et al. 2005/. The results from these analyses are commented on in Section 8.6.6.

8.6.3 Comparisons with measured data

Premises for comparisons

Hydraulic properties are generally estimated from the evaluation of hydraulic test results related to the geological domains as shown in Section 8.4. The next phase is to set up a numerical groundwater flow model by combining the geometric information associated with the geological domains with the preliminary hydraulic properties and evaluate the flow model results versus relevant data sets, e.g. natural heads, interference tests, tracer tests, and hydrogeochemical profiles. Some of these data sets come into play as calibration targets during the course of the development of the hydrogeological model. However, at this point the matching of simulations against detailed measurements is above all indicative as a regional model domain is treated with a significant imperfection in terms of detailed discretisation. For instance, the bedrock hydrogeological model treats a flow system that is 2.1 km deep, 15 km long and 11 km wide, hence much of the attention of the flow model by definition prioritises what is going on at repository depth in the regional perspective. In order to cope with this huge volume, the current numerical simulation models use coarse grid resolutions of 50–100 m. It is important to recall these shortcomings when comparing simulation results with detailed measurements.

Among the different implications associated with using a coarse grid resolution of 50–100 m the following ones are of particular concern for the integration with surface hydrology data, near-surface hydrogeology data, geology data and hydrogeochemistry data described in Chapters 4, 5 and 9:

- The deterministically treated deformation zones in Forsmark are significantly more conductive than the sparsely fractured rock mass in between. The deformation zones' thicknesses are generally not thicker than the grid resolution, which means that an implicit representation is used more or less frequently. A few deformations zones only are as thick or thicker.
- Most likely the body of the percolating groundwater circulates fairly high up in the rock due to the aforementioned significant depth trend in the hydraulic conductivity.
- The hydrogeochemical sampling at depth is currently restricted to deal with fractures with a transmissivity of at least $1 \times 10^{-8} \text{ m}^2/\text{s}$, a magnitude which is rarely found in individual fractures outside the deterministically treated deformation zones.
- The hydrogeochemical sampling represents water samples gathered by pumping with small flow rates from individual fractures intersecting very slim boreholes, whereas the simulated flow model concentrations represent data of a numerical continuum with flowing grid cell pore volumes of the order of 10–100 m³.
- The uppermost parts of the hydrogeochemical profiles are probably governed by the local recharge and the near-surface hydrogeological conditions as the regional topographic relief is low and the body of the bedrock is covered by Quaternary deposits of a different chemical composition and much greater porosities than the bedrock at depth. The mean thickness of the Quaternary deposits is of the order of a few metres, which means that the vertical to horizontal aspect ratio of the uppermost grid cells is poor, 0.02–0.08.

The classic conception of a calibration target for groundwater flow simulations, i.e. the difference between simulated and measured hydraulic heads, is difficult to apply in sparsely fracture rocks as it requires a superior geometric control of the positions of the flowing fractures/zones and their intercepts with the boreholes. Moreover, as most boreholes in Forsmark, from which data are available for version 1.2, are fairly new they have so far been subjected to water sampling and single-hole hydraulic tests mainly implying short time series and very few interference tests. The aforementioned drilling induced responses are useful in a qualitative sense but provide no means for a quantitative analysis unfortunately.

The primary data used for comparisons with the regional groundwater flow simulations of version 1.2 are the hydraulic and hydrogeochemical data that were available from boreholes within the candidate area. More precisely, these include the single-hole hydraulic tests, salinity profiles and mixing ratios along the trend and plunge of KFM01A–5A, under present-day conditions. It also includes concentrations of Cl⁻ (chloride), ratios of the environmental isotopes $\delta^{18}\text{O}$ and δD and, more tentatively, comparisons with the reported M3 mixing proportions. The latter two sources of data come from the hydrogeochemical measurements and models, see Chapter 9.

It should be remembered that only few samples are available from the deep core-drilled boreholes. Furthermore, only some samples are regarded as representative, see Chapter 9. Both representative and unrepresentative samples have been used by /Hartley et al. 2005/ for calibration purposes to increase the size of the otherwise sparse data set. Unrepresentative samples are not necessarily ‘bad’ samples. It simply means that some samples are considered more representative and have been picked as the best for chemical modelling purposes, see Chapter 9. /Follin et al. 2005/ decided to use data classified as representative only. Also data from percussion-drilled boreholes close to the cored boreholes were included in the work by /Hartley et al. 2005/ as an additional qualitative indication of near-surface data, typically in the top 100 m. However, the data from percussion holes have to be treated with caution since these water samples are taken from extracted water at relatively high pumped flow-rates compared with the cored boreholes. /Follin et al. 2005/ decided to not include the near-surface data.

It is also vital to remember that the hydrogeochemical sampling at depth currently is restricted to deal with fractures with a transmissivity of at least 1×10^{-8} m²/s, a magnitude which is rarely found in individual fractures outside the deterministically treated deformation zones. This means that the hydrogeochemical data gathered below c. 100 m depth by and large represents the water composition in the deformation zones. It is important to note that there are no hydrogeochemical data available for version 1.2 that clearly represents hydrogeochemical conditions in the rock mass fracturing or in the rock matrix pore water.

The salinity data are still quite limited in quantity and few are from larger depth. For instance, there are samples from near one kilometre depth only in KFM03A, where presumably a significant amount of Brine has been encountered. The next deepest sample location is at 512 m depth in KFM02A, where data suggest a small proportion of Brine at the base. Hence, data on the dense saline water are quite sparse. From a regional perspective there is a risk of bias if the comparison of salinity is made with data from just one or two deep boreholes. In addition, most of the boreholes are located near to the coast in very low topographic areas. So, there is an additional risk of bias due to sampling essentially in a single hydrogeological environment.

Due to the uncertainties associated with the limited quantity of hydrogeochemical data as well as the aforementioned uncertainties associated with the coarse grid resolution of the numerical simulation model, /Hartley et al. 2005/ aimed at calibrating their flow model against as much of the measured data as possible using a grid resolution of 50 m. In particular, the comparison performed considered the most conservative, and/or representative, measured data (Cl, $\delta^{18}\text{O}$ and Mg), and the water types with larger fractions in the M3 mixing approach where the $\pm 10\%$ error margin is less significant (cf. Chapter 9). The measurement error in $\delta^{18}\text{O}$ is approximately $\pm 0.2\%$, and $\pm 1\%$ in δD . In comparison, /Follin et al. 2005/ aimed at a traditional calibration of salinity (% by weight), while checking the effects for Cl, $\delta^{18}\text{O}$ and δD .

Comparison with measured hydraulic data

While developing the hydrogeological DFN, see Section 8.4, the DFN hydraulic properties were matched in a statistical sense against relatively small-scale hydraulic measurements, i.e. individual fracture transmissivities from the PFL-f tests or 5 m test section transmissivity data from the PSS tests. The unconditional statistical matching implies that a distribution of parameter values is fitted, but no specific attention was paid to the location of the individual measurements. It is difficult to calibrate an unconditional hydrogeological DFN model without a better representation of the geometry of inflows along the borehole. In conclusion, calibration of the DFN model was not performed by any of the two modelling teams mainly because it has only a secondary effect on regional-scale flow. Rather, the objective was to ensure the overall magnitude of the rock mass hydraulic conductivity of the correct low magnitude.

During the simulations it was found that the trend models for the deformation zone transmissivities suggested by equations (8-7a) and (8-7b) were a problem, as it was difficult to match both the hydraulic conductivity and hydrogeochemistry measurements without adjusting a few particular borehole-deformation zones intercepts in the simulation model to the measured transmissivity values of the sections where the hydrogeochemical data were sampled. This observation suggests that the spatial variability as suggested by Figure 8-33 is important, and that the hydrogeochemistry data, as we currently know them, by and large are governed by the hydrodynamic properties of the deterministically treated deformation zones.

A hydraulic calibration of the deformation zones intersecting the rock mass is possible by considering hydraulic properties on larger scales, e.g. compare the simulated hydraulic conductivity along the boreholes in the model with the long interval PSS data. As the grid resolution was 50–100 m in numerical simulation models, the modelling teams found it appropriate to compare with the available 100 m hydraulic conductivity data. PSS data on contiguous 100 m intervals are available for KFM01A (above c. 600 m depth), KFM02A and KFM03A. For KFM01A (below c. 600 m depth), KFM04A and KFM05A PFL flow anomaly data are available. The transmissivities inferred from the PFL flow anomalies can be grouped to approximate bulk hydraulic conductivities for 100 m intervals although these are likely to have a higher measurement limit than the PSS data (cf. Figure 8-6).

Comparison with measured hydraulic conductivities in deep boreholes

Figure 8-53 shows a comparison of hydraulic conductivity in KFM01A–5A for the EPM Reference Case, see Table 8-20. In all boreholes except KFM03A the measured hydraulic conductivity is lower than that produced by the EPM Reference Case model. The good match with KFM03A is perhaps unsurprising, since the hydrogeological DFN was based on the PFL/PSS data for this borehole, i.e. Volume E in Figure 8-36.

Figure 8-54 shows a comparison of hydraulic conductivity in KFM01A–3A for the CPM Reference Case, see Table 8-20. The good match at depth is unsurprising since a multicomponent CPM was used. However, the matches near surface are fairly poor, i.e. in KFM01A above 500 m borehole length, in KFM02A above 300 m borehole length and in KFM03A above 100 m borehole length.

Comparison with measured salinities in shallow and deep boreholes

Figure 8-55 shows the comparison with measured salinities in boreholes KFM01A–04A for the EPM Reference Case model. By superimposing the data from the boreholes, a reasonably consistent and smooth measured trend of salinity with depth is observed. The only significant anomaly in the measured data is that freshwater is measured near the surface in KFM02A whereas salinities similar to that of sea water are measured in KFM01A, KFM03A and KFM04A.

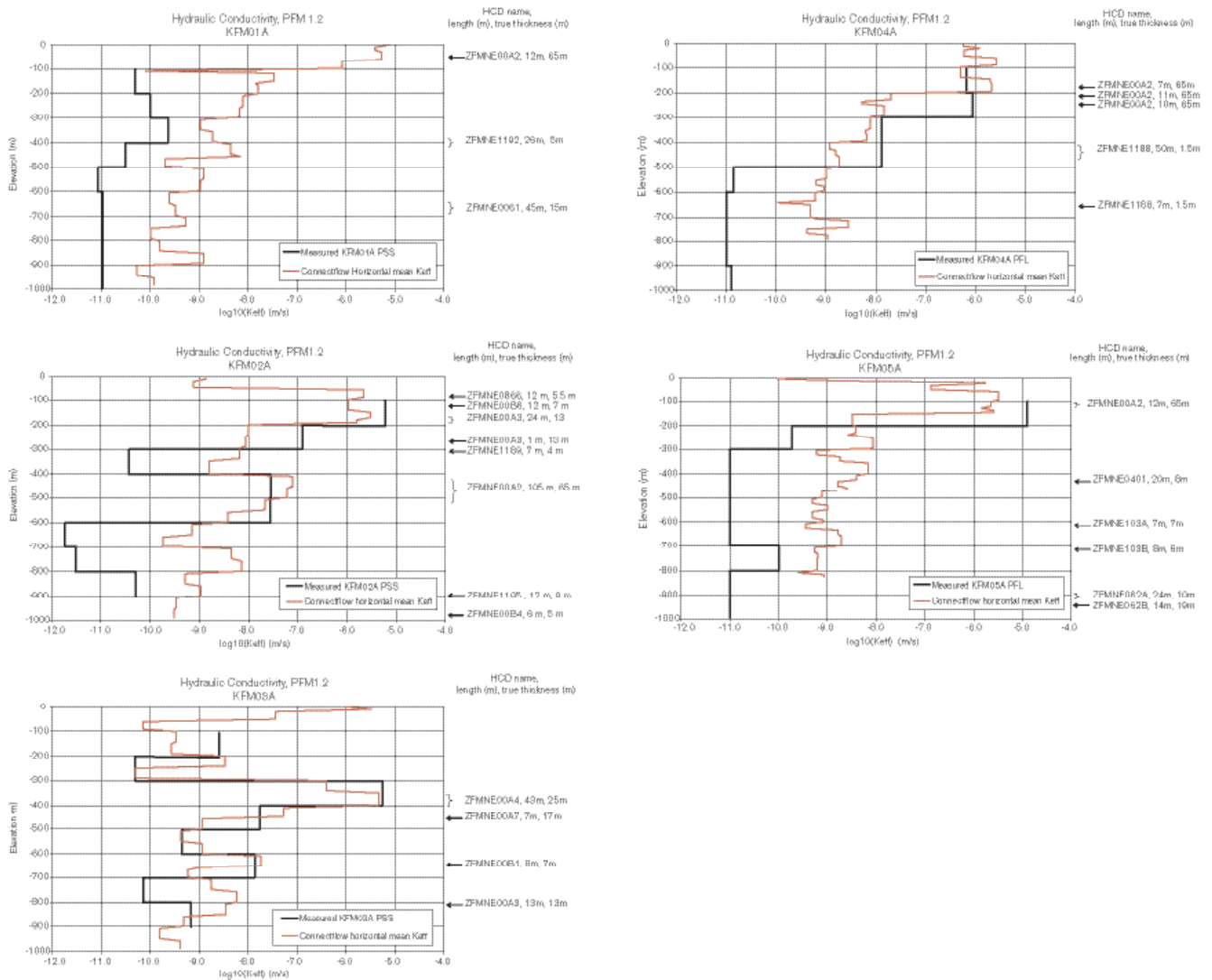


Figure 8-53. Comparison with hydraulic conductivity in KFM01A–KFM05A for the EPM reference Case model treated by /Hartley et al. 2005/. Values simulated in the model are shown by brown lines, whereas the measured values in 100 m intervals are shown in black /Hartley et al. 2005/.

The model simulations also predict similar profiles down the boreholes, except that KFM02A and KFM03A perhaps have higher salinity between depths of 200–700 m than KFM01A and KFM04A. This is interesting as KFM01A and KFM04A are in the less hydraulically conductive area below deformation zone ZFMN00A2. Above 200 m, the model strongly under-predicts salinity (except at KFM02A maybe). If correct, this creates a conceptual problem since it is hard to reconcile having sufficient hydraulic conductivity to allow infiltration of a Littorina pulse without a following infiltration of freshwater once the site was exposed to precipitation about 1,000 years ago. This may just be a question of having to fine-tune surface hydraulic, transport properties and boundary conditions to obtain a good match. The salinity at 1 km depth, as seen in KFM03A, is over-predicted despite the very gradual rise in Brine specified in the initial condition that gives about 30% Brine at one kilometres depth. It would suggest that the Brine is located even deeper. This interpretation is supported by the findings reported by /Ludvigson et al. 2004; Ludvigson and Levén, 2005/, who looked at the salinity issues in detail.

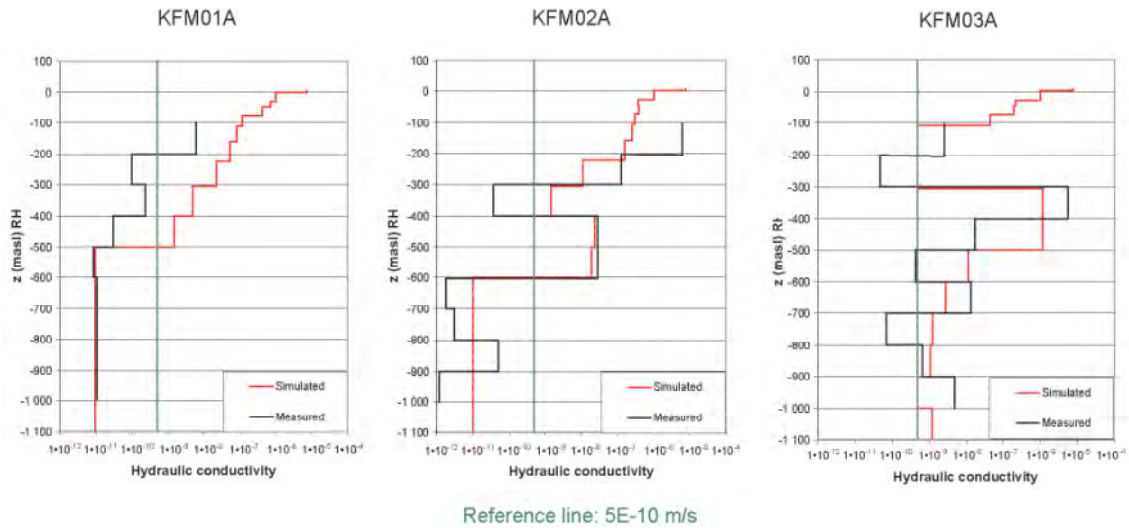


Figure 8-54. Comparison of hydraulic conductivity in KFM01A–KFM03A for the CPM Reference Case model treated by /Follin et al. 2005/. Values simulated in the model are shown by red lines, whereas the measured values on 100 m intervals are shown in black. The green reference line is inserted for ease of comparisons /Follin et al. 2005/.

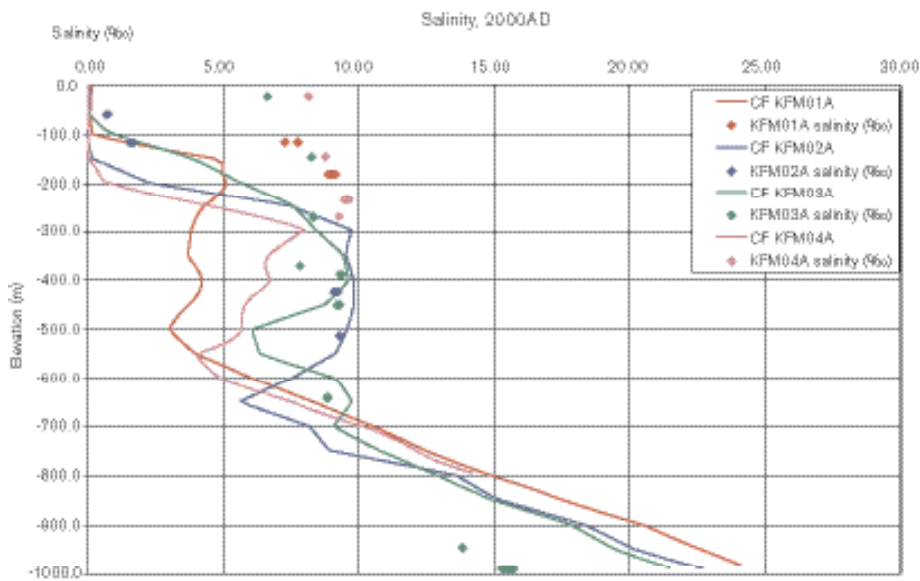


Figure 8-55. Comparison with measured salinities (TDS) in KFM01A–KFM04A for the EPM Reference Case model treated by /Hartley et al. 2005/. The salinity in the model's advective (fracture) component is shown as solid lines, and the data as points. The salinity in the diffusive (matrix) component is not shown. The data represent sampling intervals located in deformation zones.

Figure 8-56 shows the comparison with measured salinities in boreholes KFM01A–03A for the CPM Reference Case model. The less number of data points in Figure 8-56 reflects the decision to use only the high quality hydrogeochemical data in the CPM Reference Case model. An interesting difference is that the CPM Reference Case model did not use any matrix diffusion, whereas the EPM Reference Case model did. The reason for the poor matches near surface are probably due to the mismatch in hydraulic conductivity already commented on above.

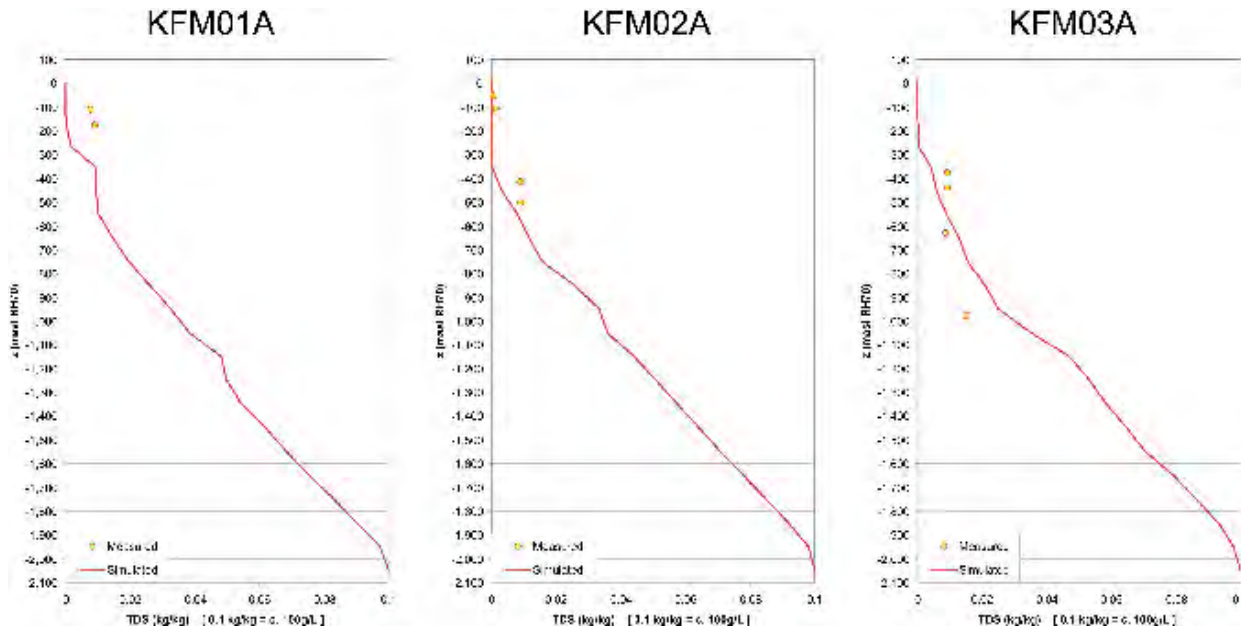


Figure 8-56. Comparison with measured salinities (TDS) in KFM01A–KFM03A for the CPM Reference Case model treated by /Follin et al. 2005/. The simulated salinities are shown by solid lines and the measured data by points. The data represent sampling intervals located in deformation zones. The simulations did not include matrix diffusion.

Comparison with reference waters in shallow and deep boreholes

The groundwater composition may be described using a simplified system of four reference (or end-member) waters; Brine, Glacial, Marine and Rain 1960, see Chapter 9. The end-member mixing fractions give several different tracers that have entered the groundwater system at different times and with different densities. As such, they give the possibility to quantify sensitivities of transient simulations to initial conditions, boundary conditions and hydraulic properties, which are not possible with salinity data alone. Salinity gives an indication of the balance in driving forces between hydraulic gradients at the surface and buoyancy effects of the dense brine, and how this balance has changed over time due to land rise. Hence, it acts as a natural tracer for transient variable-density flow.

The reference water (end-member) mixing fractions give us several different tracers that have entered the groundwater system at different times and with different densities. As such, they give the possibility to quantify sensitivities of transient simulations to initial conditions, boundary conditions and hydraulic properties not possible with salinity data alone. Salinity gives an indication of the balance in driving forces between hydraulic gradients at the surface and buoyancy effects of the dense brine, and how this balance has changed over time due to land rise. Hence, it acts as a natural tracer for transient variable-density flow.

/Hartley et al. 2005/ solved four density driven advection-dispersion equations in parallel. The groundwater density and viscosity were taken to be functions of the total groundwater salinity (and pressure and temperature). The total salinity was calculated from the pooled dissolved solids of the four reference waters.

/Follin et al. 2005/ solved a single density driven advection-dispersion equation, where the variable-density flow was governed by specified initial and boundary conditions for the salinity. The transport of water parcels representing different water types (note the difference in the wording) was made by solving several independent non-reactive advection-dispersion equations in parallel, one for each water type. The concentration of a particular constituent at any point and time in the model was the sum of the products of each water type fraction with the concentration of the constituent of the corresponding reference water.

Figure 8-57 shows the comparison with M3 calculations in boreholes KFM01A–03A for the EPM Reference Case model. The data for KFM01A are sparse between depths of 100–200 m. In this limited depth range, the model compares very well with the reference water fractions with a sharp transition from Rain 1960 water to Marine and about 20% Glacial water. Below 200 m, there are no data to support a comparison of the model. The model predicts a lens of Marine water between about 100 m and 500 m depth, reaching a maximum of about 45% at 200 m depth. Below this, it predicts a lens of Glacial water and a weak gradient towards Brine starting at 500 m.

The match for KFM02A is more interesting, since there are many more data from this borehole and it goes deeper. The model predicts a sharp transition from Rain 1960 to Marine water around 200–300 m depth, whereas the M3 calculations suggest a more gradual transition between 100–500 m depth. Since the site emerged from the sea only about a thousand years ago, the data indicate a faster transport of precipitation than the model does. The model predicts a lens of Marine water descending through the model domain between 200–600 m depth up to a fraction of 80%. Glacial water is simulated correctly to be in the range 10–20% until 500 m depth, and then rises sharply, although there are no data to confirm this trend.

KFM03A provides the greatest abundance of data. The M3 data for KFM03A near the surface are curious since they suggest 50% Marine water, but the ground is at an elevation of about 8 m and so, based on land-rise rates, has been subject to precipitation for around 1,000 years. The percussion-drilled boreholes give the expected precipitation near surface, but this under pumped conditions. According to the M3 calculations, Marine gradually decreases to about 20% below 600 m. The model suggests a gradual rise in Marine water up to about 80% at 300 m depth and then falls-off at 700 m depth, with spikes corresponding to zones ZFMNE00A4 and ZFMNE00B1. The model gives a good comparison with the Glacial water composition at the data points. Even at the base of the borehole, Brine is only just above the M3 resolution uncertainty, 10–15%, and so it is hard to calibrate Brine at Forsmark based on M3 results.

The comparisons of the EPM Reference Case model with the M3 reference water profiles were performed with rock matrix diffusion activated. This explains why the mixing fraction in both the fracture system and the rock matrix are shown in Figure 8-57. The two sets of fractions are generally similar since good communication between the fractures and matrix is assumed. It is vital to note that the deep hydrogeochemistry data underpinning the M3 reference water and mixing proportion calculations at depth are preferentially from groundwater sampled in deformation zones. There is very little flow in the rock mass between the deformation zones, and so the chemistry data represent discrete samples. Hence, although lines have been drawn linking the data points down the boreholes this continuity of water composition in the background rock is highly speculative. Therefore, the matching should only really be judged at depths where there are data. Moreover, the reference water calculations using M3 do not invoke matrix diffusion.

Figure 8-58 shows the water type profiles for the CPM Reference Case model together with the calculated M3 mixing proportions for boreholes KFM01A–03A. The data points represent positions where high quality hydrogeochemical data were sampled, but it is noted that the M3 calculations were based on all data. The flow simulations behind Figure 8-58 did not include matrix diffusion.

Comparison with major ions and environmental isotopes

Since there is an additional interpretation uncertainty associated with the M3 calculations, the hydrogeological modelling teams proposed to compare with some basic constituents. The full range of major ions as well as the $\delta^{18}\text{O}$ isotope ratio and δD isotope ratios were considered by /Hartley et al. 2005/ including non-conservative constituents, whereas /Follin et al. 2005/ considered conservative constituents only.

$\delta^{18}\text{O}$ and δD allows for a differentiation between Meteoric/Rain 1960 and Glacial freshwaters by larger negative ratio for the latter. However, the interpretation is not definitive as a large negative ratio is also observed for marine waters. Cl indicates the presence of Brine and/or Marine water. For this reason, /Hartley et al. 2005/ also incorporated comparisons with Mg as Mg differentiates between saline Marine (high Mg) and saline Brine (low Mg). However, Mg is not conservative, which leaves the issue of usefulness open for discussion. Nevertheless, it is noted that /Hartley et al. 2005/ found calibrating against Mg useful when treating it as a conservative trace.

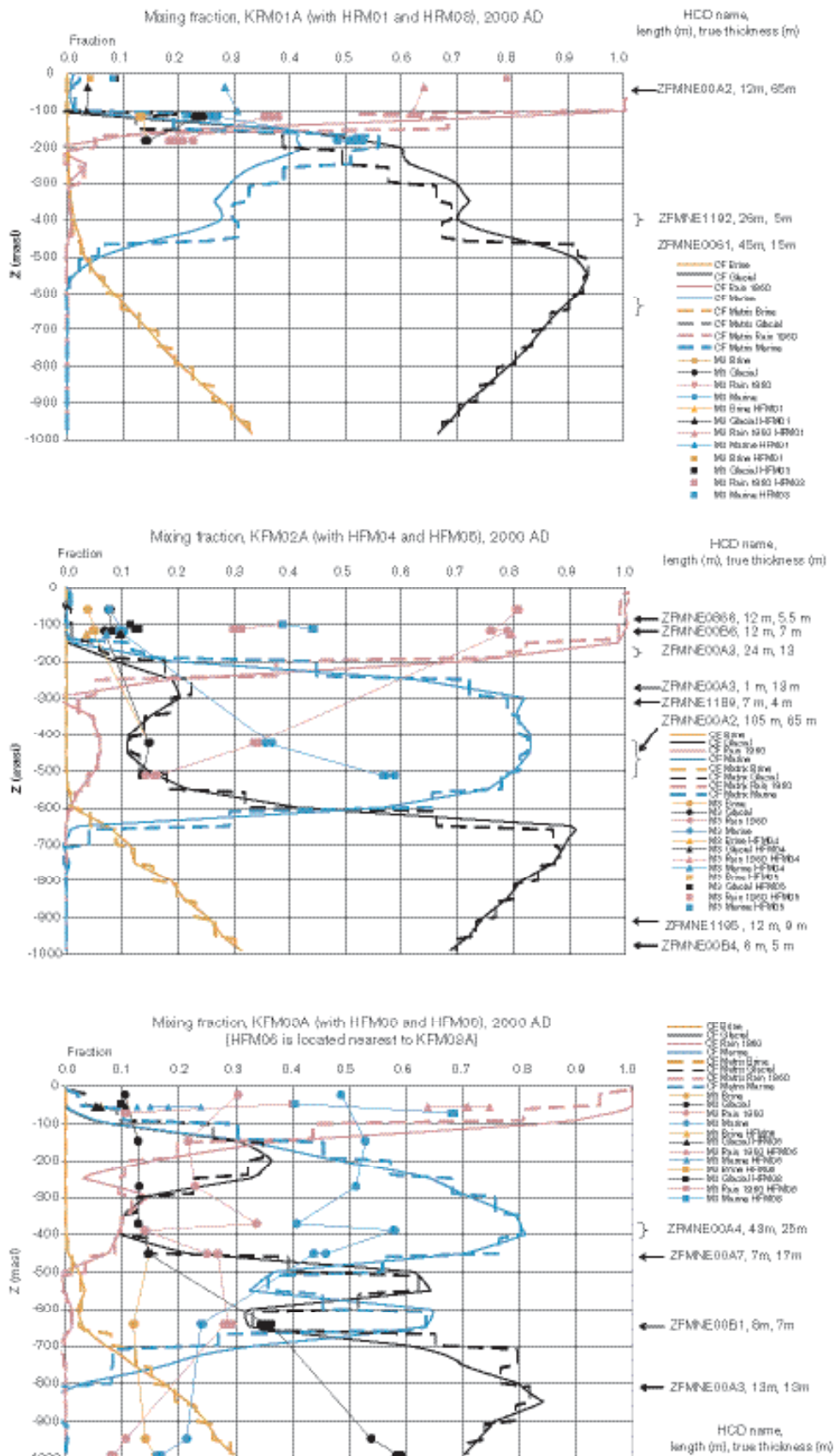


Figure 8-57. Comparison with M3 mixing proportions in KFM01A–KFM03A for the EPM Reference Case model treated by /Hartley et al. 2005/. The mixing fractions in the model’s advective (fracture) component are shown as solid lines. The diffusive (matrix) component is dashed and the M3 data have both points and lines.

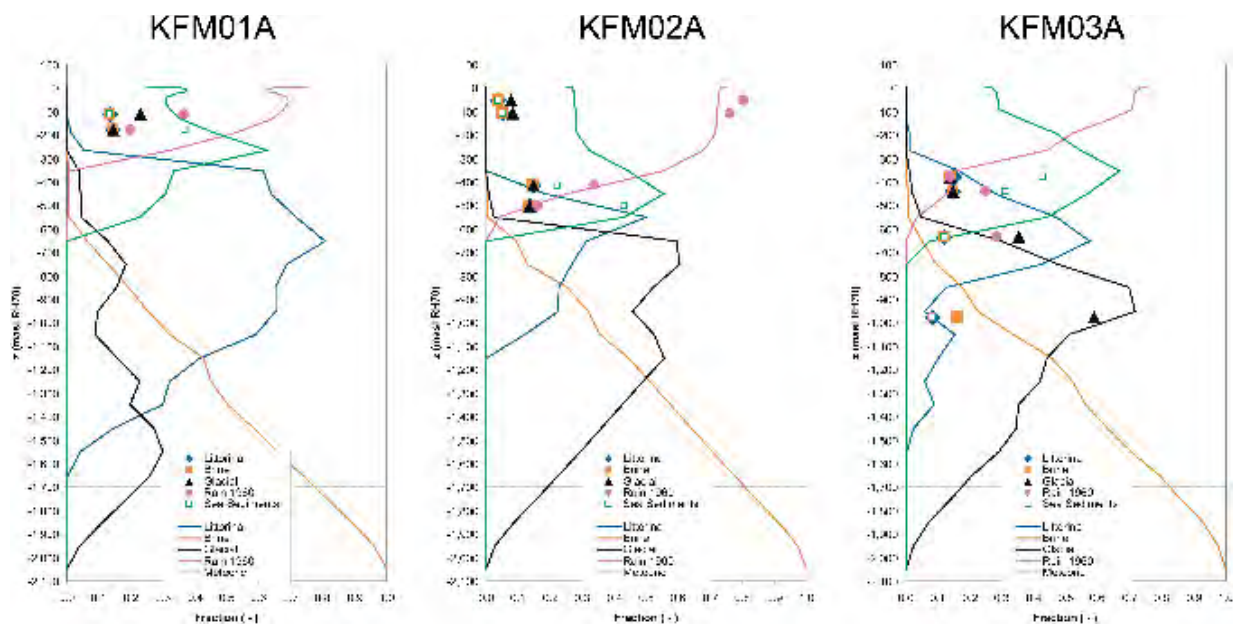


Figure 8-58. Comparison with 4+1 water types (the meteoric flushing was divided into two events, before and after 1960) in KFM01A–3A for the CPM Reference Case model treated by /Follin et al. 2005/. The water type fractions in the flow model's advective component are shown by solid lines and the mixing proportions calculated by M3 by points. The flow simulations did not include matrix diffusion.

Figure 8-59 shows the comparison with $\delta^{18}\text{O}$, Cl and Mg in KFM01A–KFM04A for the EPM Reference Case model. The error bars indicate the laboratory analysis uncertainty of about 5%. It is again interesting to observe that the profiles are generally consistent between boreholes and generally suggest a smooth trend down the boreholes. They are less spiky than the M3 profiles which are prone to being sensitive to which reference waters that have been identified as the dominant waters, as this can change from point to point.

For $\delta^{18}\text{O}$, the model predictions are generally good where there are corresponding data, but suggest Glacial spikes in the background rock where no data are available. Cl correlates to salinity, so the comments made in the previous section hold. Mg allowed /Hartley et al. 2005/ to differentiate salinity from Brine below about 500 m depth from salinity from Marine water infiltration above 500 m depth. This transition from Marine to Brine originating salinity is correctly simulated in the model. Mg also gives evidence for water of Marine origin in the shallower parts of KFM01A, KFM03A and KFM04A.

Since these three basic constituents, $\delta^{18}\text{O}$, Cl and Mg, give smoother profiles and are less prone to uncertainty than the M3 calculation, they were used to compare and calibrate the variants treated by /Hartley et al. 2005/.

Figure 8-60 shows the profiles of $\delta^{18}\text{O}$ and δD in KFM01A–3A for the CPM Reference Case model. The data points represent positions where high quality hydrogeochemical data were sampled. The flow simulations behind Figure 8-60 did not include a diffusion (matrix) component.

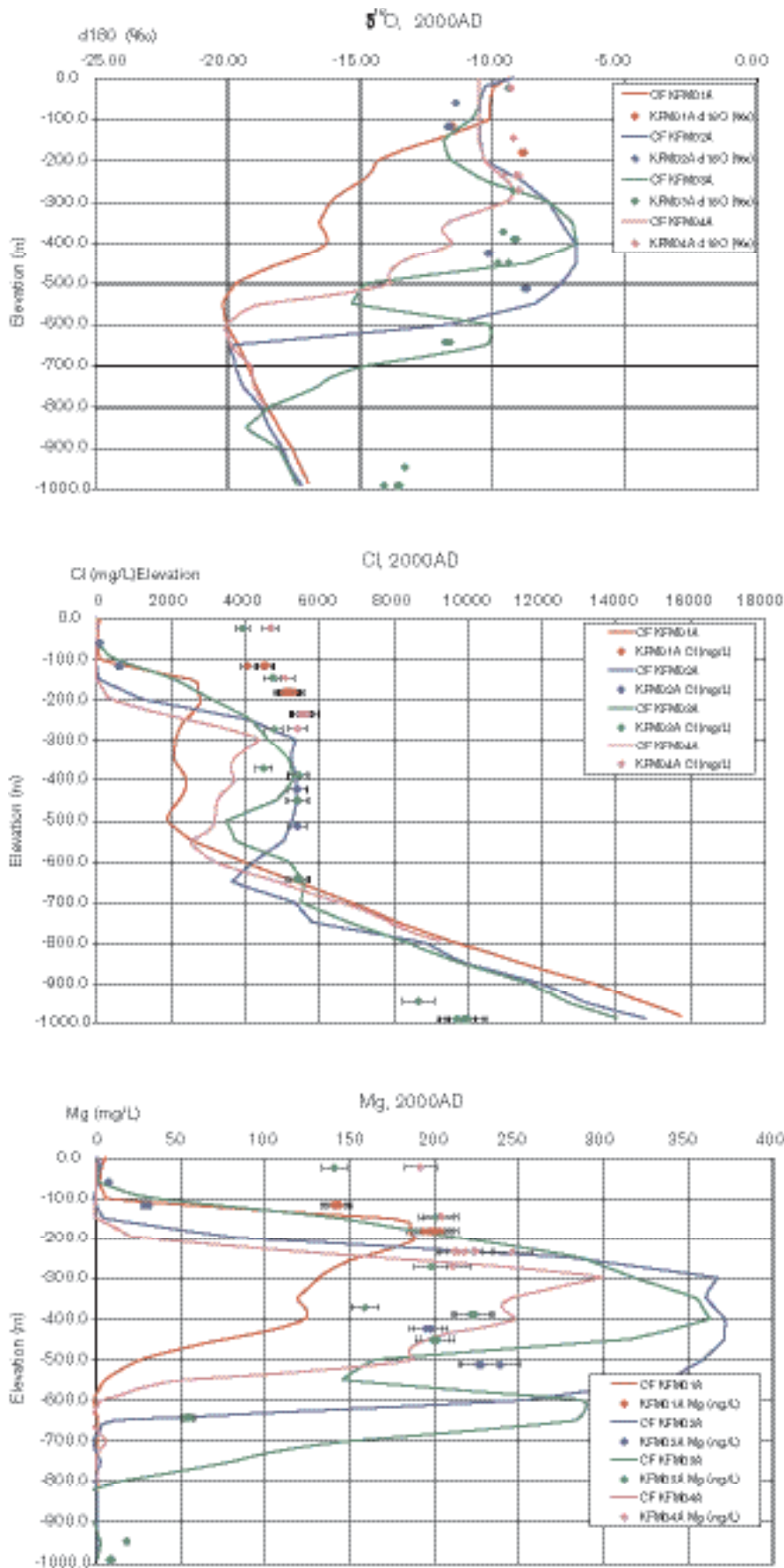


Figure 8-59. Comparison with $\delta^{18}O$, Cl and Mg in KFM01A–KFM04A for the EPM Reference Case model treated by /Hartley et al. 2005/. Values for the model’s advective (fracture) component are shown by solid lines and the data by points.

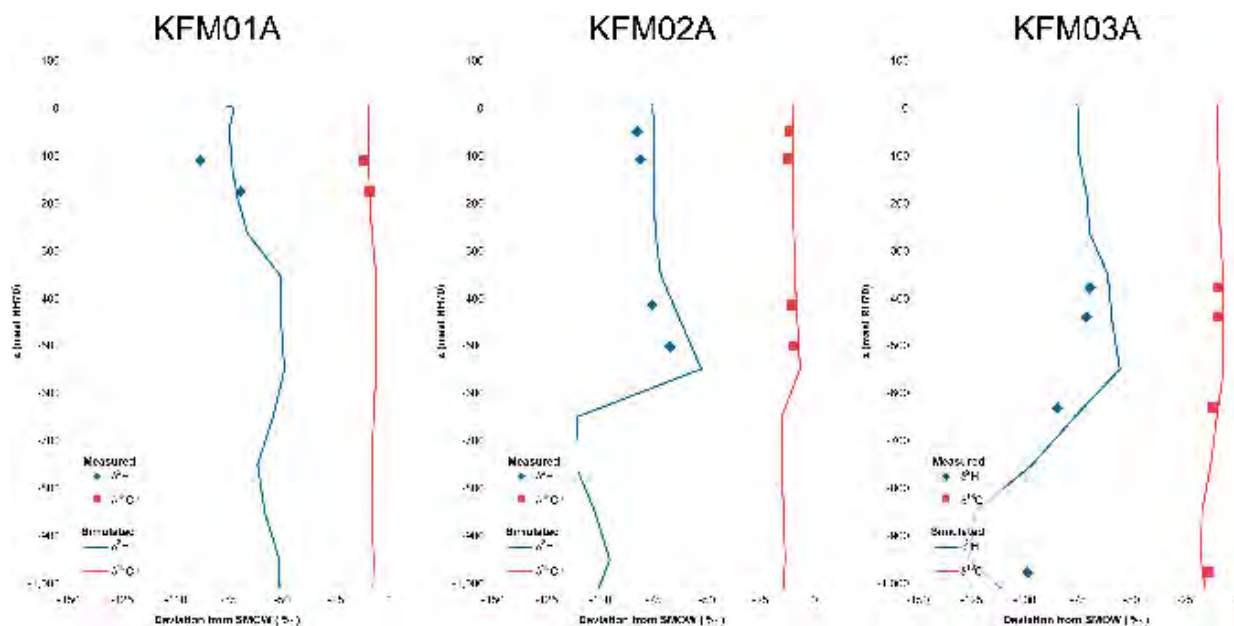


Figure 8-60. Comparison with $\delta^{18}\text{O}$ and δD in KFM01A–KFM04A for the CPM Reference Case model treated by /Follin et al. 2005/. Values from the model's advective component are shown by solid lines and the data by points. The flow simulations did not include a (matrix) diffusion component.

8.6.4 Palaeo-hydrogeological evolution

This section shows some of the results from the palaeo-hydrogeological simulations. The results shown treat the EPM Reference Case. The concept for flow outside RFM029, which is one of the objectives of the description of the past evolution, was treated quite similar by the two modelling teams, cf. Figure 8-52.

The simulations started at 8,000 BC and ran for 10,000 years, i.e. to 2,000 AD, corresponding to present-day conditions. At 8,000 BC, the last glaciation had ended and the modelled area is assumed to have been covered with water from the melted ice, here referred to as Glacial water. Initially, there are only two types of water in the model. The upper part of the model is filled with Glacial water and underneath this there is a fraction of Brine that increases with depth.

The past evolution of the Brine and Marine water is shown in Figure 8-61. Plots of the other components are provided in /Hartley et al. 2005/. The distributions of the different water types are presented in vertical slices at three times corresponding to: 5,000 BC, 0 BC and 2,000 AD (present day).

As already mentioned, the Brine distribution is very stable for the whole simulation time. This is due to the low hydraulic conductivity at depth, which is a consequence of the depth dependency in HCD properties that approach the rock mass hydraulic conductivity below about 700 m depth. Therefore, the Brine profile just reflects the initial condition. Marine water enters the system when the land is covered by the Littorina and later Baltic seas up to about 1,000 years ago. The mechanism for infiltration of Marine water is from the fact that it is denser than the underlying Glacial melt water and hence gradually sinks downwards as a pulse through the system toward the dense Brine. The pulse will sink heterogeneously around the deformation zones since advection is more rapid. This effect can be seen in Figure 8-61 where the Marine water clearly enters some sub-horizontal zones sloping south-east. The Marine pulse is generally found in the top 500 m.

The results further show that Glacial water initially sits on top of Brine and that gradually some parts of the top 500 m or so are flushed by Marine water especially in the sub-horizontal zones that dip south-east. Most of this flushing process has occurred by 0 BC, probably due to a greater head of dense Marine water lying across the site in the early Littorina phase, partly because the water was denser and also the sea was deeper then. Precipitation (Rain 1960 water) only just starts to enter the very south-west of the model at 0 BC when parts of the site are just emerging from the sea.

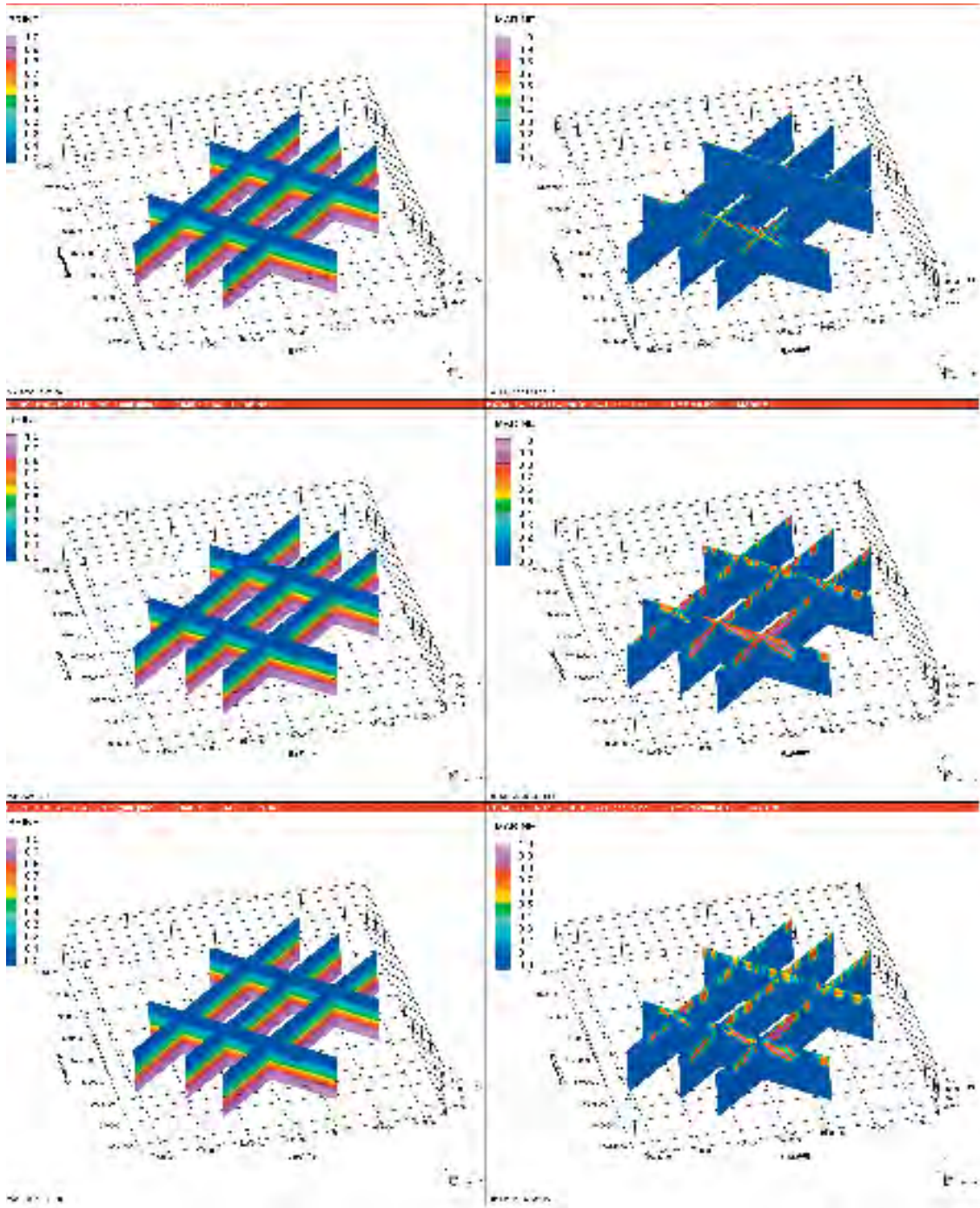


Figure 8-61. Distribution of Brine (left) and Marine water (right) in vertical slices at times equal to (from top to bottom) 5,000 BC, 0 BC and 2,000 AD (present-day), for the EPM Reference Case Model /Hartley et al. 2005/.

As the land continues to rise up to the present-day level, more of the site is exposed to infiltration of precipitation that leads to a flushing of the preceding Marine water in the top 100–300 m in the south of the model. Again, this is happening most rapidly in the deformation zones that are gently dipping towards south-east.

The TDS distribution is the result of mixing between Brine and Marine water, which has a time-varying concentration of salt. The shape of the TDS distribution suggests that the dominant part of the salt originates from the Brine with a pulse of TDS of around 10 g/L near the top associated with the Littorina pulse. The distribution of the vertical Darcy velocity shows a highly heterogeneous

flow field confirming the presence of local flow cells. There is an intuitive general trend of downward flow in the south where the higher ground is, and upward flow near the coast, although there are many local areas of downward flow near the coast also.

8.6.5 Flow path simulations and exit locations

This section presents results from flow paths simulations using the Reference Case parameter settings. The purpose of the flow-path analysis is twofold. First, it provides a set of performance measures for quantifying the current groundwater flow situation that can be used to compare variants and quantify uncertainties. Secondly, the identification of discharge areas (exit locations) is important for the Preliminary Safety Evaluation.

The location of the particle release area within the target volume used by /Follin et al. 2005/ is visualised in Figure 8-62. The particle tracking was made for 2,814 particles during 30,000 years to ensure a sufficient sampling statistics. Apart from that, the 30,000 years is useless information, since the hydrogeological conditions were fixed to represent the state of the system as modelled at 2,000 AD. The particles were released just below 400 m depth in a regular grid using a spacing of 50 m. No action was made if a particle's start position coincided with a deformation zone, see e.g. deformation zone ZFMNE00A1 (A1) in Figure 8-62.

Simulated flow paths and exit location determined by particle tracking assuming fixed hydrogeological conditions are shown in Figure 8-63. The upper left inset shows a cross-section of the CPM Reference Case and the upper right inset shows the exit locations in plan view for the EPM Reference Case. The reason for this is that the body of the particles of the CPM Reference Case get stuck. In order to make the particle tracking feasible using a multicomponent CPM, it was necessary to increase the hydraulic conductivity of the CPM Reference Case within the target volume (cf. CPM-3 in Figure 8-51) by a factor of 50, from 1×10^{-11} m/s to 5×10^{-10} m/s (cf. KFM01A in Figure 8-54). This CPM Modified Case (cf. Table 8-20) was used for the execution of a series of sensitivity tests checking the need for detailed far-field realism in the numerical simulations by means of particle tracking (cf. the second objective in Section 8.6.2). The resulting particle tracks are shown at the lower part of Figure 8-63.

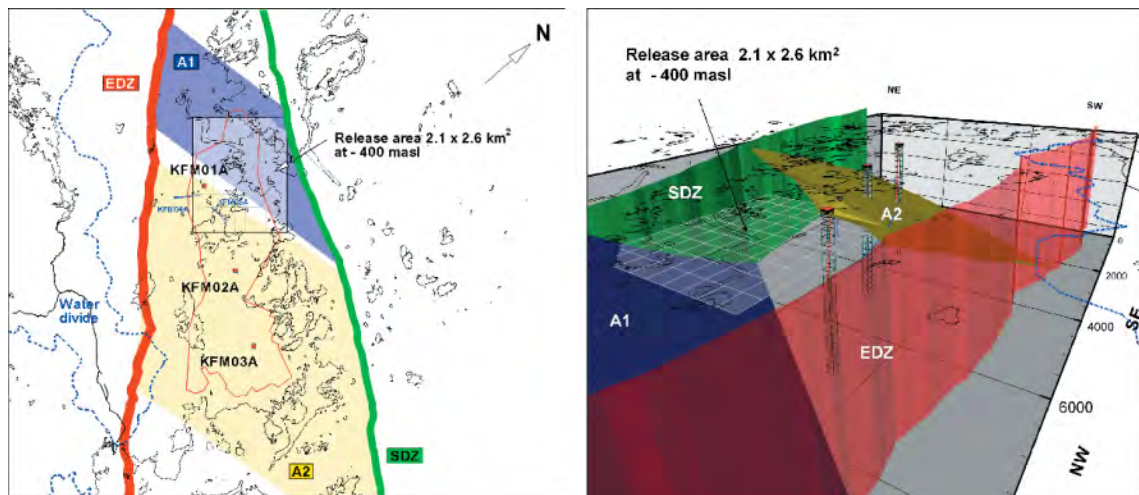


Figure 8-62. Close-up views of the area between the Eckarfjärden deformation zone (EDZ) and the Singö deformation zone (SDZ). The gently dipping deformation zones ZFMNE00A1 (A1) and ZFMNE00A2 (A2) are also shown. The release area for the particle tracking is indicated together with locations of boreholes KFM01A–KFM03A /Follin et al. 2005/.

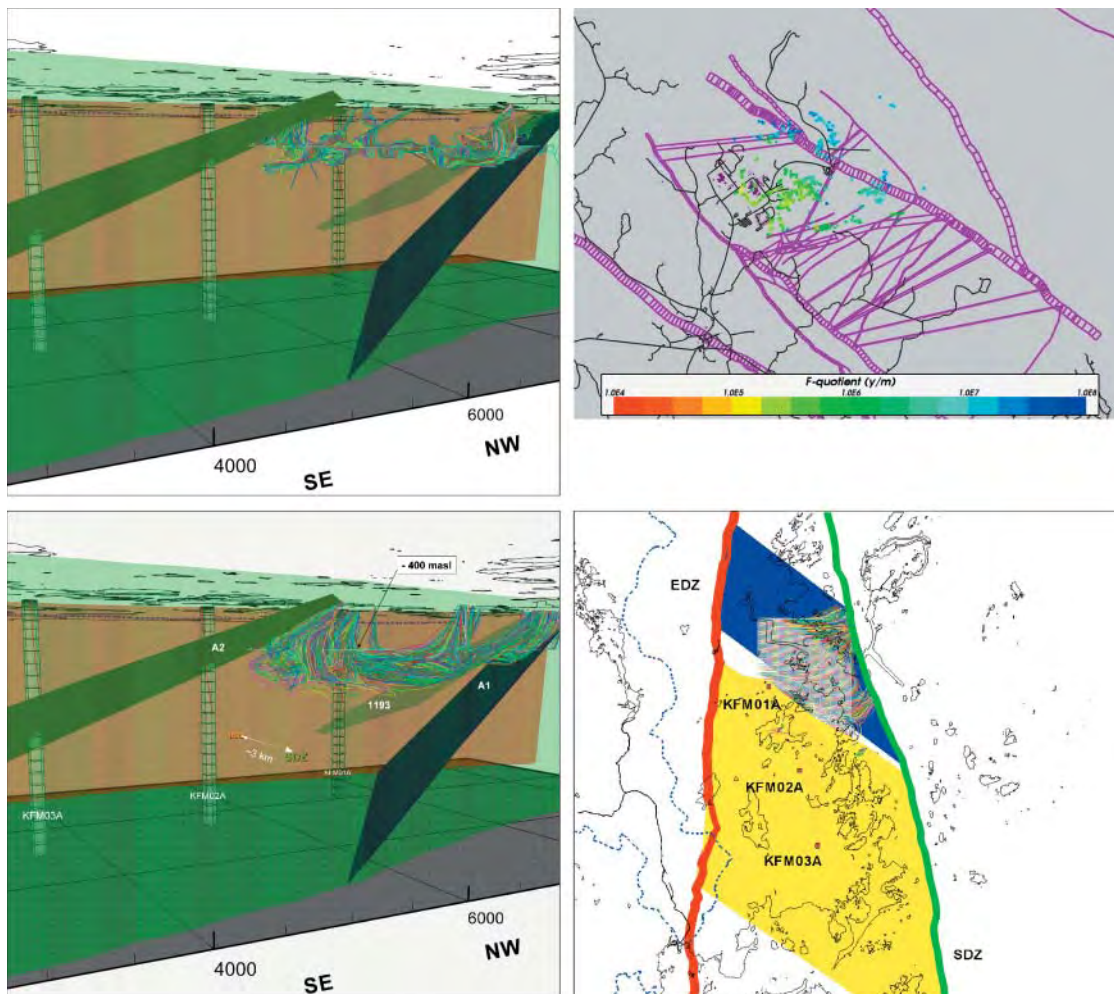


Figure 8-63. Flow paths and exit location determined by particle tracking. Upper left and right: Flow paths for the CPM Reference Case and the EPM Reference Case, respectively. Lower left and right: Flow paths and exit locations for the CPM Modified Case /Follin et al. 2005; Hartley et al. 2005/.

The hydraulic conductivity of the CPM Modified Case, 5×10^{-10} m/s, is quite close to the 100 m EPM effective hydraulic conductivity of 3×10^{-10} m/s (cf. Table 8-13). However, there is a slight difference in the particle tracking results between the EPM Reference Case model and the CPM Modified Case. In the former conception some of the exit locations are more or less right above the source, probably due to the heterogeneity and anisotropy of the underpinning DFN, although the body of the particles discharges close to the shoreline. In comparison, the flow field is more “continuum looking” in the CPM Modified Case with almost no local flow cells and with more or less all particles discharging close to the shoreline. Important deformation zones making shortcuts in the CPM Modified Case are the Singö deformation zone (SDZ) and the gently dipping deformation zones ZFMNE00A1, ZFMNE00A2 and ZFMNE1193. The lattermost is interpreted to intersect borehole DBT-1 at c. 320 m depth.

In the CPM Modified Case, almost all particles arrive at the surface exit locations within 10,000 years. The median travel time is 183 years. The CPM Modified Case assumed a matrix diffusion component and a relatively high salinity gradient (full brine at 1,450 m depth). In the CPM Reference Case, less than 20% of the particles exited within 30,000 years, thus implying a median travel time of at least 30,000 years. No matrix diffusion was assumed and full brine was specified at 1,950 m depth in this latter case.

The motive by /Follin et al. 2005/ for not activating a matrix diffusion component in the CPM Reference Case flow model does not mean that there is no matrix diffusion. Matrix diffusion was excluded solely in order to achieve a better performance of the particle tracking. That is, although the particle tracking is a purely advective process and has nothing to do with matrix diffusion (which concerns the salinity migration), the velocity field that governs the particle tracking is significantly affected by the initial conditions for the salinity, the assigned hydraulic diffusivity, and the magnitude of salinity stored in the matrix and available for diffusion.

The absence of pore water hydrogeochemistry data for model version 1.2 means that it was not possible to make conclusive judgements regarding the role of matrix diffusion for the migration of salinity. If one assumes, as it has been done in version 1.2, that the initial salinity profile in the fracture system is in equilibrium with the initial salinity profile throughout the entire low-conductive matrix, there will be diffusion of salt out from the matrix into the transmissive zones as the latter gets flushed out by the meteoric water during the shoreline displacement. This flux of salt is subjected to gravitation. The point made by /Follin et al. 2005/ is that variable-density effects rendered poorer matches in the hydrogeochemical calibration and quite peculiar flow paths.

For the same reason it was necessary to include matrix diffusion and even use a steeper gradient (sharper interface) in order to prohibit a total washout for the CPM Modified Case, since the hydraulic conductivity was much greater.

For the sake of comparison, a median travel time of 475 years was obtained with 76% of the particles exiting within 30,000 years for a variant where matrix diffusion was included in the CPM Reference Case. In comparison, the median travel time for the EPM Reference Case is 284 years accompanied with a huge variability. In these calculations, the simulation time of the particle tracking was not limited, however.

In summary, transport calculations with present-day flow paths have been performed by both modelling teams. The conclusions drawn are fairly similar. It is important to note that the shoreline displacement within the coming 10,000 years will elevate the ground surface by some 40 m /Hedenström and Risberg, 2003/. This means that the hydrogeological conditions within the target volume will change from discharging to recharging conditions giving different particle exit locations to the ones indicated in Figure 8-63. /Follin et al. 2005/ provided an example of how the future may look like at a time slice of 5,000 AD. The basic picture is that the location of the exit positions follows the position of the shoreline.

8.6.6 Sensitivity analyses

Besides the reference cases, /Follin et al. 2005/ and /Hartley et al. 2005/ also carried out a series of sensitivity analyses, mainly exploring to what extent the flow within the target area would be affected by uncertainties in properties, boundaries and boundary conditions in the regional domain.

The sensitivity cases (SC) treated by /Follin et al. 2005/, using the CPM Modified Case as the comparison case (CC), encompassed comparisons of:

- A. model domain size and boundary conditions,
- B. the base, alternative and variant models,
- C. the initial conditions for the salinity and the reference waters,
- D. a random deformation zone transmissivity besides the anticipated depth trend,
- E. hydraulic anisotropy in the near surface,
- F. the position of the groundwater table,
- G. uncertainties in the position of low-confidence lineaments interpreted as deformations in the alternative model,

- H. a higher frequency of gently dipping deformation zones outside the tectonic lens, and
- I. a combination of the cases listed above including a greater hydraulic conductivity of the rock mass outside the tectonic lens.

Each sensitivity case was run for 10,000 years and particles were released in the target area in the same fashion as described in Section 8.6.5.

Choice of model domain and deformation zone model

Modelling transient flow coupled to transport of four reference waters creates significant computational demands, and hence it is important to limit the size of the model where possible. To minimise the computational efforts, /Hartley et al. 2005/ used a smaller model domain with a higher discretisation in the target area than the pre-set rectangular regional model domain (cf. Figure 8-52). The model domain chosen followed regional-flow divides onshore and approximate trends of maximum depth in the sea floor, see Figure 8-64. This model domain covers a large area currently under the sea, which may be expected to have little influence on the present-day groundwater flow at the site. However, this area was retained since Safety Assessment for the SKB SR-Can project will assess a repository at Forsmark, which means that the model must consider flow conditions into the future when the shoreline is likely to retreat away from the site.

As the results from a numerical groundwater flow model are more or less affected by the size of the model domain, the boundary conditions used and the chosen resolution of the computational grid, it is necessary to demonstrate the effects and, if needed, make appropriate changes. For this reason, /Follin et al. 2005/ tested different model domains, one of which emphasized the position of the upstream no-flow boundary, see Figure 8-64. That is, the upstream no-flow boundary was moved 5 km to the SW, i.e. circa ten times the depicted repository depth.

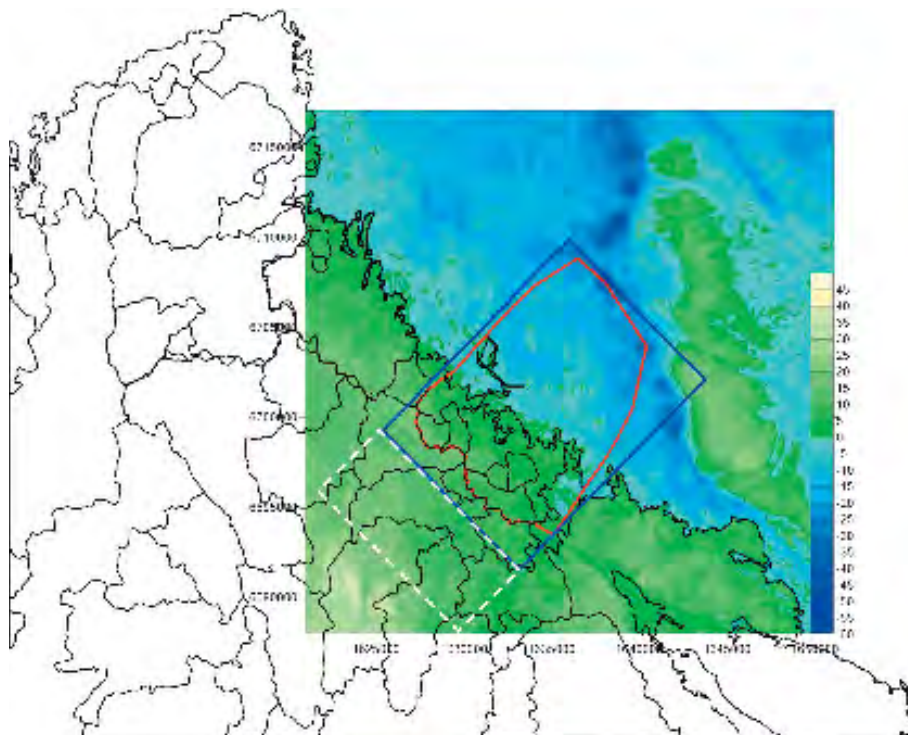
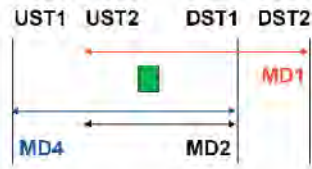


Figure 8-64. Topographic data and water divides (black lines) together with the regional model domain (blue rectangle), the reduced domain used by /Hartley et al. 2005/ (red line) and the enlarged model domain studied by /Follin et al. 2005/ (white dashes).



Model domain 1 = 15 x 11 ; UST2 – DST2

Model domain 4 = 15 x 11 ; UST1 – DST1

Model domain 2 = 10 x 11 ; UST2 – DST1


 = release area 2.1 x 2.6 km² (fixed location in all models)

Figure 8-65. Illustration showing the approach used to test the sensitivity to the size of the model domain. UST and DST mean ‘upstream boundary’ and ‘downstream boundary’, respectively. There are two of each corresponding to the different model domains, MD1, MD2 and MD4. MD1 represents the regular regional model domain of version 1.2. MD2 represents a diminished model domain with a different downstream boundary than MD1. MD4 is as large as MD1 but shifted 5 km to the SW (Figure 8-64). The green area in the centre has the same location in all model domains. Within this area particles were released at the time slice 2,000 AD /Follin et al. 2005/.

Figure 8-65 shows the approach used to test the sensitivity to the size of model domain. UST and DST mean ‘upstream boundary’ and ‘downstream boundary’, respectively. There are two of each corresponding to the different model domains, MD1, MD2 and MD4. MD1 represents the regular regional model domain of Forsmark version 1.2. MD2 represents a diminished model domain with a different downstream boundary than MD1. MD4 is as large as MD1, but shifted 5 km to the SW. The green area in the centre of Figure 8-65 has the same location in all model domains. Within this area, 2,184 particles were released at the time slice 2,000 AD, i.e. at the end of the 10,000 year long simulation period. During the particle tracking, all boundary conditions were held constant in time, i.e. no further shoreline displacement was considered.

Table 8-21 shows the outcome in terms of the relative difference between medians (*MED*), the distance between mass centres (*DMC*) and the mean of all particle to particle differences (*MPP*) for the travel times, t_w , lengths of the flow paths, L , and the Darcy velocities at the start positions, q_{Darcy} . Besides showing the results for cases MD1, MD2 and MD4, Table 8-21 also provide performance measures for a comparison between the base (Base Case, BC) and alternative (Alternative Case, AC) models. The observations made from Table 8-21 are:

- The differences in median travel time and in the median travel length are small when the no-flow boundaries are changed for the BC model. The only notable difference is that the median travel time is a bit shorter when the small model domain (MD2) is compared against the original domain (MD1).
- For the AC model, the upstream model domain (MD4) results in slightly longer travel times, whereas modelling with the smaller domain (MD2) makes the travel times become slightly shorter. The difference in flow path is negligible for both comparisons.
- The distance between mass centres and the mean of all particle to particle differences are both small, which suggests that the modelled area is sufficiently large for the studied area.
- A comparison between the BC and the AC models results in approximately the same differences regardless of the model domain used. This shows that the choice of structural model is more important for the performance measures than the choice of model domain. The AC model renders c. 25% shorter travel times and almost 20% shorter travel lengths due to the great number of low-confidence deformation zones. In addition, the discharge points move about 400 m. However, it is the low-confidence zones inside the candidate area that affect the performance measures.

Table 8-21. Performance measures for a comparison between model domains MD1, MD2 and MD4 and between the base model (BC) and the alternative model (AC). MED t_w , L , q_{Darcy} denote relative differences between the sensitivity case (SC) and the comparison case (CC) in median advective travel time, path length, and Darcy velocity (at the starting positions), respectively. DMC and MPP denote “distance between SC and CC mass centres” and “mean of all SC particle to CC particle differences” /Follin et al. 2005/.

Object	SC	CC	MED t_w (%)	MED L (%)	MED q_{Darcy} (%)	DMC (m)	MPP (m)
BC	MD4	MD1	-1.8	-1	1.2	14	65
BC	MD2	MD1	-2.9	1	1.7	14	123
AC	MD4	MD1	4.4	-4.2	-10.4	44	173
AC	MD2	MD1	4.4	3.4	-1.2	14	102
MD1	AC	BC	-26.5	-27.6	42.6	419	649
MD4	AC	BC	-21.8	-29.9	26.2	372	582
MD1	AC	BC	-21.0	-25.8	38.4	438	661

Properties of deformation zones in the “target volume”

Among the nine sensitivity cases studied by /Follin et al. 2005/, Case D and Case I were the only cases (besides the aforementioned comparison between the base and alternative models in Table 8-21) that rendered a significant difference in the defined particle tracking performance measures. The cases are illustrated in Figure 8-66.

Sensitivity case D accounts for the possibility of a random heterogeneity in the deformation zone transmissivity besides the anticipated depth trend, Figure 8-33. As the discretisation of the deformation zones consists of a large number of small triangles, each triangle is assigned a random deviate from the mean trend. The results show that this procedure causes new flow paths to open up, but the travel lengths do not change much and the discharge positions differ a little only. The main differences are in flux at the starting points and in the overall travel time.

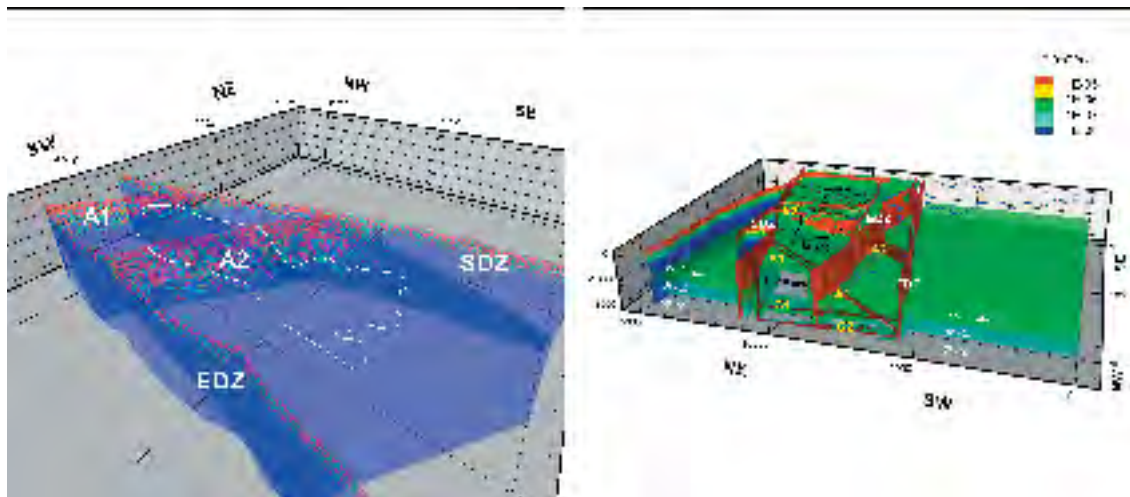


Figure 8-66. Left: In Sensitivity Case D all HCDs assigned non-correlated random deviate transmissivities as provided by (8a) and (8b). The inset shows a close-up of four of the deterministically treated deformation zones of the base model. Right: In Sensitivity Case I a combination of far-field parameter settings were used to study the effect on the particle tracking in the target area /Follin et al. 2005/.

Sensitivity Case I takes a number of interesting parameter settings into consideration, namely:

1. The base variant model (VC), which has 4 gently dipping deformation zones extended all the way to the Forsmark deformation zone.
2. A fixed deformation zone transmissivity of 1×10^{-5} m²/s at all depths in all major deformation zones in the area, i.e. the steeply dipping Eckarfjärden, Forsmark and the Singö deformation zones, and the gently dipping deformation zones denoted by ZFMNE00A1, ZFMNE00A2, ZFMNE00C1, and ZFMNE00C2.
3. 10–100 times greater hydraulic conductivity of the rock mass outside the tectonic lens.
4. A lower position of the groundwater table in all recharge areas as a means of decreasing the impact of local flow cells.
5. A shifted model domain with a different upstream boundary in order to further pronounce the regional gradient.

However, the combined effect of all these parameter settings on the travel time is quite moderate, c. 10% lower median advective travel time. The major effect is seen in the statistics of the exit positions, with a mean offset from the CPM Modified Case of c. 260 m in terms of difference in mass centre, and c. 600 m in terms of mean particle to particle difference.

HRD properties in RFM029

/Hartley et al. 2005/ explored some variants mainly concerned with assessing the various (upscaled) models of HRD. It is concluded that HRD block-scale properties of the DFN in RFM029 are more sensitive to the fracture transmissivity model than to the fracture length distribution, provided that the other fracture parameters are calibrated to the hydraulic data in a consistent methodology. Stochastic variations of the DFN have only a small influence on flow and transport compared with more important conditions such as the HCD positions and properties.

8.7 Evaluation of uncertainties

Uncertainties in hydraulic properties, boundary conditions and initial conditions to variable extent govern the overall uncertainty of the hydrogeological description and in particular the results of the numerical groundwater flow simulations. From a Safety Assessment point of view, however, their relative difference in importance calls for an assessment of which of the uncertainties that are necessary to resolve in greater detail and which may be left behind as open issues of scientific interest mainly.

8.7.1 Overburden and the upper parts of the bedrock

The flow and transport simulations conducted based on the Reference Case settings show that the current models work pretty unsatisfactory when it comes to hydrogeochemical comparisons with the findings in the upper parts of the bedrock. Below follows a discussion about possible sources for this discrepancy. The discussion begins with the overburden and continues with the upper parts of the bedrock.

The overburden consists of glacial till mainly, ranging from sandy till in the NW to clayey till in the SE. The thickness of the glacial till shows an irregular pattern over short distances despite of a gently varying topography. This suggests varying bedrock topography. The clayey till in the SE is generally considerable thicker than the sandy till in the NW. Data from near surface and near bedrock surface slug tests in the sandy till indicate higher hydraulic conductivity than the intermediate deep slug test data. The role of this variability of the overburden properties for the bedrock hydrogeological model is not assessed in the current model version. The work conducted by the two modelling teams is associated with several simplifications.

Considering the relatively recent turnover from marine to terrestrial conditions, salt in the overburden that has not yet been washed out by the precipitation is a possible remaining source of influence. In particular under lakes, which are generally filled with quite low-conductive gyttja-clay sediments. This possibility is not modelled and thus remains as an unresolved uncertainty of particular concern.

The uppermost parts of bedrock are often found to be more conductive than the glacial till and, equally important, quite heterogeneous and anisotropic with the principal value in the horizontal plane. This has been verified by a large number of pumping tests and flow logging in percussion-drilled boreholes, drilling-induced pressure responses between core-drilled and percussion-drilled boreholes far away from one another, cross-hole tests in both gently dipping and vertical deformation zones, and, finally, by the huge fracture aperture intercepts seen in almost every borehole drilled within the candidate area. The latter are sometimes completely filled with fine-grained sediments making them quite low transmissive and sometimes fully open with apertures of several centimetres, in which case flow transmissivities up to $2 \times 10^{-3} \text{ m}^2/\text{s}$ have been inferred, cf. Figure 8-14. Impeller flow logging conducted in 17 percussion-drilled boreholes throughout the candidate area show that the uppermost 100 m of the bedrock on the average contains c. three high transmissive intercepts. Hence, the horizontal fracturing seems to occur all over the candidate area and most likely it is in contact with the Baltic Sea. In between the intercepts, the rock mass is often of good quality and poorly fractured. The strong heterogeneity and anisotropy in the superficial rock properties call for a greater concern than given by the current modelling, and should probably be coupled to a much higher resolution in the computational grid.

In conclusion, hydrogeochemical sampling in the percussion-drilled boreholes in several cases indicate a sill in the salinity at c. 100 m depth above which the groundwater generally is fresher, cf. Figure 8-55. Above 200 m depth, the models strongly under-predicts salinity. If correct, this creates a conceptual problem since it is hard to reconcile having sufficient hydraulic conductivity to allow infiltration of a Littorina pulse without a following infiltration of freshwater once the site was exposed to precipitation about 1,000 years ago. This uncertainty may just be a question of having to ‘fine-tune’ the geometric and hydraulic representation of the surface hydraulic, transport properties and boundary conditions to obtain a good match, or, it may be an indicator of a missing “source term”, e.g. delayed release (washout) of salt stored in the overburden.

8.7.2 Deformation zones

There is a fairly good confidence in the existence of many of the suggested base model deformation zones within the candidate area based on the hydraulic tests conducted. However, this condition does not imply that the hydraulic uncertainties in the details are low. It is important to note that the observations made represent the positions in space where they were made primarily. That is, there is a substantial interpolation and extrapolation invoked in the regional flow modelling for version 1.2 as the model volume is much larger than the candidate area. The simulations show, however, that far-field hydrogeological uncertainties are less important for the target volume characterisation than the local heterogeneities in transmissivity and thickness of the identified deformation zones.

Current data from the site show that the hydraulic properties of the deformation zones treated as deterministic in the base model are subjected to significant trends towards depth possibly due to the prevailing stress situation. The observations made indicate that the greatest transmissivities are observed in the gently dipping deformation zones, followed by the steeply dipping deformation zones having strikes normal to the smallest principal stress. However, there is a substantial spatial variability within each category, which was found to have an impact on the hydrogeochemical matching of the flow models against the hydrogeochemical data as well as on the particle tracking.

There is no evidence that the deformation zones become impermeable below 1,000 m depth and there are no boreholes that exceed this depth. Moreover, borehole KFM03A has a few unresolved high transmissivities below c. 950 m depth. It has been suggested based on injection tests and core mapping that these features form a connected steeply dipping system away from the borehole. During the difference flow logging conducted soon after the completion of the drilling of KFM03A, an increase in the groundwater salinity was noticed in these fractures. Possibly this was a result of

the high flushing rates used during the drilling, causing an upconing of more saline groundwater below the base of KFM03A.

In conclusion, the transmissivity, storativity and kinematic porosity of any deformation zone can be expected to vary along the “plane” of the deformation zone, and as most zones are larger than one kilometre, one can expect that there will always be great difficulties to obtain a high confidence in the spatial variability of the hydrodynamic properties by means of drilling and borehole testing.

For both models it was important to get the representation of the deterministically treated deformation zones in the computational grid as correct as possible. Using the geological model together with the given HCD1 hydraulic properties it was difficult to produce a reasonable overall match to the data sets available for comparisons by changing parameters globally. A better match for individual boreholes could only be achieved by making localised changes to the hydraulic and geometric properties of specific deformation zones seen in or near the boreholes. The observations above suggest that the grid resolution is an important component for the outcome of the flow simulations. It is vital to note that the horizontal grid resolution of the EPM Reference Case model was 50 m within RFM029, whereas the horizontal grid resolution of the CPM Reference Case model was 100 m. The vertical grid resolution was also different between the two Reference Case models.

8.7.3 Rock mass

A major observation from the hydrogeological DFN analysis is that it is possible to come to different results concerning the connected fracture area per unit volume when calibrating against the borehole fracture intensity depending on the value used for the minimum feature size. However, by comparing the findings of the two modelling teams it appears as if the overall interpretation gets more constrained. Still, the reference fracture size issue is an open question of considerable conceptual concern and has an impact on the numerical simulations.

The hydrogeological DFN properties give block-scale hydraulic conductivities of the correct order of magnitude to predict hydrogeochemistry. The uncorrelated transmissivity model suggests higher values that do not give a match. This observation indirectly supports that the deformation zone transmissivities have some kind of correlation to size. However, this does not exclude the possibility for large apertures also in small fractures.

The differences between the multicomponent CPM model and the EPM model are fairly small when it comes to direct comparisons with borehole measurements, hydrogeological as well as hydrogeochemical. Concerning the particle tracking simulations, some very minor differences between the two model conceptions are noted in terms of exit locations. These differences cannot be evaluated, however, as there are no field data to compare with.

8.7.4 Boundary and initial conditions

A common conclusion of the two modelling teams is that the lateral no-flow hydraulic boundaries of the regional model domain are probably sufficiently far away from the target volume for a confident hydrogeological description of present-day conditions. However, it is important to note that the shoreline displacement within the next 10,000 years will elevate the ground surface with c. 40 m. This means that the hydrogeological condition within the target volume will change from discharging to recharging giving different particle exit locations than the ones presented in this study. The basic picture is that the location of the exit positions will follow the position of the shoreline.

From a simulation point of view, a specified topographic head or specified infiltration give similar results for a maximum potential infiltration of c. 200 mm/year and the HSD properties considered. However, more variants on the HSD properties need to be considered to see whether an improved match in salinity near the surface can be achieved. These variations should probably be coupled to a specified infiltration type boundary condition and a much higher resolution in the computational grid.

The absence in model version 1.2 of hydrogeochemistry data from the pore water in the rock matrix

means that it is not possible to make conclusive judgements regarding the role of matrix diffusion for salinity. The assumption made by the modelling teams was that the initial conditions of the salinity profile in the kinematic porosity field were in equilibrium with the salinity profile in the matrix porosity field. It is also desirable to learn more about the depth distribution of the salinity in the rock mass fracturing both within and outside RFM029.

The assumed Brine distribution was found to be very stable for the whole simulation time due to the low hydraulic conductivity at depth. This is reinforced by the depth dependency in HCD properties that approach the background conductivity below about 700 m depth. Therefore, whatever Brine profile assumed initially, later time slices will just reflect the initial condition. This does not imply, however, that all deformation zones become impervious at greater depth. There may still be several transmissive zones at depth, e.g. below the bottom of the tectonic lens (cf. the discussion above).

8.8 Feedback to other disciplines

Geology

Matters of particular interest/concern for hydrogeology are:

- An improved geological understanding/description of the high transmissive features encountered at the bottom of KFM03A.
- A confirmation of the position, strike and dip of the deformation zones ZFMNE00A1 and ZFMNE1193.
- An elaborated structural explanation of the isolated flow anomalies seen at depth in KFM02A, KFM04A and, more tentatively, KFM05A.
- Data from core-drilled boreholes across the Singö deformation zone.
- Assessment of the uncertainties in the geological DFN modelling, in particular the coupling between size and intensity.

Hydrogeochemistry

Matters of particular interest/concern for hydrogeology are:

- More data of all depths. Available hydrogeochemical data are insufficient to constrain the numerical simulations carried out by the two modelling teams; the current data may represent the hydrogeochemistry in the deformation zones mainly.
- Determinations of rock matrix pore water chemistry.
- Hydrogeochemical profiles outside the tectonic lens, in particular below the Baltic Sea.
- Hydrochemical data at various depths below the gyttja-clay sediments.
- Assessment of the Brine interface at depth.

9 Bedrock hydrogeochemistry

The data evaluation and modelling of hydrogeochemical data consists of manual evaluation, expert judgment and mathematical modelling, which must be combined when evaluating groundwater information. The results of the detailed hydrogeochemical modelling are used to produce a hydrogeochemical site descriptive model. The background hydrogeochemical report /SKB, 2005b/ describes in great detail the hydrogeochemical data evaluation and modelling carried out for the Forsmark site descriptive model version 1.2. The modelling methodology applied is described in the SKB strategy report /Smellie et al. 2002/. The outcome of the hydrogeochemical modelling is used in e.g. the hydrogeological modelling, transport modelling and safety assessment modelling.

9.1 State of knowledge at the previous model version

The first model of the Forsmark area was the site descriptive hydrogeochemical model version 0 /SKB, 2002a/. Although there were few data from the Forsmark area to support a detailed hydrogeochemical site descriptive model, postglacial events believed to have affected the groundwater evolution and chemistry at Forsmark were described in a conceptual model.

Model version 1.1 /Laaksoharju et al. 2004a/ represented the first evaluation of the available Forsmark groundwater analytical data. The complex groundwater evolution and patterns at Forsmark were modelled to be a result of many factors such as: a) the flat topography and proximity to the Baltic Sea, b) past changes in hydrogeology related to glaciation/deglaciation and land uplift associated with repeated marine/lake water regressions/transgressions, and c) organic or inorganic alteration of the groundwater composition caused by microbial processes and/or water/rock interactions. The sampled groundwaters reflected various degrees of modern or ancient water/rock interactions and mixing processes.

Based on both the general geochemical character and apparent age, two major water types were identified at Forsmark: fresh-meteoric waters with a bicarbonate imprint and low residence times (tritium values above detection limit), and brackish-marine waters with Cl contents up to 6,000 mg/L and longer residence times (tritium values below detection limit). The meteoric water was found at the surface and at shallow depths and the marine water was found closer to the coast and at depths affected by Baltic Sea water and probably old Littorina Sea water.

The 1.1 model version knowledge of the reactive system was that the main water-rock interaction processes influencing the chemistry in the fresh meteoric waters were: 1) decomposition of organic matter, 2) calcite, plagioclase, biotite and sulphide dissolution, 3) Na-Ca ion exchange, and 4) phyllosilicate precipitation (probably extremely slow in the present environment). For the brackish-saline groundwaters in contrast, water/rock interaction processes seemed to be less important although this was not well established because of a lack of data. Multiple end-member mixing between especially marine water, glacial meltwater and a deeper saline water was believed to play a significant role.

9.2 Hydrogeochemical data

This section describes the evaluation of the primary hydrogeochemical data. Most of these data are from waters sampled at various surface locations and from groundwaters in a few boreholes. The evaluation essentially aims at identifying representative datasets for use in the further analysis and to eventually provide a conceptualisation of the origin and evolution of the Forsmark groundwaters.

The Forsmark hydrogeochemical data used in model version 1.2 are listed in Appendix 6 in /SKB, 2005b/. Data from other Fennoscandian sites such as Simpevarp, Finnsjön, SFR and Olkiluoto were compiled in the 'Nordic Table' and these data also have been evaluated with respect to properties and representativeness (cf. Appendix 7 in /SKB, 2005b/).

The Forsmark 1.2 dataset is based on 1,131 water samples. Samples reflecting surface conditions (precipitation, streams, lakes and sea water) comprise a total of 735 samples. Of the remaining 396 samples, 84 samples are from percussion-drilled boreholes, 168 from core-drilled boreholes and 144 from shallow soil pipes; some of these borehole samples represent repeated sampling from the same isolated packed-off location or samples from open boreholes (50 tube samples).

From the total dataset, only 171 surface water samples and 210 groundwater samples had been analysed for all major elements, stable isotopes and tritium at the time of the data freeze 1.2. There are some samples with additional information, mainly on colloids, dissolved gases and microbes, which are also listed in Appendix 6 of /SKB, 2005b/. This means that 33.7% of the samples could be used for a detailed evaluation concerning the origin of the waters. The other samples are not necessarily rejected from the modelling exercise as they are used for background and comparison purposes and may play an important role in the understanding of the variability of the samples.

The detailed representativity check of the samples (Appendix 1 in /SKB, 2005b/) shows that only 182 out of 381 samples with complete chemical data have been considered representative. The representative data are labelled in Appendix 6 in /SKB, 2005b/. How this dataset has been used in the different models is listed in Table 2-5 and in Appendix 8 in /SKB, 2005b/.

Analysed data include the same set of parameters as in the previous stages (cf. Appendix 6 in /SKB, 2005b/). The pH and electrical conductivity values used in the evaluation were those determined in the laboratory. There are no data for Eh and temperature for the surface waters, but data do exist from some continuous logging of Eh, pH and temperature from several boreholes at different depths. The selected Eh, pH and temperature values are included in the table of the chemical analysis.

9.2.1 Groundwater chemistry data sampled in boreholes

The main focus of this Forsmark version 1.2 evaluation is on boreholes KFM01A, KFM02A, KFM03A and KFM04A, systematically drilled to provide a good coverage of the geology and hydrogeology of the candidate site. The borehole sampling locations are shown in Figure 9-1. Of the percussion boreholes indicated, borehole HFM01 supplied flushing water to the drilling of borehole KFM01A, HFM05 for borehole KFM02A, HFM06 for borehole KFM03A, and HFM10 for borehole KFM04A. The remaining percussion boreholes were used mainly for hydraulic (e.g. groundwater flow monitoring) and hydrochemical information and structural (e.g. lineaments; deformation zones) confirmation and identification.

The sampling and analytical data have been reported for the groundwaters by /Nilsson et al. 2003; Nilsson, 2003a,b; Berg and Nilsson, 2004/ and draft versions of P-reports were available at the time of the data freeze. The analytical programme included: major cations and anions (Na, K, Ca, Mg, Si, Cl, HCO_3^- , SO_4^{2-} , S^{2-}), trace elements (Br, F, Fe, Mn, Li, Sr, DOC, N, PO_4^{3-} , U, Th, Sc, Rb, In, Cs, Ba, Tl, Y and REEs) and stable (^{18}O , ^2H , ^{13}C , ^{37}Cl , ^{10}B , ^{34}S) and radioactive-radiogenic (^3H , ^{226}Ra , ^{228}Ra , ^{222}Rn , ^{238}U , ^{235}U , ^{234}U , ^{232}Th , ^{230}Th and ^{228}Th) isotopes, microbes, gases and colloids. (cf. Appendix 6 in /SKB, 2005b/).

The different analytical results obtained using contrasting analytical techniques for Fe and S have been confirmed with speciation-solubility calculations and checking their effects on the charge balance. The values selected for modelling were those obtained by ion chromatography (SO_4^{2-}) and spectrophotometry (Fe) assuming no colloidal contribution. The selected pH and Eh values correspond to available downhole data (cf. Appendix 6 in /SKB, 2005b/).

9.2.2 Representativeness of the data

By definition, a high quality sample is considered to be that which best reflects the undisturbed hydrological and geochemical in-situ conditions for the sampled section. A low quality sample may contain in-situ, on-line, at-line, on-site or off-site errors such as arise from contamination from tubes of varying compositions, air contamination, losses or uptake of CO_2 , long storage times prior to analysis, analytical errors etc. The quality may also be influenced by the rationale in locating the borehole and selecting the sampling points. Some errors are easily avoided, others are difficult or impossible to avoid. Furthermore, chemical responses to these influences are sometimes, but not always, apparent.



Figure 9-1. The groundwater sampling locations at Forsmark. The dotted lines indicate the orientation of the cutting planes (NW-SE and NE-SW) used for the visualisations.

Forsmark site

The Forsmark groundwater analytical data compiled in the SICADA database, which form the basis of the hydrochemical evaluation, will have already undergone an initial screening process by field and laboratory personnel based on sampling, sample preparation and analytical criteria. The next stage in the hydrogeochemical site descriptive process, the focus of this report, is to assess these screened data in more detail to derive a standard set of representative groundwater data for hydrogeochemical modelling purposes.

For this assessment, the initial most important stage is to check for groundwater contamination. To accomplish this stage, an intimate knowledge of the borehole site is required which entails borehole geology and hydrogeology and a detailed log of borehole activities. These latter activities are a major source of groundwater contamination and include:

- drilling and borehole cleaning,
- open-hole effects,
- downhole geophysical/geochemical logging,
- downhole hydraulic logging/testing/pumping, and
- downhole sampling of groundwaters.

In Appendix 1 in /SKB, 2005b/ these potential sources of contamination have been addressed and documented systematically for each borehole drilled and for each borehole section sampled. The degree of contamination has been judged, for example, by plotting tritium against percentage drilling water and using measured values with specifically defined limits, i.e. charge balance ($\pm 5\%$) and drilling water component ($< 1\%$), and supported qualitatively by expert judgement based on detailed studies of the distribution and behaviour of the major ions and isotopes. The final selection of data which best represents the sampled borehole section is based on identifying as near as possible a complete set of major ion and isotope (particularly tritium, ^{18}O and deuterium) analytical data. This is not always the case, however, and a degree of flexibility is necessary in order to achieve an adequate dataset to work with. For example: A charge balance of $\pm 5\%$ was considered acceptable.

In some cases groundwaters exceeding this range were chosen to provide a more representative selection of groundwaters. These groundwaters should therefore be treated with some caution when used in the modelling exercises.

Also in many cases the drilling water content was either not recorded or not measured. Less than 1% drilling water was considered acceptable. In some cases, groundwaters were chosen that exceeded this value to provide a more representative selection of groundwaters. These groundwaters have to be treated with some caution when used in the modelling exercises.

Some of the older tritium data were analysed with a higher detection limit of 8 TU; the detection limit lies around 0.02 TU for recent analyses. For some groundwaters, an approximate tritium value is suggested where no recorded value is available. This value is selected normally from the same borehole section, but represents an earlier or later sample.

Resulting from this assessment, two groundwater sample types are highlighted in Appendix 6 in /SKB, 2005b/: one type considered representative, the other type less representative, but suitable when used with caution.

The drilling event is considered to be the major source for contamination of the formation groundwater. During drilling, large hydraulic pressure differences can occur due to uplifting/lowering of the equipment, pumping and injection of drilling fluids. These events can facilitate unwanted mixing and contamination of the groundwater in the fractures, or the cutting at the drilling head itself can change the hydraulic properties of the borehole fractures. It is therefore of major importance to analyse the drilling events in detail. From this information not only can the uranium spiked drilling water be traced, but also the major risk of contamination and disturbance from foreign water volumes can be directly identified. Insufficient or excessive extraction of water from a deformation zone prior to sampling can be determined by applying DIS (Drilling Impact Study) modelling /Gurban and Laaksoharju, 2002/.

A hydraulically active deformation zone in one isolated section in borehole KFM02A: 509–516 m was the subject of the DIS modelling. The modelling carried out for this deformation zone was based on the DIFF (differential flow meter logging) measurements and the main aim was to model the amount of the contamination for this particular deformation zone (cf. Appendix 4 in /SKB, 2005b/). The result from the sampling shows 22% remaining drilling water in the first chemical sample after pumping a volume of 3.8 m³, and 6% remaining drilling water in the last sample after pumping an additional 205 m³. The duration of the pumping, with some interruptions, was approximately 130 days. The amount of drilling water removed was approximately 22 m³. The DIS calculations show that pumping should have continued further in order to remove an additional 12.6 m³. The study identified that there are uncertainties in the dosing and control of the uranium during the drilling process.

One fundamental question in modelling is whether the uncertainties lead to a risk of misunderstanding the information in the data. Generally, the uncertainties from the analytical measurements are lower than the uncertainties caused by the modelling, but the variability during sampling is generally higher than the model uncertainties.

Nordic sites

The Nordic sites, in addition to Forsmark, comprise Laxemar and Simpevarp and all remaining Swedish sites studied over the last 20–25 years; Olkiluoto in Finland is also included (for more information see Appendix 1 in /SKB, 2005b/). Most of these sites have undergone earlier detailed assessments as to groundwater quality and representativeness, e.g. Gideå, Kamlunge, Klipperås, Fjällveden, Svartboberget, Finnsjön /Smellie et al. 1985, 1987; Smellie and Wikberg, 1989/, Lansjärv /Bäckblom and Stanfors, 1989/ and Olkiluoto /Pitkänen et al. 1999, 2004a/. Based on this information, the Nordic Table has been highlighted with respect to representative and less representative groundwater samples (Appendix 7 in /SKB, 2005b/). The ‘less’ representative groundwaters do not meet all of the criteria for representativeness but are sufficiently important to be included. The importance of early or ‘First Strike’ samples is emphasised in the evaluation discussed in Appendix 1 and listed in Appendix 7 in /SKB, 2005b/. These are coloured green in the Nordic Table and involve one or more of the following deviations from being considered ‘representative’:

- lack of important ions – especially Br,
- lack of ^{18}O and deuterium data,
- variation in salinity during the time-series measurements, and
- few, or absence of time-series measurements.

The representative groundwaters are highlighted in the Nordic Table in orange (Appendix 7 in /SKB, 2005b/).

9.2.3 Explorative analysis

A commonly used approach in groundwater modelling is to start the evaluation by explorative analysis of different groundwater variables and properties. The degree of mixing, the type of reactions and the origin and evolution of the groundwater can be indicated by applying such analyses. Also of major importance is to relate, as far as possible, the groundwaters sampled to the near-vicinity geology and hydrogeology.

Borehole properties

Figure 9-2, Figure 9-3, Figure 9-4 and Figure 9-5 show a schematic representation of boreholes KFM01A, KFM02, KFM03A and KFM04A and the intercepted structures and their hydraulic conductivities. Groundwater sampling locations are indicated and the sampled chloride contents are shown. The results from drillcore mapping, BIPS measurements, differential flow measurements and electric conductivities, together with groundwater quality and representativeness of the samples, are discussed in detail for all investigated boreholes in Appendix 1 in /SKB, 2005b/.

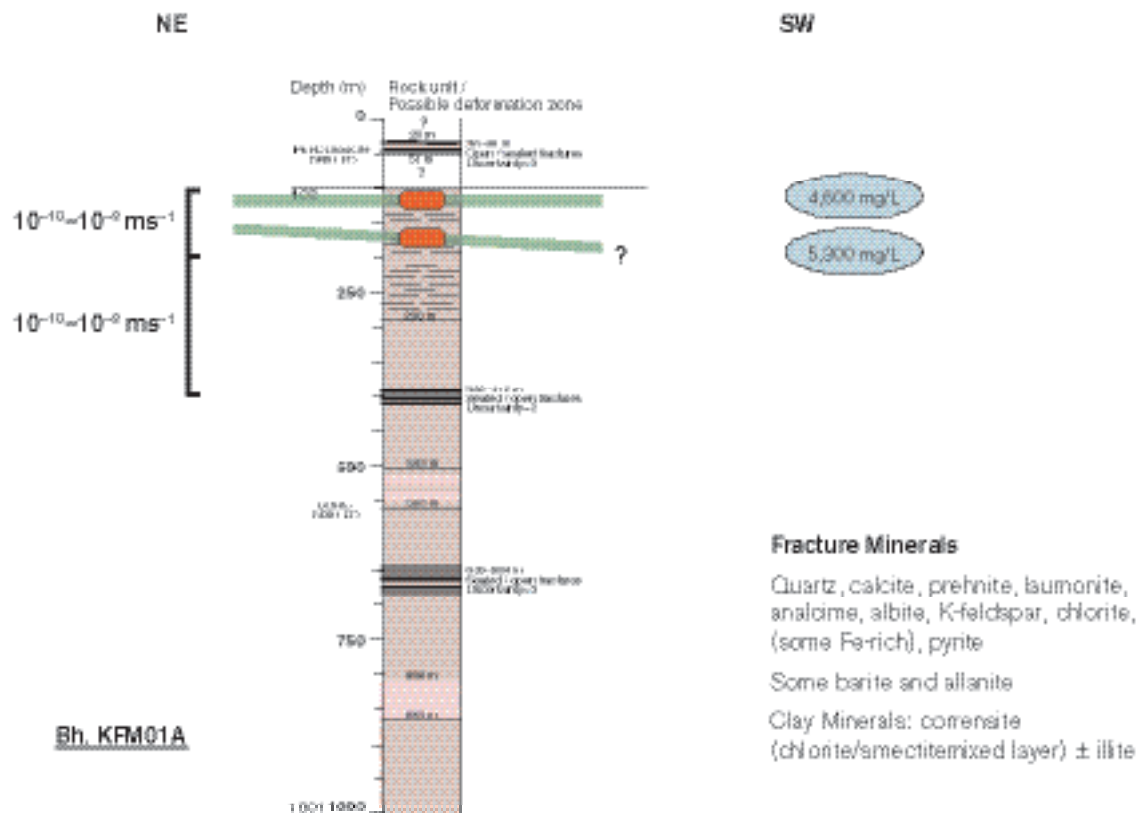


Figure 9-2. Relation of borehole KFM01A to the identified sampled deformation zones (in green) and hydraulic parameters; groundwater sampling locations are indicated in red with the mg/L chloride content in blue. The questionmark represents an uncertain deformation zone.

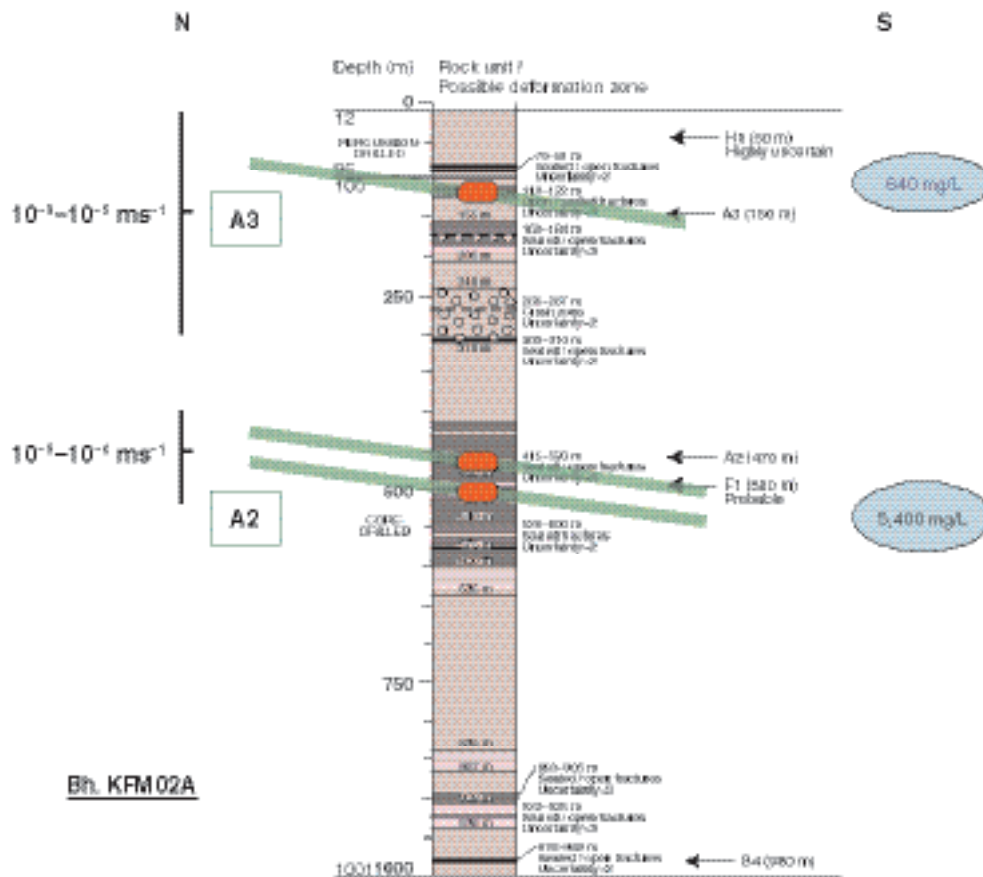


Figure 9-3. Relation of Borehole KFM02A to the known major structures (A2 and A3 in green) and hydraulic parameters; groundwater sampling locations are indicated in red with the mg/L chloride contents in blue.

Evaluation of scatter plots

The hydrochemical data have been expressed in several X-Y plots to derive trends that may facilitate interpretation. Since chloride is generally conservative in normal groundwater systems, its use is appropriate to study hydrochemical evolution trends when coupled to ions, ranging from conservative to non-conservative, to provide information on mixing, dilution, sources/sinks etc. Many of the X-Y plots therefore involve chloride as one of the variables.

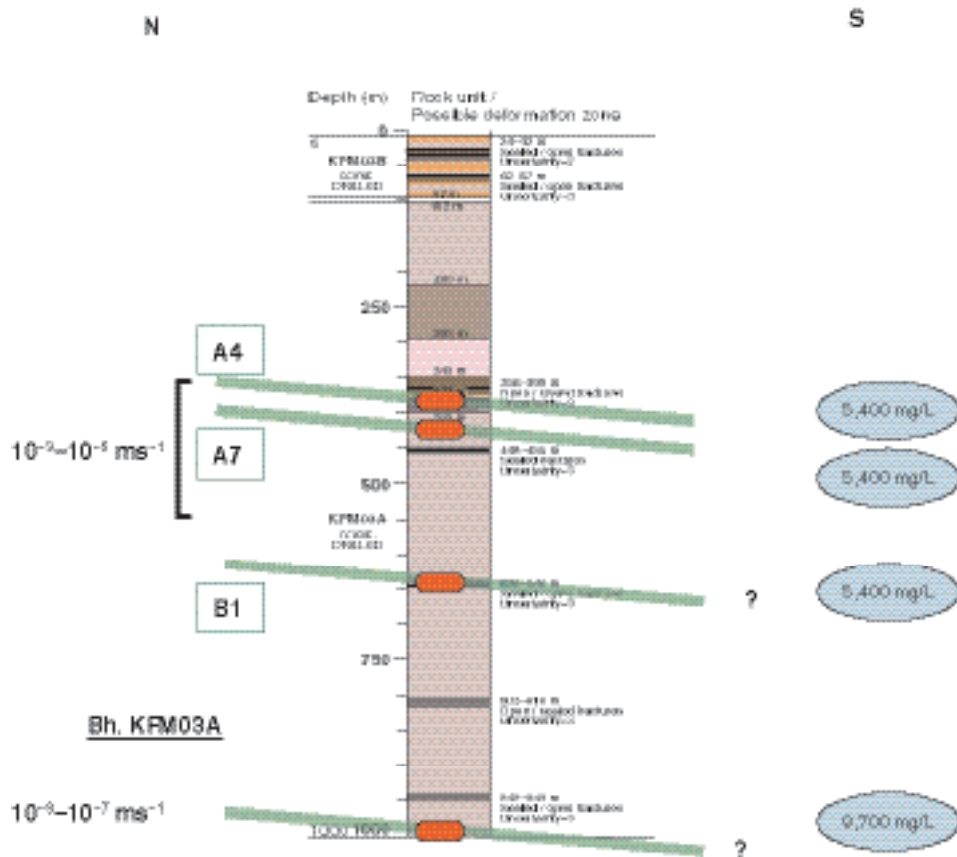


Figure 9-4. Relation of Borehole KFM03A to the known major structures (in green) and hydraulic parameters; groundwater sampling locations are indicated in red with the mg/L chloride contents in blue. The questionmarks represent uncertain deformation zones.

The hydrogeochemical evaluation presented below follows the systematic approach described in the SKB strategy report /Smellie et al. 2002/ commencing with traditional plots (e.g. Piper Plots) to group the main groundwater types characterising the Forsmark site and to identify general evolutionary or reaction trends. Comparisons are made with hydrochemical information from other Swedish and Nordic sites. Importantly, the hydrogeochemistry is related also to the regional and local geology and hydrogeology in order to understand the overall (i.e. large- and small-scale) dynamics and evolution of the groundwater systems that characterise the Forsmark site. A more detailed evaluation of the major components and isotopes can be found in Appendices 1 and 3 in /SKB, 2005b/. Discussion of many of the reactive elements is presented in the modelling part of this report (Section 9.5) and also in Appendix 3 in /SKB, 2005b/.

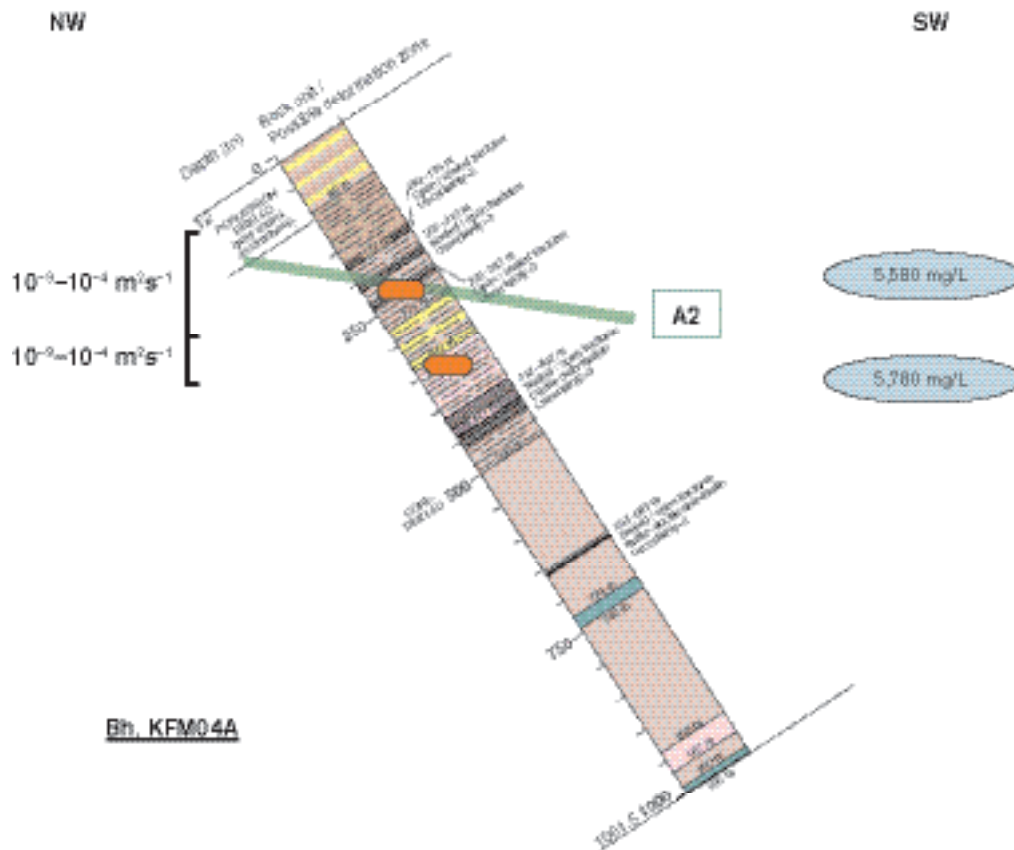


Figure 9-5. Relation of borehole KFM04A to the known major structures (in green) and hydraulic parameters; groundwater sampling locations are indicated in red with mg/L chloride contents in blue.

Piper Plot

Water classification is presented in Appendices 1 and 4 in /SKB, 2005b/. The main groundwater groups characterising Forsmark are: a) shallow (< 200 m) Na-HCO₃ to Na-HCO₃(SO₄) to Na(Ca)-HCO₃ to Na(Ca)-HCO₃-Cl(SO₄) to Na(Ca)-Cl-SO₄(HCO₃) to Na(Ca, Mg)-Cl-SO₄(HCO₃) types, b) intermediate (approx. 200–600 m) Na(Ca, Mg)-Cl(SO₄) to Na-Ca(Mg)-Cl(SO₄) types, and c) deep (> 600 m) Na-Ca-Cl to Ca-Na-Cl types. The variation in compositions, especially in the upper 200 m of the bedrock, is due to local hydrodynamic flow conditions leading to mixing of varying proportions. Microbially mediated reactions are also important in influencing both HCO₃ and SO₄, especially in the upper 600 m, as well as ion exchange reactions.

The Piper and Langelier Ludwig plots from the Forsmark site, shown in Figure 9-6, emphasise distinct groupings representing: a) the deeper cored borehole groundwaters, b) the shallow cored borehole and percussion borehole groundwaters, and c) the Baltic Sea waters. There is an overall lack of distinction between the Lake and Stream waters and many of the shallow Soil Pipe groundwaters, although most represent more dilute water types. There is some overlapping (i.e. mixing trends) between the main Baltic Sea cluster and some of the percussion borehole groundwaters and, as mentioned above, widespread overlapping between the surface and near-surface Lake and Stream waters and some of the shallow Soil Pipe groundwaters.

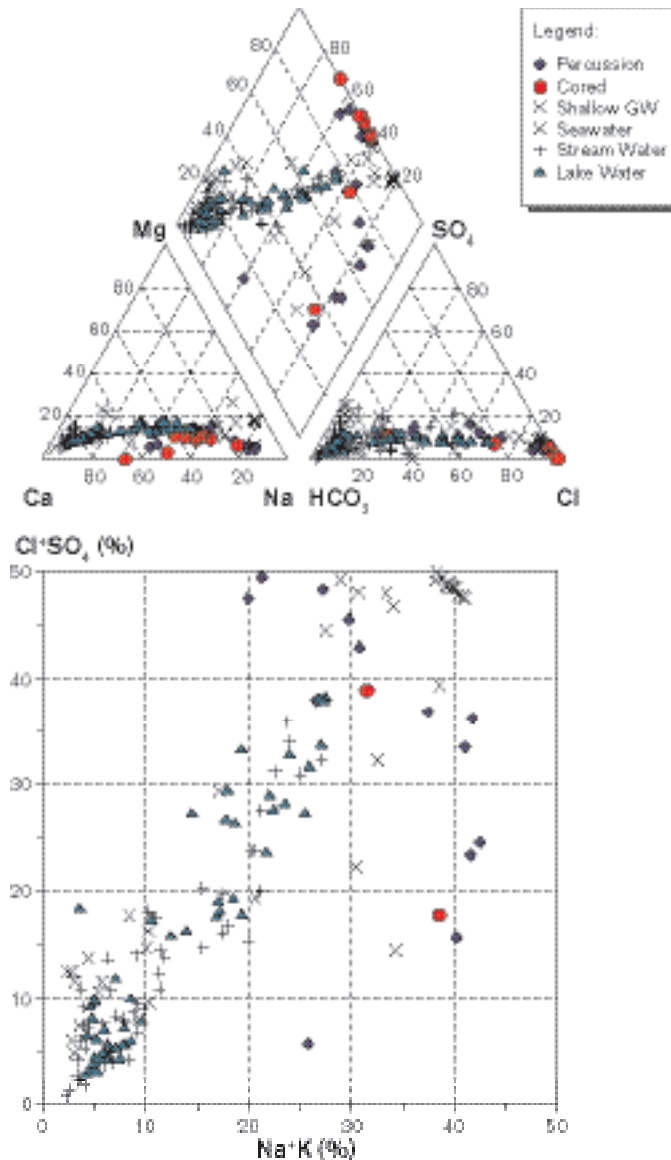


Figure 9-6. Piper and Ludwig-Langelier plots of surface, near-surface and groundwaters from Forsmark.

General comparison of Cl vs. depth with other sites

Comparison of the Forsmark chloride data with some of the other Fennoscandian sites is shown in Figure 9-7. These Fennoscandian sites, i.e. Finnsjön, SFR and Olkiluoto, provide excellent comparisons since both Finnsjön and SFR are close to the Forsmark site and Olkiluoto is the Finnish counterpart to Forsmark in terms of palaeoevolution (coastal location) and also in terms of geological and present-day climatic conditions.

Figure 9-7 for all sites shows a similar transition from dilute groundwaters (< 1,000 mg/L Cl) to brackish groundwaters (~ 5,000–6,000 mg/L Cl) at slightly varying depths ranging from 50–200 m. Finnsjön also indicates bedrock areas where local hydrodynamics appear to have transported dilute groundwaters to around 500–550 m although some contamination cannot be ruled out.

The transition from brackish to more saline groundwaters differs between the sites. At Forsmark (represented by KFM03A), this transition to saline appears to occur at depths greater than 650 m. At Olkiluoto, it is clearly at around 500 m, below which the salinity increases dramatically to a maximum of > 40,000 mg/L Cl at approx. 850 m depth, whereas at Forsmark the salinity only increases to ~ 10,000 mg/L Cl at 1,000 m depth. Both the Finnsjön and SFR sites lack groundwater data from great depth.

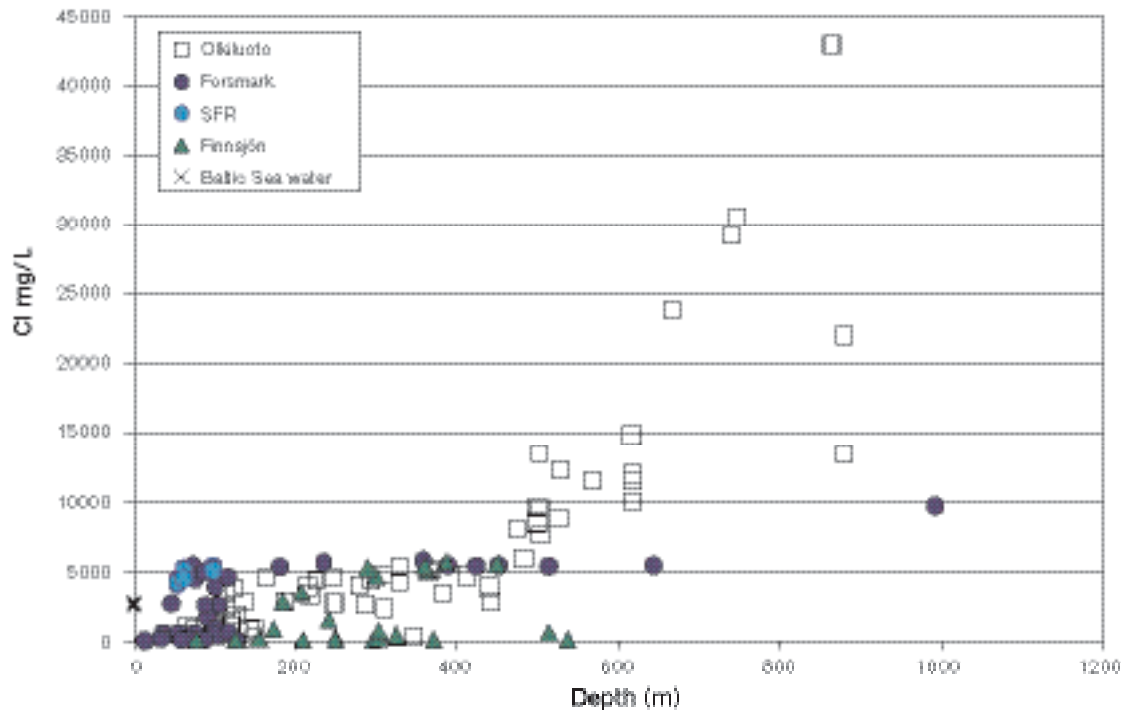


Figure 9-7. Depth comparison of chloride with other Fennoscandian sites.

Tritium

Tritium produced by the bomb tests during the early 1960's is a good tracer for waters recharged within the past four decades. As part of an international monitoring campaign, peak values between 1,000 and 4,300 TU were recorded at Huddinge near Stockholm in the years 1963–1964 and values reaching almost 6,000 TU were recorded at Arjeplog and Kiruna in northern Sweden (IAEA database). Due to decay (half life of 12 years) and dispersion, in addition to a cessation of the nuclear bomb tests, precipitation tritium values decreased so that measurements carried out at Huddinge during 1969 showed that values had dropped to between 74 and 240 TU.

Present-day surface waters from the Simpevarp and Forsmark sites show values of 7–20 TU with exceptions of a few Lake and Stream water samples from Forsmark (Figure 9-8). Generally, the Baltic Sea samples (10.3–19.3 TU) show somewhat higher values compared with the meteoric surface waters (7.8–15 TU) for precipitation. The Forsmark Baltic Sea samples show some values that are higher than the Simpevarp Baltic Sea samples, but the spread is large for both sites. The successive lowering of tritium contents with time elapsed since the bomb tests may explain the higher values in the Baltic Sea (due to reservoir effects) compared with precipitation. The difference between the Simpevarp and Forsmark Baltic Sea samples can be a north-south effect, with higher tritium values in the north compared with the south. However this is not demonstrated by the precipitation values (Figure 9-8). Moreover, the ^{14}C content in the Baltic Sea water is relatively similar between the two sites (Figure 9-9).

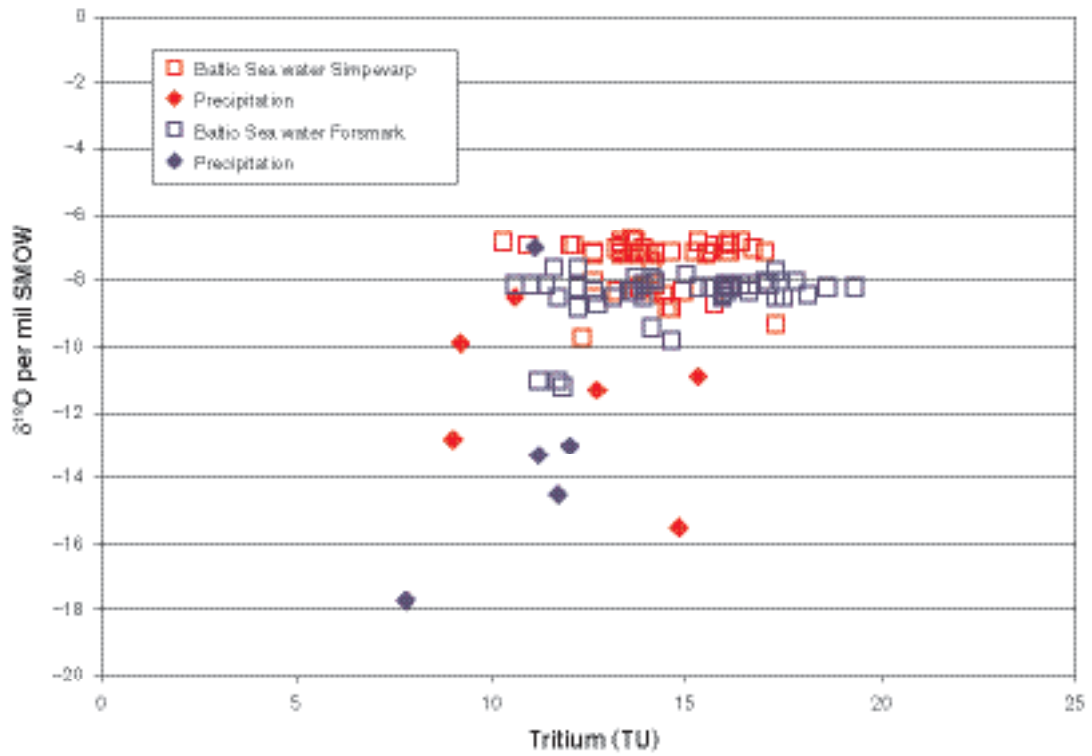


Figure 9-8. Plot of $\delta^{18}O$ versus tritium in surface water samples from the Forsmark and Simpevarp sites.

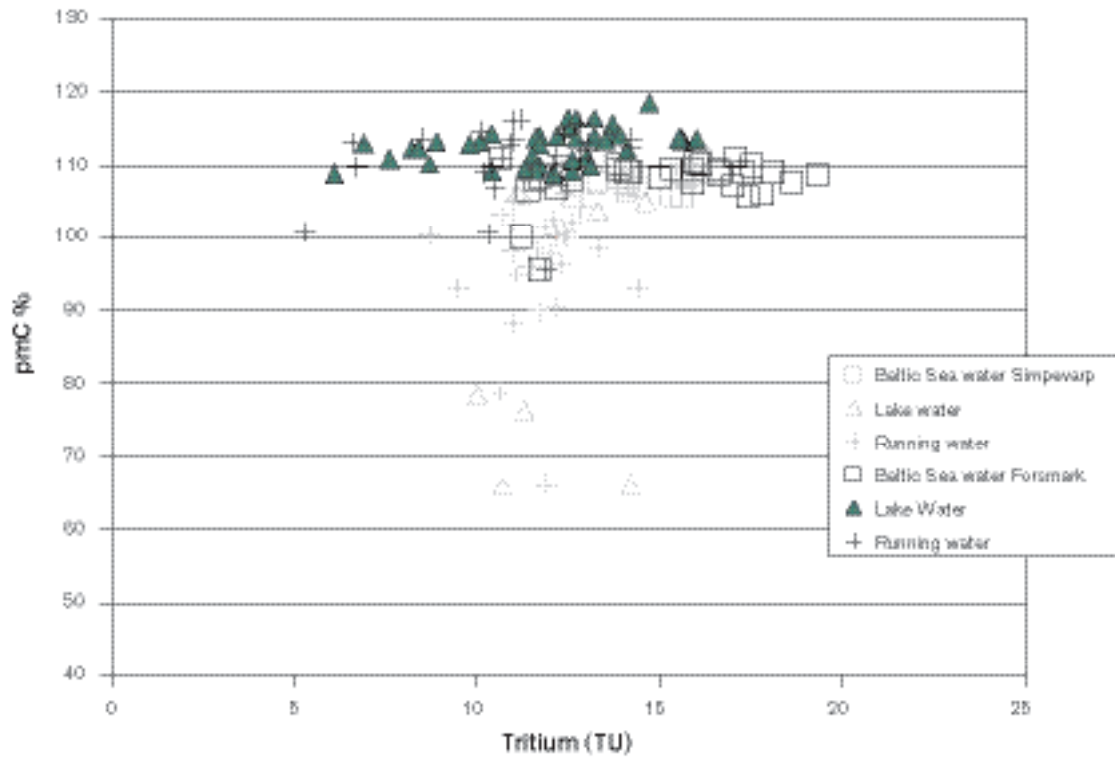


Figure 9-9. ^{14}C content, given as percentage modern carbon (pmC%) versus tritium content for surface waters from Forsmark.

The measured tritium contents in the precipitation and Baltic Sea water at each site may also contain some tritium locally produced by the nuclear power plants, i.e. that emitted both as vapour to the atmosphere and that contained in the cooling water discharged to the Baltic Sea. This contribution is probably very low but the possibility should not be completely ruled out at the moment until background environmental tritium data become available. It should be emphasised that the precipitation values are very few, show a large variation in tritium and therefore are not considered very conclusive. Continued systematic sampling of precipitation (rain and snow) for tritium analysis therefore is encouraged.

One problem in using tritium for the interpretation of near-surface recharge/discharge is, as mentioned above, the variation in content in recharge water over time. This implies that near-surface groundwaters with values around 15 TU can be 100% recent, or a mixture of old meteoric (tritium free) water, and a small portion (10%) of water from the sixties at the height of the atmospheric nuclear bomb tests.

The plot of tritium vs. ^{14}C for surface waters from Forsmark and Simpevarp shows large differences concerning the lake and stream waters at the two sites (Figure 9-9). At Simpevarp, many of the lake and stream waters show a distinctly lower ^{14}C content whereas the tritium values are the same or show a small decrease. This may be explained by the addition to the waters of HCO_3 that originates either from calcites devoid of ^{14}C , or, due to microbial oxidation of organic material with lower (or no) ^{14}C . This is the pattern expected for near-surface waters. At Forsmark, in contrast, most lake and stream waters have higher ^{14}C values than Baltic Sea waters, whereas the tritium values range from 5–15 TU for all three water sources. Since tritium contents are naturally largely variable and sometimes close to detection, the analytical data used in groundwater modelling have to be carefully scrutinised for any signs of contamination. Since it can be concluded that subsurface in-situ production of tritium is expected to be negligible in the Forsmark granitoids, the major sources of contamination will be related to drilling waters or surface waters that may have entered the borehole.

Figure 9-10 shows tritium vs. percentage drilling water content in the cored boreholes from Forsmark. The drilling water used from the percussion boreholes varied in tritium content from a minimum of 1.9 TU for HFM10 to a maximum of 5.7 TU for HFM06. However, there is no correlation between percentage drilling water and tritium values in the sampled representative groundwaters, which indicates that the drilling water was successfully removed prior to sampling.

All available tritium values from groundwaters (percussion boreholes, cored boreholes and soil pipes) are plotted versus depth in Figure 9-11. In the cored boreholes, the tritium content decreases significantly in the upper 200 m but varies considerably in the percussion boreholes. Tritium-free groundwater was collected in HFM05 (25–200 m), HFM08 (0–144 m), HFM12 (0–210 m) and HFM14 (0–151 m).

Below 200 m depth, tritium values under 3 TU were detected for all samples. For the sections sampled below 300 m, the groundwaters systematically collected from each section generally show no detectable tritium. In two cases, however, a few tritium units have been measured in the last sample in the sequence collected which for other reasons has been selected as most representative. Since at the moment it not clear why these water samples show detectable tritium contents, it is suggested that these values are used with some caution until more analyses become available.

One of the near-surface samples from KFM03A (0–46 m) shows a very high tritium content of 41 TU indicative of a significant portion of recharge from the sixties or seventies when the recharge tritium contents were much higher than at present. There is therefore the possibility that the observed tritium values in some of the sampled borehole sections reflect some contamination by these tritium-enhanced waters entering into water-conducting fracture systems during open hole borehole activities. This would help to explain the presence of low, but non-zero, tritium values and an absence of drilling water.

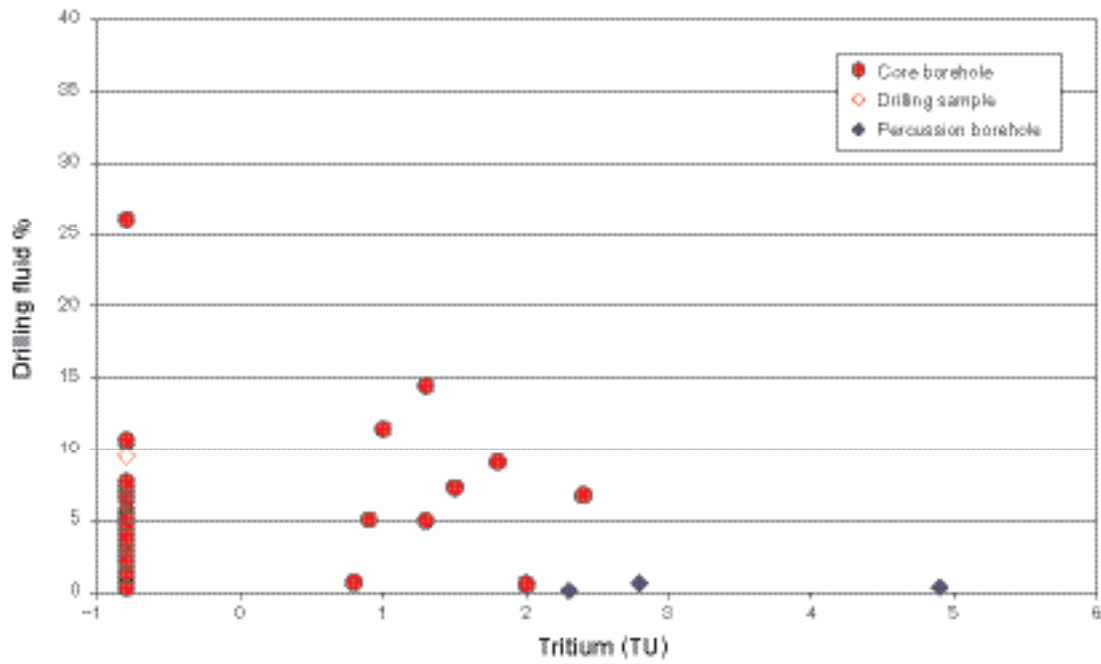


Figure 9-10. Tritium (TU) versus drilling fluid (%) for boreholes HFM05, KFM01A, KFM02A, KFM03A and KFM04A. Negative TU values are below the limit of detection.

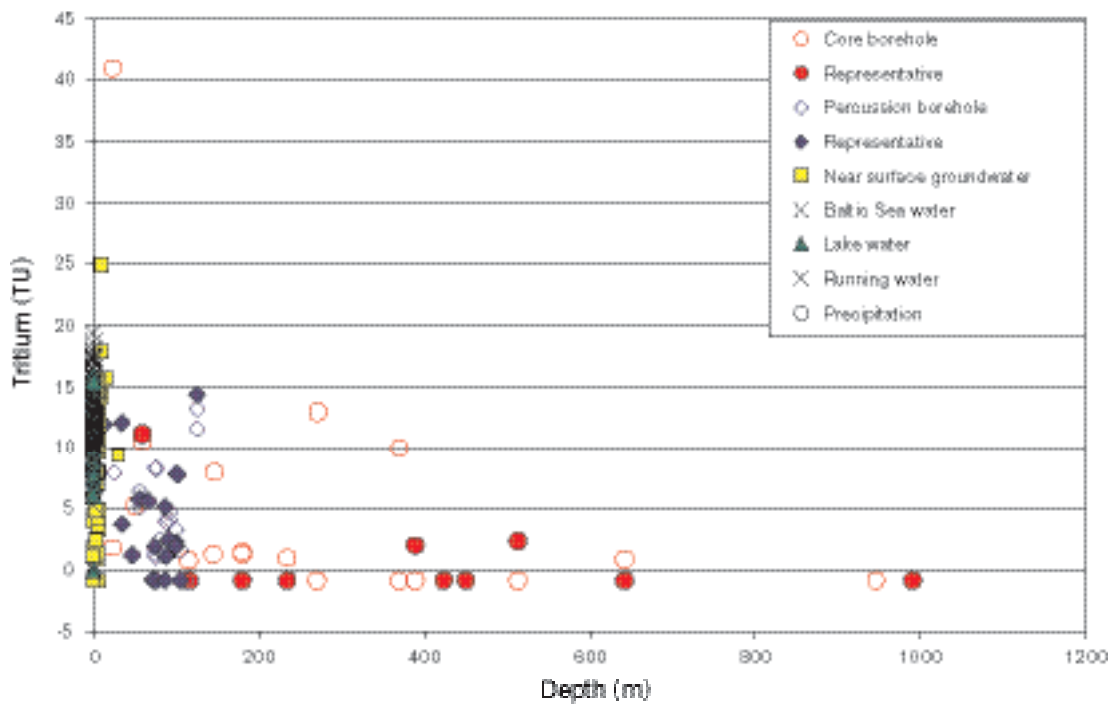


Figure 9-11. Tritium (TU) versus depth (m) for a) groundwaters from cored boreholes, percussion boreholes and soil pipes, b) Baltic Sea, Lake and Stream waters, and c) precipitation.

Tracing the Littorina Sea signature with Mg, Br, and $\delta^{18}\text{O}$

The Littorina stage in the postglacial evolution of the Baltic Sea commenced when the passage to the Atlantic Ocean opened through Öresund in the southern part of the Baltic Sea. The relatively high sea level together with the early stages of isostatic land uplift led to a successively increasing inflow of marine water into the Baltic Sea. Salinities twice as high as those of the modern Baltic Sea have been estimated for a time period of about 2,000 years starting some 7,000 years ago (cf. Chapter 3). Based on shore displacement curves, it is clear that the Forsmark area has been covered by the Littorina Sea for a long period of time (8,000 to 9,000 years) and the low topography implies that it reached several tens of kilometres further inland for a considerable part of that time. The present meteoric recharge stage following uplift and emergence has only prevailed for less than 1,000 years, implying that any flushing out of the Littorina Sea component is relatively limited. Strong evidence of a Littorina Sea water signature can therefore be expected in groundwaters at Forsmark, which is also confirmed by the hydrochemical interpretations.

The Simpevarp/Laxemar area, in contrast, was only partly covered by the Littorina Sea. Due to the topography of the area and the on-going isostatic land uplift, the Laxemar area was probably influenced only to a small degree, whereas the Simpevarp peninsula was covered for several thousands of years until eventual emergence during uplift initiated a recharge meteoric water system some 4,000 to 5,000 years ago. This recharge system effectively flushed out much of the Littorina Sea water.

Comparison of Forsmark data with those from the Simpevarp area (i.e. Äspö, Laxemar and Oskarshamn sites) indicates large differences in the character and origin of the groundwaters, especially for brackish groundwaters with chloride contents of around 4,000–6,000 mg/L Cl. This is exemplified in three plots showing chloride versus magnesium, bromide and $\delta^{18}\text{O}$ (Figure 9-12, Figure 9-13 and Figure 9-14). For a more detailed discussion and plots showing data from individual boreholes see Appendix 1 in /SKB, 2005b/.

The magnesium versus chloride plot (Figure 9-12) clearly shows the difference between the Forsmark and Simpevarp groundwaters characterised by chloride contents up to 5,500 mg/L Cl; characteristically the Forsmark samples closely follow the modern marine (Baltic Sea) trend. Those few groundwaters that plot within the Simpevarp area group are from greater depths in the bedrock and, as such, have been influenced by mixing with deeper non-marine saline groundwaters. A few samples from Äspö (KAS06 and HAS02; Figure 9-12) also show relatively high Mg contents, although not as high as in the Forsmark groundwaters with similar chloride contents. Most of the Simpevarp area groundwaters show low Mg values although small increases are observed for samples in the chloride interval 4,000–6,300 mg/L.

The bromide versus chloride plot (Figure 9-13) underlines the marine signature for most of the Forsmark groundwaters with salinities up to brackish values ($\sim 5,500$ mg/L), with the exception of sample KFM03A: 638–644 m which shows a mixed origin (already commented upon in previous sections), whereas marine signatures are obtained only in a few of the Oskarshamn sub-area groundwaters. This observation is strengthened in the $\delta^{18}\text{O}$ versus chloride plot (Figure 9-14) which shows deviating groundwater trends for Forsmark and Simpevarp.

Generally, with a few exceptions, the brackish groundwaters up to 5,500 mg/L Cl at Forsmark show indications of a marine origin in terms of: a) Br/Cl ratios, b) Mg values ≥ 100 mg/L, and c) $\delta^{18}\text{O}$ values higher than meteoric waters (due to in-mixing of marine waters). In contrast, for the Äspö-Simpevarp-Laxemar samples these criteria are only fulfilled in samples from KAS06 and one sample in KSH03A. In both cases, the groundwater samples have been collected from deformation zones outcropping close to the shoreline or under the Baltic Sea.

The chloride content and $\delta^{18}\text{O}$ value for the Littorina Sea at maximum salinity is difficult to determine precisely. Interpretations of salinities based on fossil fauna together with $\delta^{18}\text{O}$ analyses of the fossils has resulted in suggested salinities around 6,500 mg/L Cl and $\delta^{18}\text{O}$ values $\sim -4.5\text{‰}$ SMOW /Pitkänen et al. 2004a/. In Figure 9-15 (Cl versus $\delta^{18}\text{O}$) groundwaters from the Forsmark, SFR and Simpevarp areas with Br/Cl ratios < 0.0045 and magnesium values > 100 mg/L are shown. For comparison, data from Olkiluoto /Pitkänen et al. 2004a/ are included. The top three mixing lines in Figure 9-15 represent Oceanic/Littorina/meteoric, Oceanic/Baltic (Simpevarp)/meteoric

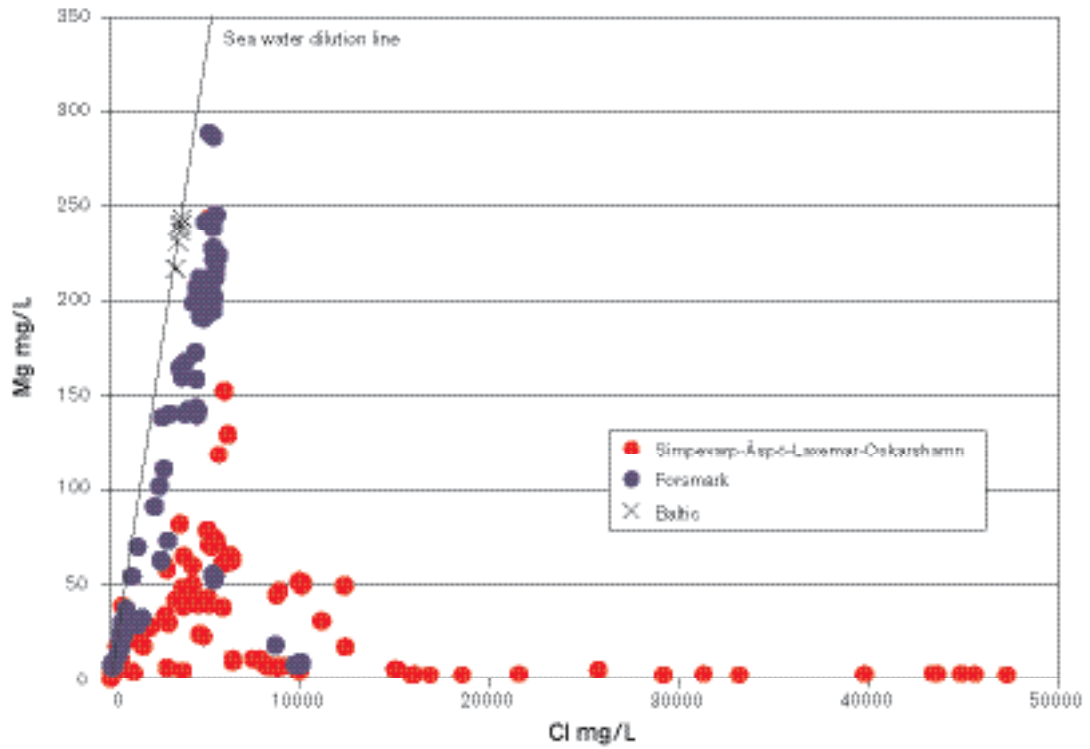


Figure 9-12. Mg versus Cl for groundwaters from Forsmark and the Simpevarp area (Simpevarp-Åspö-Laxemar-Oskarshamn (KOV01)). Baltic Sea waters from Simpevarp and Forsmark are included for reference.

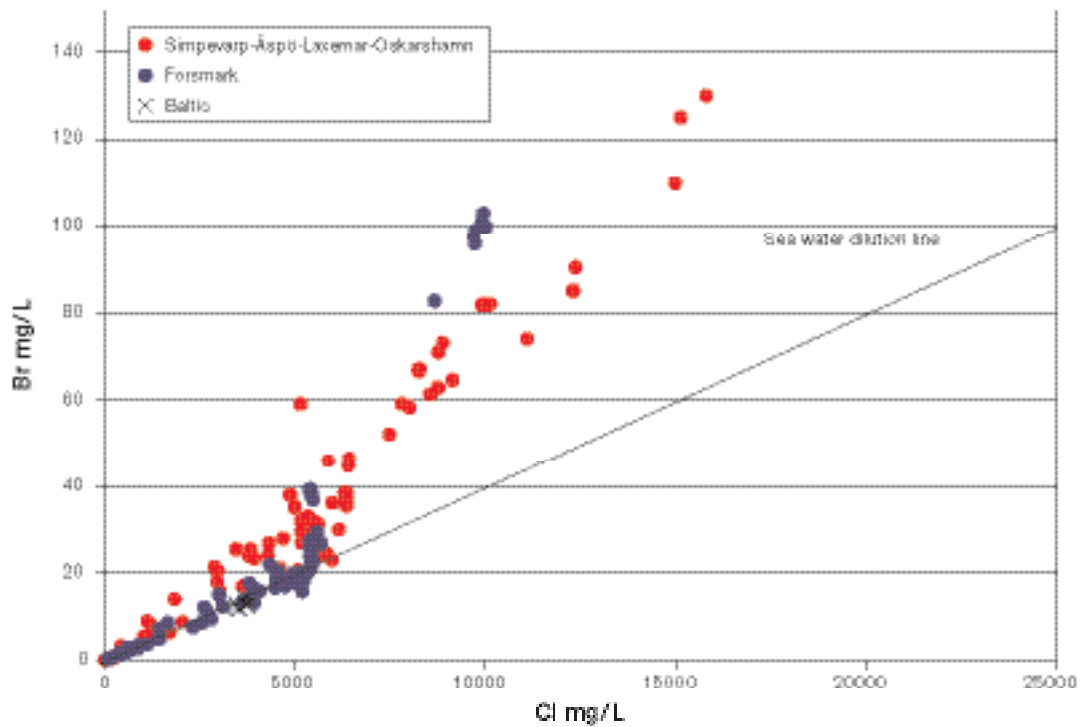


Figure 9-13. Br versus Cl for groundwater samples from Forsmark and the Simpevarp area (Simpevarp-Åspö-Laxemar-Oskarshamn (KOV01)). Baltic Sea waters from Forsmark and Simpevarp are included for reference.

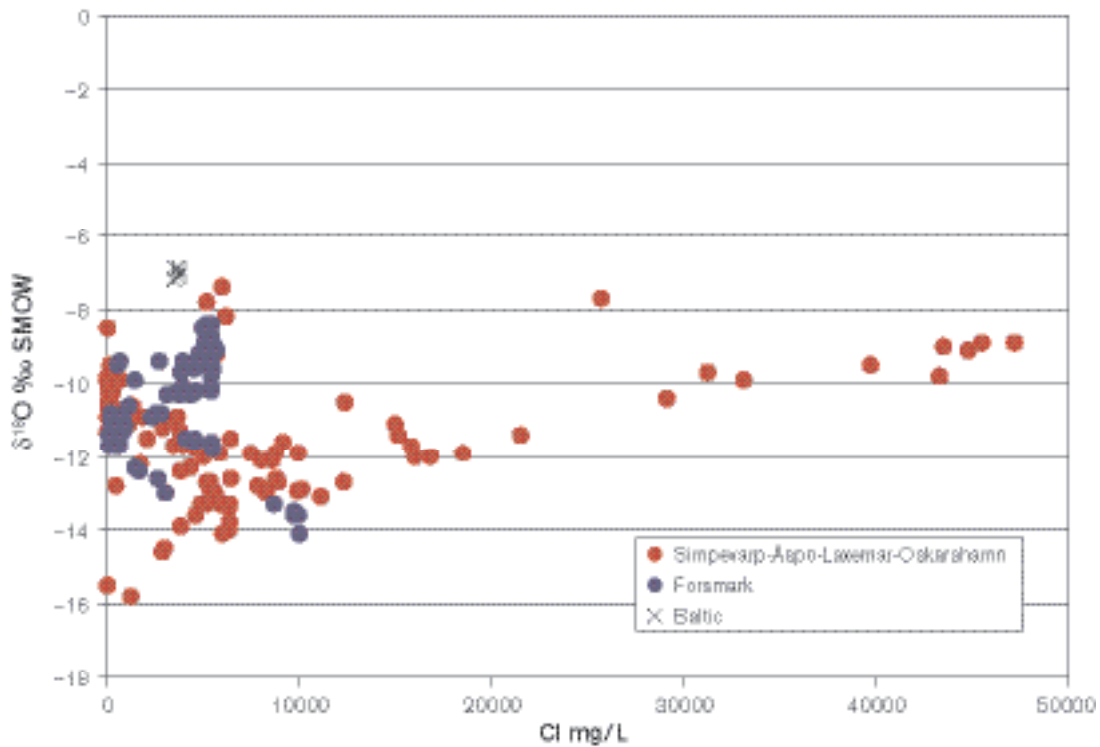


Figure 9-14. $\delta^{18}\text{O}$ versus Cl for groundwaters from Forsmark and the Simpevarp area (Simpevarp-Äspö-Laxemar-Oskarshamn (KOV01)). Baltic Sea waters from Simpevarp are included for reference.

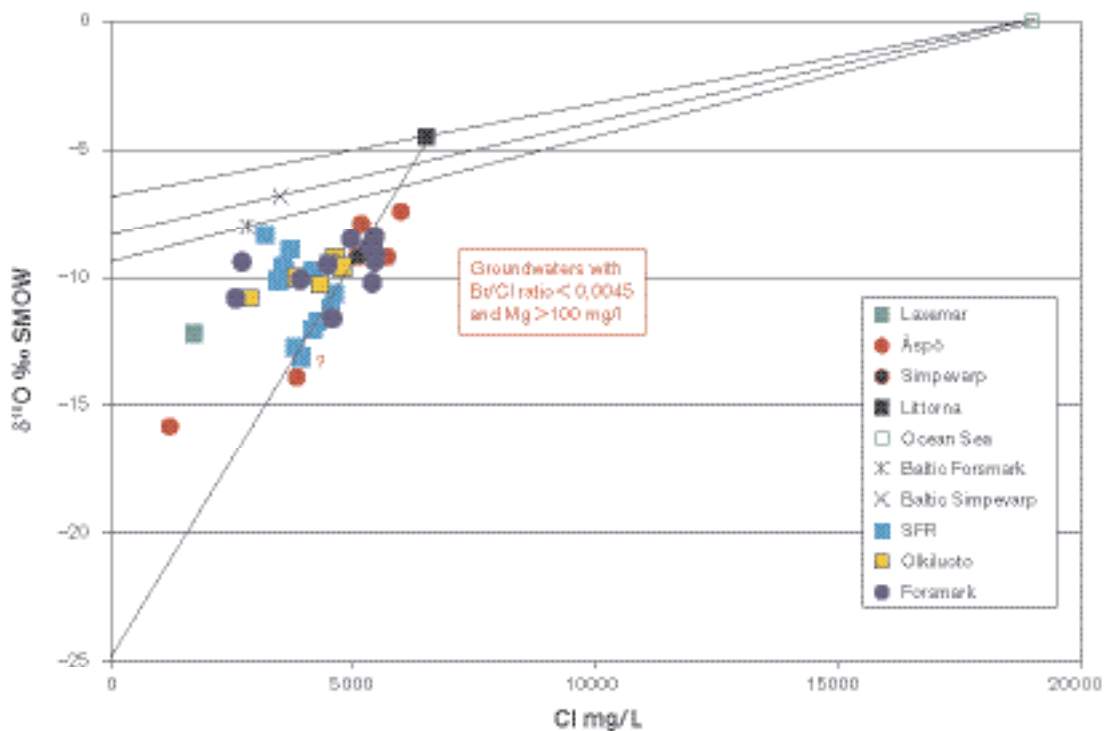


Figure 9-15. $\delta^{18}\text{O}$ versus chloride content for potential marine groundwaters from Simpevarp, Äspö, Forsmark and Olkiluoto, the last from Pitkänen et al. 2004a/. The top three mixing lines represent Oceanic/Littorina/meteoric, Oceanic/Baltic (Simpevarp)/meteoric and Oceanic/Baltic (Forsmark)/meteoric. The sub-vertical mixing line represents Littorina/glacial. Most of the plotted groundwaters reflect mixtures of varying proportions comprising the four end-members: Glacial, Littorina Sea, Baltic Sea and Meteoric waters.

and Oceanic/Baltic (Forsmark)/meteoric. The sub-vertical mixing line represents Littorina/glacial. Most of the plotted groundwaters reflect mixtures of varying proportions comprising the four end-members: Glacial, Littorina Sea, Baltic Sea and Meteoric waters.

Assuming that the suggested Littorina Sea water is the product of simple mixing between Ocean Sea water and a meteoric component, then this meteoric water had heavier $\delta^{18}\text{O}$ values than associated with present-day mixing processes that have given rise to the Baltic Sea close to Forsmark and Simpevarp (Figure 9-15). It is well known that climatic conditions were warmer during parts of the Littorina Sea period and therefore heavier $\delta^{18}\text{O}$ signatures in the meteoric water during that stage were probably applicable. However, it is probable that both the salinity and $\delta^{18}\text{O}$ were variable during the entire Littorina Sea period such that none of the sampled groundwaters at any of the sites studied is fully representative of the Littorina Sea composition.

Based on the post-glacial scenario a successive replacement of the glacial water by the denser Littorina Sea water has occurred giving rise to the sub-vertical Littorina/glacial mixing line in Figure 9-15. As can be seen, a number of waters from Forsmark and SFR cluster along this mixing line together with samples representing the brackish SO_4 type water from Olkiluoto, interpreted by /Pitkänen at al. 2004a/ to represent large portions of Littorina water.

From the Simpevarp area, there are samples from KAS06 and also one sample from KSH03 that show a large component of Littorina Sea water. Weaker indications are also found in a KAS02 sample from 200 m depth, where the magnesium content is low but the Br/Cl ratio is marine.

Figure 9-15 shows the following: 1) The uppermost heavier $\delta^{18}\text{O}$ values plot along the Oceanic Sea mixing line joining the Littorina Sea with precipitation values at that time of $\sim 7\text{‰}$ SMOW, and 2) The Littorina Sea water subsequently mixed with the older, dilute glacial meltwaters as it slowly descended into the bedrock. This has given rise to 'Littorina Sea' waters of varying chemical and isotopic composition. One such example is the narrow range of composition that characterises many of the SFR groundwaters which plot along the present-data mixing line shown in Figure 9-15.

In conclusion, of the groundwaters sampled in the cored boreholes KFM01A, KFM02A, KFM03A and KFM04A in the Forsmark area, six out of ten sampled sections plot along the Littorina/glacial mixing line. These waters represent depths ranging from 110 m in borehole KFM01A to 520 m in borehole KFM02A. Section 640 m in borehole KFM03A indicates a mixed origin comprising a Littorina/glacial and a deep saline component. Also, the groundwaters sampled from KFM04A show inmixing of a deeper saline component based on the Br/Cl ratio, even though a large portion of Littorina Sea is present. Of the 17 percussion boreholes where chemical data are available, three show values that plot along the Littorina Sea mixing line; HFM08 (0–144 m), HFM 10 (0–150 m) and HFM19 (0–173 m). The others show inmixing of today's meteoric and/or modern Baltic Sea to various degrees with the Littorina Sea/glacial mixture. This is also the case for some of the SFR groundwaters; a number of which approach Baltic Sea values (Figure 9-15).

If applying simple regularity for the mixing between the glacial and Littorina Sea waters (and assuming that the suggested Littorina Sea and glacial end member values are at least approximately correct) then the glacial components in the Forsmark samples vary from 18 to 33%, and the highest proportion of glacial water at 42% is found in the SFR groundwaters. This only concerns the glacial-Littorina mixing; the deep saline/glacial mixing which preceded this event is not addressed here.

Redox indicators

Manganese (Mn^{2+}), one of the potential redox indicators in groundwater systems, is mainly produced by microbes during the oxidation of organic material under anaerobic conditions (cf. Appendix 2 in /SKB, 2005b/). It should be emphasised, however, that the presence of Mn^{2+} is a strong indicator of reducing conditions but its absence (or very low content) in deep groundwaters cannot be taken as an indicator of oxidising conditions.

Figure 9-16 plots all available data against depth. The manganese values vary from very low contents up to 1 mg/L in the surface and near-surface waters and also in the groundwaters sampled down to approx. 100 m depth. This indicates various redox conditions and also different intensities in activity of the Mn-reducing bacteria. In the brackish groundwaters characterised with a marine signature sampled between 150 and 550 m depth, the manganese values are in the range of 1 to 3 mg/L. The deeper groundwaters show lower values (< 0.5 mg/L), which indicates a smaller contribution of microbially reduced manganese to these waters. Collectively, these data once again support the interpretation of a more active groundwater system down to approximately 600 m depth.

The Mn-reducing bacteria do not only produce Mn²⁺ but at the same time also HCO₃ due to oxidation of organic material. The plot of Mn versus HCO₃ in the analysed waters shows, however, no specific trend (Figure 9-17). The surface waters and near-surface groundwaters which have the highest bicarbonate contents (up to 800 mg/L) show Mn values < 1 mg/L suggesting that Mn-reducing bacteria are not the main contributors to HCO₃ production in these waters. In the deeper groundwaters, in contrast, there are higher manganese values in the waters where HCO₃ contents range between 90 to 125 mg/L.

As indicated in the plot of Mn versus Cl (Figure 9-18) the highest manganese values are found in waters where chloride contents are between 1,500 to 6,000 mg/L, i.e. those brackish groundwaters with a significant Littorina Sea component. With respect to uranium (cf. discussion below and Appendix 1 in /SKB, 2005b/), high amounts are found in groundwaters where manganese contents exceed 1 mg/L, thus supporting the inferred reducing conditions in these brackish groundwaters.

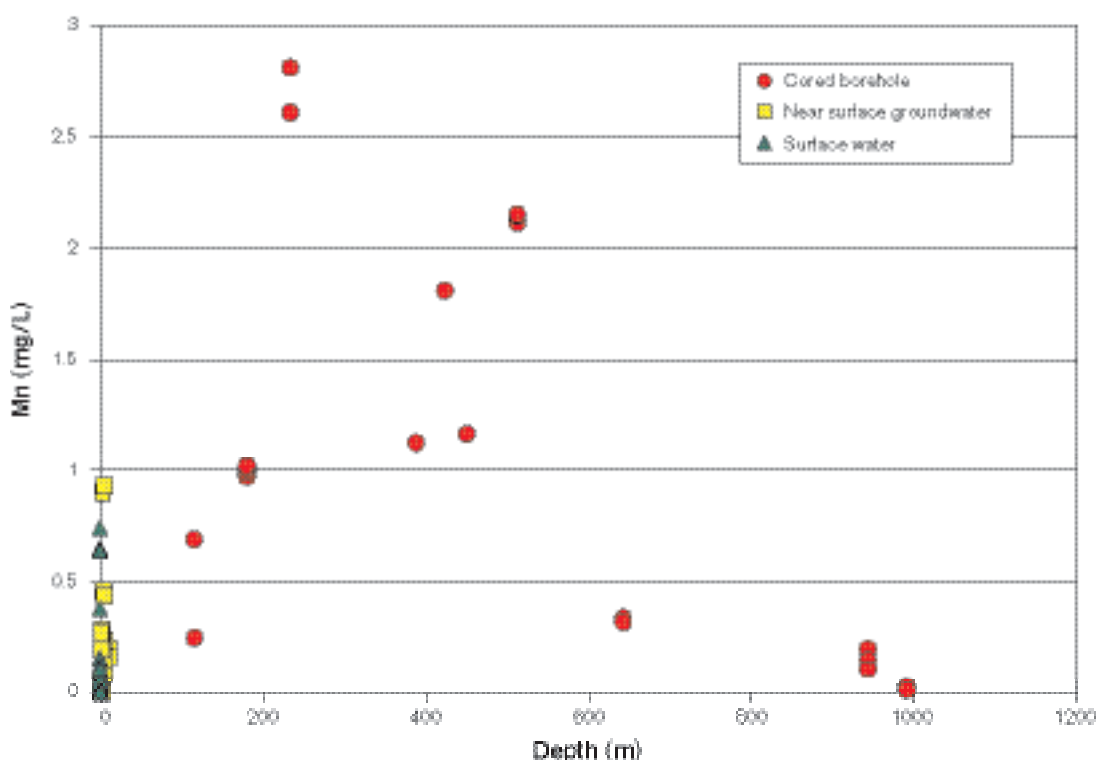


Figure 9-16. Mn versus depth in surface waters, near-surface groundwaters and groundwaters from cored boreholes in the Forsmark area.

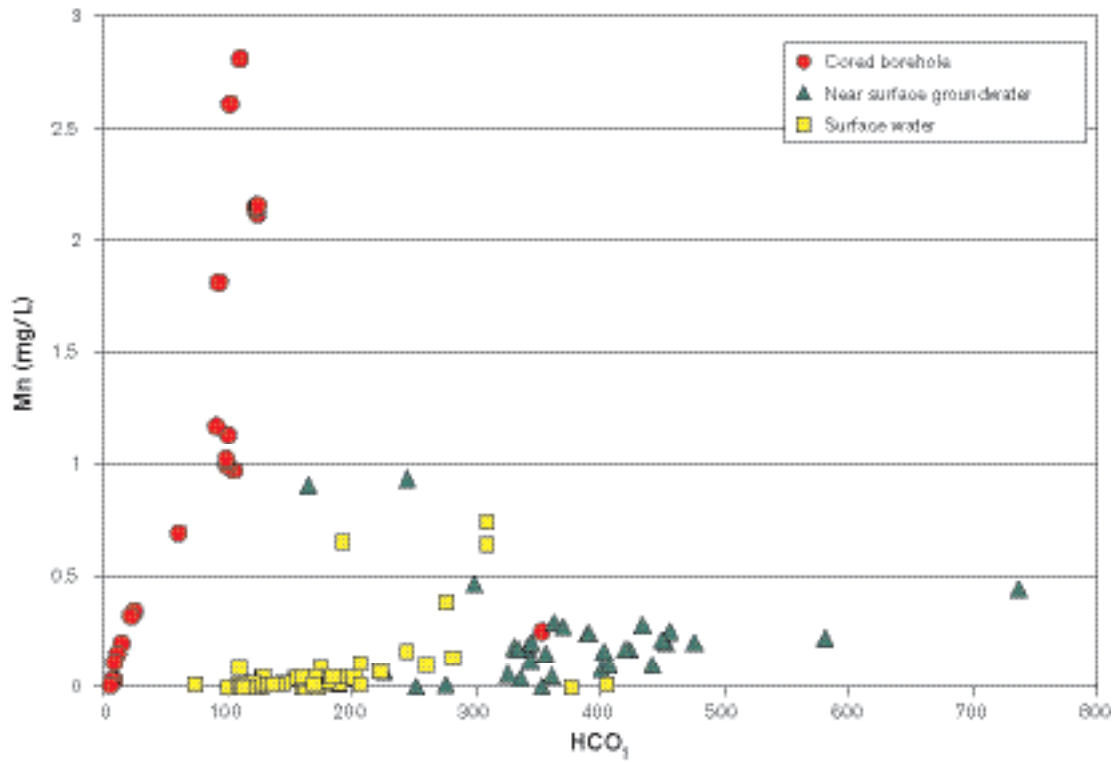


Figure 9-17. Mn versus HCO_3^- in surface waters, near-surface groundwaters and groundwaters from cored boreholes in the Forsmark area.

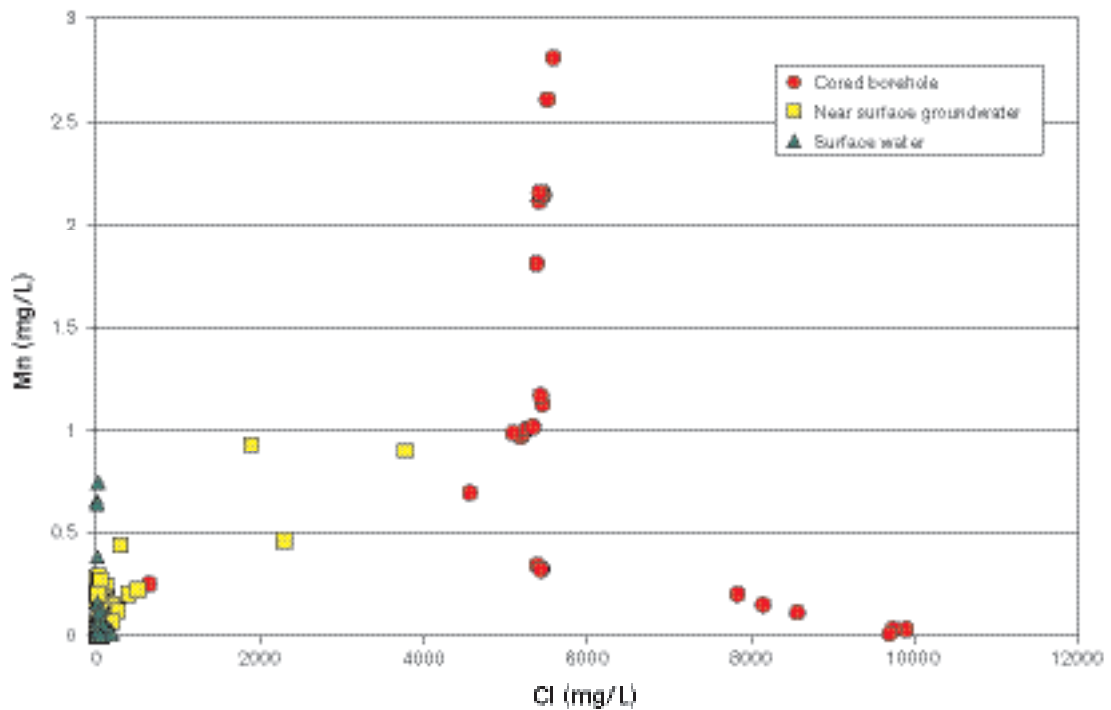


Figure 9-18. Mn versus Cl in surface waters, near-surface groundwaters and deeper groundwaters from cored boreholes in the Forsmark area.

Uranium

Uranium contents have been analysed in surface waters (Lake and Stream waters), in near-surface groundwaters from Soil Pipes and in groundwaters from the percussion and cored boreholes. The surface and near-surface waters are characterised by values between 0.05 and 28 µg/L (Figure 9-19). Large variations in uranium content in surface waters are common and are usually ascribed to various redox states (oxidation will facilitate mobilisation of uranium) and various contents of complexing agents, normally bicarbonate (which will keep the uranium mobile). The plot of uranium versus bicarbonate for the waters (Figure 9-20) shows no clear trend although there is a tendency for higher uranium contents in the surface and near-surface groundwaters associated with increasing bicarbonate up to 400 mg/L. For the few near-surface waters with higher bicarbonate contents the uranium content tends to be lower, which may be due to very low redox potentials in these waters caused by the microbial reactions producing the bicarbonate (probably to large extent sulphate reducers).

Lower uranium content with depth is expected due to decreasing redox potential and decreasing HCO₃. The groundwaters sampled in the cored boreholes, in contrast, show no such depth trend. Instead, most of the groundwaters show high values (> 30 µg/L) at depths between 200 m and 600 m (Figure 9-19). Groundwaters with the highest uranium content have bicarbonate contents around 100–125 mg/L with the exception of three samples which all originate from borehole section 639–646 m in KFM03A. This borehole section indicates a mixed groundwater origin (marine and deep saline; cf. discussion in Appendix 1 in /SKB, 2005b/).

Uranium versus chloride (Figure 9-21), shows that the highest uranium contents are found in the waters with chloride values around 5,000–5,500 mg/L, i.e. the brackish groundwaters dominated by a Littorina Sea water component.

Uranium isotope measurements have been carried out in a number of groundwater samples from Forsmark, but the reported values are questionable. To resolve this issue an interlaboratory study of reference samples has been initiated and no uranium isotope data are evaluated in this Forsmark version 1.2 reporting stage. However, a few measurements carried out at Glasgow University indicate that the uranium ²³⁴U/²³⁸U activity ratios are within the range of 2 to 4, which conforms with groundwaters from other sites.

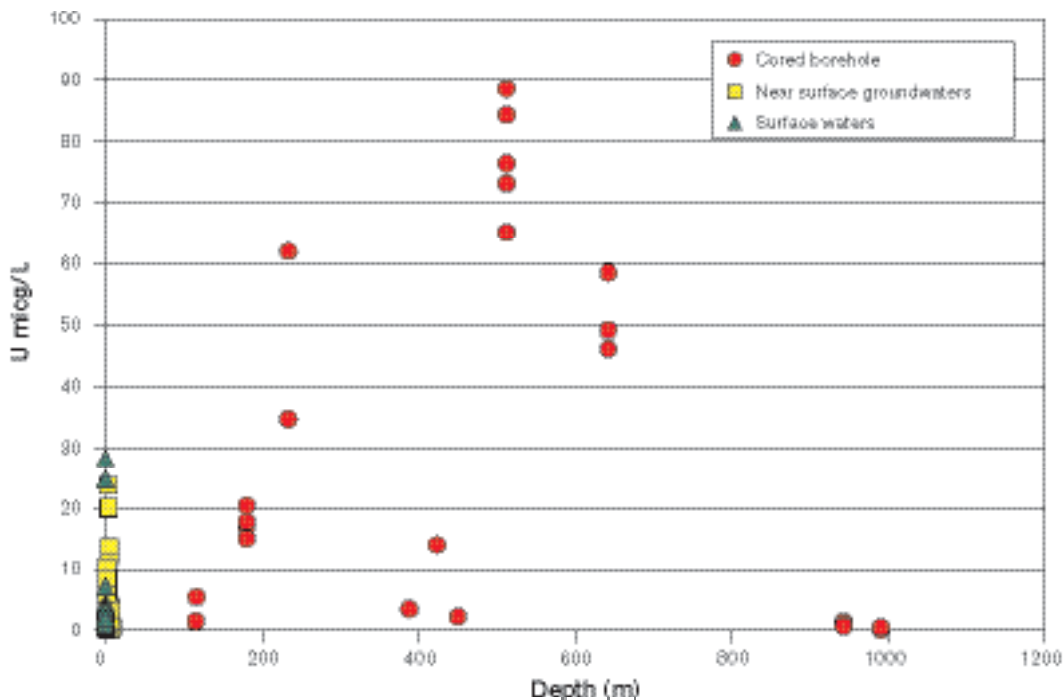


Figure 9-19. Uranium content (µg/L) in surface and groundwaters from the Forsmark area.

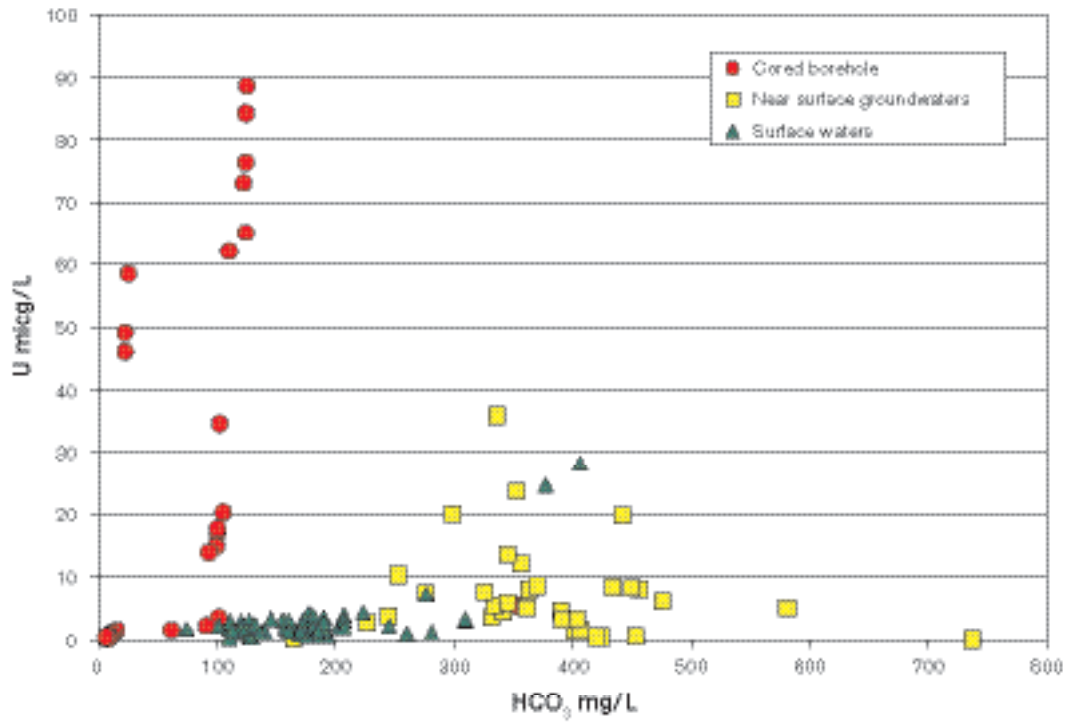


Figure 9-20. Uranium ($\mu\text{g/L}$) versus HCO_3 (mg/L) in surface and groundwaters from the Forsmark area.

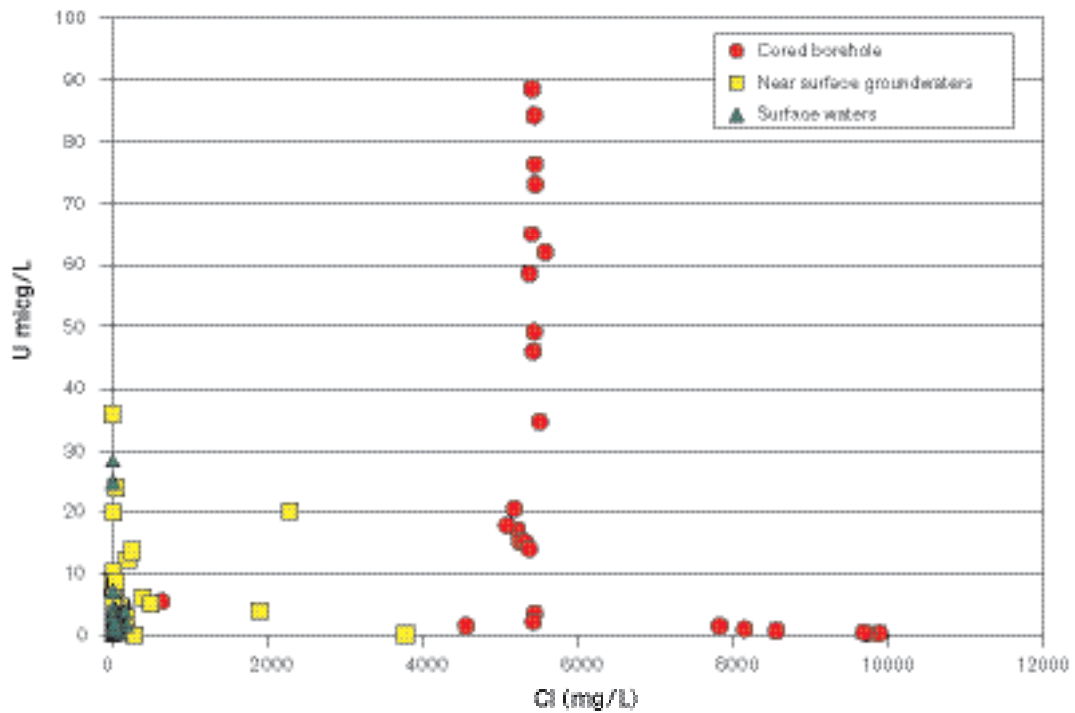


Figure 9-21. Uranium ($\mu\text{g/L}$) versus Cl (mg/L) in surface and groundwaters from the Forsmark area.

Carbon isotopes

The stable carbon isotope ratios, expressed as $\delta^{13}\text{C}\text{‰ PDB}$, radiocarbon contents (^{14}C) expressed as pmC (percentage modern carbon), and HCO_3^- , have been analysed from surface waters and groundwaters (cf. Figure 9-22 and Figure 9-23). The tritium versus ^{14}C for surface waters has been discussed already.

Baltic Sea waters have ^{14}C values around 110 pmC and $\delta^{13}\text{C}$ values mostly between -2 and -7‰ produced by equilibration with atmospheric CO_2 . The lake and stream waters show increasing input of biogenic carbon seen as increased HCO_3^- contents, decreased $\delta^{13}\text{C}$ values and, somewhat surprisingly, a small increase in ^{14}C (110–120 pmC are measured in many of the lake and stream waters). The stable carbon isotopes indicate exchange with biogenic CO_2 and it is therefore reasonable to assume that breakdown of ^{14}C -enriched organic material has contributed to the somewhat higher values. Several reasons for the ^{14}C enrichments in the organic material at Forsmark are possible, but the main candidate is uptake of radioactive CO_2 emitted into the atmosphere by the nearby nuclear power plant (cf. /Eriksson, 2004/). Part of this radioactive CO_2 is incorporated in plants (due to photosynthesis), and successive microbial breakdown of this material will contribute ^{14}C -rich CO_2 to the lake and stream waters.

The highest HCO_3^- values are produced in the near-surface groundwaters and in some of the percussion boreholes (cf. Figure 9-23). HCO_3^- contents between 300 and 500 mg/L are common in these waters and the $\delta^{13}\text{C}$ values are generally between -10 to -17‰ indicating a dominantly biogenic carbon source. However, the ^{14}C contents in these waters are lower, ranging from 80–100 pmC for most surface waters and 60–80 pmC for the high bicarbonate waters sampled in the percussion boreholes. Also, a few shallow samples from the cored boreholes are included in this group. Most of the high bicarbonate waters have detectable tritium values (cf. Figure 9-24) and ^{14}C decay effects are therefore regarded as insignificant. Instead, breakdown of older organic material or contribution of dissolved carbonate minerals (with no ^{14}C) is suggested.

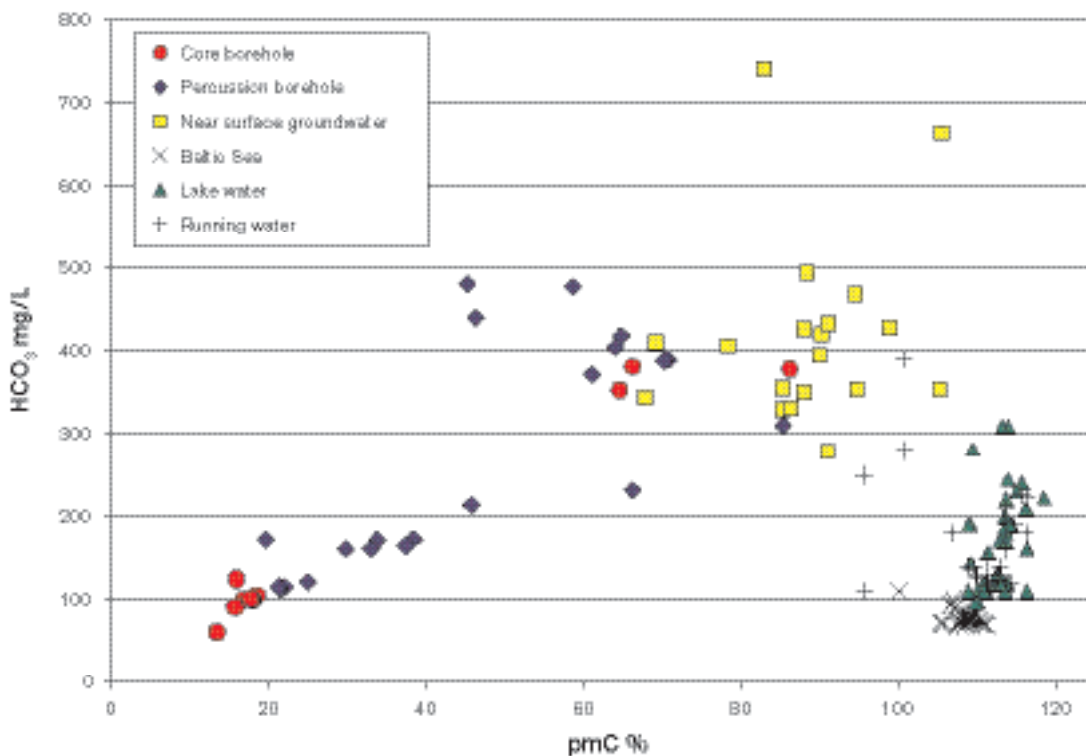


Figure 9-22. pmC (HCO_3^-) versus HCO_3^- in surface and groundwaters from the Forsmark area.

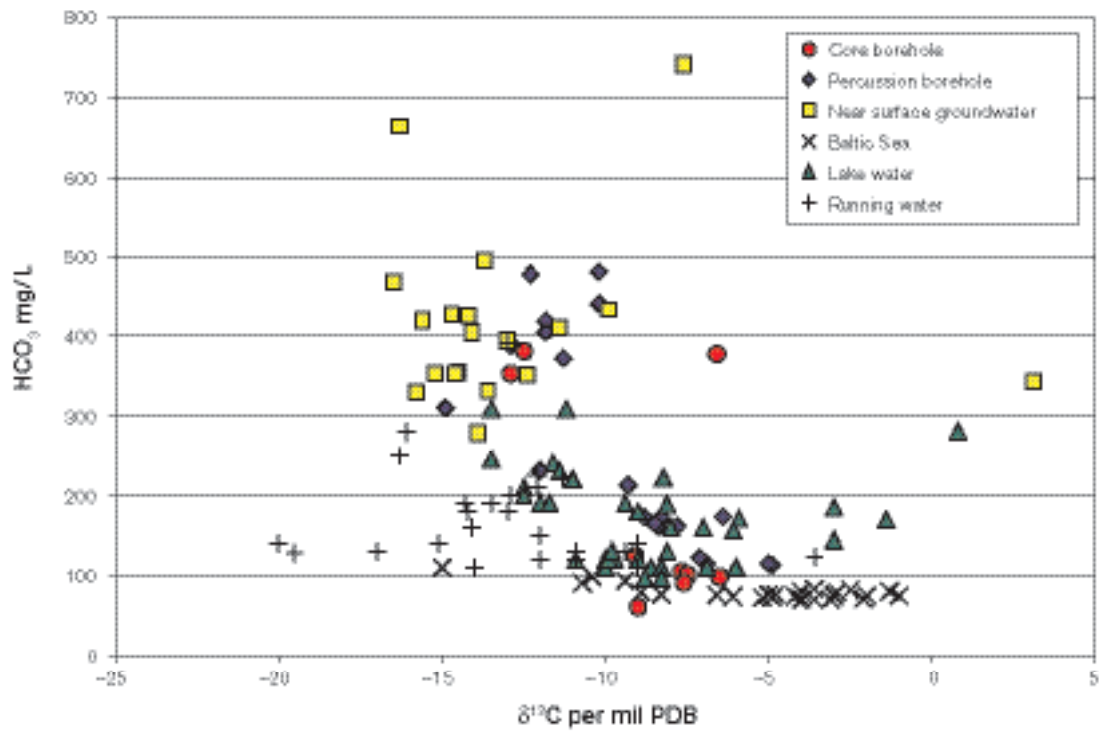


Figure 9-23. $\delta^{13}\text{C}$ (HCO₃) versus HCO₃ in surface and groundwaters from the Forsmark area.

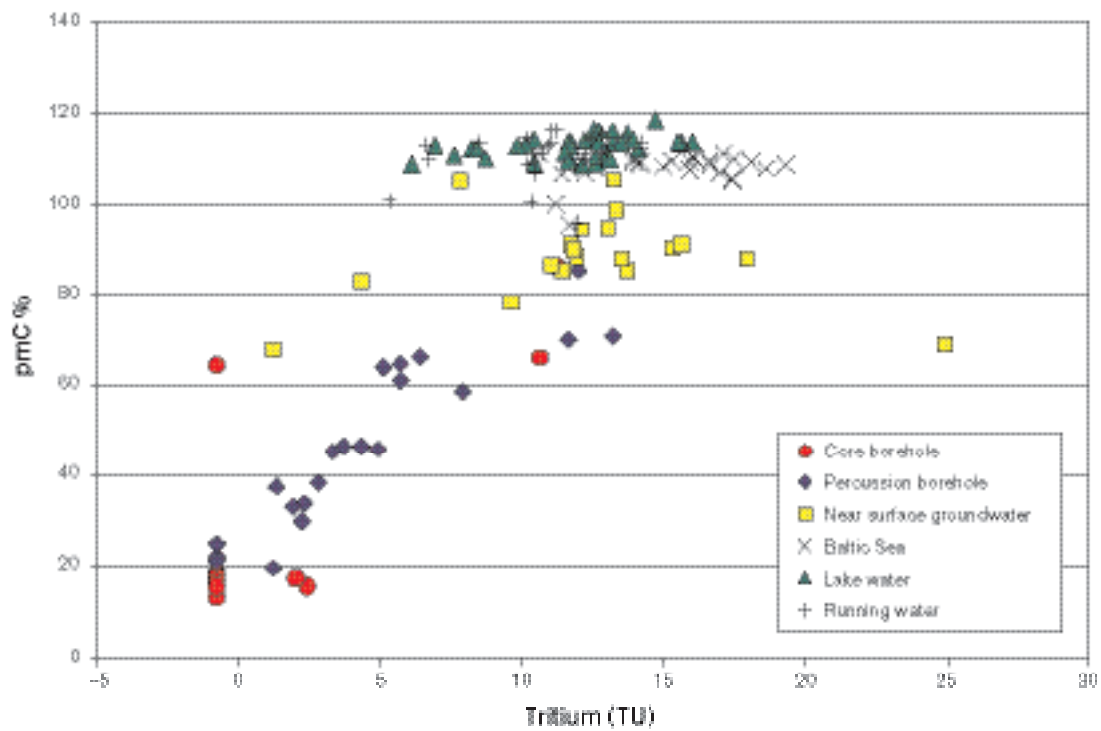


Figure 9-24. pmC (HCO₃) versus tritium in surface and groundwaters from the Forsmark area.

The tritium-free groundwaters from Forsmark show ^{14}C values in the range 14–25 pmC and these waters have generally low HCO_3 contents ($< 150 \text{ mg/L}$) and $\delta^{13}\text{C}$ values between -10 and -5‰ . Figure 9-25 for ^{14}C (expressed as pmC) versus $\delta^{13}\text{C}\text{‰}$, shows that groundwaters from the percussion and cored boreholes indicate a mixing trend between: a) HCO_3 -rich waters with low $\delta^{13}\text{C}$ and high ^{14}C content, and b) deeper groundwaters with lower HCO_3 contents, higher $\delta^{13}\text{C}$ values and lower ^{14}C . To date there are no groundwaters analysed from below depths of 550 m.

The groundwaters showing the lowest ^{14}C values have chloride contents ranging from 4,500–5,500 mg/L (Figure 9-26); these indicate marine signatures, i.e. they represent waters with a dominant Littorina Sea component. In terms of ‘relative age’, the measured pmC values indicate 11,000–16,000 years which is significantly older than the Littorina Sea period. This can be explained by an addition of older bicarbonate, probably by dissolution of older carbonate and/or mixing by glacial water (supported by low $\delta^{18}\text{O}$ in at least some of these groundwaters).

The plot of ^{14}C content versus depth (Figure 9-27) shows, as expected, a decreasing trend with depth. All groundwaters deeper than 200 m show values below 20 pmC. Together, the distribution of ^{14}C and tritium versus depth supports the occurrence of an upper 100–200 m hydraulically dynamic section and a significantly less dynamic situation at greater depth. This is further supported by the major ion chemistry.

Two organic material samples from KFM01A (110 m and 177 m) have been analysed for ^{14}C resulting in values of 53.20 and 46.4 pmC respectively. These values are much higher than those measured on HCO_3 samples from the same sampled borehole sections, i.e. 13.4 and 16.7 pmC, respectively. Earlier interpretation of these waters as being mainly mixtures of glacial and Littorina Sea water is not contradicted by these results, but indicates also the possibility of a Littorina Sea origin for the organic material and support of a more mixed origin for the bicarbonate.

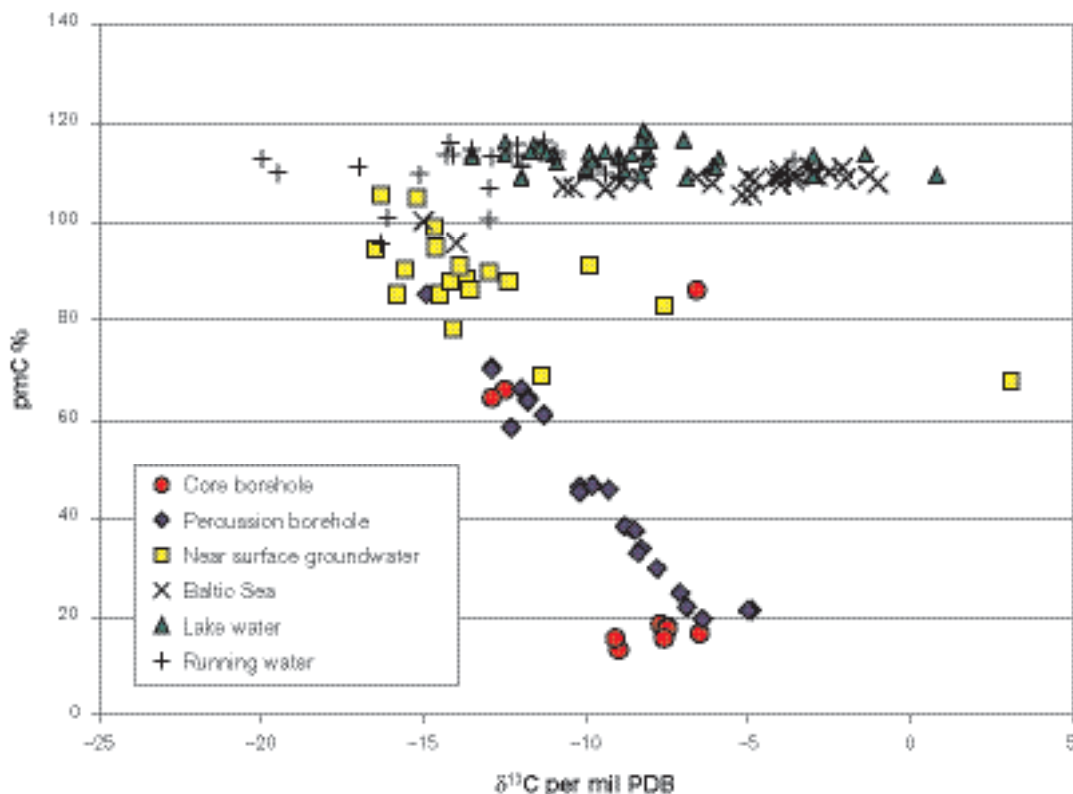


Figure 9-25. $\delta^{13}\text{C}$ versus ^{14}C (pmC) in bicarbonates in surface and groundwaters from the Forsmark area.

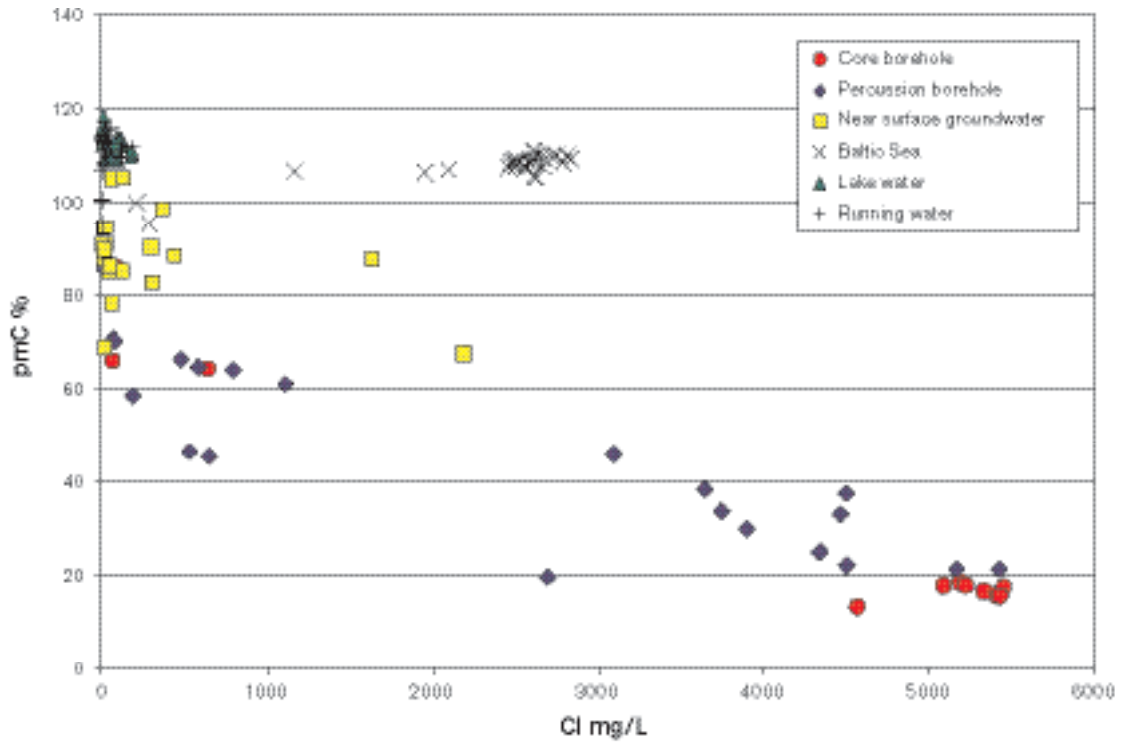


Figure 9-26. $^{14}\text{C}(\text{HCO}_3)$ versus Cl in surface and groundwaters from the Forsmark area.

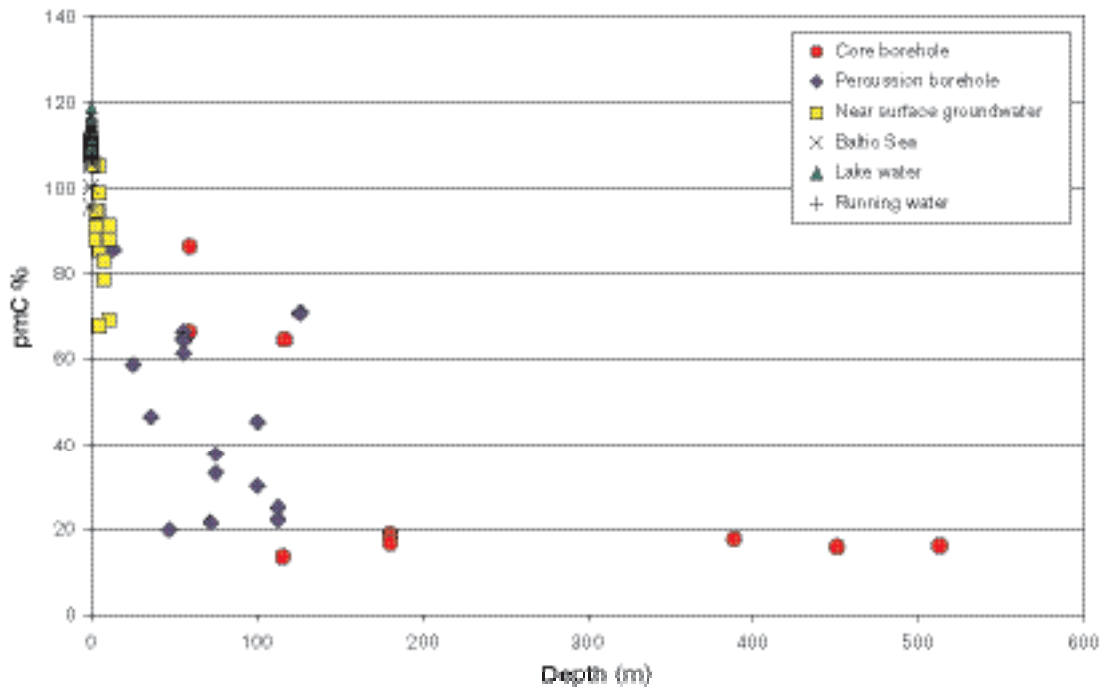


Figure 9-27. $^{14}\text{C}(\text{HCO}_3)$ versus depth in surface and groundwaters from the Forsmark area.

Sulphur isotopes

Sulphur isotope ratios, expressed as $\delta^{34}\text{S}\text{‰ CDT}$, have been measured in dissolved sulphate in groundwaters, surface Lake and Stream waters and Baltic Sea waters from the Forsmark area. Some 73 analyses have been performed of which 33 are groundwaters from cored and percussion boreholes. The isotope results are plotted against SO_4 (Figure 9-28) and Cl (Figure 9-29).

The recorded values (Figure 9-28) vary within a wide range (-11 to $+30\text{‰ CDT}$) indicating different sulphur sources for the dissolved SO_4^{2-} . For the surface waters (lake and stream waters) the SO_4 content is usually below 35 mg/L and the $\delta^{34}\text{S}$ is relatively low but variable (-1 to $+11\text{‰ CDT}$) with most of the samples in the range 2 to 8‰ CDT . These relatively low values indicate atmospheric deposition and oxidation of sulphides in the overburden as being the origin for the SO_4 . Unfortunately there are no isotopic analyses of sulphides in the overburden, but a few (6) $\delta^{34}\text{S}$ values of pyrites in fracture coatings have been analysed and show a large spread in values (5.4 to 31.5‰ CDT ; /Sandström et al. 2004/). The Baltic Sea samples cluster around 20‰ CDT with some less saline Baltic samples showing lower $\delta^{34}\text{S}$ values resulting from inmixing of surface water.

As discussed in Appendix 1 in /SKB, 2005b/, the deeper groundwaters show $\delta^{34}\text{S}$ values in the range $+12$ to $+26\text{‰ CDT}$ where all samples with SO_4 contents greater than 250 mg/L show $\delta^{34}\text{S}$ values higher than $+20\text{‰ CDT}$. Such values are usually interpreted to result from sulphate-reducing bacterial (SRB) activity in the bedrock aquifer. The Cl versus $\delta^{34}\text{S}$ plot (Figure 9-29) shows a clear trend with higher $\delta^{34}\text{S}$ values for groundwaters with higher salinities than present Baltic Sea waters ($2,800\text{ mg/L Cl}$). If the $\delta^{34}\text{S}$ values in the marine groundwaters are modified by SRB during closed conditions then a clear trend of more positive $\delta^{34}\text{S}$ values with decreasing sulphate content should be the result. This is not seen and therefore several processes need to be considered. The groundwater with the highest salinity showed a relatively low sulphate content (64 mg/L) and a $\delta^{34}\text{S}$ value of $+23\text{‰ CDT}$. However, this was a tube sample (not plotted) and is probably the product of mixing. The only identified sulphate minerals so far are minute grains of barite found in a few fracture coatings /Sandström et al. 2004/.

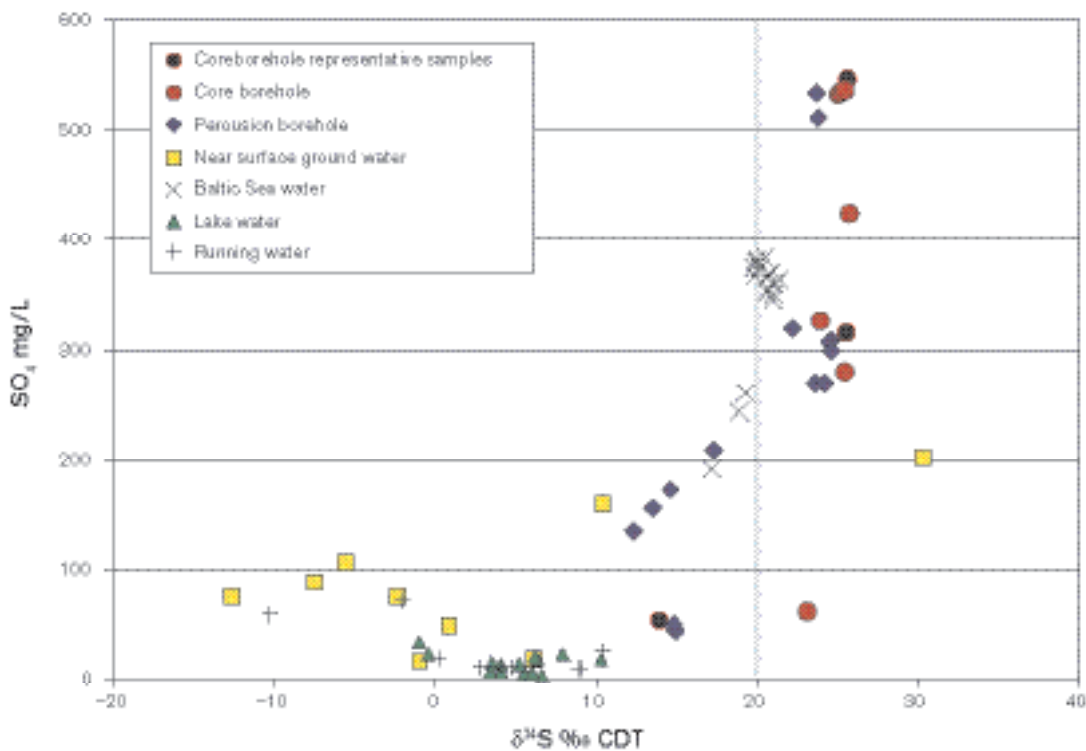


Figure 9-28. Plot of $\delta^{34}\text{S}$ (‰ CDT) versus SO_4^{2-} content for groundwaters and surface waters from the Forsmark area. The grey line indicates the marine median value at around 20‰ CDT .

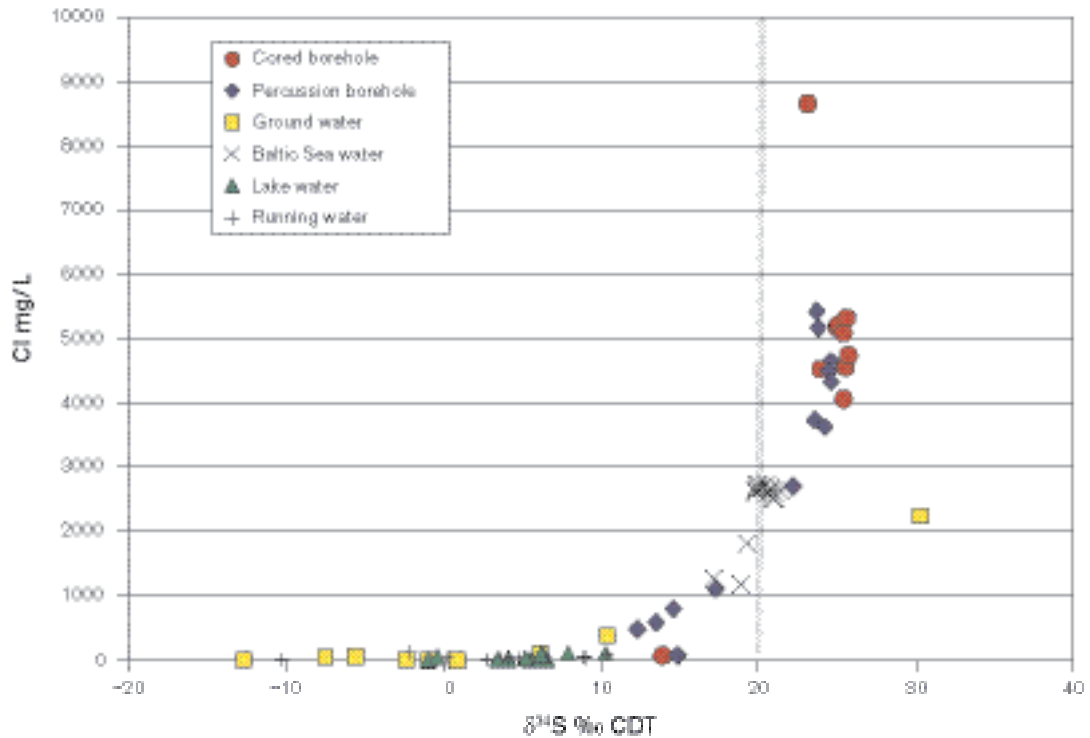


Figure 9-29. Plot of $\delta^{34}\text{S}$ (‰ CDT) versus Cl in surface waters and groundwaters from the Forsmark area. The grey line indicates the marine value at around 20‰ CDT.

Amongst the Soil Pipe near-surface groundwaters, one more brackish sample (2,200 mg/L Cl) showed a relatively high $\delta^{34}\text{S}$ value (+30‰ CDT). This originates from Bolundsfjärden (sample 0012) which is believed to have a typical discharge character. Other near-surface groundwater samples showed values similar in range, or even lower, than surface waters. The cause of these very low values is not fully understood at the moment.

Strontium isotopes

Strontium isotope ratios ($^{87}\text{Sr}/^{86}\text{Sr}$) have been measured in surface waters and groundwater samples from the Forsmark area and these are plotted against Sr content in Figure 9-30. The surface waters and especially the near-surface groundwaters show large variations in Sr isotope ratios. Most of the samples show values within the range 0.718 to 0.729 whereas a few near-surface groundwaters have lower values indicating mixing with marine water and a few have significantly higher values indicating local exchange with Rb-rich minerals. The groundwaters sampled in the percussion and cored boreholes show Sr isotope ratios varying within a narrower range (0.717 to 0.721). Some of these higher values relate to the group of four brackish groundwaters of low strontium values (cf. Figure 9-30) associated with Littorina Sea signatures.

A common way to evaluate mixing between different strontium origins is to plot $1/\text{Sr}$ versus $^{87}\text{Sr}/^{86}\text{Sr}$ (Figure 9-31); no significant trends can be observed. It should, however, be pointed out that relatively few deep sections have been analysed so far. The groundwaters sampled from borehole KFM01A (110–121 and 177–184 m) show somewhat higher Sr isotope ratios than the other groundwater samples which probably relates to the mineralogical compositions along the pathways. Since many of the groundwaters have dominant portions of a marine origin (i.e. Littorina Sea component), a marine input could have been expected. However, this is not recognised in the plot.

From the calcium versus strontium diagram for the groundwater samples (Figure 9-32), calcium and strontium correlate and both have been added to the original Na-Cl dominated water so that the original Sr content (~ 2 mg/L, i.e. twice the values measured in present day Baltic Sea) has increased to 6–10 mg/L Sr. Leaching of minerals and ion exchange are the reasons for this.

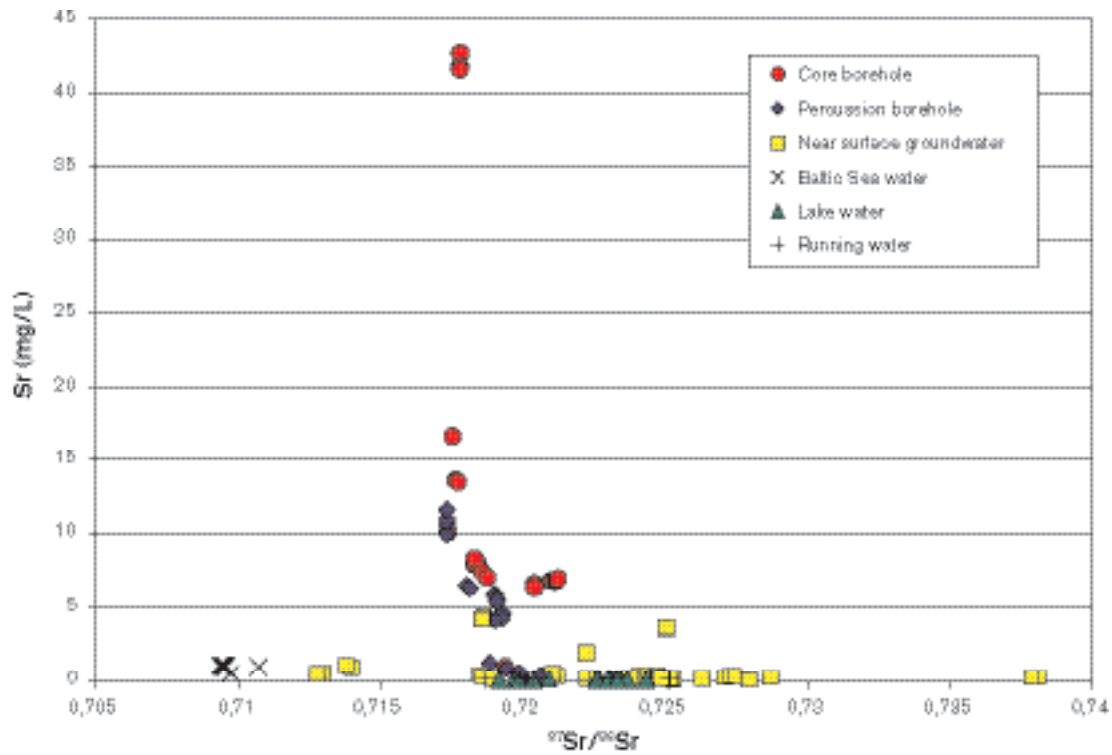


Figure 9-30. Plot of $^{87}\text{Sr}/^{86}\text{Sr}$ ratios versus Sr for Baltic Sea waters, surface waters and groundwater samples from the Forsmark area.

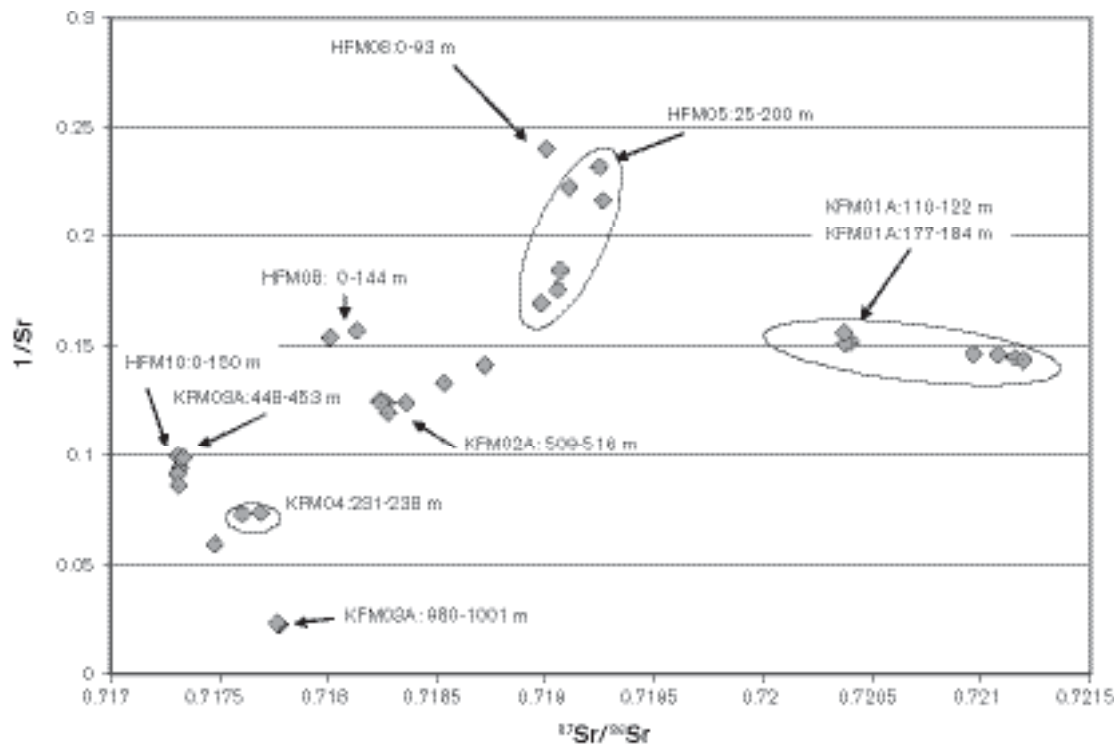


Figure 9-31. $^{87}\text{Sr}/^{86}\text{Sr}$ ratio plotted versus $1/\text{Sr}$ in groundwater samples from the Forsmark area.

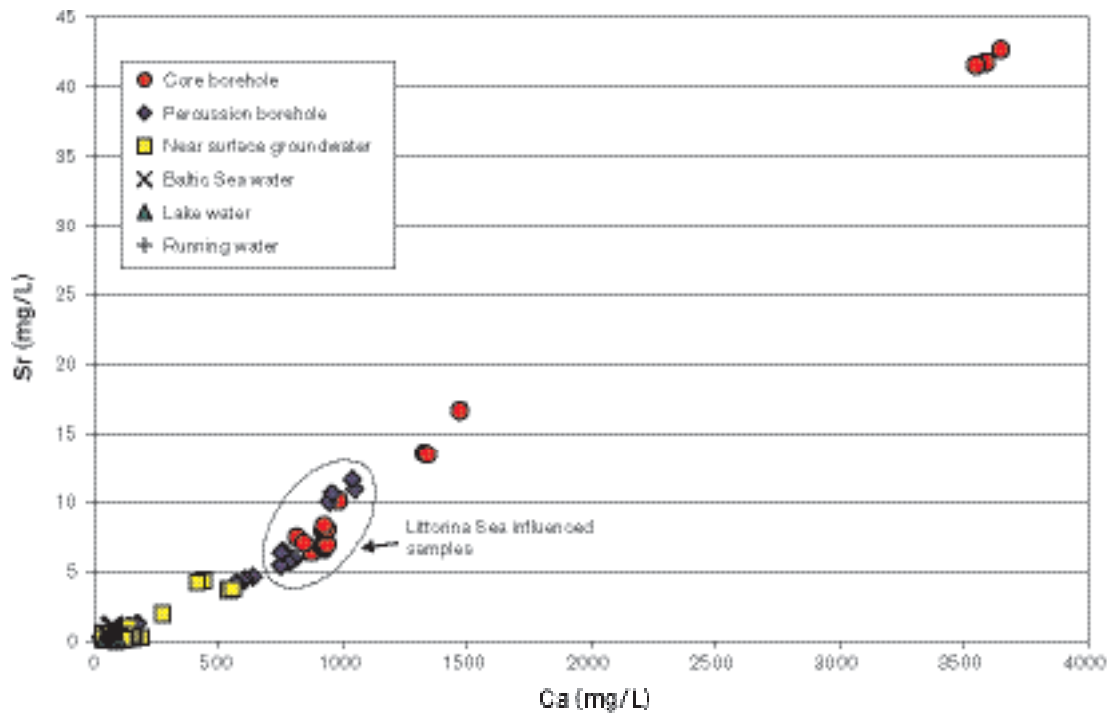


Figure 9-32. Sr versus Ca in surface waters, Baltic sea waters and groundwaters from the Forsmark area.

In conclusion, the strontium isotope values of surface and near-surface waters show relatively large variations in isotope ratios whereas the deeper groundwaters vary within a more limited range. All the isotope values deviate from those measured in the Baltic Sea samples, in that they have higher radiogenic strontium, which in turn is due to water/rock interactions, probably in large part to ion-exchange processes.

The relatively few fracture calcites so far analysed for Sr-isotopes show values below 0.718 supporting that they are not precipitated from today's groundwater and that calcite dissolution has had little influence on the Sr-isotope ratios in the groundwater. Other minerals are more important and analysis of fracture minerals and host rock samples is recommended to achieve a better understanding of the Sr (and Ca) system.

Figure 9-33 compares the Forsmark site with the Simpevarp, Laxemar and Ävrö sites, together with modern Baltic Sea waters. The relatively small variation in Sr-isotope ratios within each area suggests that ion exchange with clay minerals along the flow paths is an important process. For the Laxemar-Simpevarp sites there is a tendency towards higher contents of radiogenic Sr in the groundwaters with highest salinities (and thus highest Sr content). It is not, however, possible from the few data available to give any explanation for this. There seems not to be any major change in mineralogy that can explain a shift, but one possibility may be the increased residence times for these waters leading to more extensive mineral/water interactions. The higher $^{87}\text{Sr}/^{86}\text{Sr}$ ratios in the Forsmark samples are most probably due to differences in the composition of the bedrock and fracture minerals compared with Simpevarp. The possibility of tracing marine components using Sr-isotopes is often discussed; however the influence of clay minerals in the fractures may undermine such interpretations. For example, the strong Littorina Sea imprint in the Forsmark waters has not resulted in any detectable marine Sr isotope values in the groundwaters. Instead, modification of the Sr isotope values probably by ion exchange has taken place.

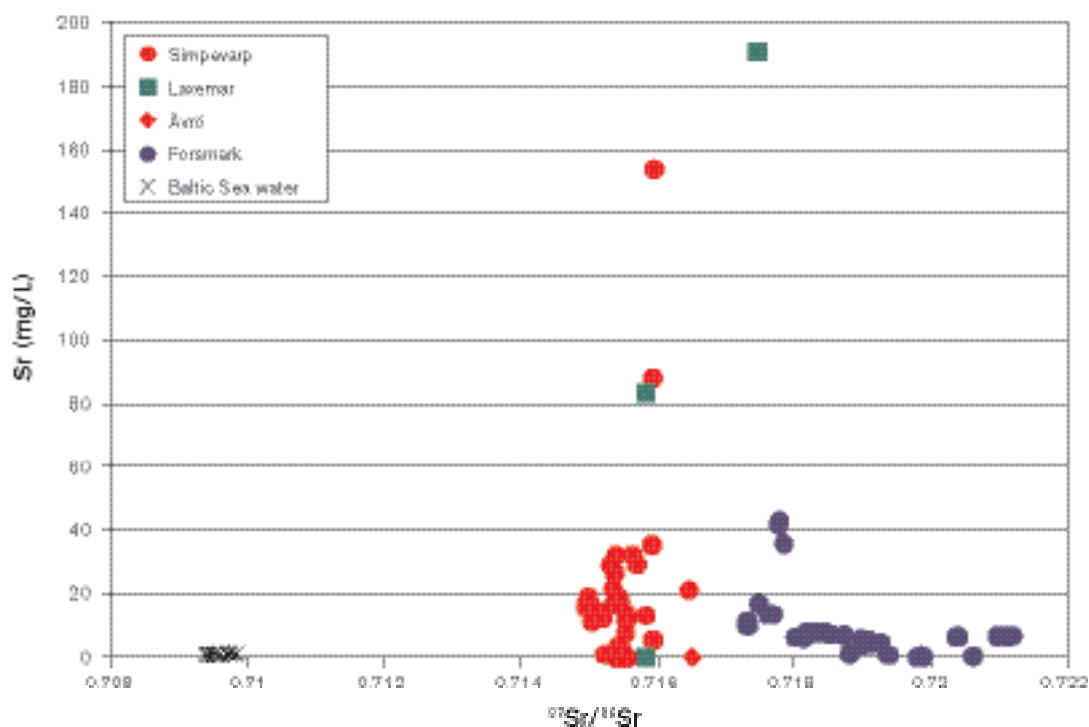


Figure 9-33. $^{87}\text{Sr}/^{86}\text{Sr}$ versus Sr for groundwaters from Forsmark, Simpevarp, Laxemar and Ävrö. Baltic Sea waters sampled from the Forsmark and Laxemar/Simpevarp sites are also plotted.

Chlorine isotopes

Stable chlorine isotopes have been analysed in waters from the Forsmark area and the results are plotted against chloride in Figure 9-34. This shows that most of the surface and Baltic Sea waters have values within the range -0.28 to $+0.34\text{‰}$ SMOC. The surface waters and the near-surface groundwaters have the greatest spread (-0.6 to $+2\text{‰}$ SMOC) where most of the samples are within the interval -0.2 to $+0.5\text{‰}$ SMOC. The majority of the Baltic Sea samples values are close to 0‰ SMOC or slightly higher (up to $+0.3\text{‰}$ SMOC), a few samples show also lower values down to -0.6‰ SMOC.

Waters from the cored and percussion boreholes are between -0.2 to $+0.6\text{‰}$ SMOC and demonstrate no relation with increasing chloride content. Given the analytical uncertainty of around $\pm 2\text{‰}$ SMOC /Frape et al. 1996/, the groundwater values correspond to a slight emphasis on a water/rock origin.

The $\delta^{37}\text{Cl}$ values in groundwaters from Forsmark and Laxemar/Simpevarp have been compared with chloride (Figure 9-35) together with additional Baltic Sea samples from the Simpevarp area. For brackish groundwaters with chloride contents around $5,000$ mg/L there is a large variation in $\delta^{37}\text{Cl}$ values; most of the Forsmark samples have slightly negative values whereas the Simpevarp samples have values on the positive side. In groundwaters with higher chloride contents ($> 6,000$ mg/L) the Simpevarp and Laxemar samples have values higher than 0.3‰ SMOC. The Forsmark sample (only one available so far) shows 0.09‰ SMOC.

Br/Cl versus $\delta^{37}\text{Cl}$ (Figure 9-36) shows that waters significantly enriched in bromide compared with marine waters display positive $\delta^{37}\text{Cl}$ values. The groundwaters at Forsmark, characterised by marine Br/Cl ratios, also cluster around 0‰ SMOC, although a similar spread is also shown by the Baltic Sea samples.

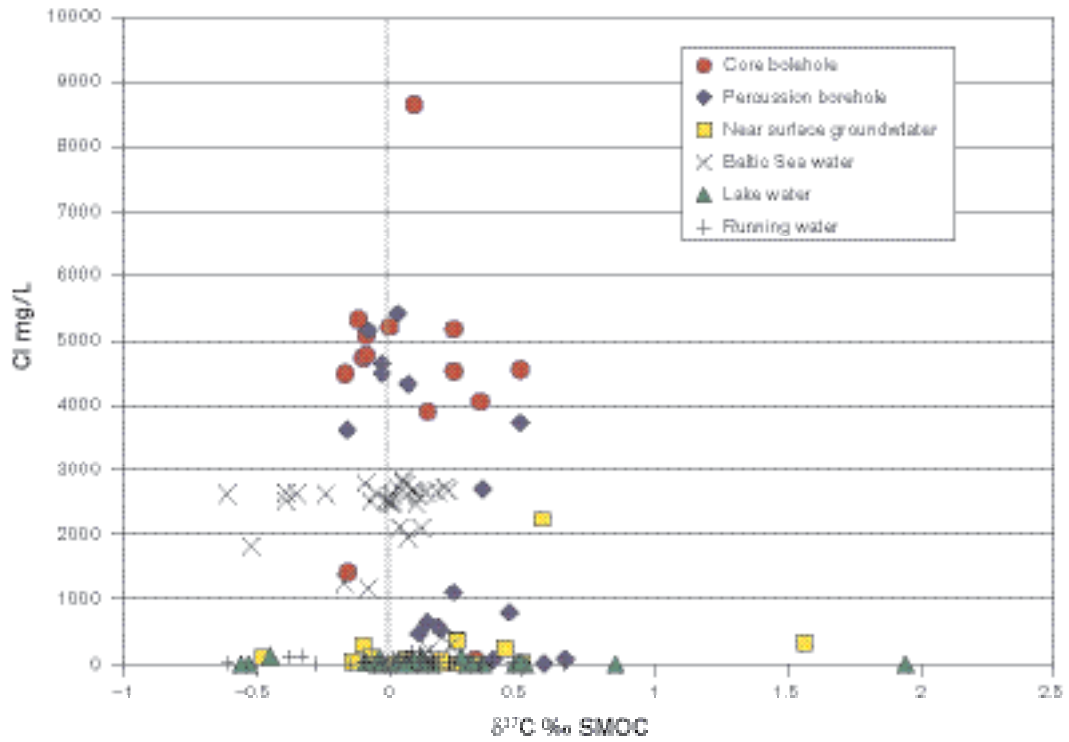


Figure 9-34. $\delta^{37}\text{Cl}$ (expressed as per mille deviation from the standard SMOC) versus Cl in surface waters, groundwaters and Baltic Sea waters from Forsmark.

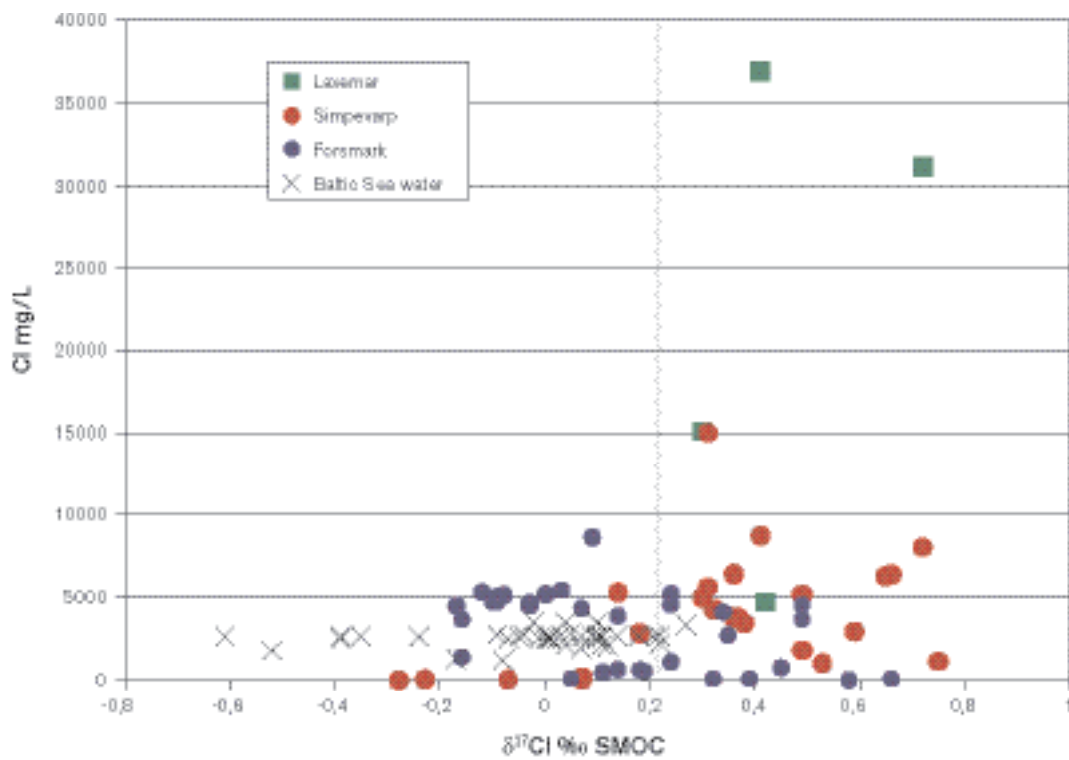


Figure 9-35. $\delta^{37}\text{Cl}$ versus Cl in groundwaters from Forsmark and Laxemar/Simpevarp and Baltic Sea waters from Simpevarp and Forsmark.

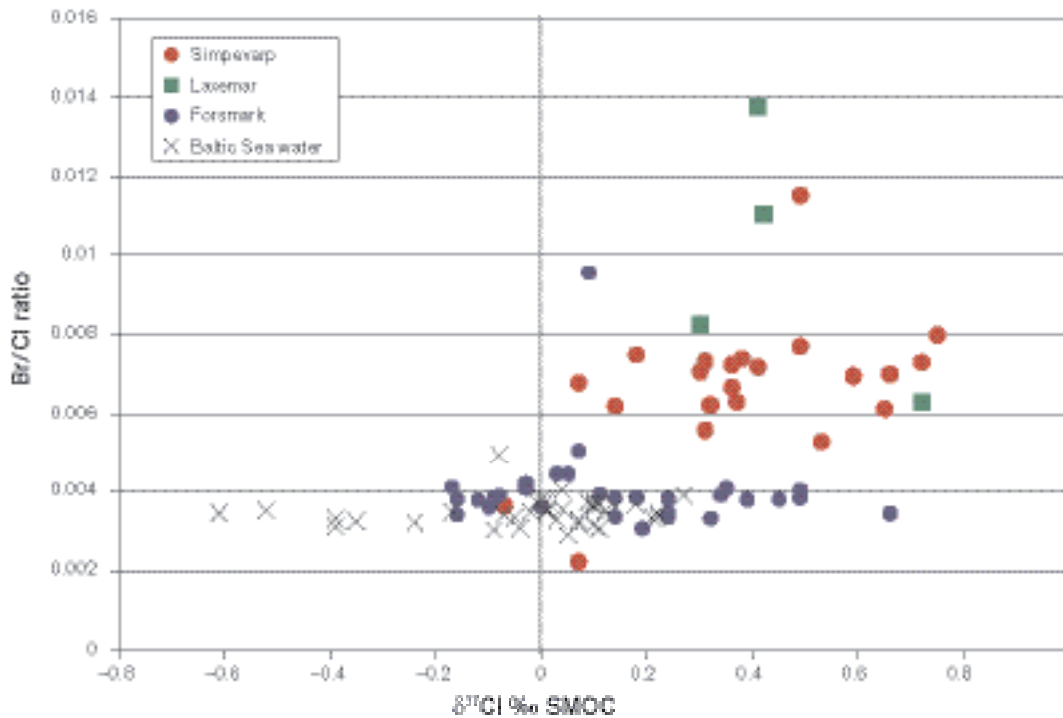


Figure 9-36. $\delta^{37}\text{Cl}$ versus Br/Cl in groundwaters from Forsmark and Laxemar/Simpevarp and Baltic Sea waters from Simpevarp and Forsmark.

Trace elements

Only a few data exist for the majority of groundwaters and even some of these are incomplete (cf. Appendix 1 in /SKB, 2005b/). The following was concluded from the evaluation.

Li, Rb and Cs (and to a lesser extent Y) from the cored and percussion boreholes show a sharp increase from low values (shallow surface to near-surface waters) to high values at approx. 100 m depth. This is followed by a levelling off (i.e. in the brackish groundwaters) until around 500 m when a decrease to moderate values occurs. Strontium, although reflecting a similar trend for the upper 500 m, increases significantly towards depth.

La and Ce from the cored and percussion boreholes are close to the detection limit, apart from approximately 400–500 m depth where a significant peak can be observed.

Shallow groundwaters from the Soil Pipes show a wide range of values for Ce, La and Y.

Calcites

In order to sort out different calcite generations and to provide palaeohydrogeological information, 54 samples have been analysed for $\delta^{13}\text{C}/\delta^{18}\text{O}$, of which 16 were selected for $^{87}\text{Sr}/^{86}\text{Sr}$ and a smaller set (7 samples) analysed for chemical composition. The calcites represent examples from both sealed and open fractures. In some of the latter, it has been possible to sample calcites formed in open spaces and showing euhedral crystal forms. When possible, observations have been noted on crystal morphology, since a correlation has been demonstrated between calcite morphology (long and short C-axis) and groundwater salinity. Most of the Forsmark calcites (from depths of 0–500 m) show short C-axis and equant crystal forms, indicating fresh or brackish water precipitates.

A sequence of at least three different calcite generations, which can be correlated to the fracture mineralogical subdivision, has been documented. These are described below.

Hydrothermal calcites with mostly low $\delta^{18}\text{O}$ -values (down to -18‰) and high $\delta^{13}\text{C}$ (-5 to -2‰). These calcites are found together with prehnite and laumontite and thereby support a close relationship between these two generations (Generation 2 and 3). Support that these two generations form

part of the same prolonged event is indicated by the tailing in $\delta^{18}\text{O}$ from -18 to at least -14% . This may be due to precipitation from a hydrothermal fluid during decreasing temperatures and/or changes in water-rock ratio during a hydrothermal event. The connection between the calcite in the prehnite and laumontite generations is in accordance with earlier observations from Finnsjön.

Calcites with extremely low $\delta^{13}\text{C}$ values (down to -36%) and $\delta^{18}\text{O}$ values of around -12% . These are found together with quartz fracture coatings (Generation 4). These mineralisations must have been precipitated during lower temperatures than the preceding laumontite formation, although it is reasonable to assume that it was still hydrothermal ($< 200^\circ\text{C}$ is suggested). The very low $\delta^{13}\text{C}$ values are usually interpreted as due to in-situ microbial activity which implies that the temperature was not significantly above 100°C when the carbon isotope signature was modified. However, the temperature evolution during this period of fracture mineralisation is not yet known. Based on Sr-isotope values this period is clearly separated from the prehnite-laumontite formation, either in time (the radiogenic ^{87}Sr is much higher in the latter generation), or the chemistry of the hydrothermal fluid was significantly different and preferred dissolution of K-Rb minerals occurred.

Euhedral calcites formed possibly as the latest phase on the quartz adularia coatings; usually found together with pyrite (Generation 5). $\delta^{18}\text{O}$ values range from -11 to -10% and the $\delta^{13}\text{C}$ -values are in the range of -18 to -20% .

It has not yet been possible to relate several calcite precipitates to any specific fracture mineralisation event. For example, a group of calcites from borehole KFM02A (110–118 m) shows significantly positive $\delta^{13}\text{C}$ values ($+6$ to $+8\%$) and $\delta^{18}\text{O}$ values of -8 to -11% . There is also a cluster of samples that may include relatively late (Quaternary) fresh water precipitates. More analyses are therefore needed in order to better identify this group. For further discussion see Appendix 1 in /SKB, 2005b/.

Microbes

Microbes from the Forsmark site have been evaluated (Appendix 2 in /SKB, 2005b/) and Figure 9-37 shows the distribution of the different microbial groups found at the six levels sampled in Forsmark and the measured intervals of redox potentials. The redox potentials varied from -140 to -250 mVd, but there is no obvious connection between these values and depth within the dataset.

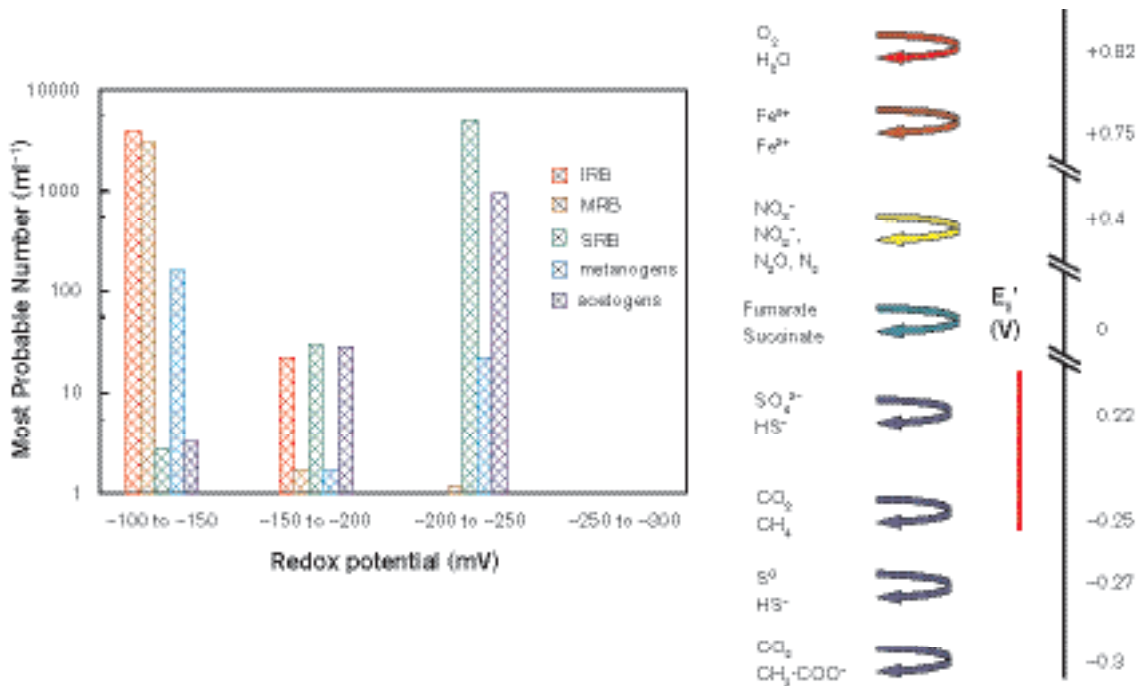


Figure 9-37. The sums of the most probable number (MPN) of microorganisms versus intervals of redox values in borehole groundwaters from the Forsmark area.

To the right in Figure 9-37 is a so-called redox ladder with different microbial respiration redox couples placed at their respective E_0' intervals. The vertical red line in this figure marks the redox interval measured at Forsmark. These redox values coincide with the positions where iron-, manganese- and sulphate-reducers, together with methanogens and acetogens, can be found. They correlate very well with the most probable number (MPN) results for this area.

Figure 9-38 shows also the MPN numbers but in relation to depth. Here it can be seen that iron- and manganese reducers only are present at shallow depth, above 300 m. These groups are absent at greater depth where methanogens, acetogens and SRB dominate. However it must be remembered that there are no data of methanogens available from KFM01A, 115.4 and 180.4 m. The overall picture of the distribution with depth is therefore incomplete.

Figure 9-39 shows a schematic representation of the biogeochemical redox variation related to the 6 groundwater sampling levels in boreholes KFM01A, KFM02A and KFM03A. In the shallow levels represented by KFM01A, the iron- and manganese-reducing bacteria dominate and this correlates well with the measured redox values at this depth. Here the sulphate-reducing bacteria (SRB) were absent.

Sulphate-reducing bacteria, on the other hand dominate at the deepest levels, represented by KFM03A, together with acetogens. These two groups could have established a relation where SRBs utilise acetic acid produced by the acetogens. The same kind of relationship has been suggested by /Pitkänen et al. 2004a/ to exist in deep groundwaters at Olkiluoto but for methanogens and SRB. That sulphate-reducing bacteria can oxidise methane anaerobically with sulphate as electron acceptor has still to be proved, but environmental studies suggest that this microbial reaction does exist.

At intermediate levels (i.e. KFM02A, 512.5 m and KFM03A, 642.5 m) the microbial populations seem to be more diverse and not dominated by any special group or groups. If the flow in these sections is low and no mixing of groundwater occurs, the beneficial electrochemical gradients will not have been established and therefore the activity of certain microbial groups will be less.

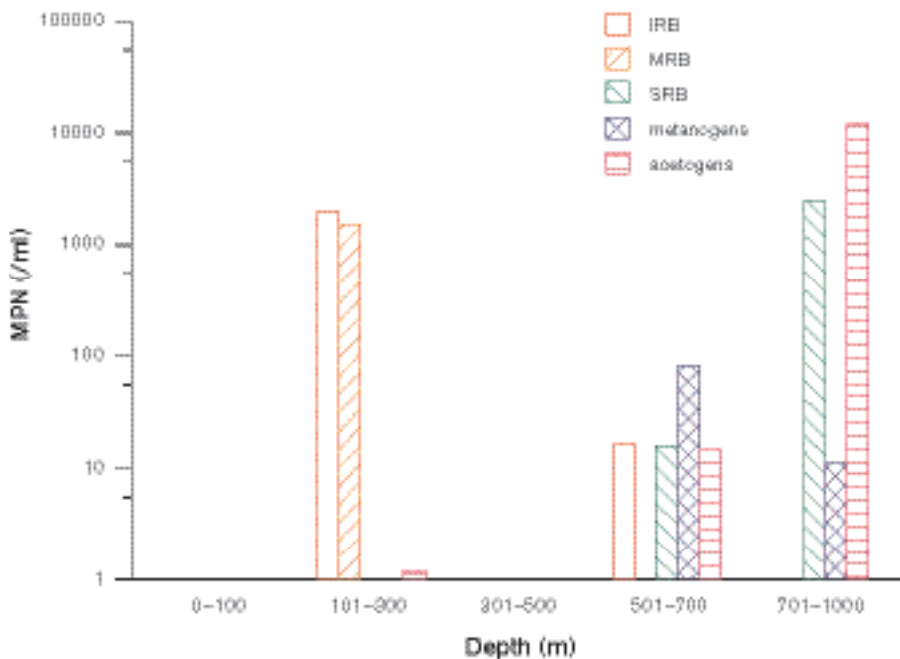


Figure 9-38. The sums of the most probable number (MPN) of microorganisms versus depth interval in borehole groundwaters from the Forsmark area.

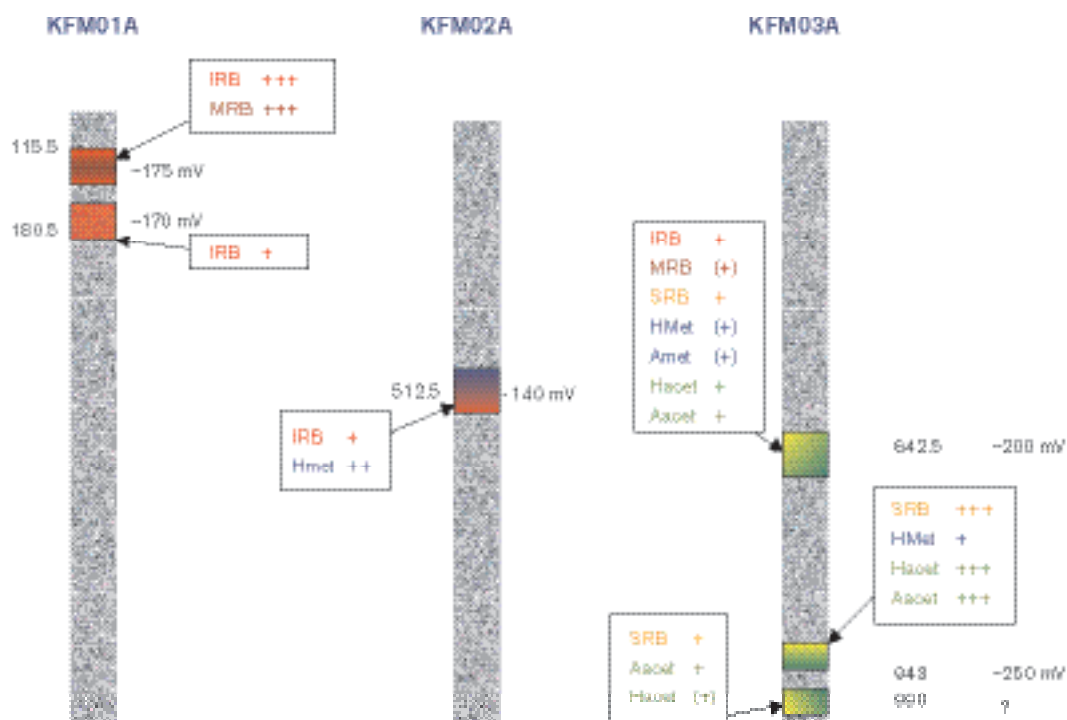


Figure 9-39. Schematic representation of the biogeochemical redox variation related to the 6 groundwater sampling levels from three boreholes in the Forsmark area.

Colloids

Colloid compositional data have been evaluated from the Forsmark site (Appendix 2 in /SKB, 2005b/). Figure 9-40 shows the composition of the colloids sampled from different depths in the three boreholes; sulphur is shown also. No data from KFM02A are shown because of broken filters. In Figure 9-41, the sulphur values have been omitted and in both figures the calcite is omitted since it is considered as an artefact due to pressure changes during sampling.

In Figure 9-40 and Figure 9-41 it can be seen that manganese oxides are very rare in all of the three boreholes; small amounts were found in KFM03A only. Significant iron oxides were found in KFM01A and aluminium, here represented as K-Mg-Illite, was present at all sampling depths although this may also be an artefact from borehole drilling. The amount of calcium is not high in any of the samples.

The filtration data available seems to agree with the numbers of colloids earlier reported from Äspö and Bangombé in Gabon /Laaksoharju et al. 1995b; Pedersen, 1996/. The new sampling and filtering methods seem to have worked well since the amounts of calcium carbonates were very low. This suggests a rethinking of the interpretation of the sulphur colloids since they might have initially existed as colloids present in the groundwater and then probably as iron sulphides. The silicon values from KFM01A, 115.4 m most likely represent sampling artefacts.

The fractionation data show that there should not be any colloids in the size range $> 1,000$ D but $< 5,000$ D. Although this is in contradiction to the filtration results, it could be closer to the truth. There are no sulphur values reported from this method; it would be interesting to carry out a comparison with the filtration method since the presence of iron sulphides could be one explanation for the low sulphide values found in groundwater, even where SRBs are thought to be present (cf. Appendix 2 in /SKB, 2005b/).

Data for the numbers of particles could increase the value of colloid analyses by making it possible to calculate the number of binding sites for radionuclides in the different colloid fractions.

The two methods, filtration and fractionation, needs to be further evaluated (cf. Appendix 2 in /SKB, 2005b/).

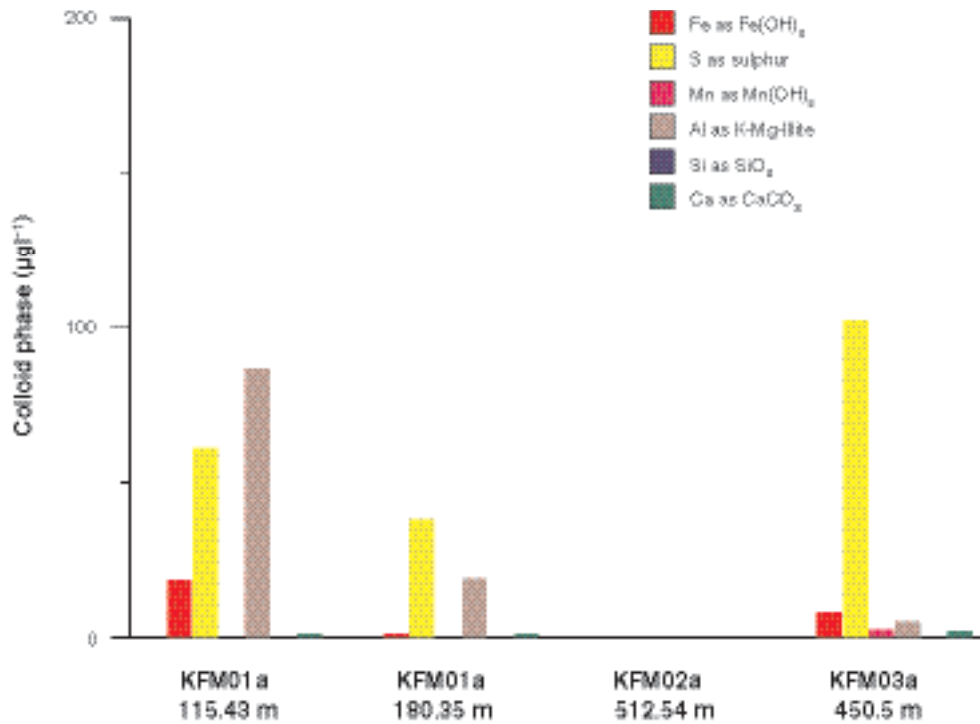


Figure 9-40. Composition of colloids sampled from boreholes KFM01A, KFM02A and KFM03A in the Forsmark area. Calcite is omitted in this figure and also the values of silica in borehole KFM01A, 115.4 m.

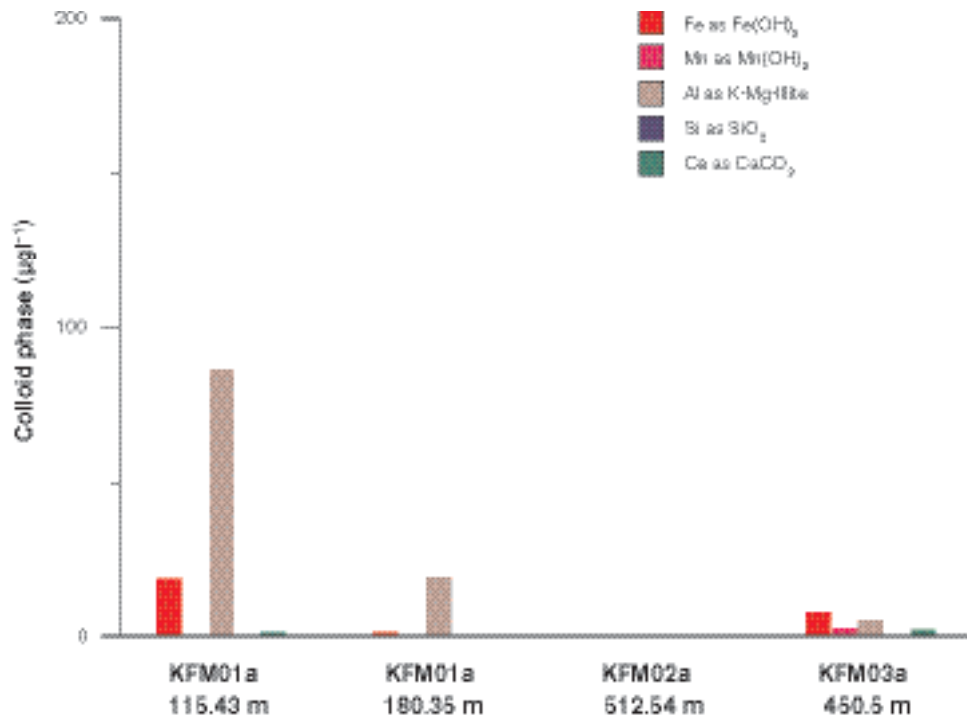


Figure 9-41. The composition of colloids sampled from boreholes KFM01A, KFM02A and KFM03A in the Forsmark area. Calcite sulphur values are omitted and also the values of silica in borehole KFM01A, 115.4 m.

Gas

The gas contents were analysed in groundwaters sampled from 5 depths in boreholes KFM01A, KFM02A and KFM03A (Appendix 2 in /SKB, 2005b/). Up to 12 gases were analysed: helium, argon, nitrogen, carbon dioxide, methane, carbon monoxide, oxygen, hydrogen, ethylene, ethene, ethane and propane. Figure 9-42 shows the total volume of gas for all groundwater samples versus depth; a clear linear correlation is indicated. An increasing amount of gas with depth is observed with the greatest volume, 127.5 ml l⁻¹, originating from the deepest level at 990.6 m in KFM03A. In comparison, the shallowest groundwater recorded 57.8 ml l⁻¹ gas.

As an example, Figure 9-43 shows that the amount of nitrogen, the dominant gas in all the groundwaters, increases with depth reflecting the overall total gas distribution. This corresponds to the gas content in groundwaters recorded from Olkiluoto, Finland, which also showed an increasing trend with depth down to 1,100 m /Pitkänen et al. 2004a/. The highest nitrogen concentration measured at Forsmark was 4.7 mM (KFM03A: 990.5 m) and the lowest was 2.4 mM (KFM01A: 180.4 m).

Helium concentrations in the Forsmark area showed similar depth trends to nitrogen, varying between 460 µM and 924 µM, a trend also reflected at Olkiluoto. The origin of nitrogen and helium in the groundwaters is considered to result from crustal degassing of the bedrock; helium can also be produced by radioactive decay in the bedrock. For more details see Appendix 2 in /SKB, 2005b/.

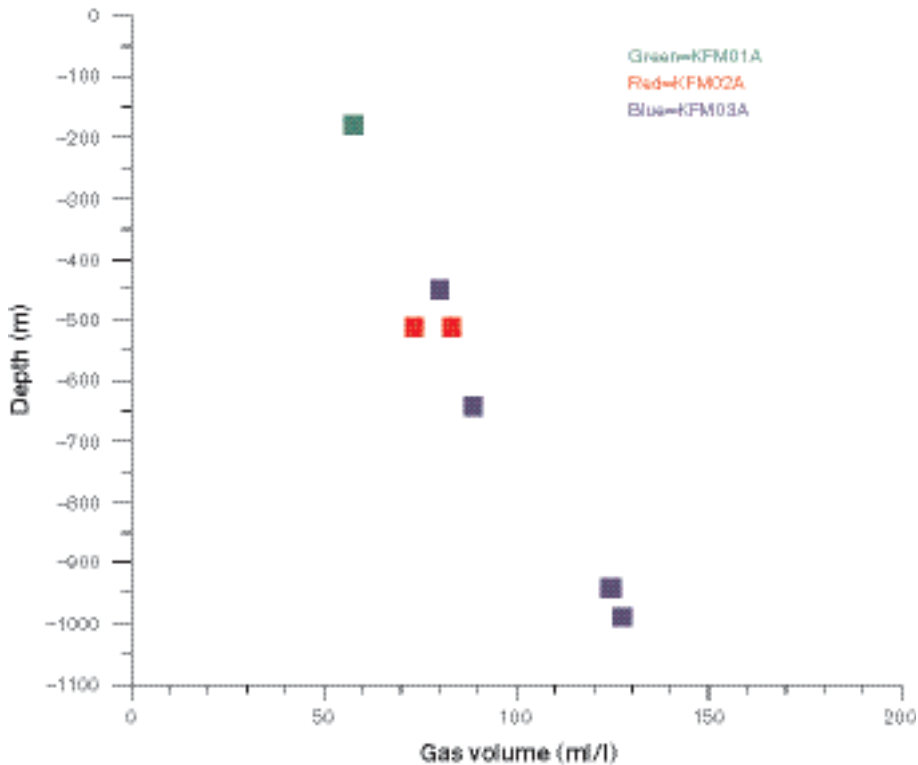


Figure 9-42. Total volume of gas for samples from groundwaters in the Forsmark area.

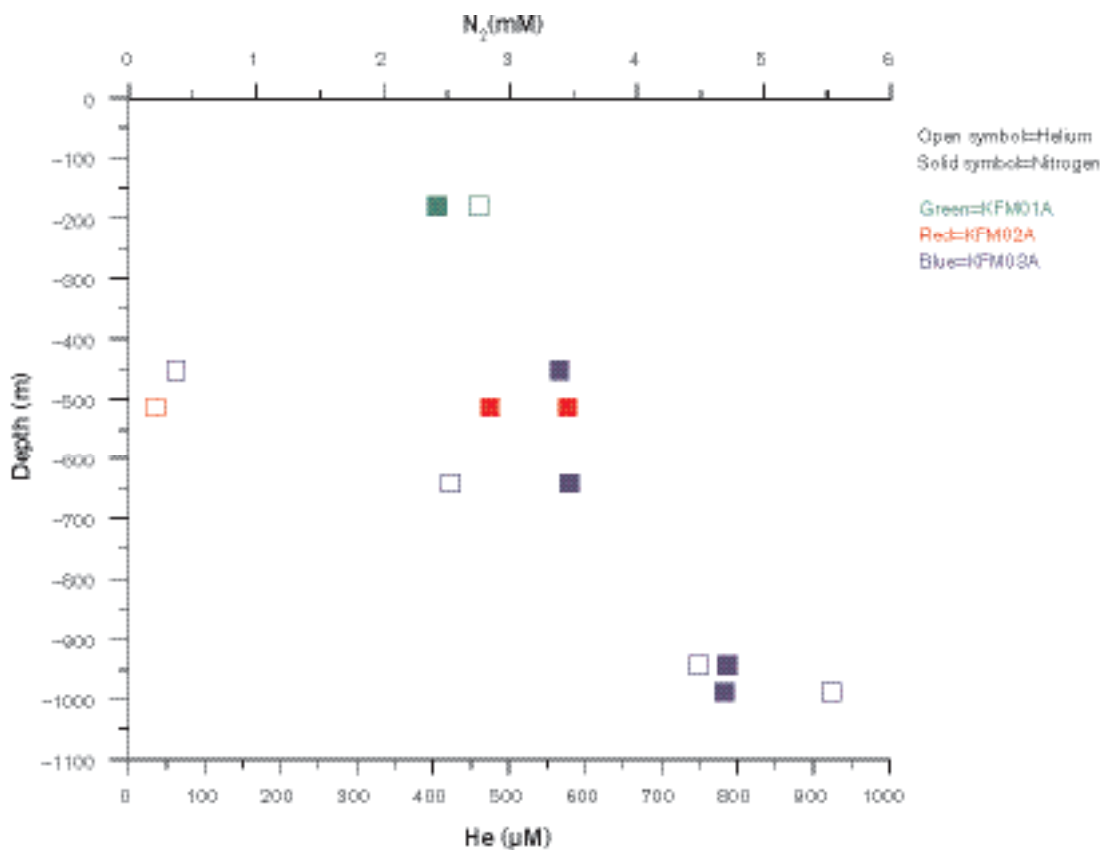


Figure 9-43. Nitrogen and helium versus depth in groundwater samples from boreholes in the Forsmark area.

9.3 Modelling assumptions and input from other disciplines

The main modelling assumption is that the obtained groundwater compositions are a result of mixing and reactions including different water types. The water types are a result of palaeohydrogeological events and modern hydrodynamic conditions (see Figure 3-15). A schematic presentation of how a site evaluation/modelling is performed, its components and the interaction with other geo-scientific disciplines, is shown in Figure 9-44. The methodology applied in this report is described in detail in the SKB strategy report /Smellie et al. 2002/.

For the groundwater chemical calculations and simulations the following standard modelling tools were used.

For evaluation and explorative analyses of the groundwater:

- AquaChem: Aqueous geochemical data analysis, plotting and modelling tool (Waterloo Hydrogeologic).

Mathematical simulation tools:

- PHREEQC with the database WATEQ4F: Chemical speciation and saturation index calculations, reaction path, advective-transport and inverse modelling /Parkhurst and Appelo, 1999/.
- M3: Mixing and Massbalance Modelling /Laaksoharju et al. 1999/.
- Flow and reactive transport simulations: CORE^{2D} /Samper et al. 2000/.

Visualisation/animation:

- TECPLOT: 2D/3D interpolation, visualisation and animation tool (Amtec Engineering Inc.).

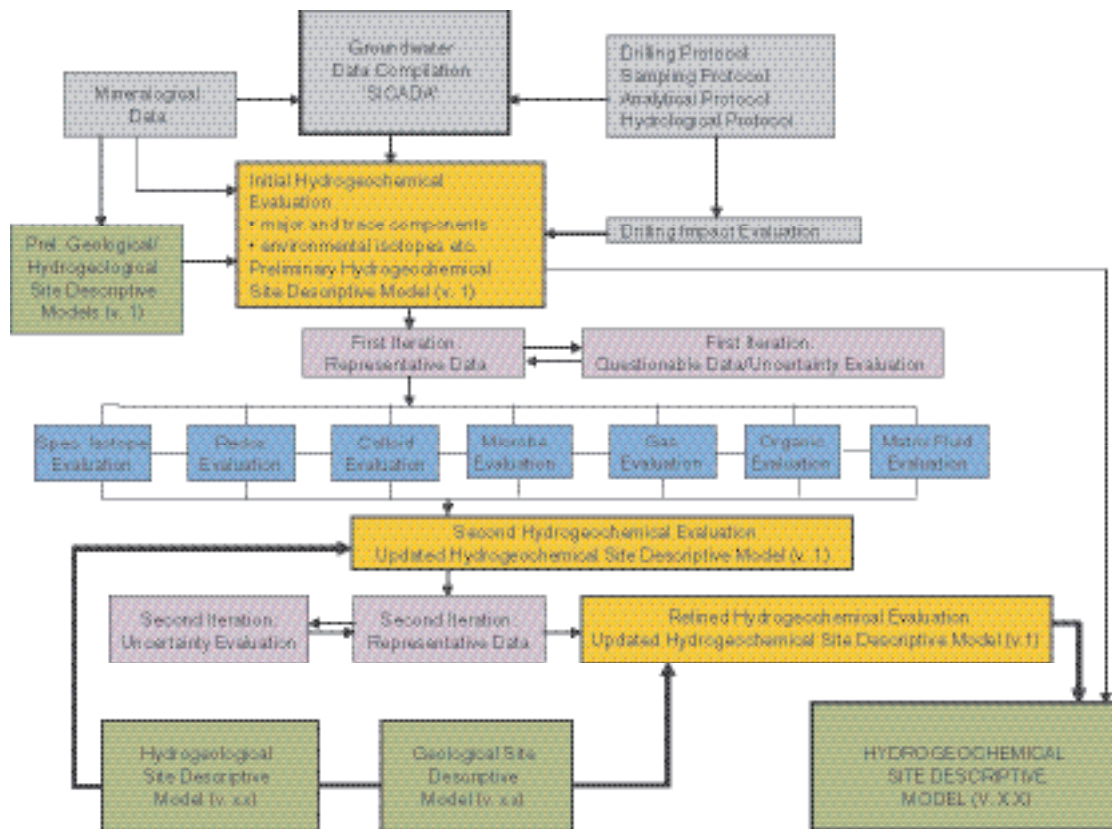


Figure 9-44. The evaluation and modelling steps used for Forsmark model version 1.2 (after /Smellie et al. 2002/).

Hydrogeochemical modelling involves the integration of different geoscientific disciplines such as geology and hydrogeology. This information is used as background information, supporting information or as independent information when models are constructed or compared (cf. Appendix 5 in /SKB, 2005b/).

Geological information is used in hydrogeochemical modelling as direct input in mass-balance modelling, but also to judge the feasibility of the results from, for example, saturation index modelling. For this particular modelling exercise, geological data were summarised, the information was reviewed and the relevant rock types, fracture minerals and mineral alterations were identified (cf. Appendix 1 and 3 in /SKB, 2005b/).

The underlying geostructural model provides important information on water-conducting fractures used for the understanding and modelling of the hydrodynamics. The cross section used for visualisation of groundwater properties is generally selected with respect to the geological model and the hydrogeological simulations (cf. Appendix 1 and 4 in /SKB, 2005b/). The available hydrogeological information and the results from hydrogeological modelling are directly used in the coupled flow and transport modelling (cf. Appendix 5 in /SKB, 2005b/). The measured values of Cl, ^{18}O , ^2H , ^{14}C and the results from the M3 mixing calculations were provided as input data for hydrodynamic modelling simulations (cf. Appendix 4 in /SKB, 2005b/). The mixing models used are descriptive and do not include advection or diffusion processes. However, these models can indicate effects of transport processes or reactions in a simplified way.

9.4 Conceptual model with potential alternatives

The conceptual hydrogeochemical model for the Forsmark site is the paleohydrogeological model shown in Figure 3-15. Much of the hydrogeochemical work focus on tracing effects of the paleohydrogeological events, but also on how mixing and reactions have altered the groundwater composition. The alternative conceptual models tested included different reference waters and local and regional models and different mathematical solutions to calculate the mixing proportions (cf. Appendix 4 in /SKB, 2005b/); various modelling tools and approaches were applied on the data set. In addition, the concept in which the water composition is modelled by using PHREEQC and the M4 approach is discussed in Appendix 3 in /SKB, 2005b/. M4 is a new method to calculate mixing proportions in multivariate space, see /SKB, 2005b/.

9.5 Hydrogeochemical modelling

Hydrogeochemical modelling has been carried out with PHREEQC /Parkhurst and Appelo, 1999/ using the WATEQ4F thermodynamic database. The modelling focussed on speciation-solubility calculations (carbonate, silica and sulphate systems), mass balance and mixing calculations, reaction path modelling (for the aluminosilicate system) and redox system analysis. These calculations were used to investigate the processes that control water composition at Forsmark. A detailed description of the modelling performed can be found in Appendix 3 in /SKB, 2005b/. The mineral phases assumed for the calculations have been identified as fracture fillings, see Appendices 1 and 3 in /SKB, 2005b/.

A further modelling approach, which is useful in helping judge the origin, mixing and major reactions influencing groundwater samples is the M3 modelling concept (Multivariate Mixing and Mass-balance calculations) detailed in /Laaksoharju et al. 1995a; Laaksoharju et al. 1999/ and applied on the Forsmark 1.1 data in /Laaksoharju et al. 2004a/.

9.5.1 Calcium carbonate system

Under this heading the evaluation of the main parameters controlling the carbonate system (pH, alkalinity, CO₂ and calcium) is included. Some PHREEQC modelling results (saturation indexes and pCO₂ values) are also included here in order to simplify the description and make the interpretation clearer.

Surficial fresh waters show a wide range of pH values as a consequence of their multiple origins (Figure 9-45a). The lowest values are associated with waters with a marked influence of atmospheric and biogenic CO₂; the highest values (up to 8.5 pH units) are associated with the most diluted groundwater. Overall this gives a decreasing trend with chloride when the rest of the groundwater samples are taken into account, although this trend inverts at depth, so that the more saline groundwaters have slightly higher values. Nevertheless, all these values are affected by uncertainties in pH measurements in the laboratory and there are not enough data from continuous logging pH measurements (apart from the analysis reported in Forsmark version 1.1) to check them.

Broadly speaking, the main features of the pH trend can be correlated with other Scandinavian sites with similar waters (e.g., Simpevarp area and Olkiluoto /Laaksoharju et al. 2004b; Pitkänen et al. 1999/) and also affected by uncertainties in pH.

Alkalinity (HCO₃⁻) is, together with chloride and sulphate, the third major anion in the system, and is the most abundant in the non-saline waters. Its concentration is highest in the shallower groundwaters (Figure 9-46a,b) as a result of atmospheric and biogenic CO₂ influence and/or calcite dissolution. The alkalinity content reaches equilibrium (or oversaturation) with calcite in the fresh waters (Figure 9-46a,b) and then decreases dramatically with depth as it is consumed by calcite precipitation, whereas calcium continues to increase as a result of mixing (Figure 9-46c,d).

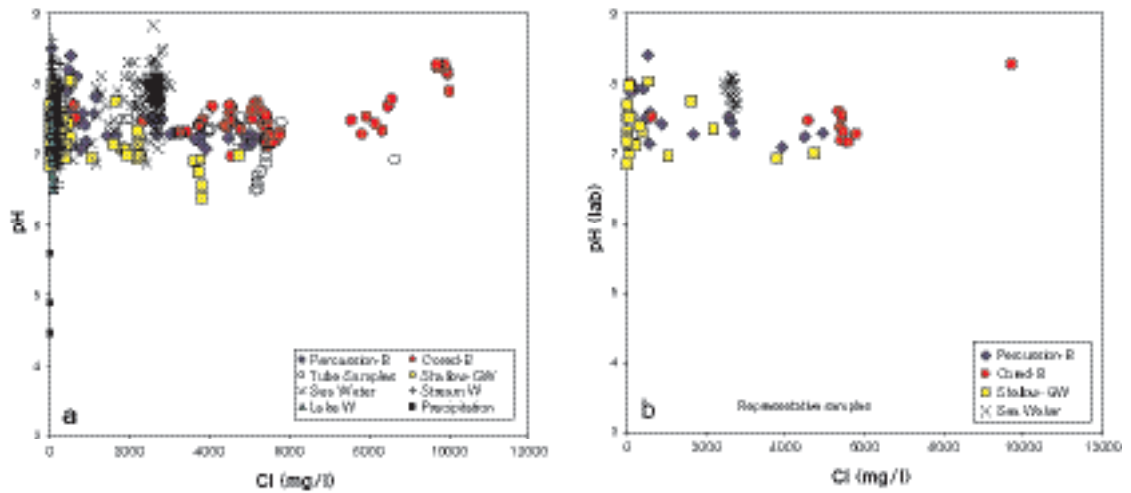


Figure 9-45. pH versus chloride content in mg/L (increasing with depth) in Forsmark waters. (a) All samples. (b) Representative samples.

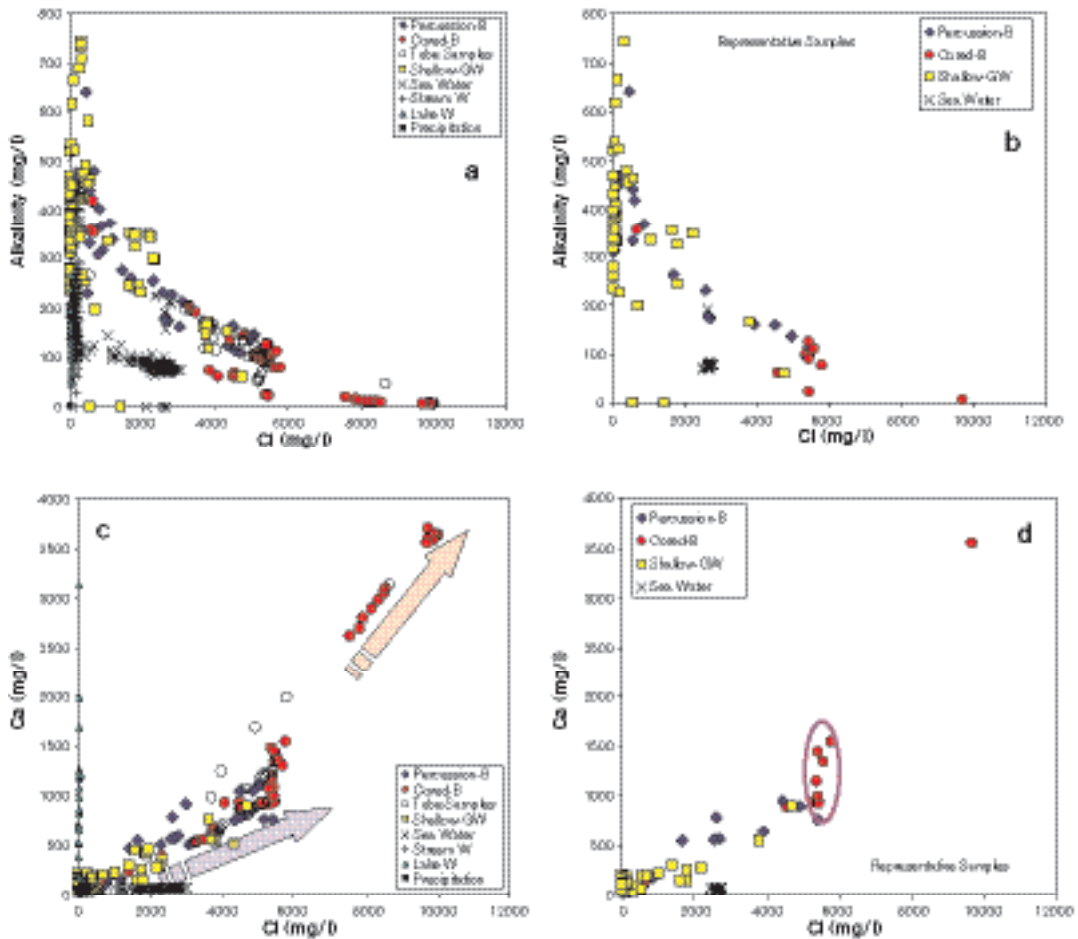


Figure 9-46. Alkalinity and calcium versus Cl in waters from the Forsmark area. (a) Alkalinity evolution in all waters. (b) Alkalinity evolution in the representative waters. (c) Calcium content in all waters. (d) Calcium content in the representative waters.

As can be seen in Figure 9-46c,d, calcium shows the same two trends (one with an important Littorina Sea component, and the other with a higher contribution of a brine component) as the rest of the cations. In general, it shows a good positive correlation with increasing chloride content, mainly in the most saline groundwaters, suggesting that mixing is the main process controlling the concentration of this element in the Forsmark waters. In spite of the extent of reequilibrium with calcite affecting Ca, the high Ca content of the mixed waters (coming from saline end members) obliterates the effects of mass transfer with respect to this mineral. This fact justifies the assumption of quasi-conservative behaviour of calcium, at least in groundwaters with chloride contents higher than 5,000 mg/L. Simple theoretical simulations of mixing between a brine end member and a dilute water, with and without calcite equilibration, have shown the negligible influence of reequilibrium on the final dissolved calcium contents /Laaksoharju et al. 2004a/.

Figure 9-47 shows the calcite saturation index in the Forsmark waters. The alkalinity trend described above can be readily explained by this plot. The uncertainty associated with the saturation index calculation (± 0.5) is higher than that usually considered (± 0.3). This is due to problems during the laboratory measurements of pH (CO_2 outgassing and ingassing), as described in Forsmark version 1.1 /Laaksoharju et al. 2004a/ and also in Simpevarp 1.2 /SKB, 2004d/.

As for CO_2 , Figure 9-47c and d shows the trend of decreasing partial pressure with increasing depth, reaching values well below atmospheric in the more saline groundwaters.

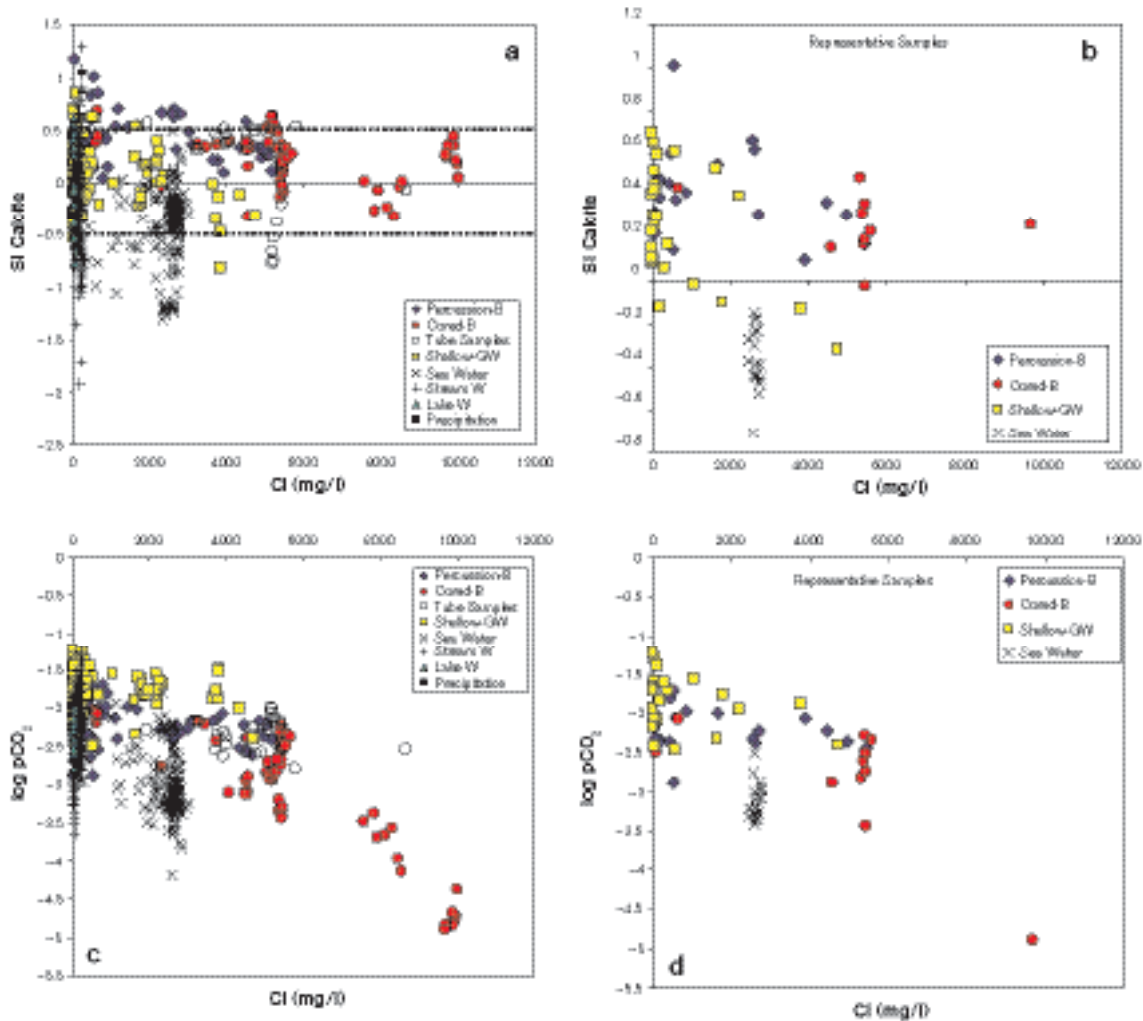


Figure 9-47. Calculated calcite saturation indexes and partial pressure of CO_2 versus chloride for waters from the Forsmark area. The dashed lines represent the uncertainty associated with SI calculations. (a) and (b) Calcite SI in all waters and in representative waters, respectively. (c) and (d) $\log p\text{CO}_2$ in all waters and in the representative waters, respectively.

9.5.2 Silica system

The content of dissolved SiO_2 in surface waters indicates a typical trend of weathering, while in groundwaters it has a narrower range of variation indicative of partial reequilibration (Figure 9-48a and b). Also in this case, the brackish groundwaters ($\text{Cl} \sim 5,500 \text{ mg/L}$) show different silica contents for the same chloride concentration. The general process evolves from an increase in dissolved SiO_2 by dissolution of silicates in surface waters and shallow groundwaters to a progressive decrease related to the participation of silica polymorphs and aluminosilicates which control dissolved silica as the residence time of the waters increases. This can be clearly seen in Figure 9-48c and d.

The weathering of rock-forming minerals is the main source of dissolved silica. Surficial waters have a variable degree of saturation with respect to silica phases (quartz and chalcedony), compatible with the weathering hypothesis, and a rather unclear control by secondary phases. This is a rough generalisation, useful for this general description, but it should be noted that surface waters come from diverse systems (streams, lakes and soil zones) involving contrasting processes (evaporation, biological uptake, etc. /Laaksoharju et al. 2004b/ that affect silica concentrations.

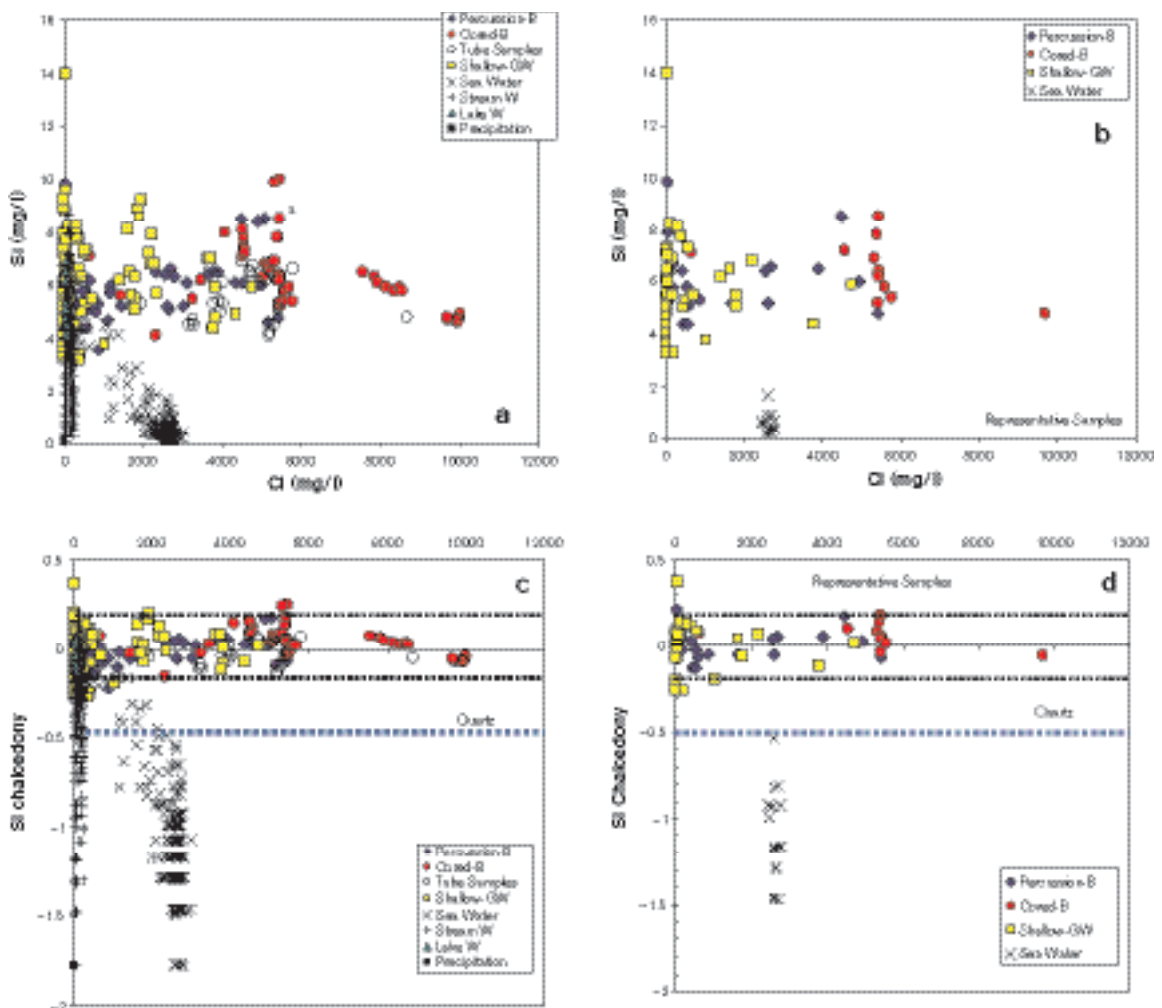


Figure 9-48. (a) Plot of SiO_2 versus Cl for all Forsmark waters and for the representative waters (b). (c) Saturation indexes of chalcedony and quartz as a function of Cl in all Forsmark waters and in the representative waters (d). The dashed lines represent the uncertainty associated with SI calculations /Deutsch et al. 1982/.

Groundwaters are oversaturated with respect to quartz and close to equilibrium with chalcedony (Figure 9-48c,d). Saturation indices are relatively constant and independent of chloride content; this suggests that the groundwater has already reached, at least, an apparent equilibrium state associated with the formation of aluminosilicates or secondary siliceous phases like chalcedony, which seems to be controlling dissolved silica.

9.5.3 Sulphate system

Figure 9-49a, showing SO_4 versus Cl, suggests three possible trends.

- a) An obvious modern Baltic Sea water dilution line, including sea water samples and some shallow groundwaters (soil pipes and percussion boreholes).
- b) A borehole brackish groundwater dilution trend moving away from (a) towards very high sulphate values, suggesting, as in the previous phase, some Littorina Sea influence /Laaksoharju et al. 2004a/. Some shallow groundwaters (soil pipe samples) are also included in this trend.
- c) A decreasing SO_4 trend as chloride increases from 6,000 mg/L to more saline values. In general, these groundwater data lend support to the absence of a significant postglacial marine component, suggesting instead a mixing with deeper, more saline waters of non-marine origin.

There is even an additional low chloride-low sulphate dilution trend incorporating some shallow groundwaters and some Lake/Stream waters. The greater scatter of sulphate at lower chloride levels may partly reflect some modern Baltic Sea water influence, some near-surface oxidation of sulphides, and also the variable effects of microbially mediated reactions (e.g. effect of sulphate-reducing bacteria) below and above the geosphere/biosphere interface.

Perhaps the most interesting aspect of the Forsmark waters is their different evolution, as shown by the sulphate content, with respect to sulphate behaviour in the Simpevarp area /SKB, 2004d/. Figure 9-49e shows the sulphate contents in waters from Simpevarp and Olkiluoto. The Forsmark data are more limited in salinity than the Olkiluoto data, but they appear to be following the same trend. In both cases, after an initial increase in sulphate (reaching the maximum values when salinity is around 5,000–6,000 mg/L of Cl) there is a clear decrease towards zero. On the contrary, for the same chloride content, sulphate concentration in the Simpevarp area is clearly higher (Figure 9-49e).

This contrasting behaviour must be related to the process controlling sulphate content in these waters. Analysing the saturation state of the groundwaters with respect to gypsum some conclusions can be drawn. This analysis was also carried out for Simpevarp and included in Simpevarp 1.2 report /SKB, 2004d/. In both cases (Simpevarp 1.2 and Forsmark 1.2) the range of salinity in the samples has increased since the previous data freeze, and a more complete evolution can be observed.

The Forsmark groundwaters are undersaturated with respect to gypsum but they evolve towards equilibrium with gypsum as chloride increases to 6,000 mg/L (Figure 9-49c,d). Then, the more saline groundwaters evolve towards more undersaturated state than the shallow groundwaters. The same behaviour can be seen in the Olkiluoto groundwaters. However, in the Simpevarp groundwaters the gypsum SI trend indicates a clear evolution towards equilibrium (Figure 9-49f) which is reached at chloride values of 10,000 mg/L and maintained even in the most saline groundwaters /Laaksoharju et al. 2004b/.

9.5.4 Massbalance and mixing calculations using PHREEQC and M4

In the previous evaluation of the Forsmark groundwaters, two different trends were identified and ascribed to two representative mixing processes: the first one giving rise to Littorina-rich waters and the second producing waters with an important participation of a brine end member /Laaksoharju et al. 2004a/. Subsequently, the presence of very shallow groundwaters with compositional features representative of discharge zones of old groundwaters has now been identified as a separate group.

These three groups of samples have been processed through the mass balance capabilities of PHREEQC in order to check the hypothesis advanced above on the influence of the different end members on their chemistry. Additionally, mixing proportions obtained by PHREEQC for selected samples have been compared with the results obtained with a modified version of M3, called M4,

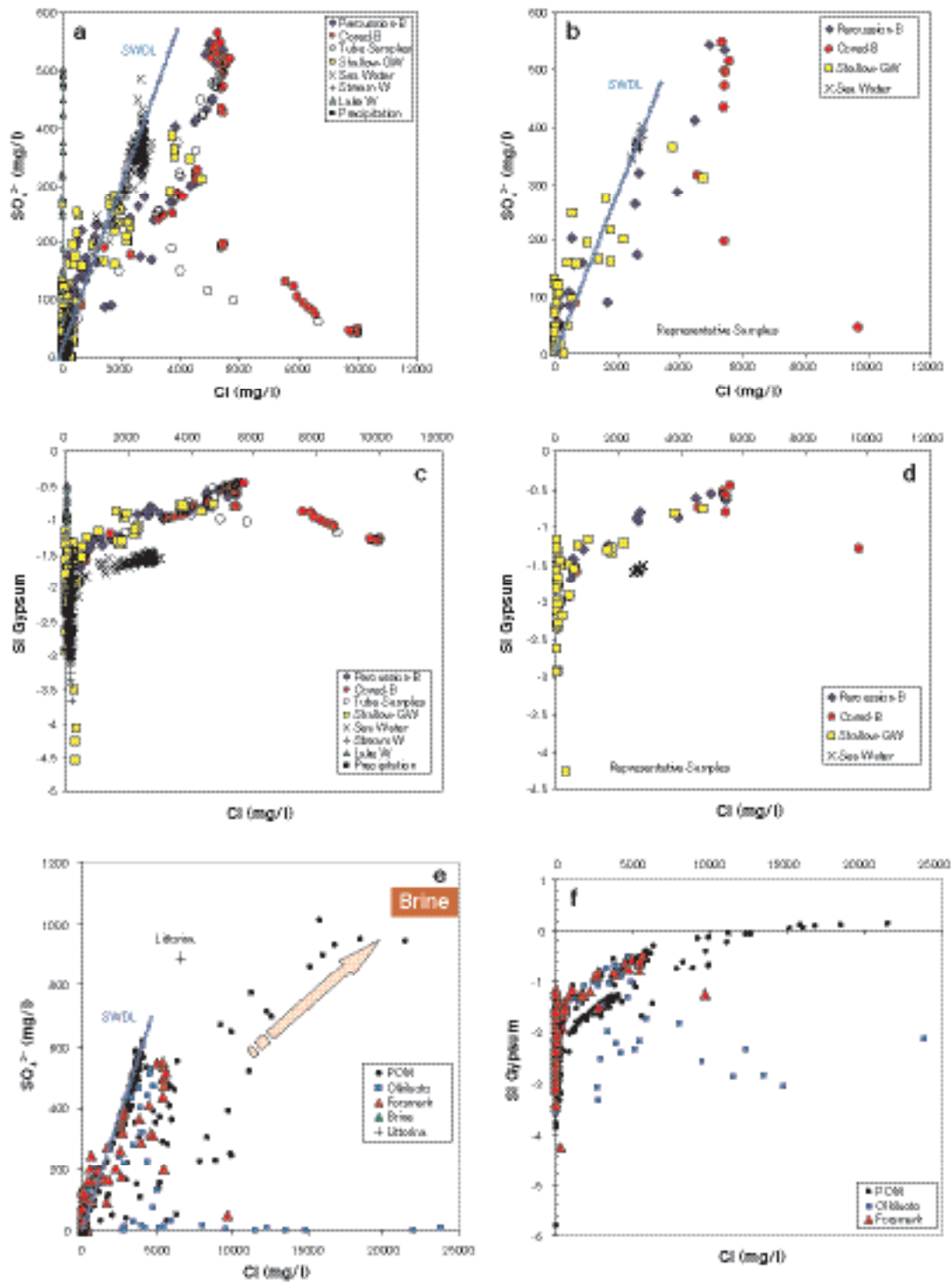


Figure 9-49. (a) and (b) SO₄ versus Cl for all Forsmark waters and for the representative ones, respectively. (c) and (d) Gypsum saturation index (SI) versus Cl for all Forsmark waters and the representative ones, respectively. (e) and (f) SO₄ and Gypsum SI versus Cl comparing Forsmark data with samples from the Simpevarp area (POM) and Olkiluoto.

developed by the University of Zaragoza team, in order to validate the code. Some additional comparisons between M3 and M4 are presented in Appendix 4 in /SKB, 2005b/. Appendix 3 in /SKB, 2005b/ gives a summary of the code, together with a sensitivity analysis carried out with both synthetic and real samples. The methodology used for inverse modelling is described in Appendix 3 in /SKB, 2005b/.

Table 9-1 summarises the PHREEQC and M4 results, showing good agreement between the two approaches (see also Appendix C in Appendix 3 in /SKB, 2005b/ for an in-depth validation of M4). PHREEQC results give the maximum and minimum values among all the successful mixing models for each sample.

Samples of Group 1 have *Littorina* proportions ranging from 35 to 51% (only the two samples with the most extreme *Littorina* mixing proportions are shown in the table: 4538 and 8016). In detail, the sample with the lowest chloride content (4,538 mg/L) has a similar proportion of *Littorina* and Glacial end-members, whereas the other samples (represented in Table 9-1 by sample #8016) have a higher *Littorina* proportion (50%) and a much lower Glacial proportion. Brine percent is consistently low (< 5%) and Precipitation is in the range 20–23%. Therefore, this set of samples shows a clear *Littorina* contribution but, in some cases, Glacial proportions can also be important.

The only sample representative of Group 2 (the most saline groundwaters found in Forsmark, #8152), reveals an important Brine contribution (16.02%; cf. < 5% in Group 1 samples) and a lower (or null) participation of *Littorina* (< 9%). The most important contribution comes from the Glacial end member (48%). These values are consistent with the results obtained for other groundwaters at similar depths elsewhere in Sweden /SKB, 2004d/ and correspond to waters representative of old (> 10,800 BP) mixing events with Brine and Glacial end-member waters, with little modification by more recent mixing processes.

Finally, Group 3 samples (shallow groundwaters in discharge zones, #8078 and 8252) are characterized by a high *Littorina* percentage, similar in general to the value reported for Group 1 samples. The other end-members have also similar contributions to the ones in Group 1. Therefore, they could represent genuine discharge zones of old, deep groundwaters.

The main reaction processes associated with these mixing models include decomposition of organic matter; dissolution of plagioclase, biotite and Fe(OH)₃; precipitation of calcite, K- and Mg-phyllosilicates, silica (chalcedony), and sulphides; and ionic exchange between Na and Ca. Mass transfers

Table 9-1. PHREEQC and M4 mixing proportions (%) for the groundwaters representative of three different trends in the Forsmark area.

Sample	Code	Brine	<i>Littorina</i>	Glacial	Precipitation
Brackish-saline					
4538	PHREEQC	3.8–5.1	27.9–35.2	27.8–31.6	29.4–39.0
Cl = 4,563 mg/L	M4	2.6	35.7	40.8	20.8
Depth: 115 m					
8016	PHREEQC	3.3–4.3	50–54	12.2–14.3	28.6–33.5
Cl = 5,410 mg/L	M4	1.6	50.8	24.4	23.2
Depth: 512 m					
Saline					
8152	PHREEQC	17.5–19.5	0–15	34–42	24–42
Cl = 9,690 mg/L	M4	16.02	9.2	47.9	26.9
Depth: 990 m					
Discharge					
8078	PHREEQC	3.5–4.8	30.5–38.5	27.2–32	28.2–33.5
Cl = 4,730 mg/L	M4	2.7	39	39.4	18.9
Depth: 3 m					
8252	PHREEQC	1.3–2.4	50.9–55	11.6–15.9	27.2–34
Cl = 3,780 mg/L	M4	0	51.4	26.3	22.4
Depth: 3.8 m					

associated with dissolution-precipitation reactions are small (< 0.1 mmol) and slightly higher for cation exchange processes (in the range of 1 mmol), especially for groundwaters with high Littorina Sea signature.

Reactions involving redox species are not well constrained in these types of calculations because the end members lack a proper redox characterisation. Nevertheless, most of the models obtained for Group 2 groundwaters predict a significant precipitation of sulphides (mass transfer rates similar to non-redox minerals). This result is consistent with the redox and microbiological character of these waters.

In conclusion, brackish groundwaters (with chloride around 5,000 mg/L) show an important Littorina Sea signature, usually being the dominant end member, with mixing proportions around 45–50%. Locally, the Littorina contribution is lower (35%) and then the Glacial end member becomes dominant (40%). These groups of groundwaters are scattered in depth, from 100 to 500 m, and therefore deeper than previously assumed in Forsmark version 1.1 /Laaksoharju et al. 2004a/. At depths below 200 m, these brackish groundwaters are located at the same level as the fresh-non saline groundwaters found in other boreholes. In fact, some soil pipe samples (Group 3 samples, < 3 m depth) show the same compositional characteristics and mixing proportions as the deeper brackish groundwaters, suggesting the existence in the system of discharge zones for these old, Littorina-dominated groundwaters.

The deepest saline groundwaters (1,000 m depth) show a clear Brine signature, a low (or null) Littorina Sea contribution and a dominance of the Glacial end-member. These Group 2 groundwaters represent the remnant of a very old mixing process (Baltic Ice Lake Stage, > 10,800 BP) when glacial melt water flushed the bedrock and mixed with ancient Brine groundwaters. It can therefore be concluded that the forced introduction of glacial melt water in Forsmark reached at least a depth of 1,000 m.

9.5.5 Reaction-path modelling

As it has been commented on above, the mineralogical study of boreholes KFM01B, KFM02A, KFM03A and KFM04A has demonstrated the presence of a complex sequence of fracture fillings. Besides the granite rock-forming minerals, most fracture filling phases are aluminosilicate minerals with which waters have been in contact during their geochemical evolution. Therefore, they are important water-rock interaction phases. However, as already pointed out, the lack of aluminium data for Forsmark groundwaters precludes a speciation-solubility analysis, limiting the analysis to a graphical representation of stability diagrams.

The accuracy of the stability diagrams depends on pH and is therefore affected by uncertainties in its value. Uncertainties in the equilibrium constants of the aluminosilicates (especially the phyllosilicates) also affect the conclusions drawn from these diagrams and from the ensuing theoretical models based on them (e.g. /Laaksoharju and Wallin, 1997; Trotignon et al. 1997, 1999/. As a consequence, the study of aluminosilicate phases has been restricted to those with low uncertainties, using thermodynamic data already tested and verified in comparable systems. That means that the “aluminosilicate system” as defined here reduces to the set adularia, albite, kaolinite, laumontite, prehnite and chlorite. The selected thermodynamic data are taken from /Grimaud et al. 1990/ at 15°C in their study of Stripa groundwaters.

The following description includes a general evaluation of Forsmark groundwaters from their position in the stability diagrams and a discussion on the effects of mixing and reaction on the chemistry¹ of the groundwater. This discussion is illustrated by means of a theoretical equilibrium modelling. The origin of the saline groundwaters (Littorina Sea and/or Brine end members) is not discussed here, as the model assumes that they are already in the system, participating in the mixing process. Nevertheless, in the Simpevarp 1.2 report /SKB, 2004d/, the potential use of this modelling approach to predict the chemical characteristics of these old saline groundwaters is described.

¹ In this section different diagrams and computer simulations for Forsmark waters are presented, in some of the cases together with other sites (Stripa, Olkiluoto and Simpevarp area).

Stability diagrams

Following the same procedure developed for Simpevarp 1.2 /SKB, 2004d/, the Forsmark waters have been plotted in different stability diagrams (see Appendix D of Appendix 3 in /SKB, 2005b/). The set of thermodynamic data utilised to construct the stability diagrams was calibrated for Stripa groundwaters /Grimaud et al. 1990/, and the presentation and explanation of the original diagrams can be found in /SKB, 2004d/.

The analysis of Forsmark waters uses the kaolinite-albite-adularia stability diagram because it is the most suitable for discriminating waters that have undergone mixing, and because many Fenoscandian groundwaters plot near the albite-adularia boundary line, suggesting a true or apparent equilibrium with both phases.

Figure 9-50 shows the kaolinite-albite-adularia diagram for the Forsmark waters. Green and blue arrows mark the two main trends that can be distinguished. **The first trend** (green arrows) starts inside the kaolinite stability field and evolves towards the kaolinite-adularia boundary. This trend is defined by modern surface waters and shallow groundwaters with low chloride contents and whose geochemical evolution is mainly the result of water-rock interactions.

The evolution path of these waters in the kaolinite field has a slope of around 2, similar to other weathering/alteration processes in granitic materials and represents the effects of a progressive dissolution of the rock forming minerals calcite, biotite, plagioclase, K-feldspars, etc. Along this process, partial reequilibration with phyllosilicates (represented by, e.g., kaolinite) can be reached. Ionic exchange and, in later stages, calcite precipitation can also take place. Waters close to or on the kaolinite-adularia boundary would correspond to the most evolved samples in this water-rock interaction process.

Some shallow groundwaters (soil pipes) and lake waters from Forsmark do not plot inside the kaolinite field, as expected, but inside the adularia stability field instead. Some of these samples (samples close to the adularia-albite limit, see below) show clear evidence of mixing with modern Baltic Sea, and even with another older marine (Littorina Sea) and saline (non marine) end members. Therefore, they could be waters whose chemistry is not only controlled by water-rock interactions and plot together with groundwaters characterised by mixing. The rest of the soil pipe and lake samples plot in the adularia field further away from the adularia-albite limit. They have low chloride contents but anomalously high K, Mg, SO_4^{2-} , etc. These samples could be the result of water-rock

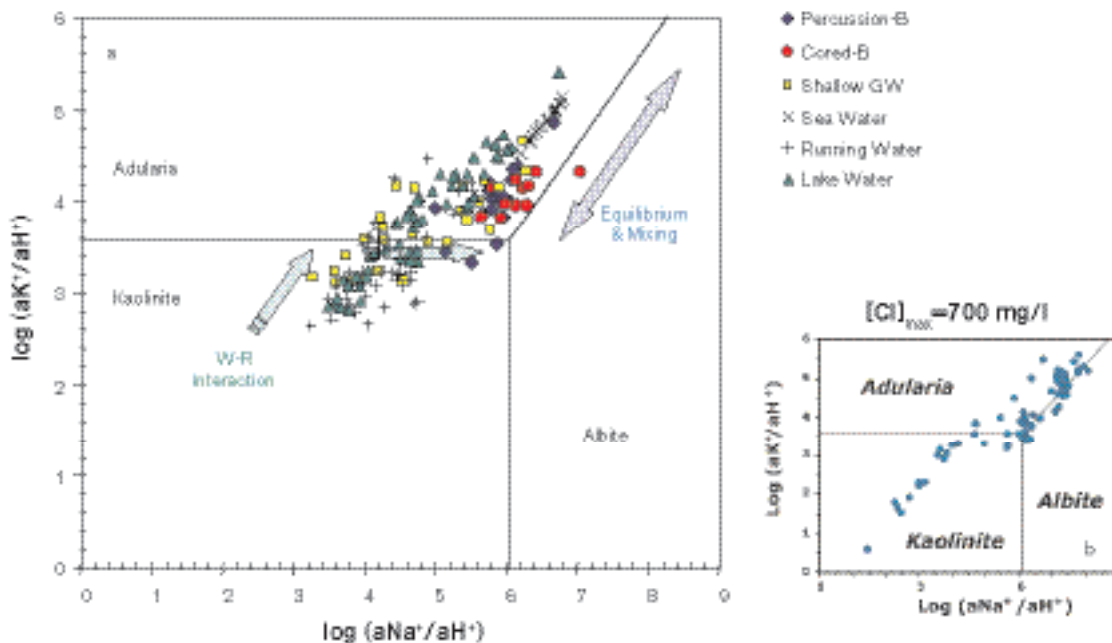


Figure 9-50. Kaolinite-adularia-albite stability diagram for Forsmark representative surface and groundwaters (a) and for Stripa groundwaters (b).

interactions in the detritic overburden or could even represent some kind of contribution from an old marine component, as they are geographically associated to what seems to be discharge zones in the system. More data would be needed to determine the origin of these waters.

The second trend (blue arrow), followed by all Forsmark brackish and saline groundwaters, runs parallel to the adularia-albite limit, indicating an equilibrium (or near equilibrium) situation. This result is very similar to that at Stripa (compare the figures and the scale) but with an important difference: the maximum chloride content in Stripa reaches only 700 mg/L, whereas Forsmark groundwaters, plotted in the same position, have Cl contents up to 10,000 mg/L. The residence time of Stripa groundwaters has been estimated at roughly 100,000 years /Fontes et al. 1989/, meaning that water-rock interaction processes can only provide up to 700 mg/L of chloride over such a large time span. It is clear, therefore, that an additional source of salinity is needed to justify the existence of much younger waters with much higher chloride concentrations at Forsmark. This source of chlorine comes from mixing with a saline component of marine and/or non marine origin. This points again to mixing as the key process controlling the chemistry of these waters, as has been repeatedly reported in previous works /Laaksoharju and Wallin, 1997; Laaksoharju et al. 1999; Laaksoharju et al. 2004b/.

In Figure 9-51 the Forsmark samples have been plotted together with those of Olkiluoto /Pitkänen et al. 2004a/ and of the Simpevarp area /SKB, 2004d/. The Olkiluoto waters occupy, in general, the same position as the Forsmark waters. The Olkiluoto samples in the kaolinite stability field and on the kaolinite-adularia boundary correspond to subsurface or shallow groundwaters whose chemistry is controlled by water-rock interactions. Samples located on the adularia-albite boundary correspond to brackish and saline groundwaters characterised by having undergone complex mixing processes (between Meteoric, Littorina, Glacial and Saline end members /Pitkänen et al. 2004a/). Results for Simpevarp groundwaters are similar, although in this case the number of samples in the adularia stability field is smaller than is the cases for Forsmark and Olkiluoto.

The position of the theoretical end members is also shown in Figure 9-51 (Brine, Littorina Sea and Glacial; Meteoric is close to Glacial). It is fairly clear that the evolution path of these waters is the result of: (a) reaction between the rock and diluted waters (surface and shallow groundwaters),

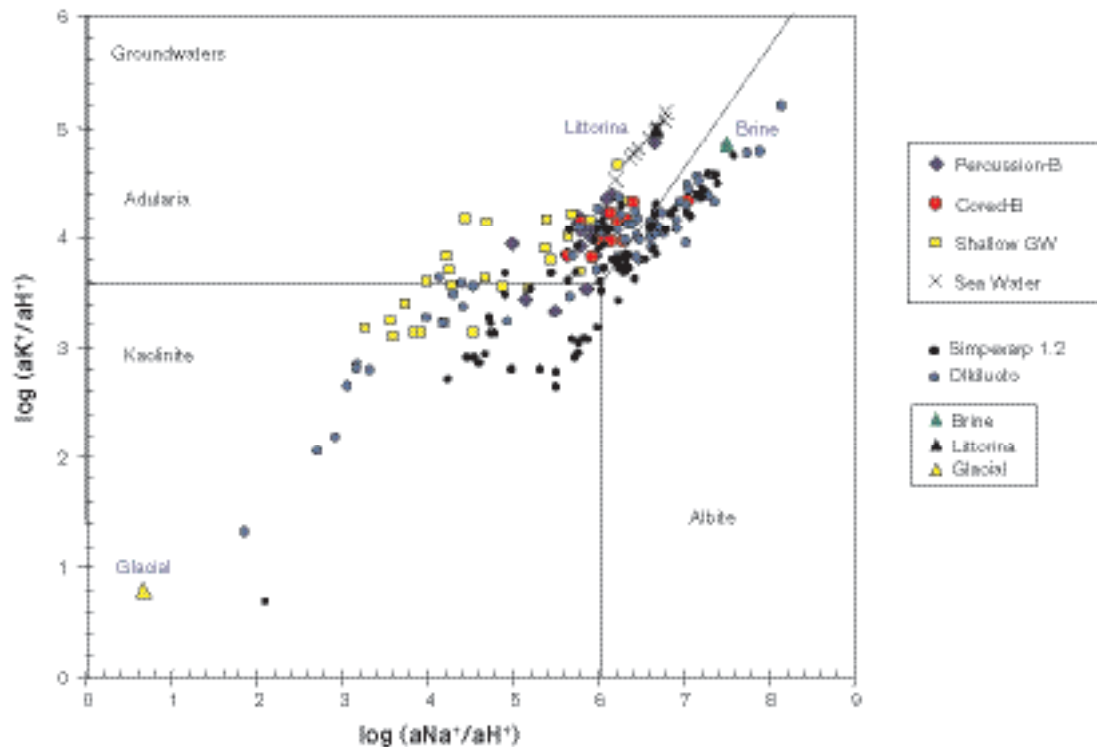


Figure 9-51. Kaolinite-adularia-albite stability diagram. Together with the Forsmark representative groundwaters, the Olkiluoto /Pitkänen et al. 2004a/ and Simpevarp area groundwaters, and also the theoretical end members (Brine, Littorina and Glacial), have been plotted in this diagram.

(b) mixing at depth with more saline groundwaters in different proportions, as a function of location and residence time, and (c) the simultaneous interaction of these deep waters with the rock.

An identical result has been found in Simpevarp 1.2 /SKB, 2004d/. However, in this case there are a substantial number of samples located close to the adularia-albite boundary but inside the adularia field, showing a clear trend towards the Littorina Sea end member. The uncertainty of the modelling is discussed in Appendix 3 in /SKB, 2005b/.

Simulating the water composition

As shown above, the Forsmark, Simpevarp area and Olkiluto groundwaters on the adularia-albite boundary and inside the adularia stability field, but close to the boundary, include samples of broadly different salinities, chemical contents and depths, but reflecting an apparently similar equilibrium situation. In a first approximation, they could be interpreted as the result of different mixing episodes between different end members at different times during the site evolution. Alongside this main process, there would be re-equilibration periods (reaction with the rock) following the disequilibrium created by the successive mixing episodes.

The chemistry of the groundwaters is then the result of a complex sequence of mixing and reaction. Following the procedure developed in the Simpevarp 1.2 report, a direct mixing and reaction calculation has been chosen in order to evaluate the relative contribution of the two processes.

The modelling performed for Simpevarp 1.2 was focussed on the assessment of the oldest mixing episode between the saline and glacial end members (8,000–10,000 BC) and is entirely valid as an explanation of the more saline waters at Forsmark (see a detailed description in /Laaksoharju et al. 2004b/). Therefore, the simulations reported here are focussed on the next mixing episode, involving the previously mixed waters and a certain amount of Littorina Sea water end member.

The simulation flow chart is shown in Figure 9-52. From previously calculated (Simpevarp 1.2) mixing proportions between Brine and Glacial (the two extreme cases analysed: 63% Brine and 37% Glacial, 5% Brine and 95% Glacial), equilibrium with different mineral assemblages was imposed. Equilibrium with calcite, chalcedony, albite, and adularia has been chosen here only as an example, but models with other mineral assemblages have also been run. The resulting water (final solutions 1 and 2 in Figure 9-52) was mixed with different proportions of Littorina (between two extreme cases: 10% and 70%). The new mixed waters are named Mix 1, 2, 3 and 4. The final step consists of imposing again equilibrium with different mineral assemblages. The equilibria with calcite-chalcedony and calcite-chalcedony-albite-kaolinite have been chosen here as examples.

Figure 9-53 shows the location of final solutions 1 and 2 after mixing with Brine and Glacial and in equilibrium with the selected minerals (black squares and orange diamonds). They plot on the adularia-albite boundary very close together. They represent the final result of the simulations performed in Simpevarp 1.2 and the starting point of this new calculation.

The next modelling step is a mixing calculation. Each of the already calculated final solutions was mixed with the Littorina Sea end member in two different proportions: 10% and 70%. The position of these mixed waters is plotted in the stability diagrams (cf. Appendix 3 in /SKB, 2005b/). After mixing, the equilibrium of the mixed waters with different combinations of calcite, chalcedony, albite, adularia and kaolinite was simulated in order to measure the effects on the final composition of the waters.

Detailed description of the modelling and its uncertainties can be found in Appendix 3 in /SKB, 2005b/. Examples of the calculated mass transfers are listed in Table 9-2.

As a summary, these results indicate that re-equilibrium reaction processes are important in the control of some parameters such as pH (as well as Eh, and some minor-trace elements), moving the waters towards the adularia-albite boundary. However, the main compositional changes, and even the extent of re-equilibration processes², are controlled by the extent of the mixing process.

² Calculated mass transfers for the same equilibrium situation change by more than one order of magnitude depending on the considered mixing proportions.

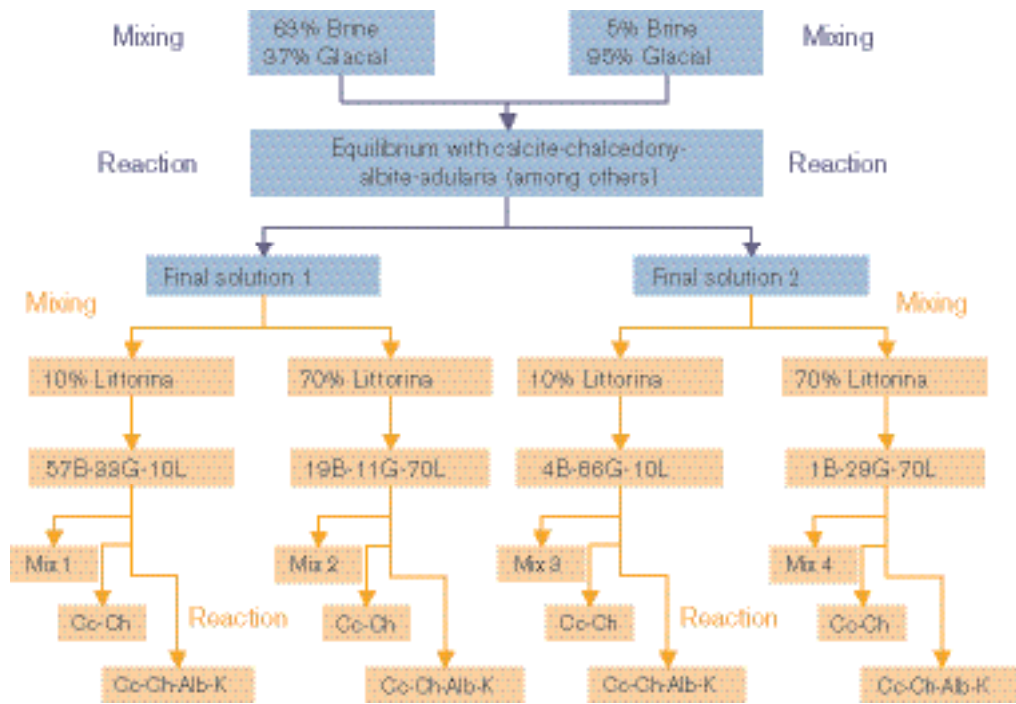


Figure 9-52. Simulation procedure for the assessment of the mixing episode between Littorina Sea and a saline groundwater (result of a previous mixing process between Brine and Glacial end members and the equilibrium with a mineral assemblage).

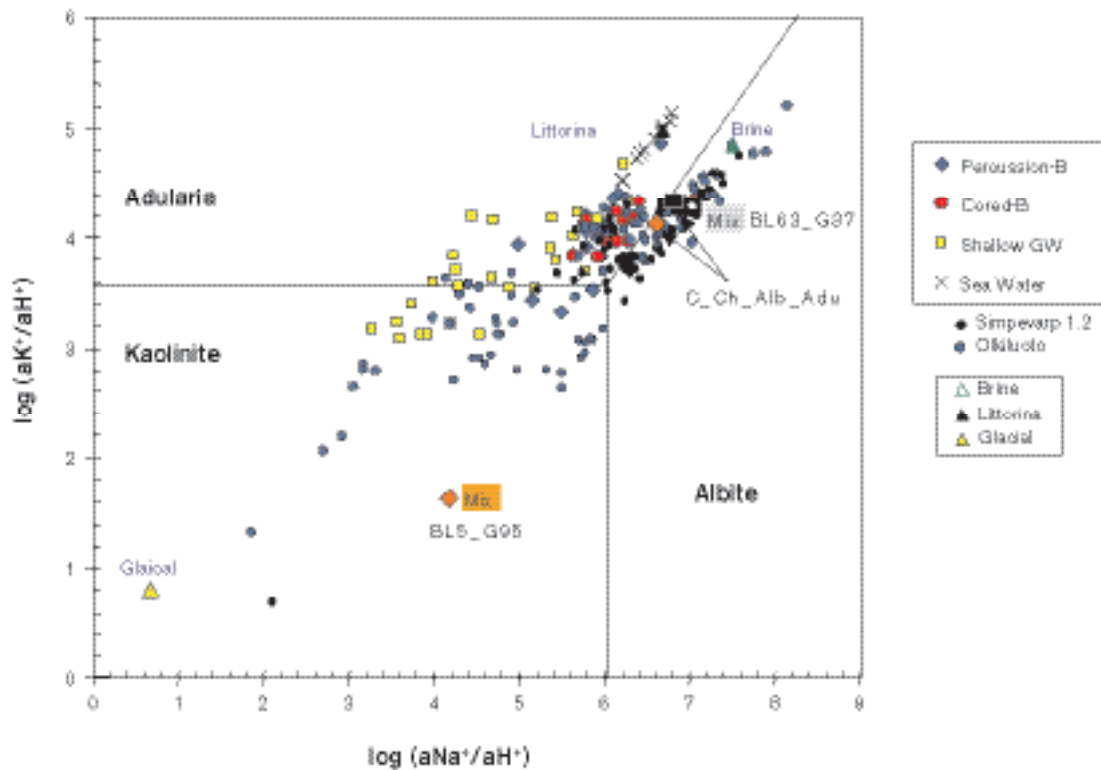


Figure 9-53. Starting point for the simulation of the mixing episode between Littorina Sea and a saline groundwater result of a previous mixing process between Brine and Glacial end members (Mix points in the plot), and the equilibrium with a mineral assemblage (C_Ch_Alb_Adu in the plot).

Table 9-2. Calculated mass transfers (mol/L) in the four mixing proportions as discussed above. Only two examples are shown here: the equilibrium with calcite (Cc) and chalcedony (Ch), and the equilibrium with calcite, chalcedony, kaolinite (Kaol) and albite (Alb).

Mass Transfers	90% (63Brine – 37Glacial) 10%Litt.		30% (63Brine – 37Glacial) 70%Litt.		90% (5Brine – 95Glacial) 10%Litt.		30% (5Brine – 95Glacial) 70%Litt.	
	57B+33G+10L		19B+11G+70L		4B+86G+10L		1B+29G+70L	
	Cc-Ch	Cc-Ch-Kaol-Alb	Cc-Ch	Cc-Ch-Kaol-Alb	Cc-Ch	Cc-Ch-Kaol-Alb	Cc-Ch	Cc-Ch-Kaol-Alb
Calcite (C)	6.6×10 ⁻⁶	2.2×10 ⁻⁴	1.1×10 ⁻⁴	4.7×10 ⁻⁴	4.3×10 ⁻⁶	1.1×10 ⁻⁴	5.6×10 ⁻⁶	1.4×10 ⁻³
Chalcedony (Ch)	8.1×10 ⁻⁶	5.1×10 ⁻⁴	6.0×10 ⁻⁵	8.2×10 ⁻⁴	5.3×10 ⁻⁶	2.5×10 ⁻⁴	6.0×10 ⁻⁵	3.3×10 ⁻³
Kaolinite (K)		1.3×10 ⁻⁴		2.2×10 ⁻⁴		6.1×10 ⁻⁵		8.1×10 ⁻⁴
Albite (Alb)		2.5×10 ⁻⁴		4.4×10 ⁻⁴		1.2×10 ⁻⁴		1.6×10 ⁻³

9.5.6 Redox modelling

In this section, the results from the modelling of the redox state in the Forsmark area are presented (cf. Appendix 3 in /SKB, 2005b/ for more details and methodology). For version 1.2, the amount of suitable data for a redox study is slightly greater than for version 1.1 and, therefore, this study is somewhat more complete. The two possibilities suggested in previous studies about the redox state of the groundwaters have been revisited, namely: (a) the iron system controls the redox state /Grenthe et al. 1992/; and (b) the sulphur system controls the redox state (e.g. /Nordstrom and Puigdomenech, 1986/).

For this modelling exercise, only samples with enough redox data were selected. This includes Eh and pH³ data from continuous logging, concentrations of Fe²⁺, S²⁻ and CH₄, and microbiological information. The selection criteria have drastically reduced the number of suitable samples for the redox characterisation of the system. In spite of this, the selected samples cover a wide range of depths (115 to 990 m; Figure 9-54) in three boreholes KFM01, KFM02 and KFM03. Moreover, they all have continuous Eh logging, redox pair concentrations and even microbiological information (in some cases) and thus, a combination of these three data sets can be made.

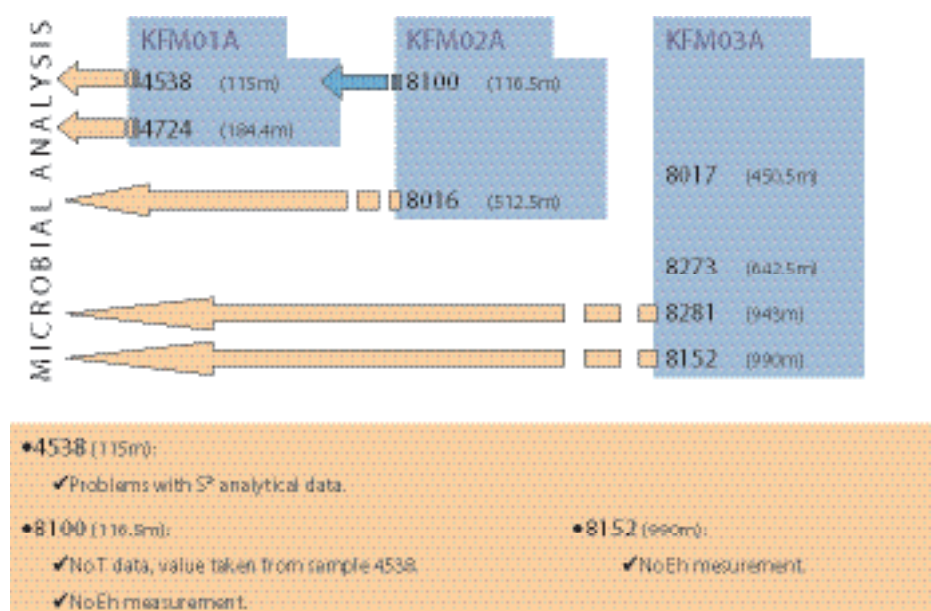


Figure 9-54. Selected groundwater samples for the redox modelling indicating their depths and the kind of available information. The analytical problems associated with sample 4538 are detailed in Appendix D in /SKB, 2005b/.

³ In order to minimise the pH uncertainty effects on the redox calculations /Laaksoharju et al. 2004a,b; SKB, 2004d/.

Redox pair calculations

The results from the redox pair calculations (cf. Appendix 3 in /SKB, 2005b/) are summarised in Figure 9-55 and Figure 9-56. The Eh calculated with the $\text{Fe}(\text{OH})_3/\text{Fe}^{2+}$ redox pair and Grenthe's calibration agrees reasonably well with the Eh values measured in the deepest samples⁴. The Eh calculated with the same redox pair for microcrystalline $\text{Fe}(\text{OH})_3$ is much more oxidising. In contrast, the microcrystalline phase gives better results in the shallower samples (4538), whereas Grenthe's calibration gives a much more reducing Eh value (Figure 9-56). This observation was already made in the previous version (Forsmark 1.1 /Laaksoharju et al. 2004a/). In some samples (4724, 8100, 8016) none of the iron calibrations provide good results. This suggests that the groundwater redox state can be controlled by iron oxides and oxyhydroxides with different degrees of crystallinity.

Except for a few samples, the different "sulphur system" redox pairs provide Eh values coincident with the potentiometrically measured Eh. The $\text{SO}_4^{2-}/\text{S}^{2-}$ homogeneous redox pair gives Eh values similar to the ones obtained from the heterogeneous pairs (Pyrite/ SO_4^{2-} and $\text{FeS}/\text{SO}_4^{2-}$; Figure 9-55 and Figure 9-56) as calculated with WATEQ4F thermodynamic data. A sensitivity analysis carried out comparing these data to /Bruno et al. 1999/ shows only minor differences.

As expected, Eh values obtained with the CH_4/CO_2 pair are very similar to those obtained with the $\text{SO}_4^{2-}/\text{S}^{2-}$ pair (and to the remaining sulphur redox pairs). Therefore, they also agree well with the potentiometrically measured Eh.

Redox pairs results for samples with noisy Eh measurements (8100 and 8152) are not so easy to interpret, but it seems that the measured Eh in sample 8100 agrees well with the Eh value from the sulphur pairs. However, Eh values from these pairs obtained for sample 8152 agree well with the ones from CH_4/CO_2 , but all of them are more reducing than the measured Eh value.

There is an overall good agreement between the potentiometrically measured Eh and the values calculated using the heterogeneous sulphur pairs, the homogeneous sulphur pair and the CH_4/CO_2 pair, even taking into account the low concentrations of S^{2-} and CH_4 . Grenthe's calibration for

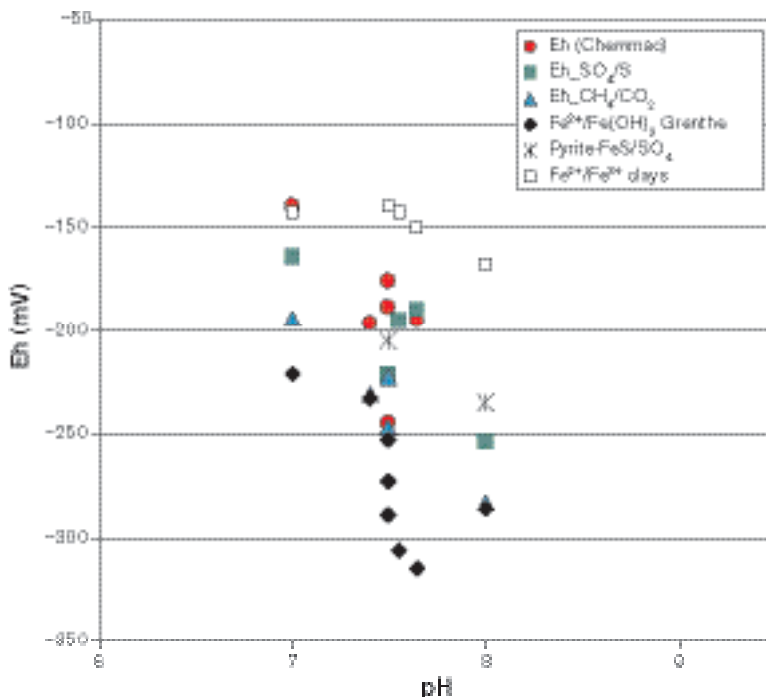


Figure 9-55. Comparison of redox results for different redox pairs in the Forsmark selected groundwaters.

⁴ In the case of sample 8152, the result must be taken with caution. Fe^{2+} concentration in this sample (0.026 mg/L or 4.6×10^{-7} mol/L) is below the lower limit (10^{-6} molar) for successful Eh measurements when iron pairs control the redox potential /Grenthe et al. 1992/.

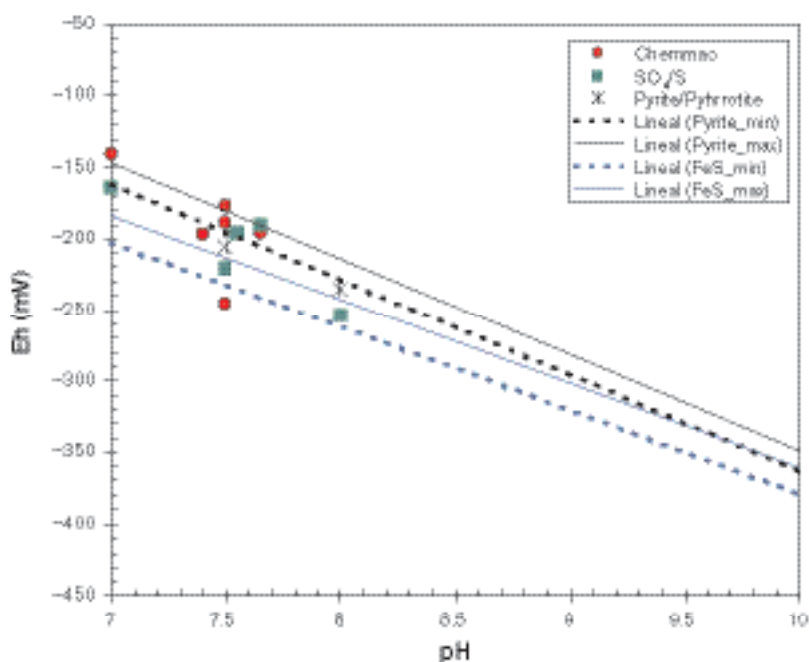


Figure 9-56. Eh-pH diagram showing the calculated Eh values for the Forsmark samples. Potentiometrically measured values are shown as red circles. The Eh values from the $\text{SO}_4^{2-}/\text{S}^{2-}$ redox pair are represented with green squares and the values obtained with the pyrite-pyrrhotite/ SO_4^{2-} pair, with an asterisk. “Pyrite_min” and “Pyrite_max” lines represent the equilibrium situation for the range of SO_4^{2-} and Fe^{2+} concentrations found in Forsmark groundwaters. The same is valid for the $\text{FeS}/\text{SO}_4^{2-}$ equilibrium.

$\text{Fe}(\text{OH})_3/\text{Fe}^{2+}$, provides Eh values in good agreement with the measured Eh for the deepest waters but in the shallowest samples the iron system seems to be controlled by a microcrystalline hydroxide and not by an intermediate phase, as Grenthe’s calibration assumes.

This suggests that the sulphur system is the main controller of the groundwater redox state, as reported previously /Nordstrom and Puigdomenech, 1986; Glynn and Voss, 1997; Laaksoharju et al. 2004 a,b/, or at least that it is the most suitable (together with the CH_4/CO_2 redox pair) to characterize the redox state of these groundwaters. The variable results obtained with the $\text{Fe}(\text{OH})_3/\text{Fe}^{2+}$ pair do not mean that the iron system does not participate in the redox control of these waters, but the variable crystallinity of the phases involved hinders a clear and general assessment. The uncertainty of the modelling is discussed in Appendix 3 of /SKB, 2005b/.

Conceptual model for the redox system

Microbial analysis of the Forsmark groundwaters has identified Sulphate-reducing Bacteria (SRB) at depths from 642.5 m (sample 8273) to 990 m (sample 8152), and their number is specially high at 943 m, in sample 8281. At these depths, the lowest values of SO_4^{2-} and the highest values of S^{2-} from all the analysed waters are found, which is consistent with the metabolic activity of SRB. However, there is no correlation between the number of SRB and dissolved sulphide; moreover, sulphide concentrations (0.03–0.06 mg/L) are too low for the high SRB number found and the expected intensity of the sulphate reduction process.

This fact, together with the low ferrous iron concentration, could indicate the presence of active iron-sulphide precipitation in fractures. This process can maintain dissolved sulphide at the low levels detected, even though sulphate reduction might produce substantial amounts of sulphide. And it can be active if a source of Fe^{2+} (iron oxyhydroxides) exists. This source can explain the low iron concentrations in samples at 642.5 and 943 m depth, but it has apparently been exhausted in the deepest groundwaters (at 990 m).

In summary, most lines of evidence support that the sulphur system, microbiologically mediated, is the main redox controller in the deepest and most saline groundwaters. On the other hand, Littorina-rich brackish groundwaters show variable and very high iron contents, in agreement with what has been observed in similar groundwaters elsewhere (e.g. at Olikiluoto; cf. /Pitkänen et al. 1999/). The microbial analysis only found trace amounts of SRB in samples 4538 and 8016 (115.5 and 512.5 m depth, respectively), but very high numbers of iron-reducing bacteria (IRB), mainly in sample 4538. However, there is no correlation between Fe^{2+} concentration and the number of IRB in these groundwaters. Moreover, they show very low but detectable contents of dissolved S^{2-} and the $\delta^{34}\text{S}$ values are very homogeneous (around 25‰) and clearly higher than in present Baltic Sea, indicating that sulphate reduction has operated. These observations could support the existence of an iron-sulphide precipitation process in these groundwaters but not intense enough to effectively limit Fe^{2+} solubility. The question then arises as when did it happen?

The high Fe^{2+} concentration in these groundwaters and the main episode of sulphate reduction could have happened during Littorina Sea water infiltration through sea bottom sediments during the Littorina Sea stage. Sedimentological studies support the existence of sulphate reduction processes at that time in the organic-rich sediments (e.g. /Albi and Winterhalter, 2001/). Later on, the mixing of this Littorina Sea water with pre-Littorina groundwaters was not able to provide enough organic carbon to keep the sulphate reduction process going with the necessary intensity to completely reduce the high Fe^{2+} concentration in these waters /Pitkänen et al. 1999/. At present, sulphate reduction could be limited by the lack of nutrients or by competition with other organisms.

Finally, methanogens were found at 512.5 and 642.5 m depth but not in the deepest samples⁵. Besides, there are no isotopic data for the measured methane and, therefore an organic control on the CH_4/CO_2 redox pairs for Forsmark groundwaters cannot be established.

9.5.7 Mixing modelling using M3

The M3 method consists of 4 steps, where the first step is a standard principal component analysis (PCA), selection of reference waters, followed by calculations of mixing proportions, and finally mass balance calculations (for more details see Appendix 4 in /SKB, 2005b/).

The reference waters used in the M3 modelling have been identified from: a) previous site investigations (e.g. Äspö and Laxemar), b) evaluation of the Forsmark primary data set, and c) selecting possible compositions of end-members which according to the post-glacial conceptual model (Figure 3-15) may have affected the site. The selected reference waters are more extreme than actually present at Forsmark (e.g. Rain-60 or Littorina Sea). Their function is: a) to be able to compare differences/similarities of the Forsmark groundwaters with possible end-members, b) to be available to describe all data used in the local and regional model, and c) to facilitate comparison with the results from the hydrogeological modelling. The analytical compositions of the selected reference waters are listed in Appendix 4 in /SKB, 2005b/. The reference waters should not be regarded as point sources of flow but rather as possible contributors to the obtained water type. The reference waters have the following features.

- **Brine water:** Represents the sampled deep brine type ($\text{Cl} = 47,000 \text{ mg/L}$) of water found in KLX02: 1,631–1,681 m /Laaksoharju et al. 1995a/. An old age for the Brine is suggested by the measured ^{36}Cl values indicating a minimum residence time of 1.5 Ma for the Cl component /Laaksoharju and Wallin, 1997/. The sample contains some tritium (TU 4.2) which is believed to be contamination from borehole activities. In the modelling 0 TU was used for this sample.
- **Glacial water:** Represents a possible melt-water composition from the last glaciation > 13,000 BP. Modern sampled glacial melt water from Norway was used for the major elements and the $\delta^{18}\text{O}$ isotope value (–21‰ SMOW) was based on measured values of $\delta^{18}\text{O}$ in calcite surface deposits /Tullborg and Larsson, 1984/. The $\delta^2\text{H}$ value (–158‰ SMOW) is a calculated value based on the equation ($\delta\text{H} = 8 \times \delta^{18}\text{O} + 10$) for the global meteoric water line.

⁵ Unfortunately no data for the shallowest depths are available.

- **Littorina Sea:** Represents old marine water and its calculated composition has been based on /Pitkänen et al. 1999/. This water is used for modelling purposes to represent past Baltic Sea water composition.
- **Modified Sea water (Sea sediment):** Represents sea water affected by microbial sulphate reduction.
- **Precipitation:** Corresponds to infiltration of meteoric water (the origin can be rain or snow) from 1960. Sampled modern meteoric water with a modelled high tritium (2,000 TU) content was used to represent precipitation from that period.

The results of the PCA modelling are shown at the regional scale (Forsmark data are compared with Simpevarp data and other Nordic sites data) in Figure 9-57. In Appendix 4 in /SKB, 2005b/ the local scale using only the Simpevarp data is shown also.

The M3 modelling shown in Figure 9-57 indicates that the Forsmark samples are affected by the reference waters: Meteoric, Marine and Glacial. The surface meteoric water types show seasonal variations and closer to the coast the influence of marine water (Baltic Sea) is detected in the shallow samples. Several samples from Forsmark show a possible Littorina Sea water influence which is much stronger at Forsmark compared with data from the Simpevarp area. Only a few samples at depth from Forsmark indicate a Glacial-Brine component. The deviation calculations in the M3 mixing calculations show potential for organic decomposition/calcite dissolution in the shallow waters. Indications of ion exchange and sulphate reduction have been modelled. These M3 results support the initial evaluation of primary data and general modelling results described in previous chapters.

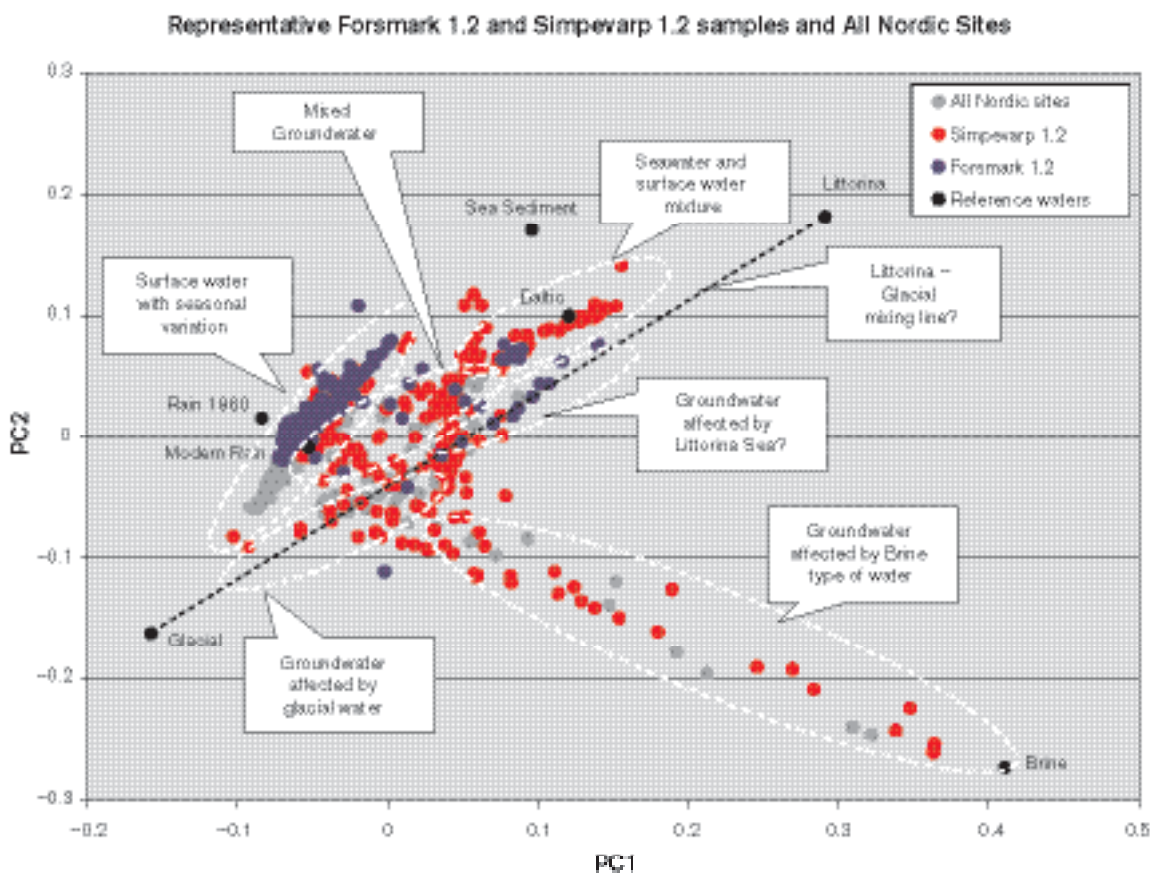


Figure 9-57. PCA modelling of the representative Forsmark (blue dots), Simpevarp area (red dots) and Nordic data (grey dots). The reference waters used in the modelling are shown and the possible influences from different end-members on the samples are indicated.

9.5.8 Visualisation of the groundwater properties

Measured Cl content and the calculated M3 mixing proportions based on representative samples are shown for two core boreholes within the modelling domain in Figure 9-58. The results for all the boreholes are shown in Appendix 4 in /SKB, 2005b/. The purpose of the plots is to show the water type, changes with depth, and to facilitate comparison of the hydrochemical results with the hydrogeological results. Due to the fact that the hydrogeologists use only 4 reference waters, the marine components (Littorina and Sea Sediment reference waters) were combined and referred to as Marine water.

The 3D/2D visualisation of the Forsmark Cl values was performed using the Tecplot code. Figure 9-59 shows the 3D interpolation and 2D visualisation of Cl at the sampling points for all the samples (both representative and non-representative samples) and for the M3 mixing proportions. The relatively few observations in the 3D space result in uncertainties; only in the near-vicinity of the observations are the uncertainties low. There are relative few samples from depths larger than 600 m and the interpolation below this depth is therefore associated with large uncertainties. However, the interpolations can still be used to indicate the major occurrence of the different water types at the site. For example: a) Meteoric water is dominant in the north-west part and in the central part of the cutting plane, b) Marine water is found towards the coast in the east part of the cutting plane, c) Glacial influences are found in the deeper part of the boreholes KFM02A and KFM03A. The glacial component found in the NW is due to cold water influences in some of the shallow samples, and d) Brine type water is increasing with depth.

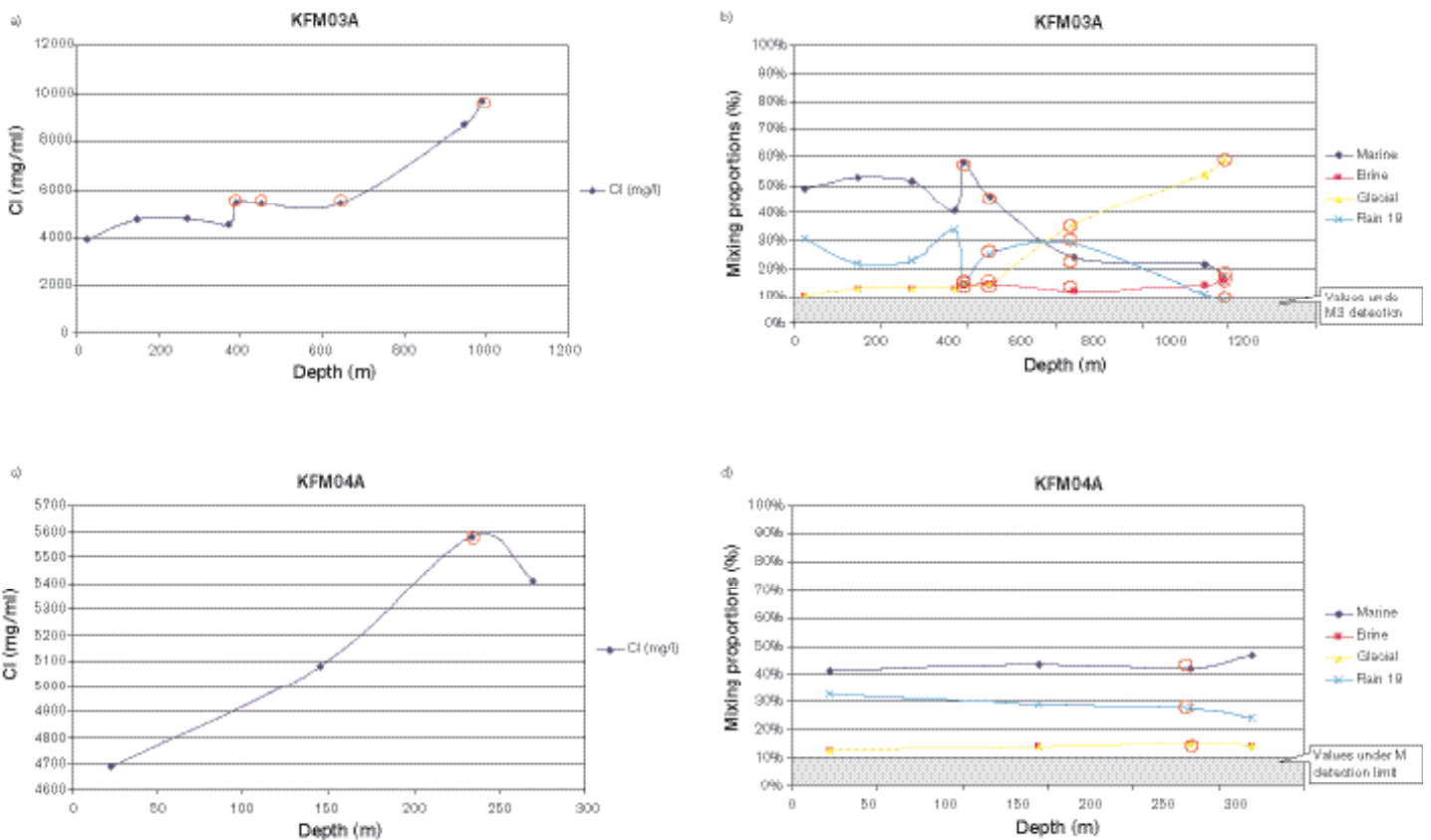


Figure 9-58. (a) and (b) scatter plots of the Cl content and mixing proportions with depth for borehole KFM03A. (c) and (d) scatter plots of the Cl content and mixing proportions with depth of borehole KFM04. The samples with red circles indicate representative samples. A mixing proportion of less than 10% is regarded as being under the detection limit of the M3 method and is therefore shaded. The mixing proportions have an uncertainty range of ± 0.1 mixing units. (The colours for the four mixing proportion plots need to be explained.)

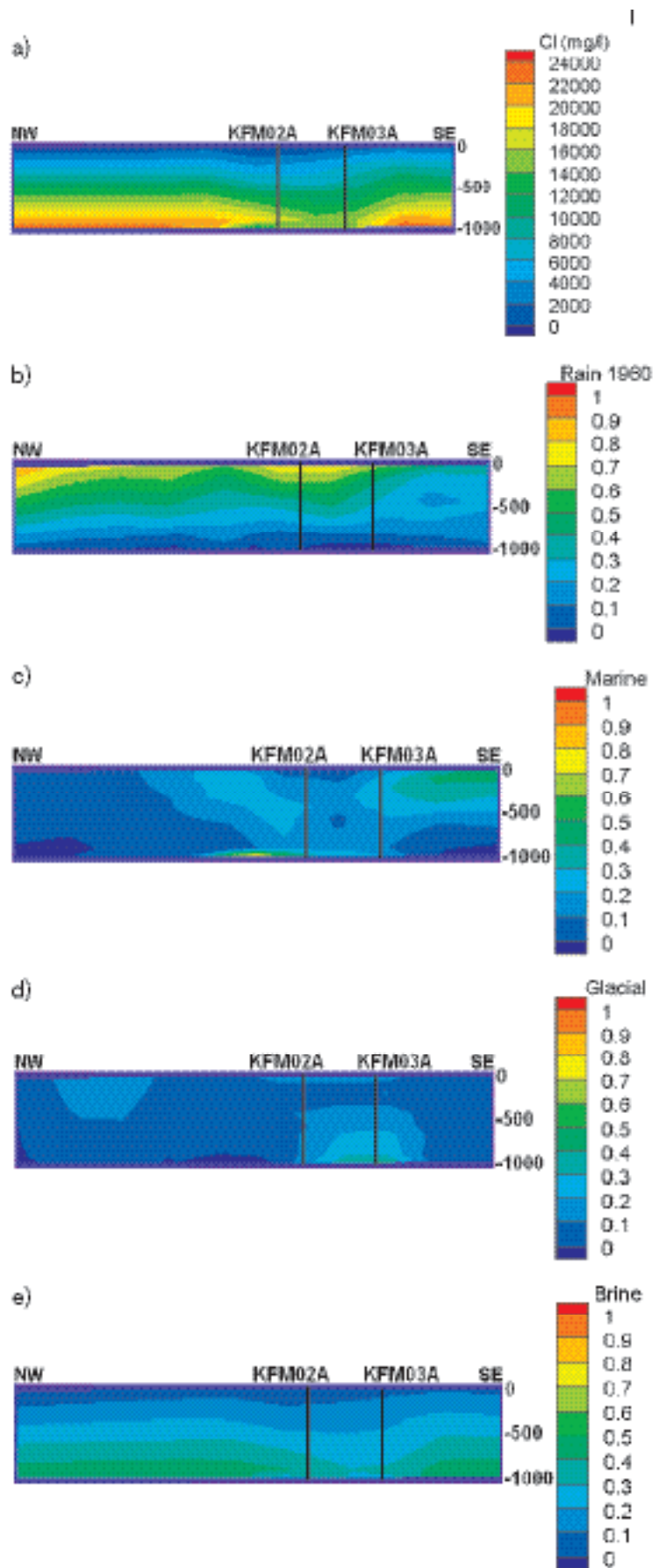


Figure 9-59. 3D interpolation and 2D visualisation of the groundwater properties along the NW-SE cutting plane (for orientation see Figure 9-1). (a) Cl interpolation, Figures b, c, d, and e show the mixing proportions for the water types Rain 1960, Marine, Glacial and Brine. The elevation is in metres.

Figure 9-60 show an example of the comparison between the different mixing proportions calculated with the M3 versus the M4 codes. The M4 calculation code (cf. Appendix 3 in /SKB, 2005b/) performs the mixing calculations in multidimensional space and therefore the uncertainties associated with the mixing proportion calculations can be reduced. For the local PCA model, 295 samples can be calculated with M3 but only 106 samples with M4. A higher accuracy is obtained with the M4 calculation, but there is the risk of loss of information through use of a reduced number of observations. Further comparisons between the codes will be conducted in future phases of the project.

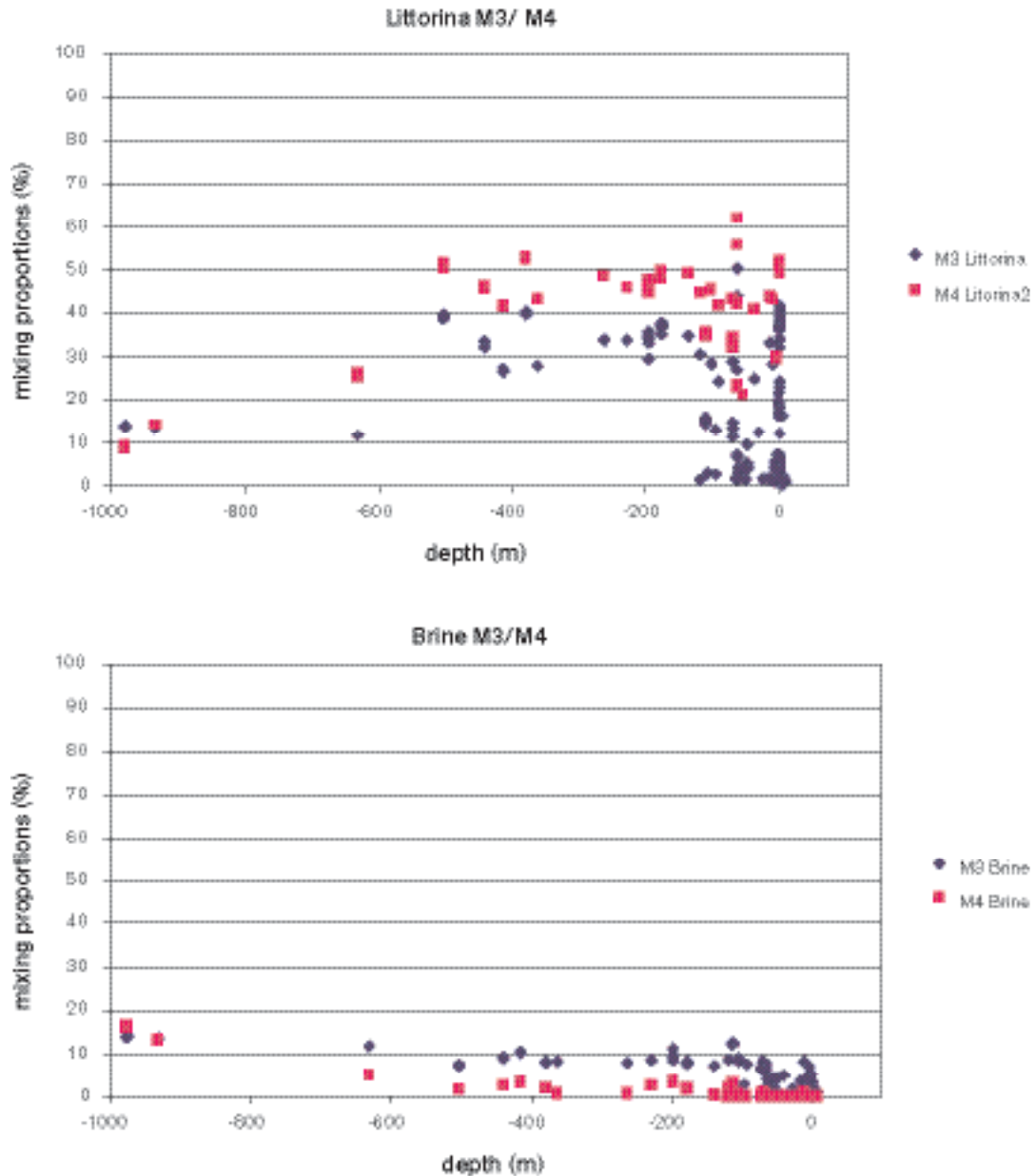


Figure 9-60. Comparison of the Littorina Sea and Brine mixing proportions obtained with M3 versus M4 codes.

9.5.9 Conclusions used for the site descriptive model

Descriptive and modelled observations are included in the hydrogeochemical site descriptive model (see, Chapter 11) and they are fundamental to the overall hydrochemical understanding of the site. The most important features, summarised in previous sections and described in detail in /SKB,2005b/, are highlighted below. The final task of the hydrogeochemical evaluation is to assess that the site meets the SKB hydrogeochemical suitability criteria. These parameters are discussed in the last part of this subsection.

Descriptive observations – Main elements

- General depth trends show increasing TDS with depth; also there is an increase in Ca/Na and Br/Cl ratios.
- Three main depth-related hydrochemical subdivisions can be recognised: a) shallow (0–150 m) dilute groundwaters (< 1,000 mg/L Cl), b) intermediate (~ 150–600 m) brackish groundwaters (5,000–6,000 mg/L Cl), and c) deep (> 600 m) saline groundwaters (~ 10,000 mg/L Cl).
- The dilute shallow region is characterised mainly by Na-HCO₃-type groundwaters, but subordinate Na-HCO₃(SO₄) to Na(Ca)-HCO₃-Cl(SO₄) groundwater types also occur.
- The intermediate groundwater region is dominated by Na(Ca, Mg)-Cl(SO₄) to Na-Ca(Mg)-Cl(SO₄) groundwater types. A strong Littorina Sea signature is apparent in this brackish region.
- The deep groundwater region comprises Na-Ca-Cl to Ca-Na-Cl groundwater types.
- The marked deviation of the deep groundwater from all other groundwaters can be explained by increased mixing with an older deep saline component of a non-marine or non-marine/old marine origin. This is clearly shown by the Na/Ca/Mg and Br/Cl ratios versus Cl content. Only one deep groundwater sample so far exists, that from borehole KFM03A at 980–1,001 m. This borehole is characterised by deformation zones A4, A7 and B1 within the depth interval of 350–550 m. It would seem that this structural interval hydraulically separates brackish groundwaters partly of old and/or new marine origin, from deeper increasingly saline groundwaters of non-marine/old marine origin.
- Compared with other Fennoscandian sites, Forsmark shows close similarities with the nearby Finnsjön and SFR sites and also with the Olkiluoto site in Finland. The similarity with Olkiluoto, especially down to 500 m, is particularly relevant as the brackish groundwaters at that site also have a strong Littorina Sea signature.
- The Littorina Sea signature at Forsmark is indicated mainly by increases in Mg and SO₄, both of which decrease rapidly below 500–600 m depth. A marine origin is further supported by the Br/Cl ratios. Although HCO₃ decreases markedly below 150 m depth, it persists at around the 100 mg/L level within the Littorina-type brackish groundwaters before dropping to very low values at depths greater than 500 m.

Descriptive observations – Isotopes

- The stable isotope data plot on or close to the Global Meteoric Water Line (GMWL) indicating a meteoric origin for the Forsmark waters. Values range from $\delta^{18}\text{O} = -13.6$ to -8.4‰ SMOW and $\delta\text{D} = -98.5$ to -66.1‰ SMOW with the most negative isotopic signatures (i.e. cold climate meteoric input) corresponding to the deepest groundwater sampled at 980–1,001 m.
- Plotting oxygen-18 against chloride further details the three distinct groups of groundwaters present at Forsmark: a) shallow, dilute groundwaters with a narrow range of $\delta^{18}\text{O}$ (-12 to -10‰ SMOW), close to present day precipitation, b) a wider range of values ($\delta^{18}\text{O} = -12$ to -8‰ SMOW) for the more brackish groundwaters, where the larger variability in $\delta^{18}\text{O}$ is explained by mixing between glacial and Littorina Sea (characterised by heavier isotope values) groundwaters, and c) the deepest outlier ($\delta^{18}\text{O} = -13.6$ SMOW) representing the most saline groundwater.

- One problem in using tritium for the interpretation of near-surface recharge/discharge is its variation in recharge water over time. This implies that near-surface groundwaters with values around 15 TU can be 100% recent, or a mixture of old meteoric (tritium free) water, and also a small portion (10%) of water from the late fifties and early sixties at the height of the atmospheric nuclear bomb tests.
- Below 200 m depth, tritium values under 3 TU are detected for all samples. For the borehole sections sampled below 300 m there are samples with no detectable tritium, but in two cases a few tritium units have been measured in the last sample collected in the time sequence of sampling. One of the near-surface samples KFM03A (0–46 m) shows a very high tritium content of 41 TU indicative of a significant portion of recharge from the sixties or seventies when tritium contents were much higher than at present. There is therefore the possibility that the observed tritium values in some of the deeper sampled borehole sections reflect some contamination by these tritium-enhanced waters entering into water-conducting fracture systems during open-hole borehole activities.
- Tritium contents in surface and near-surface waters need to be carefully interpreted. For example, the measured tritium contents in the precipitation and Baltic Sea water at Forsmark may incorporate some tritium locally produced by the nuclear power plants, i.e. that emitted as vapour to the atmosphere and that contained in the cooling water discharged to the Baltic Sea.
- The plot of tritium versus ^{14}C for surface waters from Forsmark shows that most lake and stream waters have higher ^{14}C values compared with Baltic Sea waters, whereas the tritium values range from 10–15 TU for all three water sources, although generally there is higher tritium in the Baltic Sea waters (due to reservoir effects).
- The tritium-free groundwaters from Forsmark show ^{14}C values in the range 14–25 pmC and these waters have generally low HCO_3^- contents (< 150 mg/L) and $\delta^{13}\text{C}$ values between –10 and –5‰. A plot of ^{14}C (expressed as pmC) versus $\delta^{13}\text{C}$ ‰, shows that groundwaters from the percussion and cored boreholes indicate a mixing trend between: a) HCO_3^- -rich waters with low $\delta^{13}\text{C}$ and high ^{14}C content, and b) deeper groundwaters with lower HCO_3^- contents, higher $\delta^{13}\text{C}$ values and lower ^{14}C .
- The groundwaters showing the lowest ^{14}C values have chloride contents ranging from 4,500–5,500 mg/L; these indicate marine signatures, i.e. they represent waters with a dominant Littorina Sea component. (Note: no ^{14}C analyses are available from the deep saline groundwaters). In terms of ‘relative age’, the measured pmC values indicate 11,000–16,000 years which is significantly older than the Littorina Sea period. This can be explained by an addition of older bicarbonate, probably by dissolution of older carbonate and/or mixing with glacial water (supported by low $\delta^{18}\text{O}$ in at least some of these groundwaters).
- The $\delta^{34}\text{S}$ data have a wide range (–11 to +30‰ CDT) indicating different sulphur sources for the dissolved SO_4 . For the surface waters (lake and stream waters) the SO_4 content is usually below 35 mg/L and the $\delta^{34}\text{S}$ is relatively low but variable (–1 to +11‰ CDT), with most of the samples in the range 2 to 8‰ CDT. These relatively low values indicate atmospheric deposition and oxidation of sulphides in the overburden as being the origin for the SO_4 . The Baltic Sea samples cluster around 20‰ CDT with some less saline Baltic samples showing lower $\delta^{34}\text{S}$ values resulting from inmixing of surface water.
- The deeper groundwaters show $\delta^{34}\text{S}$ values in the range +12 to +26‰ CDT where all samples with SO_4 contents greater than 250 mg/L show $\delta^{34}\text{S}$ values higher than +20‰ CDT. Such values are usually interpreted to result from sulphate-reducing bacterial activity in the bedrock aquifer.
- The Cl versus $\delta^{34}\text{S}$ plot shows a clear trend with higher $\delta^{34}\text{S}$ values for groundwaters with higher salinities than present Baltic Sea waters (2,800 mg/L Cl). If the $\delta^{34}\text{S}$ values in the marine groundwaters are modified by sulphate-reducing bacteria during closed conditions then a clear trend of more positive $\delta^{34}\text{S}$ values with decreasing sulphate content should be the result. This is not seen and therefore several processes need to be considered.
- The relatively few fracture calcites so far analysed for Sr-isotopes show values below 0.718 supporting that they are not precipitated from today’s groundwater and that calcite dissolution has had little influence on the Sr-isotope ratios in the groundwater.

- Plotting $\delta^{37}\text{Cl}$ against chloride shows that most of the surface, near-surface and Baltic Sea waters have values within the range -0.28 to $+0.34\text{‰}$ SMOC. The surface waters have the greatest spread (-0.6 to $+2\text{‰}$ SMOC) where most of the samples are within the interval -0.2 to $+0.5\text{‰}$ SMOC. The majority of the Baltic Sea samples values are close to 0‰ SMOC or slightly higher (up to $+0.3\text{‰}$ SMOC); a few samples show also lower values down to -0.6‰ SMOC.
- $\delta^{37}\text{Cl}$ in groundwaters from the cored and percussion boreholes are between -0.2 and $+0.6\text{‰}$ SMOC and demonstrate no relation with increasing chloride content. Given the analytical uncertainty of around $\pm 2\text{‰}$ SMOC, the groundwater values correspond to a slight emphasis on a water/rock origin.
- The presence of uranium in surface and near-surface waters is characterised by values between 0.05 and $28 \mu\text{g/L}$. Large variations in uranium content in surface waters are common and are usually ascribed to various redox states and various contents of complexing agents, normally bicarbonate.
- Uranium versus bicarbonate for the waters shows no clear trend although there is a tendency of higher uranium contents in the surface and near-surface groundwaters associated with increasing bicarbonate up to 400 mg/L . For the few near-surface waters with higher bicarbonate contents the uranium tends to decrease, which may be due to very low redox potential in these waters caused by the microbial reactions producing the bicarbonate (probably to a large extent sulphate reducers).
- Uranium versus chloride shows that the highest uranium contents are found in the waters with chloride values around $5,000$ – $5,500 \text{ mg/L}$, i.e. the brackish groundwaters dominated by a Littorina Sea water component.
- These high but variable uranium contents at Forsmark are accompanied by increased ^{226}Ra and ^{222}Rn indicating that uranium and radium along the fracture pathways have been mobilised to various degrees by the slowly descending Littorina Sea waters. One possible scenario is that the glacial melt water is accompanied by oxidised uranium into the (near-surface?) deformation zones and subsequently easily remobilised by the reducing but bicarbonate (and DOC) rich Littorina Sea water. The mobilised uranium was then transported to greater depths during the density turnover. The reducing character of the Littorina Sea water is supported by, for example, the high Mn^{2+} contents (1 – 3 mg/L ; resulting from Mn-reducing bacteria) recorded for most of the uranium-rich water samples.
- The primary origin of the oxidised and remobilised uranium may have been the uranium mineralisations found at several localities in Uppland. For example, pitchblende vein fillings in skarn have been documented only some kilometres from the Forsmark site.

Descriptive observations – Microbes, colloids and gases

Three boreholes were sampled at six different depths and the data were used in a two-dimensional descriptive biogeochemical model.

- Redox potentials in the boreholes differed from -140 mV to -250 mV .
- At the shallowest depths with the relatively high redox potential, iron- and manganese-reducing bacteria dominated.
- The number of methanogens was high in KFM02A at 512.5 m .
- Sulphate-reducing bacteria together with acetogens dominated at one of the deep levels (KFM03A at 943 m).
- The abundance and activity of microbial species in the Forsmark boreholes seem to be closely correlated with the redox potential.
- A high percentage of cultivable microorganisms with the MPN method was found in KFM01A at 115.4 m (iron- and manganese-reducing bacteria) and in KFM03A at 943 m (sulphate-reducing bacteria and acetogens).

- An explanation for the different amounts of cultivable cells could be differences in flow and mixing of groundwaters at the sampled sites. Thorough mixing of two or more groundwaters resulting in a gradient of different redox pairs would promote growth and activity of microorganisms with a suitable metabolism.
- The filtration data available seems to agree with the numbers of colloids earlier reported from Äspö and Bangombé, Gabon /Laaksoharju et al. 1995b; Pedersen, 1996/. The new sampling and filtering methods seemed to work well since the amounts of calcium carbonates were very low. This suggests a rethinking of the content of sulphur colloids since they might have initially existed as colloids present in the groundwater and then probably as iron sulphides. The silicon values from KFM01A, 115.4 m most likely represent sampling artefacts.
- The fractionation data show that there should not be any colloids in the size range $> 1,000$ D but $< 5,000$ D. Although this is in contradiction to the filtration results, it could be closer to the truth. There are no sulphur values reported by this method; it would be interesting to carry out a comparison with the filtration method, since the presence of iron sulphides could be an explanation for the low sulphide values found in groundwater, even if SRBs (sulphate-reducing bacteria) are present.
- Data for the numbers of particles could increase the value of colloid analyses by making it possible to calculate the number of binding sites for radionuclides in the different colloid fractions.
- Comparison of the two methods, filtration and fractionation, needs to be further evaluated.
- Up to 12 gases were analysed: helium, argon, nitrogen, carbon dioxide, methane, carbon monoxide, oxygen, hydrogen, ethylene, ethene, ethane and propane. So far, the amounts of gas data are limited and exclude any substantive analysis of the impact of gases on geochemistry and microbiology, but there is a clear trend with increasing volumes of gas per unit volume of groundwater towards depth.
- The available gas data for the Forsmark area show that the gas content is in the same order of magnitude as in most of the Nordic sites studied.
- The gases are probably mostly mantle-generated.
- Gases are probably oversaturated in relation to atmospheric pressure but not at depth.

Modelled observations – Mass balance modelling with PHREEQC

Groundwaters in Forsmark can be divided into three groups based on their salinity.

(1) **Saline groundwaters** with a brine signature (only 1 representative sample: #8152). Mixing between Brine and Glacial end members is responsible, directly or indirectly, for most of their chemical content, especially for Cl concentrations higher than 7,000 mg/L. A Littorina component is absent or in a very low percentage. Their alkalinity is low, and controlled by equilibrium with calcite. pH is controlled by calcite equilibrium and, possibly, by reactions with aluminosilicate minerals. These old mixed waters tend, with time, to re-equilibrate with the complex mineral assemblage identified as fracture fillings at Forsmark. Both mass balance and thermodynamic calculations predict low reaction mass transfers between these waters and the aluminosilicates, although more work is needed, due to the wide variety of aluminosilicates detected. Fast cation exchange reactions are also possible, but, in groundwaters with long residence times, these exchange processes may cause irreversible changes in the clay minerals /Pitkänen et al. 1999/, favouring an apparent solubility control.

The redox state is mainly controlled by the sulphur system. The existence of active sulphate-reduction processes and sulphide precipitation is in agreement with the presence of high numbers of sulphate-reduction bacteria (SRB) detected in the microbiological analysis.

Finally, the high contribution of the Glacial end member points to the forced introduction of glacial melt water in Forsmark which reached at least a depth of 1,000 m. This penetration depth is greater than at Olkiluoto, but similar to that reported in other Swedish sites /Puigdomenech, 2001/.

(2) **Brackish groundwaters** with an important and relatively constant Littorina Sea component. These are widely distributed in the Forsmark area, from very shallow levels (discharge areas?) to 500 m depth. A combination of slow and fast chemical reactions has influenced the mixed groundwaters. Calcite re-equilibrium and Ca-Na exchange reactions are the kinetically most favoured processes. Re-equilibrium with different aluminosilicates is also possible, although the mass transfers involved are low even when “forcing” pure equilibrium situations.

As in other Littorina-rich groundwaters /Pitkänen et al. 2004a/, the iron concentration is variable, but usually high, whereas dissolved sulphide, although detectable, is present in very low concentrations. This suggests that sulphate reduction is of minor importance (in agreement with microbial studies) and that iron does not have a strict solubility limit through sulphide precipitation. In this situation, the good results provided by the sulphur redox pairs in characterising the redox state of these groundwaters deserve further attention.

The penetration depth of Littorina Sea waters (500 m) is greater than presumed in the previous work (Forsmark 1.1; /Laaksoharju et al. 2004a/), and slightly more than that deduced for Olkiluoto /Pitkänen et al. 1999, 2004a/. However, this penetration depth appears to be similar to that calculated for the Äspö area /Puigdomenech, 2001/.

(3) **Non-saline dilute groundwaters** in Forsmark cover a wide range of chloride concentrations and show different trends (Ca-Na-HCO₃, Na-HCO₃-Cl, Na-Cl-HCO₃, etc). The compositional character of the most dilute groundwaters is controlled by weathering reactions (dissolution of calcite, plagioclase, biotite, sulphides, etc) induced by atmospheric and biologically produced dissolved gases (CO₂ and O₂). More concentrated waters show an additional and variable mixing contribution with a marine component (some of them with a clear modern Baltic Sea signature) that gradually promotes Na-Ca exchange and the precipitation of calcite.

Modelled observations – Mixing modelling with M3 and drilling impact study (DIS) modelling

M3 modelling helped to summarise and understand the data in terms of origin, mixing proportions and reactions.

The surface meteoric type waters show seasonal variations and closer to the coast the influence of marine water is indicated. Several samples from Forsmark show a possible Littorina Sea water influence; this signature is much clearer at Forsmark than in data from the Simpevarp area. Only a few samples at depth from Forsmark indicate a Glacial-Brine component. The deviation calculations in the M3 mixing calculations show the potential for organic decomposition/calcite dissolution in the shallow waters. Indications of ion exchange and sulphate reduction have been modelled. These M3 results support the initial evaluation of primary data and general modelling results.

The 3D/2D visualisations indicate that meteoric water is dominant in the northwest part and in the middle part of the site. Marine water is found towards the coast in the eastern part of the site. Glacial influence is found in the deeper part of the boreholes KFM02A and KFM03A. A brine type water component increases with depth.

DIS evaluation can help to judge the representativeness of the sampled data. The section 509–516 m in KFM02A was investigated and the results showed that pumping should have continued further in order to remove an additional 12.6 m³ water still influenced by flushing water contamination. The study identified that there are uncertainties in the dosing and control of the uranine during the drilling process.

Hydrochemical suitability criteria

The modelling indicates that the groundwater composition at repository depths is such that the representative samples from KFM02A: 509–516 m and KFM03A: 448–453 m can meet the SKB chemical suitability criteria (Table 9-3) for Eh, pH, TDS, DOC and Ca+Mg (see /Anderson et al. 2000/).

Table 9-3. The hydrochemical suitability criteria defined by SKB are satisfied by the analysed values of the representative samples KFM02A: 509–516 m and KFM03A: 448–453 m.

	Eh (mV)	pH (units)	TDS (g/L)	DOC (mg/L)	Colloids (mg/L)	Ca+Mg (mg/L)
Criterion	< 0	6–10	< 100	< 20	< 0.5	> 4
KFM02A 509–516 m	–140	7.0	9.2	2.1	< 0.1	1,160
KFM03A 448–453 m	–250	7.5	9.2	1.2	< 0.1	1,187

9.6 Evaluation of uncertainties

At every phase of the hydrogeochemical investigation programme – drilling, sampling, analysis, evaluation, modelling – uncertainties are introduced which have to be accounted for, addressed fully and clearly documented to provide confidence in the end result, whether it will be the site descriptive model or repository safety analysis and design /Smellie et al. 2002/. Handling the uncertainties involved in constructing a site descriptive model has been documented in detail by /Andersson et al. 2002a/. The uncertainties can be conceptual uncertainties, data uncertainties, spatial variability of data, chosen scale, degree of confidence in the selected model, and error, precision, accuracy and bias in the predictions. The results of the different evaluations and modelling carried out within hydrogeochemistry are summarised in Chapter 11. Many of the uncertainties are difficult to judge, since they are results of different steps ranging from expert judgement to mathematical modelling and not result of a single model, such as in hydrogeology. Some of the identified uncertainties recognised during the modelling exercise are discussed below.

The following data uncertainties have been estimated, calculated or modelled for the Forsmark data; these are based on models used for the 1.1 model versions and based on the Äspö modelling where similar uncertainties are believed to affect the present modelling:

- Temporal disturbances from drilling may be ± 10 –70% (cf. DIS modelling in Appendix 4 in /SKB, 2005b/).
- Effects from drilling during sampling is < 5%.
- Sampling; may be ± 10 %.
- Influence associated with the uplifting of water may be ± 10 %.
- Sample handling and preparation; may be ± 5 %.
- Analytical error associated with laboratory measurements is ± 5 % (the effects on the modelling were tested in Appendix 1 in /SKB, 2005b/).
- Mean groundwater variability during groundwater sampling (first/last sample) is about 25%.
- M3 model uncertainty is ± 0.1 units within 90% confidence interval (the effects on the modelling were tested in Appendix 4 in /SKB, 2005b/).

Conceptual errors can occur in, for example, the palaeohydrogeological conceptual model. This occurrence and influence of old water end members in the bedrock can only be indicated by using certain element or isotopic signatures. The uncertainty therefore generally increases with the age of the end member. The relevance of an end member participating in groundwater formation can be tested by introducing alternative end member compositions or by using hydrodynamic modelling to test if old water types can reside in the bedrock during prevailing hydrogeological conditions. In this model version, a measure of validation is obtained by comparison with hydrogeological simulations.

Uncertainties in the PHREEQC code depend on which code version is being used. Generally the analytical uncertainties and uncertainties concerning the thermodynamic data bases are of importance (in speciation-solubility calculations). Care also is required to select mineral phases which are realistic (even better if they have been positively identified) for the systems being modelled.

These errors can be addressed by using sensitivity analyses, alternative models and descriptions. A sensitivity analysis was performed concerning the calculations of activity coefficients in waters with high ionic strength and also the uncertainties of the stability diagrams and redox modelling are discussed in Appendix 3 in /SKB, 2005b/.

The uncertainty due to 3D interpolation and 2D/3D visualisation depends on various issues, i.e. data quality, distribution, model uncertainties, assumptions and limitations introduced. The uncertainties are therefore often site specific and some of them can be tested such as the effect of 2D/3D interpolations. The site-specific uncertainties can be tested by using quantified uncertainties, alternative models, and comparison with independent models such as hydrogeological simulations.

The discrepancies between different modelling approaches can be due to differences in the boundary conditions used in the models or in the assumptions made. The discrepancies between models should be used as an important validation and confidence building opportunity to guide further modelling efforts. In this work, the use of different modelling approaches starting from manual evaluation to advanced coupled modelling can be seen as a tool for confidence building. The same type of process descriptions independent of the modelling tool or approach increases confidence in the modelling.

9.7 Comparison between the hydrogeological and hydrogeochemical models

Since the understanding of hydrogeology and hydrogeochemistry are based on the same geological and hydrodynamic properties, these two disciplines should complement and mutually sustain each other when describing/modelling the groundwater system. Testing such an integrated modelling approach was the focus of a SKB project with international participation (Task 5) based on the Äspö HRL /Wikberg 1998; Rhén and Smellie, 2003/. The advantages with such an approach were identified as follows:

- Hydrogeological models will be constrained by an additional independent data set. If, for example, the hydrogeological model, which treats advection and diffusion processes in highly heterogeneous media, cannot reproduce the presence of Meteoric water at a certain depth and the hydrogeochemical data does, then the model parameters and/or processes have to be revisited.
- Hydrogeological models are fully three dimensional and transient processes such as shoreline displacement and variable-density flow can be treated, which means that the spatial variability of flow-related hydrogeochemical processes can be modelled, visualised and communicated. In particular, the role of the nearby borehole hydraulic conditions for the chemical sampling can be described.
- Hydrogeochemical models generally focus on the effects of chemical reactions on the groundwater composition rather than on effects of transport. An integrated modelling approach can describe flow directions and hence help to understand the origin of the groundwater. The turnover time of the groundwater system can indicate the age of the groundwater and, knowing the flow rate, can be used to indicate the reaction rate. The groundwater chemistry is a result of reactions and solute transport, and therefore only an integrated description can be used to correctly describe the measurements.
- By comparing two independent modelling approaches, a consistency check can be made. As a result greater confidence in active processes, geometrical description and material properties can be gained.

The current 1.2 modelling has further developed the comparison and integration between hydrochemistry and hydrogeology. The conceptual model for groundwater flow is a double porosity description, with flow taking place in a connected fracture network and with immobile water in the rock mass between the flowing fractures. Solutes can access the immobile water through diffusion into dead-end fractures and by matrix diffusion. The salinity of the water implies that density driven flow needs to be considered. Thus, salt both affects the groundwater flow characteristics in the mobile water phase, and may diffuse into the immobile water phase. Conservative and reactive tracer transport as well as transport of water types can be modelled, but reactive tracer transport has not

been considered in the hydrogeological modelling for Forsmark 1.2, see Chapter 8. The hydrogeological model can thus provide predictions of the groundwater components and isotopes, such as Cl, ^{18}O and ^2H , in the connected rock matrix and in the flowing groundwater. It can also be used for dynamic predictions over time for the different water types (meteoric, marine, glacial and brine). Furthermore, the groundwater flow model can, independently from chemistry, predict the salinity features at any point within the modelled rock volume, and the predictions can be compared with direct hydrogeochemical measurements or calculations.

Figures 8-64 to 8-67 in Chapter 8 show comparisons between predicted and measured water-conservative constituents and M3 mixing fractions. The deviation between the predicted and measured values are generally higher in the model proposed by /Hartley et al. 2005/ compared with the model proposed by /Follin et al. 2005/. The uncertainties in the M3 mixing calculations are on the order of ± 0.1 (10%) of the reported value and a mixing proportion less than 0.1 (10%) is regarded to be under the detection limit of the method /Laaksoharju et al. 1999/. Because of this uncertainty in resolution, it is difficult to compare the hydrogeological simulations with M3 results for end-members of small mixing proportions. Therefore, water-conservative constituents were used for calibration in Forsmark model version 1.2. In the M3 modelling, the same water-conservative constituents were used to establish model uncertainties.

The difficulties encountered in the integration and comparison work between the two disciplines are also due to few water samples available from depth and from the bedrock volume between the deterministically modelled deformation zones. Because of the tight bedrock in Forsmark, water sampling has been possible only from larger zones with a transmissivity of at least $1 \times 10^{-8} \text{ m}^2/\text{s}$.

Compared with model version 1.1, great progress has been made in the integration work between hydrogeology and hydrochemistry. Hydrogeological modelling has shown that it is possible to simulate the observed water composition in the bedrock at Forsmark by assuming different initial conditions for Brine and Glacial end-members and boundary conditions of infiltration of Littorina and Sea water in accordance with the conceptual palaeohydrogeological model of the site (Figure 3-15). This gives support to the conceptual model used within the hydrogeochemical modelling work.

Integrated models will increase the understanding of the origin, transport, mixing and reactions processes in the groundwater and will also provide a tool for predicting future chemical changes due to climate changes. For the next versions of the site descriptive modelling, various conceptual models and processes have to be tested against measured hydrogeological and hydrogeochemical data. More specifically, the following hydrogeochemical aspects will be tested.

- Simulations with a local M3 model that includes samples only from Forsmark rather than using the current regional M3 model that includes all samples taken at Nordic sites.
- To consider only samples taken from the bedrock, in order to reduce the model scatter caused by the inclusion of samples taken in the overburden and at the surface.
- Effects of using new end-members, such as Meteoric before and after 1960 (high and low tritium), and to exclude the “Sea Sediment” end-member, with the purpose to search for end-members that fits both hydrogeological and hydrogeochemical simulations.
- A new way of calculating mixing proportions, the M4 method, which may reduce the uncertainties in the mixing calculations, since the contribution from insignificant end-members can be removed and the most suitable end-members can be tested.

10 Bedrock transport properties

The main objectives of the investigations and modelling of the transport properties of the bedrock are to provide parameters to the radionuclide transport calculations performed by Safety Assessment, and to present a description of the site-specific transport conditions that can be used to support the selection of processes and parameters in radionuclide transport models developed by Safety Assessment and others. In relation to Safety Assessment, the role of the site modelling is to describe the site-specific parameters and conditions; Safety Assessment may use other parameters, depending on the scenarios investigated. In addition, the results of the transport properties modelling are used as qualitative and/or quantitative input to transport modelling within site descriptive hydrogeological and hydrogeochemical modelling.

10.1 State of knowledge at previous model version

In model version 1.1, the lack of site-specific data on retention properties constituted the main limitation. However, porosity values were provided based on the geological model and an estimate on formation factors was given using a correlation between porosity and formation factor based on data from the Finnsjön study site.

Contrary to model version 1.1, flow-related transport parameters, such as transport resistance (F factor) and advective travel time, are not reported in model version 1.2. These types of results will be presented within a safety assessment context.

10.2 Modelling methodology and input from other disciplines

The process of site descriptive modelling of transport properties is described by /Berglund and Selroos, 2004/. Essentially, the description consists of the following three parts.

- Description of the rock matrix, fractures in the rock mass, and deformation zones, including relevant processes and conditions affecting radionuclide transport. The description should express the understanding of the site and provide evidence supporting the proposed model for radionuclide transport and retention. This can be achieved by e.g. process-based modelling of sorption processes and coupled geochemical and solute transport modelling.
- Retardation model: Identification and description of “typical” rock materials, rock mass fractures and deformation zones, including parameterisation.
- Transport properties model: Parameterisation of the 3D geological model and assessment of understanding, confidence and uncertainties.

The methods used within the transport programme of the site investigations produce primary data on rock matrix porosity, θ_m , effective diffusivity, D_e , and the linear equilibrium sorption coefficient, K_d . These retardation parameters are evaluated, interpreted and presented in the form of a retardation model; the strategy for laboratory measurements, data evaluation and development of retardation models is described by /Widestrand et al. 2003/. In the three-dimensional transport properties modelling, the retardation model is used to parameterise the various geological “elements” (rock matrix, rock mass fractures and deformation zones) in the site descriptive geological and/or hydrogeological models.

The development of retardation models relies to a large extent on interactions with other disciplines, primarily geology, hydrogeochemistry and hydrogeology. Specifically, geology provides lithological and structural models where the rock types, rock mass fractures and deformation zones are described, as well as the mineralogical compositions of intact and altered materials. Hydrogeochemical information is used as a basis for the selection of water compositions in laboratory measurements of retardation parameters. The development of the transport properties model requires close interaction with the development of the hydrogeological model; specifically,

correlations between properties of water-conducting structures and elements of the retardation model are investigated. Also, a consistency check between the conceptualisation and parameterisation of rock matrix diffusion for salt (in the hydrogeological models) and solutes (in the solute transport models) is performed.

10.3 Conceptual model with potential alternatives

The base case conceptual model of solute transport in discretely fractured rock comprises transport in mobile and immobile volumes, respectively. The mobile zones are fractures and deformation zones where groundwater flow and advective transport take place. Immobile zones mainly comprise the intact rock matrix, fracture surface and fracture filling materials, and fractures with stagnant water, where solutes can be retained from the mobile water /Berglund and Selroos, 2004/. A schematic illustration of such immobile zones in a fracture, based on experiences from Äspö HRL, is presented in Figure 10-1.

In the safety assessment framework, which provides the basis for identification of retention parameters in the site descriptive models, retention is assumed to be caused by diffusion and linear equilibrium sorption. These processes are reversible and are here referred to as retardation processes. It is further noted that in a safety assessment context, a broad international consensus exists between involved implementers and regulators concerning the retention mechanisms to consider /RETROCK, 2004/.

The above presented conceptual model is based on previous experience, and has been implemented in the evaluation of earlier tracer experiments at Äspö HRL, i.e. in the TRUE project /Winberg et al. 2000; Poteri et al. 2002/. The very sparse water-conducting fracture network encountered at repository depth below the gently dipping deformation zone ZFMNE00A2, see Chapter 8, and the rather tight rock matrix characterised by low diffusivity, may imply that the proposed conceptual model needs to be somewhat modified in order to be applicable for Forsmark conditions. Some parts of rock domain RFM029 can be described as connected and water-conducting fracture networks, whereas other parts are less amenable to a DFN description. One may hypothesise that transport in these discretely fractured rock masses takes place primarily through slow advection and

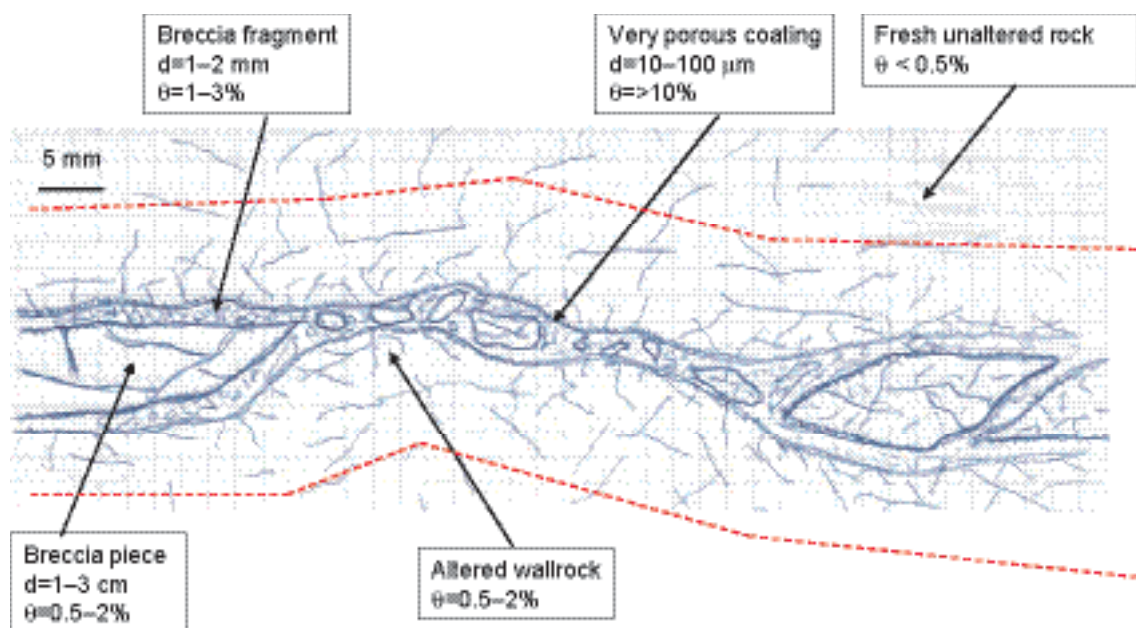


Figure 10-1. Schematic illustration of immobile volumes in a natural fracture (d and θ refer to the extent and porosity of the different volumes, respectively). Based on observations in /Andersson et al. 2002c/.

diffusion coupled with sorption on the rock surfaces. However, once a repository is built (outside the scope of this report), transport is likely to take place primarily through the tunnel system. The overall conceptual model of transport would then be from the canisters through the engineered system (back-filled tunnels and engineering damaged zone) to the first larger deformation zone and subsequently up to the surface.

For radionuclide retention, consideration of alternative representations of sorption (process-based sorption models) and additional retention processes (e.g., precipitation and co-precipitation) are of particular interest. However, no results from process-based modelling are provided in model version 1.2.

10.4 Description of input data

The evaluation of transport data available for Forsmark version 1.2 is presented in a supporting report /Byegård et al. 2005/. In the sections below, the supporting report is summarised.

10.4.1 Data and models from other disciplines

Geology

The following summary and evaluation of geological data of relevance for the transport modelling is based on the version 1.2 geological description, as presented in Chapter 5 and associated models and databases.

The major rock type in the candidate area is a medium-grained, biotite-bearing granite to granodiorite, metamorphic rock (rock code 101057). The focus is on rock domain RFM029 as it constitutes the major part of the local site. However, a few other domains are also of interest as indicated below. Thus, the domains considered comprise the following.

RFM029 = dominantly granite to granodiorite, metamorphic (84%), subordinate pegmatite (2%), fine- to medium grained granite (1%), fine- to medium-grained granodiorite, tonalite and granite (10%), amphibolite (3%).

RFM012 = dominantly granite to granodiorite, metamorphic (68%), subordinate fine- to medium-grained granodiorite, tonalite and granite (24%), pegmatite (4%), amphibolite (2%) and felsic to intermediate volcanic rock (2%).

RFM017 = dominantly tonalite to granodiorite, metamorphic, subordinate pegmatite and fine- to medium-grained granodiorite, tonalite and granite.

RFM018 = dominantly tonalite to granodiorite, metamorphic, subordinate granite to granodiorite, granodiorite, felsic to intermediate volcanic rock, amphibolite, fine- to medium-grained granodiorite, tonalite and granite.

The conceptual rock mass fracture model consists of four sub-vertical sets and one sub-horizontal set cf. Section 5.5. These sets are suggested based upon structural geometry data and partly upon their fracture fillings. The steeply dipping fracture sets trend in N-S, NE-SW, NW-SE and E-W. There is no consistent variation of fracture intensity with depth. However, the number of transmissive fractures intersected by the boreholes is much lower below 300 m depth. The four steeply dipping sets are probably part of a much larger deformation system that also includes structural lineaments. The latter consists of swarms of small fractures.

Most of the single fractures in the Forsmark area at depths larger than 100–150 m show low transmissivity, but still open and partly open fractures are mapped throughout the entire drill cores. It is therefore believed that the mineralogical composition of the fracture coatings is important as well as the presence or absence of an altered zone in the wall rock adjacent to the conductive fractures as these fractures constitute possible flow paths or more probable diffusion path ways. Wall rock alteration is not very common around the open fractures (according to mapping less than 8%) but around the fractures that are water conducting (based on flow log measurements) alteration seems to be much more common, although no figure is available. It is important to note and possibly also

to further investigate that the number of mapped open fractures is very large (272–1,125) compared with the fractures identified as water conducting by the flow log (a few tens of that number or even fewer). A more detailed evaluation of Bore map data, hydraulic tests and the flow logging should provide important input to the transport modelling as it is believed that not all fracture types are equally transmissive, cf. Chapter 8.

Concerning deformation zones four sets have been identified (cf. Chapter 5).

- Vertical and steeply, SW-dipping deformation zones that strike WNW-NW, and are dominated by sealed fractures. These zones initiated their development in the ductile regime but continued to be active in the brittle regime. On the basis of their length, both regional and local major zones are present. The model also includes one local minor zone, which has been recognised with high confidence, as well as subordinate zone segments that are situated close to, and are attached to, regional and local major zones. These segments are both local minor and local major in character.
- Vertical and steeply dipping deformation zones that strike NE and are also dominated by sealed fractures. These zones formed in the brittle regime and length estimates indicate that no zones are longer than 10 km. Two local minor zones, which have been recognised with high confidence, have also been modelled. Furthermore, the model includes two subordinate zone segments that are local minor in character, and are situated close to, and are attached to, two local major zones. A zone that does not extend to the surface has also been included.
- Vertical and steeply dipping deformation zones that strike NS and are also dominated by sealed fractures. These zones formed in the brittle regime and length estimates indicate that no zones are longer than 10 km. With the exception of one local minor zone, which has been identified with medium confidence, all zones have been recognised with low confidence. Relative to the other three sets, this set is of subordinate significance in the regional model volume.
- Gently SE- and S-dipping deformation zones that formed in the brittle regime and that, relative to the other sets, contain a higher frequency of open fractures. Length estimates indicate that no zones are longer than 10 km. However, due to truncation of their gentle dip, several of these zones fail to reach the surface inside the regional model volume.

For the retardation model, the hydraulically conductive parts of the zones are of greatest interest since not all geologically identified deformation zones are found to be hydraulically conductive. In addition, there is a significant heterogeneity observed among conductive zones. Based on the interpretations from the boreholes it has been possible to identify (and partly also to sample) three different sets of conductive deformation zones.

1. The NW trending zones characterised by ductile deformation (presence of mylonites) and altered wall rock as well as later brittle deformation. The water-conducting fractures are coated with chlorite and clay minerals \pm calcite \pm epidote. This type of zone type is intersected in boreholes HFM11 and HFM12 (Eckarfjärden deformation zone). However, it also includes the Singö deformation zone that was studied in older investigations at Forsmark.
2. The NE trending steep brittle deformation zones characterised by laumontite sealed brecciated wall rock with a few open fractures coated with laumontite \pm chlorite and calcite. This zone type is present e.g. in KFM05A. Results from the hydro tests indicate that this zone type has lower transmissivity than zone type 1 and 3. However, higher transmissivity closer to the surface may be expected.
3. The SE gently dipping brittle deformation zones characterised by a higher frequency of open fractures. The open water-conducting fractures are coated with chlorite and clay minerals \pm quartz \pm adularia \pm calcite. The wall rock is altered and often cataclastic. These are the zones with high transmissivities regardless of depth. This type of zone is e.g. present in KFM02A and KFM03A.

In addition, a superficial interval of sub-horizontal “fractures” is encountered in several boreholes in the upper 100–150 m, predominantly in the north-western part of the candidate area. Some of these features are found to be fully open and highly transmissive. Others are completely filled with gouge-like material or, if they are very close to surface, with fine grained sediments, in which cases they are of very low transmissivity. The explanation of these shallow sub-horizontal “fractures” and their possible relation to the set of deformation zones in group 3 is not fully resolved at present.

The gouge-like material in the shallow structures contains quartz, adularia, chlorite and mixed layer clays. The wall rock is altered.

Detailed information about the zones, such as flow patterns within the zone (e.g. channelling etc) and internal structure (e.g. amounts of soft and fine grained material and its structure in-situ), is not available for this model version.

Hydrogeochemistry

The hydrogeochemical modelling of the Forsmark area is based on data from the cored boreholes KFM01A–KFM04A and from the percussion boreholes HFM01–HFM19. The results are presented in Chapter 9 of this report.

Water of salinity close to the one measured at repository depth has been used for the diffusivity measurements. A water composition (described as type II below) was chosen, but only the major components (i.e., Ca^{2+} , Na^+ , Cl^- and SO_4^{2-}) were included for the diffusion experiments.

For the batch sorption experiments, the groundwater composition is considered to be more important, and four different groundwater compositions have therefore been selected, as follows:

- I. Fresh diluted Ca-HCO₃ water; groundwater now present in the upper 100 m of the bedrock, but also a water type that can be found at larger depths during late phases of glacial periods.
- II. Groundwater with marine character, Na-(Ca)-Mg-Cl (5,000 mg/L Cl); this water constitutes a large portion of the groundwaters found at 150 to 600 m depth at Forsmark and is assumed to originate, in part, from the Littorina stage of the postglacial Baltic Sea.
- III. Saline groundwater of Na-Ca-Cl type (5,400 mg/L Cl); this is a water with higher Ca and lower Mg than the type II water.
- IV. Brine-type water of very high salinity, Ca-Na-Cl type water with Cl content of 45,000 mg/L; during a glacial period, brine type waters can be forced to shallower levels than at present.

10.4.2 Transport data

Rock samples for the laboratory measurements were selected from KFM01A, KFM02A, KFM03A, KFM04A, KFM05A and KFM06A in accordance with /Widestrand et al. 2003/. In order to describe the heterogeneity of the retardation parameters and possible effects of stress release, rock samples were selected from different depths in the boreholes. The selection of samples from rock mass fractures and deformation zones has mainly been controlled by the indications of water flow, as recorded in flow logs.

The sample collection consist of about 320 rock samples, from the major rock types, rock mass fractures and deformation zones, but it also includes altered bedrock and minor rock types.

10.5 Evaluation of transport data

10.5.1 Methods and parameters

The different methods used in the laboratory programme are described in /Widestrand et al. 2003/. In the current model version, only results from methods for determining porosity, diffusion and specific surface area (BET /Brunauer et al. 1938/) are used.

The method used for determination of porosity consists of water saturation of the sample, followed by a drying step. The drying of the samples is done at a temperature of 70° C. This method thus differs from the porosity measurements done within the geology programme where a higher temperature is used.

The diffusivity is quantified through the formation factor, F_m , which is related to the diffusivity as $F_m = D_e/D_w$ (D_w is the free diffusivity in water). Formation factors are obtained from through-diffusion experiments and electrical resistivity measurements. The resistivity can be measured both

in laboratory experiments (where the rock samples are saturated with 1 M NaCl) and in borehole in-situ experiments. For obvious reasons, no saturation of the rock matrix with a known electrolyte can be done in in-situ experiments. In that case, the composition of the pore liquid must be estimated based on hydrochemical sampling and analysis, commonly assuming the same composition in the matrix as in the groundwater in neighbouring fractures. A further complication is that a lower salinity than 1 M NaCl, which is likely to be present in the pores in in-situ rock according to /Ohlsson and Neretnieks, 1997/, attributes a significant part of the conductivity to the surface ion mobility.

Measurements of specific surface area (BET) have been performed on site-specific materials according to the ISO 9277 standard method.

10.5.2 Porosity

The results of the porosity measurements are summarised in Table 10-1. A presentation on a detailed sample level is given in /Byegård et al. 2005/. The geological characterisation under a binocular microscope shows a great number of small cracks that are 3–15 mm in length and with a width of ≤ 0.5 mm, in both fresh and altered rock samples.

Different factors may affect the measured porosity. One factor is the alteration of the rock, another is the length of the rock sample. For this reason, samples with observed alteration were studied separately and an indication of increased porosity for these samples can be observed. The strongly altered episyenetic samples show, not very surprisingly, a very significantly larger porosity than all other rock types included in this study.

Table 10-1. Porosities (vol %) of different rock types from the Forsmark area (number of samples within parenthesis). Mean value \pm one standard deviation; in italic logarithmic scale (\log_{10} of the data).

Rock type (SKB code)	All rock samples (n)	Rock samples without visible cracks (n)
Granite, granodiorite and tonalite, metamorphic, fine- to medium-grained (101051)	0.30 ± 0.27 (30)	0.25 ± 0.11 (28)
	-0.60 ± 0.23 (30) only altered samples: 0.50 ± 0.51 (7)	-0.64 ± 0.17 (28) only altered samples: 0.30 ± 0.18 (5)
Granite to granodiorite, metamorphic, medium-grained, episyenetic samples excluded. (101057)	0.24 ± 0.12 (105)	0.22 ± 0.09 (95)
	-0.66 ± 0.17 (105) only altered samples: 0.31 ± 0.20 (18)	-0.68 ± 0.15 (95) only altered samples: 0.26 ± 0.20 (12)
Granite to granodiorite, metamorphic, medium-grained, episyenite (101057)	14 ± 6 (15)	No samples excluded
	1.05 ± 0.36 (15)	
Pegmatite, pegmatitic granite (101061)	0.42 ± 0.23 (3)	No samples excluded
	-0.41 ± 0.22 (3)	
Amphibolite (102017)	1.8 ± 4.0 (6)	0.21 ± 0.12 (5)
	-0.46 ± 0.76 (6)	-0.75 ± 0.28 (5)
Granodiorite, metamorphic (101056)	0.34 ± 0.21 (2)	No samples excluded
	-0.52 ± 0.28 (2)	
Felsic to intermediate volcanic rock, metamorphic (103076)	0.78 (1)	No samples excluded
	-0.11 (1)	

Sample lengths of 0.5, 1.0, 3.0, and 5.0 cm have been used. An effect of sample length on porosity has been observed and indicates that the measurement method gives an increase in measured porosity values with shorter sample lengths. The observation of increased measured porosity with shorter sample length is supported by earlier porosity measurements in connection with diffusion experiments /Johansson et al. 1997/. The statistics in Table 10-1 are based on all values resulting from all sample lengths.

10.5.3 Diffusion

Results from only a few samples have as yet been obtained from the through-diffusion experiments. The results indicate formation factors in the interval 1.0×10^{-4} to 1.5×10^{-4} for the granite, granodiorite and tonalite, metamorphic, fine- to medium-grained sampled at 555 m in KFM02A and for the granite to granodiorite, metamorphic, medium-grained sampled at 313 m in KFM01A. The granite to granodiorite, metamorphic, medium-grained sample from 281 m has a formation factor that is significantly higher than all other measured formation factors. This is not surprising, since this is a sample with episyenetic alteration, i.e., having a porosity of $\sim 10\%$. Any dependence of the measured diffusivity on sample length is difficult to observe with the relatively low number of sample used (cf. Figure 10-2).

Electrical resistivity is measured both in the laboratory and in situ. The results are reported in /Löfgren and Neretnieks, 2005/ and also summarised in /Byegård et al. 2005/. The comparison between laboratory resistivity measurements and through-diffusion measurements on samples from a similar location indicate a clear correlation between these measurements, possibly with a tendency of the formation factor from the through-diffusion experiments being somewhat lower than from the electrical resistivity measurements. However, the number of through diffusion measurements is too low to draw definitive conclusions. As expected, a tendency of increased formation factor with increasing porosity can be observed in the results.

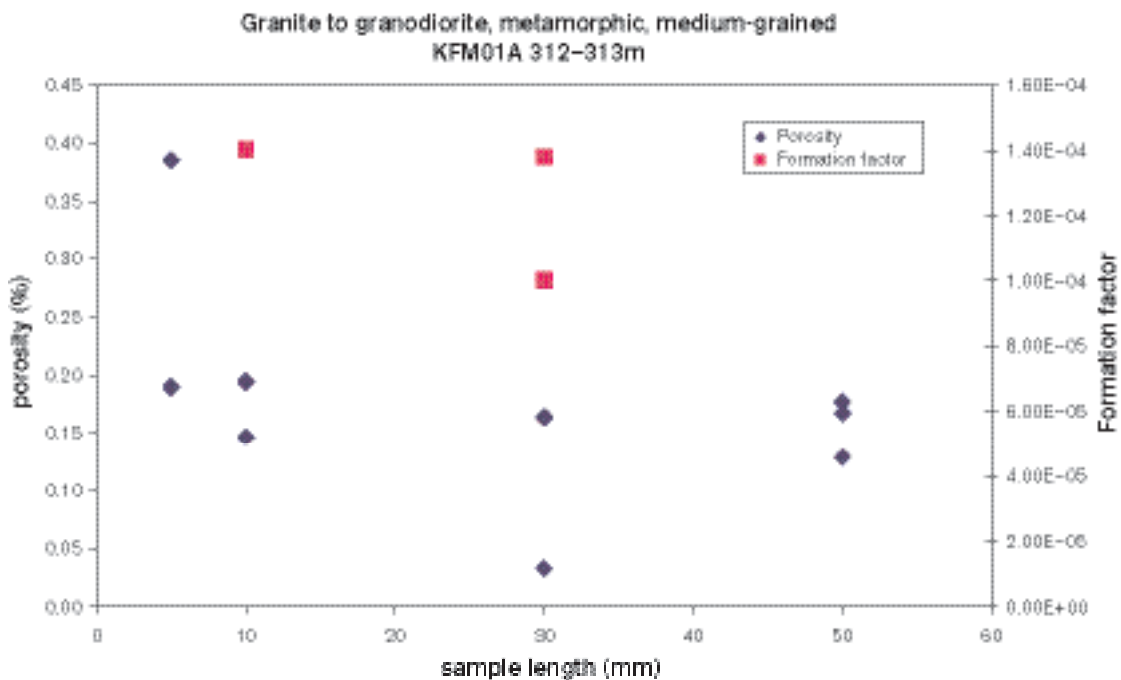


Figure 10-2. Measured porosity and formation factor (obtained by through diffusion experiment) as a function of the length of the sample used in the measurements.

For the in situ measurements, a selection of data has been made, so that only measurements that have a corresponding laboratory value, taken at the same location, are included in the analysis. A comparison indicates that the in situ measurements give a considerably lower formation factor than the corresponding laboratory measurements, see Figure 10-3 and Table 10-2. Furthermore, for the laboratory resistivity measurements, a tendency of increasing formation factor with increasing borehole depth is observed. No such increase can be observed for the in situ results, which could be interpreted as sampling causing stress release of the rock samples and a following “opening up” of the pores. According to this interpretation, the stress release of the laboratory samples should cause an overestimation of the porosity and the diffusivity. However, a slight contradiction to this interpretation is that no tendency of increased porosity with increased sampling depth can be observed for borehole KFM02A and that the general correlation of increasing porosity and diffusivity with sample depth is rather poor. A possible explanation is that rock stress is higher for borehole KFM01A than for KFM02A. This explanation is also supported by the rock mechanics analysis, see Chapter 6. Furthermore, in the rock mechanics analyses, comparisons are made of the characteristics of the P-wave measurements of the drill cores and the corresponding formation factor and porosity measurements. It is found that a good correlation of increased P-wave velocity and increased formation factor can be observed for the results on the drill cores. This is a further indication of sample disturbance caused by stress release of the drilled samples.

Comparing results for the different rock types, a slight tendency can be observed for the granite to granodiorite, metamorphic, medium-grained rock type having slightly higher formation factor than the granite, granodiorite and tonalite, metamorphic, fine- to medium-grained rock type. This is not unexpected since a more fine-grained rock type is likely to be less diffusive than a less fine grained. However, one should keep in mind that the difference is not very high and that there is a large spread between samples for each of these rock types.

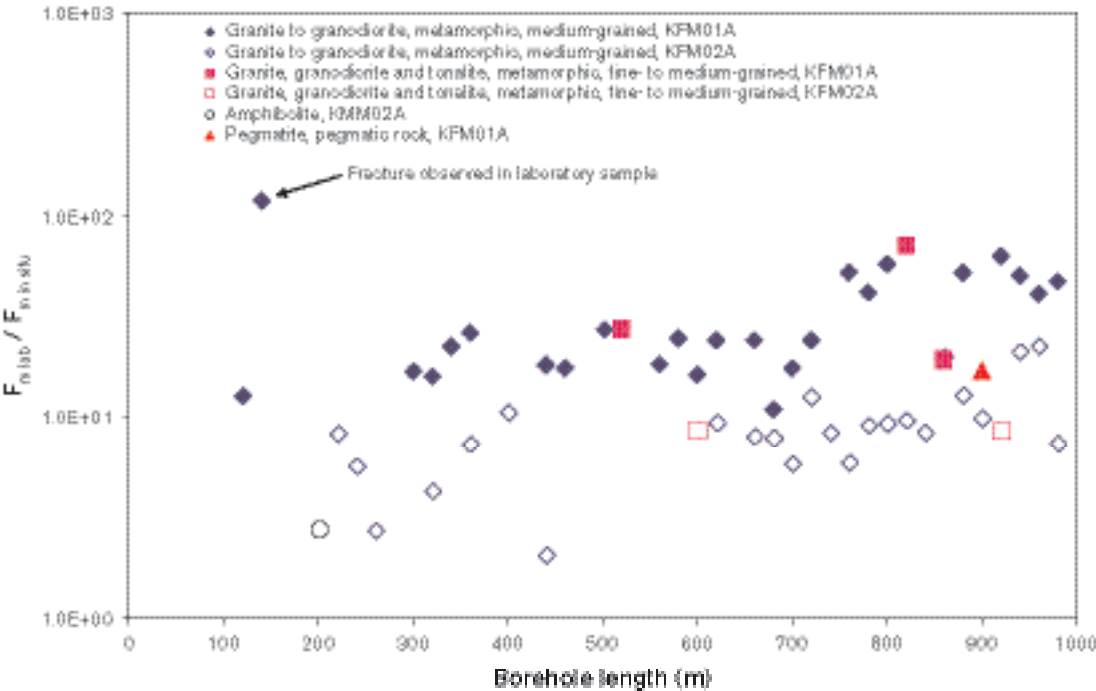


Figure 10-3. Ratio of the formation factor measured in the laboratory and in situ with electrical resistivity versus the borehole length.

Table 10-2. Summary of formation factors for the some of the Forsmark rock types. Mean value \pm one standard deviation; in italics logarithmic scale (\log_{10} of the data).

Method	Granite, granodiorite and tonalite, metamorphic, fine-to medium-grained (101051)	Granite to granodiorite, metamorphic, medium-grained (101057)	Granite to granodiorite, metamorphic, medium-grained, episyenite (101057)	Pegmatite, pegmatitic granite (101061)	Amphibolite (102017)
HTO through-diffusion	$(1.3 \pm 0.2)E-4$	$(1.9 \pm 1.3)E-4$	$5.9E-3$	Pending	$(> 1.2E-5)^1$
Log-normal distribution	-3.90 ± 0.08	-3.78 ± 0.24	-2.23	Pending	$> -4.94^1$
Electrical resistivity, lab	$(2.9 \pm 2.3)E-4$	$(3.2 \pm 1.7)E-4$	Pending	$2.5E-4$	$> 4.5E-5$
Log-normal distribution	-3.63 ± 0.30	-3.56 ± 0.24	Pending	-3.60	> -4.44
Electrical resistivity, in-situ	$(1.2 \pm 0.2)E-5$	$(2.4 \pm 1.3)E-5$	Pending	$1.5E-5$	$2.6E-5$
Log-normal distribution	-4.93 ± 0.08	-4.68 ± 0.24	Pending	-4.83	-4.58

¹ Steady state diffusion rate not reached, only minimum diffusion rate evaluated.

10.5.4 Sorption

No results on site-specific K_d measured in the laboratory are available for model version 1.2. In version 1.1, it was suggested that an import of data from the Finnsjön site could be attempted. Since version 1.1, a better geological and hydrogeochemical description has been obtained and this is now used as the basis for the set-up of the on-going laboratory batch sorption experiments with site-specific Forsmark material. Based on the improved description and an examination of the available Finnsjön sorption data, it has been concluded that the Finnsjön data base cannot be used. This is due to the early Finnsjön analyses not being sufficiently similar to the on-going batch sorption experiments.

Measurements of BET surface area have been performed within the version 1.2 work. The quantification of available surface areas is an important estimation of the sorption capacity of the rock material. Although at this stage no method is available for establishing a quantitative relationship between specific surface areas and sorption parameters, results of BET surface area measurements are included in the retardation model as qualitative data important for the understanding of the sorption processes.

Two types of measurements have so far been performed for the Forsmark site specific material.

1. For samples taken from drill core, crushing and sieving has been performed. The size fractions 63–125 μm and 2–4 mm were measured in duplicate samples for each fraction.
2. For natural fracture samples, scraping of the fracture surfaces was performed and the $< 125 \mu\text{m}$ fraction was isolated through sieving of the scraped material and measured in duplicate samples.

A general observation is that comparatively high BET surface areas can be found for materials associated with rock mass fractures and deformation zones.

10.6 Transport properties of rock domains, rock mass fractures and deformation zones

10.6.1 Methodology

The developed retardation model consists of two parts only, one for the major rock types and one for the rock mass fractures and deformation zones combined. This is a simplification of the general methodology as outlined in /Widstrand et al. 2003/, and is motivated by the scarcity of data.

10.6.2 Rock domains

Table 10-3 presents the selected transport parameters for the fresh and altered rock types. It is noted that the formation factors are based on the in situ electrical measurements. This is motivated by the fact that these measurements are believed to be most representative of virgin conditions, since they are not subject to stress release, even though some borehole interference effects cannot be excluded. The uncertainty implied by an assumed matrix water composition, which is needed for the in situ method (see /Byegård et al. 2005/ for details), is believed to be smaller than the uncertainty related to stress release. For performance assessment applications one should be aware of a possible overestimation of the porosity and formation factor values due to sample disturbances.

Table 10-3. Suggested transport parameters (water saturation measured porosity and in-situ electrical resistivity measured formation factor) for the common rock types at the Forsmark area. Logarithmic scale (\log_{10} of the data), mean value \pm one standard deviation.

Rock type (SKB code)	Porosity (vol %)	Formation factor (-)
Granite to granodiorite, metamorphic, medium-grained (101057)	-0.68 ± 0.15	-4.68 ± 0.24
Granite to granodiorite, metamorphic, medium-grained (101057), episyenetic samples	1.05 ± 0.36	-2.23^A
Granite, granodiorite and tonalite, metamorphic, fine- to medium-grained (101051)	-0.64 ± 0.17	-4.93 ± 0.08
Pegmatite, pegmatic granite (101061)	-0.41 ± 0.22	-4.83
Amphibolite (101217)	-0.75 ± 0.28	-4.58
Granodiorite metamorphic (101056)	-0.52 ± 0.28	Pending
Felsic to intermediate volcanic rock, metamorphic (103076)	-0.11	Pending

^A Based on through-diffusion experimental result.

10.6.3 Rock mass fractures and deformation zones

According to the presently available data, the presence of different fracture coatings cannot be related to specific rock types. This is important for the application of the identified fracture types in transport models. Concerning the host rock, only a minor portion of the fractures are accompanied by altered wall rock (< 10% of the open fractures according to the core logging).

Generalising the information from the core mapping and the more detailed fracture mineral studies, the following quantification and description of different rock mass fracture types is suggested.

- A. 50% have chlorite +/- calcite as fracture coating (max 0.5 mm thick on each side) and fresh wall rock.
- B. 10% have chlorite + clay minerals (+/- epidote, prehnite or calcite) as fracture coating (max 1 mm thick on each side). All of these fractures have altered wall rock > 3 cm (on each side of the coating).
- C. 15% have chlorite +/- epidote +/- prehnite as coating (max 0.5 mm thick on each side); all of these fractures have altered wall rock wall rock c. 1 cm on each side of the coating*.
- D. 15% have laumontite + chlorite + calcite as fracture coating (max 0.5 mm thick on each side); all of these fractures have altered wall rock \geq 5 cm (on each side of the coating).
- E. 10% quartz + calcite + pyrite (max 0.5 mm thick on each side) and fresh wall rock.

* The wall rock alteration is not always visible as red staining or bleaching of feldspars, but is present as alteration of plagioclase and chlorite formation due to breakdown of biotite. The density of micro fractures may also be increased in the altered zone causing increased porosity.

The descriptions of the identified rock mass fracture types, including the available retardation parameters, are given in Table 10-4 to Table 10-8. It has not yet been possible to formulate a retardation model for the deformation zones due to data scarcity.

Table 10-4. Retardation model for Fracture type A.

	Fracture coating	Fresh host rock
Distance	Max 0.5 mm	0.5 mm –
Porosity	Pending	According to Table 10-3
Formation factor	Pending	According to Table 10-3
Mineral content	Chlorite, ± calcite	See geological description
Grain size	Pending	Pending
Portion of open structures	50%	
Transmissivity interval	Pending	
Direction	Pending	

Table 10-5. Retardation model for Fracture type B.

	Fracture coating	Altered wall rock	Fresh host rock
Distance	Max 1 mm	1 mm – 3 cm	≥ 3 cm –
Porosity	Pending	Pending	According to Table 10-3
Formation factor	Pending	Pending	According to Table 10-3
Mineral content	Chlorite, clay minerals ± epidote ± prehnite ± calcite	See geological description	See geological description
Grain size	Pending	Pending	Pending
Portion of open structures	10%		
Transmissivity interval	Pending		
Direction	Pending		

Table 10-6. Retardation model for Fracture type C.

	Fracture coating	Altered wall rock	Fresh host rock
Distance	Max 0.5 mm	0.5 mm – 1 cm	≥ 1 cm –
Porosity	Pending	Pending	According to Table 10-3
Formation factor	Pending	Pending	According to Table 10-3
Mineral content	Chlorite, ± epidote ± prehnite	See geological description	See geological description
Grain size	Pending	Pending	Pending
Portion of open structures	15%		
Transmissivity interval	Pending		
Direction	Pending		

Table 10-7. Retardation model for Fracture type D.

	Fracture coating	Altered wall rock	Fresh host rock
Distance	Max 0.5 mm	0.5 mm – ≥ 1 cm	≥ 1 cm –
Porosity	Pending	Pending	According to Table 10-3
Formation factor	Pending	Pending	According to Table 10-3
Mineral content	Laumontite, chlorite, calcite, hematite	See geological description	See geological description
Grain size	Pending	Pending	Pending
Portion of open structures	15%		
Transmissivity interval	Pending		
Direction	Pending		

Table 10-8. Retardation model for Fracture type E.

	Fracture coating	Fresh host rock
Distance	Max 0.5 mm	≥ 0.5 mm –
Porosity	Pending	According to Table 10-3
Formation factor	Pending	According to Table 10-3
Mineral content	Chlorite, calcite, clay minerals	See geological description
Grain size	Pending	Pending
Portion of open structures	10%	
Transmissivity interval	Pending	
Direction	Pending	

10.7 Evaluation of uncertainties

The uncertainties relevant for the present description of transport properties can be categorised as follows.

- Uncertainties in the data and models obtained from other disciplines, primarily geology and hydrogeochemistry.
- Uncertainties in the interpretations and use of data and models from other disciplines, i.e., in interpretations of the relations between transport properties and various underlying properties, and the simplifications made when identifying and parameterising “typical” materials and fractures.
- Data uncertainties related to measurements and spatial variability of transport parameters, including the “extrapolation” of small-scale measurements to relevant model scales.
- Conceptual uncertainties related to transport-specific processes and process models.

This model provides quantitative information on transport data uncertainties only. Uncertainty ranges, in most cases taken directly from the experimental data, are given in the data tables above. Essentially, these ranges incorporate both random measurement errors and the spatial variability associated with the particular dataset.

Regarding the uncertainties related to spatial variability and scale, it may be noted that a large extent of the measurements providing data to the retardation model have been obtained in the laboratory, on a millimetre- to centimetre-scale. The proper means of “upscaling” these parameters is by integrating them along flow paths in groundwater flow models, implying that the scale of the flow model is the relevant model scale. The approach is here to present the data on the measurement scale, thereby providing a basis for further analysis in connection with the numerical flow and transport modelling.

10.8 Feedback to other disciplines

It is noted that the porosity and diffusivity values presented as part of the Forsmark model version 1.2 are consistent with corresponding values presented in /Hartley et al. 2005/ performed as part of the hydrogeological modelling in Forsmark version 1.2 (see also Chapter 8). Specifically, in the calibrated base case of /Hartley et al. 2005/, matrix porosity values (for rock matrix diffusion of salt) in the range $2.5\text{--}6 \times 10^{-3}$ and effective diffusivities in the range $1\text{--}5 \times 10^{-13} \text{ m}^2\text{s}^{-1}$ are presented. If the free diffusivity in water is assumed to be $1 \times 10^{-9} \text{ m}^2\text{s}^{-1}$, a formation factor range of $1\text{--}5 \times 10^{-4}$ is obtained. These values can be compared with the values presented as part of the transport model above, where a porosity of 2×10^{-3} and a formation factor around 2×10^{-5} are advocated for the main rock type. Thus, the data presented in the transport model lend credibility to the application of diffusion modelling within the hydrogeology and hydrogeochemistry disciplines.

11 Resulting description of the Forsmark site

This chapter provides a condensed account of the version 1.2 of the site descriptive model for the Forsmark site. The resulting description follows the consecutive order of the discipline-wise presentation in preceding chapters.

11.1 Surface properties and ecosystems

11.1.1 Quaternary deposits and other regoliths

All known Quaternary deposits in the Forsmark area were formed during or after the latest glaciation. The oldest deposits are of glacial origin, deposited directly from the inland ice or by water from the melting ice. The whole area is located far below (> 120 m) the highest coastline, which means that the area has been located under the sea during the major part of the Holocene (cf. Section 3.3). Fine-grained sediment has been deposited in local depressions such as the bottom of the lakes and on the present sea floor. Wave action and currents have partly eroded the upper surface of the overburden.

The isostatic uplift in Forsmark is still ongoing (6 mm/year), resulting in new land areas emerging from the Baltic. The most notable change in the Quaternary deposits in areas uplifted from the Baltic is the formation of organic soils, for example sedimentation of gyttja in lakes and formation of peat in wetlands. The minerogenic Quaternary deposits will be affected by coastal- and soil forming processes at the surface, but no major redistribution will take place after the area has been isolated from the Baltic. For a more comprehensive description of the present knowledge of the Quaternary deposits in the Forsmark area, see /Lindborg, 2005/.

Surface and stratigraphical distribution

The upper surface of the Forsmark area is flat, dominated by glacial till. Unconsolidated Quaternary deposits cover c. 85% of the land area in the regional model area and artificial fill c. 3%. Exposed bedrock occupies c. 13% of the land area in the regional model area.

Glacial till is the oldest known Quaternary deposit in the Forsmark area, deposited directly from the inland ice. The major part of the model area, especially in the west and south, is dominated by sandy till with medium boulder frequency. At Storskäret and on the island of Gräsö, clayey till with low boulder frequency dominates. At Storskäret, the clayey till is used as arable land and the frequency of bedrock outcrops is generally low (see Figure 4-2). The observed thickness of the Quaternary deposits within the investigated area varies between 0 and 17 m /e.g. Johansson, 2003/. The largest thickness is generally found in areas covered by clayey till.

The distal glaciofluvial sediments in the area consist of glacial clay. These sediments have been deposited in stagnant water at some distance from the retreating inland ice. These deposits are concentrated to local depressions, such as the bottom of lakes and small ponds. Moreover, glaciofluvial sediments are deposited in a small esker, the Börstilåsen esker, with a flat crest reaching c. 5 m above the present sea level. Postglacial sediments have been eroded and re-deposited by waves and streams during the last c. 10,000 years, and clay, gyttja clay, sand and peat are common in the superficial Quaternary deposits and cover many small (less than 50×50 m) areas (see Figure 4-2).

Lake sediments and marine Quaternary deposits

In a majority of the investigated lakes, the total thickness of the sediments (excluding glacial till) is less than 2 m, and only two lakes contain sediments thicker than 4.5 m, namely Lake Eckarfjärden and Lake Fiskarfjärden. The sedimentary sequence in the Forsmark lakes is fairly uniform. Generally the till is covered by a layer of sand, followed by, in turn, gyttja clay and gyttja. Uppermost, there is often a layer of recent calcareous gyttja /Hedenström, 2004/.

Compared with Quaternary deposits on land areas, the sea floor is to a larger extent covered by sediments. Offshore Quaternary deposits are dominated by glacial and post-glacial clay, together covering c. 55% of the sea floor. The thickness of the offshore Quaternary deposits varies considerably, from < 2.5 m to > 10 m /Carlsson et al. 1985/. The terrestrial area covered by glacial till is c. 75%, whereas the corresponding figure for the sea floor is c. 30%. The difference between land and the sea floor is partly a result of erosion and re-deposition of fine-grained material, e.g. postglacial clay, to the deeper parts still situated below the sea level.

Soil types

The soils in the Forsmark area are typically poorly developed soil types on till or sedimentary parent material, which are influenced by the calcareous content of the substrate /Lundin et al. 2004/. The poor soil development is a result of their young age, since most of the candidate area emerged from the sea during the last 1,500 years. The calcareous soil material has yielded nutrient-rich conditions, which can be observed in the rich and diverse flora of the area. This can also be seen in the predominant humus forms of mull type and of the intermediate moder type, which indicate a rich soil fauna. Because of the young age of the soils, the Forsmark area exhibits less soil of the Podsol type than most similar areas in Sweden /Lundin et al. 2004/. Instead, the typical soil types are the less developed Regosols, together with Gleysols and Histosols, which are formed under moist conditions (see Figure 4-4).

11.1.2 Climate, hydrology and hydrogeology

The conceptual and descriptive modelling of the meteorological, surface hydrological and near-surface hydrogeological conditions in the Forsmark area is presented in /Johansson et al. 2005/. The model area is characterised by a low relief and a small-scale topography; almost the whole area is located below 20 m above sea level. The corrected mean annual precipitation is 600–650 mm and the mean annual evapotranspiration has been estimated to be slightly more than 400 mm, leaving approximately 200 mm/year for runoff. In total, 25 “lake-centred” catchments, ranging in size from 0.03 to 8.67 km² have been delineated and described within the model area. The 25 mapped lakes range in size from 0.006 to 0.752 km². The lakes are very shallow with maximum depths ranging from 0.4 m to 2.0 m. No major water courses flow through the model area. Wetlands are frequent and cover 10–20% of the areas of the three major catchments, and up to 25–35% of some sub-catchments.

As described above, till is the dominating Quaternary deposit covering approximately 75% of the area. In most of the area, the till is sandy. Based on site-specific and generic data, a three-layer model is proposed for the hydraulic properties of the dominating till. The uppermost layer is assigned relatively high hydraulic conductivity (1.5×10^{-5} m/s) and porosity (total: 35%, effective: 15%) values due to the impact of soil forming processes. The middle layer is given lower values of both conductivity (1.5×10^{-7} – 1.5×10^{-6} m/s) and porosity (total: 25%, effective: 3–5%), in agreement with both site-specific and generic data. The bottom layer, resting on the bedrock, is in accordance with site-specific data assigned a higher conductivity value (1.5×10^{-5} m/s) than the middle layer.

Direct groundwater recharge from precipitation is the dominant source of groundwater recharge. The groundwater is very shallow, with groundwater levels within one metre below ground as an annual mean for almost all groundwater monitoring wells. Also, the annual groundwater level amplitude is less than 1.5 m for most wells. The shallow groundwater levels mean that there is a strong interaction between evapotranspiration, soil moisture and groundwater. In the modelling, surface water and near-surface groundwater divides are assumed to coincide. The small-scale topography implies that many local, shallow groundwater flow systems are formed in the Quaternary deposits, overlaying more large-scale flow systems associated with groundwater flows at greater depths.

In order to provide input to the ecological system modelling, a GIS model was used to calculate flow directions and mean discharges in the regional model area, based on topographical data (the DEM) and regional data on the specific discharge. The MIKE SHE modelling tool was used for detailed process modelling of near-surface groundwater flow and surface water flow within a modelling area covering most of the land area within the regional model boundaries. The water balance for the Forsmark area, as calculated with the MIKE SHE modelling tool using regional meteorological data,

agrees with the presented conceptual and descriptive models of the flow system. The transient model simulations for the selected reference year (1988) result in an annual total runoff of 226 mm and a total actual evapotranspiration of 441 mm. These values, which are average values for the considered model area, are judged to be reasonable for the Forsmark area. At present, however, they cannot be tested against site-specific measurements.

In the flow modelling reported by /Johansson et al. 2005/, near-surface groundwater levels and the hydrogeological interactions between the Quaternary deposits and the fractured rock were also investigated. Particle-tracking simulations, in which particles were introduced in the rock at a depth of c. 150 m, were also performed. For the aspects of the model that were tested, it was found that the quantitative modelling provided evidence supporting the descriptive model of the site. However, this support should be regarded as qualitative, since no calibration exercises or other quantitative comparisons with field data were carried out.

11.1.3 Chemistry

Surface water

Similar to most surface waters in the north-eastern parts of Uppland, the lakes and streams in the Forsmark model area are characterised by high pH, high concentrations of major ions and high electrical conductance. This is a combined effect of the calcium rich deposits in the area, and of recent emergence from the Baltic Sea. Due to interacting chemical and biological processes in the lake water, the amounts of nutrients, e.g. phosphorus (P), transported to the lakes may be effectively reduced by precipitation of calcium-rich particulate matter. Because of this, the P concentration in lakes and streams is generally low. The nitrogen concentration, on the other hand, tends to be high, or even very high, due to a combination of high input and low biotic utilisation /Brunberg and Blomqvist, 1999, 2000/. Taken together, these conditions give rise to a unique type of lake in the Forsmark area, the oligotrophic hardwater lake.

Several of the Forsmark lakes are still not completely isolated from the Baltic Sea because of the small altitude differences in the area. The lakes Norra Bassängen and Bolundsfjärden are both strongly affected by episodic intrusions of brackish water, and there were also indications of intruding brackish water in Lake Fiskarfjärden during the site investigations.

Near surface groundwater

There are two main factors which determine the characteristic chemical composition of the groundwater in the Forsmark region. The first factor is the occurrence of relict saline water, which remains since the sea covered the area. The lowest topographical areas were quite recently covered by the sea, which explains the high concentrations of e.g. Cl in some of the wells. The second factor affecting the chemical characteristics is the occurrence of CaCO₃ in most of the Quaternary deposits. Weathering processes are dissolving the calcite, causing a high pH and high concentrations of Ca and HCO₃.

Generally, the groundwater in northern Uppland is characterised by relatively high pH and high Ca and Cl concentrations /Naturvårdsverket, 1999/. Median concentrations of Ca, Mg and especially Cl and HCO₃ in the Forsmark area are, however, even above the median values for Uppland.

11.1.4 Ecosystem description

The surface ecosystem is described using a large number of properties which, when combined, will constitute the ecosystem site descriptive model /cf. Löfgren and Lindborg, 2003/. The surface ecosystem is divided into different subsystems based on the presence of system-specific processes and properties, and also on the collection, measurement and calculation of data that may differ between different subsystems. Accordingly, three different subsystems are characterised: (1) the *terrestrial system* which includes all land and wetland areas, (2) the *limnic system*, i.e. lakes and rivers, and (3) the *marine system*. The amount of data describing both the abiotic and the biotic parts of the ecosystem has increased considerably since the previous version of the site descriptive model, and these data are presented in detail in /Lindborg, 2005/. A brief summary of our present knowledge of the different subsystems is given below.

A detailed carbon budget has been developed for each of the three subsystems and these budgets are presented in Section 4.8. The drainage area of Lake Bolundsfjärden (Forsmark 2) was chosen as the model area when developing the terrestrial and limnic ecosystem models (see Figure 4-16). The total drainage area is 8.7 km² and the surface area of Lake Bolundsfjärden is 0.6 km². Ecosystem models were developed for both Lake Bolundsfjärden and for Lake Eckarfjärden, which is also situated within the drainage area Forsmark 2, but the model for Lake Eckarfjärden is described only in /Lindborg, 2005/.

The Forsmark marine ecosystem has been divided into seven basins, shown in Figure 4-14. Two of these basins, Basin Stånggrundsfjärden and Basin SAFE-area, were used for the marine modelling. These two basins are recipients of the drainage area Forsmark 2. The model for Basin SAFE-area is described only in /Lindborg, 2005/. The ecosystem models were developed as stand-alone models. No efforts have been made in this version to connect the models.

Terrestrial system

Generally, the vegetation is strongly influenced by the type of bedrock, the overburden and the human land management. The bedrock in the area mainly consists of granites and the Quaternary deposits are mainly wave-washed till covered with conifer forests. Scotch pine and Norway spruce dominate the forests. In depressions, a deeper regolith layer is found, typically with fairly high lime content. The lime influence is typical for the NE part of Uppland and is manifested in the flora. The field layer is characterised by herbs and broad-leaved grasses along with a number of orchid species. The Forsmark area has a long history of forestry and this is also seen today as a fairly high percentage of younger and older clear-cuts in the landscape. The spatial distribution of different vegetation types is presented by /Boresjö-Bronge and Wester, 2002/.

The most common mammal species in the Forsmark regional model area is roe deer (9.4 deer/km²) /Cederlund et al. 2004/. Moose is also fairly common (1.2 moose/km²), but unevenly distributed, which is normal for this part of Sweden due to hunting pressure, variations in snow depth and distribution of food. European and mountain hare are fairly low in abundance, compared with other regions (see Table 4-5). In total, 96 bird species were found during investigations in the regional model area, compared with 86 in 2002. The most common bird species are Chaffinch (sw. *Bofink*) and Willow warbler (sw. *Lövsångare*). A more comprehensive description of terrestrial mammals and birds is found in /Lindborg, 2005/.

Limnic system

The Forsmark regional model area contains more than 20 more or less permanent pools of water which could be characterised as lakes. Only three of these, Lake Fiskarfjärden, Lake Bolundsfjärden and Lake Eckarfjärden, are larger than 0.2 km², and most of them are considerably smaller. All lakes in the area are very shallow; none has an average depth exceeding 1 m. Accordingly, all bottom areas of the lakes are exposed to light and none of the lakes will evolve a stable thermal stratification during the summer. Because of the flat relief and the small drainage areas in the Forsmark area, most of the streams in the area periodically show very low discharge, or are even ephemeral.

The larger lakes in the area, and probably also the smaller ones which have not been investigated, can be classified as oligotrophic hardwater lakes. This means that they show very unusual chemical conditions, with high alkalinity, conductivity, pH value, and nitrogen concentrations, very high concentrations of slightly coloured DOC, whereas phosphorus concentrations are very low. Phytoplankton and bacterioplankton biomasses are low, and the microbial community (including both autotrophs and heterotrophs) is mainly confined to the sediments where a 10–15 cm thick microbial mat, mainly consisting of cyanobacteria, is found. Preliminary primary production measurements in the lakes show that while the production in the pelagial is always low, the production in the microbial mat may potentially be very high /Blomqvist et al. 2002/.

Most lakes are surrounded by extended reed belts which constitutes a major biomass pool and where much of the primary production occurs. Another important group of primary producers in the lakes is the stoneworts (*Chara spp.*). Large parts of the bottoms of the larger lakes in the area are covered with *Chara*. The biomass of benthic fauna is low compared with other Swedish lakes /Andersson

et al. 2003/ and the benthic fauna is dominated by herbivores, both in terms of number of individuals and in terms of biomass.

Marine system

The marine ecosystem at Forsmark has a varied bathymetry, with a few enclosed bays clearly affected by fresh water effluence, a shallow but exposed archipelago and open sea areas heavily exposed to currents and wave action. As a result, elements discharged into the marine environment from the adjacent terrestrial and limnic environments will have a different fate depending on where they enter the marine system.

The marine system in the Forsmark area is a relatively productive coastal area in a region of otherwise fairly low primary production. This is due to upwelling along the mainland /Eriksson et al. 1977/. The seabed is dominated by erosion and transport bottoms with heterogeneous and mobile sediment consisting mainly of sand and gravel with varying fractions of glacial clay /Mo and Smith, 1988/.

The major groups among primary producers in the Forsmark area are macrophytes (including macroalgae), microphytobenthos and phytoplankton. The macrophyte species that contribute most to the biomass in the benthic community in Forsmark are the red alga *Polysiphonia nigrescens*, the brown algae *Fucus vesiculosus* and *Sphacelaria arctica* and the vascular plant *Potamogeton filiformis* /Kautsky et al. 1999/.

The phytoplankton are strongly dominated by diatoms and dinoflagellates during springtime, whereas the plankton community in summer and autumn mainly consists of blue-green algae and small flagellates /Lindahl and Wallström, 1980/.

The zooplankton community has low species diversity with two copepod species comprising about 80% of the zooplankton biovolume /Persson et al. 1993/. The most common fish species in Öregrundsgrepen are herring (*Clupea harengus*), roach (*Rutilus rutilus*) and perch (*Perca fluviatilis*) /Neuman, 1982/.

11.1.5 Humans and land use

The Forsmark regional model area is uninhabited, but there are five holiday houses and three farms within the Forsmark area, indicating that the area has a small holiday population. There is only one active farm property within the area, situated at Storskäret. The agricultural area in the Forsmark area is only 4% of the total area, considerably lower than in the County of Uppsala as a whole where it represents 25%. The forest area represents as much as 72.5% of the land area. The land use is dominated by forestry; wood extraction is the only significant outflow of biomass from the area.

11.2 Bedrock geological description

The bedrock geological model consists of three components; the rock domain model, the deterministic deformation zone model, and the statistical description of fractures and possible deformation zones inferred from lineaments, the discrete fracture network (DFN) model. One or more of these components provides a foundation for the modelling work in rock mechanics, thermal properties, hydrogeology (bedrock) and, to less extent, even hydrogeochemistry (bedrock) and transport properties (bedrock). All components of the geological model have a direct impact on the location and design of the repository volume. They also provide a significant input for certain aspects of the safety analysis.

As in model version 1.1, the rock domain and deterministic deformation zone models are presented for the whole regional model volume. The DFN model has utilised fractures from essentially within the local model volume and addresses possible deformation zones inferred from lineaments in the mainland area. Only fractures that are situated outside deformation zones have been included in the DFN model.

Each rock domain is identified with the help of the three letters RFM followed by three digits. For example, the major part of the candidate area at Forsmark is situated within rock domain 29, i.e. RFM029. In a similar manner, each deformation zone is identified with the three letters ZFM followed by six codes that consist of a combination of letters and digits. The first two letters indicate to which orientation set the zone belongs, i.e. NW, NE or NS. The properties of each rock domain and each deterministic deformation zone are presented in tabular format in Appendices 1 and 3, respectively. Confidence assessments for these two geological entities are presented in Sections 5.3 and 5.4, respectively.

11.2.1 Rock domain model

A substantial quantity of geological data, both at the surface and from depth in the form of information from cored (5,600 m at six sites) and percussion (2,850 m at 19 sites) boreholes (see Figure 5-38), underpins the establishment of the rock domain model, version 1.2 for Forsmark. Since cored borehole data confirm that the character of the bedrock at c. 1,000 m depth inside the candidate volume is identical to that observed at the surface, it is clear that the more abundant surface data remain critical for the establishment of the rock domain model for the site. Notwithstanding the radical increase in data, the rock domain model version 1.2 is similar to model version 1.1.

Meta-igneous rocks with crystallisation ages in the time span pre-1,886 to 1,840 million years build the bedrock at the Forsmark site. These rocks formed during both phase 1 and phase 2 in the geological evolution of the crystalline bedrock in the Fennoscandian Shield (see Section 3.1). The structural framework for the rock domains, which was established during model version 1.1, remains.

The candidate volume at Forsmark is situated within a tectonic lens that extends along the Uppland coast from north-west of the nuclear power plant south-eastwards to Öregrund. Strongly deformed rocks, which are both foliated and lineated and which are, in part, also banded and inhomogeneous, comprise the rock domains along the south-western (e.g. RFM012, RFM018) and north-eastern (e.g. RFM021, RFM032) margins of the tectonic lens (Figure 11-1). The candidate volume is situated inside the lens and is dominated by rock domain RFM029 (Figure 11-1). Major folding and the development of less deformed rocks that are more lineated than foliated characterise the bedrock inside the lens. The tectonic lens developed when the rock units were situated at mid-crustal depths and were affected by penetrative but variable degrees of ductile deformation and metamorphism.

The results from borehole KFM04A confirm that the rock domains to the south-west of the tectonic lens dip steeply to the south-west (Figure 11-1). This borehole intersects the boundaries between three different domains that are, in successive order from top to bottom, RFM018, RFM012 and RFM029. Drilling along KFM03A and HFM18 constrains the geometry of the metatonalite in rock domain RFM017. This body forms a large xenolith within domain RFM029 (Figure 11-1). Furthermore, the data in borehole KFO01 provide constraints at depth on the geometry of the contact between a metadiorite to metagabbro body (RFM007), which is modelled as a rod-like structure, and a major pluton that is dominated by metatonalite to metagranodiorite (RFM023).

A medium-grained metagranite (SKB rock code 101057) that crystallised $1,865 \pm 3$ million years ago prevails in rock domain RFM029 (84% of the domain volume). Subordinate fine- to medium-grained metagranodiorite or metatonalite (101051, 10% of the domain volume), amphibolite (102017, 3%), pegmatitic granite or pegmatite (101061, 2%) and fine- to medium-grained granite (111058, 1%) are also present. The estimates for the proportion of these rock types are calculated from borehole data and the values do not include rock occurrences that are less than 1 m in borehole length. Except for the amphibolite and four samples (of 17) from rock type 101051, all the surface and borehole samples of these rock types at the site have yielded quartz contents that lie in the interval 23–46%. The medium-grained metagranite has a quartz content that lies in the interval 28–46% (46 samples over the site), a density of $2,657 \pm 15$ (64 samples), a uranium content of 4.9 ± 2.3 ppm (66 samples) and a natural exposure rate of 12.4 ± 2.0 microR/h (66 samples, $1R = 0.01$ Gray).

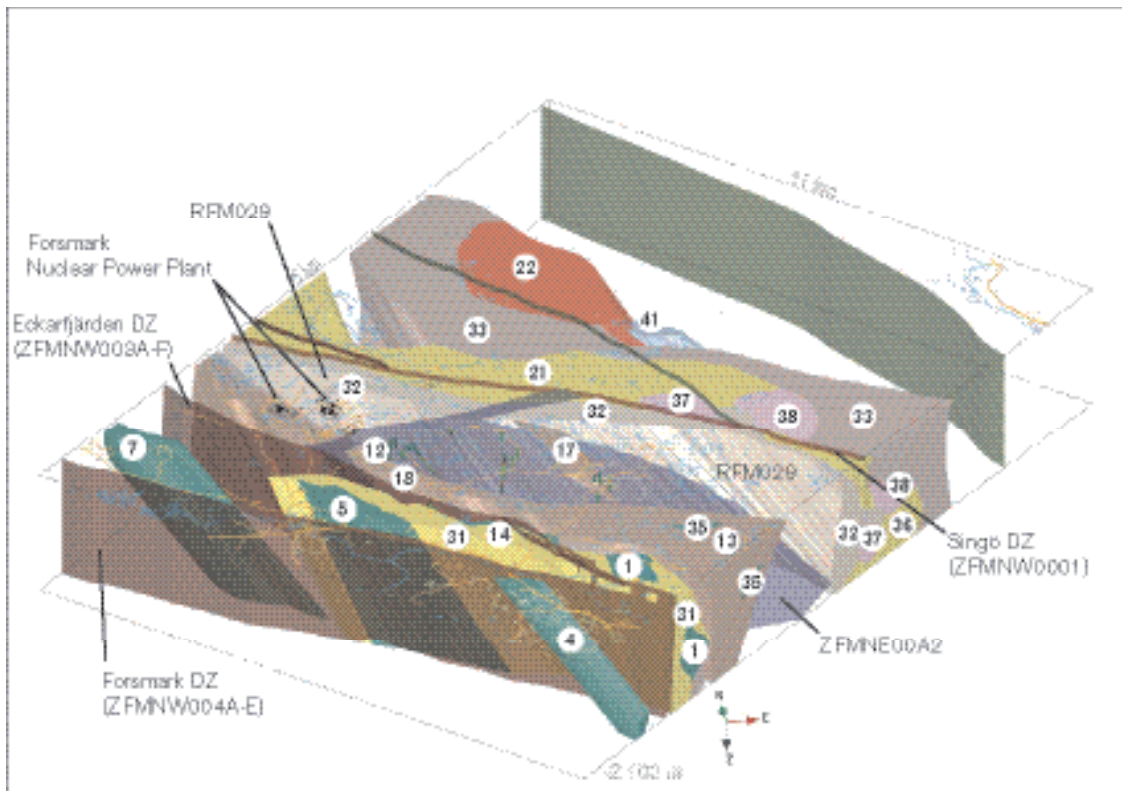


Figure 11-1. Rock domains (numbered), regional vertical and steeply dipping deformation zones, and the gently dipping zone ZFMNE00A2 in the version 1.2 geological model for Forsmark. View to the north. Rock domain RFM029 is unshaded in order to show the major folding within the tectonic lens at the Forsmark site. Other domains are unshaded in order to show the modelled, south-eastern elongation of several domains. The dominant rock type in each domain is illustrated with the help of different colours (see Figure 5-54). Regional deformation zones in brown shades are high confidence zones and in green shades are medium confidence zones. Zone ZFMNE00A2 is shown in blue and has been adopted from the base model (see below).

Virtually all the lineation data at the site, including a mineral stretching lineation and fold axes, plunge moderately or gently to the south-east. On this basis, several ultramafic to intermediate bodies, especially to the south-west of the candidate volume (e.g. RFM007), have been modelled as rods drawn out parallel to the mineral stretching lineation (Figure 11-1). The folding inside the tectonic lens deforms the tectonic foliation and affects the boundaries between several domains (Figure 11-1). North-west of Asphällsfjärden, an inhomogeneous unit dominated by aplitic meta-granite, felsic metavolcanic rocks and pegmatitic granite, with an inferred higher degree of ductile strain (RFM032), is folded in a synformal structure with a moderate to steep plunge to the south-east (126/65°). Close to Lillfjärden, a domain that is dominated by metatonalite (RFM017) is folded in an open antiform that shows a gentler plunge in the same direction (126/23). A component of dextral horizontal movement has been detected in rocks affected by strong ductile strain and such highly deformed rocks are also folded.

Age determinations at the site indicate that the penetrative ductile deformation, including fabric development and folding, occurred during the time interval 1,868–1,846 million years ago, i.e. during the early part of phase 2 in the geological evolution (see Section 3.1). The geodynamic regime was dextral transpressive in character. Oblique collision against an older continental margin to the north-east, with bulk crustal shortening in a N to NNW direction, has been inferred.

The following more significant uncertainties remain after the development of the rock domain model, version 1.2:

- The composition, degree of homogeneity and degree of ductile deformation in the rock domains at the surface in the sea areas, especially Öregrundsgrepen.

- The location of the boundaries between rock units in the north-western and south-easternmost parts of the candidate area, i.e. under Asphällsfjärden that lies between the nuclear power plant and Lake Bolundsfjärden, and around Storskäret.
- The extension at depth of all rock domains except RFM017, RFM029 and to some extent RFM007, RFM012, RFM018 and RFM023.
- The quantitative estimates of the proportions of different rock types in all rock domains except RFM012 and RFM029.

11.2.2 Deterministic deformation zone models

Data input

The substantial increase in the quantity of cored and percussion borehole data (see Figure 5-38), in combination with a better understanding of the geological significance of the seismic reflectors at the site, have provided a sound foundation for a radically more detailed deterministic structural model, compared with model version 1.1. A complementary interpretation of lineaments, which is based predominantly on new topographic and bathymetric information, has also been carried out. Furthermore, the relationship between lineaments and the available surface geophysical data has been assessed. However, an alternative interpretation of lineaments by an independent working group, within and immediately around the candidate area, has raised important questions concerning the recognition of lineaments, as well as the judgements made concerning especially their length and level of uncertainty. As for version 1.1, there also remains considerable uncertainty concerning both the along-strike and down-dip extensions of especially the gently dipping, brittle deformation zones. For these reasons, three different deterministic zone models have been generated in version 1.2. These are referred to as the *base model*, the *base model variant* and the *alternative model* (Figure 11-2).

Character of the deterministic deformation zone models

In the *base model* (Figure 11-2a), vertical or steeply-dipping deformation zones that are generally longer than 1,000 m have been determined using both fixed point intersections along boreholes and lineaments at the surface. The lineament information is supportive rather than foundational in character. This approach is viable in essentially two small areas close to Lake Bolundsfjärden and SFR. Outside these areas, only vertical and steeply-dipping zones that are generally longer than 4,000 m are included in the base model. Attention here has been focused on the longer lineaments that are based on either magnetic data or a combination of magnetic and other data. This approach questions the general use of lineaments as a tool to recognise deformation zones (see also Section 5.2.3). It differs considerably from the approach used in model version 1.1 at Forsmark. All these zones have been assigned high and medium levels of confidence in the base model.

Gently dipping zones in the base model have been recognised using both fixed point intersections in boreholes and seismic reflection data. This approach is only viable in essentially the candidate area and its continuation towards the north-west. In the base model, several of these zones have been truncated along their strike against regional, vertical or steeply dipping zones with WNW-NW strike. The *base model variant* (Figure 11-2b) only differs from the base model where it concerns which WNW-NW zone four gently-dipping zones (ZFMNE00A1, ZFMNE00A2, ZFMNE00C1, ZFMNE00C1) have been truncated against. Thus, the difference between these two models only concerns the strike-length of these four zones. All the gently dipping zones in the base model and its variant have also been assigned high and medium levels of confidence.

The *alternative model* (Figure 11-2c) follows more closely the procedures adopted in model version 1.1 for Forsmark. In this model, vertical and steeply dipping zones that are generally longer than 1,000 m have been assessed deterministically within the whole regional model volume. Outside the detailed Bolundsfjärden and SFR areas, virtually all the vertical or steeply dipping zones correspond solely to lineaments that are based on either magnetic or a combination of magnetic and other data. Most of the zones that have been recognised in this manner have been assigned a low level of confidence. The gently dipping zones in the alternative model have been determined in the same manner as in the base model.

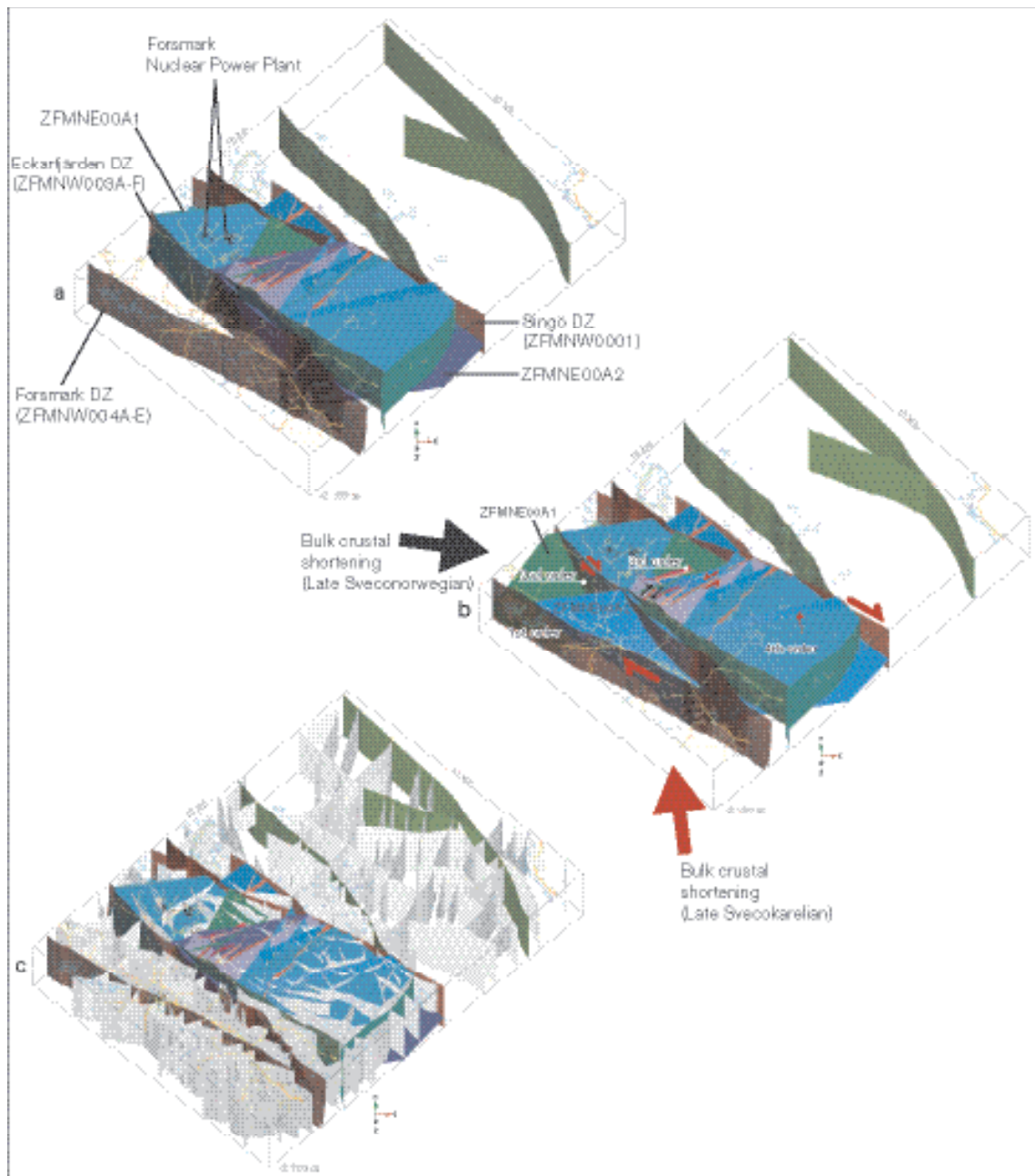


Figure 11-2. a) Base model for deterministic deformation zones, version 1.2, viewed to the north. The zones coloured in red and brown shades are vertical and steeply dipping zones with high confidence, the zones coloured in blue shades are gently dipping zones with high confidence, and the zones coloured in green shades are medium confidence zones irrespective of their dip. b) Base variant model for deterministic deformation zones, version 1.2, viewed to the north. The figure is identical to the base model in (a) apart from the along-strike extension of the gently dipping zones ZFMNE00A1, ZFMNE00A2, ZFMNE00C1 (not visible) and ZFMNE00C2 (not visible) to the south-west. c) Alternative model for deterministic deformation zones, version 1.2, viewed to the north. The zones coloured in red and brown shades are vertical and steeply dipping zones with high confidence, the zones coloured in blue shades are gently dipping zones with high confidence, the zones coloured in green shades are medium confidence zones irrespective of their dip, and the zones coloured in grey shades are vertical and steeply dipping zones with low confidence. The inferred sense of displacement and orientation of the bulk crustal shortening direction, during both the formation and an important phase of reactivation of these structures, are shown in (b). These events are inferred to have occurred during the waning stages of the Svecokarelian (red symbols) and Sveconorwegian (black symbols) orogenies, respectively.

Properties of zones and general conceptual model

Three major sets of deformation zones with distinctive orientations – WNW-NW, NE and gently dipping – have been recognised with high confidence at the Forsmark site. The bedrock in all three sets is affected by oxidation with the development of a fine-grained hematite dissemination. Clay minerals are more prominent in the gently dipping set but are, nevertheless, present along fractures in some zones in the other sets. These sets are described in more detail below.

- Vertical and steeply, SW-dipping zones with WNW-NW strike are regional and local major structures that show both ductile and brittle deformation, i.e. they are composite structures. They define important marginal structures to the candidate volume at the Forsmark site (Figure 11-2). Low-temperature mylonites are restricted to these zones, while cataclastic rocks, cohesive crush breccias and a dominance of sealed fractures are also distinctive features. Epidote together with quartz, chlorite and calcite occur as mineral filling along fractures in the zones.
- Vertical and steeply dipping, brittle deformation zones with NE strike are local major (and local minor) in character. They transect the candidate volume at Forsmark and are prominent in the Bolundsfjärden area (Figure 11-2). The zones contain cohesive crush breccias and are strongly dominated by sealed fractures. Laumontite in combination with chlorite, calcite, prehnite, quartz and, occasionally, epidote occur as mineral fillings along the fractures in the zones.
- Gently SE- and S-dipping brittle deformation zones are local major in character and are prominent in the south-eastern part of the candidate volume (Figure 11-3). Relative to the other three sets, there is an increased frequency of open fractures and incoherent fault breccias along the gently dipping set. Chlorite, calcite and clay minerals, occasionally in combination with epidote, quartz, prehnite and laumontite, are present along the fractures in these zones.

A fourth set of zones that strikes NS and is vertical or steeply dipping has also been recognised. However, only one local minor zone with a medium confidence of existence and a subordinate amount of zones with a low confidence of existence have been included in model version 1.2. Relative to the other three sets, there is a reduced number of zones and a higher degree of uncertainty concerning the existence of this set of deformation zones.

Based on the orientation of fractures in the deformation zones and the character of mineral fillings along the fractures in them, it is suggested that the three major sets formed close to each other in time. Nevertheless, the regional zones with WNW-NW strike represent the oldest set, with first-order structures in a WNW direction (e.g. Forsmark deformation zone, Singö deformation zone) and second-order splays in a NW direction (e.g. Eckarfjärden deformation zone). The earliest deformation along these discrete zones was ductile in character and occurred under greenschist facies (< 500–550°C) metamorphic conditions. Later deformation occurred in the brittle regime. The zones in the NE and gently dipping sets represent third- and fourth-order structures, respectively. They formed when the bedrock had cooled sufficiently to respond to deformation in the brittle regime. Ductile deformation is not present along these zones.

It is suggested that the conceptual model for the formation of the deformation zones at the site involves a strike-slip fault system with an important component of dextral horizontal movement along the WNW-NW set (see Figure 5-58). Formation in response to bulk crustal shortening in a N to NNW direction is envisaged (Figure 11-2b). Furthermore, it is suggested that a sinistral component of horizontal movement occurred initially along the NE zones and a reverse movement along the gently dipping zones (Figure 11-2b). Age determinations at the site indicate that low temperature ductile deformation along discrete zones occurred after 1,856 million years ago, that cooling beneath c. 500°C had initiated c. 1,830 million years ago and that cooling beneath c. 300°C had initiated c. 1,700 million years ago. Bearing in mind these results, it is suggested that the different sets of deformation zones at the Forsmark site formed during the waning stages of the Svecokarelian orogeny, i.e. during phase 2 of the geological evolution of the crystalline bedrock of the Fennoscandian Shield (see Section 3.1). In this model, the deformation zones formed in response to the same tectonic regime as the older, penetrative ductile structures (see Section 11.2.1).

The conspicuous growth of laumontite and even prehnite along fractures in the NE set suggests a selective, major reactivation of this set after the oldest possible age for the cooling below c. 300°C, i.e. after 1,704 million years ago. On the basis of the geological evolutionary model (see Section 3.1), it is inferred that this deformation occurred in response to a new tectonic regime.

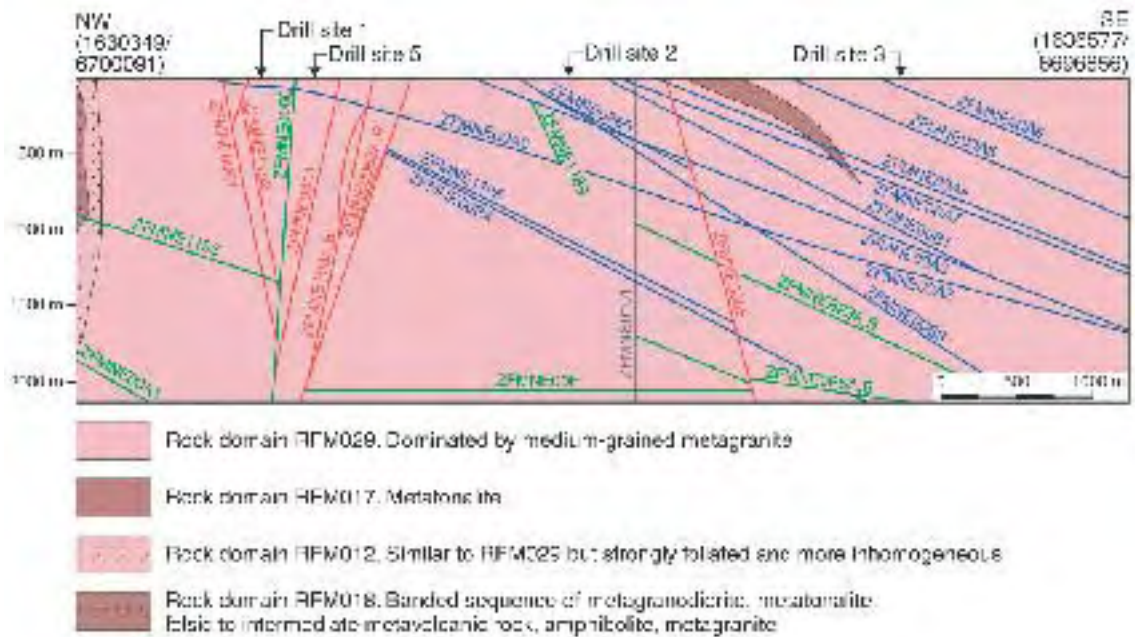


Figure 11-3. NW-SE cross-section that passes close to drill sites 1, 2, 3 and 5 inside the candidate volume. This two-dimensional structural model shows the steeply dipping deformation zones that strike NE and the gently dipping zones that dip to the south-east and south. All these zones transect the candidate volume and are sandwiched between first and second order, vertical and steeply dipping deformation zones that strike WNW-NW (not present in this cross-section). The zones coloured in red shades are vertical and steeply dipping zones with high confidence, the zones coloured in blue shades are gently dipping zones with high confidence, the zones coloured in green shades are medium confidence zones irrespective of their dip, and the zone coloured in a grey shade is a vertical zone with low confidence.

Since dextral horizontal movement has been observed along one of the zones (ZFMNE1188), reactivation during the Sveconorwegian orogeny in response to bulk crustal shortening in an ESE direction (see Section 3.1) is tentatively inferred (Figure 11-2b). At the present stage, it cannot be excluded that the zones in the NE set, with a predominance of lower temperature minerals, actually formed later than c. 1,700 million years ago.

The disturbance of the sub-Cambrian peneplain along the Forsmark deformation zone indicates an even later phase of reactivation of at least some of the deformation zones in the area, possibly during the Phanerozoic. Furthermore, there is evidence at the Forsmark site for a possible exhumation event that occurred after c. 300 million years ago. By contrast, evidence for late- or post-glacial faulting during the Quaternary period, which gave rise to earthquakes with a magnitude > 7 on the Richter scale in, for example, northern Fennoscandia, is lacking at the Forsmark site.

Several younger events that are not necessarily related to faulting have also occurred at the site. Horizontal and sub-horizontal sheet joints with large apertures, which are more or less parallel to the ground surface, are present. It is suggested that these fractures either formed or were reactivated in connection with unloading of a thick sedimentary cover, and that they are restricted to the uppermost part of the bedrock. Changes in the stress field are possible in connection with the removal of ice during the waning stages of the last glaciation /Carlsson, 1979/ and these changes may have occurred in combination with the effects of hydraulic lifting /Pusch et al. 1990/. The release of stress could also have occurred at an earlier stage, in connection with the removal of the Phanerozoic sedimentary cover that includes relatively dense, Ordovician limestone. It is also possible that both these geological events have triggered the creation or reactivation of horizontal and sub-horizontal fractures at the site and the development of fractures with larger apertures.

Secondly, fractures that lie close to the ground surface are filled with asphaltite or glacial sediment. Movement of fluids downwards from sediments that originally covered the crystalline bedrock is apparent. Upper Cambrian oil shale is a potential source for the asphaltite. To what extent fluid movement was related to loading during build-up of a cover sequence (see, for example, /Röshoff and Cosgrove, 2002/) or to unloading and stress release during removal of a cover sequence remains unresolved. Infilling of fractures with glacial sediment has been related to removal of the ice cover during the Quaternary period /Carlsson, 1979/.

Finally, the reactivation of structures opens a key question concerning the present character of the fractures at the site. This question concerns to what extent the increased frequency of open fractures and the common occurrence of clay minerals along the gently dipping zones is controlled by the favourable orientation of this set to reactivation, with respect to the present orientation of principal stresses (see Section 6.4).

Remaining uncertainties

The following more significant uncertainties remain following the development of the deterministic deformation zone models, version 1.2.

- The presence of undetected deformation zones.
- The characters of the geological feature that are represented in many of the inferred lineaments.
- The length and down-dip extension, the dip and the thickness of deformation zones interpreted with the help of linked lineaments. This uncertainty is of major significance in the alternative deformation zone model, where many lineaments have been interpreted as low-confidence deformation zones.
- The length and down-dip extension, and the thickness of the gently dipping zones that are based, to a large extent, on the seismic reflection data.

11.2.3 Discrete fracture network (DFN) model

The DFN model is described in detail in /La Pointe et al. 2005/. The conceptual framework of the model was derived from appropriate statistical testing of initial hypotheses that concern salient aspects of the model geometry and the geological controls on this geometry. These analyses gave rise to the following model aspects and considerations.

1. The DFN model consists of four sub-vertical sets and one sub-horizontal set of fractures. The four sub-vertical sets strike in the same direction as the trend of the structural lineaments that are inferred to represent deformation zones and that are treated as single fractures in the statistical analysis. The size distribution parameters of these four sets of fractures are consistent with the size distribution parameters of the inferred deformation zones, suggesting that there are four sub-vertical sets with sizes varying from centimetres to kilometres. It is not known if the sub-horizontal set is related to any of the sets of inferred deformation zones. The fracture sets appear to be old, dating back to the early deformational phases prior to 1,700 million years ago. Recent processes, such as deglaciation and crustal rebound, do not appear to be responsible to any significant extent for the observed fracturing.
2. The fracture intensity and the presence or absence of particular sets vary by rock domain. They also can vary significantly within a specific rock domain. There are sections of relatively constant orientation and intensity in boreholes on the scale of hundreds of metres within individual rock domains. However, the variations among these sections can be quite significant. The geological reasons for these volumes of relatively constant fracture intensity are not currently understood.
3. The sizes of the four sub-vertical sets are relatively well constrained, at least for rock domain RFM029 for which there are abundant data. The size statistics are more poorly known for other domains and, in fact, are not known at all for several rock domains. Particularly important is the possible sizes of the sub-horizontal fractures. Present data do not indicate whether these fractures may have radii of tens of metres, hundreds of metres or even kilometres. Clearly, this uncertainty could have a major impact on regional flow modelling.

The values of the DFN parameters are based on analyses described in Section 5.5. A summary of the model parameters and their best estimate values is provided in Table 11-1 (see also Tables 5-34 and 5-35 for ranges in parameter values). However, in order to fully appreciate the content of Table 11-1 and associated uncertainties in the parameter values, users of the DFN model should take part of the supporting report by /La Pointe et al. 2005/ and the DFN model summary in the SKB model database Simone.

Table 11-1. Summary of DFN model parameters.

Model summary					
Number of sets	5	Four sub-vertical associated with lineament trends; one sub-horizontal			
Orientation of sets		Probability distribution model	Mean Pole trend/ Plunge	Dispersion	Major Axis Trend/ Plunge (if applicable)
	NS	Bivariate Fisher	92.4/5.9	19.31, 19.69	355.3/50.2
	NE	Bivariate Bingham	137.3/3.7	-17.09, -9.1	38.1/68.2
	NW	Fisher	40.6/2.2	23.9	
	EW	Fisher	190.4/0.7	30.63	
	HZ	Fisher		8.18	
Size	Set	Probability distribution model	Exponent	Minimum radius (m)	
	NS	Power Law	2.88	0.28	
	NE	Power Law	3.02	0.25	
	NW	Power Law	2.81	0.14	
	EW	Power Law	2.95	0.15	
	HZ	Power Law	2.92	0.25	
Spatial	Poissonian within each Rock Domain				
Rock Domain	Set	Fracture intensity – P₃₂ (m²/m³)			
		Open fractures	Partly open	Sealed	Total
RFM029	NS	0.12	0.01	0.47	0.60
	NE	0.46	0.05	1.56	2.07
	NW	0.16	0.01	0.27	0.45
	EW	0.05	0.00	0.17	0.23
	HZ	0.34	0.01	0.26	0.61
	All	1.13	0.09	2.73	3.95
RFM018	NS	0.26	0.05	0.43	0.74
	NE	1.01	0.18	1.43	2.62
	NW	0.36	0.05	0.25	0.66
	EW	0.11	0.02	0.15	0.29
	HZ	0.73	0.04	0.24	1.01
	All	2.47	0.34	2.50	5.31
RFM017	NS	0.01	0.01	0.51	0.53
	NE	0.02	0.04	1.70	1.77
	NW	0.01	0.01	0.30	0.32
	EW	0.00	0.00	0.18	0.19
	HZ	0.02	0.01	0.28	0.31
	All	0.06	0.08	2.98	3.12
RFM012	NS	0.22	0.10	1.04	1.36
	NE	0.84	0.37	3.46	4.67
	NW	0.30	0.11	0.60	1.01
	EW	0.09	0.04	0.37	0.51
	HZ	0.61	0.09	0.57	1.27
	All	2.06	0.71	6.05	8.82

11.3 Rock mechanics description

The rock mechanics description of the site comprises the mechanical properties of the rock mass and its components (i.e. intact rock and fractures) and the stress conditions in the model volume. The determinations of these properties are based on geomechanical information, geological and rock mechanics conceptual models, laboratory and in-situ testing, and construction experience. The estimated mechanical properties and rock stresses combined with the hydraulic conditions provide the ground for design and safety assessments of a possible repository at the Forsmark site.

11.3.1 Mechanical properties

The basis for the rock mechanics modelling is the present version of the geological models for the site, i.e. the rock domain model, the deformation zone models and the discrete fracture network (DFN) model. These models specify: i) the partitioning of the rock mass into geologically homogeneous rock domains; ii) the position and geological description of the deformation zones and; iii) the orientation, size and frequency of the natural rock fractures. All this information is used in the rock mechanics modelling to determine the deformability and strength properties of the rock mass. The geological information is complemented by newly acquired laboratory data from the Forsmark site investigation programme. The tests providing these data were: 68 uniaxial compressive tests, 59 triaxial compressive tests, 143 tensile strength tests, and 218 P-wave velocity determinations on intact rock. In addition, 96 shear tests on 28 samples and 142 tilt tests were carried out on natural rock fractures.

Based on the laboratory results, the mechanical properties of the intact rock are summarised for the two dominant rock types at Forsmark: granite to granodiorite, and tonalite to granodiorite. The frequency distributions from the laboratory results of uniaxial compressive and tensile strength, cohesion and friction angle, Young's modulus and Poisson's ratio and "crack initiation stress" are approximated with truncated normal distributions. The average uniaxial strength is 225 MPa for the granite and 156 MPa for the tonalite (cf. Table 6-2). The crack initiation stress is about 53% of the uniaxial compressive strength. The average Young's modulus of the two rock types is very similar and ranges between 72 and 76 GPa (Table 6-2). The Poisson's ratio of the tonalite (average 0.27) is larger than that of the granite (average 0.24) (cf. Table 6-2).

Samples of natural rock fractures were tested and cohesion, basic and peak friction angle, normal and shear stiffness were determined. The data indicate that the differences between the properties of the different fracture sets are small and can be neglected.

Based on the geological loggings along four boreholes (KFM01A, KFM02A, KFM03A and KFM04A), the characterisation of the rock mass was carried out for depths between 100 and 1,000 m by means of the empirical characterisation systems RMR and Q (empirical approach, Figure 11-4). From the values of RMR and Q, the mechanical properties of the rock mass were determined by means of empirical relations. A series of parallel analyses was also numerically performed to predict the mechanical properties of the rock mass by the Distinct Element Method (theoretical approach). The same stress levels as for the empirically determined parameters were adopted when this was possible. The results of the empirical and theoretical approach were then merged to produce a set of representative mechanical properties of the rock mass (e.g. deformation modulus in Figure 11-5). The process of merging the results of the two approaches allows the quantification of the uncertainty on the rock mass properties. For rock domains RFM012, RFM017, RFM018 and the deformation zones intercepting the boreholes, no DFN model parameters were available, thus, numerical analyses were not carried out. The empirical approach alone was used for the characterisation of the rock mass in these domains. For the regional deformation zones (Singö, Forsmark and Eckarfjärden zones), information available from the excavations for the SFR repository and for the construction of the Forsmark power plant was used.

The mechanical properties of the rock mass, interpreted as a continuum equivalent medium at tunnel scale (about 30 m), are given as truncated normal distributions. The apparent uniaxial compressive strength, cohesion and friction angle, tensile strength, deformation modulus and Poisson's ratio of the rock mass were determined.

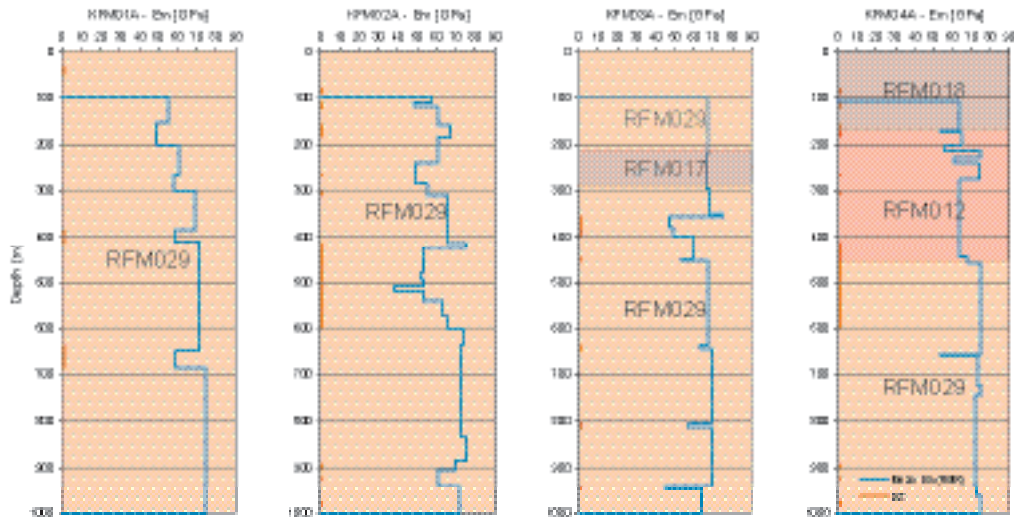


Figure 11-4. Deformation modulus of the rock mass (E_m) from the empirical relations with RMR along the boreholes. The rock domains and deformation zones are also indicated.

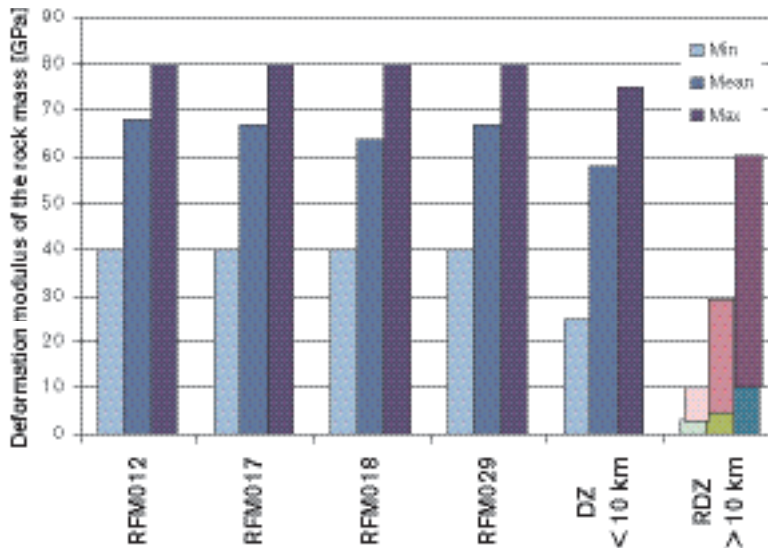


Figure 11-5. Deformation modulus of the rock mass in the rock domains and deformation zones. The values in blue apply for all confinement stresses. For the regional deformation zones (length > 10 km), the deformation modulus for low confinement (green) and for confinement larger than 10 MPa (violet) is shown.

The rock mechanics modelling results for the competent rock mass in rock domains RFM012, RFM017, RFM018 and RFM029 indicate high strength and low deformability (Table 6-7). The apparent friction angle ranges between 46° and 49° , and the cohesion between 20 and 24 MPa for all rock domains. Also, the deformation modulus is rather high (average between 64 and 68 GPa) and, for this reason, it is assumed to be independent of the rock stresses.

The deformation zones are classified into two groups based on their length: zones longer and shorter than 10 km. To the first group belong the regional deterministic zones (Singö, Forsmark and Eckarfjärden zones). Their deformation modulus is estimated to be on average 5 GPa, for low stresses, and about 30 GPa for confinement stresses larger than 10 MPa, respectively (cf. Table 6-8). The friction angle of the regional zones was estimated to be around 35° . To the second group belong the deterministic deformation zones and the minor deformation zones within the rock domains shorter than 10 km. Their deformation modulus is estimated to be on average 58 GPa (cf. Table 6-8).

This relatively high value is considered independent of the confinement stress. The strength parameters of the deterministic deformation zones did not differ much from that of the competent rock. The friction angle, for example, was evaluated to vary between 35° and 51°.

The rock mechanics model also quantifies the variability and uncertainty of the rock mass mechanical properties. The variability of the geomechanical input parameters is considered as well as the cumulative effect of several independent parameters (e.g. intact rock strength, fracture strength, mineral infilling, fracture orientation and length). The spatial variability of the mechanical properties is then represented by the standard deviations of their normal distributions. An attempt to quantify the uncertainty induced by the assumed conceptual models was also made. In fact, the results from the empirical approach, based on experience, and theoretical approach, based on constitutive models, are compared and merged. The differences between the two approaches are used to quantify the conceptual uncertainties. For the competent rock mass in the rock domains, the uncertainties on the mean parameters were estimated to be: i) between $\pm 10\%$ and $\pm 32\%$ on the strength (except for the friction angle where it was between $\pm 1\%$ and $\pm 5\%$) and; ii) between $\pm 3\%$ and $\pm 15\%$ for the deformability. In the same way, the uncertainties on the mean parameters of the deformation zones shorter than 10 km were evaluated to be: i) between $\pm 17\%$ and $\pm 45\%$ on the strength (except for the friction angle where it was $\pm 7\%$) and; ii) about 20% for the deformability. For the regional deformation zones, the uncertainties were judged to be double those for the other deformation zones.

11.3.2 In-situ stress state

While the characterisation of the rock mass focuses on the rock mass mechanical properties, the state of stress determines the mechanical boundary conditions to which the rock mass at the site is subjected. Besides the old overcoring measurements in boreholes DBT-1 and DBT-3, the state of stress is estimated based on new overcoring and hydrofracturing results obtained in boreholes KFM01A, KFM01B, KFM02A and KFM04A. The data were complemented by the results of a review study on the regional stress state around Forsmark (Finnsjön, Stockholm, Björkö, Olkiluoto). The influence of the deformation zones and their kinematics on the stress field at Forsmark was analysed by means of DEM numerical models. Moreover, new studies were also carried out to improve the understanding of the phenomena of microcracking and core disking.

Based on these data and new studies, it can be concluded that the rock stresses at Forsmark are relatively high compared with typical central Scandinavian sites. The principal directions are in line with the regional NW-SE trend for Fennoscandia (Figure 11-6) and the major principal stress is aligned with the overall direction of the tectonic lens and the associated regional deformation zones. For a depth of 500 m, an average maximum horizontal stress of 45 MPa is estimated (Table 6-10). The stress gradient of this stress component with depth between 250 and 650 m is probably small (0.02 MPa/m) compared with the gradient at shallow depths. The variations in stress orientation and magnitude in the upper 100 to 200 m of the rock are believed to depend on local variability of the frequency and orientation of the fracture structures.

The rather flat topography of the site also suggests that the principal stresses are confined to the horizontal plane and the vertical direction. The in-situ measurements indicate that the vertical stress can be obtained from the weight of the overburden. The model gives a stress gradient of the minimum horizontal stress of 0.025 MPa/mm, thus larger than the gradient of the maximum horizontal stress. This result seems to match well the in-situ measurements.

The state of stress is modelled based on results independently obtained from direct and indirect measures of the stresses in the rock mass. Similarly to the mechanical properties, the uncertainties in the magnitude and orientation of the stress components were quantified. For rock domain RFM029, the value of the stress magnitudes is expected to vary within $\pm 10\%$ for the maximum horizontal stress and $\pm 20\%$ for the minimum horizontal stress, whereas the mean value of the orientations of the stresses could vary about $\pm 10^\circ$.

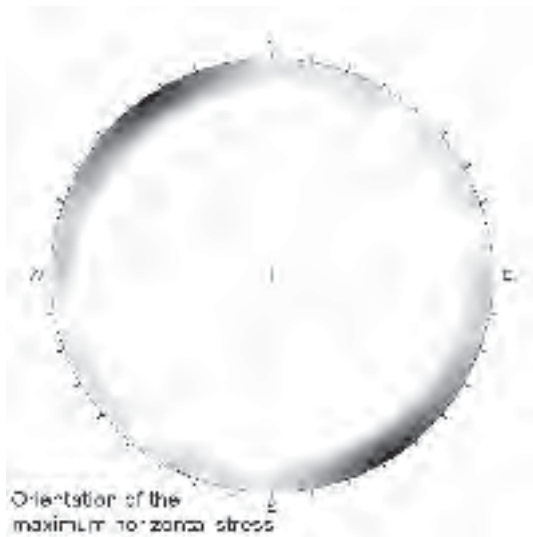


Figure 11-6. Pole density plot of the orientation of maximum horizontal stress at Forsmark.

11.4 Bedrock thermal properties

11.4.1 In-situ temperature

In-situ temperature has been measured in boreholes. The mean of the temperature loggings in 4 boreholes are 11.7°C at 500 m depth, see Section 7.2.8. Temperature versus depth is presented in Figure 7-3 and Table 7-11. The temperature increases with depth at a rate of approximately 1°C/100 m in the depth interval 400 to 600 m. However, the uncertainty in temperature at a specified depth is of the same magnitude.

Possible sources of uncertainty in the temperature logging results include the timing of the logging after drilling, water movements along the boreholes, and measured inclination of the boreholes.

11.4.2 Thermal properties

Thermal conductivity at canister scale was modelled for two rock domains with different modelling approaches. Results indicate that the mean of thermal conductivity is expected to exhibit a rather small variation between the different domains, from 3.46 W/(m·K) in rock domain RFM012 to 3.55 W/(m·K) in RFM029 (Table 7-13). The standard deviation varies according to the scale considered and for a possible relevant scale for the canister it is expected to range from 0.22 to 0.28 W/(m·K) (Table 7-12). Consequently, the lower confidence limit for the relevant scale is within the range 2.9–3.1 for the two domains under the assumption of a normal distribution.

The temperature dependence for the dominant rock type gives a decrease in thermal conductivity of 6.2–12.3% per 100°C increase in temperature. Parts of the dominant rock type have a clear foliation/lineation that results in anisotropy in the thermal transport properties. Laboratory measurements indicate that the difference in thermal conductivity in the two principal directions is about 40%, but the results have some uncertainties and the results may be both over- and under-estimated (see Table 7-9). There is also anisotropy at a larger scale caused by the orientation of subordinate rock types.

There are a number of important uncertainties associated with these results. One important consideration is the methodological uncertainties associated with the upscaling of thermal conductivity from cm-scale to canister scale. In addition, the representativeness of rock samples is uncertain and also the representativeness of the boreholes for the domains.

The estimated mean thermal conductivity for rock domain RFM029 is higher than previously estimated in Forsmark model version 1.1 (Table 7-14). The difference is about 4%.

The mean values of heat capacity for the two modelled domains is 2.17 MJ/(m³·K) with a standard deviation of about 0.15 MJ/(m³·K). Heat capacity exhibits rather large temperature dependence. For the dominant rock type the increase in heat capacity is 27.5% per 100°C temperature increase. The mean of the coefficient of thermal expansion was determined to be 7.0 to 8.0×10⁻⁶ m/(m·K) for the dominant rock types (Table 7-10).

11.5 Bedrock hydrogeological description

11.5.1 Hydraulic properties

The bedrock hydrogeological description treats rock domains RFM017 and RFM029 mainly, which cover large parts of the candidate area and, in particular, the target volume in northwest. RFM017 is quite small in comparison with RFM029 and the two rock domains may be treated as one domain. The candidate area is located at the coast of the Baltic Sea between the Eckarfjärden and Singö deformation zones, which are steeply dipping and parallel with the shoreline.

Hydraulic Conductor Domains, HCD

The HCDs are assumed identical to the *base model* deformation zones, (see Figure 11-2). A majority (27) of the 44 deformation zones are hydraulically tested and attributed transmissivity values. The hydraulic single-hole testing is done with two different test methods, injection tests and difference flow logging, and the results show a reasonable consistency on various measurement scales.

There is very limited in-situ information concerning HCD storage coefficients, kinematic porosities and transport apertures. In /Rhén et al. 1997b; Rhén and Forsmark, 2001; Andersson et al. 2000b; Andersson et al. 1998/ and /Dershowitz et al. 2003/ these parameters were estimated. Following these estimations, the aforementioned properties are modelled as different power-law functions of the interpreted transmissivities.

The zones' hydraulic thicknesses are estimated from the hydraulically active part of the zones' geological thicknesses as inferred from the single-hole geological interpretations. A cross-plot of the geological thicknesses versus the trace lengths of the outcropping deformation zone lineaments suggests that geological thickness correlates to trace length by a power-law function (see /Follin et al. 2005/).

Two significant observations made by correlating deformation zone transmissivity to deformation zone dip and depth are that gently dipping deformation zones generally have greater transmissivities than steeply dipping at comparative depths and that both gently and steeply dipping deformation zones have much greater transmissivities close to ground surface than at depth (see Figure 8-22).

Due to (i) the difference in transmissivity between gently and steeply dipping deformation zones, (ii) the spatial variability observed within individual zones, and (iii) the assumed dependencies of other hydraulic parameters on the transmissivity, it was decided to begin the regional flow simulations with simple deterministic trend models for the transmissivity assignment and then gradually include more sophisticated concepts such as random heterogeneity and local conditioning.

Hydraulic Rock Domains, HRD

Based on the core drilling results, the single-hole geological interpretations, the results from the hydraulic measurements with two different methods it is concluded that the rock mass at repository depth below the gently dipping deformation zone ZFMNE00A2 appears to be quite low-conductive and of very low kinematic porosity. This concept is based on the analysis of data from four core-drilled boreholes, KFM01A, KFM02A, KFM04A and KFM05A. Low-transmissive flowing features may exist below the lower measurement limit, but high-transmissive features probably occur in a very discrete fashion (large spacing) only.

Above repository depth, but still below the gently dipping deformation zone ZFMNE00A2, the rock mass is more fractured. The spatial variability of this increase is not known. The conditions observed in boreholes KFM01A and KFM05A suggest a sparsely fractured rock mass of low hydraulic conductivity rock in the depth range 200–360 m. Above c. 200 m depth, the rock mass fracturing and the hydraulic conductivity appears to increase rapidly.

Above the gently dipping deformation zone ZFMNE00A2, the hydrogeological conditions appear to be very different compared with the conditions below. The rock mass in between the deformation zones still has low fracture intensity, but the fractures are considerably more transmissive. Also, deformation zones are much more abundant, some of which have very high transmissivities and appear to be in good hydraulic contact with ground surface. This concept is based on the analysis of data from two core-drilled boreholes, KFM02A and KFM03A.

From a conceptual point of view, these findings opened up for different descriptions of groundwater flow and several conceptualisations were used in parallel to address the uncertainties invoked. The integrated analysis of the statistical description of the rock mass fracturing (cf. Section 11.2.3) and single-hole hydraulic measurements comprises many uncertainties and assumptions. These are described in detail in Chapter 8. The hydrogeological DFN analysis results in an interpretation where rock domain RFM029 consists of several HRDs of quite different characteristics from a hydrogeological point of view.

In model version 1.1, a direct correlation between fracture transmissivity and size was assumed. In order to illustrate the implications of this assumption, three alternative concepts were considered in model version 1.2:

1. Transmissivity uncorrelated to fracture size but with a log-normal variability (mean, $\mu_{\log(T)}$, and standard deviation, $\sigma_{\log(T)}$).
2. Transmissivity correlated to fracture size (by a factor, a and an exponent b).
3. Transmissivity semi-correlated to fracture size with random log-normal spread about a mean based on a correlated function (factor, a , exponent, b , and standard deviation, $\sigma_{\log(T)}$).

Each of the three concepts has an associated set of parameters, as given in the parentheses above, and it has been the objective of the hydrogeological DFN modelling to explore what ranges of parameter values that are required in the DFN simulations in order to obtain a match to hydrogeological data.

The conclusion drawn from the numerical simulations of flow to a borehole is that the three transmissivity models can be used as alternative cases with the parameterisation derived for the analysis of the PFL and PSS data presented in Chapter 8. However, the random variability of the uncorrelated transmissivity model makes the geometric mean of the hydraulic conductivity larger and the variance smaller for the 20 m block than for the 100 m block. This is one of several reasons that makes the uncorrelated transmissivity model unattractive. In contrast, the values obtained for the correlated model scale as expected. One argument for the correlated transmissivity model is that, at least for deformation zones, the zone width often increases with length (cf. above), and thus generally the number of individual conductive fractures associated with the zone. If the transmissivity distribution for individual fractures is the same, then, based on the assumption of parallel flow, the effective transmissivity for the fracture zone should increase with the length of the fracture zone.

Depending on which part of rock domain RFM029 that is considered, different block-scale properties are inferred (cf. Tables in Section 8.4.4). Above the gently dipping deformation zone ZFMNE00A2, the anisotropy in horizontal block-scale hydraulic conductivity appears to strike NW, whereas a NE strike seems to be present below this zone. Furthermore, the vertical block-scale hydraulic conductivity appears to fall in between the principal horizontal components. However, given the many uncertainties and assumptions involved, these simulation results are considered tentative.

In the regional scale analyses, different descriptions (conceptualisations) of groundwater flow are treated ranging from a homogeneous continuous porous medium (CPM) to a heterogeneous and anisotropic equivalent porous medium (EPM). The strategy adopted was to develop the HRD description with simple models and few parameters in order to gradually quantify parameter sensitivities before incorporating more complexity such as dependence on rock domains and DFN models with stochastic fractures. The following three stages were defined.

- *HRD1*: the rock mass within the entire regional model domain was simulated with a fixed hydraulic conductivity in the range 5×10^{-11} – 5×10^{-10} m/s. This range was based mainly on the PSS data for 100 m intervals in the rock outside the deformation zones. The purpose of the HRD1 model was to carry out a sensitivity analysis to bulk properties for a simple homogeneous CPM model.
- *HRD2*: the rock mass outside rock domain RFM029 was simulated with a hydraulic conductivity that was 10–100 times higher than the hydraulic conductivity within RFM029. This contrast was motivated by the PSS data reported from the investigations in the Finnsjön area. The purpose of the HRD2 model was to carry out a sensitivity analysis to bulk properties for a simple heterogeneous CPM model.
- *HRD3a*: the rock inside RFM029 was simulated as a multicomponent CPM. This is a moderately sophisticated alternative conception that invokes a simplistic treatment of the hydrogeological DFN findings.
- *HRD3b*: the rock inside RFM029 was simulated as a heterogeneous and anisotropic EPM based on five different fracture sets following the geological DFN model. This is a much more sophisticated model than HRD3a that can take different details of the hydrogeological DFN findings into account depending on the grid resolution.

11.5.2 Boundary and initial conditions

The initial conditions for the salt water distribution and water types at the end of the last glaciation are not known and different assumptions are tested. A best fit of simulated results to available measured data was obtained by employing freshwater conditions, mainly of glacial type, down to c. 500 m depth, with a linear increase of saline groundwater, mainly of brine type, below that to 10% by weight at a depth of c. 2,000 m. This gradient is perhaps too large as it gives an over-prediction of Brine at the base of KFM03A. The corresponding conditions below the gently dipping deformation zone are unknown.

Different top boundary conditions were tested ranging from a specified topographic head, a less undulating specified head and a specified flux type boundary condition. For the infiltration and surface properties considered, the water table was close to ground surface so the differences in results were very small.

Different sizes of the regional model domain were tested, both larger and smaller than the regional model volume, each of which was associated with no flow lateral boundary conditions. Very small differences in the characterisation of the present-day flow within rock domain RFM029 were noticed between the different model domains tested. There are several plausible explanations to this finding, e.g.:

- the low-conductive rock mass within RFM029,
- the low magnitude of the regional topographic gradient within the artificial boundaries of the regional model domain, and
- the existence of a regional surface water divide in the proximity of the candidate area.

This suggests that the size of the current regional model domain is sufficient for the present-day description. For description of future conditions it is concluded that the shoreline displacement process drastically will change the position of the shoreline, which in turn probably will affect the flow field within RFM029 to change from discharging to recharging conditions. However, the modelling of this process is outside the scope of this model version.

11.5.3 Groundwater flow and salt transport

Flow distribution

Various parameter sensitivity tests were carried out in order to study the impact on the flow field. For this purpose, particle tracking was used and particles were released from a fictive area within the target area of rock domain RFM029. The sensitivity tests addressed all three stages of the modelling – HRD1, HRD2 and HRD3. The main results from the sensitivity tests are summarised as follows:

- The presence and properties of deformation zones outside RFM029 have little effect on flow and salt transport inside the target area,
- Stochastic variations of the DFN have only a small influence on flow and transport compared to more important conditions such as the HCD positions and properties; this may justify the sufficiency of relatively few realisations of each HRD case,
- Deformation zone heterogeneity within the candidate area has a clear effect on the local flow distribution.

Matches with hydrogeochemical data

The two main conceptual models of the rock mass treated in model version 1.2, HRD3a and HRD3b, both give reasonable matches to the hydrogeochemistry data from boreholes KFM01A–KFM04A. However, three important observations are made, which are listed below.

- In general, both models make poorer matches with the measured chloride concentration in the upper one hundred of metres of most boreholes compared with the matches at larger depths.
- It was difficult to match the hydrogeochemistry measurements at depth without conditioning particular deformation zones to their measured transmissivity and thickness values at the borehole intersection where the groundwater water was sampled.
- Brine distribution is very stable for the whole simulation time due to the low hydraulic conductivity at depth, which is a consequence of the depth dependency in HCD properties that approach the rock mass hydraulic conductivity below about 700 m depth. Therefore, the Brine profile at 2,000 AD just reflects the initial condition assumed at the start of the simulation period, 8,000 BC.

The intuitive interpretations of these three observations are the following.

- Further simulations of how to best model alternative or spatial variable surface properties are required. In particular, the possible improvement of using a higher discretisation should be evaluated as it allows for a better description of the spatial variability of the overburden-bedrock interface. Of particular concern here is the hypothesis that the low permeability of the clay and gyttja-clay sediments together with the gently undulating topography limit the flushing of Littorina water stored in the rock and in the glacial till beneath the lakes.
- The hydrogeochemical measurements at depth, available for an integrated interpretation by hydrogeology, may reflect chemical properties of a flow system governed by the high transmissive deformation zones.
- The current hydrogeochemical data set is not sufficient for constraining the number of possible conceptual flow models that can be matched. However, it was noted that the uncorrelated transmissivity model gave higher block-scale hydraulic conductivities with a poorer match to the hydrogeochemical data than the correlated model.

The quality of the matching of the hydrogeological simulations with the mixing proportions calculated with the M3 varied between the kinds of reference water considered. The hydrogeochemical data are sparse, especially at depth, so it was difficult to constrain model variants and parameters with confidence. The uncertainties in the interpretation led to discussions between the modelling teams on how to best integrate with hydrogeochemistry. Concerning the use of hydrogeochemical information, it was found most convenient to define boundary and initial conditions in terms of reference water fraction, but for the calibration to compare the simulations against borehole profiles for $\delta^{18}\text{O}$, Cl and, more tentatively, Mg, to avoid additional uncertainties associated with the M3 interpretation.

11.6 Bedrock hydrogeochemical description

The results of the hydrogeochemical modelling, as described in Chapter 9, have been used to produce a hydrogeochemical site descriptive model. This is a conceptual hydrochemical model of the site that summarises most of the important findings. The model is visualised in the form of a vertical cross-section through the Forsmark site local model area, oriented in a NW-SE direction (for orientation see Figure 9-1). The cross-section, which is based on topographical and hydrogeological criteria and the locations of the site characterisation boreholes, is not positioned to approximate the main regional topographic gradient direction in the Forsmark local model area, which trends SW-NE. Instead, it was chosen parallel and fairly close to the coastline in order to represent some of the groundwater flow directions diverted along several of the major gently dipping deformation zones. Furthermore, it best illustrates the structural complexity of the site by intercepting the SW-NE trending steeply dipping deformation zones together with the suite of gently dipping deformation zones (e.g. A1, A2, A3 etc) in the south-eastern part of the candidate area. Therefore, the cross-section is extended down to a depth of approximately 2,000 m depth in order to accommodate the geological features identified (see also Figure 11-3).

The approach to locating and constructing this cross-section as well as another one is described in Appendix 1 in /SKB, 2005b/. Based on existing geological and hydrogeological information and in collaboration with the site hydrogeologists and geologists, schematic manual versions of these cross-sections were produced to facilitate illustrating the most important structures/deformation zones and their potential hydraulic impact on the groundwater flow (Appendix 1 in /SKB, 2005b/). This hydraulic information was then integrated with the results of the hydrogeochemical evaluation and modelling results to show the vertical and lateral changes in the groundwater chemistry. Figure 11-7 shows the major structural features with the main groundwater flow directions and relative velocities and the observed hydrochemistry along the NW-SE cross-section.

The local groundwater flow regimes within the candidate area are considered to extend down to depths of around 600 m, depending on the hydraulic conditions. Close to the Baltic Sea coastline where topographical variation is even less, groundwater flow penetration to depth will consequently be less marked and such areas will tend to be characterised by groundwater discharge. The conditions below 1,000 m depth within the candidate area as well as upstream the candidate area are not investigated, but are assumed to be more regional.

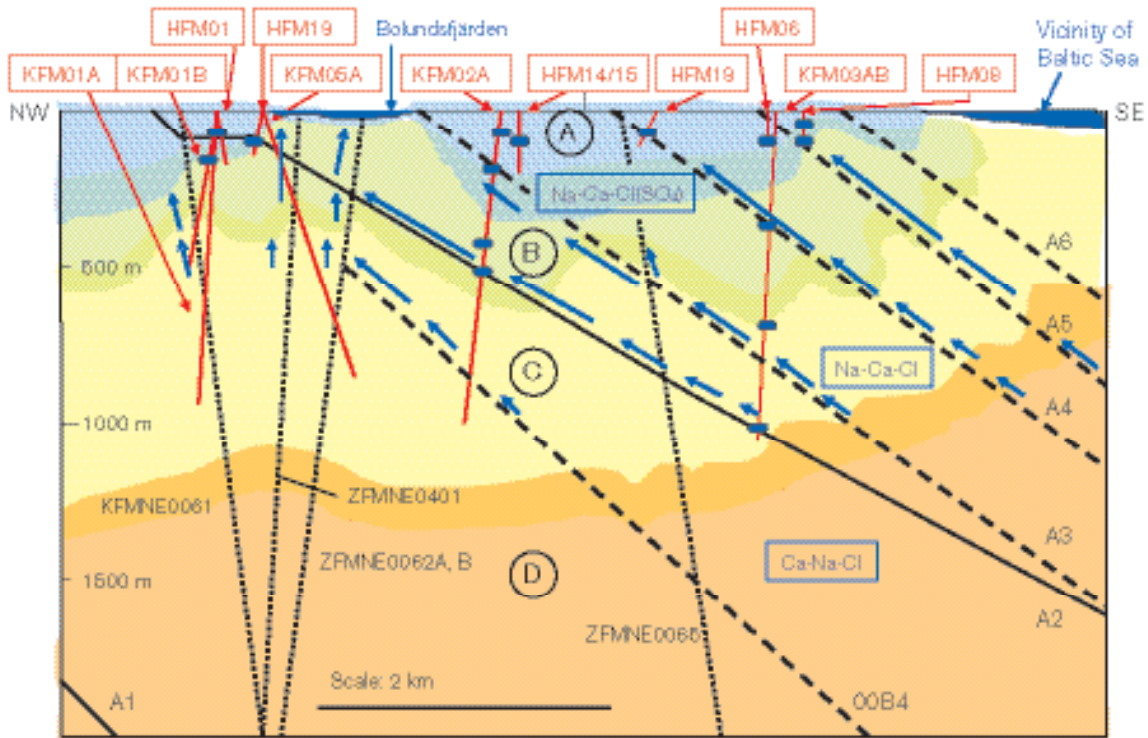
The complex groundwater evolution and patterns at Forsmark are a result of many factors such as: a) the present-day topography and proximity to the Baltic Sea, b) past changes in hydrogeology related to glaciation/deglaciation, land uplift and repeated marine/lake water regressions/transgressions, and c) organic or inorganic modification of the groundwater composition caused by microbial processes and water/rock interactions. The sampled groundwaters reflect to various degrees processes relating to modern or ancient water/rock interactions and mixing.

Four main groundwater types, Types A, B, C and D, are present (see Figure 11-7).

- A. Recent to young (0–15 TU) Na-HCO₃ type groundwaters of meteoric origin ($\delta^{18}\text{O} = \sim -11.7$ to -9.5‰ SMOW; $\delta\text{D} = \sim -85$ to -76‰ SMOW).
- B. Old (~ 13 – 22 pmC) Na-Ca-Cl(SO₄) type brackish groundwaters of Littorina Sea origin ($\delta^{18}\text{O} = \sim -11.5$ to -8.5‰ SMOW; $\delta\text{D} = \sim -85$ to -65‰ SMOW); some mixing with present meteoric water and/or cold climate water (glacial origin) is also characteristic.
- C. Saline Na-Ca-Cl type groundwaters, but devoid of a Littorina Sea signature (i.e. low Mg and SO₄), are present at greater depth (KFM03A; 645 m). It probably represents a mixing of deeper saline groundwater (Ca-Na-Cl) and a cold climate glacial water component ($\delta^{18}\text{O} = -11.6$ to -13.6‰ SMOW; $\delta\text{D} = -98.5$ to -84.3‰ SMOW) which continues to at least 1,000 m depth.
- D. Strongly saline, non-marine Ca-Na-Cl type of groundwater of deep origin is probably dominating at still greater depth ($> 1,000$ m). At the moment, this is suggested only by field observations during pumping tests.

Water type A: Dilute 0.5–2 g/L TDS; $\delta^{18}\text{O} = -11.7$ to -9.5‰ SMOW; Na-HCO₃; mainly Meteoric
Main reactions: Weathering, ion exchange, dissolution of calcite, redox reactions, microbial reactions
Redox conditions: Oxidising – reducing

Water type B: Brackish 5–10 g/L TDS; $\delta^{18}\text{O} = -11.5$ to -8.5‰ SMOW; Na(Ca,Mg)-Cl(SO₄) to Ca-Na(Mg)-Cl(SO₄); Marine (Strong Littorina Sea component) ± Meteoric; Glacial ± Deeper Saline component.
Main reactions: Ion exchange, pptn. of calcite, redox and microbial reactions
Redox conditions: Reducing



Water type C: Saline 10–15 g/L TDS; $\delta^{18}\text{O} = -11.6$ to -13.6‰ SMOW (only 3 samples); Na-Ca-Cl to Ca-Na-Cl; Glacial – Deeper Saline mixture
Main reactions: Ion exchange, microbial reactions
Redox conditions: Reducing

Water type D: Strongly saline > 20 g/L TDS; Ca-Na-Cl; Deep saline origin (Field observations)
Main reactions: Long term water rock interactions
Redox conditions: Reducing

Figure 11-7. Schematic 2-D cross-section integrating the major structures, the major groundwater flow directions and the variation in groundwater chemistry (Types A–D) from the sampled boreholes (indicated in blue). The cross-section is located parallel and fairly close to the current shoreline. The blue arrows are estimated groundwater flow directions close to the shoreline and their respective lengths reflect relative groundwater flow velocities (short = low flow; longer = greater flow. Note that in reality some of the boreholes are located at some distance from the transect (tens of metres) and have therefore been projected to their present position in the model (see Figure 9-1). Also, boreholes HFM01 and HFM02 (close to KFM01B) and HFM14 and HFM15 (close to KFM05A) are not indicated in the cross-section, but they have been taken into consideration.

The shallow Na-HCO₃ (Type A) groundwaters form a distinctive horizon at the centre of the cross-section, which lenses out towards the SE Baltic Coast where discharge of deeper groundwater probably occurs (Figure 11-7). From Bolundsfjärden to the NW, a less marked horizon is indicated, but data are few. In addition, the influence of the deformation zone A2 on the groundwater chemistry is not clear at this near-surface locality, but may represent some kind of boundary between Type A and the deeper Type B Littorina groundwaters.

Bordering the shallow Na-HCO₃ groundwaters, and extending from close to the surface (near the SE coast) to depths of around 500 m (e.g. along the gently dipping deformation zone A2), are the Type B Littorina Sea groundwaters. The shallow occurrence of Littorina Sea waters is supported by a soil pipe groundwater sample (SFM0023) collected under Lake Bolundsfjärden, which showed

elevated content of Mg and SO₄. An explanation to the preservation of Littorina water beneath Lake Bolundsfjärden can be the low permeability of the bottom sediments of the lake which together with the flat topography would limit flushing out of the water from the rock.

The distribution of the deeper, more saline groundwaters is based on few data, but these appear to represent much older groundwaters of deep origin (> 1,000 m) that have undergone mixing with cold climate glacial waters at least down to around 1,000 m depth. Lack of data prohibits a more specific interpretation.

Most lines of evidence support that the sulphur system, microbiologically mediated, is the main redox controller in the deepest and most saline groundwaters. On the other hand, Littorina-rich brackish groundwaters show variable and very high iron contents, in agreement with what has been observed in similar groundwaters elsewhere. The microbial analyses found only trace amounts of sulphate reducing bacteria (SRB) in these samples, but very high numbers of iron-reducing bacteria (IRB). However, there is no correlation between Fe²⁺ concentration and the number of IRB in these groundwaters. Moreover, they show very low but detectable contents of dissolved S²⁻ and the δ³⁴S values are very homogeneous (around 25‰) and clearly higher than in the present Baltic Sea, indicating that sulphate reduction has occurred. These observations could support the existence of an iron-sulphide precipitation process during the Littorina Sea phase of these groundwaters, but not being intense enough to effectively limit Fe²⁺ solubility.

A modelling approach, where observed fracture mineral phases were considered, was used to simulate the current composition of the groundwater in the Forsmark area by modelling the evolution when introducing Littorina Sea water. These results indicate that re-equilibrium reaction processes are important in the control of some parameters such as pH (as well as Eh, and some minor-trace elements), moving the waters towards the adularia-albite boundary. However, the main compositional changes, and even the extent of re-equilibration processes, are controlled by the extent of the mixing process.

The hydrogeochemical modelling also indicates that the groundwater composition at repository depth is such that representative samples from boreholes KFM02A: 509–516 m and KFM03A: 448–453 m meet the SKB chemical suitability criteria for Eh, pH, TDS, DOC and Ca+Mg.

In summary, the salinity distribution, mixing processes and the major reactions altering the groundwaters have been modelled down to a depth of 1,000 m, and an updated hydrogeochemical site descriptive model version 1.2 has been produced. Groundwater and isotopic data have, together with microbial information and data on colloids and gases, provided additional site descriptive information. Finally, the comparison with hydrogeological simulation results has supported the assumption that the groundwater composition can be modelled as results of mixtures between different water types affected by the paleohydrogeological development.

11.7 Bedrock transport properties

The strategy for site descriptive modelling of transport properties has been changed between model versions 1.1 and 1.2, such that flow-related transport parameters are not presented as a part of the version 1.2 site description. This implies that the site descriptive model considers parameters related to retardation (porosity, diffusivity and sorption coefficient) only.

Site investigation data from porosity measurements and diffusion experiments (in-situ and in the laboratory) have been available for model version 1.2. The work has included evaluation of data from the geological and hydrogeochemical descriptions, in addition to the evaluation of transport data. The version 1.2 transport model is described in a background report /Byegård et al. 2005/, which is summarised in Chapter 10.

11.7.1 Summary of observations

The main observations from the evaluation of transport data and data from other relevant disciplines can be summarised as follows.

- The major rock type in the candidate area is a medium-grained, biotite-bearing granite to granodiorite, metamorphic rock. The focus is on rock domain RFM029 as it constitutes the major part of the local site.
- Wall rock alteration is not common around open fractures (according to mapping less than 8% of open fractures). However, around water-conducting fractures alteration is much more common, although no exact figure can be given.
- The presence of different fracture coatings cannot be related to specific rock types at this stage.
- A mean porosity value of approximately 2×10^{-3} has been measured for the main rock type when all samples are considered. However, rock alteration was shown to influence porosity with increased porosity for altered samples. The strongly altered episyenetic samples show a very significant increase in porosity (porosity of $\sim 10\%$) compared with all other rock types included in the study.
- Laboratory resistivity measurements and through-diffusion measurements (on samples from similar location) indicate a clear correlation. A tendency of increased formation factor with increasing porosity can also be observed.
- The in-situ measurements yield a considerably lower formation factor than the corresponding laboratory measurements. Furthermore, for the laboratory resistivity measurements, a tendency of increasing formation factor with increasing borehole depth is observed. No such increase is observed for the in-situ results, which could be interpreted as sampling causing stress release and opening of the pores of the laboratory rock samples. Thus, it is advocated that diffusivities based on the in-situ resistivity measurements are used for the version 1.2 transport properties description. A formation factor of approximately 2×10^{-5} is thus reported for the main rock type.
- No sorption data are reported in version 1.2; however, available BET surface area measurements indicate that materials associated with rock mass fractures and deformation zones have high sorption properties.

11.7.2 Retardation model

The developed retardation model consists of two parts only, one for the major rock types, and one for the fractures and deformation zones combined. This is a simplification of the general methodology as outlined in /Widestrand et al. 2003/, and is motivated by the scarcity of data. The retardation model for the different rock types is given in Table 11-2.

Table 11-2. Suggested transport parameters (water saturation measured porosity and in-situ electrical resistivity measured formation factor) for the common rock types of the Forsmark area. Logarithmic scale (\log_{10} of the data), mean value \pm one standard deviation.

Rock type (SKB code)	Porosity (vol %)	Formation factor (-)
Granite to granodiorite, metamorphic, medium grained (101057)	-0.68 ± 0.15	-4.68 ± 0.24
Granite to granodiorite, metamorphic, medium grained (101057), episyenetic samples	1.05 ± 0.36	-2.23^A
Granite, granodiorite and tonalite, metamorphic, fine- to medium-grained (101051)	-0.64 ± 0.17	-4.93 ± 0.08
Pegmatite, pegmatic granite (101061)	-0.41 ± 0.22	-4.83
Amphibolite (101217)	-0.75 ± 0.28	-4.58
Granodiorite metamorphic (101056)	-0.52 ± 0.28	Pending
Felsic to intermediate volcanic rock, metamorphic (103076)	-0.11	Pending

^A Based on through-diffusion experiment result.

Generalising the information from core mapping and the more detailed fracture mineral studies, the following classification of different rock mass fracture types is presented as part of the retardation model.

- A. 50% have chlorite +/- calcite as fracture coating (max 0.5 mm thick on each side) and fresh wall rock.
- B. 10% have chlorite + clay minerals (+/- epidote, prehnite or calcite) as fracture coating (max 1 mm thick on each side). All of these fractures have altered wall rock > 3 cm (on each side of the coating).
- C. 15% have chlorite +/- epidote +/- prehnite as coating (max 0.5 mm thick on each side); all of these fractures have altered wall rock wall rock c. 1 cm on each side of the coating.
- D. 15% have laumontite + chlorite + calcite as fracture coating (max 0.5 mm thick on each side); all of these fractures have altered wall rock \geq 5 cm (on each side of the coating).
- E. 10% have quartz + calcite + pyrite (max 0.5 mm thick on each side) and fresh wall rock.

In Chapter 10, tables presenting parameterisations in terms of porosity and formation factor are given for fracture coating, altered wall rock, and fresh host rock of the different rock mass fracture types. It is observed that all data for fracture coatings are pending, and that no data on how the fracture types can be characterised in terms of direction or transmissivity interval exists.

It has not yet been possible to formulate a retardation model for the deformation zones due to data scarcity in version 1.2. Thus, at this stage the transport properties description is incomplete, since both the deformation zone description is lacking, and the description in terms of correlations to other parameters and properties of the system also is lacking. The presented model can, at this stage, primarily be used as a basic structure that can be subject to further discussion and development.

11.7.3 Implications for further work

A complicating factor in the present analysis is that considerable systematic differences are obtained between the in-situ formation factor measurements and the corresponding laboratory measured formation factors. Both methods involve methodological uncertainties; for the in-situ measurements there is only very limited information concerning the pore liquid composition, whereas laboratory samples have been exposed to stress release. Additional information and analysis is needed for better quantification of the uncertainties involved in the different methods.

The porosity measurements indicate a large spread in data, even for samples taken very close to each other. In forthcoming site descriptions it is foreseen that results from porosity measurements with alternative methods will be available, thus enabling sample heterogeneity to be addressed. It is also foreseen that a better description of site-specific sorption properties will be provided in forthcoming site descriptions of Forsmark.

12 Overall confidence assessment

The site descriptive modelling involves uncertainties and it is necessary to assess the confidence in the modelling. Based on the SKB integrated strategy report /Andersson, 2003/, and experience gained in version 1.1, procedures (protocols) have been further developed for assessing the overall confidence in the modelling. These protocols concern whether all data are considered and understood, uncertainties and the potential for alternative interpretations, consistency between disciplines, and consistency with understanding of past evolution, as well as comparisons with previous model versions. These protocols have been used in a technical auditing exercise as a part of the overall modelling work. This chapter reports the conclusions reached after that audit.

12.1 How much uncertainty is acceptable?

A site descriptive model will always contain uncertainties, but a complete understanding of the site is not needed. As set out in the geoscientific programme for investigation and evaluation of sites /SKB, 2000b/, the site investigations should continue until the reliability of the site description has reached such a level that the body of data for safety assessment and repository engineering is sufficient, or until the body of data shows that the site does not satisfy the requirements. Even if the construction and detailed investigation phase does not imply potential radiological hazards, it would still be required that no essential safety issues remain that could not be solved by local adaptation of layout and design.

12.1.1 Safety assessment needs

The Safety Assessment planning suggests that only certain site properties are really important for assessing the safety. These are:

- the intensity and size distribution of deformation zones and fractures within the potential repository volume,
- whether there is ore potential,
- the intact rock strength and coefficient of thermal expansion within the potential repository volume,
- the rock thermal conductivity within the potential repository volume,
- the distribution of hydraulic conductivity (or the transmissivity distribution of the DFN-model) in the repository volume,
- the spatial distribution of the hydraulically connected features to the extent that it allows assessment of the transport resistance along potential migration paths,
- the chemical composition of the groundwater, especially absence of dissolved oxygen and TDS levels below 100 g/L, at repository depth,
- the distribution of transport resistance, and
- the porosity and diffusivity of the rock matrix.

Generally, these properties are connected to the preferences and requirements already stated in /Andersson et al. 2000a/. Consequently, there is a need to ensure that the site modelling is able to produce qualified uncertainty estimates of these properties.

Furthermore, it is necessary to develop sufficient *understanding* of the processes and mechanisms governing the general evolution of the site. Such understanding would aid in addressing questions such as whether there can be fast flow paths due to channelling, what is the source of the brine at depth, what is the impact of rock stresses on available sorption surfaces in the rock, do we understand the impact of the mixing processes during the chemical sampling etc. However, full understanding of all aspects of a site is neither attainable nor needed. For example, some properties,

like thermal conductivity or rock matrix diffusivity, could show a high variability on the local scale, but the impact on performance, i.e. heat flow or resulting retention, depends on larger scale averages. Thus seemingly large variabilities will not have much impact in such cases and it is not necessary to determine the details of the small scale variation.

12.1.2 Repository Engineering needs

According to current thoughts within Repository Engineering, there are essentially three design issues to be addressed during the Site Investigation phase:

- Is there enough space?
- How could the layout be adapted with respect to mechanical stability and water inflow and how would such adaptation affect the degree of utilisation?
- Are critical tunnel locations (e.g. of problematic deformation zones) properly assessed?

The overriding issue of whether there is enough space for the repository may be divided into determining the generally available space and the degree of utilisation within that generally available space. The factors controlling the generally available space are the position and geometry of regional and local major deformation zones. Deposition tunnels must not be placed closer than a certain respect distance from such zones. Working definitions of respect distances exist, but some refinement work is still going on regarding what should be appropriate respect distances, see e.g. /SKB, 2004e/.

The repository layout is not only controlled by the regional and local major deformation zones. For example, deposition holes connected to large fractures or high inflows will not be used and the thermal rock properties affect the minimum allowable distances between deposition tunnels and deposition holes. During site investigations, this is handled in the design by estimating a “degree of utilisation” for the deposition panels already adjusted to the regional and local major deformation zones. Final selection of deposition holes and tunnels will be made locally, underground, during the construction and detailed investigation phase. Distribution of inflow to the deposition tunnels is an important aspect of the degree of utilisation. Apart from water, other factors affect the degree of utilisation. These include heat conductivity and rock mechanics properties affecting bedrock stability and the potential for rock spalling.

For the engineering planning and selection of the surface access point, it is necessary to identify and characterise potentially difficult tunnel locations (i.e. where the tunnel would pass close to or through deformation zones) in the rock. The information needed will be quite detailed, which means that the site description only will be used to identify potential access locations. At these locations there will later be a need to drill some additional exploration boreholes in order to assess the actual critical passages.

12.1.3 Assessing the importance of the uncertainties

As further discussed by e.g. /Andersson et al. 2004/ there are several planned occasions during the Site Investigation when Safety Assessment will be able to provide organised feedback as regards the sufficiency of the site investigations. The SR-Can project delivered its first interim report in mid 2004 /SKB, 2004e/, but the actual assessment will be published in 2006. Preliminary Safety Evaluations /SKB, 2002b/ of the investigated sites will be made using the respective version 1.2 SDM as input. Quantitative feedback from Safety Assessment could not be obtained before these studies, but the type of feedback to be obtained can still be assessed in relation to its potential impact on decisions related to the site investigation programme.

The overall confidence assessment presented in this chapter concerns i) whether all data are considered, understood, and what is the accuracy of, and biases in, the data, ii) what are the uncertainties in the models, their causes, potential for alternative interpretations and what further characterisation would reduce uncertainty, iii) consistency between disciplines, iv) consistency with understanding of past evolution, and v) comparison with previous model versions, Figure 12-1.

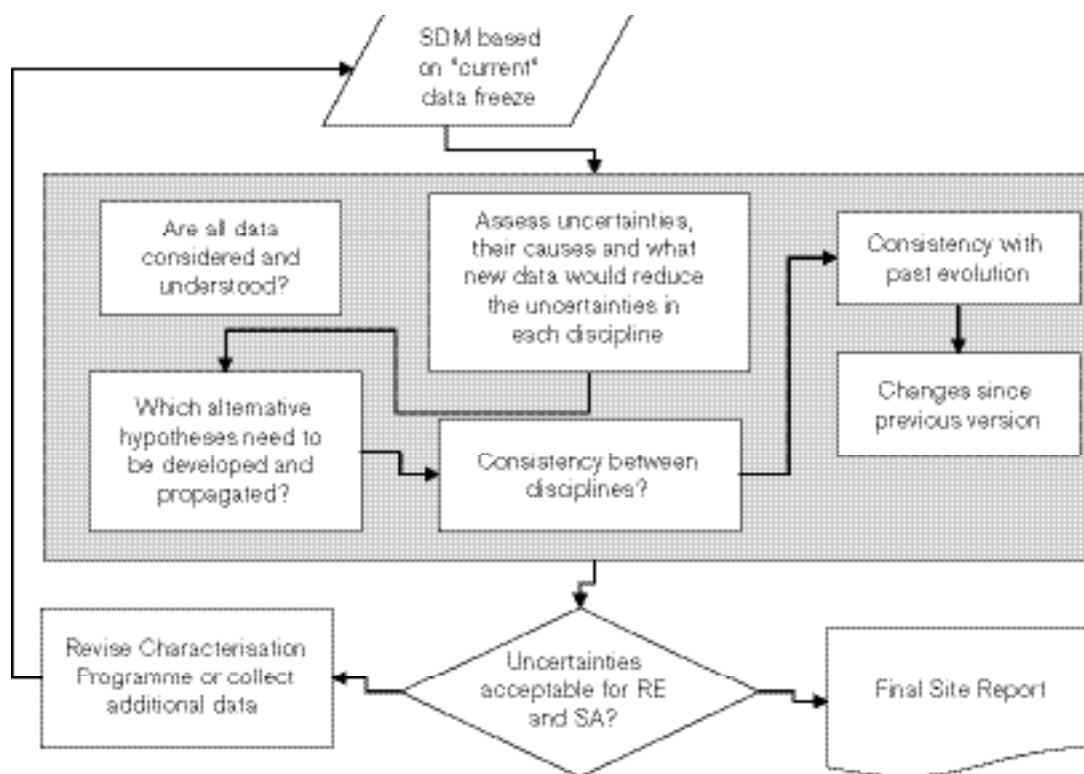


Figure 12-1. The overall confidence assessment presented in this chapter concerns the various aspects inside the grey box in the flow chart above.

Less emphasis is put on the importance of the uncertainties. Such an assessment could strictly only be done by the users and is a planned part of the design and safety assessment activities where the site descriptive model is input. Still, some general remarks based on the overall list of important issues as listed above can be made. A more comprehensive discussion on implications for further work is presented in Chapter 13. That discussion is based on the assessment presented in this chapter.

12.2 Are all data considered and understood?

Checking whether all data are considered and understood is the first step in the overall uncertainty and confidence assessment (see Figure 12-1). A similar and unbiased treatment of all data and interpretations that explain several different observations enhances confidence.

12.2.1 Answers to auditing protocol

A protocol has been developed for checking the use of available data sources. It concerns:

- Data that have been used for the current model version (by referring to tables in Chapter 2).
- Available data that have not been used and the reason for their omission (e.g. not relevant, poor quality, ...).
- If applicable – What would have been the impact of considering the non-used data?
- How accuracy is established (e.g. using QA procedures) for the different data (essentially by reference to tables in Chapter 2).
- For data (types) where accuracy is judged low – whether accuracy is quantified (with reference to applicable sections of this report or supporting documents).
- If biased data are being produced, can the bias be corrected?

The filled in auditing protocols are provided in Appendix 4. It should be noted that the questions sometimes produce long answers, but this does not necessarily mean grave impacts on the uncertainty for key features of the Forsmark site. The answers suggest the following overall observations.

Use of data

The database for the modelling is well defined and is accounted for in the tables of Chapter 2. Generally, all data available at the time of the data freeze 1.2 and as listed in the tables of Chapter 2 have been considered in the modelling. There are some exceptions, but these are judged to only have moderate or minor impact on the modelling.

In the *geological modelling*, regional gravity data reported in /Aaro, 2003/ have not been used. The data are of regional character, have been judged to be of insufficient resolution for reliable geophysical modelling and are judged to be of subordinate impact. Estimations of the dip of magnetic anomalies have not been used. These estimations were not available at the time of modelling, but would potentially have provided some insight in defining both the rock domain and deterministic structural models. Fracture data from boreholes and tunnels close to the nuclear power plant and SFR received lower priority, since virtually all these boreholes and tunnels have generated only near-surface data and there is no control on the strike and dip of fractures from these borehole data. The unused scan-line mapping of fractures at the five detailed mapped outcrops would not produce much more information on orientation and size than the detailed surface mapping, but the scan-line mapping of fractures carried out in connection with the bedrock mapping programme could provide information concerning the spatial variability of fracture intensity, pattern and orientation.

Rock mechanics data from percussion boreholes have not been used directly and previous characterisations of the rock mass at SFR, which concern shallow depths, have only been used for comparison. Available old rock mechanics data cover the area of the SFR and of the power plant and are thus marginal for the candidate area. Also, the laboratory tests have been used for comparison with the new laboratory results. However, a back analysis of the convergence measurements from tunnelling at SFR and through the Singö deformation zone could reduce the uncertainty of the mechanical properties of the regional deformation zones and of the rock stress field.

For the other disciplines, the impacts of the unused data are judged to be minor – if any. In the *thermal analysis*, anisotropy measurements presented in /Adl-Zarabbi, 2003/ have not been used due to uncertainties in the method. Modal analyses, where the sum of minerals differs to a large extent from 100%, have been excluded (few samples) and density loggings have not been used since there is no valid relationship between density and thermal conductivity for rock types in the Forsmark area. It has not been possible to go into detail regarding the evaluations of the *hydraulic* tests in boreholes drilled at SFR, Forsmark power plant and Finnsjön. Some old *hydrogeochemistry* data from Finnsjön were excluded already in version 1.1, see /SKB, 2004a/, due to differences in methods compared with the methods decided to be generally established for the site investigation, but the data have been used for comparison and for conceptual modelling. Also observations are excluded from the detailed modelling when there are representativity problems or when not being completely reported at the time of data freeze. *Near-surface chemical data* have not been used for modelling of temporal and spatial processes. Irrelevant or inaccurate data have also been omitted. Some geophysics on the *Quaternary deposits* has not been used in this version. These data will eventually allow better knowledge of the Quaternary deposits at depth.

Accuracy

Accuracy in field data and interpretation has generally been established using well-defined procedures, as is explained in detail in previous chapters of this report. In general, the data are taken from the SICADA database and have been subject to Quality Assurance in accordance with methods descriptions. Furthermore, the potential for inaccuracy stemming from inaccuracies in the field data is assessed and is judged to be a minor source of uncertainty in the resulting model description.

With the exceptions of the historic data (SFR and Forsmark power plant) that lack QA procedures, the accuracy of the *geology* data have been assessed in accordance with the QA procedures set out in the methodology. Furthermore, the reasonableness of data is checked on an “ad-hoc” basis.

For example, modellers have a dialogue with e.g. the Boremap core logging team, and also make their own inspections of the core and discuss their observations with the mapping team. Modellers are also involved in both the assembly and interpretation of surface data and in the development of single-hole interpretations. The following observations are made.

- The assessments of rock type and especially the character of mineral filling along fractures in the percussion boreholes are judged to be of significantly lower quality than the equivalent assessments in the cored boreholes, and the assessment of fracture intensity along such boreholes is judged to be of too low quality for use in model development.
- Minor mistakes could go undetected when coding the Boremap information.
- There are errors in orientation of the BIPS image in the deviation measurements of the inclined boreholes ranging from 1 to 8 degrees.
- Radar reflectors have low accuracy both in direction and in detecting fractures and are thus not used very much.
- Judgements involved in producing co-ordinated and linked lineaments give rise to major uncertainties in lineament length. Also the interpretation of lineaments in the vicinity of the nuclear power plant is judged to be of low accuracy.

Accuracy in the *rock mechanics data* have been assessed in accordance with the QA procedures set out in the methodology. It should also be noted that independent laboratory testing of intact rock was performed on a set of samples for quality assessment. The following observations are made.

- Accuracy can be low for the determination of the normal and shear stiffness of the rock fractures. A new correction during the processing of the data has been introduced.
- Accuracy of the tilt test results was judged lower than for direct shear tests on fractures. The tilt test results were used for comparison purposes only.
- The accuracy of the rock mass quality and rock mass mechanical properties was quantified in this model version. Q-logging was carried out by two consultants for the same borehole (KFM01A) with good agreement of the results. The smaller rock domains analysed have lower accuracy as do the deformation zones.
- The accuracy of the minimum horizontal stress from HF (Hydraulic Fracturing) is high, but the accuracy of the determination of the maximum (horizontal) stress from HF and HTPF (Hydraulic Testing of Pre-existing Fractures) methods is judged low, but has not been quantified. Accuracy of the determination of the stresses by means of OC (Over Coring) is also modest when the pre-existent deformations in the rock mass exceed the elasticity limit of the intact rock, whereas the accuracy of the orientation of the maximum principal stress is judged to be rather good. Comparison of the results from Forsmark and URL (Canada) has increased the confidence on the estimation of the stresses by using different measuring methods.

Accuracy in the *thermal data* has been assessed in accordance with the QA procedures set out in the methodology. Furthermore, reasonableness checks while working with the data have been carried out and results from different laboratories have been compared. The following observations are made.

- Temperature loggings from different boreholes show a variation in temperature at canister level. The difference is not large, but even such small differences could influence the design. Possible explanations are time of logging after drilling (drilling adds heat), water movements in the boreholes, an uncertainty in the temperature logging or errors in inclination measurements for the boreholes.
- For domains other than RFM029 and RFM012, there are not enough borehole data to adequately represent the domains, which limits the domain modelling of thermal properties. There is poor representativity of samples measured with TPS in rock types other than granite (101057) within the candidate volume.

With the exception of historic data from SFR, Forsmark Power Plant and Finnsjön, which were not obtained under approved QA procedures, accuracy in the *hydrogeology data* has been assessed in accordance with the QA procedures set out in the methodology. Furthermore, consistency checks

between different types of hydraulic tests have been performed. The following observations are made.

- Results from WL-tests and airlift-pumping generally have less accuracy than other hydraulic tests, due to the prevailing low permeability conditions.
- The measurement threshold of the PFL test is found to be sensitive to high flow rates in the upper part of the cored boreholes. A quantification of the inaccuracy is available.
- The interpretation of pumping tests and flow logging in percussion-drilled boreholes is highly sensitive to changes in the drill bit diameter due to wear. A quantification of the inaccuracy is available.
- Sediment-filled fractures may influence transmissivity values in the upper c. 50–100 m, see Chapter 8.

Accuracy in the *hydrogeochemistry* data has been assessed in accordance with the QA procedures set out in the methodology and the magnitudes of errors have been quantified. The effect of these errors on the interpretation is checked in the section on Explorative analysis (see Chapter 9).

Accuracy in the *transport* data has been assessed in accordance with the QA procedures set out in the methodology. The following observations are made.

- Accuracy in in-situ resistivity measurements depends on assumed water composition of the pore liquid. This composition is uncertain, but there is an ongoing programme to investigate the pore water composition in both Forsmark and Laxemar.
- There is low accuracy/precision in correlation between through-diffusion experiment results and data from resistivity measurements.

Accuracy in the *near surface* data has been assessed in accordance with the QA procedures set out in the methodology. Accuracy is judged low for the following data:

- Elements and compounds where concentrations are near the detection limits.
- Simple discharge measurements.
- The soil type map based on the regional Quaternary deposit map, but the classification errors are known.
- Production of biomass and standing stocks of biomass in the sea.
- Various biotic data.

As can be seen, most of the noted issues are not sources of uncertainty in the model description because they have been recognised as subject to error and therefore not used. Furthermore, this has not necessarily resulted in data gaps as the methods previously used have been replaced by alternatives.

Biases

There are some biases in the version 1.2 data, but many of the biases noted in version 1.1 data are now reduced. Some important examples are discussed here, but completed tables in Appendix 4 provide a fuller picture.

As pointed out in version 1.1, there is a bias concerning the more common recognition of lineaments and, in consequence, possible deformation zones in the land area compared with the sea area. This bias has been reduced by the incorporation of new data sets (e.g. bathymetric data in the Öregrundsgrepen area) in version 1.2. The bias has more or less been eliminated for lineaments longer than 1,000 m. However, it remains for the shorter lineaments. For this reason, this bias only has an affect on the stochastic interpretation of fractures and deformation zones. The bias has been eliminated by restricting the stochastic DFN model to essentially the land area.

There is also a bias in the lineament data due to truncation at the border of the regional model volume. This has been assessed by studying the influence of truncation on size and orientation.

There are several biases in the fracture data. As pointed out in version 1.1, there is a bias towards the recognition of different fracture orientation sets from boreholes and from surface outcrop data. The bias concerns an overemphasis of flat-lying fractures in sub-vertical boreholes and an overemphasis of steeply dipping fractures in surface outcrop data. A low variation in borehole orientation tends to emphasise this type of bias. This problem can be and has been reduced with the help of a Terzaghi orientation correction. The problem has been reduced further in version 1.2, since the subsurface data comes from boreholes with a variable trend and an inclination that is either sub-vertical or 60°. There is also bias, not assessed in the fracture data from outcrops, due to truncation at the border of the stripped outcrops. Another bias is caused by mapping only fractures longer than 0.5 m, but this bias has been assessed by studying all fractures at one outcrop.

Reflection seismic data from the surface focuses attention mainly on the occurrence of flat-lying structures in the bedrock. VSP (Vertical Seismic Profile) data from boreholes should help to rectify this imbalance. Such data were not planned for version 1.2, but will be available for version 2.1.

Bias in the rock mechanics interpretation is introduced because the boreholes are sub-vertical. Corrections have been applied to the fracture orientation and thickness of the deformation zones. However, some directional features and properties might have been overlooked. Sampling for mechanical testing has prioritised the homogeneous sections, as partly required by the testing method. This means that the measured spread in data is less than the actual spatial variation. Biases are also due to the limited extent over which surface rock mechanics logging has been carried out compared with the extent of the candidate area, but the relevance of the surficial information to rock mechanics is limited. Bias in the laboratory test results has been reduced by letting two different laboratories perform similar tests and comparing the results. New laboratory data are not available for the rock types sparsely occurring in the candidate area (e.g. pegmatite, gabbro, aplite). Moreover, there might be a tendency toward sampling specimens of good rock. This bias was partially corrected by inferring the mechanical properties of the weaker and/or underrepresented rock types, or using data from SFR. Bias in the sampling of rock fractures has been reduced by having access to a larger set of specimens and to specimens from an inclined borehole (KFM04A) and is not judged important for the model at this stage. Bias in old available data has been removed by using old data only for comparison. Bias due to uneven coverage of the Forsmark candidate area is judged low, thanks to the even spread of the boreholes over the rock volume of interest. As there is a strong bias in the maximum (horizontal) stress as estimated from the HF and HTPF methods, these data have not been used when analysing this component of the rock stress field.

Temperature logging has a possible bias from disturbance (from drilling and drilling fluid) during drilling. The effect has not been assessed, but would depend on the time after drilling (logging is usually done soon after the drilling). There is an unknown bias resulting from using modal data in the SCA (Self Consistent Approximation) method. Thus, SCA data are judged to be more uncertain than direct measurements (when available). SCA data have been compared with TPS data and, where possible, a correction of SCA data has been made. Generally, there is unknown representativity of modal analyses and TPS data due to possible biased sample selection. Sample selection has not been fully probabilistic. Samples were taken in order to characterise the general rock type – not to find odd varieties. Bias in data may be reduced (unknown on how much), but can be eliminated only for new data using probabilistic sample selection. The risk of systematic error in the determination of properties has been reduced by using different laboratories for the measurements.

Also, hydraulic data are sensitive to the trend and plunge of the fracturing relative to the orientations of the boreholes. However, for model version 1.2 there are data from several boreholes in different directions, which reduces the problem significantly. This effect will be further reduced in the future by incorporating more boreholes with other orientations.

Contamination from drilling fluid is a potential source of bias in the hydrochemistry data. Such biased data can be corrected by using back-calculations, but the representativity may still be in question.

For the transport data, there is a potential impact from disturbance (stress release) of laboratory samples. This would imply too high diffusivities etc in the laboratory samples compared with in-situ and there are some indications of this when comparing in-situ and laboratory formation factor data. However, the accuracy of the in-situ data needs also be considered.

Biases in the near surface data includes a lack of hydrogeochemical investigations of wetlands, over-representation of groundwater observation wells in local depression areas, over-representation of hydraulic conductivity values of the contact zone till/bedrock, under-representation of measurements of hydraulic conductivities of sediments and peat, and under-representation of stratigraphical investigations of wetlands compared with lake sediments. Complementary investigations are planned. Also, peat chemistry data only come from two different mires, which may not be representative for wetlands in the area. Corrections are not possible without complementary investigations. Most limnic data are from Lake Eckarfjärden, but corrections are not judged necessary since lakes in the area are very similar.

12.2.2 Overall judgement

In general most available data have been analysed and treated according to good practices. Inaccuracy and biases are understood and accounted for in the subsequent modelling. Inaccuracy and bias in the field data are, with some exceptions, judged to be a minor source of uncertainty in the resulting model description.

12.3 Uncertainties and potential for alternative interpretations?

The next step in the overall uncertainty and confidence assessment, see Figure 12-1, is to assess the uncertainties in the different discipline-specific analyses and modelling. Small estimated uncertainties and inability to produce many different alternative interpretations from the same database are indications of confidence – although not a strict proof. A related issue is whether new measurements or other tests could resolve uncertainties or distinguish between alternatives and thereby further enhance confidence.

12.3.1 Auditing protocol

The site descriptive model represents an integrated characterisation of a natural rock mass. Uncertainties are an inherent aspect of any such characterisation and thus also of the site descriptive model. There are different types or origins of the uncertainties. Some are conceptual and may depend on unresolved scientific issues or on inadequate understanding (and/or modelling) of the geological, physical or chemical properties or behaviour of the rock mass. Other uncertainties have to do with limitations in the available database due to spatial variations, temporal variations, measurement accuracy, quality of data or the lack of some data. Uncertainties cannot be avoided. It must be kept in mind that some uncertainties are more important than others, see Section 12.1. All main uncertainties should be identified, but efforts on quantifying and reducing uncertainty should primarily be focused on the important uncertainties.

The uncertainties need to be identified and the causes of uncertainty should be determined. Are the uncertainties mainly caused by inaccuracy in data, poor information density or is there limited process understanding. Specifically, confidence in the description could be high, even if there are few measurements, if the geological understanding is high (e.g. if there is a homogenous and evident geology), but could also be low, even with a ‘wealth’ of data, if the geological understanding is poor.

An important support for confidence in a model aspect (parameter/geometry or process) is to what extent it is based on support from different (independent) data rather than being based on “simple” extrapolation of a single measurement. A related issue is whether the selected conceptual model (model processes) with associated parameters have been determined through a calibration or validation exercise.

Another issue is whether a particular uncertainty could influence the assignment of uncertainty to another parameter. If two aspects of the site descriptive model (or of the input data) are correlated they cannot be estimated independently of each other. Addressing this issue will also provide input for assessing the need to consider interdisciplinary model interactions (see Section 12.4).

In order to assess the importance of an uncertainty it needs to be quantified. The quantification needs to consider the different causes of uncertainty.

One way of expressing uncertainty is to formulate an alternative representation. In a first step, potential alternative hypotheses are listed. These are then further evaluated – see Section 12.3.3.

Finally, the uncertainty assessment provides input to the question of if and how the site investigation programme should be continued. Among issues to consider are the questions of whether there are already available, but unused, data, which could be used to reduce uncertainty, and what new data would potentially help reduce or resolve uncertainty.

Thus, a common philosophy is required for addressing uncertainty and the implementation needs to be audited. There is a need to consider how uncertainties can be identified through uncertainty elicitation. Thus, a protocol has been developed for checking this. It concerns:

- Listing the main uncertainties in the different disciplines.
- Identifying the cause of the uncertainty (e.g. data inaccuracy, information density, uncertainty in other discipline model or process understanding), also indications from new data not yet fully analysed is a valid cause.
- Whether the uncertainty has been assessed considering information from more than one data source or through a calibration or validation exercise (a positive answer would be an argument in support of the adequacy of quantification of the uncertainty).
- Assessing the impact on other uncertainties (in all disciplines).
- Quantification of the uncertainty (with reference to applicable section of the site descriptive model report).
- Whether there is a potential for an alternative representation and whether an alternative actually has been developed.
- Whether there are unused data that could be used to reduce the uncertainty.
- What new data would potentially help resolve the uncertainty and are these new data already considered in the plans (“CSI programme”) for the Complete Site Investigations at Forsmark /SKB, 2005a/.

The filled-in auditing protocols are provided in Appendix 4. It should be noted that only some of the listed uncertainties would be of concern for Safety Assessment or Rock Engineering. As already explained, assessing the importance of these uncertainties lies outside the scope of the current report, but a general comment on this issue is made below.

12.3.2 Main uncertainties

Bedrock geological model

As already identified and discussed in Chapter 5, and as listed in Table A4-3 of Appendix 4, the main uncertainties in the version 1.2 *bedrock geological model of rock domains* concern:

- Composition, degree of inhomogeneity and degree of ductile deformation of rock domains at the surface in the sea areas, especially Öregrundsgrepen.
- Location of boundaries between the rock domains in the vicinity of Asphällsfjärden, within the area that has been selected as a “target area” for continued site investigations.
- Extension at depth of rock domains outside the NW part of the candidate area, selected as the “target area” for repository location.
- Numerical estimates of the proportions of different rock types in especially the inhomogeneous rock domains.

Since only magnetic anomaly data are available in the sea areas, there is considerable uncertainty in the composition, degree of inhomogeneity and degree of ductile deformation of rock domains at the surface in these areas. Due to restricted outcrop data, there is an uncertainty in the location of boundaries between rock domains in the vicinity of Asphällsfjärden that lies within the “target area”. Due to lack of data there is also uncertainty in the extension at depth of the rock domains outside the “target area”, i.e. in all domains except RFM017, RFM029 and to some extent RFM007, RFM012

and RFM018. Uncertainties in the numerical estimates of the proportions of different rock types, especially in the inhomogeneous rock domains, are due to questionable representativity of the data in RFM029 and absence of, or few, data in other rock domains. The uncertainty especially affects the thermal model. Borehole data are available to semi-quantitatively assess uncertainty for critical parts (“target volume”) of rock domain RFM029 (see Section 5.2.7). Bearing in mind the nature of these uncertainties, there is little justification for developing alternative models. All these uncertainties could possibly impact the regional model for rock mechanics properties and hydrogeology, but, apart from the uncertainty in rock type composition in the local volume affecting the thermal model, there are only very minor impacts on the models in the local model volume.

None of the uncertainties in the rock domain model are of significant importance for Safety, and they are only of limited importance for Repository Engineering. More detailed gravity data and seismic reflection data, would reduce uncertainties in the extension at depth of rock domains outside the “target area”, and a proposal is included in the CSI programme /SKB, 2005a/. The uncertainties would also be reduced by a dense network of shallow drilling into the bedrock beneath Öregrundsgrepen, drilling of bedrock along deeper boreholes and by estimates at selected outcrops in each rock domain. However, such characterisations are not justified, bearing in mind the needs related to the local model volume, and are not considered in the CSI programme /SKB, 2005a/.

As already identified and discussed in Chapter 5 and as listed in Table A4-3 of Appendix 4, the main uncertainties in the version 1.2 *bedrock geological* model of *deformation zones* concern:

- Presence of undetected deformation zones.
- Character of the geological features that are represented in inferred lineaments.
- Continuity, dip and thickness of deformation zones interpreted with the help of linked lineaments.
- Continuity and thickness of the gently dipping zones that are based, to a large extent, on the seismic reflection data.

Presence of undetected deformation zones is uncertain, since there is a strong focus in the geological programme on indirect data (interpretation of airborne and ground geophysical data, topographic and bathymetric data, and seismic reflection data), and a limited amount of direct data (poor exposure of deformation zones at the surface and limited borehole data). The uncertainty is assessed from different sources, through the independent alternative lineament interpretation and through independent checks concerning the interpretation of seismic reflection data. The larger deformation zones (> 3 km) are probably already all found and an alternative interpretation of lineaments has been completed to test the reproducibility of this interpretation work. Alternative structural models have been developed for the steeply dipping zones outside the areas where the data resolution is relatively high. A more stochastic approach has been adopted in the base model and a more deterministic approach has been adopted in the alternative model. The uncertainty has large impacts on the hydrogeology model and also affects rock mechanics. Indirectly, there are substantial implications for Repository Engineering and Safety Assessment.

The character of the geological feature that is represented by an inferred lineament is uncertain since various geological processes can explain the formation of a lineament. For some lineaments, the uncertainty is limited by using information from excavations and from percussion and cored boreholes through the inferred lineaments. For other lineaments, especially those outside the local model volume, it is uncertain whether they actually represent deformation zones, some do others do not. For this reason, an alternative model is set up, see previous paragraph. The uncertainty impacts the rock mechanics and hydrogeology models

Uncertainty in continuity, dip and thickness of deformation zones interpreted with the help of linked lineaments is of major significance in the alternative deterministic structural model, where many lineaments have been interpreted as low confidence deformation zones. There are poor constraints on the termination of some linked lineaments upon which the lengths of deformation zones are partly or entirely based. For down-dip extension, the conceptual model relating depth to length of lineament is uncertain. For dip and thickness, there are restricted amounts of data. In the “target volume”, the uncertainty is limited, since some percussion and cored boreholes go through some of the deformation zones based, to some extent, on the interpretation of linked lineaments. No such assessment is possible outside the “target area”. The uncertainty is provided as ranges for the position, orientation, thickness and length of all the medium and high confidence deformation zones documented in the

tables of the properties of deformation zones (see Section 5.4.4). Bearing in mind the broad nature of this uncertainty, there is little justification to develop alternative models. The uncertainty impacts the uncertainties in the models for rock mechanics and especially hydrogeology. Indirectly, there is a strong impact on Repository Engineering and Safety Assessment.

The continuity and thickness of the gently dipping zones that are based, to a large extent, on the seismic reflection data, are uncertain. There are poor constraints on the termination of seismic reflectors upon which deformation zones are sometimes based and there are limited thickness data. There are also different concepts to explain thickness variation. For some of these deformation zones the uncertainty is reduced since they are intersected by percussion and cored boreholes. The uncertainty is provided as ranges for the position, orientation, thickness and length of all the medium and high confidence deformation zones documented in the tables of the properties of deformation zones (see Section 5.4.4). Alternative structural models for the along-strike extension of the major, gently dipping zones (ZFMNE00A1, -A2, -C1 and -C2) have been developed (base model and base model variant). The uncertainty impacts the uncertainties in the models for rock mechanics and especially hydrogeology. Indirectly, there is a strong impact on Repository Engineering and Safety Assessment.

Uncertainties in the deformation zones have both Safety and Engineering implications, especially if these uncertainties relate to characteristics inside potential repository volumes. Uncertainties outside the target have little influence on the flow, as clearly demonstrated in Chapter 8. It should also be noted that the uncertainties are comparatively lower inside the “target area”, which means that eventually the uncertainty in deformation zones could be reduced to acceptable levels. The presence of deformation zones would be more certain if based on more fracture data from boreholes and tunnels close to the nuclear power plants and SFR. Excavation of representative lineaments at the surface, seismic refraction data at the surface, interpretation of the dip of magnetic anomalies and new borehole data from the bedrock close to these lineaments would reduce uncertainties in the character of lineaments and would also reduce uncertainties in continuity, dip and thickness of deformation zones interpreted with the help of linked lineaments. New seismic reflection data coupled with new boreholes in the marginal areas to the candidate area would reduce uncertainty in the continuity and thickness of the gently dipping zones. All these activities are proposed in the CSI programme /SKB, 2005a/.

As already identified and discussed in Chapter 5 and as listed in Table A14-3 of Appendix 4 the main uncertainties in the version 1.2 *bedrock geological discrete fracture network* model concern:

- The assumption that all lineaments represent brittle deformation zones.
- Size distribution.
- Size of sub-horizontal fractures.
- Spatial model of fracturing with depth.
- Variation of fracture orientation and size in the different rock domains.
- Fracture intensity and its variability in the model volume.
- Representativity of near-surface, sub-horizontal (stress-release) fractures for use in the DFN-model.

The assumption that all lineaments represent brittle deformation zones has already been discussed above. This assumption has a large impact on the *size* and *intensity* distribution and thus on the entire DFN-model. Extrapolating data from surface outcrops to several 100 m depths is coupled to considerable uncertainty, and the validity of the DFN cannot be fully addressed until detailed underground fracture mapping, and analyses thereof, has been performed. However, as further discussed in Chapter 5, the fracturing pattern was essentially established quite early in the geologic history. The oldest fractures are judged to have formed prior to 1,700 million years ago when the present rock surface was at a few km depths. Experiences from the Äspö HRL are that although the intensity of the surface fractures might be augmented by e.g. glacial processes, the relative length distribution, the orientations and the few surviving mineral fillings very well match the fracture array mapped some hundred metres below in the rock. Outcrop fractures can thus be used in the DFN, although uncertain, especially for obtaining the length distributions. A possibly more problematic issue is the conceptual uncertainty regarding whether lineaments and fractures from outcrop mapping belong to the same statistical size distribution. Interpolation between these data sets is necessary to bridge the

gap in data in the range 25 m to 1,000, where there are few direct measurements. Also, the size of sub-horizontal fractures is uncertain, due to poor information. At the current stage, these uncertainties in the DFN-model are only partly quantified. The DFN-analysis in Section 5.5 focuses on one alternative. However, other alternatives appear possible.

The *spatial model* of fracturing with depth is uncertain, since the orientation of fractures and the intensity changes with depth but the conceptual model (i.e. is fracturing related to lithology, proximity to DZ or just depth). The uncertainties are quantified as ranges of intensities, based on P10 and P21 in different borehole sections and outcrops, see Section 5.5. Section 5.5 also notes that alternative spatial models would be a possibility, based on the role of the deformation zone ZFMNE00A2 as a boundary between high and low fracturing intensities and where the near-surface rock is defined as a subdomain of its own. Such alternatives are developed within the hydrogeological modelling in order to match the fracturing with the observed strong variation in hydraulic properties of the rock. However, the exact spatial distribution of the variation is not fully established.

The variation of fracture orientation and size in the different rock domains is also uncertain. There are few orientation data in rock domains other than RFM029 and the size distribution is based on lineaments taken from all rock domains. In RFM029, there are different bounds defined to cover the specific variations in the different outcrops.

All uncertainties in the discrete fracture network model affect uncertainties in the rock mechanics and hydrogeological models. Indirectly, these uncertainties also affect Safety Assessment and Repository Engineering.

Uncertainties in the DFN-model have direct Safety and Engineering implications. Further characterisation efforts for reducing these uncertainties and already considered in the CSI programme /SKB, 2005a/ include: capturing old SFR-mapping data, trenches over lineaments in the “target volume”, evaluating fracture data with respect to lithology, mineralogy and proximity of deformation zones in each borehole (see also kinematics under evolutionary aspects below), more spatially representative borehole data, scan-line mapping in connection with bedrock mapping and more percussion holes and more outcrop mapping. Excavating and mapping larger areas (100 m × 100 m) of rock would enhance confidence, but have severe practical implications and is not part of the CSI programme. Mapping on outcrops with topographic relief, would in theory reduce uncertainty in the sub-horizontal fractures, but such outcrops do not exist at the site. Data from other rock domains than RFM029 are not planned in CSI and are perhaps not important – but would enhance understanding.

Finally, there is also some uncertainty in the *geological evolution*. There is poor control on the tectonic history in the brittle régime after c. 1,750 million years, due to limited process understanding that especially affects the timing. This impacts the uncertainties in the models for deterministic structures, rock mechanics and hydrogeology.

A more comprehensive analysis of the data concerned with mineral fillings along fractures in coming models may provide some new constraints on this problem. Closer interplay between data pertaining to the mineral fillings along fractures and the brittle structures at the site, especially fracture orientation sets, kinematic data along brittle deformation zones, reflection seismic data that may provide markers for relative ages of movement and geochronological data would enhance the understanding and reduce uncertainties. Proposals for all these studies have been included in the CSI programme /SKB, 2005a/.

Rock mechanics

As already identified in Chapter 6 and Table A4-4 of Appendix 4, the main uncertainties in the version 1.2 *rock mechanics stress* model concern:

- Rock stress magnitudes and their spatial and depth distribution.
- Rock stress orientation.
- High stresses under sub-horizontal deformation zones.
- Spatial variability of bedrock mechanics properties.

- Effects of pore pressure and stress on rock mass properties.
- Bedrock mechanics properties of deformation zones.
- Scale effects on the mechanical properties.

The rock stress magnitudes and their spatial and depth distribution are uncertain, since measured stresses are at the upper limit of applicability of the measurement methods. Different measurement and interpretation methods have been used: overcoring OC, hydraulic fracturing HF, core disk and transient strain analysis. The uncertainty ranges for stress magnitude are given in Chapter 6. No alternatives are given, since the estimated ranges are judged to be sufficiently accurate. The uncertainty affects rock mass parameters depending on stress, and indirectly also repository design.

There is some, but low, uncertainty in the rock stress orientation, due to limited data resolution (spatial). However, both regional and local measurement data have been analysed and the observations are considered to be understood. Uncertainty ranges, with no alternatives, are provided in Chapter 6 and the uncertainty is judged to be low. Thus, the uncertainty has a very limited impact on other disciplines.

There is uncertainty in the high stresses under sub-horizontal deformation zones. This stress increase has been observed in the boreholes and it is also indicated by numerical modelling. That is, the observed distinction is not really uncertain, but is not verified for all the sub-horizontal deformation zones. Uncertainty ranges are provided in Chapter 6, with no alternatives, since the observation is understood. This correlation observed in data and resulting from modelling improves confidence in the deformation zone model.

The spatial variability of bedrock mechanics properties is well known in rock domain RFM029 (“target volume” in granite to granodiorite, code 101057), but more uncertain outside, where there are few data. However, new laboratory data show small differences compared with the values in model version 1.1, which were based on data from SFR, i.e. data outside RFM029. Thus, there is some basis to suggest that the property values could be extrapolated outside RFM029. The mechanical properties of the rock mass for RFM029 were determined both by empirical methods and numerical modelling. The uncertainties of the derived mechanical properties have been quantified, see Chapter 6. There is no need for alternative models since uncertainties are considered sufficiently quantified. There are no consequences of the uncertainty on the other disciplines, but there is some impact on repository design.

There is an uncertainty in the constitutive relation as to how pore pressure and stress on rock affects rock mass properties. These effects can partially be considered by empirical methods and the theoretical/numerical modelling can explicitly take into account pore pressure and rock stress. However, neither of the two approaches has been tried so far and the uncertainty is not quantified. There are no consequences for the other disciplines, but some impact on repository design.

Rock mechanics properties of the deformation zones are uncertain since there are no laboratory data available on samples from the deformation zones. The mechanical properties of the rock mass for a number of local deformation zones (length < 10 km) were determined based on empirical methods. Regional deformation zones (length > 10 km) were characterised based on experience from SFR and the Forsmark Power Plant. The analysed deformation zones do not allow distinctions to be made between the properties of ductile and brittle zones. The determination is based either on just the empirical methods or on historical data. Furthermore, more realistic mechanical parameters could improve the rock stress model that, at present, assumes very low strength parameters. Uncertainty for local deformation zones was assessed by means of the empirical methods and quantification is given in Chapter 6. There is no need for alternative models, apart from the alternatives given in the alternative geological deformation zone models. There is no DFN-model available for the deformation zones. Thus, no numerical modelling of the rock mechanics properties of the deformation zones could be carried out. Had such modelling been carried out, it may improve the confidence of the deformation zone description. Otherwise, there are no consequences of the uncertainty on other disciplines, but there is an impact on repository design.

The scale effect on the mechanical properties is uncertain, since the fracture network properties may vary depending on the scale at which they are evaluated. This implies that the empirical and numerical methods are sensitive to the size of the rock mass block/borehole section analysed for rock mass characterisation. Neglecting this aspect can lead to uncertainty in the parameter determination. As further discussed in Chapter 6, the scale dependency of the Q and RMR values is analysed for four boreholes. RMR seems to be rather insensitive to scale. For borehole KFM01A, the deformation modulus obtained from Q might diminish up to 30% when passing from borehole sections of 5 m to sections of 20 m (see Chapter 6). Two potential alternatives could originate if the rock mass parameters derived from either Q or RMR are used, but for the current SDM, RMR is used as it is less sensitive to scale effects. There are no consequences of the uncertainty on other disciplines, but there is an impact on repository design.

Uncertainty in stress has great importance for Rock Engineering. The uncertainties would reduce from more stress measurements near the surface to estimate the stress gradient and by further checking the stress increase below sub-horizontal deformation zones. Furthermore, new data will probably confirm the present understanding of the stress orientations. Proposals for these studies are included in the CSI programme /SKB, 2005a/.

To improve confidence, measurements should be taken by means of overcoring and hydraulic methods at the same depth. The use of new independent methods for the determination of the rock stresses is also considered useful. One of the methods suggested by /Sjöberg et al. 2005/ is the sampling of cores of different diameters in relation to extensive core diskings. This method, although dependent on the occurrence of the core diskings, is completely independent of the other stress measurements and covers a range of stresses that the other methods usually fail to determine.

The CSI programme also includes new laboratory tests that together with characterisation of the rock mass outside rock domain RFM029 will reduce uncertainty of the rock mechanics properties outside RFM029. The new data will probably confirm the present results on the scale effects on the mechanical properties.

Different constitutive models on pore pressure effects on strength and deformability are available in the literature. No tests are included in the CSI. Uncertainty in rock mechanics properties of the deformation zones would possibly be reduced by back- analysing convergence measurements from the SFR construction. More data from deformation zones would certainly further reduce the uncertainties, but the question is if there is a need of lower uncertainty for planning construction. However, the deformation zones intercepted during construction should be explored (not included in the CSI).

Thermal model

As already identified in Chapter 7 and Table A4-4 of Appendix 4, the main uncertainties in the version 1.2 *thermal* model concern:

- Thermal conductivity, its spatial variability, scaling and anisotropy.
- Thermal properties in deformation zones.
- Heat capacity.
- In-situ temperature.
- Thermal expansion.

Uncertainty in thermal conductivity occurs at different scales ranging from uncertainty within rock types, uncertainty in upscaling laboratory size data to larger (e.g. canister) scales, spatial variability within rock types and rock type variability within rock domains. The spatial variability of mineralogy within a rock type is uncertain, as the representativity of the SCA and TPS data is uncertain. Anisotropy is also suggested in the data, but the interpretation is uncertain; it may be overestimated at the small scale measurements relative to its significance at the canister scale. Upscaling within the rock domain is also uncertain due to uncertainty in the spatial distribution of secondary rock types within the domain. The upscaling, including the anisotropy, depends on the structure, orientation and size distribution of these secondary rock types, and not only on their relative proportions.

Furthermore, the 3D geometry of most of the rock domains is uncertain. There are also uncertainties in the modelling approach. However, the uncertainty in SCA data has been evaluated by comparison with TPS data and by sensitivity studies. Different approaches are used to evaluate the variability in thermal conductivity. The spatial variability is quantified and discussed in Section 7.3.3. The impact of subordinate rock types in RFM029 is also quantified, so there is no need for alternatives. The uncertainty is captured as a distribution; with ranges in parameter values estimated by considering different approaches, see Section 7.3.3. The uncertainty does not affect other disciplines, but is of great importance for Repository Engineering and Safety Assessment.

The thermal properties in the deformation zones are uncertain, since there are no thermal data from them. However, the uncertainty is judged to be of limited importance (unless a zone is close to a deposition tunnel and then it ought to be assessed underground).

Heat capacity is uncertain due to the uncertain representativity of the TPS data. Still, a range is provided, see Section 7.3.3. The uncertainty only has limited impact on the thermal development.

The in-situ temperature is uncertain due to uncertainty in temperature data, possibly because of disturbance from the drilling and drilling fluid, convection in the boreholes, short-circuited flows in the boreholes, etc. The problem can be observed from differences between boreholes. A range is provided, see Section 7.3.3, and there is no reason for alternatives. The uncertainty does not affect other disciplines, and is in fact small, but is still important for Repository Engineering and layout.

Uncertainty in thermal expansion is possibly due to data inaccuracy. A comparison between methods and laboratories has been done but not yet reported. Also, stress dependence has not been assessed. The data are obtained from stress-released samples. A range is provided, see Section 7.3.3, and there is no reason for alternative models, but it is not determined whether the expansion is linear with T or not. The uncertainty does not affect other disciplines, but effects rock mechanics evolution due to heating.

The uncertainties have few direct implications for Safety, but are possibly important for Repository Engineering as further reduction in the uncertainty on the variability of thermal conductivity and also on the initial temperature would enable more efficient use of the rock volume. However, given the high thermal conductivity of the rock, it is likely that the thermal properties would not be the factor limiting the volume between canisters.

Representative direct measurements of thermal conductivity, data from more boreholes, more samples with both density and thermal conductivity measurements and measurements at a relevant scale will reduce uncertainty in the scaling of thermal conductivity. Large-scale tests of thermal conductivity in different directions would reduce uncertainty in anisotropy. These actions are already in the current CSI programme /SKB, 2005a/. Also, improved confidence in the rock domain model would help. The uncertainty would be further reduced by extensive sampling of other rock types to produce variograms of spatial variability and by more data from subordinate rock types (from existing or planned cores). Representative measurements of heat capacity would reduce uncertainty in heat capacity. Uncertainty in in-situ temperature may be reduced by reassessing the existing database and evaluate the possible effects of disturbance. Useful new data would be temperature logs at more representative (less disturbed) times. It may also be possible to reconsider the measurement procedure in order to mitigate the effects of long term thermal convection. Laboratory test method development, already underway, will reduce the uncertainty in thermal expansion.

Hydrogeology

As already identified in Chapter 8 and in Table A4-5 of Appendix 4, the main uncertainties in the version 1.2 *hydrogeological* model concern:

- Geometry and connectivity of deformation zones and the transmissivity distribution, spatial variability and depth dependence in deformation zones, especially outside the candidate area volume.
- Geometry and connectivity of the discrete fracture network (DFN) between the deterministically modelled deformation zones, and resulting transmissivity distribution in these fractures, including depth dependence and set dependence (anisotropy).

- Bedrock topography.
- Matrix porosity and salinity in matrix porosity (see transport properties).
- Boundary conditions.
- Processes: shoreline displacement, evapotranspiration, upconing, surface runoff.
- Palaeohydrogeology, initial conditions, in particular, the salinity profiles in the deformation zones, in the DFN and in the matrix.

The uncertainty in geometry and connectivity of deformation zones, as already discussed, also implies uncertainty as to how these modelled structures are coupled to structures of hydrogeological significance. Apart from the uncertainty in the geological model, this uncertainty is due to lack of hydrogeological data testing to determine whether there is a hydraulic contact between the rock inside the candidate area and rock outside, e.g. through gently dipping deformation zones. This also means that the transmissivity distribution and its spatial variability in deformation zones outside the candidate area are uncertain since there are few, if any, hydraulic measurements in these zones. Existing data from zones in the target area show spatial variability between zones and indications of a strong depth trend, but this trend is different for the gently dipping and steeply dipping deformation zones. This uncertainty could potentially affect the strength of the hydraulic contact between the rock inside the candidate area and the rock outside. The calibration against hydrogeochemistry data (palaeohydrogeology, see Chapter 8) provides some means of testing the current model. In principle, the uncertainty has a fundamental impact on the modelling of the regional groundwater flow and hydrogeochemical system. However, the uncertainty is explored by analysing the sensitivity to the transmissivity distribution in the regional groundwater flow modelling and by testing two alternative models for deformation zones in the regional domain, see Chapter 8. It is there concluded that the flow inside the target area is essentially insensitive to the regional uncertainties treated, whereas the spatial variability of the transmissivity for the zones inside the target volume would have an impact on the detailed flow in this volume.

There are several related uncertainties in the hydraulic properties of the rock mass between the modelled deformation zones. This concerns *division into volumes* of different hydraulic properties, the *connectivity* of the discrete fracture network (DFN), the *transmissivity* distribution in these fractures, *anisotropy* and the *spatial variability in the fractures*.

- As discussed in Chapter 8, the hydraulic data from the boreholes strongly suggest that the rock mass, also inside rock domain RFM029, should be divided into volumes of different hydraulic properties. Noteworthy is the volume below deformation zone ZFMNE00A2 and below about the –360 m level (denoted Volume D or G by the different modelling teams, see Figure 8-39), where there are essentially no measured hydraulic responses in the data. However, since there are few boreholes, the exact division of the different volumes remains to be defined.
- As already discussed, there is an uncertainty in the intensity of fractures in the size range 100–1,000 m. This is an important issue to be resolved by the geologists. This causes uncertainty in the connectivity of the fracture network, which also affects the assignment of transmissivity distributions to the fractures and the resulting block-scale hydraulic conductivities. The different volumes may be modelled as percolating networks of discrete features, however, with quite different hydrogeological DFN properties depending on the assumptions of the intensity of larger fractures in the DFN-model. In the low percolating networks it is necessary to set the transmissivity higher in order to match the total measured transmissivity in the different boreholes. Of special interest is volume D (or G). In this volume, there is no recorded transmissivity from the hydraulic tests. Depending on the assumptions made, alternative interpretations are possible ranging from a non-percolating fracture network, suggesting impervious rock matrix properties, to a poorly percolating fracture network with transmissivities that are low and below the lower measurement limit of the hydraulic test equipment. In the case of a non-percolating fracture network, flow and advective transport would essentially take place only in the deterministically modelled deformation zones, possibly with the addition of a very low hydraulic conductivity of the rock matrix itself. Current hydraulic data cannot be used to determine whether such a low conductivity exist in the rock matrix.

- In the hydraulic analysis, the main assumption is to correlate fracture size and transmissivity. However, alternative models, with no correlation or with some correlation, have also been applied to the data. These alternatives result in quite different block properties and are possibly less realistic, but cannot be excluded at this point.
- Whether fractures of different orientation have different transmissivity distribution (i.e. anisotropy) has been analysed. Data only suggest moderate anisotropy, but since there are few data this issue is still uncertain.
- Finally, there is likely to be a spatial variability of the transmissivity in the plane of each fracture. This will cause channelling and could also have an impact on the connectivity analysis. This uncertainty is not resolved in the site modelling, but is left for further analysis within safety assessment. However, it should be remembered that any assumption on channelling still must be consistent with the hydraulic observations.

Overall, the uncertainty in the hydraulic properties of the rock mass in the target area is at least partly quantified, and especially by considering alternative models of fracture network connectivity, and fracture transmissivity distribution. The uncertainty in the different volumes can, at this point, be represented by considering the range of properties for the different volumes. The uncertainties have direct implications for the groundwater composition, and the transport analysis in Safety Assessment.

The integrated evaluation presented in Chapter 8 of the near-surface and upper bedrock conditions together with hydrogeochemistry show that the thickness and hydraulic properties of the overburden as well as the highly transmissive and anisotropic uppermost parts of the bedrock probably needs a better discretisation in the regional bedrock hydrogeological model.

Matrix porosity and salinity in matrix porosity are uncertain due to lack of data from the rock matrix. The implications of the uncertainty are assessed in the palaeohydrogeology analyses by sensitivity studies. These uncertainties have an impact on the flow model and the integration with hydrogeochemistry and radionuclide migration.

There is uncertainty in various hydrological processes like the shoreline displacement, Littorina occurrence, evapotranspiration, up-coning and surface runoff. There is an evolving data base, and new models for shoreline displacement and Littorina occurrence are implemented and used. The importance of the uncertainty (sensitivity) is discussed in Chapter 8. It has an impact on the flow model and on transport paths and on the integrated evaluation together with hydrogeochemistry.

The impact of groundwater flow driven by regional topographic gradients is a matter of concern that has been treated by the modelling teams. The various sensitivity cases analysed, see Chapter 8, suggest that the regional model domain is sufficiently large for describing the hydrogeological conditions within the target volume where the impact on the flow is very small. The reasons for this interpretation are the existence of a major water divide in the proximity of the target area and the quite low-conductive rock at depth within the target area. The former governs the local flow pattern down to several hundreds of metres depth and the latter governs the flux of the (super) regional flow field. It is vital to note, that because of the shoreline displacement and the vicinity of the aforementioned major water divide, the hydrogeological conditions in Forsmark will change from discharge to recharge within the next couple of hundred of years.

The initial conditions (in particular, the salinity profile) used in the palaeohydrogeology analyses are uncertain. It could be questioned whether the current model of the shoreline displacement and the occurrence of the Littorina Sea period is sufficiently well understood and there will, by necessity, never be any data on the initial conditions. There is also a lack of hydrogeochemical data at depth due to sampling difficulties. There is a comparison between approaches at the sites in Sweden and in Finland. To assess the uncertainty, a few cases have been tested, but data indicate that the conditions at depth are reasonably well defined.

The uncertainties in the hydraulic DFN model have implications for the assessment of safety. The current description, with its alternatives, is judged appropriate to get a handle on the situation, but reducing the uncertainties is needed. New borehole data VSP, more reflection seismics, interference and cross-hole tests, Boremap, BIPS and PFL data for zones outside the “target area” and further

integration with geology may decrease uncertainty in the hydraulics of deformation zones. Such characterisation is planned in the current CSI programme /SKB, 2005a/. Existing PSS and PFL data can be used to test the transmissivity distribution in the discrete fractures by simulating existing tests performed at various scales. To some extent this is already made in the current model version. Data to resolve the geometry of fractures would come from more boreholes and single-hole interference tests could reduce uncertainty in the hydraulics of the discrete fractures. Such characterisation is planned in the current CSI programme /SKB, 2005a/. Detailed hydraulic tests 0–100 m below surface, may also be useful, but are not in the current CSI plan. The other discussed uncertainties would be reduced by new samples for estimating salinity in the rock matrix, new time series of near-surface hydrology data and boreholes in nearby boundaries and in the Baltic Sea from the bottom of the SFR. Such characterisation is planned in the current CSI programme /SKB, 2005a/.

Hydrogeochemistry

As already identified in Chapter 9 and in Table A4-5 of Appendix 4, the main uncertainties in the version 1.2 *hydrogeochemical* model concern:

- Spatial variability of hydrochemistry in 3D at depth.
- Temporal (seasonal) variability in surface water chemistry, which ultimately impacts the identification of discharge and recharge areas.
- Model uncertainties (e.g. equilibrium calculations, migration and mixing).
- Identification and selection of end-member waters, noting that there is a judgemental aspect of the M3 (principal components) analysis.
- Groundwater composition in the rock matrix.

The spatial variability of hydrochemistry in 3D at depth is uncertain, as the information density concerning borehole groundwater chemistry is low. Groundwater sampling causes mixing at the sampling point and the samples represent an average composition. However, a validation test has been conducted in which representative/non-representative samples have been utilised. Locally, there were samples containing as much as 50% drilling fluid, but if these unrepresentative samples were included in the site-scale interpolation the impact on the result was only in the order of $\pm 10\%$, see Section 9.6. Alternative representations are also discussed, but not quantified in Section 9.6. The uncertainty may cause uncertainties in the salinity interface in e.g. hydrogeological modelling and transport modelling and also contributes to the uncertainties in the overall hydrogeochemical understanding of the site.

Uncertainty in temporal (seasonal) variability in surface-water chemistry, which ultimately impacts the identification of discharge and recharge areas, occurs, since the processes are slow and the sampling may not describe the seasonal variation and samples may be taken at different time intervals at the surface relative to the shallow boreholes. The effects of seasonal variation have not been quantified, but they are identified, see Section 9.3. Different modelling approaches are applied to the same data set to describe the same processes, but there is no need for alternatives. The uncertainty can cause uncertainty in the interaction between surface waters and groundwaters and may affect transport modelling. The amount of reactions taking place at the surface may not be properly described.

There are model uncertainties in e.g. equilibrium calculations and in migration and mixing calculations. These uncertainties occur due to inaccurate pH measurements, inaccuracies in the thermodynamic databases, wrong mineral phase selections, wrong end-member selections, and model uncertainties. However, validation analyses are made where different modelling approaches are applied on the same data set. One unit error in the pH measurements may cause one unit error in the saturation index calculations. The uncertainties in the proportion of the different end-members in the M3-modelling are $\pm 10\%$, see Section 9.2, 9.5 and 9.6. Also, different modelling approaches are applied on the same data set to describe the same processes thereby confidence is built into the description, but there is no other need for different alternative models. The uncertainty may cause uncertainties in transport modelling and hydrogeological modelling and also contributes to the uncertainties in the overall hydrogeochemical understanding of the site.

There is a judgemental aspect of the M3 (principal components) analysis and the identification and selection of end-member waters, combined with a poor understanding of the palaeohydrogeology events. However, there is integration with hydrogeology to identify and use the same end-members. Different end-members have been selected in the regional/local models, but no other quantification of the uncertainty has been conducted, see Section 9.5 and 9.6. Different modelling approaches are applied on the same data set to describe the same processes for confidence building. The uncertainty may cause uncertainties in the chemical process description and in the integration with hydrogeology and also contributes to the uncertainties in the overall hydrogeochemical understanding of the site.

The groundwater composition in the rock matrix is uncertain since there are few measurements. The uncertainty is not quantified, and there is no reason for alternative models. The uncertainty may affect the hydrogeological modelling and transport modelling and the description of the interaction between high and low conductive groundwaters systems.

There are no direct Safety or Engineering implications stemming from the uncertainties in the hydrogeochemical model. The listed groundwater compositions are well within the bounds of the preferred conditions, see Chapter 9 and 11. Still, reducing the uncertainties would enhance understanding and thus the capability of predicting the future evolution. The uncertainties would be reduced by more data observations from deep boreholes, analyses of rock matrix samples, electromagnetic data for regional characterisation and data from extreme end-member waters. Samples for rock matrix determination have already been collected and the results will be available for model version 2.1. These characterisations are also part of the CSI programme /SKB, 2005a/. The planned deep regional boreholes, e.g. at SFR, are useful and the use of additional regional boreholes should be weighted against the information from already existing (Finnsjön, SFR) or planned sources. Whether there is a need to revise the sampling of near surface waters will be planned later.

Bedrock transport properties

As already identified in Chapter 10 and Table A4-5 of Appendix 4, the main uncertainties in the version 1.2 model of the *bedrock transport properties*¹ concern:

- Spatial variability and correlation between matrix transport properties and flow paths.
- Sorption and, to some extent, diffusion properties of the matrix.
- Sorption properties, diffusivities and porosities of the geologic material representative of the fractures (e.g., fracture rim zone, gouge material and fracture filling).
- Fracture representation in different fracture and minor/major zones and their correlation to rock migration properties.

The spatial variability and correlation between matrix transport properties and flow paths is uncertain since the data set is limited. There is also the question about the applicability of data collected in the laboratory to field conditions. However, generally the expectation is that the correlation between matrix and flow path properties is low, but with higher correlation between fracture surface and flow path properties. A range of properties for each different rock type is given, see Chapter 10. Correlation is hard to establish. Alternatives are not justified.

There is uncertainty in matrix retention properties, especially concerning sorption, due to spatial variability and the limited data set (no site specific sorption data). There is also the question of the potential impact of stress release on core samples and on the conceptual model of sorption. However, diffusion properties are assessed with electrical resistivity in both laboratory and field combined with through-diffusion experiments. The impact of stress release on core samples is assessed by comparing lab and in-situ tests. The uncertainty is quantified as a range of properties, see Chapter 10. Alternative descriptions are not relevant – uncertainty in the sorption process as such is assessed within Safety Assessment, e.g. in SR-Can. Uncertainty in diffusion properties also implies an uncertainty for hydrogeological salt modelling (matrix diffusion of salt).

¹ It should be noted that uncertainty in transport resistance is not analysed in the SDM but in the Safety Assessment context.

Sorption properties, diffusivities and porosities of geologic material representative of the fractures (e.g., fracture rim zone, gouge material and fracture filling) are uncertain as there is a shortage of relevant material and, so far, no performed measurements. These uncertainties imply an uncertainty for hydrogeological salt modelling (matrix diffusion of salt), but are of limited importance for Safety Assessment.

The fracture representation in different fracture and minor/major zones, based on the concept in the SKB strategy report for transport properties /Widestrand et al. 2003/, is uncertain due to the low numbers of hydraulically transmissive fractures and due to difficulties of presenting the data according to the proposed retardation model. In fact, it is unclear whether the correlation of transport properties to different fracture types and deformation zones could be resolved. The relevance of the deformation zone classification defined in the strategy report /Widestrand et al. 2003/ needs reconsideration. It is not evident that e.g. fracture size or transmissivity and the fracture filling mineralogy should be related. The uncertainty imply an uncertainty for hydrogeological salt modelling (matrix diffusion of salt), but is of limited importance for Safety Assessment.

The uncertainties are of importance for Safety but not for Engineering. The current description, with its alternatives, is judged appropriate to get a handle on the situation, especially by further uncertainty assessment within Safety Assessment, but reducing the uncertainties would be useful. More laboratory data will be produced during the CSI programme /SKB, 2005a/. This will reduce uncertainty in matrix retention properties and in sorption properties, diffusivities and porosities of geologic material representative to the fractures. More borehole data may also improve understanding of the potential correlation between fractures and migration properties, but the expectations are rather low.

Surface and near surface

As already identified in Chapter 4 and in Table A4-6 of Appendix 4 the main uncertainties in the version 1.2 model of *the surface system* are related to the lack of some types of data. Specifically, the most important gaps in the present database concern:

- The soil depth model.
- Stratigraphic distribution and character of organic deposits.
- Off-shore Quaternary deposits – character and thickness of sediments.
- Salinity variation in the Baltic.
- Spatial and temporal variability in meteorological data.
- Spatial and temporal variability in discharge.
- Surface water and groundwater levels.
- Evapotranspiration.
- Interactions between surface and bedrock systems.
- Transport of matter in the surface system.
- Chemistry in the regolith.
- Chemistry in groundwater from the Quaternary deposits.
- Biomass and production (flora and fauna).
- Chemical composition of biota.
- Occurrence of marsh gas.

These uncertainties will be reduced as additional data becomes available. Furthermore, uncertainties related to the understanding of site-specific processes will be analysed in future model versions. It is also worth remembering that there is a general conceptual uncertainty in that what is observed in the surface system at the present day may not be representative, even if climate conditions would not evolve, and that it may be desirable to adopt a modified description (e.g. more cautious) for Safety Assessment.

12.3.3 Alternatives

As discussed in the SKB strategy report for integrated evaluation /Andersson, 2003/ alternatives may both concern:

- an alternative geometrical framework (e.g. the geometry of deformation zones and rock domains), and
- alternative descriptions (models such as DFN or SC – or parameter values) within the same geometrical framework.

Alternative model generation should be seen as an aspect of model development in general and as a mean of exploring confidence. At least in early stages, when there is little information, it is evident that there will be several different possible interpretations of the data, but this may not necessitate that all possible alternatives are propagated through the entire analysis chain including Safety Assessment (SA). Combining all potential alternatives with all its permutations leads to an exponential growth of calculation cases – variant explosion – and a structured and motivated approach for omitting alternatives at early stages is therefore a necessity.

Compared with model version 1.1 there is an increased attention to alternatives in version 1.2. As can be seen from Tables A4-3 to A4-6 in Appendix 4, some alternative hypotheses have actually been developed into alternative models. Furthermore, the alternative hypotheses are all assessed in order to decide on their treatment. This assessment is based on addressing the following set of questions for each potential alternative identified:

- Is the alternative “resolved in version 1.2? (Only concerns hypotheses raised in version 1.1).
- Will the alternative affect other site descriptive models (or aspects of those models)?
- What are judged to be the important implications for Engineering in phase D1?
- What are judged to be the important implications for Safety Assessment analyses in PSE (Preliminary Safety Evaluation) and SR-Can?
- What are judged to be the implications for investigations to “resolve” alternatives?

Finally, based on the answers to these questions a recommendation is made whether the alternative should be developed and propagated, be discarded or be put “on hold”, by applying the following criteria:

Reasons to develop/propagate now:

- Potentially large impact on Safety Analysis or Repository Engineering.
- Potentially very expensive to resolve by further data collection.
- Issue judged to be good to put “at rest” early.

Reasons not to propagate/develop:

- “Old hypothesis” which is now resolved.
- Shown to have little impact on Safety Assessment or Repository Engineering (can be directly discarded).
- Could be factored into quantified uncertainty.

Reasons to wait with development/propagation:

- Judged to have limited impact on Safety Assessment or Repository Engineering.
- Will be resolved through expected investigations in later data freezes.

Alternative hypotheses not explored will be “kept on the list” for further scrutiny.

The judgements made for the different alternative hypotheses are summarised in Table 12-1. The judgements regarding importance for Safety Assessment and Engineering are preliminary, but have been reviewed by experts within the Safety Assessment and Rock Engineering teams.

Table 12-1. Assessment of alternatives.

Potential "Primary" alternatives in SDM	Is the need for alternative resolved in 1.2? (Only concerns hypotheses raised in version 1.1)	Is there a need to propagate the alternative to other SDM models (or aspects of these models)?	Implications for Engineering in phase D1	Implications for PSE analyses in PSE and SR-Can	Implications for investigations to "resolve" alternative	Handling in version 1.2
Surface and near surface description						
None	Little conceptual uncertainty.					No alternatives will be developed. The prime objective is to derive a model.
Bedrock geology						
Alternative lineament interpretation.	Raised in 1.1, assessed in 1.2 but not fully resolved.	May affect deformation zone model (if alter-native lineament interpretation is really different compared with "original" lineament interpretation). See also next row.	See next row.	See next row.	Careful examination (excavations, boreholes, etc) of lineaments in target volume to determine which lineaments are deformation zones.	An alternative interpretation of lineaments has been completed to test the reproducibility of this interpretation work.
Presence of undetected deformation zones outside "target area".	New	May affect stress calculations (more for understanding). Affects hydrogeology in large scale sensitivity calculations.	Probably NO IMPACT (although if this results in new stress model – see next row).	Probably NO IMPACT (possibly on future developments).	Significant characterisation efforts would be needed to resolve, see Table 4-3 in Appendix 4.	Alternative structural models have been developed for the steeply dipping zones outside the areas where the data resolution is relatively high. A more stochastic approach has been adopted in the base model and a more deterministic approach has been adopted in the alternative model. Will provide important input to selection of local model domain for version 2.1.
Changes of geometry deformation zones (extent and directions) in "target area".	Raised in 1.1 and assessed in version 1.2, but not fully resolved.	New rock mechanics model (minor update). New hydrogeologic model (major update – all calibrations should be remade with this structure in mind).	Yes, new design – changed repository volume.	Yes, new set of migration calculations (due to new hydro-geological model). May also affect assessment of rock mechanics impacts and respect distances.	Several additional deep boreholes. More reflection seismics etc, see Table 4-3 in Appendix 4.	No need to propagate to RE. Implications for hydrogeology are assessed in Chapter 8 and shown to be small, see below. Alternative structural models for the along-strike extension of the major, gently dipping zones (ZFMNE00A1, -A2, -C1 and -C2) have been developed (base model and base model variant). These alternatives are potentially important to propagate – and should be assessed by Repository Engineering. Implications for Safety Assessment are relatively straightforward. The issue will anyway be resolved later in the investigations.

Potential "Primary" alternatives in SDM	Is the need for alternative resolved in 1.2? (Only concerns hypotheses raised in version 1.1)	Is there a need to propagate the alternative to other SDM models (or aspects of these models)?	Implications for Engineering in phase D1	Implications for analyses in PSE and SR-Can	Implications for investigations to "resolve" alternative	Handling in version 1.2
Continuity, dip and thickness of deformation zones interpreted with the help of linked lineaments.	Raised in version 1.1, but covered by previous row. Will not be retained on the list.	New rock mechanics model (minor update). New hydrogeological model (major update) – all calibrations should be remade with this structure in mind).	Yes, new design – changed repository volume.	Yes, new set of migration calculations (due to new hydro-geological model). May also affect assessment of rock mechanics impacts and respect distances.	Several additional deep boreholes. More reflection seismics, etc; see Table 4-3 in Appendix 4.	This uncertainty is of major significance in the alternative deterministic structural model, where many lineaments have been interpreted as low confidence deformation zones. Bearing in mind the broad nature of this uncertainty, there is little justification to develop alternative models. The alternative is covered by the previous row "Changes of geometry deformation zones".
Alternative DFN-geometry	Raised in version 1.1. In version 1.2 some alternatives are formulated but issue not fully resolved.	Rock mechanics model (see further discussion under rock mechanics). Hydrogeology: (see further discussion under hydrogeology).	May affect space and degree of utilisation.	Yes, new set of calculations for RN-transport. Also affects mechanical stability of deposition holes.	See Table 4-3 in Appendix 4.	Alternatives should be assessed within hydrogeology and rock mechanics. Should also be directly considered within Safety Assessment.
Rock mechanics						
Rock mechanics Properties	Empirical and theoretical approaches are affected by different DFN, Rock Domain and Deformation Zone Models. The alternatives derive directly from those of the Geological Models. The possibility of dividing RFM029 into a RD above and below ZFMNE00A2 was considered.	They are already considered.	Minor impact expected since the degree of utilisation more depends on the intact rock strength and on the level of stress. The DZ Model could be an issue for utilisation. The amount of key blocks may be affected by alternative DFN-models. The extrapolation of the properties to data-void volumes is affected by the shape of the Geological Models.	No – or minor impact expected.		Confirm the robustness and predicting capability of the actual RM Model. Validate the assumed models for stress dependency of the rock mass mechanical properties. No need to propagate to SA.
Thermal properties	There is no need for an alternative thermal model					

Potential "Primary" alternatives in SDM	Is the need for alternative resolved in 1.2? (Only concerns hypotheses raised in version 1.1)	Is there a need to propagate the alternative to other SDM models (or aspects of these models)?	Implications for Engineering in phase D1	Implications for analyses in PSE and SR-Can	Implications for investigations to "resolve" alternative	Handling in version 1.2
Hydrogeology	Raised in version 1.1, some alternatives assessed in version 1.2, but issue not fully resolved.	New regional hydrogeologic model – affects palaeohydro-geological model.	Minor, would e.g. not affect inflow or grouting needs.	Minor, groundwater flow in repository and migration from it depends on the conditions in the local domain, but the migration paths from a repository may extend outside the target volume. Also large scale hydrogeology is of importance for understanding the long term evolution of the groundwater composition.	Significant, and un-realistic, characterisation efforts would be needed to resolve the uncertainties, see Table 4-5 in Appendix 4.	Assessment of the impact of the alternative structural models developed within geology combined with assessment of the importance of the location of boundaries and the uncertainty in the transmissivity distribution in the deformation zones, see Chapter 8. There is no need to further propagate this uncertainty to Engineering, but the impact on the end-points of migration paths should be considered within the Safety Assessment. Also the implications for long-term predictions of groundwater compositions should be addressed. Thus, it is thus suggested to propagate the alternative models in the regional domain also to the Safety Assessment.
Hydraulic properties of the fracture network of a scale less than the deterministic deformation zones. Alternatives concern whether there is non-connected fracture network, alternative transmissivity vs. size correlation, channelling inside fractures, depth dependence and transmissivity correlation to orientation.	Raised in version 1.1, some alternatives assessed in version 1.2, but issue not fully resolved.	The uncertainty may affect large scale transport and thus could affect the palaeohydrogeology calibration efforts.	May affect space and degree of utilisation.	Yes, new set of calculations for RN-transport.	See Table 4-5 in Appendix 12.	Important to get a handle on the impact of the different alternatives as they concern main safety function (retention) and it is unclear whether issues can be resolved by more investigations during the Site Investigation phase.
Hydro-geochemistry	Raised in version 1.1.	May affect "palaeo-hydrogeological" simulations.	NO IMPACT	Predictions of future groundwater composition (and thus resulting migration data).		Various alternatives are explored, see Chapter 8. Alternatives shown to have different hydraulic properties should be considered within the Safety Assessment. However, these alternatives may not cover the full uncertainty range, and especially the issue on channelling could need additional analyses within the Safety Assessment Framework.
Alternative hypotheses as to groundwater composition and processes.	Raised in version 1.1.					Alternative representations are discussed in Section 9.6. Different modelling approaches are applied on the same data set to describe the same processes, thereby confidence is built into the description. To be considered in the long term prediction of groundwater composition.
Transport	There are no alternative models.					Uncertainty in the migration processes (e.g. sorption, diffusion etc) are assessed within Safety Assessment (SR-Can).

Bedrock geological model

As further explained in Table A4-3 in Appendix 4, identified hypotheses for alternative models of the bedrock geology concern:

- Alternative lineament interpretation.
- Presence of undetected deformation zones outside the “target area”.
- Changes of geometry of deformation zones (extent and direction) in the “target area”.
- Continuity, dip and thickness of deformation zones interpreted with the help of linked lineaments.
- Alternative DFN model.

Some of these alternative hypotheses have been further assessed, whereas others are discarded or kept, as summarised in Table 12-1.

Alternative lineament interpretation was raised in version 1.1 and in version 1.2 an alternative interpretation has been carried out, as discussed in Chapter 5. As lineaments are an important input to the deformation zone (and DFN) model, an alternative interpretation has been carried out by an independent team. As discussed in Chapter 5, the resulting lineaments are similar, but there are also important differences. These differences put the usefulness of lineaments into question. As a consequence, the plan is now to carefully examine (from excavations, boreholes, etc) questionable lineaments inside the target volume to determine which of them are deformation zones. In the regional domain, the differences have inspired an alternative deformation zone model.

The presence of undetected deformation zones outside the “target area” was of course considered as a possibility already in version 1.1, but not directly discussed. However, the deformation zones in the regional domain only have limited importance. They may affect stress calculations (more for understanding), but more importantly they could affect the regional scale hydrogeology. There is little direct impact on Repository Engineering or Safety Assessment, although the large-scale hydrogeology is of importance for understanding the long-term evolution of the groundwater composition. Significant, and unrealistic, characterisation efforts would be needed to resolve the uncertainties. Instead, alternative structural models have been developed for the steeply dipping zones outside the areas of relatively high data resolution. A more stochastic approach has been adopted in the base model and a more deterministic approach has been adopted in the alternative model. This will provide important input to the selection of a local model domain for model version 2.1. There is no need to propagate this uncertainty to Engineering. Implications for hydrogeology are assessed in Chapter 8 and are shown to be small.

Uncertainty in geometry, extent and directions of deformation zones inside the “target area” was raised in 1.1. Alternative geometries would imply a minor update of the rock mechanics model and a major update of the hydrogeology model. Alternative geometry directly affects Repository Engineering (design) and Safety Assessment. A new set of migration calculations due to new hydrogeological model and possibly also a new assessment of rock mechanics impacts would be the result. The characterisation efforts to resolve uncertainties include several additional deep boreholes, more reflection seismics etc, as listed in Table A4-3 in Appendix 4. Alternative structural models for the along-strike extension of the major, gently dipping zones (ZFMNE00A1, -A2, -C1 and -C2) have been developed (base model and base model variant). These alternatives are potentially important to propagate – and should be assessed by Repository Engineering. Implications for Safety Assessment are relatively straightforward. The issue will anyway be resolved later in the investigations.

The possibility for alternative models for continuity, dip and thickness of deformation zones, interpreted with the help of linked lineaments, was raised in version 1.1. However, this hypothesis is covered by the previous issue and will not be retained on the list.

Hypotheses on alternative DFN-geometry were raised already in version 1.1. The DFN model affects the rock mechanics model and hydrogeology. It has a large impact on Repository Engineering, affecting space and degree of utilisation, and on Safety Assessment. In version 1.2, some alternatives are formulated, but they do possibly not cover the complete uncertainty range. The need to propagate these alternatives to rock mechanics and hydrogeology are discussed below.

Rock mechanics

In version 1.1 it was not judged meaningful to discuss alternative models of rock mechanics. This view is strengthened in version 1.2. The listed uncertainties are sufficiently captured by the uncertainty distributions provided. However, there is a need to consider how to handle the alternatives in the geological model.

The rock mechanics properties, as assessed by the empirical and theoretical approaches, are affected by different DFN, rock domain and deformation zone models. However, the impact on Rock Engineering is still regarded minor, since the degree of utilisation, from a rock mechanics standpoint, is more dependent on the intact rock strength and on the level of stress. There is little impact on Safety Assessment. The deformation zone model could be an issue for further consideration. The assessed size and disposition of key blocks may be affected by alternative DFN-models. The extrapolation of the properties to data-void volumes is affected by the shape of the geological models. Analysing the alternative geological input can be used to confirm the robustness and predictive capability of the rock mechanics model and possibly to complete the model with the properties of some of the minor rock types.

Thermal model

In version 1.1, it was not judged meaningful to discuss alternative thermal models. This view is strengthened in version 1.2. The listed uncertainties are sufficiently captured by the uncertainty distributions provided.

Hydrogeological model

As further explained in Table A4-5 in Appendix 4, identified hypotheses for alternative models of the bedrock hydrogeology concern:

- Geometry, connectivity and transmissivity of deformation zones and the geological discrete fracture network model in the regional domain,
- Hydraulic properties of the fracture network on a scale less than the deterministic deformation zones. Alternatives concern whether there is non-connected fracture network, alternative transmissivity vs. size correlation, depth dependence and transmissivity correlation to orientation and channelling within the fracture plane.

Alternative geometry, connectivity and transmissivity of deformation zones and fractures in the regional domain were raised already in version 1.1. These alternatives could affect the regional groundwater flow, the selection of proper boundary conditions and thus also the assessment of palaeohydrogeology. There is little direct impact on Repository Engineering or Safety Assessment, although the large-scale hydrogeology is of importance for understanding the long-term evolution of the groundwater composition. Furthermore, the migration paths from a repository may extend outside the target volume. Substantial, and unrealistic, characterisation efforts would be needed to resolve the uncertainties. Instead, an assessment is made of the impact of the alternative structural models developed within geology combined with assessment of the importance of the location of boundaries and the uncertainty in the transmissivity distribution in the deformation zones, see Chapter 8. There is no need to further propagate this uncertainty to Engineering, but the impact on the end-points of migration paths should be considered within the Safety Assessment. Also the implications for long-term predictions of groundwater compositions should be addressed. It is thus suggested to propagate the alternative models in the regional domain also to the Safety Assessment.

There are several different hypotheses for the description of the hydraulic properties of the fracture network (hydrogeological DFN). These include different assumption on the connectivity, if the properties are different in different parts of the domain and if there is a correlation between size and transmissivity, and channelling inside fractures. These hypotheses were raised already in version 1.1 and have been further developed. The uncertainty may affect large-scale transport and thus could affect the palaeohydrogeology calibration efforts. It may also affect the distribution of inflow to the repository and is thus of importance for Rock Engineering. An even larger impact is expected on migration properties of importance for Safety Assessment. Table A4-5 in Appendix 4 lists possible characterisation efforts that would reduce the uncertainties, but it is judged to be important to get a

handle on the impact of the different alternatives as they concern a main safety function (retention) and it is unclear whether issues can be resolved by more investigations during the Site Investigation phase. Therefore, various alternatives on the spatial distribution of properties, of the connectivity and transmissivity distributions are explored. The alternatives should be propagated and explored within the Safety Assessment (SR-Can). However, these alternatives may not cover the full uncertainty range, and especially the issue on channelling could need additional analyses within the Safety Assessment framework.

Hydrogeochemical model

Alternative hypotheses in groundwater composition and processes were raised in version 1.1. These may affect “palaeohydrogeological” simulations and thus also impact the predictions of future groundwater composition in Safety Assessment. There is no impact on Repository Engineering. Alternative representations are discussed in Section 9.6. Different modelling approaches are applied on the same data set to describe the same processes, thereby confidence is built into the description. To be considered in the long-term prediction of groundwater composition in Safety Assessment.

Bedrock transport properties

There are no alternative models for the bedrock transport properties. There is uncertainty in the migration processes like sorption and matrix diffusion. However, these uncertainties are assessed within the Safety Assessment (SR-Can) framework and are primarily to be discussed in the SR-Can (and later SR-Site) Process Report.

Surface system

Formulation and analyses of alternative models is not judged a necessary or useful approach at the present stage of surface and near-surface systems modelling. Due to the rapid development of the surface system, Safety Assessment applies a more stylised approach. Also, as the surface system is much more accessible than the subsurface, there is less room for overall conceptual uncertainty and most uncertainty can be mapped onto parameter variation.

12.3.4 Overall assessment

Compared with version 1.1, more of the uncertainties are now quantified or explored as alternatives. Only some of the uncertainties have direct implications for Safety Assessment or Repository Engineering. However, it will also be important to obtain the feedback from the users of the site descriptive model as to which of these uncertainties really require additional efforts. Such feedback is expected in particular from the preliminary design work and the Preliminary Safety Assessments. More data from the CSI will allow for further quantification and may also reduce many of these uncertainties.

12.4 Consistency between disciplines

Another prerequisite for confidence is consistency (i.e. no conflicts) between the different discipline model interpretations. This is checked in the next step of the Overall Uncertainty and Confidence Assessment (see Figure 12-1). A protocol has been developed using an interdisciplinary interaction matrix for documentation. For each interaction, the following questions have been addressed.

- Which aspects of the “source” discipline would it be valuable to consider in developing the “target” discipline model? The answer should be based on overall process understanding and the answers to the questions on impacts on uncertainties and alternatives provided in Tables A4-3 to A4-6 in Appendix 4 and in Table 12-1.
- Which aspects of the “source” discipline have actually been used when developing the “target” model?
- Are there any discrepancies between answers to the first and second question, and if so why?

It should be noted that this protocol is an expansion of a similar type of protocol used in version 1.1. There, only the second question, which aspects were considered, was asked.

Discrepancies between what it would be valuable to consider and what actually is considered affects confidence in the model. Again, it is primarily for the users to determine whether these discrepancies are grave or acceptable. However, an overview of this issue is provided at the conclusion of this section.

12.4.1 Important and actually considered interactions

Table 12-2 provides an overview of the interactions judged to be important (green) and to what extent these were actually considered (black) in Forsmark version 1.2. Table A4-7 in Appendix 4 lists them in full. In addressing the questions, the efforts is spent primarily on issues judged to be important and not in explaining why unimportant interactions indeed are so.

Impacts on bedrock geology

As can be seen from Table A4-7 in Appendix 4, many disciplines are judged to provide important feedback to the geological modelling. However, it is noted that the geological modelling up till now has not fully used such feedback. On the other hand, an essential part of the modelling philosophy is to base the geometrical framework on geological information and reasoning and not to “fit” the geological model to the other models. Still, the geological model should be useful to other disciplines and could use data from other disciplines as indications, among others, for e.g. identifying deformation zones.

Feedback from *rock mechanics* on stress orientations in relation to fracture sets could give additional confidence in the deformation zone and DFN model. The analysis of rock mechanics properties could affect the division of rock domains and deformation zones (e.g. less reason to split between domains or reason to split an existing domain). In version 1.2, the feedback on deformation zones and fracture sets has been discussed, but is not formally considered. It must also be kept in mind that the different fracture sets are geologically old structures and the current stress field is different from the stress field that formed the fractures. The rock domains in Forsmark are well defined. The possibility of identifying a new rock domain below ZFMNE00A2 was considered, but has not been propagated at this stage.

Also the *thermal modelling* could provide feedback on the description of rock domains. The geological modelling could enhance the utility of its predictions by considering what is really used and shown to be critical for the thermal modelling. In version 1.2, this feedback has been discussed, but not formally considered in the geological modelling. However, the mineralogy of different rock types is presented with thermal properties in focus.

Hydrogeology could provide confirmation of and indications of the properties of deformation zones (i.e. are there hydraulic contacts or not) and control of the hydraulic applicability of the DFN-model. Assessing the applicability of the geological DFN-model is part of the hydrogeological DFN-analysis. Future work is needed concerning an understanding of the discrete fracture network model, especially below the deformation zone ZFMNE00A2. Indications of water in the single-hole interpretation have affected identification of deformation zones, but other indicators are primarily used. However, more systematic re-check and more use of hydraulic data could be carried out. The regional hydrogeological analyses suggest that the different variants of the deformation zones in the regional domain have relatively little importance for the flow in the target volume, but the variants are nevertheless retained for assessment within Safety Analysis. It is possible that also this analysis would further support a relatively low ambition level in describing the deformation zones in the regional domain.

Data on post-glacial tectonics are used in the descriptive model.

Table 12-2. Summary of interactions judged to be important (green) and to what extent these were actually considered (black) in version 1.2. (There is a clockwise interaction convention in the matrix, e.g. influence of geology on rock mechanics is located in Box 1,2, whereas the influence of rock mechanics on geology is located in Box 2,1).

Bedrock Geology	Yes/Yes	Yes/Yes (partly)	Yes/Yes (could be more developed).	Yes/Yes	Yes/Yes	No need	No need	No need	Yes/Yes	No need
Yes/Yes but could possibly be more developed	Rock mechanics (in the bedrock)	Some/yes	Yes/Yes, but could be more developed	No need	No need	No need	No need	No need	No need	No need
Yes/Yes, but possibly could be more developed	Thermal (in the bedrock)	Thermal (in the bedrock)	Yes/Judged unimportant	No need	No need	No need	No need	No need	No need	No need
Yes/Yes, but possibly could be more developed	Some/Yes	Some/Yes	Hydrogeology in the bedrock	Yes/Yes	Yes/Yes	Yes/Yes, but possibly could be more developed	Yes/Yes, but possibly could be more developed	Yes/Yes, but possibly could be more developed	No need	No need
No need	No need	No need	Yes/Yes	Hydrogeo-chemistry in the bedrock	Yes/Yes, but possibly could be more developed	No need	Yes/Yes, but possibly could be more developed	No need	No need	No need
No need	No need	No need	Yes/Yes, but possibly could be more developed	Yes/Yes	Yes/Yes, but possibly could be more developed	No need	No need	No need	No need	No need
No need	No need	No need	Yes/Yes	Yes/Yes	Yes/Yes	No need	Hydrogeo-chemistry (surface and near surface)	Yes/Yes	Yes/Yes	Yes/Yes
No need	No need	No need	Yes/Yes, but possibly could be more developed	Yes/Yes	Yes/Yes	No need	Yes/Yes, but possibly could be more developed	Surface hydrology and near surface hydrogeology	Yes/Yes	Yes/Yes
Yes/Yes	No need	No need	Yes/Yes	Yes/Yes, but possibly could be more developed	Yes/Yes	No need	Yes/Yes	Yes/Yes	Quaternary Deposits and topography	Yes/Yes
No need	No need	No need	No need	Yes/Yes, but possibly could be more developed	Yes/Yes, but possibly could be more developed	No need	Yes/Yes	Yes/Yes	Yes/Yes	Biota

Impacts on rock mechanics model

As can be seen from Table A4-7 in Appendix 4, it is mainly the *bedrock geology* model that impacts the rock mechanics model through the rock domains, deformation zones and DFN-model. This input is used within the rock mechanics modelling.

In principle also *hydrogeology* would impact the rock mechanics description, since water pressures reduce the rock stress to effective stress. However, this coupling has little effect on the parameters predicted, but is of course considered by Repository Engineering. Furthermore, the coupling is relatively trivial to take into account since water pressures are close to hydrostatic, i.e. no special hydraulic modelling is needed. Another possible coupling is whether the stress magnitudes and orientations are consistent with the anisotropy of hydraulic conductivity. Clearly, the anisotropy above deformation zone ZFMNE00A2 and the small amount of water conductive features below the zone support the stress model. However, HM-couplings also have many uncertainties.

Impacts on thermal model

As can be seen from Table A4-7 in Appendix 4, it is mainly the *bedrock geology* model that impacts the thermal model through the rock type descriptions etc of the rock domains. This input is used within the thermal modelling. However, it is noted that foliation could impact anisotropy in thermal properties. There are indications of anisotropy in the thermal data, but the anisotropy is not yet fully assessed, especially not at relevant scales.

A *rock mechanics* input to the thermal data is whether there is a bias when measuring thermal expansion on stress-released samples. This issue is discussed, but not analysed.

Thermal convection and other groundwater flows (i.e. a formal impact from *hydrogeology*) affect uncertainty in measurement of initial temperature. These effects are discussed when assessing uncertainty in in-situ temperature values.

Impacts on hydrogeology model

As can be seen from Table A4-7 in Appendix 4, many disciplines should inform the hydrogeological modelling and most of this input is considered.

Bedrock geology provides the geometrical framework in terms of rock domains, deformation zones and DFN-geometry for the hydrogeological models. This input is certainly used. However, the DFN is close to the percolation threshold and, especially below ZFMNE00A2, the hydraulic conceptual model could be questioned, see Chapter 8. Possibly, only the deformation zones are hydraulically interesting. Also, the potential differences in deformation zone pattern and fracturing within rock domain RFM029 (NW vs. SE) are possibly not fully assessed and the analysis is concentrated on rock domain RFM029 and has not assessed variation in other rock domains (there are few data for these domains).

Stress orientation, i.e. a *rock mechanics* input, is expected to affect hydraulic anisotropy. Above ZFMNE00A2 there is clear hydraulic anisotropy. Only three fracture sets are conductive. The sub-horizontal set is the most conductive and orthogonal to the minimum principal stress ($\sigma_3 = \sigma_h$) and parallel to the maximum principal stress ($\sigma_1 = \sigma_H$), i.e. possibly a rock mechanics explanation. σ_1 is also very high close to the surface, which appears to be a good explanation for the highly conductive sub-horizontal features close to surface. At depth, i.e. below ZFMNE00A2, the lack of hydraulic conductive features is reasonable in relation to the stress situation, although no formal analysis has been undertaken.

Temperature affects water density and viscosity. This impact is considered and judged unimportant.

There is a strong coupling between hydrogeology and *hydrogeochemistry*, since it is suggested that mixing is the main process for groundwater evolution. Furthermore, density differences, created by varying salinity, affect the flow regime. These couplings are considered in the modelling work. Present-day salinity and water type distribution are “calibration targets” for simulation and the

hydrogeologic modelling considers density effects. However, it is not always trivial to match the hydrogeological model to the chemical data, and vice versa. For example, it was not possible to fully match the rather high salinity in some of the boreholes. The chemical data could be rather insensitive to key aspects of the hydrogeological model (i.e. the flow characteristics in the repository volume), but very sensitive to other aspects – like the details of the near-surface hydrogeology or the initial conditions at the time of the past glaciation. Further enhancement of the interaction is warranted, but it is also important to understand the limitations in achieving full integration.

The regional simulations of past groundwater evolution involve modelling of salt migration. The migration properties should be consistent with assessed migration properties of the *transport model*. Such a test is made, but it is also concluded that the migration of salt is not very sensitive to migration properties of the rock matrix.

There are also interactions with the *surface system*. The identification of water types and boundary conditions in the near-surface hydrogeochemistry provides input to the surface water type considered in the modelling. Also, surface hydrology and near-surface hydrogeology as well as topography and the description of the Quaternary deposits provide input to the formulation of the top boundary conditions. All these interactions are considered in the modelling, although simplifications are made.

Impacts on hydrogeochemistry model

As can be seen from Table A4-7 in Appendix 4, many disciplines are judged to provide important feedback to the hydrogeochemical modelling and most of this input is considered.

Fracture mineralogy and the chemical composition of the bedrock, as provided by the *geological model*, require consideration. In particular, consideration of hydraulically important deformation zones helps to explain the origin and characteristics of the water.

As already noted, there is a strong coupling between *hydrogeology* and hydrogeochemistry and between hydrogeochemistry and the *transport model*. These couplings are considered in the modelling work, as explained above. However, much work remains, e.g. what is meant by different water types and how to handle uncertainty in pore water composition.

There are also interactions from the *surface system*. Surface and near-surface hydrogeochemistry and hydrology and hydrogeology influence the waters in the bedrock. Some data are used in a simplified coupled/integrated model and the measured near-surface data are used as reference water in mixing calculations. Also the description of the Quaternary deposits provides input to selection of water types and input to coupled modelling.

Impacts on transport model

As can be seen from Table A4-7 in Appendix 4, many disciplines are judged to provide important feedback to the transport modelling and most of this input is considered.

The rock domains of the *bedrock geology* provide the main tool for extrapolating the transport property data into three dimensions. This coupling is considered to the extent possible.

It is necessary to consider the impact of stress release (i.e. influence from *rock mechanics*) on the intact rock samples taken for laboratory diffusion and sorption measurements. This consideration is also part of the data evaluation. Formation factor logs suggest a stress impact on diffusivities, but there are also uncertainties (rock type, pore fluid) in the in-situ formation factor data (see Table 4-6 in Appendix 4). Therefore, there is an ongoing programme to investigate the pore water composition in both Forsmark and Laxemar. Impacts of stress release on other transport data are more difficult to assess.

Hydrogeology should identify the potential flow paths where the transport description is needed. Flow logs are considered in identification of “flowing fractures”, but it is unclear whether “type fractures” can be identified (see Table A4-6 in Appendix 4).

The groundwater composition (i.e. *hydrogeochemistry*) affects sorption and (to a less extent diffusivity) values. These couplings are considered. The groundwater composition is set as input to process-based retention modelling and the groundwater composition (identified water types) are used to set up laboratory tests and in the parameterisation of the retardation model.

Surface system

As shown in Table A4-7 in Appendix 4, many interactions take place among the different surface disciplines, which is why an integrated modelling approach is adopted for the surface system. However, the table also indicates that these interactions are only partially performed in this model version (cf. the frequent use of “some” in the table). It is also evident from the table that many feedbacks are required, and also made, in order to produce consistent, integrated models within the disciplines where modelling is performed for both the surface system and the deep rock. Also in these cases, interactions need to be further developed.

12.4.2 Overall assessment

Table A4-7 in Appendix 4 demonstrates the integrated character of the site descriptive modelling. Different disciplines depend on the outcome of other disciplines and provide important feedbacks to those disciplines. Furthermore, to a large extent the interactions judged to be important are also considered in the modelling, and the current discrepancies between the needed interactions and the interactions considered is not assessed as a major problem for confidence in the site descriptive model of Forsmark.

Still, some further improvements are identified as being useful. In particular, it is observed that the geological modelling could enhance its use of feedback from especially rock mechanics, hydrogeology and hydrogeochemistry, but this also stresses the needs for these latter disciplines to clearly formulate this feedback in a form useful for the geological modelling.

12.5 Consistency with understanding of past evolution

For confidence, it is essential that the naturally ongoing processes considered being important can explain – or at least not contradict – the model descriptions. The distribution of the groundwater compositions should, for example, be reasonable in relation to rock type distribution, fracture minerals, current and past groundwater flow and other past changes. Such ‘paleohydrogeologic’ arguments may provide important contributions to confidence even if they may not be developed into ‘proofs’.

Table 12-3 lists how the current model is judged to be consistent with the overall understanding of the past evolution of the site, as outlined in Chapter 3. The following are noted.

- The geological model is consistent with the regional geological evolutionary model up to the Quaternary period. However, there are few constraints, both at Forsmark and in the whole Fennoscandian Shield, on the younger geological history (after c. 1,750 million years). It would be potentially interesting to couple the geological evolution and the formation of the different fracture sets by determining the age of fracture minerals. Such studies when performed at Äspö were rather inconclusive, but further work in this area could nevertheless provide some insights into the validity of the conceptual model for groundwater flow and hydrogeochemical development, and are therefore planned for the CSI programme at Forsmark /SKB, 2005a/. The new data in 1.2 do not require an update of the evolutionary model, but the new data allow for a refinement of the model and an enhanced understanding.
- Assessment of potential glacio-isostatic faulting is underway. Currently, there are no positive indications of such faulting, but it cannot be totally ruled out, as there are disturbances in some sediments, see Chapter 5. However, the observations at drilling site 5 show indications of boulder formation and not faulting.

- The stress modelling does not take into account the kinematics and genesis of the deformation zones. This allows for capturing the present conditions, but not the historical evolution. The quite straight forward geometrical conceptual model explains current stress magnitudes and orientations and is thus consistent with any development during the Quaternary period.
- The existing regional palaeohydrogeology model seems to describe the observed water types fairly well. Groundwater flow and salinity transport simulations start at 8,000 BC, which coincides with the Ancylus Lake period. At this time, the Forsmark area was covered by c. 115 m of fresh water. The simulations explore the impact of various assumptions such as the initial penetration depth of the glacial melt water, the distribution of material property heterogeneity, model size and boundary conditions. In general, analysing the impact of potential changes after 8,000 BC on the current day groundwater flow and distribution of groundwater composition supports the conceptual groundwater model. The interaction between the evolution of the surface water composition and the evolution of the groundwater composition is described concerning both processes and the origin of various water types (e.g. meteoric water, glacial melt water, Littorina water, brine). However, the modelling points to many uncertainties, especially in what were the conditions at the onset of the de-glaciation period.
- Also, the ongoing investigation of the fracture minerals may provide indication of the variation in water chemistry over time. However, this has not yet been thoroughly analysed.
- There is a fairly good understanding of the last 10,000 years of development of the surface system. The description of this historical development is consistent with the description of the present system.

In general, the site descriptive model of Forsmark is found to be consistent with the current understanding of the past evolution. In fact, as the investigations proceed, the findings from the site contribute more and more to an improved understanding of the past evolution of the site.

Table 12-3. Consistency with past evolution.

Site descriptive model (SDM) technical audit: consistency with past evolution		
Time period and subject	Is SDM consistent with evolution in this time period?	Are there findings from the modelling suggesting a need to update the Evolutionary model?
1,900 million years to the Quaternary		
Bedock geology	<p>Geological model is consistent with the regional geological evolutionary model. However, there are few constraints, both at Forsmark and in the whole Fennoscandian Shield, on the younger geological history (after c. 1,750 million years).</p> <p>It would be potentially interesting, i.e. not carried out in SDM version 1.2, to couple the geological evolution and the formation of the different fracture sets by determining the age of fracture minerals. However, such studies performed at Äspö were rather inconclusive, but could nevertheless provide some insights into the validity of the conceptual model for groundwater flow and hydrogeochemical development. Planned for CSI.</p>	The new data in 1.2 do not require an update of the evolutionary model, but the new data allow refinement of the model and an enhanced understanding. Geological modeling at Forsmark is at the leading edge!

Site descriptive model (SDM) technical audit: consistency with past evolution

Time period and subject	Is SDM consistent with evolution in this time period?	Are there findings from the modelling suggesting a need to update the Evolutionary model?
Rock mechanics	<p>There is no need of consistency of the mechanical properties of the rock mass with the historical evolution of the Site. The properties of interest are evaluated at the present time.</p> <p>For the Stress Model, a numerical modelling was carried out on a simplified version of the DZ Model. The modelling did not take into account the kinematics and genesis of the DZs. The geometry and the simulated state of stress can, for this reason, capture the present conditions but not the historical evolution. Until a conceptual model for the formation of the DZs and the fracture sets at the Site is set up, the historical evolution of the stress field at Forsmark cannot be completely understood.</p>	
During the Quaternary period		
Bedrock geology	<p>Assessment of potential glacio-isostatic faulting is underway. Currently, no positive indications of faulting, but cannot be totally ruled out as there are disturbances in some sediments, see Chapter 5.</p> <p>Observations at Drill Site 5 shows Indications of boulder formation and not faulting.</p>	Improved understanding of significance of "surface disturbances.
Rock mechanics	The quite straight forward geometrical conceptual model explains current stress magnitudes and orientations.	
Thermal model	N/A	
Hydrogeology and hydrogeochemistry	<p>Groundwater flow and salinity transport simulations start at 8,000 BC, which coincides with the Ancylus Lake period. At this point of time the Forsmark area was covered by c. 115 m of fresh water. The simulations explore the impact of various assumptions such as, the initial penetration depth of the glacial melt water, the distribution of material property heterogeneities, and model size/boundary conditions.</p> <p>In general, analysing the impact of potential changes after 8,000 BC on the current day groundwater flow and distribution of groundwater composition will affect and support the conceptual GW model.</p> <p>The interaction between the evolution of the surface water composition and the evolution of the groundwater composition, is described concerning processes and origin of various water types (e.g. meteoric water, glacial melt water, Littorina water, brine).</p>	<p>Modelling has identified many uncertainties, especially in what were the conditions at the onset of the de-glaciation period.</p> <p>Ongoing investigation of the fracture minerals may provide indication of the variation in water chemistry over time. However, this has not yet been thoroughly analysed.</p>
Surface System	We have a fairly good understanding of the last 10,000 years of development of the surface system, and the description of this historical development is consistent with the description of the present system.	No

12.6 Comparison with previous model versions

The final evaluation of confidence envisaged in the flow chart of Figure 12-1 concerns to what extent measurement results from later stages of the investigation compare with previous predictions. This is important for discussing the potential benefit of additional measurements. Clearly, if new data compare well with a previous prediction, the need for yet additional data may even further diminish.

12.6.1 Auditing protocol

Again, a protocol has been developed for checking this. It concerns:

- changes compared with the previous model version (i.e. version 1.1 /SKB, 2004a/),
- whether there were any “surprises” associated to these changes, and
- whether changes are significant or only concern details.

Table 12-4 lists the answers to these questions.

Table 12-4. Comparison with previous model version.

List changes compared to previous model version (i.e. version 1.1)	
Geology	<p><i>Rock domain (RD) model</i></p> <p>Small changes in RD model despite significant amount of new data. These include steeper fold structure between SFR and nuclear power plants, and extent of rock domains RFM012, RFM029 and RFM032 in the vicinity of the nuclear power plants. Stable model (enhanced confidence). Awaits an independent test with the help of geophysical modelling.</p> <p><i>Deformation zone (DZ) model</i></p> <p>Significant increase in the number of high confidence deformation zones (some lower confidence zones now high confidence + entirely new zones). Note common occurrence of gently dipping zones, especially in the south-eastern part of the candidate area. Main sets are NW-steep, NE-steep, NE-gentle – as in version 1.1, but few NS-steep. Zones based on topographic lineaments (e.g. NS) in version 1.1 have not been confirmed by new data. DZ model is stabilising and can be treated with enhanced confidence, especially in “target area”. However, significant modifications are expected in future models.</p> <p>The “uncritical” interpretation of lineaments as DZ seriously questioned. Confident control concerning the geological significance of gently dipping seismic reflectors. Occurrence of vuggy metagranite.</p> <p><i>DFN</i></p> <p>Assessment of the new fracture data shows that spatial variability in size, intensity and properties is large. There is possibly a need for a new conceptual model or new domain below ZFMNE00A2? Orientation (number of fracture sets) similar to version 1.1. However, model is not yet stable.</p>
Rock mechanics	<p>The RM Model makes better use of the DZ Model. Moreover, the DFN Model is also used for inferring the mechanical properties of the rock mass numerically.</p> <p>The mechanical properties in SDM version 1.1 were assessed from SFR-data only. The new site specific data confirm the presence of strong and stiff intact rock. The new mechanical tests on intact rock samples seem to be in line with the laboratory results on SFR samples. Moreover, all the fracture sets present very similar strength properties.</p> <p>The empirical and numerical methods seem to indicate that the deformation modulus of the rock mass at Forsmark is not very sensitive to the rock stresses because it is close to the Young's modulus of the intact rock thanks to low fracture frequency (at least below 100 m depth).</p> <p>The RM Model appears to be rather stable in the sense that the ranges of mechanical properties are mainly confirmed. A better spatial coverage of the Target Area is also achieved. Some DZs are also characterised by empirical methods.</p> <p>The stress field is now based on more measurements and a simplified geometrical concept based on the DZ Model was set up.</p>

Thermal	The current model version contains considerable more measured thermal conductivity data. New modelling approaches have been applied. Anisotropy exists for thermal conductivity.
Hydrogeology	Much more data both near surface and at depth. Data are possibly understood, but questions arise as to whether current modelling concepts are appropriate. The impression from the version 1.1 model with very few water conductive features below 400 m is further enhanced but with more details and relations to the DZ model. The improved DZ-models (from geo) make the hydro-interpretations much more constrained. Hydrogeological DFN needs to handle the low permeable region below Deformation zone A2. Model is not fully stable yet.
Hydrogeochemistry	The 1.2 model contains considerable more data from the depth and also measurements on microbes, gases and colloids that were not available during 1.1. New modelling approaches, such as integrated transport and geochemical modelling, have been applied on the 1.2 data. Better description of the hydrochemical system and chances to compare/integrate the results with the hydrogeological modelling. Not yet a stable model.
Transport	Site specific data on porosity and formation factor.
Surface systems	The previous model presented the limited dataset available at that time, without integration of different disciplines or system descriptions. The 1.2 model contains considerably more site-specific data, and a first attempt is made at an integrated description of the surface system.

Address whether there were any “surprises” connected to these changes

Geology	Abundance of gently dipping DZ in the south-eastern part of the candidate area. So far little support that the NS lineaments represent deformation zones. Developments concerning interpretation of lineaments. Occurrence of vuggy metagranite in one borehole.
Rock mechanics	Boreholes KFM02A and KFM03A do not show a clear decrease of the rock mass quality in the upper 300 m. In borehole KFM01A, the presence of ZFMNE00A2 at the surface might have enhanced the natural increase of fractures towards the surface. A stress jump due to the presence of gently dipping DZs could be very likely at the Site.
Thermal	No real change, although indications of anisotropy would need further assessment.
Hydrogeology	No real surprise, but the picture of very low hydraulic conductivity at depth is strengthened from the new borehole data.
Hydrogeochemistry	More measurements indicate a strong Littorina signature at depth compared with e.g. Simpevarp.
Transport	No real surprise.
Surface system	The improved understanding of the site has not lead to any major changes in the conceptualisation of the different subsystems or other “surprises”.

Address whether changes are significant or only concern details

Geology	Changes in RD model concern details. Changes in DZ model are significant.
Rock mechanics	The RM Model appears to be rather stable in the sense that the ranges of mechanical properties are mainly confirmed. A better spatial coverage of the Target Area is also achieved. Some DZs are also characterised by empirical methods.
Thermal	Anisotropy in thermal conductivity may influence design.
Hydrogeology	The hydrogeological model with its alternatives is significantly different from version 1.1. This is especially true for the alternative with no conducting fracture network, apart from distinct deformation zones, below the –400 m level i.e. below deformation zone ZFMNE00A2. There it may be a need for a new conceptual model.
Hydrogeochemistry	The changes are significant since the model will describe the groundwater evolution down to 1,000 m depth rather than down to 200 m depth as in the version 1.2.
Transport	Details – main difference is now that there are some site specific data.
Surface system	No comparison could be made.

12.6.2 Assessment

As can be seen from Table 12-4 there are significant changes in version 1.2 compared with version 1.1 /SKB, 2004a/, but there are no substantial surprises.

Compared with version 1.1 the main changes in the *geological* model are:

- Small changes in the rock domain model, including steeper fold structure between SFR and nuclear power plants, and extent of rock domains RFM012, RFM029 and RFM032 in the vicinity of the nuclear power plants, despite a significant amount of new data.
- Significant increase in the number of high confidence deformation zones (some lower confidence zones now high confidence + entirely new zones) (Note especially the common occurrence of gently dipping zones, especially in the south-eastern part of the candidate area).
- Deformation zones based on topographic lineaments (e.g. NS) in version 1.1 have not been confirmed by new data: the “uncritical” interpretation of lineaments as deformation zones is seriously questioned.
- Confident control concerning the geological significance of gently dipping seismic reflectors.
- Occurrence of vuggy metagranite.
- DFN-assessment of the new fracture data shows that spatial variability in size, intensity and properties is large and there is possibly a need for a new conceptual model or new domain below ZFMNE00A2.

The rock domain model appears quite stable, but awaits an independent test with the help of geophysical modelling. The deformation zone model is stabilising and can be treated with enhanced confidence, especially in the “target area”. However, significant modifications are expected in future models. There is possibly a need for a new conceptual DFN model or new domain below ZFMNE00A2.

Compared with version 1.1 the main changes in the *rock mechanics* model are:

- Better use of the deformation zone model and the DFN model is also used for inferring the mechanical properties of the rock mass numerically (the mechanical properties in version 1.1 were assessed from SFR-data only).
- The new site-specific data confirm the presence of strong and stiff intact rock.
- The stress field is now based on more measurements and a simplified geometrical concept based on the deformation zone model was set up. A stress jump due to the presence of gently dipping deformation zones could be very likely at the site.

The rock mechanics model appears to be rather stable in the sense that the ranges of mechanical properties are mainly confirmed. A better spatial coverage of the “target area” is also achieved. Some deformation zones are also characterised by empirical methods. The new mechanical tests on intact rock samples seem to be in line with the laboratory results on SFR samples. Moreover, all the fracture sets present very similar strength properties. The empirical and numerical methods seem to indicate that the deformation modulus of the rock mass at Forsmark is not very sensitive to the rock stresses because it is close to the Young’s modulus of the intact rock thanks to low fracture frequency (at least below 100 m depth). However, it was somewhat surprising that boreholes KFM02A and KFM03A did not show a clear decrease of the rock mass quality in the upper 300 m. In borehole KFM01A, the presence of ZFMNE00A2 at the surface might have enhanced the natural increase of fractures towards the surface.

Compared with version 1.1 the main changes in the *thermal model* are:

- Inclusion of considerably more measured thermal conductivity data.
- Use of new modelling approaches.
- Recognition that anisotropy exists for thermal conductivity.

These changes are not significant and the model appears rather stable although indications of anisotropy need further assessment.

Compared with version 1.1 the main changes in the *hydrogeological model* are:

- Much more data from both near surface and at depth: these data are possibly understood, but raise questions as to whether current modelling concepts are appropriate.
- The impression from the version 1.1 model with very few water conductive features below 400 m is further enhanced, but with more details and relations to the deformation zone model.
- The improved geological deformation zone models make the hydro-interpretations much more constrained.
- The hydrogeological DFN model needs to handle the low permeable region below deformation zone ZFMNE00A2. Different conceptual models are suggested.

There are no real surprises, but the picture of very low hydraulic conductivity at depth is strengthened from the new borehole data. The hydrogeological model with its alternatives is significantly different from that in version 1.1. This is especially true for the description below deformation zone ZFMNE00A2. The model is not yet stable.

Compared with version 1.1 the main changes in the *hydrogeochemical model* are:

- The 1.2 model contains considerable more data from the depth and also measurements on microbes, gases and colloids that were not available during 1.1.
- New modelling approaches such as integrated transport and geochemical modelling has been applied on the 1.2 data.
- There is a better description of the hydrochemical system and there has been the opportunity to compare/integrate the results with the hydrogeological modelling.

There are no real surprises, but the new measurements indicate a much stronger Littorina signature at depth compared with e.g. Simpevarp. The changes are significant since the model describes the groundwater evolution down to 1,000 m depth rather than down to 200 m depth as in version 1.1.

Compared with version 1.1 the main changes in the *transport model* are:

- There now exist site-specific data on matrix porosity and the formation factor.

There are no real surprises in the data.

Compared with version 1.1 the main changes in the *surface system model* are:

- The previous model presented the limited dataset available at that time, without integration of different disciplines or system descriptions.
- The 1.2 model contains considerably more site specific data, and a first attempt is made to provide an integrated description of the surface system.

The improved understanding of the site has not lead to any major changes in the conceptualisation of the different subsystems or other “surprises”.

13 Conclusions

This chapter provides a summary of the present understanding of the Forsmark site and the current status of the Forsmark site descriptive model. Achievements made in the analysis/modelling work are brought forward together with changes in the site description since the previous model version. The main features of the Forsmark site is summarised together with uncertainties and confidence in the site description, as evaluated in Chapter 12. Important steps to be taken in future modelling in order to reduce the uncertainty in the site description are identified. Finally, implications of the remaining uncertainties in the site description for the on-going site investigations are discussed.

13.1 Major developments since previous model version

There are considerable developments in model version 1.2 as compared with model version 1.1. The obvious reason for this is the substantial increase in site-specific data, both surface and sub-surface, which has allowed for more elaborate analyses and modelling. This has significantly contributed to major advances in the local site description. Important modelling achievements and developments since the previous model version are summarised below.

- The major developments in the geological model concern the increased number of high confidence deformation zones in the local model volume. Sub-surface data have confirmed the gently dipping seismic reflectors as representing gently dipping zones. This has resulted in the inclusion of gently dipping zones, especially in the south-eastern part of the candidate area, which were not present in model version 1.1. These developments have contributed to the selection of a target area for the complete site investigations, referred to as the priority site in /SKB, 2005a/, in the north-western part of the candidate area.
- Uncertainties with respect to the interpretation of lineaments and whether they correspond to deformation zones or not are still high. An alternative geological model for low confidence deformation zones interpreted solely from lineaments has been defined and treated.
- A conceptual model for the formation of deformation zones has been developed that complements the conceptual model for rock domains presented in version 1.1.
- The increase in number of boreholes has provided a much larger database for the discrete fracture network (DFN) modelling of the rock mass fracturing. The assessment of the new fracture data shows that spatial variability in size, intensity and properties is large and that there is probably a need, in the first instance, to distinguish between rock mass fracturing above and below the gently dipping deformation zone ZFMNE00A2.
- Despite the large amount of new data, there are only small changes to the rock domain model. These changes include a more steeply plunging fold structure between SFR and the nuclear power plant, and the extent of rock domains RFM012, RFM029 and RFM032 in the vicinity of the nuclear power plant.
- The rock mechanics properties in version 1.1 were assessed from SFR data alone, whereas site-specific data have been utilised in version 1.2 together with both the deformation zone and the DFN models. This has confirmed the range of mechanical properties and has given a better spatial coverage over the target area for the complete site investigations.
- The stress field is based on more measurements and on a simplified geometrical concept based on the base case deformation zone model. Compared with model version 1.1, a smaller stress gradient with depth is estimated for rock domain RFM029.
- The modelling of thermal properties is based on many more data and a new approach has been applied compared with the previous model. There are no significant changes in thermal properties compared with model version 1.1. Some measurement data indicate anisotropy in thermal conductivity, but the interpretation is uncertain.

- Collected hydraulic data from the boreholes have strengthened the picture of fewer water conducting features at depth below deformation zone ZFMNE00A2 than above this zone. The same data have provided a more detailed input to the assessment of hydraulic DFN properties. Together with the improved deformation zone models, the available hydraulic data have allowed for more elaborated hydrogeological analyses and interpretations. The hydraulic data from the boreholes strongly suggest that the rock mass, also within rock domain RFM029, should be divided into volumes of different hydraulic properties. However, the exact division of the different volumes remains to be defined.
- There is a strong coupling between hydrogeology and hydrogeochemistry and the coupling are considered in the modelling work. In the hydrogeological modelling, density effects are accounted for and simulation results are compared with the present day salinity and water type distribution. However, it is not always trivial to match the hydrogeological model to the chemical data, and vice versa. For example, it was not possible to fully match the rather high salinity in some of the boreholes. The chemical data could be rather insensitive to key aspects of the hydrogeological model (i.e. the flow characteristics in the target volume), but very sensitive to other aspects – like the details of the near-surface hydrogeology or the initial conditions at the time of the past glaciation.
- The hydrogeochemical model is based on considerably more hydrogeochemical data from depth and also on measurements on microbes, gases and colloids that were not available previously. For example, the microbial characterisation has given direct support to the redox modelling. New modelling approaches, such as integrated transport and geochemical modelling, have been applied to the data. Despite the significant increase in the amount of data, it is noted that deep data are far from abundant.
- The descriptive hydrogeochemical model has been updated to include descriptions of the distribution of salinity, mixing and a more detailed description of major reactions/processes down to a vertical depth of 1,000 m, compared with 200 m in model version 1.1. This has provided several data sets suitable for comparisons with regional flow simulations and thus allowed for integration between hydrogeochemistry and hydrogeology to an extent that was not possible before.
- Site-specific data have allowed for parameterisation of rock mass porosity and diffusivity, giving similar values as previously evaluated in version 1.1.
- A first attempt has been made to provide an integrated description of the surface system. Quantitative modelling of Quaternary cover thickness, shallow groundwater and surface water has been undertaken that supports earlier conceptual models. Terrestrial, limnic and marine ecosystem models have been developed for the drainage area of Lake Bolundsfjärden, which is located within the target area.

13.2 Current understanding of the site

The following sections summarise the current understanding of the Forsmark area and comment on the associated uncertainties and present confidence in the site description.

13.2.1 Main features of the Forsmark site

In planning the execution programme for the Forsmark area /SKB, 2002b/ some important site-specific questions were formulated. They concerned the *three-dimensional shape of the tectonic lens, the potential for ore occurrence at depth, the occurrence of gently dipping deformation zones and the occurrence of high rock stresses*. These issues are addressed together with other important issues and aspects in the following summary of the current understanding of the characteristics of the Forsmark site.

Topography and surface system

The topography resembles that of northern Uppland in general. It is gently undulating and of quite moderate elevations. Still, the regional model domain encompasses a significant regional water divide located between the candidate area and the Forsmark deformation zone. The overburden is dominated by glacial till of different character. Unconsolidated Quaternary deposits cover c. 85% of the land area in the regional model area and these deposits were formed during or after the latest glaciation. Despite the modest topography, the upper surface of the bedrock is found to undulate over small distances implying large variations in thickness of the Quaternary cover (between 0 and c. 17 m).

The Quaternary deposits are rich in CaCO₃. This together with the recent emergence of the area from the Baltic Sea affects the chemistry of surface and shallow groundwaters giving rise to high pH and high alkalinity. Furthermore, the surface waters are high in nitrogen and low in phosphorus, giving rise to the special characteristics of the oligotrophic hardwater lakes in the Forsmark area. Shallow groundwater is at places affected by marine water giving rise to locally high Cl concentrations (see further below).

Results from modelling of the surface hydrology and near-surface hydrogeology indicate that recharge areas occupy large parts of the regional model area, but also that there are large temporal variations in the distribution of recharge and discharge areas between wet and dry periods. The penetration depth of the local flow cells is probably short-circuited by the high horizontal transmissivities observed in the uppermost part of the bedrock.

The integrated ecosystem modelling indicates that by far the largest pool of carbon in the ecosystem is stored in soil and sediments and that the largest flux of carbon is driven by the exchange of water between the marine basins and between the marine basins and the open Baltic Sea. The longest turnover times for carbon are found in soil and sediments, ranging from some hundreds of years in marine bays to several thousands of years for the lake and terrestrial ecosystems. This is of importance for understanding transport and accumulation of radionuclides in the ecosystem.

Geology

The bedrock within the candidate volume of the rock is situated within the north-western part of a major tectonic lens that trends NW-SE along the coastal area of the Uppland. The candidate volume is dominated by one lithological domain, defined as rock domain RFM029. The dominant rock type in this domain is a medium-grained metagranite (84% of the domain volume). Subordinate rock types are fine- to medium-grained metagranodiorite or metatonalite, amphibolite, pegmatitic granite or pegmatite and fine- to medium-grained granite. These rocks extend downwards to a depth of at least 1,000 m. Except for the amphibolite and some samples from the fine- to medium-grained metagranodiorite or metatonalite, all the surface and borehole samples of these rock types at the site have yielded quartz contents that lie in the interval 23–46%. A foliation within the metagranite is folded and both fold axis and mineral stretching lineations plunge towards the south-east. Rock domains with strongly deformed, and also in part, banded and inhomogeneous rocks occur along the south-western (e.g. RFM012, RFM018) and the north-eastern (e.g. RFM021, RFM032) margins of the lens. The rocks in these marginal domains dip steeply towards the south-west.

An assessment of the potential of the Forsmark area for exploration for metallic and industrial mineral deposits has shown that there is no such mineralisation encountered within the candidate area. A potential for iron oxide mineralisation and possibly base metals was recognised in an area south-west of the candidate area, but the mineralisations in the Forsmark area are small and have no economic value.

Three major sets of deformation zones have been recognised with high confidence at the Forsmark area. Vertical and steeply, SW-dipping zones with WNW-NW strike, form important structures at the boundary of the candidate volume, where the ductile strain is also high. These are regional and local major structures that show complex, ductile and brittle deformation. The zones with WNW-NW strike represent the oldest set, with first-order structures in a WNW direction (e.g. Forsmark and Singö deformation zones) and second order splays in a NW direction (e.g. Eckarfjärden deformation

zone). Vertical and steeply-dipping, brittle deformation zones with NE strike are local major (and local minor) in character. They transect the candidate volume at Forsmark and are prominent in the Bolundsfjärden area. Gently SE- and S-dipping brittle deformation zones are local major in character and occur more frequently in the south-eastern part of the candidate volume. Relative to the other three sets, there is an increased frequency of open fractures along the gently dipping set. These gently dipping zones seem to play an important role in determining the properties of the Forsmark site (see further below). There is evidence for reactivation of each set of deformation zones after their formation, which is suggested to have occurred prior to c. 1,700 million years ago. So far, no high confidence deformation zones have been identified that correspond to the NS lineaments at the Forsmark site.

Statistical analyses of rock mass fractures in between deformation zones indicate a large spatial variability in the size, intensity and properties between different rock domains, but also within rock domain RFM029. In general, the fracture frequency is low in rock domain RFM029. However, the fracturing shows no consistent depth dependence, but may be affected by the proximity to deformation zones. This is indicated, for example, by the higher frequency of fractures close to the gently dipping zone ZFMNE00A2 in one of the boreholes and very few fractures at larger depths below this zone.

The upper few tens of metres of the bedrock contain fractures with a large aperture that are more or less parallel to the ground surface. Some of these fractures are filled with glacial sediments. It is suggested that these structures formed or reactivated as a result of stress release in connection with the removal of ice during the last glaciation and/or, at an earlier stage, in connection with the removal of the Phanerozoic sedimentary cover. However, there is no evidence of faulting or major earthquakes since the disappearance of the last inland ice sheet.

Thermal and rock mechanics properties

The rock types in rock domain RFM029 have high quartz contents and thermal properties that are favourable for a potential repository. Much of the rock has a mean value for the thermal conductivity of approximately 3.6 W/(m·K), whereas a minor part of the rock in rock domain RFM029 has a lower value, approximately 3 W/(m·K). There are also some indications of anisotropy in thermal conductivity in lineated/foliated parts of the rock. The thermal properties of rock domain RFM012 (southwest of RFM029) seem to be similar to those of rock domain RFM029.

The rock mass in domain RFM029 has mechanical properties favourable for a potential repository, with high strength and low deformability. Furthermore, the deformation modulus is rather high (on average 64–68 GPa), indicating no dependence on the rock stresses. The rock mass in domains RFM012 and RFM018 (along the south-western margin of the lens) and in RFM017 (inside the lens) have similar mechanical properties to the rock mass in domain RFM029.

The mechanical strength of deformation zones shorter than 10 km seems to be comparable to that of the rock mass. In a similar manner as the rock mass, the deformation modulus is high (on average 58 GPa), indicating no dependence on rock stress. The deformation modulus for regional deformation zones that are longer than 10 km and strike NW-SE (e.g. Forsmark, Singö, Eckarfjärden zones) is lower and is dependent on the rock stress, on average 5 GPa for low stresses and about 30 GPa for confinement stresses above 10 MPa.

The rock stresses at Forsmark are relatively high compared with typical central Scandinavian sites. The major principal stress direction trends approximately 142°. An average maximum horizontal stress of 45 MPa has been estimated at the depth of 500 m. The stress gradient of this stress component at depths between 350 and 650 m is probably small (0.02 MPa/m) compared with the gradient at shallow depths. The variations in stress orientation and magnitude in the upper 100 to 200 m are believed to depend on local variability of the frequency and orientation of the rock fracture structures.

Hydrogeology, hydrogeochemistry and transport properties

The rock mass between the deformation zones in the candidate volume appears to be of very low permeability beneath the gently dipping deformation zone ZFMNE00A2 at depths below about the –360 m level. In contrast, the upper part of the rock mass is rather permeable. Also, the transmissivity of deformation zones seems to vary with depth and dip, with higher transmissivity in the gently dipping zones than in the steeply dipping zones at comparable depths. However, down to c. 60 m depth, the zones are hydraulically very heterogeneous with transmissivities that vary over three orders of magnitude. However, since there are few boreholes, the exact division of volumes of different hydraulic properties remains to be defined.

The near-surface rock seems to be in good hydraulic contact over long distances, possibly because of the near-surface vertical or steeply dipping deformation zones and outcropping gently dipping zones. The numerical simulations carried out indicate that the groundwater flow inside the candidate volume predominantly is determined by the location, geometry and hydraulic properties of the deformation zones within this volume.

The groundwater evolution and patterns at Forsmark are complex and are the result of several factors including: a) the present-day topography and proximity to the Baltic Sea, b) past changes in hydrogeology related to glaciation/deglaciation, land uplift and repeated marine/lake water regressions/transgressions, and c) organic or inorganic alteration of the groundwater composition caused by microbial processes or water/rock interactions.

Four main groundwater types are present at the Forsmark site. Recent to young meteoric (Na-HCO₃ type) waters are found at shallow depths (0–150 m). Old brackish water of marine origin (Na-Ca-Cl(SO₄) type) with a Littorina Sea and glacial signature are found at depths between c. 150 and 500 m. At larger depths (KFM03A: 645 m), an older meteoric saline (Na-Ca-Cl type) groundwater with a small glacial component is found. At still greater depth (KFM03A: 990 m) the groundwater changes to a higher saline Ca-Na-Cl type characterised by an even greater glacial signature.

Meteoric water dominates in the north-west part and in the middle part of the site. Marine water is found towards the coast in the eastern part of the site. Signatures of Littorina Sea water are found at shallow depths close to the Baltic Sea coastline and shallow groundwaters below Bolundsfjärden show elevated salinity. Factors of potential importance for the preservation of Littorina Sea water at shallow depths in the Forsmark area are that the area quite recently rose above sea level and that the flat topography and hydraulic properties of the Quaternary sediments seem to limit the effective recharge and the flushing out of water from the rock.

Modelling results indicate that re-equilibration reaction processes have been important for the establishment of the present groundwater composition, following the intrusion of Littorina Sea water into the rock. However, the main compositional changes, and even the extent of re-equilibration processes, seem to have been controlled by the extent of mixing.

Most lines of evidence suggest that the sulphur system, microbiologically mediated, is the main redox controller in the deepest and most saline groundwater. Furthermore, the groundwater composition at repository depth is such that it fulfils the SKB chemical suitability criteria for all the principal components, i.e. Eh, pH, TDS, DOC and Ca+Mg.

The major fracture-coating materials in water-conducting fractures in the candidate volume are chlorite, calcite and clay minerals. The gently dipping deformation zones and the shallow sub-horizontal fractures are highly water conductive. They are rich in gouge and contain quartz and adularia in addition to chlorite and mixed-layer clays. In addition, the rock beneath the coating in the water-conducting fractures in the gently dipping deformation zones and in the shallow sub-horizontal fractures is altered. The sorption properties of these fracture coatings are presently not known, but available data on specific surface area (BET) indicate that materials associated with fractures and deformation zones have high sorption capacities. The porosity of the rock matrix is approximately 0.2% and the formation factor approximately 2×10^{-5} . Furthermore, there are indications that the formation factor (and the porosity) are dependent on the rock stress, which means that field tests and laboratory results do not provide the same answer.

The base case conceptual model of solute transport in discretely fractured rock comprises transport in mobile and immobile volumes, respectively. The mobile zones are fractures and deformation zones where groundwater flow and advective transport takes place. The immobile zones mainly comprise the intact rock matrix, fracture surface and fracture filling materials, and fractures with stagnant water where solutes can be retained from the mobile water. Based on the present indications of very low conductive rock mass between the deformation zones in the target area at depth and the rather tight rock matrix (low matrix diffusivity), it is possible that the basic concept for solute transport in a discrete fracture network needs to be somewhat modified in order to be applicable for the Forsmark site. Specifically, it will be essential to capture transport characteristics in the sparsely fractured rock with likely channelled flow and limited access to the rock matrix for transported solutes.

13.2.2 Uncertainties and confidence

As discussed in Chapter 12, most of the available data have been analysed and treated according to acceptable practices. In addition, inaccuracies and biases are understood and accounted for in the subsequent modelling. Inaccuracies and biases in the field data are, with some exceptions, judged to be a minor source of uncertainty in the resulting model description.

Important modelling steps have been taken and more of the uncertainties are now quantified or explored as alternatives. However, several hypotheses remain to be tested and some uncertainties remain un-quantified. Some uncertainties are related solely to the understanding of the site and do not have direct implications for safety assessment or repository engineering, whereas others have significant implications. Important uncertainties that have direct implications for safety assessment or repository engineering concern:

- The occurrence, continuity, dip and thickness of deformation zones and the heterogeneity of their transmissivity, mainly in the target area.
- The size, intensity and transmissivity of fractures in the rock mass between deformation zones, mainly in the target area, including spatial variability and the possibility of dividing the rock mass into volumes with different hydraulic properties.
- The spatial and depth distribution of stress magnitudes and rock mechanics properties, mainly in the target area.
- Spatial variability in rock transport properties and correlations with flow paths.

Uncertainties related to spatial variability, potential anisotropy and up-scaling of thermal conductivity have implications for repository engineering, but may not be very important because of the high thermal conductivity values that generally apply within the target area. The groundwater composition at the Forsmark site fulfils the present suitability criteria by a substantial margin, and uncertainties may not be of direct importance for safety assessment. However, these uncertainties are of importance for the understanding of the past evolution and, thereby also, for predictions of future evolution of water chemistry at the site.

Uncertainties in rock mechanics properties, rock stresses and thermal properties are quantified. Uncertainties in the occurrence and geometry of deformation zones have been illustrated by providing alternative models, which have been explored in the hydrogeological modelling. The hydrogeological modelling has also involved a number of sensitivity analyses to illustrate the importance of uncertainties in e.g. boundary conditions, the hydraulic properties of the deformation zones, and the hydraulic properties of the fractures between the deformation zones. Uncertainties in the hydrogeochemical description have been explored by applying different modelling approaches to the same data set.

As demonstrated in Section 12.4, there are many important interactions between the different disciplines and many of these have been considered in the development of version 1.2 of the site descriptive model. It is obvious that geology provides an important input to many of the other disciplines by defining the geometrical framework and geological properties of rock domains, deformation zones and rock mass fracturing. However, to assure consistency in the site model there

is also feedback from other disciplines to geology that should be utilised to improve confidence in the geological model. This has to some extent been applied in developing model version 1.2, but there are possibilities for further improvements in this area. An example of an important feedback during the development of model version 1.2 is the hydraulic confirmation that gently dipping deformation zones are major features for groundwater flow. Other important interactions concern the interplay between hydrogeology and hydrogeochemistry. This coupling is considered in the work, but improvements can be made in order to address remaining uncertainties.

The formation of a NET group for making an integrated analysis of the surface system has ensured that interactions between the abiotic and biotic systems are well covered. Interactions between the surface system and the bedrock system are also considered, but could be further developed. For example, surface and near-surface hydrogeochemistry as well as hydrology and hydrogeology are relevant to the nature and distribution of the waters in the bedrock, and the surface hydrology has been assessed incorporating information relating to the upper part of the bedrock, although still using version 1.1 of the hydrogeology model.

In general, the Forsmark 1.2 site descriptive model is in agreement with the current understanding of the past evolution as described in Chapter 3. As the investigations proceed, the findings from the site continue to improve our understanding of the past conditions, as exemplified in Section 12.5.

Our current understanding of the site has been primarily confirmed by the outcome of the version 1.2 modelling and no major surprises have occurred. The fact that much more sub-surface data have implied only minor changes in the rock domain model has significantly increased the confidence in the lithological description. Enhanced confidence in rock mechanics and thermal properties has also been achieved since the analyses and modelling, now based on a larger data set and site-specific data, confirm the ranges obtained in model version 1.1.

Sub-surface data have confirmed the existence of deformation zones and supported the significance of seismic reflectors as representing gently dipping zones. The deformation zone model is stabilising and can be treated with enhanced confidence in the local model volume. This also increases the confidence in the hydrogeological description, although much uncertainty still remains regarding the hydraulic properties of the deformation zones and of the fracture network in the rock mass between the deformation zones. However, the picture of very low hydraulic conductivity at depth is strengthened by the new data and, to some extent, also supported by the hydrogeochemistry of the site. Since the structure of the fracture network in the rock mass between deformation zones and the hydraulic properties of the fractures are of major importance for repository engineering and safety assessment, resolving these uncertainties related to flow in a sparsely fractured rock mass and the potential impacts on solute transport is of high priority.

13.3 Implications for further modelling

The model version presented in this report completes the site descriptive modelling based on data gathered within the Initial Site Investigation phase. Ongoing field work is now largely focused on the north-western part of the candidate area, which is the selected target area for the location of a potential repository. The arguments for the selection of this area as well as a programme for the investigations that will be carried out during the Complete Site Investigation (CSI) phase have been presented /SKB, 2005a/.

According to the present plans for site descriptive modelling, three modelling steps will be carried out during CSI. The scope of the two first modelling steps is limited, whereas the third and final step will result in a complete site description. However, an important component of all three steps is to address and continuously try to resolve uncertainties of importance for repository engineering and safety assessment (see Figure 12-1). The following sections address important aspects for further modelling, set in relation to the aim and scope of especially the first modelling step during CSI (model version 2.1).

13.3.1 Technical aspects

The modelling step 2.1 will make use of all data available on the 1st of August, 2005, i.e. data freeze 2.1. The primary objective with the 2.1 modelling is to provide a feedback to the site concerning potential revisions of the current CSI programme /SKB, 2005a/. In addition, the geological models will be updated. Modelling within the other disciplines will focus on resolving specific issues without any requirements on producing complete updated models.

One important aspect for further modelling concerns the size of the local model volume. Already in model version 1.1, it was concluded that the size of this volume needs to be reduced in order to increase the resolution and decrease the uncertainty in the description. The work with model version 1.2, together with the focussing of the site investigation work to the target area in the north-western part of the candidate area, has further strengthened this need. Therefore, the size of the local model volume will be reduced, or descriptions with different resolution within the local model volume will be developed. In this way, it will be possible to obtain higher resolution and to illustrate the variability in the geology and rock mechanics descriptions of the area that has been prioritised for the location of a potential repository. Both a local geological model for the target area and an updated regional geological model are foreseen in the 2.1 modelling.

Other important geological aspects to be considered in the forthcoming modelling concern:

- The division of rock domain RFM029 into sub-domains in order to assess, for example, the spatial variability in fracturing above and below deformation zone ZFMNE00A2.
- The geological significance of lineaments in the target area that are longer than 1,000 m.
- Utilise new geochronological and kinematic data in order to improve the understanding of the timing and sequence of formation of different sets of deformation zones.
- Carry out an assessment of all available reflection seismic data, from both surface and borehole measurements, in order constrain better the geometry of especially the gently dipping deformation zones.

It is essential that all identified feedback from the modelling in rock mechanics, hydrogeology etc, is incorporated in the development of the next version of the geological model. This concerns for example:

- Feedback from bedrock hydrogeology that can provide confirmation and indications of deformation zones and control of the hydraulic applicability of the DFN model.
- Carry out a more comprehensive analysis of the data concerned with mineral fillings along fractures, in order to couple the geochemical history of fracture fillings to tectonic history and to assess the relevance of this feature for the explanation of the low transmissivity of steep structures.

The hydrogeological modelling has further strengthened the picture of very low conductive rock at depth and that the water flows in deformation zones, whereas the rock mass between the zones is virtually non-conducting. This in turn has raised a question regarding the applicability of the present conceptual model for solute transport, which to a large extent is influenced by earlier experience, e.g. from Äspö. This highlights the importance of obtaining a more detailed description of the hydrogeology in the target volume for the repository location, including also the thickness and hydraulic properties of the overburden as well as the highly transmissive and anisotropic uppermost parts of the bedrock.

Examples of other aspects to consider for future modelling are:

- Extending the modelling of evolution of water chemistry to include concentration of different species, in addition to water types.
- Incorporating additional geochemical processes, geological heterogeneity and the deeper saline water system in coupled, reactive transport modelling.
- Calculating groundwater mixing proportions using alternative models to M3 and other variants of end-member waters.

13.3.2 Modelling procedures and organisation of work

A great deal of experience has been gained on procedures and organisation of the modelling work during the Forsmark 1.2 modelling. Interdisciplinary modelling is a continuous learning process which will continue to develop throughout the site descriptive modelling. This implies that the strategy/methodology described in the developed strategy documents may become out of date, or need revision/amendment. One such example is the development of the document which details an updated methodology for geological DFN modelling /Munier, 2004/.

Capturing and evaluating the primary field data is a very demanding effort. This has become more burdensome because of the large amount of data available for model version 1.2. In data freeze 2.1, still more data will be available. Even if the increase is not as large as between model versions 1.1 and 1.2, the effort needed in future modelling should not be underestimated.

The interaction and information exchange between site modelling and site investigation as well as between site modelling and the clients of the site descriptive model, repository engineering and safety assessment, has been further improved during the work with model version 1.2. The establishment of the discipline-specific NET-groups has facilitated this close interplay between the site investigation, the modelling project and safety assessment, since representatives from these different areas are members of these groups. In addition, representatives from repository engineering actively follow the progress of the modelling work by participating in project group meetings.

Large improvements have also been made in the integration between disciplines in the modelling work. Since the NET-groups handle most of the discipline-specific questions, it has been possible for the project group to focus on integration issues. This increases the possibility for further improvement regarding important integration aspects of the site descriptive modelling.

Another important component supporting integration and information exchange has been the workshops held for assessing uncertainty and confidence. These types of workshops will continue, but with objectives and participation adapted to the focus of the current modelling. For example, a workshop during modelling step 2.1 could focus on identifying remaining uncertainties that require additional field data, with participation from the modelling project, the site investigation team and also from repository engineering and safety assessment. The prime aim of such a workshop would be to capture relevant feedbacks from the results of the design work and safety assessments based on Forsmark model version 1.2.

13.4 Implications for the ongoing site investigation programme

The recommendations arising from the work with model version 1.2 are divided firstly into recommendations or feedback that have been given to the site investigation organisation during the course of the modelling work, and secondly into recommendations that have emerged predominantly from the uncertainties in the model version 1.2.

13.4.1 Recommendations provided during the modelling work

An important feedback that was completed during the modelling work concerned recommendations to the site during the production of the programme for the complete site investigation phase /SKB, 2005a/. Several members of the modelling team were actively involved in the development of the CSI programme. In this way, information and data needs for future model developments were effectively implemented.

During the work with model version 1.2, the project group has had continuous information exchanges with the site investigation team, amongst other things concerning questions related to the field investigation programme. These questions have been both more profound in character (e.g. location of drilling sites, location and orientation of cored boreholes, programme for verification of lineaments in the target area) and of a more detailed character (e.g. sampling procedures and methods).

Recommendations given on the siting of new drill holes have been documented in decision papers (see below). Recommendations and feedback from the hydrogeochemical modelling work are provided in their reporting of model version 1.2 /SKB, 2005b/. However, much of the feedback to the site investigation team has been given in a more “informal“ form via mail, via telephone, in meetings and so forth, not necessarily associated with documentation of the contents of the feedback. A log is kept to keep track of this “informal” feedback and it was established during the work with model version 1.1.

Recommendations concerning drilling of new boreholes

In April 2004, a decision was taken by SKB to focus continued core drilling activities to the north-western part of the candidate area. These drilling activities aim to answer a number of questions regarding the suitability of the north-western part of the candidate area for the location of the repository.

Together with representatives for repository engineering, members of the modelling team provided a recommendation for the location of drill sites 7 and 8, a recommendation for the position and orientation of cored boreholes KFM06B and 06C at drill site 6, cored boreholes KFM07A and 07B at drill site 7 and cored boreholes KFM08A and 08B at drill site 8, and a recommendation for the position and orientation of three percussion boreholes. These recommendations were documented as an appendix to a SKB decision paper (Appendix 5). Subsequently, a recommendation for a modification of the length and orientation of borehole KFM08B was included as an appendix in a new decision paper (Appendix 6). Finally, a motivation for the drilling of cored borehole KFM08C and a recommendation for its orientation were completed in a separate SKB decision paper (Appendix 7).

13.4.2 Recommendations based on uncertainties in the integrated model

Even though progress has been made on the site-specific critical issues that were raised in FUD-K /SKB, 2001b/ and later in the planning of the site investigations at Forsmark /SKB, 2002b/, see Section 13.2.2, uncertainties in the site description still remain. These uncertainties are noted and discussed in Section 12.3, where it is also stated whether additional data can resolve these uncertainties. In cases where additional data were assessed as important for reducing uncertainty, a formal check was made against the programme for site investigations, which is planned to be carried out during the complete site investigation phase /SKB, 2005a/. The result of this check (see Section 12.3) showed that the planned investigation programme covered the identified additional data needed, with a few exceptions that had to be added to the site investigation programme. This was not surprising bearing in mind once again the input from several members of the modelling team in the writing of the CSI programme. A summary of the important aspects of the feedback to the CSI programme, based on the evaluation compiled in Chapter 12, as well as some additional considerations that are of significance for the site investigation programme are listed below.

Location of boreholes

As already described above, recommendations concerning location of boreholes have been provided and included in the CSI programme. The locations are selected in order to answer questions concerning e.g. the north-west extension of rock domain RFM029, the lithological, structural, rock mechanical, hydrogeological and hydrogeochemical characteristics of the bedrock in the north-western part of the candidate area, and the presence of possible undetected deformation zones in this area (see Appendix 5).

New boreholes at the boundaries of the candidate volume should also help in reducing uncertainties in the continuity and thickness of the gently dipping zones (see below) and in determining the hydraulic properties of these zones. Such boreholes are included in the CSI programme and include boreholes in the sea area close to SFR. It is also of interest to learn whether the hydraulic properties of the rock mass outside the tectonic lens, south-west of the candidate area, are significantly different from those inside the tectonic lens.

Measurement of the orientation of linear mineral fabrics at depth

There is a need for a systematic measurement of the orientation of linear mineral fabrics in the bedrock in the cored boreholes. Data that are lacking include the measurement of the orientation of both mineral lineation in the bedrock and slickenside striations along minor fault planes.

The justification for the acquisition of linear mineral fabric data is to demonstrate how much the mineral lineation varies in orientation with depth. This is an intrinsic feature of the rock domain model for the site and the assumption that the orientation of this structure is constant with depth needs to be tested. Measurements of slickensides are necessary when data on the kinematics of deformation zones are attained. Measurements of the orientation of mineral lineation should be completed in all new cored boreholes and possibly along a number of selected sections along the boreholes KFM02A, KFM03A and KFM05A. Measurements of the orientation of slickenside striations should be completed along all the deformation zones.

Occurrence, geometry and properties of deformation zones

The excavation and detailed mapping of representative linked lineaments at the surface, seismic refraction data obtained from the surface, the interpretation of the dip of magnetic anomalies, and new borehole data from the bedrock close to these lineaments would considerably reduce uncertainty in the character of lineaments. Such data would also reduce uncertainty in the continuity, dip and thickness of deformation zones interpreted with the help of linked lineaments. New seismic reflection data coupled with new boreholes at the boundaries to the candidate volume would reduce uncertainty in the continuity and thickness of the gently dipping zones. All these activities are proposed in the CSI programme /SKB, 2005a/. The confidence in the identification of deformation zones may also be improved by a deeper analysis of fracture data from boreholes and tunnels close to the nuclear power plant and SFR. However, only a limited amount of new information can be attained from these data.

An improved understanding of the tectonic history in the brittle regime, which initiated at the Forsmark site prior to c. 1,700 million years ago, may be achieved by the assembly of kinematic data along brittle deformation zones. Furthermore, geochronological data are required that shed light on the timing of mineral growth along fractures, and that provide information on the cooling and exhumation history of the site. Proposals for all these studies, including a closer integration of the studies of mineral fillings along fractures and the structural characteristics of brittle deformation zones, have been included in the CSI programme /SKB, 2005a/.

There is also a need for a more detailed documentation of the properties of deformation zones that have been identified in the single hole interpretations. This characterisation should be carried out prior to the integration and parameterisation of deformation zones in the modelling work. It is recommended that this procedure is applied to all the deformation zones that have so far been recognised in the single hole interpretations. Naturally, it should also be applied to all the zones recognised in forthcoming single hole interpretations.

Fracture statistics and DFN modelling

The present DFN model is associated with large uncertainties (see Section 12.3). Further characterisation efforts for reducing these uncertainties include: capturing old SFR-mapping data, data from trenches over lineaments in the target area, evaluating fracture data with respect to lithology, mineralogy and proximity of deformation zones in each borehole, more spatially representative borehole data, scan-line mapping in connection with bedrock mapping, and more outcrop mapping, especially beneath deformation zone ZFMNE00A2. These types of investigations form a part of the CSI programme /SKB, 2005a/.

The excavating and mapping of larger areas (100×100 m) of rock would enhance confidence, but have severe practical and environmental implications and has not been included in the CSI programme. The mapping of outcrops with topographic relief would, in theory, reduce uncertainty in the occurrence and character of sub-horizontal fractures, but such outcrops do not exist at the site.

Data from rock domains other than RFM029 are of uncertain value for repository engineering and safety assessment and are not planned in the CSI program. However, such data would enhance our understanding of the site.

Detailed mineralogy of rock and fracture minerals

The redox buffering capacity of the geosphere is important information for safety assessment. In order to evaluate this entity, detailed mineralogical data on Fe(II) and sulphide content of the rock and fracture minerals are needed.

Rock stress distribution – rock mechanics properties

The rock stress magnitudes and their spatial and depth distribution are uncertain, since measured stresses are at the upper limit of applicability of the measurement methods. The uncertainties would reduce from more stress measurements near the surface to estimate the stress gradient and by further checking the stress increase below gently dipping deformation zones. However, new data will probably confirm the present understanding of the stress orientations. Proposals for these studies are included in the CSI programme /SKB, 2005a/.

To improve confidence, measurements should be taken by means of overcoring and hydraulic methods at the same depth. The use of new independent methods for the determination of the rock stresses is also helpful. The general observation of low frequency of core diskings in the deep boreholes at the Forsmark site has initiated the question of at what stress conditions core diskings is likely to occur. An answer to this could give input to estimations of an upper bound for the state of stress at the site. A special study on this matter has been initiated at the Äspö Hard Rock Laboratory, at the location of the so-called Äspö Pillar Stability Experiment (APSE), where a well-controlled high stress environment has been developed in the floor of a tunnel /Andersson, 2003/.

New laboratory tests together with characterisation of the rock mass outside rock domain RFM029 will reduce uncertainty of the rock mechanics properties at the site. Such tests are included in the CSI programme and new data will probably confirm the present results concerning the effects of scale on the mechanical properties.

Bedrock thermal properties

Representative direct measurements of thermal conductivity, data from more boreholes, and measurements at a relevant scale will reduce uncertainty in the scaling of thermal conductivity. Large-scale tests of thermal conductivity in different directions would reduce uncertainty in anisotropy. These activities are already included in the current CSI programme /SKB, 2005a/. The uncertainty would be further reduced by extensive sampling of other rock types to produce variograms of spatial variability and by more data from subordinate rock types (from existing or planned cored boreholes). Such activities are part of the CSI programme /SKB, 2005a/.

Representative measurements of heat capacity would reduce uncertainty. Uncertainty in in-situ temperature measurements may be reduced by reassessing the existing database and by evaluating the possible effects of disturbances. Useful new data would include temperature logs at more representative (less disturbed) times. It may also be possible to reconsider the measurement procedure in order to mitigate effects of long-term thermal convection. Laboratory test method development, already underway, will reduce the uncertainty in thermal expansion values.

Transmissivity distribution – hydraulic tests

The variability in the hydraulic properties of deformation zones will be better addressed by new borehole data, more seismic reflection data from boreholes and the surface, interference and cross-hole tests, as well as Boremap, BIPS and PFL data for zones outside the target area. Such characterisation is planned in the current CSI programme /SKB, 2005a/.

Existing PSS data can be used to test the transmissivity distribution in discrete fractures by simulating existing tests performed at various scales. Data to resolve the geometry of fractures using inclined boreholes and single-hole interference tests (interference tests between nearby cored boreholes are not possible) would reduce uncertainty in the hydraulics of the discrete fractures. Such characterisation is planned in the current CSI programme /SKB, 2005a/.

Other uncertainties in the hydrogeological model are related to processes and conditions affecting the palaeohydrogeological evolution and thus the present hydrogeological and hydrogeochemical conditions at the site. These uncertainties would be reduced by new samples for estimating salinity in the rock matrix, new time series of near-surface hydrology data and new boreholes at or just outside the boundaries of the target area including the Baltic Sea area from the bottom of SFR. Dilution tests in gently dipping zones are also of interest as they provide information about the natural gradients. Such characterisation is planned in the current CSI programme /SKB, 2005a/.

Some of the results of the Forsmarks 1.2 hydrogeological modelling highlight the need for an improved integration between the bedrock and the near-surface hydrogeology. Detailed hydraulic tests 0–100 m below the surface would probably be quite useful for that purpose by providing near-surface properties to the bedrock hydrogeological model. Such tests are not included in the current CSI plan.

Groundwater composition – rock matrix pore water

Uncertainties in the hydrogeochemical model that can be reduced by additional field activities concern: uncertainties in the spatial variability of hydrochemistry in 3D at depth, uncertainties related to the composition of water in the rock matrix and the exchange between high and low conductive groundwater systems and uncertainties in temporal (seasonal) variability in surface water chemistry, which impacts the identification of discharge and recharge areas.

The listed groundwater compositions are well within the bounds of the preferred conditions, see Chapters 9 and 11. However, reducing the uncertainties would enhance our understanding of the site and, thus, the possibilities to predict the future evolution. The uncertainties would be reduced by more data observations from deep boreholes, analyses of rock matrix samples, electromagnetic data for regional characterisation, and data from extreme end-member waters. Samples for rock matrix determination have already been collected and the results will be available for model version 2.1. These various characterisations are part of the CSI programme /SKB, 2005a/. The planned boreholes, e.g. at SFR, are likely to be useful for understanding of the groundwater composition in a regional context and the use of additional boreholes in the region should be weighted against the information from already existing sources (Finnsjön, SFR). Whether there is a need to revise the sampling of near-surface waters will be assessed at a later stage.

Bedrock transport properties

Uncertainty in matrix retention properties and in sorption properties, diffusivities and porosities of representative geological material along fractures will be reduced by more laboratory data and by Single Well Injection Withdrawal (SWIW) tests. These activities are included in the CSI programme /SKB, 2005a/. More borehole data may also improve our understanding of the potential correlation between fractures and migration properties, but the expectations of significant progress in this area are rather low.

Surface system

The main uncertainties in the version 1.2 model of the surface system are related to the lack of some types of data (see Section 12.3.2.). These uncertainties will be reduced as additional data become available. Activities that will generate these data are included in the current CSI programme.

13.5 General conclusions

Regarding the specific objectives stated for the version 1.2 modelling of the Forsmark area, as given in Chapter 1, the following general conclusions can be made.

- Primary data available at data freeze 1.2 have been analysed as part of the Forsmark 1.2 modelling procedure, including older data from construction of the nuclear power plant and SFR.
- Three-dimensional descriptive models of rock domains and deformation zones have been updated. These models focus on the regional scale model volume, but include the local scale model volume. The geological models have formed the basis for the parameterisation of the models in other disciplines. They have also formed the geometrical and structural basis for subsequent hydrogeological flow modelling and the ongoing repository design work.
- Confidence in the developed models has been treated in a systematic way, as presented in Chapter 12, including assessment of uncertainties, and interactions and feedback between disciplines. Significant progress is noted in the coupling between hydrogeochemistry and hydrogeological modelling. The feedback from other disciplines to the geological modelling should continue and be further formalised in future modelling work.
- Possible alternative models have been screened and prioritised in relation to the needs of repository engineering and safety assessment. Several of these alternative models have also been tested in order to explore uncertainties in the site description. For example, alternative structural models developed for the geometry of deformation zones have been propagated into the hydrogeological modelling. In addition, various alternatives concerning the hydraulic properties of the fracture network in the rock mass between the deformation zones have been explored. However, these alternatives may not cover the full uncertainty range, and especially the issue on channelling could need additional analyses within the safety assessment framework.
- Site-specific issues have been addressed and our understanding of the site has developed, as a result of the Forsmark 1.2 modelling and as demonstrated in the preceding sections. No new important site-specific issues have been raised, but the occurrence of very low conductive rock at depth has been confirmed and has become an issue of major interest.
- Modelling results and identified uncertainties have been used as input to the current Complete Site Investigation programme /SKB, 2005a/ and for a formal check of the content of the CSI programme prior to decision concerning its implementation.

14 References

- Aaltonen J, Gustafsson C, 2004.** RAMAC and BIPS logging in borehole KFM01A. Forsmark site investigation. SKB P-03-45, Svensk Kärnbränslehantering AB.
- Aaro S, 2003.** Regional gravity survey in the Forsmark area, 2002 and 2003. SKB P-03-42, Svensk Kärnbränslehantering AB.
- Abrahamsson T, 2003.** Vegetation inventory in part of the municipality of Östhammar. SKB P-03-81. Svensk Kärnbränslehantering AB.
- Adl-Zarrabi B, 2003.** Outcrop samples from Forsmark. Determination of thermal properties by the TPS-Method, SKB P-03-08, Svensk Kärnbränslehantering AB.
- Adl-Zarrabi B, 2004a.** Drill hole KFM03A. Thermal properties: heat conductivity and heat capacity determined using the TPS method and mineralogical composition by modal analysis. Forsmark site investigation, SKB P-04-162, Svensk Kärnbränslehantering AB.
- Adl-Zarrabi B, 2004b.** Drill hole KFM04A. Thermal properties: heat conductivity and heat capacity determined using the TPS method and mineralogical composition by modal analysis. Forsmark site investigation, SKB P-04-199, Svensk Kärnbränslehantering AB.
- Adl-Zarrabi B, 2004c.** Drill hole KFM01A. Thermal properties: heat conductivity and heat capacity determined using the TPS method and mineralogical composition by modal analysis. Forsmark site investigation, SKB P-04-159, Svensk Kärnbränslehantering AB.
- Adl-Zarrabi B, 2004d.** Drill hole KFM02A. Thermal properties: heat conductivity and heat capacity determined using the TPS method and mineralogical composition by modal analysis. Forsmark site investigation, SKB P-04-161, Svensk Kärnbränslehantering AB.
- Ahlbom K, Andersson J-E, Andersson P, 1992.** Finnsjön study site. Scope of activities and main results. SKB TR 92-33, Svensk Kärnbränslehantering AB.
- Albi K, Winterhalter B, 2001.** Authigenic mineralisation in the temporally anoxic Gotland Deep, the Baltic Sea. *Baltica*, 14, 74–83.
- Allen H L, Ocevski B T, 1981.** Comparative primary productivity of algal epiphytes on three species of macrophyte in the littoral zone of Lake Ohrid, Yugoslavia. *Holarctic Ecology* 4:155–160.
- Amadei B, Stephansson O, 1997.** Rock stress and its measurement. Chapman and Hall, London, p. 490.
- Ambrosiani Garcia K, 1990.** Macrofossils from the till-covered sediments at Öje, central Sweden. In: Late Quaternary Stratigraphy in the Nordic Countries 150,000–15,000 B.P. (Andersen B.G. & Königsson L.-K. Eds.). *Striae* 34, 1–10.
- Andersson J-E, Nordqvist R, Nyberg G, Smellie J, Tirén S, 1991.** Hydrogeological conditions in the Finnsjön area. Compilation of data and conceptual model. SKB TR-91-24, Svensk Kärnbränslehantering AB.
- Andersson P, Andersson J-E, Gustafsson E, Nordqvist R, Voss C, 1993.** Site characterisation in fractured crystalline rock – A critical review of geohydrologic measurement methods. Site-94. SKI Technical Report 93:23, Statens Kärnkraftinspektion.
- Andersson P, Ludvigsson J-E, Wass E, 1998.** Äspö Hard Rock Laboratory, True Block Scale Project, Preliminary characterisation. Combined interference tests and tracer tests. SKB IPR-01-44, Svensk Kärnbränslehantering AB.
- Andersson J, Ström A, Svemar C, Almén K-E, Ericsson L O, 2000a.** What requirements does the KBS-3 repository make on the host rock? Geoscientific suitability indicators and criteria for siting and site evaluation. SKB TR 00-12, Svensk Kärnbränslehantering AB.
- Andersson P, Ludvigsson J-E, Wass E, Holmqvist M, 2000b.** Äspö Hard Rock Laboratory, True Block Scale Project, Tracer test stage. Interference tests, dilution tests and tracer tests. SKB IPR-00-28, Svensk Kärnbränslehantering AB.

- Andersson J, Berglund J, Follin S, Hakami E, Halvarson J, Hermanson J, Laaksoharju M, Rhén I, Wahlgren C-H, 2002a.** Testing the methodology for site descriptive modelling. Application for the Laxemar area. SKB TR-02-19, Svensk Kärnbränslehantering AB.
- Andersson J, Christiansson R, Hudson J, 2002b.** Site Investigations. Strategy for Rock Mechanics Site Descriptive Model. SKB TR-02-01, Svensk Kärnbränslehantering AB.
- Andersson P, Byegård J, Dershowitz B, Doe T, Hermanson J, Meier P, Tullborg E-L, Winberg A, 2002c.** Final report of the TRUE Block Scale project, 1. Characterisation and model development, SKB TR-02-13. Svensk Kärnbränslehantering AB.
- Andersson C, 2003.** Äspö Pillar Stability Experiment. Summary of preparatory work and predictive modelling. SKB R-03-02, Svensk Kärnbränslehantering AB.
- Andersson J, 2003.** Site descriptive modelling – strategy for integrated evaluation. SKB R-03-05, Svensk Kärnbränslehantering AB.
- Andersson E, Tudorancea M-M, Tudorancea C, Brunberg A-K, Blomqvist P, 2003.** Water chemistry, biomass and production of biota in Lake Eckarfjärden during 2002. SKB R-03-27, Svensk Kärnbränslehantering AB.
- Andersson J, Munier R, Ström A, Söderbäck B, Almén K-E, Olsson L, 2004.** When is there sufficient information from the Site Investigations? SKB R-04-23, Svensk Kärnbränslehantering AB.
- Andrén T, Björck J, Johnsen S, 1999.** Correlation of the Swedish glacial varves with the Greenland (GRIP) oxygen isotope stratigraphy. *Journal of Quaternary Science* 14, 361–371.
- Andrén C, 2004a.** Forsmark site investigation, Amphibians and reptiles. SKB P-04-07. Svensk Kärnbränslehantering AB.
- Andrén C, 2004b.** Underlag till Energiflöden i ekosystem med grod- och kräldjur. Nature – Artbevarande & Foto.
- Aronsson M, 1993.** Projekt Upplands Flora. *Daphne* 1993:1.
- Arvidsson R, 1996.** Fennoscandian earthquakes: Whole crustal rupturing related to postglacial rebound. *Science* 274, 744–746.
- Axelsson C-L, Hansen L M, 1997.** Update of structural models at SFR nuclear waste repository, Forsmark, Sweden. SKB R-98-05, Svensk Kärnbränslehantering AB.
- Axelsson C-A, Ekstav A, Lindblad Påsse A, 2002.** SFR – Utvärdering av hydrogeologi. SKB R-02-14, Svensk Kärnbränslehantering AB.
- Balu L, Cosma C, 2005.** Estimation of 3D positions and orientations of reflectors based on an updated interpretation of Stage 1 reflection seismic data. Preliminary site description of the Forsmark area – version 1.2. SKB R-05-39, Svensk Kärnbränslehantering AB.
- Barton N, Lien R, Lunde J, 1974.** Engineering classification of rock masses for the design of tunnel support. *Rock Mech.*, Vol. 6, pp. 189-236.
- Barton N, 2002.** Some new Q-value correlations to assist in site characterisation and tunnel design. *Int. J. Rock Mech. & Min. Sci.*, Vol. 39, p. 185–216.
- Barton N, 2003.** KFM01A. Q-logging. SKB P-03-29, Svensk Kärnbränslehantering AB.
- Barton N, 2004.** Q-logging of surface exposure in Forsmark. SKB P-04-187, Svensk Kärnbränslehantering AB.
- Bein A, Arad A, 1992.** Formation of saline groundwaters in the Baltic region through freezing of seawater during glacial periods. *Journal of Hydrology*, 140, pp. 75-87.
- Berg C, Nilsson A-C, 2004.** Hydrochemical logging of KFM04A. Forsmark site investigation. SKB P-04-47.
- Berggren J, Kyläkorpi L, 2002.** Ekosystemen i Forsmarksområdet. Sammanställning av befintlig information, SKB R-02-08, Svensk Kärnbränslehantering AB.
- Bergkvist M, Ekström L, Eriksson K, Hammarlund E, Hollsten M, Lind A-L, Lundholm K, 2003.** Kallrigafjärden, NO Uppland. Områdets historia, nuläge samt framtida landskapsutveckling. SKB R-03-26. Svensk Kärnbränslehantering AB.

- Berglund B E, Digerfeldt G, Engelmark R, Gaillard M-J, Karlsson S, Miller U, Risberg J, 1996.** Palaeoecological events during the last 15,000 years, Regional syntheses of palaeoecological studies of lakes and mires in Europe – Sweden. In Berglund, B.E., Birks, H.J.B., Ralska-Jasiewiczowa, M. and Wright, H.E. (eds.): IGCP Project 158B 233-280.
- Berglund S, Selroos J-O, 2004.** Transport Properties Site Descriptive Model. Guidelines for evaluation and modelling. SKB R-03-09, Svensk Kärnbränslehantering AB.
- Berglund J, Petersson J, Wängnerud A, Danielsson P, 2004.** Boremap mapping of core drilled borehole KFM01B. Forsmark site investigation. SKB P-04-114, Svensk Kärnbränslehantering AB.
- Bergman S, Bergman T, Johansson R, Stephens M, Isaksson H, 1998.** Förstudie Östhammar. Delprojekt jordarter, bergarter och deformationszoner. Kompletterande arbeten 1998. Del 1: Fältkontroll av berggrunden inom Forsmarks- och Hargshamnssområdena. SKB R-98-57, Svensk Kärnbränslehantering AB.
- Bergman S, Sjöström H, 1994.** The Storsjön-Edsbyn Deformation Zone, central Sweden. Unpublished research report, Sveriges Geologiska Undersökning.
- Bergman S, Isaksson H, Johansson R, Lindén A, Persson Ch, Stephens M, 1996.** Förstudie Östhammar. Jordarter, bergarter och deformationszoner. SKB PR-D-96-016, Svensk Kärnbränslehantering AB (in Swedish).
- Bergman T, Isaksson H, Johansson R, Lindén A H, Lindroos H, Rudmark L, Stephens M, 1999.** Förstudie Tierp. Jordarter, bergarter och deformationszoner. SKB R-99-53, Svensk Kärnbränslehantering AB.
- Bergman T, Andersson J, Hermansson T, Zetterström E, Albrecht L, Stephens M B, Petersson J, Nordman C, 2004.** Bedrock mapping. Stage 2 (2003) – bedrock data from outcrops and the basal parts of trenches and shallow boreholes through the Quaternary cover. Forsmark site investigation. SKB P-04-91, Svensk Kärnbränslehantering AB.
- Bergström E, 2001.** Late Holocene distribution of lake sediment and peat in NE Uppland, Sweden. SKB R-01-12, Svensk Kärnbränslehantering AB.
- Beunk F F, Page L M, 2001.** Structural evolution of the accretional continental margin of the Paleoproterozoic Svecofennian orogen in southern Sweden. *Tectonophysics* 339.
- Bieniawski ZT, 1989.** Engineering rock mass classifications. John Wiley & Sons.
- Björck S, 1995.** A review of the history of the Baltic Sea 13-8 ka. *Quaternary International* 27, 19-40.
- Björck S, Kromer B, Johnsen S, Bennike O, Hammarlund D, Lemdahl G, Possnert G, Lander Rasmussen T, Wohlfarth B, Hammer C H, Spurk M, 1996.** Synchronized Terrestrial-atmospheric deglacial records around the North Atlantic. *Science* 274, 1155–1160.
- Björck J, 1999.** The Alleröd-younger Dryas pollen zone in an 800-years varve chronology from southeastern Sweden. *Geologiska Föreningens i Stockholm Förhandlingar* 121, 287–292.
- Björnbom S, 1979.** Clayey basal till in central and northern Sweden. A deposit from an old phase of the Würm glaciation. *SGU C 753*, Sveriges Geologiska Undersökning.
- Blomqvist P, Nilsson E, Brunberg A-K, 2002.** Habitat distribution, water chemistry, and biomass and production of pelagic and benthic microbiota in Lake Eckarfjärden, Forsmark. SKB R-02-41, Svensk Kärnbränslehantering AB.
- Boresjö Bronge L, Wester K, 2002.** Vegetation mapping with satellite data of the Forsmark and Tierp region. SKB R-02-06, Svensk Kärnbränslehantering AB.
- Borgiel M, 2004.** Sampling and analyses of surface sediment in lakes and shallow bays. Forsmark site investigation. SKB P-04-05, Svensk Kärnbränslehantering AB.
- Bratt P (ed.), 1998.** Forntid i ny dager – Arkeologi i Stockholmstrakten, Raster Förlag, Stockholm (in Swedish).
- Brunauer S, Emmett P H, Teller E, 1938.** Adsorption of gases in multimolecular layers. *J Amer Chem Soc* 60: 309-319.

- Brunberg A-K, Blomqvist P, 1999.** Characteristics and ontogeny of oligotrophic hardwater lakes in the Forsmark area, central Sweden. SKB R-99-68, Svensk Kärnbränslehantering AB.
- Brunberg A-K, Blomqvist P, 2000.** Post-glacial, land rise-induced formation and development of lakes in the Forsmark area, central Sweden. SKB-TR-00-02, Svensk Kärnbränslehantering AB.
- Brunberg A-K, Blomqvist P, 2003.** Ontogeny of lake ecosystems in the Forsmark area – chemical analyses of deep sediment cores. SKB R-03-28, Svensk Kärnbränslehantering AB.
- Brunberg A-K, Carlsson T, Blomqvist P, Brydsten L, Strömgren M, 2004.** Identification of catchments, lake-related drainage parameters and lake habitats. Forsmark site investigation. SKB P-04-25, Svensk Kärnbränslehantering AB.
- Brunberg L, 1995.** Clay-varve chronology and deglaciation during the Younger Dryas and Pre-boreal in the easternmost part of the Middle Swedish Ice Marginal Zone. Stockholm university, Quaternaria A2, 94 pp.
- Bruno J, Cera E, Grivé M, Rollin C, Ahonen L, Kaija J, Blomqvist R, El Aamrani F.Z, Casas I, de Pablo J, 1999.** Redox Processes in the Palmottu uranium deposit. Redox measurements and redox controls in the Palmottu system. Draft. Informe 64023. ENRESA, 76 p.
- Brydsten L, 1999.** Shore line displacement in Öregrundsgrepen. SKB TR-99-16, Svensk Kärnbränslehantering AB.
- Brydsten L, 2004.** A method for construction of digital elevation models for site investigation program at Forsmark and Simpevarp. SKB P-04-03, Svensk Kärnbränslehantering AB.
- Brydsten L, Strömgren, M, 2004.** Water depth soundings in shallow bays in Forsmark. SKB P-04-125, Svensk Kärnbränslehantering AB.
- Byegård J, Gustavsson E, Tullborg E-L, Selroos J-O, 2005.** Bedrock transport properties. Preliminary site description Forsmark area – version 1.2. SKB R-05-XX, Svensk Kärnbränslehantering AB.
- Bäckblom G, Stanfors R, 1989.** Interdisciplinary study of post-glacial faulting in the Lansjärv area, northern Sweden. SKB TR-89-31, Svensk Kärnbränslehantering AB.
- Canhem C D, Pace M L, Papaik M J, Primack A G B, 2004.** A spatially explicit watershed-scale analysis of dissolved organic carbon in Adirondack lakes. Ecological Application 14(3):839-854.
- Carlsson A, Olsson T, 1977.** Water leakage in the Forsmark tunnel, Uppland, Sweden. SGU C 734, Geological Survey of Sweden.
- Carlsson A, 1979.** Characteristic features of a superficial rock mass in southern central Sweden – Horizontal and subhorizontal fractures and filling material. Striae 11.
- Carlsson L, Carlsten S, Sigurdsson T, Winberg A, 1985.** Hydraulic modelling of the final repository for reactor waste (SFR). Compilation and conceptualization of available geological and hydrogeological data. Edition 1. SKB Progress Report SFR 85-06, Svensk Kärnbränslehantering AB.
- Carlsson A, Christiansson R, 1987.** Geology and tectonics at Forsmark, Sweden. SKB SFR-87-04, Svensk Kärnbränslehantering AB.
- Carlsson L, 2004.** Drill hole KFM02A: Extensometer measurement of the coefficient of thermal expansion of rock. Forsmark site investigation, SKB P-04-164, Svensk Kärnbränslehantering AB.
- Carlsten S, Petersson J, Stephens M, Mattsson H, Gustafsson J, 2004a.** Geological single-hole interpretation of KFM01A, KFM01B and HFM01–03 (DS1). Forsmark site investigation. SKB P-04-116, Svensk Kärnbränslehantering AB.
- Carlsten S, Petersson J, Stephens M, Mattsson H, Gustafsson J, 2004b.** Geological single-hole interpretation of KFM02A and HFM04–05 (DS2). Forsmark site investigation. SKB P-04-117, Svensk Kärnbränslehantering AB.
- Carlsten S, Petersson J, Stephens M, Thunehed H, Gustafsson J, 2004c.** Geological single-hole interpretation of KFM03B, KFM03A and HFM06–08 (DS3). Forsmark site investigation. SKB P-04-118, Svensk Kärnbränslehantering AB.

- Carlsten S, Petersson J, Stephens M, Mattsson H, Gustafsson J, 2004d.** Geological single-hole interpretation of KFM04A and HFM09-10 (DS4). Forsmark site investigation. SKB P-04-119, Svensk Kärnbränslehantering AB.
- Carlsten S, Petersson J, Stephens M, Thunehed H, Gustafsson J, 2004e.** Geological single-hole interpretation of HFM11-13 and HFM16-18. Forsmark site investigation. SKB P-04-120, Svensk Kärnbränslehantering AB.
- Carlsten S, Petersson J, Stephens M, Thunehed H, Gustafsson J, 2004f.** Geological single-hole interpretation of KFM05A, HFM14-15 and HFM19 (DS5). Forsmark site investigation. SKB P-04-296, Svensk Kärnbränslehantering AB.
- Cederlund G, Hammarström A, Wallin K, 2004.** Surveys of mammal populations in the areas adjacent to Forsmark and Oskarshamn. Results from 2003. SKB P-04-04. Svensk Kärnbränslehantering AB.
- Chapin F S, Matson P A, Mooney H A, 2002.** Principles of Terrestrial Ecosystem Ecology. Springer Verlag New York, Inc. ISBN 0-387-95439-2.
- Christiansson R, Hudson J A, 2003.** ISRM suggested methods for rock stress estimation – Part 4: Quality control of rock stress estimation. I.J.R.M. and Min. Sci., vol 40, p 1021-25.
- Clark D A, Brown S, Kicklighter D W, 2001.** Measuring net primary production in forests: concepts and field methods. Ecological applications 11(2):356-370.
- Claesson L-Å, Nilsson G, 2004a.** Drilling of the telescopic borehole KFM01A at drillsite DS1. Forsmark site investigation. SKB P-03-32, Svensk Kärnbränslehantering AB.
- Claesson L-Å, Nilsson G, 2004b.** Drilling of borehole KFM01B at drilling site DS1. Forsmark site investigation. SKB P-04-302, Svensk Kärnbränslehantering AB.
- Claesson L-Å, Nilsson G, 2004c.** Drilling of a flushing water well, HFM01, and two groundwater monitoring wells, HFM02 and HFM03 at drillsite DS1. Forsmark site investigation. SKB P-03-30, Svensk Kärnbränslehantering AB.
- Claesson L-Å, Nilsson G, 2004d.** Drilling of the telescopic borehole KFM02A at drillsite DS2. Forsmark site investigation. SKB P-03-52, Svensk Kärnbränslehantering AB.
- Claesson L-Å, Nilsson G, 2004e.** Drilling of a flushing water well, HFM05, and a groundwater monitoring well, HFM04 at drillsite DS2. Forsmark site investigation. SKB P-03-51, Svensk Kärnbränslehantering AB.
- Claesson L-Å, Nilsson G, 2004f.** Drilling of the telescopic borehole KFM03A and the core drilled borehole KFM03B at drilling site DS3. Forsmark site investigation. SKB P-03-59, Svensk Kärnbränslehantering AB.
- Claesson L-Å, Nilsson G, 2004g.** Drilling of a flushing water well, HFM06, and two groundwater monitoring wells, HFM07 and HFM08 at drillsite DS3. Forsmark site investigation. SKB P-03-58, Svensk Kärnbränslehantering AB.
- Claesson L-Å, Nilsson G, 2004h.** Drilling of a flushing water well, HFM10, a groundwater monitoring well in solid bedrock, HFM09 and a groundwater monitoring well in soil, SFM0057, at drilling site DS4. Forsmark site investigation. SKB P-04-76, Svensk Kärnbränslehantering AB.
- Claesson L-Å, Nilsson G, 2004i.** Drilling of a flushing water well, HFM13, two groundwater monitoring wells in solid bedrock, HFM14-15 and one groundwater monitoring well in soil, SFM0058, at and close to drilling site DS5. Forsmark site investigation. SKB P-04-85, Svensk Kärnbränslehantering AB.
- Claesson L-Å, Nilsson G, 2004j.** Drilling of five percussion holes, HFM11-12 and HFM17-19, on different lineaments. Forsmark site investigation. SKB P-04-106, Svensk Kärnbränslehantering AB.
- Claesson L-Å, Nilsson G, 2004k.** Drilling of a monitoring well, HFM16, at drilling site DS6. Forsmark site investigation. SKB P-04-94, Svensk Kärnbränslehantering AB.
- Claesson L-Å, Nilsson G, 2004l.** Drilling of the telescopic borehole KFM04A and the percussion drilled borehole KFM04B at drilling site DS4. Forsmark site investigation. SKB P-03-82, Svensk Kärnbränslehantering AB.

- Claesson L-Å, Nilsson G, 2004m.** Drilling of the telescopic borehole KFM05A at drilling site DS5. Forsmark site investigation. SKB P-04-222, Svensk Kärnbränslehantering AB.
- Claesson L-Å, Nilsson G, 2004l.** P-04-67.
- Claesson L-Å, Nilsson G, 2004m.** P-04-152.
- Cobbold P R, Quinquis H, 1980.** Development of sheath folds in shear zones. *Journal of Structural Geology* 2.
- Cosma C, Balu L, Enescu N, 2003.** Estimation of 3D positions and orientations of reflectors identified in the reflection seismic survey at the Forsmark area. SKB R-03-22, Svensk Kärnbränslehantering AB.
- Cousins S A O, 2001.** Plant species diversity patterns in a Swedish rural landscape. Effects of the past and consequences for the future. Doctoral thesis, No. 17. Department of Physical Geography and Quaternary Geology, Stockholm University.
- Dagan G, 1981.** Analysis of flow trough heterogeneous random aquifers by the method of embedding matrix, 1, Steady flow, *Water resources res.*, 17 (1), 107–121.
- Darcel C, Davy P, Bour O, de Dreuzy J-R, 2004.** Alternative DFN model based on initial site investigations at Simpevarp. SKB R-04-76, Svensk Kärnbränslehantering AB.
- Debon, Le Fort, 1983.** A chemical-mineralogical classification of common plutonic rocks and associations. *Transactions of the Royal Society of Edinburgh, Earth Sciences* 73.
- Dershowitz W, Winberg A, Hermanson J, Byegård J, Tullborg E-L, Andersson P, Mazurek M, 2003.** Äspö Task Force on modelling of groundwater flow and transport of solutes. Task 6c. A semi-synthetic model of block scale conductive structures at the Äspö HRL. Äspö Hard Rock Laboratory, International Progress Report IPR-03-13, Svensk Kärnbränslehantering AB.
- Deutsch W J, Jenne E A, Krupka K M, 1982.** Solubility equilibria in basalt aquifers: The Columbia Plateau, Eastern Washington, U.S.A. *Chemical Geology*, 36, 15-34.
- Dinges C, 2004.** Drill hole KFM04A, Thermal properties: Anisotropic thermal conductivity and thermal diffusivity determined using the Hot Disk thermal constants analyser (the TPS technique). Forsmark site investigation, Svensk Kärnbränslehantering, Report in progress.
- Eklund S, 2004.** Nyckelbiotoper och högre naturvärden inom prioriterade områden i Uppsala och Södermanlands län. SKB P-04-33. Svensk Kärnbränslehantering AB.
- Ekman L, 1996a.** Data sammanställning från kärnborrhål KFO01 vid Forsmark. SKB PR-D-96-025. Svensk Kärnbränslehantering AB.
- Ekman M, 1996b.** A consistent map of the postglacial uplift of Fennoscandia. *Terra-Nova* 8/2, 158–165.
- Elhammer et al, 2005.** Forsmark site investigation. Detailed marine geological mapping (in prep.) SKB P-03-101, Svensk Kärnbränslehantering AB.
- Eriksson S, Sellei C, Wallström K, 1977.** The structure of the plankton community of the Öresundsgrepen (southwest Bothnian Sea). *Helgoländer wiss. Meeresunters.* Vol. 30: p. 582-597.
- Eriksson L, 2004.** Miljörapport 2003. Utsläpp av radioaktiva ämnen. Forsmarks Kraftgrupp. Rep. Nr. FQ-2004-78.
- Fairbanks R, 1989.** A 17,000-year glacio-eustatic sea level record: influence of glacial melting rates on the Younger Dryas event and deep-ocean circulation. *Nature* 342, 637–642.
- Follin S, Stigsson M, Svensson U, 2005.** Regional hydrogeological simulations for Forsmark – Numerical modelling using DarcyTools. Preliminary site description Forsmark area – version 1.2. SKB R-05-60, Svensk Kärnbränslehantering AB.
- Follin S, Stigsson M, Svensson U, 2005b.** Variable-density groundwater flow simulations and particle tracking – Numerical modelling using DarcyTools. Preliminary site description Simpevarp subarea – version 1.2. SKB R-05-11, Svensk Kärnbränslehantering AB.

- Fontes J-Ch, Louvat D, Michelot J-L, 1989.** Some constraints on geochemistry and environmental isotopes for the study of low fracture flows in crystalline rocks – The Stripa case. In: International Atomic Energy Agency (Eds.) *Isotopes techniques in the study of the Hydrology of Fractured and Fissured Rocks*. IAEA, Vienna, Austria.
- Forsman I, Zetterlund M, Rhén I, 2004.** Correlation of Posiva Flow Log anomalies to core mapped features in Forsmark (KFM01A to KFM05A). SKB R-04-77, Svensk Kärnbränslehantering AB.
- Franzén I, 2002.** Bolundsfjärden – en sjö under bildning. En naturvärdes- och skadebedömning. *Scripta Limnologica Upsaliensia* 2002 B:2.
- Frape S K, Byrant G, Blomqvist R, Ruskeeniemi T, 1996.** Evidence from stable chlorine isotopes for multiple sources of chloride in groundwaters from crystalline shield environments. In: *Isotopes in Water Resources Management, 1966*. IAEA-SM-336/24, Vol. 1, 19–30.
- Fredén C (ed.), 2002.** Berg och jord. Sveriges nationalatlas. Tredje upplagan.
- Fredriksson D, 2004.** Forsmark site investigation – Peatland investigation Forsmark. SKB P-04-127.
- Fredriksson A, Olofsson I, 2005.** Theoretical modelling – Forsmark Rock Mechanics site descriptive model – Version 1.2, R-04-YY in preparation, Svensk Kärnbränslehantering AB.
- Frietsch R, 1975.** Brief outline of the metallic mineral resources of Sweden. SGU C 718, Sveriges Geologiska Undersökning.
- Geir J E, Axelsson C-E, Hässler L, Benabderrahmane A, 1992.** Discrete fracture modelling of the Finnsjön rock mass: Phase 2. SKB TR-92-07, Svensk Kärnbränslehantering AB.
- Gessner M O, Schieferstein B, Müller U, Barkmann S, Lenfers U A, 1996.** A partial budget of primary organic carbon flows in the littoral zone of a hardwater lake. *Aquatic Botany* 55: 93–106.
- Glynn P D, Voss C I, 1997.** Geochemical characterization of Simpevarp ground waters near Äspö Hard Rock Laboratory. SITE-94 SKI Report 96:29, Statens Kärnkraftinspektion.
- Gower S T, Kucharik C J, Norman J M, 1999.** Direct and indirect estimations of Leaf Area Index, fAPAR, and Net Primary Production of terrestrial ecosystems. *Remote Sensing of Environment* 70:29-51.
- Green M, 2003.** Fågelundersökningar inom SKB:s platsundersökningar 2002 – Forsmark. SKB P-03-10, Svensk Kärnbränslehantering AB.
- Green M, 2004.** Bird monitoring in Forsmark 2002-2003. Forsmark site investigation. SKB P-04-30. Svensk Kärnbränslehantering AB.
- Gregersen S, 1992.** Crustal Stress Regime in Fennoscandia from Focal Mechanisms, *J. Geoph. Research*, Vol. 97, No. B8, 11, p. 821–827.
- Grenthe I, Stumm W, Laaksoharju M, Nilsson A C, Wikberg P, 1992.** Redox potentials and redox reactions in deep groundwater systems. *Chem. Geol.*, 98, 131–150.
- Grimaud D, Beaucaire C, Michard G, 1990.** Modeling of the evolution of ground waters in a granite system at low temperature: the Stripa ground waters, Sweden. *Applied Geochemistry*, 5, 515–525.
- Gurban I, Laaksoharju M, 2002.** Drilling Impact Study (DIS); Evaluation of the influences of drilling, in special on the changes on groundwater parameters. SKB Report PIR-03-02, Svensk Kärnbränslehantering AB.
- Gustafsson C, Nilsson P, 2003.** Forsmark site investigation. Geophysical, radar and BIPS logging in boreholes HFM01, HFM02, HFM03 and the percussion drilled part of KFM01A. SKB P-03-39, Svensk Kärnbränslehantering AB.
- Gustafsson B, 2004a.** Millennial changes of the Baltic Sea salinity – studies of the salinity to climate change. SKB TR-04-12. Svensk Kärnbränslehantering AB.
- Gustafsson B, 2004b.** Sensitivity of the Baltic Sea salinity to large perturbations in climate. *Climate research*, 27: 237-251.

- Gustafsson J, Gustafsson C, 2004a.** RAMAC and BIPS logging in borehole KFM01B and RAMAC directional re-logging in borehole KFM01A. Forsmark site investigation. SKB P-04-79, Svensk Kärnbränslehantering AB.
- Gustafsson J, Gustafsson C, 2004b.** RAMAC and BIPS logging in borehole KFM02A. Forsmark site investigation. SKB P-04-40, Svensk Kärnbränslehantering AB.
- Gustafsson J, Gustafsson C, 2004c.** RAMAC and BIPS logging in borehole KFM03A and KFM03B. Forsmark site investigation. SKB P-04-41, Svensk Kärnbränslehantering AB.
- Gustafsson J, Gustafsson C, 2004d.** RAMAC and BIPS logging in borehole KFM04A, KFM04B, HFM09 and HFM10. Forsmark site investigation. SKB P-04-67, Svensk Kärnbränslehantering AB.
- Gustafsson J, Gustafsson C, 2004e.** RAMAC and BIPS logging in borehole HFM13, HFM14 and HFM15. Forsmark site investigation. SKB P-04-68, Svensk Kärnbränslehantering AB.
- Gustafsson J, Gustafsson C, 2004f.** RAMAC and BIPS logging in borehole HFM11 and HFM12. Forsmark site investigation. SKB P-04-39, Svensk Kärnbränslehantering AB.
- Gustafsson J, Gustafsson C, 2004g.** RAMAC and BIPS logging in borehole KFM06A, HFM16, HFM17, HFM18 and HFM19. Forsmark site investigation. SKB P-04-69, Svensk Kärnbränslehantering AB.
- Gustafsson J, Gustafsson C, 2004h.** RAMAC and BIPS logging in borehole KFM05A. Forsmark site investigation. SKB P-04-152, Svensk Kärnbränslehantering AB.
- Gylling B, Walker D, Hartley L, 1999.** Site-scale groundwater flow modelling of Beberg. SKB TR-99-18, Svensk Kärnbränslehantering AB.
- Gölke M, Coblenz D, 1996.** Origins of the European regional stress field, *Tectonophysics*, No. 266, p. 11–24.
- Haimson B C, Cornet F H, 2003.** ISRM Suggested Methods for rock stress estimations – Part 3: hydraulic fracturing (HF) and/or hydraulic testing of pre-existing fractures (HTPF). *Int. J. Rock. Mech. & Min. Sci.* 40, No 7-8, pp 1011-1020.
- Hakala M, 1999.** Numerical study on core damage and interpretation of in-situ state of stress, Report 99-25, POSIVA, Finland.
- Hakala M, Hudson J A, Christiansson R, 2003.** Quality control of overcoring stress measurement data. *Int. J. Rock. Mech. Min. Sci.*, 40, No 7-8, pp 1141-1159.
- Hakami E, Hakami H, Cosgrove J, 2002.** Strategy for a Rock mechanics Site Descriptive Model. Development and testing of an approach to modelling the state of stress. SKB R-02-03, Svensk Kärnbränslehantering AB.
- Hansen L, 1989.** Bedrock of the Forsmark area. Technical Report, Swedish State Power Board, Stockholm.
- Hartley L J, Holton D, 2003.** ConnectFlow (Release 2.0) Technical Summary Document. SERCO/ERRA-C/TSD02V1.
- Hartley L J, Hoch A R, Cliffe K A C, Jackson C P, Holton D, 2003a.** NAMMU (Release 7.2) Technical Summary Document. SERCO/ERRA-NM/TSD02V1.
- Hartley L J, Holton D, Hoch A R, 2003b.** NAPSAC (Release 4.4) Technical Summary Document. SERCO/ERRA-N/TSD02V1.
- Hartley L, Cox I, Hunter F, Jackson P, Joyce S, Swift B, Gylling B, Marsic N, 2005.** Regional hydrogeological simulations for Forsmark – Numerical modelling using CONNECTFLOW. Preliminary site description of the Forsmark area. SKB R-05-32, Svensk Kärnbränslehantering AB.
- Hartley L, Hoch A, Hunter F, Marsic N, 2005b.** Regional hydrogeological simulations – Numerical modelling using ConnectFlow. Preliminary site description Simpevarp subarea – version 1.2. SKB R-05-12, Svensk Kärnbränslehantering AB.
- Hedenström A, 2001.** Shore displacement in south eastern Uppland during the early Litorina Sea stage. *Quaternaria Ser A*. No 10, paper IV. 48 pp.

- Hedenström A, Risberg J, 2003.** Shore displacement in northern Uppland during the last 6500 calendar years. SKB TR-03-17, Svensk Kärnbränslehantering AB.
- Hedenström A, 2004.** Forsmark site investigation. Investigation of marine and lacustrine sediments in lakes. Stratigraphical and analytical data. SKB P-04-86. Svensk Kärnbränslehantering AB.
- Hermanson J, Hansen L, Olofsson J, Sävås J, Vestgård J, 2003a.** Detailed fracture mapping at the KFM02 and KFM03 drill sites. Forsmark. SKB P-03-12, Svensk Kärnbränslehantering AB.
- Hermanson J, Hansen L, Vestgård J, Leiner P, 2003b.** Detailed fracture mapping of the outcrops Klubbudden, AFM001098 and drill site 4, AFM001097. Forsmark site investigation. SKB P-03-115, Svensk Kärnbränslehantering AB.
- Hermanson J, Hansen L, Olofsson J, Sävås J, Vestgård J, 2004.** Detailed fracture mapping of excavated rock outcrop at drilling site 5. Forsmark site investigation. SKB P-04-90, Svensk Kärnbränslehantering AB.
- Hoch A R, Hartley L J, 2003.** NAMMU (Release 7.2) Verification Document. SERCO/ERRA-NM/VD02V1.
- Hoch A R, Hartley L J, Holton D, 2003.** NAPSAC (Release 4.3) Verification Document. SERCO/ERRA-NM/VD02V1.
- Hoek E, Brown ET, 1997.** Practical estimates of rock mass strength. *International Journal of Rock Mechanics and Mining Sciences*, Vol. 34, No. 8, pp. 1165–1186.
- Hoek E, Carranza-Torres C, Corkum B, 2002.** The Hoek-Brown Failure Criterion – 2002 Edition. 5th North American Rock Mechanics Symposium and 17th Tunneling Association of Canada Conference: NARMS-TAC, p.267-271.
- Holmén J G, Stigsson M, 2001.** Modelling of future hydrogeological conditions at SFR. SKB R-01-02, Svensk Kärnbränslehantering AB.
- Horai K, 1971.** Thermal conductivity of rock-forming minerals. *J. Geophys. Res.* 76, p. 1278–1308.
- Huononen R, Borgiel M, 2005.** Forsmark site investigation: Sampling of phyto- and zooplankton in sea water. Abundances and carbon biomasses. SKB P-05-72, Svensk Kärnbränslehantering AB.
- Hättestrand C, Stroeven A, 2002.** A preglacial landscape in the centre of Fennoscandian glaciation: geomorphological evidence of minimal Quaternary glacial erosion. *Geomorphology*, 44, 127–143.
- Högdahl K, 2000.** Late-orogenic, ductile shear zones and protolith ages in the Svecofennian Domain, central Sweden. *Meddelande från Stockholms Universitets Institution för Geologi och Geokemi* 309.
- Ingmar T, Moreborg K, 1976.** The leaching and original content of calcium carbonate in till in northern Uppland, Sweden. *Geologiska Föreningen i Stockholm Förhandlingar*, 98, 120–132.
- Isaksson H, 2003.** Forsmark site investigation. Interpretation of topographic lineaments 2002. SKB P-03-40, Svensk Kärnbränslehantering AB.
- Isaksson H, Keisu M, 2005.** Interpretation of airborne geophysics and integration with topography. Stage 2 (2002-2004). Forsmark site investigation. SKB P-04-282, Svensk Kärnbränslehantering AB.
- Isaksson H, Mattson H, Thunehed H, Keisu M, 2004a.** Interpretation of petrophysical surface data. Stage 1 (2002). SKB P-03-102, Svensk Kärnbränslehantering AB.
- Isaksson H, Thunehed H, Mattson H, Keisu M, 2004b.** Interpretation of airborne geophysics and integration with topography. Stage 1 (2002). SKB P-04-29, Svensk Kärnbränslehantering AB.
- Isaksson H, Thunehed H, Keisu M, 2004c.** Interpretation of airborne geophysics and integration with topography. Forsmark site investigation. SKB P-04-29, Svensk Kärnbränslehantering AB.
- Jansson U, Berg J, Björklund A, 2004.** A study on landscape and the historical geography of two areas - Oskarshamn and Forsmark. SKB R-04-67. Svensk Kärnbränslehantering AB.
- Jerling L, Isæus M, Lanneck J, Lindborg T, Schüldt R, 2001.** The terrestrial biosphere in the SFR region. SKB R-01-09, Svensk Kärnbränslehantering AB.

- Johansson H, Byegård J, Skarnemark G, Skålberg M, 1997.** Matrix diffusion of some alkali and alkaline earth metals in granitic rock. *Mat. Res. Soc. Symp. Proc.* 465: 871–878.
- Johansson P-O, 2003.** Forsmark site investigation. Drilling and sampling in soil. Installation of groundwater monitoring wells and surface water level gauges. SKB P-03-64, Svensk Kärnbränslehantering AB.
- Johansson R, 2005.** A comparison of two independent interpretations of lineaments from geophysical and topographical data at the Forsmark site. SKB R-05-23, Svensk Kärnbränslehantering AB.
- Johansson P-O, Werner K, Bosson E, Berglund S, Juston J, 2005.** Description of climate, surface hydrology, and near-surface hydrogeology. Forsmark 1.2. SKB R-05-06. Svensk Kärnbränslehantering AB
- Jonsell B, Jonsell L, 1995.** Floran i Hållnäs socken (Vascular plants in the parish of Hållnäs, N. Uppland, Sweden). *Svensk Botanisk Tidskrift* 89:257–312.
- Juhlin C, Bergman B, Palm H, 2002.** Reflection seismic studies in the Forsmark area – stage 1. SKB R-02-43, Svensk Kärnbränslehantering AB.
- Juhlin C, Bergman B, 2004.** Reflection seismics in the Forsmark area. Updated interpretation of Stage 1 (previous report R-02-43). Updated estimate of bedrock topography (previous report P-04-99). SKB P-04-158, Svensk Kärnbränslehantering AB.
- Jönsson S, Ludvigson J-E, Svensson T, 2004.** Forsmark site investigation. Hydraulic interference tests. Boreholes HFM11 and HFM12. SKB P-04-200, Svensk Kärnbränslehantering AB.
- Kautsky H, Plantman P, Borgiel M, 1999.** Quantitative distribution of aquatic plant and animal communities in the Forsmark-area. SKB R-99-69, Svensk Kärnbränslehantering AB.
- Keisu M, Isaksson H, 2004.** Acquisition of geological information from Forsmarkverket. Information from the Vattenfall archive, Räcksta. Forsmark site investigation. SKB P-04-81, Svensk Kärnbränslehantering AB.
- Klee G, Rummel F, 2004.** Rock stress measurements with hydraulic fracturing and hydraulic testing of pre-existing fractures in boreholes nos. KFM01A, KFM01B, KFM02A and KFM04A, SKB P-04-YY, (in preparation) , Svensk Kärnbränslehantering AB.
- Knutsson G, Morfeldt C-O, 2003.** Grundvatten – teori & tillämpning, Svensk Byggtjänst, Stockholm.
- Koistinen T, Stephens M B, Bogatchev V, Nordgulen O, Wennerström M, Korhonen J, 2001.** Geological map of the Fennoscandian Shield, scale 1:2 000 000. Geological Surveys of Finland, Norway and Sweden and the North-West Department of Natural Resources of Russia.
- Korhonen K, Paananen M, Paulamäki S, 2004.** Interpretation of lineaments from airborne geophysical and topographic data. An alternative model within version 1.2 of the Forsmark modelling project. SKB P-04-241, Svensk Kärnbränslehantering AB.
- Kristiansson J, 1986.** The ice recession in the south-eastern part of Sweden. University of Stockholm. Department of Quaternary Research 7, 132 pp.
- Kufel L and Kufel I, 2002.** Chara beds acting as nutrient sinks in shallow lakes- a review. *Aquatic Botany* 72(3-4): 249–260.
- Kuivamäki A, Vuorela P and Paananen M, 1998.** Indications of postglacial and recent bedrock movements in Finland and Russian Karelia. Geological Survey of Finland, Report YST-99.
- Kyläkorpi L, 2005.** Tillgänglighetskartan. SKB report, in press. Svensk Kärnbränslehantering AB.
- Källgården J, Ludvigson J-E, Hjerne C, 2004.** Forsmark site investigation. Single-hole injection tests in borehole KFM03A. SKB P-04-194, Svensk Kärnbränslehantering AB.
- Laaksoharju M, Smellie J, Nilsson A-C, Skårman C, 1995a.** Groundwater sampling and chemical characterisation of the Laxemar deep borehole KLX02. SKB TR 95-05, Svensk Kärnbränslehantering AB.

- Laaksoharju M, Degueldre C, Skårman C, 1995b.** Studies of colloids and their importance for repository performance assessment SKB TR-95-24, Svensk Kärnbränslehantering AB.
- Laaksoharju M, Wallin B (eds.), 1997.** Evolution of the groundwater chemistry at the Äspö Hard Rock Laboratory. Proceedings of the second Äspö International Geochemistry Workshop, June 6–7, 1995. SKB International Co-operation Report ISRN SKB-ICR-91/04-SE. ISSN 1104-3210 Stockholm, Sweden.
- Laaksoharju M, Skårman C, Skårman E, 1999.** Multivariate Mixing and Mass-balance (M3) calculations, a new tool for decoding hydrogeochemical information. Applied Geochemistry Vol. 14, #7, 1999, Elsevier Science Ltd., pp. 861–871.
- Laaksoharju M (ed.), Gimeno M, Smellie J, Tullborg E-L, Gurban I, Auqué L, Gómez J, 2004a.** Hydrogeochemical evaluation of the Forsmark site, model version 1.1. SKB R-04-05, Svensk Kärnbränslehantering AB.
- Laaksoharju M (editor), Smellie J, Gimeno M, Auqué L, Gomez , Tullborg E-L and Gurban I, 2004b.** Hydrochemical evaluation of the Simpevarp area, model version 1.1. SKB R 04-16, Svensk Kärnbränslehantering AB.
- Lagerbäck, 1979.** Neotectonic structures in northern Sweden. Geologiska Föreningens i Stockholm Förhandlingar 100, 263–269.
- Lagerbäck R, Robertsson A-M, 1988.** Kettle holes – stratigraphical archives for Weichselian geology and palaeoenvironment in northernmost Sweden. Boreas, vol 17, 439–468.
- Lagerbäck, 1990.** Late Quaternary faulting and paleoseismicity in northern Fennoscandia, with particular reference to the Lansjärv area, northern Sweden. Geologiska Föreningens i Stockholm Förhandlingar 112, 333–354.
- Lagerbäck R, Sundh M, 2003.** Forsmark site investigation. Searching for evidence of late- or post-glacial faulting in the Forsmark region. Results from 2002. SKB P-03-76, Svensk Kärnbränslehantering AB.
- Lagerbäck R, Sundh M, Johansson H, 2004.** Searching for evidence of late- or post-glacial faulting in the Forsmark region. SKB P-04-123, Svensk Kärnbränslehantering AB.
- Lanaro F, Röshoff K, Christiansson, R, 2004.** Effect of scale on rock mass empirical characterisation, Proc. EURO-Conf. on Rock Phys. Geomech., (eds. Dresen G, Shapiro S, Stephansson O), GFZ: Potsdam, Germany, P51.
- Lanaro F, 2005.** Rock mechanics characterisation of the rock mass – Empirical approach. Preliminary site description Forsmark area – version 1.2. SKB R-05-XX, Svensk Kärnbränslehantering AB.
- Lanaro F, 2005a.** Rock Mechanics characterisation of borehole KFM01A, Forsmark Site Investigations, P-05-112, Svensk Kärnbränslehantering AB.
- Lanaro F, 2005b.** Rock Mechanics characterisation of borehole KFM02A, Forsmark Site Investigations, P-05-113, Svensk Kärnbränslehantering AB.
- Lanaro F, 2005c.** Rock Mechanics characterisation of borehole KFM03A, Forsmark Site Investigations, P-05-114, Svensk Kärnbränslehantering AB.
- Lanaro F, 2005d.** Rock Mechanics characterisation of borehole KFM04A, Forsmark Site Investigations, P-05-115, Svensk Kärnbränslehantering AB.
- Lanaro F, Fredriksson A, 2005.** Forsmark Site Investigation v.1.2: Summary of the primary data, P-04-GG, Svensk Kärnbränslehantering AB.
- La Pointe P R, Cladouhos T, Follin S, 1999.** Calculation of displacement on fractures intersecting canister induced by earthquakes: Aberg, Beberg and Ceberg examples. SKB TR-99-03, Svensk Kärnbränslehantering AB.
- La Pointe P R, Olofsson I, Hermanson J, 2005.** Statistical model of fractures and deformation zones for Forsmark. Preliminary site description Forsmark area – version 1.2. SKB R-05-26, Svensk Kärnbränslehantering AB.

- Larsson W, 1973.** Forsmark kraftstation, aggregat 1 och 2, avloppstunneln: Berggeologiska förhållanden efter tunnellen. Technical Report, Swedish State Power Board, Stockholm.
- Le Bas M J, Le Maitre R W, Woolley A R, 1986.** A chemical classification of volcanic rocks based on the total alkali–silica diagram. *Journal of Petrology*, 27.
- Lidmar-Bergström K, 1994.** Morphology of the bedrock surface. In C. Fredén (ed.), *Geology. National Atlas of Sweden*.
- Lidmar-Bergström K, Olsson S, Olvmo M, 1997.** Paleosurfaces and associated saprolites in southern Sweden. *Geological Society* 120, 95–124.
- Liedberg L, 2004.** Drill hole KFM03A: Extensometer measurement of the coefficient of thermal expansion of rock. Forsmark site investigation, SKB P-04-165, Svensk Kärnbränslehantering AB.
- Lindahl G, Wallström K, 1980.** Växtplankton i Öregrundsgrepen, SV Bottenhavet. Meddelande från Växtbiologiska Institutionen, Uppsala Universitet, 1980:8 (in Swedish).
- Lindborg T, Schüldt R, 1998.** The biosphere at Aberg, Beberg and Ceberg – a description based on literature concerning climate, physical geography, ecology, land use and environment. SKB TR-98-20, Svensk Kärnbränslehantering AB.
- Lindborg T (ed.), 2005.** Description of the surface systems, Forsmark area – version 1.2. SKB R-05-03. Svensk Kärnbränslehantering AB.
- Lindfors U, Perman F, Sjöberg J, 2004.** Evaluation of the overcoring results from borehole KFM01B, SKB P-04-301 (in press), Svensk Kärnbränslehantering AB.
- Lindroos H, Isaksson H, Thunehed H, 2004.** The potential for ore and industrial minerals in the Forsmark area. SKB R-04-18, Svensk Kärnbränslehantering AB.
- Lohm U, Persson T, 1979.** Levande Jord. Aktuell biologi 3. Esselte studium.
- Ludvigson J-E, Hansson K, Rouhiainen P, 2001.** Methodology study of Posiva difference flow meter in borehole KLX02 at Laxemar. SKB R-01-52, Svensk Kärnbränslehantering AB.
- Ludvigson J-E, 2002.** Brunnsinventering i Forsmark. SKB R-02-17, Svensk Kärnbränslehantering AB.
- Ludvigson J-E, Jönsson S, 2003.** Forsmark site investigation. Hydraulic interference tests. Boreholes HFM01, HFM02 and HFM03. SKB P-03-35, Svensk Kärnbränslehantering AB.
- Ludvigson J-E, Jönsson S, Levén J, 2004a.** Forsmark site investigation. Hydraulic evaluation of pumping activities prior to hydro-geochemical sampling in borehole KFM03A – Comparison with results from difference flow logging. SKB P-04-96, Svensk Kärnbränslehantering AB.
- Ludvigson J-E, Levén J, 2005.** Comparison of measured EC in selected fractures in boreholes KFM02A, KFM03A and KFM04A from difference flow logging and hydro-geochemical characterization - Analysis of observed discrepancies in KFM03A. Forsmark site investigation, P-05-21, Svensk Kärnbränslehantering AB.
- Lundin L, Lode E, Stendahl J, Melkerud P-A, Björkvald L, Thorstensson A, 2004.** Soils and site types in the Forsmarks area. SKB R-04-08. Svensk Kärnbränslehantering AB.
- Lundqvist J, 1985.** Deep-weathering in Sweden. *Fennia* 163, 287–292.
- Lundqvist J, 1992.** Glacial stratigraphy in Sweden. Geological Survey of Finland Special paper 15. 43-59.
- Lundqvist J, Wohlfarth B, 2001.** Timing and east-west correlation of south Swedish ice marginal lines during the Late Weichselian. *Quaternary Science Reviews* 20, 1127–1148.
- Löfgren A, Lindborg T, 2003.** A descriptive ecosystem model – a strategy for model development during site investigations. SKB R-03-06, Svensk Kärnbränslehantering AB.
- Löfgren M, Neretnieks I, 2005.** Forsmark site investigation. Formation factor logging in-situ and in the laboratory by electrical methods in KFM01A and KFM02A. Measurements and evaluation of methodology. SKB P-05-29, Svensk Kärnbränslehantering AB.

- Löfman J, 1999.** Site scale groundwater flow in Olkiluoto. Posiva 99-03, Posiva OY, Helsinki.
- Majdi H, 2001.** Changes in fine root production and longevity in relation to water and nutrient availability in a Norway spruce forest stand in northern Sweden. *Tree Physiology* 21:1057–1061.
- Martin CD, Chandler, NA, 1994.** The Progressive Fracture of Lac du Bonnet Granite, *Int. J. Rock Mech. & Min. Sci.*, Vol. 31, p. 643–659.
- Martin CD, Read RS, 1996.** AECL's Mine-by Experiment: A tests tunnel in brittle rock, *Proc. 2nd North American Rock Mech. Symp.*, Montreal (Eds. Aubertin M, Hassani F and Mitri H), Balkema: Rotterdam, Vol. 1, pp. 13–24.
- Mas Ivars D, Hakami H, 2005.** Effect of a sub-horizontal fracture zone and rock mass heterogeneity on the stress field in Forsmark Area – A numerical study using 3DEC, SKB R-05-59, Svensk Kärnbränslehantering AB.
- Mattsson L, Stridberg E, 1980.** Skogens roll i svensk markanvändning. Umeå, Department of Forest Economics, Swedish Institute of Agriculture Sciences.
- Mattsson H, Isaksson H, Thunehed H, 2003.** Forsmark site investigation. Petrophysical rock sampling, measurements of petrophysical rock parameters and in-situ gamma-ray spectrometry measurements on outcrops carried out 2002. SKB P-03-26, Svensk Kärnbränslehantering AB.
- Mattsson H, Keisu M, 2004.** Interpretation of borehole geophysical measurements in KFM04A, KFM06A (0-100m), HFM10, HFM11, HFM12, HFM13, HFM16, HFM17 and HFM18. Forsmark site investigation. SKB P-04-143, Svensk Kärnbränslehantering AB.
- Mattsson H, Thunehed H, Isaksson H, Kübler L, 2004a.** Interpretation of petrophysical data from the cored boreholes KFM01A, KFM02A, KFM03A and KFM03B. Forsmark site investigation. SKB P-04-107, Svensk Kärnbränslehantering AB.
- Mattsson H, Thunehed H, Keisu M, 2004b.** Interpretation of borehole geophysical measurements in KFM01A, KFM01B, HFM01, HFM02 and HFM03. Forsmark site investigation. SKB P-04-80, Svensk Kärnbränslehantering AB.
- McClay K, 1989.** The Mapping of Geological Structures. Geological Society of London Handbook, Open University Press, Milton Keynes.
- Meulemanns J T, 1988.** Seasonal changes in biomass and production of periphyton growing upon reed in Lake Maarsseveen I. *Arch. Hydrobiol.* 112(1):21–42.
- Middlemost E A K, 1994.** Naming materials in the magma/igneous rock system. *Earth-Science Reviews* 37.
- Miliander S, Punakivi M, Kyläkorpi L, Rydgren B, 2004.** Forsmark site description: Human population and human activities. SKB R-04-10, Svensk Kärnbränslehantering AB.
- Mo K, Smith S, 1988.** Mjukbottenfaunan i Öregrundsgrepen 1978–1986. Naturvårdsverket Rapport 3467. 43 p. (in Swedish).
- Morén L, Pässe T, 2001.** Climate and shoreline in Sweden during Weichsel and the next 150,000 years. SKB TR-01-19. Svensk Kärnbränslehantering AB.
- Moye D G, 1967.** Diamond drilling for foundation exploration. *Civil. Eng. Trans., Inst. Eng. Australia*, p. 95–100.
- Muir Wood R, 1993.** A review of the seismotectonics of Sweden. SKB TR-93-13. Svensk Kärnbränslehantering AB.
- Muir Wood R, 1995.** Reconstructing the tectonic history of Fennoscandia from its margins: The past 100 million years. SKB TR-95-36, Svensk Kärnbränslehantering AB.
- Munier R, Stenberg L, Stanfors R, Milnes A G, Hermanson J, Triumpf C-A, 2003.** Geological Site Descriptive Model. A strategy for the model development during site investigations. SKB R-03-07, Svensk Kärnbränslehantering AB.
- Munier R, 2004.** Statistical analysis of fracture data, adapted for modelling Discrete Fracture Networks-Version 2. SKB R-04-66, Svensk Kärnbränslehantering AB.

- Müller B, Zoback M L, Fuchs K, Mastin L, Gregersen S, Pavoni N, Stephansson O, Ljunggren C, 1992.** Regional Patterns of Tectonic Stress in Europe, *J. Geophys. Research*, No. 97, B8, 11, p. 783-803.
- Möller C, Snäll S, Stephens M B, 2003.** Dissolution of quartz, vug formation and new grain growth associated with post-metamorphic hydrothermal alteration in KFM02A. Forsmark site investigation. SKB P-03-77, Svensk Kärnbränslehantering AB.
- Mörner N A, 2003.** Paleoseismicity of Sweden a novel paradigm. *Paleogeophysics & Geodynamics*, Stockholm.
- Naturvårdsverket, 1999.** Bedömning för miljö kvalitet. Report 4915. 140 pp.
- Neuman E, 1982.** Species composition and seasonal migrations of the coastal fish fauna in the southern Bothnian Sea, in *Coastal research in the Gulf of Bothnia*, Müller, K., Editor. 1982, Dr. W Junk Publishers.
- Nielsen U T, Ringgaard J, 2004a.** Geophysical borehole logging in borehole KFM01A, HFM01 and HFM02. Forsmark site investigation. SKB P-03-103, Svensk Kärnbränslehantering AB.
- Nielsen U T, Ringgaard J, 2004b.** Geophysical borehole logging in borehole KFM01B, HFM14, HFM15, HFM16, HFM17 and HFM18. Forsmark site investigation. SKB P-04-145, Svensk Kärnbränslehantering AB.
- Nielsen U T, Ringgaard J, 2004c.** Geophysical borehole logging in borehole KFM02A, KFM03A and KFM03B. Forsmark site investigation. SKB P-04-97, Svensk Kärnbränslehantering AB.
- Nielsen U T, Ringgaard J, 2004d.** Geophysical borehole logging in borehole KFM04A, KFM06A, HFM10, HFM11, HFM12 and HFM13. Forsmark site investigation. SKB P-04-144, Svensk Kärnbränslehantering AB.
- Nielsen U T, Ringgaard J, 2004e.** Geophysical borehole logging in borehole KFM05A and HFM19. Forsmark site investigation. SKB P-04-153, Svensk Kärnbränslehantering AB.
- Nilsson A-C, 2003a.** Forsmark site investigation. Sampling and analyses of groundwater in percussion drilled boreholes and shallow monitoring wells at drillsite DS1. Results from the percussion boreholes HFM01, HFM02, HFM03, KFM01A (borehole section 0-100m) and the monitoring wells SFM0001, SFM0002 and SFM0003. SKB P-03-47, Svensk Kärnbränslehantering AB.
- Nilsson A-C, 2003b.** Forsmark site investigation. Sampling and analyses of groundwater in percussion drilled boreholes and shallow monitoring wells at drill site DS2. Results from the percussion boreholes HFM04, HFM05, KFM02A (borehole section 0-100m) and the monitoring wells SFM0004 and SFM0005. SKB P-03-48, Svensk Kärnbränslehantering AB.
- Nilsson B, 2003c.** Element distribution in till at Forsmark – a geochemical study. Forsmark site investigation. SKB P-03-118, Svensk Kärnbränslehantering AB.
- Nilsson P, Aaltonen J, 2003.** Forsmark site investigation. Geophysical, radar and BIPS logging in boreholes HFM06, HFM07 and HFM08. SKB P-03-54, Svensk Kärnbränslehantering AB.
- Nilsson P, Gustafsson C, 2003.** Forsmark site investigation. Geophysical, radar and BIPS logging in boreholes HFM04, HFM05 and the percussion drilled part of KFM02A. SKB P-03-53, Svensk Kärnbränslehantering AB.
- Nilsson A-C, Karlsson S, Borgiel M, 2003.** Forsmark site investigations. Sampling and analyses of surface waters. Results from sampling in the Forsmark area, March 2002 to March 2003. SKB P-03-27, Svensk Kärnbränslehantering AB.
- Nitare J, Norén M, 1992.** Nyckelbiotoper kartläggs i nytt projekt vid Skogsstyrelsen. *Svensk botanisk tidskrift* volym 86: 219-226.
- NMR, 1984.** Naturgeografisk regionindelning av Norden. Nordiska ministerrådet (in Swedish).
- Nordman C, 2003a.** Boremap mapping of percussion boreholes HFM01-03. Forsmark site investigation. SKB P-03-20, Svensk Kärnbränslehantering AB.
- Nordman C, 2003b.** Boremap mapping of percussion boreholes HFM04 and HFM05. Forsmark site investigation. SKB P-03-21, Svensk Kärnbränslehantering AB.

- Nordman C, 2003c.** Boremap mapping of percussion boreholes HFM06–08. Forsmark site investigation. SKB P-03-22, Svensk Kärnbränslehantering AB.
- Nordman C, 2003d.** Boremap mapping of percussion boreholes HFM09–12. Forsmark site investigation. SKB P-04-101, Svensk Kärnbränslehantering AB.
- Nordman C, 2003e.** Boremap mapping of percussion boreholes HFM13-15 and HFM19. Forsmark site investigation. SKB P-04-112, Svensk Kärnbränslehantering AB.
- Nordman C, Samuelsson E, 2004.** Boremap mapping of percussion boreholes HFM16–18. Forsmark site investigation. SKB P-04-113, Svensk Kärnbränslehantering AB.
- Nordstrom D K, Puigdomenech I, 1986.** Redox chemistry of deep ground water in Sweden. SKB TR 86-03, Svensk Kärnbränslehantering AB.
- Näslund J O, Rodhe L, Fastook J L, Holmlund P, 2003.** New ways of studying ice sheet flow directions and glacial erosion by computer modelling-examples from Fennoscandia. *Quaternary Sciences Reviews* 22, 245–258.
- Ohlsson Y, Neretnieks I, 1997.** Diffusion data in granite – recommended values. SKB TR 97-20, Svensk Kärnbränslehantering AB.
- Olesen O, Blikra L H, Braaten A, Dehls J F, Olsen L, Rise L, Roberts D, Riis F, Faleide J I, Anda E, 2004.** Neotectonic deformation in Norway and its implications: a review. *Norwegian Journal of Geology* 84.
- Olsen L, Mejdahl V, Selvik S, 1996.** Middle and Late Pleistocene stratigraphy, Finnmark, north Norway. *NGU Bulletin* 429, 111 p.
- Page L, Hermansson T, Söderlund P, Andersson J, Stephens M B, 2004.** Bedrock mapping U/Pb, 40Ar/39Ar and (U-Th)/He geochronology. Forsmark site investigation. SKB P-04-126, Svensk Kärnbränslehantering AB.
- Parkhurst D L, Appelo C A J, 1999.** User's Guide to PHREEQC (Version 2), a computer program for speciation, batch-reaction, one-dimensional transport, and inverse geochemical calculations. U.S. Geological Survey Water-Resources Investigations Report 99-4259, 312 p.
- Passchier C W, Trouw R A J, 1998.** *Microtectonics*. Springer-Verlag, Berlin, Heidelberg.
- Pedersen K (ed.), 1996.** Bacteria, colloids and organic carbon in groundwater at the Bangombé site in the Oklo area. SKB TR-96-01, Svensk Kärnbränslehantering AB.
- Pereya-Ramos E, 1981.** The ecological role of characeae in the lake littoral. *Ekologia polska* 29 (2): 167-209.
- Perman F, Sjöberg J, 2003.** Transient strain analysis of overcoring measurements in boreholes DBT-01 and DBT-03. Forsmark site investigation. SKB P-03-119, Svensk Kärnbränslehantering AB.
- Persson C, 1985.** Jordartskarta 12I Östhammar NO med beskrivning. SGU Ae 73, Sveriges Geologiska Undersökning (in Swedish with English summary).
- Persson C, 1986.** Jordartskarta 13I Österlövsta SO/13J Grundkallen SV med beskrivning. SGU Ae 76, Sveriges Geologiska Undersökning (in Swedish with English summary).
- Persson C, 1992.** The latest ice recession and till deposits in northern Uppland, eastern central Sweden. SGU Series Ca 81, Sveriges Geologiska Undersökning.
- Persson J, Wallin M, Wallström K, 1993.** *Kustvatten i Uppsala län 1993*. Vol. 2. 1993, Uppsala, Sweden: Upplandsstiftelsen. p. 246.
- Petersson J, Wängnerud A, 2003.** Forsmark site investigation. Boremap mapping of telescopic drilled borehole KFM01A. SKB P-03-23, Svensk Kärnbränslehantering AB.
- Petersson J, Wängnerud A, Strähle A, 2004a.** Boremap mapping of telescopic drilled borehole KFM02A. Forsmark site investigation. SKB P-03-98, Svensk Kärnbränslehantering AB.
- Petersson J, Wängnerud A, Danielsson P, Strähle A, 2004b.** Boremap mapping of telescopic drilled borehole KFM03A and core drilled borehole KFM03B. Forsmark site investigation. SKB P-03-116, Svensk Kärnbränslehantering AB.

- Petersson J, Wängnerud A, Berglund J, Danielsson P, Stråhle A, 2004c.** Boremap mapping of telescopic drilled borehole KFM04A. Forsmark site investigation. SKB P-04-115, Svensk Kärnbränslehantering AB.
- Petersson J, Berglund J, Wängnerud A, Danielsson P, Stråhle A, 2004d.** Boremap mapping of telescopic drilled borehole KFM05A. Forsmark site investigation. SKB P-04-295, Svensk Kärnbränslehantering AB.
- Petersson J, Berglund J, Danielsson P, Wängnerud A, Tullborg E-L, Mattsson H, Thunehed H, Isaksson H, Lindroos H, 2004e.** Petrography, geochemistry, petrophysics and fracture mineralogy of boreholes KFM01A, KFM02A and KFM03A+B. Forsmark site investigation. SKB P-04-103, Svensk Kärnbränslehantering AB.
- Pitkänen P, Luukkonen A, Ruotsalainen P, Leino-Forsman H, Vuorinen U, 1998.** Geochemical modelling of groundwater evolution and residence time at the Kivetty site. POSIVA Report 98-07, POSIVA, Helsinki, Finland.
- Pitkänen P, Luukkonen A, Ruotsalainen P, Leino-Forsman H, Vuorinen U, 1999.** Geochemical modelling of groundwater evolution and residence time at the Olkiluoto site. POSIVA Report 98-10, POSIVA, Helsinki, Finland.
- Pitkänen T, Isaksson H, 2003.** A ground geophysical survey prior to the siting of borehole KFM04A. Forsmark site investigation. SKB P-03-55, Svensk Kärnbränslehantering AB.
- Pitkänen P, Partamies S, Luukkonen A, 2004a.** Hydrogeochemical interpretation of baseline groundwater conditions at the Olkiluoto Site. POSIVA Report 2003-07, POSIVA, Helsinki, Finland.
- Pitkänen T, Thunehed H, Isaksson H, 2004b.** A ground geophysical survey prior to the siting of borehole KFM05A and KFM06A and control of the character of two SW-NE oriented lineaments. Forsmark site investigation. SKB P-03-104, Svensk Kärnbränslehantering AB.
- Poteri A, Billaux D, Dershowitz W, Gomez-Hernandez JJ, Cvetkovic V, Hautojärvi A, Holton D, Medina A, Winberg A (ed.), 2002.** Final report of the TRUE Block Scale project. 3. Modelling of flow and transport. SKB TR-02-15, Svensk Kärnbränslehantering AB.
- Puigdomenech I (ed.), 2001.** Hydrochemical stability of groundwaters surrounding a spent nuclear fuel repository in a 100,000 year perspective. SKB TR 01-28, Svensk Kärnbränslehantering AB.
- Pusch R, Börgesson L, Knutsson S, 1990.** Origin of silty fracture fillings in crystalline bedrock. Geologiska Föreningens I Stockholm Förhandlingar 112, 209–213.
- Påsse T, 1997.** A mathematical model of past, present and future shore level displacement in Fennoscandia. SKB TR 97-28, Svensk Kärnbränslehantering AB.
- Påsse T, 2001.** An empirical model of glacio-isostatic movements and shore-level displacement in Fennoscandia. SKB R-01-41, Svensk Kärnbränslehantering AB.
- Pöllänen J, Sokolnicki M, 2004.** Forsmark site investigation. Difference flow logging in borehole KFM03A. SKB P-04-189, Svensk Kärnbränslehantering AB.
- Pöllänen J, Sokolnicki M, Rouhiainen P, 2004.** Forsmark site investigation. Difference flow logging in borehole KFM05A. SKB P-04-191, Svensk Kärnbränslehantering AB.
- Ranheden H, 1989.** Barknäre and Lingnäre, human impact and vegetational development in an area of subrecent landuplift. Striae 33.
- RETROCK, 2004.** RETROCK Project, Treatment of geosphere retention phenomena is safety assessments. Scientific basis of retention processes and their implementation in safety assessment models (WP2). SKB R-04-48, Svensk Kärnbränslehantering AB.
- Rhén I, Bäckblom G, Gustafson G, Stanfors R, Wikberg P, 1997a.** Äspö HRL – Geoscientific evaluation 1997/2. Results from pre-investigations and detailed site characterisation. Summary report. SKB TR 97-03, Svensk Kärnbränslehantering AB.
- Rhén I, Gustafson G, Stanfors R, Wikberg P, 1997b.** Äspö HRL – Geoscientific evaluation 1997/4. Results from pre-investigations and detailed site characterisation. Comparison of predictions and observations. Geohydrology, groundwater chemistry and transport of solutes. SKB TR 97-05, Svensk Kärnbränslehantering AB.

- Rhén I, Gustafson G, Stanfors R, Wikberg P, 1997c.** Äspö HRL – Geoscientific evaluation 1997/5. Models based on site characterization 1986-1995. SKB TR 97-06, Svensk Kärnbränslehantering AB.
- Rhén I, Forsmark T, 2001.** Äspö Hard Rock Laboratory. Prototype repository, Hydrogeology, Summary report of investigations before the operation phase. SKB IPR-01-65, Svensk Kärnbränslehantering AB.
- Rhén I, Smellie J, 2003.** Task force modelling of groundwater flow and transport of solutes. Task 5 summary report. (ISSN 1404-0344) SKB TR-03-01, Svensk Kärnbränslehantering AB.
- Rhén I, Follin S, Hermanson J, 2003.** Hydrogeological Site Descriptive Model. A strategy for the model development during site investigations. SKB R-03-08, Svensk Kärnbränslehantering AB.
- Ringberg B, Hang T, Kristiansson J, 2002.** Local clay-varve chronology in the Karlskrona-Hultsfred region, southeast Sweden. Geologiska Föreningens i Stockholm Förhandlingar 124, 79–86.
- Risberg J, 1991.** Palaeoenvironment and sea level changes during the early Holocen on the Södertörn peninsula, Södermanland, eastern Sweden. Stockholm University, Department of Quaternary Research. Report 20.
- Robertsson A-M, Persson Ch, 1989.** Biostratigraphical studies of three mires in Northern Uppland, Sweden. SGU C 821, Sveriges Geologiska Undersökning.
- Robertsson A-M, Svedlund J-O, Andrén T, Sundh M, 1997.** Pleistocene stratigraphy in the Dellen region, central Sweden. *Boreas*, Vol 26, pp. 237–260.
- Robertsson A-M, 2004.** Forsmark site investigation. Microfossil analyses of till and sediment samples from Forsmark, northern Uppland. SKB P-04-110. Svensk Kärnbränslehantering AB.
- Rouhiainen P, Pöllänen J, 2004a.** Forsmark site investigation. Difference flow logging in borehole KFM02A. SKB P-04-188, Svensk Kärnbränslehantering AB.
- Rouhiainen P, Pöllänen J, 2004b.** Forsmark site investigation. Difference flow logging in borehole KFM04A. SKB P-04-190, Svensk Kärnbränslehantering AB.
- Rouhiainen P, Pöllänen J, Ludvigson J-E, 2004.** Forsmark site investigation. Addendum to Difference flow logging in borehole KFM01A. SKB P-04-193, Svensk Kärnbränslehantering AB.
- Rønning H J S, Kihle O, Mogaard J O, Walker P, Shomali H, Hagthorpe P, Byström S, Lindberg H, Thunehed H, 2003.** Forsmark site investigation. Helicopter borne geophysics, Östhammar, Sweden. SKB P-03-41, Svensk Kärnbränslehantering AB.
- Röshoff K, Cosgrove J, 2002.** Sedimentary dykes in the Oskarshamn-Västervik area. A study of the mechanism of formation. SKB R-02-37, Svensk Kärnbränslehantering AB.
- Röshoff R, Lanaro F, Jing L, 2002.** Strategy for a Rock Mechanics Site Descriptive Model. Development and testing of the empirical approach. SKB R-02-01, Svensk Kärnbränslehantering AB.
- Samper J, Delgado J, Juncosa R, Montenegro L, 2000.** CORE2D v 2.0: A Code for non-isothermal water flow and reactive solute transport. User's manual. ENRESA Technical report 06/2000.
- Sandström B, Savolainen M, Tullborg E-L, 2004.** Forsmark site investigation. Fracture mineralogy. Results from fracture minerals and wall rock alteration in boreholes KFM01A, KFM02A, KFM03A and KFM03B. SKB P-04-149, Svensk Kärnbränslehantering AB.
- SBF, 1999.** Nyckelbiotopsinventeringen 1993–1998 – Slutrapport. Swedish Board of Forestry, Jönköping.
- SCB, 2003.** SCB:s Marknadsprofiler, produktkatalog mars 2003–februari 2004, Statistics Sweden.
- Schoning K, 2001.** Marine conditions in middle Sweden during the Late Weichselian and Early Holocene as inferred from foraminifera, Ostracoda and stable isotopes. Doctoral thesis. Department of Physical Geography and Quaternary Geology. Quaternaria Ser A. No 8.
- Shackelton N J, 1997.** The deep-sea sediment record and the Pliocene-Pleistocene boundary. *Quaternary International*, vol 40, 33–35.

- Shackelton N J, Berger A, Peltier W R, 1990.** An alternative astronomical calibration of the lower Pleistocene timescale based on ODP Site 677. *Transactions of the Royal Society of Edinburgh: Earth Sciences*, 81, 251–261.
- Šibrava V, 1992.** Should the Pliocene-Pleistocene boundary be lowered? *SGU Ca* 81, 327–332, Sveriges Geologiska Undersökning.
- Sibson R H, 1977.** Fault rocks and fault mechanisms. *Journal of the Geological Society (London)* 133, 191–214.
- Sigurdsson T, 1987.** Bottenundersökning av ett område ovanför SFR, Forsmark. SFR 87-07, Svensk Kärnbränslehantering AB.
- Sjöberg J, 2004.** Overcoring rock stress measurements in borehole KFM01B. Forsmark site investigation. SKB P-04-83, Svensk Kärnbränslehantering AB.
- Sjöberg J, Lindfors U, Perman F, Ask D, 2005.** Forsmark Site Investigation: Evaluation of the state of stress at the Forsmark Site, SKB R-05-35, Svensk Kärnbränslehantering AB.
- SKB, 2000a.** Förstudie Östhammar. Slutrapport. SKB. ISBN 91-972810-4-2 (in Swedish).
- SKB, 2000b.** Geoscientific programme for investigation and evaluation of sites for the deep repository. SKB TR-00-20, Svensk Kärnbränslehantering AB.
- SKB, 2001a.** Site investigations. Investigation methods and general execution programme. SKB TR-01-29, Svensk Kärnbränslehantering AB
- SKB, 2001b.** Integrated account of method, site selection and programme prior to the site investigation phase. SKB TR-01-03, Svensk Kärnbränslehantering AB.
- SKB, 2002a.** Forsmark – site descriptive model version 0. SKB R-02-32, Svensk Kärnbränslehantering AB.
- SKB, 2002b.** Preliminary safety evaluation, based on initial site investigation data. Planning document. SKB TR 02-28, Svensk Kärnbränslehantering AB.
- SKB, 2004a.** Preliminary site description. Forsmark area – version 1.1. SKB R-04-15, Svensk Kärnbränslehantering AB.
- SKB, 2004b.** Preliminary site description. Simpevarp area – version 1.1. SKB R-04-25, Svensk Kärnbränslehantering AB.
- SKB, 2004c.** Underground design premises, SKB R-04-60, Svensk Kärnbränslehantering AB.
- SKB, 2004d.** Hydrogeochemical evaluation for Simpevarp model version 1.2. Preliminary site description of the Simpevarp area. SKB-R-04-74.
- SKB, 2004e.** Interim main report of the safety assessment SR-Can. SKB TR-04-11, Svensk Kärnbränslehantering AB.
- SKB, 2005a.** Forsmark site investigation. Programme for further investigations of geosphere and biosphere. SKB R-05-14, Svensk Kärnbränslehantering AB.
- SKB, 2005b.** Hydrogeochemical evaluation for Forsmark model version 1.2. Preliminary site description of the Forsmark area. SKB-R-05-17.
- Smellie J A T, Larsson N-Å, Wikberg P, Carlsson L, 1985.** Hydrochemical investigations in crystalline bedrock in relation to existing hydraulic conditions: Experience from the SKB test-sites in Sweden. SKB TR-85-11, Svensk Kärnbränslehantering AB.
- Smellie J A T, Larsson N-Å, Wikberg P, Puigdomenech I, Tullborg E-L, 1987.** Hydrochemical investigations in crystalline bedrock in relation to existing hydraulic conditions: Klipperås test-site, Småland, southern Sweden. SKB TR-87-21, Svensk Kärnbränslehantering AB.
- Smellie J A T, Wikberg P, 1989.** Hydrochemical investigations at the Finnsjön site, central Sweden. *J. Hydrol.*, 126, 147–169.
- Smellie J, Laaksoharju M, Tullborg E-L, 2002.** Hydrogeochemical Site Descriptive Model. A strategy for the model development during site investigations. SKB R-02-49, Svensk Kärnbränslehantering AB.

- Snoeijs P, 1985.** Microphytobenthic biomass and environmental data in and around the Forsmark Biotest Basin, 1983–1985. 1985:2, Växtbiologiska Intutionen, Uppsala.
- Snoeijs P, 1986** Primary production of microphytobenthos on rocky substrates in the Forsmark biotest basin, 1984 National Swedish environmental protection board report Vol. 3216 p. 1–24.
- Snoeijs P, Mo K, 1987.** Macrofauna on rocky substrates in the Forsmark biotest basin (March 1984 – March 1985). 3397, National Swedish Environmental Protection Board.
- Sohlenius G, Hedenström A, Rudmark L, 2004.** Mapping of unconsolidated Quaternary deposits 2002–2003. Map description. SKB R-04-39. Svensk Kärnbränslehantering AB.
- Sonesten L, 2005.** Chemical characteristics of surface waters in the Forsmark area. Evaluation of data from lakes, streams and coastal sites. SKB P-05-41, Svensk Kärnbränslehantering AB.
- SSPB, 1982.** Characterisation of deep-seated rock masses by means of borehole investigations. Swedish State Power Board, Final Report, April 1982, Main Area 5, Report No 1.
- SSPB, 1986.** Large scale in-situ tests on stress and water flow relationships in fractured rock, Swedish State Power Board.
- Stanfors R, Ericsson L O, 1993.** Post-glacial faulting in the Lansjärv area, northern Sweden. Comments from the expert group on a field visit at Molberget post-glacial fault area, 1991. SKB TR-93-11, Svensk Kärnbränslehantering AB.
- Stanfors R, Erlström M, Markström I, 1997.** Äspö HRL – Geoscientific evaluation 1997/1. Overview of site characterization 1986–1995. SKB TR 97-02, Svensk Kärnbränslehantering AB.
- Stemann-Nielsen E, 1952.** The use of radio-active (^{14}C) for measuring organic production in the sea. J. Cons. perm. int. Explor. Mer. Vol. 18: p. 117–140.
- Stephansson O, Eriksson B, 1975.** Pre-Holocene joint fillings at Forsmark, Uppland, Sweden. Geologiska Föreningens i Stockholm Förhandlingar 97, 91–95.
- Stephens M B, Wahlgren C-H, Weihed P, 1994.** Geological Map of Sweden, scale 1:3,000,000. SGU Ba 52, Sveriges Geologiska Undersökning.
- Stephens M B, Wahlgren C-H, 1996.** Post-1.85 Ga tectonic evolution of the Svecokarelian orogen with special reference to central and SE Sweden. GFF 118 (extended abstract).
- Stephens M B, Wahlgren C-H, Weijermars R, Cruden A R, 1996.** Left-lateral transpressive deformation and its tectonic implications, Sveconorwegian orogen, Baltic Shield, southwestern Sweden. Precambrian Research 79.
- Stephens M B, Bergman T, Andersson J, Hermansson T, Wahlgren C-H, Albrecht L, Mikko H, 2003a.** Forsmark bedrock mapping. Stage 1 (2002) – Outcrop data including fracture data. SKB P-03-09, Svensk Kärnbränslehantering AB.
- Stephens M B, Lundqvist S, Ekström M, Bergman T, Andersson J, 2003b.** Rock types, their petrographic and geochemical characteristics, and a structural analysis of the bedrock based on stage 1 (2002) surface data. SKB P-03-75, Svensk Kärnbränslehantering AB.
- Stephens M B, 2004.** SGU (Geological Survey of Sweden), Personal communication.
- Stephens M B, Forsberg O, 2005.** Rock types and ductile structures on a rock domain basis, and fracture orientation and mineralogy on a deformation zone basis. Preliminary site description of the Forsmark area – version 1.2. SKB R-05-xx, Svensk Kärnbränslehantering AB.
- Stephens M B, Lundqvist S, Bergman T, Ekström M, 2005a.** Bedrock mapping. Petrographic and geochemical characteristics of rock types based on Stage 1 (2002) and Stage 2 (2003) surface data. Forsmark site investigation. SKB P-04-87, Svensk Kärnbränslehantering AB.
- Stephens M B, Isaksson H, Bergman T, 2005b.** Description of the bedrock geological map at the Forsmark site. Preliminary site description of the Forsmark area – version 1.2. SKB R-05-xx, Svensk Kärnbränslehantering AB.
- Stigsson M, Follin S, Andersson J, 1999.** On the simulation of variable density flow at SFR, Sweden. SKB R-99-08, Svensk Kärnbränslehantering AB.

- Stille H, Fredriksson A, Widing E, Åhrling G, 1985.** Bergmekaniska beräkningar – FEM-analys av Silo med anslutande tunnlår. SKB SFR 85-05, Svensk Kärnbränslehantering AB (in Swedish).
- Streckeisen A, 1976.** To each plutonic rock its proper name. *Earth Science Reviews* 12.
- Streckeisen A, 1978.** IUGS Subcommittee on the Systematics of Igneous Rocks. Classification and nomenclature of volcanic rock, lamprophyres, carbonatites and melilitic rocks. Recommendations and suggestions. *Neues Jahrbuch für Mineralogie* 134.
- Strömberg B, 1989.** Late Weichselian deglaciation and clay varve chronology in east-central Sweden. SGU Ca 73, Sveriges Geologiska Undersökning.
- Sundberg J, 1988.** Thermal properties of soils and rocks, Publ. A 57 Dissertation, doctoral thesis, Geologiska institutionen, Chalmers University of Technology and University of Göteborg.
- Sundberg J, 2002.** Determination of thermal properties at Äspö HRL. Comparison and evaluation of methods and methodologies for borehole KA 2599 G01. SKB R-02-27, Svensk Kärnbränslehantering AB.
- Sundberg J, 2003.** Thermal Site Descriptive Model, A Strategy for the Model Development during Site Investigations. SKB R-03-10, Svensk Kärnbränslehantering AB.
- Sundberg J, Back P-E, Bengtsson A, 2005a.** Uncertainty analysis of thermal properties at Äspö HRL prototype repository. Svensk Kärnbränslehantering AB, Report in progress.
- Sundberg J, Back P-E, Bengtsson A, Ländell M, 2005b.** Thermal modelling. Preliminary site description Forsmark area – version 1.2. SKB R-05-31, Svensk Kärnbränslehantering AB.
- Sundberg J, Back P-E, Bengtsson A, 2005c.** Thermal modelling of the Simpevarp area – Supporting document for thermal model S1.2. Svensk Kärnbränslehantering AB, Stockholm. Report in progress.
- Sundh M, Sohlenius G, Hedenström A, 2004.** Stratigraphical investigation of till in machine cut trenches. SKB P-04-34. Svensk Kärnbränslehantering AB.
- Svenonius F, 1887.** Beskrifning till kartbladen Forsmark och Björn. SGU Aa 98 och 99, Sveriges Geologiska Undersökning.
- Svensson N-O, 1989.** Late Weichselian and early Holocene shore displacement in the central Baltic, based on stratigraphical and morphological records from eastern Småland and Gotland, Sweden. *LUNDQUA*, vol 25, 181 pp.
- Svensson U, 1996.** SKB Palaeohydrogeological programme. Regional groundwater flow due to advancing and retreating glacier-scoping calculations. In: SKB Project Report U 96-35, Svensk Kärnbränslehantering AB.
- Svensson U, 2001a.** A continuum representation of fracture networks. Part I: Method and basic test cases. *Journal of Hydrology*, 250, pp. 170–186.
- Svensson U, 2001b.** A continuum representation of fracture networks. Part II: Application to the Äspö Hard Rock Laboratory. *Journal of Hydrology*, 250, pp. 187–205.
- Svensson U, 2004.** DarcyTools, Version 2.1. Verification and validation. SKB R-04-21, Svensk Kärnbränslehantering AB.
- Svensson U, Ferry M, 2004.** DarcyTools, Version 2.1. User's guide. SKB R-04-20, Svensk Kärnbränslehantering AB.
- Svensson U, Kuylenstierna H-O, Ferry M, 2004.** DarcyTools, Version 2.1. Concepts, methods, equations and demo simulations. SKB R-04-19, Svensk Kärnbränslehantering AB.
- Thiem G, 1906.** *Hydrologische Methoden*. J M Gebhardt, Leipzig.
- Thunehed H, Pitkänen T, 2002.** Markgeofysiska mätningar inför placering av de tre första kärnbränslehålen i Forsmarksområdet. SKB P-02-01, Svensk Kärnbränslehantering AB.
- Thunehed H, 2004.** Interpretation of borehole geophysical measurements in KFM02A, KFM03A, KFM03B and HFM04 to HFM08. Forsmark site investigation. SKB P-04-98, Svensk Kärnbränslehantering AB.

- Thunehed H, Keisu M, 2004.** Interpretation of borehole geophysical measurements in KFM05A, HFM14, HFM15 and HFM19. Forsmark site investigation. SKB P-04-154, Svensk Kärnbränslehantering AB.
- Thunehed H, 2005.** Inversion of helicopterborne electromagnetic measurements. Forsmark site investigation. SKB P-04-157, Svensk Kärnbränslehantering AB.
- Triumf C-A, 2004.** Oskarshamn site investigation. Joint interpretation of lineaments. SKB P-04-49, Svensk Kärnbränslehantering AB.
- Trotignon L, Beaucaire C, Louvat D, Aranyosy J F, 1997.** Equilibrium geochemical modelling of Äspö groundwaters: a sensitivity study to model parameters. In: Laaksoharju, M. and Wallin, B. (Eds.) Evolution of the groundwater chemistry at the Äspö Hard Rock Laboratory. SKB 97-04, Svensk Kärnbränslehantering AB.
- Trotignon L, Beaucaire C, Louvat D, Aranyosy J F, 1999.** Equilibrium geochemical modelling of Äspö groundwaters: a sensitivity study of thermodynamic equilibrium constants. *Appl. Geochem.*, 14, 907–916.
- Tullborg E-L, Larson S Å, 1984.** $\delta^{18}\text{O}$ and $\delta^{13}\text{C}$ for limestones, calcite fissure infillings and calcite precipitates from Sweden. *Geologiska föreningens i Stockholm förhandlingar* 106(2).
- Ukkonen P, Lunkka J P, Jungner H, Donner J, 1999.** New radiocarbon dates from Finnish mammoths indicating large ice-free areas in Fennoscandia during the Middle Weichselian. *Journal of Quaternary Science* 14, 711–714.
- van Balen R T, Heeremans M, 1998.** Middle Proterozoic-early Palaeozoic evolution of central Baltoscandian intracratonic basins: evidence for asthenospheric diapirs, *Tectonophysics* 300, p. 131–142.
- Vikström M, 2005.** Modelling of soil depth and lake sediments. An example from the Forsmark site. SKB R-05-07. Svensk Kärnbränslehantering AB.
- Wahlgren C-H, Cruden A R, Stephens M B, 1994.** Kinematics of a fan-like structure in the eastern part of the Sveconorwegian orogen, Baltic Shield, south-central Sweden. *Precambrian Research* 70.
- Wastegård S, Andrén T, Sohlenius G, Sandgren P, 1995.** Different phases of the Yoldia Sea in the north western Baltic Proper. *Quaternary International* 27, 121–129.
- Welin E, 1964.** Uranium disseminations and vein fillings in iron ores of northern Uppland, Central Sweden. *Geologiska Föreningens i Stockholm Förhandlingar* 86.
- Welinder S, Pedersen E A, Widgren M, 1998.** Det svenska jordbrukets historia: Jordbrukets första femtusen år. Natur och Kultur/LTs förlag, Borås (in Swedish).
- Werner K, Johansson P-O, 2003.** Slug tests in groundwater monitoring wells in soil. Forsmark site investigation. SKB P-03-65, Svensk Kärnbränslehantering AB.
- Werner K, Lundholm L, Johansson P-O, 2004.** Forsmark site investigation. Drilling and pumping test of wells at Börstilåsen. SKB P-04-138, Svensk Kärnbränslehantering AB.
- Westman P, Wastegård S, Schoning K, Gustafsson B, Omstedt A, 1999.** Salinity change in the Baltic sea during the last 8,500 years: evidence, causes and models. SKB TR-99-38, Svensk Kärnbränslehantering AB.
- Wetzel R G, 2001.** *Limnology: Lake and River Ecosystems*. 3rd Edition, Academic Press, San Diego. 1006 pp.
- Wickman F E, Åberg G, Levi B, 1983.** Rb-Sr dating of alteration events in granitoids. *Contributions to Mineralogy and Petrology* 83.
- Widstrand H, Byegård J, Ohlsson Y, Tullborgh E-L, 2003.** Strategy for the use of laboratory methods in the site investigations programme for the transport properties of the rock. SKB R-03-20, Svensk Kärnbränslehantering AB.
- Widgren M, 1983.** Settlement and farming systems in early Iron Age. A study of fossil agrarian landscapes in Östergötland, Sweden. *Stockholm studies in Human Geography* 3, Dissertation in Human geography. Almquist & Wiksell International, Stockholm. 132 pp.

- Wikberg P, 1998.** Äspö Task Force on modelling of groundwater flow and transport of solutes. SKB progress report HRL-98-07, Svensk Kärnbränslehantering AB.
- Wiklund S, 2002.** Digitala ortofoton och höjdm modeller. Redovisning av metodik för platsundersökningsområdena Oskarshamn och Forsmark samt förstudieområdet Tierp Norra. SKB P-02-02, Svensk Kärnbränslehantering AB.
- Winchester J A, Floyd P A, 1977.** Geochemical discrimination of different magma series and their differentiation products using immobile elements. *Chemical Geology*, 20.
- Winberg A, Andersson P, Hermansson J, Byegård J, Cvetkovic V, Birgersson L, 2000.** Äspö Hard Rock Laboratory. Final report on the first stage of the tracer retention understanding experiments. SKB TR-00-07. Svensk Kärnbränslehantering AB.
- Åkerman C, 1994.** Ores and mineral deposits. In C. Fredén (ed.), *Geology. National Atlas of Sweden*.
- Åkesson U, 2004a.** Drill hole KFM01A: Extensometer measurement of the coefficient of thermal expansion of rock. Forsmark site investigation, SKB P-04-163, Svensk Kärnbränslehantering AB.
- Åkesson U, 2004b.** Drill hole KFM02A: Extensometer measurement of the coefficient of thermal expansion of rock. Forsmark site investigation, SKB P-04-164, Svensk Kärnbränslehantering AB.
- Åkesson U, 2004c.** Drill hole KFM03A: Extensometer measurement of the coefficient of thermal expansion of rock. Forsmark site investigation, SKB P-04-165, Svensk Kärnbränslehantering AB.

Properties of rock domains (RFM001 to RFM042) in the regional model volume

The construction of these tables is described in Section 5.3. The orientation of planar structures (tectonic foliation, banding) is given in the form of strike and dip using the right-hand-rule method. For example, 108/75 corresponds to a strike and dip of N72°W/75°SW. Fisher mean and K values are calculated from the poles to planes. In some cases, the pole to a best-fit great circle through the poles to a group of planar structures is provided. The orientation of linear structures (mineral stretching lineation, fold axis) is given in the form of trend and plunge. For example, 124/36 corresponds to a trend of S34°E and a plunge of 36°.

RFM001				
Property	Character	Quantitative estimate	Confidence	Comment
Dominant rock type	Ultramafic rock, metamorphic (101004)		High	Outcrop data, N=29
Mineralogical composition (%). Only the dominant minerals are listed	Pyroxene	46.6–61.2	Low	Data from outcrop samples, N=2. Range
	Hornblende (actinolite)	9.6–31.0		
	Olivine (serpentine)	0–35.2		
Grain size	Medium-grained		High	Outcrop data, N=29
Age (million years)		1,891–1,861	High	Regional correlation. Range. Age probably 1,886±1
Structure	Isotropic or weakly lineated and foliated		High	Outcrop data, N=29
Texture	Equigranular		High	Outcrop data, N=29
Density (kg/m ³)		3,045	Low	Data from a single outcrop sample, N=1
Porosity (%)		1.04	Low	Data from a single outcrop sample, N=1
Magnetic susceptibility (SI units)		0.04572	Low	Data from a single outcrop sample, N=1
Electric resistivity in fresh water (ohm m)		52	Low	Data from a single outcrop sample, N=1
Uranium content based on gamma ray spectrometric data (weight ppm)		0.0	Low	Outcrop data, N=1
Natural exposure rate (microR/h)		0.0	Low	Outcrop data, N=1
Subordinate rock type(s) Only the more important components are listed	Diorite, quartz diorite and gabbro, metamorphic (101033)		High	Outcrop data, N=29. Gabbro dominates in the northeastern part of the domain
Degree of inhomogeneity	Low		High	Outcrop data, N=29
Metamorphism/alteration	1. Local serpentinisation 2. Amphibolite-facies metamorphism		High	Outcrop data, N=29
Mineral fabric (type/orientation)				Insufficient data

RFM002

Property	Character	Quantitative estimate			Confidence	Comment
Dominant rock type	Diorite, quartz diorite and gabbro, metamorphic (101033)				High	Outcrop data, N=27
Mineralogical composition (%). Only the dominant minerals are listed	Plagioclase feldspar	40.4–64.6	51.3	5.0	High	Data from outcrop samples, N=11. Range/mean/standard deviation
	Hornblende	10.6–50.6	27.6	11.5		
	Biotite	0–14.2	8.3	5.0		
	Quartz	0–24.6	8.3	7.7		
Grain size	Medium-grained				High	Outcrop data, N=27
Age (million years)		1,891–1,861			High	Regional correlation. Range. Age probably 1,886±1
Structure	Lineated and weakly foliated				High	Outcrop data, N=27
Texture	Equigranular				High	Outcrop data, N=27
Density (kg/m ³)		2,738–3,120	2,934	100	High	Data from outcrop samples, N=14. Range/mean/standard deviation
Porosity (%)		0.25–0.54	0.37	0.07	High	Data from outcrop samples, N=14. Range/mean/standard deviation
Magnetic susceptibility (SI units)		0.00036–0.05592	0.00293	0.01914/0.00254	High	Data from outcrop samples, N=14. Range/geometric mean/standard deviation above/below mean
Electric resistivity in fresh water (ohm m)		5,412–34,227	15,315	12,575/6,905	High	Data from outcrop samples, N=14. Range/geometric mean/standard deviation above/below mean
Uranium content based on gamma ray spectrometric data (weight ppm)		0.0–2.8	1.2	0.9	High	Outcrop data, N=14. Range/mean/standard deviation
Natural exposure rate (microR/h)		0.2–6.4	2.7	1.9	High	Outcrop data, N=14. Range/mean/standard deviation
Subordinate rock type(s) Only the more important components are listed	Ultramafic rock, metamorphic (101004)				High	Outcrop data, N=27
	Amphibolite (102017)				High	
	Pegmatite, pegmatitic granite (101061)				High	
	Granitoid, metamorphic (111051)				High	
Degree of inhomogeneity	Low				High	Outcrop data, N=27
Metamorphism/alteration	Amphibolite-facies metamorphism				High	Outcrop data, N=27
Mineral fabric (type/orientation)	Mineral stretching lineation	124/36	47		Medium	Outcrop data, N=5. Fisher mean. Trend/plunge and K value

RFM003						
Property	Character	Quantitative estimate			Confidence	Comment
Dominant rock type	Felsic to intermediate volcanic rock, metamorphic (103076)				High	Outcrop data, N=17
Mineralogical composition (%). Only the dominant minerals are listed	Quartz	5.2–39.2	26.0	10.3	High	Data from outcrop samples, N=15. Range/mean/standard deviation
	K-feldspar	0–12.6	3.4	4.1		
	Plagioclase feldspar	29.2–53.2	48.6	6.5		
	Biotite	0–22.8	12.0	8.0		
	Hornblende	0–35.6				
Grain size	Fine-grained				High	Outcrop data, N=17
Age (million years)		1,906–1,891			High	Regional correlation. Range
Structure	Banded, foliated and lineated				High	Outcrop data, N=17
Texture	Equigranular				High	Outcrop data, N=17
Density (kg/m ³)		2,648–2,946	2,732	79	High	Data from outcrop samples, N=19. Range/mean/standard deviation
Porosity (%)		0.20–0.62	0.37	0.11	High	Data from outcrop samples, N=19. Range/mean/standard deviation
Magnetic susceptibility (SI units)		0.00006–0.24000	0.00235	0.04163/0.00222	High	Data from outcrop samples, N=19. Range/geometric mean/standard deviation above/below mean
Electric resistivity in fresh water (ohm m)		1,725–81,878	14,374	22,146/8,716	High	Data from outcrop samples, N=19. Range/geometric mean/standard deviation above/below mean
Uranium content based on gamma ray spectrometric data (weight ppm)		2.5–6.8	4.3	1.0	High	Outcrop data, N=19. Range/mean/standard deviation
Natural exposure rate (microR/h)		5.2–13.4	9.4	2.5	High	Outcrop data, N=19. Range/mean/standard deviation
Subordinate rock type(s) Only the more important components are listed	Pegmatite, pegmatitic granite (101061)				High	Outcrop data, N=17
	Diorite, quartz diorite and gabbro, metamorphic (101033)				High	
	Amphibolite (102017)				High	
	Granitoid, metamorphic (111051)				High	
Degree of inhomogeneity	High				High	Outcrop data, N=17
Metamorphism/alteration	Amphibolite-facies metamorphism				High	Outcrop data, N=17
Mineral fabric (type/orientation)	Tectonic foliation/banding	108/75	35		Medium	Outcrop data, N=8. Fisher mean. Strike/dip and K value
	Mineral stretching lineation	136/40	240		Medium	Outcrop data, N=8. Fisher mean. Trend/plunge and K value

RFM004

Property	Character	Quantitative estimate	Confidence	Comment
Dominant rock type	Ultramafic rock, metamorphic (101004)		High	Outcrop data, N=8
Mineralogical composition (%). Only the dominant minerals are listed	Pyroxene	46.6–61.2	Low	Data from outcrop samples, N=2. Range
	Hornblende (actinolite)	9.6–31.0		
	Olivine (serpentine)	0–35.2		
Grain size	Medium-grained		High	Outcrop data, N=8
Age (million years)		1,891–1,861	High	Regional correlation. Range. Age probably 1,886±1
Structure	Isotropic or lineated and weakly foliated		High	Outcrop data, N=8
Texture	Equigranular		High	Outcrop data, N=8
Density (kg/m ³)		3,045	Low	Data from a single outcrop sample, N=1
Porosity (%)		1.04	Low	Data from a single outcrop sample, N=1
Magnetic susceptibility (SI units)		0.04572	Low	Data from a single outcrop sample, N=1
Electric resistivity in fresh water (ohm m)		52	Low	Data from a single outcrop sample, N=1
Uranium content based on gamma ray spectrometric data (weight ppm)		0.0	Low	Outcrop data, N=1
Natural exposure rate (microR/h)		0.0	Low	Outcrop data, N=1
Subordinate rock type(s) Only the more important components are listed	Diorite, quartz diorite and gabbro, metamorphic (101033)		High	Outcrop data, N=8
	Pegmatite, pegmatitic granite (101061)		High	
	Amphibolite (102017)		High	
	Tonalite to granodiorite, metamorphic (101054)		High	
Degree of inhomogeneity	Low		High	Outcrop data, N=8
Metamorphism/alteration	Amphibolite-facies metamorphism		High	Outcrop data, N=8
Mineral fabric (type/orientation)				No data

RFM005						
Property	Character	Quantitative estimate			Confidence	Comment
Dominant rock type	Diorite, quartz diorite and gabbro, metamorphic (101033)				High	Outcrop data, N=21
Mineralogical composition (%). Only the dominant minerals are listed	Plagioclase feldspar	40.4–64.6	51.3	5.0	High	Data from outcrop samples, N=11. Range/mean/standard deviation
	Hornblende	10.6–50.6	27.6	11.5		
	Biotite	0–14.2	8.3	5.0		
	Quartz	0–24.6	8.3	7.7		
Grain size	Medium-grained				High	Outcrop data, N=21
Age (million years)		1,891–1,861			High	Regional correlation. Range. Age probably 1,886±1
Structure	Lineated and weakly foliated				High	Outcrop data, N=21
Texture	Equigranular				High	Outcrop data, N=21
Density (kg/m ³)		2,738–3,120	2,934	100	High	Data from outcrop samples, N=14. Range/mean/standard deviation
Porosity (%)		0.25–0.54	0.37	0.07	High	Data from outcrop samples, N=14. Range/mean/standard deviation
Magnetic susceptibility (SI units)		0.00036–0.05592	0.00293	0.01914/0.00254	High	Data from outcrop samples, N=14. Range/geometric mean/standard deviation above/below mean
Electric resistivity in fresh water (ohm m)		5,412–34,227	15,315	12,575/6,905	High	Data from outcrop samples, N=14. Range/geometric mean/standard deviation above/below mean
Uranium content based on gamma ray spectrometric data (weight ppm)		0.0–2.8	1.2	0.9	High	Data from outcrop samples, N=14. Range/mean/standard deviation
Natural exposure rate (microR/h)		0.2–6.4	2.7	1.9	High	Data from outcrop samples, N=14. Range/mean/standard deviation
Subordinate rock type(s) Only the more important components are listed	Pegmatite, pegmatitic granite (101061)				High	Outcrop data, N=21
	Ultramafic rock, metamorphic (101004)				High	
	Amphibolite (102017)				High	
	Tonalite to granodiorite, metamorphic (101054)				High	
Degree of inhomogeneity	Low				Medium	Outcrop data, N=21
Metamorphism/alteration	Amphibolite-facies metamorphism				High	Outcrop data, N=21
Mineral fabric (type/orientation)	Tectonic foliation/banding	136/89	15		Medium	Outcrop data, N=11. Fisher mean. Strike/dip and K value
	Mineral stretching lineation	137/41	60		Medium	Outcrop data, N=4. Fisher mean. Trend/plunge and K value

RFM006

Property	Character	Quantitative estimate			Confidence	Comment
Dominant rock type	Granite to granodiorite, metamorphic (101057)				High	Outcrop data, N=21
Mineralogical composition (%). Only the dominant minerals are listed	Quartz	27.8–45.8	35.6	4.2	High	Data from outcrop samples (N=29) and borehole samples from KFM01A (N=5), KFM02A (N=6) and KFM03A (N=6). Range/mean/standard deviation
	K-feldspar	0.2–36.0	22.5	8.6		
	Plagioclase feldspar	24.0–63.8	35.6	8.5		
	Biotite	0.8–8.2	5.1	1.6		
Grain size	Medium-grained				High	Outcrop data, N=21
Age (million years)		1,891–1,861			High	Regional correlation. Range. Age probably 1,865±3
Structure	Lineated and weakly foliated				High	Outcrop data, N=21
Texture	Equigranular				High	Outcrop data, N=21
Density (kg/m ³)		2,639–2,722	2,657	15	High	Data from outcrop samples (N=45) and borehole samples from KFM01A (N=5), KFM02A (N=8) and KFM03A (N=6). Range/mean/standard deviation
Porosity (%)		0.28–0.66	0.43	0.08	High	Data from outcrop samples (N=45) and borehole samples from KFM01A (N=5), KFM02A (N=8) and KFM03A (N=6). Range/mean/standard deviation
Magnetic susceptibility (SI units)		0.00007–0.02548	0.00442	0.01591 / 0.00346	High	Data from outcrop samples (N=45) and borehole samples from KFM01A (N=5), KFM02A (N=8) and KFM03A (N=6). Range/geometric mean/standard deviation above/below mean
Electric resistivity in fresh water (ohm m)		3,352–54,100	14,727	11,237 / 6,374	High	Data from outcrop samples (N=45) and borehole samples from KFM01A (N=10), KFM02A (N=15) and KFM03A (N=12). Range/geometric mean/standard deviation above/below mean
Uranium content based on gamma ray spectrometric data (weight ppm)		0.8–19.0	4.9	2.3	High	Outcrop data (N=47) and borehole samples from KFM01A (N=5), KFM02A (N=8) and KFM03A (N=6). Range/mean/standard deviation
Natural exposure rate (microR/h)		6.3–19.3	12.4	2.0	High	Outcrop data (N=47) and borehole samples from KFM01A (N=5), KFM02A (N=8) and KFM03A (N=6). Range/mean/standard deviation

RFM006					
Property	Character	Quantitative estimate		Confidence	Comment
Subordinate rock type(s) Only the more important components are listed	Tonalite to granodiorite, metamorphic (101054)			High	Outcrop data, N=21
	Pegmatite, pegmatitic granite (101061)			High	
	Amphibolite (102017)			High	
	Felsic to intermediate volcanic rock, metamorphic (103076)			High	
Degree of inhomogeneity	Low			High	Outcrop data, N=21
Metamorphism/alteration	Amphibolite-facies metamorphism			High	Outcrop data, N=21
Mineral fabric (type/orientation)	Tectonic foliation/banding	127/77	37	High	Outcrop data, N=13. Fisher mean. Strike/dip and K value
	Mineral stretching lineation	143/44	128	High	Outcrop data, N=17. Fisher mean. Trend/plunge and K value

RFM007

Property	Character	Quantitative estimate			Confidence	Comment
Dominant rock type	Diorite, quartz diorite and gabbro, metamorphic (101033)	90%			High	Outcrop data, N=18. Borehole data, 0–270.70 m in KFO01. Quantitative estimate based on borehole log in SKB report PR D-96-025
Mineralogical composition (%). Only the dominant minerals are listed	Plagioclase feldspar	40.4–64.6	51.3	5.0	High	Data from outcrop samples, N=11. Range/mean/standard deviation
	Hornblende	10.6–50.6	27.6	11.5		
	Biotite	0–14.2	8.3	5.0		
	Quartz	0–24.6	8.3	7.7		
Grain size	Medium-grained				High	Outcrop data, N=18
Age (million years)		1,891–1,861			High	Regional correlation. Range. Age probably 1,886±1
Structure	Lineated and weakly foliated				High	Outcrop data, N=18
Texture	Equigranular				High	Outcrop data, N=18
Density (kg/m ³)		2,738–3,120	2,934	100	High	Data from outcrop samples, N=14. Range/mean/standard deviation
Porosity (%)		0.25–0.54	0.37	0.07	High	Data from outcrop samples, N=14. Range/mean/standard deviation
Magnetic susceptibility (SI units)		0.00036–0.05592	0.00293	0.01914/0.00254	High	Data from outcrop samples, N=14. Range/geometric mean/standard deviation above/below mean
Electric resistivity in fresh water (ohm m)		5,412–34,227	15,315	12,575/6,905	High	Data from outcrop samples, N=14. Range/geometric mean/standard deviation above/below mean
Uranium content based on gamma ray spectrometric data (weight ppm)		0.0–2.8	1.2	0.9	High	Outcrop data, N=14. Range/mean/standard deviation
Natural exposure rate (microR/h)		0.2–6.4	2.7	1.9	High	Outcrop data, N=14. Range/mean/standard deviation
Subordinate rock type(s) Only the more important components are listed	Granite to granodiorite, metamorphic (101057)	5%			High	Outcrop data, N=18. Borehole data, 0–270.70 m in KFO01. Quantitative estimates based on borehole log in SKB report PR D-96-025
	Pegmatite, pegmatitic granite (101061)	4%			High	
	Granite, fine- to medium-grained (111058)	1%			High	
Degree of inhomogeneity	Low				Medium	Outcrop data, N=18
Metamorphism/alteration	Amphibolite-facies metamorphism				High	Outcrop data, N=18
Mineral fabric (type/orientation)	Mineral stretching lineation	147/34	61		Medium	Outcrop data, N=17. Fisher mean. Trend/plunge and K value

RFM008						
Property	Character	Quantitative estimate			Confidence	Comment
Dominant rock type	Diorite, quartz diorite and gabbro, metamorphic (101033)				High	Outcrop data, N=11
Mineralogical composition (%). Only the dominant minerals are listed	Plagioclase feldspar	40.4–64.6	51.3	5.0	High	Data from outcrop samples, N=11. Range/mean/standard deviation
	Hornblende	10.6–50.6	27.6	11.5		
	Biotite	0–14.2	8.3	5.0		
	Quartz	0–24.6	8.3	7.7		
Grain size	Medium-grained				High	Outcrop data, N=11
Age (million years)		1,891–1,861			High	Regional correlation. Range. Age probably 1,886±1
Structure	Foliated and lineated				High	Outcrop data, N=11
Texture	Equigranular				High	Outcrop data, N=11
Density (kg/m ³)		2,738–3,120	2,934	100	High	Data from outcrop samples, N=14. Range/mean/standard deviation
Porosity (%)		0.25–0.54	0.37	0.07	High	Data from outcrop samples, N=14. Range/mean/standard deviation
Magnetic susceptibility (SI units)		0.00036–0.05592	0.00293	0.01914/0.00254	High	Data from outcrop samples, N=14. Range/geometric mean/standard deviation above/below mean
Electric resistivity in fresh water (ohm m)		5,412–34,227	15,315	12,575/6,905	High	Data from outcrop samples, N=14. Range/geometric mean/standard deviation above/below mean
Uranium content based on gamma ray spectrometric data (weight ppm)		0.0–2.8	1.2	0.9	High	Outcrop data, N=14. Range/mean/standard deviation
Natural exposure rate (microR/h)		0.2–6.4	2.7	1.9	High	Outcrop data, N=14. Range/mean/standard deviation
Subordinate rock type(s) Only the more important components are listed	Pegmatite, pegmatitic granite (101061)				High	Outcrop data, N=11
Degree of inhomogeneity	Low				Medium	Outcrop data, N=11
Metamorphism/alteration	Amphibolite-facies metamorphism				High	Outcrop data, N=11
Mineral fabric (type/orientation)	Tectonic foliation/banding	133/82	39		Medium	Outcrop data, N=12. Fisher mean. Strike/dip and K value
	Mineral stretching lineation	137/41	61		Medium	Outcrop data, N=11. Fisher mean. Trend/plunge and K value

RFM011						
Property	Character	Quantitative estimate			Confidence	Comment
Dominant rock type	Granite to granodiorite, metamorphic (101057)				High	Outcrop data, N=17
Mineralogical composition (%). Only the dominant minerals are listed	Quartz	27.8–45.8	35.6	4.2	High	Data from outcrop samples (N=29) and borehole samples from KFM01A (N=5), KFM02A (N=6) and KFM03A (N=6). Range/mean/standard deviation
	K-feldspar	0.2–36.0	22.5	8.6		
	Plagioclase feldspar	24.0–63.8	35.6	8.5		
	Biotite	0.8–8.2	5.1	1.6		
Grain size	Medium-grained				High	Outcrop data, N=17
Age (million years)		1,891–1,861			High	Regional correlation. Range. Age probably 1,865±3
Structure	Lineated and weakly foliated				High	Outcrop data, N=17
Texture	Equigranular				High	Outcrop data, N=17
Density (kg/m ³)		2,639–2,722	2,657	15	High	Data from outcrop samples (N=45) and borehole samples from KFM01A (N=5), KFM02A (N=8) and KFM03A (N=6). Range/mean/standard deviation
Porosity (%)		0.28–0.66	0.43	0.08	High	Data from outcrop samples (N=45) and borehole samples from KFM01A (N=5), KFM02A (N=8) and KFM03A (N=6). Range/mean/standard deviation
Magnetic susceptibility (SI units)		0.00007–0.02548	0.00442	0.01591/ 0.00346	High	Data from outcrop samples (N=45) and borehole samples from KFM01A (N=5), KFM02A (N=8) and KFM03A (N=6). Range/geometric mean/standard deviation above/below mean
Electric resistivity in fresh water (ohm m)		3,352–54,100	14,727	11,237/ 6,374	High	Data from outcrop samples (N=45) and borehole samples from KFM01A (N=10), KFM02A (N=15) and KFM03A (N=12). Range/geometric mean/standard deviation above/below mean
Uranium content based on gamma ray spectrometric data (weight ppm)		0.8–19.0	4.9	2.3	High	Outcrop data (N=47) and borehole samples from KFM01A (N=5), KFM02A (N=8) and KFM03A (N=6). Range/mean/standard deviation
Natural exposure rate (microR/h)		6.3–19.3	12.4	2.0	High	Outcrop data (N=47) and borehole samples from KFM01A (N=5), KFM02A (N=8) and KFM03A (N=6). Range/mean/standard deviation

RFM011						
Property	Character	Quantitative estimate			Confidence	Comment
Subordinate rock type(s) Only the more important components are listed	Amphibolite (102017)				High	Outcrop data, N=17
	Pegmatite, pegmatitic granite (101061)				High	
Degree of inhomogeneity	Low				High	Outcrop data, N=17
Metamorphism/alteration	Amphibolite-facies metamorphism				High	Outcrop data, N=17
Mineral fabric (type/orientation)	Mineral stretching lineation	141/46	185		Medium	Outcrop data, N=10. Fisher mean. Trend/plunge and K value

RFM012						
Property	Character	Quantitative estimate			Confidence	Comment
Dominant rock type	Granite to granodiorite, metamorphic (101057)	68%			High	Outcrop data, N=7. Borehole data, 177–500 m in KFM04A and boreholes close to nuclear power plant 3. Quantitative estimate from borehole data (KFM04A)
Mineralogical composition (%). Only the dominant minerals are listed	Quartz	27.8–45.8	35.6	4.2	High	Data from outcrop samples (N=29) and borehole samples from KFM01A (N=5), KFM02A (N=6) and KFM03A (N=6). Range/mean/standard deviation
	K-feldspar	0.2–36.0	22.5	8.6		
	Plagioclase feldspar	24.0–63.8	35.6	8.5		
	Biotite	0.8–8.2	5.1	1.6		
Grain size	Fine- to medium-grained				High	Outcrop data, N=7. Borehole data, 177–500 m in KFM04A and boreholes close to nuclear power plant 3
Age (million years)		1,891–1,861			High	Regional correlation. Range. Age probably 1,865±3
Structure	Foliated, lineated, ductile high-strain zones				High	Outcrop data, N=7. Borehole data, 177–500 m in KFM04A and boreholes close to nuclear power plant 3
Texture	Equigranular				High	Outcrop data, N=7. Borehole data, 177–500 m in KFM04A and boreholes close to nuclear power plant 3
Density (kg/m ³)		2,639–2,722	2,657	15	High	Data from outcrop samples (N=45) and borehole samples from KFM01A (N=5), KFM02A (N=8) and KFM03A (N=6). Range/mean/standard deviation
Porosity (%)		0.28–0.66	0.43	0.08	High	Data from outcrop samples (N=45) and borehole samples from KFM01A (N=5), KFM02A (N=8) and KFM03A (N=6). Range/mean/standard deviation

RFM012						
Property	Character	Quantitative estimate			Confidence	Comment
Magnetic susceptibility (SI units)		0.00007–0.02548	0.00442	0.01591/0.00346	High	Data from outcrop samples (N=45) and borehole samples from KFM01A (N=5), KFM02A (N=8) and KFM03A (N=6). Range/geometric mean/standard deviation above/below mean
Electric resistivity in fresh water (ohm m)		3,352–54,100	14,727	11,237/6,374	High	Data from outcrop samples (N=45) and borehole samples from KFM01A (N=10), KFM02A (N=15) and KFM03A (N=12). Range/geometric mean/standard deviation above/below mean
Uranium content based on gamma ray spectrometric data (weight ppm)		0.8–19.0	4.9	2.3	High	Outcrop data (N=47) and borehole samples from KFM01A (N=5), KFM02A (N=8) and KFM03A (N=6). Range/mean/standard deviation
Natural exposure rate (microR/h)		6.3–19.3	12.4	2.0	High	Outcrop data (N=47) and borehole samples from KFM01A (N=5), KFM02A (N=8) and KFM03A (N=6). Range/mean/standard deviation
Subordinate rock type(s) Only the more important components are listed	Granitoid, metamorphic, fine- to medium-grained (101051)	24%			High	Outcrop data, N=7. Borehole data, 177–500 m in KFM04A and boreholes close to nuclear power plant 3. Quantitative estimates from borehole data (KFM04A)
	Pegmatite, pegmatitic granite (101061)	4%			High	
	Amphibolite (102017)	2%			High	
	Felsic to intermediate volcanic rock, metamorphic (103076)	2%			High	
Degree of inhomogeneity	Low				High	Outcrop data, N=7. Borehole data, 177–500 m in KFM04A and boreholes close to nuclear power plant 3
Metamorphism/alteration	Amphibolite-facies metamorphism				High	Outcrop data, N=7. Borehole data, 177–500 m in KFM04A and boreholes close to nuclear power plant 3
Mineral fabric (type/orientation)	Tectonic foliation/ ductile high-strain zone	139/79	36		High	Outcrop data, N=13. Borehole data, 177–500 m in KFM04A, N=95. Fisher mean. Strike/dip and K value
	Mineral stretching lineation	155/37	125		High	

RFM013						
Property	Character	Quantitative estimate			Confidence	Comment
Dominant rock type	Tonalite to granodiorite, metamorphic (101054)				High	Outcrop data, N=45
Mineralogical composition (%). Only the dominant minerals are listed	Quartz	0–45.4	23.4	9.1	High	Data from outcrop samples (N=24) and a borehole sample from KFM03A (N=1). Range/mean/standard deviation
	K-feldspar	0–21.8	5.9	5.4		
	Plagioclase feldspar	19.6–61.4	47.4	9.1		
	Biotite	0–15.6	9.5	4.7		
	Hornblende	0–41.8	10.0	9.1		
Grain size	Medium-grained				High	Outcrop data, N=45
Age (million years)		1,891–1,861			High	Regional correlation. Range. Age probably 1,883±3
Structure	Lineated and weakly foliated				High	Outcrop data, N=45
Texture	Equigranular				High	Outcrop data, N=45
Density (kg/m ³)		2,674–2,831	2,737	43	High	Data from outcrop samples (N=20) and a borehole sample from KFM03A (N=1). Range/mean/standard deviation
Porosity (%)		0.31–0.53	0.40	0.07	High	Data from outcrop samples (N=20) and a borehole sample from KFM03A (N=1). Range/mean/standard deviation
Magnetic susceptibility (SI units)		0.00020–0.03507	0.00185	0.01049/0.00157	High	Data from outcrop samples (N=20) and a borehole sample from KFM03A (N=1). Range/geometric mean/standard deviation above/below mean
Electric resistivity in fresh water (ohm m)		5,921–25,249	14,380	6,715/4,578	High	Data from outcrop samples (N=20) and a borehole sample from KFM03A (N=2). Range/geometric mean/standard deviation above/below mean
Uranium content based on gamma ray spectrometric data (weight ppm)		1.2–7.4	3.6	1.4	High	Outcrop data (N=20) and a borehole sample from KFM03A (N=1). Range/mean/standard deviation
Natural exposure rate (microR/h)		4.7–10.9	7.8	1.8	High	Outcrop data (N=20) and a borehole sample from KFM03A (N=1). Range/mean/standard deviation
Subordinate rock type(s) Only the more important components are listed	Granodiorite (101056)				High	Outcrop data, N=45
	Pegmatite, pegmatitic granite (101061)				High	
	Diorite, quartz diorite and gabbro, metamorphic (101033)				High	
	Amphibolite (102017)				High	

RFM013

Property	Character	Quantitative estimate		Confidence	Comment
Degree of inhomogeneity	High			High	Outcrop data, N=45
Metamorphism/alteration	Amphibolite-facies metamorphism			High	Outcrop data, N=45
Mineral fabric (type/orientation)	Tectonic foliation/ banding	112/57	12	High	Outcrop data, N=31. Fisher mean. Strike/dip and K value
	Mineral stretching lineation	144/36	39	High	Outcrop data, N=41. Fisher mean. Trend/plunge and K value

RFM014						
Property	Character	Quantitative estimate			Confidence	Comment
Dominant rock type	Diorite, quartz diorite and gabbro, metamorphic (101033)				High	Outcrop data, N=8
Mineralogical composition (%). Only the dominant minerals are listed	Plagioclase feldspar	40.4–64.6	51.3	5.0	High	Data from outcrop samples, N=11. Range/mean/standard deviation
	Hornblende	10.6–50.6	27.6	11.5		
	Biotite	0–14.2	8.3	5.0		
	Quartz	0–24.6	8.3	7.7		
Grain size	Medium-grained				High	Outcrop data, N=8
Age (million years)		1,891–1,861			High	Regional correlation. Range. Age probably 1,886±1
Structure	Lineated and weakly foliated				High	Outcrop data, N=8
Texture	Equigranular				High	Outcrop data, N=8
Density (kg/m ³)		2,738–3,120	2,934	100	High	Data from outcrop samples, N=14. Range/mean/standard deviation
Porosity (%)		0.25–0.54	0.37	0.07	High	Data from outcrop samples, N=14. Range/mean/standard deviation
Magnetic susceptibility (SI units)		0.00036–0.00592	0.00293	0.01914/0.00254	High	Data from outcrop samples, N=14. Range/geometric mean/standard deviation above/below mean
Electric resistivity in fresh water (ohm m)		5,412–34,227	15,315	12,575/6,905	High	Data from outcrop samples, N=14. Range/geometric mean/standard deviation above/below mean
Uranium content based on gamma ray spectrometric data (weight ppm)		0.0–2.8	1.2	0.9	High	Outcrop data, N=14. Range/mean/standard deviation
Natural exposure rate (microR/h)		0.2–6.4	2.7	1.9	High	Outcrop data, N=14. Range/mean/standard deviation
Subordinate rock type(s) Only the more important components are listed	Ultramafic rock, metamorphic (101004)				High	Outcrop data, N=8
	Pegmatite, pegmatitic granite (101061)				High	
	Granitoid, metamorphic (111051)				High	
	Felsic to intermediate volcanic rock, metamorphic (103076)				High	
Degree of inhomogeneity	Low				High	Outcrop data, N=8
Metamorphism/alteration	Amphibolite-facies metamorphism				High	Outcrop data, N=8
Mineral fabric (type/orientation)	Mineral stretching lineation	145/41	26		Medium	Outcrop data, N=4. Fisher mean. Trend/plunge and K value

RFM016

Property	Character	Quantitative estimate			Confidence	Comment
Dominant rock type	Diorite, quartz diorite and gabbro, metamorphic (101033)				High	Outcrop data, N=60
Mineralogical composition (%). Only the dominant minerals are listed	Plagioclase feldspar	40.4–64.6	51.3	5.0	High	Data from outcrop samples, N=11. Range/mean/standard deviation
	Hornblende	10.6–50.6	27.6	11.5		
	Biotite	0–14.2	8.3	5.0		
	Quartz	0–24.6	8.3	7.7		
Grain size	Medium-grained				High	Outcrop data, N=60
Age (million years)		1,891–1,861			High	Regional correlation. Range. Age probably 1,886±1
Structure	Lineated and weakly foliated, ductile high strain-zones				High	Outcrop data, N=60
Texture	Equigranular				High	Outcrop data, N=60
Density (kg/m ³)		2,738–3,120	2,934	100	High	Data from outcrop samples, N=14. Range/mean/standard deviation
Porosity (%)		0.25–0.54	0.37	0.07	High	Data from outcrop samples, N=14. Range/mean/standard deviation
Magnetic susceptibility (SI units)		0.00036–0.05592	0.00293	0.01914/0.00254	High	Data from outcrop samples, N=14. Range/geometric mean/standard deviation above/below mean
Electric resistivity in fresh water (ohm m)		5,412–34,227	15,315	12,575/6,905	High	Data from outcrop samples, N=14. Range/geometric mean/standard deviation above/below mean
Uranium content based on gamma ray spectrometric data (weight ppm)		0.0–2.8	1.2	0.9	High	Outcrop data, N=14. Range/mean/standard deviation
Natural exposure rate (microR/h)		0.2–6.4	2.7	1.9	High	Outcrop data, N=14. Range/mean/standard deviation
Subordinate rock type(s) Only the more important components are listed	Pegmatite, pegmatitic granite (101061)				High	Outcrop data, N=60
	Amphibolite (102017)				High	
Degree of inhomogeneity	Low				High	Outcrop data, N=60
Metamorphism/alteration	Amphibolite-facies metamorphism				High	Outcrop data, N=60
Mineral fabric (type/orientation)	Tectonic foliation/banding	334/74	6		Medium	Outcrop data, N=17. Fisher mean. Strike/dip and K value. Variable orientation, reflected in very low K value
Mineral fabric (type/orientation)	Mineral stretching lineation	163/27	18		High	Outcrop data, N=36. Fisher mean. Trend/plunge and K value

RFM017

Property	Character	Quantitative estimate			Confidence	Comment
Dominant rock type	Tonalite to granodiorite, metamorphic (101054)				High	Outcrop data, N=40. Borehole data, HFM18 and 220–293 m in KFM03A. No quantitative estimate is provided. Short borehole section in KFM03A is not considered to be representative for the domain
Mineralogical composition (%). Only the dominant minerals are listed	Quartz	0–45.4	23.4	9.1	High	Data from outcrop samples (N=24) and a borehole sample from KFM03A (N=1). Range/mean/standard deviation
	K-feldspar	0–21.8	5.9	5.4		
	Plagioclase feldspar	19.6–61.4	47.4	9.1		
	Biotite	0–15.6	9.5	4.7		
	Hornblende	0–41.8	10.0	9.1		
Grain size	Medium-grained				High	Outcrop data, N=40. Borehole data, HFM18 and 220–293 m in KFM03A
Age (million years)		1,883	3		High	U-Pb (zircon) age using SIMS technique from sample at 6698336/1634013. 95% confidence interval
Structure	Lineated and weakly foliated				High	Outcrop data, N=40. Borehole data, HFM18 and 220–293 m in KFM03A
Texture	Equigranular				High	Outcrop data, N=40. Borehole data, HFM18 and 220–293 m in KFM03A
Density (kg/m ³)		2,674–2,831	2,737	43	High	Data from outcrop samples (N=20) and a borehole sample from KFM03A (N=1). Range/mean/standard deviation
Porosity (%)		0.31–0.53	0.40	0.07	High	Data from outcrop samples (N=20) and a borehole sample from KFM03A (N=1). Range/mean/standard deviation
Magnetic susceptibility (SI units)		0.00020–0.03507	0.00185	0.01049/0.00157	High	Data from outcrop samples (N=20) and a borehole sample from KFM03A (N=1). Range/mean/standard deviation
Electric resistivity in fresh water (ohm m)		5,921–25,249	14,380	6,715/4,578	High	Data from outcrop samples (N=20) and a borehole sample from KFM03A (N=2). Range/geometric mean/standard deviation above/below mean

RFM017

Property	Character	Quantitative estimate			Confidence	Comment
Uranium content based on gamma ray spectrometric data (weight ppm)		1.2–7.4	3.6	1.4	High	Outcrop data (N=20) and a borehole sample from KFM03A (N=1). Range/geometric mean/standard deviation above/below mean
Natural exposure rate (microR/h)		4.7–10.9	7.8	1.8	High	Outcrop data (N=20) and a borehole sample from KFM03A (N=1). Range/mean/standard deviation
Subordinate rock type(s) Only the more important components are listed	Pegmatite, pegmatitic granite (101061)				High	Outcrop data, N=40. Borehole data, HFM18 and 220–293 m in KFM03A. No quantitative estimate is provided. Short borehole section in KFM03A is not considered to be representative for the domain
	Granitoid (tonalitic), metamorphic, fine- to medium-grained (101051)				High	
Degree of inhomogeneity	Low				High	Outcrop data, N=40. Borehole data, HFM18 and 220–293 m in KFM03A
Metamorphism/alteration	Amphibolite-facies metamorphism				High	Outcrop data, N=40. Borehole data, HFM18 and 220–293 m in KFM03A
Mineral fabric (type/orientation)	Tectonic foliation	126/23 (pole to best-fit great circle)			High	Outcrop data, N=31. Borehole data, 220–293 m in KFM03A, N=2. Foliation folded. Pole to best-fit great circle provided
	Mineral stretching lineation	134/32	21		High	Outcrop data, N=31. Fisher mean. Trend/plunge and K value

RFM018						
Property	Character	Quantitative estimate			Confidence	Comment
Dominant rock type	Tonalite to granodiorite, metamorphic (101054)				High	Outcrop data, N=99. Borehole data, HFM09, HFM10, 12–177 m in KFM04A and boreholes close to power plant 3. No quantitative estimate is provided. Short borehole sections are not considered to be representative for the domain
Mineralogical composition (%). Only the dominant minerals are listed	Quartz	0–45.4	23.4	9.1	High	Data from outcrop samples (N=24) and a borehole sample from KFM03A (N=1). Range/mean/standard deviation
	K-feldspar	0–21.8	5.9	5.4		
	Plagioclase feldspar	19.6–61.4	47.4	9.1		
	Biotite	0–15.6	9.5	4.7		
	Hornblende	0–41.8	10.0	9.1		
Grain size	Fine- to medium-grained				High	Outcrop data, N=99. Borehole data, HFM09, HFM10, 12–177 m in KFM04A and boreholes close to power plant 3.
Age (million years)		1,891–1,861			High	Regional correlation. Range. Age probably 1,883±3
Structure	Foliated, banded and lineated				High	Outcrop data, N=99. Borehole data, HFM09, HFM10, 12–177 m in KFM04A and boreholes close to power plant 3.
Texture	Equigranular				High	Outcrop data, N=99. Borehole data, HFM09, HFM10, 12–177 m in KFM04A and boreholes close to power plant 3.
Density (kg/m ³)		2,674–2,831	2,737	43	High	Data from outcrop samples (N=20) and a borehole sample from KFM03A (N=1). Range/mean/standard deviation
Porosity (%)		0.31–0.53	0.40	0.07	High	Data from outcrop samples (N=20) and a borehole sample from KFM03A (N=1). Range/mean/standard deviation
Magnetic susceptibility (SI units)		0.00020–0.03507	0.00185	0.01049/0.00157	High	Data from outcrop samples (N=20) and a borehole sample from KFM03A (N=1). Range/geometric mean/standard deviation above/below mean
Electric resistivity in fresh water (ohm m)		5,921–25,249	14,380	6,715/4,578	High	Data from outcrop samples (N=20) and a borehole sample from KFM03A (N=2). Range/geometric mean/standard deviation above/below mean
Uranium content based on gamma ray spectrometric data (weight ppm)		1.2–7.4	3.6	1.4	High	Outcrop data (N=20) and a borehole sample from KFM03A (N=1). Range/mean/standard deviation

RFM018

Property	Character	Quantitative estimate			Confidence	Comment
Natural exposure rate (microR/h)		4.7–10.9	7.8	1.8	High	Outcrop data (N=20) and a borehole sample from KFM03A (N=1). Range/mean/standard deviation
Subordinate rock type(s) Only the more important components are listed	Granite to granodiorite, metamorphic (101057)				High	Outcrop data, N=99. Borehole data, HFM09, HFM10, 12–177 m in KFM04A and boreholes close to power plant 3. No quantitative estimate is provided. Short borehole sections are not considered to be representative for the domain
	Granodiorite, metamorphic (101056)				High	
	Felsic to intermediate volcanic rock, metamorphic (103076)				High	
	Pegmatite, pegmatitic granite (101061)				High	
	Amphibolite (102017)				High	
	Granitoid, metamorphic, fine- to medium-grained (101051)				High	
	Diorite, quartz diorite and gabbro, metamorphic (101033)				High	
	Granite, fine- to medium-grained (111058)				High	
	Magnetite mineralisation associated with calc-silicate rock (109014)				High	Mineralisations in felsic metavolcanic rocks where mining or exploration activity has taken place in historical time
Degree of inhomogeneity	High				High	Outcrop data, N=99. Borehole data, 12–177 m in KFM04A and boreholes close to power plant 3.
Metamorphism/alteration	Amphibolite-facies metamorphism				High	Outcrop data, N=99. Borehole data, 12–177 m in KFM04A and boreholes close to power plant 3.
Mineral fabric (type/orientation)	Tectonic foliation/banding/ductile high-strain zone	141/81	44		High	Outcrop data, N=87. Borehole data, 12–177 m in KFM04A, N=26. Fisher mean. Strike/dip and K value.
	Mineral stretching lineation	143/35	84		High	Outcrop data, N=87. Borehole data, 12–177 m in KFM04A, N=26. Fisher mean. Trend/plunge and K value

RFM020						
Property	Character	Quantitative estimate			Confidence	Comment
Dominant rock type	Granite, metamorphic, aplitic (101058)				Medium	Outcrop data, N=7. Tunnel data. Borehole data along tunnels
Mineralogical composition (%). Only the dominant minerals are listed	Quartz	30.8–44.4	37.3	4.4	High	Data from outcrop samples, N=7. Range/mean/standard deviation
	K-feldspar	4.0–47.0	22.9	15.9		
	Plagioclase feldspar	18.8–58.2	37.1	15.8		
	Biotite	0–2.0	1.1	0.9		
Grain size	Fine-grained (and leucocratic)				Medium	Outcrop data, N=7. Tunnel data. Borehole data along tunnels
Age (million years)		1,891–1,861			High	Regional correlation. Range. Age possibly 1,865±3
Structure	Lineated and weakly foliated				Medium	Outcrop data, N=7. Tunnel data. Borehole data along tunnels
Texture	Equigranular				Medium	Outcrop data, N=7. Tunnel data. Borehole data along tunnels
Density (kg/m ³)		2,620–2,646	2,635	9	Medium	Data from outcrop samples, N=7. Range/mean/standard deviation
Porosity (%)		0.36–0.48	0.40	0.05	Medium	Data from outcrop samples, N=7. Range/mean/standard deviation
Magnetic susceptibility (SI units)		0.00179–0.01722	0.00657	0.00691/0.00337	Medium	Data from outcrop samples, N=7. Range/geometric mean/standard deviation above/below mean
Electric resistivity in fresh water (ohm m)		11,467–27,915	15,876	5,288/3,967	Medium	Data from outcrop samples, N=7. Range/geometric mean/standard deviation above/below mean
Uranium content based on gamma ray spectrometric data (weight ppm)		3.3–7.6	5.3	1.4	Medium	Outcrop data, N=9. Range/mean/standard deviation
Natural exposure rate (microR/h)		8.3–18.9	12.8	3.3	Medium	Outcrop data, N=9. Range/mean/standard deviation
Subordinate rock type(s) Only the more important components are listed	Pegmatite, pegmatitic granite (101061)				Medium	Outcrop data, N=7. Tunnel data. Borehole data along tunnels
	Granite to granodiorite, metamorphic (101057)				Medium	
	Amphibolite (102017)				Medium	
Degree of inhomogeneity	High				Medium	Outcrop data, N=7. Tunnel data. Borehole data along tunnels
Metamorphism/alteration	Amphibolite-facies metamorphism				High	Outcrop data, N=7. Tunnel data. Borehole data along tunnels
Mineral fabric (type/orientation)	Tectonic foliation/banding	120/84	87		Medium	Outcrop data, N=5. Fisher mean. Strike/dip and K value
	Mineral stretching lineation	123/40	87		Medium	Outcrop data, N=7. Fisher mean. Trend/plunge and K value

RFM021

Property	Character	Quantitative estimate			Confidence	Comment
Dominant rock type	Felsic to intermediate volcanic rock, metamorphic (103076)				High	Outcrop data, N=98. Tunnel data. Borehole data along tunnels. Includes SFR
Mineralogical composition (%). Only the dominant minerals are listed	Quartz	5.2–39.2	26.0	10.3	High	Data from outcrop samples, N=15. Range/mean/standard deviation
	K-feldspar	0–12.6	3.4	4.1		
	Plagioclase feldspar	29.2–53.2	48.6	6.5		
	Biotite	0–22.8	12.0	8.0		
	Hornblende	0–35.6				
Grain size	Fine-grained				High	Outcrop data, N=98. Tunnel data. Borehole data along tunnels. Includes SFR
Age (million years)		1,906–1,891			High	Regional correlation. Range
Structure	Foliated, lineated, in part banded, folded				High	Outcrop data, N=98. Tunnel data. Borehole data along tunnels. Includes SFR
Texture	Equigranular				High	Outcrop data, N=98. Tunnel data. Borehole data along tunnels. Includes SFR
Density (kg/m ³)		2,648–2,946	2,732	79	High	Data from outcrop samples, N=19. Range/mean/standard deviation
Porosity (%)		0.20–0.62	0.37	0.11	High	Data from outcrop samples, N=19. Range/mean/standard deviation
Magnetic susceptibility (SI units)		0.00006–0.24000	0.00235	0.04163/ 0.00222	High	Data from outcrop samples, N=19. Range/geometric mean/standard deviation above/below mean
Electric resistivity in fresh water (ohm m)		1,725–81,878	14,374	22,146/ 8,716	High	Data from outcrop samples, N=19. Range/geometric mean/standard deviation above/below mean
Uranium content based on gamma ray spectrometric data (weight ppm)		2.5–6.8	4.3	1.0	High	Outcrop data N=19. Range/mean/standard deviation
Natural exposure rate (microR/h)		5.2–13.4	9.4	2.5	High	Outcrop data, N=19. Range/mean/standard deviation

RFM021						
Property	Character	Quantitative estimate		Confidence	Comment	
Subordinate rock type(s) Only the more important components are listed	Pegmatite, pegmatitic granite (101061)			High	Outcrop data, N=98. Tunnel data. Borehole data along tunnels. Includes SFR	
	Diorite, quartz diorite and gabbro, metamorphic (101033)			High		
	Amphibolite (102017)			High	Outcrop data, N=98. Tunnel data. Borehole data along tunnels. Includes SFR	
	Granitoid, metamorphic (111051)			High		
	Granite, fine- to medium-grained (111058)			High		
	Granitoid, metamorphic, fine- to medium-grained (101051)			High		
Degree of inhomogeneity	High			High	Outcrop data, N=98. Tunnel data. Borehole data along tunnels. Includes SFR	
Metamorphism/alteration	1. In part, pre-metamorphic K-Na alteration. 2. Amphibolite-facies metamorphism			High	Outcrop data, N=98. Tunnel data. Borehole data along tunnels. Includes SFR	
Mineral fabric (type/orientation)	Tectonic foliation/banding	124/64		(pole to best-fit great circle)	High	Outcrop data in subarea NW, northwest of SFR, N=52. Foliation/banding folded. Pole to best-fit great circle provided
	Tectonic foliation/banding	127/83	20		High	Outcrop data in subarea SE, N=35. Fisher mean Strike/dip and K value
	Mineral stretching lineation	132/31	7		High	Outcrop data in entire domain, N=27. Fisher mean. Trend/plunge and K value. Variable plunge steers low K value
	Fold axis	134/58	7		High	Outcrop data in subarea NW, N=18. Fisher mean. Trend/plunge and K value
Mineral fabric (type/orientation)	Fold axis	135/37	19		High	Outcrop data in subarea SE, N=20. Fisher mean. Trend/plunge and K value

RFM022

Property	Character	Quantitative estimate			Confidence	Comment
Dominant rock type	Granite, fine- to medium-grained (111058)				Medium	Outcrop data, N=18
Mineralogical composition (%). Only the dominant minerals are listed	Quartz	25.4–42.8	32.4	6.4	High	Data from outcrop samples (N=4) and a borehole sample from KFM03A (N=1). Range/mean/standard deviation
	K-feldspar	22.6–37.8	29.6	5.6		
	Plagioclase feldspar	22.0–46.2	33.0	9.3		
	Biotite	0.6–4.4	2.7	1.6		
Grain size	Fine- to medium-grained				Medium	Outcrop data, N=18
Age (million years)		1,851	5		Medium	Regional correlation. Age and 95% confidence interval
Structure	Isotropic or weakly lineated and foliated				Medium	Outcrop data, N=18
Texture	Equigranular				Medium	Outcrop data, N=18
Density (kg/m ³)		2,627–2,645	2,638	9	Low	Data from outcrop samples (N=2) and a borehole sample from KFM03A (N=1). Range/mean/standard deviation
Porosity (%)		0.48–0.69	0.50	0.02	Low	Data from outcrop samples (N=2) and a borehole sample from KFM03A (N=1). Range/mean/standard deviation
Magnetic susceptibility (SI units)		0.00010–0.00573	0.00085	0.00408/0.00070	Low	Data from outcrop samples (N=3) and a borehole sample from KFM03A (N=1). Range/geometric mean/standard deviation above/below mean
Electric resistivity in fresh water (ohm m)		6,974–13,017	8,849	2,770/2,115	Low	Data from outcrop samples (N=2) and borehole samples from KFM03A (N=2). Range/geometric mean/standard deviation above/below mean
Uranium content based on gamma ray spectrometric data (weight ppm)		3.4–14.9	8.3	3.8	Low	Outcrop data (N=5) and a borehole sample from KFM03A (N=1). Range/mean/standard deviation
Natural exposure rate (microR/h)		12.7–22.9	19.0	3.6	Low	Outcrop data (N=5) and a borehole sample from KFM03A (N=1). Range/mean/standard deviation
Subordinate rock type(s) Only the more important components are listed	Pegmatite, pegmatitic granite (101061)				Medium	Outcrop data, N=18
	Felsic to intermediate volcanic rock, metamorphic (103076)				Medium	
Degree of inhomogeneity	Low				Medium	Outcrop data, N=18
Metamorphism/alteration						Outcrop data, N=18. Uncertain

RFM022						
Property	Character	Quantitative estimate			Confidence	Comment
Mineral fabric (type/orientation)	Tectonic foliation	319/72	15		Medium	Outcrop data, N=7. Fisher mean. Strike/plunge and K value
	Mineral stretching lineation	137/22	19		Medium	Outcrop data, N=7. Fisher mean. Trend/plunge and K value

RFM023						
Property	Character	Quantitative estimate			Confidence	Comment
Dominant rock type	Tonalite to granodiorite, metamorphic (101054)				High	Outcrop data, N=77. Borehole data, 270.70– 478.30 m in KFO01
Mineralogical composition (%). Only the dominant minerals are listed	Quartz	0–45.4	23.4	9.1	High	Data from outcrop samples (N=24) and a borehole sample from KFM03A (N=1). Range/mean/standard deviation
	K-feldspar	0–21.8	5.9	5.4		
	Plagioclase feldspar	19.6–61.4	47.4	9.1		
	Biotite	0–15.6	9.5	4.7		
	Hornblende	0–41.8	10.0	9.1		
Grain size	Medium-grained				High	Outcrop data, N=77. Borehole data, 270.70– 478.30 m in KFO01
Age (million years)		1,891–1,861			High	Regional correlation. Range. Age probably 1,883±3
Structure	Lineated and weakly foliated				High	Outcrop data, N=77. Borehole data, 270.70– 478.30 m in KFO01
Texture	Equigranular				High	Outcrop data, N=77. Borehole data, 270.70– 478.30 m in KFO01
Density (kg/m ³)		2,674– 2,831	2,737	43	High	Data from outcrop samples (N=20) and a borehole sample from KFM03A (N=1). Range/mean/standard deviation
Porosity (%)		0.31–0.53	0.40	0.07	High	Data from outcrop samples (N=20) and a borehole sample from KFM03A (N=1). Range/mean/standard deviation
Magnetic susceptibility (SI units)		0.00020– 0.03507	0.00185	0.01049/ 0.00157	High	Data from outcrop samples (N=20) and a borehole sample from KFM03A (N=1). Range/geometric mean/ standard deviation above/ below mean
Electric resistivity in fresh water (ohm m)		5,921– 25,249	14,380	6,715/ 4,578	High	Data from outcrop samples (N=20) and a borehole sample from KFM03A (N=2). Range/geometric mean/ standard deviation above/ below mean

RFM023						
Property	Character	Quantitative estimate			Confidence	Comment
Uranium content based on gamma ray spectrometric data (weight ppm)		1.2–7.4	3.6	1.4	High	Outcrop data (N=20) and a borehole sample from KFM03A (N=1). Range/mean/standard deviation
Natural exposure rate (microR/h)		4.7–10.9	7.8	1.8	High	Outcrop data (N=20) and a borehole sample from KFM03A (N=1). Range/mean/standard deviation
Subordinate rock type(s) Only the more important components are listed	Pegmatite, pegmatitic granite (101061)				High	Outcrop data, N=77. Borehole data, 270.70–478.30 m in KFO01
	Granite to granodiorite, metamorphic (101057)				High	
	Diorite, quartz diorite and gabbro, metamorphic (101033)				High	
	Amphibolite (102017)				High	
	Granitoid, metamorphic, fine- to medium-grained (101051)				High	
	Granite, Fine- to medium-grained (111058)				High	
Degree of inhomogeneity	Low				Medium	Outcrop data, N=77. Borehole data, 270.70–478.30 m in KFO01
Metamorphism/alteration	Amphibolite-facies metamorphism				High	Outcrop data, N=77. Borehole data, 270.70–478.30 m in KFO01
Mineral fabric (type/orientation)	Tectonic foliation/banding	140/25 (pole to best-fit great circle)			High	Outcrop data, N=34. Foliation/banding folded. Pole to best-fit great circle provided
	Mineral stretching lineation	144/33	36		High	Outcrop data, N=97. Fisher mean. Trend/plunge and K value

RFM024						
Property	Character	Quantitative estimate			Confidence	Comment
Dominant rock type	Tonalite to granodiorite, metamorphic (101054)				High	Outcrop data, N=228
Mineralogical composition (%). Only the dominant minerals are listed	Quartz	0–45.4	23.4	9.1	High	Data from outcrop samples (N=24) and a borehole sample from KFM03A (N=1). Range/mean/standard deviation
	K-feldspar	0–21.8	5.9	5.4		
	Plagioclase feldspar	19.6–61.4	47.4	9.1		
	Biotite	0–15.6	9.5	4.7		
	Hornblende	0–41.8	10.0	9.1		
Grain size	Medium-grained				High	Outcrop data, N=77
Age (million years)		1,891–1,861			High	Regional correlation. Range. Age probably 1,883±3
Structure	Lineated and weakly foliated				High	Outcrop data, N=228
Texture	Equigranular, locally porphyritic				High	Outcrop data, N=228

RFM024						
Property	Character	Quantitative estimate			Confidence	Comment
Density (kg/m ³)		2,674– 2,831	2,737	43	High	Data from outcrop samples (N=20) and a borehole sample from KFM03A (N=1). Range/mean/standard deviation
Porosity (%)		0.31–0.53	0.40	0.07	High	Data from outcrop samples (N=20) and a borehole sample from KFM03A (N=1). Range/mean/standard deviation
Magnetic susceptibility (SI units)		0.00020– 0.03507	0.00185	0.01049/ 0.00157	High	Data from outcrop samples (N=20) and a borehole sample from KFM03A (N=1). Range/geometric mean/standard deviation above/below mean
Electric resistivity in fresh water (ohm m)		5,921– 25,249	14,380	6,715/ 4,578	High	Data from outcrop samples (N=20) and a borehole sample from KFM03A (N=2). Range/geometric mean/standard deviation above/below mean
Uranium content based on gamma ray spectrometric data (weight ppm)		1.2–7.4	3.6	1.4	High	Outcrop data (N=20) and a borehole sample from KFM03A (N=1). Range/mean/standard deviation
Natural exposure rate (microR/h)		4.7–10.9	7.8	1.8	High	Outcrop data (N=20) and a borehole sample from KFM03A (N=1). Range/mean/standard deviation
Subordinate rock type(s) Only the more important components are listed	Granodiorite, metamorphic (101056)				High	Outcrop data, N=228
	Granite to granodiorite, metamorphic (101057)				High	
	Diorite, quartz diorite and gabbro, metamorphic (101033)				High	
	Pegmatite, pegmatitic granite (101061)				High	
	Amphibolite (102017)				High	
	Granite, metamorphic, aplitic (101058)				High	
Degree of inhomogeneity	Low				High	Outcrop data, N=228
Metamorphism/alteration	Amphibolite-facies metamorphism				High	Outcrop data, N=228
Mineral fabric (type/orientation)	Tectonic foliation/banding	118/73	18		High	Outcrop data, N=69. Fisher mean. Strike/dip and K value
	Mineral stretching lineation	131/38	45		High	Outcrop data, N=247. Fisher mean. Trend/plunge and K value

RFM025						
Property	Character	Quantitative estimate			Confidence	Comment
Dominant rock type	Diorite, quartz diorite and gabbro, metamorphic (101033)				High	Outcrop data, N=43
Mineralogical composition (%). Only the dominant minerals are listed	Plagioclase feldspar	40.4–64.6	51.3	5.0	High	Data from outcrop samples, N=11. Range/mean/standard deviation
	Hornblende	10.6–50.6	27.6	11.5		
	Biotite	0–14.2	8.3	5.0		
	Quartz	0–24.6	8.3	7.7		
Grain size	Medium-grained				High	Outcrop data, N=43
Age (million years)		1,886	1		High	U-Pb (zircon) age using TIMS technique from sample at 6699652/1630093. 95% confidence interval
Structure	Lineated and weakly foliated				High	Outcrop data, N=43
Texture	Equigranular				High	Outcrop data, N=43
Density (kg/m ³)		2,738–3,120	2,934	100	High	Data from outcrop samples, N=14. Range/mean/standard deviation
Porosity (%)		0.25–0.54	0.37	0.07	High	Data from outcrop samples, N=14. Range/mean/standard deviation
Magnetic susceptibility (SI units)		0.00036–0.05592	0.00293	0.01914/0.00254	High	Data from outcrop samples, N=14. Range/geometric mean/standard deviation above/below mean
Electric resistivity in fresh water (ohm m)		5,412–34,227	15,315	12,575/6,905	High	Data from outcrop samples, N=14. Range/geometric mean/standard deviation above/below mean
Uranium content based on gamma ray spectrometric data (weight ppm)		0.0–2.8	1.2	0.9	High	Outcrop data, N=14. Range/mean/standard deviation
Natural exposure rate (microR/h)		0.2–6.4	2.7	1.9	High	Outcrop data, N=14. Range/mean/standard deviation
Subordinate rock type(s) Only the more important components are listed	Pegmatite, pegmatitic granite (101061)				High	Outcrop data, N=43
	Amphibolite (102017)				High	
	Tonalite to granodiorite, metamorphic (101054)				High	
Degree of inhomogeneity	Low				High	Outcrop data, N=43
Metamorphism/alteration	Amphibolite-facies metamorphism				High	Outcrop data, N=43
Mineral fabric (type/orientation)	Tectonic foliation/banding	146/88	44		High	Outcrop data, N=47. Fisher mean. Strike/dip and K value
	Mineral stretching lineation	145/42	33		High	Outcrop data, N=23. Fisher mean. Trend/plunge and K value

RFM026						
Property	Character	Quantitative estimate			Confidence	Comment
Dominant rock type	Granite to granodiorite, metamorphic (101057)				High	Outcrop data, N=144. Borehole data, HFM11, HFM12
Mineralogical composition (%). Only the dominant minerals are listed	Quartz	27.8–45.8	35.6	4.2	High	Data from outcrop samples (N=29) and borehole samples from KFM01A (N=5), KFM02A (N=6) and KFM03A (N=6). Range/mean/standard deviation
	K-feldspar	0.2–36.0	22.5	8.6		
	Plagioclase feldspar	24.0–63.8	35.6	8.5		
	Biotite	0.8–8.2	5.1	1.6		
Grain size	Medium-grained				High	Outcrop data, N=144. Borehole data, HFM11, HFM12
Age (million years)		1,891–1,861			High	Regional correlation. Range. Age probably 1,865±3
Structure	Foliated, lineated, ductile high-strain zones				High	Outcrop data, N=144. Borehole data, HFM11, HFM12
Texture	Equigranular				High	Outcrop data, N=144. Borehole data, HFM11, HFM12
Density (kg/m ³)		2,639–2,722	2,657	15	High	Data from outcrop samples (N=45) and borehole samples from KFM01A (N=5), KFM02A (N=8) and KFM03A (N=6). Range/mean/standard deviation
Porosity (%)		0.28–0.66	0.43	0.08	High	Data from outcrop samples (N=45) and borehole samples from KFM01A (N=5), KFM02A (N=8) and KFM03A (N=6). Range/mean/standard deviation
Magnetic susceptibility (SI units)		0.00007–0.02548	0.00442	0.01591/0.00346	High	Data from outcrop samples (N=45) and borehole samples from KFM01A (N=5), KFM02A (N=8) and KFM03A (N=6). Range/geometric mean/standard deviation above/below mean
Electric resistivity in fresh water (ohm m)		3,352–54,100	14,727	11,237/6,374	High	Data from outcrop samples (N=45) and borehole samples from KFM01A (N=10), KFM02A (N=15) and KFM03A (N=12). Range/geometric mean/standard deviation above/below mean
Uranium content based on gamma ray spectrometric data (weight ppm)		0.8–19.0	4.9	2.3	High	Outcrop data (N=47) and borehole samples from KFM01A (N=5), KFM02A (N=8) and KFM03A (N=6). Range/mean/standard deviation

RFM026

Property	Character	Quantitative estimate			Confidence	Comment
Natural exposure rate (microR/h)		6.3–19.3	12.4	2.0	High	Outcrop data (N=47) and borehole samples from KFM01A (N=5), KFM02A (N=8) and KFM03A (N=6). Range/mean/standard deviation
Subordinate rock type(s) Only the more important components are listed	Granite, metamorphic, aplitic (101058)				High	Outcrop data, N=144. Borehole data, HFM11, HFM12
	Granodiorite, metamorphic (101056)				High	
	Pegmatite, pegmatitic granite (101061)				High	
	Diorite, quartz diorite and gabbro, metamorphic (101033)				High	
	Felsic to intermediate volcanic rock, metamorphic (103076)				High	
	Amphibolite (102017)				High	
Degree of inhomogeneity	Low				High	Outcrop data, N=144. Borehole data, HFM11, HFM12
Metamorphism/alteration	Amphibolite-facies metamorphism				High	Outcrop data, N=144. Borehole data, HFM11, HFM12
Mineral fabric (type/orientation)	Tectonic foliation/ banding/ ductile high-strain zone	138/87		23	High	Outcrop data, N=91. Fisher mean. Strike/dip and K value
	Mineral stretching lineation	139/41		50	High	Outcrop data, N=83. Fisher mean. Trend/plunge and K value

RFM029

Property	Character	Quantitative estimate			Confidence	Comment
Dominant rock type	Granite to granodiorite, metamorphic (101057)	84%			High	Outcrop data, N=488. Tunnel data. Borehole data including KFM01A, KFM01B, KFM02A, KFM03A except 220–293 m, KFM03B, 500–1001.5 m in KFM04A, and boreholes close to nuclear power plants 1–2, barrack area and tunnels. Quantitative estimate from all the KFM boreholes except KFM03B
Mineralogical composition (%). Only the dominant minerals are listed	Quartz	27.8–45.8	35.6	4.2	High	Data from outcrop samples (N=29) and borehole samples from KFM01A (N=5), KFM02A (N=6) and KFM03A (N=6). Range/mean/standard deviation
	K-feldspar	0.2–36.0	22.5	8.6		
	Plagioclase feldspar	24.0–63.8	35.6	8.5		
	Biotite	0.8–8.2	5.1	1.6		
Grain size	Medium-grained				High	Outcrop data, N=488. Tunnel data. Borehole data including KFM01A, KFM01B, KFM02A, KFM03A except 220–293 m, KFM03B, 500–1001.5 m in KFM04A, and boreholes close to nuclear power plants 1–2, barrack area and tunnels
Age (million years)		1,865	3		High	U-Pb (zircon) age using SIMS technique from sample at 6699740/1632290. 95% confidence interval
Structure	Lineated and weakly foliated. More strongly foliated along southwestern and northeastern margins. In part folded				High	Outcrop data, N=488. Tunnel data. Borehole data including KFM01A, KFM01B, KFM02A, KFM03A except 220–293 m, KFM03B, 500–1001.5 m in KFM04A, and boreholes close to nuclear power plants 1–2, barrack area and tunnels
Texture	Equigranular				High	Outcrop data, N=488. Tunnel data. Borehole data including KFM01A, KFM01B, KFM02A, KFM03A except 220–293 m, KFM03B, 500–1001.5 m in KFM04A, and boreholes close to nuclear power plants 1–2, barrack area and tunnels
Density (kg/m ³)		2,639–2,722	2,657	15	High	Data from outcrop samples (N=45) and borehole samples from KFM01A (N=5), KFM02A (N=8) and KFM03A (N=6). Range/mean/standard deviation

RFM029

Property	Character	Quantitative estimate			Confidence	Comment
Porosity (%)		0.28–0.66	0.43	0.08	High	Data from outcrop samples (N=45) and borehole samples from KFM01A (N=5), KFM02A (N=8) and KFM03A (N=6). Range/mean/standard deviation
Magnetic susceptibility (SI units)		0.00007–0.02548	0.00442	0.01591/0.00346	High	Data from outcrop samples (N=45) and borehole samples from KFM01A (N=5), KFM02A (N=8) and KFM03A (N=6). Range/geometric mean/standard deviation above/below mean
Electric resistivity in fresh water (ohm m)		3,352–54,100	14,727	11,237/6,374	High	Data from outcrop samples (N=45) and borehole samples from KFM01A (N=10), KFM02A (N=15) and KFM03A (N=12). Range/geometric mean/standard deviation above/below mean
Uranium content based on gamma ray spectrometric data (weight ppm)		0.8–19.0	4.9	2.3	High	Outcrop data (N=47) and borehole samples from KFM01A (N=5), KFM02A (N=8) and KFM03A (N=6). Range/mean/standard deviation
Natural exposure rate (microR/h)		6.3–19.3	12.4	2.0	High	Outcrop data (N=47) and borehole samples from KFM01A (N=5), KFM02A (N=8) and KFM03A (N=6). Range/mean/standard deviation
Subordinate rock type(s) Only the more important components are listed	Granitoid, metamorphic, fine- to medium-grained (101051)	10% (Suspected to be overestimated in the boreholes)			Medium	Outcrop data, N=488. Tunnel data. Borehole data including KFM01A, KFM01B, KFM02A, KFM03A except 220–293 m, KFM03B, 500–1001.5 m in KFM04A, and boreholes close to nuclear power plants 1–2, barrack area and tunnels. Occurs as small, irregular and dyke-like bodies. Uniformly distributed. Quantitative estimate from all boreholes except KFM03B

RFM029

Property	Character	Quantitative estimate	Confidence	Comment
	Amphibolite (102017)	3%	High	Outcrop data, N=488. Tunnel data. Borehole data including KFM01A, KFM01B, KFM02A, KFM03A except 220–293 m, KFM03B, 500–1001.5 m in KFM04A, and boreholes close to nuclear power plants 1–2, barrack area and tunnels. Occurs as small, irregular and dyke-like bodies. Uniformly distributed. Quantitative estimate from all boreholes except KFM03B
Subordinate rock type(s) Only the more important components are listed	Pegmatite, pegmatitic granite (101061)	2%	High	Outcrop data, N=488. Tunnel data. Borehole data including KFM01A, KFM01B, KFM02A, KFM03A except 220–293 m, KFM03B, 500–1001.5 m in KFM04A, and boreholes close to nuclear power plants 1–2, barrack area and tunnels. Occurs as small irregular bodies and dykes. Volumetrically more significant at shallow depths in the southeastern part of the candidate area (e.g. <100 m at drillsite 3). Quantitative estimate from all boreholes except KFM03B
	Granite, fine- to medium-grained (111058)	1% (Suspected to be underestimated in the boreholes)	Medium	Outcrop data, N=488. Tunnel data. Borehole data including KFM01A, KFM01B, KFM02A, KFM03A except 220–293 m, KFM03B, 500–1001.5 m in KFM04A, and boreholes close to nuclear power plants 1–2, barrack area and tunnels. Occurs as narrow dykes. Contacts sealed. Uniformly distributed. Quantitative estimate from all boreholes except KFM03B
	Granite, metamorphic, aplitic (101058)	Not observed in sufficient quantity in the boreholes	High for occurrence	Outcrop data, N=488. Occurs as small, irregular bodies. Volumetrically significant at the surface in the northwesternmost part of the candidate area and close to the nuclear power plants 1–2

RFM029

Property	Character	Quantitative estimate		Confidence	Comment
Degree of inhomogeneity	Low			High	Outcrop data, N=488. Tunnel data. Borehole data including KFM01A, KFM01B, KFM02A, KFM03A except 220–293 m, KFM03B, 500–1001.5 m in KFM04A, and boreholes close to nuclear power plants 1–2, barrack area and tunnels
Metamorphism/alteration	1. In part, pre-metamorphic K-Na alteration. 2. Amphibolite-facies metamorphism			High	Outcrop data, N=488. Tunnel data. Borehole data including KFM01A, KFM01B, KFM02A, KFM03A except 220–293 m, KFM03B, 500–1001.5 m in KFM04A and boreholes close to nuclear power plants 1–2, barrack area and tunnels. Pre-metamorphic K-Na alteration is conspicuous close to RFM032, in the northwesternmost part of the candidate area and close to the nuclear power plants 1–2. Some indications also in KFM01A
Mineral fabric (type/orientation)	Tectonic foliation	143/45 (pole to best-fit great circle)		High	Outcrop data, N=338. Foliation folded. Pole to best-fit great circle provided
	Tectonic foliation/ ductile high-strain zone	163/41 (pole to best-fit great circle)		High	Borehole data from KFM01A, KFM01B, KFM02A, KFM03A except 220–293 m, KFM03B and 500–1001.5 m in KFM04A N=300. Foliation and ductile high-strain zones folded. Pole to best-fit great circle provided
Mineral fabric (type/orientation)	Tectonic foliation/ ductile high-strain zone	154/45 (pole to best-fit great circle)		High	Outcrop data (N=338) combined with borehole data from KFM01A, KFM01B, KFM02A, KFM03A except 220–293 m, KFM03B and 500–1001.5 m in KFM04A (N=300). Foliation and ductile high-strain zones folded. Pole to best-fit great circle provided
	Mineral stretching lineation	142/38	62	High	Outcrop data, N=248. Fisher mean. Trend/plunge and K value
	Fold axis	126/38	26	High	Outcrop data, N=6. Fisher mean. Trend/plunge and K value

RFM030						
Property	Character	Quantitative estimate			Confidence	Comment
Dominant rock type	Tonalite to granodiorite, metamorphic (101054)				High	Outcrop data, N=274
Mineralogical composition (%). Only the dominant minerals are listed	Quartz	0–45.4	23.4	9.1	High	Data from outcrop samples (N=24) and a borehole sample from KFM03A (N=1). Range/mean/standard deviation
	K-feldspar	0–21.8	5.9	5.4		
	Plagioclase feldspar	19.6–61.4	47.4	9.1		
	Biotite	0–15.6	9.5	4.7		
	Hornblende	0–41.8	10.0	9.1		
Grain size	Medium-grained, locally fine-grained				High	Outcrop data, N=274
Age (million years)		1,891–1,861			High	Regional correlation. Range. Age probably 1,883±3
Structure	Banded, foliated and lineated. In part folded				High	Outcrop data, N=274
Texture	Equigranular, locally porphyritic				High	Outcrop data, N=274
Density (kg/m ³)		2,674–2,831	2,737	43	High	Data from outcrop samples (N=20) and a borehole sample from KFM03A (N=1). Range/mean/standard deviation
Porosity (%)		0.31–0.53	0.40	0.07	High	Data from outcrop samples (N=20) and a borehole sample from KFM03A (N=1). Range/mean/standard deviation
Magnetic susceptibility (SI units)		0.00020–0.03507	0.00185	0.01049/0.00157	High	Data from outcrop samples (N=20) and a borehole sample from KFM03A (N=1). Range/geometric mean/standard deviation above/below mean
Electric resistivity in fresh water (ohm m)		5,921–25,249	14,380	6,715/4,578	High	Data from outcrop samples (N=20) and a borehole sample from KFM03A (N=2). Range/geometric mean/standard deviation above/below mean
Uranium content based on gamma ray spectrometric data (weight ppm)		1.2–7.4	3.6	1.4	High	Outcrop data (N=20) and a borehole sample from KFM03A (N=1). Range/mean/standard deviation
Natural exposure rate (microR/h)		4.7–10.9	7.8	1.8	High	Outcrop data (N=20) and a borehole sample from KFM03A (N=1). Range/mean/standard deviation

RFM030

Property	Character	Quantitative estimate		Confidence	Comment
Subordinate rock type(s) Only the more important components are listed	Granodiorite, metamorphic (101056)			High	Outcrop data, N=274
	Diorite, quartz diorite and gabbro, metamorphic (101033)			High	
	Pegmatite, pegmatitic granite (101061)			High	
	Amphibolite (102017)			High	
	Granite to granodiorite, metamorphic (101057)			High	
	Felsic to intermediate volcanic rock, metamorphic (103076)			High	
	Granitoid, metamorphic, fine- to medium-grained (101051)			High	
	Granite, fine- to medium-grained (111058)			High	
	Sulphide mineralisation (109010)			High	Mineralisation where mining or exploration activity has taken place in historical time
Degree of inhomogeneity	High			High	Outcrop data, N=274
Metamorphism/alteration	Amphibolite-facies metamorphism			High	Outcrop data, N=274
Mineral fabric (type/orientation)	Tectonic foliation/banding	126/81	24	High	Outcrop data, N=217. Fisher mean. Strike/dip and K value
	Mineral stretching lineation	136/40	62	High	Outcrop data, N=194. Fisher mean. Trend/plunge and K value
	Fold axis	144/39	9	High	Outcrop data, N=12. Fisher mean. Trend/plunge and K value

RFM031

Property	Character	Quantitative estimate			Confidence	Comment
Dominant rock type	Felsic to intermediate volcanic rock, metamorphic (103076)				High	Outcrop data, N=129
Mineralogical composition (%). Only the dominant minerals are listed	Quartz	5.2–39.2	26.0	10.3	High	Data from outcrop samples, N=15. Range/mean/standard deviation
	K-feldspar	0–12.6	3.4	4.1		
	Plagioclase feldspar	29.2–53.2	48.6	6.5		
	Biotite	0–22.8	12.0	8.0		
	Hornblende	0–35.6				
Grain size	Fine-grained				High	Outcrop data, N=129
Age (million years)		1,906–1,891			High	Regional correlation. Range
Structure	Banded, foliated, lineated. In part folded				High	Outcrop data, N=129
Texture	Equigranular				High	Outcrop data, N=129

RFM031						
Property	Character	Quantitative estimate			Confidence	Comment
Density (kg/m ³)		2,648– 2,946	2,732	79	High	Data from outcrop samples, N=19. Range/mean/standard deviation
Porosity (%)		0.20–0.62	0.37	0.11	High	Data from outcrop samples, N=19. Range/mean/standard deviation
Magnetic susceptibility (SI units)		0.00006– 0.24000	0.00235	0.04163/ 0.00222	High	Data from outcrop samples, N=19. Range/geometric mean/standard deviation above/below mean
Electric resistivity in fresh water (ohm m)		1,725– 81,878	14,374	22,146/ 8,716	High	Data from outcrop samples, N=19. Range/geometric mean/standard deviation above/below mean
Uranium content based on gamma ray spectrometric data (weight ppm)		2.5–6.8	4.3	1.0	High	Outcrop data, N=19. Range/mean/standard deviation
Natural exposure rate (microR/h)		5.2–13.4	9.4	2.5	High	Outcrop data, N=19. Range/mean/standard deviation
Subordinate rock type(s) Only the more important components are listed	Amphibolite (102017)				High	Outcrop data, N=129
	Tonalite to granodiorite, metamorphic (101054)				High	
	Pegmatite, pegmatitic granite (101061)				High	
	Diorite, quartz diorite and gabbro, metamorphic (101033)				High	
Subordinate rock type(s) Only the more important components are listed	Granodiorite, metamorphic (101056)				High	Mineralisations where mining or exploration activity has taken place in historical time
	Magnetite mineralisation associated with calc-silicate rock (109014)				High	
Degree of inhomogeneity	High				High	Outcrop data, N=129
Metamorphism/alteration	1. In part, pre-metamorphic K-Na alteration. 2. Amphibolite-facies metamorphism				High	Outcrop data, N=129
Mineral fabric (type/orientation)	Tectonic foliation/banding	131/85	24		High	Outcrop data, N=94. Fisher mean Strike/dip and K value
	Mineral stretching lineation	139/41	51		High	Outcrop data, N=44 Fisher mean. Trend/plunge and K value
	Fold axis	146/41	59		High	Outcrop data, N=16 Fisher mean. Trend/plunge and K value

RFM032

Property	Character	Quantitative estimate			Confidence	Comment
Dominant rock type	Granite, metamorphic, aplitic (101058)				High	Outcrop data, N=99. Tunnel data. Borehole data along tunnels
Mineralogical composition (%). Only the dominant minerals are listed	Quartz	30.8–44.4	37.3	4.4	Medium	Data from outcrop samples, N=7. Range/mean/standard deviation
	K-feldspar	4.0–47.0	22.9	15.9		
	Plagioclase feldspar	18.8–58.2	37.1	15.8		
	Biotite	0–2.0	1.1	0.9		
Grain size	Fine-grained (and leucocratic)				High	Outcrop data, N=99. Tunnel data. Borehole data along tunnels
Age (million years)		1,891–1,861			High	Regional correlation. Range. Age possibly 1,865±3
Structure	Banded, foliated and lineated. In part folded				High	Outcrop data, N=99. Tunnel data. Borehole data along tunnels
Texture	Equigranular				High	Outcrop data, N=99. Tunnel data. Borehole data along tunnels
Density (kg/m ³)		2,620–2,646	2,635	9	Medium	Data from outcrop samples, N=7. Range/mean/standard deviation
Porosity (%)		0.36–0.48	0.40	0.05	Medium	Data from outcrop samples, N=7. Range/mean/standard deviation
Magnetic susceptibility (SI units)		0.00179–0.01722	0.00657	0.00691/0.00337	Medium	Data from outcrop samples, N=7. Range/geometric mean/standard deviation above/below mean
Electric resistivity in fresh water (ohm m)		11,467–27,915	15,876	5,288/3,967	Medium	Data from outcrop samples, N=7. Range/geometric mean/standard deviation above/below mean
Uranium content based on gamma ray spectrometric data (weight ppm)		3.3–7.6	5.3	1.4	Medium	Outcrop data, N=9. Range/mean/standard deviation
Natural exposure rate (microR/h)		8.3–18.9	12.8	3.3	Medium	Outcrop data, N=9. Range/mean/standard deviation
Subordinate rock type(s) Only the more important components are listed	Granite to granodiorite, metamorphic (101057)				High	Outcrop data, N=99. Tunnel data. Borehole data along tunnels
	Pegmatite, pegmatitic granite (101061)				High	
	Amphibolite (102017)				High	
Subordinate rock type(s) Only the more important components are listed	Granitoid, metamorphic, fine- to medium-grained (101051)				High	Outcrop data, N=99. Tunnel data. Borehole data along tunnels. U-Pb (zircon) age of 1,864±3 million years, using SIMS technique from sample at 6700532/1632663. Age given with 95% confidence interval

RFM032						
Property	Character	Quantitative estimate			Confidence	Comment
	Granite, fine- to medium-grained (111058)				High	Outcrop data, N=99. Tunnel data. Borehole data along tunnels. U-Pb (zircon) age of 1,851±5 million years, using SIMS technique from sample at 6700655/1632484. Age given with 95% confidence interval
	Felsic to intermediate volcanic rock, metamorphic (103076)				High	Outcrop data, N=99. Tunnel data. Borehole data along tunnels
Degree of inhomogeneity	High				High	Outcrop data, N=99. Tunnel data. Borehole data along tunnels
Metamorphism/alteration	1. In part, pre-metamorphic K-Na alteration. 2. Amphibolite-facies metamorphism				High	Outcrop data, N=99. Tunnel data. Borehole data along tunnels
Mineral fabric (type/orientation)	Tectonic foliation/banding	126/65 (pole to best-fit great circle)			High	Outcrop data, N=124. Foliation/banding folded. Pole to best-fit great circle provided
	Mineral stretching lineation	118/37	33		High	Outcrop data, N=45. Fisher mean. Trend/plunge and K value
	Fold axis	116/40	57		High	Outcrop data, N=8. Fisher mean. Trend/plunge and K value

RFM033						
Property	Character	Quantitative estimate			Confidence	Comment
Dominant rock type	Granite to granodiorite, metamorphic (101057)				Medium	Outcrop data, N=18
Mineralogical composition (%). Only the dominant minerals are listed	Quartz	27.8–45.8	35.6	4.2	High	Data from outcrop samples (N=29) and borehole samples from KFM01A (N=5), KFM02A (N=6) and KFM03A (N=6). Range/mean/standard deviation
	K-feldspar	0.2–36.0	22.5	8.6		
	Plagioclase feldspar	24.0–63.8	35.6	8.5		
	Biotite	0.8–8.2	5.1	1.6		
Grain size	Medium-grained				Medium	Outcrop data, N=18
Age (million years)		1,891–1,861			High	Regional correlation. Range. Age probably 1,865±3
Structure	Lineated and weakly foliated				Medium	Outcrop data, N=18
Texture	Equigranular				Medium	Outcrop data, N=18
Density (kg/m ³)		2,639–2,722	2,657	15	High	Data from outcrop samples (N=45) and borehole samples from KFM01A (N=5), KFM02A (N=8) and KFM03A (N=6). Range/mean/standard deviation

RFM033						
Property	Character	Quantitative estimate			Confidence	Comment
Porosity (%)		0.28–0.66	0.43	0.08	High	Data from outcrop samples (N=45) and borehole samples from KFM01A (N=5), KFM02A (N=8) and KFM03A (N=6). Range/mean/standard deviation
Magnetic susceptibility (SI units)		0.00007–0.02548	0.00442	0.01591/0.00346	High	Data from outcrop samples (N=45) and borehole samples from KFM01A (N=5), KFM02A (N=8) and KFM03A (N=6). Range/geometric mean/standard deviation above/below mean
Electric resistivity in fresh water (ohm m)		3,352–54,100	14,727	11,237/6,374	High	Data from outcrop samples (N=45) and borehole samples from KFM01A (N=10), KFM02A (N=15) and KFM03A (N=12). Range/geometric mean/standard deviation above/below mean
Uranium content based on gamma ray spectrometric data (weight ppm)		0.8–19.0	4.9	2.3	High	Outcrop data (N=47) and borehole samples from KFM01A (N=5), KFM02A (N=8) and KFM03A (N=6). Range/mean/standard deviation
Natural exposure rate (microR/h)		6.3–19.3	12.4	2.0	High	Outcrop data (N=47) and borehole samples from KFM01A (N=5), KFM02A (N=8) and KFM03A (N=6). Range/mean/standard deviation
Subordinate rock type(s) Only the more important components are listed	Pegmatite, pegmatitic granite (101061)				Medium	Outcrop data, N=18
	Amphibolite (102017)				Medium	
	Granitoid, metamorphic, fine- to medium-grained (101051)				Medium	
	Granite, fine- to medium-grained (111058)				Medium	
	Granite, metamorphic, aplitic (101058)				Medium	
Degree of inhomogeneity	Low				Medium	Outcrop data, N=18
Metamorphism/alteration	Amphibolite-facies metamorphism				High	Outcrop data, N=17
Mineral fabric (type/orientation)	Mineral stretching lineation	129/24	71		Medium	Outcrop data, N=22. Fisher mean. Trend/plunge and K value

RFM035						
Property	Character	Quantitative estimate			Confidence	Comment
Dominant rock type	Diorite, quartz diorite and gabbro, metamorphic (101033)				Medium	Outcrop data, N=6
Mineralogical composition (%). Only the dominant minerals are listed	Plagioclase feldspar	40.4–64.6	51.3	5.0	High	Data from outcrop samples, N=11. Range/mean/standard deviation
	Hornblende	10.6–50.6	27.6	11.5		
	Biotite	0–14.2	8.3	5.0		
	Quartz	0–24.6	8.3	7.7		
Grain size	Medium-grained				Medium	Outcrop data, N=6
Age (million years)		1,891–1,861			High	Regional correlation. Range. Age probably 1,886±1
Structure	Lineated and weakly foliated				Medium	Outcrop data, N=6
Texture	Equigranular				Medium	Outcrop data, N=6
Density (kg/m ³)		2,738–3,120	2,934	100	High	Data from outcrop samples, N=14. Range/mean/standard deviation
Porosity (%)		0.25–0.54	0.37	0.07	High	Data from outcrop samples, N=14. Range/mean/standard deviation
Magnetic susceptibility (SI units)		0.00036–0.05592	0.00293	0.01914/0.00254	High	Data from outcrop samples, N=14. Range/geometric mean/standard deviation above/below mean
Electric resistivity in fresh water (ohm m)		5,412–34,227	15,315	12,575/6,905	High	Data from outcrop samples, N=14. Range/geometric mean/standard deviation above/below mean
Uranium content based on gamma ray spectrometric data (weight ppm)		0.0–2.8	1.2	0.9	High	Outcrop data, N=14. Range/mean/standard deviation
Natural exposure rate (microR/h)		0.2–6.4	2.7	1.9	High	Outcrop data, N=14. Range/mean/standard deviation
Subordinate rock type(s) Only the more important components are listed	Pegmatite, pegmatitic granite (101061)				Medium	Outcrop data, N=6
	Amphibolite (102017)				Medium	
Degree of inhomogeneity	Low				Medium	Outcrop data, N=6
Metamorphism/alteration	Amphibolite-facies metamorphism				High	Outcrop data, N=6
Mineral fabric (type/orientation)	Mineral stretching lineation	137/32		179	Medium	Outcrop data, N=4. Fisher mean. Trend/plunge and K value

RFM036

Property	Character	Quantitative estimate			Confidence	Comment
Dominant rock type	Felsic to intermediate volcanic rock, metamorphic (103076)				Low	Outcrop data, N=2
Mineralogical composition (%). Only the dominant minerals are listed	Quartz	5.2–39.2	26.0	10.3	High	Data from outcrop samples, N=15. Range/mean/standard deviation
	K-feldspar	0–12.6	3.4	4.1		
	Plagioclase feldspar	29.2–53.2	48.6	6.5		
	Biotite	0–22.8	12.0	8.0		
	Hornblende	0–35.6				
Grain size	Fine-grained				Low	Outcrop data, N=2
Age (million years)		1,906–1,891			High	Regional correlation. Range
Structure	Banded, foliated and lineated. In part folded				Low	Outcrop data, N=2
Texture	Equigranular				Low	Outcrop data, N=2
Density (kg/m ³)		2,648–2,946	2,732	79	High	Data from outcrop samples, N=19. Range/mean/standard deviation
Porosity (%)		0.20–0.62	0.37	0.11	High	Data from outcrop samples, N=19. Range/mean/standard deviation
Magnetic susceptibility (SI units)		0.00006–0.24000	0.00235	0.04163/0.00222	High	Data from outcrop samples, N=19. Range/geometric mean/standard deviation above/below mean
Electric resistivity in fresh water (ohm m)		1,725–81,878	14,374	22,146/8,716	High	Data from outcrop samples, N=19. Range/geometric mean/standard deviation above/below mean
Uranium content based on gamma ray spectrometric data (weight ppm)		2.5–6.8	4.3	1.0	High	Outcrop data, N=19. Range/mean/standard deviation
Natural exposure rate (microR/h)		5.2–13.4	9.4	2.5	High	Outcrop data, N=19. Range/mean/standard deviation
Subordinate rock type(s) Only the more important components are listed	Pegmatite, pegmatitic granite (101061)				Low	Outcrop data, N=2
	Amphibolite (102017)				Low	
	Granite, fine- to medium-grained (111058)				Low	
	Granite, metamorphic, aplitic (101058)				Low	
Degree of inhomogeneity	High				Low	Outcrop data, N=2
Metamorphism/alteration	Amphibolite-facies metamorphism				High	Outcrop data, N=2
Mineral fabric (type/orientation)						Insufficient data

RFM037						
Property	Character	Quantitative estimate			Confidence	Comment
Dominant rock type	Granitoid, metamorphic, fine- to medium-grained (101051)				Medium	Outcrop data, N=17
Mineralogical composition (%). Only the dominant minerals are listed	Quartz	15.4–35.4	27.3	5.6	High	Data from outcrop samples (N=17) and borehole samples from KFM01A (N=2), KFM02A (N=3) and KFM03A (N=1). Range/mean/standard deviation
	K-feldspar	0–38.0	12.2	12.0		
	Plagioclase feldspar	29.4–67.0	46.4	10.0		
	Biotite	1.8–19.4	9.1	4.8		
	Hornblende	0–25.2				Range. Hornblende only present in 10 of the 23 samples
Grain size	Fine- to medium-grained				Medium	Outcrop data, N=17
Age (million years)		1,864	3		High	Regional correlation. Age and 95% confidence interval
Structure	Lineated and weakly foliated				Medium	Outcrop data, N=17
Texture	Equigranular				Medium	Outcrop data, N=17
Density (kg/m ³)		2,642–2,832	2,715	52	High	Data from outcrop samples (N=10) and borehole samples from KFM01A (N=3), KFM02A (N=2) and KFM03A (N=1). Range/mean/standard deviation
Porosity (%)		0.28–0.59	0.45	0.09	High	Data from outcrop samples (N=10) and borehole samples from KFM01A (N=3), KFM02A (N=2) and KFM03A (N=1). Range/mean/standard deviation
Magnetic susceptibility (SI units)		0.00014–0.02539	0.00096	0.00445/0.00079	High	Data from outcrop samples (N=11) and borehole samples from KFM01A (N=3), KFM02A (N=2) and KFM03A (N=1). Range/geometric mean/standard deviation above/below mean
Electric resistivity in fresh water (ohm m)		5,862–18,252	9,932	4,220/2,962	High	Data from outcrop samples (N=10) and borehole samples from KFM01A (N=6), KFM02A (N=4) and KFM03A (N=2). Range/geometric mean/standard deviation above/below mean
Uranium content based on gamma ray spectrometric data (weight ppm)		1.9–8.2	4.1	1.8	High	Outcrop data (N=15) and borehole samples from KFM01A (N=3), KFM02A (N=2) and KFM03A (N=1). Range/mean/standard deviation

RFM037						
Property	Character	Quantitative estimate			Confidence	Comment
Natural exposure rate (microR/h)		5.7–22.8	11.0	4.6	High	Outcrop data (N=15) and borehole samples from KFM01A (N=3), KFM02A (N=2) and KFM03A (N=1). Range/mean/standard deviation
Subordinate rock type(s) Only the more important components are listed	Pegmatite, pegmatitic granite (101061)				Medium	Outcrop data, N=17
	Felsic to intermediate volcanic rock, metamorphic (103076)				Medium	
	Granite, fine- to medium-grained (111058)				Medium	
	Amphibolite (102017)				Medium	
Degree of inhomogeneity	Low				Medium	Outcrop data, N=17
Metamorphism/alteration	Amphibolite-facies metamorphism				Medium	Outcrop data, N=17
Mineral fabric (type/orientation)	Mineral stretching lineation	129/25	18		Medium	Outcrop data, N=7. Fisher mean. Trend/plunge and K value

RFM038						
Property	Character	Quantitative estimate			Confidence	Comment
Dominant rock type	Granitoid, metamorphic, fine- to medium-grained (101051)				Medium	Outcrop data, N=9
Mineralogical composition (%). Only the dominant minerals are listed	Quartz	15.4–35.4	27.3	5.6	High	Data from outcrop samples (N=17) and borehole samples from KFM01A (N=2), KFM02A (N=3) and KFM03A (N=1). Range/mean/standard deviation
	K-feldspar	0–38.0	12.2	12.0		
	Plagioclase feldspar	29.4–67.0	46.4	10.0		
	Biotite	1.8–19.4	9.1	4.8		
	Hornblende	0–25.2				Range. Hornblende only present in 10 of the 23 samples
Grain size	Fine- to medium-grained				Medium	Outcrop data, N=9
Age (million years)		1,864	3		High	Regional correlation. Age and 95% confidence interval
Structure	Lineated and weakly foliated				Medium	Outcrop data, N=9
Texture	Equigranular				Medium	Outcrop data, N=9
Density (kg/m ³)		2,642–2,832	2,715	52	High	Data from outcrop samples (N=10) and borehole samples from KFM01A (N=3), KFM02A (N=2) and KFM03A (N=1). Range/mean/standard deviation

RFM038						
Property	Character	Quantitative estimate			Confidence	Comment
Porosity (%)		0.28–0.59	0.45	0.09	High	Data from outcrop samples (N=10) and borehole samples from KFM01A (N=3), KFM02A (N=2) and KFM03A (N=1). Range/mean/standard deviation
Magnetic susceptibility (SI units)		0.00014–0.02539	0.00096	0.00445/0.00079	High	Data from outcrop samples (N=11) and borehole samples from KFM01A (N=3), KFM02A (N=2) and KFM03A (N=1). Range/geometric mean/standard deviation above/below mean
Electric resistivity in fresh water (ohm m)		5,862–18,252	9,932	4,220/2,962	High	Data from outcrop samples (N=10) and borehole samples from KFM01A (N=6), KFM02A (N=4) and KFM03A (N=2). Range/geometric mean/standard deviation above/below mean
Uranium content based on gamma ray spectrometric data (weight ppm)		1.9–8.2	4.1	1.8	High	Outcrop data (N=15) and borehole samples from KFM01A (N=3), KFM02A (N=2) and KFM03A (N=1). Range/mean/standard deviation
Natural exposure rate (microR/h)		5.7–22.8	11.0	4.6	High	Outcrop data (N=15) and borehole samples from KFM01A (N=3), KFM02A (N=2) and KFM03A (N=1). Range/mean/standard deviation
Subordinate rock type(s) Only the more important components are listed	Pegmatite, pegmatitic granite (101061)				Medium	Outcrop data, N=9
	Granite, fine- to medium-grained (111058)				Medium	
	Amphibolite (102017)				Medium	
Degree of inhomogeneity	Low				Medium	Outcrop data, N=9
Metamorphism/alteration	Amphibolite-facies metamorphism				Medium	Outcrop data, N=9
Mineral fabric (type/orientation)	Mineral stretching lineation	126/24	18		Medium	Outcrop data, N=11. Fisher mean. Trend/plunge and K value

RFM039

Property	Character	Quantitative estimate			Confidence	Comment
Dominant rock type	Granite, metamorphic, aplitic (101058)				Medium	Outcrop data, N=9
Mineralogical composition (%). Only the dominant minerals are listed	Quartz	30.8–44.4	37.3	4.4	High	Data from outcrop samples, N=7. Range/mean/standard deviation
	K-feldspar	4.0–47.0	22.9	15.9		
	Plagioclase feldspar	18.8–58.2	37.1	15.8		
	Biotite	0–2.0	1.1	0.9		
Grain size	Fine-grained (and leucocratic)				Medium	Outcrop data, N=9
Age (million years)		1,891–1,861			High	Regional correlation. Range. Age possibly 1,865±3
Structure	Banded, foliated, lineated. In part folded				Medium	Outcrop data, N=9
Texture	Equigranular				Medium	Outcrop data, N=9
Density (kg/m ³)		2,620–2,646	2,635	9	Medium	Data from outcrop samples, N=7. Range/mean/standard deviation
Porosity (%)		0.36–0.48	0.40	0.05	Medium	Data from outcrop samples, N=7. Range/mean/standard deviation
Magnetic susceptibility (SI units)		0.00179–0.01722	0.00657	0.00691/0.00337	Medium	Data from outcrop samples, N=7. Range/geometric mean/standard deviation above/below mean
Electric resistivity in fresh water (ohm m)		11,467–27,915	15,876	5,288/3,967	Medium	Data from outcrop samples, N=7. Range/geometric mean/standard deviation above/below mean
Uranium content based on gamma ray spectrometric data (weight ppm)		3.3–7.6	5.3	1.4	Medium	Outcrop data, N=9. Range/mean/standard deviation
Natural exposure rate (microR/h)		8.3–18.9	12.8	3.3	Medium	Outcrop data, N=9. Range/mean/standard deviation
Subordinate rock type(s) Only the more important components are listed	Pegmatite, pegmatitic granite (101061)				Medium	Outcrop data, N=99
	Amphibolite (102017)				Medium	
	Granite to granodiorite, metamorphic, medium-grained (101057)				Medium	
Subordinate rock type(s) Only the more important components are listed	Granitoid, metamorphic, fine- to medium-grained (101051)				Medium	
Degree of inhomogeneity	High				Medium	Outcrop data, N=9
Metamorphism/alteration	1. In part, pre-metamorphic K-Na alteration. 2. Amphibolite-facies metamorphism				High	Outcrop data, N=9

RFM039					
Property	Character	Quantitative estimate		Confidence	Comment
Mineral fabric (type/orientation)	Tectonic foliation/ banding	303/81	33	Medium	Outcrop data, N=6. Fisher mean. Strike/dip and K value
	Mineral stretching lineation	133/29	96	Medium	Outcrop data, N=9. Fisher mean. Trend/plunge and K value
	Fold axis	128/26	151	Medium	Outcrop data, N=5. Fisher mean. Trend/plunge and K value

RFM040					
Property	Character	Quantitative estimate		Confidence	Comment
Dominant rock type	Granite to granodiorite, metamorphic, veined to migmatitic (111057)			Medium	Outcrop data, N=13
Mineralogical composition (%). Only the dominant minerals are listed					No data available. The rock affected by veining and migmatization is similar to the dominant rock type in, for example, RFM029 (rock code 101057)
Grain size	Medium-grained			Medium	Outcrop data, N=13
Age (million years)		1,891–1,861		High	Regional correlation. Range. Age probably 1,865±3
Structure	Lineated. In part folded			Medium	Outcrop data, N=13
Texture	Equigranular			Medium	Outcrop data, N=13
Density (kg/m ³)					No data available. The rock affected by veining and migmatization is similar to the dominant rock type in, for example, RFM029 (rock code 101057)
Porosity (%)					No data available. The rock affected by veining and migmatization is similar to the dominant rock type in, for example, RFM029 (rock code 101057)
Magnetic susceptibility (SI units)					No data available. The rock affected by veining and migmatization is similar to the dominant rock type in, for example, RFM029 (rock code 101057)
Electric resistivity in fresh water (ohm m)					No data available. The rock affected by veining and migmatization is similar to the dominant rock type in, for example, RFM029 (rock code 101057)

RFM040

Property	Character	Quantitative estimate		Confidence	Comment
Uranium content based on gamma ray spectrometric data (weight ppm)					No data available. The rock affected by veining and migmatization is similar to the dominant rock type in, for example, RFM029 (rock code 101057)
Natural exposure rate (microR/h)					No data available. The rock affected by veining and migmatization is similar to the dominant rock type in, for example, RFM029 (rock code 101057)
Subordinate rock type(s) Only the more important components are listed	Pegmatite, pegmatitic granite (101061)			Medium	Outcrop data, N=13
	Granitoid, metamorphic, fine- to medium-grained (101051)			Medium	
	Granite, metamorphic, aplitic (101058)			Medium	
	Amphibolite (102017)			Medium	
	Granite, fine- to medium-grained (111058)			Medium	
	Felsic to intermediate volcanic rock, metamorphic (103076)			Medium	
Degree of inhomogeneity	High			High	Outcrop data, N=13
Metamorphism/alteration	Amphibolite-facies metamorphism			High	Outcrop data, N=13
Mineral fabric (type/orientation)	Mineral stretching lineation	123/32	25	High	Outcrop data, N=21. Fisher mean. Trend/plunge and K value
	Fold axis	126/27	52	High	Outcrop data, N=7. Fisher mean. Trend/plunge and K value

RFM041					
Property	Character	Quantitative estimate		Confidence	Comment
Dominant rock type	Sedimentary rock, metamorphic, veined to migmatitic (106001)			Medium	Outcrop data, N=9
Mineralogical composition (%) Only the dominant minerals are listed					No data available
Grain size	Fine-grained			Medium	Outcrop data, N=9
Age (million years)					No data available
Structure	Banded, lineated and folded			Medium	Outcrop data, N=9
Texture	Equigranular			Medium	Outcrop data, N=9
Density (kg/m ³)		2,691		Low	Data from a single outcrop sample, N=1
Porosity (%)		0.48		Low	Data from a single outcrop sample, N=1
Magnetic susceptibility (SI units)		0.00270		Low	Data from a single outcrop sample, N=1
Electric resistivity in fresh water (ohm m)		10,888		Low	Data from a single outcrop sample, N=1
Uranium content based on gamma ray spectrometric data (weight ppm)		5.3		Low	Outcrop data, N=1
Natural exposure rate (microR/h)		9.2		Low	Outcrop data, N=1
Subordinate rock type(s) Only the more important components are listed	Pegmatite, pegmatitic granite (101061)			Medium	Outcrop data, N=9
	Granitoid, metamorphic, fine- to medium-grained (101051)			Medium	
	Granite, fine- to medium-grained (111058)			Medium	
	Amphibolite (102017)			Medium	
Degree of inhomogeneity	High			Medium	Outcrop data, N=9
Metamorphism/alteration	Amphibolite-facies metamorphism			High	Outcrop data, N=9
Mineral fabric (type/orientation)	Mineral stretching lineation	122/29	54	Medium	Outcrop data, N=5. Fisher mean. Trend/plunge and K value
	Fold axis	116/30	15	Medium	Outcrop data, N=6. Fisher mean. Trend/plunge and K value

RFM042

Property	Character	Quantitative estimate	Confidence	Comment
Dominant rock type	Granitoid, metamorphic (111051)		Low	No data available. Based on bedrock geological map compilation over Gräsö, presented in SKB report PR D-96-016 and SDM version 0
Mineralogical composition (%). Only the dominant minerals are listed				No data available
Grain size				No data available
Age (million years)		1,891–1,861	High	Regional correlation. Range
Structure	Lineated and weakly foliated			No data available. Based on bedrock geological map compilation over Gräsö, presented in SKB report PR D-96-016 and SDM version 0
Texture				No data available
Density (kg/m ³)				No data available
Porosity (%)				No data available
Magnetic susceptibility (SI units)				No data available
Electric resistivity in fresh water (ohm m)				No data available
Uranium content based on gamma ray spectrometric data (weight ppm)				No data available
Natural exposure rate (microR/h)				No data available
Subordinate rock type(s) Only the more important components are listed	Pegmatite, pegmatitic granite (101061)		Low	No data available. Based on bedrock geological map compilation over Gräsö, presented in SKB report PR D-96-016 and SDM version 0
	Granite, fine- to medium-grained (111058)		Low	
Degree of inhomogeneity	Low		Low	No data available. Based on bedrock geological map compilation over Gräsö, presented in SKB report PR D-96-016 and SDM version 0
Metamorphism/alteration	Amphibolite-facies metamorphism		High	No data available. Based on bedrock geological map compilation over Gräsö presented in SKB report PR D-96-016 and SDM version 0
Mineral fabric (type/orientation)				No data available

Dominant and subordinate rock types in rock domains – codes and nomenclature

The table below translates the various rock codes in the rock domain tables to rock names. The different groups (A to D), that are essentially a stratigraphic classification of the rocks, are described in Section 5.2.1. The oldest rocks of supracrustal character are included in Group A. The rocks in Groups B and C belong to different generations of younger, calc-alkaline intrusive rocks. The youngest intrusive rocks are included in Group D.

Rock code	Rock composition	Complementary characteristics		
Rock codes and rock names adopted by SKB				
111058	Granite		Fine- to medium-grained	Group D
101061	Pegmatite, pegmatitic granite			Group D
101051	Granite, granodiorite and tonalite	Metamorphic	Fine- to medium-grained	Group C
111051	Granitoid	Metamorphic		Group B
101058	Granite	Metamorphic	Aplitic	Group B
111057	Granite to granodiorite	Metamorphic, veined to migmatitic		Group B
101057	Granite to granodiorite	Metamorphic	Medium-grained	Group B
101056	Granodiorite	Metamorphic		Group B
101054	Tonalite to granodiorite	Metamorphic		Group B
101033	Diorite, quartz diorite, gabbro	Metamorphic		Group B
102017	Amphibolite			Group B
101004	Ultramafic rock	Metamorphic		Group B
108019	Calc-silicate rock (skarn)			Group A
109014	Magnetite mineralisation associated with calc-silicate rock (skarn)			Group A
109010	Sulphide mineralisation			Group A
103076	Felsic to intermediate volcanic rock	Metamorphic		Group A
106001	Sedimentary rock	Metamorphic, veined to migmatitic		Group A
106000	Sedimentary rock	Metamorphic		Group A
Additional rock codes and rock names of strongly subordinate character				
1051	Granitoid	Metamorphic	Uncertain classification 101051, 111051	Group B or Group C
1053	Tonalite	Metamorphic	Uncertain classification 101051 or 101054	Group B or Group C
1054	Tonalite to granodiorite	Metamorphic	Uncertain classification 101051 or 101054	Group B or Group C
1056	Granodiorite	Metamorphic	Uncertain classification 101051 or 101056	Group B or Group C
1057	Granite to granodiorite	Metamorphic	Uncertain classification 101051 or 101057	Group B or Group C
1058_120	Granite	Metamorphic	Uncertain classification 101057 or 101058	Group B
1058	Granite		Uncertain classification 101051, 101057, 101058 or 111058	Group B, Group C or Group D
1059	Leucocratic granite		Uncertain classification 101058 or 111058	Group B or Group D

Rock code	Rock composition	Complementary characteristics	
1062	Aplite	Uncertain classification 101058 or 111058	Group B or Group D
111058_101051	Granite	Uncertain classification 101051 or 111058	Group C or Group D
5103	Felsic rock	Metamorphic Uncertain classification 103076 or 101058	Group A or Group B
6053	Quartz-hematite rock		
8003	Cataclastic rock		
8004	Mylonite		
8011	Gneiss		
8020	Hydrothermal vein or segregation		
8021	Quartz-rich hydrothermal vein or segregation		
8023	Hydrothermally altered rock		

Properties of all deformation zones included in the regional model volume

The construction of these tables is described in Section 5.4. The tables listed here are for the zones in the alternative model. This model has been selected since it includes all the zones that have been assessed deterministically in the version 1.2 modelling work. It only differs from the base model and its variant by the inclusion of low confidence zones that are vertical or steeply dipping. The orientations of deformation zones and fractures are given in the form of strike and dip using the right-hand-rule method. For example, 108/75 corresponds to a strike and dip of N72°W/75°SW. Fisher mean and K values for fractures are calculated from the poles to fractures.

Vertical and steeply, SW-dipping brittle and ductile deformation zones with WNW-NW strike ZFMNW0001 (Singö deformation zone) – high confidence zone					
Property	Quantitative estimate	Span	Confidence level	Basis for interpretation	Comments
Position		20 m	High	Intersections along tunnels 1–2, 3 and SFR, and boreholes along tunnels, seismic refraction data, linked lineament XFM0803A0	Span refers to the general position of the zone core on the surface. Span reduces to ± 1 m in the bedrock volume close to the tunnels and boreholes. Lineament based on magnetic and bathymetric data
Orientation (strike/dip, right-hand-rule)	120/90	$\pm 10/\pm 10$	High for strike, medium for dip	Intersections along tunnels 1–2, 3 and SFR, and boreholes along tunnels, linked lineament XFM0803A0	Model version 0
Thickness	200 m	± 50 m	Medium	Intersections along tunnels 1–2, 3 and SFR, and boreholes along tunnels	/Carlsson and Christiansson 1987/. Thickness refers to total zone thickness (transition zone and core)
Length	30 km	+ 25 km	Medium	Linked lineament XFM0803A0	Total length. Extends outside regional model volume. Model version 0 used to obtain estimate of the extension outside this volume
Ductile deformation			High	Intersections along tunnels 1–2, 3 and SFR, and boreholes along tunnels	Present
Brittle deformation			High	Intersections along tunnels 1–2, 3 and SFR, and boreholes along tunnels	Present
Alteration			Medium	Character of linked lineament XFM0803A0	Oxidized bedrock with fine-grained hematite dissemination
Fracture orientation (strike/dip, right-hand-rule)	125/80 (schistosity), 140/80 (schistosity), 210/75, 055/75, 170/40, sub-horizontal		High	Intersections along tunnels 1–2, 3 and SFR, and boreholes along tunnels	/Carlsson and Christiansson, 1987/
Fracture frequency	10 m ⁻¹	± 4 m ⁻¹	High	Intersections along tunnels 1–2, 3 and SFR, and boreholes along tunnels	
Fracture filling			High	Intersections along tunnels 1–2, 3 and SFR, and boreholes along tunnels	Chlorite, calcite, quartz, clay minerals, sandy material

Vertical and steeply, SW-dipping brittle and ductile deformation zones with WNW-NW strike ZFMNW0002 (splay from Singö deformation zone through tunnel 3) – high confidence zone

Property	Quantitative estimate	Span	Confidence level	Basis for interpretation	Comments
Position		± 20 m	High	Intersection along tunnel 3, seismic refraction data, linked lineament XFM0804A0	Span refers to the general position of the zone core on the surface. Span reduces to ± 1 m in the bedrock volume close to tunnel 3. Lineament based on magnetic and bathymetric data
Orientation (strike/dip, right-hand-rule)	135/90	± 10/± 10	High for strike, medium for dip	Intersection along tunnel 3, linked lineament XFM0804A0	Model version 0
Thickness	75 m	± 10 m	Medium	Intersection along tunnel 3	Thickness refers to total zone thickness (transition zone and core)
Length	13 km	± 1 km	Medium	Linked lineament XFM0804A0. Truncated to the south-east against ZFMNW0001	Total length. Extends to the north-west outside regional model volume. Model version 0 used to obtain estimate of the extension outside this volume
Ductile deformation			High	Intersection along tunnel 3	Present. Zones of foliated rocks and chlorite schist documented during mapping of tunnel 3
Brittle deformation			Medium	Intersection along tunnel 3	Present. However, note low fracture frequency
Alteration			High	Intersection along tunnel 3, character of linked lineament XFM0804A0	Chloritization, oxidized bedrock with fine-grained hematite dissemination
Fracture orientation (strike/dip, right-hand-rule)	NW/70S, NE/90, NNW/90		High	Intersection along tunnel 3	
Fracture frequency	1 m ⁻¹	0.5 m ⁻¹	Low	Intersection along tunnel 3	
Fracture filling			High	Intersection along tunnel 3	Chlorite, calcite

Vertical and steeply, SW-dipping brittle and ductile deformation zones with WNW-NW strike ZFMNW003A, B, C, D, E, F (Eckarfjärden deformation zone)¹ – high confidence zone

Property	Quantitative estimate	Span	Confidence level	Basis for interpretation	Comments
Position		± 20 m	High	Intersections along HFM11 (DZ1) and HFM12 (DZ1), linked lineament XFM0015A0	Span refers to general position of the zone core on surface. Span reduces to ± 1 m in the bedrock volume close to the two boreholes. Zone can possibly be extended from borehole depth 170 m in HFM12 down to borehole depth 179 m. Lineament based on magnetic, electrical, topographic and bathymetric data
Orientation (strike/dip, right-hand-rule)	140/85	± 10/± 10	High for strike, medium for dip	Intersections along HFM11 (DZ1) and HFM12 (DZ1), linked lineament XFM0015A0	
Thickness	60 m	± 20 m	Medium	Intersections along HFM11 (DZ1) and HFM12 (DZ1)	Thickness refers to total zone thickness (transition zone and core). Span attempts to take into account variation along the whole zone.
Length	35 km	± 5 km	Medium	Linked lineament XFM0015A0	Total length. Extends outside regional model volume. Model version 0 used to obtain estimate of the extension outside this volume
Ductile deformation			High	Surface geology and intersections along HFM11 (DZ1) and HFM12 (DZ1)	Present. Strong, low-temperature ductile deformation throughout the zone with the development of mylonites. Also situated in broader belt with strong, high-temperature ductile deformation
Brittle deformation			High		Present
Alteration			High	Surface geology and intersections along HFM11 (DZ1) and HFM12 (DZ1), character of linked lineament XFM0015A0	Oxidized bedrock with fine-grained hematite dissemination. Consistent with low magnetic anomaly
Fracture orientation (strike/dip, right-hand-rule)	Mean of NW fracture set = 130/88	K value of NW fracture set = 17	Medium	Intersections along HFM11 (DZ1) and HFM12 (DZ1), N = 482	Only orientation of dominant fracture set is provided. Sub-horizontal and steeply-dipping fracture sets are also present. Fracture sets defined from DFN analysis

Vertical and steeply, SW-dipping brittle and ductile deformation zones with WNW-NW strike ZFMNW003A, B, C, D, E, F (Eckarfjärden deformation zone)¹ – high confidence zone

Property	Quantitative estimate	Span	Confidence level	Basis for interpretation	Comments
Fracture frequency	Mean 3 m ⁻¹	Span 0–14 m ⁻¹	Medium	Intersections along HFM11 (DZ1) and HFM12 (DZ1)	Dominance of sealed fractures. Quantitative estimate and span exclude sealed fracture network at 98–99 m in HFM11 and several sealed fracture networks in the upper part of HFM12. Higher average fracture frequency in the 83–116 m interval in HFM11 (4 m ⁻¹) and the 147–170 m interval in HFM12 (5 m ⁻¹), i.e. the south-western side of the zone
Fracture filling			High	Surface geology and intersections along HFM11 (DZ1) and HFM12 (DZ1)	Epidote, quartz, calcite, chlorite

¹ Composite deformation zone with main and subordinate zone segments. Properties are only provided for the main zone segment, ZFMNW003A, that corresponds at the surface to lineament XFM0015A0. The other zone segments (ZFMNW003B–F) are local minor zones that, together with ZFMNW003A, form an anastomosing network around inferred less-deformed segments within the zone. Zones ZFMNW003B–F correspond at the surface to lineaments XFM0015A1–5, respectively.

Vertical and steeply, SW-dipping brittle and ductile deformation zones with WNW-NW strike ZFMNW004A, B, C, D, E (Forsmark deformation zone)¹ – high confidence zone

Property	Quantitative estimate	Span	Confidence level	Basis for interpretation	Comments
Position		± 20 m	High	Linked lineament XFM0014A0	Span estimate refers to the general position of the central part of the zone on the surface. Lineament based on magnetic, electrical, topographic and bathymetric data
Orientation (strike/dip, right-hand-rule)	125/90	± 10/± 10	High for strike, low for dip	Strike based on linked lineament XFM0014A0. Dip by comparison with ZFMNW0001	
Thickness	200 m	± 50 m	Low	Comparison with ZFMNW0001	Thickness refers to total zone thickness (transition zone and core)
Length	70 km	± 5 km	Medium	Linked lineament XFM0014A0	Total length. Extends outside regional model volume. Model version 0 used to obtain estimate of the extension outside this volume
Ductile deformation			High	Surface geology	Present
Brittle deformation			High	Surface geology outside regional model volume	Present. See summary in model version 0
Alteration			High	Surface geology outside regional model volume, character of linked lineament XFM0803A0	Oxidized bedrock with fine-grained hematite dissemination. See summary in model version 0. Consistent with low magnetic anomaly
Fracture orientation (strike/dip, right-hand-rule)					
Fracture frequency					
Fracture filling					

¹ Composite deformation zone with main and subordinate zone segments. Properties are provided for the main zone segment, ZFMNW004A, that corresponds at the surface to lineament XFM0014A0. The other zone segments (ZFMNW003B–E) are local minor zones that, together with ZFMNW004A, form an anastomosing network around inferred less-deformed segments within the zone. Zones ZFMNW004B–E correspond at the surface to lineaments XFM0014A1–4, respectively.

Vertical and steeply, SW-dipping brittle and ductile deformation zones with WNW-NW strike ZFMNW0805 (Zone 8, SFR; splay from Singö deformation zone) – high confidence zone

Property	Quantitative estimate	Span	Confidence level	Basis for interpretation	Comments
Position		± 20 m	High	Borehole intersections, seismic refraction data, linked lineament XFM0805A0	Span refers to general position on surface. Span reduces to ± 1 m in the bedrock volume close to SFR. Lineament based on magnetic and bathymetric data
Orientation (strike/dip, right-hand-rule)	135/90	± 10/± 10	High	Borehole intersections, linked lineament XFM0805A0	NW/steep NE in /Axelsson and Hansen, 1997/
Thickness	10 m	± 5 m	Low	Borehole intersections	Thickness refers to total zone thickness (transition zone and core). Uncertainty concerning the thickness and significance of this zone. Compare /Carlsson et al. 1986, Axelsson and Hansen, 1997/
Length	3,632 m	± 200 m	Medium	Linked lineament XFM0805A0. Truncated to the south-east against ZFMNW0001	
Ductile deformation			Low	Borehole intersections	Present. Degree of foliation development is uncertain. See /Axelsson and Hansen, 1997/
Brittle deformation			High	Borehole intersections	Present
Alteration			Medium	Character of linked lineament XFM0805A0	Oxidized bedrock with fine-grained hematite dissemination
Fracture orientation (strike/dip, right-hand-rule)					
Fracture frequency	15 m ⁻¹	± 5 m ⁻¹	Medium	Borehole intersections	Uncertain to which zone highly fractured bedrock is related. See /Axelsson and Hansen, 1997/
Fracture filling					

Vertical and steeply, SW-dipping brittle and ductile deformation zones with WNW-NW strike ZFMNW1194 (DZ2 in KFM01B) – high confidence zone

Property	Quantitative estimate	Span	Confidence level	Basis for interpretation	Comments
Position		± 1 m	High	Intersection along KFM01B (DZ2)	Span estimate refers to the position of the central part of the zone close to borehole KFM01B
Orientation (strike/dip, right-hand-rule)	145/81	± 5/± 5	Medium	Orientation of fractures in KFM01B (DZ2)	
Thickness	3 m		Medium	Intersection along KFM01B (DZ2)	Thickness refers to total zone thickness (transition zone and core)
Length	379 m	± 25 m	Medium	Estimated length at surface after truncation against ZFMNE0060 and ZFMNE0061	
Ductile deformation			High	Intersection along KFM01B (DZ2)	Not present
Brittle deformation			High	Intersection along KFM01B (DZ2)	Present
Alteration			High	Intersection along KFM01B (DZ2)	Oxidized bedrock with fine-grained hematite dissemination
Fracture orientation (strike/dip, right-hand-rule)	Mean of gently-dipping fracture set = 168/11 Mean of NW fracture set = 145/81	K value of gently-dipping fracture set = 21 K value of NW fracture set = 21	Medium	Intersection along KFM01B (DZ2), N = 226	Sub-horizontal fractures form dominant fracture set. Subordinate set composed of fractures that strike NW and dip steeply to the SW. Gently- to moderately-dipping fractures with variable strike are also present. Fracture sets defined from DFN analysis
Fracture frequency	Mean 8 m ⁻¹	Span 5–13 m ⁻¹	Medium	Intersection along KFM01B (DZ2)	Dominance of sealed fractures. Quantitative estimate and span exclude abundant sealed fracture networks
Fracture filling			Medium	Intersection along KFM01B (DZ2)	Chlorite, calcite, epidote, quartz, clay minerals

**Vertical and steeply, SW-dipping brittle and ductile deformation zones with WNW-NW strike, based solely on lineament and comparison studies
ZFMNW017A, B C^{1,2} – medium confidence zone**

Property	Quantitative estimate	Span	Confidence level	Basis for interpretation	Comments
Position		± 20 m	High	Linked lineament XFM0017A0	Span estimate refers to the general position of the central part of the zone on the surface. Lineament based on magnetic, electrical, topographic and bathymetric data
Orientation (strike/dip, right-hand-rule)	127/90	± 10/± 10	High for strike, low for dip	Strike based on trend of linked lineament. Dip based on comparison with high confidence, vertical and steeply-dipping zones with NW strike	
Thickness	130 m	± 70 m	Low	Comparison with high confidence, vertical and steeply-dipping, regional zones with NW strike	Thickness refers to total zone thickness (transition zone and core)
Length	7,223 m	± 500 m	Medium	Linked lineament XFM0017A0. Truncated against ZFMNW003A and ZFMNE0828	
Ductile deformation			Low	Comparison with high confidence, vertical and steeply-dipping zones with NW strike	Assumed to be present
Brittle deformation			Low	Comparison with high confidence, vertical and steeply-dipping zones with NW strike	Assumed to be present
Alteration			Medium	Character of linked lineament XFM0017A0	Oxidized bedrock with fine-grained hematite dissemination
Fracture orientation (strike/dip, right-hand-rule)					
Fracture frequency					
Fracture filling					

¹ *Motivation lineament to deformation zone:* Lineament is long (> 7,000 m), is based on several data sets and has a weighted uncertainty factor that lies between 1.5 and 2.

² Composite deformation zone with main and subordinate zone segments. Properties are provided for the main zone segment, ZFMNW017A, that corresponds at the surface to lineament XFM0017A0. The other zone segments (ZFMNW017B–C) are local minor zones that, together with ZFMNW017A, form an anastomosing network around inferred less-deformed segments within the zone. Zones ZFMNW017B–C correspond at the surface to lineaments XFM0017A1–2, respectively.

**Vertical and steeply, SW-dipping brittle and ductile deformation zones with WNW-NW strike, based solely on lineament and comparison studies
ZFMNW0806 (splay from Singö deformation zone)¹ – medium confidence zone**

Property	Quantitative estimate	Span	Confidence level	Basis for interpretation	Comments
Position		± 20 m	High	Linked lineament XFM0806A0	Span estimate refers to the general position of the central part of the zone on the surface. Lineament based on magnetic and bathymetric data
Orientation (strike/dip, right-hand-rule)	146/90	± 10/± 10	High for strike, low for dip	Strike based on trend of linked lineament. Dip based on comparison with high confidence, vertical and steeply-dipping zones with NW strike	
Thickness	130 m	± 70 m	Low	Comparison with high confidence, vertical and steeply-dipping, regional zones with NW strike	Thickness refers to total zone thickness (transition zone and core).
Length	16 km	± 2 km	Medium	Linked lineament XFM0806A0. Truncated to the south-east against ZFMNW0001	Total length. Extends to the north-west outside regional model volume. Results of feasibility study (Tierp) used to estimate total length
Ductile deformation			Low	Comparison with high confidence, vertical and steeply-dipping zones with NW strike	Assumed to be present
Brittle deformation			Low	Comparison with high confidence, vertical and steeply-dipping zones with NW strike	Assumed to be present
Alteration			Medium	Character of linked lineament XFM0806A0	Oxidized bedrock with fine-grained hematite dissemination
Fracture orientation (strike/dip, right-hand-rule)					
Fracture frequency					
Fracture filling					

¹ *Motivation lineament to deformation zone:* Lineament is long (16 km), is based on several data sets and has a weighted uncertainty factor that lies between 1.5 and 2.

Vertical and steeply, SW-dipping brittle and ductile deformation zones with WNW-NW strike, based solely on lineament and comparison studies
ZFMNW0853¹ – medium confidence zone

Property	Quantitative estimate	Span	Confidence level	Basis for interpretation	Comments
Position		± 20 m	High	Linked lineament XFM0853A0	Span estimate refers to the general position of the central part of the zone on the surface. Lineament based on magnetic data
Orientation (strike/dip, right-hand-rule)	117/90	± 5/± 10	High for strike, low for dip	Strike based on trend of linked lineament. Dip based on comparison with high confidence, vertical and steeply-dipping zones with NW strike	
Thickness	10 m	± 5 m	Low	Comparison with ZFMNW0805	Thickness refers to total zone thickness (transition zone and core). ZFMNW0805 and ZFMNW0853 are similar in length
Length	4,348 m	± 200 m	Medium	Linked lineament XFM0853A0. Truncated to the east against ZFMNW0854	
Ductile deformation			Low	Comparison with high confidence, vertical and steeply-dipping zones with NW strike	Assumed to be present
Brittle deformation			Low	Comparison with high confidence, vertical and steeply-dipping zones with NW strike	Assumed to be present
Alteration			Medium	Character of linked lineament XFM0853A0	Oxidized bedrock with fine-grained hematite dissemination
Fracture orientation (strike/dip, right-hand-rule)					
Fracture frequency					
Fracture filling					

¹ *Motivation lineament to deformation zone:* Lineament is long (> 4,000 m), is based on magnetic data and has a weighted uncertainty factor that is < 1.5.

**Vertical and steeply, SW-dipping brittle and ductile deformation zones with WNW-NW strike, based solely on lineament and comparison studies
ZFMNW0854¹ – medium confidence zone**

Property	Quantitative estimate	Span	Confidence level	Basis for interpretation	Comments
Position		± 20 m	High	Linked lineament XFM0854A0	Span estimate refers to the general position of the central part of the zone on the surface. Lineament based on magnetic data
Orientation (strike/dip, right-hand-rule)	147/90	± 10/± 10	High for strike, low for dip	Strike based on trend of linked lineament. Dip based on comparison with high confidence, vertical and steeply-dipping zones with NW strike	
Thickness	130 m	± 70 m	Low	Comparison with high confidence, vertical and steeply-dipping, regional zones with NW strike	Thickness refers to total zone thickness (transition zone and core)
Length	26 km	± 2 km	Medium	Linked lineament XFM0854A0	Total length. Extends both to the north-west and to the south-east outside regional model volume. Results of feasibility study (Tierp) used to estimate total length
Ductile deformation			Low	Comparison with high confidence, vertical and steeply-dipping zones with NW strike	Assumed to be present
Brittle deformation			Low	Comparison with high confidence, vertical and steeply-dipping zones with NW strike	Assumed to be present
Alteration			Medium	Character of linked lineament XFM0854A0	Oxidized bedrock with fine-grained hematite dissemination
Fracture orientation (strike/dip, right-hand-rule)					
Fracture frequency					
Fracture filling					

¹ *Motivation lineament to deformation zone*: Lineament is long (26 km), is based on magnetic data and has a weighted uncertainty factor that is 1.0.

Vertical and steeply, SW-dipping brittle and ductile deformation zones with WNW-NW strike, based solely on lineament and comparison studies
Group of 79 low confidence zones

Property	Quantitative estimate	Span	Confidence level	Basis for interpretation	Comments
Position		± 20 m	High	Linked lineament	Span estimate refers to the general position of the central part of the zone on the surface. Lineament based on magnetic data or a combination of magnetic data and topographic/bathymetric and/or electrical data. Initial assessment also of older seismic refraction data
Orientation (strike/dip, right-hand-rule)	Strike in interval 85–154/dip 90	± 10/± 10	High for strike, low for dip	Strike based on trend of linked lineament. Dip based on comparison with high confidence, vertical and steeply-dipping zones with NW strike	
Thickness	10 m	± 5 m	Low	Comparison with high confidence, vertical and steeply-dipping, local major zones with NW strike	Thickness refers to total zone thickness (transition zone and core)
Length	In interval 1,000–8,000 m (ZFMNW025B is 355 m)	± 200 m	Medium	Linked lineament	
Ductile deformation			Low	Comparison with high confidence, vertical and steeply-dipping zones with NW strike	Assumed to be present
Brittle deformation			Low	Comparison with high confidence, vertical and steeply-dipping zones with NW strike	Assumed to be present
Alteration					
Fracture orientation (strike/dip, right-hand-rule)					
Fracture frequency					
Fracture filling					

**Steeply-dipping brittle deformation zones with NE strike
ZFMNE0061 (DZ3 in KFM01A) – high confidence zone**

Property	Quantitative estimate	Span	Confidence level	Basis for interpretation	Comments
Position		± 20 m	High	Intersection along KFM01A (DZ3), linked lineament XFM0061A0	Span estimate refers to the general position of the central part of the zone on the surface. Lineament based on magnetic, electrical and topographic data
Orientation (strike/dip, right-hand-rule)	068/81	± 5/± 10	High	Intersection along KFM01A (DZ3), linked lineament XFM0061A0	
Thickness	15 m		Medium	Intersection along KFM01A (DZ3)	Thickness refers to total zone thickness (transition zone and core)
Length	1,727 m	± 100 m	Medium	Linked lineament XFM0061A0. Truncated at depth against ZFMNE0060	
Ductile deformation			High	Intersection along KFM01A (DZ3)	Not present
Brittle deformation			High	Intersection along KFM01A (DZ3)	Present
Alteration			High	Intersection along KFM01A (DZ3), character of linked lineament XFM0061A0	Oxidized bedrock with fine-grained hematite dissemination along 60 m borehole section (20 m perpendicular to the zone boundaries). Alteration occurs along and in the footwall of the deformation zone. Consistent with low magnetic anomaly
Fracture orientation (strike/dip, right-hand-rule)	Mean of NE fracture set = 040/76	K value of NE fracture set = 69	Medium	Intersection along KFM01A (DZ3), N = 246	Only one fracture set in a NE strike direction is prominent. Other fracture orientations are present. Fracture set defined from DFN analysis
Fracture frequency	Mean 5.5 m ⁻¹	Span 0–18 m ⁻¹	Medium	Intersection along KFM01A (DZ3)	Dominance of sealed fractures
Fracture filling			Medium	Intersection along KFM01A (DZ3)	Laumontite, chlorite, hematite, calcite, quartz

**Steeply-dipping brittle deformation zones with NE strike
ZFMNE062A, B (DZ5 and DZ4, respectively, in KFM05A) – high confidence zone**

Property	Quantitative estimate	Span	Confidence level	Basis for interpretation	Comments
Position		± 20 m	High	Intersections along KFM05A (DZ4 and DZ5), linked lineament XFM0062A0	Span estimate refers to the general position of the central part of the zone on the surface. Span reduces to ± 1 m in the bedrock volume close to KFM05A. Modelled as two separate sub-zones that enclose at depth a minor, less-deformed bedrock block. Sub-zones labelled as ZFMNE062A in borehole depth interval 936–950 m (DZ5) and ZFMNE062B in borehole depth interval 892–916 m (DZ4). ZFMNE062A can possibly be extended down to borehole depth 992 m. Lineament based on magnetic, electrical and topographic data
Orientation (strike/dip, right-hand-rule)	234/73	± 5/± 10	Strike high, dip medium	Intersections along KFM05A (DZ4 and DZ5), linked lineament XFM0062A0	A steeper dip will be obtained if ZFMNE062A is extended down to 992 m
Thickness	10 m in sub-zone ZFMNE062A and 19 m in sub-zone ZFMNE062B		Medium	Intersections along KFM05A (DZ4 and DZ5)	Thickness refers to total zone thickness (transition zone and core)
Length	3,704 m	± 200 m	Medium	Linked lineament XFM0062A0. Truncated against ZFMNW0001 and ZFMNW017A	
Ductile deformation			High	Intersections along KFM05A (DZ4 and DZ5)	Not present
Brittle deformation			High	Intersections along KFM05A (DZ4 and DZ5)	Present
Alteration			High	Intersections along KFM05A (DZ4 and DZ5), character of linked lineament XFM0062A0	Oxidized bedrock with fine-grained hematite dissemination. Consistent with low magnetic anomaly
Fracture orientation (strike/dip, right-hand-rule)	Mean of NE fracture set = 241/90	K value of NE fracture set = 33	Medium	Intersections along KFM05A (DZ4 and DZ5), N = 244	Only one fracture set in a NE strike direction is prominent. Other fracture orientations are present. Fracture set defined from DFN analysis
Fracture frequency	Mean = 6 m ⁻¹ in sub-zone ZFMNE062A and 7 m ⁻¹ in sub-zone ZFMNE062B	Span = 0–6 m ⁻¹ in sub-zone ZFMNE062A and 0–12 m ⁻¹ in sub-zone ZFMNE062B	Medium	Intersections along KFM05A (DZ4 and DZ5)	Dominance of sealed fractures. Quantitative estimate and span exclude abundant sealed fracture networks in both sub-zones
Fracture filling			Medium	Intersections along KFM05A (DZ4 and DZ5)	Laumontite, chlorite, calcite, hematite, quartz

**Steeply-dipping brittle deformation zones with NE strike
ZFMNE0065 (DZ3 in HFM18) – high confidence zone**

Property	Quantitative estimate	Span	Confidence level	Basis for interpretation	Comments
Position		± 20 m	High	Intersection along HFM18 (DZ3), linked lineament XFM0065A0	Span estimate refers to the general position of the central part of the zone on the surface. Span reduces to ± 1 m in the bedrock volume close to HFM18. Lineament based on magnetic, electrical and topographic data. ZFMNE00A7 also modelled to intersect HFM18 in the borehole depth interval 119–148 m (DZ3)
Orientation (strike/dip, right-hand-rule)	036/75	± 5/± 10	High	Intersection along HFM18 (DZ3), linked lineament XFM0065A0	
Thickness	23 m		Medium	Intersection along HFM18 (DZ3)	Thickness refers to total zone thickness (transition zone and core). ZFMNE00A7 also modelled to intersect HFM18 in the borehole depth interval 119–148 m (DZ3)
Length	3,895 m	± 200 m	Medium	Linked lineament XFM0065A0. Truncated against ZFMNW0001 and ZFMNW017A	
Ductile deformation			High	Intersection along HFM18 (DZ3)	Not present
Brittle deformation			High	Intersection along HFM18 (DZ3)	Present
Alteration			High	Intersection along HFM18 (DZ3), character of linked lineament XFM0065A0	Oxidized bedrock with fine-grained hematite dissemination beneath 130 m borehole depth. Consistent with low magnetic anomaly. ZFMNE00A7 also modelled to intersect HFM18 in the borehole depth interval 119–148 m (DZ3)
Fracture orientation (strike/dip, right-hand-rule)	Mean of NE fracture set with steep dip to the south-east = 030/77	K value of NE fracture set with gentle to moderate dips to the south-east = 13	Medium	Intersection along HFM18 (DZ3), N = 132	Fractures with a variable dip to the south-east dominate. ZFMNE00A7 also modelled to intersect HFM18 in the borehole depth interval 119–148 m (DZ3)
Fracture frequency	Mean 4.5 m ⁻¹	Span 0–11 m ⁻¹	Medium	Intersection along HFM18 (DZ3), N = 132	Open and sealed fractures. Quantitative estimate and span exclude sealed fracture network at 144–145 m depth interval. ZFMNE00A7 also modelled to intersect HFM18 in the borehole depth interval 119–148 m (DZ3)
Fracture filling			Medium	Intersection along HFM18 (DZ3)	Chlorite, calcite, quartz. ZFMNE00A7 also modelled to intersect HFM18 in the borehole depth interval 119–148 m (DZ3)

**Steeply-dipping brittle deformation zones with NE strike
ZFMNE103A, B (712–720 m and 609–616 m levels, respectively, within DZ3 in KFM05A) – high confidence zone**

Property	Quantitative estimate	Span	Confidence level	Basis for interpretation	Comments
Position		± 20 m	High	Intersections along KFM05A (609–616 m and 712–720 m borehole depth intervals in DZ3), linked lineament XFM0103A0	Span estimate refers to the general position of the central part of the zone on the surface. Span reduces to ± 1 m in the bedrock volume close to KFM05A. Modelled as two separate sub-zones that enclose at depth a minor, less-deformed bedrock block. Sub-zones labelled as ZFMNE103A in borehole depth interval 712–720 m in DZ3 and ZFMNE103B in borehole depth interval 609–616 m in DZ3. Lineament based on magnetic and topographic data
Orientation (strike/dip, right-hand-rule)	232/79	± 5/± 10	High	Intersections along KFM05A (609–616 m and 712–720 m borehole depth intervals in DZ3), linked lineament XFM0103A0	
Thickness	7 m in sub-zone ZFMNE103A and 6 m in sub-zone ZFMNE103B		Medium	Intersections along KFM05A (609–616 m and 712–720 m borehole depth intervals in DZ3)	Thickness refers to total zone thickness (transition zone and core)
Length	1,542 m	± 100 m	Medium	Linked lineament XFM0103A0. ZFMNE103A truncated against ZFMNW017A and at depth against ZFMNE0060 and ZFMNE0062	
Ductile deformation			High	Intersections along KFM05A (609–616 m and 712–720 m borehole depth intervals in DZ3)	Not present
Brittle deformation			High	Intersections along KFM05A (609–616 m and 712–720 m borehole depth intervals in DZ3)	Present
Alteration			High	Intersections along KFM05A (609–616 m and 712–720 m borehole depth intervals in DZ3), character of linked lineament XFM0103A0	Oxidized bedrock with fine-grained hematite dissemination. Consistent with low magnetic anomaly

**Steeply-dipping brittle deformation zones with NE strike
ZFMNE103A, B (712–720 m and 609–616 m levels, respectively, within DZ3 in KFM05A) – high confidence zone**

Property	Quantitative estimate	Span	Confidence level	Basis for interpretation	Comments
Fracture orientation (strike/dip, right-hand-rule)	Mean of NE fracture set = 227/87 Mean of NS fracture set = 182/87	K value of NE fracture set = 15 K value of NS fracture set = 15	Medium	Intersections along KFM05A (609–616 m and 712–720 m borehole depth intervals in DZ3), N = 102	Fracture set with NE strike direction is dominant. Subordinate fracture set with NS strike as well as fractures with more gentle dips are also present. Fracture sets defined from DFN analysis
Fracture frequency	Mean = 6 m ⁻¹ in sub-zone ZFMNE103A and 8 m ⁻¹ in sub-zone ZFMNE103B	Span = 0–11 m ⁻¹ in sub-zone ZFMNE103B	Medium	Intersections along KFM05A (609–616 m and 712–720 m borehole depth intervals in DZ3)	Dominance of sealed fractures. Quantitative estimate and span exclude sealed fracture networks along major part of ZFMNE103B and along the whole part of ZFMNE103A
Fracture filling			Medium	Intersections along KFM05A (609–616 m and 712–720 m borehole depth intervals in DZ3)	Laumontite, chlorite, calcite, hematite, quartz

**Steeply-dipping brittle deformation zones with NE strike
ZFMNE0401 (DZ2 in KFM05A/DZ1 in HFM13) – high confidence zone**

Property	Quantitative estimate	Span	Confidence level	Basis for interpretation	Comments
Position		± 20 m	High	Intersections along KFM05A (DZ2) and HFM13 (DZ1), linked lineament XFM0401A0	Span estimate refers to the general position of the central part of the zone on the surface. Span reduces to ± 1 m in the bedrock volume close to KFM05A. Lineament based on magnetic and topographic data
Orientation (strike/dip, right-hand-rule)	239/80	± 5/± 10	High	Intersections along KFM05A (DZ2) and HFM13 (DZ1), linked lineament XFM0401A0	
Thickness	8 m	± 2 m	Medium	Intersections along KFM05A (DZ2) and HFM13 (DZ1)	Thickness refers to total zone thickness (transition zone and core)
Length	965 m	± 50 m	Medium	Linked lineament XFM0401A0. Truncated at depth against ZFMNE0060	
Ductile deformation			High	Intersections along KFM05A (DZ2) and HFM13 (DZ1)	Not present
Brittle deformation			High	Intersections along KFM05A (DZ2) and HFM13 (DZ1)	Present
Alteration			High	Intersections along KFM05A (DZ2) and HFM13 (DZ1), character of linked lineament XFM0401A0	Oxidized bedrock with fine-grained hematite dissemination. Consistent with low magnetic anomaly
Fracture orientation (strike/dip, right-hand-rule)	Mean of NE fracture set = 239/81	K value of NE fracture set = 33	Medium	Intersections along KFM05A (DZ2) and HFM13 (DZ1), N = 226	Fracture set with NE strike direction is dominant. Subordinate fracture set with NW to NS strike as well as fractures with more gentle dips are also present. Fracture sets defined from DFN analysis
Fracture frequency	Mean 7 m ⁻¹	Span 0–17 m ⁻¹	Medium	Intersections along KFM05A (DZ2) and HFM13 (DZ1)	Dominance of sealed fractures in KFM05A (DZ2). Approximately equal amounts of open and sealed fractures in HFM13 (DZ1). Quantitative estimate and span exclude sealed fracture networks at several locations along KFM05A (DZ2)
Fracture filling			Medium	Intersections along KFM05A (DZ2) and HFM13 (DZ1)	Chlorite, calcite, prehnite, epidote, laumontite, hematite, quartz, clay minerals in KFM05A (DZ2) Chlorite, calcite in HFM13 (DZ1)

**Steeply-dipping brittle deformation zones with NE strike
ZFMNE0869 (Zone 3, SFR) – high confidence zone**

Property	Quantitative estimate	Span	Confidence level	Basis for interpretation	Comments
Position		± 1 m	High	Intersection along SFR tunnel and boreholes, seismic refraction data	Span estimate refers to the position of the central part of the zone in SFR tunnel and boreholes
Orientation (strike/dip, right-hand-rule)	020/90	± 10/± 10	Medium	Intersection along SFR tunnel	SSW/steep W in /Axelsson and Hansen, 1997/
Thickness	10 m	± 1 m	High	Intersection along SFR tunnel	Composite zone consisting of several narrower high-strain segments (sub-zones) that diverge and converge in a complex pattern (see /Axelsson and Hansen, 1997/). Thickness refers to total zone thickness (transition zone and core)
Length	1,077 m	± 50 m	High	Intersection along SFR tunnel and boreholes	Truncated along strike against ZFMNW0001 and ZFMNW0805. Extended to 1,100 m depth
Ductile deformation			High	Intersection along SFR tunnel and boreholes	Not present
Brittle deformation			High	Intersection along SFR tunnel and boreholes, seismic refraction data	Present
Alteration					
Fracture orientation (strike/dip, right-hand-rule)					
Fracture frequency	15 m ⁻¹	± 5/ m	High	Intersection along SFR boreholes	
Fracture filling					

**Steeply-dipping brittle deformation zones with NE strike
ZFMNE0870 (Zone 9, SFR) – high confidence zone**

Property	Quantitative estimate	Span	Confidence level	Basis for interpretation	Comments
Position		± 1 m	High	Intersection along SFR tunnel and boreholes	Span estimate refers to the position of the central part of the zone in SFR tunnel and boreholes
Orientation (strike/dip, right-hand-rule)	050/90	± 10/± 10	Medium	Intersection along SFR tunnel	ENE/steep in /Axelsson and Hansen, 1997/
Thickness	2 m	± 1 m	High	Intersection along SFR tunnel and boreholes	Thickness refers to total zone thickness (transition zone and core)
Length	1,029 m	± 50 m	High	Intersection along SFR tunnel and boreholes	Truncated along strike against ZFMNW0001 and ZFMNW0805. Extended to 1,100 m depth
Ductile deformation			Low	Intersection along SFR tunnel	Mylonite present. Significance uncertain
Brittle deformation			High	Intersection along SFR tunnel and boreholes	Present. Water-bearing, clayey gouge
Alteration					
Fracture orientation (strike/dip, right-hand-rule)					
Fracture frequency	15 m ⁻¹	± 5/ m	High	Intersection along SFR boreholes	
Fracture filling			High	Intersection along SFR tunnel	Clay minerals, chlorite, calcite, Fe-bearing mineral

**Steeply-dipping brittle deformation zones with NE strike
ZFMNE1188 (surface at drill site 4/DZ4 and DZ5 in KFM04A) – high confidence zone**

Property	Quantitative estimate	Span	Confidence level	Basis for interpretation	Comments
Position		± 1 m	High	Surface geology (drill site 4) and intersections along KFM04A (DZ4, DZ5)	Span estimate refers to the position of the central part of the zone at drill site 4 and close to borehole KFM04A. Zone also passes close to DZ1, DZ2 and DZ3 in KFM04A, i.e. the zone strikes close to the trend of KFM04A
Orientation (strike/dip, right-hand-rule)	220/88	± 5/± 5	High	Surface geology (drill site 4) and intersections along KFM04A (DZ4, DZ5)	
Thickness	1.5 m	± 0.5 m	High	Surface geology (drill site 4) and intersections along KFM04A (DZ4, DZ5)	Thickness refers to total zone thickness (transition zone and core)
Length	741 m	± 50 m	Medium	Estimated length at surface after truncation along strike against ZFMNE0060 and ZFMNW017A, and down-dip at 1,100 m	
Ductile deformation			Low	Surface geology (drill site 4) and intersections along KFM04A (DZ4, DZ5)	Present along both DZ4 and DZ5 in KFM04A. NW strike. Uncertain significance
Brittle deformation			High	Surface geology (drill site 4) and intersections along KFM04A (DZ4, DZ5)	Present. Dextral horizontal component of movement
Alteration			High	Intersections along KFM04A (DZ4, DZ5)	Oxidized bedrock with fine-grained hematite dissemination
Fracture orientation (strike/dip, right-hand-rule)	Mean of NW fracture set = 139/84 Mean of NE fracture set = 237/84	K value of NW fracture set = 27 K value of NE fracture set = 12	Medium	Intersections along KFM04A (DZ4, DZ5), N = 423	Fracture set with NW strike dominates. Fracture set with NE strike and more gently-dipping fractures are also present. Difficulties to interpret significance of fracture orientation data since zone strike and borehole trend are close to each other. Fracture sets defined from DFN analysis
Fracture frequency	Mean 8.5 m ⁻¹	Span 2–20 m ⁻¹	Medium	Intersections along KFM04A (DZ4, DZ5)	Dominance of sealed fractures. Quantitative estimate and span exclude sealed fracture networks along both DZ4 and DZ5
Fracture filling			Medium	Intersections along KFM04A (DZ4, DZ5)	Laumontite, chlorite, calcite, quartz, epidote, prehnite, hematite, clay minerals, zeolites in DZ4 in KFM04A Chlorite, calcite, epidote, prehnite, quartz, hematite, laumontite in DZ5 in KFM04A

**Steeply-dipping brittle deformation zones with NE strike
ZFMNE1189 (DZ5 in KFM02A; spatial association with vuggy metagranite) – medium confidence zone¹**

Property	Quantitative estimate	Span	Confidence level	Basis for interpretation	Comments
Position		± 1 m	High	Intersection along KFM02A (DZ5)	Span estimate refers to the position of the central part of the zone close to borehole KFM02A. Zone can possibly be extended from 310 m borehole depth in KFM02A down to borehole depth 314 m
Orientation (strike/dip, right-hand-rule)	040/65	± 10/± 10	Low	Orientation of fractures in KFM02A (DZ5)	Low number of fractures in the set (20)
Thickness	4 m		Medium	Intersection along KFM02A (DZ5)	Thickness refers to total zone thickness (transition zone and core)
Length					ZFMNE1189 does not extend to the surface. Truncated at depth against ZFMNE00A2, ZFMNE00A3 and ZFMNE00B6, and along strike against the downward projection (90°) of two arbitrarily chosen lineaments XFM0047A0 and XFM0101A0
Ductile deformation			High	Intersection along KFM02A (DZ5)	Not present
Brittle deformation			High	Intersection along KFM02A (DZ5)	Present
Alteration			High	Intersection along KFM02A (DZ5)	ZFMNE1189 occurs at the base of an intense alteration zone with quartz dissolution and development of vuggy metagranite, combined with albitisation and strong oxidation with fine-grained hematite dissemination. This alteration zone extends from 240–310 m borehole length in KFM02A and is c. 40 m thick measured perpendicular to ZFMNE1189
Fracture orientation (strike/dip, right-hand-rule)	Mean of NE fracture set = 038/65	K value of NE fracture set = 33	Medium	Intersection along KFM02A (DZ5), N = 36	Fracture set with NE strike and steep dip to the south-east is present. More gently-dipping fractures are also present. Low number of fractures. Fracture set defined from DFN analysis
Fracture frequency	Mean 5 m ⁻¹	Span 3–8 m ⁻¹	Medium	Intersection along KFM02A (DZ5)	Dominance of sealed fractures
Fracture filling			Medium	Intersection along KFM02A (DZ5)	Chlorite, calcite, quartz, hematite

¹ The relatively low fracture frequency has motivated a reduction in the degree of confidence.

**Steeply-dipping brittle deformation zones with NE strike
ZFMNE1192 (DZ2 in KFM01A) – high confidence zone**

Property	Quantitative estimate	Span	Confidence level	Basis for interpretation	Comments
Position		± 1 m	High	Intersection in KFM01A (DZ2)	Span estimate refers to the position of the central part of the zone close to borehole KFM01A. Zone possibly initiates at 376 m depth in KFM01A. Predicted to intersect KFM01B (DZ3), if not truncated by ZFMNE1194 (see also ZFMNS0404)
Orientation (strike/dip, right-hand-rule)	073/82	± 5/± 5	Medium	Orientation of fractures in KFM01A (DZ2)	
Thickness	5 m		Medium	Intersection in KFM01A (DZ2)	Thickness refers to total zone thickness (transition zone and core)
Length	1,326 m	± 50 m	Medium	Estimated length at surface after truncation against ZFMNE0060 and ZFMNW1194	
Ductile deformation			High	Intersection in KFM01A (DZ2)	Not present
Brittle deformation			High	Intersection in KFM01A (DZ2)	Present
Alteration			High	Intersection in KFM01A (DZ2)	Oxidized bedrock with fine-grained hematite dissemination
Fracture orientation (strike/dip, right-hand-rule)	Mean of NE fracture set = 067/81	K value of NE fracture set = 87	Medium	Intersection in KFM01A (DZ2), N = 113	Fracture set with NE strike and steep dip to the south-east is prominent. Fracture set defined from DFN analysis
Fracture frequency	Mean 4.5 m ⁻¹	Span 1–8 m ⁻¹	Medium	Intersection in KFM01A (DZ2)	Sealed and open fractures
Fracture filling			Medium	Intersection in KFM01A (DZ2)	Laumontite, chlorite, calcite, hematite, quartz

Vertical and steeply-dipping brittle deformation zones with NE strike, based solely on lineament and comparison studies
ZFMNE0060¹ – medium confidence zone

Property	Quantitative estimate	Span	Confidence level	Basis for interpretation	Comments
Position		± 20 m	High	Linked lineament XFM0060A0	Span estimate refers to the general position of the central part of the zone on the surface. Lineament based on magnetic, electrical and topographic data
Orientation (strike/dip, right-hand-rule)	242/87	± 5/– 10	High for strike, low for dip	Strike based on trend of linked lineament. Dip based on comparison with high confidence, steeply-dipping zones with NE strike and lack of intersection in the boreholes at drill site 1	
Thickness	10 m	± 5 m	Low	Comparison with high confidence, steeply-dipping zones with NE strike	Thickness refers to total zone thickness (transition zone and core)
Length	3,012 m	± 200 m	Medium	Linked lineament XFM0060A0. Truncated against ZFMNW017A	
Ductile deformation			Low	Comparison with high confidence, steeply-dipping zones with NE strike	Assumed not to be present
Brittle deformation			Low	Comparison with high confidence, steeply-dipping zones with NE strike	Assumed to be present
Alteration			Medium	Character of linked lineament XFM0060A0	Oxidized bedrock with fine-grained hematite dissemination
Fracture orientation (strike/dip, right-hand-rule)					
Fracture frequency					
Fracture filling					

¹ *Motivation lineament to deformation zone:* Lineament is long (> 3,000 m), is based on several data sets and has a weighted uncertainty factor that is < 1.5. Furthermore, it belongs to a family of lineaments that cross-cut the tectonic lens at Forsmark, all of which show a similar trend, length and character. Several of these lineaments have been successfully linked to borehole intersections in the present structural model. They are inferred, with high confidence, to be brittle deformation zones dominated by sealed fractures and sealed fracture networks.

Vertical and steeply-dipping brittle deformation zones with NE strike, based solely on lineament and comparison studies

ZFMNE0828¹ – medium confidence zone

Property	Quantitative estimate	Span	Confidence level	Basis for interpretation	Comments
Position		± 20 m	High	Linked lineament XFM0828A0	Span estimate refers to the general position of the central part of the zone on the surface. Lineament based on magnetic, topographic and bathymetric data
Orientation (strike/dip, right-hand-rule)	216/90	± 5/± 10	High for strike, low for dip	Strike based on trend of linked lineament. Dip based on comparison with high confidence, steeply-dipping zones with NE strike	
Thickness	10 m	± 5 m	Low	Comparison with high confidence, steeply-dipping zones with NE strike	Thickness refers to total zone thickness (transition zone and core)
Length	4,402 m	± 200 m	Medium	Linked lineament XFM0828A0. Truncated against ZFMNW0001	
Ductile deformation			Low	Comparison with high confidence, steeply-dipping zones with NE strike	Assumed not to be present
Brittle deformation			Low	Comparison with high confidence, steeply-dipping zones with NE strike	Assumed to be present
Alteration			Medium	Character of linked lineament XFM0828A0	Oxidized bedrock with fine-grained hematite dissemination
Fracture orientation (strike/dip, right-hand-rule)					
Fracture frequency					
Fracture filling					

¹ *Motivation lineament to deformation zone*: Lineament is long (> 4,000 m), is based on several data sets and has a weighted uncertainty factor that is < 1.5. Furthermore, it belongs to a family of lineaments that cross-cut the tectonic lens at Forsmark, all of which show a similar trend, length and character. Several of these lineaments have been successfully linked to borehole intersections in the present structural model. They are inferred, with high confidence, to be brittle deformation zones dominated by sealed fractures and sealed fracture networks.

Vertical and steeply-dipping brittle deformation zones with NE strike, based solely on lineament and comparison studies

Group of 51 low confidence zones

Property	Quantitative estimate	Span	Confidence level	Basis for interpretation	Comments
Position		± 20 m	High	Linked lineament	Span estimate refers to the general position of the central part of the zone on the surface. Lineament based on magnetic data or a combination of magnetic data and topographic/bathymetric and/or electrical data. Initial assessment also of older seismic refraction data
Orientation (strike/dip, right-hand-rule)	Strike in interval 20–84/dip 90	± 10/± 10	High for strike, low for dip	Strike based on trend of linked lineament. Dip based on comparison with high confidence, steeply-dipping zones with NE strike	
Thickness	10 m	± 5 m	Low	Comparison with high confidence, steeply-dipping zones with NE strike	Thickness refers to total zone thickness (transition zone and core)
Length	In interval 1,000–7,000 m	± 200 m	Medium	Linked lineament	
Ductile deformation			Low	Comparison with high confidence, steeply-dipping zones with NE strike	Assumed not to be present
Brittle deformation			Low	Comparison with high confidence, steeply-dipping zones with NE strike	Assumed to be present
Alteration					
Fracture orientation (strike/dip, right-hand-rule)					
Fracture frequency					
Fracture filling					

**Steeply-dipping brittle deformation zones with NS strike
ZFMNS0404(DZ3 in KFM01B) – medium confidence zone¹**

Property	Quantitative estimate	Span	Confidence level	Basis for interpretation	Comments
Position		± 20 m	High	Intersection along KFM01B (DZ3), linked lineament XFM0404A0	Span estimate refers to the general position of the central part of the zone on the surface. Span reduces to ± 1 m in the bedrock volume close to KFM01B. Linked lineament XFM0404A0 is based solely on topographic data
Orientation (strike/dip, right-hand-rule)	352/85	± 5/± 10	High	Intersection along KFM01B (DZ3), linked lineament XFM0404A0	
Thickness	16 m		Medium	Intersection along KFM01B (DZ3)	Thickness refers to total zone thickness (transition zone and core)
Length	336 m	± 25 m	Medium	Linked lineament XFM0404A0. Truncated against ZFMNE0060, ZFMNE0061 and ZFMNW1194	
Ductile deformation			High	Intersection along KFM01B (DZ3)	Not present
Brittle deformation			High	Intersection along KFM01B (DZ3)	Present
Alteration			High	Intersection along KFM01B (DZ3)	Oxidized bedrock with fine-grained hematite dissemination
Fracture orientation (strike/dip, right-hand-rule)	Mean of NS fracture set = 347/86 Mean of sub-horizontal fracture set = 074/7	K value of NS fracture set = 33 K value of sub-horizontal fracture set = 13	Medium	Intersection along KFM01B (DZ3), N = 258	Fracture set with NS strike and steep dip to the east is dominant. A subordinate fracture set that is sub-horizontal and fractures with steeper, more variable orientation are also present. Fracture sets defined from DFN analysis
Fracture frequency	Mean 7 m ⁻¹	Span 1–14 m ⁻¹	Medium	Intersection along KFM01B (DZ3)	Dominance of sealed fractures. Quantitative estimate and span exclude sealed fracture networks and two crush zones in the lower central part of the zone
Fracture filling			Medium	Intersection along KFM01B (DZ3)	Laumontite, chlorite, calcite, prehnite, quartz, epidote, hematite, goethite

¹ The alteration observed in DZ3 along KFM01B does not agree with the character of lineament XFM0404A0 at the surface. Bearing in mind this consideration, the occurrence of laumontite in the fracture fillings and the observation that ZFMNE1192 will intersect KFM01B at DZ3, if truncation by ZFMNW1194 is not carried out, it is possible that zone ZFMNS0404 does *not* exist. If this is correct, DZ3 in KFM01B is the same zone as DZ2 in KFM01A, i.e. ZFMNE1192. However, the orientations of the fractures along these two zones are distinctly different. In summary, the considerations presented here motivate retention of ZFMNS0404 in the structural model with caution. For this reason, a lower degree of confidence has been placed on this zone.

Vertical and steeply-dipping brittle deformation zones with NS strike, based solely on lineament and comparison studies

Group of 41 low confidence zones

Property	Quantitative estimate	Span	Confidence level	Basis for interpretation	Comments
Position		± 20 m	High	Linked lineament	Span estimate refers to the general position of the central part of the zone on the surface. Lineament based on magnetic data or a combination of magnetic data and topographic/bathymetric and/or electrical data. Initial assessment also of older seismic refraction data
Orientation (strike/dip, right-hand-rule)	Strike in interval 335–19/dip 90	± 10/± 10	High for strike, low for dip	Strike based on trend of linked lineament. Dip based on comparison with ZFMNS0404	
Thickness	10 m	± 5 m	Low	Comparison with high confidence, vertical and steeply-dipping, local major zones	Thickness refers to total zone thickness (transition zone and core)
Length	In interval 1,000–5,500 m	± 200 m	Medium	Linked lineament	
Ductile deformation			Low	Comparison with ZFMNS0404	Assumed not to be present
Brittle deformation			Low	Comparison with ZFMNS0404	Assumed to be present
Alteration					
Fracture orientation (strike/dip, right-hand-rule)					
Fracture frequency					
Fracture filling					

**Gently SE- and S-dipping brittle deformation zones
ZFMNE00A2 (type intersection DZ6 in KFM02A) – high confidence zone**

Property	Quantitative estimate	Span	Confidence level	Basis for interpretation	Comments
Position		± 15 m	High	Borehole intersections along KFM01A (DZ1), KFM01B (DZ1), KFM02A (DZ6), KFM04A (DZ1, DZ2 and DZ3), KFM05A (DZ1), HFM01 (DZ1), HFM02 (DZ1), HFM14 (DZ1 and DZ2), HFM15 (DZ1), HFM16 (DZ1), HFM19 (DZ1 and DZ2) in combination with seismic reflector A2	ZFMEW0865 in model version 1.1 included as a sub-zone within ZFMNE00A2. Seismic reflector F1 may also be a sub-zone related to ZFMNE00A2. Furthermore, the bedrock c. 75 m beneath ZFNE00A2 (measured perpendicular to the zone) contains a high frequency of fractures that dip moderately to the north-west (DZ7 in the single-hole interpretation). ZFMNE00A2 is predicted to pass under but close to the base of KFM03A. For this reason, DZ5 in KFM03A may also be related to ZFMNE00A2 (cf. /Juhlin et al. 2004/). Span estimate refers to the general position of the central part of the zone and is based on /Cosma et al. 2003/. Span reduces to ± 1 m in the bedrock volume close to the boreholes
Orientation (strike/dip, right-hand-rule)	080/24	+ 15/- 10	High	Seismic reflector A2 in combination with borehole intersections listed against "Position"	Strike and dip after /Juhlin et al. 2002/. Span estimate based on both /Juhlin et al. 2002/ and /Cosma et al. 2003/
Thickness	65 m	± 35 m	High	Borehole intersections along KFM02A (DZ6), KFM04A (DZ1, DZ2 and DZ3), HFM14 (DZ1 and DZ2). Other borehole intersections listed against "Position" start or finish within the zone	Composite zone consisting of several narrower high-strain segments (sub-zones) that are inferred to diverge and converge in a complex pattern. These sub-zones separate less deformed bedrock segments. In KFM02A, the uppermost (415–430 m) and lowermost (480–520 m) parts display bedrock alteration and highest fracture frequency. In KFM04A, three separate sub-zones that vary in thickness from 5–10 m are present over an interval of 67 m perpendicular to the zone. Thus, thickness refers to total zone thickness (transition zones and cores)
Length	4,874 m in base model. 7,894 m in variant of base model	± 200 m ± 500 m	Medium	Seismic reflector A2 and borehole intersections listed against "Position". Truncated against ZFMNW0001 and ZFMNW003A in base model and against ZFMNW0001 and ZFMNW004A in variant of base model. Uncertain whether ZFMNE00A2 extends as far as KFM03A (see /Juhlin et al. 2004/)	

**Gently SE- and S-dipping brittle deformation zones
ZFMNE00A2 (type intersection DZ6 in KFM02A) – high confidence zone**

Property	Quantitative estimate	Span	Confidence level	Basis for interpretation	Comments
Ductile deformation			High	Borehole intersections listed against "Position"	Not present
Brittle deformation			High	Borehole intersections listed against "Position"	Present
Alteration			High	Borehole intersections listed against "Position"	Oxidized bedrock with fine-grained hematite dissemination
Fracture orientation (strike/dip, right-hand-rule)	Mean of gently-dipping fracture set = 027/11 Mean of NE fracture set = 053/75 Mean of NW fracture set = 313/88	K value of gently-dipping fracture set = 18 K value of NE fracture set = 10 K value of NW fracture set = 13	High	Borehole intersections along KFM02A (DZ6), KFM04A (DZ1, DZ2 and DZ3) and HFM19 (DZ1 and DZ2), N = 1,058	Data from deeper borehole intersections to avoid influence of sub-horizontal sheet joints parallel to the topography. Three fracture sets are apparent; a gently-dipping fracture set and steeply-dipping NE and NW sets. Fracture sets defined from DFN analysis
Fracture frequency	Mean 9 m ⁻¹	Span 0–26 m ⁻¹	High	Borehole intersections listed against "Position"	Open and sealed fractures. In the cored boreholes, the highest fracture frequency is present in KFM04A. Furthermore, crush zones have been observed at different depths in KFM01A, KFM01B, KFM02A and KFM05A. One crush zone is also present in KFM04A. Sealed fracture networks are present in KFM01B, KFM04A, KFM05A. Quantitative estimate and span exclude crush zones and sealed fracture networks
Fracture filling			High	Borehole intersections listed against "Position"	Chlorite, calcite, clay minerals, asphaltite goethite, prehnite, laumontite, hematite, epidote, quartz. Asphaltite only observed along ZFMNE00A2 in KFM01B (DZ1) and KFM05A (DZ1), i.e. above c. 100 m

Gently SE- and S-dipping brittle deformation zones

ZFMNE00A3 (DZ3 in KFM02A/DZ4 in KFM03A; association with vuggy metagranitoid) – high confidence zone

Property	Quantitative estimate	Span	Confidence level	Basis for interpretation	Comments
Position		± 15 m	High	Intersections along KFM02A (DZ3) and KFM03A (DZ4), seismic reflector A3	Span estimate refers to the general position of the central part of the zone and is based on /Cosma et al. 2003/. Span reduces to ± 1 m in the bedrock volume close to the boreholes
Orientation (strike/dip, right-hand-rule)	055/23	± 10/± 2	High	Seismic reflector A3	Mean value and span from /Cosma et al. 2003/. Consistent with orientation estimate from /Juhlin et al. 2002/
Thickness	13 m	± 9	Medium	Intersections along KFM02A (DZ3) and KFM03A (DZ4)	Thickness refers to total zone thickness (transition zone and core)
Length	3,889 m	± 200 m	Medium	Intersections along KFM02A (DZ3) and KFM03A (DZ4), seismic reflector A3. Truncated against ZFMNW0001, ZFMNW017A, ZFMNE0828 and ZFMNE00A2	
Ductile deformation			High	Intersections along KFM02A (DZ3) and KFM03A (DZ4)	Not present
Brittle deformation			High	Intersections along KFM02A (DZ3) and KFM03A (DZ4)	Present
Alteration			Medium	Intersections along KFM02A (DZ3) and KFM03A (DZ4)	Oxidized bedrock with fine-grained hematite dissemination in central part of the zone in KFM02A. Association here with vuggy metagranitoid
Fracture orientation (strike/dip, right-hand-rule)	Mean of gently-dipping fracture set = 034/4	K value of gently-dipping fracture set = 13	Medium	Intersections along KFM02A (DZ3) and KFM03A (DZ4), N = 224	Gently-dipping fractures dominate. Gently-dipping fracture set defined from DFN analysis
Fracture frequency	Mean 6 m ⁻¹	Span 0–15 m ⁻¹	Medium	Intersections along KFM02A (DZ3) and KFM03A (DZ4)	Sealed and open fractures. Quantitative estimate and span exclude crush zone in the upper part of the zone in KFM02A
Fracture filling			Medium	Intersections along KFM02A (DZ3) and KFM03A (DZ4)	Chlorite, calcite, clay minerals, hematite, quartz, prehnite, pyrite

**Gently SE- and S-dipping brittle deformation zones
ZFMNE00A4 (DZ1 in KFM03A/DZ2 in HFM18) – high confidence zone**

Property	Quantitative estimate	Span	Confidence level	Basis for interpretation	Comments
Position		± 15 m	High	Intersections along KFM03A (DZ1) and HFM18 (DZ2), seismic reflector A4	Span estimate refers to the general position of the central part of the zone and is based on /Cosma et al. 2003/. Span reduces to ± 1 m in the bedrock volume close to the boreholes
Orientation (strike/dip, right-hand-rule)	061/25	± 4/± 1	High	Seismic reflector A4	Strike from /Cosma et al. 2003/, dip from /Juhlin et al. 2002/. Span from both sources
Thickness	25 m	± 13 m	Medium	Intersections along KFM03A (DZ1) and HFM18 (DZ2)	Composite zone consisting of several narrower high-strain segments (sub-zones) that are inferred to diverge and converge in a complex pattern. These sub-zones separate less deformed bedrock segments. In KFM03A, sections with a higher fracture frequency occur along < 5 m thick intervals at c. 370 m, at c. 390 m and at 399 m borehole depths Thickness refers to total zone thickness (transition zones and cores)
Length	4 298 m	± 200 m	Medium	Intersections along KFM03A (DZ1) and HFM18 (DZ2), seismic reflector A4. Truncated against ZFMNW0001, ZFMNE0828 and ZFMNW017A	
Ductile deformation			High	Intersections along KFM03A (DZ1) and HFM18 (DZ2)	Not present
Brittle deformation			High	Intersections along KFM03A (DZ1) and HFM18 (DZ2)	Present
Alteration			Medium	Intersection along HFM18 (DZ2)	Oxidized bedrock with fine-grained hematite dissemination observed in the lower part of the zone in HFM18 (beneath 42 m borehole depth)
Fracture orientation (strike/dip, right-hand-rule)	Mean of gently-dipping fracture set = 042/4	K value of gently-dipping fracture set = 13	Medium	Intersections along KFM03A (DZ1) and HFM18 (DZ2), N = 216	Gently-dipping fractures dominate. Gently-dipping fracture set defined from DFN analysis
Fracture frequency	Mean 4 m ⁻¹	Span 0–21 m ⁻¹	Medium	Intersections along KFM03A (DZ1) and HFM18 (DZ2)	Open and sealed fractures. Quantitative estimate and span exclude crush zones. In KFM03A, sections with a fracture frequency > 10 m ⁻¹ and/or crush zones occur at c. 370 m, at c. 390 m and at 399 m borehole depths
Fracture filling			Medium	Intersections along KFM03A (DZ1) and HFM18 (DZ2)	Chlorite, calcite, laumontite

**Gently SE- and S-dipping brittle deformation zones
ZFMNE00A5 (DZ1 and DZ2 in KFM03B/DZ1 in HFM06/DZ1 in HFM08) – high confidence zone**

Property	Quantitative estimate	Span	Confidence level	Basis for interpretation	Comments
Position		± 15 m	High	Intersections along KFM03B (DZ1), KFM03B DZ2), HFM06 (DZ1) and HFM08 (DZ1), seismic reflector A5	ZFMNE0867 in model version 1.1 has been renamed to ZFMNE00A5. Span estimate refers to the general position of the central part of the zone and is based on /Cosma et al. 2003/. Span reduces to ± 1 m in the bedrock volume close to the boreholes. Possible correlation with linked lineament XFM0067A0
Orientation (strike/dip, right-hand-rule)	075/31	± 1/± 2	High	Seismic reflector A5	Mean value and span based on /Juhlin et al. 2002/ and /Cosma et al. 2003/
Thickness	10 m	± 5 m	Medium	Intersections along KFM03B (DZ1), HFM06 (DZ1) and HFM08 (DZ1)	Thickness refers to total zone thickness (transition zone and core). DZ2 in borehole section 62–67 m in KFM03B is c. 4 m thick and is situated c. 20 m beneath the base of DZ1 in the same borehole. It is interpreted as a separate sub-zone to ZFMNE00A5
Length	5,116 m	± 200 m	Medium	Intersections along KFM03B (DZ1), HFM06 (DZ1) and HFM08 (DZ1). Truncated against ZFMNE00A4, ZFMNW0001, ZFMNW017A and ZFMNE0828	
Ductile deformation			High	Intersections along KFM03B (DZ1), KFM03B DZ2), HFM06 (DZ1) and HFM08 (DZ1)	Not present
Brittle deformation			High	Intersections along KFM03B (DZ1), KFM03B DZ2), HFM06 (DZ1) and HFM08 (DZ1)	Present
Alteration			Medium	Intersections along KFM03B (DZ1), KFM03B DZ2), HFM06 (DZ1) and HFM08 (DZ1)	Partly oxidized bedrock with fine-grained hematite dissemination
Fracture orientation (strike/dip, right-hand-rule)	Mean of gently-dipping fracture set = 038/14	K value of gently-dipping fracture set = 12	Medium	Intersections along KFM03B (DZ1), KFM03B DZ2), HFM06 (DZ1) and HFM08 (DZ1), N = 155	Gently-dipping fractures dominate. Gently-dipping fracture set defined from DFN analysis
Fracture frequency	Mean 4 m ⁻¹	Span 0–13 m ⁻¹	Medium	Intersections along KFM03B (DZ1), KFM03B DZ2), HFM06 (DZ1) and HFM08 (DZ1)	Sealed and open fractures. Quantitative estimate and span exclude crush zones. Crush zones at 67 m in KFM03B (DZ2) and at 61 m and 70 m in HFM06 (DZ1)
Fracture filling			Medium	Intersections along KFM03B (DZ1), KFM03B DZ2), HFM06 (DZ1) and HFM08 (DZ1)	Chlorite, calcite, clay minerals, quartz, prehnite, hematite

**Gently SE- and S-dipping brittle deformation zones
ZFMNE00A6 (DZ1 in HFM07) – high confidence zone**

Property	Quantitative estimate	Span	Confidence level	Basis for interpretation	Comments
Position		± 15 m	High	Intersection along HFM07 (DZ1), seismic reflector A6	ZFMNE0868 in model version 1.1 has been renamed to ZFMNE00A6. Span estimate refers to the general position of the central part of the zone and is based on /Cosma et al. 2003/. Span reduces to ± 1 m in the bedrock volume close to borehole HFM07
Orientation (strike/dip, right-hand-rule)	075/31	± 2/± 1	High	Seismic reflector A6	Strike from /Juhlin et al. 2002/, dip from /Cosma et al. 2003/. Span from both sources
Thickness	10 m		Medium	Intersection along HFM07 (DZ1)	Thickness refers to total zone thickness (transition zone and core).
Length	5,091 m	± 200 m	Medium	Intersection along HFM07 (DZ1), seismic reflection A6. Truncated against ZFMNW0001, ZFMNW017A and ZFMNE0828	
Ductile deformation			High	Intersection along HFM07 (DZ1)	Not present
Brittle deformation			High	Intersection along HFM07 (DZ1)	Present
Alteration			Medium	Intersection along HFM07 (DZ1)	Oxidation (fine-grained hematite dissemination), chloritization
Fracture orientation (strike/dip, right-hand-rule)	Mean of NE fracture set = 045/70	K value of NE fracture set = 11	Medium	Intersections along KFM03B (DZ1), KFM03B DZ2, HFM06 (DZ1) and HFM08 (DZ1), N = 98	Fractures that strike NE and dip moderately- to steeply to the south-east dominate. NE fracture set defined from DFN analysis
Fracture frequency	Mean 7.5 m ⁻¹	Span 3–14 m ⁻¹	Medium	Intersection along HFM07 (DZ1)	Open and sealed fractures
Fracture filling			Medium	Intersection along HFM07 (DZ1)	Chlorite, calcite

**Gently SE- and S-dipping brittle deformation zones
ZFMNE00A7 (DZ2 in KFM03A/DZ3 in HFM18) – high confidence zone**

Property	Quantitative estimate	Span	Confidence level	Basis for interpretation	Comments
Position		± 15 m	High	Intersections along KFM03A (DZ2) and HFM18 (DZ3), seismic reflector A7	Span estimate refers to the general position of the central part of the zone and is based on /Cosma et al. 2003/. Span reduces to ± 1 m in the bedrock volume close to the boreholes. ZFMNE0065 also modelled to intersect HFM18 in the depth interval 119–148 m (DZ3)
Orientation (strike/dip, right-hand-rule)	055/23	– 10/– 7	High	Seismic reflector A7	Strike and dip based on /Juhlin et al. 2004/. Span based on /Juhlin et al. 2004/ and /Cosma et al. in manuscript/
Thickness	17 m	± 10 m	Medium	Intersections along KFM03A (DZ2) and HFM18 (DZ3)	Thickness refers to total zone thickness (transition zone and core). ZFMNE0065 also modelled to intersect HFM18 in the depth interval 119–148 m (DZ3)
Length	4,090 m	± 200 m	Medium	Intersections along KFM03A (DZ2) and HFM18 (DZ3), seismic reflector A7. Truncated against ZFMNE00A4, ZFMNW0001, ZFMNW017A and ZFMNE0828	
Ductile deformation			High	Intersections along KFM03A (DZ2) and HFM18 (DZ3)	Not present
Brittle deformation			High	Intersections along KFM03A (DZ2) and HFM18 (DZ3)	Present
Alteration			Medium	Intersections along KFM03A (DZ2) and HFM18 (DZ3)	Oxidized bedrock with fine-grained hematite dissemination. ZFMNE0065 also modelled to intersect HFM18 in the depth interval 119–148 m (DZ3)
Fracture orientation (strike/dip, right-hand-rule)	Mean of NE fracture set with gentle to moderate dips to the south-east = 028/34	K value of NE fracture set with gentle to moderate dips to the south-east = 15	Medium	Intersections along KFM03A (DZ2) and HFM18 (DZ3), N = 180	Fractures with a variable dip to the south-east dominate. ZFMNE0065 also modelled to intersect HFM18 in the depth interval 119–148 m (DZ3)
Fracture frequency	5 m ⁻¹	Span 0–13 m ⁻¹	Medium	Intersections along KFM03A (DZ2) and HFM18 (DZ3)	Open and sealed fractures. Quantitative estimate and span exclude sealed fracture network at 144–145 m depth interval in HFM18. ZFMNE0065 also modelled to intersect HFM18 in the depth interval 119–148 m (DZ3)
Fracture filling			Medium	Intersections along KFM03A (DZ2) and HFM18 (DZ3)	Chlorite, calcite, clay minerals, quartz, hematite, prehnite. ZFMNE0065 also modelled to intersect HFM18 in the depth interval 119–148 m (DZ3)

**Gently SE- and S-dipping brittle deformation zones
ZFMNE00B1 (DZ3 in KFM03A) – high confidence zone**

Property	Quantitative estimate	Span	Confidence level	Basis for interpretation	Comments
Position		± 15 m	High	Intersection along KFM03A (DZ3), seismic reflector B1	Span estimate refers to the general position of the central part of the zone and is based on /Cosma et al. 2003/. Span reduces to ± 1 m in the bedrock volume close to borehole KFM03A
Orientation (strike/dip, right-hand-rule)	032/27	± 2/± 2	High	Seismic reflector B1	Strike and dip after /Cosma et al. 2003/. Span based on /Juhlin et al. 2002/ and /Cosma et al. 2003/
Thickness	7 m		Medium	Intersection along KFM03A (DZ3)	Thickness refers to total zone thickness (transition zone and core).
Length	2,208 m	± 100 m	Medium	Intersection along KFM03A (DZ3), seismic reflector B1. Truncated against ZFMNE00A3, ZFMNE00A7, ZFMNE00A4, ZFMNW017A and ZFMNE0828	
Ductile deformation			High	Intersection along KFM03A (DZ3)	Not present
Brittle deformation			High	Intersection along KFM03A (DZ3)	Present
Alteration			Medium	Intersection along KFM03A (DZ3)	Oxidized bedrock with fine-grained hematite dissemination
Fracture orientation (strike/dip, right-hand-rule)	Mean of gently-dipping fracture set = 128/12	K value of gently-dipping fracture set = 9	Medium	Intersection along KFM03A (DZ3), N = 46	Gently-dipping fractures dominate. Gently-dipping fracture set defined from DFN analysis
Fracture frequency	Mean 6 m ⁻¹	Span 1–10 m ⁻¹	Medium	Intersection along KFM03A (DZ3)	Sealed and open fractures
Fracture filling			Medium	Intersection along KFM03A (DZ3)	Chlorite, calcite, clay minerals, quartz, prehnite, laumontite, hematite, epidote

**Gently SE- and S-dipping brittle deformation zones
ZFMNE00B4 (DZ10 in KFM02A) – high confidence zone**

Property	Quantitative estimate	Span	Confidence level	Basis for interpretation	Comments
Position		± 15 m	High	Intersection along KFM02A (DZ10), seismic reflector B4	Span estimate refers to the general position of the central part of the zone and is based on /Cosma et al. 2003/. Span reduces to ± 1 m in the bedrock volume close to borehole KFM02A
Orientation (strike/dip, right-hand-rule)	050/29		High	Seismic reflector B4	Strike and dip after /Cosma et al. 2003/. Consistent with /Juhlin et al. 2002/. Only 1° difference in dip value in these two contributions
Thickness	5 m		Medium	Intersection along KFM02A (DZ10)	Thickness refers to total zone thickness (transition zone and core).
Length					ZFMNE00B4 does not extend to the surface Truncation against ZFMNW0001 in the north-east, against ZFMNW017A in the south-west and against ZFMNE0062 in the north-west. Truncation to the north-west takes account of recommendation in /Juhlin et al. 2004/
Ductile deformation			High	Intersection along KFM02A (DZ10)	Not present
Brittle deformation			High	Intersection along KFM02A (DZ10)	Present
Alteration			Medium	Intersection along KFM02A (DZ10)	Oxidized bedrock with fine-grained hematite dissemination
Fracture orientation (strike/dip, right-hand-rule)	Mean of all fractures = 068/52	K value of all fractures = 9	Medium	Intersection along KFM02A (DZ10), N =27	Most fractures dip gently- to moderately to the south-east and south. Low number of measurements
Fracture frequency	4.5 m ⁻¹	Span 1–11 m ⁻¹	Medium	Intersection along KFM02A (DZ10)	Sealed and open fractures
Fracture filling			Medium	Intersection along KFM02A (DZ10)	Chlorite, prehnite, calcite

**Gently SE- and S-dipping brittle deformation zones
ZFMNE00B6 (DZ2 in KFM02A/DZ2 in HFM04) – high confidence zone**

Property	Quantitative estimate	Span	Confidence level	Basis for interpretation	Comments
Position		± 15 m	High	Intersections along KFM02A (DZ2) and HFM04 (DZ2), seismic reflector B6	Span estimate refers to the general position of the central part of the zone and is based on /Cosma et al. 2003/. Span reduces to ± 1 m in the bedrock volume close to the boreholes
Orientation (strike/dip, right-hand-rule)	030/32		High	Seismic reflector B6	/Cosma et al. in manuscript/. Consistent with /Juhlin et al. 2004/
Thickness	7 m	± 4 m	Medium	Intersections along KFM02A (DZ2) and HFM04 (DZ2)	Thickness refers to total zone thickness (transition zone and core)
Length	2,950 m	± 200 m	Medium	Intersections along KFM02A (DZ2) and HFM04 (DZ2), seismic reflector B6. Truncated against ZFMNW0001 and ZFMNW017A	
Ductile deformation			High	Intersections along KFM02A (DZ2) and HFM04 (DZ2)	Not present
Brittle deformation			High	Intersections along KFM02A (DZ2) and HFM04 (DZ2)	Present
Alteration			Medium	Intersections along KFM02A (DZ2) and HFM04 (DZ2)	Strong clay alteration. Oxidized bedrock with fine-grained hematite dissemination in the lower part of the zone (DZ2) in KFM02A
Fracture orientation (strike/dip, right-hand-rule)	Mean of gently-dipping fracture set = 038/15	K value of gently-dipping fracture set = 15	Medium	Intersections along KFM02A (DZ2) and HFM04 (DZ2), N = 105	Gently- to moderately-dipping fractures dominate. Gently-dipping fracture set defined from DFN analysis
Fracture frequency	Mean 6 m ⁻¹	Span 1–15 m ⁻¹	Medium	Intersections along KFM02A (DZ2) and HFM04 (DZ2)	Open and partly open fractures dominate. Quantitative estimate and span exclude crush zones that are prominent in the lower part of DZ2 in KFM02A
Fracture filling			Medium	Intersections along KFM02A (DZ2) and HFM04 (DZ2)	Chlorite, calcite, clay minerals, hematite

**Gently SE- and S-dipping brittle deformation zones
ZFMNE0866 (DZ1 in KFM02A/DZ1 in HFM04/DZ1 in HFM05) – high confidence zone**

Property	Quantitative estimate	Span	Confidence level	Basis for interpretation	Comments
Position		± 1 m	High	Intersections along KFM02A (DZ1), HFM04 (DZ1) and HFM05 (DZ1)	Span estimate refers to the position of the central part of the zone close to the boreholes.
Orientation (strike/dip, right-hand-rule)	061/31	± 5/± 5	High	Intersections along KFM02A (DZ1), HFM04 (DZ1) and HFM05 (DZ1)	
Thickness	5.5 m	± 4.5 m	Medium	Intersections along KFM02A (DZ1), HFM04 (DZ1) and HFM05 (DZ1)	Thickness refers to total zone thickness (transition zone and core)
Length	2,417 m	± 100 m	Medium	Intersections along KFM02A (DZ1), HFM04 (DZ1) and HFM05 (DZ1). Truncated against ZFMNE00A3, ZFMNE00B6 and ZFMNE0065	
Ductile deformation			High	Intersections along KFM02A (DZ1), HFM04 (DZ1) and HFM05 (DZ1)	Not present
Brittle deformation			High	Intersections along KFM02A (DZ1), HFM04 (DZ1) and HFM05 (DZ1)	Present
Alteration			Medium	Intersections along KFM02A (DZ1), HFM04 (DZ1) and HFM05 (DZ1)	Oxidation (fine-grained hematite dissemination), chloritization
Fracture orientation (strike/dip, right-hand-rule)	Mean of gently-dipping fracture set = 001/11	K value of gently-dipping fracture set = 13	Medium	Intersections along KFM02A (DZ1), HFM04 (DZ1) and HFM05 (DZ1), N = 58	Gently-dipping fractures dominate. Steeply-dipping fractures with variable strike are also present. Gently-dipping fracture set defined from DFN analysis
Fracture frequency	Mean 4 m ⁻¹	Span 1–13 m ⁻¹	Medium	Intersections along KFM02A (DZ1), HFM04 (DZ1) and HFM05 (DZ1)	Sealed and open fractures. Quantitative estimate and span exclude crush zone in HFM05 (DZ1)
Fracture fillings			Medium	Intersections along KFM02A (DZ1), HFM04 (DZ1) and HFM05 (DZ1)	Chlorite, calcite

**Gently SE- and S-dipping brittle deformation zones
ZFMNE0871 (Zone H2, SFR) – high confidence zone**

Property	Quantitative estimate	Span	Confidence level	Basis for interpretation	Comments
Position		± 1 m	High	Intersection along SFR tunnel and boreholes	Span estimate refers to the position of the central part of the zone in SFR tunnel and boreholes Projection to surface differs in /Axelsson and Hansen, 1997/ and /Holmén and Stigsson, 2001/. Possible correlation with linked lineament XFM0137B0 that has been recognised on the basis of magnetic and bathymetric data
Orientation (strike/dip, right-hand-rule)	048/16	± 5/± 15	Medium	Intersection along SFR tunnel	ENE/20 in /Axelsson and Hansen, 1997/. NE/15–20 in /Holmén and Stigsson, 2001/
Thickness	10 m	± 9 m	High	Intersection along SFR tunnel and boreholes	Thickness refers to total zone thickness (transition zone and core)
Length	1,168 m	± 100 m	Medium	Intersection along SFR tunnel and boreholes. Truncated against ZFMNW0001, ZFMNW0002 and ZFMNW0805	
Ductile deformation			High	Intersection along SFR tunnel and boreholes	Not present
Brittle deformation			High	Intersection along SFR tunnel and boreholes	Present
Alteration			High	Intersection along SFR boreholes	Present
Fracture orientation (strike/dip, right-hand-rule)					
Fracture frequency	15 m ⁻¹	± 5 m ⁻¹	High	Intersection along SFR boreholes	
Fracture filling			High	Intersection along SFR boreholes	Clay minerals

**Gently SE- and S-dipping brittle deformation zones
ZFMNE1187 (DZ1 in HFM09/DZ2 in HFM10) – high confidence zone**

Property	Quantitative estimate	Span	Confidence level	Basis for interpretation	Comments
Position		± 1 m	High	Intersections along HFM09 (DZ1) and HFM10 (DZ2)	Span estimate refers to the position of the central part of the zone close to the boreholes. Intersects also KFM04A (c. 75 m) and KFM04B (c. 80 m). Report during drilling
Orientation (strike/dip, right-hand-rule)	032/15	± 5/± 5	High	Intersections along HFM09 (DZ1) and HFM10 (DZ2)	Intersects also KFM04A (c. 75 m) and KFM04B (c. 80 m). Report during drilling
Thickness	7 m		Medium	Intersections along HFM09 (DZ1) and HFM10 (DZ2)	Thickness refers to total zone thickness (transition zone and core)
Length	911 m	± 100 m	Medium	Intersections along HFM09 (DZ1) and HFM10 (DZ2). Truncated against ZFMNE00A2, ZFMNW017A and ZFMNE062A	
Ductile deformation			High	Intersections along HFM09 (DZ1) and HFM10 (DZ2)	Not present
Brittle deformation			High	Intersections along HFM09 (DZ1) and HFM10 (DZ2)	Present
Alteration			Medium	Intersections along HFM09 (DZ1) and HFM10 (DZ2)	Oxidized bedrock with fine-grained hematite dissemination
Fracture orientation (strike/dip, right-hand-rule)	Mean of gently-dipping fracture set = 037/12 Mean of NE fracture set = 231/78	K value of gently-dipping fracture set = 28 K value of NE fracture set = 34	Medium	Intersections along HFM09 (DZ1) and HFM10 (DZ2), N = 68	Two fracture sets that are gently-dipping to the south-east and steeply-dipping to the north-west. Fracture sets defined from DFN analysis
Fracture frequency	Mean 3 m ⁻¹	Span 0–19 m ⁻¹	Medium	Intersections along HFM09 (DZ1) and HFM10 (DZ2)	Open and sealed fractures. Quantitative estimate and span exclude two crush zones in HFM09 (DZ1) and a sealed fracture network in HFM10 (DZ2)
Fracture filling			Medium	Intersections along HFM09 (DZ1) and HFM10 (DZ2)	Chlorite, calcite, epidote

**Gently SE- and S-dipping brittle deformation zones
ZFMNE1193 (316–322 m level in DBT1/KFK001) – high confidence zone**

Property	Quantitative estimate	Span	Confidence level	Basis for interpretation	Comments
Position		± 1 m	High	Intersection along borehole length 316–322 m in DBT1 (KFK001)	Span estimate refers to the position of the central part of the zone close to borehole DBT1 (KFK001). Data from borehole drilled during construction of nuclear power plant
Orientation (strike/dip, right-hand-rule)	080/27	± 5/± 5	High	Comparison with ZFMNE00A2. Minor modification in dip so as to avoid intersection in DBT3 (KFK003)	
Thickness	5 m		Medium	Intersection along borehole length 316–322 m in DBT1 (KFK001)	Thickness refers to total zone thickness (transition zone and core)
Length	3,288 m	± 200 m	Medium	Intersection along borehole length 316–322 m in DBT1 (KFK001). Truncated against ZFMNW0001, ZFMNW003A, ZFMNW0017A and ZFMNE0060	
Ductile deformation			High	Intersection along borehole length 316–322 m in DBT1 (KFK001)	Not present
Brittle deformation			High	Intersection along borehole length 316–322 m in DBT1 (KFK001)	Present
Alteration					
Fracture orientation (strike/dip, right-hand-rule)					
Fracture frequency					
Fracture filling					

**Gently SE- and S-dipping brittle deformation zones
ZFMNE1195 (DZ8 in KFM02A) – high confidence zone**

Property	Quantitative estimate	Span	Confidence level	Basis for interpretation	Comments
Position		± 1 m	High	Intersection along KFM02A (DZ8)	Span estimate refers to the position of the central part of the zone close to borehole KFM02A. The minor zone DZ9 that occurs in the 922–925 m depth interval in KFM02A, 17 m borehole length beneath DZ8, is possibly a sub-zone related to ZFMNE1195
Orientation (strike/dip, right-hand-rule)	080/39	± 5/± 5	Low	Orientation of fractures in KFM02A (DZ8)	Low number of fractures in the set (24)
Thickness	9 m		Medium	Intersection along KFM02A (DZ8)	Thickness refers to total zone thickness (transition zone and core)
Length					ZFMNE1195 does not intersect the surface. Truncated against ZFMNE0062, ZFMNE0065, ZFMNE00A2, ZFMNE00B4 and ZFMNE00B6
Ductile deformation			High	Intersection along KFM02A (DZ8)	Not present
Brittle deformation			High	Intersection along KFM02A (DZ8)	Present
Alteration					
Fracture orientation (strike/dip, right-hand-rule)	Mean of dominant gently- to moderately-dipping fracture set = 080/40	K value of gently-dipping fracture set = 28	Medium	Intersection along KFM02A (DZ8), N = 57	Gently- to moderately- and southerly-dipping fractures form the most prominent fracture set. Fractures with other orientations are also present
Fracture frequency	Mean 5 m ⁻¹	Span 0–20 m ⁻¹	Medium	Intersection along KFM02A (DZ8)	Dominance of sealed fractures
Fracture filling			Medium	Intersection along KFM02A (DZ8)	Chlorite, calcite

Gently SE- and S-dipping brittle deformation zones, based solely on seismic reflection data and comparison study ZFMNE00A1 – medium confidence zone

Property	Quantitative estimate	Span	Confidence level	Basis for interpretation	Comments
Position		± 15 m	High	Seismic reflector A1/A0	Span estimate refers to the general position of the central part of the zone. Estimate based on /Cosma et al. 2003/. Possible correlation with linked lineament XFM0137A0 that has been recognised on the basis of magnetic, electrical, topographic and bathymetric data
Orientation (strike/dip, right-hand-rule)	082/45	– 7± 5	High	Seismic reflector A1/A0	Strike and dip based on /Cosma et al. 2003/. Span estimate makes use of both /Juhlin et al. 2002/ and /Cosma et al. 2003/
Thickness	65 m	± 35 m	Medium	Comparison with ZFMNE00A2	Thickness refers to total zone thickness (transition zone and core)
Length	3,213 m in base model 3,669 m (minimum) in variant of base model	± 200 m	Medium	Seismic reflector A1/A0. Alternative models: Truncated against ZFMNW0001 and ZFMNW003A in base model and against ZFMNW0001 and ZFMNW004A in variant of base model. ZFMNE00A1 in the variant of the base model extends outside the regional model volume. Only a minimum length can be determined	
Ductile deformation			Medium	Comparison with high confidence, gently-dipping zones	Not present
Brittle deformation			High	Comparison with high confidence, gently-dipping zones	Present
Alteration					
Fracture orientation (strike/dip, right-hand-rule)					
Fracture frequency					
Fracture filling					

Gently SE- and S-dipping brittle deformation zones, based solely on seismic reflection data and comparison study ZFMNEB23A, B – medium confidence zone

Property	Quantitative estimate	Span	Confidence level	Basis for interpretation	Comments
Position		± 15 m	High	Seismic reflectors B2 and B3	Seismic reflectors B2 and B3 have been treated together to form a single zone. This zone has been divided into two segments (A and B) separated by ZFMNE0065. Span estimate refers to the general position of the central part of the zone. Estimate based on /Cosma et al. 2003/
Orientation (strike/dip, right-hand-rule)	028/24	± 3/± 3	High	Seismic reflectors B2 and B3	/Cosma et al. 2003/. Consistent with /Juhlin et al. 2002/
Thickness	15 m	± 10 m	Medium	Comparison with high confidence, gently-dipping zones except ZFMNE00A2	Thickness refers to total zone thickness (transition zone and core)
Length					ZFMNEB23A, B does not intersect the surface. Truncated against ZFMNW0001, ZFMNW017A, ZFMNE0062 and arbitrarily against the downward projection (90°) of lineament XFM0101A0
Ductile deformation			Medium	Comparison with high confidence, gently-dipping zones	Not present
Brittle deformation			High	Comparison with high confidence, gently-dipping zones	Present
Alteration					
Fracture orientation (strike/dip, right-hand-rule)					
Fracture frequency					
Fracture filling					

Gently SE- and S-dipping brittle deformation zones, based solely on seismic reflection data and comparison study ZFMNE0B5A, B – medium confidence zone

Property	Quantitative estimate	Span	Confidence level	Basis for interpretation	Comments
Position		± 15 m	High	Seismic reflector B5	This zone has been divided into two segments (A and B) separated by ZFMNE0065. Span estimate refers to the general position of the central part of the zone. Estimate based on /Cosma et al. 2003/.
Orientation (strike/dip, right-hand-rule)	050/9 for ZFMNE0B5A and 062/26 for ZFMNE0B5B		High	Seismic reflector B5	Strike and dip after /Cosma et al. 2003/
Thickness	15 m	± 10 m	Medium	Comparison with high confidence, gently-dipping zones except ZFMNE00A2	Thickness refers to total zone thickness (transition zone and core)
Length					ZFMNE0B5A, B does not intersect the surface. Truncated against ZFMNW0001, ZFMNW017A, ZFMNE0062 and arbitrarily against the downward projection (90°) of lineament XFM0101A0
Ductile deformation			Medium	Comparison with high confidence, gently-dipping zones	Not present
Brittle deformation			High	Comparison with high confidence, gently-dipping zones	Present
Alteration					
Fracture orientation (strike/dip, right-hand-rule)					
Fracture frequency					
Fracture filling					

Gently SE- and S-dipping brittle deformation zones, based solely on seismic reflection data and comparison study ZFMNE00B7 – medium confidence zone

Property	Quantitative estimate	Span	Confidence level	Basis for interpretation	Comments
Position		± 15 m	High	Seismic reflector B7	Span estimate refers to the general position of the central part of the zone. Estimate based on /Cosma et al. 2003/
Orientation (strike/dip, right-hand-rule)	025/20	– 9/+ 2	High	Seismic reflector B7	Strike and dip after /Juhlin et al. 2004/. Span estimate makes use of both /Juhlin et al. 2004/ and /Cosma et al. in manuscript/
Thickness	15 m	± 10 m	Medium	Comparison with high confidence, gently-dipping zones except ZFMNE00A2	Thickness refers to total zone thickness (transition zone and core)
Length	1,999 m	± 100 m		Does not appear to intersect boreholes to the south-east of ZFMNE0060. Truncated against ZFMNW0001, ZFMNE0060 and ZFMNE00A2	
Ductile deformation			Medium	Comparison with high confidence, gently-dipping zones	Not present
Brittle deformation			High	Comparison with high confidence, gently-dipping zones	Present
Alteration					
Fracture orientation (strike/dip, right-hand-rule)					
Fracture frequency					
Fracture filling					

Gently SE- and S-dipping brittle deformation zones, based solely on seismic reflection data and comparison study ZFMNE00C1 – medium confidence zone

Property	Quantitative estimate	Span	Confidence level	Basis for interpretation	Comments
Position		± 15 m	High	Seismic reflector C1	Span estimate refers to the general position of the central part of the zone. Estimate based on /Cosma et al. 2003/
Orientation (strike/dip, right-hand-rule)	037/18	– 22/+ 2	High	Seismic reflector C1	Strike and dip after /Cosma et al. 2003/. Span estimate makes use of both /Juhlin et al. 2002/ and /Cosma et al. 2003/
Thickness	65 m	± 35 m	Medium	Comparison with ZFMNE00A2	Thickness refers to total zone thickness (transition zone and core)
Length					ZFMNE00C1 does not intersect the surface. Alternative models after comparison with ZFMNE00A1 and ZFMNE00A2: In the base model, ZFMNE00C1 is truncated against ZFMNW0001 and ZFMNW003A. In the variant of the base model, ZFMNE00C1 is truncated against ZFMNW0001 and ZFMNW004A
Ductile deformation			Medium	Comparison with high confidence, gently-dipping zones	Not present
Brittle deformation			High	Comparison with high confidence, gently-dipping zones	Present
Alteration					
Fracture orientation (strike/dip, right-hand-rule)					
Fracture frequency					
Fracture filling					

Gently SE- and S-dipping brittle deformation zones, based solely on seismic reflection data and comparison study ZFMNE00C2 – medium confidence zone

Property	Quantitative estimate	Span	Confidence level	Basis for interpretation	Comments
Position		± 15 m	High	Seismic reflector C2	Span estimate refers to the general position of the central part of the zone. Estimate based on /Cosma et al. 2003/.
Orientation (strike/dip, right-hand-rule)	035/13	– 40/– 3	High	Seismic reflector C2	Strike and dip after /Cosma et al. 2003/. Span estimate makes use of both /Juhlin et al. 2002/ and /Cosma et al. 2003/
Thickness	65 m	± 35 m	Medium	Comparison with ZFMNE00A2	Thickness refers to total zone thickness (transition zone and core)
Length					ZFMNE00C2 does not intersect the surface. Alternative models after comparison with ZFMNE00A1 and ZFMNE00A2. In the base model, ZFMNE00C2 is truncated against ZFMNW0001 and ZFMNW003A. In the variant of the base model, ZFMNE00C2 is truncated against ZFMNW0001 and ZFMNW004A
Ductile deformation			Medium	Comparison with high confidence, gently-dipping zones	Not present
Brittle deformation			High	Comparison with high confidence, gently-dipping zones	Present
Alteration					
Fracture orientation (strike/dip, right-hand-rule)					
Fracture frequency					
Fracture filling					

Gently SE- and S-dipping brittle deformation zones, based solely on seismic reflection data and comparison study ZFMNW00E1 – medium confidence zone

Property	Quantitative estimate	Span	Confidence level	Basis for interpretation	Comments
Position		± 15 m	High	Seismic reflector E1	Span estimate refers to the general position of the central part of the zone. Estimate based on /Cosma et al. 2003/
Orientation (strike/dip, right-hand-rule)	297/12	– 27/– 3	High	Seismic reflector E1	Strike and dip after /Cosma et al. 2003/. Span estimate makes use of both /Juhlin et al. 2002/ and /Cosma et al. 2003/
Thickness	15 m	± 10 m	Medium	Comparison with high confidence, gently-dipping zones except ZFMNE00A2	Thickness refers to total zone thickness (transition zone and core)
Length					ZFMNE00E1 does not intersect the surface. Truncated against ZFMNW017A, ZFMNE0062 and ZFMNE0065
Ductile deformation			Medium	Comparison with high confidence, gently-dipping zones	Not present
Brittle deformation			High	Comparison with high confidence, gently-dipping zones	Present
Alteration					
Fracture orientation (strike/dip, right-hand-rule)					
Fracture frequency					
Fracture filling					

Overall confidence assessment

Table A4-1. Protocol for use of available data and potential biases in the bedrock description.

Question	Geology	Rock mechanics	Thermal	Hydrogeology	Hydrogeochemistry	Transport
Which data have been used for the current model version (refer to tables in Chapter 2 of the report).	A detailed summary of data used (including P-report references) is available in Table 2-1 in Chapter 2. Furthermore, the data are referred to under the relevant section in Chapter 5.	See Table 2-2. <i>From the geology:</i> – Geological “single-hole interpretation” of 4 boreholes (KFM01A, KFM02A, KFM03A, KFM04A). <i>From the Laboratory:</i> – BOREMAP data from 4 drill cores (KFM01A, KFM02A, KFM03A, KFM04A). – Laboratory tests on intact rock; Uniaxial compression tests, Triaxial compression tests, Indirect tensile tests, P-wave velocity measurements on the core. – Laboratory tests on rock fractures; Normal loading tests, Direct shear tests, Tilt tests. From In situ Measurements: – HF and HTPF (KFM01A, KFM01B, KFM02A, KFM04A). – OC (KFM01B). – Core diskling information. <i>From pre-existent investigations:</i> – Laboratory tests on intact rock and fractures (SFR). – Old data from tunnelling through Singö deformation zone provide an estimation of the mechanical properties of the regional deformation zones.	See Table 2-3. Thermal conductivity, heat capacity and density measurements (at different temperatures) measurement on bore cores. Comparing TPS measurements with different laboratories. Two separate anisotropy measurements of thermal properties. Modal analyses. Data from previous model version with reclassified rock codes and new modal analyses from boreholes. Thermal expansion measurements. Temperature and gradient loggings. Lithological model and Boremap core logging from the geological model.	Listed in Table 2-4. Single-hole difference flow logging in cored boreholes KFM01A–KFM05A. Single-hole Injection tests in cored boreholes KFM01A–KFM03A. Single-hole pumping tests and flow logging in percussion-drilled boreholes HFM01–19. Cross-hole pumping tests and responses between bedrock boreholes during pumping and other interferences. Reports describing results of hydraulic tests in boreholes drilled at SFR, Forsmark power plant and Finnsjön. Bedrock overburden interface, see Table A4-2.	Listed in Table 2-5. KFM01A, KFM02A, KFM03A; KFM04A Complete chemical characterisation (class 4 and 5), sampling during drilling, Uranine analyses. Percussion-drilled boreholes HFM01–HFM19. Environmental monitoring boreholes PFM000001-7-9-910-39-2942-4778. Soil pipes, BAT tubes. Sea Water, Running water, Lake Water. Other available data: Swedish and Nordic site data.	Data from Transport programme (Table 2-6): Resistivity lab KFM01A, KFM02A (delivered). In situ formation factor KFM01A, KFM02A (delivered). BET-area, crushed material KFM01A, KFM02A, KFM03A, KFM04A. Through diffusion KFM01A, KFM02A (partial delivery Dec. 2004). Data from other programmes: Porosity (matrix) (geology/mechanics?) Lithological data (geology) Mineralogical data (geology) Water chemical composition (groundwater chemistry) Fracture length and orientation (geology) Fracture transmissivity (hydrogeology) Fracture frequency (borehole log, geology) Sorpton, diffusivity and porosity from Finnsjön investigation.

Question	Geology	Rock mechanics	Thermal	Hydrogeology	Hydrogeochemistry	Transport
		<ul style="list-style-type: none"> Independent Q-loggings of rock outcrops and KFM01A. Re-interpretation of pre-existent HF measurements (DBT1.) Re-interpretation of regional stress data (Finnsjön, Björkö, Stockholm, Olkiluoto, etc). 				
<p>If available data have not been used</p> <p>– what is the reason for their omission (e.g. not relevant, poor quality, lack of time, ...)</p> <p>A) <i>Regional gravity data</i> reported in P-03-42 have not been used. The data are of regional character and have been judged to be of insufficient resolution for reliable geophysical modelling. Modelling of geophysical data has so far not been carried out at Forsmark.</p> <p>B) <i>Estimations of the dip of magnetic anomalies</i> reported in P-04-283 have not been used. These estimations were not available at the time of modelling. Report P-04-283 only became available at the end of 2004.</p> <p>C) <i>Fracture data from boreholes and tunnels close to the nuclear power plant and SFR.</i> These data have received lower priority, since virtually all these boreholes and tunnels have generated only near-surface data. There are few data from depths > 100 m. Secondly, there is no control on the strike and dip of fractures from these borehole data.</p> <p>D) <i>Minor DZ in the old construction areas.</i> These DZ are too small to be included in the regional model version.</p>	<ul style="list-style-type: none"> Information from percussion boreholes has not been directly used (is however considered in the geological model). Previous characterisations of the rock mass at SFR have been used for comparison. Reasons for the omission: <ul style="list-style-type: none"> The empirical methods require frequency, orientation, aperture, roughness and infillings of the fracture that are not provided by percussion boreholes. The theoretical approach makes use of the DFN Model. The DFN Model does not consider percussion borehole information. The percussion boreholes reach shallow depth (around 100 m). Previous characterisation at SFR are also at shallow depth. 	<p>Anisotropy measurements presented in P-03-08 have not been used due to uncertainties in the method. Modal analyses where the sum of minerals differs to a large extent from 100 % have been excluded (few samples).</p> <p>Density loggings have not been used since there is no valid relationship between density and thermal conductivity for rock types in the Forsmark area.</p>	<p>It has not been possible to go into detail regarding the evaluations of the hydraulic tests in boreholes drilled at SFR, Forsmark power plant and Finnsjön.</p>	<p>Swedish site data, used for comparison and for conceptual modelling.</p> <p>Nordic site data, used for comparison and for conceptual modelling.</p> <p>Many observations excluded (particularly concerning surface samples which are used for background information) from the detailed modelling due to representativity problems or not being completely reported at the time of data freeze.</p>	<p>Some old Finnsjön data were excluded already in version 1.1, see /SKB, 2004a/, due to:</p> <ul style="list-style-type: none"> Differences in methods compared to the methods decided to be generally established for the site investigation investigations. Incomplete geological and/or hydrochemical information. 	

Question	Geology	Rock mechanics	Thermal	Hydrogeology	Hydrogeochemistry	Transport
	<p>E) <i>Scan line mapping of fractures at the five detailed mapped outcrops.</i> Partly because they would not produce much more information on orientation and size than the detailed surface mapping.</p> <p>F) <i>Scan line mapping of fractures carried out in connection with the bedrock mapping programme.</i> Partly because they are not part of the same "data set".</p>					
<p>(If applicable) What would have been the impact of the non-used data?</p>	<p>A) <i>Regional gravity data:</i> Subordinate impact. The data are only of broad regional significance.</p> <p>B) <i>Dip of magnetic anomalies:</i> Would potentially have provided some help to both the rock domain and deterministic structural models.</p> <p>C) <i>Fracture data from older boreholes:</i> Additional information at depths predominantly down to c. 100 m for fracture intensity and character of fracture filling.</p> <p>D) <i>Minor DZ in the old construction areas.</i> Negligible.</p> <p>E) <i>Scan line mapping of fractures at the five detailed mapped outcrops:</i> These data may help to fill the gap of fractures from 0.2 up to 0.5 m, and confirm what is observed from surface mapping.</p> <p>F) <i>Scan line mapping of fractures carried out in connection with the bedrock mapping programme:</i> These data could provide information concerning the spatial variability of fracture intensity, pattern and orientation.</p>	<p>Old rock mechanics data available cover the area of the SFR and of the power plant. Thus, it is marginal for the candidate area. The laboratory tests have been used for comparison with the new laboratory results. The data neglected for this model analysis concern shallow depths. A back analysis of the convergence measurements from tunnelling at SFR and through Singö deformation zone could reduce the uncertainty of the mechanical properties of the regional deformation zones and of the rock stress field.</p>	<p>The impact when considering the extra modal analyses is small. Using the density loggings gives a large scale spatial distribution of the rock type.</p>	<p>Minor, if any.</p>	<p>The impact of using non-representativity data has been checked by means of visualisation. The results indicate that the results can make a difference of $\pm 50\%$ locally, at site scale on the order of $\pm 10\%$.</p>	<p>Some more "site-specific" data, but the data are too uncertain to be of real value.</p>

Question	Geology	Rock mechanics	Thermal	Hydrogeology	Hydrogeochemistry	Transport
How is data accuracy established (e.g. using QA procedures) for the different data? (Essentially just refer to tables in Chapter 2).	The data used in the geological modelling are listed in Table 2-1, Chapter 2. Data stored in SICADA follows standard QA procedures as set out in the method descriptions. Deviations have been handled accordingly. Exceptions are historic data (SFR and Forsmark power plant) that lack QA procedures.	BOREMAP data have been used as stored in SICADA after removing double values. QA according to the methodology. Laboratory tests on intact rock have been used as stored in SICADA. Independent testing was performed on a set of samples for quality assessment. QA according to the methodology.	For details about data collection and accuracy reference is given to the individual reports. Except quality assurance mentioned in reports, reasonableness check has been made when working with data. Modal analyses have been compared with TPS measurements to evaluate the validity.	According to standard QA procedures. Deviations have been handled accordingly. Exceptions are historic data from SFR, Forsmark power plant and Finnsjön, which lack QA procedures. Consistency checks between different types of hydraulic tests have been performed, e.g. PFL vs. PSS, and single hole tests vs. interference tests.	According to standard QA procedures. Deviations have been handled accordingly. Measurement errors are on the order of (\pm 5–10%), see Section 9.2.	Site Investigation Transport data: QA according to Method Descriptions. QA of data from other disciplines as described in Chapter 2 and references cited there. Accuracy in Finnsjön data established by evaluation of the raw data according to the Method descriptions.
	Reference to individual P-reports is necessary. The evaluation of these data is provided in Chapter 5 (Section 5.2). Reasonableness of data checked on an "ad-hoc" basis. For example, modellers have a dialogue with e.g. the BOREMAP core logging team, and also make their own inspections of the core and discuss this with the mapping team. Modellers are also involved in both the assembly and interpretation of data at the surface and in the development of single-hole interpretations.	Laboratory tests on rock fractures have been used as stored in SICADA. Some problems in the determination of the normal and shear stiffness were encountered due to the fact that the compressibility of the rock walls was neglected. QA according to the actual methodology (correction made on same results). Tilt test results were used as stored in SICADA. QA according to the methodology. P-wave velocity on the core was used as stored in SICADA. QA according to the methodology. Q-logging was carried out by different consultants for the same borehole (KFM01A) with good agreement in the results. The uncertainty of the rock mechanics properties of the rock mass are quantified in this model version. QA according to the methodology.	In cases where the data reports not yet were finished, contact with the report producers has been established. Comparison between different laboratories.			

Question	Geology	Rock mechanics	Thermal	Hydrogeology	Hydrogeochemistry	Transport
		OC, HF and HTPF data were used as stored in SICADA. QA according to the methodology. For the analysis of rock stresses, some of the measurement results were neglected because they were judged to be at the limit of applicability of OC, HF and HTPF techniques, respectively.				
List data (types) where accuracy precision is judged low – and answer whether inaccuracy is quantified (with reference to applicable sections of this report or supporting documents).	<i>Percussion borehole data:</i> The assessment of rock type and especially the character of mineral filling along fractures in the percussion boreholes are judged to be of significantly lower quality than the equivalent assessments in the cored boreholes. Furthermore, since the recognition of fractures within the percussion boreholes is based solely on BIPS information, the assessment of fracture intensity along such boreholes is judged to be too low. These inaccuracies have not been quantified but are important for the consideration of the quality of data generated from percussion relative to cored boreholes.	<i>Mechanical properties</i> Accuracy can be low for the determination of the normal and shear stiffness of the rock fractures. A new correction during the processing of the data has been introduced. This will lead to a modification of the methodology for normal and shear stiffness determination on fractures. QA was carried out according to the actual methodology (without correction). Accuracy of the tilt test results was judged lower than for direct shear tests on fractures. The tilt test results were used for comparison. The accuracy of the rock mass quality and rock mass mechanical properties was quantified in this model version. The estimated accuracy of the mean values of the rock mass quality for rock domain RFM029 might vary as follows (see Chapter 6): – Q: ±10% – RMR: ±1%	Temperature loggings from different boreholes show a variation in temperature at canister level. The difference is not large, but also small differences influence the design. Possible explanations are time of logging after drilling (drilling adds heat), water movements in the boreholes, an uncertainty in the temperature logging or inclination measurements in boreholes. For domains other than RFM029 and RFM012 there is not enough borehole data to reflect the domain, which limits the domain modelling of thermal properties. Poor representativity of samples measured with TPS in other rock types than granite to granodiorite within the candidate volume (101057).	Results from WL-tests and airlift-pumping generally have less accuracy than other hydraulic tests due to the prevailing low permeability conditions. No quantification of inaccuracy available at present! The measurement threshold of the PFL test is found to be sensitive to high flow rates in the upper part of the cored boreholes. A quantification of the inaccuracy is available. The interpretation of pumping tests and flow logging in percussive-drilled boreholes is highly sensitive to changes in the drill bit diameter due to wearing. A quantification of the inaccuracy is available. Sediment-filled fractures may influence transmissivity values in the upper c. 50–100 m, see Chapter 8.	Major components, stable isotopes (± 5–10%). The effect of these errors on the interpretation is checked in the section of Explorative analysis (see Chapter 9).	General uncertainties included in the evaluation concept for sorption coefficients and diffusivities are addressed and discussed in /R-03-20/ Accuracy in in situ resistivity measurement depends on assumed water composition of the pore liquid. This composition is uncertain. Low accuracy/precision in correlation between through-diffusion experiment results and data from resistivity measurements /Appendix in R-03-20/.
	<i>Errors in the coding of the BOREMAP information.</i> Major errors probably detected, but minor mistakes could go undetected. <i>Errors in orientation of the BIPS image.</i> Range 1–8 degrees.					

Question	Geology	Rock mechanics	Thermal	Hydrogeology	Hydrogeochemistry	Transport
<p><i>Errors in the deviation measurements of the inclined boreholes.</i></p> <p><i>Orientation of radar reflectors:</i> The documented orientation of radar reflectors is judged to be of low accuracy. Inaccuracy not quantified. Method-specific problem. Radar reflectors not consistent with fracture information.</p> <p><i>Judgements involved in producing co-ordinated and linked lineaments.</i> Gives rise to a major uncertainty in lineament length.</p> <p>The interpretation of lineaments in the vicinity of the nuclear power plant has made use of <i>old seismic refraction data</i> that were available prior to the site investigation programme and <i>old topographic information</i> that was available prior to the construction of the nuclear power plant. The accuracy in the positioning of these data is questionable and is judged here to be low. Inaccuracy not quantified.</p>	<p>The accuracy of the rock mass quality reflects on the accuracy of the mean value of the derived mechanical properties of the rock mass. These can be quantified, for the same rock domain, in:</p> <ul style="list-style-type: none"> - deformation modulus: $\pm 7\%$ - uniaxial compressive strength: $\pm 8\%$. <p>For the rock domains with much less available data, these accuracies should be increased by a factor between 3 and 4.</p> <p>The size of the rock volume in relation to the number of available data also influences the accuracy. The smaller rock domains analysed have lower accuracy as well as the deformation zones.</p> <p>The depth in BOREMAP and the depth at which the rock and fracture samples have been collected are used as stored in SICADA.</p>	<p><i>Stress Model</i></p>	<p>Accuracy of the minimum (horizontal) stress from HF is high.</p>	<p>Accuracy of the determination of the maximum (horizontal) stress from HF and HFTP methods is judged low, but has not been quantified. QA according to the methodology.</p>		

Question	Geology	Rock mechanics	Thermal	Hydrogeology	Hydrogeochemistry	Transport
		<p>Accuracy of the determination of the stresses by means of OC is also modest when the pre-existent deformations in the rock mass exceed the elasticity limit of the intact rock. QA according to the methodology.</p> <p>Accuracy of the orientation of the maximum principal stress is judged to be rather good.</p> <p>The comparison of the results from Forsmark and URL (Canada) has increased the confidence on the estimation of the stresses by using different measuring methods.</p> <p>The depth of the rock stress measurements is used as stored in SICADA.</p>				
<p>If biased data are being produced, can these be corrected for the bias?</p>	<p>As pointed out in version 1.1, there is a bias concerning the more common recognition of lineaments and, by consequence, possible deformation zones in the land area compared with the sea area. This bias has been reduced by the incorporation of new data sets (e.g. bathymetric data in the Öregrundsgräpen area) in version 1.2.</p>	<p>Bias is introduced because the boreholes are sub-vertical. Corrections have been applied to the fracture orientation and thickness of the deformation zones. However, some directional features and properties might have been overlooked.</p>	<p>Temperature logging has possible bias from disturbance (from drilling and drilling fluid) during drilling. Effect not assessed, but would depend on time after drilling (logging is usually done close after the drilling).</p>	<p>Data from cored boreholes are sensitive to the trend and plunge of the fracturing relative to the orientations of the boreholes. However, we have for version 1.2 several boreholes in different directions, which relaxes the problem significantly. This effect will be further reduced in the future by incorporating more boreholes with other orientations.</p>	<p>Potential sources of bias include contamination from drilling fluid. Such biased data can be corrected by using back-calculations, but the representativity may still be put in question.</p>	<p>Potential impact from disturbed (stress release) of laboratory samples. This would imply too high diffusivities etc in the laboratory samples compared with in situ results. Possibly some indications of degree of bias by comparing in situ and laboratory formation factor data (but accuracy in in situ data needs also be considered, see above).</p>

Question	Geology	Rock mechanics	Thermal	Hydrogeology	Hydrogeochemistry	Transport
<p>The bias has more or less been eliminated for the lineaments longer than 1,000 m. However, it remains for the shorter lineaments. For this reason, this bias only has an affect on the stochastic interpretation of fractures and deformation zones. The bias has been eliminated by restricting the stochastic DFN model to essentially the land area.</p> <p>There is also a bias in the lineament data due to truncation at the border of the regional model volume. This has been assessed by studying the influence of truncation on size and orientation.</p> <p>As pointed out in version 1.1, there is a bias towards the recognition of different fracture orientation sets from boreholes and from surface outcrop data. The bias concerns an over-emphasis of flat-lying fractures in sub-vertical boreholes and an over-emphasis of steeply dipping fractures in surface outcrop data. Furthermore, a low variation in borehole orientation also gives rise to this type of bias.</p>	<p>Sampling for mechanical testing has prioritised the homogeneous sections (in rock unit 101057) – partly required by the testing method. This means that the measured spread in data is less than actual spatial variation.</p> <p>Bias are also due to the limited extension on which surface rock mechanics logging has being carried out compared with the extension of the candidate area. (On the other hand one could question the relevance of the surficial information).</p> <p>Bias in the laboratory test results has been reduced by letting two different laboratories perform similar tests and comparing the results.</p> <p>New laboratory data are not available for the rock types sparsely occurring in the candidate area (e.g. pegmatite, gabbro, aplite). Moreover, there might be a tendency of sampling specimens of good rock. This bias was partially corrected for by inferring the mechanical properties of the weaker and/or under-represented rock types, or using data from SFR.</p>	<p>Unknown bias resulting from using modal data in the SCA method. Thus SCA data are judged to be more uncertain than direct measurements (when available). SCA data have been compared with TPS data and where possible, a correction of SCA data have been made.</p> <p>Generally, unknown representativity of modal analyses and TPS data due to possible biased sample selection. Sample selection has not been fully probabilistic. However, samples were taken in order to characterise the rock type – not to find odd varieties. Bias in data may be reduced (unknown how much) but can be eliminated only for new data (probabilistic sample selection).</p> <p>Risk for systematic error has been reduced by using different laboratories.</p>				

Question	Geology	Rock mechanics	Thermal	Hydrogeology	Hydrogeochemistry	Transport
	<p>The problem has been reduced in version 1.2, since the subsurface data comes from boreholes with a variable trend and an inclination that is either sub-vertical or 60°.</p> <p>There is a bias in the fracture data from outcrops due to truncation at the border of the stripped outcrops. This is not assessed. Sensitivity studies could have been made.</p> <p>Another bias is caused by the mapping of fractures longer than 0.5 m. The bias has been assessed by studying all fractures in one outcrop.</p> <p>All fracture data from outcrops have been derived from within or from the hanging wall of ZFMNE00A2. No surface data are available from the foot wall of this deformation zone.</p> <p>Reflection seismic data from the surface focuses attention on the occurrence of flat-lying structures in the bedrock. VSP data from boreholes should help to rectify this imbalance. Such data were not planned for version 1.2 but will be available for version 2.1.</p>	<p>Bias in the sampling of rock fracture has being reduced by having access to a larger set of specimens and to specimens from an inclined borehole (KFM04A). (Not judged important for the model at this stage).</p> <p>Bias in old available data has been removed by using old data only for comparison.</p> <p>Bias due to uneven coverage of the candidate area is judged low, thanks to the even spread of the boreholes over the rock volume of interest.</p> <p>As there is a strong bias in the maximum (horizontal) stress as estimated from the HF and HTPF methods, these data have not been used when analysing this component of the rock stress field.</p>				

Table A4-2. Protocol for use of available data and potential biases in the description of the near surface.

Question	Hydrogeochemistry	Hydrology and hydrogeology	Quaternary deposits (Overburden)	Biota
Which data have been used for the current model version (refer to tables in Chapter 2 of the SDM report).	Environmental monitoring boreholes SFM – Class 3 + isotopes. Surface water sampling – Class 3–5 + biosupplements + sonde measurements. Precipitation – Class 3 + isotopes.	Regional meteorological data. Local meteorological data, from May 2003 (SICADA). Regional discharge data Local discharge data (SICADA). Topography on land and bathymetry of the Baltic sea; Geometric data on catchment areas, lakes and water courses (SICADA). Surface water levels. Groundwater levels (SICADA). Hydraulic properties of Quaternary deposits. Regional oceanographic data (TR-02-02). Local oceanographic data (TR-99-11, TR-00-01).	Detailed map of QD in the central part of the model area. Less detailed map of QD in outer parts of the model area. Marine geology (map of QD). Soil type (soil classification). Stratigraphical distribution of till and sediments. Textural composition of till and sediments. Chemical composition of till, sediments and peat. Mineral composition of till and sediments. Pollen content of glacial sediments. Total depth of QD along geophysical profiles in the central model area.	Terrestrial producer model: Vegetation map, Vegetation inventory, National Forest Inventory, Primary production and biomass, Key biotopes, Dead wood, Soil type (soil and site type classification). Terrestrial consumer model: Bird inventory, Mammal inventory, Inventory of amphibians and reptiles. Aquatic producer model: Classification of lake habitats, Limnic producer biomass and production, Inventory of marine vegetation. Aquatic consumer model: Limnic fish inventory, Limnic consumer biomass and production, Marine benthic fauna.
If available data have not been used – what is the reason for their omission (e.g. not relevant, poor quality, lack of time, ...)	Chemical data have not been used for modelling of temporal and spatial processes. Observations without isotope data are excluded from the hydrochemical model. Trace elements – not relevant for modelling (baseline data). Organic pollutants in sediments – not relevant for modelling (baseline data). Data from private wells. Sonde measurements – some parameters (redox, chlorophyll, turbidity, light) may have low accuracy.	Some geophysics has not been used in this model version.	All site specific data have been used.	

Question	Hydrogeochemistry	Hydrology and hydrogeology	Quaternary deposits (Overburden)	Biota
(If applicable) What would have been the impact of considering the non-used data?	Description of temporal and spatial chemical processes.	Better knowledge of QD depth.		
How is data accuracy established (e.g. using QA procedures) for the different data? (Essentially just refer to tables in Chapter 2).	<p>Charge balance ($\pm 5\text{--}10\%$). Comparisons between laboratories and between methods.</p> <p>Consistency checks of data by plotting.</p> <p>Expert judgements.</p>	<p>Meteorological data measured and quality assured according to SMHI standard procedures.</p> <p>Regional discharge measurements quality assured according to SMHI standard procedures.</p> <p>Local discharge measurements according to SKB MD.</p> <p>Catchment areas interpreted from maps and checked in the field.</p> <p>Automatic measurements of surface and ground water levels, calibrated and checked by manual field measurements.</p> <p>Hydraulic properties measured by standard methods according to SKB MD.</p>	<p>Field classification and sampling according to national standard methods. Calibration between experts. Field classification compared with laboratory analyses.</p> <p>The marine geological interpretations are verified by sampling.</p> <p>Soil classification according to international standard.</p> <p>Detailed QD map compared with regional QD map.</p>	Data accuracy evaluated by statistical description, and by comparison with generic values (expert judgement) of parameters in each model.
List data (types) where accuracy is judged low – and answer whether accuracy is quantified (with reference to applicable sections of this report or supporting documents).	Accuracy may be low for elements and compounds where concentrations are near the detection limits.	<p>Simple discharge measurements – accuracy is not quantified.</p> <p>Hydraulic conductivity values from grain size distribution – comparisons are made with slug test data.</p>	Soil type map based on regional QD map with known classification errors.	Production of biomass and standing stocks of biomass in the sea – accuracy is not quantified.
If biased data are being used, can these be corrected for the bias?	Hydrogeochemical investigations of wetlands are lacking – complementary investigations planned.	<p>Meteorology: Precipitation data corrected for measurement errors by standard procedure.</p> <p>Hydrogeology: Groundwater observation wells over-represented in local depression areas – supplementary wells will be located on local heights.</p> <p>Hydraulic conductivity values of the contact zone till/bedrock are over-represented compared to values from till only – correction has been made by comparison with generic data.</p> <p>Measurements of hydraulic conductivities of sediments and peat are under-represented – complementary investigations planned.</p>	<p>Stratigraphical investigations of wetlands are under-represented compared to lake sediment data – complementary investigations planned.</p> <p>Peat chemistry data only from two different mires – data may not be representative for wetlands in the area.</p> <p>Correction not possible without complementary investigations.</p>	Most limnic data are from Lake Eckarfjärden – corrections are not judged necessary (with some exceptions) since lakes in the area are very similar.

Table A4-3. Protocol for assessing uncertainty in the bedrock geology aspects of the SDM.

Aspect of SDM	Uncertainty	Cause (e.g. data inaccuracy, information density, uncertainty in other discipline models or process understanding)	Has uncertainty been assessed considering information from more than one data source or through a calibration or validation exercise?	Impact on other uncertainties (in all disciplines)	Quantification (provide reference to applicable section of the SDM report)	Potential Alternative representation. (Is there reason for this and has one been developed)	Are there unused data which could be used to reduce uncertainty	What new data would potentially help resolve uncertainty? (Are they considered in current KPLU programme)
Geology – rock domain model	Composition, degree of inhomogeneity and degree of ductile deformation of rock domains at the surface in the sea areas, especially Öregrundsgrepen.	Only magnetic anomaly data.	Not relevant.	Impact on the regional model for rock mechanics properties and hydrogeology. Only very minor impact on the models in the local model volume.	Not relevant.	Bearing in mind the nature of this uncertainty, there is little justification to develop alternative models.	No.	Dense network of shallow drilling into the bedrock beneath Öregrundsgrepen. Poorly motivated, bearing in mind the needs in the local model volume. Not considered in the CSI programme.
	Location of rock domain boundaries, Asphällsfjärden (part of "target area").	Lack of data.	Not relevant.	Impact on the regional and local models for rock mechanics properties and hydrogeology. Impact on repository design.	Not relevant.	Will possibly be needed when local model is developed in version 2.1.	No.	Drilling of bedrock along one or more deeper boreholes. Proposal included in the CSI programme.
	Extension at depth of all rock domains except RFM017, RFM029 and to some extent RFM007, RFM012 and RFM018.	Lack of data.	Not relevant.	Impact on the regional model for rock mechanics properties and hydrogeology. Only very minor impact on the models in the local model volume.	Not relevant.	Bearing in mind the nature of this uncertainty, there is little justification to develop alternative models.	Possibly, geophysical modelling of the regional gravity data and seismic reflection data.	Drilling of bedrock along deeper boreholes. Poorly motivated, bearing in mind the needs in the local model volume. More detailed gravity data and seismic reflection data. Proposal included in the CSI programme.
	Numerical estimates of the proportions of different rock types in especially the inhomogeneous rock domains.	In RFM029, representativity of data could be questioned. Absence or little data in other rock domains.	Not relevant.	Impact on the regional model for rock mechanics properties and hydrogeology. Only very minor impact on the models in the local model volume.	Borehole data are available to semi-quantitatively assess uncertainty for critical parts ("target volume") of rock domain RFM029 (see Section 5.2.7). Otherwise not relevant.	Bearing in mind the nature of this uncertainty, there is little justification to develop alternative models.	No.	Numerical estimates at selected outcrops in each rock domain. Poorly motivated, bearing in mind the needs in the local model volume. Not considered in the CSI programme.

Aspect of SDM	Uncertainty	Cause (e.g. data inaccuracy, information density, uncertainty in other discipline models or process understanding)	Has uncertainty been assessed considering information from more than one data source or through a calibration or validation exercise?	Impact on other uncertainties (in all disciplines)	Quantification (provide reference to applicable section of the SDM report)	Potential Alternative representation. (Is there reason for this and has one been developed)	Are there unused data which could be used to reduce uncertainty	What new data would potentially help resolve uncertainty? (Are they considered in current KPLU programme)
Geology – structural model	Presence of undetected deformation zones.	Strong focus in the geological programme on indirect data (interpretation of airborne and ground geophysical data, topographic and bathy-metric data, and seismic reflection data), and limited amount of direct data (poor exposure of deformation zones at the surface and limited borehole data).	Yes. Alternative lineament interpretation. Independent check concerning the interpretation of seismic reflection data.	Impact on the uncertainties in the models for rock mechanics and especially hydro-geology. Impact for design and safety assessment.	The larger DZ (>3 km) are probably already found.	An alternative interpretation of lineaments has been completed to test the re-productibility of this interpretation work. Alternative structural models have been developed for the steeply dipping zones outside the areas where the data resolution is relatively high. A more stochastic approach has been adopted in the base model and a more deterministic approach has been adopted in the alternative model.	Fracture data from boreholes and tunnels close to the nuclear power plants and SFR.	New borehole data. A proposal for new boreholes has been included in the CSI programme.
	Character of the geological feature that is represented in an inferred lineament.	Various geological processes can explain the formation of a lineament. Uncertainty concerning which of these processes is the cause of a particular lineament.	Yes. Percussion and cored boreholes through some of the inferred lineaments.	Impact on the uncertainties in the models for rock mechanics and especially hydro-geology. Impact for design and safety assessment.	Not relevant.		No.	Excavation of representative lineaments at the surface, seismic refraction data at the surface, and new borehole data from the bedrock close to these lineaments. Proposals for all these studies have been included in the CSI programme.

Aspect of SDM	Uncertainty	Cause (e.g. data inaccuracy, information density, uncertainty in other discipline models or process understanding)	Has uncertainty been assessed considering information from more than one data source or through a calibration or validation exercise?	Impact on other uncertainties (in all disciplines)	Quantification (provide reference to applicable section of the SDM report)	Potential Alternative representation. (Is there reason for this and has one been developed)	Are there unused data which could be used to reduce uncertainty	What new data would potentially help resolve uncertainty? (Are they considered in current KPLU programme)
	Continuity, dip and thickness of deformation zones interpreted with the help of linked lineaments. This uncertainty is of major significance in the alternative deterministic structural model, where many lineaments have been interpreted as low confidence deformation zones.	<i>Length:</i> Poor constraints on the termination of a linked lineament upon which a deformation zone is partly or entirely based. <i>Down-dip extension:</i> Conceptual model relating depth to length of lineament is uncertain. <i>Dip:</i> Restricted amount of data. <i>Thickness:</i> Restricted amount of data. Also different concepts to explain thickness variation.	Yes. In the "target volume", percussion and cored boreholes through some of the DZ based, to the interpretation of linked lineaments. No assessment possible outside the "target area".	Impact on the uncertainties in the models for rock mechanics and especially hydrogeology. Impact for design and safety assessment.	Provided as ranges for the position, orientation, thickness and length of all the medium and high confidence deformation zones. Have been documented in the tables for the properties of deformation zones (see Section 5.4.4).	Bearing in mind the broad nature of this uncertainty, there is little justification to develop alternative models.	Interpretation of the dip of magnetic anomalies.	Excavation of representative lineaments at the surface, seismic refraction data at the surface, and new borehole data from the bedrock close to these lineaments. Proposals for all these studies have been included in the CSI programme (see also Evolutionary aspects).
	Continuity and thickness of the gently dipping zones that are based, to a large extent, on the seismic reflection data.	<i>Continuity:</i> Poor constraints on the termination of a seismic reflector upon which a deformation zone is based. <i>Thickness:</i> Restricted amount of data. Also different concepts to explain thickness variation.	Yes. Percussion and cored boreholes through some of the DZ based, to a large extent, on the seismic reflection data.	Impact on the uncertainties in the models for rock mechanics and especially hydrogeology. Impact for design and safety assessment.	Provided as ranges for the position, orientation, thickness and length of all the medium and high confidence deformation zones. Have been documented in the tables for the properties of deformation zones (see Section 5.4.4).	Alternative structural models for the along-strike extension of the major, gently dipping zones (ZFMNE00A1, -A2, -C1 and -C2) have been developed (base model and base model variant).	No.	New seismic reflection data coupled with new boreholes in the marginal areas to the candidate area. Proposals for these studies have been included in the CSI programme (see also Evolutionary aspects).

Aspect of SDM	Uncertainty	Cause (e.g. data inaccuracy, information density, uncertainty in other discipline models or process understanding)	Has uncertainty been assessed considering information from more than one data source or through a calibration or validation exercise?	Impact on other uncertainties (in all disciplines)	Quantification (provide reference to applicable section of the SDM report)	Potential Alternative representation. (Is there reason for this and has one been developed)	Are there unused data which could be used to reduce uncertainty	What new data would potentially help resolve uncertainty? (Are they considered in current KPLU programme)
Geology – DFN model	Assumption that all lineaments represent brittle deformation zones.	Data inaccuracy, uncertainty from DZ model.	See DZ model.	Impact on length distribution.	Section 5.5.	Uncertainty is not quantified, but directly relates to the uncertainty in the DZ-model. See Section 5.5.	No.	More accurate DZ model. See also next row.
	Size distribution.	Conceptual uncertainty regarding whether lineaments and fractures from outcrop mapping belong to the same statistical size distribution. This is in turn caused by the absence of data in the range c. 25 to 1,000 m.	No, but simulations show it is possible to obtain consistency between fracture frequency in boreholes and on outcrops.	Large impact on hydrogeological DFN and Safety Assessment and repository design.	Only partly quantified. Range in "k", x0 could possibly be estimated depending on how to interpolate or extrapolate in the trace length-frequency diagram.	The DFN-analysis in Section 5.5 focuses on one alternative. However, putting more weight on the longer fractures and lineaments with resulting increase in connectivity of the fracture network, is also developed. The latter alternative is further explored in the hydrogeology assessment in Chapter 8.	Possibly some old SFR-mapping data.	Intermediate scale of resolution giving information on fracture size. Trenches over lineaments in the "target volume" (see above), in CSI-programme. Larger areas (100 m x 100 m) of uncovered rock for mapping. (Not considered in CSI).
	Size of sub-horizontal fractures.	Poor information Distribution can only be assessed by assumptions.	Not relevant.	Connectivity which affects resulting properties in rock mechanics and hydrogeology.	Not really possible – uncertainty is larger than for sub-vertical sets.	Not quantified. It is assumed that the size distribution is the same as for the sub-vertical sets.	No	Mapping on outcrops with topographic relief, but they do not exist! (Issue will remain until Underground exploration).

Aspect of SDM	Uncertainty	Cause (e.g. data inaccuracy, information density, uncertainty in other discipline models or process understanding)	Has uncertainty been assessed considering information from more than one data source or through a calibration or validation exercise?	Impact on other uncertainties (in all disciplines)	Quantification (provide reference to applicable section of the SDM report)	Potential Alternative representation. (Is there reason for this and has one been developed)	Are there unused data which could be used to reduce uncertainty	What new data would potentially help resolve uncertainty? (Are they considered in current KPLU programme)
	Spatial model of fracturing with depth. Fracture intensity and its variability in the model volume.	The orientation of fractures changes with depth but the conceptual model (i.e. is fracturing related to lithology, proximity to DZ or just depth) is presently not understood. Intensity also changes with depth, but the exact division of the variation is not fully established.	No.	Affects resulting properties in rock mechanics and hydrogeology.	Range of intensities, based on P10 and P21 in different borehole sections and outcrops, see Section 5-5.	Section 5.5 notes that an alternative spatial model based on the position of the DZ ZFMNE00A2 and to place the near-surface rock into its own subdomain would be a possibility. Such alternatives are developed within the hydrogeological modelling in order to match the fracturing with the observed strong variation in hydraulic properties of the rock.	Yes. Evaluate fracture data with respect to lithology, mineralogy and proximity of DZ in each borehole, see kinematics under evolutionary aspects.	More spatially representative borehole data (probably covered in CSI-programme). Detailed fracture mapping in carefully selected outcrops (e.g. foot wall of DZ ZFMNE00A2).
	Variation of fracture orientation and size in the different rock domains.	Orientation: Still too few data in other rock domains than RFM029. Size: all lineaments used for distribution.	Not relevant.	As above, but possibly of minor importance outside RFM029.	In RFM029 different bounds defined to cover the specific variations in the different outcrops. Outside RFM029 there is no statistics-uncertainty estimated by assumptions of similarities.	No.	No.	For RFM029, see above. Data from other rock domains than RFM029 (not in CSI). Perhaps not important – but would enhance understanding.

Aspect of SDM	Uncertainty	Cause (e.g. data inaccuracy, information density, uncertainty in other discipline models or process understanding)	Has uncertainty been assessed considering information from more than one data source or through a calibration or validation exercise?	Impact on other uncertainties (in all disciplines)	Quantification (provide reference to applicable section of the SDM report)	Potential Alternative representation. (Is there reason for this and has one been developed)	Are there unused data which could be used to reduce uncertainty	What new data would potentially help resolve uncertainty? (Are they considered in current KPLU programme)
Geology – evolutionary aspects	Poor control on the tectonic history in the brittle regime after c. 1,750 million years.	Process understanding, especially timing.	Not relevant.	Impact on the uncertainties in the models for deterministic structures, rock mechanics and hydrogeology. Impact for safety assessment.	Not relevant.	Not relevant.	A more thorough analysis of the data concerned with mineral fillings along fractures in coming models may provide some new constraints on this problem.	<p>Closer interplay between data pertaining to the mineral fillings along fractures and the brittle structures at the site, especially fracture orientation sets. Kinematic data along brittle deformation zones. Reflection seismic data may provide markers for relative ages of movement. Geochronological data (cooling ages from sites at different positions relative to the regional deformation zones; ages of mineral fillings along fractures). Proposals for all these studies have been included in the CSI.</p>

Table A4-4. Protocol for assessing uncertainty in the rock mechanics and thermal property aspects of the SDM.

Aspect of SDM	Uncertainty	Cause (e.g. data inaccuracy, information density, uncertainty in other discipline model or process understanding)	Has uncertainty been assessed considering information from more than one data source or through a calibration or validation exercise?	Impact on other uncertainties (in all disciplines),	Quantification (provide reference to applicable section of the SDM report)	Potential Alternative representation. (Is there reason for this and has one been developed).	Are there unused data which could be used to reduce uncertainty	What new data would potentially help resolve uncertainty? (Are they considered in current KPLU-programme).
Bedrock in situ stress state	Rock stress magnitudes and their spatial and depth distribution.	Stresses at the upper limit of the applicability of the measurement methods.	Different measurement and interpretation methods have been used (overcoming, hydraulic, core disk, transient strain analysis).	On rock mass parameters depending on stress. (Impact on design.)	The uncertainty ranges for stress magnitude are given in Chapter 6.	No alternatives. The estimated ranges are judged to be sufficiently accurate.	No.	More measurement near the surface to estimate the stress gradient (already in CSI).
	Rock stress orientation.	Data resolution (spatial and depth).	Regional and local measurement data have been analysed.	(Impact on design.)	Yes, see Chapter 6. The uncertainty is judged to be low, thus with low impact on other disciplines.	No alternatives. The observation is considered understood.	No.	New data will probably confirm the present results.
	High stresses under sub-horizontal deformation zones.	This stress increase has been observed in the boreholes and it is also indicated by numerical modelling. The connection is not really uncertain but is not verified for all the sub-horizontal deformation zones.	Measurements and numerical modelling were considered.	This correlation improves the confidence of the DZ-model. (Impact on design.)	Yes, see Chapter 6. The observation is understood.	No alternatives. The observation is understood.	No.	The stress increase should be checked under other sub-horizontal zones at the site (already part of CSI).
Bedrock mechanics properties	Spatial variability.	Well known in rock domain RFM029 ("target volume" in granite to granodiorite, code 101057). Few data outside the target volume (e.g. tonalite, granodiorite).	The new laboratory data show small differences compared to the values in version 1.1, which were based on data from SFR. This could be extrapolated to the spatial variation of the properties outside RFM029. The mechanical properties of the rock mass for RFM029 were determined/validated from the results of empirical methods and numerical modelling.	No consequences for the other disciplines. (Impact on design.)	Uncertainty was not evaluated on data from the laboratory. The uncertainty of the derived mechanical properties was quantitatively evaluated in Chapter 6.	No need of alternative models due to the uncertainties. The uncertainties are considered sufficiently quantified.	No.	New laboratory tests are planned together with characterisation of the rock mass (already in CSI). This will reduce the uncertainty of the properties outside RFM029.

Aspect of SDM	Uncertainty	Cause (e.g. data inaccuracy, information density, uncertainty in other discipline model or process understanding)	Has uncertainty been assessed considering information from more than one data source or through a calibration or validation exercise?	Impact on other uncertainties (in all disciplines),	Quantification (provide reference to applicable section of the SDM report)	Potential Alternative representation. (Is this and has one been developed).	Are there unused data which could be used to reduce uncertainty	What new data would potentially help resolve uncertainty? (Are they considered in current KPLU-programme).
	Effect of pore pressure and stress on rock mass properties.	The uncertainty of the pore pressure and rock stresses affects the values of the rock mass mechanical properties that depend on them.	These effects can partially be considered by empirical methods. Theoretical/numerical modelling can explicitly take into account pore pressure and rock stress. Neither of the two attempts was done during characterisation. Rock stresses and pore pressure have to be considered for design.	No consequences for the other disciplines. (Impact on design.)	No quantification of pore pressure and rock stress uncertainty on the mechanical properties was attempted.	Reflected by the alternatives in the DZ-model and hydro-geological model.	Probably historical data.	Hydro-mechanical laboratory testing of rock fracture does not have an established SKB methodology. Constitutive models including pore pressure effects on strength and deformability are available in the literature. No tests are included in CSI.
	Deformation zones.	No laboratory data are available on samples from the deformation zones. The mechanical properties of the rock mass for a number of local deformation zones (lengths > 10 km) were determined based on empirical methods. Regional deformation zones (length > 10 km) were characterised based on experiences from SFR and the Forsmark power plant. The analysed DZ do not allow discerning between the properties of ductile and brittle zones.	No. The determination is based either on just the empirical methods or on historical data. There is no DFN available for the deformation zones. Thus, no numerical modelling could be carried out.	These determinations may improve the confidence of the DZ-model. Furthermore, more realistic mechanical parameters could improve the rock stress model that, at present, assumes very low strength parameters. No consequences are expected for other disciplines. (Impact on design.)	Uncertainty was assessed by means of the empirical methods on local deformation zones. Quantification is given in Chapter 6.	Reflected by the alternatives in the DZ-Model.	Possibility of back-analysing convergence measurements from the SFR construction.	More data from DZ would certainly reduce the uncertainties. The question is if there is a need of lower uncertainty for planning the construction. However, the DZs intercepted during construction should be explored (not included in CSI).

Aspect of SDM	Uncertainty	Cause (e.g. data inaccuracy, information density, uncertainty in other discipline model or process understanding)	Has uncertainty been assessed considering information from more than one data source or through a calibration or validation exercise?	Impact on other uncertainties (in all disciplines),	Quantification (provide reference to applicable section of the SDM report)	Potential Alternative representation. (Is there reason for this and has one been developed).	Are there unused data which could be used to reduce uncertainty	What new data would potentially help resolve uncertainty? (Are they considered in current KPLU-programme).
	Scale effects on the mechanical properties.	Fracture network properties may vary depending on the scale at which they are evaluated. This implies that the empirical and numerical methods are sensitive to the size of the rock mass block/bore-hole section analysed for rock mass characterisation. Neglecting this aspect can lead to uncertainty in the parameter determination.	The scale dependency of the Q and RMR values was analysed for four boreholes. RMR seems to be rather insensitive to scale. The deformation modulus of the rock mass was evaluated from RMR values.	(Impact on design.)	The effect of scale on the deformation modulus was quantified. For borehole KFM01A, the deformation modulus obtained from Q might diminish up to 30% when passing from bore-hole sections of 5 m to sections of 20 m (see Chapter 6).	Two potential alternatives could originate if the rock mass parameters derived from either Q or RMR are used. In this version of the SDM, RMR is used for reducing scale effects.	No.	New data will probably confirm the present results.
Bedrock thermal properties	Thermal conductivity – rock type.	Spatial variability of mineralogy within rock type Uncertain representativity for SCA and TPS data. SCA calculations from modal analysis (thermal conductivity of mineral and modal composition), see Table A4-1. Anisotropy suggested in data, but uncertain interpretation. May be overestimated in small scale.	Uncertainty in SCA data has been evaluated by comparison with TPS data and by sensitivity studies.	None, except for design.	Spatial variability is quantified, see below. Uncertainty in spatial variability is discussed in Section 7.3.3.	No, uncertainty captured as distribution.	No.	Representative direct measurements of thermal conductivity. More samples with both density and thermal conductivity measurements (101057). Extensive sampling of other rock types to produce variograms of spatial variability. Measurements in relevant scale (in CSI programme).

Aspect of SDM	Uncertainty	Cause (e.g. data inaccuracy, information density, uncertainty in other discipline model or process understanding)	Has uncertainty been assessed considering information from more than one data source or through a calibration or validation exercise?	Impact on other uncertainties (in all disciplines),	Quantification (provide reference to applicable section of the SDM report)	Potential Alternative representation. (Is there reason for this and has one been developed).	Are there unused data which could be used to reduce uncertainty	What new data would potentially help resolve uncertainty? (Are they considered in current KPLU-programme).
Thermal properties – spatial variability.	Uncertainties in transformation between different scales e.g. measurement scale to canister scale.	TPS and SCA data are used. TPS data have been used to analyse the spatial variability within 101057.	None, except for design.	Spatial variability within 101057 is quantified and uncertainty in spatial variability is discussed in Section 7.3.3.	No.	Measurements in relevant scale (in CSI programme).		
Thermal conductivity – rock domains.	Uncertainties in large scale variations inside domains with medium or low presence of 101057 (See geology). Problem with representativity of borehole – domain. 3D geometry of most of the rock domains is also uncertain. Uncertainties in the modelling approach. Anisotropy depending on frequency and orientation of subordinate rock types.	Different approaches are used to evaluate the variability in thermal conductivity.	None, except for design.	Spatial variability within target volume rock type (101057) is quantified and uncertainty in spatial variability is discussed in Section 7.3.3. Impact of subordinate rock types RFM029 is also quantified.	No, but ranges are estimated by considering different approaches, see Section 7.3.3.	Need of more data from subordinate rock types (from existing or planned cores) to evaluate the spatial variability with higher confidence. (Not yet in CSI). The representativity problem can be resolved with more boreholes. Also, improved confidence in rock domain model would help. Large scale test of thermal conductivity in different directions would reduce uncertainty in anisotropy (in CSI).		

Aspect of SDM	Uncertainty	Cause (e.g. data inaccuracy, information density, uncertainty in other discipline model or process understanding)	Has uncertainty been assessed considering information from more than one data source or through a calibration or validation exercise?	Impact on other uncertainties (in all disciplines),	Quantification (provide reference to applicable section of the SDM report)	Potential Alternative representation. (Is there reason for this and has one been developed).	Are there unused data which could be used to reduce uncertainty	What new data would potentially help resolve uncertainty? (Are they considered in current KPLU-programme).
	Thermal properties in DZ.	No thermal data from DZ.	No.	No.	A range could be set.	No reason.	No.	Measurements in relevant scale. Uncertainty judged to be of less importance (unless zone close to deposition tunnel – to be assessed underground).
	Heat capacity.	Uncertain representativity for TPS data.	No.	No.	A range is provided (see Section 7.3.3).	No.	No.	Representative measurements of heat capacity.
	In-situ temperature.	Uncertainty in temperature data, possibly due to disturbance from the drilling and drilling fluid, convection in the boreholes, etc. Short-circuited flows in the borehole.	Difference between boreholes.	No (the differences are small – but are important for Engineering and layout).	A range is provided (see Section 7.3.3).	No reason.	Re-assess existing database and evaluate the possible effect of disturbance.	Temperature logs at more representative (less disturbed) times. Possibly reconsider measurement procedure to mitigate effect of long term thermal convection.
	Thermal expansion.	Possible data inaccuracy. Stress dependence not assessed, measured on stress-released sampled.	Not yet – but comparison between methods and laboratories is done but not reported.	No, but effects rock mechanics evolution due to heating.	A range is provided (see Section 7.3.3).	Not yet. It could be discussed whether the expansion is linear with T or not.	No.	Laboratory test method development (is already underway).

Table A4-5. Protocol for assessing uncertainty in the hydrogeology, hydrogeochemistry and transport property aspects of the SDM.

Aspect of SDM	Uncertainty	Cause (e.g. data inaccuracy, information density, uncertainty in other discipline models or process understanding)	Has uncertainty been assessed considering information from more than one data source or through a calibration or validation exercise?	Impact on other uncertainties (in all disciplines)	Quantification (provide reference to applicable section of the SDM report)	Potential Alternative representation. (Is there reason for this and has one been developed)	Are there unused data which could be used to reduce uncertainty	What new data would potentially help resolve uncertainty? (Are they considered in current KPLU-programme)
Bedrock hydro-geology	<p>Geometry and connectivity of deformation zones and the transmissivity distribution, spatial variability and depth dependence in deformation zones, especially outside the candidate area/ volume.</p> <p>Hydraulics of the rock mass; Division into volumes of different hydraulic properties.</p>	<p>Uncertainty in the geological model. Lack of hydro-geological data testing whether there is a hydraulic contact between the rock inside the candidate area and rock outside.</p> <p>Support for a hydrogeological modelling of stochastic deformation zones in the size range 100 – 1,000 m is based on assumptions on upscaling.</p>	<p>Calibration against hydrogeochemistry data.</p>	<p>Fundamental impact on our modelling of the regional groundwater flow and hydrogeochemical system (paleohydro-geology).</p> <p>Direct implications for migration and groundwater composition.</p>	<p>Handled by alternatives and by sensitivity studies. The sensitivity to the T-distribution is dealt with in the regional groundwater flow modelling, see Chapter 8.</p> <p>No – but the uncertainty in the different volumes can at this point be represented by considering the range of properties for the different volumes.</p>	<p>There are alternative DZ models in the regional domain. Sensitivity study of importance of T-distribution.</p>	<p>No.</p>	<p>Boremap, BIPS and PFL data for a number of zones and some interference tests within these zones in current CSI-programme.</p> <p>Data to resolve the geometry of fractures using inclined boreholes. In current CSI-programme. Detailed hydraulic tests 0–100 m below surface (Interference tests between nearby cored boreholes are not possible). Single-hole interference tests (to test connectivity). In current CSI-programme.</p>

Aspect of SDM	Uncertainty	Cause (e.g. data inaccuracy, information density, uncertainty in other discipline models or process understanding)	Has uncertainty been assessed considering information from more than one data source or through a calibration or validation exercise?	Impact on other uncertainties (in all disciplines)	Quantification (provide reference to applicable section of the SDM report)	Potential Alternative representation. (Is there reason for this and has one been developed)	Are there unused data which could be used to reduce uncertainty	What new data would potentially help resolve uncertainty? (Are they considered in current KPLU-programme)
	Hydraulics of the rock mass; Connectivity of the discrete fracture network.	Few boreholes, the exact division of the different volumes remains to be defined.		Direct implications for migration and groundwater composition.	By different alternatives.	The different volumes may be modelled as percolating networks of discrete features, however with quite different hydro-geological DFN properties depending on the assumptions of the intensity of larger fractures in the DFN-model. In the low percolating networks it is necessary to set the transmissivity higher in order to match the total measured transmissivity in the different boreholes.		See above.
	Hydraulics of the rock mass; Transmissivity distribution in DFN.	Unknown correlation between size and T.		Direct implications for migration and groundwater composition.	By different alternatives.	Alternative models, with no correlation or with some correlation are also applied to the data. These alternatives results in quite different block properties and are possibly less realistic, but cannot be excluded at this point.		See above.

Aspect of SDM	Uncertainty	Cause (e.g. data inaccuracy, information density, uncertainty in other discipline models or process understanding)	Has uncertainty been assessed considering information from more than one data source or through a calibration or validation exercise?	Impact on other uncertainties (in all disciplines)	Quantification (provide reference to applicable section of the SDM report)	Potential Alternative representation. (Is there reason for this and has one been developed)	Are there unused data which could be used to reduce uncertainty	What new data would potentially help resolve uncertainty? (Are they considered in current KPLU-programme)
	Hydraulics of the rock mass; Anisotropy in the Hydro-DFN.	Limited data.		Direct implications for migration and groundwater composition.	Data only suggest moderate anisotropy, but since there are few data this issue is still uncertain.	No need.		See above.
	Hydraulics of the rock mass; Spatial variability (channelling) in the fractures.	There is likely to be a spatial variability of the transmissivity in the plane of each fracture, but it is very hard to measure.		Direct implications for migration and groundwater composition.	This uncertainty is not resolved in the site modelling, but is left for further analysis within safety assessment. However, it should be remembered that any assumption on channelling still must be consistent with the hydraulic observations.			See above.
	Bedrock topography.	Possibly higher resolution would be needed to capture near-surface hydrology.	No.	Yes Implications for: - near surface hydrology.	Different suggestions exist but will not be used in 1.2, see Chapter 8.	Not relevant.	No.	Hardly any. No correlation between known and unknown data points. Make use of monitoring data.
	Matrix porosity and salinity in matrix porosity.	Lack of data on matrix salinity.	No.	It has an impact on the flow model and the integration with hydrogeochemistry and radionuclide migration.	See Chapter 8. The implication of the uncertainty is assessed in the palaeohydrogeology analyses by sensitivity analysis.	No.	No.	New samples for estimating salinity in rock matrix, see hydrogeochemistry, In CSI.
	Boundary conditions.	The chosen model domain has artificial boundaries.	Yes.	Has potential impact on the flow model and then transport paths and the integrated evaluation with hydrogeochemistry.	See Chapter 8. A few cases have been tested suggesting that the regional domain is large enough not to impact flow in the target volume.	No, although the sensitivity to the alternative deformation zone models are explored.	No.	Borehole nearby boundaries. In current CSI-programme.

Aspect of SDM	Uncertainty	Cause (e.g. data inaccuracy, information density, uncertainty in other discipline models or process understanding)	Has uncertainty been assessed considering information from more than one data source or through a calibration or validation exercise?	Impact on other uncertainties (in all disciplines)	Quantification (provide reference to applicable section of the SDM report)	Potential Alternative representation. (Is there reason for this and has one been developed)	Are there unused data which could be used to reduce uncertainty	What new data would potentially help resolve uncertainty? (Are they considered in current KPLU-programme)
Palaeo-hydro-geology	Initial conditions (in particular, the salinity profile).	By necessity, there will never be any data on the initial conditions. There is also lack of hydrogeochemical data at depth due to sampling difficulties.	Comparison between approaches at the sites in Sweden and in Finland.	See above.	See Chapter 8. A few cases have been tested but data indicate that the conditions at depth are pretty firm.	No.	No.	Borehole in the Baltic Sea and from the bottom of the SFR. In current CSI-programme.
Hydrogeo-chemistry	Spatial variability of hydrochemistry in 3D at depth.	The information density concerning borehole groundwater chemistry is low. The samples are mixed and represent an average composition.	A validation test has been conducted where representative/non-representative samples has been interpolated.	This may cause uncertainties concerning the salinity interface in e.g. hydrogeological modelling and transport modelling. Causes uncertainties in overall hydrogeochemical understanding of the site.	Local uncertainty on the order of $\pm 50\%$ site scale uncertainty on the order of $\pm 10\%$, see Section 9.6.	Alternative representation discussed in Section 9.6.	No	More data observations from deep boreholes. Rock matrix samples. Discuss very deep borehole in relation to difficulties and supply of data from other sources (Finnsjön, SFR...). Consider use of electromagnetic data for regional characterisation. Part of CSI programme.
	Temporal (seasonal) variability in surface water chemistry, which ultimately impacts the identification of discharge and recharge areas. Temporal averaging follows from processes being slow..	The sampling may not describe the seasonal variation and samples may be taken at different time intervals from the surface versus the shallow boreholes.	No, this has not been done, but a detailed surface hydrogeological modelling may be helpful for this type of exercise.	Can cause uncertainty concerning the interaction between surface and groundwaters and may affect transport modelling. The amount of reactions taking place at the surface may not be properly described.	The effect from seasonal variation has not been quantified but the effects have been identified, see Section 9.3.	Different modelling approaches are applied on the same data set to describe the same processes.	No.	Sampling reflecting seasonal variation from selected surface and borehole locations in identified recharge/discharge areas. To be planned later.

Aspect of SDM	Uncertainty	Cause (e.g. data inaccuracy, information density, uncertainty in other discipline models or process understanding)	Has uncertainty been assessed considering information from more than one data source or through a calibration or validation exercise?	Impact on other uncertainties (in all disciplines)	Quantification (provide reference to applicable section of the SDM report)	Potential Alternative representation. (Is there reason for this and has one been developed)	Are there unused data which could be used to reduce uncertainty	What new data would potentially help resolve uncertainty? (Are they considered in current KPLU-programme)
	Model uncertainties (e.g. equilibrium calculations, migration and mixing).	Inaccurate pH measurements, inaccuracy in the thermodynamic data bases, wrong mineral phase selections, wrong end-members selection, model uncertainties.	Yes. For validation different modelling approaches are applied on the same data set.	May cause uncertainties in transport modelling and hydrogeological modelling. Causes uncertainties in overall hydrogeochemical understanding of the site.	One unit error in the pH measurements may cause one unit error in the equilibrium calculations. The uncertainties of the mixing modelling is $\pm 10\%$, see Sections 9.2, 9.5 and 9.6.	Different modelling approaches are applied on the same data set to describe the same processes thereby confidence is built into the description.	No.	No new data needed.
	Identification and selection of end-member waters. There is a judgemental aspect of the M3 (principal components) analysis.	Poor understanding of the palaeohydrogeology events.	Integration with hydrogeology to identify and use same end-members.	May cause uncertainties in the chemical process description and in the integration with hydrogeology. Causes uncertainties in overall hydrogeochemical understanding of the site.	Different end-members have been selected in the regional/local models, no quantification has been conducted, see Sections 9.5 and 9.6.	Different modelling approaches are applied on the same data set to describe the same processes for confidence building.	No.	Data from extreme waters. Part of CSI programme. Deep borehole from SFR.
	Groundwater composition in the rock matrix.	Few measurements.	No.	May affect the hydrogeological modelling and transport modelling. The description of the interaction between high and low conductive groundwaters systems will be uncertain.	No.	No.	No.	Samples for rock matrix determination have been collected and the results will be available for version 2.1. Part of CSI programme.

Aspect of SDM	Uncertainty	Cause (e.g. data inaccuracy, information density, uncertainty in other discipline models or process understanding)	Has uncertainty been assessed considering information from more than one data source or through a calibration or validation exercise?	Impact on other uncertainties (in all disciplines)	Quantification (provide reference to applicable section of the SDM report)	Potential Alternative representation. (Is there reason for this and has one been developed)	Are there unused data which could be used to reduce uncertainty	What new data would potentially help resolve uncertainty? (Are they considered in current KPLU-programme)
Transport properties	Spatial variability and correlation between matrix transport properties and flow paths.	There is uncertainty in matrix retention properties. Reason spatial variability, limited data set, and transfer of information from lab to field. Generally expectation of low correlation between matrix and flow path properties; higher correlation between fracture surface and flow path properties.			A range of properties for each different rock type are given, see Chapter 10. Correlation hard to establish.	Not justified.	No.	Potentially, more borehole data can establish a relation (however, low expectations).
	Diffusion properties of the matrix.	There is uncertainty in matrix retention properties, especially concerning the sorption properties. Reason spatial variability, limited data set. Impact of stress release on core samples.	Diffusion assessed with electrical resistivity in both lab and field combined with through diffusion experiment. Multiple samples and sample lengths for all lab experiments. Impact of stress release on core samples assessed by comparing laboratory and in situ tests.	Uncertainty in diffusion properties implies an uncertainty for hydrogeological salt modelling (matrix diffusion of salt).	Through distributions (resistivity), intervals and/or quantifications of uncertainty observed in the measurement.	No.	No.	More laboratory data will be produced during the CSI.

Aspect of SDM	Uncertainty	Cause (e.g. data inaccuracy, information density, uncertainty in other discipline models or process understanding)	Has uncertainty been assessed considering information from more than one data source or through a calibration or validation exercise?	Impact on other uncertainties (in all disciplines)	Quantification (provide reference to applicable section of the SDM report)	Potential Alternative representation. (Is there reason for this and has one been developed)	Are there unused data which could be used to reduce uncertainty	What new data would potentially help resolve uncertainty? (Are they considered in current KPLU-programme)
	Sorption properties of the matrix.	Reason spatial variability, limited data set (no site specific sorption data). Conceptual model of sorption.	No.	No.	Through intervals and/or quantifications of uncertainty observed in the measurement.	No (uncertainty in sorption process as such assessed within Safety Assessment, SR-Can).		More laboratory data will be produced during the CSI.
	Sorption properties, diffusivities and porosities of the geologic material representative to the fractures (e.g., fracture rim zone, gouge material and fracture filling).	Shortage of relevant material and, so far, no performed measurements.		Uncertainty in diffusion properties implies an uncertainty for hydrogeological salt modelling (matrix diffusion of salt). Limited importance for Safety Assessment.	Not quantified. Part of the calibration work in the palaeohydro-geology simulations.		Possible, if one would allow import from other sites (e.g., Åspö data).	More laboratory data will be produced during the CSI.
	Fracture representation in different fracture and minor/major zones according to the concept in R-03-20.	Low numbers of hydraulically transmissive fractures. Difficulties of presenting the data according to the proposed retardation model.			Unclear whether the correlation of transport properties to different type fractures and DZ could be resolved. Relevance of DZ classification in R-03-20 could also be discussed. Not evident that e.g. fracture size or transmissivity and the fracture filling mineralogy should be related.		No.	Potentially, more boreholes can give more data that motivates the fracture classification.

Table A4-6. Protocol for assessing uncertainty in the near surface aspects of the SDM.

Aspect of SDM	Uncertainty	Cause (e.g. data inaccuracy, information density, uncertainty in other discipline models or process understanding)	Has uncertainty been assessed considering information from more than one data source or through a calibration or validation exercise?	Impact on other uncertainties (in all disciplines).	Quantification (provide reference to applicable section of the SDM report)	Potential Alternative representation. (Is there reason for this and has one been developed).	Are there unused data which could be used to reduce uncertainty	What new data would potentially help resolve uncertainty? (Are they considered in current KPLU-programme).
Surface system – Quaternary deposits	Soil depth model.	Low information density in parts of the regional model area.	Soil depth based on geophysical methods validated by comparison with borehole data.	Hydrological, hydrogeological and transport modelling (flow of matter). Bedrock surface mapping. Hydrogeochemistry modelling. Ecosystem descriptions and models.	No.	A simplified soil depth model is used in deep hydrogeological modelling.	Data from airborne geophysics may be used to improve soil depth model.	Additional information from areas with low information density. New data from e.g. seismic profiles will be available in later model versions, part of CSI.
	Stratigraphic distribution and character of organic deposits.	Low information density.	No.	Hydrological, hydrogeological and transport modelling (flow of matter). Hydrogeochemistry modelling. Ecosystem descriptions and models.	No.	No.	No.	Additional information from areas with low information density – campaign is planned.
	Off-shore Quaternary deposits – character and thickness of sediments.	Low information density.	No.	Hydrological, hydrogeological and transport modelling (flow of matter). Hydrogeochemistry modelling. Ecosystem descriptions and models.	No.	No.	No.	Additional information from areas with low information density – interpretation of marine geophysical data is planned.
Post-glacial history	Salinity variation in the Baltic.	No site-specific data.	No.	Hydrogeological and hydrogeochemical modelling.	No.	No.	No.	Data from biostratigraphical investigations on sediment core (planned).

Aspect of SDM	Uncertainty	Cause (e.g. data inaccuracy, information density, uncertainty in other discipline models or process understanding)	Has uncertainty been assessed considering information from more than one data source or through a calibration or validation exercise?	Impact on other uncertainties (in all disciplines),	Quantification (provide reference to applicable section of the SDM report)	Potential Alternative representation. (Is there reason for this and has one been developed).	Are there unused data which could be used to reduce uncertainty	What new data would potentially help resolve uncertainty? (Are they considered in current KPLU-programme).
Surface system – Surface hydrology, near-surface hydrogeology	Spatial and temporal variability in meteorological data.	Only short time-series of site specific data available.	Evaluation of data from different SMHI stations in the region (performed in v0; TR-02-02). Comparison between local and regional data for short time series.	Hydrological, hydrogeological and transport modelling (near surface and deep rock). Oceanographic models. Ecosystem models.	No. Longer site-specific time series are necessary.	No.	No.	Longer site-specific time series will be available.
	Spatial and temporal variability in discharge.	Only results of "simple" measurements available; no data from discharge stations in F1.2.	No.	Hydrological models (comparison/calibration). Hydrogeological models (basis for setting BCs). Transport/flow of matter. Ecosystem models.	No.	No.	No.	Site specific data – measurements initiated 2004, but relevant time series will not be available until after F1.2.
	Surface water and groundwater levels.	Short time series and topographical bias.	No.	Hydrological models (basic description, comparison/calibration). Hydrogeological models (basis for setting BCs). Transport/flow of matter. Ecosystem models.	No.	No.	No.	Monitoring in observation wells and surface water level gauges since spring 2003. Some additional observation wells will be installed.
	Evapotranspiration.	Short time series calculation of potential evapotranspiration and no measurement of actual evapotranspiration.	Yes, calculation by two different methods for calculation of potential evapotranspiration.	Hydrological models (basic description, comparison/calibration). Hydrogeological models (basis for setting BCs). Transport/flow of matter. Ecosystem models.	Yes, sensitivity analyses of selected parameters in evapotranspiration equations.	No.	No.	Longer time series of meteorological data for calculation of pot. evapotranspiration. Local measurement of evapotranspiration will be performed.

Aspect of SDM	Uncertainty	Cause (e.g. data inaccuracy, information density, uncertainty in other discipline models or process understanding)	Has uncertainty been assessed considering information from more than one data source or through a calibration or validation exercise?	Impact on other uncertainties (in all disciplines),	Quantification (provide reference to applicable section of the SDM report)	Potential Alternative representation. (Is there reason for this and has one been developed).	Are there unused data which could be used to reduce uncertainty	What new data would potentially help resolve uncertainty? (Are they considered in current KPLU-programme).
	Interactions between surface and bedrock systems.	Insufficient data and models/descriptions of hydraulic properties and flow conditions in overburden and uppermost rock. Surface system model based on old (version 1.1) bedrock model.	Yes, comparison of slug tests, pumping tests and grain size distribution data for calculation of hydraulic conductivity.	Hydrogeological models (recharge to rock, effects of repository drawdown). Transport/flow of matter (incl. radionuclide transport models). Ecosystem models.	No.	Alternative models for vertical distribution of hydraulic properties in QD may be useful. Not developed yet.	No.	Geologic (e.g. stratigraphy) and hydrogeologic (e.g. hydraulic properties, groundwater levels) data. Investigations are planned.
Surface system – Chemistry	Transport of matter.	Lack of discharge data.	No.	Transport/flow of matter. Ecosystem models.	No.	No.	No.	Site specific data – measurements initiated 2004, but relevant time series will not be available until after F1.2.
	Chemistry in regolith.	Uncertainty in which parameters that are relevant for transport processes.	No.	Transport/flow of matter. Ecosystem models.	No.	No.	No.	Site specific data – investigations are planned.
	Chemistry in QD groundwater.	Uncertainty in groundwater origin and flow paths.	No.	Hydrological and hydrogeological models (basic description, comparison/calibration). Transport/flow of matter.	No.	No.	No.	Site specific data – investigations are planned.
Ecosystems – biotic	Biomass and production (flora and fauna).	Limited site data density.	No.	Sedimentation and accumulation of matter.	No.	No.	No.	Site specific biomass and production data – investigations are planned.
	Chemical composition of biota.	Samples exist, but not yet analysed.	No.	No.	No.	No.	No.	Site data – investigations are planned.
	Occurrence of marsh gas.	No investigations performed.	No.	No.	No.	No.	No.	Site data – presently no investigations are planned.

Table A4-7. Interactions judged to be important (green) and to what extent these where actually considered (black).

<p>Bedrock geology</p>	<p>Spatial distribution of properties based on rock domains. DFN geometry is used to infer properties in theoretical approach. Both effects are considered.</p>	<p>Spatial distribution of properties based on rock types and their distribution in the rock domains. Foliation could impact anisotropy in thermal properties. Modal analyses is used as (one) input. Is partly done. Anisotropy not yet assessed.</p>	<p>Rock domains, deformation zones and DFN-geometry is the geometrical framework. DZ geometry alternatives used as input. Assessment of hydrogeological reasonableness of using geological DFN as input – Hydrogeological DFN close to percolation threshold. Especially below DZ A2 the hydraulic conceptual model could be questioned see Chapter 8. Possibly only the DZ are hydraulically interesting. Potential differences in DZ pattern and fracturing within RFM029 (NW vs. SE) possibly not fully assessed. Analysis concentrated on RFM029, not assessed variation in other RD (also little data there).</p>	<p>Fracture mineralogy and chemical composition of bedrock should be considered. Hydraulically important DZ would explain origin of water. Is done.</p>	<p>Spatial distribution of properties based on rock domains (identified rock types in rock domain model). Porosity measurements on surface and borehole samples. Fracture mineralogy and hydrothermal alteration. Is done to the extent possible.</p>	<p>No need.</p>	<p>No need.</p>	<p>Data on geometry (rock surface, fracture zones, etc), mineralogy and geochemistry. Is considered.</p>	<p>No need.</p>
-------------------------------	---	--	--	---	---	-----------------	-----------------	--	-----------------

<p>A) Stress orientations in relation to fracture sets could give additional confidence i DZ and DFN models.</p> <p>B) Reason for division of RD and DZ could be reassessed (less reason to split between domains or reason to split existing domain).</p> <p>A) Not used, but is planned. Must keep in mind that the different fracture sets can be geologically old structures and the current stress field is different from the stress field that formed the fractures.</p> <p>B) The RDs in Forsmark are well defined. The possibility of identifying a new RD below ZFMNE00A2 was considered.</p>	<p>Rock mechanics (in the bedrock)</p>	<p>Is thermal expansion measured on stress released samples OK? Possibly discussed.</p>	<p>Stress orientation expected to affect hydraulic anisotropy field.</p> <p>Above DZ A2 there is clear hydraulic anisotropy. Only three fracture sets are conductive. The SubH set is the most conductive and orthogonal to the minimum principal stress ($\sigma_3 = \sigma_h$) and parallel to the maximum principal stress ($\sigma_1 = \sigma_H$), i.e. possibly a RM-explanation. σ_1 is also very high close to the surface, which appears to be a good explanation for the highly conductive SubH features close to surface.</p> <p>At depth (below DZ A2). Lack of hydraulic conductive features is reasonable in relation to the stress situation (no formal analysis).</p>	<p>No need (only indirectly from hydrogeology and transport properties).</p>	<p>Consider stress impact on "intact" rock samples for laboratory measurements.</p> <p>Formation factor logs suggest a stress impact on diffusivities, but there are also uncertainties (rock type, pore fluid) in the in situ formation factor data (see Table A4-1). Stress release impact on other transport data more difficult to assess.</p>	<p>No need.</p>	<p>No need.</p>	<p>No need.</p>	<p>No need.</p>
<p>Enhance the utility of the data by considering what is really used and shown to be critical for the thermal modelling.</p> <p>Mineralogy of different rock types presented with thermal properties in focus.</p>	<p>No need (thermal expansion analysis is outside SDM see Table A4-4).</p>	<p>Thermal (in the bedrock)</p>	<p>Temp. affects some hydraulic properties.</p> <p>Is considered and judged unimportant.</p>	<p>No need.</p>	<p>No need.</p>	<p>No need.</p>	<p>No need.</p>	<p>No need.</p>	<p>No need.</p>

<p>A) Confirmation and indications of structures (i.e. are there hydraulic contacts or not).</p> <p>B) Control of the hydraulic applicability of the DFN-model.</p> <p>A) Indications of water in single hole interpretation have affected identification of DZ, but other indicators primarily used. However, more systematic re-check and more use of hydraulic data could be carried out.</p> <p>Importance of the different variants in the regional domain should affect future (v2.1) ambition level for the DZ regional model.</p> <p>B) Noted that the three conductive fracture sets also are the dominant part of geological DFN. Future work is needed concerning the understanding of DFN below DZ A2.</p>	<p>Water pressure reduces the rock stress to effective stress.</p> <p>Assess consistency between stress magnitudes as well as stress orientations and hydraulic conductivity.</p> <p>Observed anisotropy above A2 and the small amount of water conductive features below A2 supports the model of stress model. However, HM-couplings also have many uncertainties.</p>	<p>Thermal convection affects uncertainty in measurement of initial temperature.</p> <p>Discussed.</p>	<p>Hydrogeology in the bedrock</p>	<p>Mixing is considered as the main mechanism for distribution and evolution of groundwater composition.</p> <p>Simulation of past salinity and, distribution of end-member waters, evolution, predicted salinity distribution and possibility to compare predicted and measured.</p>	<p>Identification of potential flow paths where description is needed.</p> <p>Correlation between transport and hydrogeological parameters.</p> <p>Flow logs considered in identification of "flowing fractures".</p> <p>Unclear whether "type fractures" could be identified (see Table A4-5).</p>	<p>Input to coupled hydrogeological/hydrogeochemic modelling of the surface system.</p> <p>No such modelling has been done.</p>	<p>Integrated models and description.</p> <p>Boundary condition in surface system models.</p> <p>Common hydraulic properties in overlapping domain, bottom boundary condition provided. However, based on version 1.1 bedrock hydrogeology model.</p>	<p>No need.</p>	<p>No need.</p>
--	--	--	---	---	---	---	---	-----------------	-----------------

No need (current hydrogeochemistry has very little impact on mineralogy).	No need (for the site description).	No need.	<p>Hydrogeo-chemistry in the bedrock</p> <p>Hypothesis of palaeo-evolution. Density affects flow.</p> <p>Present day salinity and water type distribution are "calibration targets" for simulation. Models consider density effects.</p> <p>Very uncertain data on pore water composition in the matrix.</p>	<p>Groundwater composition affects sorption parameters (salinity could also affect diffusivity but a minor impact).</p> <p>Input to process-based retention modelling.</p> <p>Groundwater composition (identified water types) used to set up laboratory tests and in parameterisation of retardation model.</p>	<p>Integrated models and description.</p> <p>Boundary condition and water types in surface system models.</p> <p>Some comparisons are made, but no detailed modelling.</p>	No need.	No need.	No need.
No need.	No need.	No need.	<p>Bedrock Transport Properties</p> <p>Modelling salt migration should be consistent with assessed migration properties.</p> <p>Consistency check as regards porosities and mass transfer parameters used in palaeo-simulations should be done.</p>	<p>Bedrock Transport Properties</p>	No need.	No need.	No need.	No need.
No need.	No need.	No need.	<p>Identification of water types and boundary conditions.</p> <p>Input of surface water type considered in the modelling.</p>	No need.	<p>Hydrogeo-chemistry (surface and near surface)</p>	<p>Supporting analyses (evaluation of specific chem. parameters, coupled modelling).</p> <p>Used in descriptive model.</p>	<p>Specific processes, e.g. precipitation-dissolution.</p> <p>Is considered in the description of soil forming processes.</p>	<p>Chemical composition of soil and waters.</p> <p>Used in modelling and validation of flow of matter in limnic ecosystem descriptions.</p>

No need.	No need.	No need.	No need.	Integrated models and description. Identification of boundary conditions. Simplified description used in deep rock model.	Input to deep rock model (e.g., GW recharge to rock). Hydraulic properties and boundary conditions in coupled models. Is considered.	No need.	Flow pattern, input to mass balance and mass transport modelling. Performed to some extent, based on regional data.	Surface hydrology and near surface hydrogeology	Soil forming processes (erosion, sedimentation, peat accumulation) Is considered.	Flow rates, volumes of surface waters and groundwater. Used in biomass, production and transport calculations, based on regional data.
Post-glacial tectonics. Data on post-glacial tectonics used in descriptive model.	No need.	No need.	No need.	QD description provides basis for derivation of boundary conditions. e.g. recharge/discharge, shoreline displacement. Salinity variation and shoreline displacement are used in modelling.	QD description provides input to selection of water types and input to coupled modelling. Salinity variation and shoreline displacement are used in modelling.	No need.	Type of QD affects chemical composition (description, process models). QD/water chemistry correlation studied, but no detailed modelling.	Geological model (QD map and stratigraphic model) used as a basis for numerical model. Hydrogeological properties (comparison/consistency check). Is done.	Quaternary Deposits and topography	Geological model (QD map and stratigraphic model) and soil type model used as modelling inputs. Is done.
No need.	No need.	No need.	No need.	No need.	Modelling of biogeochemical processes. Assignment of boundary conditions to deep rock model. Carbon transport processes identified, but not quantified.	No need.	Modelling of biogeochemical processes. Included in conceptual model, no detailed modelling performed.	Input data to water balance modelling (interception and evapotranspiration) Is considered.	Turbation, soil type and accumulation processes. Is considered.	Biota

Motivation and selection of site for cored boreholes KFM07A, KFM07B KFM08A, KFM08B, KFM06B, KFM06C, and the associated group of percussion boreholes HFM20, HFM21 and HFM22 (Appendix to SKB Decision paper 1024611)

Background

A recent decision has been taken by SKB to focus cored drilling activity during the second half of 2004 and the first half of 2005 in the north-western part of the candidate area (see SKB document 023661, 2004-04-14/. This decision is in line with the strategic observation noted in connection with the establishment of the site descriptive model, version 1.1, that there is a need for a reduction in the prioritised area at Forsmark /SKB, 2004/. However, it was also noted in this report that sufficient geological data that are necessary to motivate the selection of such an area will only have been analysed after establishment of the site descriptive model, version 1.2. For this reason, aspects of repository design, construction and operation have steered selection of the north-western area during the next round of drilling activities, pending presentation of the site descriptive model version 1.2 during the early part of 2005 /see SKB document 023661, 2004-04-14/.

Rock domains and structural scenario within and marginal to the north-western part of the candidate area

The area within and marginal to the north-western part of the candidate area consists of four separate rock domains (Figure 1). These were referred to as RFM012, RFM018, RFM029 and RFM032 in the version 1.1 geological model for the Forsmark site /SKB, 2004/. Rock domain RFM029 forms the most important bedrock component in the rock volume that includes the candidate area (Figure 1). A brief description of these rock domains is provided here. A more detailed documentation of the geological characteristics of these domains is provided in the site descriptive model, version 1.1 /SKB, 2004; see especially Appendices 5-1, 5-2 and 7-1/.

Rock domain 12 (RFM012). This rock domain forms a minor bedrock component outside the candidate area, directly south and west of the barrack area (Figure 1). It consists predominantly of medium-grained metagranite, similar to that observed in the candidate area, but with an inferred higher degree of ductile deformation. However, there are few outcrops in this domain and no available old borehole data. The paucity of data gives rise to some uncertainty concerning how or even whether or not this domain should be separated from RFM029 inside the candidate area (see below). For this reason, important question marks remain concerning the volume of bedrock that is suitable for repository purposes in this area.

Rock domain 18 (RFM018). This rock domain is situated to the south-west and west of the candidate area (Figure 1). It consists of a tectonically banded sequence of different types of metagranitoid, fine-grained felsic meta-igneous rocks that are inferred to be volcanic in origin, amphibolite, and pegmatite or pegmatitic granite. This intensely banded sequence strikes NW and dips steeply to the south-west. The rocks in this strongly inhomogeneous domain show both planar and linear, mineral grain-shape fabrics and were affected by an inferred high degree of ductile strain. A type outcrop for this domain is exposed at drill site 4. Furthermore, the upper part of KFM04A has penetrated the rocks in this domain and confirmed the poor suitability of this domain as a repository host rock.

Rock domain 29 (RFM029). Rock domain 29 forms the most important bedrock component in the rock volume that includes the candidate area (Figure 1). Cored boreholes KFM01A, KFM01B, KFM02A, KFM03B and a large part of cored boreholes KFM03A and KFM04A have been drilled through the bedrock in this rock domain. It consists predominantly of medium-grained metagranite that has yielded a U-Pb (zircon) age of 1,866 million years. The metagranite displays a mineral grain-shape fabric that is predominantly linear in character. However, a stronger planar grain-shape

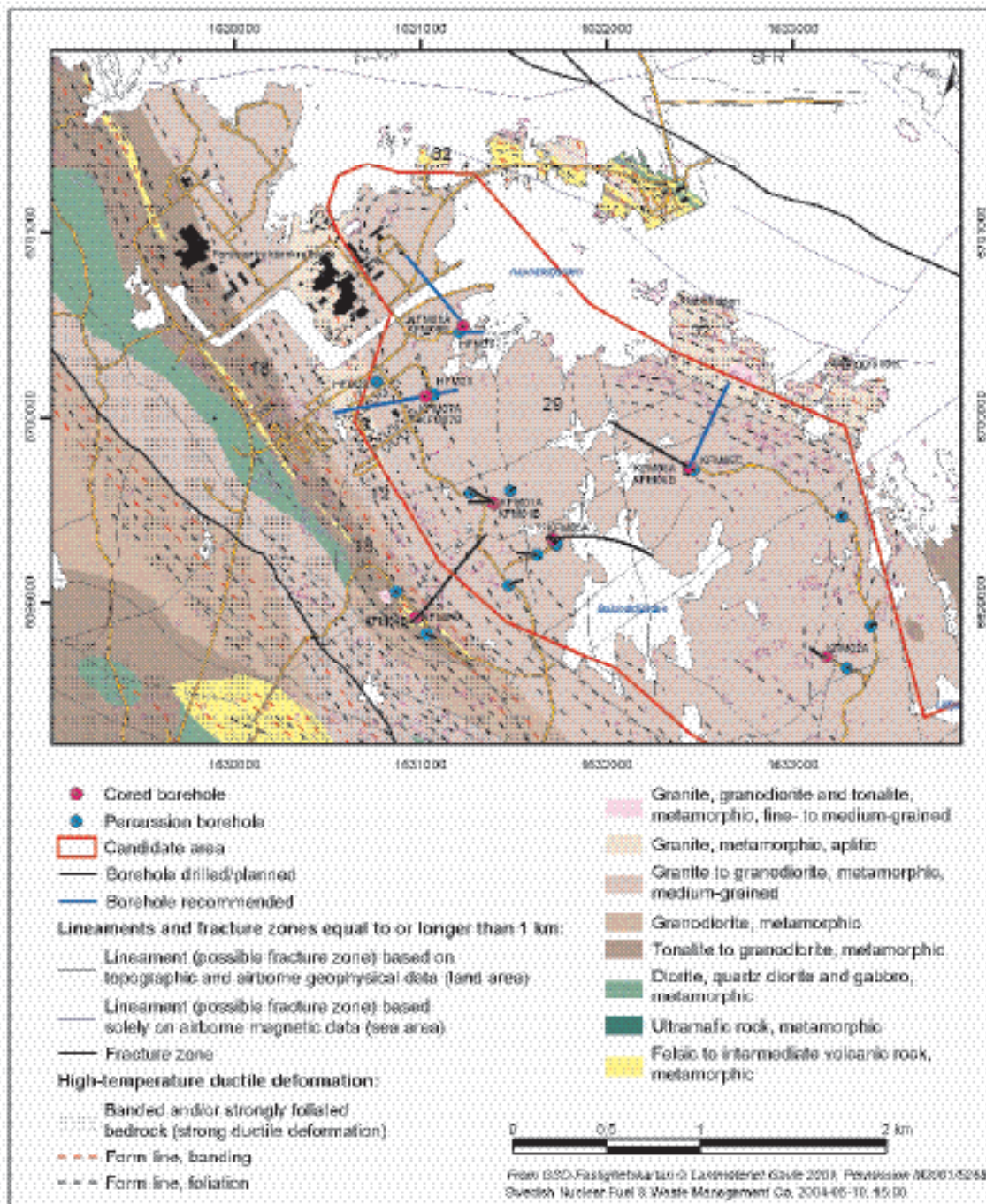


Figure 1. Geological map of the north-western part of the candidate area and its surroundings with boreholes.

fabric is conspicuous closer to the contacts with the marginal rock domains to the west (RFM012), south-west and west (RFM018), and both north-west and north-east (RFM032). It is inferred that this change is related to an increase in the degree of ductile deformation towards the contacts of the metagranite with other rock units.

Rock domain 32 (RFM032). This rock domain forms a folded bedrock component directly to the north-west and to the north-east of the candidate area (Figure 1). It consists of fine-grained and leucocratic (i.e. aplitic) metagranite, banded fine-grained felsic meta-igneous rocks that are inferred to be volcanic in origin, amphibolite, and pegmatite or pegmatitic granite. Geological mapping at Klubbudden and close to the nuclear power plants 1 and 2, as well as an inspection of shallow cored boreholes from this nuclear power plant site, have shown that this domain also contains a

whitish grey, felsic meta-intrusive rock with biotite flecks. This lithology is inferred to be an altered (albitised?), medium-grained metagranite, similar to that observed in RFM029.

This inhomogeneous packet of commonly fine-grained, meta-igneous rocks dips moderately to the south-east beneath RFM29 in the hinge of the major synform west of Asphällsfjärden (Figure 2). To the north-east of the candidate area, the rocks within this domain strike north-west and dip steeply to the south-west beneath RFM029. Fracture mapping at Klubbudden has demonstrated a higher frequency of fractures relative to that observed in the medium-grained metagranite inside the candidate area. These results provide support to the preliminary assessment carried out during the Östhammar feasibility study that the bedrock represented in the coastal strip, north-east of the candidate area, is not suitable as a repository host-rock.

What are the key questions to be solved with the drilling?

Both the ongoing, preliminary repository layout work as well as the geological considerations discussed above awaken the following key questions and, thereby, motivate a drilling campaign in the north-western part of the candidate area.

- How far can the volume of potentially suitable bedrock for a repository, which is known to occur within rock domain 29, be extended to the west, north-west and north-east?
- What are the lithological, structural, rock mechanical, hydrogeological and hydrogeochemical characteristics of the bedrock in the north-western part of the candidate area?
- Are there any significant lithological, structural, rock mechanical, hydrogeological and hydrogeochemical changes in rock domain RFM029 in the hinge versus the flanks of the major synformal fold structure that passes west of Asphällsfjärden.
- Are there any so far undetected fracture zones with NS or NE strike that pass through the north-western part of the candidate area? It is important to keep in mind that the topography in this area has been disturbed during the building activity around the nuclear power plants. Furthermore, new (2002) airborne geophysical data are not available in the vicinity of the nuclear power plants.

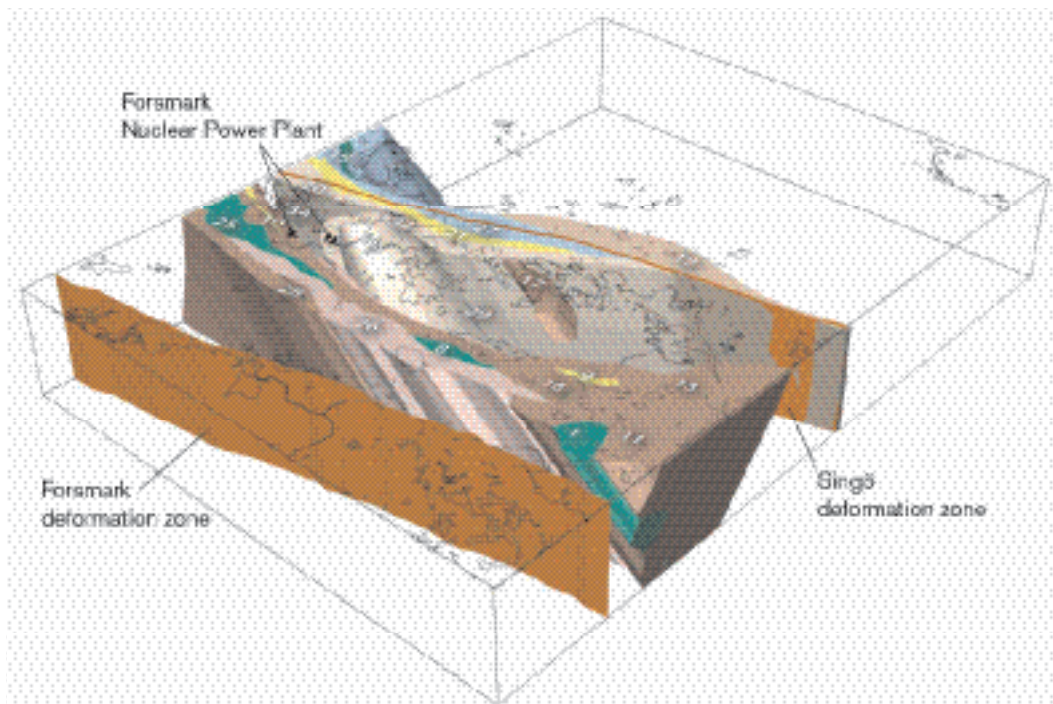


Figure 2. Rock domain model viewed to the north. Domains RFM029 and RFM034 are unshaded in order to show the major folding within the tectonic lens at the Forsmark site. The domains southwest of domain RFM026 are unshaded in order to show the modelled southeasterly elongation of the bedrock at Forsmark.

- The repository layout work carried out so far suggests that communication shafts and common facilities at repository level (central area) should be located more or less below the present barrack area. In order to obtain a reasonable, early-stage assessment of the feasibility of such a layout, the drilling campaign should provide information about the rock engineering characteristics of the bedrock in this area, in particular with respect to geomechanical conditions.

Finally, there is a need to complement the new telescoped boreholes with short, additional cored boreholes in order to provide a cored column for the uppermost 100 metres.

Boreholes – motivation, choice of site and orientation

In order to provide answers to the key questions that have been raised above, it is recommended that six cored boreholes and three percussion boreholes are drilled at four separate sites in the north-western part of the candidate area. Three of these sites are located within the Forsmark industrial area. These sites will be denoted as drill site 7, where the two cored boreholes KFM07A and KFM07B as well as the percussion borehole HFM21 will be drilled, and drill site 8, where the cored boreholes KFM08A and KFM08B as well as the percussion borehole HFM22 will be drilled. The third percussion borehole referred to as HFM20 will be drilled c. 300 m to the west-north-west of drill site 7. In order to minimise the effects of environmental disturbance, it is recommended that all these boreholes are placed alongside minor roads. The fourth site has been placed at the already established drill site close to the small lake Puttan that is referred to as drill site 6. The cored boreholes KFM06B and KFM06C will be drilled at this site.

Cored boreholes

Table 1 summarizes the position, orientation and length of the six cored boreholes. The locations are also shown in Figure 1. They are listed in the table in the recommended order of drilling. It is noted that three boreholes (KFM07A, KFM08A and KFM06C) should be drilled at a dip angle of 60° and with a borehole length of 1000 m and thereby extend 500 m in a horizontal direction. The other three boreholes (KFM06B, KFM07B and KFM08B) are subvertical with borehole lengths of 100 m, 500 m and 100 m, respectively.

Table 1. Position, dip, direction and borehole length of the planned cored boreholes in the north-western part of the candidate area. The co-ordinates listed below refer to the position of the drill site.

Borehole	Drill site	N-S co-ordinates	E-W co-ordinates	Dip (°)	Direction (°)	Borehole length (m)
KFM06B	6	6699730	1632440	85	300	100
KFM07A	7	6700127	1631031	60	260	1000
KFM08A	8	6700469	1631221	60	320	1000
KFM08B	8	6700469	1631221	85	320	100
KFM06C	6	6699730	1632440	60	025	1000
KFM07B	7	6700127	1631031	85	260	500

Borehole KFM06B. This borehole should be drilled at site 6 down to 100 m borehole length, at an angle of 85° and in the same direction as KFM06A, i.e. 300°. Drill site 6 is situated at the end of the minor road that passes KFM02A and terminates close to the small lake Puttan (Figure 1). This borehole will complement borehole KFM06A with cored borehole material in the hydrogeologically critical interval of 0-100 m.

Borehole KFM07A. This borehole should be drilled at site 7 in the eastern part of the barrack area (Figure 1). The borehole should be drilled down to 1000 m borehole length, at an angle of 60° and in the direction 260°. This borehole will enter the bedrock in rock domain 29 on the south-western flank of the synformal structure that plunges moderately to the south-east. The borehole will help

to constrain the boundary of potentially suitable bedrock in a westerly direction. It will also provide better constraints on the bedrock geology in the poorly-exposed area around the barrack area and penetrate diagonally through the rock volume that is of interest for communication shafts and associated facilities, according to the ongoing layout work.

Borehole KFM08A. This borehole should be drilled at site 8 at the end of a minor road that passes westwards out to Asphällsfjärden (Figure 1). The borehole should be drilled down to 1000 m borehole length, at an angle of 60° and in the direction 320°. This borehole will enter the bedrock in rock domain 29 in the hinge of the major synformal structure that plunges moderately to the south-east. The borehole will help to constrain the boundary of potentially suitable bedrock in a north-westerly direction and provide more information concerning the geometry of the boundary between rock domains RFM029 and RFM032.

Borehole KFM08B. This borehole should be drilled at site 8 (Figure 1) down to 100 m borehole length, at an angle of 85° and in the same direction as KFM08A, i.e. 320°. This borehole will complement KFM08A with cored borehole material in the hydrogeologically critical interval of 0-100 m.

Borehole KFM06C. This borehole should be placed at drill site 6 (Figure 1). The borehole should be drilled down to a borehole length of 1000 m, at an angle of 60° and in the direction 025°. It will enter the bedrock in rock domain 29 on the north-eastern flank of the major synformal structure that plunges moderately to the south-east. The borehole will help to constrain the boundary of potentially suitable bedrock in a northerly to north-easterly direction and will provide more information concerning the geometry of the boundary between rock domains RFM029 and RFM032.

Borehole KFM07B. This borehole is preliminary in character, and should be drilled provided that data from the boreholes listed above, especially KFM07A, do not provide key information that argue against execution of the drilling. Pending this assessment, it should be drilled at site 7 (Figure 1), adjacent to KFM07A, at an angle of 85° in the same direction as KFM07A, i.e. 260°. One purpose of the drilling is to complement KFM07A and provide a cored column for the uppermost 100 m. Furthermore, it is envisaged that data on rock mass quality, state of stress and hydrogeological conditions down to repository depth will be of high priority, since the borehole penetrates through or near to the target volume for shafts and common facilities of a potential repository at Forsmark. This is the main argument for extending the borehole to c. 500 m depth. In addition, the borehole will contribute to the understanding of some of the geological key questions listed above.

Following the drilling campaign outlined here, the north-western part of the candidate area will have been penetrated with inclined boreholes with a 1000 m borehole length in the directions 045° (KFM04A), 080° (KFM05A), 300° (KFM06A), 260° (KFM07A), 320° (KFM08A) and 025° (KFM06C), as well as with five subvertical boreholes with a borehole length of 500 m or 1000 m (KFM01A, KFM01B, KFM02A and KFM07B). This variation in borehole orientation should minimise the biases that can arise in the documentation of both fractures and the occurrence of vuggy metagranite.

Percussion boreholes

Table 2 summarizes the position, orientation and length of the three percussion boreholes (HFM20, HFM21 and HFM22). The locations are also shown in Figure 1.

Table 2. Position, dip, direction and borehole length of the planned percussion boreholes in the north-western part of the candidate area.

Borehole	Drill site	N-S co-ordinates	E-W co-ordinates	Dip (°)	Direction (o)	Borehole length (m)
HFM20	–	6700191	1630769	85	350	300
HFM21	7	6700125	1631077	60	080	250
HFM22	8	6700460	1631210	60	090	250

Borehole HFM20 should be drilled subvertically (85°) in a direction that is approximately at a right angle to the two other percussion boreholes. A borehole length of 300 m is recommended provided that bedrock and groundwater conditions permit drilling to this depth. This borehole will be drilled in the same area as the other percussion boreholes but at some distance from HFM21 and HFM22.

HFM21 and HFM22, both 250 m in length, will be drilled to supply drill sites 7 and 8, respectively, with water during the core drilling. Thus, they are located close to these two sites. However, their location, orientation and length have also been selected in order to investigate the character at depth of two separate lineaments that trend c. north-south and that are possible deformation zones. For this reason, it is recommended that both boreholes HFM21 and HFM22 should be drilled at an angle of 60° in the directions 080° and 090°, respectively.

Together, these three boreholes will form a geometrical array that will permit a detailed, cross-hole hydraulic investigation of the superficial part of the bedrock (0 to c. 200 m) in this part of the investigation area.

Reference

SKB, 2004. Preliminary site description. Forsmark area – version 1.1. SKB R-04-15, Svensk Kärnbränslehantering AB.

Michael Stephens

Bengt Leijon

Sven Follin

Forsmark, 2004-05-10

Revision of the recommended length and orientation of borehole KFM08B (Appendix to SKB decision paper 1038014)

Background

A decision was taken by SKB to focus cored drilling activity during the second half of 2004 and 2005 in the north-western part of the candidate area /SKB document 023661, 2004-04-14/. This decision is in line with the strategic observation noted in connection with the establishment of the site descriptive model, version 1.1, that there is a need for a reduction in the prioritised area at Forsmark /SKB, 2004/. It is also strongly supported by the results of the geological modelling in the ongoing site descriptive model programme, version 1.2. The results of the version 1.2 geological modelling were presented to the site investigation team at Forsmark on the 20th September, 2004. As a consequence of the earlier decision and the need for planning of drilling activity during the period 2004-2005, a document was completed that summarised the key questions that need to be solved by a drilling campaign in the north-western part of the candidate area /SKB document 1024611, 2004-05-13/. This campaign involved six cored boreholes (KFM06B, KFM06C, KFM07A, KFM07B, KFM08A and KFM08B) as well as three percussion boreholes (HFM20, HFM21, HFM22). The motivation concerning the choice of site for and the orientation of all these boreholes was also included in this document.

Previous motivation for KFM08B and subsequent developments

Since the upper part of the bedrock at several sites of investigation at Forsmark is hydraulically highly conductive, it is important that the telescoped boreholes at each drill site are complemented with short, additional cored boreholes in order to provide a cored column for the uppermost 100 metres. With this motivation in mind, it was decided to drill KFM08B at drill site 8 down to 100 metres borehole length, at an angle of 85° and in the same direction as KFM08A, i.e. 320° /SKB document 1024611, 2004-05-13/.

One of the major uncertainties for the establishment of a structural model at the Forsmark site concerns how well lineaments that have been recognised at the surface represent deformation zones. This uncertainty was pointed out in the site descriptive model, version 1.1 /SKB, 2004/ and, with the establishment of alternative lineament models for the site, is even more relevant in the structural model for the site, version 1.2. Furthermore, the international panel of experts that assist SKI in their detailed scrutiny of the site investigation work at both Forsmark and Oskarshamn (INSITE) have also pointed out the need for more information concerning the structural geological significance of lineaments. For these reasons, it is judged necessary to modify the borehole length and orientation of borehole KFM08B in order to improve our understanding of the geological significance of the lineaments in the Forsmark area.

Revised assessment for the length and orientation of KFM08B

The area around Bolundsfjärden in the north-western part of the Forsmark site is transected by several lineaments. The most conspicuous orientation sets in this area are NS and NE (Figure 1). These lineaments can be followed northwards to the coastal area and lineaments with NS trend are present in the vicinity of drill site 8 (Figure 2). Under the pre-condition that borehole KFM08B should be used to improve our understanding of lineaments, in addition to the necessary completion of cored drilling in the uppermost 100 metres of the bedrock, this borehole needs to be drilled either westwards or eastwards.

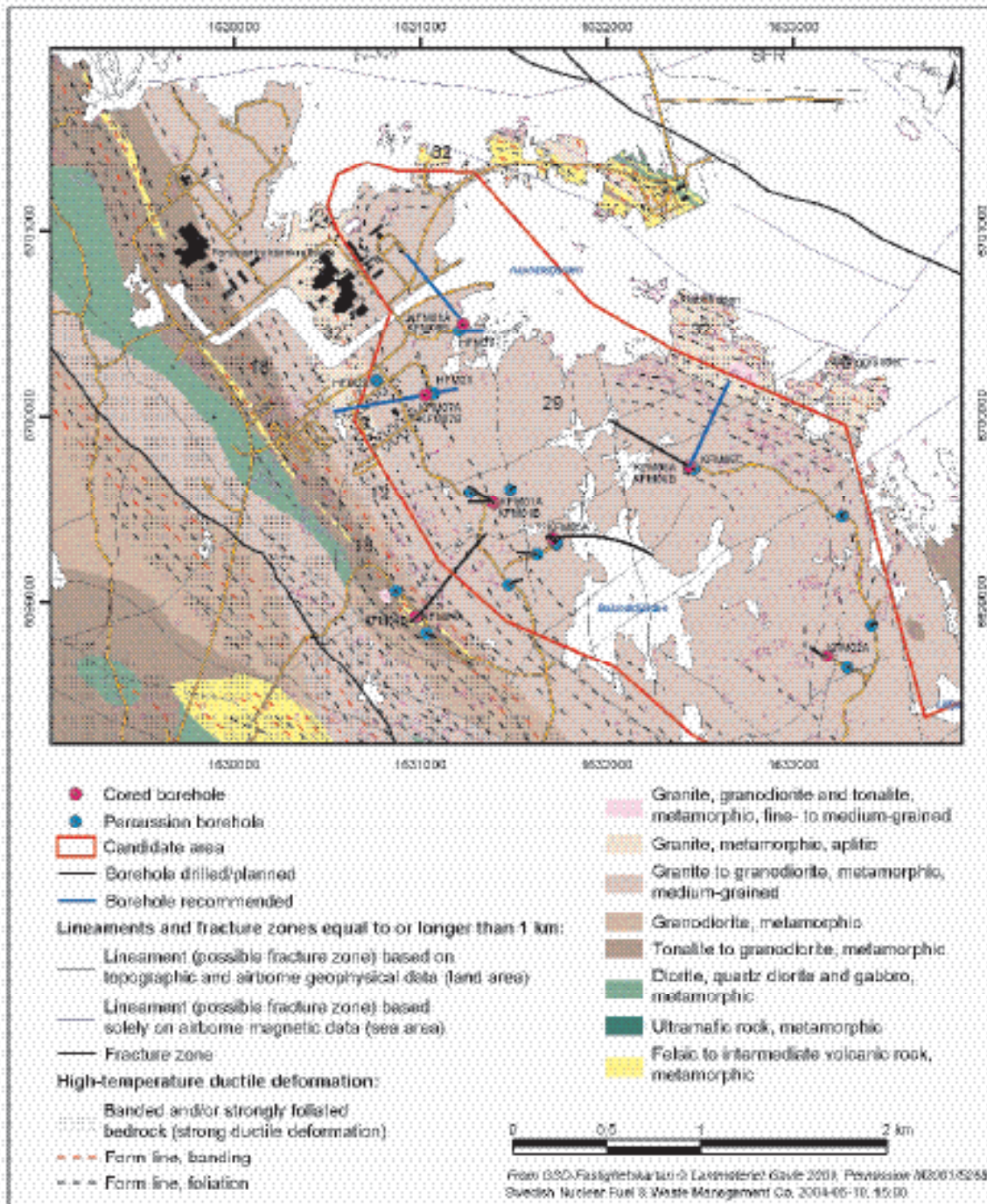


Figure 1. Geological map of the north-western part the candidate area and its surroundings with boreholes. This figure has been extracted from SKB document 1024611.

One of the aims of the drilling activities in the complete site investigation programme is to investigate the extension of the favourable rock domain 29 in the north-western part of the area. For this reason, a third borehole from drill site 8 may well be necessary and will need to be directed in a north-easterly direction towards the inferred north-eastern boundary of this rock domain. Bearing in mind this consideration, it is recommended that the short borehole KFM08B is directed to the west with the aim to provide information concerning the minor lineaments XFM0430A0 and XFM1063A0 that trend NW and NS, respectively. Both these lineaments have been defined solely on the basis of topographic data. In order to improve the chances to intersect deformation zones that are possibly related to these two lineaments, it is recommended that borehole KFM08B is drilled to a borehole length of 200 m.

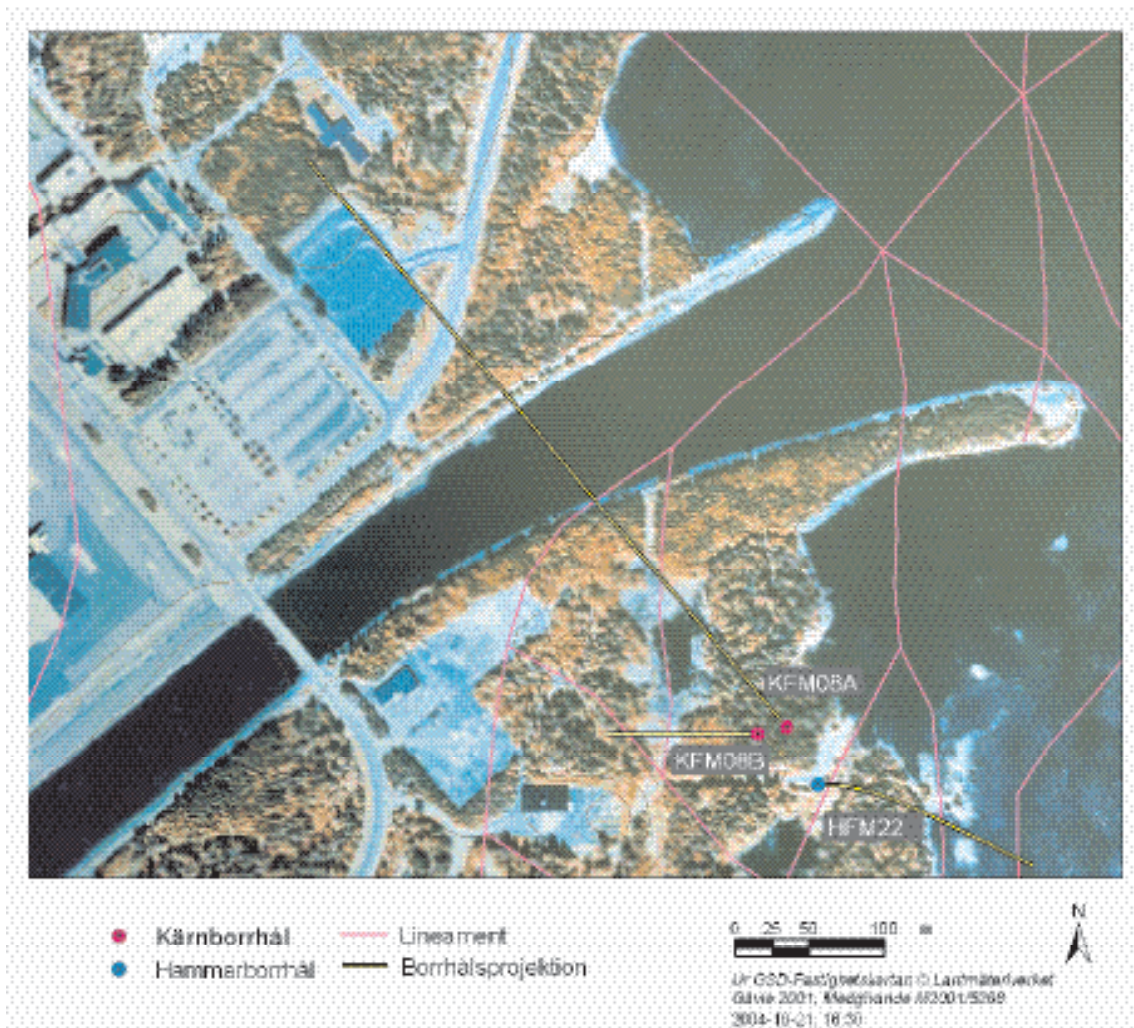


Figure 2. Lineaments in the vicinity of drill site 8. The position of boreholes KFM08A, KFM08B (this document) and HFM22 are also shown.

Conclusion

The borehole length and orientation of borehole KFM08B as recommended in SKB document 1024611 is modified according to Table 1:

Table 1. Position, dip, direction and borehole length of the planned cored borehole KFM08B in the north-western part of the candidate area.

Borehole	Drill site	N-S co-ordinates	E-W co-ordinates	Dip (°)	Direction (°)	Borehole length (m)
KFM08B	8	6700491	1631178	60	270	200

The position of boreholes KFM08A, KFM08B and HFM22 and their relationship to the infrastructure in the coastal area are shown in Figure 3.

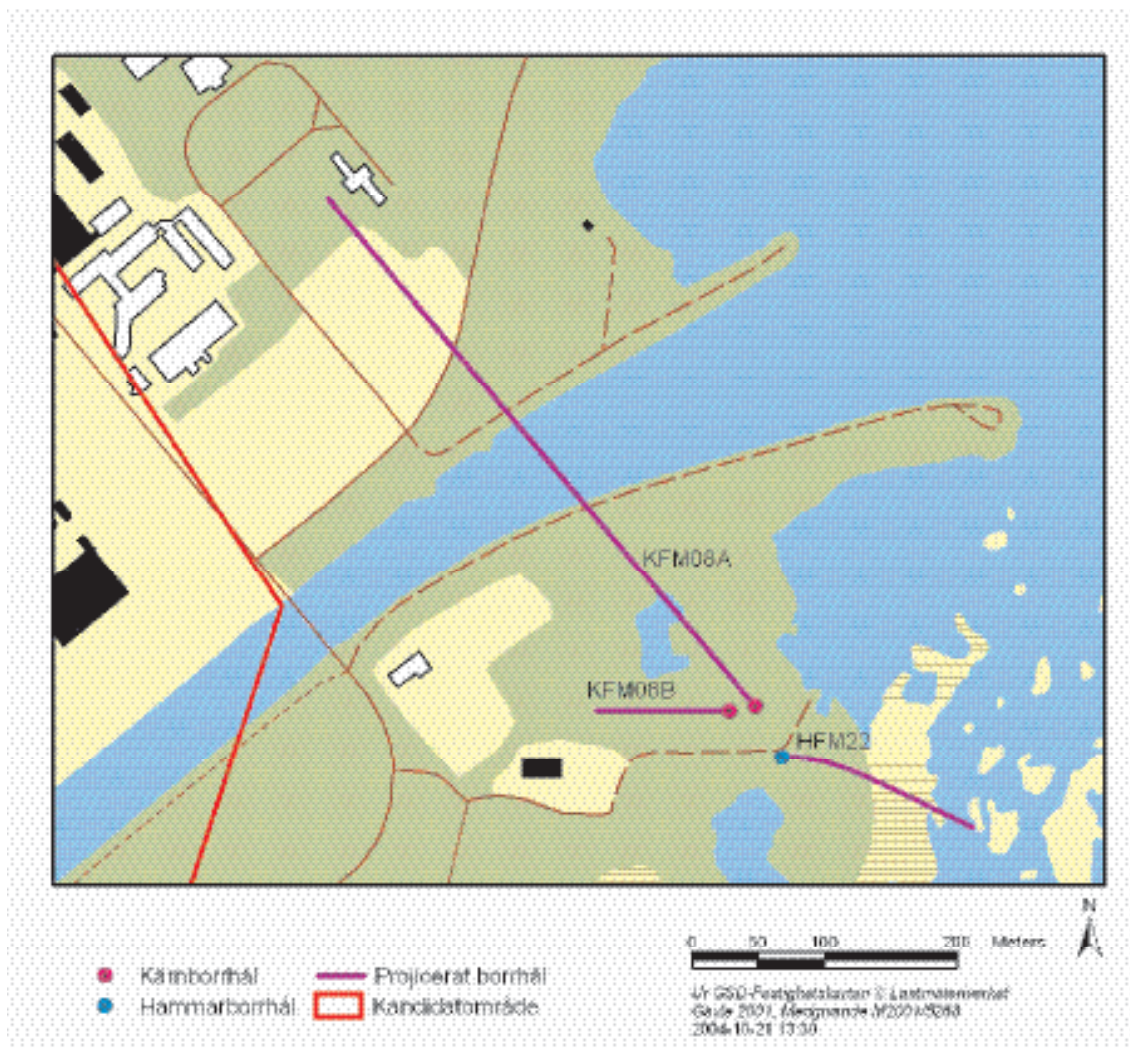


Figure 3. Position of boreholes KFM08A, KFM08B and HFM22 and their relationship to the local infrastructure.

Reference

SKB, 2004. Preliminary site description. Forsmark area – version 1.1. SKB R-04-15, Svensk Kärnbränslehantering AB.

Michael Stephens

Uppsala, 2004-12-15

Motivation for and orientation of cored borehole KFM08C (Appendix to SKB decision paper 1038090)

Background

In accordance with the results of the initial site investigation (ISI) at Forsmark, including the site descriptive model (SDM), version 1.2 /SKB, 2005a/, a decision has been taken by SKB to focus the complementary site investigation (CSI) in the north-western part of the candidate area /SKB, 2005b/. In the document where the CSI programme is motivated and described /SKB, 2005b/, this area is referred to as the priority site (Figure 1).

In the latest motivation for the selection of boreholes /SKB documents 1024611 and 1033089/, the location, orientation and programme for six cored boreholes (KFM06B, KFM06C, KFM07A, KFM07B, KFM08A and KFM08B) at three separate sights were presented. All these sites are situated in the prioritised area and two of them (drill sites 7 and 8) are located in the area north-west of the steeply dipping deformation zone ZFMNE0061 (Figure 1) and the gently dipping zone ZFMNE00A2.

A short description of the four rock domains RFM012, RFM018, RFM029 and RFM032 (Figure 2) and the structural scenario within and marginal to the priority site was presented in SKB document 1024611. These domains occur within and immediately adjacent to the prioritised area. A more detailed documentation of the characteristics of these rock domains as well as the deformation zones that transect the priority site is provided in SDM model, version 1.2 /SKB, 2005a; see especially Appendices 5-1, 5-2 and 5-3/. The present document addresses the motivation for and the orientation of a new, cored borehole with a borehole length of 1000 m within the prioritised area.

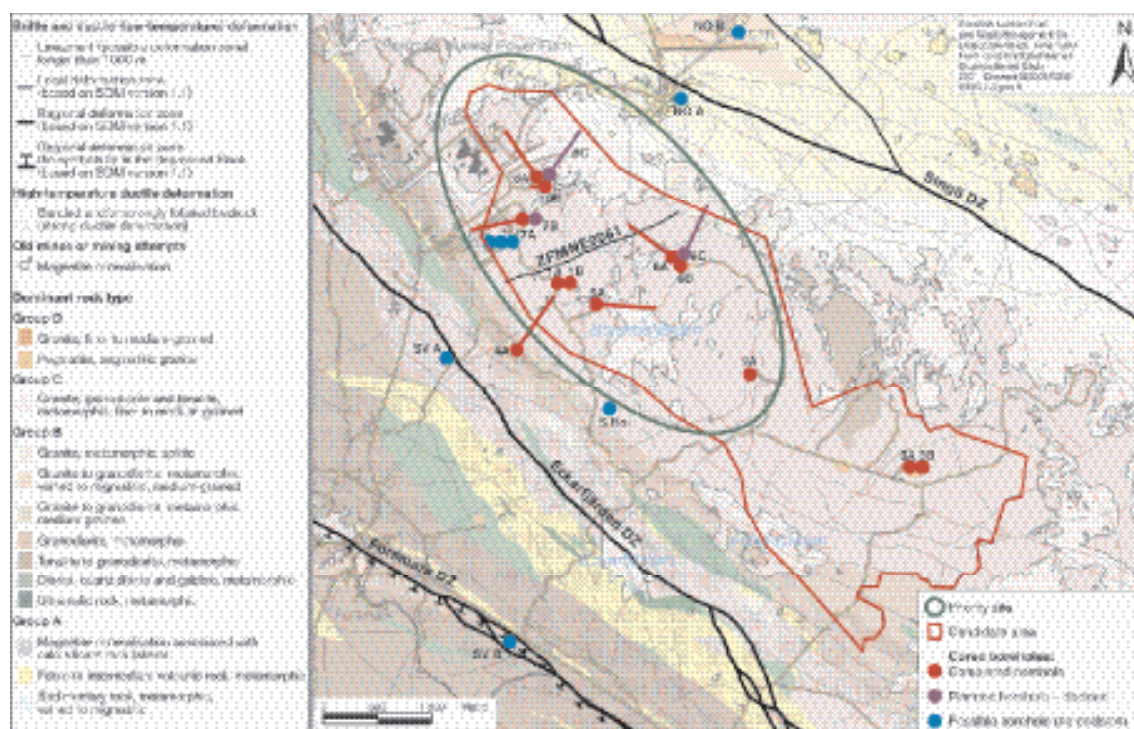


Figure 1. Geological map of the bedrock inside and immediately around the candidate area at Forsmark. Completed, planned and possible cored boreholes as well as the priority site are also shown (modified after /SKB, 2005b/).

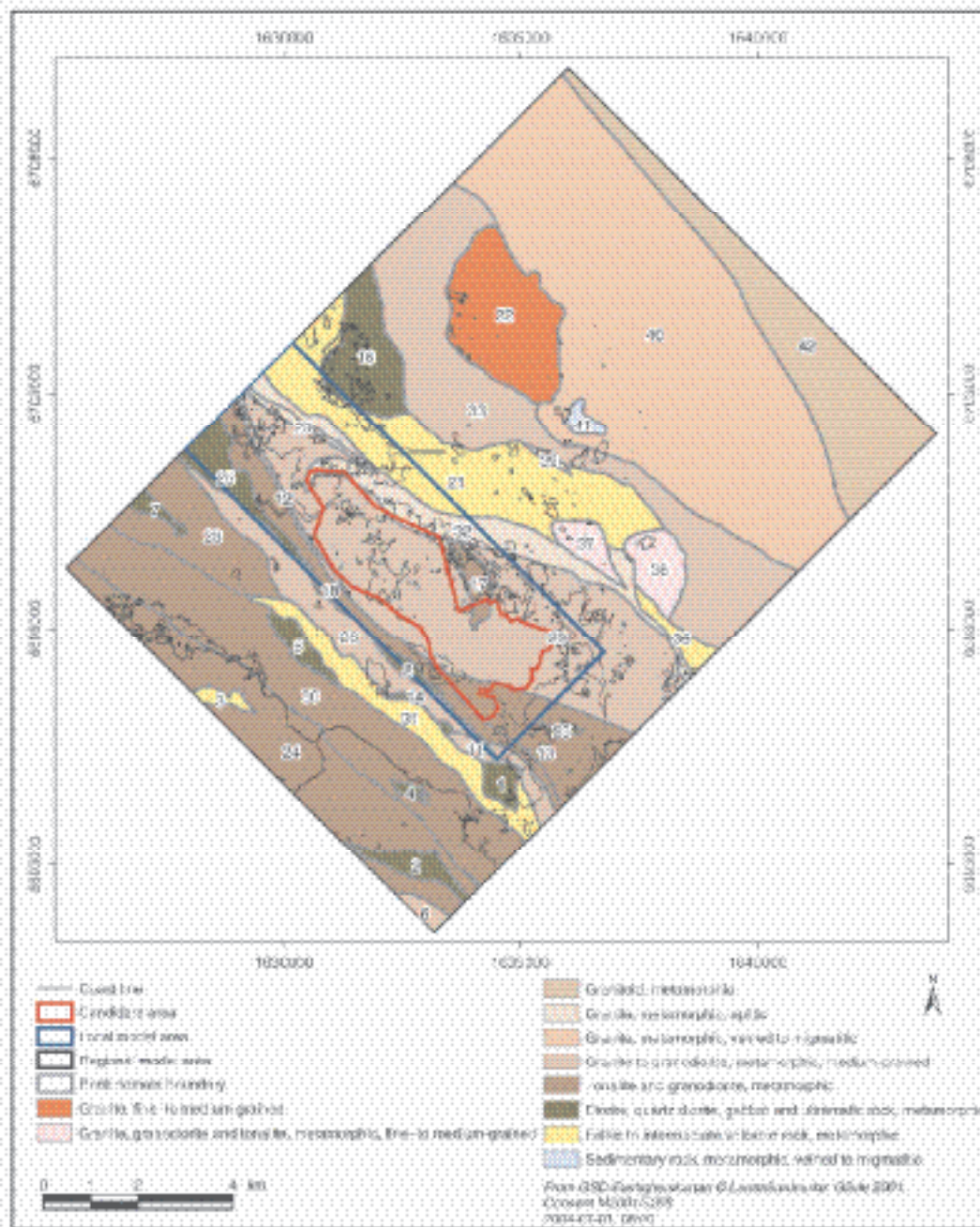


Figure 2. Rock domains at the Forsmark site numbered from 1-42 (after /SKB, 2005a/). Rock domains have been defined on the basis of rock composition and grain size, and degree of homogeneity and ductile deformation. The colours correspond to rock units in Figure 1.

Motivation

What are the key questions to be solved with the drilling

On the basis of the priority decision and the results of the version 1.2 modelling work, a possible layout for a repository has been designed at a depth of 400 m in the north-western part of the candidate area /layout version from Ramböll to SKB, February 2005, see Figure 3/. An important motivation for the 1000 m long boreholes KFM04A, KFM07A and KFM08A concerned how far the volume of potentially suitable bedrock for a repository, which the ISI has demonstrated is present in rock domain 29 (RFM29), extends to the west and north, i.e. though the western and northern parts of the proposed layout area. These boreholes also provide key lithological, structural, hydrogeological and hydrogeochemical data in this part of the priority site. No information is available in the north-eastern part of the prioritised area, beneath Aspfallsfjärden (Figure 3).



Figure 3. Possible repository layout at 400 m depth in the prioritised area /layout version from Ramböll to SKB, February 2005/. This design is based on the results of SDM, version 1.2. Boreholes (including KFM06C, KFM07B and KFM08C) are also shown with known or predicted orientation diversions.

Since outcrops are very sparse in the Asphällsfjärden area, there is considerable uncertainty in the position of the boundary between rock domains RFM029 and RFM032 (Figure 2) and, as a consequence of this, the extension of established, potentially suitable bedrock in the north-eastern part of the priority site. This area is also transected by several lineaments that trend NW, NE and NS. The lineament that trends NS (XFM1064A0) appears to show a low velocity (≤ 4000 m/s) refraction seismic anomaly along a part of its length (RSLV04 in Figure 5-32 in SKB, 2005a). It also possibly connects up with the lineament referred to as XFM0099A0 that trends west of Bolundsfjärden.

Both the preliminary repository layout as well as the geological considerations discussed above awaken the following key questions and, thereby, motivate a drilling campaign under Asphällsfjärden.

- How far can the volume of potentially suitable bedrock for a repository, which is known to occur within rock domain RFM029, be extended to the north-east under Asphällsfjärden?
- What are the lithological, structural, rock mechanical, hydrogeological and hydrogeochemical characteristics of the bedrock in the north-eastern part of the priority site?
- What is the character of the lineaments that transect Asphällsfjärden?
- Are there any so far undetected deformation zones that pass through the north-eastern part of the priority site?

Choice of site and borehole orientation

On the basis of the considerations listed above and in order to minimise the effects of environmental disturbance, it is recommended that the new borehole, with a length of 1000 m, is placed at an already established site (drill site 8). It is also recommended that the borehole is drilled in a north-easterly direction beneath Asphällsfjärden. Such a borehole will penetrate the bedrock in rock domain RFM029 and is directed towards the contact with rock domain RFM032.

Rock domain RFM029 is dominated by a medium-grained, biotite-bearing metagranite that is commonly lineated. Amphibolite and minor intrusions of metatonalite, metagranodiorite, pegmatitic granite, pegmatite and granite form subordinate components. The pegmatitic rocks and the minor intrusions of granite commonly show higher natural gamma radiation values relative to all the other rocks. In contrast, rock domain RFM032 consists of an heterogeneous, banded complex of aplitic metagranite, amphibolite, felsic metavolcanic rocks, medium-grained metagranite, and minor intrusions of metagranodiorite, pegmatitic granite, pegmatite and granite.

The compromise, for environmental considerations, to utilise an existing drill site has important consequences. The present geological model for the site predicts that the borehole will not enter rock domain RFM032. For this reason, the answer to the first question raised above, which concerns the extension of rock domain RFM029 to the north-east, will probably involve a minimum estimate. Notwithstanding this limitation, the borehole will radically improve our understanding of the characteristics of the north-eastern part of the priority site.

It is recommended that KFM08C is drilled at an angle of 60°. In order to explore the north-eastern margin of the prioritised area, a drilling direction of 035° is also recommended. The position, dip, direction and length of borehole KFM08C are summarised in Table 1.

Table 1. Position, dip, direction and borehole length of the planned cored borehole KFM08C.

Borehole	Drill site	Dip (°)	Direction (°)	Borehole length (m)
KFM08C	8	60	035	1000

Following the drilling campaign outlined here, the prioritised area will have been penetrated with boreholes in directions 045° (KFM04A), 080° (KFM05A), 300° (KFM06A), 025° (KFM06C), 260° (KFM07A), 320° (KFM08A) and 035° as well as with five subvertical boreholes (KFM01A, KFM01B, KFM02A, KFM06B and KFM07B). This variation in borehole orientation should minimise the biases that can arise in the documentation of both fractures and the occurrence of various rock types.

References

SKB, 2005a. Preliminary site description. Forsmark area – version 1.2. In manuscript, Svensk Kärnbränslehantering AB.

SKB, 2005b. Forsmark site investigation. Programme for further investigations of geosphere and biosphere. SKB R-05-14, Svensk Kärnbränslehantering AB.

Michael Stephens

Uppsala, 2004-04-14